

FAA CENTER OF EXCELLENCE FOR ALTERNATIVE JET FUELS & ENVIRONMENT

Annual Technical Report

2018

For the period

October 1, 2017 – September 30, 2018

Boston University
Georgia Institute of Technology
Massachusetts Institute of Technology
Missouri University of Science and Technology
Oregon State University
Pennsylvania State University
Purdue University
Stanford University
University of Dayton
University of Hawaii
University of Illinois
University of North Carolina
University of Pennsylvania
University of Tennessee
University of Washington
Washington State University



This work was funded by the US Federal Aviation Administration (FAA) Office of Environment and Energy as a part of ASCENT Project AJFE under FAA Award Number 13-C. Any opinions, findings, and conclusions or recommendations expressed in this material are those of the authors and do not necessarily reflect the views of the FAA or other ASCENT Sponsors.



Table of Contents

Overview Michael Wolcott and R. John Hansman, Center Directors	1
Project 001(A) | Alternative Jet Fuel Supply Chain Analysis Lead Investigators: Michael Wolcott, Michael Gaffney, Manuel Garcia-Perez, Xiao Zhang	4
Project 001(B) | Alternative Jet Fuel Supply Chain Analysis Lead Investigators: Scott Q. Turn	17
Project 001(C) | Alternative Jet Fuel Supply Chain Analysis Lead Investigators: Wallace E. Tyner	30
Project 001(D) | Alternative Jet Fuel Supply Chain Analysis Lead Investigators: Saurabh Bansal, Tom Richard	36
Project 001(E) | Alternative Jet Fuel Supply Chain Analysis Lead Investigators: Burton C. English, Timothy Rials	42
Project 001(F) | Alternative Jet Fuel Supply Chain Analysis Lead Investigators: Steven R. H. Barrett, Raymond L. Speth	72
Project 002 | Ambient Conditions Corrections for Non-Volatile PM Emissions Measurements Lead Investigator: Phil Whitefield	91
Project 003 | Cardiovascular Disease and Aircraft Noise Exposure Lead Investigator: Junenette Peters	99
Project 005 | Noise Emission and Propagation Modeling Lead Investigators: Kai-Ming Li, Victor W. Sparrow	105
Project 008 | Noise Outreach Lead Investigator: Kathleen K. Hodgdon	108
Project 010 | Aircraft Technology Modeling and Assessment Lead Investigators: Dimitri Mavris, William Crossley, Jimmy Tai, Daniel A. DeLaurentis	113
Project 011(A) | Development of Rapid Fleet-Wide Environmental Assessment Capability Using a Response Surface Modeling Approach Lead Investigators: R. John Hansman	166
Project 017 | Pilot Study on Aircraft Noise and Sleep Disturbance Lead Investigator: Mathias Basner	170
Project 018 | Health Impacts Quantification for Aviation Air Quality Tools Lead Investigator: Kevin J. Lane, Jonathan Levy	173



Project 019 | Development of Aviation Air Quality Tools for Airport-Specific Impact Assessment: Air Quality Modeling Lead Investigator: Saravanan Arunachalam	190
Project 020 | Development of NAS wide and Global Rapid Aviation Air Quality Lead Investigator: Steven R. H. Barrett	225
Project 021 | Improving Climate Policy Analysis Tools Lead Investigator: Steven R.H. Barrett, Florian Allroggen	233
Project 022 | Evaluation of FAA Climate Tools Lead Investigator: Donald Wuebbles	241
Project 023 | Analytical Approach for Quantifying Noise from Advanced Operational Procedures Lead Investigators: Philip J. Morris, R. John Hansman	248
Project 024(B) | Emissions Data Analysis for CLEEN, ACCESS, and Other Recent Tests Lead Investigators: Randy Vander Wal	253
Project 025 | National Jet Fuels Combustion Program – Area #1: Chemical Kinetics Combustion Experiments Lead Investigator: Ronald K. Hanson	267
Project 027(A) | National Jet Fuels Combustion Program – Area #3: Advanced Combustion Tests Lead Investigators: Tonghun Lee	272
Project 027(B) | National Jet Fuels Combustion Program – Area #3: Advanced Combustion Tests Lead Investigators: Tim Lieuwen	286
Project 028 | National Jet Fuels Combustion Program – Area #4: Combustion Model Development and Evaluation Lead Investigators: Mohan Gupta, Suresh Menon, Matthias Ihme	301
Project 029 (A) | National Jet Fuels Combustion Program – Area #5: Atomization Tests and Models Lead Investigators: Robert P. Lucht	319
Project 031(A) | Alternative Jet Fuels Test and Evaluation Lead Investigators: Steven Zabarnick	348
Project 033(A) | Alternative Fuels Test Database Library Lead Investigator: Tonghun Lee	356
Project 034 | National Jet Fuels Combustion Program – Area #7: Overall Program Integration and Analysis Lead Investigators: Joshua S. Heyne, Tonghun Lee	365
Project 036 | Parametric Uncertainty Assessment for AEDT2b Lead Investigators: Dimitri Mavris, Dongwook Lim, Yongchang Li	481



Project 037 | CLEEN II Technology Modeling and Assessment Lead Investigators: Dimitri Mavris	514
Project 038 | Rotorcraft Noise Abatement Procedures Development Lead Investigator: Kenneth Brentner	516
Project 039 | Naphthalene Removal Assessment Lead Investigator: Steven R. H. Barrett	525
Project 040 | Quantifying Uncertainties in Predicting Aircraft Noise in Real-world Situations Lead Investigators: Kai-Ming Li, Victor W. Sparrow	536
Project 041 | Identification of Noise Acceptance Onset for Noise Certification Standards of Supersonic Airplanes Lead Investigator: Victor W. Sparrow, Kathleen K. Hodgdon	553
Project 042 | Acoustical Model of Mach Cut-off Lead Investigator: Victor W. Sparrow	561
Project 043 | Noise Power Distance Re-Evaluation Lead Investigator: Dimitri N. Mavris	583
Project 045 | Takeoff/Climb Analysis to Support AEDT APM Development Lead Investigators: Michelle R. Kirby, Dimitri N. Mavris	631
Project 046 | Surface Analysis to Support AEDT APM Development Lead Investigator: Hamsa Balakrishnan	663
Project 048 | Analysis to Support the Development of an Engine nvPM Emissions Standards Lead Investigator: Steven R. H. Barrett	672
Publications Index	677
Funding Tables	690



Overview

This report covers the period October 1, 2017 through September 30, 2018. The Center was established by the authority of FAA solicitation 13-C-AJFE-Solicitation. During that time the ASCENT team launched a new website, which can be viewed at ascent.aero. The next meeting will be hosted by the Georgia Institute of Technology, April 18-19, 2019 in Atlanta.

Over the last year, the ASCENT team has made great strides in research, outreach, and education. The team's success includes the following:

- **32 research projects.**

The projects can be divided into five categories: tools, operations, noise, emissions, and alternative fuels. See the project category descriptions for more detail on each category and a summary of the projects. Funding for these projects comes from the FAA in partnership with Transport Canada.

- **179 publications, reports, and presentations by the ASCENT team.**

Each project report includes a list of publications, reports, and presentations published between June 2015 and December 2018. A comprehensive list of the publications, reports, and presentations is available in the publications index on page 726.

- **116 students participated in aviation research with the ASCENT team.**

Each project report includes the names and roles of the graduate and undergraduate students in the investigator's research. Students are selected by the investigators to participate in this research.

- **72 industry partners involved in ASCENT.**

ASCENT's industry partners play an important role in the Center. The 72members of the ASCENT Advisory Board provide insight into the view of stakeholders, provide advice on the activities and priorities of the Center's co-directors, and ensure research will have practical application. The committee does not influence FAA policy. Industry partners also play a direct role in some of the research projects, providing resources and expertise to the project investigators.

Leadership

Dr. Michael Wolcott
Center Director and Technical Lead for Alternative Jet Fuels Research
Washington State University
(509) 335-6392
wolcott@wsu.edu

Dr. R. John Hansman
Center Co-Director and Technical Lead for Environmental Research
Massachusetts Institute of Technology
(617) 253-2271
rjhans@mit.edu

Dr. John Holladay
Federal Research Laboratories and Agency Liaison
john.holladay@pnnl.gov

Dr. James Hileman
Chief Scientific and Technical Advisor for Environment and Energy
Office of Environment and Energy
Federal Aviation Administration
james.hileman@faa.gov

Research Topics

Research projects within ASCENT are divided into five categories: tools, operations, noise, emissions, and alternative fuels.

Tools

Research within the tools category involves researching current systems to understand the short- and long-term effects of new technologies. The ASCENT ream is working to develop tools to model and assess new and existing aircraft technology.

Projects include:

- 010 - Aircraft Technology Modeling and Assessment
- 011 - Rapid Fleet-wide Environmental Assessment Capability
- 036 – Parametric Uncertainty Assessment for AEDT 2b
- 037 – CLEEN II Technology Modeling and Assessment
- 045 – Takeoff/Climb Analysis to Support AEDT APM Development
- 046 – Surface Analysis to Support AEDT APM Development

Operations

Research within the operations category involves improving aviation operations to reduce negative impacts on local communities, the environment, and the economy. The ASCENT team is working to develop efficient gate-to-gate aircraft operations, develop evaluation tools for aircraft performance, and explore new operations procedures.

Projects include:

- 023 - Analytical Approach for Quantifying Noise from Advanced Operational Procedures

Noise

Research within the noise category involves researching noise pollution caused by the aviation industry. The ASCENT team is working to understand the impact of noise pollution on health, create tools for analyzing aircraft noise, understand how specific variables impact noise, and conduct outreach and education about aircraft noise reduction.

Projects include:

- 003 - Cardiovascular Disease and Aircraft Noise Exposure
- 005 - Noise Emission and Propagation Modeling
- 008 - Noise Outreach
- 017 - Pilot Study on Aircraft Noise and Sleep Disturbance
- 023 - Analytical Approach for Quantifying Noise from Advanced Operational Procedures
- 038 – Rotorcraft Noise Abatement Procedures Development
- 040 – Quantifying Uncertainties in Predicting Aircraft Noise in Real-world Situations
- 041 – Identification of Noise Acceptance Onset for Noise Certification Standards of Supersonic Airplane
- 042 – Acoustical Mode of Mach Cut-off
- 043 – Noise Power Distance Re-Evaluation

Emissions

Research within the emissions category focuses on reducing emissions from the aviation industry. The ASCENT team is working to analyze data and improve models to better understand the effect of airplane emissions, create and refine analysis techniques, and understand how policy changes could affect emissions.

Projects include:



- 002 - Ambient Conditions Corrections for Non-Volatile PM Emissions Measurements
- 018 - Health Impacts Quantification for Aviation Air Quality Tools
- 019 - Development of Aviation Air Quality Tools for Airport-Specific Impact Assessment: Air Quality Modeling
- 020 - Development of NAS wide and Global Rapid Aviation Air Quality
- 021 - Improving Climate Policy Analysis Tools
- 022 - Evaluation of FAA Climate Tools
- 024 - Emissions Data Analysis for CLEEN, ACCESS, and Other Recent Tests
- 039 – Naphthalene Removal Assessment
- 048 – Analysis to Support Development of an Engine nvPM Emissions Standards

Alternative Fuels

Research within the alternative fuels category addresses the challenges associated with the creation and accessibility of alternative fuels. The ASCENT team is working to improve the feasibility of renewable fuels, understand how alternative fuels will affect emissions, air quality, and performance, and create standards for alternative fuel certification.

Projects include:

- 001 - Alternative Jet Fuel Supply Chain Analysis
- 021 - Improving Climate Policy Analysis Tools
- 024 - Emissions Data Analysis for CLEEN, ACCESS, and Other Recent Tests
- 025 - National Jet Fuels Combustion Program – Area #1: 027 - National Jet Fuels Combustion Program – Area #3: Advanced Combustion Tests
- 027 - National Jet Fuels Combustion Program – Area #3: Advanced Combustion Tests
- 028 - National Jet Fuels Combustion Program – Area #4: Combustion Model Development and Evaluation
- 029 - National Jet Fuels Combustion Program – Area #5: Atomization Tests and Models
- 030 - National Jet Fuels Combustion Program – Area #6: Referee Swirl-Stabilized Combustor Evaluation/Support
- 031 - Alternative Jet Fuels Test and Evaluation
- 033 - Alternative Fuels Test Database Library
- 034 - National Jet Fuels Combustion Program – Area #7: Overall Program Integration and Analysis



Project 001(A) Alternative Jet Fuel Supply Chain Analysis

Washington State University

Project Lead Investigator

Michael P. Wolcott
Regents Professor
Department of Civil & Environmental Engineering
Washington State University
PO Box 642910
Pullman, WA 99164-2910
509-335-6392
wolcott@wsu.edu

University Participants

Washington State University

- P.I.(s): Michael P. Wolcott, Regents Professor; Christina Sanders, Acting Director, DGSS; Manuel Garcia-Perez, Associate Professor; and Xiao Zhang, Associate Professor
- FAA Award Number: 13-C-AJFE-WaSU-013
- Period of Performance August 1st, 2017 to July 31st, 2018
- Task(s):
    - WSU 1. Design cases– Garcia-Perez, Zhang
    - WSU 2. Evaluation of the most promising biorefinery concepts for AJF production. Garcia-Perez, Zhang
    - WSU 3. Supplement and maintain the current inventory of biorefinery infrastructure identified in the conversion design cases that are useful for production of AJF. Wolcott
    - WSU 4. Community Social Asset Assessment Gaffney
    - WSU.5 Refine and deploy the facility siting tools for determining regional demand and potential conversion sites to be used in regional analyses. Wolcott
    - WSU.6 Refinery to Wing Stakeholder Assessment. Gaffney
    - WSU.7 Supply Chain analysis. Wolcott-Garcia-Perez
    - WSU. 8 Analytical support for regional CAAFI and USDA jet fuel project. Wolcott

Project Funding Level

$396,037 FAA funding and $396,037 matching funds. State committed graduate school contributions for four PhD students. Faculty time for Michael Wolcott, Manuel Garcia-Perez and Xiao Zhang are contributing to cost share.

Investigation Team

- Michael Wolcott, Project Director/Principal Investigator
- Christina Sanders, Co-Project Director(s) /Co-Principal Investigator (Co-PI)
- Season Hoard, Co-Project Director(s)/Co-Principal Investigator (Co-PI)
- Manuel Garcia-Perez, Co-project Director(s)/Co-Principal Investigator
- Xiao Zhang, Co-project Director(s)/Co-principal Investigator
- Paul Smith, Faculty
- Michael Gaffney, faculty
- Kristin Brandt, Staff Engineer
- Natalie Martinkus, Staff Engineer
- Scott Geleynse, post-doctoral
- Dane Camenzind, Graduate Student
- Lina Pilar Martinez Valencia, Graduate Student
- Tanzil Abid Hossain, Graduate Student



- Anamaria Paiva, Graduate Student
- Daniel Mueller, Graduate Student
- Kelly Nguyen, Graduate Student

Collaborating Researchers

- Burton English, University of Tennessee
- Kristin C. Lewis, Volpe

Project Overview

As part of an effort to realize an "aviation system in which air traffic will move safely, swiftly efficiently, and seamlessly around the globe", the Federal Aviation Administration (FAA) has set a series of goals and supporting outcomes, strategies, and performance metrics (Hileman et al 2013). The goal entitled, "Sustaining our Future" outlines a number of strategies that are collectively aimed at reducing the environmental and energy impacts of the aviation system. To achieve this goal, the FAA set an aspirational goal of aviation utilizing 1 billion gallons of alternative jet fuel (AJF) by the year 2018. This goal was created from an economic, emissions, and overall feasibility perspective (Richard 2010, Staples et al. 2014).

Current approaches to supply chain analysis for AJF optimize transportation logistics of feedstocks-to-refinery and refinery-to-wing (Bond et al 2014). One of the largest barriers to large scale production of all alternative jet fuels is the high capital cost of greenfield facilities translating to risk in the investment community (Huber et al 2007). The capital cost of cellulosic ethanol plants ranges from $10-13/gal capacity (Hileman and Stratton, 2014). The additional process steps required to convert the intermediate to a drop-in AJF could increase this cost to over $25/gal capacity (Hileman 2014).

The realities of these initial commercialization efforts into second-generation alternative jet fuel have led to studies that envision alternate conversion scenarios including transitioning existing facilities (Brown 2013). Gevo is employing retrofit strategies of corn ethanol plants for producing isobuthanol, a potential intermediate for the alcohol-to-jet process of producing iso-paraffinic kerosene (Pearlson 2011, Pearlson et al 2013). Research to envision scenarios to achieve the FAA aspirational goal of AJF consumption relied upon "switching" scenarios where existing and planned capacity would be used for producing the drop-in fuel (Malina et al 2012). All of these approaches require identifying existing industrial assets to target for future AJF production. Siting becomes, not just an exercise of optimizing feedstock transportation, but aligning this critical factor with a host of existing infrastructure, markets within regions with the proper social capital for developing this new industry (Seber et al 2014, Henrich et al 2007).

Up to now all the published AJF supply chain analyses have been limited to standalone jet fuel production technologies that do not generate bio-products. The potential techno-economic and environmental benefits of using existing industrial infrastructure and the production of coproducts on the development of jet fuel production scenarios has to be considered in future studies.

The design cases of the standalone AJF production facilities will be used in supply chain evaluations. Community Social Asset Modeling (CAAM): Social Asset modeling is not well-developed and efforts are likely hampered by the difficulty in quantifying social assets when compared to improved environmental performance or a reduction in alternative jet fuel costs that may be observed by optimizing economic and environmental constraints. However, considering the community characteristics of a potential site is important when determining preferred locations for a new biorefinery. Community resistance or enthusiasm for the alternative jet fuels industry can play a large role in the success or failure of a facility (Martinkus et al 2014). CAAM efforts conducted within this project will inform disciplinary applications and advances. It is clear that social factors can have a significant effect – positive or negative – on project adoption and implementation, especially high technology or energy-related projects (Lewis et al 2012, Martinkus et al 2012). Accounting for social factors to inform selection of sites and implementation decisions to maximize positive social support and minimize opposition and social negatives can significantly enhance project success. The CAAM model originally piloted in the NARA project is designed to provide a quantitative rating of select social factors at the county level (Martinkus et al 2014).

This research is targeted at identifying the key barriers, in regional supply chains, that must be overcome to produce 1-billion gallons of alternative jet fuel. This overall goal is addressed by developing tools to support the AJF supply chain assessment by the Volpe Center. Our effort will provide facility siting analyses that assess (a) conversion design cases combined with (b) regional supply chain assets and (c) social capacity assessments for communities to act collectively for



development goals. Finally, a refinery-to-wing stakeholder assessment will support modeling and accounting of AJF distribution for downstream fuel logistics.

Task 1- Design Cases

Washington State University

Objective(s)

Continuation from previous years

Our team will complete the reviews and final report of the design cases for six standalone AJF technologies and four important industries (sugarcane, pulp and paper, corn ethanol and petroleum refineries) developed in previous years and will start developing the design cases for targeted co-products that could improve the economic viability of AJFs.

New Tasks

1. New case design report "Alternative Jet Fuel Supply Chain Analysis: hydrothermal liquefaction processing of tall oil for jet fuel production". This work involved collecting primary data, establishing process flow diagram and conducting a detailed TEA. This task will be carried out in collaboration with PNNL HTL group.
2. Conduct detailed TEA analyses of integrating lignin co-products technologies in Alcohol-to-Jet pathway to determine the potential to lower fuel cost to $2.00/gge.
3. New design case reports on technology review and process evaluation of lipid conversion processes (HEFA, CH, SBI, Forge, Tyton, decarboxylation) and new technologies for the production of alternative lipids (HTL and sugars to lipid).
4. Conduct detailed TEA analysis integrating lignin co-products technologies in biorefinery cases integrated with the corn ethanol, and the sugarcane industry

Research Approach

Background

The design cases developed for AJFs and for existing industrial infrastructure are being used in the development of supply chains and the identification of synergisms that could eventually lead to the construction of integrated systems of AJF production that take advantage of the infrastructure in a given region. Analysis of the location of existing infrastructure showed that the United States can be divided in regions by dominant biomass of the region. So, we believe that a viable approach to evaluate the synergism between the AJF pathways, the existing infrastructure and the co-products is to generate advanced biorefinery concepts around the Petroleum Refineries, Pulp and Paper Mills, Sugar Cane Mills, and Corn Ethanol Mills. Then we will compare the biorefinery concepts developed for each of these technologies to decide the most promising ones. The most promising biorefinery concepts for the synergistic production of AJFs and co-products with these industries will then be used in the supply chain analyses.

Standalone design case reports are generated by conducting reviews of research related to each in academic literature and public information available from commercial interests developing the technology. The reports are meant to detail the processes involved in each conversion pathway and outline the technology readiness and particular barriers to implementation. Publically available information on the commercial processes and research literature will provide the foundation of information later used in modeling efforts. Where detailed process engineering information is lacking, new models will be built to estimate the parameters needed to complete assessments such as techno-economic modeling, lifecycle analysis and supply chain modeling. Aspen Plus is primarily used to generate process models and details including mass balances, energy balances, energy requirements, and equipment size and cost. These results will also aim to provide the basis for comparative analysis between design cases, identifying key advantages and markets for each technology.

Each design case has the following components:

1. Feedstock requirement (availability and feedstock composition)
2. Flow diagram of technology
3. Companies commercializing the technology (level of maturity)
4. Current location of units in the United States (In case of an existing technology it will be the inventory of units that could be retrofitted)
5. Literature review on papers reporting data relevant to the operation of the technology (operating conditions, type of reactor used, catalysts, yield of products)



6. Properties of jet fuel produced
7. Identification of potential intermediates (bio-oil, sugars, densified feedstock); current and potential uses of wastes and effluents; and co-products (biochemicals, carbon, etc.) that can be obtained from the technology.

Last year we submitted the MS Word technical reports and the MS Excel files, with mass and energy balances and techno-economic analyses, (TEA) for the pathways listed below. All files are available on shared drives for the Project 01 team members. Where indicated, TEAs are still undergoing internal review.

- Pyrolysis-bio-oil hydro-treatment concept (Hydro-treated Depolymerized Cellulosic Jet HDCJ).
- Synthetic Kerosene and Synthetic Aromatic Kerosene (SK&SAK). [Under review]
- Alcohol to Jet (ATJ)- A manuscript with the information for the mass and energy balances and its TEA was recently published. [The TEA of Direct Sugars to Hydrocarbons (DSHC) is under internal review.]
- Syngas Fischer Tropsch (FT)- Design cases were prepared for biomass gasification. The first one was for micro-reactors. The second design was for a technology using large standard reactors. [The TEAs for general FT and micro-FT are under internal review.]
- HEFA Mass and Energy Balances and the TEA. [Under review].

We are currently working on a manuscript comparing the economic and environmental performance of the alternative jet fuel technologies discussed above. Last year we also made progresses in design cases for the existing industries that could be used to reduce production cost of alternative jet fuels.

A very preliminary technical report with information of mass and energy balances and TEA of the petroleum refinery are still being developed for the corn ethanol and sugarcane design cases. We have made major progress on the analysis of corn ethanol, and sugarcane biorefineries for jet fuel production. Two papers in this area are under internal review.

We are working with PNNL to complete a case design report on HTL for AJF conversion. This work involved collecting primary data, establishing process flow diagrams for several feedstocks including, municipal wastewater (primary and secondary sludge), algae and tall oil, and conducting a detailed TEA. We have discussed the draft report with PNNL. We will also work with PNNL to help identify ways to improve HTL conversion efficiency.

A summary report on several lipid conversion pathways including SBI, Forge, Tyton, decarboxylation and co-processing was prepared. We have also revised the design case for the Catalytic Hydrothermolysis (CH) process and a manuscript "Techno-economic analysis of Catalytic Hydrothermolysis Pathway for Jet Fuel Production was prepared. The manuscript reviews the technological development and commercialization progress of CH pathway and assess the advantages of the CH pathway to utilize a wider range of feedstocks including edible and non-edible vegetable oils as well as fats, oils, and greases (FOGs) and generate a broader mix of hydrocarbons. Potential cost savings for the use of low-cost feedstocks like FOGs are assessed considering the added costs for preconditioning and feedstock availability. A draft manuscript has been reviewed by Agrisoma. We plan to complete the manuscript revision and submission by January 31, 2019.

Milestone(s)

Completed the Excel file with TEAs of all the alternative jet fuel technologies. The design cases for the corn ethanol and the sugarcane industry are still under review by the standardization team.We are still working on the design case for the petroleum refinery. We completed the analysis of corn-ethanol alternatives for jet fuel production.

Major Accomplishments

Models were developed for the main AJF production technologies and for relevant technologies that can be used as baseline for the synthesis of biorefinery concepts. The methodology for these models is provides data to form a baseline for comparative analysis with other design cases. Key process variations have been identified in several design cases and have been modeled to determine their effects on process economics and viability, as well as to identify the key barrier toward commercialization in complete biorefinery concepts.



Data generated from the design cases were also supplied to A01 partners to assist with supply chain, techno-economic models by improving the conversion and cost figures database values. Evaluations of the effects of process variations on the chemical properties of products generated are being used to provide insight into the challenges that will be faced when blending the AJFs into commercial jet fuel.

Publications

Scott Geleynse, Kristin Brandt, Manuel Garcia-Perez, Michael Wolcott, Xiao Zhang, The Alcohol to Jet Conversion Pathway for Drop-In Alternative jet fuels: Techno-Economic Evaluation. ChemSusChem, 11,3728 –3741 (2018).

Outreach Efforts

During the preparation of design case reports, we have closely interacted with industrial companies including Gevo, LanzaTech and Agrisoma. These companies have also helped us review the reports and draft manuscripts.

Awards

The publication listed above was selected as a VIP (very important paper) and invited for cover art and cover profile in ChemSusChem.

Student Involvement

Several graduate (Scott Geleynse, Mond Guo, Carlos Alvarez Vasco, Ruoshui Ma, Kelly Nguyen, Tanzil Hossain, Anamaria Paiva, Lina Martinez) and undergraduate students participated in the creation, editing and updating of the design cases for standalone AJF technologies, for relevant existing infrastructure and for co-products from lignin.

Plans for Next Period

Release the final version of all design cases for standalone AJF production technologies, for relevant infrastructure (corn ethanol, sugarcane, pulp and paper and petroleum refinery)

Task 2- Evaluation of the Most Promising Biorefinery Concepts for AJF Production

Washington State University

Objective(s)

Continuation from previous years

This year we will complete the evaluation of biorefinery scenarios for AJF production in corn ethanol, sugarcane, pulp and paper mills and petroleum refineries. Last year we advanced the analysis for corn ethanol and pulp and paper mills. This year we should complete the analysis for sugarcane and petroleum refineries.

New Tasks

Conduct detailed TEA analyses of integrating lignin co-products technologies with the Alcohol to Jet pathway to determine the potential to lower fuel cost to $2.00/gge.

Research Approach

Background

In this task we are using the design cases of existing infrastructure, AJF production technology and co-products identified to generate new biorefinery concepts for Petroleum Refineries, Pulp and Paper Mills, Sugarcane Mills and Corn Ethanol Mills. The results from this effort will allow us to identify and select the most commercially feasible biorefinery concepts. Major technical gaps/barriers toward commercialization of each of the biorefinery concepts will also be revealed from the results of this study.

Integration of process technologies through a similar approach to the standalone design cases is assessed. Further evaluation of integration concepts will be developed by pairing standalone cases with these opportunities to evaluate the economic and environmental advantage of the integration approaches. During this period, we conducted detailed analyses of alcohol to jet conversion (ATJ) and integration with pulp mill operations. We have also investigated the potential of lignin co-products contribution to the overall process economy.



A dry grind corn ethanol mill (DGCEM) with a capacity of 80 million gallons of ethanol per year (MGY) was studied in order to evaluate potential biorefinery scenarios for AJF production. Five alternative jet fuel (AJF) technologies were studied: Virent's BioForming, "Gevo" alcohol to jet (ATJ), direct sugar to hydrocarbon (DSHC), fast pyrolysis (FP) and Fischer-Tropsch (FT). A standardized methodology was adopted to evaluate twelve integration scenarios between DGCEM and AJF technologies in terms of minimum fuel selling price (MFSP) and greenhouse gas (GHG) emission. We are currently conducting similar analyses for a corn ethanol plant and petroleum refineries. The comparison of sugarcane bio-refinery concepts for aviation fuel production has progressing well.

We will complete a draft paper of integration of ATJ technologies in pulp mill infrastructure this year. We will then apply this methodology for analyzing other advanced fermentation technology (direct sugar to hydrocarbon by Amyris) in pulp mill next year. We will also expand the lignin co-product analysis to all other AJF pathways.

Major Accomplishments

Economic models and Life Cycle Assessments were used to support the selection of the most promising biorefinery concepts for the corn ethanol plant, sugarcane and pulp and paper. Manuscripts on corn ethanol, sugarcane and pulp and paper bio-refineries for jet fuel production will be submitted shortly. We are now working on the petroleum refinery biorefinery concepts.

Publications

None

Outreach Efforts

Scott Geleynse, Xiao Zhang. Techno-Economic Assessment of Pulp Mill Infrastructure Integration with the Alcohol-to-Jet Pathway for Aviation Fuel Production. International Bioenergy & Bioproducts Conference, October 30, 2018

Awards

None

Student Involvement

Graduate students Scott Geleynse, Senthil Subramaniam, Kelly Nguyen, Abid Tanzil Houssain, Lina Martinez Valencia, Anamaria Paiva, and Ruoshui Ma have received trained working in this project. An undergraduate student, Kitana Kaiphanliam, funded under an NSF REU grant assisted with building techno-economic models for co-products production scenarios.

Plans for Next Period

Next period Dr. Garcia-Perez's team will focus on the potential cost reductions if alternative jet fuels are integrated with a petroleum refinery.

Task 3- Supplement and Maintain the Current Inventory of Biorefinery Infrastructure Identified in the Conversion Design Cases that are Useful for Production of AJF

Washington State University

Objective(s)

Continuation from previous years

This task requires annual evaluation of the database to add or eliminate new and closed facilities in each category so that the geospatially specific assets are current with reality.

Research Approach

Utilizing existing infrastructure assets is key to retrofit approaches to developing the industry. In order to differentiate between the relative value of different options, the specific assets must be valued with respect to their potential use within



a conversion pathway. Regional databases of industrial assets that might be utilized by a developing AJF industry, have been assessed on a national level. These baseline databases are compiled from a variety of sources that include industry associations, universities, and news outlets. These databases will be expanded, refined, and validated as the conversion design cases articulate additional needs for the regional analyses.

Milestone(s)

National databases are compiled, geolocated, validated and shared for biodiesel, corn ethanol, energy pellet, pulp & paper, and sugar mill production. We are evaluating the database to add or eliminate new and closed facilities in each category so that the geospatially specific assets are current with reality.

Geospatially specific facility databases, waste feedstocks estimates, and forest residual inventories were developed and prepared with the Volpe Center in their FTOT analysis. FTOT analysis of specific scenarios are compared to similar versions analyzed with the National Renewable Energy Laboratory's (NREL) Alternative jet fuels Scenario Model (BSM) to estimate adoption of alternative jet fuel technologies for determining potential national targets.

Major Accomplishments

The national databases have been compiled, validated, and shared with the A01 teams. All of the metadata is complete for use in the regional analyses.

Publications

Databases were used in the following publication submitted for peer review in BioFPR:

Lewis, Kristin C., Emily K. Newes, Steven O. Peterson, Matthew N. Pearlson, Emily A. Lawless, Kristin Brandt, Dane Camenzind et al. US alternative jet fuel deployment scenario analyses identifying key drivers and geospatial patterns for the first billion gallons. Biofuels, Bioproducts and Biorefining. 2018. Doi:10.1002/bbb.1951

Outreach Efforts

None

Awards

None – these are shared assets for later analyses

Student Involvement

Dane Camenzind, Master's student in Civil Engineering, validated the operating status of previously identified production facilities, compiled and geolocated MSW incinerators and landfill gas to energy facilities and worked to assemble and update all county level feedstock information.

Plans for Next Period

None

Task 4- Continue Work on Social Asset Decision Tools Developed in Phase 1 for Plant Siting (Community Asset & Attribute Model—CAAM); Including Additional Validation and Incorporation of Multi-decision Making Tools. Extend Application to Another US Region in Coordination with Other Team Members (Inland Northwest, Appalachian Region). Prepare for Extension Nationally & Replication in Select Countries.

Washington State University

Objective(s)

Expand and refine social asset decision tools for biorefinery plant siting (Community Asset & Attribute Model—CAAM) through addition of political capital. Prepare for extension nationally and replication for Canada and select EU countries.



Research Approach

Based on key measures of social, cultural, human, and political capitals, WSU has developed and finalized a Community Asset and Attribute Model (CAAM). The first tool was initially applied to the NARA region in the Pacific Northwest, and the refined tool that added more complete measures of social, cultural, and human capital was deployed in two sub-regions of NARA. The initial measure of political capital has now been added to the CAAM and the tool can be used across the continental United States. The refined CAAM (excluding the political capital) has been used to assess social capacity for biorefinery siting in two separate studies, including retrofitting paper mill facilities in the Pacific Northwest. Ground-truthing analysis was used to assess the role of social, cultural and human capitals in the success or failure of alternative jet fuel related projects in both the NARA and BANR regions. This ground-truthing analysis supported the role of CAAM measures in project success, and suggested opportunities to further improve the CAAM which are completed. The final CAAM includes measurements for political capital, and the ways in which each capital is measured were altered for each capital. We have also completed the strategic application model which combines the final CAAM with supplementary data to make strategic recommendations for community engagement to increase the likelihood of project success. Efforts to validate the final CAAM and strategic application are currently underway, and involve application in the BANR region and the inland Northwest. We are also using past case-studies in the Pacific Northwest to help validate the strategic application model.

Milestone(s)

The validated CAAM model based on county-level comparative rankings on Social, Human Cultural, and Political Capitals is tested and available for use.

Major Accomplishments

The final CAAM model with the addition of social capital is completed. The strategic application model has been created based off the final, completed CAAM and the addition of supplementary data. The supplementary data includes diversity and segregation data at the county-level to assess the type of social capital for the community, and necessary strategic approaches based on this information. We have developed a codebook for the final dataset to help researchers utilize the CAAM and create their own scores tailored to their specific regions. The papers submitted based on previous CAAMs have been published: the development of the CAAM prior to the addition of political capital was published by Politics and the Life Sciences in 2017, the manuscript details the model's measurements of cultural, human, and social capital and presents validation of the model based on case studies from the Pacific Northwest. The site-selection manuscript combining this refined model was also published in 2017 by Biomass and Bioenergy. Significant research collaborations have been organized to further test the CAAM's effectiveness, including in areas outside aviation alternative jet fuel and refinery site selection (namely, climate change resiliency and community vulnerability to climate change). A third manuscript is also currently being written that further demonstrates the validity of the CAAM through a case study analysis in the Pacific Northwest.

Publications

Martinkus, N., Rijkoff, S.A.M., Hoard, S.A., Shi, W., Smith, P., Gaffney, M. & Wolcott, M. (2017). Biorefinery site selection using a stepwise biogeophysical and social analysis approach. Biomass and Bioenergy, 97, 139-148. doi:10.1016/j.biombioe.2016.12.022

Rijkhoff, S.A.M., Hoard, S., Gaffney, M.J. & Smith, P.M. (2017). Communities ready for takeoff: Integrating social assets for alternative jet fuel site-selection modeling. Politics and the Life Sciences, 36(1):14-26. doi:10.1017/pls.2017.6

Outreach Efforts

Mueller, D., Hoard, S., Sanders, C. & Gaffney, M. *From Field to Flight: Using Community Capitals to Predict Sustainable Aviation Alternative jet fuel Scale-Up*. Washington State University Academic Showcase. Pullman, WA.

Mueller, D., Hoard, S., Sanders, C., & Gaffney, M. *From Field to Flight: Using Community Capitals to Predict Sustainable Aviation Alternative jet fuel Scale-Up*. Northwest Climate Conference. Tacoma, WA.

Awards

None



Student Involvement

Daniel Mueller, Ph.D. candidate in political science at WSU and research assistant on this project, will continue validation efforts for the CAAM and has finalized measurements for political capital and finished developing strategic applications of the CAAM. Future work includes further validation of the CAAM and testing the model through various collaborative research efforts.

Plans for Next Period

The final CAAM and strategic application will be validated in the Inland Northwest and BANR regions. This approach will include incorporating in multi-method decision-making tools, and appropriate weighting of the capitals based on their correlation.

Task 5- Refine and Deploy the Facility Siting Tools for Determining Regional Demand and Potential Conversion Sites to be Used in Regional Analyses

Washington State University

Objective(s)

Continuation from last year

Develop readiness level tools for regional projects.

Research Approach

The CAAM model, developed under the NARA project and refined for ASCENT applications, provides county-level data collected from national datasets to conduct a preliminary assessment of community characteristics for four (Cultural, Social, Human, Political) of the seven "Community Capitals" developed by Emery and Flora 2006.

To help improve facility siting tools, prior CAAM models (focusing on 3 assets: social, cultural, and human capital) were added to economic assets to assess the suitability of communities in the Pacific Northwest for bio-refineries. Expanding on these analyses, our CAAM measures have been added to a decision support tool (DST) to assess the repurpose potential of pulp mills in the Pacific Northwest for a biorefinery. An additional manuscript has been written on the effectiveness of this tool and will be submitted for review. These approaches have been utilized for cellulosic Alcohol-to-Jet supply chains in the Pacific Northwest, and we will work to demonstrate the tool for supply chain siting analyses for alternative jet fuel production using HEFA conversion technology and FOGs as feedstock in the Inland Northwest.

Milestone(s)

CAAM has been updated with four capitals, and readiness level tools for regional projects have been developed.

Major Accomplishments

During this reporting period, a manuscript combining CAAM with economic indicators to assess site-selection in the Cascades-to-Pacific region (western Oregon and western Washington) was developed and will be submitted. Supplementary data for strategic application has been added to strategic recommendations model which we plan to integrate with future DSTs.

Publications

Martinkus, Natalie, Greg Latta, Kristin Lynne Brandt, and Michael P. Wolcott. 2018. A Multi-Criteria Decision Analysis Approach to Facility Siting in a Wood-Based Depot-and-Biorefinery Supply Chain Model. Frontiers in Energy Research, 6:124. Doi: 10.3389/fenrg.2018.00124

Outreach Efforts

None

Awards

None



Student Involvement

Daniel Mueller, Ph.D. candidate in Political Science, now holds a funded Research Assistant appointment working on this project, and has been primarily responsible for acquisition of new primary data, and continuing validation of the model.

Plans for Next Period

In the next year, the latest iteration of the CAAM will be further validated and applied in the Inland Northwest and BANR regions, with expansion to at least one additional U.S. region (Inland Northwest and potentially Central Appalachian Region in cooperation with team members). This model is based upon the addition of measurements for political capital, development of more refined measurement of capital comparative ranking beyond dichotomous outperform/under-perform ratings using standard deviations to examine distance from regional average and impact on successful development and implementation of alternative measurements for cultural capital and slight changes in measurements for human and social capitals, additional supplementary demographic data to enhance the nuance of the model, and final validation, after statistical confirmation, using selected case studies to confirm the efficacy of the model.

The updated CAAM is available for use nationally, allowing comparison of counties against defined regional norms on cultural, social, human, and political capital scales that have been statistically tested and validated through triangulated testing with external data. The new version of the CAAM allows for further enhancing predictive capacity through the development of strategic applications of the model, including, for example, the level of political support for alternative jet fuels in any given community. Finalized codebooks for this model have been developed and made available and will continue to be refined as the model is further validated.

Task 6- Refinery-to-Wing Stakeholder

Washington State University
This is a shared task lead by Penn State University. The reporting is provided in Award No. 13-C-AJFE-PSU-002.

Objective(s)

Continuation from last year
Extend Stakeholder assessment to a limited sample of informed stakeholders in the remaining sections of the country to provide insight into market & industry dynamics which will help optimize successful outcomes.

Research Approach

The team will collect primary data via surveys to better understand the awareness, opinions, and perspectives of key aviation fuel supply chain stakeholders regarding to the potential impacts and key success factors for an economically viable biojet fuel production industry in the United States. These aviation fuel supply chain stakeholders include airport management, FBOs, other aviation fuel handlers, relevant airlines, and CAAFI personnel. Data collection to assess aviation fuel supply chain stakeholder opinions, awareness, and perceptions regarding factors impacting the adoption and diffusion of AJF in the Pacific Northwest region has been completed, and Midwest region analysis is continuing. A national survey of aviation management has been developed and has been distributed to several hundred stakeholders across the United States. This survey replaced efforts to conduct interviews due to low response rates and is currently ongoing. As respondents submit their answers, further outreach efforts will be conducted to improve the survey response rate, primarily by calling directly recipients of the survey who have not yet completed it.

Milestone(s)

Assessment in the Pacific Northwest region of stakeholder perceptions using interviews and a survey of airport management have been completed, resulting in one previously published paper and a second paper soon to be published in late 2018. Interview protocols have been completely converted into surveys, and a national survey has been distributed to stakeholders across every region of the country. Responses continue to be collected, and further outreach to enhance survey completion will start soon.

Major Accomplishments

The team has written a second manuscript describing airport management opinions on aviation alternative jet fuel in the Pacific Northwest. The paper has been accepted for publication in the International Journal of Aviation Management. Interview protocols have been converted into a national survey, which has been distributed to hundreds of aviation fuel stakeholders at airports across the country.



Publications

Mueller, D., Hoard, S., Smith, P. M., Sanders, C., & Gaffney, M. (2019). Airport Management Perspectives on Aviation Biofuels: Drivers, Barriers, and Policy Requirements in the U.S. Pacific Northwest. *International Journal of Aviation Management*. https://doi.org/10.1504/IJAM.2019.098380

Outreach Efforts

None

Awards

None

Student Involvement

Daniel Mueller, Ph.D. candidate in political science at WSU and research assistant on this project, has helped develop the national survey and is currently administrating this survey. He will also be assisting in outreach to survey recipients to improve response rates.

Plans for Next Period

The next year will see the completion of the national stakeholder assessment, with the team continuing to gather responses from across the country and analyzing the incoming data. When data gathering and analysis is complete, the team will begin drafting a manuscript reporting survey results.

Task 7- Supply Chain Analysis

Washington State University-Volpe

Objective(s)

Continuation from previous years

Oilseeds production and use for production of AJF using HEFA refining is one potential pathway to production of fuels in the Pacific and Inland Northwest. A logistical optimization routine is used to assess the most likely supply chain scenarios that may result in this region.

Research Approach

Oilseed production is estimated based upon previous USDA-funded research addressing sustainable agricultural practices in the dry-land farming area of the Inland Northwest. The yield and rotation information from this project, called REACCH (reacchpna.org), was used to assess 50% and 100% of maximum sustainable oilseed production in this region as a rotation crop to traditional wheat production. A variety of storage facility types (country, shuttle, and barge elevators) and transportation modes (road, rail, and barge) were assessed. Siting methods in this report were used to determine potential locations for oilseed crushing. Plant oil refining for biodiesel production at the REG facility in Grays Harbor, WA and coproduction of alternative jet fuel at an oil refinery near Anacortes, WA were considered for supplying diesel and jet fuel demands in the Greater Seattle and Portland markets. The location of crushing facilities and transportation modes/routes were determined using optimization routines that considered both plant oil and oilseed meal delivery. The oilseed meal was assumed to be used regionally as a protein source for cattle and diary production.

Milestone(s)

Analysis is complete and an MS thesis is completed.

Major Accomplishments

WSU and the Volpe AFTOT analysis team has teamed with the NREL BSM team for a joint analysis of the ability to reach 1-billion gallon of AJF production in the US.

Publications

Camenzind, D. 2018. Supply Chain Analysis for the Production of Alternative Jet Fuel from Oilseeds produced within the U.S. Pacific Northwest. MS Thesis. Washington State University.



Outreach Efforts
None

Awards
None

Student Involvement
Dane Camenzind, MS Environmental Engineering, Washington State University

Plans for Next Period
Compare optimized supply chains to those assessed by Volpe using FTOT.
Utilize regional supply chain tools in assessing forest residuals to alternative jet fuels using pyrolysis methods in Task 8 below.

Task 8- Analytical Support for Regional CAAFI and USDA Jet Fuel Project
Washington State University

Objective(s)
Continuation from previous years
Develop a readiness level tool to assess the status of regional alternatives jet production projects. In addition, use the supply chain and standalone design cases to support the USDA BANR project in TEA and supply chain analysis. This regional CAP project focuses on the use of softwood forest salvage feedstock for fuels via a catalyzed pyrolysis conversion pathway.

Research Approach
We will develop readiness level tools for regional projects to assess their status of developing fuel project and assist in understanding critical missing components. This tool will take similar form and approaches to the CAAFI Feedstock and Fuel Readiness Levels and will be used to assist CAAFI in understanding the stage of development for projects of interest and assess critical gaps. In addition, we will assist the regional USDA BANR team in deploying TEA and Supply Chain analysis to their project. This effort is structured around using softwood forest salvage feedstock with a thermochemical conversion process to produce fuels and coproducts.

Milestone(s)
We are progressing on the use of the supply chain and standalone design cases to support the USDA BANR project in TEA and supply chain analysis. We have supported the BANR team in creating TEAs for the technologies under consideration.

Major Accomplishments
In collaboration with the USDA BANR project and attending their annual meeting to coordinate analysis. We currently await their completion of beetle-killed softwood estimates to complete the supply chain analysis.

Publications
None

Outreach Efforts
None

Awards
None

Student Involvement
Dane Carmenzind, MS Environmental Engineering, Washington State University
Lina Martinez, PhD Biosystems Engineering, Washington State University



Plans for Next Period

Analysis of the BANR Region is ongoing and will be complete within the project year.

References

Bond JQ, Upadhye AA, Olcay H, Tompsett GA, Jae J, Xing R, Alonso DM, Wang D, Zhang T, Kumar R, Foster A, Sen SM, Maravalias CT, 13 R, Barret SR, Lobo R, Wayman CE, Dumesic JA, Huber GW. (2014). Production of renewable jet fuel range alkanes and commodity chemicals from integrated catalytic processing of biomass. Energy Environ. Sci, 7:1500.

Brown, N. (2013). FAA Alternative Jet Fuel Activities. Overview. Presented to: CLEEN Consortium, November 20, 2013.

Henrich E. (2007). The status of FZK concept of biomass gasification. 2nd European Summer School on Renewable Motor Fuels. Warsaw, Poland 29-31, August 2007.

Hileman JI, De la Rosa-Blanco E, Bonnefoy PA, Carter NA: The carbón dioxide challenge facing aviation. (2013). Progress in Aerospace Sciences. 63:84-95.

Hileman, J. I., and R. W. Stratton. (2014). "Alternative jet fuel feasibility." Transport Policy, 34:52-62.

Hileman J. (2013). Overview of FAA Alternative Jet Fuel Activities. Presentation to the Biomass R&D Technical Advisory Committee, Washington DC, August 14, 2013.

Huber GW, Corma A. (2007). Synergies between Bio- and Oil Refineries for the Production of Fuels from Biomass. Angewandte Chemie. 46(38):7184-7201.

Lewis, K; S Mitra, S Xu, L Tripp, M Lau, A Epstein, G Fleming, C Roof. (2012) Alternative jet fuel scenario analysis report. No. DOT/FAA/AEE/2011-05.(http://ntl.bts.gov/lib/46000/46500/46597/DOT-VNTSC-FAA-12-01.pdf) (Retrieved on 2014-07)

Malina R. (2012). HEFA and F-T jet fuel cost analyses. Laboratory for Aviation and the Environment. MIT, Nov 27, 2012.

Martinkus, N., Kulkarni, A., Lovrich, N., Smith, P., Shi, W., Pierce, J., & Brown, S. An Innovative Approach to Identify Regional Bioenergy Infrastructure Sites. Proceedings of the 55th International Convention of Society of Wood Science and Technology, August 27-31, 2012 - Beijing, CHINA.

Martinkus, N., Shi, W., Lovrich, N., Pierce, J., Smith, P., and Wolcott, M. (2014). Integrating biogeophysical and social assets into biomass-to-alternative jet fuel supply chain siting decisions. Biomass and Bioenergy, 66:410-418.

Pearlson MN. (2011). A Techno-economic and Environmental Assessment of Hydroprocessed Renewable Distillate Fuels. MSc Thesis in Technology and Policy, MIT.

Pearlson M, Wollersheim C, Hileman J. (2013). A techno-economic review of hydroprocessed renewable esters and fatty acids for het fuel production. Alternative jet fuels, Bioproducts and Biorefining, 7(1):89-96.

Richard TL: Challenges in Scaling Up Alternative jet fuels Infrastructure. (2010). Science, 329:793.

Seber G, Malina R, Pearlson MN, Olcay H, Hileman JI, Barret SRH. (2014). Environmental and Economic Assessment of Producing hydroprocessed jet and diesel fuel from waste oil and tallow. Biomass and Bioenergy 67:108-118.

Spath P, Aden A, Eggeman M, Ringer B, Wallace B, Jechura J. (2005). Biomass to Hydrogen Production detailed Design and Economic Utilizing the Battelle Columbus Laboratory Indirectly Heated Gasifier. Technical Report NREL/TP-510-37408.

Staples MD, Malina R, Olcay H, Pearlson MN, Hileman JI, Boies A, Barrett SRH. (2014). Lifecycle greenhouse gas footprint and minium selling price of renewable diesel and jet fuel from fermentation and advanced fermentation technologies. Energy & Environmental Science, 7:1545.



Project 001(B) Alternative Jet Fuel Supply Chain Analysis

University of Hawaii

Project Lead Investigator

University of Hawaii Lead
Scott Q. Turn
Researcher
Hawaii Natural Energy Institute
University of Hawaii
1680 East-West Rd., POST 109; Honolulu, HI 96822
(808) 956-2346
sturn@hawaii.edu

University Participants

University of Hawaii

- P.I.(s): Scott Q. Turn, Researcher
- FAA Award Number: 13-C-AJFE-UH, Amendment 005
- Period of Performance: 10/1/15 to 9/30/18
- Task(s):
    1. Informing Regional Supply Chains
    2. Identification of Supply Chain Barriers in the Hawaiian Islands

University of Hawaii

- P.I.(s): Scott Q. Turn, Researcher
- FAA Award Number: 13-C-AJFE-UH, Amendment 007
- Period of Performance: 10/1/16 to 9/30/18
- Task(s):
    1. Informing Regional Supply Chains
    2. Support of Indonesian Alternative Jet Fuel Supply Initiatives

University of Hawaii

- P.I.(s): Scott Q. Turn, Researcher
- FAA Award Number: 13-C-AJFE-UH, Amendment 008
- Period of Performance: 8/1/17 to 9/30/18
- Task(s):
    1. National lipid supply availability analysis
    2. Hawaii regional project

Project Funding Level

Under **FAA Award Number 13-C-AJFE-UH, Amendment 005**, the Alternative Jet Fuel Supply Chain Analysis-Tropical Region Analysis project received $75,000 in funding from the FAA and cost share funding of $75,000 from the State of Hawaii.

Under **FAA Award Number 13-C-AJFE-UH, Amendment 007**, the Alternative Jet Fuel Supply Chain Analysis-Tropical Region Analysis project received $100,000 in funding from the FAA and cost share funding of $75,000 from the State of Hawaii and $25,000 of in-kind cost match in the form of salary support for Scott Turn from the University of Hawaii.

Under **FAA Award Number 13-C-AJFE-UH, Amendment 008**, the Alternative Jet Fuel Supply Chain Analysis-Tropical Region Analysis project received $125,000 in funding from the FAA and cost share funding of $125,000 from the State of Hawaii.



Investigation Team

Lead
Scott Turn – University of Hawaii

Other Lead Personnel
Tim Rials and Burt English (UT Co-PIs)
Manuel Garcia-Perez (WSU Co-PI)
Kristin Lewis (Volpe PI)
Michael Wolcott (WSU PI)

UH Investigation Team
Under **FAA Award Number 13-C-AJFE-UH, Amendment 005**, Task 1 and Task 2 includes
Dr. Scott Turn, Researcher, Hawaii Natural Energy Institute, UH
Dr. Trevor Morgan, Assistant Researcher, Hawaii Natural Energy Institute, UH
Dr. Richard Ogoshi, Assistant Researcher, Department of Tropical Plant and Soil Sciences, UH
Dr. Adel H. Youkhana, Junior Researcher, Department of Tropical Plant and Soil Sciences, UH

Under **FAA Award Number 13-C-AJFE-UH, Amendment 007**, Task 1 and Task 2 includes
Dr. Scott Turn, Researcher, Hawaii Natural Energy Institute, UH
Dr. Trevor Morgan, Assistant Researcher, Hawaii Natural Energy Institute, UH
Dr. Richard Ogoshi, Assistant Researcher, Department of Tropical Plant and Soil Sciences, UH
Dr. Adel H. Youkhana, Junior Researcher, Department of Tropical Plant and Soil Sciences, UH
Dr. Curtis Daehler, Professor, Department of Botany, UH
Ms. Sharon Chan, Junior Researcher, Hawaii Natural Energy Institute, UH

Under **FAA Award Number 13-C-AJFE-UH, Amendment 008**, Task 1 and Task 2 includes
Dr. Scott Turn, Researcher, Hawaii Natural Energy Institute, UH
Dr. Trevor Morgan, Assistant Researcher, Hawaii Natural Energy Institute, UH
Dr. Jinxia Fu, Assistant Researcher, Hawaii Natural Energy Institute, UH
Ms. Sabrina Summers, undergraduate student, Bioengineering Department, UH
Mr. Kyle Marcelino, undergraduate student, Bioengineering Department, UH
Mr. Taha Elwir, undergraduate student, Chemistry Department, UH

Project Overview

Under **FAA Award Number 13-C-AJFE-UH, Amendment 005**, the research effort has two objectives. The first objective is to develop information on regional supply chains for use in creating scenarios of future alternative jet fuel production in tropical regions. Outputs from this project may be used as inputs to regional supply chain analyses being developed by the FAA and Volpe Center. The second objective is to identify the key barriers in regional supply chains that must be overcome to produce significant quantities of alternative jet fuel in the Hawaiian Islands and similar tropical regions.

The **FAA Award Number 13-C-AJFE-UH, Amendment 005** project goals are to:

- Review and summarize:
  - the available literature on biomass feedstocks for the tropics,
  - the available literature on pretreatment and conversion technologies for tropical biomass feedstocks,
  - the available literature on geographic information systems data sets available for assessment of alternative jet fuel production systems in the tropics.
- Identify alternative jet fuel supply chain barriers in the Hawaiian islands

Under **FAA Award Number 13-C-AJFE-UH, Amendment 007**, the research effort has two objectives. The first objective is to develop information on regional supply chains for use in creating scenarios of future alternative jet fuel production in tropical regions. Outputs from this project may be used as inputs to regional supply chain analyses being developed by the FAA and Volpe Center. Included in this objective is the development of fundamental property data for tropical biomass resources to support supply chain analysis. The second objective is to support the Memorandum of Understanding



between the Federal Aviation Administration (FAA) and Indonesian Directorate General of Civil Aviation (DGCA) to promote developing and using sustainable, alternative aviation fuels.

The **FAA Award Number 13-C-AJFE-UH, Amendment 007** project goals are to:

- Support the Volpe Center and Commercial Aviation Alternative Fuels Initiative (CAAFI) Farm to Fly 2.0 supply chain analysis.
- Use GIS-based estimates of fiber crop production potential to develop preliminary technical production estimates of jet fuel in Hawaii.
- Develop fundamental property data for tropical biomass resources.
- Transmit data and analysis results to other ASCENT Project 1 researchers to support improvement of existing tools and best practices.
- Support Indonesian alternative jet fuel supply initiatives.

Under **FAA Award Number 13-C-AJFE-UH, Amendment 008**, the research effort has two objectives. The first objective is to support a national lipid supply availability analysis that will inform industry development and guide policy. The second objective is to conduct a targeted supply chain analysis for alternative jet fuel production facility based on a Hawaii regional project.

The **FAA Award Number 13-C-AJFE-UH, Amendment 008** project goals are to:

- Support ASCENT partners conducting the national lipid supply availability analysis by contributing information on tropical oilseed availability.
- Evaluate supply chains for targeted waste streams and purpose grown crops in Hawaii to a location in the principal industrial park on the island of Oahu.

Task 0.1 – Informing Regional Supply Chains

University of Hawaii

Objective(s)

This task included two activities, (1) a review of the archival literature on existing tropical crops and potential new crops that could provide feedstocks for AJF production and (2) a review of relevant pretreatment and conversion technology options and experience with feedstocks identified in (1).

Research Approach

Activity 1. The archival literature will be reviewed to construct an updated database of relevant citations for the tropical crops; new potential energy crops will be identified and added to the database. Available information on agronomic practices, crop rotations, and harvest techniques will be included. The database will be shared with and serve as a resource for the Project 1 team and Volpe Center analyses of regional supply chains.

Activity 2. A database of relevant pretreatment and conversion technology options and experience with potential tropical feedstock materials will be assembled from the archival literature and from existing Project 1 team shared resources. Of particular interest are inventories of material and energy flows associated with the pretreatment and conversion unit operations, fundamental to the design of sustainable systems and the underlying analysis. Pairings of pretreatment and conversion technology options provide the starting point for evaluation of tropical biorefineries that can be integrated into ASCENT Project 1 team and Volpe Center activities.

Milestone(s)

Task 1, Activity 1: Identify target list of databases to search for relevant literature.
Task 1, Activity 1: Interim report summarizing progress on literature search.
Task 1, Activity 2: Identify target list of databases to search for relevant literature.
Task 1, Activity 2: Interim report summarizing progress on literature search.
Task 1, Activity 3: Identify target list of databases to search for relevant literature.
Task 1, Activity 3: Interim report summarizing progress on literature search.



Major Accomplishments
This work is largely completed. A report was produced for each of the two activities. The two reports were combined to form a manuscript that has been submitted for publication in the journal *Energy & Fuels*. Reviewer comments were received and are being addressed by the authors.

Publications
Morgan, T.M., A. Youkhana, R. Ogoshi, S. Turn, and M. Garcia-Perez. Review of biomass resources and conversion technologies for alternative jet fuel production in Hawai'i and tropical regions. *Energy & Fuels*. Reviewed and under revision.

Outreach Efforts
On February 21, 2108, the PI participated in a ThinkTech Hawaii broadcast focused on alternative jet fuels with collaborators from WSU and CAAFI, see https://www.youtube.com/watch?v=Ci4oWITPRKQ&feature=youtu.be

Awards
None

Student Involvement
None

Plans for Next Period
During the next period, the manuscript will be revised and published.

Task 0.2- Identification of Supply Chain Barriers in the Hawaiian Islands
University of Hawaii

Objective(s)
Identify the key barriers in regional supply chains that must be overcome to produce significant quantities of alternative jet fuel in the Hawaiian Islands and similar tropical regions.

Research Approach
UH developed the Hawaii Bioenergy Master Plan for the State of Hawaii [1]. Completed in 2009, UH was tasked with determining whether Hawaii had the capability to produce 20% of land transportation fuels and 20% of electricity from bio-based resources. Toward this end, the plan included assessments of (1) land and water resources that could support biomass feedstock production, (2) potential biomass resources and their availabilities, (3) technology requirements, (4) infrastructure requirements to support logistics, (5) economic impacts, (6) environmental impacts, (7) availability of human capital, (8) permitting requirements, and (9) limitations to developing complete value chains for biomass based energy systems. In keeping with the stakeholder driven development of the Hawaii Bioenergy Master Plan, barriers to development of regional supply chains for ASCENT will be identified by interacting with key stakeholder groups. Green Initiative for Fuels Transition Pacific (GIFTPAC) meetings are held quarterly and are attended by biofuel development interests in Hawaii including representatives of large landowners, producers of first generation biofuels, petroleum refiners, electric utilities, the State Energy Office, U.S. Pacific Command, biofuel entrepreneurs, county government officials, and the University of Hawaii. Additional stakeholders are invited as necessary to fill information and value chain gaps. These meetings are excellent opportunities to receive stakeholder input, identify barriers to supply chain development, and organize data collection efforts that span supply chain participants.

Milestone(s)
Include a description of any and all milestones reached in this research according to previously indicated timelines.

Task 2: Introduce activities at next regularly scheduled GIFTPAC meeting after contract executed.
Task 2: Interim report outlining two tropical supply chain scenarios developed in consultation with Project 1 team, and with input from GIFTPAC participants.



Major Accomplishments

This task is largely completed. A stakeholder meeting was held and documented in a report. The stakeholders identified barriers to alternative jet fuel production in Hawaii and ranked the barriers in order of importance as indicated below:

Economic constraints (e.g., high costs of entry for production factors such as land) throughout the whole production chain

- Issues associated with access to capital including high initial risks and uncertain return on investment
- Insufficient government support in the form of incentives and favorable policies to encourage long-term private investment
- Cost, availability and competition for water
- Alternative jet fuel production technologies are emerging but have not yet demonstrated full commercial viability
- Insufficient or inadequate infrastructure (e.g., harbors, roads, fuel distribution infrastructure, irrigation systems) to support the whole production chain

Several of the barriers are held in common with other locations in the continental U.S. but those related to water and infrastructure bear unique characteristics of an island state.

Publications

None

Outreach Efforts

This activity engaged stakeholders to identify barriers to alternative jet fuel production in Hawaii. Preparation included reviewing stakeholder lists from previous activities. Facilitators appropriate to the stakeholder group were retained. The stakeholder meeting included a presentation about the larger ASCENT program's scope and goals and the other aspects of the UH ASCENT project.

Awards

None

Student Involvement

None

Plans for Next Period

This task is complete but stakeholder outreach activities will continue under other tasks outlined below.

Task 0.3- Informing Regional Supply Chains

University of Hawaii

Objective(s)

Building on FY16 activities, additional supporting analysis will be conducted for proposed supply chains in Hawaii, including:

0.3.1 -Support Volpe Center and Commercial Aviation Alternative Fuels Initiative (CAAFI) Farm to Fly 2.0 supply chain analysis.

0.3.2- Use GIS-based estimates of fiber crop production potential to develop preliminary technical production estimates of jet fuel in Hawaii.

0.3.3- Develop fundamental property data for tropical biomass resources.

0.3.4- Transmit data and analysis results to support improvement of existing tools (e.g. POLYSIS).



Research Approach

Activity 0.3.2 has been conducted using geographic information system (GIS) data to identify areas suitable for purpose grown crop production of feedstocks for AJF production in Hawaii. The approach has been to use GIS layers for land capability class (LCC), slope and zoning as preliminary screens for suitability. Lands are classified by NRCS with ratings from 1 to 6. LCC's from 1 to 3 are generally suitable for agricultural production and LCC of 4 can be productive with proper management. LCC's of 5 or 6 can support less intensive production and could be suitable for forestry. The slopes of terrains impact aspects of production including mechanization and erodibility. An elevation GIS layer was used to derive a slope layer. Zoning layers were acquired from State and County GIS offices. Only agricultural zoning was deemed suitable for this analysis.

The EcoCrop model was used to develop yield models for the crops selected in Task 0.1 based on the annual rainfall and mean minimum monthly temperature data. EcoCrop includes model parameters on sugarcane, banagrass, 5 species of eucalyptus, leucaena, pongamia, jatropha, and sorghum. The parameters for sugarcane will be used to provide a base case assessment for comparison with historical sugar cane acreage and yield. Using sensitivity analysis, the model can be tuned to account for the differences between parameters developed from global sugar production and a century of production experience in Hawaii that was refined through plant breeding to adapt sugarcane varieties to a wide variety of agro-ecosystems. Model results across all of the potential feedstocks will be used to identify land use patterns that would match plants with environmental conditions toward maximizing productivity in support of AJF production.

Pongamia will be the initial focus of Activity 0.3.3. Pongamia is an oil seed bearing, leguminous tree that has production potential in Hawaii and Florida. The tree produces pods containing oil bearing seeds. Pods, oil seed cake, and oil will be evaluated from a number of trees growing on the island of Oahu. Fundamental measurements of chemical composition will be conducted and reported. Development of coproducts from the pods and oil seed cake will be explored.

Milestone(s)

- Identify target opportunities to augment POLYSYS, AFTOT, and conversion modules.
- Review previously developed GIS information layers for tropical fiber crops and identify updating requirements.
- Preliminary estimates of AJF technical potential in Hawaii based on previously developed GIS information layers.

Major Accomplishments

The GIS based analysis of AJF production potential is ongoing. The assessment of potential lands meeting requirements for land capability class, slope, and land use zoning was completed. The EcoCrop model is being implemented to predict yield as a function of the minimum mean monthly temperature and the annual rainfall. This will allow prescription of potential AJF feedstock crops on land areas capable of supporting their production under both rain-fed and irrigated conditions. This analysis will provide information necessary in determining cropping patterns and assessing transport costs to processing facility locations. The EcoCrop model's prediction of sugarcane potential was determined and the results were compared with historic sugarcane acreage, both rainfed and irrigated. EcoCrop's upper and lower values for temperature and rainfall that support optimal sugarcane production were varied to calibrate the prediction against historic acreage. The difference between the EcoCrop values and those representative of Hawaii conditions can be attributed to improvements due to plant breeding and unique combinations of environmental conditions. An example of the latter is the relatively young volcanic soils present in high rainfall areas on the island of Hawaii that allow for high drainage rates and accommodate sugar production. Similar analysis has begun with for *Eucalyptus grandis* and *Eucalyptus saligna*, the former suited for planting at lower, warmer, wetter locations and the latter better suited for cooler, drying sites.

Calibration of the EcoCrop model using historic sugarcane planted acreages was completed in 2018. This effort used a confusion matrix approach to validation (resulting in a Kappa value >0.4) and identified the annual mean temperature as being a better indicator of environmental capability than the minimum mean monthly temperature recommended by the EcoCrop developers. This effort highlights the need to adapt models to local conditions. Comparison of the model predictions for suitable cropping with current land uses is also being conducted to provide another indicator of agreement.

Dr. Curtis Daehler of the University of Hawaii, Department of Botany, completed a report assessing the invasiveness of pongamia. Retrospective analyses show that predictive weed risk assessment (WRA) systems correctly identify many major pest plants, but WRA predictions are not 100% accurate. The purpose of this study was to make field observations of pongamia planted around Oahu in order to look for direct evidence that pongamia is escaping from plantings and becoming an invasive weed on Oahu. Seven field sites were visited in varying environments across Oahu. Although some



pongamia seedlings were found in the vicinity of some pongamia plantings, particularly in wetter, partly shaded environments, almost all observed seedlings were restricted to areas directly beneath the canopy of mother trees. This finding suggests a lack of effective seed dispersal away from pongamia plantings. Based on its current behavior in the field, pongamia is not invasive or established outside of cultivation on Oahu. Because of its limited seed dispersal and low rates of seedling establishment beyond the canopy, risk of pongamia becoming invasive can be mitigated through monitoring and targeted control of any rare escapes in the vicinity of plantings. Seeds and seed pods are water dispersed, so future risks of pongamia escape and unwanted spread would be minimized by avoiding planting at sites near flowing water, near areas exposed to tides, or on or near steep slopes. Vegetative spread by root suckers was not observed around plantings on Oahu, but based on reports from elsewhere, monitoring for vegetative spread around plantations is recommended; unwanted vegetative spread might become a concern in the future that could be addressed with localized mechanical or chemical control.

Pods, oil seed cake, and oil were evaluated from a number of trees growing on the island of Oahu. Fundamental measurements of chemical composition were made for seeds, pods, extracted oil, and post-extraction seed material. Measured values included C, H, N, S elemental composition; energy content; volatile matter, fixed carbon, and ash content; and trace element composition. Oils were characterized for peroxide value, iodine value, fatty acid profile, free fatty acid content, flash point, density, viscosity, and phase transition temperatures. Development of coproducts from the pods and oil seed cake will be explored.

Publications
None

Outreach Efforts
Outreach in this task has focused on interactions with Terviva, a startup company that has identified pongamia germplasm production and marketing as the central focus of their business plan.

The PI and ASCENT collaborators from WSU and UT participated in a Bioeconomy Modelers Workshop organized by NREL.

Awards
None

Student Involvement
Three undergraduate student are involved in the project with primary responsibility for processing and analyzing samples of biomass materials selected for evaluation as potential alternative jet fuel feedstocks.

Plans for Next Period
The GIS analysis of AJF production potential will be completed to include State-wide working maps for each of the species will be developed and summarized in a report.

Analysis of coproduct development based on pongamia oil seeds and husks will be continued.

Task 0.4- Support of Indonesian Alternative Jet Fuel Supply Initiatives
University of Hawaii

Objective(s)
This task supports the Memorandum of Understanding between the Federal Aviation Administration (FAA) and Indonesian Directorate General of Civil Aviation (DGCA) to promote development and use of sustainable, alternative aviation fuels. Under the coordination of the FAA, efforts to establish points of contact and coordinate with Indonesian counterparts are ongoing.

Research Approach
This task will support the Memorandum of Understanding between the Federal Aviation Administration (FAA) and Indonesian Directorate General of Civil Aviation (DGCA) to promote development and use of sustainable, alternative



aviation fuels. This will begin with working with the FAA to establish points of contact to coordinate efforts with Indonesian counterparts. The Indonesian Aviation Biofuels and Renewable Energy Task Force (ABRETF) membership includes Universitas Indonesia, Institut Teknologi Bandung, and Universitas Padjadjaran. A prioritized list of tasks will be developed in consultation with Indonesian counterparts and data required to inform sustainability and supply analyses and potential sources of information will be identified. This could include data collection on Indonesian jet fuel use and resources for alternative jet fuel production, airport locations and annual and monthly jet fuel consumption patterns. Characterization of sustainable biomass resources with potential for use in producing alternative jet fuel supplies could include developing preliminary GIS mapping information of their locations and distributions and preliminary estimates of their technical potentials.

Milestone(s)

- Identify points of contact at Indonesian universities participating in ABRETF.
- Identify research needs and develop project plan.
- Develop data on potential project.

Major Accomplishments

The PI travelled to Jakarta in the first week of August 2017 and met with the following individuals:

- Cesar Velarde Catolfi-Salvoni (ICAO)
- Wendy Aritenang (ICAO)
- Dr. Ridwan Rachmat (Head of Research Collaboration, Indonesian Agency for Agricultural Research and Development)
- Sylvia Ayu Bethari (Head of Aviation Fuel Physical & Chemical Laboratory, Research and Development Centre for Oil and Gas Technology)
- Dr. Ina Winarni (Forest Product Research and Development Center, Ministry of Environment and Forestry)
- Dr. SD Sumbogo Murti (Center of Technology Energy Resources and Chemical Industry, Agency for the Assessment and Application of Technology)

The activities of the tropical supply chain analysis effort were presented to the group followed by a general discussion. The conclusion from this introductory meeting was that the Indonesian counterparts would seek agreement on how to move forward with future cooperation.

Publications

None

Outreach Efforts

Outreach efforts by the PI are described in the Major Accomplishments section above.

The PI is scheduled to travel to Jakarta at the end of November 2018, and meet with Dr. Wendy Aritenang of the International Civilian Aviation Organization Jakarta office to discuss the current activities. The same trip will include meetings with Universitas Indonesia representatives to the Association of Asia Pacific Rim Universities to establish a Cluster on Renewable Energy under its auspices.

Awards

None

Student Involvement

None

Plans for Next Period

The PI will continue to develop the cooperative research agenda between UH and Indonesian universities through continued dialog with FAA, ICAO, and the Indonesian Directorate General of Civil Aviation.

Task 2.2- National Lipid Supply Availability Analysis

University of Hawaii

Objective(s)

Activities under this task will support ASCENT partners working on a national lipid supply availability analysis by sharing data on tropical oilseed availability developed under previous year's activities.

Research Approach

Activities under this task will support ASCENT partners working on a national lipid supply availability analysis by sharing data on tropical oilseed availability developed under previous year's activities. This support will include estimates of pongamia production capability in the State in addition to assessments of waste cooking oil and tallow.

Milestone(s)

Milestones will coincide with lead institution, WSU, schedule for the national lipid supply analysis.

Major Accomplishments

Additional seeds and pods were collected from the pongamia tree on the University of Hawaii campus, Foster Botanical Garden and the Ke`ehi Lagoon Beach Park. Large (tens of kg) quantities of material were acquired from TerViva's plantings on Oahu's north shore for use in oil evaluation. Two oil seed presses were acquired and safety documents were developed. Pods, oil seed cake, and oil were evaluated from a number of trees growing on the island of Oahu. Fundamental measurements of chemical composition were made for seeds, pods, extracted oil, and post-extraction seed material. Measured values included C, H, N, S elemental composition; energy content; volatile matter, fixed carbon, and ash content; and trace element composition. Oils were characterized for peroxide value, iodine value, fatty acid profile, free fatty acid content, flash point, density, viscosity, and phase transition temperatures. Development of coproducts from the pods and oil seed cake will be explored.

Publications

None

Outreach Efforts

The PI presented information about this task to stakeholders attending the Green Initiative for Fuels Transition Pacific and CAAFI Hawaii quarterly conference call on September 5, 2018.

Awards

None

Student Involvement

Three undergraduate student are involved in the project with primary responsibility for processing and analyzing samples of biomass materials selected for evaluation as potential alternative jet fuel feedstocks.

Plans for Next Period

Efforts in the next period will include conducting production estimates of oil seed crops in Hawaii and assessing waste oil supplies. Information will be provided to the lead institution, WSU.

Task 3.2- Hawaii Regional Project

University of Hawaii

Objective(s)

A supply chain based on fiber feedstocks transported to a conversion facility located at Campbell Industrial Park (CIP) on Oahu will be evaluated (Figure 1). CIP is the current site of two oil refineries. Construction and demolition (C&D) wood waste from PVT Landfill could be the primary source of feedstock. Other sources will be evaluated from elsewhere on Oahu and from outer islands, including MSW stream from outer islands and mining of current stocks of waste in place.

Waste streams and purpose grown crops form the basis for a hub and spoke supply system with the hub located on Oahu. Pipelines for jet fuel transport are in place from CIP to Daniel K. Inouye International Airport and adjacent Joint Base Pearl Harbor/Hickam. Other coproduct off-takers for alternative diesel fuel (ADF) include Hawaiian Electric Co. and several military bases (Schofield Barracks (~50 MW alternative fuel-capable power plant under development), Kaneohe Marine Corp Base, etc.). Hawaii Gas (local gas utility) is also seeking alternative sources of methane if methane or feedstock suitable for methane production is available as a coproduct. Hawaii Gas currently off takes feedstock (naphtha) from refinery.



Figure 1. Possible locations of value chain participants for fiber based AJF production facility located at Campbell Industrial Park, Oahu.

Research Approach

Task 3.2.G1. Analysis of feedstock-conversion pathway efficiency, product slate (including co-products), maturation

Building on activities from previous years, additional supporting analysis will be conducted for proposed supply chains in Hawaii, including:

- 3.2.G1.1 Assess feedstock suitability for conversion processes (characterization, conversion efficiencies, contaminants, etc.) [UH and WSU (Manuel Garcia-Perez)]
- 3.2.G1.2 Acquire data re. feedstock size reduction, particle size of materials, bulk densities [UH, WSU (Manuel Garcia-Perez)]
- 3.2.G1.3 Evaluate coproducts at every step of the supply chain. [A01 team]



Task 3.2.G2. Scoping of techno-economic analysis (TEA) issues
This task will determine the current TEA status of targeted AJF production technologies that use fiber feedstocks as production inputs. [UH, WSU (Manuel Garcia-Perez), Purdue (Wally Tyner)]

Task 3.2.G3. Screening level greenhouse gas (GHG) life cycle assessment (LCA)
This task will conduct screening level GHG LCA on the proposed target supply chains and AJF conversion technologies.

Sub-tasks:
- 3.2.G3.1 Assess MIT waste based GHG LCA tools in context of Hawaii application. [MIT (Mark Staples)]
- 3.2.G3.2 Assess requirements to link previously completed eucalyptus energy and GHG analysis to the edge of the plantation with available GHG LCA info for conversion technology options. [MIT (Mark Staples), UH]
- 3.2.G3.3 Identify and fill information/data gaps

Task 3.2.G4. Identification of supply chain participants/partners

Sub-tasks:
- 3.2.G4.1 Define C&D landfill case
- 3.2.G4.2 Identify eucalyptus in existing plantations – landowners, leaseholder/feedstock producer, harvesting contractor, trucking, etc. [UH]
- 3.2.G4.3 Define other feedstock systems as identified. [A01 Team]

Task 3.2.G5. Develop appropriate stakeholder engagement plan

Sub-tasks:
- 3.2.G5.1 Review stakeholder engagement methods and plans from past work to establish baseline methods [UH, WSU (Season Hoard)].
- 3.2.G5.2 Identify and update engagement strategies based on updated CAAM/Outreach support tool [UH, WSU (Season Hoard)]

Task 3.2.G6. Identify and engage stakeholders

Sub-tasks:
- 3.2.G6.1 Identify stakeholders along the value chain and create database based on value chain location. [UH]
- 3.2.G6.2 Conduct stakeholder meeting using instruments developed in Task 3.2G5. [UH, WSU (Season Hoard)]
- 3.2.G6.3 Analyze stakeholder response and feedback to process. [UH, WSU (Season Hoard)]

Task 3.2.G7. Acquire transportation network and other regional data needed for FTOT and other modeling efforts

Sub-tasks:
- 3.2.G7.1 Acquire necessary data to evaluate harbor capacities and current usage. [UH, Volpe (Kristin Lewis), WSU (Mike Wolcott)]
- 3.2.G7.2 Acquire data on interisland transport practices. [UH, Volpe (Kristin Lewis), WSU (Mike Wolcott)]

Task 3.2.G8. Evaluate infrastructure availability

Sub-tasks:
- 3.2.G8.1 Evaluate interisland shipping options and applicable regulation. [UH, Volpe (Kristin Lewis), WSU (Mike Wolcott)]
- 3.2.G8.2 Evaluate transport or conveyance options from conversion location to end user and applicable regulation. [UH, Volpe (Kristin Lewis), WSU (Mike Wolcott)]

Task 3.2.G9. Evaluate feedstock availability

Sub-tasks:
- 3.2.G9.1 Refine/groundtruth prior evaluations of options for purpose grown feedstock supply [UH]



3.2.G9.2 Conduct projections of C&D waste supply moving forward and mining of waste in place on Oahu, MSW and mining of waste in place on other islands [UH]

Task 3.2.G10. Develop regional proposal
This task will use the information collected in Tasks 3.2.G1 through 3.2.G9 to develop a regional project proposal.

Milestone(s)
One milestone is associated with each of the subtask activities identified in the research approach section above.

Major Accomplishments
Characteristics of the feedstock generated at the landfill is the first piece of information needed to provide a basis for the ensuing analysis. The feedstock received at the landfill is an inhomogeneous mixture of construction and demolition. PVT is currently also mining the waste-in-place from the existing landfill and processing it to produce a feedstock stream. Both sources of waste (material arriving in trucks and mined waste-in-place) produce feedstock with highly variable fuel properties. ASTM sampling methods for refuse derived fuels have been reviewed and adapted to the current circumstances. Samples of feedstock particles (≤6 inches) will be sampled from a drop point in a processing conveyor. Approximately 2 ft^3 will be acquired at a time and this volume will be reduced to particles ≤0.25 inches that can be further subdivided using a riffler. A final representative sample of one kg will be retained for analysis and archiving. Analysis will include ultimate analysis, proximate analysis, higher heating value, analysis of ash chemical composition, bulk density, ash deformation temperature. PVT Land Company and the University of Hawaii have signed an agreement allowing UH personnel to locate equipment at the landfill, to obtain samples from the feedstock processing line, and to preprocess the samples to a particle size suitable for further work in a laboratory environment. Equipment has been moved to the site and off-grid power has been located for operating equipment.

Publications
None

Outreach Efforts
A presentation outlining the project was made to stakeholders attending the Commercial Aviation Alternative Fuels Initiative Seminar on Alternatives to Petroleum Jet webinar on February 23, 2018.

The PI presented information about this task to stakeholders attending the Green Initiative for Fuels Transition Pacific and CAAFI Hawaii quarterly conference call on September 5, 2018.

Awards
None

Student Involvement
Two undergraduate students have been involved in the development of the sample preparation strategy.



Plans for Next Period

During the next period, activities will begin toward completing subtasks identified in the research approach section above. A postdoctoral fellow will begin work on this project on March 1, 2019. The table below includes plans for each task moving forward.

Task Identifier	Task Title	Activity Moving Forward
3.2.G1	Analysis of feedstock-conversion pathway efficiency, product slate (including co-products), maturation	This task is in progress and will continue into the coming year to provide time series data on feedstock properties and on specific types of feedstock materials, e.g. construction, demolition, "mined" material, etc. Property data will inform the other tasks.
3.2.G2	**Scoping of techno-economic analysis (TEA) issues**	Based on TEA previously conducted by ASCENT collaborators (Manuel Garcia-Perez, Wally Tyner), a list of data needs for conducting TEA will be assembled and data availability will be assessed.
3.2.G3	Screening level greenhouse gas (GHG) life cycle assessment (LCA)	Based on GHG analysis previously conducted by ASCENT collaborators (Mark Staples), a list of data needs for conducting GHG analysis of the project will be assembled and data availability will be assessed.
3.2.G4	Identification of supply chain participants/partners	The anchor supply chain participants have been identified, but potential participants needed to complete the supply chain will be identified.
3.2.G5	Develop appropriate stakeholder engagement plan	Based on the supply chain participants and the stakeholders identified in Task 3.2.G6, a stakeholder engagement plan will be drafted in cooperation with Season Hoard.
3.2.G6	Identify and engage stakeholders	Stakeholder lists from previous biomass energy planning efforts in Hawaii will be reviewed and revised as needed. Stakeholder engagement will ensue as Tasks 3.2.G1 to G4 results are developed.
3.2.G7	Acquire transportation network and other regional data needed for FTOT and other modeling efforts	In consultation with ASCENT partners Kristin Lewis and Mike Wolcott, contacts from the State of Hawaii, Department of Transportation, Harbors Division will be engaged to initiate data collection on pipeline use and interisland barge movement of fuels.
3.2.G8	Evaluate infrastructure availability	Based on information and data developed in 3.2.G7, availability of existing infrastructure and options to target infrastructure expansion will be developed
3.2.G9	Evaluate feedstock availability	Refinement and groundtruthing of purpose grown crops will be approached by identifying existing plantings of candidate crops in botanical gardens and experiment stations and assessing them in their environment. Opportunities to establish additional plantings will be identified. After reviewing solid waste management plans, meetings will be held with the Solid Waste Divisions in each County to explore options for waste diversion opportunities.



Project 001(C) Alternative Jet Fuel Supply Chain Analysis

Purdue University

Project Lead Investigator

Wallace E. Tyner
James and Lois Ackerman Professor
Department of Agricultural Economics
Purdue University
403 West State Street
West Lafayette, IN 47907-2056
765-494-0199
wtyner@purdue.edu

University Participants

Purdue University

- Wallace E. Tyner, James and Lois Ackerman Professor
- FAA Award Number: 13-C-AJFE-PU
- Period of Performance: July 14, 2014 – August 31, 2018
- Task(s):

1. **Lead: Tyner; supported by graduate students)** – Develop stochastic techno-economic models for relevant pathways and identify key stochastic variables to be modeled for assessing risk in conversion pathways. This work will lead to our capability to compare pathways, their expected economic cost plus the inherent uncertainty in each pathway.
2. **Lead: Tyner; supported by Taheripour, Zhao, and Malina (Hasselt University)** – Life cycle analysis of alternative aviation biofuel pathways in coordination with ICAO CAEP/AFTF. Work with the CAEP/AFTF life cycle assessment group on issues such as system boundaries, induced land use change, LCA methodology, and pathway GHG emissions assessment.
3. **Lead**: **Tyner; supported by Zhao and Taheripour** – Develop estimates of land use change associated emissions for aviation biofuels for the ICAO Alternative Fuels Task Force. This task is closely related to Task #2,
4. **Lead: Tyner** - **P**rovide support for the other ASCENT universities on aviation biofuels policy analysis.
5. **Lead: Tyner** – Provide support for the Farm to Fly initiative as needed.

Project Funding Level

Amendment 3 - $250,000, Amendment 6 - $110,000, Amendment 10 - $230,000, Amendment 15 - $373,750, Amendment 19 - $400,000.
Current cost sharing for this project year was from Oliver Wyman

Investigation Team

Wallace E. Tyner – PI – James and Lois Ackerman Professor
Farzad Taheripour – Research Associate Professor – involved in several aspects of the project, but especially life cycle analysis and land use change
Xin Zhao – PhD student Purdue University – stochastic techno-economic analysis and GTAP ILUC analysis
Elspeth McGarvey – MS student, Purdue University - stochastic techno-economic analysis
Jeremiah Stevens – MS student, Purdue University – stochastic techno-economic analysis

Project Overview

This project has five main components. First is advancement of stochastic techno-economic analysis for aviation biofuel pathways. Second is life cycle and production potential analysis of alternative aviation biofuel pathways in coordination with ICAO-AFTF. The third component also involves working with ICAO-AFTF but specifically on estimation of land use



change associated emissions for aviation biofuels. The fourth and fifth components are smaller. The fourth is to provide support for the policy sub-group in AFTF. The fifth will be providing support for "Farm to Fly 2.0" (F2F2). F2F2 is a collaboration of government and industry to enable commercially viable, sustainable bio-jet fuel supply chains in the U.S. at the state and regional level that are able to support the goal of one billion gallons of bio-jet fuel production capacity and use by 2018.To support this effort, Purdue would provide necessary analytical support to this process.

Task 1- Develop Stochastic Techno-economic Models for Relevant Pathways and Identify Key Stochastic Variables for Assessing Risk in Conversion Pathways

Purdue University

Objective(s)

Develop stochastic techno-economic models for relevant pathways and identify key stochastic variables to be modeled for assessing risk in conversion pathways. This work will lead to our capability to compare pathways, their expected economic cost, plus the inherent uncertainty in each pathway.

Research Approach

For each pathway being evaluated, we develop a stochastic model that covers the entire pathway so that it can be used for both techno-economic and life cycle analysis. Over this period, we have evaluated alcohol-to-jet and the Catalytic Hydrothermolysis (CH) processes. We have also developed some new approaches to stochastic TEA.

Milestone(s)

We continue to get refereed journal papers published in the area of stochastic techno-economic analysis. See the publications in the publications section below.

Major Accomplishments

See the publications section below.

Publications

Yao, Guolin, Mark D. Staples, Robert Malina, and Wallace E. Tyner. "Stochastic techno-economic analysis of alcohol-to-jet fuel production." *Biotechnology for Biofuels* 10:18 (2017), 13 pages.

McGarvey, Elspeth, and Wallace E. Tyner (2018). "A Stochastic Techno-Economic Analysis of the Catalytic Hydrothermolysis Aviation Biofuel Technology." *Biofuels, Bioproducts, & Biorefining* DOI: 10.1002/bbb.1863.

Outreach Efforts

Tyner made a presentation on stochastic TEA for aviation biofuels at the ASCENT meeting in Boston in April 2018.

Awards

None

Student Involvement

Elspeth McGarvey – MS student, Purdue University
Jeremiah Stevens – MS student, Purdue University
These students have worked on the stochastic techno-economic analysis during this project year.

Plans for Next Period

We will continue stochastic TEA, with the next pathway to be completed being pennycress to jet fuel. We also anticipate an analysis on camelina based jet fuel.



Task 2- Life Cycle Analysis of Alternative Aviation Biofuel Pathways in Coordination with ICAO-AFTF

Purdue University

Objective(s)

Work with the CAEP/AFTF life cycle assessment committee (WP3) on issues such as system boundaries, induced land use change, LCA methodology, and pathway GHG emissions assessment.

Research Approach

There are many varied assignments and pieces under this task. For life cycle analysis, working with other team members, we use standard approaches for consequential LCA. For system boundaries, we have investigated the consequences of different approaches to defining system boundaries. For estimating induced land use change, we use the GTAP-BIO model and have modified it to improve land allocation at the extensive and intensive margins (see task 3).

In addition, Tyner has been working with Dr. Brad Saville on low-risk for induced land use change.

Tyner is co-chair of the AFTF induced land use change group.

Milestone(s)

Tyner and Zhao participated in the AFTF meetings in Brasilia in October 2017 and in Montreal in April and September 2018. They have been involved in many of the tasks and document preparation for the meetings. In Brasilia, Tyner and Zhao gave presentations on the improvements in induced land use change modeling and the work plan for the ILUC sub-group. In April in Montreal they provided a comparison of the GTAP-BIO and GLOBIOM models and the progress that had been made in reconciling differences between the two models. In September 2018, AFTF reached agreement on the approach to calculating induced land use change emissions that would be recommended to CAEP.

Major Accomplishments

AFTF has agreed on the induced land use change emissions to be included in CORSIA.

Publications

See the list is Task #3.

Outreach Efforts

None

Awards

None

Student Involvement

Xin Zhao has been involved in the AFTF ILUC work. He completed his PhD in August 2018.

Plans for Next Period

In the next period, we will be doing further model improvements and additional test simulations for multiple aviation biofuel pathways and regions. We have also been working with the International Institute for Applied Systems Analysis on comparing model results from their GLOBIOM model with GTAP-BIO. That work will continue in 2018-2019 assuming funding is available.



Task 3- Develop Estimates of Land Use Change Associated Emissions for Aviation Biofuels for the ICAO Alternative Fuels Task Force

Purdue University

Objective(s)

Develop estimates of land use change associated emissions for aviation biofuels for the ICAO Alternative Fuels Task Force

Research Approach

We use the updated and modified GTAP-BIO model to produce estimates of induced land use change for AFTF. We are also working with IIASA and Hugo Valin to evaluate differences between results obtained with GTAP-BIO and GLOBIOM. We reached concurrence in the September 2018 AFTF meeting on ILUC emissions for CORSIA.

Milestone(s)

See the milestone list under Task #2.

Major Accomplishments

Most of the accomplishments under this task are in the form of work progress of ICAO/CAEP/AFTF. Some of the working papers and information papers we have produced in 2017/18 are listed in this section and in the overall publication list at the end of this report.

Publications

There have been numerous working papers and information papers produced for the AFTF work:

CAEP/11-AFTF/05-WP/04 – "Updates on Preliminary GTAP-BIO and GLOBIOM Results for Aviation Biofuels Induced Land use change Emission Values," Brasilia, October 2017.

CAEP/11-AFTF/06-IP/04 – "GTAP-BIO Progress on Estimating Aviation Biofuel Induced Land Use Change Emission Values," Montreal, April 2018.

CAEP/11-AFTF/06-WP/03 – "Updates on Preliminary Aviation Biofuel Induced Land Use Change Emission Values from GTAP-BIO and GLOBIOM," Montreal, April 2018.

CAEP/11-AFTF/07-IP/05 – "GTAP-BIO Updates on Estimating Aviation Biofuel Induced Land Use Change Emission Values," Montreal, September 2018.

CAEP/11-AFTF/07-IP/06 – "Sensitivity Analysis for Key Data and Parameters in GTAP-BIO and AEZ-EF," Montreal, September 2018.

CAEP/11-AFTF/07-IP/07 – "Discussion of Creating Global or Regional Values for Aviation Biofuel Induced Land Use Change Emissions," Montreal, September 2018.

CAEP/11-AFTF/07-IP/08 – "Updates of Comparisons between GTAP-BIO and GLOBIOM for Aviation Biofuels Induced Land Use Change Emissions," Montreal, September 2018.

In addition, the following journal paper was published related to land use change research:

Chen, Rui, Zhangcai Qin, Jeongwoo Han, Michael Wang, Farzad Taheripour, Wallace E. Tyner, Don O"Connor, James Duffield (2018). "Life cycle energy and greenhouse gas emission effects of biodiesel in the United States with induced land use change impacts." *Bioresource Technology* 251, pp. 249-258, https://doi.org/10.1016/j.biortech.2017.12.031.

Outreach Efforts

Xin Zhao made a poster presentation of the aviation biofuels induced land use change work at the April 2018 ASCENT meeting.



Awards
None

Student Involvement
Xin Zhao – PhD student, Purdue University

Plans for Next Period
We will continue working with ICAO on induced land use change emission estimates assuming availability of funding.

Task 4- Provide Support for the other ASCENT Universities on Aviation Biofuels Policy Analysis
Purdue University

Objective(s)
To provide support for the other ASCENT universities on aviation biofuels policy analysis.

Research Approach
We develop spreadsheet models of various pathways incorporating risk analysis. The output of the risk analysis is the distribution of net present value (NPV), internal rate of return (IRR), and the probability the investment will lose money. Being able to provide a distribution of financial outputs is immensely valuable to private sector investors and other players. The analysis outputs can also be used to help target future research to areas where the research outcome could be expected to have a high payoff. We have been working with WSU on stochastic TEA and expect in the next year to work with WSU, PSU, Hawaii, and Tennessee on stochastic TEA and risk analysis.

Tyner has joined the Southeast Partnership for Advanced Renewables from Carinata (SPARC) project funded by USDA and will be working with them on stochastic TEA of different pathways.

In addition, we now can develop distributions of breakeven prices that reflect the uncertainty in the input distributions. A distribution of breakeven prices is a very effective way to communicate the relative level of pathway cost as well as its uncertainty.

Any of the stochastic techno-economic analyses can be used with policy overlays to conduct evaluations of alternative policy options. The stochastic models can also be used to examine the impacts of alternative feedstock contracting mechanisms for feedstocks without effective hedging alternatives available, such as the cellulosic feedstocks or new lipids such as pennycress. We have worked with the ICAO/AFTF policy sub-group to develop such policy case studies.

Milestone(s)
We have published papers on stochastic TEA (see the publications in task #1) and are now assisting researchers at other universities in doing this type of analysis using the approaches we have developed.

Major Accomplishments
We have provided guidance to ASCENT partners and have helped them to build stochastic TEA models for their pathways under investigation.

Publications
None

Outreach Efforts
None

Awards
None



Student Involvement
Elspeth McGarvey – MS student, Purdue University
Jeremiah Stevens – MS student, Purdue University

Plans for Next Period
We will be working with researchers at other universities to do stochastic TEA and to develop policy overlays for the models.

Task 5- Provide Support for the Farm to Fly Initiative as Needed
Purdue University

Objective(s)
To provide support for the Farm to Fly initiative as needed.

Research Approach
This activity is a general support for other initiatives. Our main role is to consult with other projects and activities and provide assistance as needed.

Milestone(s)
There has been little activity under this task in this reporting period.

Major Accomplishments
None

Publications
None

Outreach Efforts
None

Awards
See Task 1.

Student Involvement
None

Plans for Next Period
We will continue to be available to other projects and universities as needed in the regional and national analysis related to "Farm to Fly."



Project 001(D) Alternative Jet Fuel Supply Chain Analysis

The Pennsylvania State University

Project Lead Investigator

Saurabh Bansal
Associate Professor of Supply Chain Management
Department of Supply Chain and Information Systems
The Pennsylvania State University
405 Business
University Park, PA 16802
814.863.3727
Sub32@psu.edu

Other Lead Personnel

- Kristin Brandt– WSU
- Tim Rials – UT, Burt English – UT
- Lara Fowler – PSU
- Gabrielle Gilbeau - PSU

University Participants

The Pennsylvania State University

- Other researchers: Lara Fowler – PSU, Gabrielle Gilbeau - PSU
- FAA Award Number: FAA Cooperative Agreement No. 13-C-AJFE-PSU, Amendment 028
- Period of Performance: October 1, 2017 – September 30, 2018

Project Funding Level

FAA Funding: $200,000.
Matching: Penn State - $200,000
Total Funding: $400,000

Investigation Team

1.3.1 **(Lead: Bansal;** supported by Brandt, and English) – Risk-reward profit sharing modeling for first facilities

1.3.2 **(Lead: Bansal; supported by Brandt, and English)** – Additional quantification of risk and uncertainties in supply chains (foundational part of task above)

1.3.3 **(Lead: Bansal; supported by Brandt, and English)** – Supply chain risk analysis tools for farmer adoption

1.4.1 **(Lead: Fowler; supported by Gilbeau)** – National survey of current and proposed state and federal programs that monetize ecosystem services

1.4.3 **(Lead: Fowler; supported by Gilbeau)** – Help support stakeholder engagement efforts



Project Overview

Task 1.3.1-Risk-Reward Profit Sharing Modeling for First Facilities

Pennsylvania State University

Objective(s)

Develop a transparent risk-sharing tool to provide an understanding of cash flows and risks faced by all supply chain partners, to all partners.

Research Approach

We first collected a large number of risk sharing tools that have been proposed in the supply chain literature. Subsequently, we narrowed down the list of 9-12 mechanisms. We created an Excel-based framework in which the cash flows of all supply chain partners are modeled, using the numbers from the TEA analyses developed by WSU. This framework incorporates the risk sharing mechanisms.

Milestone(s)

Developed the prototype Excel model, in collaborations with the TEA models from WSU.

Major Accomplishments

We have the Excel tool ready to be used with some guidelines that explain the use of the tool.

Publications

We anticipate publishing a paper based on combined work from the last year and the coming year.

Outreach Efforts

The tool has been discussed at three avenues at the ASCENT enterprise.

Awards

None

Student Involvement

None

Plans for Next Period

We intend to run some focus group and laboratory studies to quantify the expected benefit from the tool. We will also develop a video that provide guidelines on using the tool.

References

None

Task 1.3.2- Additional Quantification of Risk and Uncertainties in Supply Chains (foundational part of task above)

Pennsylvania State University

Objective(s)

Develop methods to rely on expert judgments to quantify uncertainties associated with biofuel supply chains.

Research Approach

We developed a new econometric approach to quantify probability distributions of uncertain quantities such as yield or demand when a panel of experts provide judgments for the most likely values. This approach exploits the well-known



theory of generalized least squares in statistics, for the context in which historical data are available to calibrate expert judgments or when these data are not available.

Milestone(s)
We have captured the method in two manuscripts. One of them is finished and submitted for peer review while the second one is in progress.

Major Accomplishments
Theoretical development and numerical study shows the promise of this approach.

Publications
One paper is under review. The second manuscript will be finished in a few months.

Outreach Efforts
None

Awards
None

Student Involvement
None

Plans for Next Period
The second paper will be finished. Any revisions required for the first paper will also be made in the next one-two years.

References
None

Task 1.3.3- Supply Chain Risk Analysis Tools for Farmer Adoption
Pennsylvania State University

Objective(s)
Understand farmers' risk preferences over a long duration and how it impacts their decisions to adopt crops that can support AJF supply chains.

Research Approach
The research is in two parts: (i) survey farmers to understand their risk preferences over extended durations and (ii) use this information as an input to prescriptive models.

Milestone(s)
We have initiated conversation with farmers to develop an understanding for (i) above.

Major Accomplishments
Our work thus far suggests that farmers do indeed plan for long term and they have other objectives beyond monetary returns. In a set of interactions with farmers with Centre County in Pennsylvania, we found that farmers value a stability in cash flows over 5-10 years, keeping land within the family for the next generation, and environmental issues that may impact their next generation's ownership of land. We plan on continuing this work during the coming year.

Publications
None



Outreach Efforts
None

Awards
None

Student Involvement
None

Plans for Next Period
The work for this objective is expected to continue in the coming year as we talk to more farmers and understand their decisions for crop adoption.

References
None

Task 1.4.1- National Survey of Current and Proposed State and Federal Programs that Monetize Ecosystem Services
Pennsylvania State University

Objective(s)
Conduct a survey and summarize current and proposed state and federal programs to monetize economic systems.

Research Approach
This task builds on and continues the work done under ASCENT Project 01, Task 8.1,that focused on the biomass and water quality benefits to the Chesapeake Bay watershed. Under this task, we examined the biofuel law and policy landscape of the Pacific Northwest and Southeast regions, as well as the state of Hawaii. We also researched federal biofuel law and policy.

Milestone(s)
We have captured this research in three regional white papers describing the biofuel law and policy incentives, and the ecosystem services drivers for the sub-regions defined by:

- Project 01A, Tasks 3.1, the Pacific Northwest
- Project 01B, Task 3.2, Hawaii
- Project 01E, the Southeast

Major Accomplishments
We have captured this research in three regional white papers describing the biofuel law and policy incentives, and the ecosystem services drivers for the sub-regions described in the Milestones section above.

Publications
The white papers will be published in the upcoming ASCENT funding year.

Outreach Efforts
Economic model to motivate land use conversion has been demonstrated at CAAFI meetings. In addition, we have provided presentations and posters at several meetings, including the following.

- Presentation by Lara B. Fowler, Gaby Gilbeau: U.S. Biofuel Law & Policy: Biomass Production + Ecosystem Services= Support for the Biofuel Industry? MABEX Annual Conference, University Park, PA (Sept. 13, 2017)



- Poster by Gaby Gilbeau, Lara B. Fowler, U.S. Biofuel Law & Policy: Biomass Production, Water Quality, and Support for the Biofuel Industry, MABEX Annual Conference, University Park, PA (Sept. 2017).
- Presentation by Gaby Gilbeau, Lara B. Fowler, Nationwide Environmental Services Assessment, ASCENT Team Webinar (Nov. 2017).
- Presentation by Kate Zipp: Analysis of ecosystem service valuation, law and policy drivers, and potential policy design of water quality improvements associated with perennial grasses and cover crops, ASCENT Project Meeting, Boston, MA (April 2018).
- Presentation by Lara Fowler, Gaby Gilbeau: The Legal & Regulatory Landscape of the Biofuels Industry, ASCENT Fall Meeting, Alexandria, VA (Oct. 9, 2018)
- Poster by Gaby Gilbeau and Lara Fowler, Biofuel Law & Policy: The Legal & Regulatory Landscape of the Biofuels Industry, CAAFI Fall Meeting, Alexandria, VA (Dec. 2018)

Awards
None

Student Involvement
None

Plans for Next Period
The research moving forward in the next two years will expand upon these regional and national overviews to explore law and policy drivers in additional regions of interest for the ASCENT program, a more in-depth national examination, and expansion of the research beyond water, looking at other environmental service and credit-trading markets. This will help support work identified by other ASCENT team members.

References
None

Task 1.4.3- Help Support Stakeholder Engagement Efforts
Pennsylvania State University

Objective(s)
Facilitate dialogue between producers, industry, government, and other affected stakeholders.

Research Approach
Our work under this objective focused on stakeholder engagement and facilitation of effective dialogue to help bridge the gap between producers, industry, government, and other affected stakeholders. Our work under Objective 1.4.3 included a "Stakeholder Engagement 101" training session for the ASCENT 01 project team members.

Milestone(s)
These efforts supported the stakeholder engagement efforts led by other teams, including but not limited to the regional partners identified in ASCENT Project 01, Tasks 3.1, 3.2 and 3.3.

Major Accomplishments
We provided a stakeholder engagement presentation for ASCENT partners during a regularly scheduled team meeting on April 30, 2018.

In addition, we have held initial conversations with partners in Tennessee but these have been delayed due to constraints for the Tennessee partners.



Publications
None

Outreach Efforts
Economic model to motivate land use conversion has been demonstrated at CAAFI meetings.

Awards
None

Student Involvement
None

Plans for Next Period
Future work on this task involves identifying potential stakeholders and developing guidelines for facilitate discussion among various stakeholders using the model developed in Task 1.3.1. This work will also help support regional analyses under D6. Work going forward under this objective includes presenting to the project partners on facilitation skills and tactics. Additional support for regional projects will be offered as needed, for facilitation and stakeholder engagement sessions as the regional projects move to the deployment stage.

References
Daly, C., Halbleib, M., Hannaway, D., & Eaton, L. (n.d.). Environmental Limitation Mapping of Potential Biomass Resources across the Conterminous United States. *Global Climate Change Biology-Bioenergy*.

Environmental Protection Agency. (2010). *Chesapeake Bay TMDL Document*.

Fackler, P. L. (2008). Solving Optimal Switching Models. *Working Paper. North Carolina State University*. Retrieved from http://www4.ncsu.edu/unity/users/p/pfackler/www/ECG766/switch.pdf

Hunter-Davenport, B., Brady, T., & Shader, N. (2016). Pennsylvania Unveils Comprehensive Strategy to Improve Water Quality in state and Chesapeake Bay Watershed. Retrieved November 3, 2017, from http://www.media.pa.gov/pages/Agriculture_details.aspx?newsid=385

Miranda, M. J., & Fackler, P. L. (2002). *Applied Computational Economics and Finance*. Cambridge: MIT Press.

Song, F., Zhao, J., & Swinton, S. M. (2011). Switching to Perennial Energy Crops Under Uncertainty and Costly Reversibility. *American Journal of Agricultural Economics*, *93*(3), 768–783. https://doi.org/10.1093/ajae/aar018



Project 001(E) Alternative Jet Fuel Supply Chain Analysis

University of Tennessee

Project Lead Investigator

Timothy Rials
Professor and Director
Center for Renewable Carbon
University of Tennessee
2506 Jacob Dr. Knoxville, TN 37996
865-946-1130
trials@utk.edu

University Participants

University of Tennessee

- P.I.(s): Burton English, Professor
- FAA Award Number: 11712069
- Period of Performance: [August 1, 2017 to September, 30, 2018
- Task(s):
  - Task 1.1: Assess and inventory regional forest and agricultural biomass feedstock options.
  - Task 1.2: Delineate the sustainability impacts associated with various feedstock choices including land use effects.
  - Task 3: Lay the groundwork for lipid and/or biomass in TN & Southeast U.S.
  - Task 4: Biorefinery Infrastructure and Siting (Supporting Role).

Project Funding Level

Total 4-year funding/This year funding
Total Estimated Project Funding: $404,056/$225,000
Total Federal and Non-Federal Funds: $808,112/$450,000
Faculty salary was provided by The University of Tennessee, Institute of Agriculture, in support of the project.

Investigation Team

- Tim Rials – Project Director(s)/Principal Investigator (PD/PI)
- Burton English – Co-Principal Investigator (Co PD/PI)
- Chris Clark – Faculty
- Lixia He – Other Professional
- Kim Jensen – Faculty
- Dayton Lambert – Faculty
- Jim Larson – Faculty
- Ed Yu – Faculty
- Evan Markel – Graduate Student
- Katryn Pasaribu – Graduate Student
- Umama Rahman – Masters Graduate Student
- Bijay Sharma – Graduate Student
- McKenzie Thomas – Masters Graduate Student
- Ming-Jou Tsai – Maters Graduate Student



Project Overview

The University of Tennessee will lead the Feedstock Production (Task 1) component of the project. This component targets the need to assess and inventory regional forest and agricultural biomass feedstock options; and delineate the sustainability impacts associated with various feedstock choices, including land use effects. The University of Tennessee will lead the national lipid supply availability analysis employing POLYSYS to develop information on the potential impacts and feasibility of using lipids to supply aviation fuel. The team at UT will facilitate regional deployment/production of jet fuel by laying the groundwork and developing a regional proposal for deployment. Additionally, The University of Tennessee will support activities in Task 3 with information and insights on feedstocks, along with potential regional demand centers for aviation fuels and coproducts, along with information on current supply chain infrastructure, as required.

Finally, through a structured workshop, the University of Tennessee will garner stakeholder input on supply chain challenges as well as provide a forum for interdisciplinary dialogue and problem solving for alternative aviation fuels. The University of Tennessee is committed to hosting this workshop in early 2019 in Knoxville, TN. There has been valuable discussion of CAAFI perspectives and information needs, and aviation industry stakeholders have already been contacted for workshop input.

Major goals included:

1. Develop a rotation based oil seed crop scenario and evaluate potential with POLYSYS
2. Develop database on infrastructure and needs for Southeast
3. Organize and convene workshop on the alternative jet fuel supply chain for southeastern stakeholders
4. Initiate aviation fuel supply chain study in the southeast
5. Continue with sustainability work for both goals 1 and 4

Task 1.1- Assess and Inventory Regional Forest and Agricultural Biomass Feedstock Options

University of Tennessee

Objective(s)

As the markets for lignocellulosic biomass (LCB) feedstock, i.e. grasses, short-rotation woody crops, and agricultural residues, are currently not well established, it is important to evaluate the feasibility of supplying those LCB feedstocks. The opportunity cost of converting the current agricultural lands to LCB feedstocks production will be estimated. In addition, the production, harvest, storage and transportation cost of the feedstocks are included in the assessment. A variety of potential crop and biomass sources will be considered in the feedstock path including:

- **Oilseed crops:**
  - Mustard/Crambe (*Sinapsis alba/Crambe abyssinicia*)
  - Pennycress (*Thlaspi arvense*)
  - Rapeseed/Canola (*Brassica napus/B. campestris*)
  - Safflower (*Carthamus tinctorius*)
  - Sunflower (*Helianthus spp.*)
  - Soybean (*Glycine max*);
  - Camelina (*Camelina sativa*)
  - Carinata
- **Perennial grasses**:
  - Switchgrass (*Panicum virgatum*)
  - Miscanthus (*Miscanthus sinensis*)
  - Energy Cane (*Saccharum complex*)
- **Short-rotation woody crops**:
  - Poplar (*Populus species*)
  - Willow (*Salix species*)
  - Loblolly pine (*Pinus taeda*)
  - Sweetgum (*Liquidambar styraciflua*)



    - Sycamore (*Plantanus occidentalis*)
- **Agricultural residue**:
    - Wheat straw
    - Corn stover
- **Forest residue**:
    - Logging and Processing Residue

POLYSYS will be used to estimate and assess the supply and availability of these feedstock options at regional and national levels. This U.S. agricultural sector model forecasts changes in commodity prices and net farm income over time.

County level estimates of all-live total woody biomass, as well as average annual growth, removals, and mortality will be obtained from the Forest Inventory and Analysis Database (FIADB). Mill residue data will be obtained from the USFS FIA Timber Product Output (TPO) data. The ForSEAM model will be used to estimate and predict logging residues. ForSEAM uses U.S. Forest Service FIA data to project timber supply based on USGPM demand projections. Specific tasks related to this objective are outlined below. These supply curves will be placed in POLYSYS and estimates into the future will be made.

Task 1 Goals (support/continues ongoing work from previous year)

0.1 Complete the economic viability analysis on switchgrass, short rotation woody crops, crop residues, forest residues, and cover crops to assist team with theme 1.3

1.3 Assist Risk-Reward Profit Sharing modeling by providing information from past work on cellulosic supply chains to PSU

1.4.1 Assist PSU in the National Survey of current and proposed programs that incentivize ecosystem services

1.4.2 Finish environmental impact analysis for the fore-mentioned crops looking at soil, water, greenhouse gas emissions and sequestration, and direct land use change

Research Approach

1. Using an existing model, POLYSYS, the price for a commodity or annual demands for feedstock are exogenously determined and placed into the model. For this year, analysis was conducted for a model cover crop – pennycress, an oil feedstock. A solution was generated that estimated the supply curve that pennycress might take ranging from $0.00 to $0.50 per pound. The feedstock streams were placed in ASCENT 1's Database. It was presented twice before the ASCENT 1 research team.
2. Completed the development of camelina and carinata budgets.
3. Added cover crops camelina and carinata to the potential feedstock candidates list and developed fact sheets for these crops. Yields for camelina have been developed as a cover crop in most of the U.S. and as a spring crop in the Pacific NW.
4. Estimated the Standard deviation and mean and initiated a stochastic spreadsheet analysis of camelina.
5. Contacted Temple Texas for assistance in developing carinata yields using EPIC. This is ongoing.
6. Conducted an POLYSYS analysis on Camelina with the flow as indicated in Figure 1.1. This is written up in a defended thesis and will be further developed as a journal article.



Figure 1.1. Approach to estimate economic impacts of using camelina as a biofuels feedstock.

New Findings

- Camelina has the potential to supply both oil and biomass to the biofuels market.
- Camelina, like pennycress, is a winter crop that is typically planted in September and harvested the following May.
- It can be planted after corn harvest and be harvested before soybeans are planted.
- Following harvest, seed crushing and pre-processing, camelina offers a suitable oil to allow conversion to a Hydro-processed Ester and Fatty Acid (HEFA) fuel. Camelina budget presented in Table 1.1, Table 1.2, and Table 1.3. Carinata costs under review. Table 1.1 indicates that if you receive $0.28 per pound of seed, total revenue could be equal to $293/acre at a cost of $123 per acre in variable costs and $33 per acre in fixed costs, yielding a per acre profit of $137 per acre.
- Tornado diagram developed and breakeven table generated (Figure 1.2). The diagram was developed by changing the variable of interest by + or – 20%. Findings indicate that price and yields impact profitability more than any other variable ranging from $80 to $200 per acre. Breakeven prices were estimated and displayed in Table 1.2 and range from $0.07 per pound at high yields and $0.27 per pound at low yields.
- Camelina supply curve generated. A spatial Camelina yield supply curve was estimated by EPIC. The supply curve indicates that sufficient Camelina feedstock would be generated to produce 450 million gallons if the feedstock price was $0.20 per pound (Figure 1.3).



Table 1.1. 2018 Field Camelina

	Unit	Quantity	Price	Total
Revenue			**Gross Revenue ($/Acre)**	
Camelina	lbs	1050	$0.28	$293.15
		Total Revenue	**$293.15**	
Variable Expenses				
Seed	lbs	5	$2.00	$10.00
Fertilizer	Acre	1	$45.30	$45.30
Chemical	Acre	1	$27.50	$27.50
Repair & Maintenance	Acre	1	$11.76	$11.76
Fuel, Oil & Filter	Acre	1	$8.50	$8.50
Operator Labor	Acre	1	$5.95	$5.95
Machinery Cost Broadcast Planting	Acre	1	$13.40	$13.40
Crop Insurance	Acre	1	$0.00	$0.00
Operating Interest [7]	Acre	1	$0.90	$0.90
Other Variable Costs	Acre	1	$0.00	$0.00
		Total Variable Expenses	**$123.31**	
		Return Above Variable Expenses	**$169.84**	
Fixed Expenses				
Machinery				
Capital Recovery	Acre	1	$27.08	$27.08
Other Fixed Machinery Costs	Acre	1	$0.00	$0.00
Taxes, Housing & Insurance	Acre	1	$5.96	$5.96
Other Fixed Costs	Acre	1	$0.00	$0.00
		Total Fixed Expenses	**$33.04**	
Return Above All Specified Expenses			**$136.80**	

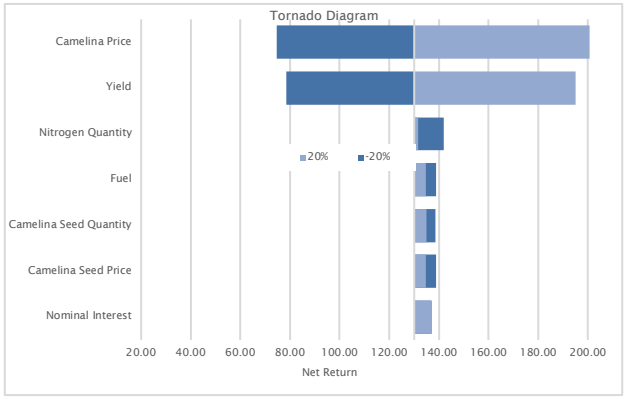


Figure 1.2. Camelina Tornado Diagram

Table 1.2. Breakeven Price for Selected Yield

Yield (lbs.)	Variable Cost ($/lbs.)	Total Specified Cost ($/lbs.)
450	$0.27	$0.35
600	$0.21	$0.26
750	$0.16	$0.21
900	$0.14	$0.17
1050	**$0.12**	**$0.15**
1200	$0.10	$0.13
1350	$0.09	$0.12
1500	$0.08	$0.10
1650	$0.07	$0.09

Table 1.3. Breakeven Yield for Selected Price

Price ($/lbs.)	Variable Cost (lbs./acre)	Total Specified Cost (lbs./acre)
$0.18	688	873
$0.20	604	766
$0.23	538	682
$0.25	485	615
$0.28	**442**	**560**
$0.30	405	514
$0.33	375	475
$0.35	348	441
$0.38	325	412

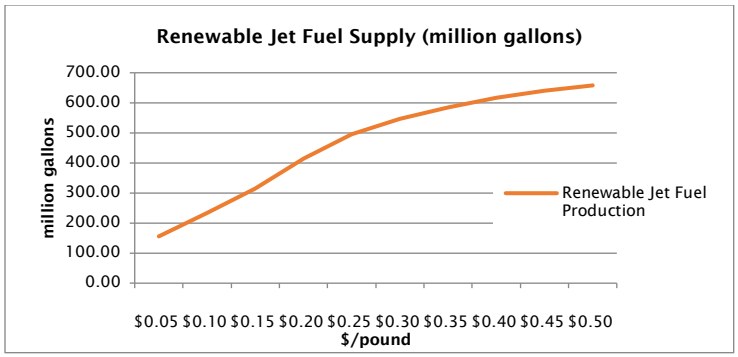


Figure 1-3. Renewable Jet fuel supply curve generated using POLYSYS assuming ASCENT HEFA conversion process

Milestone(s)

- Generated data passed on to ASCENT 01 database for camelina feedstock.
- Camelina pathway developed.
- Other cover crops costs have been derived and under review.
- Delivered pennycress and crush facility spreadsheet to PSU for use in Risk reward profit sharing modeling.

Major Accomplishments

1. Journal Article on pennycress stemming from Evan Markel's dissertation published.
2. Developed two posters examining impacts of feedstock risk.
3. Evaluated the impact of BCAP on cellulosic feedstock risk
4. Developed economic multipliers for:
    - FT-SPK; Feedstock - Conversion temp. - 1200~1600 deg. C; Product - jet and naphtha; I have an excel model of economic analysis
    - ATJ-SPK; Feedstock - yeast biocatalyst converts purified sugar to **ethanol**, followed by oligomerization and hydrogenation; Product - jet fuel.

Publications

Evan Markel, Burton C. English, Chad Hellwinckel, R. Jamey Menard (2018) Potential for Pennycress to Support a Renewable Jet Fuel Industry. in Ecology, Pollution and Environmental Science, *SciEvironm* 1:121 accessed at http://hendun.org/journals/EEO/EEO-121.php.

Outreach Efforts

None

Awards

None

Student Involvement

We have had a PhD student, Evan Markel, working on this project. He gathered information on Pennycress and developed an analysis looking at pennycress as a feedstock. Another Ph.D. student, Katryn Pasaribu, along with a Masters student, Umama Rahman, worked on the cover crop spreadsheets, and Bijay Sharma worked on risk analysis.

Plans for Next Period

Complete cover crop analysis for feedstock costs and yields. Develop POLYSYS analysis for both camelina, carinata, and winter rye. Upload information gained into Box. Present material on Webinar in March or April.

Task 1.2- Delineate the Sustainability Impacts Associated with Various Feedstock Choices Including Land Use Effects

University of Tennessee

Objective(s)

Environmental Sustainability – Regarding environmental sustainability, the impacts associated with lignocellulosic biomass (LCB) feedstock production, such as greenhouse gas (GHG) flux and soil erosion are estimated based on local geographic characteristics. The GHG flux related to land use change and LCB feedstock production is analyzed using the POLYSYS model. Different agricultural land use systems have varied effects on soil erosion or soil loss. The impact on soil erosion from different LCB feedstock productions is simulated with the Universal Soil Loss Equation and the 1997 NRI data base.

Economic/Social Sustainability – The IO analysis provides estimates of output, employment and income multipliers, which measure the response of the economy to a change in demand or production[9, 22]. The economic multipliers measure the indirect and induced effects of a change in final demand (direct effects) for a particular industry (for example, the introduction of biorefineries and preprocessing facilities in a region). The indirect effects are the secondary effects or production changes when input demands change due to the impact of the directly-affected industry (for example, construction sector, agriculture producers, and transportation sectors). The induced effects represent the response by all local industries caused by changes in expenditures by households and inter-institutional transfers generated from the direct and indirect effects of the change in final demand. Projections of changes in jobs (job creation), economic activity, The FT-SPK and ATJ-SPK multipliers have been estimated for the entire 48 contiguous states and maps developed that will allow estimation of the economic impacts of the direct investment and operating transactions to be reflected in the economic impacts of a given area within the country. The model regions are the 187 Bureau of Economic Analysis (BEA) regions in the country. This was completed and information available for Total Industry Output, Value Added, and Employment.

Research Approach

Develop impact analysis for economic and environmental parameters.

New Findings

IO Analysis

For the ASCENT TEA's developed by WSU, estimate the impacts for Total Industry Output, Value Added, and Employment. Using the Bureau of Economic Analysis (BEA) regions (Figure 1.4), develop a spatial surface of the multipliers for three indicators for both investment (one time) impacts and annual operating impacts. These impacts have been developed for the conversion facility, feedstocks, land use change, proprietor income and transportation for alcohol to jet, Fast Pyrolysis, and HEFA pathways. Economic Impacts result from changes in agricultural operations from feedstock establishment, profit, land use change, and commodity price change; investment changes in preprocessing and conversion facilities from investment expenditures, salaries and wages; transportation; and from annual operations of preprocessing and conversion facilities including operation expenditures, profit/loss including the value of the RIN less the value of the transfer payment that occurred as a result of the RIN transfer, and salaries and wages. Below are examples of these spatially-oriented economic impact layers (SEIL) that were developed for a single facility located in a particular BEA for investment (Figure 1.5-1.7) and annual operating transactions (Figures 1.8-1.10) as well as employment impacts (Figures 1.11-1.16).



Figure 1.4. Bureau of Economic Administration trading areas

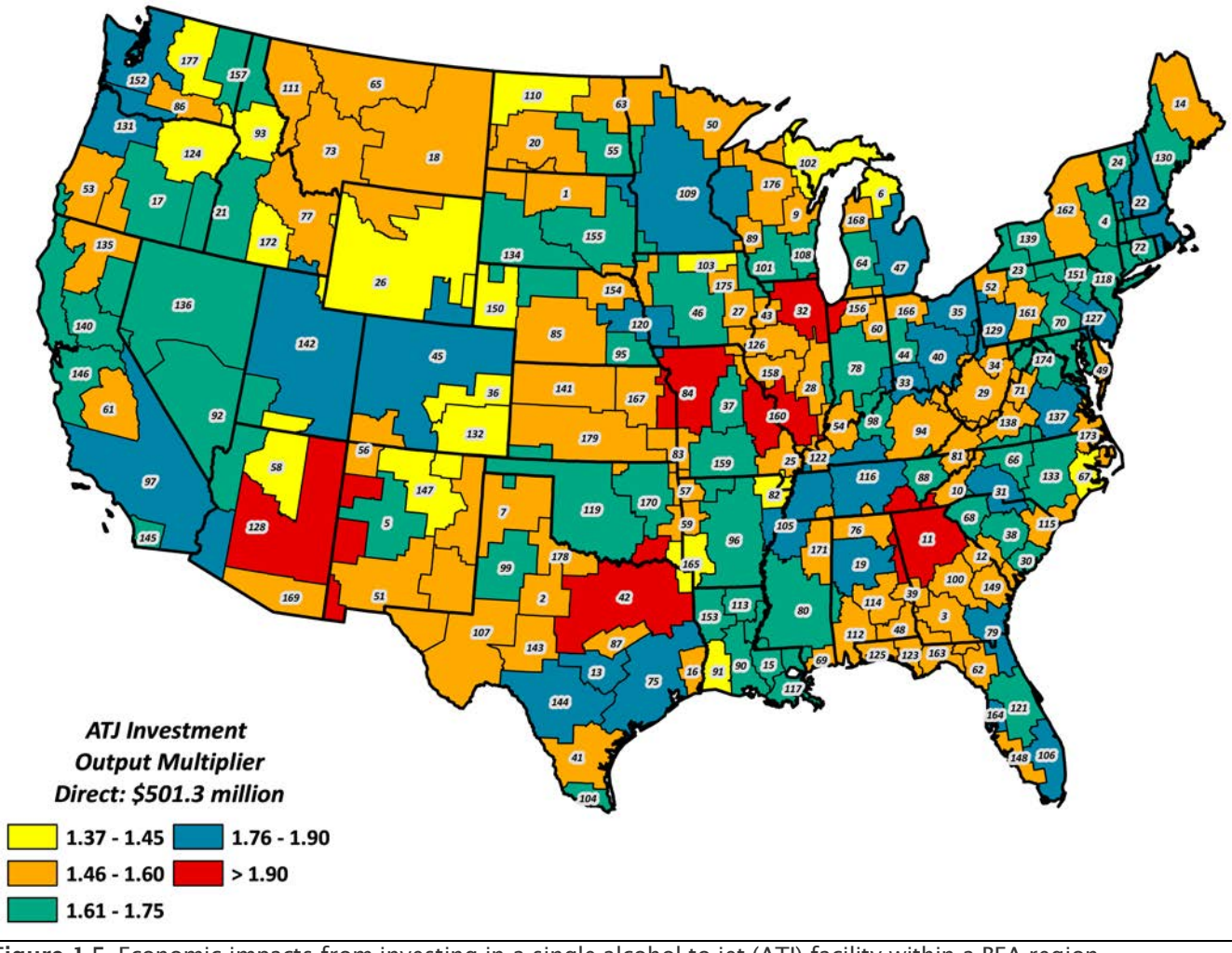


Figure 1.5. Economic impacts from investing in a single alcohol to jet (ATJ) facility within a BEA region

Projections of changes in economic activity as a result of this investment through multiplier effects are estimated using Analysis By Parts (ABP) methodology with United States IMPLAN datasets aggregated to BEA region.

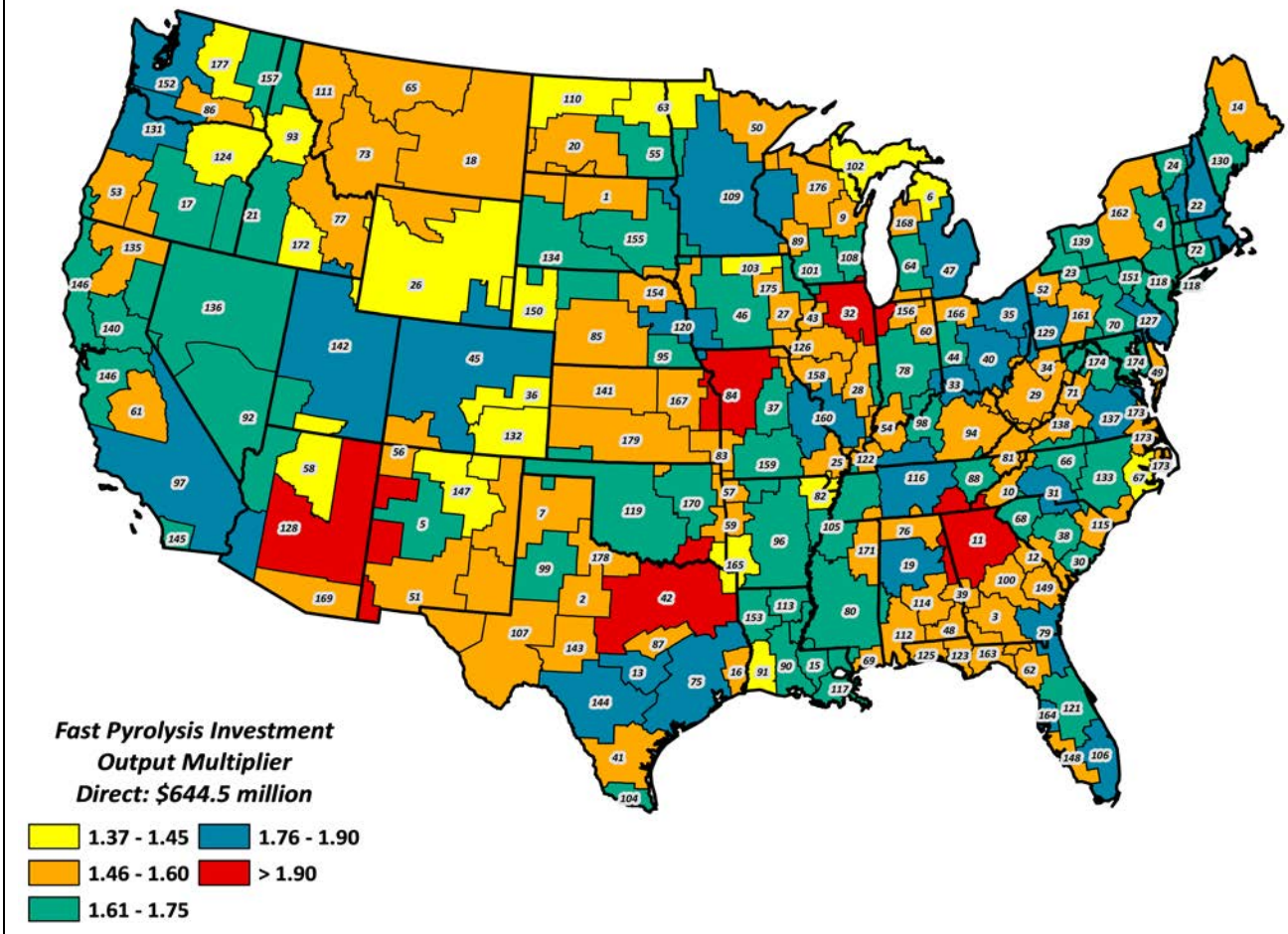


Figure 1.6. Economic impacts from investing in a single fast pyrolysis facility within a BEA region

Projections of changes in economic activity as a result of this investment through multiplier effects are estimated using Analysis By Parts (ABP) methodology with United States IMPLAN datasets aggregated to BEA region.

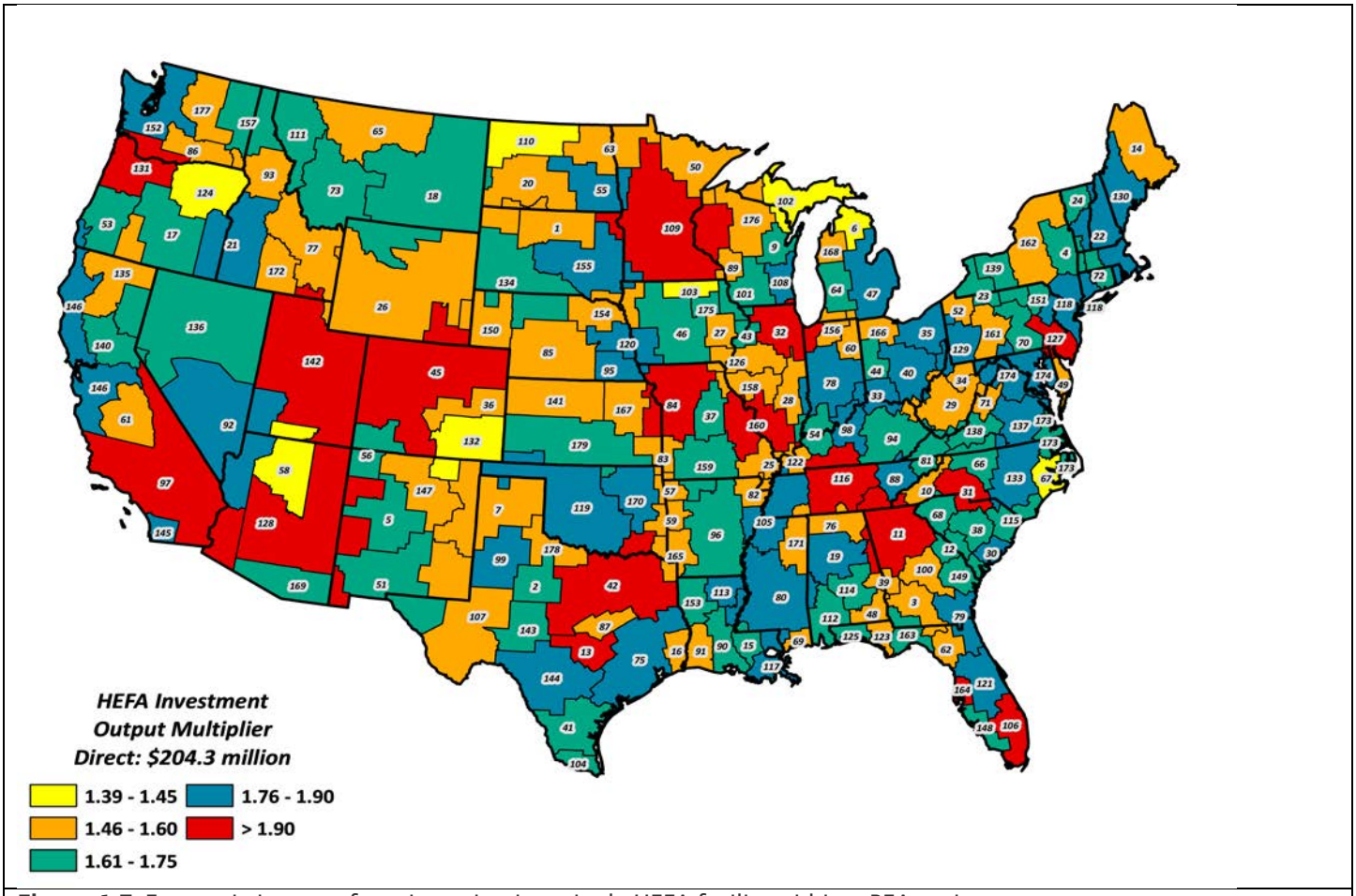


Figure 1.7. Economic impacts from investing in a single HEFA facility within a BEA region

Projections of changes in economic activity as a result of this investment through multiplier effects are estimated using Analysis By Parts (ABP) methodology with United States IMPLAN datasets aggregated to BEA region.

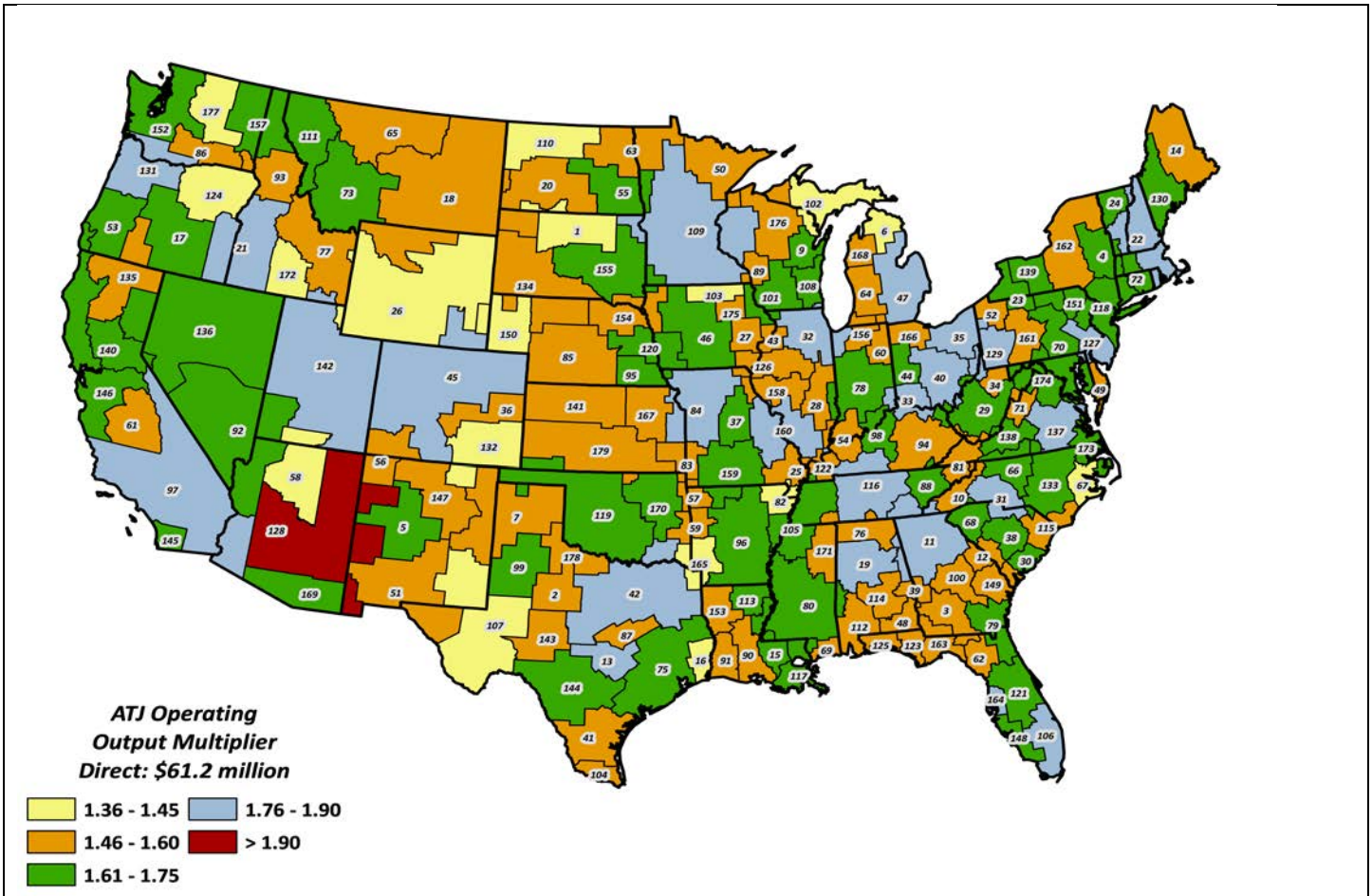


Figure 1.8. Annual Economic impacts from operating a single alcohol to jet (ATJ) facility within a BEA region Projections of changes in economic activity as a result of this investment through multiplier effects are estimated using Analysis By Parts (ABP) methodology with United States IMPLAN datasets aggregated to BEA region.

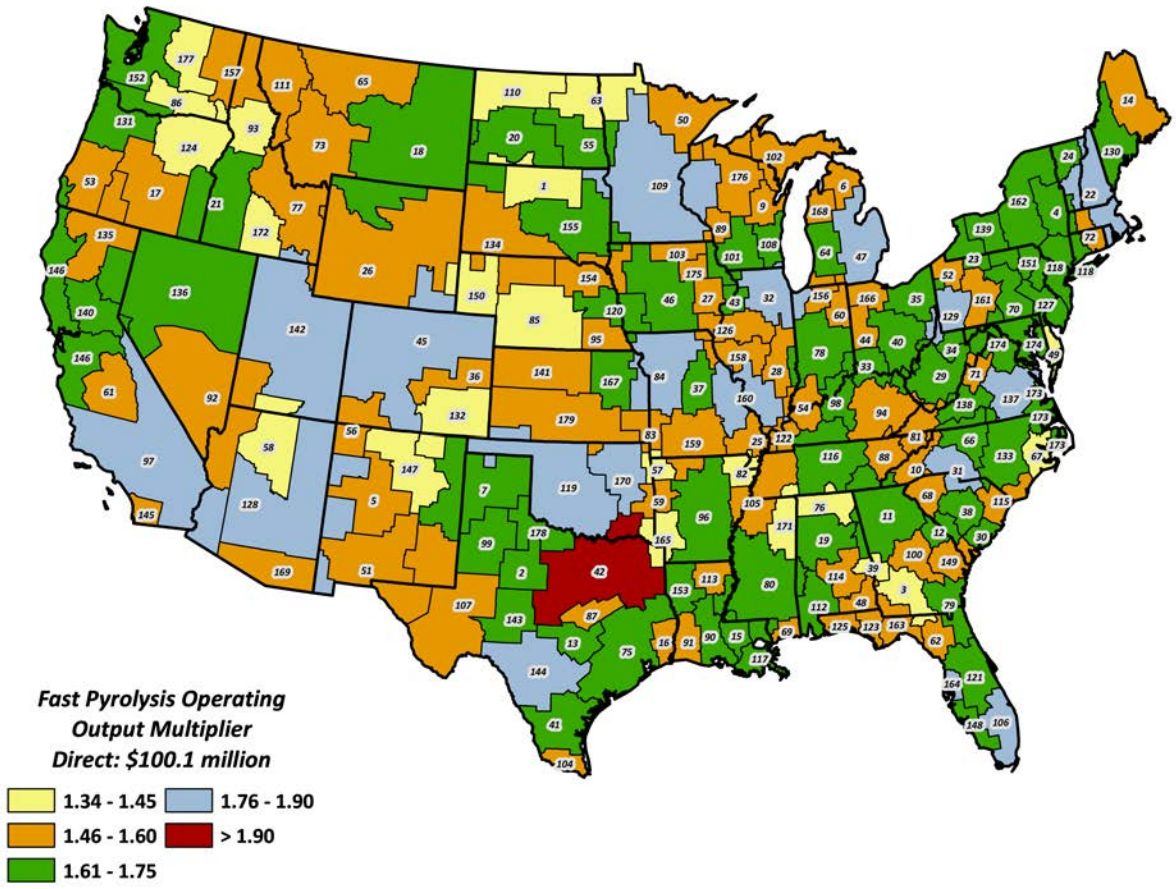


Figure 1.9. Annual Economic impacts from operating a single fast pyrolysis facility within a BEA region

Projections of changes in economic activity as a result of this investment through multiplier effects are estimated using Analysis By Parts (ABP) methodology with United States IMPLAN datasets aggregated to BEA region.

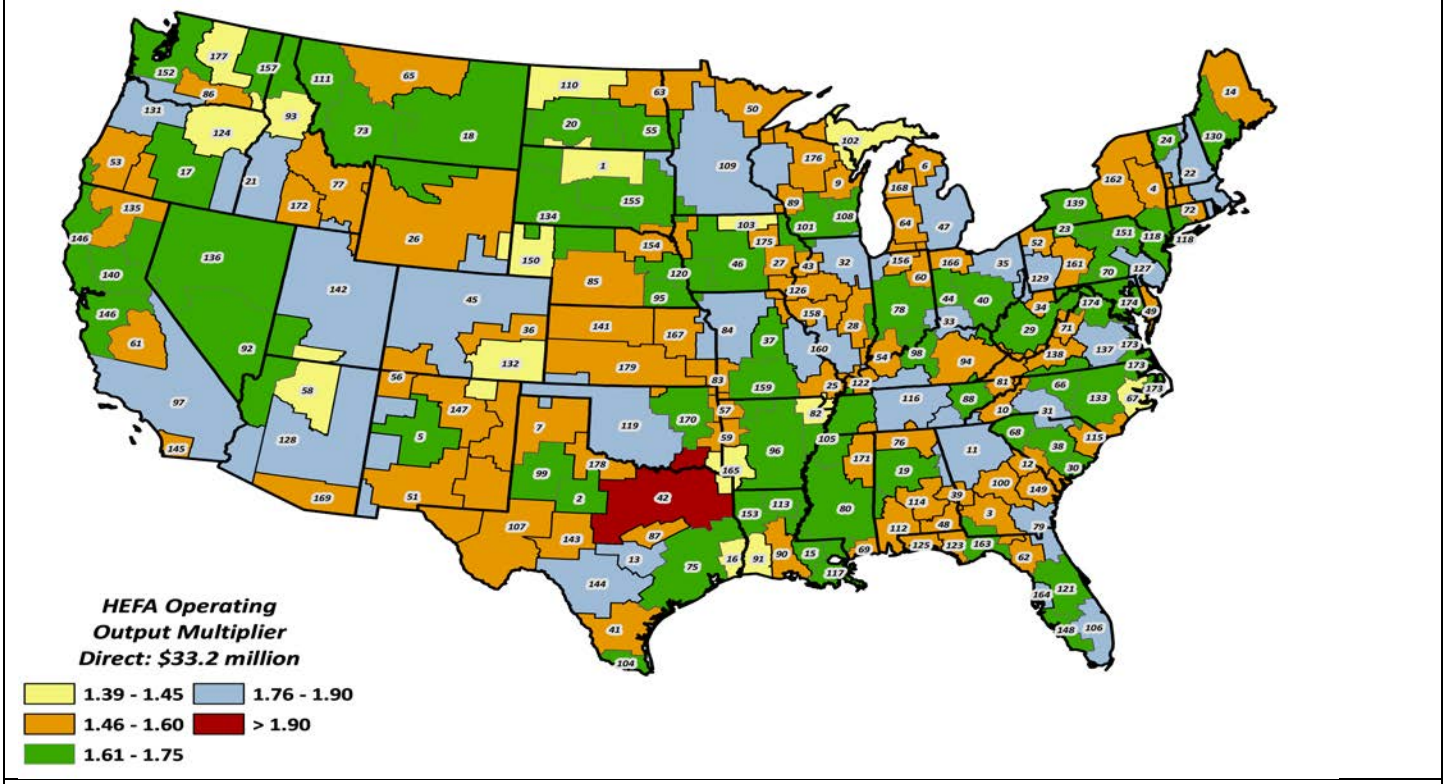


Figure 1.10. Annual Economic impacts from operating a single HEFA facility within a BEA region

Projections of changes in economic activity as a result of this investment through multiplier effects are estimated using Analysis By Parts (ABP) methodology with United States IMPLAN datasets aggregated to BEA region.

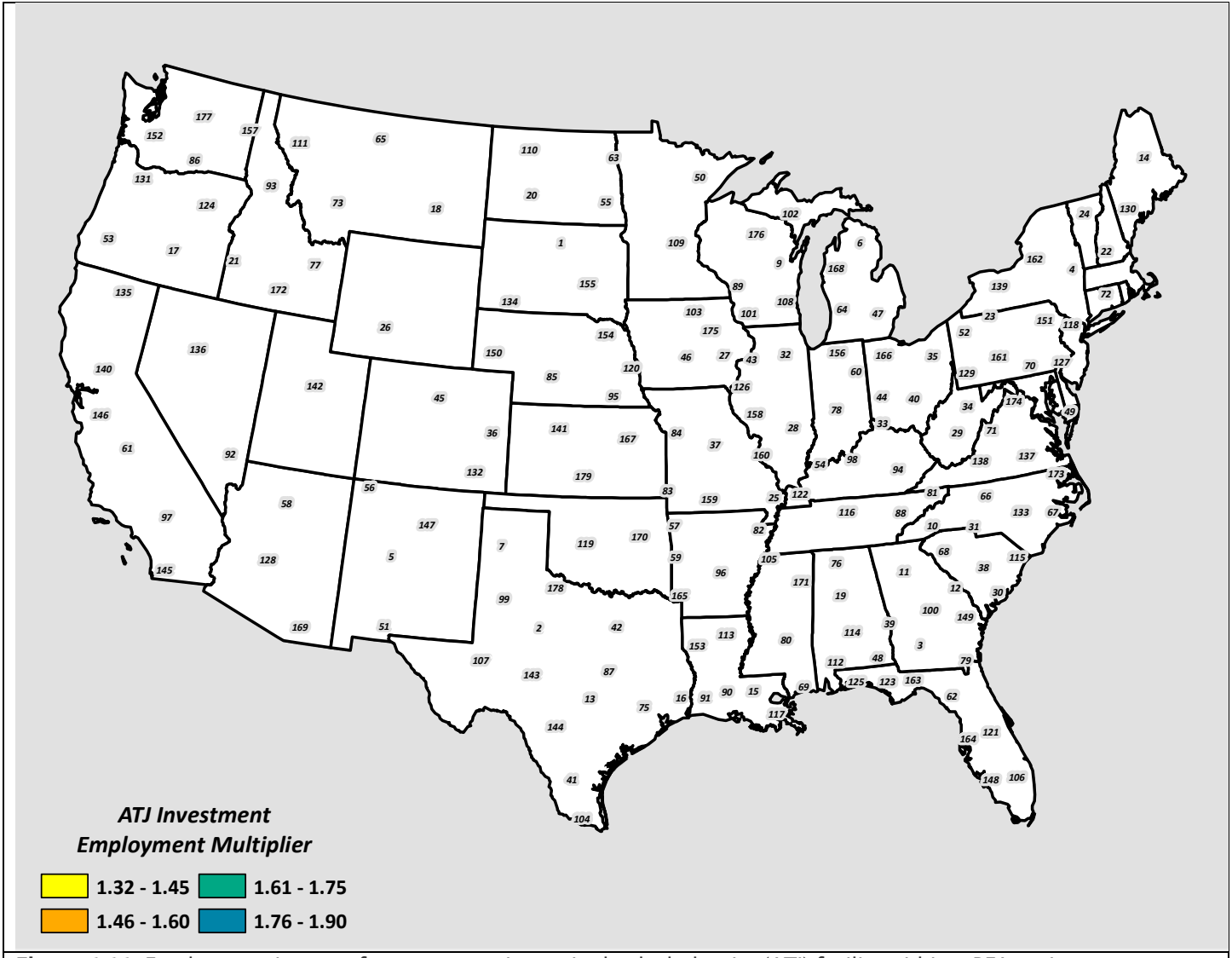


Figure 1.11. Employment impacts from constructing a single alcohol to jet (ATJ) facility within a BEA region
Projections of changes in economic activity as a result of this investment through multiplier effects are estimated using Analysis By Parts (ABP) methodology with United States IMPLAN datasets aggregated to BEA region.

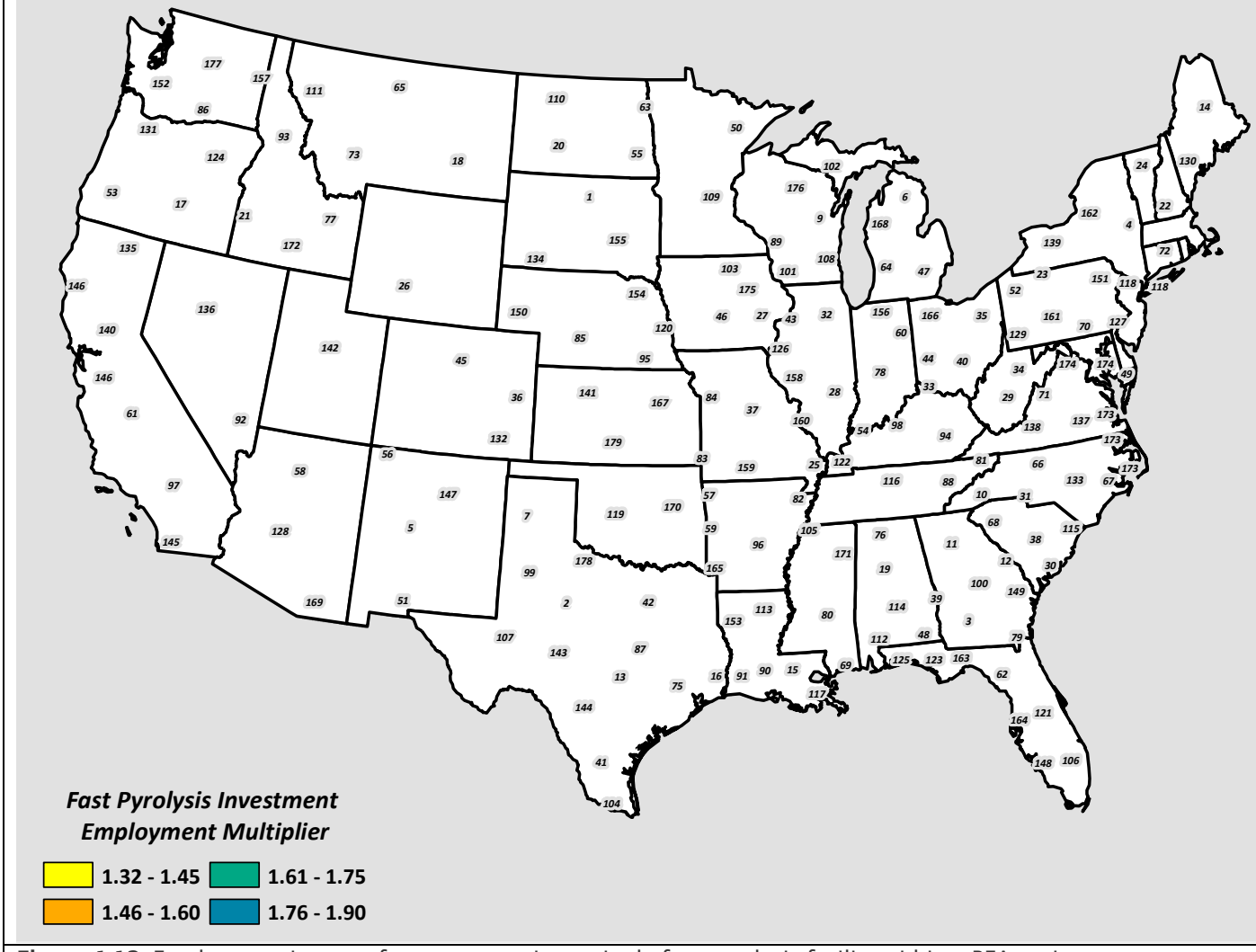


Figure 1.12. Employment impacts from constructing a single fast pyrolysis facility within a BEA region
Projections of changes in economic activity as a result of this investment through multiplier effects are estimated using Analysis By Parts (ABP) methodology with United States IMPLAN datasets aggregated to BEA region.

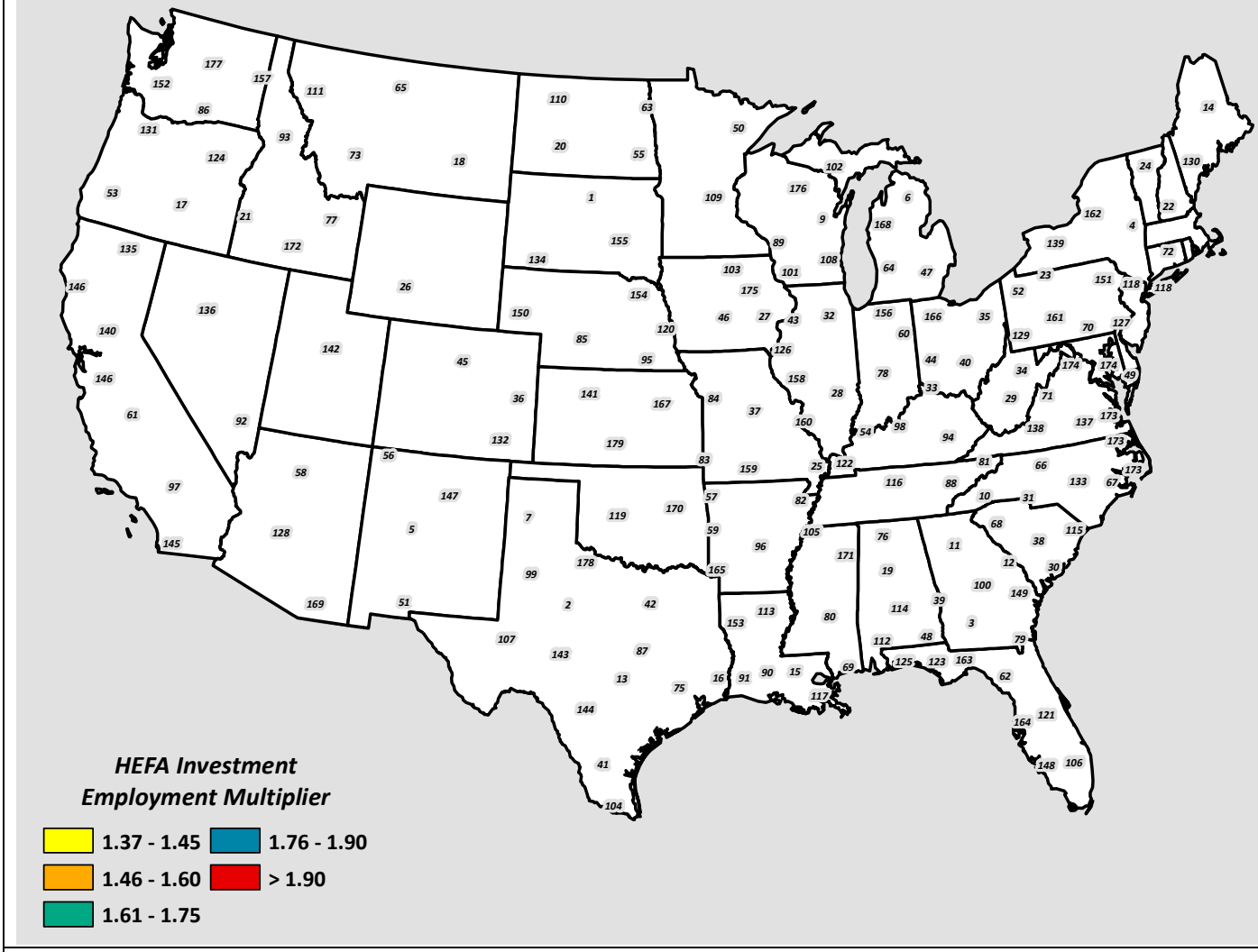


Figure 1.13. Employment impacts from constructing a single HEFA facility within a BEA region
Projections of changes in economic activity as a result of this investment through multiplier effects are estimated using Analysis By Parts (ABP) methodology with United States IMPLAN datasets aggregated to BEA region.

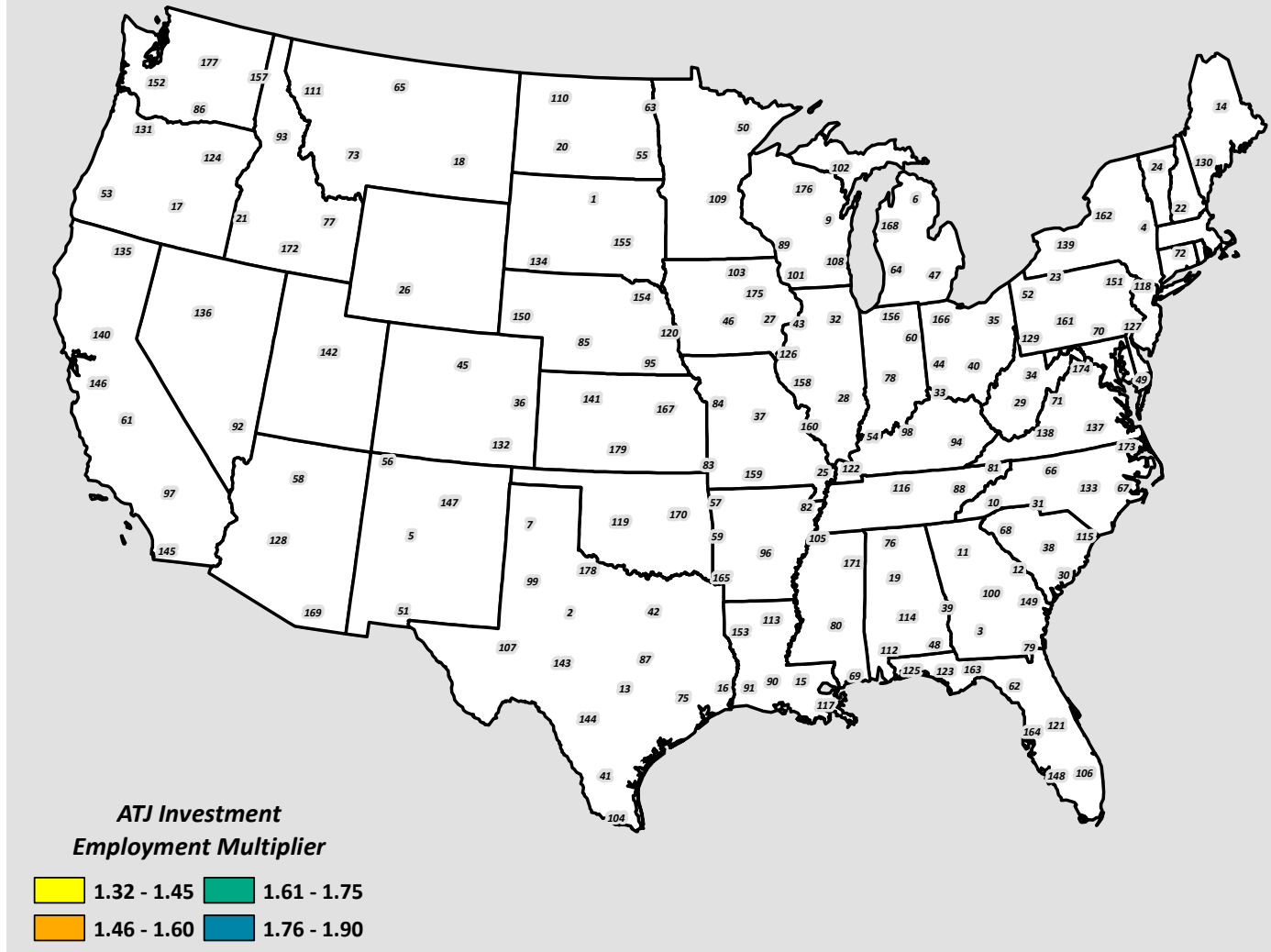


Figure 1.14. Annual operating Employment impacts from a single alcohol to jet (ATJ) facility within a BEA region
Projections of changes in economic activity as a result of this investment through multiplier effects are estimated using Analysis By Parts (ABP) methodology with United States IMPLAN datasets aggregated to BEA region.

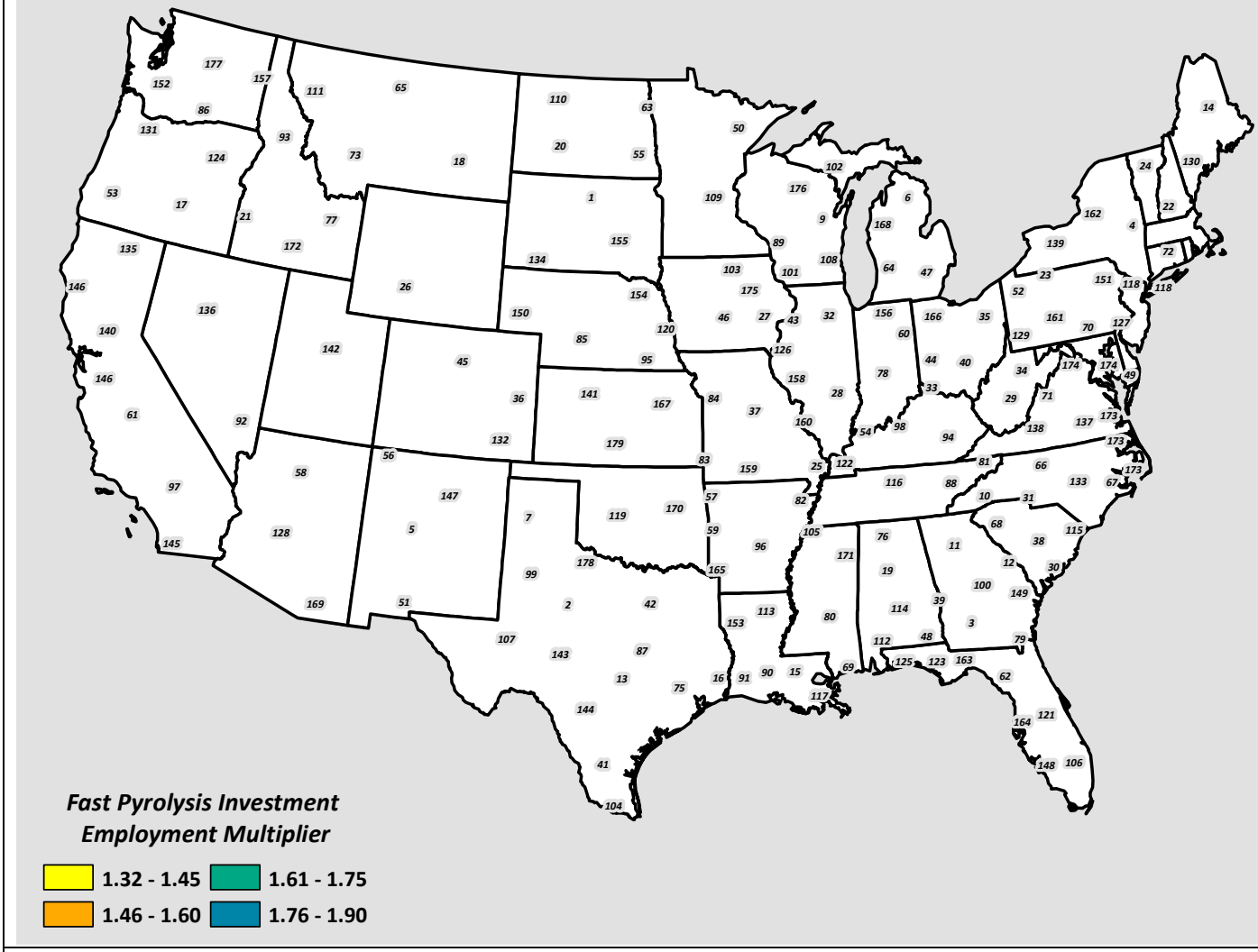


Figure 1.15. Annual operating Employment impacts from a single fast pyrolysis facility within a BEA region
Projections of changes in economic activity as a result of this investment through multiplier effects are estimated using Analysis By Parts (ABP) methodology with United States IMPLAN datasets aggregated to BEA region.

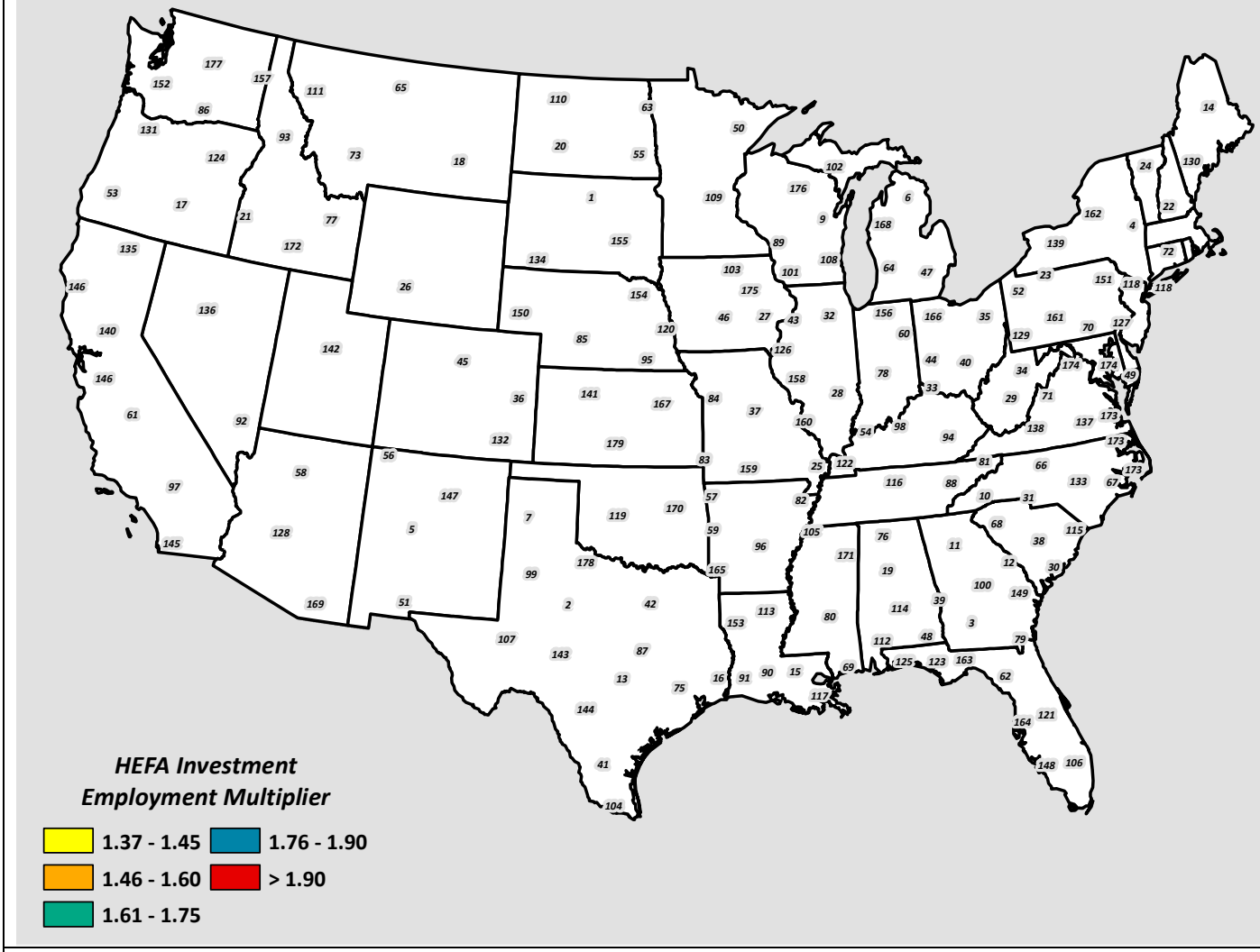


Figure 1.16. Annual operating Employment impacts from a single HEFA facility within a BEA region
Projections of changes in economic activity as a result of this investment through multiplier effects are estimated using Analysis By Parts (ABP) methodology with United States IMPLAN datasets aggregated to BEA region.



Environmental Parameters

Access database is developed with soil characteristics and climate characteristics defined (RKLS factors in the Universal Soil Loss Equation). Soils were identified for crop land, CRP land, and pasture land for each agricultural Statistical District in the U. S. using the 1997 NRI. A C factor, as defined in the Universal Soil Loss equation, was estimated for each crop from the same dataset for conventional, reduced, and no tillage practices[1]. The P factor was assumed to equal 1. For any new crop, a C factor will need to be defined. Based on information from the IBSS project, a C factor of 0.04 is used for switchgrass. Note that Schwartz found a much smaller C factor in his research. We are still researching the C factors for cover crops as they are not readily available. A C factor for a corn soybean rotation ranges from 0.1 to 0.45 depending on tillage and cover. With winter cover this range should be lower than 0.1 since the land cover is year around and not relying on residues for a portion of the year.

In examining welfare analysis of potential carbon credits, resulting from a land use change, to the renewable aviation fuel production in west TN, we found that:

- Carbon credits induced farmers to convert more crop lands with high opportunity costs into feedstock production, resulting in lower farmers' surplus.
- Carbon credits led a net welfare gain to the RJF sector, primarily due to increment in the airlines' surplus (equivalently, reduction in the processor's cost).
- The RJF and its co-products achieved a 62.5% LCA-based GHG emissions reduction. The GHG emissions reduction increased to 65% with carbon credit through displacement of the CJF and fossil fuels.
- Carbon credit had positive influence on aviation GHG emissions reduction, and net welfare of RJF sector. However, RIN credits heavily influenced the economic feasibility of RJF.
- We have carbon emissions coefficients in POLYSYS and those are available to indicate percent changes as a result of changes in land use as well as input application.
- Solutions of the Baseline Model indicate that the RJF processor's cost is $1.16 billion whereas the aggregate profit of farmers is around $16.88 million annually. A total of 657 thousand acres farmland is used for feedstock production including 382 thousand acres of pasture land (Figure 1.17). More than 57% of farmers received a margin ranging from 10 to 47 % over their opportunity costs of land conversion (Figure 1.18).

[1] The Universal Soil Loss Equation estimates annual soil erosion (A) expressed as A=RKLSCP. Four of the factors RKLS are related to the physical location of the soil and two factors C and P are related to management of the crop. A C factor is the crop management factor and provides the ratio of soil loss from land cropped under specified conditions compared to tilled continuous fallow conditions. The P factor is equal to 1 unless the land is planted on the contour, strip cropped, or terraced.

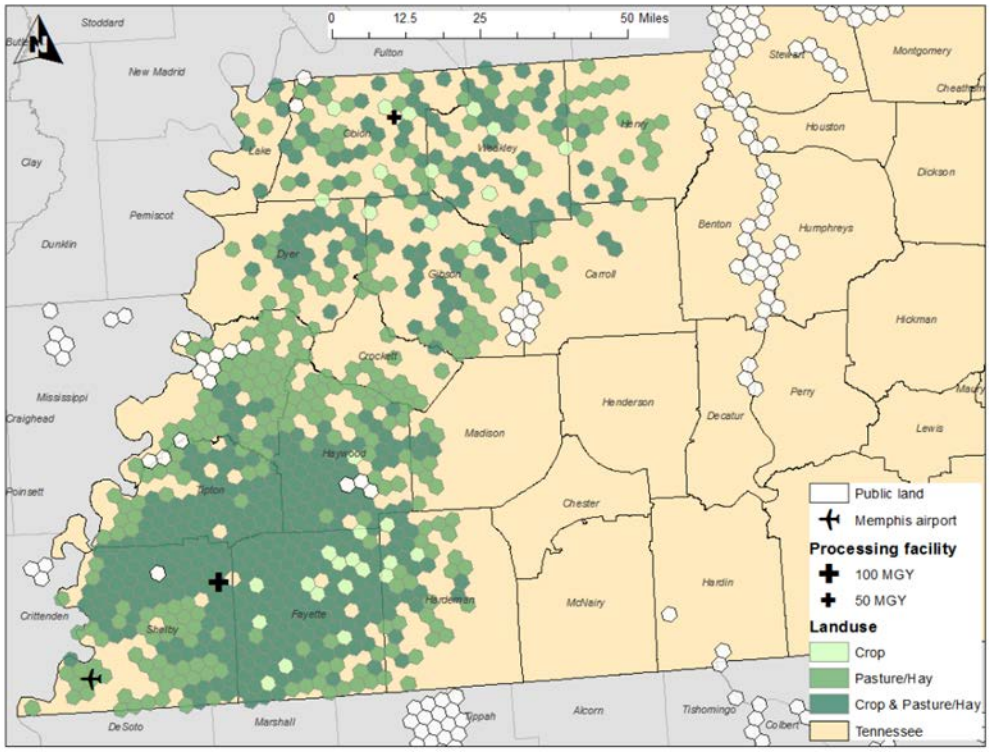


Figure 1.17 Optimal land use for switchgrass production and facility locations to deliver renewable aviation fuel to the Memphis International Airport

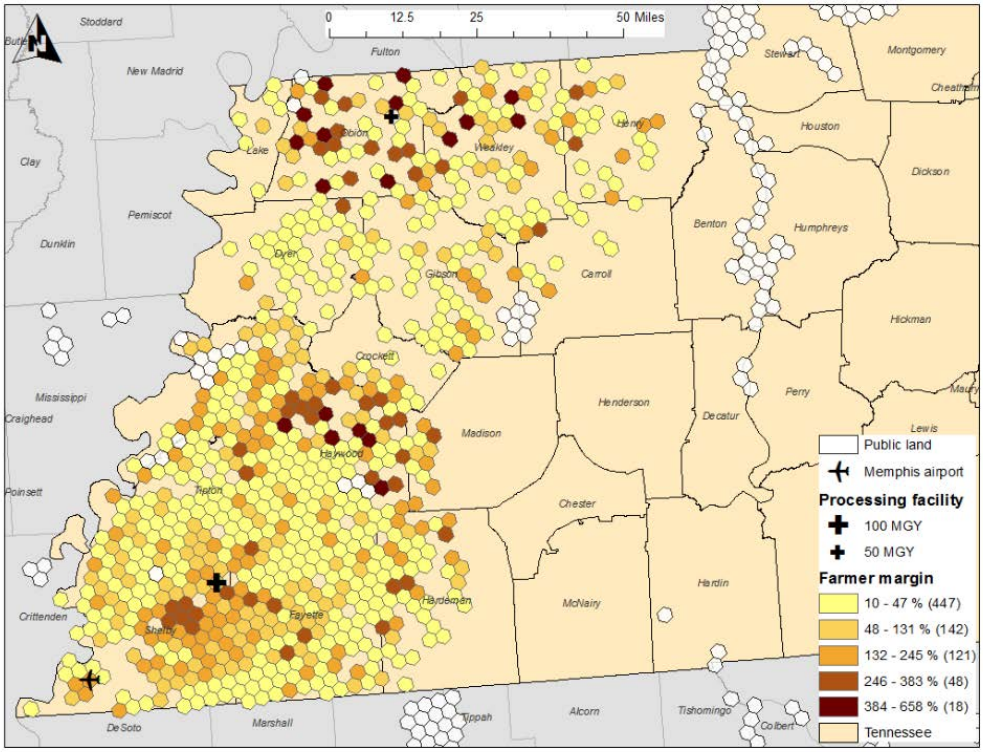


Figure 1.18. Margins of switchgrass feedstock suppliers

Milestone(s)

1. Completed conversion facility economic impact analysis for HEFA pathway.
2. A chapter in Bijay Sharma's Dissertation was completed on welfare analysis linked to carbon credits.

Major Accomplishments

National economic impact spatial analysis (NEISA) was completed for three ASCENT technologies.

Publications

None

Outreach Efforts

None

Awards

None

Student Involvement

None

Plans for Next Period

Incorporate NEISA into camelina study and the Tennessee pennycress analysis.



Task 2- Supports the Lipid Focused Comprehensive Analyses in ASCENT Project 1 Strategy

University of Tennessee

Sub Task 2.2.1 – Provide national analysis for Lipid based feedstocks

Sub Task 2.2.2 - Complete supply potential analysis for each lipid fuel pathway incorporating supply chain costs, preprocessing and conversion facility costs for selected fuel pathways incorporating social capital and environmental tradeoff components. (WSU, PSU)

Sub Task 2.3- Continue to conduct analysis on new lipid feedstocks and achieve a month turn around on national analysis with documentation to follow (contributes to subtask 2.2 as well)

Objectives

See Task 1

Research Approach

Same as in Task 1 focused on oilseed analysis

New Findings

See Task 1

Milestone(s)

1. Completed conversion facility economic impact analysis for HEFA pathway.
2. Published pennycress article
3. Thesis completed with 1 chapter focused on national analysis of camelina

Major Accomplishments

National economic impact spatial analysis (NEISA) completed for three ASCENT technologies

Publications

None

Outreach Efforts

None

Awards

None

Student Involvement

None

Plans for Next Period

Incorporate NEISA into camelina study and the Tennessee pennycress analysis

Task 3- Lay the Groundwork for Lipid and/or Biomass in Tennessee & Southeast U.S.

University of Tennessee

Objective

The University of Tennessee will lead the groundwork for lipid and/or biomass in Tennessee & the Sourtheast U.S. Supply Chain Analysis

- Identify 2 potentially viable supply chains to support a specific airport and end user in the Southeast U.S. and provide a proposal for a specific (tactical) deployment project,
- Delineate sustainability impacts associated with different feedstock choices,
- Assess viable conversion technologies,
- Identify stakeholders and partners
- Initiate a stochastic analysis of the system,
- Evaluate markets for potential co-products for Task 3 groundwork and deployment projects, and
- Assist in the development of social capital spatial analysis to be incorporated in regional analysis.

Research Approach

We used similar techniques as displayed in Task 1 but focused on the Southeast. We will develop a budget or use information from the modeling effort behind the billion ton 2016 analysis. We will use BioFLAME, a GIS model that has 5 sq. mile hexagons defined as supply regions. Information supplied by ForSEAM will be used on logging residue locations downscaling its estimates from agricultural statistical districts to the supply regions using the NASS crop supply layer as a means to achieve this. The analysis will be run to find where a sufficient supply might be available to provide a sustainable logging residue feedstock.

In examining potential coproduct markets, the research seeks to determine whether home gardeners would pay a premium for potting mix containing 25 percent biochar using the contingent valuation method. The method used follows a Random Utility framework (McFadden 1974). Responses are structured as a binary variable, with respondents choosing the base product being counted as zeroes, and those who choose the 25 percent biochar product counted as ones. Respondents are also given the option to select neither product. In the contingent valuation approach used, the prices of the base and biochar-potting mix products are provided to respondents, who may select either or neither product (Hanemann 1984). The probability of choosing the biochar product is then a function of price, demographics, expenditure patterns, and attitudes. The model is estimated as a logit model and willingness to pay is calculated using the estimates.

New Findings

1. Two feedstocks have been identified – oilseed cover crop (such as pennycress, camelina or carinata) and logging residues
2. Forest Residue
    - From a different project, logging residues are explored and facility location developed for Alabama. Pathway selected for analysis is logging residues delivered directly to ASCENT's Fast Pyrolysis' biorefinery in chipped form.
    - Biorefineries requiring 545,000 to 720,000 dry tons cannot be located in the S.E. with a maximum transportation distance of 70 miles.
    - Logging residue location determined. We quantified available logging residues using the model (ForSEAM) that supplied the 2016 Billion Ton study information forest biomass. It was decided that only softwoods would be used in the analysis (Figure 3.1).
    - If we add collection points where preprocessing can be achieved, then 5 biorefineries could be established at 720,000 dry tons/year if maximum driving distance increased to 150 miles (Figure 3.2).
    - Average feedstock cost and transportation distance for the Alabama location are still being reviewed.
    - Locating the facility in Alabama and increasing maximum transportation distance to 150 miles, the facility can run at capacity stated (Figure 3.3)

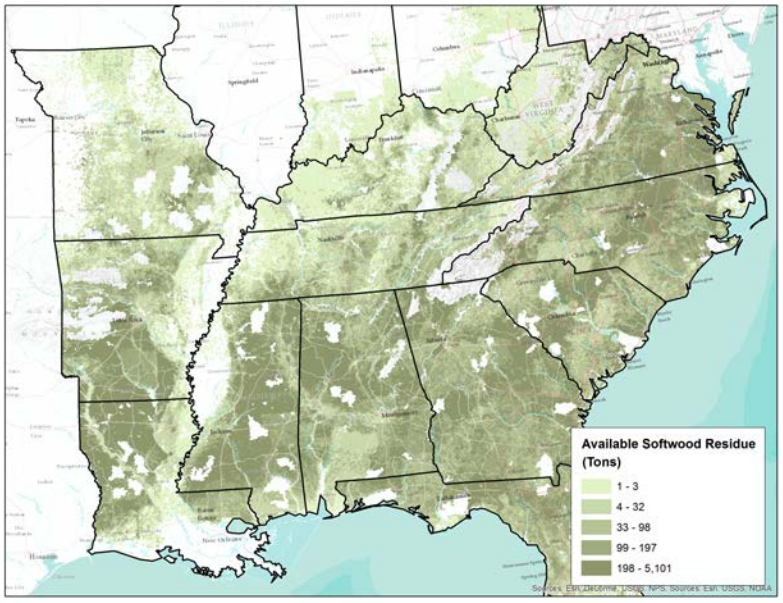


Figure 3.1. Estimated Available Logging Residues, 2020

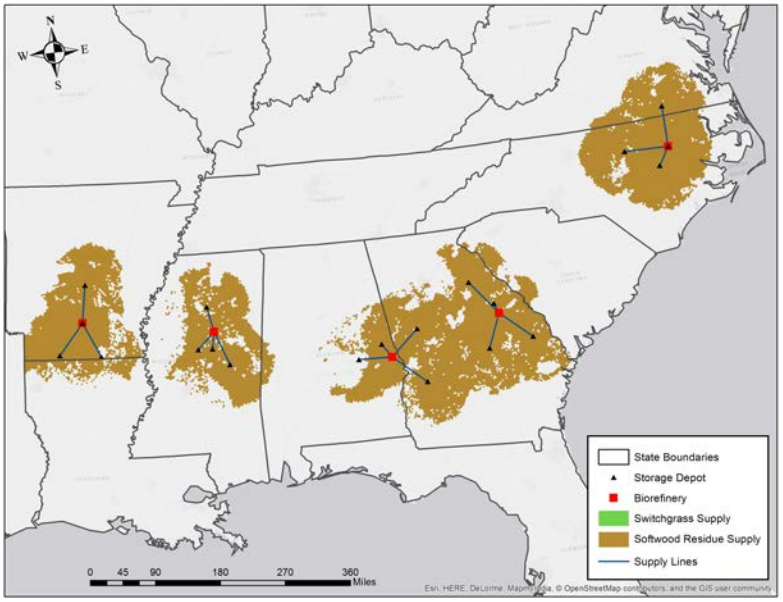


Figure 3.2. Biorefinery locations that are supported with 720,000 tons of logging residue per year.

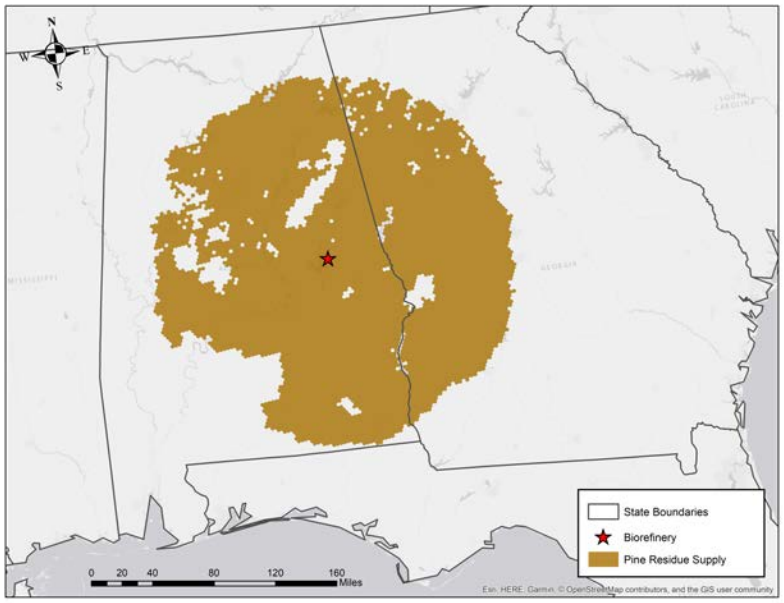


Figure 3.3. Biorefinery location in Alabama using 725,000 tons of logging residues.

3. Pennycress analysis has been conducted for middle Tennessee with fuel delivery to Nashville. This analysis is currently under review.
    - Using ASCENT HEFA technology and pennycress cover crop as a feedstock, we explored the feasibility of supplying the Nashville airport with alternative fuels.
    - Met with Southwest personnel and others in Nashville to see how fuel is stored and distributed at the airport. Discussions indicated that the Colonial Pipeline, the primary means of obtaining fuel, was running at 100% capacity and air travel growth out of Nashville would require additional fuel.
    - Designed an 800-900 ton per day mechanical crush facility which is under modification now with WSU consultation.
    - The ASCENT HEFA biorefinery requires 259,000 tons of oil/year and produces 68.2 million gallons gasoline equivalent of this, 39.9 million gallons in jet.
    - Conducted a four biorefinery analysi,s locating both the biorefineries and crush facilities (Figure 3.4). However, after examining fuel use, the Nashville airport would require 40 million gallons to replace 50% of its current fuel consumption with renewable aviation fuel.

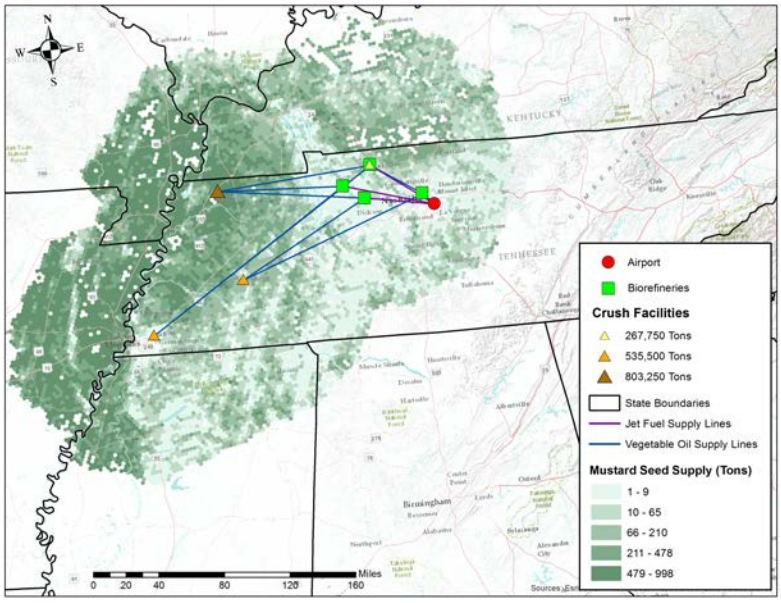


Figure 3.4. Location of biorefineries and crush plants to supply 160 million gallons of renewable aviation fuel.

4. Evaluated high investment risks and novelty of the feedstock-based conversion technologies and the barriers associated with that investment in a Dissertation that:

    - Used a two-stage stochastic model to evaluate the impact of federal subsidies in designing a switchgrass-based bioethanol supply chain in west Tennessee wherein decisions driven by minimized expected and Conditional Value-at-Risk of system cost reflected the risk-neutral and risk-averse perspective of the biofuel sector, respectively. A major contribution of this study is the impact assessment of Biomass Crop Assistance Program (BCAP) on investment decisions (including land allocation) of a risk-sensitive biofuel industry under feedstock supply uncertainty.
    - Evaluated the impacts of renewable jet fuel (RJF) production from switchgrass on farmland allocation. GHG emissions are estimated in response to fulfilling the RJF demand at the Memphis International Airport in Tennessee. A potential carbon market is used to explore the impact of hypothetical carbon credits on the GHG emissions reduction and net supply-chain welfare while addressing the economic motives of the supply-chain participants. This study highlights the importance of Renewable Identification Number (RIN) credits and tradable carbon credits in achieving the desired economic viability and emission abatement goals.
    - Examined the cost-efficiency of cost-ranked and cost-benefit-ranked auction-based payment designs for forest-based carbon sequestration with varying degree of correlation between opportunity costs of afforestation and carbon sequestration capacities, when bidders learn in multi-round procurement auctions. Simulation outcomes can guide decision makers in choosing an optimal payment design that ensures efficiency gains for auction-based payments compared to fixed-rate payments, and more importantly ensures minimal loss in cost-efficiency in a dynamic setting.

5. The need for advanced biofuels to meet the RFS, along with relatively high costs of production, has spurred interest in the economic viability of the coproducts of advanced biofuel production. The Department of Energy has identified a lack of high-value co-products as a leading barrier to large scale production of biofuels (Bozell and Peterson 2010). With pyrolysis, lignocellulose can be converted into bio-oil which then can be used to produce second-generation transportation fuels (Garcia-Perez, Lewis, and Kruger, 2010; Jones et al., 2009; Garcia-Perez et al., 2009). Along with this bio-oil, biochar is produced as a primary co-product. The objective of this analysis is to ascertain consumers' preference and willingness to pay a premium for gardening product (potting mix) that contains biochar in a 25 percent mixture. Potting mix is selected as a product because it is a commonly used household gardening product and is used by both indoor and outdoor gardeners. Mason et al (2008) note that sales of products related to container gardening have been one of the fastest growing lawn and garden categories. A potting



mix/biochar blend would provide consumers with a convenient pre-mixed product with a 25 percent blend. As part of achieving the overall objective, sub-objectives include the following:

a. Estimate WTP for a potting mix with 25 percent biochar compare to a base (conventional) product with no biochar.
b. Provide information on the impact of consumer demographics and attitudes on WTP.
c. Ascertain the relative importance of various biochar attributes on consumer preference for the potting mix with biochar.
d. Project market potential for a 25 percent biochar potting mix product based on potting mix expenditures among the survey respondents.

Results of our survey show that compared with a base price of $4.99 for conventional potting mix, respondents would pay $8.56 for an 8 quart bag of potting mix with a 25 percent biochar blend. Factors influencing this willingness to pay included age(-), percent of household income spent on gardening supplies (+), among of potting mix purchased per year (+), participating in organic gardening and recycling gardening supplies packaging (+), usually purchasing biochar at gardening centers (+), importance of biofuels development (+), and personal actions influencing the environment and environmental responsibility (+). Based upon the results, it is projected that garden centers would be a good place to initially market a biochar potting mix. If we assume that garden centers are the first to offer biochar potting mix products, about 11.44 percent usually purchased potting mix at garden centers (about 95,181 households). Overall the percentage electing to purchase the biochar potting mix was 50.11 percent (accounting for those who chose the conventional product and those who chose neither). This would suggest that 47,695 households might try a biochar mix. The responding gardeners had a median purchase of 32 quarts of potting mix per year. This would give a total of 1.53 million quarts of potting mix. The WTP for an 8 quart bag was $8.56 or $1.07 per quart. This would suggest that around 190,780 8 quart bags of biochar potting mix per year, or potential sales of $1.63 million statewide.

Milestone(s)

1. Completed conversion facility economic impact analysis for HEFA pathway.
2. Dissertation defended and several presentations made
3. Biochar for soil amendment of potential TN consumers completed

Major Accomplishments

National economic impact spatial analysis (NEISA) completed for three ASCENT technologies

Publications

Sharma, B. 2018. Analyzing the Impacts of Policy Supports and Incentive Programs on Resource Management. Ph.D. dissertation. University of Tennessee.

Sharma, B., T.E. Yu, B.C. English, and C.N. Boyer. “Economic Analysis of Renewable Jet Fuels: A Game-theoretic Approach,” Selected presentation at the 7th International Conference on Transportation and Logistics, Dalian, China. September 8-10, 2018.

Sharma, B., T.E. Yu, B.C. English, C.N. Boyer, and J.A. Larson. “Stochastic Optimization of Cellulosic Biofuel Supply Chain under Feedstock Yield Uncertainty,” Selected presentation at the 10th International Conference on Applied Energy, Hong Kong. August 22-25, 2018.

Sharma, B., T.E. Yu, B.C. English, and C.N. Boyer. “Analyzing the Economics of Renewable Jet Fuels Using a Game-theoretic Approach,” Selected Presentation at Applied and Agricultural Economics Association annual meeting, Washington D.C. August 5-7, 2018.

Thomas, McKenzie, Kimberly Jensen, Christopher Clark, Dayton Lambert, Burton English, and Forbes Walker. (2019 forthcoming). Consumer Preferences for Potting Mix with Biochar. Paper to be presented at 2019 Southern Agricultural Economics Association Meetings, Birmingham, AL.



Outreach Efforts
None

Awards
None

Student Involvement
None

Plans for Next Period
Incorporate NEISA into camelina study and the Tennessee pennycress analysis
A journal manuscript will be prepared based on the biochar survey data.
McKenzie Thomas will complete her M.S. thesis using this data.

Task 4- Biorefinery Infrastructure and Siting (Supporting Role)
Washington State University

Objective(s)
The University of Tennessee team will play a supporting role in this task. Several models are available to contribute to the effort, including: 1) BioSAT (currently available for the 33 Eastern states), 2) BioFLAME (we hope to expand its geographic scope from its current southeast U.S. regional focus to the contiguous 48 states).

Research Approach
- Provide feedstock information (location, price, quantity) to ASCENT Database
- Contact WSU for ASCENT conversion technologies
- Pennycress feedstock information provided to VOLPE and saved to shared folders available to all ASCENT Project 001 researchers
- Working with WSU on developing a TEA for the crush facility

Milestone(s)
- WSU provided HEFA, ATJ and FT – SPK TEAs for economic indicator development
- Economic indicators are developed for those three technologies.
- Have made a comparison between the two crush technologies and established basic assumptions to be used by both technologies

Major Accomplishments
None

Publications
None

Outreach Efforts
None

Awards
None

Student Involvement
None

Plans for Next Period
Complete the TEA for the crush facility and compare solvent based to mechanical based crush facilities.



Project 001(F) Alternative Jet Fuel Supply Chain Analysis

Massachusetts Institute of Technology

Project Lead Investigator

PI: Professor Steven Barrett
Raymond L. Bisplinghoff Professor of Aeronautics and Astronautics
Director, Laboratory for Aviation and the Environment
Massachusetts Institute of Technology
77 Massachusetts Ave, Building 33-322, Cambridge, MA 02139
+1 (617) 452-2550
sbarrett@mit.edu

Co-PI: Dr. Raymond L. Speth
Research Scientist
Associate Director, Laboratory for Aviation and the Environment
Massachusetts Institute of Technology
77 Massachusetts Ave, Building 33-322, Cambridge, MA 02139
+1 (617) 253-1516
speth@mit.edu

University Participants

Massachusetts Institute of Technology

- P.I.: Steven R. H. Barrett
- FAA Award Number: 13-C-AJFE-MIT, Amendment Nos. 003, 012, 016, 028, 033, 040, and 048
- Period of Performance: Aug. 1, 2014 to Aug. 31, 2019
- Tasks (note that the tasks listed here are relevant only to the reporting period, 10/01/2017 – 09/31/2018):
    1. Support U.S. participation in the International Civil Aviation Organization (ICAO) Committee on Aviation Environmental Protection (CAEP) Alternative Fuels Task Force (AFTF) to appropriately account for the use of alternative jet fuels under the Carbon Offsetting and Reduction Scheme for International Aviation (CORSIA) by calculating default core life cycle greenhouse gas (GHG) emissions values;
    2. Support FAA work to calculate induced land use change (ILUC) emissions of alternative jet fuels, and assess sustainability certification schemes for potential inclusion under CORSIA;
    3. Comprehensively quantify and assess the impact of various policy options, in isolation and in combination, on the financial viability of alternative aviation fuel in order to provide policy guidance to States that are party to CORSIA;
    4. Collaborate with ASCENT Project 21 to capture the climate impacts of non-CO_2 life cycle emissions from petroleum and alternative aviation fuels in APMT-Impacts Climate;
    5. Collaborate with WSU to facilitate development of Aspen HEFA model;
    6. Provide additional (including in-person) support to FAA for decision-making in the context of AFTF.

Hasselt University (sub-award from MIT)

- P.I.(s): Steven R.H. Barrett, Professor
- Period of Performance: Aug. 1, 2014 to Aug. 31, 2019
- Tasks (note that the tasks listed here are relevant only to the reporting period, 10/01/2017 – 09/31/2018):
    1. Support U.S. participation in the International Civil Aviation Organization (ICAO) Committee on Aviation Environmental Protection (CAEP) Alternative Fuels Task Force (AFTF) to appropriately account for the use of alternative jet fuels under the Carbon Offsetting and Reduction Scheme for International Aviation (CORSIA) by calculating default core life cycle greenhouse gas (GHG) emissions values;



2. Comprehensively quantify and assess the impact of various policy options, in isolation and in combination, on the financial viability of alternative aviation fuel in order to provide policy guidance to States that are party to CORSIA;
3. Provide additional (including in-person) support to FAA for decision-making in the context of AFTF.

Project Funding Level

$2,235,000 FAA funding and $2,235,000 matching funds. Sources of match are approximately $388,000 from MIT, plus 3rd-party in-kind contributions of $809,000 from Byogy Renewables, Inc. and $1,038,000 from Oliver Wyman Group.

Investigation Team

Principal Investigator:	Professor Steven Barrett (MIT)
Co-Principal Investigator:	Dr. Raymond Speth (MIT)
Co-Investigators:	Dr. Mark Staples, Dr. Florian Allroggen (MIT)
Graduate Research Assistants:	Timothy Galligan, Paula do Vale Pereira, Juju Wang, Uyiosa Oriakhi (MIT)

The research will partly be conducted through a sub-award with Hasselt University (Belgium), led by Prof. Robert Malina, and Hasselt University post-doctoral researcher Hakan Olcay.

Project Overview

The overall objectives of ASCENT Project 01, for the reporting period October 1, 2017 to September 30, 2018, were to:

- Derive information on regional supply chains to create scenarios for future alternative jet fuel (AJF) production;
- identify the key supply chain-related obstacles that must be overcome for commercial scale production of AJF in the near term;
- Achieve large-scale replacement of conventional jet fuel with AJF in the longer term.

Following these overall objectives, MIT's work under ASCENT Project 01 from 10/01/2017 to 09/31/2018, was focused on the following:

1. Support U.S. participation in ICAO CAEP AFTF to appropriately account for the use of alternative jet fuels under CORSIA by calculating default core lifecycle greenhouse gas (GHG) emissions values
2. Support FAA work to calculate ILUC emissions of alternative jet fuels, and assess sustainability certification schemes for potential inclusion under CORSIA
3. Comprehensively quantify and assess the impact of various policy options, in isolation and in combination, on the financial viability of alternative aviation fuel in order to provide policy guidance to States that are party to CORSIA;
4. Collaborate with the ASCENT Project 21 team to capture the climate impacts of non-CO_2 lifecycle emissions from petroleum and alternative aviation fuels in APMT-Impacts Climate;
5. Collaborate with Washington State University to facilitate development of an Aspen model of the hydroprocessed esters and fatty acids (HEFA) fuel production process
6. Provide additional (including in-person) support to FAA for decision-making in the context of AFTF.

Task 1- Default Core LCA Emissions Value Calculation and LCA Methodology Development for Use Under CORSIA

Massachusetts Institute of Technology

Objective(s)

The overall objective of this task is to provide support to the FAA for its engagement with ICAO CAEP AFTF, specifically on the development of the methodologies for appropriate accounting of AJF lifecycle GHG emissions under CORSIA, and applying the method to calculate AJF default core LCA (CLCA) emissions values for use under CORSIA.



Research Approach

Introduction
During this reporting period, significant progress was made on the work of the CLCA Task Group of AFTF. The MIT ASCENT Project 01 team has been key to this progress in terms of two primary tasks, calculation of default core LCA values for a number of pathways to be used under CORSIA and development of a method to account for avoided landfilling and recycling emissions associated with using municipal solid waste (MSW) as a feedstock for AJF production. These two items are described below.

Default core LCA calculation for CORSIA
During the reporting period, AFTF met three times: AFTF/05 from October 23-25, 2017 in Brasilia, Brasil; AFTF/06 from April 23-27, 2018 in Montreal, Canada; and AFTF/07 from September 17-21, 2018 in Montreal, Canada. In preparation for each meeting, MIT carried out LCA on a number of AJF pathways, in collaboration with researchers from the European Union Joint Research Center (JRC), Argonne National Laboratory (ANL), the University of Toronto, the Brazil Bioethanol Science and Technology Laboratory (CTBE) and Universidade Estadual de Campinas (Unicamp).

The pathways that MIT worked on in advance of each of these meetings, as well as the institutions with which MIT collaborated to verify the results, are shown in Table 1.

Table 1. Pathways for which MIT carried out default core LCA calculations during the reporting period, in the context of ICAO CAEP AFTF. The table indicates the meeting at which AFTF agreed upon the default core LCA values calculated by MIT, as well as the institutions with which MIT collaborated to verify the results presented.

Meeting	Pathway	Collaborating institutions
AFTF/05	Sugarcane SIP	JRC, Unicamp
	Sugarcane iBuOH ATJ	JRC, CTBE
AFTF/06	Corn grain EtOH ATJ	JRC
	Sugarcane EtOH ATJ	JRC, CTBE
AFTF/07	Corn grain iBuOH ATJ	JRC
	Herbaceous lignocellulosic iBuOH ATJ	JRC
	Molasses iBuOH ATJ	JRC
	Sugarbeet SIP	JRC

The GREET® (the Greenhouse gasses, Regulated Emissions, and Energy use in Transportation) (Argonne National Laboratory, 2015) model was used for the analyses by MIT. GREET is a peer-reviewed, publicly available, and editable software. JRC used the E3 Database model for their calculations (Ludwig-Bolkow Systemtechnik GMBH, 2006). Over the course of the analysis performed for AFTF, the original database was reviewed and updated to respond to AFTF-specific requirements. Lifecycle inventory datasets for the various AJF pathways were inputs for these LCA models, and were put together collaboratively based on information from experts from the difference institutions. These data are documented in detail in the following Information Papers presented to AFTF: CAEP/11-AFTF/5-IP/3; CAEP/11-AFTF/6-IP/6; and CAEP/11-AFTF/7-IP/11. The functional unit was defined as one mega joule (MJ) of delivered jet fuel energy (lower heating value), and the LCA results are presented in terms of the amount of GHG emissions for each functional unit (gCO_2e/MJ).

Previously, AFTF had agreed to a methodology for the calculation of default CLCA values. Because the development of this methodology was carried out in a previous reporting period, it is not discussed in detail here. However, some of the key facets of this methodology consist of the following:

- Core default LCA values are calculated at a global level of resolution
- A pathway is defined as a feedstock and conversion technology pairing for which emissions vary by <10% of the conventional jet fuel baseline (8.9 gCO_2e/MJ)



- Default values are calculated as the mid-point of the range of results for a given pathway

Default CLCA values calculated in advance of AFTF/05

Sugarcane SIP

The life cycle inventory (LCI) data for these pathways were brought forward by technical experts from MIT, JRC and Unicamp. The initial comparison of these three data sources revealed a number of differences in the core LCA results. One of the reasons for notable differences in the feedstock cultivation emissions was the assumed farnesene yields: MIT assumed 17% (wt.) yield of farnesene from sucrose, JRC assumed 13%, and the Unicamp analysis assumed higher farnesene yields and sugarcane quality (the exact values used in the Unicamp analysis could not be revealed due to their proprietary nature).

Following discussion amongst the experts from the three institutions, it was proposed to use harmonized MIT and JRC CLCA results, as shown in Table 2, to define the default CLCA value for the sugarcane SIP pathway. In addition, intra-continental transportation of the finished fuel product was assumed, in order to be consistent with the other pathways considered.

Table 2. Core LCA results used for sugarcane SIP default core LCA value calculation

Conversion technology	Data source	Model	Cultivation	Feedstock transp.	Fermentation and upgrading	Regional fuel transp.	Total emissions [gCO_2e/MJ]	Midpoint value [gCO_2e/MJ]
SIP	MIT	GREET	17.6	2.8	11.4	0.3	**32.1**	**32.8**
	JRC	E3db	20.9	1.9	10.4	0.3	**33.5**	

Sugarcane iBuOH ATJ

The LCI data for these pathways were brought forward by technical experts from MIT, JRC, and CTBE. All of these analyses considered isobutanol (iBuOH) as the intermediate alcohol, which is then dehydrated and oligomerized to jet fuel. To make a consistent comparison of CLCA results from these three data sources, it was proposed to harmonize the assumptions in three areas: the iBuOH transportation step was removed from the JRC results, and the jet fuel transportation emissions were assumed to be equivalent to those calculated for the sugarcane SIP pathway; the average of the jet fuel transportation emissions from the MIT and JRC results was applied to the CTBE results, in order to consistently approximate intra-continental fuel transportation emissions; and gaseous H_2 requirements from steam methane reforming from the MIT analysis was applied to the CTBE data, as modelled in GREET 2016.

The core LCA results from the three data sources, following the harmonization of these parameters, are shown in Table 3, which were to propose the default CLCA value for this pathway.

Table 3. Harmonized core LCA results for sugarcane ATJ default value calculation

Conversion technology	Data source	Model	Cultivation	Feedstock transp.	Fermentation and upgrading	Regional fuel transp.	Total emissions [gCO_2e/MJ]	Midpoint value [gCO_2e/MJ]
ATJ	MIT	GREET	12.4	1.9	6	0.3	**20.7**	**24.0**
	JRC	E3db	17.7	1.6	7.7	0.3	**27.3**	
	CTBE	GREET	13.1	1.7	6.7	0.3	**21.8**	

Default CLCA values calculated in advance of AFTF/06

Corn grain EtOH ATJ

The system boundary considered for this pathway includes corn grain cultivation and harvesting, transportation of the feedstock to a drop-in fuel production facility, fermentation to ethanol and upgrading to a drop-in fuel slate and finished jet fuel transportation and distribution. Two independent LCA sources for the corn grain EtOH AJT fuel pathway were compared:



an updated version of the pathway described in Staples et al. (2014) and modelled in GREET.net (v.1.3.0.13239) by MIT; and the same pathway as modelled by JRC in the E3db.

Table 4. Comparison of corn grain ethanol ATJ LCA data

Data source	Model	Cultivation and harvesting	Feedstock transp.	Fermentation and EtOH upgrading	Jet fuel transp.	Total emissions [gCO_2e/MJ]	Proposed default CLCA value [gCO_2e/MJ]
MIT	GREET	21.3	1.2	42.7	0.4	65.6	65.7
JRC	E3db	31.2	2.1	32.0	0.4	65.7	

The largest differences in the corn grain ethanol ATJ data from MIT and JRC were in the cultivation and harvesting, and fermentation and ethanol upgrading steps. Despite these differences, the overall LCA results from the two data sources were within 10% of the petroleum-derived jet fuel baseline (8.9 gCO_2e/MJ), and therefore these data were used to propose a default CLCA value for the pathway.

Sugarcane EtOH ATJ

The system boundary for the sugarcane EtOH ATJ pathway includes sugarcane cultivation and harvesting, transportation of the feedstock to a drop-in fuel production facility, fermentation to ethanol and upgrading to a drop-in fuel slate and finished jet fuel transportation and distribution. Three independent LCA sources for the sugarcane EtOH ATJ pathway were compared: an updated version of the pathway described in Staples et al. (2014) and modelled in GREET.net (v.1.3.0.13239) by MIT; the pathway as modelled by JRC in the E3db; a modified version of the pathway described in Bonomi et al. (2016), Chagas et al. (2016) and Klein et al. (2018) modelled by CTBE.

Table 5. Comparison of sugarcane ethanol ATJ LCA data

Data source	Model	Cultivation and harvesting	Feedstock transp.	Fermentation and EtOH upgrading	Jet fuel transp.	Total emissions [gCO_2e/MJ]	Proposed default CLCA value [gCO_2e/MJ]
MIT	GREET	13.7	1.6	4.6	0.4	20.4	24.1
JRC	E3db	17.5	1.6	7.7	0.4	27.2	
CTBE	ReCiPe	19.9	2.1	5.3	0.4*	27.7	
*Note that these emissions were not initially included in the CTBE data. Therefore, the value for jet fuel transportation emissions from the other data points were adopted to maintain consistency.							

The largest differences in the sugarcane EtOH ATJ data were in the cultivation and harvesting step and fermentation and ethanol upgrading steps. Despite these differences, the overall LCA results from the two data sources were within 10% of the petroleum-derived jet fuel baseline (8.9 gCO_2e/MJ), and therefore this data was used to propose a default CLCA value for the pathway.

<u>Default CLCA values calculated in advance of AFTF/07</u>

Corn grain iBuOH ATJ

Two independent data sources were compared for the corn grain iBuOH ATJ pathway to determine an appropriate default CLCA value: one carried out by MIT using the GREET.net model (v.1.3.0.13239) and the other by JRC using the E3db. A comparison of the results from the MIT and JRC analyses are shown in Table 6. Despite some differences, the results from the two models are within the 8.9 gCO_2e/MJ definition of a pathway. Therefore, these data were used to propose a default CLCA value for the corn grain iBuOH ATJ pathway.

Table 6. Comparison of default core LCA results for corn grain iBuOH ATJ from MIT and JRC

Conversion technology	Data source	Model	Cultivation	Feedstock transp.	Fermentation and upgrading	Jet fuel transp	Total emissions [gCO_2e/MJ]	Proposed default CLCA value [gCO_2e/MJ]
Corn grain iBuOH ATJ	MIT	GREET	15.9	0.9	38.8	0.4	56.0	55.8
	JRC	E3db	22.5	0.6	32.1	0.3	55.5	



Herbaceous lignocellulosic energy crop iBuOH ATJ

Three independent analyses were compared for this pathway to determine an appropriate default CLCA value. MIT modelled the switchgrass and miscanthus iBuOH ATJ pathways in GREET.net (v.1.3.0.13239) and JRC independently modelled the switchgrass iBuOH ATJ pathway in the E3db. The LCA results from the MIT and JRC analyses are compared in Table 6. These results are within the 8.9 gCO_2e/MJ definition of a pathway, therefore the proposed default core LCA value for the herbaceous lignocellulosic iBuOH ATJ pathway was calculated using these data.

Table 7. Comparison of default core LCA results for herbaceous lignocellulosic iBuOH ATJ from MIT and JRC

Conversion technology	Data source	Model	Cultivation	Feedstock transp.	Fermentation and upgrading	Jet fuel transp	Total emissions [gCO_{2e}/MJ]	Proposed default CLCA value [gCO_{2e}/MJ]
Miscanthus iBuOH ATJ	MIT	GREET	12.5	1.4	27.7	0.4	42.1	43.4
Switchgrass iBuOH ATJ	MIT	GREET	14.9	2.1	27.0	0.4	44.5	
	JRC	E3db	9.9	3.1	31.4	0.3	44.7	

Molasses iBuOH ATJ

Two independent analyses were used to evaluate this pathway. The JRC analysis was carried out using the E3db, and assumed that this pathway was entirely consistent with the sugarcane iBuOH ATJ pathway for which default core LCA values have already been calculated. In contrast, the MIT analysis modelled a process of sugar extraction from sugarcane, in which molasses is a by-product. This was modelled in GREET.net model (v.1.3.0.13239). The results for the MIT analysis on the molasses iBuOH AJT pathway are shown below in Table 8, and are compared to the data proposed by JRC. These data are within the definition of a pathway of 8.9 gCO_2e/MJ, therefore these data were used to determine the default CLCA value for this pathway.

Table 8. Summary of core LCA results for the molasses iBuOH ATJ pathway

Conversion technology	Data source	Model	Cultivation	Feedstock transp.	Fermentation and upgrading	Jet fuel transp	Total emissions [gCO_{2e}/MJ]	Proposed default CLCA value [gCO_{2e}/MJ]
Molasses iBuOH ATJ	JRC	E3db	17.7	1.6	7.7	0.3	27.3	27.0
	MIT	GREET	17.8	2.1	6.4	0.3	26.6	

Sugarbeet SIP

The results for the JRC and MIT analyses of the sugarbeet SIP pathway, using the E3db and GREET.net (v.1.3.0.13239) models, respectively, are shown below in Table 9. A number of factors contribute to the discrepancy between the two independent studies. The two analyses rely on differing data sources for sugarbeet cultivation. MIT assumes a lower sugar yield from sugarbeet, resulting in a 21% lower energetic yield of farnesene per unit feedstock and there are differing assumptions around biogas yield from sugarbeet pulp and electricity and heat co-generation efficiencies. Despite the differing assumptions, these results were within the definition of a pathway for AFTF of 8.9 gCO_2e/MJ, therefore the proposed default core LCA value for the sugarbeet SIP pathway was evaluated using these data.



Table 9. Default core LCA results for sugarbeet SIP

Conversion technology	Data source	Model	Cultivation	Feedstock transp.	SIP production	Jet fuel transp	Total emissions [gCO_{2e}/MJ]	Proposed default CLCA value [gCO_{2e}/MJ]
SIP from sugarbeet	JRC	E3db	11.0	0.9	16.6	0.3	28.8	32.4
	MIT	GREET	23.4	1.4	10.8	0.4	36.0	

Summary of MIT work on default CLCA value calculations

All of the results and analyses summarized above, for which MIT carried out LCA analyses, were eventually accepted by AFTF, and are to be finalized by CAEP in February 2019. A summary of the agreed upon default CLCA values are given in Table 10. In addition, Prof. Robert Malina of Hasselt University (a sub-awardee under this project) led the AFTF CLCA Task Group during this reporting period.

Table 10. Summary of AFTF-agreed default CLCA values

Meeting	Pathway	Collaborating institutions	AFTF agreed default CLCA value [gCO_2e/MJ]
AFTF/05	Sugarcane SIP	JRC, Unicamp	32.8
	Sugarcane iBuOH ATJ	JRC, CTBE	24.0
AFTF/06	Corn grain EtOH ATJ	JRC	65.7
	Sugarcane EtOH ATJ	JRC, CTBE	24.1
AFTF/07	Corn grain iBuOH ATJ	JRC	55.8
	Herbaceous lignocellulosic iBuOH ATJ	JRC	43.4
	Molasses iBuOH ATJ	JRC	27.0
	Sugarbeet SIP	JRC	32.4

Methodology development for MSW emissions crediting

During this reporting period, Dr. Mark Staples from the MIT Project 01 team led an AFTF Small Group to define a methodology for estimating avoided landfilling and recycling emissions credits associated with using MSW as a feedstock for AJF production. The progress of this small group was presented to AFTF/06 and AFTF/07 and is documented in detail in CAEP/11-AFTF/6-IP/8 and CAEP/11-AFTF/7-IP/4.

This work resulted in the proposal of a landfill emissions crediting (LEC) methodology based on the first-order decay method and adopts elements of the UNFCCC Clean Development Method (CDM) for evaluating emissions avoided from landfilling. The recycling emissions credit method that was proposed is adopted from the UNFCCC CDM.

This work also assesses the risk of double counting emissions reductions associated with emissions credits and quantifies the impacts of options to mitigate the risk. The results show that, even using very conservative assumptions, the potential magnitude of REC/LEC double claiming is less than 5% of projected international aviation CO_2 emissions in 2050. In addition, a number of approaches to mitigate the double counting risk are presented, including:

- Correcting national inventories to account for claimed LEC/REC credits (which would completely eliminate the risk of double claiming but may be difficult to implement);
- Limiting net LCA values to a minimum of 0 gCO_2e/MJ (which is shown to significantly reduce the magnitude of the potential for double claiming); and
- Defining GHG reporting requirements for SCS, to enable national authorities to check for inconsistencies.



Milestone(s)

The work described above represents the achievement of MS 1, 2 and 3, as defined in the AY 2017/2018 Grant Proposal. Progress on core LCA default value calculations, and was presented to AFTF at meetings in October 2017, April 2018, and September 2018 and documented in numerous CAEP working and information papers. In addition, significant effort was expended in development of a methodology to account for LEC/REC associated with MSW-derived AJF. This was presented to the AFTF at meetings in April 2018 and September 2018 and documented in numerous CAEP working and information papers.

Major Accomplishments

A major accomplishment was the calculation of default CLCA values for eight additional pathways under CORSIA, and the agreement of AFTF to the proposed values. This progress will enable the inclusion and use of these fuels as soon as CORSIA goes into effect. In addition, a scientifically rigorous methodology was defined for accounting for LEC/REC associated with MSW-derived AJF.

Publications

Peer reviewed publications

Suresh, P, R Malina, MD Staples, S Lizin, H Olcay, D Blazy, MN Pearlson, SRH Barrett, 2018. Life cycle greenhouse gas emissions and costs of production of diesel and jet fuel from municipal solid waste. *Environmental Science and Technology,* DOI: 10.1021/acs.est.7b04277

Staples, MD, R Malina, P Suresh, JI Hileman, SRH Barrett, 2018. Aviation CO_2 emissions reductions from the use of alternative jet fuels. *Energy Policy,* 114, p. 342-354, DOI: 10.1016/j.enpol.2017.12.007

Project 01 funding is acknowledged in both of these publications.

Written reports

CAEP/11-AFTF/5-IP/03, Progress on calculation of default core life cycle analysis (LCA) values, presented at AFTF/5, October 2017, Brasilia, Brazil

CAEP/11-AFTF/5-WP/03, Progress on the core LCA task group, presented at AFTF/5, October 2017, Brasilia, Brazil

CAEP/11-AFTF/6-IP/06, Progress on calculation of default core LCA values, presented at AFTF/6, April 2018, Montreal, Canada.

CAEP/11-AFTF/6-WP/04, Summary of the work of CLCA-TG since AFTF05, presented at AFTF/6, April 2018, Montreal, Canada.

CAEP/11-AFTF/6-IP/08, Assessing LEC and REC for MSW-derived fuels within CORSIA, presented at AFTF/6, April 2018, Montreal, Canada.

CAEP/11-AFTF/7-IP/11, Progress on calculation of default core LCA values, presented at AFTF/7, September 2018, Montreal, Canada.

CAEP/11-AFTF/7-IP/04, Report on the progress of the MSW Crediting Small Group, presented at AFTF/7, September 2018, Montreal, Canada.

CAEP/11-AFTF/7-WP/06, Core LCA progress, September 2018, Montreal, Canada.

Outreach Efforts

Progress on these tasks were communicated during weekly briefing calls with the FAA and other U.S. delegation members to AFTF, numerous AFTF teleconferences between in-person meetings, as well as at in-person meetings of AFTF in October 2017, April 2018 and September 2018. In addition, MIT presented its work under Project 01 to ASCENT at the biannual meeting in April 2018, in Cambridge, MA.

Awards

None



Student Involvement

During the reporting period of AY 2017/2018, the MIT graduate students involved in this task were Paula do Vale Pereira, Juju Wang, and Uyiosa Oriakhi. Paula do Vale Pereira and Uyiosa Oriakhi were funded partially, and Juju Wang was fully funded, under ASCENT Project 01.

Plans for Next Period

In the coming year, the MIT ASCENT Project 01 team will continue its work in AFTF. Default core LCA values will be calculated and proposed for additional pathways. In addition, Prof. Robert Malina from Hasselt University will continue to lead the core LCA Task Group, and Dr. Mark Staples will continue to lead a small group responsible for dealing with emissions credits under CORSIA. The work of the core LCA Task Group during CAEP/11 will be summarized in a series of working paper and technical reports presented to CAEP in February 2019. MIT will take a lead role in drafting a number of these papers.

References

Argonne National Laboratory. (2015) Greenhouse gases, Regulated Emissions, and Energy use in Transportation (GREET) Model. [Online]. http://greet.es.anl.gov/

Bonomi, A., O. Cavalett, M.P. Cunha, and M.A.P. Lima. "Virtual biorefinery – an optimization strategy for renewable carbon valorization." 1st Ed. Basel: Springer International Publishing, 2016.

Chagas, M.F., R.O. Bordonal, O. Cavalett, J.L.N. Carvalho, A. Bonomi Jr., and N. La Scala. "Environmental and economic impacts of different sugarcane production systems in the ethanol biorefinery." Biofuels, Bioproducts and Biorefining, 10(1), 2016: 89-106.

Klein, B.C., M.F. Chagas, T.L. Junqueira, M.C.A.F. Rezende, T.d.F. Cardoso, O. Cavalett, and A. Bonomi. "Techno-economic and environmental assessment of renewable jet fuel production in integrated Brazilian sugarcane biorefineries." Applied Energy, 209, 2018: 290-305.

Ludwig-Bolkow Systemtechnik GMBH. (2006) E3 Database. [Online]. http://www.e3database.com/

Staples, M.D. et al. (2014). Lifecycle greenhouse gas footprint and minimum selling price of renewable diesel and jet fuel from fermentation and advanced fermentation production technologies. Energy and Environmental Science, 7, 1545-1554.

Task 2- Support of ILUC Calculations and Assessment of Sustainability Certification Schemes for Potential Inclusion Under CORSIA

Massachusetts Institute of Technology

See combined Tasks 2 & 6 below.

Task 3- Stochastic Techno-Economic Assessment (TEA) to Evaluate Alternative Jet Fuel Policies in the Context of CORSIA

Massachusetts Institute of Technology & Hasselt University

Objective(s)

For AY 2017/2018 Task 3, the objective of the funded work was to quantify the impact of different policy options on the economic viability of alternative jet fuel (AJF) production. This analysis was used to inform the work of the Policy Guidance Task Group of AFTF, by providing quantitative evidence of the effectiveness of policies that CAEP Member States may be considering to support the deployment of AJF technologies. The analysis leverages techno-economic work and models that MIT has developed previously, with the assistance of FAA funding.

Research Approach

Introduction

In previous years, MIT has carried out TEA studies for a wide set of feedstock-to-fuel pathways to convert biomass or industrial and household wastes into alternative aviation fuel. The resulting literature (eg., Bann et al., 2017; Yao et al., 2017; Suresh et al. 2018; Pearlson et al., 2013, Seber et al., 2014; Bond et al., 2014; Staples et al., 2014) shows that alternative aviation fuels will remain more expensive to produce than conventional jet fuel in the short- to medium-term. However, a number of policy measures exist that could potentially improve the economic viability of these technologies. Examples of such measures include loan guarantees, public offtake agreements, alternative fuel production or use mandates, production or consumption subsidies, tax breaks, carbon taxation or carbon offsetting mandates. In the U.S., for example, alternative aviation fuel support is provided, inter alia, through the Farm-to-Fly Program and its associated loan guarantees and support for alternative aviation fuel R&D and pilot plant development, the Renewable Fuels Standard (RFS) and by offtake agreements of the U.S. military.

To date, the monetary impact of only some of these options have been studied for a limited set of feedstock-to-fuel production pathways (Bann et al., 2017; Bittner et al., 2015). The available evidence points to heterogeneity in the cost-effectiveness of these policy measures. MIT (in collaboration with Purdue University and Hasselt University) has carried out an analysis of a wide set of policy options for a number of AJF production technologies.

This work was carried out in the context of the AFTF Policy Task Group, and made use of the harmonized stochastic TEA model developed at MIT (Bann et al., 2017). The model was augmented to account for several policy measures, and quantifies the changes in net present value (i.e. financial performance of a jet fuel production facility) and jet fuel minimum selling prices resulting from these policies.

Methods

The case studies considered for the stochastic TEA analysis are summarized in Table 11.

Table 11. Case studies selected for stochastic TEA policy assessment

Process	Feedstock	Region	Company example
Micro - Fischer-Tropsch (FT)	Forest residues	North America	Velocys
Synthesized iso-parrafins (SIP)	Sugarcane	South America	Total-Amyris
Hydroprocessed esters and fatty acids (HEFA)	Waste tallow and yellow grease	North America/ Europe	Altair/Neste
Hydroprocessed esters and fatty acids (HEFA)	Palm oil/palm fatty acid distillates (PFAD)	Asia & Pacific	Pertamina
FT	Municipal solid waste	North America	Fulcrum
Alcohol to jet (ATJ) via. iBuOH	Corn	US	Gevo

To carry out the TEA of the different AJF pathway case studies outlined above, a discounted cash flow rate of return (DCFROR) model was used. The DCFROR model quantifies the economic viability of an n^{th} plant, commercial-scale fuel production facility in terms of two metrics:

- Net Present Value (NPV), which is the value of all future cash flows, discounted to nominal dollars in the base year; and



- Minimum Selling Price (MSP), which is the lowest price at which the fuel product must be sold to have a project NPV of zero at the stipulated rate of return. By comparing the calculated MSP to conventional fuel prices, the cost premium (or discount) of producing the AJF fuel can be calculated.

This analysis builds off the DCFROR model first presented in Pearlson et al. (2013) and applied to middle distillate fuel production from soybean oil using the HEFA process. This model was subsequently extended to handle additional feedstock-to-fuel AJF pathways, and to quantify uncertainty in the results as a function of uncertainty and stochasticity in the input parameters, as described in Suresh et al. (2018) and Bann et al. (2017).

Each of the pathways modelled relies on a number of updated harmonized financial assumptions. Each AJF production plant is assumed to have a 20-year lifetime, with 40% equity financing. The remainder of the financing is assumed to be from a 10-year loan with 8% interest. The plants are assumed to operate for 350 days per year, with a deterministic nameplate capacity of approximately 111 million liters/year (2000 bbl/day) of total fuel product. Actual pathway capacity used in each iteration of the model varies somewhat with stochastic changes in fuel yield. The return on equity is 15%. The income tax rate was assumed to be 16.1%. Many of the input parameters are drawn from a probability distribution or stochastic process, in order to quantify uncertainty in their values and the calculated results. These include facility capital costs, fixed operating costs, feedstock costs, utility prices (electricity and natural gas), fuel product prices, and non-fuel product prices. Parameter values are drawn from these distributions and run through the DCFROR model 10000 times, in order to generate a distribution of MSP and NPV results. Where possible, regionally specific data was used to reflect the location of the selected case studies. The parameter values and distributions, as well as the mass and energy balance data used for each of the pathways, is documented in detail in CAEP/11-AFTF/07-IP/14.

A number of policy types were implemented in the stochastic TEA model. These are summarized in Table 12. For the GHG emissions reduction-based incentive, each pathway's reduction in emissions is based on LCA values already agreed to by AFTF, or our best estimate of what the agreed default LCA values are likely to be.

Table 12. Policy types to be considered in the stochastic TEA policy assessment

Policy type	Implementation in stochastic TEA model
Input subsidy	Reduce feedstock costs seen by fuel producer by subsidy amount
Capital grant	Reduce initial capital cost by grant amount
Output based incentives	Increase prices received by fuel producer for products by incentive amount
GHG emission reduction-defined incentive	Increase prices received by fuel producer for products, as a function of GHG reduction from petroleum fuels

Results

Figure 1 shows the MSP of the six case studies modelled, and serves as a reference point when no policies have been applied. The red line indicates the median value of calculated MSP, and the bold blue line represents current market prices for petroleum-derived jet fuel.

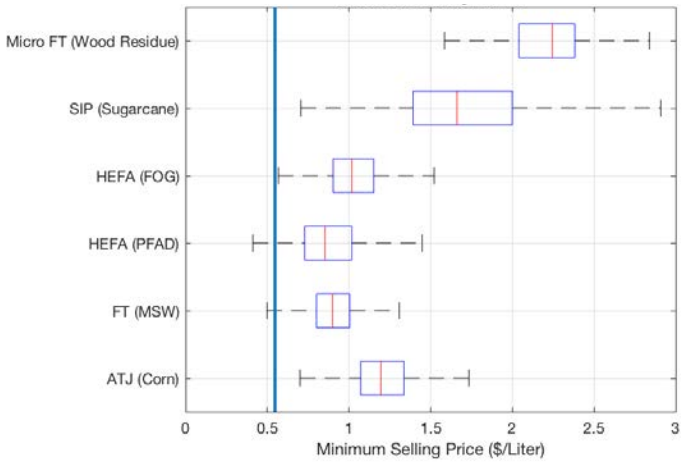


Figure 1. MSP of the six modelled case studies

Next, each of the policies described above was implemented with the same total cost to the government. In order to do this for the HEFA pathways, for example, the first policy modelled was the output subsidy at three levels: 0.10, 0.25, 0.75 USD per liter output subsidy. The average total cost to the government was calculated, and this was used to determine a comparable size for the capital grant, input subsidy, and GHG reduction-based incentive policies. Example results for the HEFA FOG pathway are shown in Table 13. The results for the other pathways are fully documented in CAEP/11-AFTF/07-IP/14.



Table 13. Policies cases for each of the 4 policy types and the resulting total policy costs and impact on fuel MSP for the HEFA FOG pathway. Mean values are provided with variance in brackets.

HEFA (FOG)			
Policy type	**Output Subsidy**		
Policy	0.10 $/liter output subsidy	0.25 $/liter output subsidy	0.75 $/liter output subsidy
Total policy cost (mil. USD) [Standard Deviation]	77 [3]	192 [8]	576 [23]
MSP ($/liter) [Standard Deviation]	0.97 [0.19]	0.82 [0.19]	0.32 [0.19]
Policy type	**Input Subsidy**		
Policy	16% subsidy on feedstock costs	40% subsidy on feedstock costs	119% subsidy on feedstock costs
Total policy cost (mil. USD) [Standard Deviation]	77 [19]	192 [50]	571 [146]
MSP ($/liter) [Standard Deviation]	0.98 [0.17]	0.81 [0.12]	0.25 [0.05]
Policy type	**Capital Grant**		
Policy	74 mil. USD capital grant	79 mil. USD capital grant*	79 mil. USD capital grant*
Total policy cost (mil. USD) [Standard Deviation]	74 [4]	79 [9]	79 [9]
MSP ($/liter) [Standard Deviation]	0.88 [0.19]	0.87 [0.19]	0.87 [0.19]
Policy type	**GHG Emissions Reduction Policy**		
Policy	CO_2 reduction credit of 48 USD/tonne	CO_2 reduction credit of 114 USD/tonne	CO_2 reduction credit of 343 USD/tonne
Total policy cost (mil. USD) [Standard Deviation]	77 [3]	192 [8]	576 [23]
MSP ($/liter) [Standard Deviation]	0.97 [0.19]	0.82 [0.19]	0.32 [0.19]

*The size of the capital grant in these cases is limited by total estimated fixed capital investment (FCI): we have not considered capital grants that exceed total FCI.

These results show that, at equivalent total policy costs, different policies have different impacts on the mean and variance of MSP. In particular, the capital grant is most effective at reducing mean MSP because the benefit of the policy to the fuel producer is not taxed. Note that this result is sensitive to the way loans are treated and paid off in the DCFROR model: in these results, the debt-to-equity ratio is assumed to remain constant, whereas in reality a capital grant may instead be used preferentially to reduce debt or equity.

In contrast, feedstock input subsidies are shown to be more effective at reducing risk (as indicated by the impact on variance in MSP) than the other policies considered here, even at the same total policy cost. Furthermore, as the size of the feedstock subsidy increases, variance in MSP decreases. This is because variability in feedstock costs is a significant contributor to uncertainty in MSP, and as the policy is implemented as a percentage of total feedstock cost, the risk of variability in feedstock costs is offloaded onto the policy. These results indicate that policy makers may wish to select different policy mechanisms depending on their objectives.

The results shown in Table 13 indicate that a large enough feedstock subsidy, output subsidy or GHG reduction-based incentive could reduce the MSP of jet fuel to be competitive with today's jet fuel market price of 0.55 USD per liter. Therefore, the magnitude of each policy type required to have a project NPV of zero was also calculated. For example, the results for the breakeven feedstock subsidy for five of the fuel production pathways are shown in Figure 2. The results indicate that

HEFA PFAD and FOG pathways would require a median feedstock subsidy of 13% and 47% percent, respectively, to have a project NPV of 0. The corn grain ATJ and sugarcane SIP pathways would require feedstock subsidies of 80% and 93%, respectively, in the median cases. The results for the forestry residue micro FT pathway are around 430% in the median case, meaning that the micro FT pathway would have to receive a subsidy of approximately 4 times the costs of feedstock in order to be profitable. Note that the black lines in the figure indicate 0-100%, and that the MSW FT case is not shown in Figure 2 because the assumption is that there is no cost associated with the feedstock.

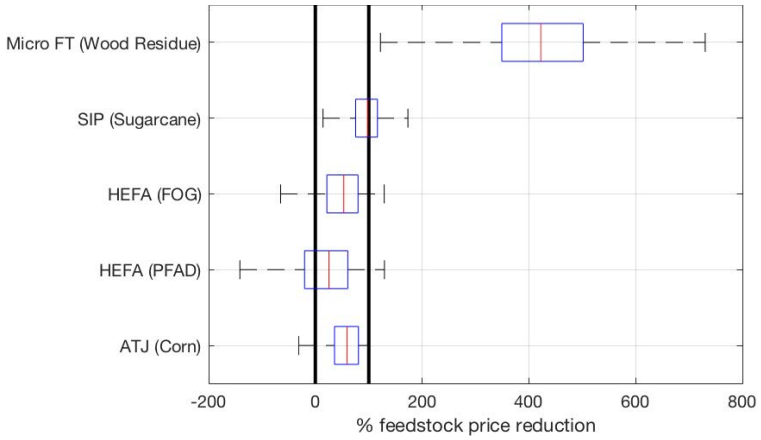


Figure 2. Breakeven feedstock subsidy for four fuel production pathways.

A similar analysis was carried out for the other policy types. In addition, the analysis included an assessment of the impact of real-world policies on the economic viability of the six feedstock-to-fuel pathways. These illustrative policies investigated included: a feedstock subsidy of 50 USD/tonne for PFAD, suggested by the technical experts from Indonesia (~approx. 27% of feedstock cost); a capital grant of 5 mil. USD (comparable to capital grants awarded under the US Department of Energy and Bioenergy Technologies Office); CO_2 emissions credits of 8 USD/tonne$_{CO2}$ in 2020, ramping up to 20 USD/tonne$_{CO2}$ by 2035 (the carbon pricing assumptions used by GMTF in a cost-benefit assessment of CORSIA); and an output subsidy of 0.25 USD/l (similar to historical highs seen for RIN prices under the US Renewable Fuels Standard (US EPA 2015)).

Milestone(s)

The work described for this task represents the achievement of MS 4 as defined in the AY 2017/2018 Grant Proposal. Progress on stochastic TEA policy analysis was presented to AFTF at meetings in April 2018 and September 2018 and documented in numerous CAEP working and information papers.

Major Accomplishments

The major accomplishments were the calculation of the stochastic TEA results for 6 feedstock-to-fuel pathways, considering 4 different policy types of various magnitudes. These data were presented to AFTF and documented in CAEP information and working papers and will ultimately be passed on to CAEP in order to inform policies being considered by Member States.

Publications

Peer reviewed publications

None

Written reports

CAEP/11-AFTF/6-IP/05, Stochastic techno-economic analysis for quantitative policy assessment, presented at AFTF/6, April 2018, Montreal, Canada

CAEP/11-AFTF/7-IP/14, Stochastic techno-economic analysis for quantitative policy assessment, presented at AFTF/7, September 2018, Montreal, Canada

Outreach Efforts

Stochastic techno-economic analysis for quantitative policy assessment. Presented by Juju Wang on the at ASCENT 1 bi-weekly teleconference on March 5, 2018.

Awards

None

Student Involvement

Juju Wang, Master's student at MIT's Department of Aeronautics and Astronautics, carried out the majority of the analysis. This work will make up the majority of her master's thesis, and she is expected to graduate in June 2019.

Plans for Next Period

In the coming year, the MIT ASCENT Project 01 team will continue its work in AFTF. The quantitative policy assessment work carried out to date will be augmented, and then documented in a working paper to be presented to CAEP in February 2019. MIT will draft this working paper.

In addition, this work will start to be prepared for submission to a peer-reviewed journal. Much of the analysis carried out for this task will be written up in a Master's thesis to be submitted by Juju Wang for anticipated graduation in June 2019.

References

Bann, S.J., Malina, R., Staples, M.D., Suresh, P., Pearlson, M., Tyner, W.E., Hileman, J.I., Barrett, S.R.H., *The costs of production of alternative jet fuel: A harmonized stochastic assessment*. Bioresource Technology, Volume 227, 2017

Bittner, A, Tyner, WE., Zhao, X, Field to flight: A techno-economic analysis of the corn stover to aviation biofuels supply chain. Biofuels, Bioprod. Bioref., 9: 201–210 (2015).

Bond, J; Upadhye, A; Olcay, H; Tompsett, G; Jae, J; Xing, R; Alonso, D; Wang, D; Zhang, T; Kumar, R; Foster, A; Sen, S; Maravelias, C; Malina, R; Barrett, S; Lobo, R; Wyman, C; Dumesic, J; Huber, G. Production of renewable jet fuel range alkanes and commodity chemicals from integrated catalytic processing of biomass, In: Energy and Environmental Science, Vol. 7 (2014).

Pearlson, M., Wollersheim, C., Hileman, J., 2013. A techno-economic review of hydroprocessed renewable esters and fatty acids for jet fuel production. Biofuels, Bioprod. Biorefin. 7, 89–96. http://dx.doi.org/10.1002/bbb.1378.

Seber, G; Malina, R; Pearlson, M; Olcay, H; Hileman, J; Barrett, S. Environmental and economic assessment of producing hydroprocessed jet and diesel fuel from waste oils and tallow, Biomass and Bioenergy Vol. 67 (2014).

Staples, M. D., Malina, R., Olcay, H., Pearlson, M. N., Hileman, J. I., Boies, A., & Barrett, S. R. H. (2014). Lifecycle greenhouse gas footprint and minimum selling price of renewable diesel and jet fuel from fermentation and advanced fermentation production technologies. Energy Environ. Sci., 7(5), 1545–1554. https://doi.org/10.1039/C3EE43655A

Suresh, P, R Malina, MD Staples, S Lizin, H Olcay, D Blazy, MN Pearlson, SRH Barrett, 2018. Life cycle greenhouse gas emissions and costs of production of diesel and jet fuel from municipal solid waste. *Environmental Science and Technology,* DOI: 10.1021/acs.est.7b04277

Yao, G; Staples, M. / Malina, R; Tyner, WE: Stochastic Techno-Economic Analysis of Alcohol- to-Jet Fuel Production, in: Biotechnology for Biofuels, Vol. 10, 18 (2017).



Task 4- Collaborate with ASCENT 21 to Incorporate Non-CO_2 Lifecycle Emissions into APMT-Impacts Climate

Massachusetts Institute of Technology

Objective(s)

The objective of this task was to collaborate with Project A021 to incorporate non-CO_2 lifecycle GHG emissions into APMT-IC and to evaluate the impact that the choice of climate metric has on results and conclusions from APMT-IC.

Research Approach

Introduction

The MIT ASCENT Project 01 team collaborated with the Project A021 team to properly represent AJF in the APMT-IC module. AMPT-IC was developed by MIT under the Partnership for AiR Transportation Noise and Emissions Reduction (PARTNER) to quantify the environmental impacts of policies influencing aircraft operations and the resulting changes in health and welfare outcomes for climate, air quality and noise. Previously, APMT-IC represented the differences between petroleum-derived jet fuels and AJF in terms of lifecycle CO_2-equivalent emissions, where the CO_2e value of CH_4 and N_2O emissions are calculated on the basis of 100-year global warming potential (GWP) equivalents. While this approach is useful as a first-order approximation to quantify the lifecycle climate impacts of different jet fuels, the use of 100-year GWP to capture non-CO_2 emissions misrepresents the climate impacts. For instance, the atmospheric background concentrations, radiative forcing, and atmospheric lifetime of CH_4 and N_2O are fundamentally different than those of CO_2. Using an equivalency metric that depends on an arbitrarily defined time horizon, such as the GWP-100, masks these physical differences, and that could distort the results at each step of the analysis. Therefore, in order to better reflect non-CO_2 lifecycle emissions in APMT-IC, it was proposed under ASCENT Project 21 to model lifecycle CH_4 and N_2O emissions to quantify their impacts on radiative forcing.

Methods

The MIT Project 01 team contributed to this improvement of APMT-IC by providing lifecycle emissions inventories for petroleum and AJF, disaggregated by emissions species, to the Project A021 team. This data was used to verify and validate the modifications made to APMT-IC. The results have been used to evaluate the impact that the choice of climate metric has on results and conclusions from APMT-IC, and to enhance the ability to assess policies influencing the use of AJF.

Results

The results obtained from the newly implemented model were verified through comparisons the Model for Greenhouse Gas Induced Climate Change (MAGICC6) (Meinshausen et al., 2011) and the global warming potential was compared to results published in the IPCC Fifth Assessment Report (Myhre et al. 2013) and Cherubini et al. (2013). In both cases the implemented model was found to align with results in the literature.

These additional capabilities enable APMT-IC to not only evaluate aviation life-cycle emissions scenarios, but also to evaluate non-aviation emissions scenarios for ground emissions of CH_4, N_2O and CO_2. In addition, the current method is capable of capturing the associated climate impacts on their characteristic time scales. These new capabilities have already been applied in a paper accepted for publication in *GCB Bioenergy*. The paper illustrates the importance of capturing the emissions time scales, especially with regard to land use change emissions.

Milestone(s)

The work on this task represents the achievement of MS 6 as defined in the AY 2017/2018 Grant Proposal. The improvements made to APMT-IC, including the differentiation of lifecycle CO_2, CH_4 and N_2O emissions, was presented at the bi-annual ASCENT meeting in April 2018, in Cambridge, MA.

Major Accomplishments

The major accomplishment during this period of performance was the incorporation of lifecycle CH_4 and N_2O into APMT-IC, so that the climate impacts of technology pathways emitting these species can be better represented in the model. In addition, the enhanced model was used in a project to evaluate the time-dependent climate impacts of different bio-energy systems, relative to fossil fuels. This study was accepted for peer reviewed publication in *GCB Bioenergy*.

Publications

de Jong, S, MD Staples, C Grobler, V Daioglou, R Malina, SRH Barrett, R Hoefnagels, A Faaij, M Junginger, 2018. Using dynamic relative climate impact curves to quantify the climate impact of bioenergy production systems over time. *GCB Bioenergy,* DOI: 10.1111/gcbb.12573

Project 01 funding is acknowledged in this publication.

Outreach Efforts

This work was presented at the ASCENT bi-annual meeting in April 2018, in Cambridge, MA.

Awards

None

Student Involvement

These modifications to APMT-IC were carried out by Carla Grobler, a graduate student at MIT, who is primarily funded by Project A021. Lifecycle emissions inventories for petroleum-derived jet fuel and AJF were provided by Tim Galligan and Juju Wang, MIT graduate students funded under ASCENT Project 01.

Plans for Next Period

None

References

Cherubini, F., Bright, R.M. and Strømman, A.H., 2013. Global climate impacts of forest bioenergy: what, when and how to measure? *Environmental Research Letters* 8(1), p.014049.

Meinshausen, M., Raper, S. C. B. and Wigley, T. M. L. (2011). Emulating coupled atmosphere-ocean and carbon cycle models with a simpler model, MAGICC6 - Part 1: Model description and calibration. *Atmospheric Chemistry and Physics* 11(4), pp. 1417–1456. doi: 10.5194/acp-11-1417-2011.

Myhre, G. et al. (2013). Anthropogenic and Natural Radiative Forcing. In: Climate Change 2013: The Physical Science Basis. Contribution of Working Group I', in Stocker, T. F. et al. (eds) *Climate Change 2013: The Physical Science Basis. Contribution of Working Group I to the Fifth Assessment Report of the Intergovernmental Panel on Climate Change*. Cambridge, United Kingdom and New York, NY, USA: Cambridge University Press.

Task 5- Collaborate with Washington State University (WSU) to Facilitate Development of an Aspen Model of the Hydroprocessed Esters and Fatty Acids (HEFA) Fuel Production Process

Massachusetts Institute of Technology

Objective(s)

The objective of this task was to collaborate with Washington State University (WSU) ASCENT Project 01 team to facilitate development of an Aspen model of the HEFA fuel production process.

Research Approach

Under this task, the MIT ASCENT Project 01 team agreed to facilitate development of an Aspen model of the HEFA fuel production process by the ASCENT Project 01 research team at WSU. The HEFA model developed by WSU leverages the knowledge gained during development of the model described in Pearlson et al. (2013). The purpose of this task was to build up a modeling tool suited for use in WSU's lipid-focused advanced supply chain deployment support project, which is Task 3.1 of the ASCENT Project 01 Regional Project Planning numbering system.

During the reporting period, the MIT Project 01 team had a number of conversations with the WSU Project 01 team led by Manuel Garcia-Perez. The state of the Aspen HEFA model described in Pearlson et al. (2013) was discussed, along with the



challenges encountered and lessons learned. Some clarifying questions regarding the data reported in the paper were also clarified. These interactions aided WSU's development of a higher fidelity Aspen model of the HEFA process.

Milestone(s)
This collaboration was discussed during the bi-weekly ASCENT Project 01 teleconference on November 13, 2017. This represents completion of MS 5 as defined in the AY 2017/2018 Grant Proposal.

Major Accomplishments
This major accomplishment of this reporting period was collaboration between MIT and WSU, to facilitate WSU's development of an Aspen HEFA model.

Publications
None

Outreach Efforts
None

Awards
None

Student Involvement
None

Plans for Next Period
None

References
Pearlson, M; Wollersheim, C; Hileman, J. A Techno-economic Review of Hydroprocessed Renewable Esters and Fatty Acids for Jet Fuel Production, Biofuels Bioprod. Biorefining 7, 89 (2013).

Tasks 2 & 6- Support of ILUC Calculations and Assessment of Sustainability Certification Schemes for Potential Inclusion Under CORSIA & Additional (including in-person) Support to FAA for Decision-Making in the Context of AFTF
Massachusetts Institute of Technology

Objective(s)
The objective of this task is to provide support to the FAA in the context of AFTF beyond the major LCA and policy analysis tasks outlined above. Specifically, this task will support the work of the induced land use change (ILUC) and sustainability task groups and provide in-person support for FAA decision-making at meetings of AFTF and CAEP.

Research Approach
ILUC Task Group
The ILUC Task Group is responsible for the calculation of ILUC emissions factors which are added to the core LCA values. Purdue University and the University of Toronto currently lead this task within AFTF. During the reporting period, the MIT ASCENT Project 01 team supported the work of the ILUC Task Group by:



- providing relevant pathway and technology-specific data (e.g. expected fuel yields, fuel product slates) and scenario assumptions (e.g. anticipated global fuel production volumes) for ILUC analysis such that the work is consistent with the work of the LCA Task Group;
- identify additional pathways for which ILUC values may be required (e.g. fuels derived from valuable by-product feedstocks, such as palm fatty-acid distillates or corn oil); and
- contributing to discussion on comparison of ILUC results from the GTAP and GLOBIOM models.

Sustainability Task Group
In order to qualify under CORSIA, AJFs have to satisfy sustainability criteria beyond the CO_2 reductions that are captured in the LCA and ILUC emissions analyses. During the reporting period, it was decided that these criteria would encompass only a limited set of environmental aspects. Therefore, the contribution of MIT ASCENT Project 01 team was smaller than anticipated because the scope of work was significantly reduced.

In-person Support
During the reporting period, the MIT ASCENT Project 01 team will provided significant in-person support for FAA decision-making for purposes of the AFTF. Prof. Robert Malina from Hasselt University served as the co-lead of the task group on core LCA emission values and the small group lead on feedstock classification and reporting requirements. Dr. Mark Staples from MIT led the modeling work of the AFTF Task Group for Core LCA and the small group on emissions credits. Team members took part in AFTF in-person meetings in October 2017, April 2018 and September 2018, as well as the ICAO Alternative Fuels Conference in Mexico in fall 2017, as requested by FAA. Team members also participated in numerous teleconferences, virtual meetings, and the preparation of CAEP information and working papers.

Milestone(s)
Participation in AFTF/05, AFTF/06, AFTF/07, and the ICAO Alternative Fuels Conference in fall 2017.

Major Accomplishments
None

Publications
Peer reviewed publications
None

Written reports
CAEP/11-AFTF/7-IP/12, Report on the progress of the feedstock classification small group, presented at AFTF/7, September 2018, Montreal, Canada

CAEP/11-AFTF/7-IP/13, Reporting requirements for actual GHG emissions LCA values, presented at AFTF/7, September 2018, Montreal, Canada

Outreach Efforts
None

Awards
None

Student Involvement
None

Plans for Next Period
In the coming year, the MIT ASCENT Project 01 team will continue its work in AFTF, the specific scope of which depends on decisions to be reached by CAEP in February 2019. The work carried out to-date will be documented in a number of working papers to be presented to CAEP at that meeting.



Project 002 Ambient Conditions Corrections for Non-volatile PM Emissions Measurements

Missouri University of Science and Technology, Aerodyne Research Inc., and Honeywell

Project Lead Investigator

Philip D. Whitefield
Professor of Chemistry and Dir. Center for Research in Energy and Environment (CREE)
Chemistry
Missouri University of Science and Technology
400 W 11th Street, Rolla, MO 65409
573-341-4420
pwhite@mst.edu

University Participants

Missouri University of Science and Technology

- Philip D. Whitefield, Professor of Chemistry and Dir. Center for Research in Energy and Environment (CREE)
- FAA Award Number: 13-C-AJFE-MST Amendments: 002,003,005,008 and 010
- Period of Performance: 9/18/2014 – 12/31/2019
- Tasks:
  1. Ambient conditions corrections measurements using the NASA LDI combustor rig
  2. Ambient conditions corrections measurements using the GEAE combustor rig
  3. Engine to engine variability at Honeywell
  4. Ground-based nvPM emissions from an IAE V2527-A5 engine burning four different fuel types

Project Funding Level

PROJECT	FUNDING	MATCHING	SOURCE
13-C-AJFE-MST-002	1,288,836.30	1,288,836.30	EMPA LETTER
	284,613.66	284,613.66	TRANSPORT CANADA
13-C-AJFE-MST-003	500,000.00	500,000.00	EMPA LETTER
13-C-AJFE-MST-005	500,000.00	500,000.00	EMPA LETTER
13-C-AJFE-MST-008	579,234.00	579,234.00	EMPA LETTER
13-C-AJFE-MST-010	725,500.00	725,500.00	EMPA LETTER

Investigation Team

Professor Philip Whitefield, Dr. Wenyan Liu, Research Chemist, Steven Achterberg, Research Technician, Max Trueblood, Research Technician, Dr. Richard Miake-Lye and Dr. Zenhong Yu (sub-contractors Aerodyne Research Inc) and Rudy Dudebout and Paul Yankowich (sub-contractors Honeywell Aerospace).

Project Overview

The International Civil Aviation Organization (ICAO) has approved publication of the revised ICAO Annex 16 Vol. II specifying a standardized sampling system for the measurement of non-volatile particulate matter (nvPM) from aircraft engines for use in certification. The Missouri University of Science and Technology (Missouri S&T) owns and operates the ICAO Annex 16 Vol. II compliant, North American mobile reference system (NARS) to measure nvPM emissions from the exhaust of aircraft engines. The work under this project exploits the use of the NARS to address issues associated with



ambient conditions corrections, engine-to-engine variability and fuel formulation sensitivity. During this reporting period work has been performed on two major tasks:

Task 1
Testing has taken place at Honeywell as part of a series of measurements to acquire certification-like data on a set of engines identified by ICAO Committee on Aviation Environmental Protection (CAEP) Working Group 3 (Emissions Technical) Particulate Matter Task Group (CAEP/WG3/PMTG to be representative of the commercial fleet, for entry into the nvPM values database. The engine-to-engine variability of nvPM emissions data from a sample of a large number of engines is required in order to assess the characteristic variability of these engines, which is critical in establishing a regulatory limit for nvPM number- and mass-based emissions. The measurement activity in this task has been undertaken by Honeywell personnel under sub-contract to MS&T. Technical oversight will be provided by the MS&T team.

Task 2
The North American Reference System (NARS) and its ancillary equipment has been used to characterize the ground-based nvPM emissions from an IAE V2527-A5 engine burning four different fuel types. This work was conducted as part of the NASA/DLR ND MAX campaign.

Task 1- Engine-to-Engine Variability at Honeywell

Missouri University of Science and Technology

Objective(s)

The objective of this effort is to gather emissions data from at least 20 Honeywell commercial propulsion engines of the same type to assess engine-to-engine variability and to derive characteristic nvPM emissions.

Research Approach

Experience has shown that manual calibration of the currently accepted standard systems for measuring nvPM from aero-engines is problematic. The current accepted method for assuring that nvPM measurements are valid is to perform a back-to-back measurement with a known good measurement system or "gold standard system." The North American reference system for nvPM, operated by MS&T has been compared with a similar European system and now serves as the reference "gold" system in the United States and Canada. In July and August, 2014, Honeywell performed a correlation test with the North American reference system at the Honeywell facility in Phoenix, Arizona. This test was performed on a development HTF7500 engine using the Honeywell Mobile Emissions Facility 2, (MES2). MES2 is equipped to measure nvPM, gaseous emissions and smoke. The North American reference system was plumbed in parallel to MES2 and nvPM results were measured sequentially from the Honeywell system and the MS&T system. Data were collected at the four International Civil Aviation Organization (ICAO) landing and take-off (LTO) conditions. Emissions samples were drawn from the Honeywell emissions sampling system (a cruciform mixed exhaust rake with 16 sampling ports on four arms at four radii) and two core engine sampling rakes with six radial ports per rake. Test results were analyzed and reported to the FAA.

In support of the anticipated 2019 ICAO/FAA Part 34 certification standard, Honeywell received a request for proposal from the FAA in January 2016 to measure engine-to-engine variability of non-volatile particulate matter emissions data from a sample of 20 Honeywell engines in order to assess the characteristic variability of these engines. The FAA proposed work included the following items:

(a) Obtain nvPM mass and number emissions from 20 turbofan engines, which contain the same model and type with the standardized draft ICAO Annex 16 Appendix 7 compliant nvPM measurement system, along with ICAO Annex 16 compliant gaseous emissions (possibly obtained during green runs).
(b) Use a single-point probe positioned at a spot in the exhaust stream that is representative of the average emissions in the exit plane. A certification-type probe is preferable, if the added cost is not prohibitive.
(c) Vary the rated thrust from idle to 100 percent at 10 percent increments. After the engine stabilizes at each thrust point, hold the throttle at that thrust point for approximately 3 minutes so that nvPM and gaseous emissions can be acquired.
(d) Use limited release Non-Disclosure Agreement (NDA) as needed. Ensure that the nvPM and gaseous emissions data are available from the 20 engines for analysis to derive characteristic nvPM mass and number emissions indices (EIs) or any other emissions metric as needed.



In response to this request, Honeywell proposed conducting nvPM emissions sampling during break-in (green run) testing of new AS907-2-1A type production engines. This required the redesign of the HTF7500 sampling rake in order for it to be compatible with the AS907-2-1A engine short mixer design. During testing, two of the existing fixed AS907-2-1A Station 6 (core exit) thermocouple (TC) probes were replaced with these new core exhaust emissions sampling rakes.

Honeywell used their existing mobile emissions facility, MES2, certified for ICAO emissions testing. Under this program, Honeywell also procured one standardized draft Annex 16 Appendix 7 compliant nvPM mass measurement system and installed it in MES2 system to support this testing. Reference 2.

Task 1.1 – Procurement of nvPM Emissions Test Equipment

Honeywell shall design and fabricate nvPM emissions rakes required to gather data from new Honeywell AS907-2-1A engines. These are Station 6 (core exit) emissions sampling rakes compatible with the AS907-2-1A engine short mixer configuration. Two rakes were installed for testing, with each rake configured with six dial sampling ports. An exhaust sample from both rakes is averaged and analyzed through the compliant Honeywell emissions measurement system MES2. Honeywell completed design drawings for the engine Station 6 exhaust emissions rakes and fabricated four, which consists of two for testing with two spares. One standardized draft Annex 16 Appendix 7 compliant nvPM mass measurement system was purchased and installed in Honeywell's existing mobile emissions facility, MES2.

Task 1.2 – Engine nvPM Emissions Testing

Honeywell shall obtain nvPM and gaseous emissions from a minimum of 20 AS907-2-1A type turbofan engines during production break-in testing, using MES2. This facility is fully compliant with the draft ICAO Annex 16 Appendix 7 nvPM measurement system and is also ICAO Annex 16 compliant for the gaseous emissions system. In addition, with nvPM and gaseous emissions, Honeywell will report derived smoke number (SN) from the optical smoke meter (OSM). Honeywell did not perform or report filter smoke measurements to minimize the analysis time per engine condition. To minimize impact on the critical HTF7000 production engine break-in test schedule, the nvPM emissions test plan aligns with the existing break-in run test schedule which includes a 3-minute hold at the end of each power point tested. This program obtained nvPM mass and gaseous emissions samples at the end of these 3-minute periods. The proposed 11-point nvPM and gaseous emissions sampling test matrix is shown in Table 1. Prior to each green run test, technicians replaced two of the fixed AS907-2-1A Station 6 (core exit) TC probes with the exhaust emissions sampling rakes.

Table 1. nvPM Mass and Emissions Sampling Test Matrix.

Test Condition/	Approximate Maximum Thrust, Percent	Stabilizing Time Prior to nvPM Sampling, minutes
Ground idle (GI)	4	3
17,600	8	3
20,600	16	3
22,600	29	3
23,600	38	3
24,600	52	3
25,600	72	3
26,300	90	3
26,900	97	3
Maximum takeoff (MTO)	100	3
1,100 lb/hr	33	3
GI	4	3

Since agreement with production is contingent on not significantly impacting or delaying the production test schedule, this task plans to gather data from 25 green run engine tests, anticipating the risk that some tests may have issues that are not identified during the test and thus will not produce acceptable data. Honeywell will reduce the analysis results following every test to validate the data, but the production engine tests cannot be delayed while waiting for data



validation completion.

The engine rated thrust was varied in increments from idle to 100 percent MTO per Table 1. The steady-state engine condition were stabilized at each point for approximately 3 minutes before obtaining the exhaust emissions data.

Task 1.3 - Data Reduction and Analysis

Honeywell will reduce and analyze the data following every test to validate that the data set is acceptable.

Task 1.4 - Project Management and Reporting

Honeywell shall manage the program activities and finances in accordance with standard Honeywell practice and provide monthly status reports to MS&T.

Honeywell is proposing completion of this work within 11 months after contract award. Honeywell estimates that it will require four months to procure, install, and check out the required nvPM test equipment before initiating nvPM engine testing.

Current production projections indicate that a sufficient number of AS907-2-1A engines will be produced during the proposed contract period to be able to conduct the 25 planned exhaust emissions tests during planned green runs. Honeywell estimates that this testing will be completed within a four-month period after the nvPM equipment has been cleared for testing.

Following these tests, Honeywell shall compile the data and prepare a draft final report documenting the test results and hold a final briefing to present results to MS&T and FAA representatives. Honeywell shall prepare a limited release draft final report, and make available the nvPM and gaseous emissions data from the engines tested for additional analysis to derive characteristic nvPM mass and number, EIs or any other emissions metrics as needed.

Honeywell shall then submit a draft final report to MS&T, and allocate 30 days for review and feedback. Honeywell shall then incorporate the comments and submit the final report to MS&T.

Milestone(s)

A final test report has been submitted by Honeywell to MS&T. It presents the results of a twenty-five-engine test campaign to sample nvPM from production engines of the same model type. The sampling systems and analysis procedures used for this test campaign conform to the guidance set forth in SAE AIR 6241 and the draft Appendix 7 to ICAO Annex 16.

Major Accomplishments

1. Total variation, including measurement system uncertainty, ambient condition variation, fuel variation and engine-to-engine variation has been assessed on one measurement train with two mass measurement systems.
2. Highest standard deviation noted at 30% power, standard deviation equal to 93% of average
3. Lowest standard deviation noted at 100% power, standard deviation equal to 16% of average
4. Modal standard deviation is higher at lower mean values
5. Generally lower variation in number measurement noted
6. Similar variation noted between system loss corrected and only thermophoretic loss corrected data
7. Excellent agreement between LII and MSS demonstrated
8. Fuel correction reduced variation by <1%
9. No significant correlation on LTO mass or number with ambient temperature or humidity
10. Standard Deviation divided by average for 21 engine testing with fuel correction:
    - LTO mass standard deviation % of mean (combined LII + MSS) = 20.4%
    - LTO number standard deviation % of mean = 11.0%

Publications

None

Outreach Efforts

This work was reported at the ASCENT advisory board meetings held in Cambridge MA in April 2018



Data provided to ICAO working group 3 Particulate Matter Task Group in paper CAEP11-WG3-PMTG7-IP01

Awards
None

Student Involvement
None

Plans for Next Period
Having completed the engine testing described above additional scope is proposed in the form of a series of new tasks for Missouri S&T and Honeywell to perform combustor rig testing with alternate fuels to establish nvPM ambient corrections designed specifically to address a set of FAA objectives:

- Set up an RQL full annular combustor rig and standardized nvPM measurement system
- Vary combustor inlet air conditions (range of ambient conditions on the ground and at altitude) and measure nvPM emissions
- Use probe designs that minimize losses and sample representatively
- Develop isokinetic sampling techniques such that particles are not over-sampled or under-sampled.
- Perform rig testing using Jet-A fuel; and three alternative fuels
- Analyze data to inform performance-based nvPM emissions modeling for all altitudes

Since the nvPM emissions from aircraft engines are affected by changing inlet conditions, a combustor rig test provides the most flexibility to quantify the impact of changing ambient or altitude conditions on the nvPM mass and number emissions and to develop correlations for use in inventory modeling or regulatory purposes.

In order to successfully complete these new tasks, the existing contracts will need an extended period of performance and will result in additional cost.

Task 2- Ground-based nvPM Emissions from an IAE V2527-A5 Engine Burning Four Different Fuel Types
Missouri University of Science and Technology

Objective(s)

1. Measure engine emissions from four different fuel types on the ground using NARS and its ancillary equipment and compare it to the NASA measurement system and where appropriate quantify differences. Specifically, the research team will:
    a. Deploy to Europe
    b. Make measurements and analyze data.
2. Contribute to planning the emissions measurements at various altitudes and evaluate cruise nvPM models.

Research Approach
The Missouri University of Science and Technology (Missouri S&T) owns and operates an Annex 16 compliant, North American mobile reference system to measure nvPM emissions from the exhaust of aircraft engines. The nvPM system consists of three sections – collection, transfer, and measurement – connected in series (Figure 1). A description of each section is provided below.

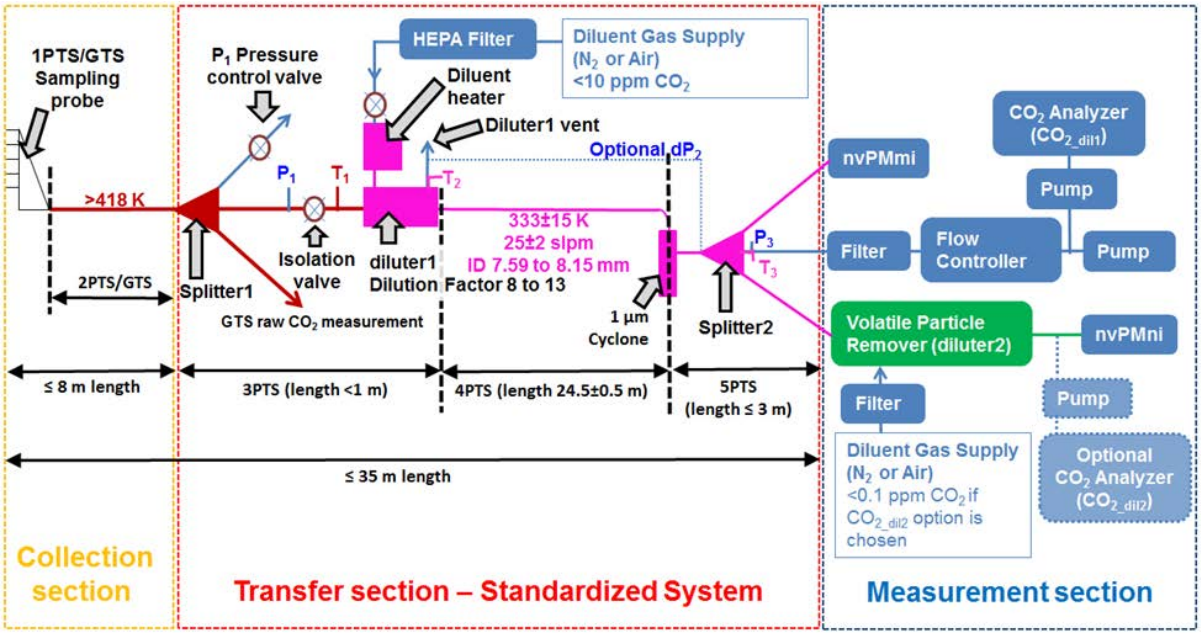


Figure 1. Components of an ICAO Annex 16 Vol.II Appendix 7 Compliant nvPM system

Collection section
The collection section consists of the probe rake system and up to 8m of stainless sample line heated to 160˚C.

Transfer section
The transfer section consists of a three-way sample splitter, a PM sample eductor/dilutor, flow controllers, and sample line heater controllers. The first sub-component of the transfer section is a three-way sample splitter which divides the total exhaust gas sample from the rake into three flow streams. The first is the required flow of exhaust for the Annex 16 combustion gas sample. The second is the PM sample and the third is an excess flow dump line controlled with a pressure relief valve. The PM sample is diluted by a factor 8-13 with dry nitrogen (heated to 60˚C) by means of an eductor/dilutor. The diluted PM sample with a flow rate 25 ± 2 SLPM is transferred by an electrically heated, temperature controlled conductive, grounded, carbon loaded PTFE PM sample transfer line 25m in length, maintained at 60˚C to a 1µm cyclone and then a second three-way splitter to direct the sample to the number and mass measurement devices in the measurement system.

Measurement section
The measurement section consists of a volatile particle remover and a particle number measurement device, a mass measurement device and a mass flow controller, pump and CO_2 detector as specified by Annex 16
As part of evaluating the methodology and the robustness of the system described in Annex 16, the North American nvPM reference system has been deployed at several OEM facilities in North America as well as the SR Technics maintenance facility in Zurich, Switzerland. These demonstration/inter-comparison studies served to provide information regarding the variability of the individual sampling and measurement systems. Additional testing at OEM facilities has also be conducted to acquire QL2 data on a set of engines identified to be representative of the commercial fleet for entry into the nvPM values database. Datasets from these initial measurement activities are being used by the ICAO Committee on Aviation Environmental Protection (CAEP) and their PM Task Group (PMTG) as they consider future aviation PM regulations. The data will be used by PMTG to develop a metric on which the regulation for nvPM emissions will be based. In this task Missouri S&T and its sub-contractor Aerodyne Research Inc. will use the North American Reference System to measure engine emissions from four different fuel types on the ground using NARS and its ancillary equipment and compare it to the NASA measurement system. And where appropriate quantify differences.



Task 4.1- Contribute to planning the emissions measurements at various altitudes and evaluate cruise nvPM models
In this task the primary objective of the MS&T team will be to work closely with the ND-MAX principal investigators to plan the logistics and test matrices of the proposed emission measurements at ground level and at altitude including an inter-comparison of the NARS data with that acquired with the NASA/DLR deployed nvPM measurement systems. The secondary objective of this task will be to evaluate models predicting cruise nvPM emissions by comparing the model results with the in-situ and ground-based measurements.

Task 2.2- Prepare the NARS and ancillary equipment for deployment to test site in Germany
In this task the NARS sub-systems will be laboratory tested at Missouri S&T and Aerodyne to assure they meet operational specification as defined in AIR6241/ARP 6320. On completion of laboratory testing the NARS and ancillary equipment will be packaged and shipped to the test site in Germany.

Task 2.3- Deploy to and set up the NARS at an airfield in Germany
In this task the MS&T team will deploy to the test site in Germany and set up the NARS and ancillary equipment and undertake sub-system check-out procedures in preparation for emissions testing.

Task 2.4- Conduct ground-based emissions measurements on four different aviation fuels
In this task the MS&T team will use the NARS and ancillary equipment to characterize the nvPM component of emissions from four separate fuels to be defined by the test matrix established in the work described in task 6.

Task 2.5- Tear-down and ship NARS and ancillary equipment to MS&T
In this task the MS&T team will tear down the NARS and ancillary equipment and package it for return shipment to the US.

Task 2.6- Reduce, analyze and report nvPM data
In this task the raw emissions data acquired during task 3 will be reduced and analyzed using the methods described in AIR6241/ARP 6320. These data will be reported to the FAA and shared with the ND-MAX participants.

Milestone(s)
The airborne and ground-based phases of the ND-MAX campaign have been successfully executed. Data analysis and interpretation is underway.

Major Accomplishments
Measured the emissions from 4 different fuels – 2 conventional sources of Jet A1 and two specifically designed sustainable alternative jet fuels (SAJFs) blended to 50% with each of the conventional fuels. The SAJFs were designed to have naphthalene contents that differed by an order of magnitude.

The two SAJFs, yielded substantial reductions in soot emissions when compared to the two unblended conventional Jet A-1 fuels. The percent reductions decrease with fuel flow rate (%N1).

The PM emissions were observed to decrease with increasing fuel hydrogen content.

No statistically significant differences in PM emissions were observed when the two SAJF blends were compared.

Organic PM emissions were found to be insensitive to fuel type and had a distinct mode at 268nm. Compositional analysis revealed the organic PM to be due to vented lubrication oil and not a product of combustor emissions.

Publications
None

Outreach Efforts
Presentations on the data analysis and interpretation to date have been made at:
- ASCENT advisory board meetings held in Cambridge MA in April 2018 and Washington DC October 2018
- AEC Roadmap Meeting held in Washington DC in May 2018



- It is scheduled to be presented at the AGU Fall Meeting in session A33K – Improving the Science of Emissions through Inventories, Observations and Models III, 12 December 2018, Washington DC.

Awards
None

Student Involvement
No graduate students were employed in this task however four undergraduate research assistants were employed in pre- and post-test activities including individual component testing and calibration and data reduction and interpretation.

Plans for Next Period
Attend ND MAX workshop in Hampton VA 17-19 October 2018. Continue with instrument inter-comparisons especially between other ground-based systems and their in-flight equivalents. Present paper at AGU Fall Meeting in DC 10-14 December 2018. Publish results Spring 2019.



Project 003 Cardiovascular Disease and Aircraft Noise Exposure

Boston University

Project Lead Investigator

Junenette L. Peters
Assistant Professor
Department of Environmental Health
Boston University School of Public Health
715 Albany St., T4W, Boston, MA 02118
617-358-2552
petersj@bu.edu

University Participants

Boston University (BU)

- P.I.(s): Jonathan Levy (University PI); Junenette Peters (Project PI)
- FAA Award Number: 13-C-AJFE-BU-002;
- Period of Performance: October 1, 2017 to September 30, 2018

Tasks:

1. Assign aircraft noise exposures over time to geocoded participant addresses for new cohorts - Nurses' Health Study (NHS), NHSII, NHS3, Health Professional Follow-up Studies (HPFS), and HPFS2.
2. Link aircraft noise exposures to participant data for NHS, NHSII, NHS3, HPFS, and HPFS2.
3. Determine the numbers of cardiovascular disease (CVD_-related outcomes of interest available in NHS, NHSII, and HPFS participants living near airports.
4. Develop and execute models for estimating CVD health risks associated with aircraft noise exposure.

Project Funding Level

Total Funding $340,000
Matching: $294,867
Source of Matching: Non-federal donors to the NHS and HPFS cohorts

Investigation Team

Junenette Peters, PI, Boston University

Dr. Peters is responsible for directing all aspects of the proposed study, including study coordination, design and analysis plans, and organizing co-investigator meetings.

Jonathan Levy, Boston University

Dr. Levy will participate in the noise exposure assessment effort and provide expertise in the area of predictive modeling and air pollution.

Francine Laden and Jamie Hart, Harvard University

Dr. Laden is our NHS and HPFS sponsor for this ancillary study. Dr. Jamie Hart's will assign aircraft noise exposures to cohorts' participant geocoded address coordinates. Dr. Laden and Dr. Hart will also assist with documentation of data from the NHS and HPFS based on previous experience working on air pollution and chronic disease outcomes research in these cohorts.



Project Overview

Aircraft noise is a considerable source of stress among near-airport communities. Exposure has been associated with sleep disturbance, physiological responses and psychological reactions, with corresponding effects on blood pressure. However, the extent to which aircraft noise increases the risk of cardiovascular disease (CVD) has not been fully elucidated. Likewise, the role of CVD risk factors in mediating an association between noise and CVD has not been assessed. Additionally, exposure assessment that includes time-varying and spatially resolved noise exposures has not been systematically incorporated into previous epidemiological studies, making it key to receive aircraft noise data over multiple years. FAA PARTNER 44 and ASCENT 03 projects provided the pilot data and collaborations necessary to successfully compete for National Institute of Health (NIH) funding to evaluate noise effects on cardiovascular outcomes in the longitudinal Women's Health Initiative (WHI) cohorts. This study proposes to extend ongoing efforts in the WHI and evaluate the effects of aircraft noise exposure on cardiovascular disease in both women and men in the longitudinal Nurses' Health Studies (NHS, NHSII, and NHS3) and companion Health Professional Follow-up Study (HPFS and HPFS2) cohorts. These studies began with the original cohort (NHS) in 1976 and is currently recruiting the third generation (NHS3), with over 330,000 total participants.

The proposed scope of this research effort would involve multiple years, with activities within Phase I providing the foundation for future activities. The objectives for this year include: 1) Determining noise exposure estimates for study participants; 2) Linking noise exposure estimates to participant data on outcomes (health effects) and other risk factors; 3) Developing and executing models to evaluate cardiovascular effect(s) of noise.

Tasks based on receiving noise data for 90 airports over time in multiple metrics:

- Initially projected timeline for receiving data for 2000, 2005 and 2010 – March 2015
- Also negotiated for noise data for additional years (1995 and 2015)

However, data was modeled by two facilities (Wyle and Volpe) using different methods and assumptions. Data for 37 airports needed to be rerun to harmonize data.

- Received data from rerun of 37 airport for key metrics – October 2017.
- Received data from rerun for remaining metrics – November 2017.
- Performed quality assurance/quality control and requested corrections.
- Received final data for all metrics – August 2018.

Task 1- Assign Aircraft Noise Exposures Over Time to Geocoded Participant Addresses

Boston University

Objective

To intersect geocoded addresses available from 1995 to 2015 with noise surfaces obtained.

Research Approach

We will intersect geocoded addresses with noise contours available from 1995 to 2015. Given the longitudinal nature of this study, noise exposures will be assigned reflecting specific residential addresses over time based on participant address histories. We will estimate the percent of participants across noise exposure categories (e.g., DNL > 55 dB) and assess overall trends in participant noise exposure levels over time.

Milestone

(Dependent on receiving noise data – originally projected for March 2015; actual date of final receipt of August 2018)

- Assign aircraft noise exposures – November 2016

Major Accomplishments

- Collaborated with Volpe to develop a final aircraft noise modeling documentation (metadata).



- Received aircraft noise data for airports for the years 1995, 2000, 2005, 2010, 2015. Metrics received include Day-Night Average Sound Level (DNL), Equivalent Sound Level (Leq) Day and Leq Night, Time above Threshold (TA) 65 dB and TA 85 dB.
- Performed quality assurance/quality control for noise contours for all 90 airports.
- Received final corrected data for 90 airports and 5 metrics and 5 years.
- Processed DNL data.
- Estimated noise exposure in DNL for participants of NHS, NHSII, HPFS.
- Estimated the number of people exposed to aircraft noise for the NHS and NHSII cohorts (Figure 1) based on those free of hypertension (see Table 2).

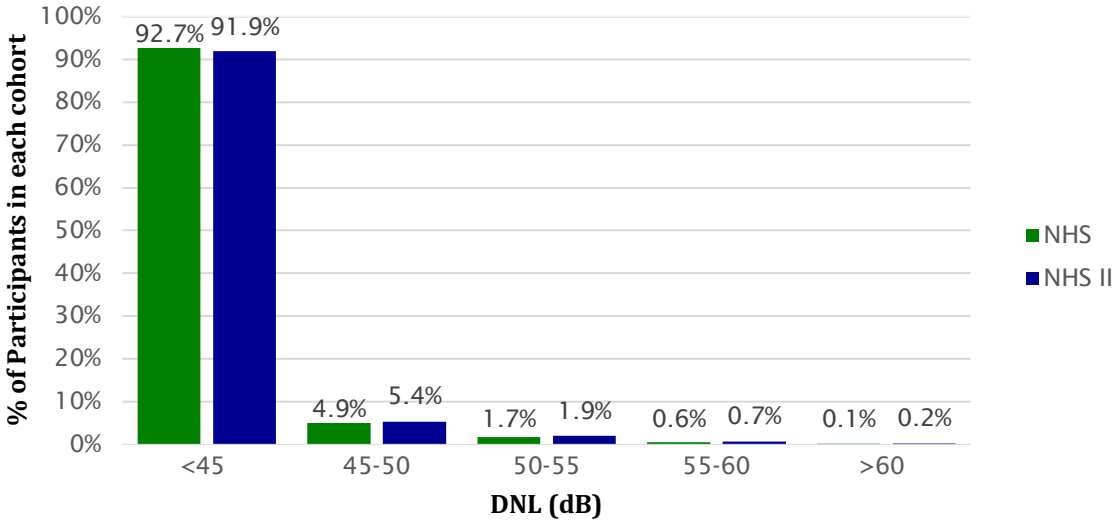


Figure 1: Distribution of aircraft noise (DNL) in those free of hypertension at baseline (1995)

Task 2- Link Aircraft Noise Exposures to Participant Data for NHS, NHSII, NHS3, HPFS, and HPFS2

Boston University

Objective

To link with the individual level information in NHS and HPFS.

Research Approach

We will link information with the wealth of individual level information on socio-demographics (e.g., age, race/ethnicity, education); lifestyle factors (e.g. physical activity/exercise, diet, smoking, alcohol consumption); and relevant outcomes (e.g., hearing and hearing loss, sleep disturbance, diabetes, CVD and CVD mortality).

Milestone

Link aircraft noise exposures to individual data for all cohorts – December 2016

Major Accomplishments

Linked aircraft noise exposures in DNL to individual cohort data for NHS and NHSII (see Tables 1 and 2).

Task 3- Determine the Numbers of CVD-Related Outcomes of Interest Available in NHS, NHSII, and HPFS Participants Living Near Airports

Boston University

Objective

To identify all cases of overall and cause-specific incident cardiovascular, cardiovascular mortality and incident hypertension.

Research Approach

We will identify all cases of overall and cause-specific incident CVD, CVD mortality, and incident hypertension among individuals in the NHS, NHSII, and HPFS living within the 45 dB contours. These cohorts have been followed over a long enough period (over two to four decades) to observe health outcomes and participants are of an age when they are at risk for CVD.

Milestones

Determine the number of cardiovascular-related outcomes among those living near airports – January 2016

Determine the number of participants at risk for cardiovascular disease (free of CVD at baseline/earliest time with available noise data [1995]).

Major Accomplishments

Determined the number of cohort participants alive and free of CVD at baseline (1995). Preliminary characteristics of participants provided in Table 1.

Table 1. Characteristics of participants alive and free of CVD at baseline (1995)

Characteristics	NHS	NHSII	HPFS
Number of Participants	96,000	115,000	50,000
	Mean ± SD or %		
Age (years)	68.6 ± 7.3	46.6 ± 7.0	63.8 ± 10.2
Body mass index (kg/m^2)	25.6 ± 7.5	21.2 ± 3.2	26.6 ± 11.5
Race (%)			
Black	2	2	6
White	94	96	91
Other/Multiple races	6	2	3
Smoking Status (%)			
Never	45	64	40
Former	45	25	41
Current	11	9	6
Family History of MI	32	22	13

Determined the number of cohort participants alive and free of hypertension (self-reported) at baseline (1995). Characteristics provided in Table 2.

- Study Period
  - NHS: 1994-2007
  - NHS II: 1995-2006
- Exclusion Criteria
  - No diagnosed hypertension at the entrance into our study
  - No missing noise or air pollution data



Table 2. Characteristics of participants alive and free of hypertension at baseline (1995)

Characteristics	NHS	NHSII
Number of Participants	61,876	94,588
	Mean ± SD or %	
Age (years)	59 ± 7	40 ± 5
Race - White (%)	95	93
Post-Menopausal (%)	88	7
Family History of Hypertension (%)	36	49
Smoking Status (%)		
Never	43	65
Former	41	24
Current	15	11
Census Track Medium Income (USD in $1000)	65 ± 26	64 ± 24

Task 4- Develop and Execute Models for Estimating CVD Risk Associated with Noise Exposure in NHS, NHSII, and HPFS

Boston University

Objective

To develop appropriate measures to evaluate the effects of aircraft noise on cardiovascular outcomes.

Research Approach

The team will develop hazard models for estimating time varying CVD risk associated with noise exposure in the vicinity of each airport. We will also explore methods to account for clustering and spatial correlation between individuals living near each airport. We will then conduct epidemiological analyses to estimate the health effects of noise exposure on each CVD outcome controlling for other risk factors thought to be related to CVD

Milestones

Develop models for estimating cardiovascular health risks associated with aircraft noise exposure – January 2016

Perform analysis of cardiovascular health risks associated with aircraft noise exposure – June 2016

Major Accomplishments

- Developed model for estimating hypertension associated with aircraft noise exposure using DNL.
    - Using time-varying Cox hazards model (allows for changes in exposure and risk factors over time)
        - dichotomizing self-reported hypertension (yes/no)
        - dichotomizing noise exposure (DNL >44, >50, >55, and >60 dB)
        - adjusting for: medication use, race, region, smoking history, area-level income, area-level housing value, air pollution, BMI, alcohol consumption, diet, menopausal status, family history of hypertension, physical activity, latitude, diabetes status
- Performed initial analysis of association of aircraft noise (DNL) and the risk of hypertension.
- Submitted abstract titled 'Time-varying aircraft noise exposure and incident hypertension in the Nurses' Health Study' to professional society conference (joint meeting of the International Society of Exposure Science [ISES] / International Society for Environmental Epidemiology [ISEE]).
- Presented preliminary analysis at the ISES/ISEE joint meeting.
    - Preliminary Results: Incidence of hypertension is increased with increased DNL, but statistically non-significant



Publications

- Peters JL, Zevitas CD, Redline S, Hastings A, Sizov N, Hart JE, Levy JI, Roof CJ, Wellenius GA. Aviation noise and cardiovascular health in the United States: a review of the evidence and recommendations for research direction, Current Epidemiology Reports 2018; 5(2):140–152. doi.org/10.1007/s40471-018-0151-2.

Outreach Efforts

Developed and submitted abstracts and presented at professional conference (joint meeting ISES/ISEE).

- Nguyen DD, Levy J, Hart JE, VoPham T, Simon MC, Malwitz A, Laden F, Peters JL. Characterizing temporal trends in aviation noise surrounding U.S. airports, ISES/ISEE 2018 Annual Joint Meeting, August 2018 (oral).
- Simon MC, Hart JE, Levy J, VoPham T, Lane KJ, Fabian MP, Nguyen DD, Laden F, Peters JL. Sociodemographic patterns of exposure to civil aircraft noise, ISES/ISEE 2018 Annual Joint Meeting, August 2018 (poster).
- Kim CS, Hart JE, Levy JI, VoPham TM, Simon MC, Nguyen DD, Malwitz A, Laden F, Peters JL. Time-varying aircraft noise exposure and incident hypertension in the Nurses' Health Study, ISES/ISEE 2018 Annual Joint Meeting, August 2018 (oral).

Awards

None

Student Involvement

Chloe Kim (doctoral candidate) dissertation includes aspects of Task 4 – developing and executing models on noise and hypertension risk. Chloe presented on 'Time-varying aircraft noise exposure and incident hypertension in the Nurses' Health Study' at the joint meeting of ISES/ISEE.

Daniel Nguyen (doctoral candidate) presented on 'Characterizing temporal trends in aviation noise surrounding U.S. airports' at the joint meeting of ISES/ISEE.

Plans for Next Period

(TBD [*awaiting funding*] to September 30, 2019)

- Assign noise exposure estimates to participants for additional metrics (Leq Day and Leq Night and TA 65dB and TA 85 dB).
- Finalize models estimating CVD-related risks factors (e.g., hypertension) associated with aircraft noise exposure and develop manuscript for publication in peer-reviewed journal.
    - Perform analysis using DNL for HPFS.
    - Perform analysis using Leq Night for all cohorts.
    - Perform meta-analysis combining the results for all three cohorts – NHS, NHSII, and HPFS.
- Execute models estimating risk of CVD associated with aircraft noise exposure.
- Develop abstracts for presentation at professional conferences.
- Determine the number of newly recruited participants (NHS3) residing near airports from whom survey questions or measurements of noise and sleep disturbance may be obtained.
- Develop suite of survey questions on built environment and noise perception.



Project 005 Noise Emission and Propagation Modeling

Pennsylvania State University
Purdue University

Project Lead Investigator

Victor W. Sparrow
Director and United Technologies Corporation Professor of Acoustics
Graduate Program in Acoustics
Penn State
201 Applied Science Bldg.
University Park, PA 16802
+1 (814) 865-6364
vws1@psu.edu

University Participants

Pennsylvania State University

- P.I.: Victor W. Sparrow, United Technologies Corporation Professor of Acoustics
- FAA Award Number: 13-C-AJFE-PSU, amendments 005, 015, 029
- Period of Performance: August 18, 2014 to December 31, 2017
- Task(s):
    1. Assess applicability of meteorological reanalysis models for possible use in FAA noise tools
    2. Assess measurement data sets for noise propagation model validation

Purdue University

- P.I.(s): Kai Ming Li, Professor of Mechanical Engineering
- FAA Award Number: 13-C-AJFE-PU, amendments 002, 007, 009, 016
- Period of Performance: June 1, 2014 to June 2017
- Task(s):
    3. Extend model for fast moving sources (completed)

Project Funding Level

FAA funding to Penn State in 2014-2015 was $132K and in 2015-2016 was $110K. FAA funding to Purdue in 2014-2015 and 2015-2016 was $80K and $90K, respectively.

In-kind cost sharing from Vancouver Airport Authority received in October 2016 was $294,500 to Penn State and $294,500 to Purdue. The point of contact for this cost sharing is Mark Cheng, mark_cheng@yvr.ca. Project support is in the form of aircraft noise and trajectory data, meteorology data, and consulting on those datasets.

Investigation Team

Penn State

Victor W. Sparrow (PI)
Graduate Research Assistant Rachel Romond (meteorological reanalysis data investigation)
Graduate Research Assistant Manasi Biwalkar (measurement data sets for model validation investigation)

Purdue

Kai Ming Li (PI)
Graduate Research Assistant Bao Tong (moving source investigation)
Graduate Research Assistant Yiming Wang (moving source investigation)



Project Overview

The FAA has been funding research efforts in developing enhanced noise emission and propagation capabilities to better support environmental impact studies at both local and national levels. The main emphasis in the near and mid-term is to increase the Research Readiness Level (RRL) of the capabilities so that they can be further matured for implementation into the FAA tools. Validation of the modeling capabilities has been the central focus of the project. Via recent US-EU research collaboration, the field measurement database (BANOERAC) is becoming available for model validation. This database contains acoustic time history of flight events from various types of commercial aircraft during cruise, climb and descent phases of the flight. In addition, the DISCOVER/AQ and Vancouver Airport Authority databases have already come on line for use in this and other FAA projects. These datasets make model validation possible. In addition, the work will make existing models ready for simulating real weather conditions via proper treatment of the meteorological input parameters and to establish a common basis for comparing US and EU models.

Task 1 - Assess applicability of meteorological reanalysis models for possible use in FAA noise tools

Task 2 - Assess measurement data sets for noise propagation model validation

Pennsylvania State University

Objective(s)

The objective of Project 5, Task 1 was to determine if meteorological reanalysis datasets and corresponding input parameters are useful for aircraft noise propagation prediction and whether the same can be integrated into the AEDT noise analysis framework. The objective of Project 5, Task 2 was to begin examination of aircraft measurement databases and ascertain their applicability for validating aircraft noise prediction tools.

Concluding Work

All of the tasks for ASCENT Project 5 have been completed. In the period October 1, 2017 until September 30, 2018 covered by this annual report, Penn State paid for and received the BANOERAC flight trajectory data from ANOTEC Engineering of Motril, Spain. BANOERAC stands for “Background noise level and noise levels from en-route aircraft” and that European project concluded in 2009. Specifically, Project 5 had funds budgeted to obtain the BANOERAC flight trajectory data through ANOTEC. Since the beginning of the project, Penn State has been working with ANOTEC Engineering to obtain suitable data sharing agreements with the European Aviation Safety Agency (EASA) for the use of the BANOERAC dataset for ASCENT research.

ANOTEC had the raw ADS-B data to calculate the flight trajectories, but never produced those trajectories under EASA funding. ASCENT Project 5 was no-cost extended to December 31, 2017 to ensure that a Penn State purchased services agreement to ANOTEC would remain in place so that ANOTEC could provide those flight trajectories.

In early 2017, the data sharing agreements were put into force, and in the spring and summer of 2017 Penn State worked with ANOTEC to establish a purchased services agreement. ANOTEC delivered the BANOERAC flight trajectory data to Penn State and Purdue on November 20, 2017.

The BANOERAC data is now being used in the ongoing ASCENT Project 40.

Milestone(s)

N/A

Major Accomplishments

The BANOERAC data, including the flight trajectory data, was received by Penn State and Purdue.

Publications

None

Outreach Efforts
None

Awards
None

Student Involvement
None

Plans for Next Period
None

References
BANOERAC Project final report, Document ID PA074-5-0, ANOTEC Consulting S.L. (2009).



Project 008 Noise Outreach

The Pennsylvania State University

University Members

Penn State Applied Research Laboratory Team Lead	Kathleen Hodgdon
Penn State Earth & Environmental Systems Institute	Bernd Haupt

Advisory Committee Members

Gulfstream Aerospace Corporation	Robbie Cowart
Port of Portland Sr. Noise Analyst	Jason Schwartz
Volpe National Transportation Systems Center	Juliet Page

Project Lead Investigator

Kathleen Hodgdon
Research Associate
Applied Research Laboratory
Pennsylvania State University
ARL North Atherton Street
P.O. Box 30 (Mail Stop 2210H)
State College PA 16804-0030
Phone: 814-865-2447
Email: kkh2@psu.edu

University Participants

Pennsylvania State University

- P.I.: Kathleen Hodgdon, Research Associate
- Researcher: Maurie Caitlin Kelly, Research Associate
- Researcher: Bernd Haupt, Senior Research Associate
- FAA Award No.:13-C-AJFE-PSU Amendment 36
- Period of Performance: July 31, 2017 to July 31, 2018
- Task(s):
  1. Stakeholders Interactions
  2. Content Development
  3. Site Navigation and Infrastructure Enhancement

Project Funding Level

This project supports the Outreach efforts at Penn State with $25K of FAA funds. Matching funds are anticipated to satisfy cost share on all tasks.

Investigation Team

For 2017-2018 the investigation team includes:
P.I.: Kathleen Hodgdon Research Associate
Researcher: Bernd Haupt Senior Research Associate

Project Overview

Aviation noise issues can be complex. The NoiseQuest website is designed to support noise mitigation through information. NoiseQuest, located at www.noisequest.psu.edu, is an international resource that is designed to implement global education on aviation noise topics. The site presents aviation noise information that provides centralized web based



educational outreach for all communities. This supports Outreach efforts for airports too small to have their own outreach programs, and provides additional outreach for airports with an existing outreach program.

The PSU Outreach team has continued to expand and enhance the NoiseQuest website. Over the last year we completed site reconfiguration and restructuring to a device agnostic format to make the site more mobile friendly. The content was reviewed and refreshed as part of the restructuring of the site to be accessible across all platforms.

Task 8.1- Stakeholders Interactions

Pennsylvania State University

Objectives

The Outreach project seeks to improve airport and community interactions by providing information and education on aviation noise topics. The team interacted with stakeholders and identified publications and concepts for content to be shared on the NoiseQuest site.

Research Approach

Interactive outreach with stakeholders was conducted to identify concerns that could be addressed by expanded content topics. Efforts to obtain additional GIS noise contour data for the NQ Explorer were not conducted during the completion of the site redesign. The site user statistics were monitored to better inform the site development.

Milestones

We communicated with aviation stakeholders to identify updates for existing content and opportunities for new content development.

Major Accomplishments

We continue to interact with airport noise managers and community groups to identify topics of interest, successful implementations of outreach, or other approaches taken to resolve aviation noise issues. We continue to monitor our site statistics to gain insights on site usage (see Appendix A for Site Statistics).

Publications

Contents are published at www.noisequest.psu.edu.

Outreach Efforts

We interact with airport noise managers and stakeholders from across the country.

Awards

None

Student Involvement

None

Plans for Next Period

We will continue to monitor site statistics to determine site usage patterns. To promote greater site usage, we will work to get additional stakeholders to link to NoiseQuest and to provide recommendations for content.

Task 8.2- Content Development

Pennsylvania State University

Objectives

This task focuses on identifying and developing content that addresses aviation noise impact and outreach education.



Research Approach
The Outreach team seeks to identify content that presents updates on aviation noise research, addresses noise issues, or meets the educational outreach needs of aviation stakeholders on specific topics.

Milestones
The team maintained existing site areas and added new content.

Major Accomplishments
The content organization was reviewed as part of site restructuring to be accessible across all platforms.
General content across the site was updated. Content on AEDT, NextGen and Performance-Based Navigation were updated and enhanced.

Publications
Site developed at www.noisequest.psu.edu

Outreach Efforts
We develop the Outreach content by reaching out to stakeholders for content ideas and development.

Awards
None

Student Involvement
None

Plans for Next Period
Content is currently in development. The plans for the future included generating enhanced content to further engage the public. The existing site content will be enhanced with content, graphics, videos and presentations. New content topics will be identified and relevant features added to the site. This would include features such as additional videos and images across site, additional Supersonics low boom "sonic thump" content, additional helicopter and rotorcraft noise abatement content, and additional GIS noise contours for NQ Explorer. We plan to add an NQ Explorer tab under Community Tools once we have more contours added to that section of the site. Other topics will be identified based on stakeholder engagement.

Task 8.3- Site Navigation and Architecture Redesign and Development
Pennsylvania State University

Objectives
Efforts under this task maintain the site architecture and enhance site navigation.

Research Approach
This effort includes website management including backups, updates, and infrastructure enhancement. The team works to assure that the information on NoiseQuest is presented in an easily navigated user-friendly format.

Milestones
Review of the site was completed and updates and new content was posted to the site. During the review, broken links were identified and addressed.

Major Accomplishments
The site was reworked, with changes to the navigation features and content areas. To monitor usage of the entire site, website statistics can be viewed using Google Analytics. Changes were made to navigational aspects of the site to facilitate the ease of use across multiple platforms.



Publications
None

Outreach Efforts
The team works to ensure that the changes resulted in clarity and ease of navigation across multiple platforms. These actions were taken to facility ease of use on mobile devices so as to increase the mobile user base.

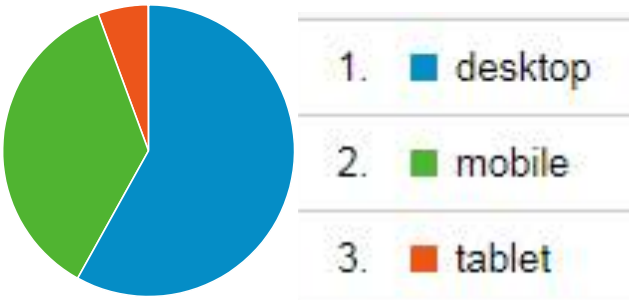
Awards
None

Student Involvement
None

Plans for Next Period
The site is now device agnostic and user-friendly on all platforms simultaneously. We need to further address some of the previously observed issues related to Google Map's API within the NQ Mapper in the NQ Explorer. The team will continue website management which includes backups, updates, and infrastructure enhancement as warranted.

Appendix A. NoiseQuest Statistics Recent Usage

NoiseQuest	Page views	% Page views	Avg. Time on Page
Most Active Pages	18,710	100	0:01:48
Noise basics-basics	3,571	19.09	0:02:26
Home page	2,809	15.01	0:01:18
National airspace-types of airp orts	2,383	12.74	0:04:07
Community tools-FAQ	1,571	8.40	0:03:01
Noise effects-reducing noise	872	4.66	0:04:40
Community tools-glossary	756	4.04	0:01:24
NQ explorer	586	3.13	0:01:38
Community tools-homebuyers	459	2.45	0:00:56
Sources of noise-overview	361	1.93	0:02:46
Noise basics-noise models	363	1.94	0:02:10



Device	Users	% Users
Category	10,431	100
desktop	6,058	58.08
mobile	3,787	36.31
tablet	585	5.61



Project 010 Aircraft Technology Modeling and Assessment

Georgia Institute of Technology and Purdue University

Project Lead Investigators

Dimitri Mavris (PI)
Regents Professor
School of Aerospace Engineering
Georgia Institute of Technology
Mail Stop 0150
Atlanta, GA 30332-0150
Phone: 404-894-1557
Email: dimitri.mavris@ae.gatech.edu

William Crossley (PI)
Professor
School of Aeronautics and Astronautics
Purdue University
701 W. Stadium Ave
West Lafayette, IN 47907-2045
Phone: 765-496-2872
Email: crossley@purdue.edu

Jimmy Tai (Co-PI)
Senior Research Engineer
School of Aerospace Engineering
Georgia Institute of Technology
Mail Stop 0150
Atlanta, GA 30332-0150
Phone: 404-894-0197
Email: jimmy.tai@ae.gatech.edu

Daniel DeLaurentis (Co-PI)
Professor
School of Aeronautics and Astronautics
Purdue University
701 W. Stadium Ave
West Lafayette, IN 47907-2045
Phone: 765-494-0694
Email: ddelaure@purdue.edu



Executive Summary

Georgia Tech and Purdue partnered to investigate the future demand for supersonic air travel and the environmental impact of supersonic aircraft. In the context of this research, environmental impacts includes direct CO_2 emissions and fuel consumption. The research was conducted as a collaborative effort in order to leverage capabilities and knowledge available from the multiple entities that make up the ASCENT university partners and advisory committee. The primary objective of this research project was to support the Federal Aviation Administration (FAA) in modeling and assessing the potential future evolution of the next generation supersonic aircraft fleet. Research under this project consisted of four integrated focus areas: (1) Developing a set of harmonized fleet assumptions for use in future fleet assessments; (2) Modeling environmental impact of supersonic vehicles expected to enter the fleet through 2050; (3) Analyzing supersonic vehicle performance using AEDT and (4) Performing vehicle and fleet level assessments based on input from the FAA and the results of (1) and (2).

To develop suitable assumptions for the fleet level analysis incorporating new supersonic vehicles, it is necessary to forecast the future demand for supersonic air travel. Georgia Tech followed a two-step approach that first examines historical data to identify current premium demand (business and first class), and then estimates how such demand would scale for supersonic travel. The first step relied heavily on data derived from the Bureau of Transportation Statistics (BTS) databases, especially the Airline Origin and Destination Survey (DB1B) database, which provided information on passenger itineraries based on a 10% sampling of airline tickets from reporting carriers. For the second step, cost data documented by Airlines for America (A4A) was utilized. The A4A Passenger Airline Cost Index (PACI) was used to establish a baseline airline cost structure based on current operating costs. That structure was then scaled to estimate that of a supersonic airliner. Together, the two steps provided a better understanding of potential demand for future commercial supersonic travel from both a passenger and an airline perspective.

In an independent, but complementary, approach to consider demand and routes for supersonic aircraft, the Purdue team developed a ticket pricing model for possible future supersonic aircraft that relies upon current as-offered business class and above fares for routes that could have passenger demand for supersonic aircraft. Via an approach that considered the size of the potential business class and above demand on a city pair route, the distance of that city pair route, and an adjustment to allow for the shortest trip time by increasing overwater distance of the route, the Purdue team identified 26 potential routes for supersonic aircraft. By providing these potential routes to the FLEET (Fleet-Level Environmental Evaluation Tool) simulation, the allocation problem in FLEET then determines how many supersonic aircraft operate on these routes, giving a prediction of which routes would see supersonic aircraft use and an idea of the number of supersonic flights operated on those routes.

To provide a preliminary estimate for the performance of supersonic vehicles, the Georgia Tech team started by establishing a reference performance for a subsonic vehicle. Quantitative estimates for the impact of supersonic vehicles on the various KEIs, especially fuel efficiency, were then derived based on literature review, future performance targets set by NASA, and engineering judgement. For an appropriate estimation, performance parameters such as cruise lift-to-drag ratio and engine-specific fuel consumption (SFC) values were required. Those values could be determined from preliminary constraint, mission and utilization analyses conducted based on the vehicle's design mission requirements. Georgia Tech developed rapid, interactive tools that incorporated such analyses. They were calibrated using publicly available data for the Concorde and utilized to estimate the impact for two concept supersonic vehicles. The first vehicle represents a 10-12 passenger business jet, while the second represents a 50-60 passenger airliner.

In order to facilitate environmental impact prediction of supersonic aircraft, it was necessary to identify modeling capabilities and potential gaps in existing tools. Georgia Tech identified existing supersonic aircraft models in the AEDT vehicle database, including the Concorde and some military aircraft. These models were reviewed as to how these aircraft were modeled. Coefficients in the AEDT vehicle modeling definitions were identified that pertain to the specifics and peculiarities of those vehicles. Publicly available data were used to gauge the accuracy of AEDT.

Georgia Tech and Purdue exercised their respective fleet analysis tools (GREAT and FLEET and produced for estimates of the fleet level impact of a potential fleet of supersonic aircraft operating in the future.

The outcome of this study is intended to provide a glimpse into the future potential state of supersonic air travel using preliminary estimates of supersonic vehicle performance. Future works should build on the current estimates to conduct more detailed vehicle and fleet performance analyses.



Table of Acronyms

AEDT	Aviation Environmental Design Tool
ANGIM	Airport Noise Grid Integration Model
APU	Auxiliary Power Unit
ASPM	Airspace System Performance Metrics
BADA	Base of Aircraft Data
BPR	Bypass Ratio
BTS	Bureau of Transportation Statistics
CAEP	Committee on Aviation Environmental Protection
CLEEN	Continuous Lower Energy, Emissions, and Noise
CMC	Ceramic Matrix Composite
CMO	Current Market Outlook
DNL	Day-Night Level
DOE	Design of Experiments
ECU	Electronic Control Unit
EDS	Environmental Design Space
EIA	Energy Information Administration
EIS	Entry into Service
EPNL	Effective Perceived Noise Level
ETS	Emissions Trading System
EU	European Union
FAA	Federal Aviation Administration
FLOPS	Flight Optimization System
FPR	Fan Pressure Ratio
GDP	Gross Domestic Product
GMF	Global Market Forecast
GREAT	Global and Regional Environmental Analysis Tool
GTF	Geared Turbofan
HPC	High Pressure Compressor
HPCPR	High Pressure Compressor Pressure Ratio
HPT	High Pressure Turbine
HWB	Hybrid Wing Body
ICAO	International Civil Aviation Organization
LPC	Low Pressure Compressor
LPCPR	Low Pressure Compressor Pressure Ratio
LSA	Large Single Aisle
LTA	Large Twin Aisle
MSC	Mission Specification Changes
NEE	Noise Equivalent Energy
NPSS	Numerical Propulsion System Simulation
nvPM	Non-volatile Particulate Matter
OEM	Original Equipment Manufacturer
OPR	Overall Pressure Ratio
PAI	Propulsion Airframe Integration
R&D	Research and Development
RJ	Regional Jet
RPM	Revenue Passenger Miles
SA	Single-Aisle (Includes both SSA and LSA Classes)
SSA	Small Single Aisle
STA	Small Twin Aisle
TRL	Technology Readiness Level
TSFC	Thrust Specific Fuel Consumption
UHC	Unburned Hydocarbons
USD	U.S. Dollars
VLA	Very Large Aircraft
WWLMINET	World Wide Logistics Management Institute Network



University Participants

Georgia Institute of Technology

P.I.(s): Dr. Dimitri Mavris (PI), Dr. Jimmy Tai (Co-PI)
FAA Award Number: 13-C-AJFE-GIT-006, -012, -022, -031, -041
Period of Performance: August 1, 2014 – August 31, 2018

Purdue University

P.I.(s): Dr. Daniel DeLaurentis (PI), Dr. William A. Crossley (Co-PI)
FAA Award Number: 13-C-AJFE-PU-004, -008, -013, -018, -026
Period of Performance: August 1, 2014 – August 31, 2018

Project Funding Level

The project was funded at the following levels: Georgia Institute of Technology ($1,547,500); Purdue University ($431,231). Cost share details for each university are below:

The Georgia Institute of Technology has agreed to a total of $1,547,500 in matching funds. This total includes salaries for the project director, research engineers, graduate research assistants and computing, financial and administrative support, including meeting arrangements. The institute has also agreed to provide tuition remission for the students paid for by state funds.

Purdue University provides matching support through salary support of the faculty PIs and through salary support and tuition and fee waivers for one of the graduate research assistants working on this project. While Purdue University provides the majority of the 1:1 cost share for the Aviation Sustainability Center of Excellence (ASCENT) 10-Purdue, an in-kind matching contribution of just under $20,000 came from a gift of the RDSwin-Pro aircraft design software from Conceptual Research Corp.

Investigation Team

Georgia Institute of Technology
Principal Investigator: Dimitri Mavris
Co-Investigator: Jimmy Tai
Fleet Modeling Technical Lead: Holger Pfaender and Mohammed Hassan
Students: Eugene Mangortey, Manon Huguenin, Patsy Jammal

Purdue University
Principal Investigator: William Crossley
Co-Investigator: Daniel DeLaurentis
Students: Kushal Moolchandani, Parithi Govindaraju, Nithin Kolencherry, Kolawole Ogunsina, Hsun Chao, Samarth Jain



Project Overview

Georgia Tech and Purdue partnered to investigate the impact of supersonic aircraft on future environmental impacts of aviation. Impacts assessed at the fleet level include direct CO_2 emissions and fuel consumption. The research was conducted as a collaborative effort in order to leverage capabilities and knowledge available from the multiple entities that make up the ASCENT university partners and advisory committee.

The primary objective of this research project was to support the Federal Aviation Administration (FAA) in modeling and assessing the potential future evolution of the next generation supersonic aircraft fleet. Research under this project consisted of four integrated focus areas: (1) Developing a set of harmonized fleet assumptions for use in future fleet assessments; (2) Modeling environmental impact of supersonic vehicles expected to enter the fleet through 2050; (3) Analyzing supersonic vehicle performance using AEDT and (4) Performing vehicle and fleet level assessments based on input from the FAA and the results of (1) and (2).

Due to extensive experience assessing the FAA Continuous Lower Energy, Emissions, and Noise project (CLEEN I), Georgia Tech was selected as the lead for all four objectives described above. Purdue supported the objectives as shown in Table 1, listing the high-level division of responsibilities.

Table 1. University Contributions

Objectives		Georgia Tech	Purdue
1	Fleet Assumptions & Demand Assessment	Identify supersonic demand drivers and supporting airports	Estimate latent demand and flight schedules for supersonic aircraft
2	Preliminary Vehicle Environmental Impact Prediction	(a) Develop estimates of Key Environmental Indicators (KEI) for supersonic aircraft relative to current technology subsonic; (b) Develop estimates of likely operating altitudes (U.S)	Support with expert knowledge
3	AEDT Vehicle Definition	Test current version of AEDT ability to analyze existing supersonic models	N/A
4	Vehicle and Fleet Assessments	Apply GREAT to estimate impact of supersonics in terms of fuel burn, water vapor, and LTO NOx	Apply FLEET to estimate impact of supersonics in terms of fuel burn, water vapor, and LTO NOx

Georgia Tech led the process of conducting literature review on potential future demand for supersonic travel for fleet and technology evolution and evaluation. This work was performed under objective 1 and the outcome was used to support objective 4. Under objective 2, Georgia Tech developed conceptual design tools to estimate the environmental impact of supersonic vehicles relative to subsonic ones. In addition, Georgia Tech used AEDT to its ability to analyze supersonic aircraft performance under objective 3. Georgia Tech also ran GREAT for multiple scenarios to assess the fleet-level impacts of supersonic vehicles.

Purdue applied their FLEET tool under objective 4, using a subset of the fleet assumptions defined in objective 1 and preliminary vehicle impact estimates from objective 2. This activity demonstrated the capabilities of FLEET for assessment of fleet-level environmental impacts as a result of new aircraft technologies and distinct operational scenarios.

Major Accomplishments

The following were the major tasks completed under ASCENT Project 10:

Fleet Assumptions & Demand Assessment

The Georgia Tech team developed preliminary estimates of potential markets and routes for supersonic aircraft based on existing market and demand data as well as a ticket price analysis. Additionally, an airline operating cost model and a



parametric aircraft cost scale model was developed in order to estimate the potential required ticket premium for airlines to be able to profitably operate a fleet of supersonic aircraft.

The Purdue team developed the approach to determine what the team calls "supersonic-eligible" routes, with several different filters that can identify routes based on distance between airports, predicted demand for supersonic flights, and percentage of the flight over water. This will provide a flexible and fast way to identify these routes.

Preliminary Vehicle Environmental Impact Prediction
Georgia Tech developed a parametric constraint and sizing environment that allows the user to define key mission parameters as well as capabilities and estimate the required engine and aircraft size and the resulting performance. This was used to estimate preliminary environmental performance metrics for several potential future concept aircraft.

AEDT Vehicle Definition
Georgia Tech investigated and identified the existing gaps in modeling supersonic aircraft in AEDT. The result was a white paper in modeling requirements and potentially required changes to the AEDT code and the associated modeling standards to improve and enable modeling specific aspects of supersonic aircraft and their environmental impacts.

Vehicle and Fleet Assessments
Georgia Tech used the GREAT and IDEA models to simulate the impact of potential supersonic vehicles on the fleet-level performance. Such impact was determined for a number of scenarios with varying underlying assumptions.

The Purdue team has also developed an approach to identify the price of currently offered business and above class tickets and then use this to develop a price for the supersonic aircraft tickets. This is important because of the inability to access reported international ticket price data of any kind. With this approach, the supersonic ticket price model allows the profit-seeking airline module and the passenger price-elasticity module to function in our FLEET simulation.

Milestone(s)

Georgia Tech had four milestones covered this year of performance.

1) The drivers of supersonic demand were identified in Task 1.
2) Using the demand estimate, a list of airports and routes that could support future supersonic aircraft was produced in Task 1.
3) Preliminary Key Environmental Indicators (KEI) for future supersonic aircraft were produced in Task 2.
4) A white paper assessing the ability of AEDT to model supersonic aircraft was developed along with a number of potential improvements needed to improve the accuracy of modeling supersonic aircraft in AEDT.

For Purdue the proposal covering this year of performances listed two milestones:

1) Complete modeling of chosen contractor's technologies.
2) Updated fleet assessment.

The Purdue team is using our own placeholder description of a potential, new supersonic transport aircraft; the representation of this in FLEET matches the most early proposed supersonic aircraft, one that will fly at Mach 2.2 but only during overwater portions of flight.

The Purdue team has also incorporated the supersonic aircraft model and performed initial fleet-level assessments of CO_2 emissions for the single "Current Trends, Best Guess" scenario.

Task 1- Fleet-Level Assumptions Setting and Demand Assessment

Georgia Institute of Technology and Purdue University

Objective(s)

This task focused on identifying and predicting significant drivers of commercial supersonic travel demand. For this year, focus was on U.S. operations. Using scenarios from prior ASCENT Project 10 work, Georgia Tech was to identify drivers of supersonic demand to and from the U.S., including domestic operations and international flight connections arriving to or departing from U.S. airports. In parallel, Purdue was to predict the latent demand for supersonic travel using the same



ASCENT 10 scenarios to bound the potential future demand. Georgia Tech was to use this latent demand to identify specific airports within the U.S. that are likely to support supersonic operations under the various previously defined scenarios. Georgia Tech was to pass this information to Purdue to generate flight schedules (# of ops) for each identified airport. This information would then be used in Task 4 to estimate the impact of supersonic travel on the U.S. aerospace system.

Research Approach – Georgia Tech

To investigate demand for commercial supersonic travel, Georgia Tech followed a two-step approach that first examines historical data to identify current premium demand (business and first class), and then estimates how such demand would scale for supersonic travel. The first step relied heavily on data derived from the Bureau of Transportation Statistics (BTS) databases, especially the Airline Origin and Destination Survey (DB1B) database, which provided information on passenger itineraries based on a 10% sampling of airline tickets from reporting carriers. For the second step, cost data documented by Airlines for America (A4A) was utilized. The A4A Passenger Airline Cost Index (PACI) was used to establish a baseline airline cost structure based on current operating costs. That structure was then scaled to estimate that of a supersonic airliner. Together, the two steps provided a better understanding of potential demand for future commercial supersonic travel from both a passenger and an airline perspective.

Current Demand for Premium Seats

In gauging demand for commercial supersonic travel, Georgia Tech attempted to identify current demand for premium seats. This is because supersonic travel, especially in the near term, is expected to cost more than subsonic travel (due to the increased time savings and increased associated costs). Historical performance of the Concorde also supports that assumption. As a result, identifying current premium passengers became a priority. The 2016 BTS DB1B database provided important information to begin this process. The database not only includes basic travel information such as origin, destination, miles flown, etc., but also includes important information such as number of passengers, fare class, fare per mile, etc. Premium passengers were identified as those who flew in the business and first classes (i.e., BTS DB1B fare classes C: unrestricted business class, D: restricted business class, F: unrestricted first class and G: restricted first class). However, there were some limitations in using the DB1B database. First, the data provided only represents a 10% sample of actual demand and not a full representation of the flying public. It was assumed that such sample was large enough to be representative of total demand. Second, the DB1B database is restricted to U.S. domestic flights only and does not include any information regarding international travel. This was a major limitation since most supersonic operations, especially in the near term, are expected to be transoceanic (for the U.S., this means the majority of international travel across the Atlantic and Pacific oceans). The Georgia Tech team inquired about a more inclusive dataset from the BTS; however, such dataset has restricted access due to proprietary concerns. To overcome this limitation, the team relied on an additional inventory of global flights for which it has access. The inventory provides information on all flights in 2015 including number of seats and number of operations, but unlike the DB1B database, does not specify fare class or number of passengers. Assumptions regarding passenger load factor and premium passenger share had to be made to conduct a preliminary demand assessment. Results for U.S. domestic (using 2016 BTS DB1B database) and global international (using 2015 inventory) demand for premium seats are presented below.

For domestic demand, the cumulative average daily premium passengers was aggregated by fare paid using the DB1B data. This was done by first filtering out all non-premium passengers (BTS DB1B fare classes U: unknown, X: restricted coach class and Y: unrestricted coach class), multiplying the number of passengers by 10 (since the DB1B is a 10% sample of total passengers) and then finally dividing by 365 (since the DB1B is annual). The x-axis of Figure 1represents the fare per mile in 2016 US dollars (calculated by dividing total fare by trip distance). The y-axis represents the cumulative average daily passengers that paid a certain fare per mile or higher. For example, the plot shows that approximately nine daily passengers paid three dollars per mile or higher in 2016 (orange square). The general trend is plotted in blue. Overall, the trend is sensible as it suggests that demand decreases as price increases. For current subsonic operations, it is estimated that the average fare per mile is in the order of 20 cents (shown in green on the plot). It is also estimated that future supersonic operations will target an average fare per mile of 100 cents (shown in red on the plot). This suggests, at least for 2016 operations, supersonic airlines can capture a daily demand of approximately 100 premium passengers (red dotted line).

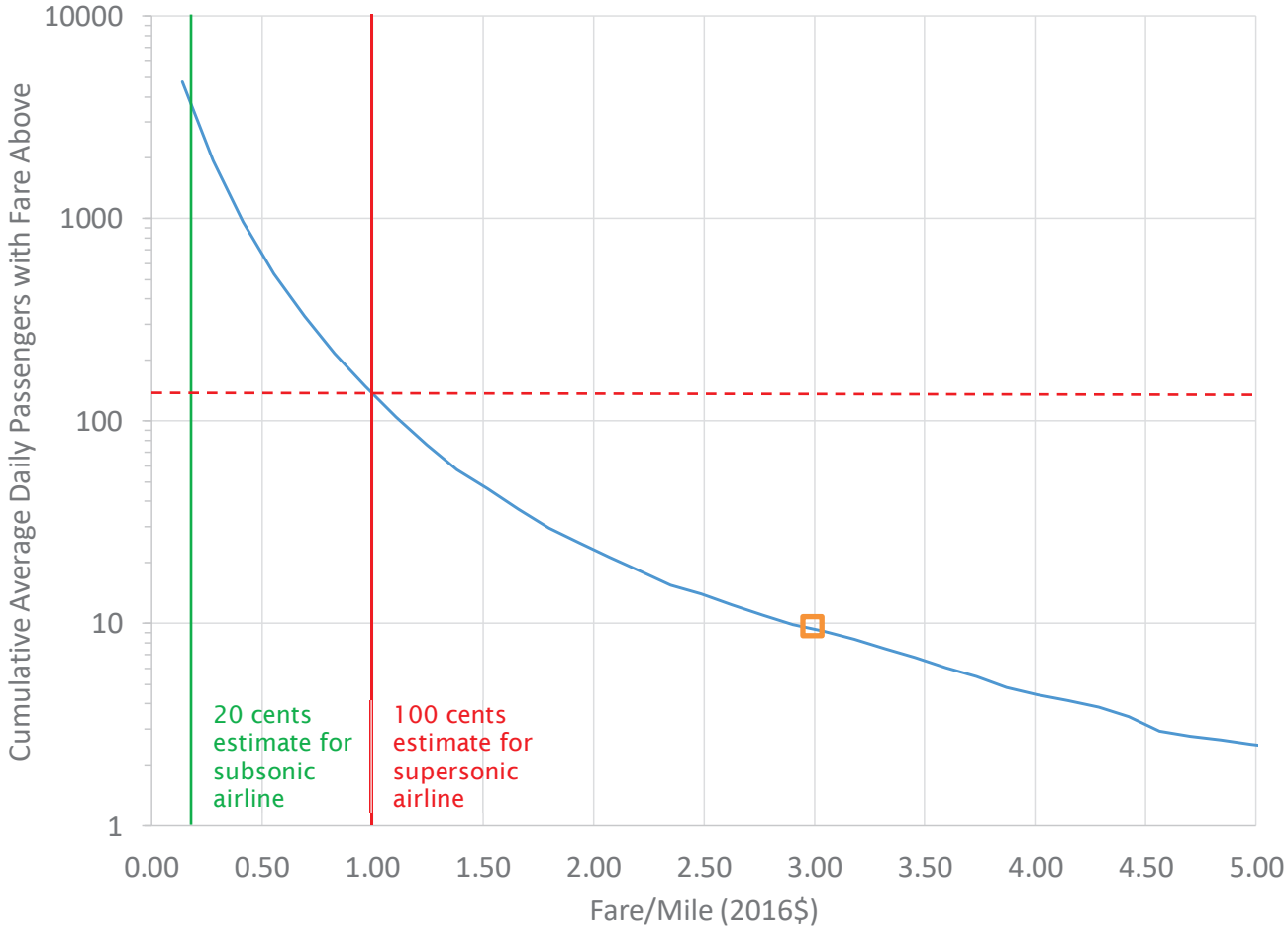


FIGURE 1. DEMAND CURVE ESTIMATION

For international demand, the premium Passengers Daily Each Way (PDEW) was plotted against flight distance for all flights (Figure 2). This was done by utilizing appropriate assumptions for passenger load factor and premium seat share to determine the number of premium passengers (since the inventory only includes number of seats) and then dividing by 365 to compute PDEW. Results from domestic demand analysis were used as a reference to estimate international demand. It is estimated that international demand for supersonic travel would target routes with PDEW values greater than 100 (area above the horizontal orange line). This would provide enough demand to fill a single 100 seat plane with a single flight per day or a 50 seat plane with two flights per day. Furthermore this shows the potential size of the market and it is therefore advisable to target markets that are large enough to support a high load factor without having to capture all of the existing potential demand because that would be unrealistic. It is estimated that supersonic flights, especially in the near term, will be long-haul ones of distances greater than 2000 nmi (area to the right of the vertical orange line). Hence, it is estimated that international supersonic demand would be for routes that lie in the shaded orange area. These routes are listed in Table 2 and plotted on the map shown in Figure 3. The thickness of the lines in the map correspond to PDEW (thicker lines indicate routes with higher PDEW).

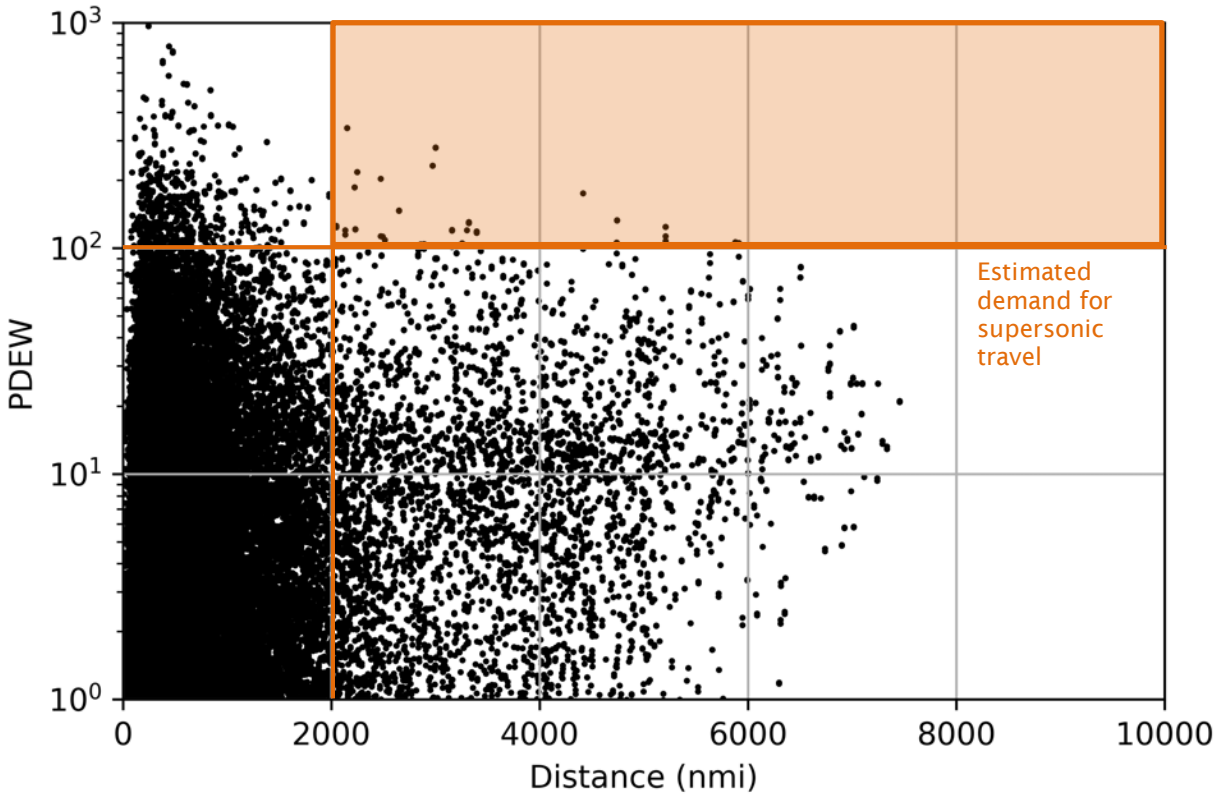


FIGURE 2. MARKET SELECTION

TABLE 2. LIST OF 50 AIRPORT PAIRS WITH OVER 100 PDEW AND OVER 2000NMI GREAT CIRCLE DISTANCE

OPS	SUM_SEATS	GRT_CIRC_DIST	DEP_APT_CODE	ARR_APT_CODE
13372	342	2151	KJFK	KLAX
13372	341	2151	KLAX	KJFK
6946	279	2999	KJFK	EGLL
6925	279	2999	EGLL	KJFK
4144	232	2973	OMDB	EGLL
4139	232	2973	EGLL	OMDB
9186	218	2247	KSFO	KJFK
9177	218	2247	KJFK	KSFO
4802	203	2473	PANC	KORD
6923	186	2221	KLAX	PHNL
7168	186	2221	PHNL	KLAX
4228	175	4415	VHHH	PANC
2545	147	2650	OMDB	VTBS
2541	146	2650	VTBS	OMDB
2965	133	4741	KLAX	EGLL
2946	133	4741	EGLL	KLAX
3476	131	3318	PHNL	RJAA
3452	129	3318	RJAA	PHNL
4092	126	2048	ZSPD	WSSS



2853	124	5209	EGLL	VHHH
2850	124	5209	VHHH	EGLL
3589	124	2048	WSSS	ZSPD
5471	122	2229	KEWR	KSFO
5498	121	2229	KSFO	KEWR
2956	121	3158	KJFK	LFPG
5451	120	2133	KEWR	KLAX
3270	120	3301	RKSI	PANC
2919	120	3158	LFPG	KJFK
3178	119	3395	WSSS	YSSY
2741	117	3395	YSSY	WSSS
5202	115	2133	KLAX	KEWR
2750	113	2473	KORD	PANC
2257	113	5209	KLAX	RKSI
2995	113	2491	RKSI	WSSS
2897	112	2491	WSSS	RKSI
3123	109	2511	VTBS	RJAA
2180	107	5209	RKSI	KLAX
2167	106	5879	WSSS	EGLL
2167	106	5879	EGLL	WSSS
2626	106	4737	RJAA	KLAX
2363	105	5909	RCGM	KLAX
2657	105	3253	YMML	WSSS
2552	105	3253	WSSS	YMML
2520	105	2511	RJAA	VTBS
2695	104	2889	WSSS	RJAA
2547	104	2857	WSSS	RJTT
2545	104	2857	RJTT	WSSS
1987	101	3157	WSSS	OMDB
1990	101	3157	OMDB	WSSS



FIGURE 3. SELECTED ROUTES



Potential Airline Market for Supersonic Travel

After analyzing the potential demand from a passenger perspective, the Georgia Tech team investigated the market for supersonic travel from an airline perspective. A4A data for airline operating costs were used to establish a baseline airline cost structure representative of subsonic operations. Specifically, Passenger Airline Cost Index (PACI) data for the fourth quarter of 2016 were used to establish the structure shown in Figure 4. As shown in the figure, 'labor' and 'fuel' costs account for approximately 50% of all airline operating costs. Other major contributors include 'aircraft rents and ownership' and 'professional services'. This baseline structure was assumed to be representative of that for a currently operational reference subsonic aircraft with certain specifications. To estimate a similar cost structure representative of operating costs for a concept supersonic aircraft, the specifications of the latter needed to be estimated relative to those of the reference aircraft. Engineering judgement was exercised, along with some feedback input based on the results of Task 2, to define the specifications of the concept supersonic vehicle. The specifications for both the subsonic and supersonic vehicles are tabulated in Table 3. Using these specifications, and by normalizing the cost structure by flight hour, the baseline airline structure could be adjusted to reflect the differences in various component costs (e.g., fuel and maintenance).

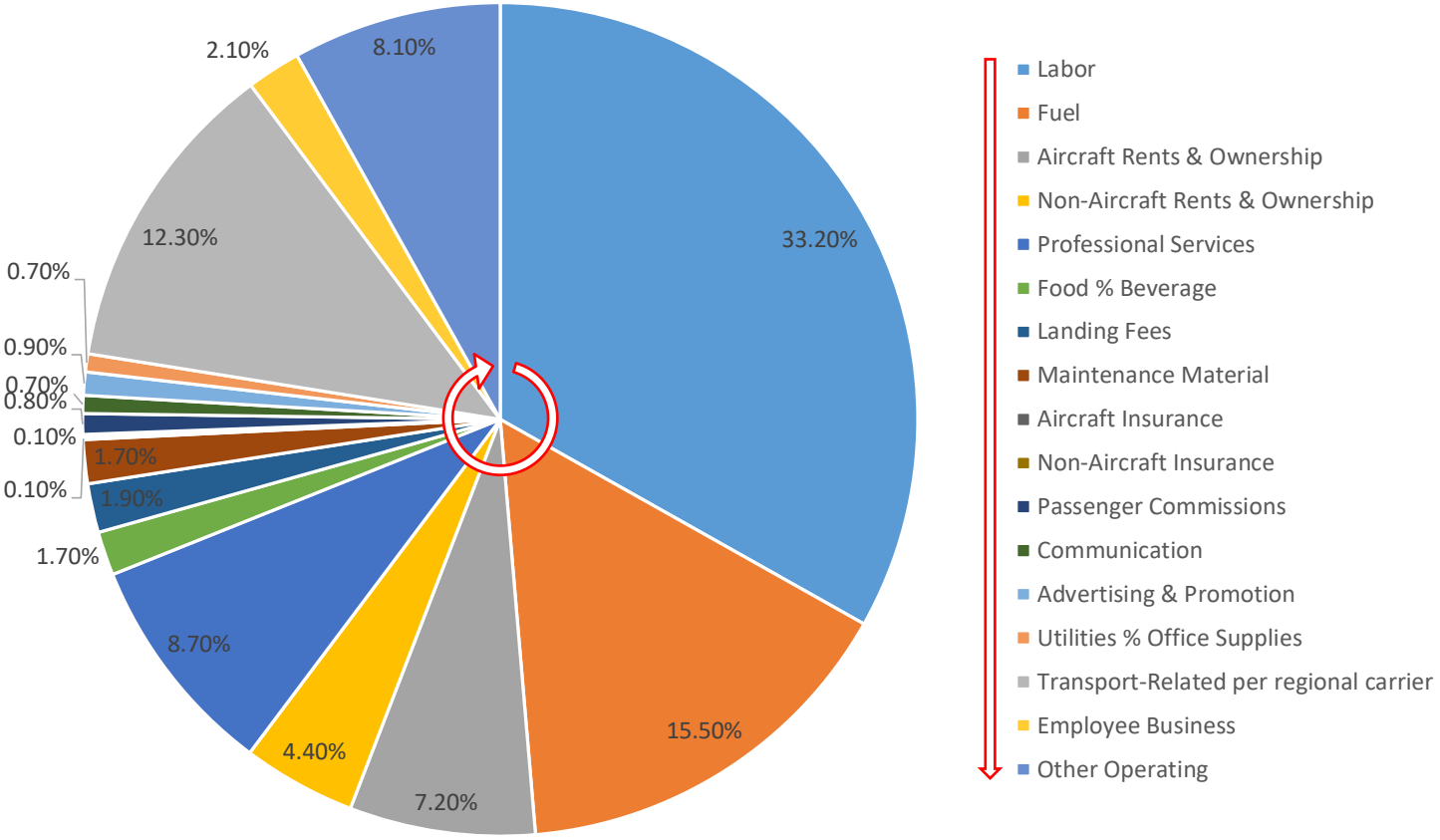


FIGURE 4. COMMERCIAL AIRLINE COST INDEX

An important parameter that was estimated using this procedure was the required yield per seat mile (i.e., the average fare per seat mile). Assuming airline profit margins remain the same as that for subsonic operations, yield directly correlates with operating costs. This parameter was estimated for different utilization and fuel consumption scaling values (Figure 5). The plot above shows the resulting trends. Generally, the more fuel is consumed, the higher the required yield should be to maintain the same profit margins. Alternatively, higher utilization allows for lower required yield values. For the concept supersonic aircraft characteristics assumed (fuel consumption 8 times that of subsonic aircraft and utilization of 1000 hours per year), it was found that required yield would have to be almost 4.5 times that of subsonic operations for airlines to maintain the same profit margins (red square). This means that, on average, airlines would have to charge passengers of supersonic flights 4.5 times more than passengers of subsonic flights.



TABLE 3. RELATIVE COST INDEX ADJUSTMENTS

	Reference Subsonic Aircraft	Concept Supersonic Aircraft
Number of Seats	180	100
Load Factor	0.8	0.8
Block Speed (miles per hour)	500	1350
Utilization (hours per year)	4500	1000
Fuel Consumption (relative per block hour)	1.0	8.0
Maintenance Costs (relative)	1.0	3.0
Acquisition Costs (relative)	1.0	2.0

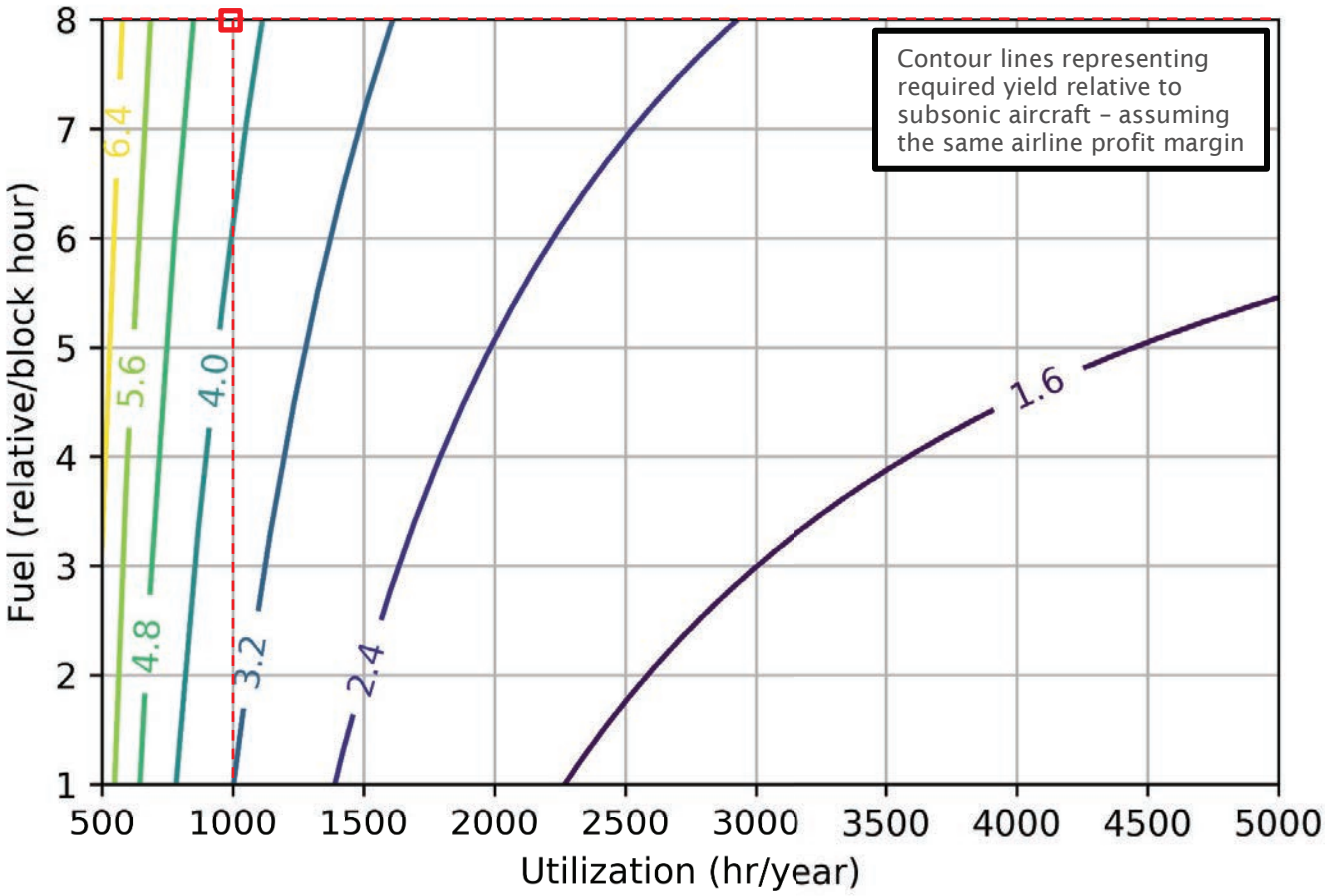


FIGURE 5: RELATIVE REQUIRED YIELD AS FUNCTION OF FUEL MULTIPLIER AND UTILIZATION

Research Approach – Purdue

FLEET Supersonic Simulation Requirements

Supersonic Ticket Price Modeling

One of the first steps in determining ticket prices for supersonic flights is identifying the potential routes where the supersonic aircraft might operate and then use available pricing information about those routes. Considering that the Boom Aerospace concept is a possible first supersonic passenger-carrying entrant that does not make an attempt at low boom flight, the initial supersonic aircraft are most likely to operate on over-ocean routes, where they can fly supersonically over



the water. This means that mostly international routes will be "supersonic eligible". Following discussion from Boom's website that indicates their aircraft could operate with a ticket price similar to current business class tickets, the Purdue team assumes that the supersonic ticket price would be similar to the current business class ticket prices. With data about historical ticket prices paid for international routes difficult to obtain, the Purdue team is dependent on the current (2017) offered "business class or above" ticket pricing data to model supersonic ticket prices for FLEET simulations.

Supersonic Ticket Price Modeling Components

The Purdue team uses offered "business class or above" ticket price data in 2018 to model the supersonic ticket fare for supersonic eligible routes. However, to use the current (2018) offered "business class or above" ticket price for supersonic aircraft on the eligible routes, FLEET needs a "reference" 2018 supersonic aircraft operating cost. With the no actual supersonic aircraft models currently available, the Purdue team has developed two placeholder strategies to estimate the supersonic aircraft operating cost using a fictitious "reference" aircraft operating cost. These placeholder approaches to model the supersonic aircraft operating cost will be replaced by the actual operating cost incurred by the supersonic aircraft model to be provided by the project partners from Georgia Institute of Technology.

Offered "business class or above" ticket price in 2018

In this work, it is assumed that the supersonic ticket price is similar to the current business ticket fare. The Purdue team employs offered "business class or above" pricing data for modeling the supersonic ticket fares in FLEET. This approach is different from the one being currently employed to model the subsonic ticket fares. In particular, the current approach used for subsonic ticket pricing utilizes data from the Bureau of Transportation Statistics (BTS) Airline Origin and Destination Survey (DB1B) [1] for finding routes with nearly homogenous aircraft size to develop a curve that estimates yield (profitability on a ticket sold to a passenger) as a function of range for each size-class of subsonic aircraft. However, this approach does not translate to supersonic aircraft, because the historical ticket prices paid for international flights from BTS DB1B database is not publicly available. Therefore, the Purdue team's FLEET model currently calculates the supersonic aircraft ticket pricing by using offered "business class or above" pricing data obtained from the ITA software website [2]. The Purdue team has collected roundtrip offered "business class or above" ticket fare data for all the origin-destination pairs (and destination-origin pairs) of the supersonic eligible routes for 02/09/2018 and selected the median of the ticket price data for every route as the current offered "business class or above" ticket fare.

Reference supersonic aircraft operating cost

To utilize the offered "business class or above" ticket fare data to model the supersonic ticket price in FLEET, a "reference" 2018 supersonic aircraft operating cost is required. The current work utilizes FLEET's existing class 5 subsonic aircraft as the "reference" aircraft to estimate the supersonic aircraft operating cost. The class 5 aircraft corresponds to a twin-aisle aircraft, which has a much larger seat capacity (approximately 250 seats) than the envisioned first-entry supersonic transports. However, the reason to select FLEET's class 5 subsonic aircraft as the "reference" aircraft is because of its ability to operate on transoceanic ranges, allowing the Purdue team to get a fairly rough estimate of an inflated operating cost per passenger fora supersonic aircraft with a much smaller payload compared to FLEET's subsonic class 5 aircraft. Currently, with the reference aircraft selected, two different placeholder ideas have been developed to estimate the supersonic aircraft operating cost.

1. The first placeholder approach assumes that the 2018 supersonic aircraft direct operating cost is equal to the direct operating cost of new-in-class 5 subsonic aircraft in FLEET.

$$DOCpax_{ref_sup,\,route} = DOC_{new-in-class\,5,\,route}/seats_{supersonic}$$

2. The alternate placeholder approach assumes that the 2018 supersonic aircraft direct operating cost is equal to the average direct operating cost of best-in-class 5 and new-in-class 5 subsonic aircraft.

$$DOCpax_{ref_sup,\,route} = \frac{\left[\left(DOC_{best-in-class\,5,\,route} + DOC_{new-in-class\,5,\,route}\right)/2\right]}{seats_{supersonic}}$$

In the simulation year 2018, FLEET has both best-in-class 5 and new-in-class 5 subsonic aircraft in service at the same time, leading to the development of the two different placeholder approaches described above. The current simulation results use



the second placeholder approach to select the "reference" supersonic aircraft operating cost as an average of the best-in- and new-in-class 5 direct operating costs.

Supersonic Ticket Price Margin Calculation Strategies

The Purdue team has developed three different strategies to model the supersonic ticket price margin. As discussed earlier, the "reference" 2018 supersonic aircraft operating cost is required to use offered "business class or above" ticket fare for calculating the supersonic flight fare margin on each route. The supersonic ticket price margin so calculated is used to determine the supersonic ticket fare for every route using one of the following ticket price models:

Ticket price margin per route

i. This approach uses a route-specific ticket price margin. The margin per passenger for a given route is calculated as the offered 2018 "business class or above" ticket fare for that route, less the fictitious 2018 "reference" supersonic aircraft direct operating cost per passenger for the route.

$$margin_{route} = CurrentOfferFare_{route} - DOCpax_{ref_sup,\,route}$$

ii. For each supersonic eligible route, the addition of the calculated margin per passenger with the direct operating cost per passenger gives the supersonic ticket fare.

$$Fare_{sup_ac,\,route} = margin_{route} + DOCpax_{sup_ac,\,route}$$

Here, the sup_ac index allows for best-in-class supersonic aircraft (EIS 2025), new-in-class supersonic aircraft (EIS 2035), and future-in-class supersonic aircraft (EIS 2045).

iii. This approach ensures that the margin for every route is independent of the other supersonic eligible routes in FLEET. This approach should potentially be able to take care of the variability in ticket fares due to the popularity/ high demand on different routes, mimicking the market behavior fairly. However, as FLEET simulation does not model the competition between different airlines (instead FLEET simulation currently models a single airline), this ticket price model could possibly lead to unrealistic results.

Constant margin across routes

i. This approach is the simplest to implement among all approaches as it is based on average margin that is independent of the route length.

ii. The average margin per passenger for all the routes is calculated as the difference between the offered 2018 "business class or above" ticket fare and the fictitious 2018 "reference" supersonic aircraft direct operating cost per passenger, averaged over all the supersonic routes.

$$margin_{avg} = \Sigma\,(CurrentOfferFare_{route} - DOCpax_{ref_sup,\,route})/n_{routes}$$

iii. For each supersonic eligible route, the sum of the average margin per passenger with the direct operating cost per passenger gives the supersonic ticket fare.

$$Fare_{sup_ac,\,route} = margin_{avg} + DOCpax_{sup_ac,\,route}$$

Here, the sup_ac index allows for best-in-class supersonic aircraft (EIS 2025), new-in-class supersonic aircraft (EIS 2035), and future-in-class supersonic aircraft (EIS 2045).

iv. This approach ensures that the margin is independent of range; the supersonic ticket fare varies only according to the direct operating cost per passenger for different routes. This implies that the profit margin for every route remains constant.



Average margin per passenger-nautical mile

i. This approach is based on using an average margin per passenger-nautical mile metric to estimate the supersonic ticket fare.

ii. The average margin per passenger-nautical mile is calculated as the difference between the offered 2018 "business class or above" ticket fare and the fictitious 2018 "reference" supersonic aircraft direct operating cost per passenger, per route length of every route, averaged over all the supersonic eligible routes.

$$margin\ per\ nm_{avg} = \Sigma \frac{CurrentOfferFare_{route} - DOCpax_{ref_sup,route}}{Range_{route}} / n_{routes}$$

iii. The supersonic ticket fare for every supersonic eligible route is calculated as the sum of the direct operating cost per passenger for the route, and the average margin per passenger-nautical mile multiplied by the route length for every route.

$$Fare_{\sup_ac,route} = \left(margin\ per\ nm_{avg} \times Range_{route}\right) + DOCpax_{\sup_ac,route}$$

Here, the sup_ac index allows for best-in-class supersonic aircraft (EIS 2025), new-in-class supersonic aircraft (EIS 2035), and future-in-class supersonic aircraft (EIS 2045).

iv. In this approach, the supersonic ticket fare is directly dependent on the supersonic route length. This implies that operating a supersonic aircraft on a longer route would lead to a higher profit margin than on a shorter route, reflecting that passengers would be willing to pay more to save more time; therefore, the allocation problem might favor supersonic aircraft on longer routes, if aircraft count, capacity and demand constraints are satisfied, to maximize profit.

Current ticket price model and future work

The Purdue team selected the third ticket price calculation strategy (average margin per nautical mile) exclusively to determine the supersonic ticket fares for eligible routes in the current FLEET simulations. The supersonic ticket prices accommodate the effect of supersonic operation range on an airline's profit margin, as this ticket price model is dependent on the route length. This implies that a supersonic passenger would be willing to pay more for a longer-range flight as there would be more time savings compared to a shorter-range flight. The team investigated and compared the fleet allocation (both subsonic and supersonic), class-wise carbon emissions, and the route-wise airline profit margin for all three ticket price models and concluded that the average margin per nautical mile ticket price estimation model is the most plausible choice for Purdue's simulation of supersonic commercial travel in FLEET. Subsequently, the development of a passenger choice model (i.e., a model that accounts for the "value of travel time" of passengers as a foundation for modeling their choice on routes when both supersonic and subsonic aircraft are available, discussed later on) will accommodate for the effect of passenger time savings on ticket pricing.

Supersonic aircraft cost and performance modeling

The supersonic aircraft modeling task is currently underway and primarily performed by Georgia Tech. In the meanwhile, to produce the initial supersonic scenario simulation results using FLEET, supersonic aircraft models are required. The Purdue team has currently developed 'placeholder' supersonic aircraft models to conduct these initial FLEET simulations. These 'placeholder' supersonic aircraft models will later be replaced by the supersonic aircraft models to be provided by the project partners from Georgia Institute of Technology.

Current supersonic aircraft model 'placeholder'

The Purdue team has developed a 'placeholder' aircraft model that enables the representation of a supersonic aircraft in the FLEET simulations using the existing subsonic aircraft models. In the 'placeholder' model, the aircraft cost and performance modeling are currently accomplished by using 'multipliers' to modify the cost and performance parameter outputs of already existing subsonic aircraft to mimic the operation of a supersonic aircraft.

Current 'multipliers' for aircraft performance

The 'placeholder' supersonic aircraft developed by the Purdue team has a seat capacity of 69 passengers, which matches the seat capacity of a subsonic class 2 aircraft in FLEET. The proposed concept from BOOM would have 55 seats; so applying



an appropriate load factor limits the supersonic to 55 seats in the results that will appear below. The fuel burn for the 'placeholder' supersonic aircraft is set to be equivalent to the fuel burn of FLEET's existing class 5 subsonic aircraft. This translates to the supersonic aircraft having approximately 3.5 times more average fuel burn per passenger-nautical mile when compared to a subsonic class 5 aircraft (refer to Table 1). This is done to account for an increased fuel burn expected for a supersonic aircraft when compared to a subsonic aircraft of the same size/class. The supersonic aircraft are expected to require increased maintenance hours, which are represented in the 'placeholder' model by implementing a multiplier of 1.5 times the subsonic class 5 maintenance hours requirement. Table 2 summarizes the 'multipliers' implemented for developing the 'placeholder' supersonic aircraft model for FLEET.

TABLE 4. COMPARISON OF AVERAGE FUEL BURN PER PASSENGER NAUTICAL MILE BETWEEN SUPERSONIC AIRCRAFT AND CLASS 5 SUBSONIC AIRCRAFT

	Representative-in-Class	Best-in-Class	New-in-Class	Future-in-Class
'Placeholder' Supersonic Aircraft [lb/nmi]	0.4745	0.4225	0.4212	0.2312
FLEET's Class 5 Subsonic Aircraft [lb/nmi]	0.1255	0.1346	0.1188	0.0652

TABLE 5. SUMMARY OF 'MULTIPLIERS' USED FOR DEVELOPING THE 'PLACEHOLDER' SUPERSONIC AIRCRAFT MODEL IN FLEET

Cost and Performance Parameters of 'Placeholder' Supersonic Aircraft	Multipliers / Modeling Characteristics
Seat Capacity	Subsonic class 2 aircraft (69 seats)
Fuel Burn	Subsonic class 5 aircraft
Block Time	Overwater calculations and subsonic class 5 aircraft (for overland segment only)
Turnaround Time	1 hour
Crew Cost	Block time calculations and subsonic class 5 aircraft
Maintenance Hours	1.5 times of subsonic Class 5 aircraft
Insurance	Subsonic Class 5 aircraft Insurance
Indirect Operating Cost	Subsonic Class 5 aircraft
Acquisition Cost	Subsonic Class 6 aircraft

In this current work, the supersonic aircraft is expected to fly supersonically overwater only, so the block time for the current 'placeholder' supersonic aircraft is computed according to how much of the flight is overwater. The placeholder model presumes that the supersonic aircraft cruises at Mach 2.2 overwater and Mach 0.95 overland; hence, the total block time considers the time contributions for both its overwater and overland flight sub-segments. For the overland flight (subsonic flight segment), the block time of the supersonic aircraft is equivalent to the block time of class 5 subsonic aircraft already existing in FLEET. The percentage of overwater flight for the supersonic aircraft is calculated using the overwater calculations detailed in the next section. The modified block time equation appears below.

$$Blocktime_{sup} = \left[Blocktime_{sub_class5}^{min_time_route} \times (1 - \%_{overwater})\right] + \left[\%_{overwater} \times \frac{min_time_distance}{Sup_cruise_spd}\right]$$

Here, the $Blocktime_{sub_class5}^{min_time_route}$ represents the block time of subsonic class 5 aircraft on the minimum time route identified using the supersonic route path adjustment strategy and overwater calculation for supersonic aircraft operation, described in the following section.



Using the updated block time calculations described above, the crew cost for the 'placeholder' supersonic aircraft is also modified to incorporate the block time reduction occurring during the supersonic overwater flight segment. The updated crew cost is a factor of the FLEET's subsonic class 5 aircraft crew cost, with the modified equation appearing below.

$$Crewcost_{sup} = Crewcost_{sub_class5} \times \frac{SeatCap_{sup}}{SeatCap_{sub_class5}} \times \frac{Blocktime_{sup}}{Blocktime_{sub_class5}^{min\ _time_route}}$$

As with the previous case, the $Blocktime_{sub_class5}^{min\ _time_route}$ represents the block time of subsonic class 5 aircraft on the minimum time route identified using the supersonic route path adjustment strategy and overwater calculation for supersonic aircraft operation.

Characterizing Supersonic Eligible Routes in FLEET

As part of the first-year effort to include supersonic aircraft, the Purdue team has developed approaches to characterize what the team calls "supersonic eligible" routes. A set of filters was developed to identify which of the 1,940 routes in the FLEET network have enough total passenger demand to support a plausible number of business class or above travelers and are within bounds on minimum range (where there is sufficient range to accelerate to supersonic speed for meaningful block time reduction) and maximum range (to reflect the projected maximum range of proposed supersonic transports). The team has also developed a simple, but credible approach to consider the percentage of each route that is "overwater". This facilitates scenarios where the supersonic aircraft can only operate above Mach 1.0 during the overwater segment. This overwater approach also considers a simple re-routing that might increase distance flown between airports over that of the great circle distance, but that resulting route minimizes flight time to take advantage of the supersonic speeds.

Route Filters based on 2016 BTS database

The Purdue team has implemented demand and World-Wide Logistics Management Institute Network (WWLMINET) airport [3] filters to determine potential supersonic eligible routes from the 2016 Bureau of Transportation Statistics (BTS) T-100 database. These filters lead to a set of 127 supersonic eligible routes for FLEET simulations. The supersonic route set will be the intersection of the subsonic route set from 2005 BTS T-100 data and the 127 supersonic eligible route set with overwater percentage filter.

Demand filter

The demand filter assumes that the potential supersonic passengers are the current "business class or above" passengers. In FLEET, the travel demand is split such that supersonic ("business class or above") demand is a fixed percentage (5%) of the total travel demand with subsonic for the remainder. In addition, the supersonic daily demand (5% of the total travel demand) should correspond to 50 passengers or more to make the route supersonic aircraft operation eligible. To determine the number of potential business-class-or-above paying passengers, the Purdue team considered typical aircraft currently flying transoceanic routes. Those aircraft have enough seats in business and above cabins that are roughly 10% of the total seat capacity, albeit with fairly significant variation. Then, the Purdue team assumes that 50% of the daily "business class or above" passengers would be willing to fly supersonic, as a coarse approximation that half of the passengers flying in business class or above cabin are paying that fare (the other half are using upgrades or similar). With the daily demand for "business class or above" travel being set to 10% of the total travel demand, the supersonic daily demand turns out as 5% of the total travel demand. Because the Bureau of Transportation Statistics provides the DB1B Coupon database sample of ticket prices paid only for domestic routes, a direct comparison is not possible. However, an indirect comparison indicates that for all domestic routes in the DB1B for 2016, 4.82% of the reported tickets were business class or above; focusing on domestic flights between 2350 nmi and 4500 nmi, 6.89% of the reported tickets were business class or above. This supports that the 5% travel demand assumption.

Supersonic route path adjustment and overwater calculation (to represent the no supersonic over-land limitation)

The current work considers that the supersonic aircraft can only operate over Mach 1.0 when it is flying overwater. The Purdue team has developed a method to estimate the overwater portion for the supersonic eligible routes, this allows the team to further identify supersonic routes that have a certain percentage of route path overwater (for example, some of our recent studies have used 75% overwater as this additional filter for supersonic eligible routes). This method includes adjusting the supersonic eligible route path from its great circle path to allow the aircraft to operate at supersonic speeds for the longest overwater route segment possible. The re-routing facilitates the selection of the supersonic eligible route path along which minimum flight time is possible (using supersonic speeds overwater and subsonic speeds over-land).

The overwater portion calculations with re-routing technique have the following characteristics:

1. These calculations consider the longest route portion over water without any land portions. The great circle distance is based on the longitudes and latitudes of airports on a spherical earth model.
2. In case small islands lie under the flight path (in the great circle path or during path re-routing), the algorithm checks if the sum of path length before and after the island is greater than 40% of the total flight path. If yes, then the small island is ignored, because we assume that an aircraft can avoid the island by flying around it (and we are interested in the longest overwater route segment).
3. The re-routing technique finds 14 alternate flight path deviations above and below the great circle path. For generating the alternate flight path, the coordinates of the mid-point of the great circle path are determined, followed by incrementing (or decrementing) the mid-point latitude by 1° for each alternate flight path, ultimately changing the departure heading of the aircraft. The 14 alternate routes generated in this study correspond to incremental deviations in departure heading to a maximum of +7° and -7° from the great circle path.
4. Among the great circle path and all the alternate flight paths generated for a route, the minimum time flight path is selected for the supersonic aircraft. The flight time is determined using different flight speeds for overwater and over-land flight operation. The minimum time flight path is hence optimal because of the discrete departure deviations. The flight time for every route is calculated using a supersonic flight speed of Mach 2.2 (at 55,000 ft) for the longest segment overwater and subsonic flight speed of Mach 0.95 (at 35,000 ft) for remaining segments. These simplistic calculations are performed using the following equation:

$$t_{flight} = \frac{P_{overwater}/100}{vel_{sup}} + \frac{1 - (P_{overwater}/100)}{vel_{sub}}$$

where, t_{flight} denotes the flight time, $P_{overwater}$ is the percentage of flight overwater, vel_{sup} is the supersonic aircraft speed (Mach 2.2 at 55,000 ft), and vel_{sub} is the subsonic aircraft speed (Mach 0.95 at 35,000 ft).

For example, considering the JFK – NRT route shown in Figure 6, the overwater portion calculation technique finds a minimum time flight path (denoted by red dotted line) with a deviation from the great circle flight path (denoted by solid red line). In this case, the minimum flight time path also has the longest segment overwater amongst all the route path deviations generated by the technique.

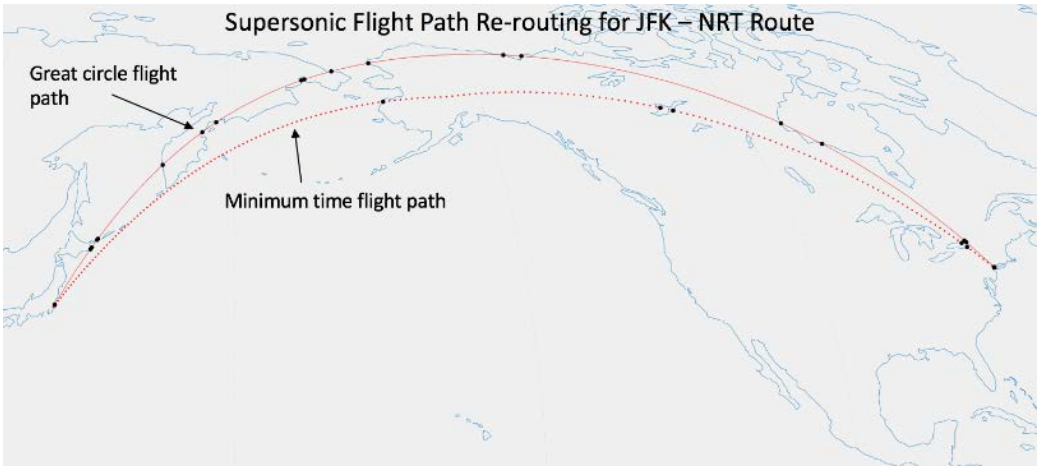


FIGURE 6. DEMONSTRATION OF SUPERSONIC FLIGHT PATH RE-ROUTING FOR JFK-NRT ROUTE TO FIND THE MINIMUM FLIGHT TIME PATH

Supersonic route network with overwater filter

In FLEET, the set of 127 supersonic eligible routes obtained after implementing the demand and airport filters undergo additional filtering with respect to their presence in the existing FLEET route network and their range. FLEET's existing route network of 1,940 routes is based on the 2005 BTS T-100 reported operations. The routes filtered from the 2016 BTS T-100 database are compared to the existing FLEET network to ensure that the supersonic eligible routes are a subset of the 1,940

routes in FLEET. This work considers routes with route lengths between 1,500 nmi and 4,500 nmi. This leads to the inclusion of transoceanic routes, because they meet the required range and have a considerable portion of the flight path over water. The set of 127 supersonic eligible routes reduces to 96 after the application of these additional filters.

For the initial studies, the simulations allow supersonic operation over water only, so the overwater calculations are employed to filter the 96 supersonic eligible routes to give routes that have more than or equal to 75% of flight path overwater. This leads to a set of 26 supersonic eligible routes, which appear on a global projection in Figure 7 where some of the simple latitude deviations for minimum flight time are visible. Table 6 lists all of these routes with distance and overwater percentages. The Purdue team has utilized this set of 26 supersonic eligible routes for producing the current simulation results. As with all routes in FLEET, the aircraft will travel a round trip on the route, so the Amsterdam Schiphol (AMS) to New York – John F. Kennedy (JFK) route also covers flights from JFK to AMS.



FIGURE 7. POTENTIAL SUPERSONIC ROUTES WITH > 75% OF FLIGHT OVER WATER IN FLEET

TABLE 6. FLEET SUPERSONIC-ELIGIBLE ROUTES WITH OVERWATER FILTER AT 75% OR MORE

Airport A	Airport B	Route Length Min Time [nmi]	Percentage of flight path overwater
AMS	JFK	3227.86	76.44
ATL	CDG	3864.97	81.71
BOS	LHR	2939.35	83.75
CDG	IAD	3413.89	88.19
CDG	JFK	3182.62	88.43
CDG	MIA	3981.58	95.40
EWR	FRA	3445.46	78.36
FCO	JFK	3769.93	80.49
FRA	IAD	3622.24	79.73
FRA	JFK	3409.91	78.64
HNL	KIX	3618.86	96.50
HNL	LAS	2397.70	88.07
HNL	LAX	2227.44	99.13
HNL	NRT	3329.67	98.32
HNL	PHX	2531.75	89.12
HNL	SEA	2326.19	96.01
HNL	SFO	2082.62	99.24



HNL	SYD	4412.18	99.27
IAD	LHR	3255.82	81.82
JFK	LHR	3093.34	87.12
JFK	MAD	3120.04	89.26
JFK	MXP	3553.73	83.03
JFK	ZRH	3454.17	81.58
LHR	MIA	3859.46	96.05
MAD	MIA	3837.72	93.71
NRT	SFO	4442.36	99.47

Task 2- Preliminary Vehicle-Level Environmental Impact Prediction

Georgia Institute of Technology and Purdue University

Objective

This task focused on providing a preliminary estimate of the environmental impact of supersonic travel. The likely performance of supersonic aircraft *relative* to existing subsonic transports, for which performance is known, was to be identified. This relative estimation was performed for a number of Key Environmental Indicators (KEI) including fuel burn, emissions, water vapor, likely cruise altitudes, and noise. KEI information was to be compiled for three supersonic aircraft types:

1. Type 1: aircraft that operate at supersonic speeds in unrestricted areas and subsonic speeds over other areas
2. Type 2: same aircraft as Type 1 except that they also have technology to fly at Mach cut-off speeds over prohibited areas. Mach cut-off is a phenomenon that takes advantage of atmospheric characteristics to prevent sonic booms from propagating to the ground (typically works from Mach 1.1 to 1.15)
3. Type 3: aircraft specifically designed to produce very low sonic boom levels during all phases of supersonic flight.

Quantitative estimates for each KEI were to be generated through an extensive literature search of previously developed concepts and active projects in industry and government using sources such as NASA contractor reports, journal and conference publications, and press releases pertaining to concepts under active development. Georgia Tech was to estimate fuel burn, noise, water vapor, and emissions as a function of vehicle size, mission, and passenger capability, using publicly available resources. These estimates were to be compared to baseline aircraft in the subsonic transport category with the goal of establishing an equivalency in each of the KEI metrics.

Research Approach

To provide a preliminary estimate for the performance of supersonic vehicles, the Georgia Tech team started by establishing a reference performance for a subsonic vehicle. Quantitative estimates for the impact of supersonic vehicles on the various KEIs, especially fuel efficiency, were then derived based on literature review, future performance targets set by NASA, and engineering judgement. The subsonic vehicle that was selected as reference was the Boeing 737-800. This aircraft was chosen based on its similar payload-range capabilities compared to both the Concorde and future supersonic vehicles. The KEIs selected were primarily fuel burn, CO2 emissions, NOx emissions and noise. The first two KEIs correlate with each other to a great extent. For NOx, a distinction was made between emissions released during cruise and emissions released in the vicinity of airports at low altitudes during Landing and Take Off (LTO). Similarly for noise, a distinction was made between airport noise and sonic boom noise. The latter is only a characteristic of supersonic vehicles since it is only produced in regimes of supersonic flow. As for targeted performance, NASA goals for supersonic vehicles were used as reference. NASA set vehicle performance goals for the mid-term (business jet size) and far-term (airliner size). Table 7 summarizes the findings.



TABLE 7. COMPARISON OF ENVIRONMENTAL METRICS FOR SUBSONIC AND SUPERSONIC AIRCRAFT

	1976 Concorde	1998 Boeing 737-800	Current Tech. Estimate	2025 NASA N+2	2035 NASA N+3	2035+ NASA N+3 Stretch
Fuel Efficiency (lb/seat/nmi)	0.53	0.10		0.30	0.29	0.22
Cruise NOx Emissions (g/kg of fuel)	23.3	-		<10.0	<5.0	<5.0
LTO NOx Emissions (g)	29,995	8,466		-	-	-
Cumulative Airport Noise Margin Stage 3 (EPNdB)	- 43.2	+ 13.0		-	20	30
Sonic Boom Noise (PLdB)	105	N/A		N/A	70-80	65-75
	Historical Performance		Supersonic	Targeted Performance		

The historical values in the table were derived from various sources. For the Concorde, flight manuals were utilized to determine fuel efficiency in terms of pounds of fuel per seat per nautical mile. Values for cruise NOx emissions and sonic boom noise were determined based on a literature search. As for LTO NOx emissions, the value was determined using the ICAO engine databank. Last, for airport noise, it was determined based on Maximum Take Off Mass (MTOM) relative to Stage 3 certification standards. It is to be noted that the Concorde did not need to meet any noise certification standards. Nevertheless, the noise margin (relative to Stage 3) was calculated for reference. For the Boeing 737-800, similar sources were utilized to gather the required information.

Once values for the Concorde and the Boeing 737-800 were gathered, preliminary estimates for current technology supersonic vehicles (Types 1/2/3) needed to be established. However, for an appropriate estimation, performance parameters such as cruise lift-to-drag ratio and engine specific fuel consumption (SFC) values were required. Those values could be determined from preliminary constraint, mission and utilization analyses conducted based on the vehicle's design mission requirements.

Constraint and Mission Analyses

Preliminary constraint and mission analyses can be conducted based on aircraft mission requirements. A constraint analysis translates a design's performance requirements into constraints on a thrust loading versus wing loading plot. It results in the definition of a feasible design space within which a design point may be selected. Alternatively, a mission analysis flies the chosen design through a mission to determine parameters such as aircraft takeoff weight, thrust requirement and wing area. Both analyses followed the methods outlined by Mattingly et al. in the "Aircraft Engine Design" book. Mission requirements for supersonic vehicles considered in the analyses were as follows:

1. Takeoff ground roll (constraint and mission analyses)
2. Initial climb with One Engine Inoperative (constraint analysis)
3. Accelerated climb (mission analysis)
4. Constant speed climb – subsonic (constraint and mission analyses)
5. Transonic acceleration (constraint and mission analyses)
6. Constant speed climb – supersonic (constraint and mission analyses)
7. Supersonic cruise (constraint and mission analyses)
8. Deceleration and descent (mission analysis)
9. Landing ground roll (constraint analysis)

For constraint analysis, the goal is to establish a relationship between the aircraft's thrust loading (defined as the ratio between sea-level thrust and take-off weight) and wing loading (defined as the ratio between take-off weight and wing area) for every mission requirement. Such relationship is typically of the following form:



$$\frac{T_{SL}}{W_{TO}} = \frac{\beta}{\alpha}\left\{\frac{qS}{\beta W_{TO}}\left[K_1\left(\frac{n\beta W_{TO}}{qS}\right)^2 + K_2\left(\frac{n\beta W_{TO}}{qS}\right) + C_{D_0} + C_{D_R}\right] + \frac{P_S}{V}\right\}$$

where T_{SL} is sea-level thrust, W_{TO} is take-off weight, S is wing area, n is load factor, $\alpha = T/T_{SL}$ is the installed full throttle thrust lapse, $\beta = W/W_{TO}$ is the ratio of instantaneous weight to takeoff weight, q is dynamic pressure, $[K_1; K_2; C_{D_0}]$ are the coefficients of the parabolic lift-drag polar, C_{D_R} represents additional drag caused by, for example, flaps or ground friction, P_S is the weight specific excess power, and V is velocity. When relationships for all mission requirements are plotted together on a thrust loading versus wing loading plot, a design space is defined in which any point selected is a feasible design that meets all requirements. An example plot is shown in Figure 8.

For mission analysis, the goal is to utilize the results of constraint analysis (mainly the selected design point in terms of thrust loading and wing loading) and calculate takeoff weight, sea-level thrust and wing area. This is done by determining the aircraft's fuel consumption throughout the different segments of a design mission:

$$\frac{W_f}{W_i} \approx \begin{cases} \exp\left\{-\dfrac{TSFC \cdot (D+R)}{W}\Delta t\right\}, & \text{if } P_S = 0 \\ \exp\left\{-\dfrac{TSFC \cdot T}{V \cdot (T-(D+R))}\Delta z_e\right\}, & \text{if } P_S > 0 \end{cases}$$

where W_f/W_i is the ratio of aircraft final weight at the end of the segment to its initial weight at the beginning of that segment, is the thrust specific fuel consumption, $[T; W; (D+R)]$ are the instantaneous thrust, weight and drag forces, respectively, V is velocity, Δt is the total segment flight time, and Δz_e is the total change in segment energy height. For segments of the first type ($P_S = 0$), all thrust work is dissipated resulting in no speed and/or altitude variation. Examples include constant speed cruise, best cruise Mach number and altitude, and loiter. For segments of the second type ($P_S > 0$), some thrust work is converted to mechanical energy in order to vary speed and/or altitude. Examples include constant speed climb, takeoff acceleration, and horizontal acceleration. An example plot of the progression in aircraft weight due to fuel consumption throughout the design mission is shown in Figure 9.

The ratio of aircraft fuel weight to takeoff weight can be determined using the fuel consumption relations of the different mission segments and accordingly, aircraft takeoff weight can be determined:

$$\frac{W_F}{W_{TO}} = 1 - \prod_{k=1}^{n}\left[\frac{W_f}{W_i}\right]_k \quad ; \quad W_{TO} = W_P \Big/ \left(1 - \frac{W_E}{W_{TO}} - \frac{W_F}{W_{TO}}\right)$$

where n is the total number of mission segments, W_P is the payload weight and W_E/W_{TO} is the ratio of aircraft empty weight to takeoff weight (typically estimated using empirical relations). Once the aircraft takeoff weight is known, sea-level thrust and wing area can be determined using the design point value in terms of thrust loading and wing loading.

Constraint and mission analyses were integrated in the form of an interactive dashboard that allows the user to parametrically vary mission requirements and underlying assumptions (Figure 10). It was created using 'Bokeh', an interactive library that allows the creation of web front-end visualizations without requiring a large amount of html or javascript development. A screenshot of the dashboard is shown below. Concorde design point and weights are embedded for reference.

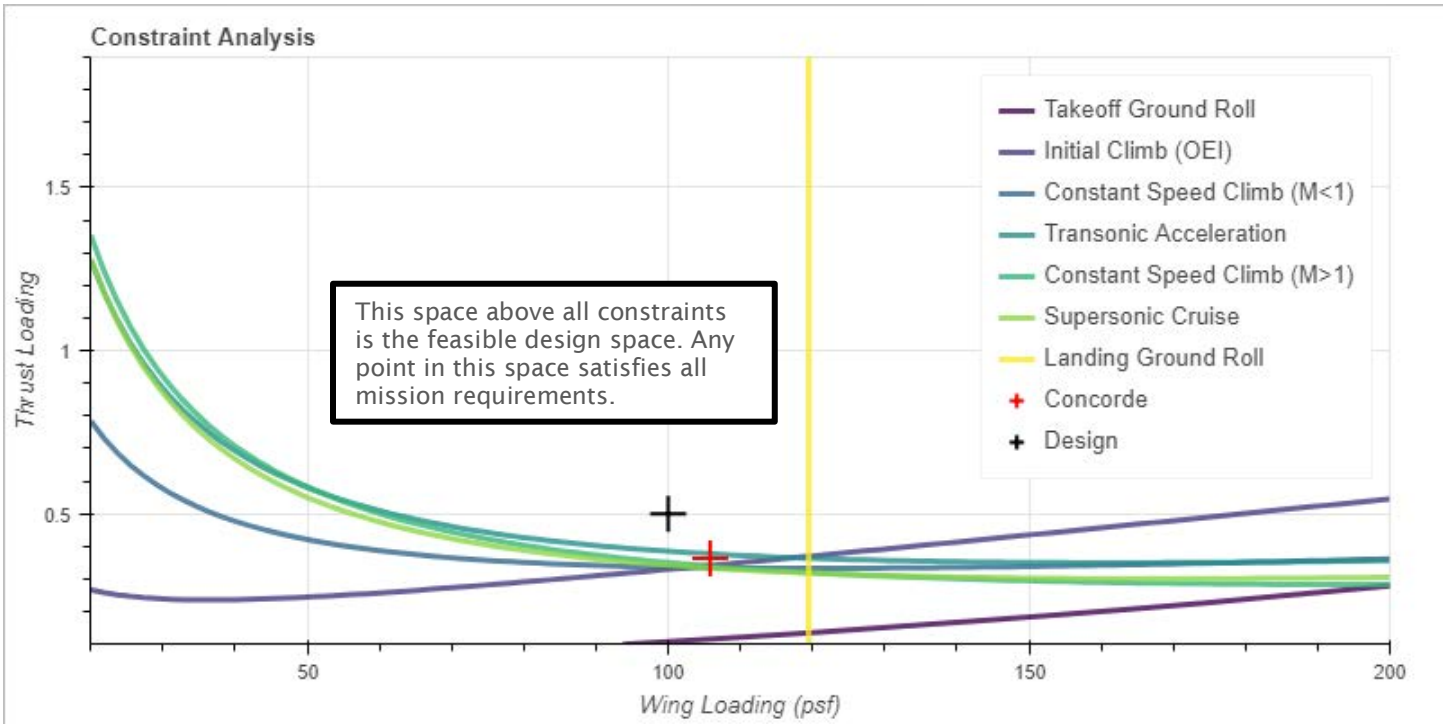


FIGURE 8. CONSTRAINT PLOT

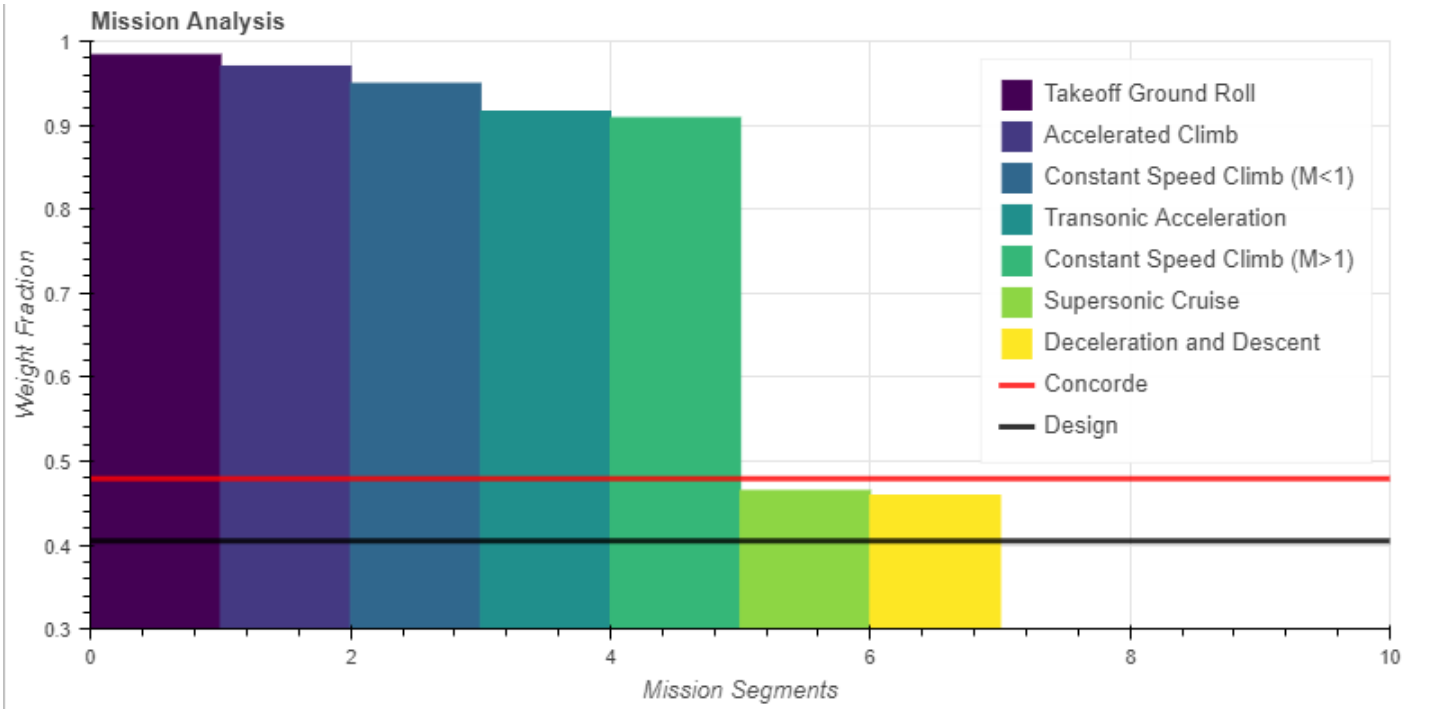


FIGURE 9. WEIGHT FRACTION ANALYSIS

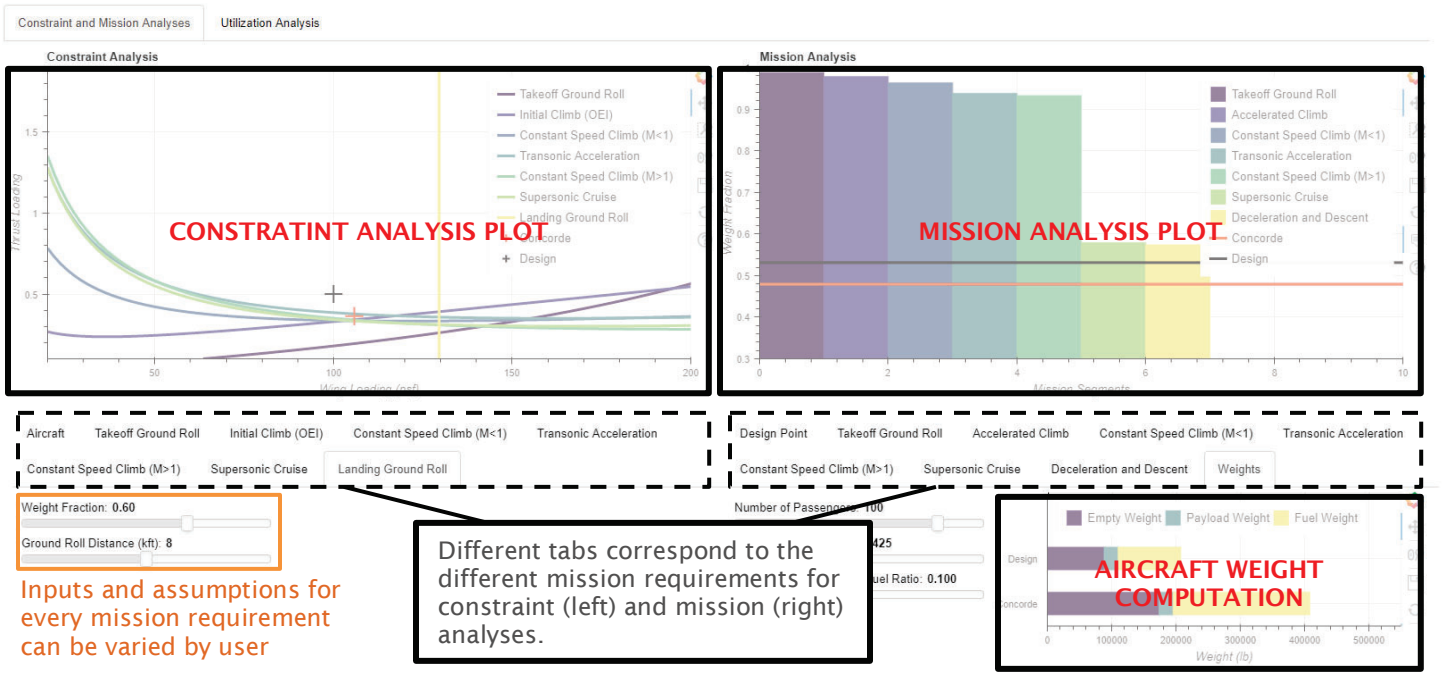


FIGURE 10. SYNTHESIS AND SIZING OVERVIEW

Using publicly available Concorde data (such as cruise lift-to-drag ratio and SFC), the underlying models of the dashboard were calibrated such that the design point and weights of the Concorde were matched (refer to the snapshot below).



FIGURE 11. MATCHING CONCORDE DESIGN

Next, using the calibrated models, and by utilizing appropriate assumptions to account for efficiency gains in terms of aerodynamics (drag polar), propulsion (SFC) and structures (empty weight fraction), a preliminary assessment of two concept

supersonic vehicles was conducted. The first vehicle represents a 10-12 passenger business jet, while the second represents a 50-60 passenger airliner. The two snapshots in Figure 12 and Figure 13 show the results for both vehicles, respectively.

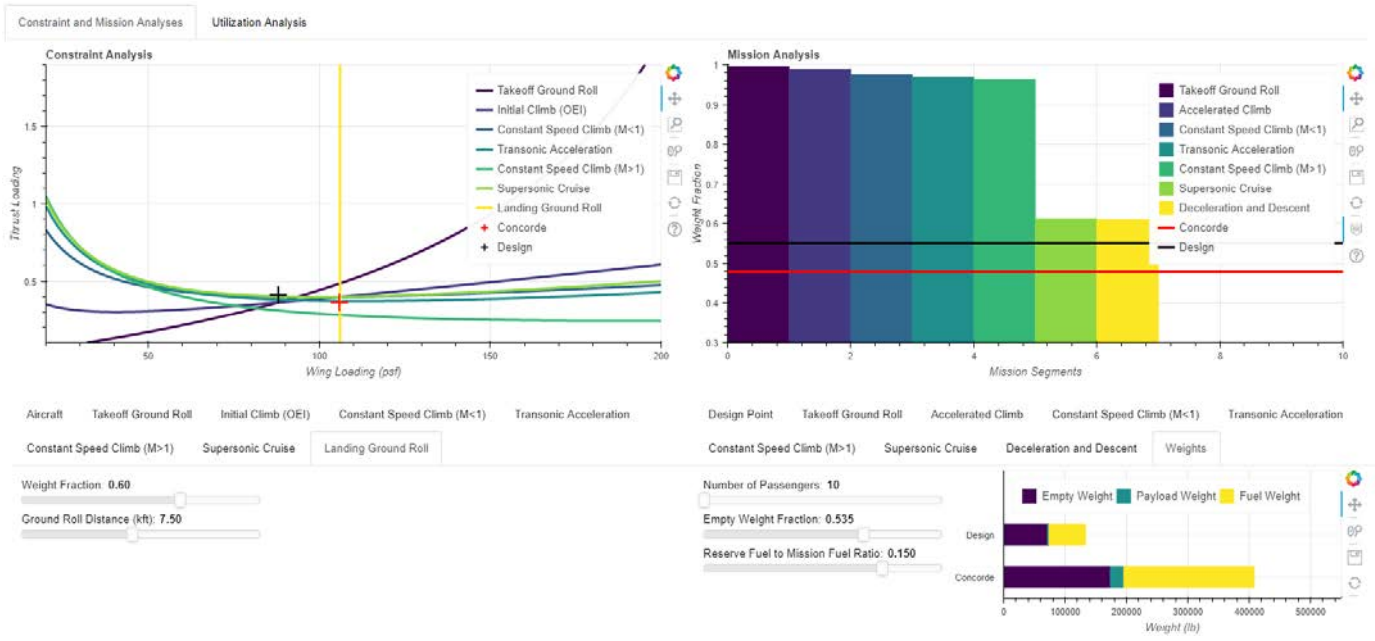


FIGURE 12. EXPLORING A SUPERSONIC BUSINESS JET DESIGN

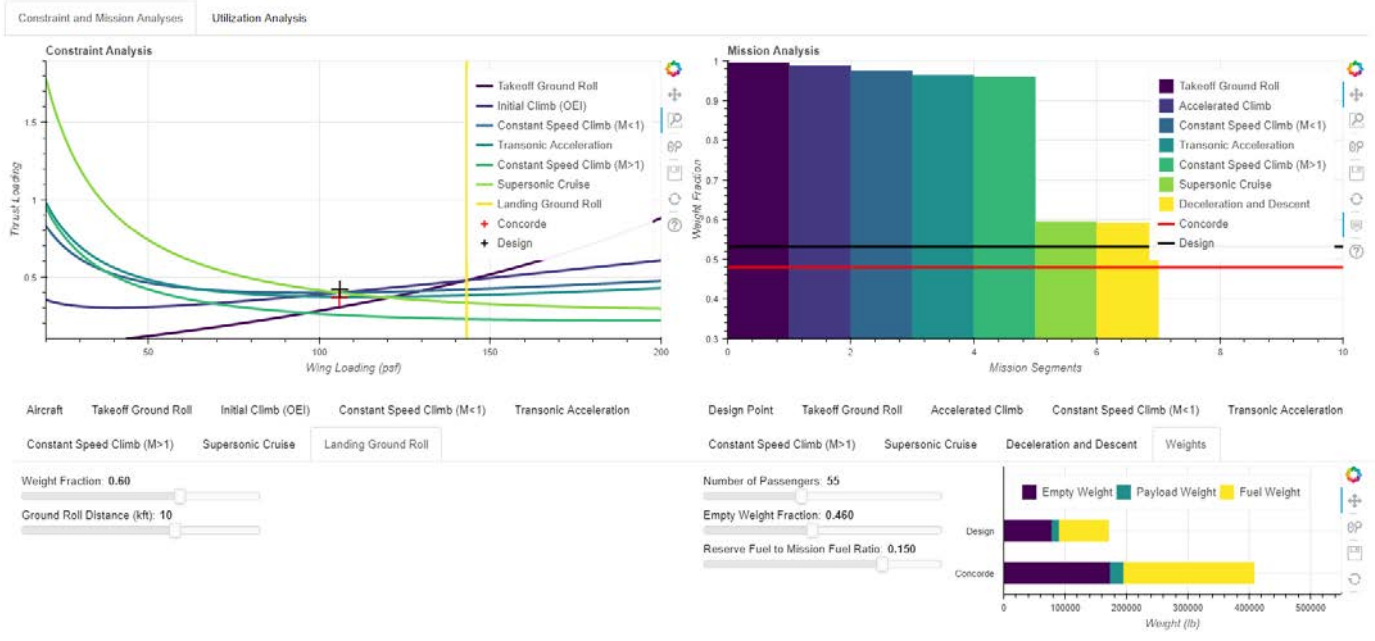


FIGURE 13. EXPLORING A 55 SEAT SUPERSONIC AIRLINER DESIGN



Aircraft Utilization

Aircraft utilization can be analyzed using general flight and aircraft characteristics. The goal of a utilization analysis is to gauge the potential productivity of an aircraft. For supersonic vehicles, productivity is assessed in terms of the potential time savings per flight (relative to a subsonic vehicle) and the maximum aircraft utilization possible within a 24-hr period. Similar to constraint and mission analyses, utilization analysis was integrated in an interactive dashboard that allows the user to parametrically vary flight and aircraft characteristics. A screenshot of the dashboard is shown in Figure 14.

Total flight time is broken into four components: time to takeoff and climb, time to descend and land, cruise time, and turnaround time (in cases where flight range exceeds maximum design range). The first two are user inputs and are assumed the same for both subsonic and supersonic vehicles. Cruise time for the subsonic vehicle is simply computed as cruise range divided by cruise speed (which is derived from user input Mach number and cruising altitude). However, for supersonic vehicles, cruise time also depends on the percentage of flight over water. This is because supersonic vehicles may be restricted to fly at subsonic speeds over land. Therefore, the percentage of flight over water along with the subsonic cruise settings (for portions of the flight over land) have been embedded in the dashboard as inputs that the user may vary, as shown in orange in Figure 15 (note: to simulate unrestricted operations, percentage over water should be set to 100).

Cruise flight time is hence calculated as:

$$t_{C,sub} = S_C / V_C$$
$$t_{C,sup} = x \cdot \left(S_C / V_{C,sup}\right) + (1 - x) \cdot \left(S_C / V_{C,sub}\right)$$

where $[t_{C,sub}; t_{C,sup}]$ are cruise times for the subsonic vehicle and supersonic vehicle, respectively, $[V_C; V_{C,sub}; V_{C,sup}]$ are the cruise speeds for the subsonic vehicle, supersonic vehicle flying subsonically, and supersonic vehicle flying supersonically, respectively, x is the percentage of flight over water, S_C is the cruise range, and $R_{C,max}$ is the maximum cruise range of the supersonic vehicle. For flights that exceed the maximum cruise range of the supersonic vehicle, it is necessary for the vehicle to descend and land, refuel and turnaround, then takeoff and climb back to cruising altitude. Therefore, for every stop that the vehicle needs to make, total flight time is increased by these additional components. The time to turnaround is also a user input (shown in green in Figure 15).

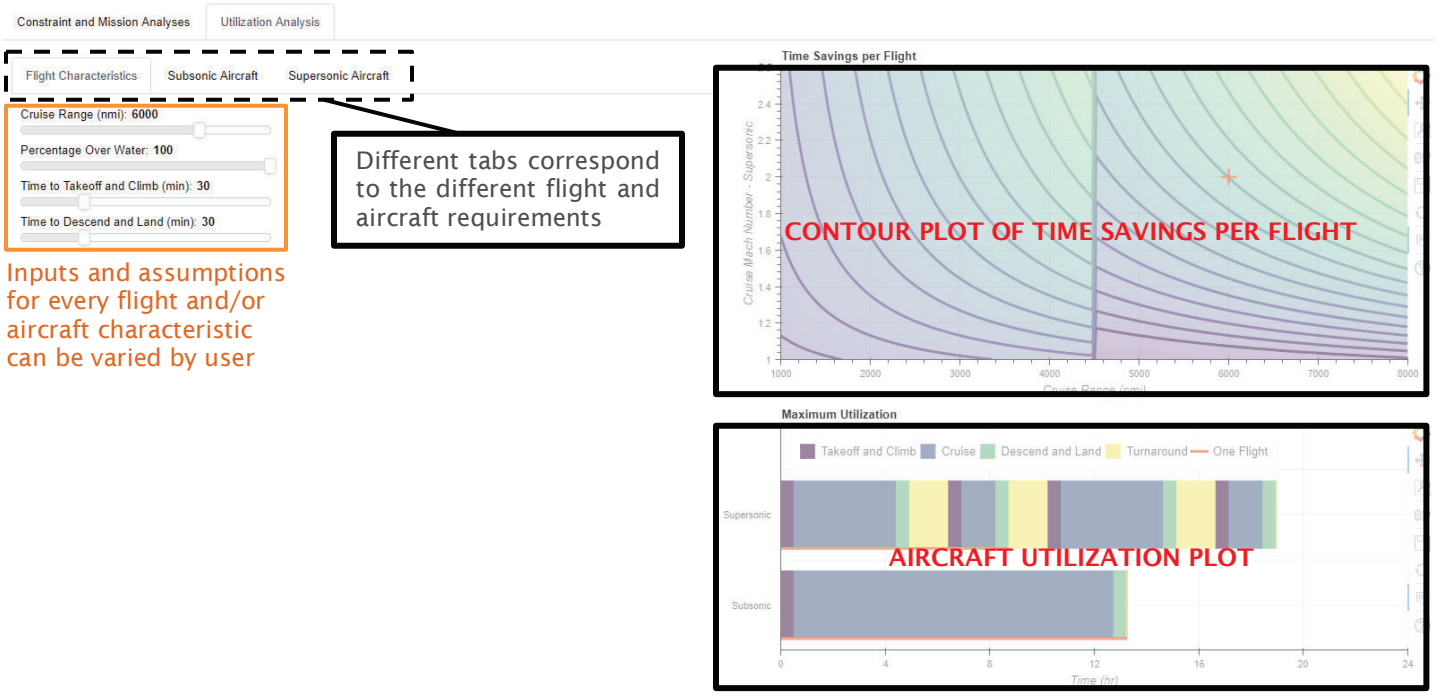


FIGURE 14. EXPLORING MISSION FREQUENCY AND UTILIZATION

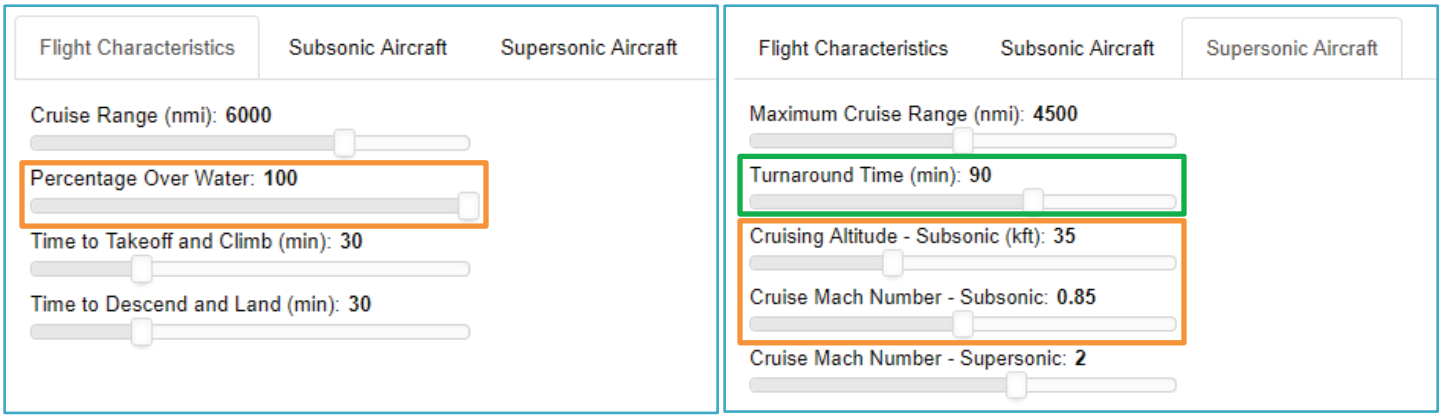


FIGURE 15. AIRLINE OPERATION ASSUMPTIONS

Based on the previous, a contour plot of time savings per flight ($t_{total,sub} - t_{total,sup}$) can be constructed as a function of cruise Mach number of the supersonic vehicle and cruise range. Figure 16and Figure 17 show two example cases (percentage over water is 100 for both). In the first example, the cruise Mach number and cruise range are set to be 2.0 and 6000 nmi, respectively (shown as the red cross in the figure), while the maximum range of the supersonic vehicle is set at 4500 nmi. This is the reason a vertical distortion in the contour lines appears at 4500 nmi since additional time is required to make a refueling stop for any range beyond that value. In this example, total time savings was 4.5 hours. In the second example, the cruise Mach number and cruise range are set to be 2.0 and 7000 nmi, respectively (again shown as the red cross in the figure), while the maximum range of the supersonic vehicle is set at 3000 nmi. In this case, two vertical distortions appear in the contour lines because one refueling stop would be required for any range between 3000 nmi and 6000 nmi and

another stop would be required for any range greater than 6000 nmi. In this example, total time savings were 3.2 hours (note: time savings per flight are displayed when the user hovers the mouse pointer over any point in the plot).

Aircraft utilization within a 24-hour period for both subsonic and supersonic vehicles can also be determined using the user input flight and aircraft characteristics. Based on the total flight time per trip, and taking into account the turnaround time on the ground, the maximum utilization can be determined. Aircraft utilization corresponding to the two example cases are shown in the figures below. As shown in the Figure 18 andFigure 19, a supersonic return flight is possible in the first case with an overall utilization of approximately 19 hours (including turnaround time). In the second case however, the supersonic aircraft requires two refueling stops to accomplish its mission in approximately 12 hours, with no time left to turnaround and complete a return flight.

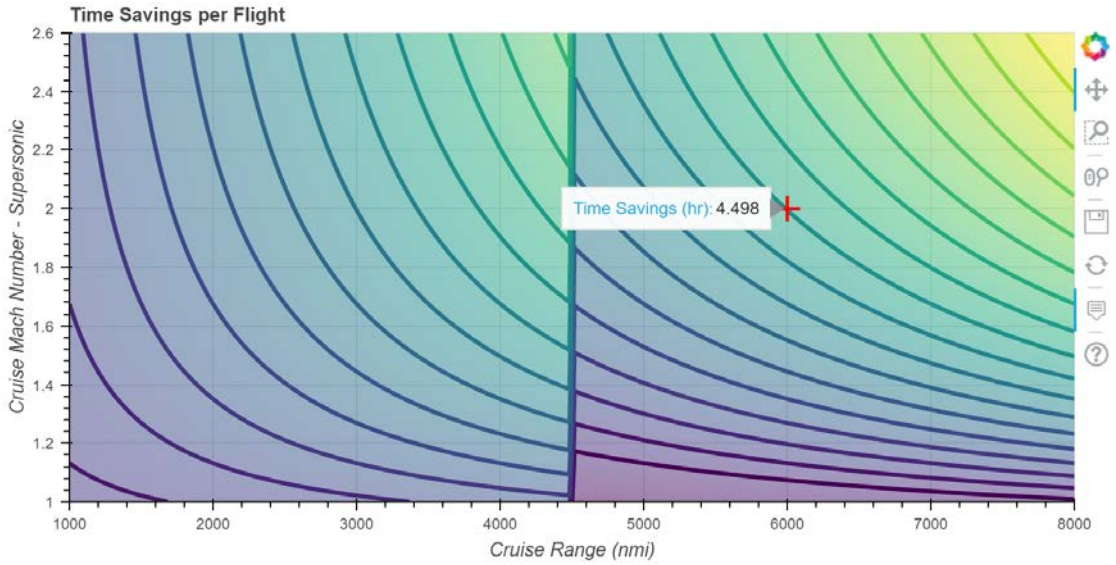


FIGURE 16. TIME SAVINGS FOR MACH 2.2 AND 4500 NMI MAXIMUM RANGE

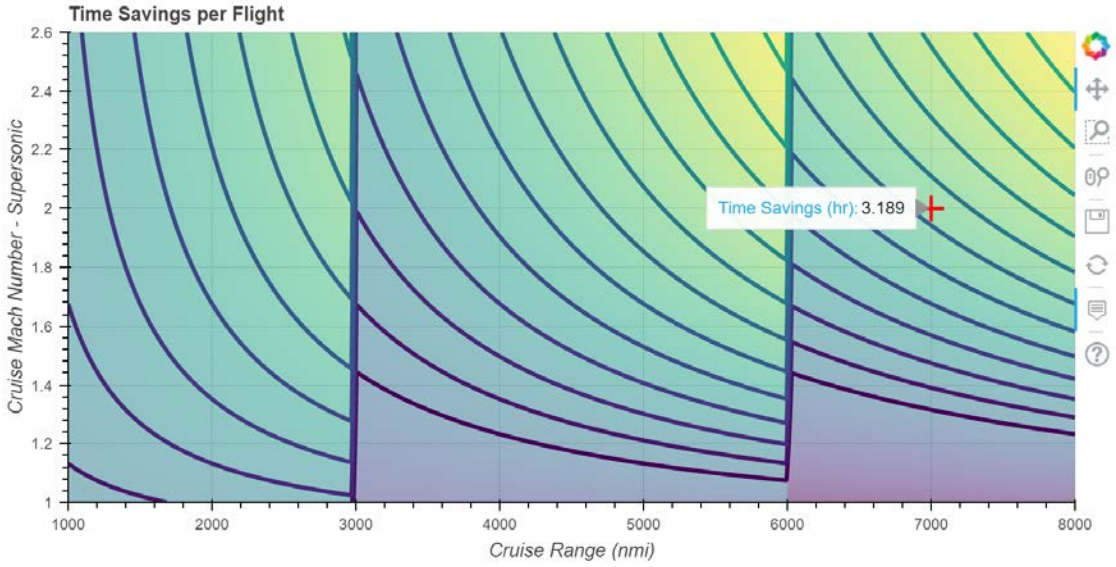


FIGURE 17. TIME SAVINGS FOR MACH 2.0 AND 3000 NMI MAXIMUM RANGE

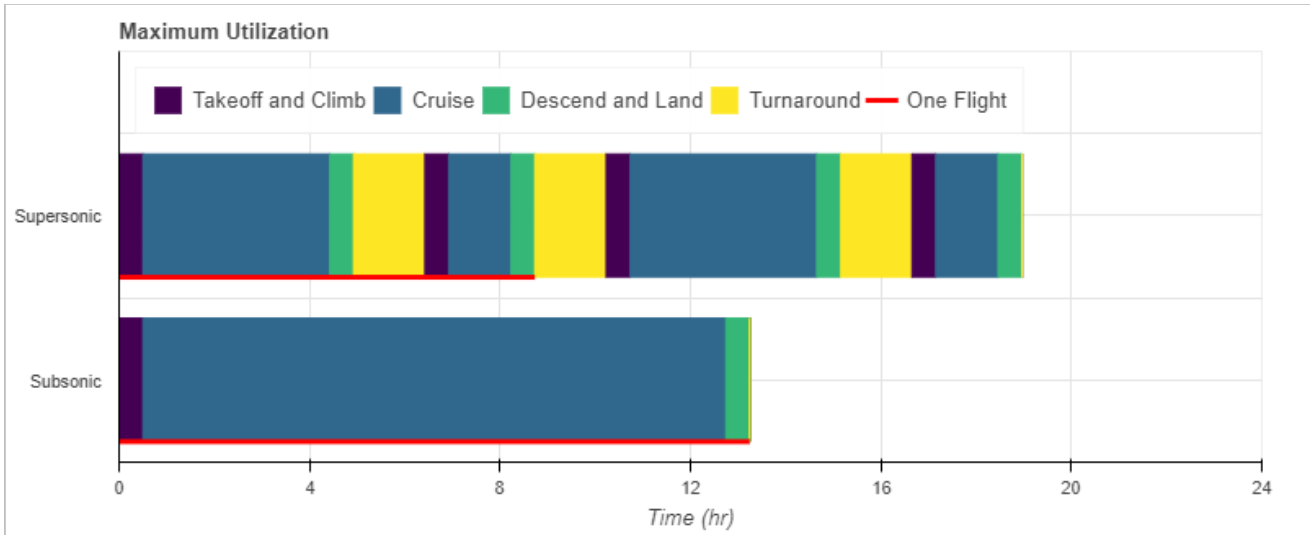


FIGURE 18. UTILIZATION FOR SUPERSONIC VS SUBSONIC MACH 1.4

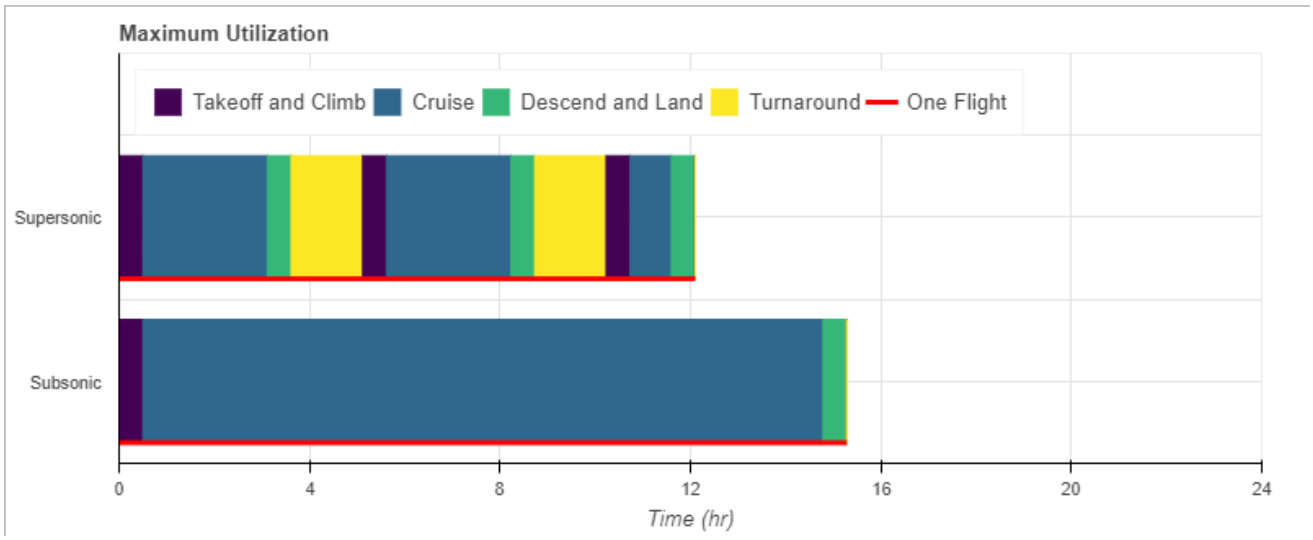


FIGURE 19. UTILIZATION FOR SUPERSONIC VS SUBSONIC MACH 2.2

A utilization analysis was conducted for the two concept supersonic vehicles that were assessed using constraint and mission analyses. For the 10-12 passenger business jet, with a cruise Mach number of 1.4 and a maximum range of 4000 nmi, a design range equal to its maximum provides aircraft utilization of approximately 21 hours (assuming percentage over water is 100). The supersonic business jet provided 3.1 hours of time savings per flight relative to the subsonic vehicle. It was able to complete three flights within a 24-hour period compared to just two for the subsonic vehicle. Similarly, for the 50-60 passenger airliner, with a cruise Mach number of 2.2 and maximum range of 4500 nmi, a design range equal to its maximum provides aircraft utilization of approximately 22.5 hours (assuming percentage over water is 100). The supersonic airliner provided 5.6 hours of time savings per flight relative to the subsonic vehicle. It was able to complete four flights (two round trips) within a 24-hour period compared to just two (one round trip) for the subsonic vehicle. The utilization plots for the two concept vehicles are shown in the figures below. The results show that for their respective design mission ranges, the two concept supersonic vehicles offer high productivity from a utilization standpoint. Both vehicles managed to perform more flights and resulted in higher utilization within 24 hours compared to their subsonic references (Figure 20 and 21).

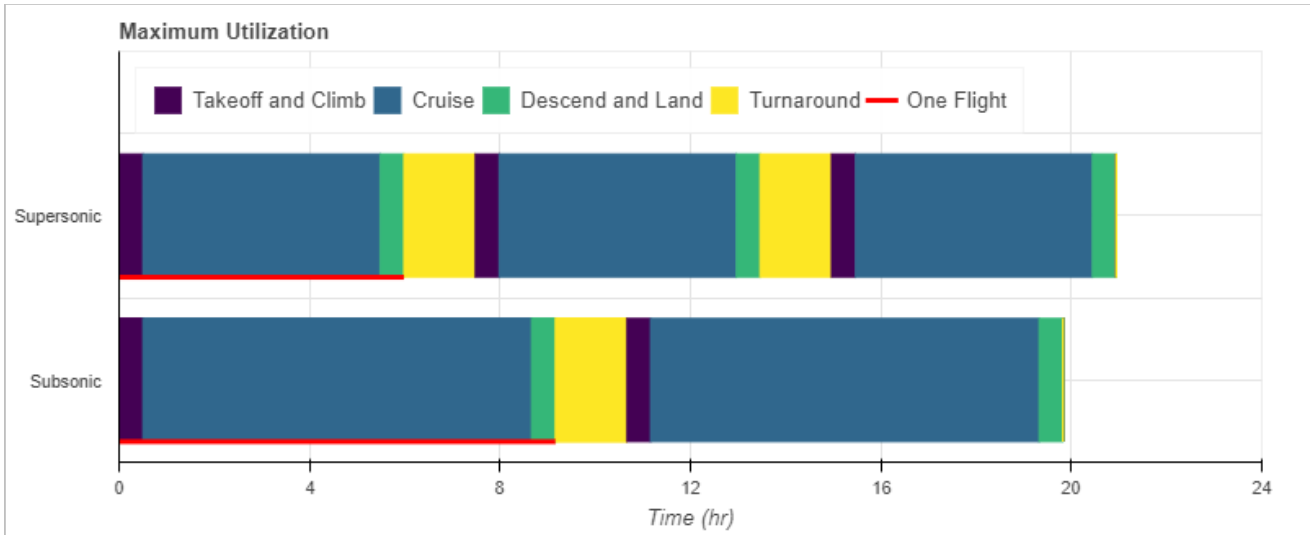


FIGURE 20. UTILIZATION FOR SUPERSONIC VS SUBSONIC MACH 1.4

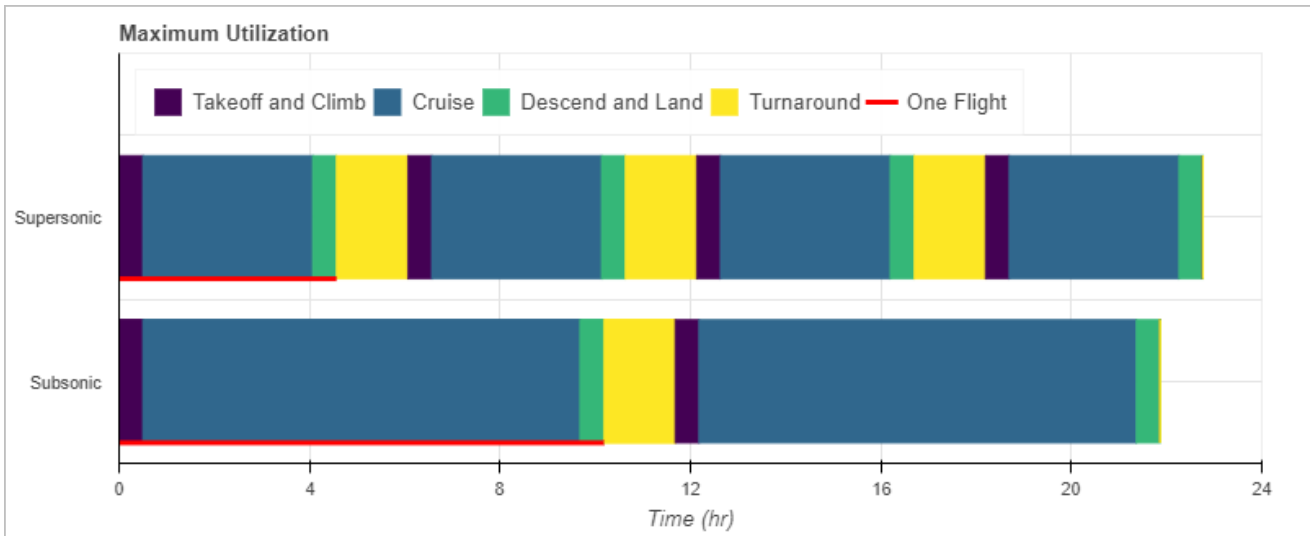


FIGURE 21. UTILIZATION FOR SUPERSONIC VS SUBSONIC MACH 2.2

Preliminary Estimates

For the two concept supersonic vehicles considered in the previous constraint, mission and utilization analyses, a preliminary estimate of fuel efficiency can be determined using number of passengers, design range and block fuel. For the supersonic business jet, fuel efficiency was computed to be 1.275 lb/seat/nmi. This value is more than double of that of the Concorde. However, that was expected based on the low number of seats. Alternatively, for the supersonic airliner, fuel efficiency was computed to be 0.275 lb/seat/nmi. This value is almost half of that of the Concorde and is in perfect alignment with the NASA near- and mid-term goals. Results for fuel efficiency are summarized in Table 8.

As for preliminary estimates for the other KEIs, such as cruise NOx emissions and airport noise, those remain to be investigated. The bulk of the effort for Task 2 was dedicated to the construction of the interactive and parametric conceptual design tools (dashboard), and the analysis of fuel efficiency. Surely, the developed tools will be utilized in a similar manner to assess the remaining KEIs in future work.



TABLE 8. SUMMARY OF CHARACTERISTICS FOR TWO SUPERSONIC AIRCRAFT CONCEPTS

	Supersonic Business Jet	Supersonic Airliner
Number of Seats	10	55
Design Ranger (nautical miles)	4000	4500
Block Fuel (pounds)	51000	68000
Fuel Efficiency (pounds per seat per nautical mile)	1.275	0.275

Task 3- Investigation of AEDT Ability to Analyze Supersonic Vehicles

Georgia Institute of Technology and Purdue University

Objective

Fleet Level Technology Assessment

This task focused on identifying the modeling capabilities and potential gaps in the tools used for aircraft environmental predictions. Georgia Tech was to identify existing models of supersonic aircraft in the AEDT vehicle database, including the Concorde and some military aircraft. AEDT studies were to be created on some routes of interest to generate single flight results for these vehicles, and their modeled KEIs were to be documented. Additionally, Georgia Tech was to update and attempt to import and generate the same information for AEDT vehicle coefficients for a 100 passenger supersonic aircraft that was previously developed for the NASA NRA "Integration of Advanced Vehicle Concepts into the NAS". In this process any potential errors or gaps in the capability were to be documented. In order to identify potential modeling gaps, coefficients in the AEDT vehicle modeling definitions that pertain to the specifics and peculiarities of those vehicles were identified. An existing known subsonic aircraft with general characteristics close to the vehicles under study were to be duplicated and coefficients used in certain aspects of modeling and phases of flight were to be adjusted to possible values for that particular supersonic aircraft. The resulting definition of this adjusted vehicle were to be run through AEDT to identify potential errors or gaps in modeling capability. This was to be documented, along with potential solutions for addressing the particular requirements of modeling supersonic aircraft.

Research Approach

To facilitate environmental impact prediction of supersonic aircraft, it is necessary to identify the modeling capabilities and potential gaps in the tools used for these predictions. As part of this task we identified existing models of supersonic aircraft in the AEDT vehicle database, including the Concorde and some military aircraft. These models were then reviewed as to how these aircraft were modeled. The next step will be to create AEDT studies on some routes of interest to generate single flight results for these vehicles and document the modeled KEI information for these aircraft types. In order to identify potential modeling gaps, coefficients in the AEDT vehicle modeling definitions were identified that pertain to the specifics and peculiarities of those vehicles.

Supersonic Vehicles in AEDT

The first step of the task was to test one of the current supersonic models existing in the AEDT database. The primary civilian aircraft that exists in AEDT's fleet database is the Concorde.

For this, a study was created in AEDT to plot the noise contour generated by a take-off of the Concorde at JFK airport. The first step is selecting the adequate equipment, which is the CONCORDE/OLY593 in the AEDT database.

TABLE 9. DEFAULT CONFIGURATION OF CONCORDE IN AEDT

Max gross landing weight (lb)	245000
Max landing distance (ft)	10600
Max gross take-off weight (lb)	400000
Number of engines	4
Max sea level static thrust (lbs/engine)	38100
Max operating speed (knots)	500
Max operating Mach number	1.2
Max operating altitude (ft)	41000
Wing surface area	181.2

To test out the Concorde noise estimates in AEDT it is necessary to select an airport in AEDT. JFK airport (KJFK), with default layout was chosen for this purpose. The operation has to be defined for the aircraft; here take-off is chosen, for the North-East track. An annualization for this operation is then defined (i.e. the frequency of such an operation). We wish to plot the contours for a single flight, so we do not repeat the operation over time. It should be noted that historically the
Next, a receptor grid has to be generated. We chose a 120x120 receptor grid, spaced out by 1.5 nautical miles each. The grid has to be centered on the airport and large enough to allow the noise contours to be closed, otherwise they will not be plotted by AEDT.

In this case the most relevant metric for noise of an aircraft c was the Single Event Level (SEL), which is the most appropriate for a noise metric for a single flight, because it is the metric that is used in aggregated form in the Day-Night-Level (DNL) for regulatory purposes. With these parameters, the simulation on AEDT gives the following noise contours shown in Figure 22. It should be noted that this is for a specific straight departure from JFK only. This does not represent in any way the departures that Concorde performed in the past, which were cognizant of the fact that in order to minimize noise exposure over land the actual tracks were heavily biased to be over water. Furthermore, this straight path does not follow any currently used tracks at JFK or in the New York airspace.

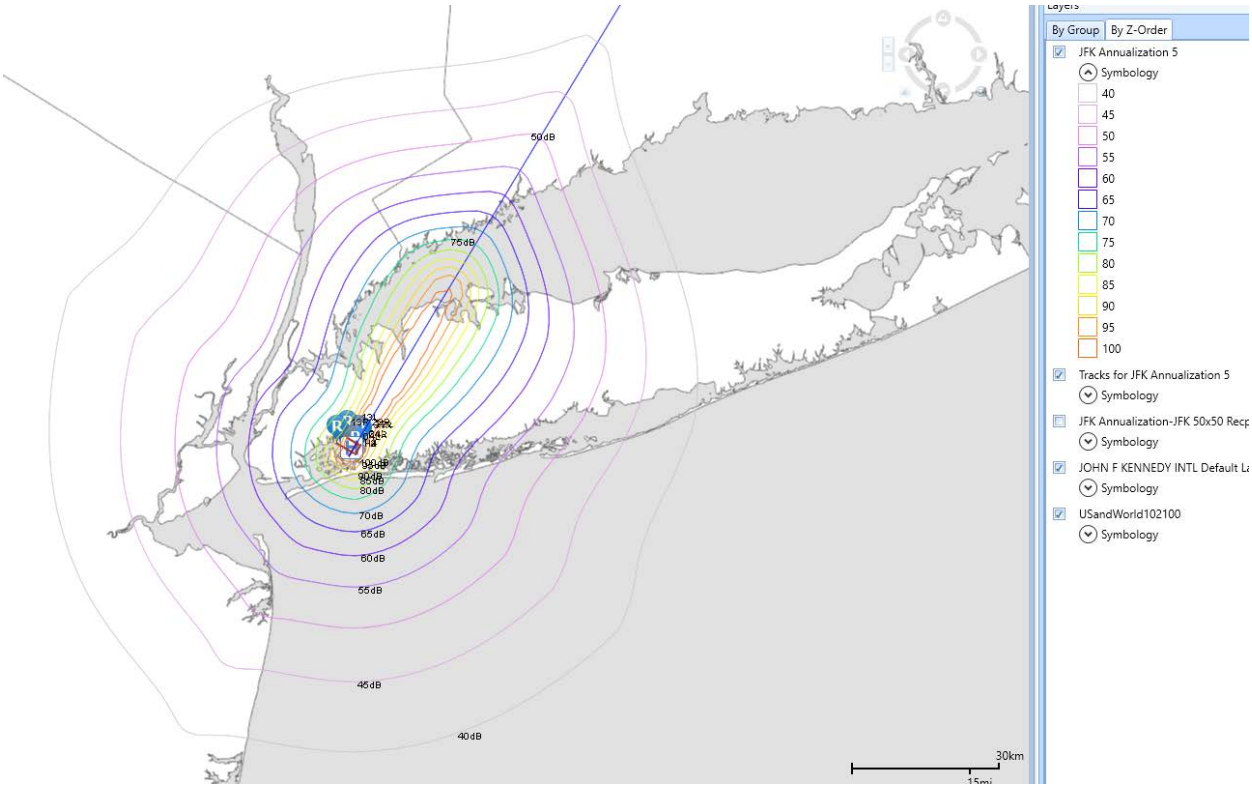


FIGURE 22. NOISE CONTOURS FOR CONCORDE TAKE-OFF AT JFK

A simulation for several flights of the Concorde were performed through the AEDT tester developed by ASDL. The tester takes all the flights combinations from AEDT database and performs the calculation for the flights suitable for the chosen aircraft.



AEDT model of the Concorde

Aircraft Noise Performance (ANP) Model
The ANP model data contain a Concorde model. This is not surprising, given that the Concorde was one of the first aircraft to undergo noise certification, which provides the necessary data to create the ANP model. The model has a few interesting features, likely due to the age of the model data. First, it only includes STANDARD procedures and no ICAO procedures, even though the Concorde did use noise abatement procedures. Another feature of the ANP model is that it includes a standard climb power thrust curve and a reheat thrust curve, which are both used in the procedures. However, it does not include alternate thrust curves for temperature variations as found in most current ANP models.

Looking and the noise model for the Concorde, there are only three thrust settings for which noise curves exist. Additionally, the highest departure thrust noise curve is at 32klbf thrust per engine, whereas the Concorde produced close to 38klbf per engine with reheat. This means that if the thrust exceeds the value of the highest thrust noise curve, the noise values will be extrapolated. In this case, even at 32klbf thrust, the noise at 200ft distance is 138db SEL, which is without reheat. Extrapolating this would push the noise close to 140dB. The spectral classes that are being used in the noise modeling for atmospheric adjustments are 106 and 206, which are the low bypass relative frequency loudness adjustments.

BADA 3
The BADA model database is used in AEDT for aircraft modeling over 10,000 ft above field elevation and especially during cruise phases. Since this model and database is relatively new, having been introduced after the retirement of the Concorde, it does not contain a Concorde model. The AEDT fleet database default substitution model is the “FGTL” (generic heavy fighter) model, which is based off the Rockwell B1 Lancer using a cruise Mach of 0.8. This substitution is likely based of the closeness in the MTOW (180,000 kgs vs 186,000 kgs) and the same number of engines with similar SLS thrust.

Engine Emissions Databank (EEDB)
The latest versions of the EEDB do not contain any information of the Olympus engines. However, the AEDT fleet database does contain an entry, which is marked “EDMS 4.5 – Rolls Royce”. Therefore, we can presume that the engine at one point existed in the EEDB and was eventually removed after the retirement of the Concorde. It should also be noted that the data does not include thrust information and it is therefore not possible to conclude from this whether the data does or does not include reheat information. Additionally, the entry contains four values for fuel flow and each emissions species. This, however, does not match the expected five sets of values for the certification of supersonic engines. Additionally, the thrust levels for each sets of points are define considerably differently and also depend on the presence of reheat capability. Therefore, it is unclear what the values represent. It is possible to assume that these values represent subsonic engine equivalents that are designed to match the definition of the four subsonic point values. This is consistent with how AEDT will interpret these values.

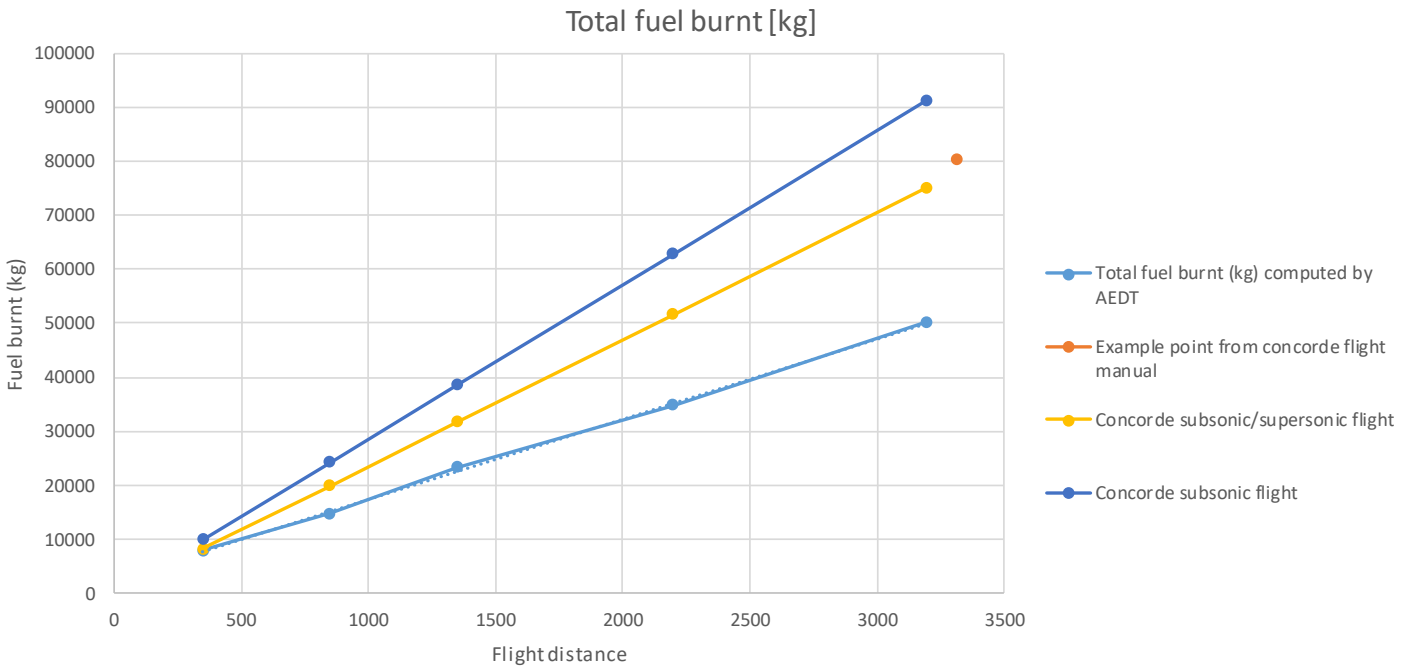


FIGURE 23. CONCORDE FUELBURN ESTIMATES BASED ON FLIGHT DISTANCE

Modeling by phase of flight

Aircraft Noise Performance (ANP) Model
The current way of modeling take-off and landing performance under 10,000 ft field elevation is to use the ANP models and the modeling methods described in ICAE Doc 9911 and previously described in SAE 1845, as well as the INM Manual. Since the modeling is derived from also modeling military aircraft, it does include provisions for aircraft whose performance characteristics are somewhat similar to high speed military aircraft, at least in the take-off and landing characteristics. Specifically, these characteristics include:

- Possible use of reheat
- Aerodynamic optimization for high speed
- Aircraft configuration changes

The possible use of reheat is addressed in a later section. The aircraft shape optimization for high efficiency at supersonic Mach numbers usually require a significant trade-off in efficiency at low speed flight. Therefore, many supersonic aircraft struggle to produce enough lift at low speeds in order to sustain flight. This means that in addition to very high angles of attack and deployable surfaces, it is often necessary to have increased speeds at take-off, such as V_1, V_R and V_2, in addition to higher speeds at low altitudes potentially in excess of 250 knots under 10,000 ft. Additionally, higher landing speeds can also be necessary. This means that the default reference speeds used in the performance modeling, but especially in the source noise modeling and data are potentially too low. The effects of this are currently being investigated in ASCENT Projects 43 and 45. Aerodynamic configurations such as additional moveable surfaces and other features that change the configuration and aerodynamics of the aircraft are implementable by defining these as additional entries into the FLAPS table and then making use of them in the corresponding procedure steps. This means that it is necessary for the manufacturer to supply this information so that it can be used during modeling.

BADA
BADA is currently used for modeling the aircraft performance over 10,000 ft above field elevation. It also only includes a single thrust and fuel curve, which might not be adequate enough to model the aircraft engine performance over a wide

variety of Mach numbers and inlet and nozzle configurations, especially in a linear fashion as is currently the standard in version 3. While the model does not explicitly cover supersonic flight, it could potentially be adopted to allow this, given additional configuration data. The current implemented version explicitly forbids Mach numbers greater than 1.0. Additionally, BADA 3 currently only provisions a single cruise configuration. This would have to be expanded to account for the difference in subsonic and supersonic configurations of the aircraft.

The climb procedure over 10,000 ft, by default, uses a defined energy share (share of potential energy contribution to altitude vs speed increases), while following a constant calibrated air speed (CAS). This is continued until a transition altitude, where the climb CAS speed equals the climb Mach number. The climb to the initial cruise altitude then continues at that constant Mach number. This mimics a relatively standard way in which conventional subsonic passenger aircraft are flown.

For supersonic aircraft, however, it is possible in the aircraft procedure coefficients to specify a second segment climb and cruise speed and Mach number such that the transition altitude occurs at a projected altitude at which the transition from subsonic to supersonic flight is expected to take place. This was tested on the 100 seat airliner model created for NASA in a previous project [4]. The result is that the current version of AEDT will handle the transition to supersonic cruise as long as the drag polar for cruise as well as the TSFC curves are designed to match cruise conditions correctly. The transition itself is handled not very well. It tends to consist of a very brief jump from subsonic to supersonic that completely misses the drag rise as well as the fuelburn and associated emissions caused by the transition. This can cause an additional modeling error on the order of a few percent of mission block fuel. However, considering the system was never designed for modeling these conditions as well as the lack of any other modeling standards, it is probably acceptable for the short term future.

Figure 24 shows that this is too simplistic for a supersonic passenger aircraft, at least the way the Concorde was supposed to be flown. Specifically, there are different procedures depending on whether a subsonic cruise or a supersonic cruise will be performed and whether or not the climb to supersonic cruise has to be delayed for overland noise rules. Additionally, the transition from subsonic flight to supersonic flight typically has to be achieved as quickly as possible in order to minimize time in very high drag conditions while not violating flight envelope and center of gravity constraints. The current number of coefficients present in the BADA procedure definition is insufficient to describe the details of this, especially if this is materially different between potential future supersonic aircraft.

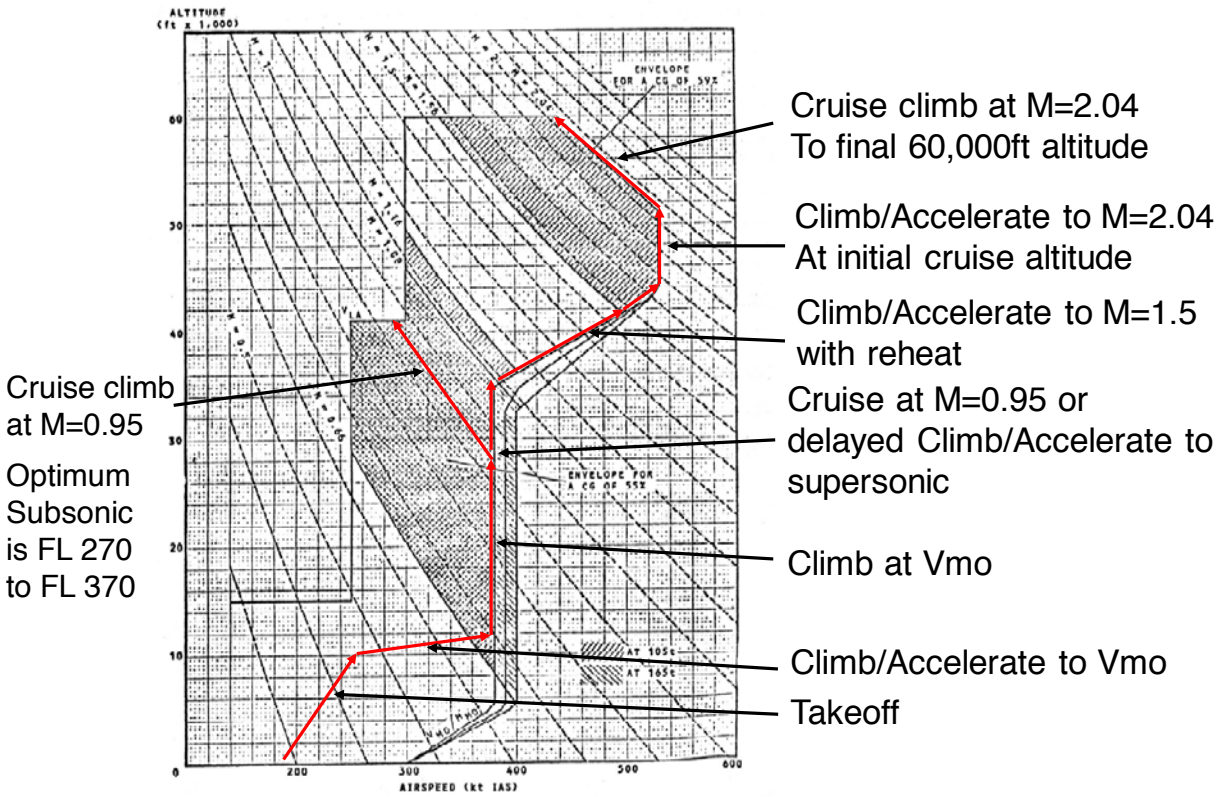


FIGURE 24. CONCORDE OPERATIONAL ENVELOPE (ALTITUDE IN FEET VERSUS INDICATED AIRSPEED IN KNOTS) WITH STANDARD CLIMB TO CRUISE PROCEDURE SHOWN[5]

Noise Modeling

The current state of noise modeling in AEDT is entirely limited to the use of Noise-Power-Distance (NPD) curves, which describe the aircraft noise signature as a function of engine thrust (power) and distance of the observer. The distance data is limited from 200 ft to 25,000 ft, but can be extrapolated – if required – using a linear method. This method is probably sufficient to properly capture the noise generated by a supersonic aircraft near and around airports but is not suited to propagating the boom noise created by the shock waves from high altitudes, nor does it capture any potential focusing or dissipating effects due to trajectory or atmospheric effects. However, there are a few research codes (such as PCBOOM), that currently allow the calculation of the boom effects on the ground. These methods and the required data will have to be integrated in AEDT, if such functionality is desired.

Emissions Modeling

AEDT uses the Fuel Flow Method v26 in order to use the ground test data obtained during engine certification and publish in the ICAO Engine Emissions Databank (EEDB). This method uses four defined throttle settings with fuel flow end emissions index (EI) values to interpolate the values over the entire flight envelope. It also adjusts the equivalent combustor inlet conditions from the sea-level static (SLS) data to the appropriate conditions at any altitude. The altitude adjustment is based on adjusting the changes in free stream conditions to equivalent changes in combustor inlet conditions using isentropic relations. Therefore, an aircraft in supersonic flight will violate this assumption due to the shocks produced by the nose and the inlet compression shocks during supersonic flight. Supersonic inlets tend to have a number of moving surfaces to optimally adjust to the required conditions and to allow the engine to operate normally and effectively during a wide range of Mach numbers. This means that the required conditions heavily depend on the specifics of the situation and the inlet configuration required. However, since it is an objective of the inlet to slow the free stream to acceptable subsonic conditions at the face of the engine inlet at all times and to minimize losses as much as possible, it is potentially possible to assign an additional inlet correction factor based the inlet total pressure recovery. This correction factor can take the form of an ideal



number based on Mach number or if available actual inlet performance. It is possible that the current combustor correction coefficients, which are based on a 1990s era CFM56 empirical correlation, have to be updated similar to the required updates for modern stage combustion engines.

The nozzle performance is an additional potential issue. Supersonic aircraft will require a much more complex nozzle compared to a simple subsonic converging exit. The Concorde utilized a secondary set of nozzles on each engine designed to improve subsonic performance. The current modeling method adjusts for installed effects with simple fixed multipliers from the ground test data. It is unclear how these multipliers will have to be adjusted due to the much larger installed effects that an integrated engine of a supersonic aircraft will present. Another potential issue is that the adjustments for speed and altitude effects compared to the static ground tests will probably have to be adjusted. The specifics of this will depend on how and which equipment will be included in the ground tests. Unlike the military aircraft noise modeling that lends itself to be adopted to supersonic passenger aircraft, there is no emissions certification requirement for military aircraft.

Reheat

The Concorde made use of reheat during take-off in order to meet certification requirements in case of engine failure, but would terminate reheat below 1000 ft if all engines continued to operate nominally. Additionally, the Concorde made use of reheat in order to minimize time spent in the transonic drag rise region during the climb to supersonic cruise.

Modern supersonic aircraft are not expected to require or include reheat due to better engine thrust and efficiency and the potential fuel penalty for not using reheat either being completely eliminated or small enough to outweigh a host of other issues, such as maintenance cost, regulatory complexity and others. It is unlikely that the capability of properly representing reheat beyond the current capabilities are required in the future.

Accomplishments

This work identified the key issues that will need to be addressed in improving the modeling of supersonic aircraft in AEDT, which are:

- Transition from subsonic to supersonic
- Supersonic cruise
- Emissions modeling
- Noise modeling
- Boom modeling

A key element in modeling a supersonic aircraft is to be able to model the transition from subsonic flight to supersonic flight. This involves crossing the highest drag regime of flight and contributes a significant amount of the fuel burn and emissions. As investigated this can currently be approximated by a sudden jump but this neglects this portion of flight almost completely. This will require modeling either through a generic transonic drag rise approximation or additional aircraft specific coefficients.

The modeling of supersonic cruise currently does work but can be improved. The atmosphere model that is used potentially has to include more sophisticated data about the actual altitudes of the atmospheric layers. Additionally, an aircraft model is currently limited to either subsonic or supersonic flight but cannot accommodate both. This is potentially necessary because supersonic cruise is currently prohibited over land and the model needs to be able to accommodate that.

After performance modeling, emissions modeling is another area for improvements. Specifically the current full flight emissions modeling method – the Boeing Fuel Flow Method (BFFM) – which is used because it avoids requiring detailed engine performance parameters. It relies on first principles physics relations for atmospheric and engine cycle approximations and empirical fits for combustor properties. This needs to be update in order to accommodate the cycle differences and the differences in operating conditions at altitude.

Finally, the modeling of aircraft noise needs to be addressed. The airport noise is not specifically different for supersonic aircraft, but will be dominated by jet noise due to the potentially high exhaust speeds that are requires for supersonic cruise. This will potentially require the de-rating for take-off in order to meet stringent noise limits. This will have to be addressed in potentially a similar way as subsonic de-rating is handled in AEDT. It will become necessary to integrate supersonic boom modeling with AEDT. This can be accomplished either through the validation and integration with existing tools – such as PcBOOM and others – or alternatively direct integration of modeling methods or code into AEDT. There is some work required before AEDT will be able to model supersonic aircraft with good fidelity, but the issues have been identified.

Task 4- Fleet-Level Environmental Assessments

Objective

This task was to quantify the fleet-level impact of supersonic aircraft. Georgia Tech was to use the GREAT fleet prediction tool to perform a preliminary assessment of the impact of supersonic aircraft using a subset of scenarios from prior ASCENT 10 work and for a subset of the KEIs and aircraft types evaluated in Task 2. Similarly, Purdue was to utilize their FLEET capability to analyze such impact.

Research Approach – Georgia Tech

To prepare modeling supersonic aircraft several changes to the modeling toolchain had to be made. First, inside GREAT and IDEA the current subsonic fleet is divided into seat classes in order to track the different sizes as well as payload-range capabilities of the current fleet of aircraft in operation. In order to model a supersonic fleet, the team decided to add a new seat class "SST", in order to track these new aircraft separately. It should be noted, however, that this means that for now there is only a single type of supersonic aircraft that is being tracked. For now this was a 55 seat commercial jet with a maximum range of approximately 4500nmi that tries to mimic one of the potential new market entrants that could enter service in the next few years. For now it was decided to set the earliest entry into service date (EIS) to 2025.

The model was also altered in two ways in order to model the potential amount of supersonic flights. First, it is now possible to simply specify an amount of the fleet that would be switched or replaced by supersonic flights. It should be noted that it is possible to specify this for all modeled regions: Domestic, Atlantic, Pacific, Latin-America, Other. Therefore, it becomes possible to investigate the implications of switching a certain amount of passengers or flights in those regions. This is especially important with regards to investigating the potential of allowing overland supersonic flights or not, since most domestic flights are almost 100% overland flights in the U.S. This also has an effect of what missions and markets a potential supersonic aircraft would be used on.

The second method that was added to the models builds on this capability by partially reusing the logic of converting production numbers into potential replacement aircraft and therefore the ability to replace a certain share of the projected operations. This allows the user to specify aircraft production rates. The produced aircraft are then inserted into the fleet to be used to replace existing aircraft. This also necessitates assuming a productivity per aircraft. This is normally a function of primarily utilization since subsonic fleet block times and speeds (the gate to gate time and average speed based on it) have been relatively constant over the last decades. However, supersonic aircraft by definition have a much higher block speed. They therefore in theory would be potentially capable of flying many more mission than a subsonic aircraft. However, based on the analysis in Task 2. It seems likely that keeping a high utilization would become a significant challenge and therefore it seems unlikely that supersonic aircraft would yield an increased productivity. So for now the assumptions were set to have an increased block speed with a lower utilization and therefore only a small change in the number of flights possible in a given time period per aircraft in the supersonic fleet. An example of the production assumption based on a study from Boyd Consulting Group [7] estimating a potential 10 year demand of up to 1300 supersonic airliners is shown in Figure 25. For the purposes of this it was also assumed that the manufacturer would face a four year production ramp up to the targeted production rate of eleven aircraft per month. The result is shown as a share of the overall fleet. The curve bends down significantly due to the large increases in the conventional fleet forecasts in the coming decades such that a constant production rate yields a diminishing share of the overall fleet.

The standard fleet turnover model applicable to all seat classes was also brought forward. This means the models have the capability to replace aircraft within their seat class with potential improved future aircraft with similar capabilities. For now it was assumed that a supersonic aircraft would be operated more similar to current wide-body aircraft in terms of time of ownership and the underlying financing and leasing durations and the expected useful economic life.

Using these production rate assumptions along with the vehicle specific performance estimates from Task 2 allows running of the fleet analysis. The scenarios develop for the subsonic projections of commercial aviation environmental impact can be used as a basis for analyzing the effect of a potential supersonic fleet. It should be noted that it is possible to independently vary the supersonic specific assumptions in terms of market share, production rate, passenger demand, and aircraft technology. This can serve as a guide as to the potential variability of these assumptions and is what was done for this phase of work. However, it is indeed plausible that those assumptions are not wholly independent of the assumptions developed for the subsonic only scenarios. For example, it is definitely plausible that engine and aircraft technology for both subsonic and supersonic vehicles would at least partly develop in tandem. It is also expected that passenger demand for air

travel with affect both subsonic and supersonic together and not be completely decoupled, except for some very specific cases.

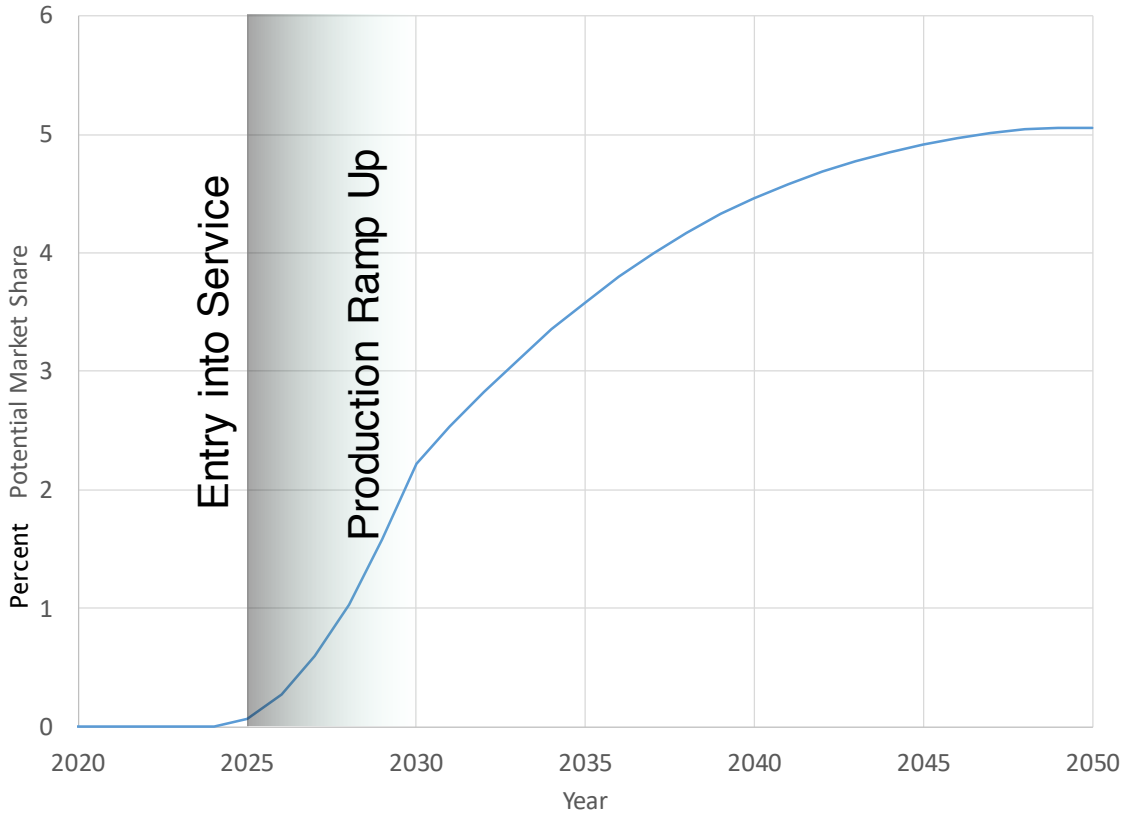


FIGURE 25. PERCENT POTENTIAL MARKET SHARE OF SUPERSONIC FLEET

The results presented here should be taken as a guide to the range of variability in the results instead of wholly consistent scenarios of the future. An example is shown in Figure 26, which shows the relative CO_2 emissions trajectories for the "Current Trends Best Guess" scenario as well as the same scenario but instead with a large fleet of operational supersonic commercial aircraft starting in 2025 using the production rate assumptions explained before.

Similar results were produced for most of the subsonic scenarios with and without supersonic aircraft being introduced. Additional metrics such as specific fleet make up as well as passenger demand and airline operating cost structure were generated in addition to the fuel burn and CO_2 emissions results. In order to summarize the results of these runs, they were aggregated as ranges of the fleet-wide delta in CO_2 emissions in 2050 that is the emissions with a supersonic fleet minus the emissions without a supersonic fleet. This shows the potential size of the resulting additional emissions a fleet of supersonic airliners could potentially produce. This is shown in Figure 27. The primary drivers of assumptions for the supersonic fleet are summarized in the three rows shown. The first row shows the impact of the market size assumption. This could range from a very limited adoption of around a dozen aircraft that only fly one to two round trips per day to the potential switch of the entire premium ticket market that is paying business, first-class, and higher passengers. This would require a large fleet of supersonic airliners, which at a multiple of fuel burn and therefore emissions would drive a significant increase in emissions. The second row shows the impact of vehicle technologies on the 2050 emissions. The worst case would be a significant fleet of current technology only aircraft – with estimates as developed in Task 2 – and the best case based on the aggressive mid- and far-term technology goals defined by NASA's supersonic vehicle project. The third row attempts to show the interaction of the primary subsonic aviation growth rates on the resultant supersonic demand. This is in effect a scaling that happens due to the overall increase or decrease – or better, high growth or low growth – of aviation

travel as a whole, of which supersonic airliners are expected to only capture a small portion. Nonetheless, it shows significant variation depending on the underlying assumptions provided by those specific scenarios.

Additionally, these ranges represent only a one-at-a-time sensitivity. There are potentially significant interactions that could take place. This means not only interactions between the scenario assumptions for subsonic and supersonic demand, technology, operations, etc, but also the interactions between the supersonic market adoption rate, aviation growth, as well as vehicle technology. This was not studied at this stage of the project, but it is envisioned to do so once better vehicle performance and demand estimates have been developed.

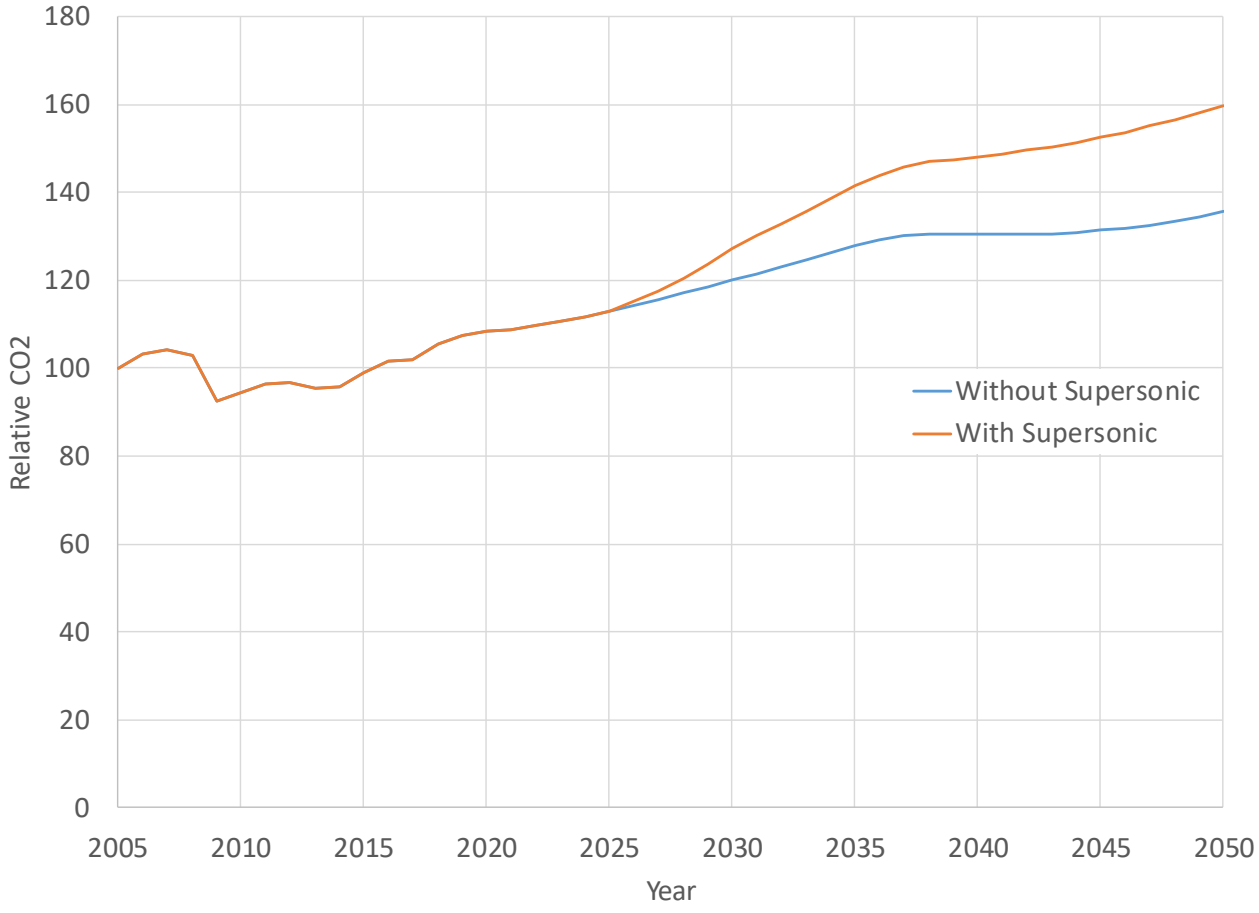


FIGURE 26. CURRENT TRENDS BEST GUESS SCENARIO EFFECT OF INCLUDING LARGE SUPERSONIC FLEET (FIGURE 25)

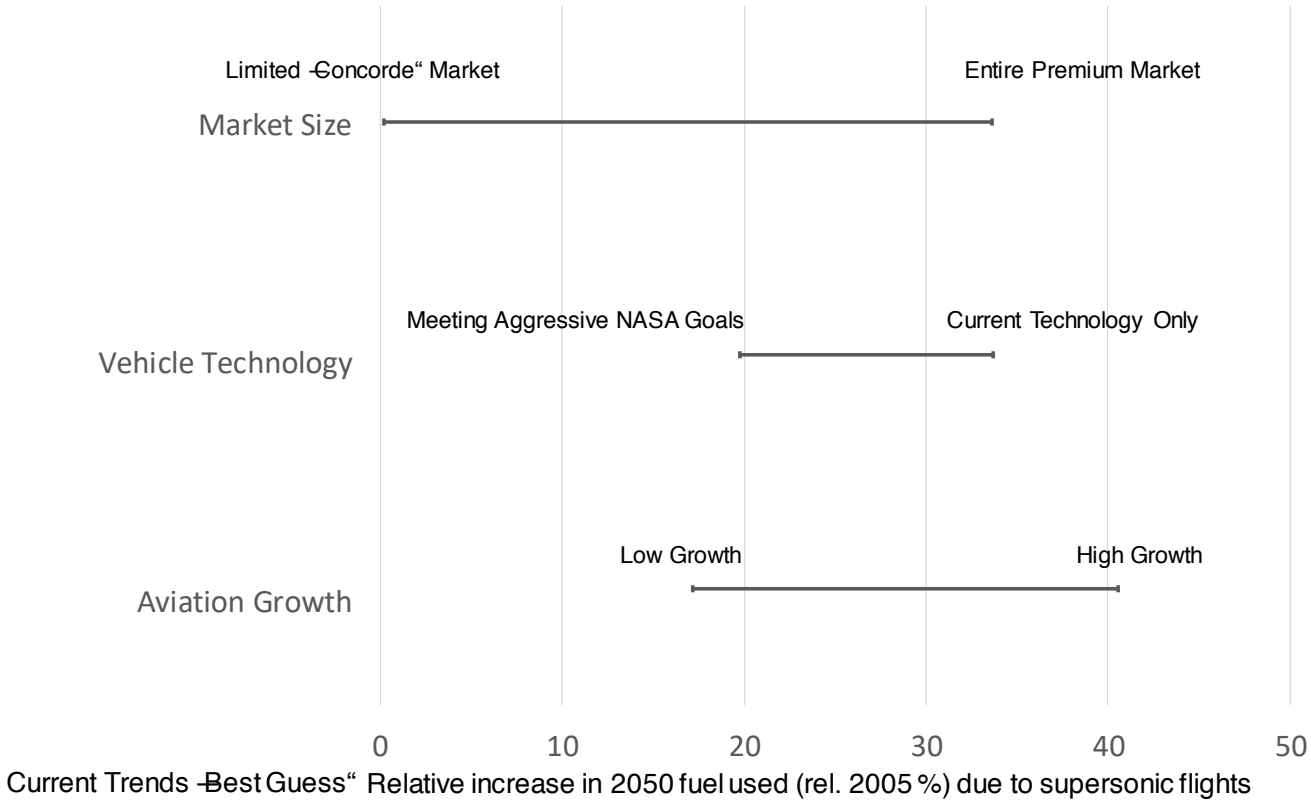


FIGURE 27. RANGE OF RESULTS DUE TO POSSIBLE ASSUMPTIONS FOR SUPERSONIC AIRCRAFT

Research Approach – Purdue

Vehicle and Fleet Assessments

Incorporating Supersonic Aircraft in FLEET Allocation Problem

In FLEET, there are two ways to conduct the airline aircraft allocation with supersonic aircraft in the airline's fleet, the sequential approach and the simultaneous approach. In the sequential allocation approach, FLEET allocated the airline's supersonic aircraft first to satisfy the identified supersonic flight demand. Then, it uses subsonic aircraft to carry the unsatisfied supersonic flight demand remaining from the supersonic allocation along with all of the subsonic demand. For both subsonic and supersonic demands, the airline cannot carry passenger more than the available market demands. This approach is consistent with the assumptions that the supersonic ticket fares are similar to the current business and first classes ticket fares, so that the supersonic flight demand come from the business and first classes demand. Passengers would generally choose a supersonic flight first because of the shorter block hours, if the supersonic ticket fare is similar to the business and first classes fares on subsonic flights. In the simultaneous allocation approach, the airline allocates the supersonic and subsonic aircraft at the same time to satisfy both supersonic and subsonic flight demands. The simultaneous approach is slightly more complicated to implement, but this would provide a more holistic approach to enforcing noise and/or airport capacity constraints, if those are desired.

Subsonic and supersonic aircraft sequential allocation approach

Figure 28 shows the flowchart of subsonic and supersonic aircraft sequential allocation approach. In each simulation year, FLEET predicts the inherent airline passenger demand growth due to the economic growth and adopts the price-demand elasticity to show the influences of airline ticket price changes from last year on demand. Subsequently, the total demand is

split into subsonic demand and supersonic demand. In the work to date, the team has been using the notion that proposed supersonic transport aircraft will operate with a ticket price roughly equivalent to business class fares. FLEET uses the assumption that 5% of the total demand on a route is the business and first-class passengers; this represents the potential supersonic aircraft demand. In FLEET, the airline first allocates its supersonic aircraft to satisfy the supersonic demand and then any unsatisfied supersonic demand is combined with the subsonic demand, and the subsonic aircraft allocation meets this demand. Finally, the airline acquires and retires aircraft based on the operations of supersonic and subsonic aircraft operations from the allocation problem.

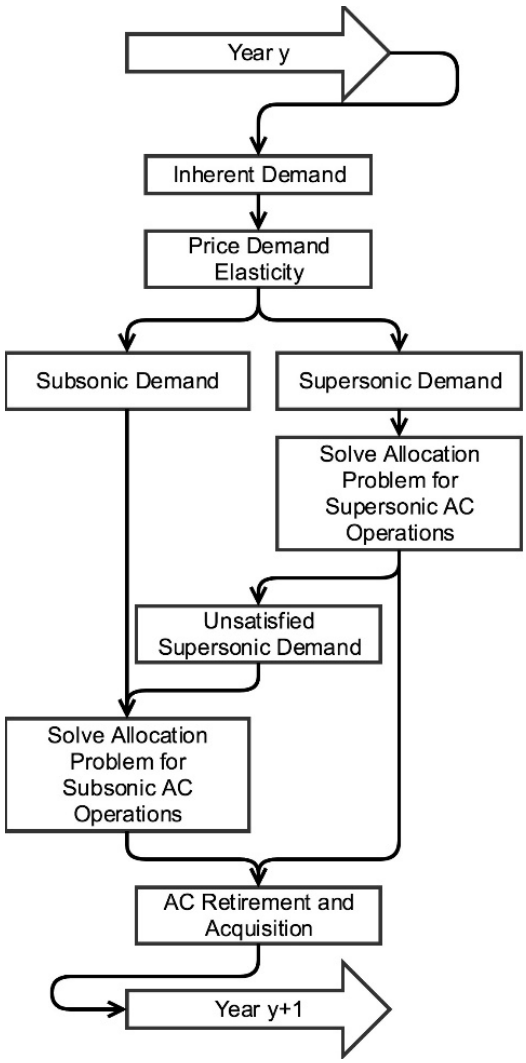


FIGURE 28. FLOWCHART OF SUBSONIC AND SUPERSONIC AIRCRAFT SEQUENTIAL ALLOCATION APPROACH

The sequential allocation approach has three advantages: it is easy to implement in FLEET; it can ensure that assumptions about the supersonic flight ticket fare and supersonic flight demand can be held; simulation results are relatively easy to analyze and provide reasoning.

The drawbacks of the sequential allocation approach include two points. The first involves implementation of airport traffic capacity constraints or airport noise constraints. Both types of constraints limit the number of aircraft operations in FLEET's aircraft allocation problem. The traffic capacity constraint limits the number of take-offs and landings, while the airport noise



constraint limits the size of the predicted total area inside a DNL contour of 65 dB. The predicted noise area is also a function of the number of operations of each type of aircraft in the airline's fleet. With the supersonic aircraft allocated before the subsonic fleet but the capacity and noise area requiring the total number of operations (meaning supersonic and subsonic aircraft) at an airport, these constraints either allow unrestricted supersonic operations (i.e., once the supersonic fleet is allocated, the subsonic fleet is limited to meet the constraints) or require an a priori estimate of how limits should be applied to the supersonic aircraft before they are allocated. The second disadvantage of the sequential approach is that this approach favors supersonic aircraft operations. The airline always allocates the supersonic aircraft on the most profitable routes to optimize revenues from only the supersonic route network instead of from the entire fleet network because the sequential allocation approach separates the consideration of supersonic and subsonic aircraft fleets. It is possible that the sum of profits from the supersonic allocation and the subsonic allocation approach could be less than the profit from the simultaneous approach, and the major reason for including the allocation model in FLEET is to represent how a profit-seeking airline would use its aircraft.

Subsonic and supersonic aircraft simultaneous allocation approach

Figure 29 shows the flowchart of a proposed subsonic and supersonic aircraft simultaneous allocation approach. After calculating the inherent demand growth with price-demand elasticity effect, FLEET evaluates the subsonic demand and supersonic demand on each route. Both demands are inputs for the simultaneous allocation problem. Subsequently, the simultaneous aircraft allocation problem evaluates both subsonic and supersonic aircraft operations. Based on the supersonic and subsonic aircraft operations, the airline in FLEET makes strategies of aircraft acquisition and retirement.

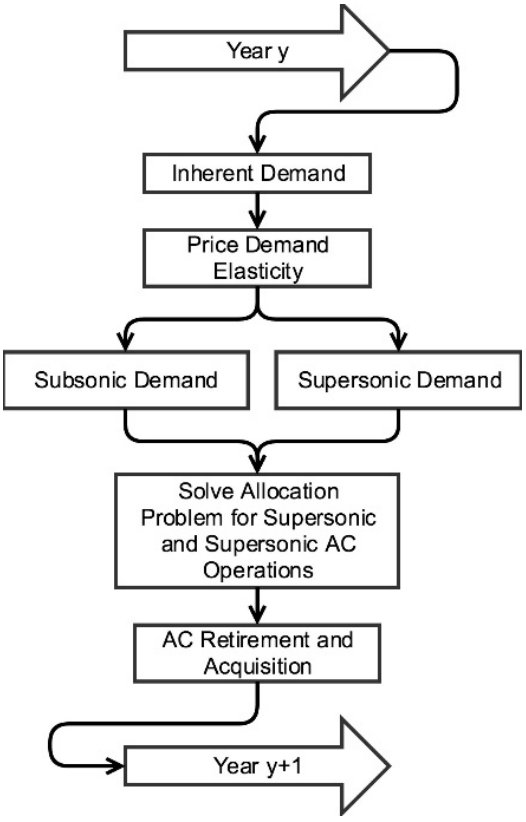


FIGURE 29. FLOWCHART OF SUBSONIC AND SUPERSONIC AIRCRAFT SIMULTANEOUS ALLOCATION APPROACH



The simultaneous aircraft allocation problem is shown as follows.

Objective function:

$$\sum_{a1,r1}(\boldsymbol{PaxSub_{a1,r1}PSub_{a1,r1}-xSub_{a1,r1}CSub_{a1,r1}})+\sum_{a2,r2}(\boldsymbol{PaxSup_{a2,r2}PSup_{a2,r2}-xSup_{a2,r2}CSup_{a2,r2}})$$

EQUATION 1

Constraint functions:

$$\sum_{r}2xSub_{a,r}(BHSub_{a,r}+MHSub_{a,r}+tSub_{a,r})\leq 24\times 3fleetSub_{a},\forall a,r\in r1$$

EQUATION 2

$$\sum_{r}2xSup_{a,r}(BHSup_{a,r}+MHSup_{a,r}+tSup_{a,r})\leq 24\times 3fleetSup_{a},\forall a,r\in r2$$

EQUATION 3

$$tranPax_{r}=\begin{cases}DemSup_{r}-\sum_{a2}PaxSup_{a2,r}\,,\ \forall r\in r1\cap r2\\ 0,\forall r\notin r1\cap r2\end{cases}$$

EQUATION 4

$$\sum_{a2}Paxsup_{a2,r2}\leq DemSup_{r2},\forall r2$$

EQUATION 5

$$0.2(DemSub_{r1})+tranPax_{r1}\leq\sum_{a1}PaxSub_{a1,r1}\leq DemSub_{r1}+tranPax_{r1},\forall r1$$

EQUATION 6

$$paxsup_{a,r}\leq xSup_{a,r}\times SupSeat_{a}\,,\forall a,r$$

EQUATION 7

$$paxsub_{a,r}\leq xSub_{a,r}\times SubSeat_{a}\,,\forall a,r$$

EQUATION 8

Equation 1 shows the objective function of the simultaneous allocation problem. $r1$ and $r2$ are sets of subsonic and supersonic routes, respectively. $PaxSub_{a1,r1}$ and $PaxSup_{a2,r2}$ show the number of passenger carried by subsonic aircraft $a1$ and supersonic aircraft $a2$ on routes $r1$ and $r2$, respectively; while $xSub_{a1,r1}$ and $xSup_{a2,r2}$ represent the number of flights of subsonic aircraft $a1$ and supersonic aircraft $a2$ on routes $r1$ and $r2$. $PSub_{a1,r1}$ and $PSup_{a2,r2}$ are the subsonic and supersonic ticket fares for taking subsonic aircraft $a1$ and supersonic aircraft $a2$ on routes $r1$ and $r2$, respectively. Finally, $CSub_{a1,r1}$ and $CSup_{a2,r2}$ are the operation costs per flight of using subsonic aircraft $a1$ and supersonic aircraft $a2$ on routes $r1$ and $r2$.

Equation 2 and Equation 3 check that the total operation hours of subsonic aircraft and supersonic aircraft are less than 72 hours, respectively. The operating hours include block hours ($BHSub_{a,r}$ and $BHSup_{a,r}$), maintenance hours ($MHSub_{a,r}$ and $MHSup_{a,r}$), and aircraft turn-over time ($tSub_{a,r}$ and $tSup_{a,r}$) for both subsonic and supersonic aircraft. $fleetSub_{a}$ and $fleetSup_{a}$ represent number of subsonic and supersonic aircraft type a in the airline's fleet. The 72-hour time window allows for completion of the longest trans-Pacific roundtrips.

Equation 4 shows the definition of the redundant variable, $tranPax_{r}$, to simplify the expression of Equation 6 and show the unsatisfied supersonic flight passenger demand. The unsatisfied supersonic flight passenger demand equals to the carried



supersonic flight passenger demand, $PaxSup_{a2,r2}$, subtracts from the total supersonic flight demand, $DemSup_r$, on the intersection of subsonic and supersonic route sets.

Equation 5 ensures that the carried supersonic flight passengers are less than the supersonic flight market demand, $DemSup_{r2}$. The unsatisfied supersonic flight demand will be included in the subsonic flight market demand. Equation 6 ensures that the airline can satisfy all unsatisfied supersonic flight demand and, at a minimum, twenty percent of the subsonic demand. This 20% limitation makes the constraint easier to address in the allocation problem; in practice, very high percentages of the available demand are satisfied (95% and above). Also, the carried subsonic flight passenger should be less than the total subsonic market demand.

Finally, both Equations 7 and 8 ensure that the carried passenger is less than the total available seats for subsonic and supersonic flight, respectively. $SupSeat_a$ and $SubSeat_a$ are the supersonic aircraft a seat capacity and subsonic aircraft a seat capacity, respectively.

The strength of the simultaneous allocation problem is that constraints for the entire airline fleet are readily incorporated in the allocation problem. Hence, it is easy to implement both the airport noise constraint and the airport operation capacity constraint without introducing biases for one type of aircraft. Also, this formulation can guarantee that the aircraft allocation is optimal for the overall airline's operations instead of optimizing for supersonic aircraft operations first and then serving remaining demand via subsonic aircraft operations.

The simultaneous allocation problem renders the choices of business class or first-class passengers to the airline. The redundant variable in Equation 4 represents numbers of business class or first-class passengers who buy the subsonic ticket price. The airline can optimize its overall profits by making the decisions for those passengers to either take the supersonic or subsonic flights.

Future Work: Allocation Problem Selection

An immediate future item for work is to determine which allocation approach to use for supersonic studies moving forward. The Purdue team will develop a passenger choice model (i.e., account for the "value of travel time" of passengers as a foundation for modeling their choice on routes when both supersonic and subsonic aircraft are available) and integrate it into the subsonic and supersonic aircraft simultaneous allocation approach, so that the business or first-class passengers have the option to choose between either supersonic or subsonic flights based on the airlines' schedules. The team will continue to utilize the supersonic and subsonic aircraft sequential allocation approach if the quality of the passenger choice model developed does not meet reasonable expectations about the choice between supersonic or subsonic travel, or if the team receives feedback that the sequential allocation might match how airlines might schedule supersonic aircraft when they enter the fleet.

Preliminary Simulation Results

Figure 29 shows a subset of scenarios developed from the first phase of the ASCENT 10 project [8] that can be readily simulated in FLEET, based upon the fidelity of the current supersonic aircraft modelling approach and the relevance of the availability of supersonic aircraft. The scenarios are listed by row in dark blue boxes, whereas the columns list the final worldview descriptors with specific settings for each scenario. Each cell is colored from low to nominal to high settings. Scenarios that we studied for the subsonic-only fleet mix with noise limitations are not part of the set of scenarios shown in Figure 29 because of the current lack of noise models for supersonic aircraft. The rest of this section describes Purdue's preliminary results from a simulation study in which supersonic aircraft become available for serving commercial air travel demand by the FLEET profit-seeking airline. The "Current Trend Best Guess" (CTBG) scenario with an all-subsonic aircraft fleet, characterized from the first phase of the ASCENT 10 project, was used to enable the comparison to the fleet mix with supersonic aircraft. Since the modeling and assumptions are still under continuous refinement and improvement, these preliminary results are primarily useful for understanding the workings of the model, the kinds of sensitivities we see when supersonic aircraft are introduced to the fleet and improving the diagnostic and analysis of the simulation data.

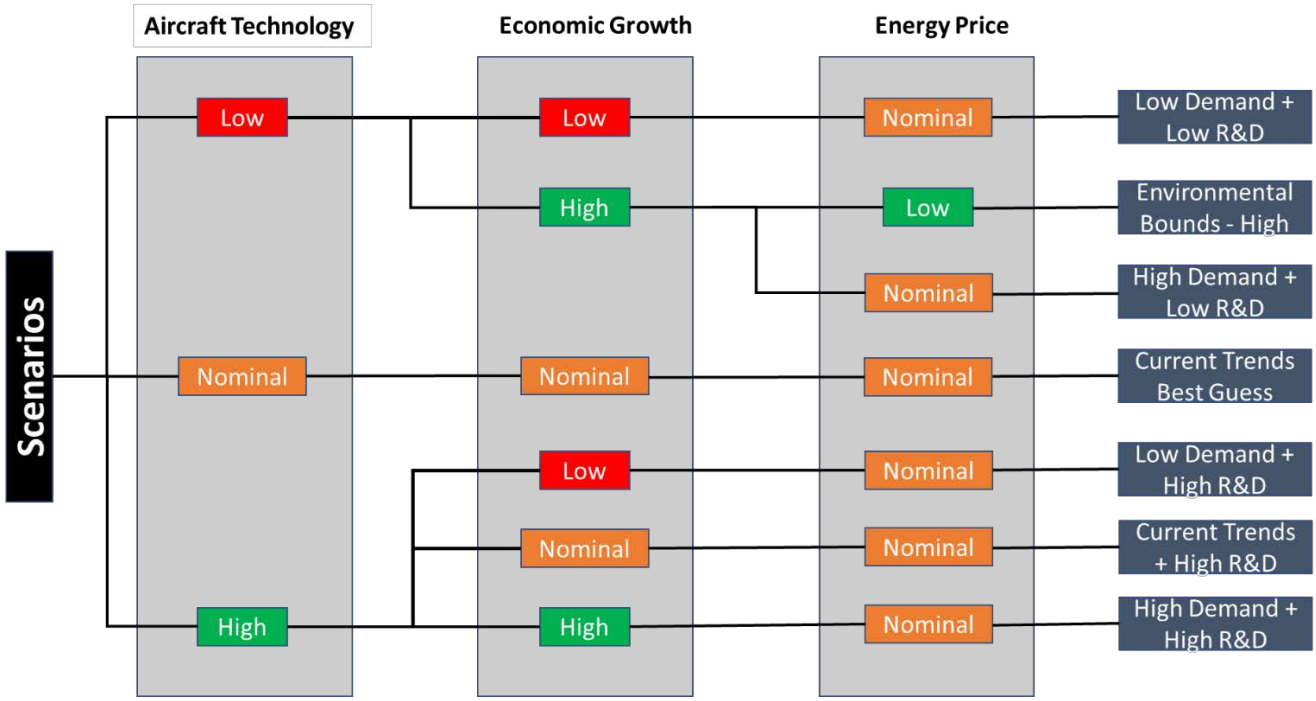


FIGURE 30. SCENARIO TREE OVERVIEW FOR SUPERSONIC STUDY

The FLEET setup for the CTBG scenario is defined as follows:

- A network of 169 airports including U.S. domestic routes and international routes that have either their origin or destination in the U.S.
- The annual gross domestic product (GDP) grows at a constant value of 4.3% in Asia, 4.2% in Latin America, 2.4% in Europe, and 2.8% for airports in the United States.
- The annual population growth rate at a constant value of 1.1% in Asia, 1.26% in Latin America, 0% in Europe, and 0.58% for the United States.
- Jet fuel prices grow according to the Energy Information Administration (EIA) reference fuel price [9] case and adjusted it to meet the ASCENT survey fuel price, $77.08/bbl, by 2050.
- Carbon emission prices grow linearly from $0/MT in 2020 to $21/MT by 2050.

TABLE 10. SUBSONIC AIRCRAFT TYPES USED IN SIMULATION

Subsonic Aircraft Types in Study				
	Representative-in-Class	Best-in-Class	New-in-Class	Future-in-Class
Class 1 (SRJ)	Canadair RJ200/RJ440	Embraer ERJ145		
Class 2 (RJ)	Canadair RJ700	Canadair RJ900	GT Gen1 DD RJ (2020)	GT Gen2 DD RJ (2030)
Class 3 (SA)	Boeing 737-300	Boeing 737-700	GT Gen1 DD SA (2017)	GT Gen2 DD SA (2035)
Class 4 (STA)	Boeing 757-200	Boeing 737-800	GT Gen1 DD STA (2025)	GT Gen2 DD STA (2040)
Class 5 (LTA)	Boeing 767-300ER	Airbus A330-200	GT Gen1 DD LTA (2020)	GT Gen2 DD LTA (2030)
Class 6 (VLA)	Boeing 747-400	Boeing 777-200LR	GT Gen1 DD VLA (2025)	GT Gen2 DD VLA (2040)

In Table 10 the aircraft labeled with "GT Gen1 DD" are the Generation 1 aircraft modeled by Georgia Tech with a 'Direct Drive' engine. The Generation 2 aircraft are labeled as "GT Gen2 DD". These include aircraft that belong to the following classes - regional jet (RJ), single aisle (SA), small twin aisle (STA), large twin aisle (LTA), and very large aircraft (VLA). Based

on the amount and speed of technology incorporated into aircraft, in each of the scenarios, the New-in-Class and Best-in-Class aircraft models will vary. Given the observation that new orders for 50-seat regional jet aircraft have diminished to zero, there are no small regional jet (SRJ) aircraft in the new- and future-in-class technology ages.

The Purdue Team tests the simulation with different supersonic ticket price models and supersonic aircraft allocation problems to assess which models result in the most possible carbon emission trends and commercial aviation industry behaviors. In this report, Purdue Team uses the previous ASCENT 10 project all-subsonic CTBG simulation results as the reference. Then, the CTBG supersonic aircraft scenario with 1) average margin per nautical mile ticket price model and 2) sequential supersonic aircraft allocation approach is used to compare the results with the all-subsonic CTBG scenario. The following sections include the simulation results and discussions.

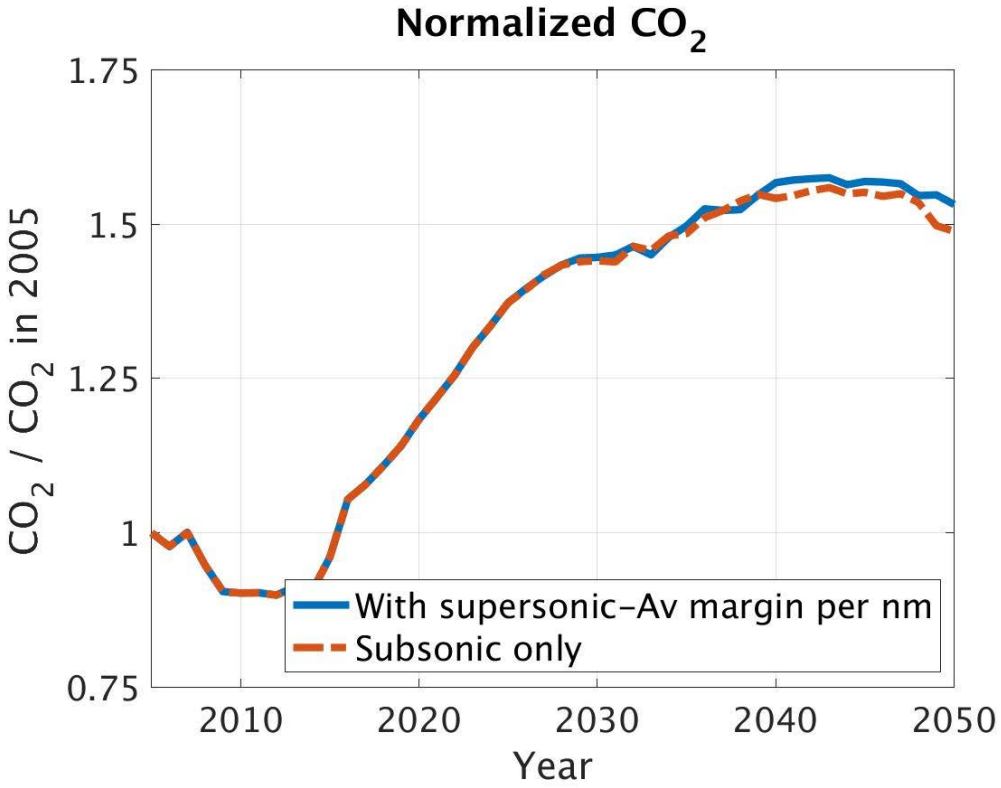


FIGURE 31. NORMALIZED FLEET-LEVEL CO_2 EMISSIONS FROM 2005 TO 2050

Figure 31 shows the predicted fleet-level CO_2 emission values for the subsonic-only airline fleet, which is the same result as in the previous phase of ASCENT 10 for the CTBG scenario definition, along with predictions for the airline fleet including the introduction of supersonic aircraft. The CO_2 emission for each year during the FLEET simulation period is normalized by the CO_2 emission value in the first simulation year of 2005. The dashed orange line represents CO_2 emission trend for the scenario in which there are no supersonic aircraft available (i.e., all subsonic aircraft only fleet) to the airline, while the solid blue line represents the CO_2 emission trend for the scenario where supersonic aircraft with cruise a Mach of 2.2 is available to the airline after year 2025. By 2050, the CO_2 emission in the subsonic-only fleet scenario increased to 1.5 times of the CO_2 emission value in 2005, while the carbon emission from the scenario with supersonic aircraft available resulted in about 1.51 times of the carbon emission in 2005. Although the scenario with supersonic aircraft available has a higher CO_2 emission value than the subsonic fleet only scenario by 2050, the scenario with supersonic aircraft has a slightly lower CO_2 emissions than the all subsonic fleet scenario at different times in the 2030s.

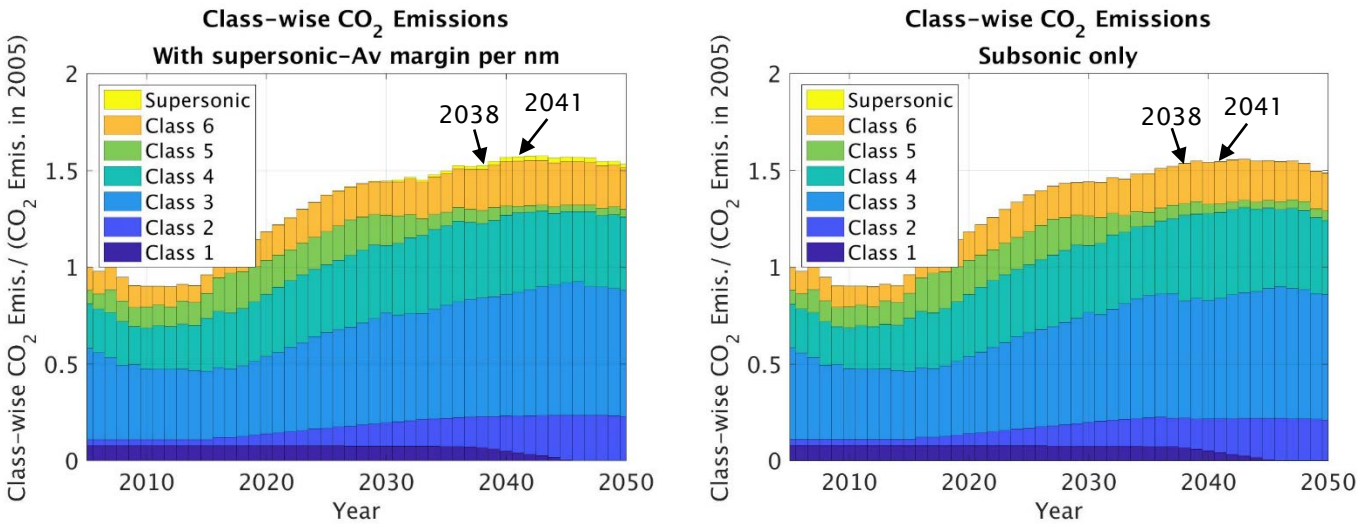


FIGURE 32. NORMALIZED CO_2 EMISSIONS BY AIRCRAFT CLASS

Figure 32 shows the CO_2 emission composition by each aircraft class in the airline fleet throughout the simulation period. Similar to Figure 30, the CO_2 emission values for each aircraft class in both scenarios are normalized by their corresponding carbon emission values for each aircraft class in 2005. Also consistent with Figure 31, Figure 32 shows that the CO_2 emission in the simulation for the scenario with available supersonic aircraft (left plot) was lower than the CO_2 emission in the all-subsonic aircraft fleet scenario (right plot) in some years in the 2030s. Conversely, the scenario with supersonic aircraft available consistently yielded a higher CO_2 emission than the all-subsonic fleet scenario after 2040. The carbon emission reduction observed in the scenario with supersonic aircraft available, when compared to the subsonic-only fleet scenario for years 2034 and 2038, is due to the different manner in which the FLEET airline utilizes its subsonic aircraft (i.e. classes 1 to 6) when supersonic aircraft are available.

Figure 33 shows the number of trips flown daily, over a three-day period by different aircraft types on supersonic-eligible routes in the FLEET airline network for both "subsonic only" and "with supersonic" fleet-mix schemes in 2038. The three-day period allows for subsonic aircraft to complete the longest round-trip trans-Pacific flights in the FLEET network. Low to high number of aircraft trips are represented by a spectrum of light blue to deep blue shades respectively, while the red-shaded cells indicate city pairs with no utilization of a certain aircraft type. For instance, of the 26 supersonic-eligible routes indicated in Figure 33, the Honolulu to Los Angeles (i.e., HNL to LAX, route number 13) has the most average number of daily trips (as evidenced by the blue shaded cells) by both subsonic and supersonic aircraft in 2038. This behavior stems from a FLEET modeling abstraction that ensures that only the travel demand by all U.S. air carriers is characterized. A lot of real-world travel demand on the HNL-LAX route are predominantly served by U.S. carriers, thus a high fraction of this demand is captured in the FLEET simulation. For routes like New York to London (i.e., JFK to LHR, route number 20) in FLEET, served by other multiple carriers from Europe and other continents, the fraction of real-world demand served by U.S. air carriers is smaller compared to the total demand served by all carriers operating on the route, thus the lower number of aircraft trips as compared to the HNL-LAX route.

Figure 33 also reveals that the FLEET airline does not utilize any subsonic best-in-class aircraft on any of the supersonic-eligible routes in 2038, for the fleet-mix scheme where supersonic aircraft is made available to the airline. In addition, unlike the fleet-mix scheme with subsonic-only aircraft where most future-in-class 3 aircraft utilization predominantly occurs on Honolulu to Osaka (i.e. HNL to KIX, route number 11), the FLEET airline utilizes future-in-class 3 aircraft, which is comparatively more fuel efficient and has more seats than older generation class 3 aircraft, in the fleet-mix scheme with supersonic aircraft available on almost all of the 26 eligible supersonic routes in 2038. The combined effect of the sparse utilization of the moderately fuel-efficient new-in-class 5 aircraft and more fuel-efficient future-in-class 3 aircraft across multiple supersonic-eligible routes in the fleet-mix scheme with supersonic aircraft available, as compared to the high density route-specific utilization observed in the subsonic-only fleet scheme, consequently results in a lower total CO_2 emission in 2038 for the scenario where supersonic aircraft is available and used by the airline.



			Fleet-mix Scheme with Supersonic Aircraft				
			Subsonic				Supersonic
			Future	New	New	New	Best
FLEET Airline City Pair			Class 3	Class 4	Class 5	Class 6	
1	AMS	JFK	0.00	3.33	0.00	0.00	0.00
2	ATL	CDG	0.67	0.67	0.67	4.00	1.33
3	BOS	LHR	0.67	5.33	1.33	0.00	1.33
4	CDG	IAD	0.00	2.67	0.67	0.67	0.67
5	CDG	JFK	0.67	11.33	0.67	0.00	2.00
6	CDG	MIA	0.67	0.00	1.33	1.33	0.00
7	EWR	FRA	0.67	2.67	0.67	0.00	0.00
8	FCO	JFK	0.67	0.00	0.67	2.67	0.67
9	FRA	IAD	0.00	8.67	1.33	0.00	1.33
10	FRA	JFK	0.67	2.00	0.67	0.00	0.00
11	HNL	KIX	0.00	0.67	1.33	7.33	0.00
12	HNL	LAS	1.33	8.00	0.67	0.00	1.33
13	HNL	LAX	3.33	56.00	0.00	0.00	8.67
14	HNL	NRT	0.00	26.00	0.67	0.67	0.00
15	HNL	PHX	1.33	6.00	0.00	0.00	1.33
16	HNL	SEA	0.67	9.33	1.33	0.00	2.00
17	HNL	SFO	1.33	33.33	0.67	0.00	5.33
18	HNL	SYD	0.00	0.67	1.33	0.00	0.00
19	IAD	LHR	0.67	12.00	0.67	0.00	2.00
20	JFK	LHR	0.67	26.67	0.00	0.00	4.00
21	JFK	MAD	0.67	2.00	0.67	0.00	0.00
22	JFK	MXP	0.67	0.67	0.67	0.67	0.00
23	JFK	ZRH	0.67	2.00	0.67	0.00	0.00
24	LHR	MIA	0.67	0.67	0.67	2.00	0.67
25	MAD	MIA	0.67	0.67	0.67	1.33	0.00
26	NRT	SFO	0.00	0.67	0.00	14.00	0.00

			Fleet-mix Scheme with Subsonic-Only Aircraft			
			Subsonic			
			Future	New	New	New
FLEET Airline City Pair			Class 3	Class 4	Class 5	Class 6
1	AMS	JFK	0.00	3.33	0.00	0.00
2	ATL	CDG	0.00	0.00	7.33	0.00
3	BOS	LHR	0.00	7.33	0.00	0.00
4	CDG	IAD	0.00	4.67	0.00	0.00
5	CDG	JFK	0.00	13.33	0.00	0.00
6	CDG	MIA	0.00	0.00	3.33	0.00
7	EWR	FRA	0.00	4.67	0.00	0.00
8	FCO	JFK	0.00	3.33	0.00	2.00
9	FRA	IAD	0.00	10.67	0.00	0.00
10	FRA	JFK	0.00	3.33	0.00	0.00
11	HNL	KIX	20.67	0.00	0.00	0.00
12	HNL	LAS	0.00	10.00	0.00	0.00
13	HNL	LAX	0.00	61.33	0.00	0.00
14	HNL	NRT	0.00	28.67	0.00	0.00
15	HNL	PHX	0.00	7.33	0.00	0.00
16	HNL	SEA	0.00	12.00	0.00	0.00
17	HNL	SFO	0.00	36.67	0.00	0.00
18	HNL	SYD	0.00	0.00	2.00	0.00
19	IAD	LHR	0.00	14.67	0.00	0.00
20	JFK	LHR	0.00	28.67	0.00	0.00
21	JFK	MAD	0.00	3.33	0.00	0.00
22	JFK	MXP	0.00	0.00	2.67	0.00
23	JFK	ZRH	4.67	0.00	0.00	0.00
24	LHR	MIA	0.00	0.00	2.00	2.00
25	MAD	MIA	0.00	0.00	0.00	2.00
26	NRT	SFO	0.00	0.00	0.00	15.33

FIGURE 33. NUMBER OF TRIPS ALLOCATED BETWEEN CITY PAIRS PER DAY OVER A REPRESENTATIVE THREE-DAY PERIOD IN 2038

Figure 34 shows the number of daily trips (over a 3-day period) flown by different aircraft types on supersonic-eligible routes in the FLEET airline network for both fleet-mix schemes in 2041. Similar to Figure 33, low to high number of aircraft trips are represented by a spectrum of light blue to deep blue shades respectively, while the red-shaded cells indicate city pairs with no utilization of a certain aircraft type. Similar to 2038 (Figure 33), Figure 34 shows that the FLEET airline utilizes a similar mix of subsonic aircraft class across different technology ages in both schemes that results in a significantly higher fleet-level carbon emissions in 2041 for the scheme with supersonic aircraft available. Furthermore, the airline also allocates available next-generation new-in-class supersonic aircraft to serve demand on different routes, thereby using more supersonic aircraft in 2041 as compared to the total supersonic aircraft utilization in 2038.

			Fleet-mix Scheme with Supersonic Aircraft						
			Subsonic					Supersonic	
			Future	New	New	Future	New	Best	New
FLEET Airline City Pair			Class 3	Class 4	Class 5	Class 5	Class 6		
1	AMS	JFK	0.00	2.67	0.67	0.00	0.00	0.00	0.67
2	ATL	CDG	0.67	0.00	0.00	0.67	4.67	0.00	1.33
3	BOS	LHR	0.67	7.33	0.00	0.00	0.00	1.33	0.00
4	CDG	IAD	0.67	3.33	0.67	0.00	0.00	0.67	0.00
5	CDG	JFK	0.67	12.67	0.67	0.00	0.00	0.67	1.33
6	CDG	MIA	0.67	0.00	0.00	0.00	1.33	0.00	0.67
7	EWR	FRA	0.67	3.33	0.67	0.00	0.00	0.67	0.00
8	FCO	JFK	0.67	0.67	0.00	0.67	2.67	0.67	0.00
9	FRA	IAD	1.33	9.33	0.00	0.00	0.67	2.00	0.00
10	FRA	JFK	3.33	1.33	0.00	0.00	0.00	0.00	0.67
11	HNL	KIX	0.67	0.00	0.00	0.67	8.67	0.00	2.67
12	HNL	LAS	7.33	5.33	0.00	0.00	0.00	1.33	0.00
13	HNL	LAX	13.33	52.00	0.00	0.00	0.00	9.33	0.00
14	HNL	NRT	1.33	29.33	0.67	0.00	0.00	0.00	4.67
15	HNL	PHX	2.00	4.67	0.00	0.00	0.00	1.33	0.00
16	HNL	SEA	10.67	4.00	0.00	0.00	0.00	2.00	0.00
17	HNL	SFO	1.33	34.00	0.00	0.00	0.00	6.00	0.00
18	HNL	SYD	0.00	0.00	0.00	2.00	0.00	0.00	0.67
19	IAD	LHR	1.33	14.00	0.00	0.00	0.00	2.67	0.00
20	JFK	LHR	3.33	27.33	0.00	0.00	0.00	4.67	0.00
21	JFK	MAD	0.00	2.00	1.33	0.00	0.00	0.67	0.00
22	JFK	MXP	0.00	2.00	0.00	0.00	0.67	0.00	0.67
23	JFK	ZRH	0.67	2.00	0.00	0.00	0.67	0.00	0.67
24	LHR	MIA	0.67	0.00	0.00	0.67	2.67	0.00	0.67
25	MAD	MIA	0.67	0.67	0.00	0.00	2.00	0.00	0.67
26	NRT	SFO	0.00	0.67	0.00	0.67	16.00	0.00	4.00

			Fleet-mix Scheme with Subsonic-Only Aircraft				
			Subsonic				
			Future	New	New	Future	New
FLEET Airline City Pair			Class 3	Class 4	Class 5	Class 5	Class 6
1	AMS	JFK	0.67	2.00	0.67	0.00	0.00
2	ATL	CDG	1.33	0.00	0.00	0.00	5.33
3	BOS	LHR	1.33	7.33	0.00	0.00	0.00
4	CDG	IAD	1.33	3.33	0.67	0.00	0.00
5	CDG	JFK	1.33	12.67	0.67	0.00	0.00
6	CDG	MIA	0.00	0.00	0.00	0.67	2.00
7	EWR	FRA	0.00	4.00	0.67	0.00	0.00
8	FCO	JFK	0.67	0.00	0.00	0.67	3.33
9	FRA	IAD	0.00	9.33	0.00	2.00	0.00
10	FRA	JFK	0.67	3.33	0.00	0.00	0.00
11	HNL	KIX	0.00	14.00	0.00	1.33	0.00
12	HNL	LAS	0.00	10.00	0.67	0.00	0.00
13	HNL	LAX	13.33	55.33	0.00	0.00	0.00
14	HNL	NRT	0.67	30.67	0.00	1.33	0.00
15	HNL	PHX	1.33	6.00	0.00	0.00	0.00
16	HNL	SEA	1.33	10.67	0.67	0.00	0.00
17	HNL	SFO	2.00	37.33	0.00	0.00	0.00
18	HNL	SYD	0.00	1.33	0.00	0.00	0.67
19	IAD	LHR	1.33	14.00	0.67	0.00	0.00
20	JFK	LHR	1.33	30.00	0.00	0.00	0.00
21	JFK	MAD	1.33	2.00	0.67	0.00	0.00
22	JFK	MXP	0.67	2.00	0.67	0.00	0.00
23	JFK	ZRH	1.33	2.00	0.00	0.67	0.00
24	LHR	MIA	0.67	0.67	0.00	0.00	2.67
25	MAD	MIA	1.33	0.00	0.00	0.00	2.00
26	NRT	SFO	0.00	0.67	0.00	1.33	16.00

FIGURE 34. NUMBER OF TRIPS ALLOCATED BETWEEN CITY PAIRS PER DAY OVER A REPRESENTATIVE 3-DAY PERIOD IN 2041



Summary and Future Work

Georgia Tech

The Georgia Tech team investigated routes that would be capable to carry enough demand to fill a 50 to 60 seat supersonic aircraft with significant time advantages. It was also demonstrated that an estimate of vehicle demand can be converted to equivalent passenger traffic in GREAT.

The preliminary modeling of supersonic vehicles developed a parametric capability to explore the design constraints for potential future supersonic aircraft design. This is valuable because it allows the user to explore specific aircraft capabilities or mission requirements and their influence on the engine and aerodynamic efficiency of the aircraft as well as a simplified mission performance and weight analysis that results in preliminary estimates of fuel efficiency for a potential aircraft. These results in multipliers of a couple of new aircraft concepts relative to a reference subsonic aircraft type. The resulting fuel intensity of these new types is in the several multiples of a standard single aisle reference aircraft.

This phase of the effort investigated the ability of AEDT to model supersonic aircraft - which it can – but is not well supported. The results obtained from existing or other aircraft developed for other research efforts show specific modeling gaps that influence the accuracy of any potential supersonic aircraft model in AEDT. These modeling gaps resulted in specific recommendations for improving the future modeling capabilities of AEDT.

The fleet analysis tools were expanded to specifically include a separate category for supersonic aircraft. The results for the fleet analysis obtained from GREAT/IDEA, which include several of the supersonic concept aircraft for the first time, are first attempts at incorporating potential supersonic aircraft into the fleet analysis frameworks. The range of the results show a relatively modest impact of CO_2 emissions for only a few daily flights on a very limited number of routes. However, following some prior market assessments of a potential demand of over a thousand supersonic aircraft over a ten year period, the results show a potentially very significant increase in CO_2 emissions of aviation.

Future work – shown in the second year proposal for the current supersonic effort – will focus on reducing the modeling uncertainty in the demand for supersonic aircraft as well as expanding the estimates for supersonic aircraft in the key environmental indicators. The team will also work with the AEDT developers in order to improve the modeling of supersonic aircraft and enable to accurate representation of them in the software. Additionally, the fleet level modeling of supersonic aircraft will focus on expanding the environmental metrics as well as incorporating new models. Finally, the team will develop high fidelity EDS models of two potential supersonic aircraft that will allow a much higher fidelity of the environmental performance of these aircraft. This also will allow investigations into the optimum design and operation of these potential new aircraft.

Purdue

The Purdue team successfully demonstrated FLEET's capabilities for modeling and analyzing the introduction of commercial supersonic aircraft to an existing all-subsonic airline fleet model. This demonstration has shown that FLEET is capable of adjusting scenarios developed by ASCENT 10 Project partners (in the first phase of the ASCENT 10 project) to accommodate for the availability of supersonic aircraft in the airline fleet, and as such, provides some unique features that benefit the FAA in tackling challenging fleet-level emissions forecasting problems.

The preliminary results from FLEET – using the placeholder supersonic aircraft model – indicate some seemingly counterintuitive trends for fleet level CO_2 emissions when comparing the subsonic only fleet mix to a mix that includes some supersonic aircraft along with subsonic aircraft. In the fleet-mix scheme where supersonic aircraft become available, the future CO_2 emissions drop below the values predicted in the corresponding scheme with all-subsonic aircraft fleet for some of the years of the simulation. In other year, the predicted fleet-level CO_2 emissions for the with supersonic fleet scheme exceeds that predicted for the subsonic only fleet by an amount that is larger than one would expect for the number of supersonic aircraft operated by the airline. The FLEET approach to use an allocation problem to represent scheduling and assignment decisions of a profit-seeking airline, combined with a retirement model to represent when the airline would retire an existing aircraft from its fleet and an acquisition model for adding new aircraft – both to replace retiring aircraft and to meet growing demand – provides a model-based coupling of these considerations. When the allocation approach first satisfies business class and above passenger demand with supersonic aircraft and subsequently satisfies remaining demand with the subsonic fleet, this coupling shows a different use, retirement and acquisition of the subsonic fleet from that



predicted in the subsonic-only fleet mix scheme. These changes lead to the (at least initially) counterintuitive fleet-level CO_2 results. At this time, the results still rely upon the simplistic placeholder supersonic aircraft model, so the predicted values for fuel burn / CO2 emissions should not be viewed with high support; the ability to find these trends via FLEET is the more important conclusion at this point in the effort.

The preliminary results presented in this report are based on the allocation approach which satisfies travel demand first by using supersonic aircraft and next by using subsonic aircraft. In the near term, the Purdue team intends to perform additional studies for the "with supersonic" fleet-mix scheme for several of the economic / technology factor scenarios described as part of the previous ASCENT 10 efforts. When the supersonic aircraft vehicle description becomes available from our Georgia Tech colleagues, we will replace our current placeholder description and repeat the various studies.

Future work (elucidated in detail in the second-year proposal for the current supersonic effort) will assess the fleet-level advantage of having different types of supersonic aircraft, defined by certain operational specifications (e.g. Mach cut-off overland), available to the FLEET airline to improve model fidelity, upon developing and revamping necessary FLEET modules to accommodate for supersonic aircraft, before subsequently running FLEET for different ASCENT 10 Project scenarios.

Publications

Ogunsina, K., Chao, H., Kolencherry, N., Jain, S., Moolchandani, K., Crossley, W. A., and DeLaurentis, D. A., "Fleet-Level Environmental Assessments for Feasibility of Aviation Emission Reduction Goals," Proceedings of CESUN Global Conference 2018, Tokyo, Japan.

Outreach Efforts

Multiple interactions with government, industry, and academia have occurred during the course of project.

ASCENT 10: Aircraft Technology Modeling and Assessment, oral presentation to ASCENT Spring Advisory Committee Meeting, MIT, Cambridge MA, April 4, 2018.

Awards

None

Student Involvement

Of the Georgia Tech students, Eugene Mangortey performed significant work under Task 2. He conducted an extensive literature search on the Concorde's historical performance and operation, and investigated the special policies and provisions that were put in place when the Concorde came into service. He analyzed the research findings and helped formulate specific recommendations and design considerations for future supersonic vehicles. Eugene is currently a Graduate Research Assistant at Georgia Tech and is expected to graduate with his Master's degree in 2019.

Manon Huguenin performed significant work under Task 3. She learned how to use AEDT and ran the required studies for the Concorde. She also analyzed AEDT outcomes and researched actual Concorde performance to identify discrepancies and help formulate recommendations for further development of AEDT. Manon is currently a Graduate Research Assistant at Georgia Tech and is expected to graduate with her Master's degree in 2019.

The Purdue team includes three graduate students in the effort, all three have been conducting tasks in support of the effort. One has just obtained his MS degree and is continuing at Purdue for PhD studies. The other two students are continuing as PhD students.

Plans for Next Period

Table 11 shows the expected objective and contributions developed between Georgia Tech, Purdue, and FAA. It shows the expected contributions by task and university.



TABLE 11. UNIVERSITY CONTRIBUTIONS FOR YEAR 2

Objectives		Georgia Tech	Purdue
1	Fleet Assumptions & Demand Assessment	Identify supersonic demand drivers and supporting airports and project demand for all scenarios Expand to international airports	Estimate latent demand and flight schedules for supersonic aircraft
2	Preliminary Vehicle Environmental Impact Prediction	Develop estimates of Key Environmental Indicators (KEI) for supersonic aircraft relative to current technology subsonic aircraft, Develop estimates of likely operating altitudes	Support with expert knowledge
3	AEDT Vehicle Definition	Test current version of AEDT ability to analyze existing supersonic models Work with AEDT developers to understand the required modifications to support supersonic vehicles	N/A
4	Vehicle and Fleet Assessments	Apply GREAT to estimate impact of supersonics in terms of fuel burn, water vapor, and LTO NOx for a combination of vehicles and scenarios	Apply FLEET to estimate impact of supersonics in terms of fuel burn, water vapor, and LTO NOx
5	EDS Vehicle Modeling	Create 2 EDS supersonic vehicle models with boom signatures	Support with expert knowledge

Table 12 highlights the plans for the next research period for Georgia Tech. Full details on these plans can be found in the second year proposal submitted earlier in the summer.

TABLE 12. LIST OF ANTICIPATED MILESTONES FOR THE NEXT RESEARCH PERIOD (GT)

Milestone	Planned Due Date
Documentation of the updated projected supersonic demand for the A10 scenarios	12/2018
Documentation of the development of key environmental Indicators (KEI) for the list of current and future subsonic aircraft by type and size class	03/2019
Updated Fleet Level Environmental Impacts for each scenario in APMT compatible format	08/2019
EDS aircraft descriptions and characteristics in Powerpoint format including fuel burn, emissions, and noise, and FLOPS output files and also engine descriptions including NPSS and Wate output files.	08/2019
A Report documenting the results of the interdependency tasks	2/2019

Table 13 highlights the plans for the next research period for Purdue. Full details on these plans can be found in the second-year proposal submitted earlier in the summer.



TABLE 13. LIST OF ANTICIPATED MILESTONES FOR THE NEXT RESEARCH PERIOD (PURDUE)

Milestone	Planned Due Date
• Develop and test passenger choice model and ticket price model; update FLEET allocation problem and supersonic route network • Document the results of these changes using a variant of the current trends best guess scenario from the subsonic-only studies as an initial view of how introducing supersonic aircraft might change fleet-level CO_2 emissions	12/2018
• Employ aircraft representations from Georgia Tech teammates – using Key Environmental Indicators and the multiplier approach – into FLEET and demonstrate FLEET studies with these models; begin to measure additional environmental metrics (e.g., NO_x, H_2O) • Document these FLEET studies to show the impact of introducing supersonic aircraft with higher resolution than the studies described above	02/2019
• Develop coefficients, estimates, and additional modules for assessing fleet-level environmental impact; study additional scenarios with FLEET, building upon the previous subsonic-only study scenarios. Incorporate improved vehicle models from Georgia Tech teammates as they become available • Document these FLEET scenario studies to show predictions of how the various environmental metrics (CO_2, NO_x, H_2O) may evolve when supersonic aircraft are available in these future scenarios	04/2019
• Conduct sensitivity studies for drivers (ticket price, passenger choice model parameters, regional fuel prices, etc.) that impact supersonic travel. • Document the sensitivity in the fleet-level environmental metrics to these parameters, which are not typically varied as part of the future scenarios	06/2019
• Coordinate with colleagues at Georgia Tech to provide a project report summarizing this second phase of work studying the introduction of supersonic aircraft	08/2019

References

1. BTS DB1B Ticket Database (https://www.transtats.bts.gov/DatabaseInfo.asp?DB_ID=125)
2. http://matrix.itasoftware.com
3. "List of WWLMINET 257 airports," Personal communications with Dou Long of LMI, 4 May 2009
4. Blake, Matt, et al. "Advanced Vehicle Concepts and Implications for NextGen." NASA/CR-2010-216397, 2010.
5. "The Concorde Flying Manual Volume II", British Airways Overseas Division, 1976 with later amendments.
6. D. Dubois and G. C. Paynter, "Fuel Flow Method 2' for Estimating Aircraft Emissions," *Sae Tech. Pap. Ser.*, no. 724, pp. 776–790, 2006.
7. Bachman, Justin, "Supersonic is coming back. Will the airlines buy it?", Bloomberg, (https://www.bloomberg.com/news/articles/2016-11-29/supersonic-is-coming-back-will-the-airlines-buy-it), 11/27/2016.
8. Mavris, D., Delaurentis, D., Crossley, W., & Alonso, J. J. (2017). Project 10 Aircraft Technology Modeling and Assessment: Phase I Report, 650–723. Retrieved from https://s3.wp.wsu.edu/uploads/sites/192/2017/10/ASCENT_P10_2017_PhaseI_Final_Report.pdf
9. U. S. Energy Information Administration, Annual Energy Outlook 2011, 2011, URL: www.eia.gov/forecasts/aeo/



Project 011(A) Development of Rapid Fleet-Wide Environmental Assessment Capability Using a Response Surface Modeling Approach

Massachusetts Institute of Technology

Project Lead Investigator

R. John Hansman
T. Wilson Professor of Aeronautics & Astronautics
Department of Aeronautics & Astronautics
Massachusetts Institute of Technology
Room 33-303
77 Massachusetts Ave
Cambridge, MA 02139
617-253-2271
rjhans@mit.edu

University Participants

Massachusetts Institute of Technology

- P.I.(s): R. John Hansman
- FAA Award Number: 13-C-AJFE-MIT, Amendment Nos. 006, 011, 014, 023, and 038
- Period of Performance: Aug. 18, 2014 to Aug. 31, 2018 (year 4 as NCE)
- Task(s):
  1. Extend And Enhance Modeling Framework
  2. Extend Fleet Gauge Sample Problem To System Level
  3. Develop Multi-stakeholder Valuation Methods To Enable Comparison And Decisions About Preferred Strategies In The Environmental Output Space
  4. Apply Fast Modeling Framework To Additional Sample Problem

Project Funding Level

$670,000 FAA funding and $670,000 matching funds. Sources of match are approximately $232,500 from MIT and $437,500 from Massachusetts Port Authority.

Investigation Team

Prof R. John Hansman (PI)
Greg O'Neill (Post Doctoral Researcher)
Luke Jensen (Post Doctoral Researcher)
Jacqueline Thomas (Graduate Student)
Clement Li (Graduate Student)
Alison Yu (Graduate Student)
Pedro Manuel Maddens-Toscano (Graduate Student)

Project Overview

The objective of the research is to continue development of an analytical framework for evaluating the environmental impact of air transportation and to use that framework on a variety of sample policy and operational problems. This framework will use fast models for aircraft-level performance, noise, and emissions, enabling broad scenario explorations and parametric analyses in environmental studies. Phase I of this research (2014-2015) consisted of general analysis framework development, sample problem selection, and surrogate model development. Phase II of this research (2015-



2016) aimed to continue model development while demonstrating the capability of the modeling approach on a specific multi-dimensional sample problem involving fleet gauge modification. Phase III of this research (2016-2017) aimed to increase the ability to evaluate local noise impacts at the system level and develop additional multi-objective sample problems to demonstrate the flexibility and extensibility of the rapid environmental analysis framework. This phase refined the relationship between local and system-level impacts arising from specific advanced operational procedures and aircraft fleet evolution.

Task 1- Extend and Enhance Modeling Framework

Massachusetts Institute of Technology

Objective(s)

The modeling framework for rapid environmental impact assessment has been developed to include local and system wide impacts for noise, emissions, and fuel consumption at specific locations based on representative or generic airports. The first two years of this research highlighted the challenge of systematically evaluating local impacts (e.g. noise and LTO emissions) which depend on location-specific elements such as procedure design, fleet mix, population density, etc. with global factors such as emissions and fuel consumption.

This task aimed to develop techniques that can capture key environmental characteristics at a system level that incorporates location-specific characteristics. In order to rapidly analyze individual airport performance, it is necessary to have a generic representation of the operating patterns and flight trajectories. This task leverages work that has been done on statistical clustering methods to identify common operations at individual airports, simplified generic profile definitions for some airports, and detailed procedure modeling for certain classes of advanced operational procedures.

Research Approach

- Expand the modeling framework and architecture developed in the initial phases of the research to add greater detail on modules and interfaces to enable implementation of specific sample problems.
- Locate and incorporate data sources for procedure definition, fleet mix, and timetable to enable rapid system-level analysis without requiring extensive manual intervention on an airport-by-airport basis.

Major Accomplishments

- Modeling framework applied for system-wide analysis of all runway ends for OEP-35 airports
- Modeling framework now integrates AEDT emissions results into analysis
- Modeling framework allows for rapid analysis of multiple flight procedures, and varying metrics are considered to communicate integrated noise exposure

Task 2- Extend Fleet Gauge Sample Problem to System Level

Massachusetts Institute of Technology

Objective(s)

In Year 2 of this effort, an initial fleet gauge sample problem was evaluated. The objective of this sample problem was to calculate the environmental impact of a 10% upgauge at a single example airport (DCA) using the 2015 operational fleet model. The aggregate noise, emissions, fuel consumption and NOx impacts were calculated, along with potential effects on passenger throughput. In Year 3, this sample problem will be expanded to a broader system level using the results of Task 1, specifically incorporating local noise analysis at the OEP 35 airports. This allowed for continued development and refinement of the modeling framework, allowing for policy valuation and comparison across multiple stakeholders and impact scales.

Research Approach

- Develop modeling capability at a specific airport (DCA) that is representative of the types of results desired for each airport in a broader system-level analysis.
- Extend the modeling capability developed for the specific airport to a small subset of the NAS to evaluate potential data and analysis implementation challenges.



- Extent modeling capability to full airport sample set of interest (initially the OEP 35 airports).

Major Accomplishments

- Noise analysis for all runway ends at OEP-35 airports considers set of possible flight procedures within RNAV and RNP criteria and not only straight in and straight out procedures.
- Noise analysis applied to all runway ends at OEP-35 airports in order to determine noise-minimum flight procedures within RNAV and RNP criteria.
- Noise metric analysis considered at multiple airports within US and internationally.

Task 3- Develop Multi-stakeholder Valuation Methods to Enable Comparison and Decisions About Preferred Strategies in the Environmental Output Space

Massachusetts Institute of Technology

Objective(s)

Environmental impacts from air transportation activities are felt across multiple stakeholders, geographic scales, and timescales. As a result, different stakeholders have different priorities and perceived valuations of possible policies and procedures. The focus of the first two years in this research effort was to generate system outputs in terms of raw environmental metrics (for noise, emissions, fuel burn, etc.). These metrics do not translate directly to a stakeholder preference structure or an improved understanding of community welfare on local and system wide scales. In this phase of the research effort, multi-stakeholder valuation methods were investigated with specific emphasis placed on an evaluation of different noise metrics to capture annoyance beyond traditional "significant" noise level definitions.

Research Approach

- Evaluate methods and metrics for assessing impact from environmental variables, particularly noise.
- Analyze and compare results using the rapid system-level analysis framework using appropriate metrics of choice.

Major Accomplishments

- Integrated AEDT fuel emissions calculations into system model for analyzing environmental impact
- Results reported in terms of noise analysis and emissions analysis
- Further development of noise metrics for population impact analysis with DNL as well as supplemental metrics for analysis such as N_{Above}.
- Initial complaint analysis for correlation of complaints and integrated noise metrics, including DNL and N_{Above}. Complaint analysis conducted at multiple airports including BOS and MSP.
- Developed methods for rapid population impact analysis of flight procedures such as dispersed flight tracks using integrated exposure metrics including DNL and N_{Above}.

Task 4- Apply Fast Modeling Framework to Additional Sample Problem

Massachusetts Institute of Technology

Objective(s)

In this task, the fast modeling architecture for local and system wide environmental analysis was applied to an additional sample problem to evaluate system-level applications for location-specific procedural changes. The objective of this task was to exercise modeling capabilities with scenarios that are relevant for multiple stakeholders, including local communities, operators, airports, and regulators.

Research Approach

- Identify methods to model flight operations in the vicinity of airports using representative trajectories based on historical radar data and published procedures



- Integrate schedule, fleet, and runway utilization data from external sources to allow calculation of noise contours at airports of interest
- Analyze noise impacts at a system level that would arise from implementing a specific advanced operational procedure of interest, or modifying procedure design criteria for specific types of PBN procedures.

Major Accomplishments

- Developed method for generating set of possible flight procedures based on RNAV and RNP procedure design criteria
- Developed method for rapidly applying noise contour analysis to tens of thousands of possible flight procedures
- Applied rapid noise analysis framework to RNAV and RNP procedures in order to determine noise-minimum procedure for each runway procedure at all OEP-35 airports

Publications

- Jensen, L., "Data-Driven Flight Procedure Simulation and Noise Analysis in a Large-Scale Air Transportation System," *MIT ICAT*, 2018. http://hdl.handle.net/1721.1/116741

Outreach Efforts

02/26/2018: Briefing to Aviation Noise Symposium
04/03/2018: Briefing to ASCENT Advisory Board
04/19/2018: Briefing to FAA Joint University Program research update meeting
06/15/2018: Collaboration with NASA discussion
07/12/2018: Collaboration with MSP airport discussion
07/23/2018: Briefing to FAA Joint University Program research update meeting
10/09/2018: Briefing to ASCENT Advisory Board
10/22/2018: Briefing to FAA Joint University Program research update meeting
11/08/2018: Briefing to Airline Industry Consortium
In-person outreach and collaboration with TASOPT aircraft performance model development team at MIT.
In-person outreach and collaboration with Volpe noise tool development team.

Awards

None

Student Involvement

Graduate students have been involved in all aspects of this research in terms of analysis, documentation, and presentation.

Plans for Next Period

The next phase of this project will involve further analysis of metrics to best communicate noise results for multi-stakeholder situations. The noise analysis framework will be applied to further examples in analyzing potential concepts for flight procedures including dispersed flight tracks. The framework will be applied at a system-level, analyzing not only a single flight procedure but rather a set of flight procedures and the impacts to the communities.

Project 017 Pilot Study on Aircraft Noise and Sleep Disturbance

University of Pennsylvania

Project Lead Investigator

Mathias Basner, MD, PhD, MSc
Associate Professor of Sleep and Chronobiology
Department of Psychiatry
University of Pennsylvania
1019 Blockley Hall, 423 Guardian Dr.
Philadelphia, PA 19104-6021
215-573-5866
basner@pennmedicine.upenn.edu

University Participants

University of Pennsylvania

- P.I.: Mathias Basner, Associate Professor
- FAA Award Number: 13-C-AJE-UPENN-006
- Period of Performance: October 01, 2017 to September 30, 2018
- Task(s):
    - ATL Pilot Sleep Study: Data analysis

Project Funding Level

The funding amount for this period was $135,306.00. The cost sharing requirement for this project was met by our international collaborators at the German Aerospace Center (DLR).

Investigation Team

- Principal Investigator: Mathias Basner
- Postdoctoral researcher: Michael Smith
- Research Assistant: Sarah Rocha

Project Overview

The long-term goal of this line of research is to derive exposure-response relationships for aircraft noise-induced sleep disturbance that are representative of the exposed U.S. population. As studies will have to investigate samples around multiple airports, it will not be possible to use polysomnography (i.e., simultaneous recording of the electroencephalogram, electromyogram, and electrooculogram) to monitor sleep, as this method requires trained personnel at the measurement site in the evening and in the morning and is thus too costly. An alternative methodology of using a single channel electrocardiogram (ECG) and actigraphy to monitor sleep has been examined. This methodology allows the investigation of larger subject samples at lower cost as individuals can be taught how to apply the electrodes themselves. Also, unlike polysomnography, awakenings can be identified automatically. As part of previous research, an algorithm for identifying EEG arousals (Basner, Griefahn, Müller et al., 2007) based on increases in heart rate was refined in order to only identify those arousals greater than or equal to 15 seconds in duration, which is the most agreed upon indicator of noise-induced sleep disturbance. High agreement between EEG visually scored arousals and arousals identified using the refined ECG based algorithm was obtained. The methodology of using ECG and actigraphy to monitor sleep has been implemented in two pilot field studies to evaluate the quality of data that can be obtained for unattended physiological and noise measurements. Based on lessons learned, the study protocol is being refined in order to inform the design and cost of a potential multi-airport study on the effects of noise on sleep.



Objectives

(1) Finish acquisition and analysis of acoustical and physiological data of the PHL study;
(2) Refine and, to the extent possible, automatize the methodology to identify aircraft noise events and maximum sound pressure levels in complex acoustical signals;
(3) Inform the design and cost of a potential large-scale field study on the effects of aircraft noise on sleep around multiple US airports based on lessons learned from the current field studies;
(4) Continue our collaboration with colleagues at the German Aerospace Center (DLR) to compare, combine, and publish findings from US and German field studies.

Research Approach

Based on lessons learned in the Philadelphia Sleep study, the methodology has been refined and a second pilot study is currently being conducted to evaluate its feasibility. The airport for this study was selected in consultation with the FAA and has relevant amounts of nighttime air traffic and a sufficient population from which to sample. To determine the sample regions around the airport, L_{Night} noise contours were provided by the FAA. Additionally, we calculated L_{Night} contours for 84 weekdays based on flight track data. For the study we have 10 sampling regions, 5 east and west of the airport of the following noise categories: < 40 dB (control region), 40-45 dB, 45-50 dB, 50-55 dB, and >55 dB L_{Night}.

To recruit participants for the study, brief surveys were mailed to randomly selected households within each of the 10 sampling frames. The primary purpose of the survey is determining the eligibility of individuals to take part in an in-home sleep study. The survey contains questions on the individual's health, sleep, and noise sensitivity. To increase the response rate to the recruitment survey, different incentives, such as a promised gift card and a pre-paid $2.00 were examined. Additionally, survey length and number of follow-up surveys were varied to determine their effect on response rate. The target number of completed surveys is 200 per 5dB noise category, for a total of 1000 surveys.

In the survey, participants indicate their interest in taking part in the in-home sleep study, which consists of 5 nights of unattended ECG and actigraphy measurements and indoor sound recordings. The equipment is mailed to the participants' homes and instruction manuals and videos on how to setup and use the equipment are provided. Mailing the equipment eliminated the need for staff in the field which significantly reduces the study cost. In addition, mailing the equipment may increase the response rate as staff does not enter the participants' homes. For enrolling in the in-home sleep study, participants received varying amounts of compensation. For survey mailing rounds 1-5, participants received $20 per night in which measurements were completed. Compensation was increased to $30 per night for mailing rounds 6-9, and to $40 per night for rounds 10-17. The purpose of increasing the compensation was to evaluate how response rate changes as compensation increases. This will help determine a cost-effective compensation for a future multiple airport study. The outcomes for this study are to determine the response rates for both the mail and in-home study, assess the feasibility of mailing equipment, and evaluate the quality of data that can be obtained.

Milestones

The following are milestones that were achieved during the past 12 months:
(1) Data collection for the second pilot sleep study was completed in 11/2017.
(2) Analysis of the acoustical and physiological data of the PHL study was completed.
(3) Analysis of the acoustical and survey data of the ATL study was completed.
(4) The physiologic and acoustical analysis methodology was refined.

Major Accomplishments

The approach for recruiting participants for in-home sleep measurements was refined. In collaboration with Dr. Uwe Müller from the German Aerospace Center, software to convert recorded audio signals to calibrated sound pressure levels was developed. Data collection for the second pilot study around ATL was completed, with 407 surveys received and 34 participants completing the in-home study of aircraft noise exposure and heart rate and body movements. Analysis of the surveys was completed, nighttime noise (L_{Night}) was significantly associated with worse overall sleep quality; L_{Night} also increased the likelihood of frequently having trouble sleeping due to nighttime awakenings, and having greater difficulty staying awake during the day. Residents in higher L_{Night} neighborhoods were more likely to report that their sleep was highly disturbed due to aircraft noise, and that they felt highly annoyed to aircraft noise over the past 12 months. The findings have been drafted into a manuscript that will be submitted to a peer reviewed journal in late 2018. Analysis of the ATL



acoustical and physiological data was ongoing at the end of the project period, the reason for a no-cost extension, and expected to be completed in November 2018.

Statistical analysis of the most effective approaches for receiving completed surveys and recruiting participants for the field study was completed. Personalizing the address, enclosing a $2 cash incentive with initial questionnaire mailing and repeated follow-up mailings were effective at increasing response rate. Although these approaches were more expensive than other approaches in terms of per household mailed, the higher response rates meant that they were more cost-effective overall for obtaining an equivalent number of responses. Although no effect of the different strategies on the likelihood that respondents would eventually participate in the field study was observed, pre-issued cash incentives and sending follow-up waves would maximize the numbers of people from which to recruit, and may be an effective strategy for improving recruitment into the field studies. The total cost to receive a completed survey was around $30 for the most cost-effective approaches. The total cost to recruit a single participant into the field study was around $400 for the most cost-effective approaches.

Publications

Basner, M., Clark, C., Hansell, A., Hileman, J.I., Janssen, S., Shepherd, K., Sparrow, V.: Aviation noise impacts: state of the science. Noise and Health 19(87): 41-50, 2017.

Basner, M., McGuire, S.: Pilot study examining the effects of aircraft noise on sleep in communities near Philadelphia International airport. Presentation at the 12th ICBEN Congress on Noise as a Public Health Problem, Zurich, Switzerland, June 18-22, 2017.

Müller, U., Elmenhorst, E.-M., Mendolia, F., Quehl, J., Basner, M., McGuire, S., Aeschbach, D.: A comparison of the effects of night time air traffic noise on sleep at Cologne/Bonn and Frankfurt Airport after the night flight ban. Presentation at the 12th ICBEN Congress on Noise as a Public Health Problem, Zurich, Switzerland, June 18-22, 2017.

McGuire, S., Müller, U., Elmenhorst, E.-M., Mendolia, F., Aeschbach, D., Basner, M.: Cross-country comparison of aircraft noise-induced sleep disturbance. Poster at the 12th ICBEN Congress on Noise as a Public Health Problem, Zurich, Switzerland, June 18-22, 2017.

McGuire, S., Basner, M.: Development of a methodology for field studies on the effects of aircraft noise on sleep. Presentation at the 173rd Meeting of the Acoustical Society of America and the 8th Forum Acusticum, Boston, MA, June 25-29, 2017.

Smith, M., Witte, M., Rocha, S., Basner, M.: Effectiveness of incentives and follow-up on increasing survey response rates and participation in field studies. Manuscript currently under FAA project manager review, to be submitted to Public Opinion Quarterly.

Basner, M., Witte, M., McGuire, S.: Aircraft noise effects on sleep – results of a pilot study near Philadelphia International Airport. Manuscript currently under FAA project manager review, to be submitted to the International Journal of Environmental Research and Public Health.

Rocha, S., Witte, M., Smith, M., Basner, M.: Survey results from a pilot sleep study near Atlanta international airport. Manuscript to be submitted to International Journal of Environmental Research and Public Health, in preparation.

Outreach Efforts

None

Awards

None

Student Involvement

None

Plans for Next Period

The analyses of acoustic and physiological data from the ATL pilot study will be finalized. We will continue our collaboration with colleagues at the German Aerospace Center (DLR) to compare findings from US and German field studies and to prepare joint publications.

References

Basner M, Griefahn B, Müller U, Plath G, Samel A. An ECG-based algorithm for the automatic identification of autonomic activations associated with cortical arousal. Sleep 2007; 30(10):1349-61.

Project 018 Community Measurements of Aviation Emissions Contribution to Ambient Air Quality

Boston University School of Public Health

Project Lead Investigator

Kevin J. Lane
Assistant Professor
Department of Environmental Health
Boston University School of Public Health
715 Albany St. T4W, Boston, MA 02118
617-414-8457
klane@bu.edu

Jonathan I. Levy (through 9/30/17)
Interim Chair and Professor
Department of Environmental Health
Boston University School of Public Health
715 Albany St. T4W, Boston, MA 02118
617-358-2460
jonlevy@bu.edu

University Participants

Boston University School of Public Health

- P.I.(s): Kevin J. Lane, Assistant Professor and Jonathan I. Levy, Professor and Associate Chair
- FAA Award Number: 13-C-AJFE-BU, Amendment 7
- Period of Performance: October 1, 2017 – September 30, 2018
- Task(s):
    1. Construct regression models to determine the contributions of aircraft arrivals to UFP and BC concentrations measured during our 2017 monitoring campaign.
    2. Conduct site selection for our 2018 monitoring campaign by analyzing our 2017 measurements and by considering optimal sites to determine multiple types of aviation source contributions.
    3. Measure UFP and other air pollutants at sites near Boston Logan International Airport selected under Task 2.
    4. Develop platforms that would allow for comparisons between atmospheric dispersion models implemented by collaborators on ASCENT Project 19 and monitored pollutant concentrations from Project 18.

Project Funding Level

$270,000. Matching funds provided by non-federal donor to the Women's Health Initiative (WHI) cohort studies, provided as cost share support to Boston University through Project 3.

Investigation Team

ASCENT BUSPH Director and Project 18 Co-Investigator: Jonathan I. Levy, Sc.D. (Professor of Environmental Health, Chair of Department of Environmental Health, Boston University School of Public Health). Dr. Levy is the Boston University PI of ASCENT. He initiated ASCENT Project 18 and serves the director of BUSPH ASCENT research.

ASCENT Project 18 Principal Investigator: Kevin J. Lane, Ph.D. (Assistant Professor of Environmental Health, Department of Environmental Health, Boston University School of Public Health). Dr. Lane joined the Project 18 team in July 2017. Dr. Lane has expertise in ultrafine particulate matter exposure assessment, geographic information systems, and statistical modeling of large datasets, along with cardiovascular health outcomes associated with air pollution exposures. He has



contributed to study design and data analysis strategies, and as of 10/1/17, took over the primary responsibility for project execution and contributes to manuscripts and reports produced.

Post-doctoral researcher: Matthew Simon, Ph.D. Dr. Simon joined the Project 18 team in September 2017, and is involved in data analyses, field study design and implementation, and scientific manuscript preparation.

Graduate Student: Chloe Kim, MPH. Ms. Kim is a doctoral student in the Department of Environmental Health at BUSPH. She has taken the lead on organizing and implementing the air pollution monitoring study and will be responsible for the design and execution of related statistical analyses.

Research Assistant: Claire Schollaert. Ms. Schollaert provides field support for the air pollution monitoring study, including design and implementation of monitoring platforms.

Project Overview

The primary goal was to conduct new air pollution monitoring underneath flight paths to and from Boston Logan International Airport, using a protocol specifically designed to answer the question of the magnitude and spatial distribution of ultrafine particulate matter (UFP) in the vicinity of arrival flight paths. Data was collected that would address the question of whether aircraft emissions, and in particular arrival emissions, can contribute significantly to UFP concentrations at appreciable distances from the airport. Task 1 was an extension of ongoing air pollution monitoring and statistical analysis work under the current ASCENT Project 18. Tasks 2 and 3 leverage the infrastructure developed for our field campaign to collect measurements to address a broader set of research questions than those evaluated under Task 1, with some additional data collection on UFP size distributions and including a new air pollutant (NO/NO2). These Tasks have provided a strong foundation for Task 4, which has increased the potential for future collaborative efforts with Project 19 in which we interpret the measurements collected and use them to inform ongoing modeling efforts at UNC.

A summary of 2017 project methods and data collection have been included below to inform on the continuation of Project 18 data into bivariate statistical analysis and multiple regression model development conducted under Task 1 and was used to inform new site selection for Task 2.

Project 18 Task 1 for the 2016-2017 funding cycle focused on designing and implementing an air pollution monitoring study that would allow us to determine contributions from arriving aircraft to ambient air pollution in a near-airport setting. The objective of this task was to address the question of whether aircraft emissions, and in particular arrival emissions, can contribute significantly to ultrafine particulate matter (UFP) concentrations at appreciable distances from the airport.

An air pollution monitoring campaign was conducted at six sites at varying distances from the airport and the arrival flight path to runway 4R (Figure P.1). Site 1 = Office of Department of

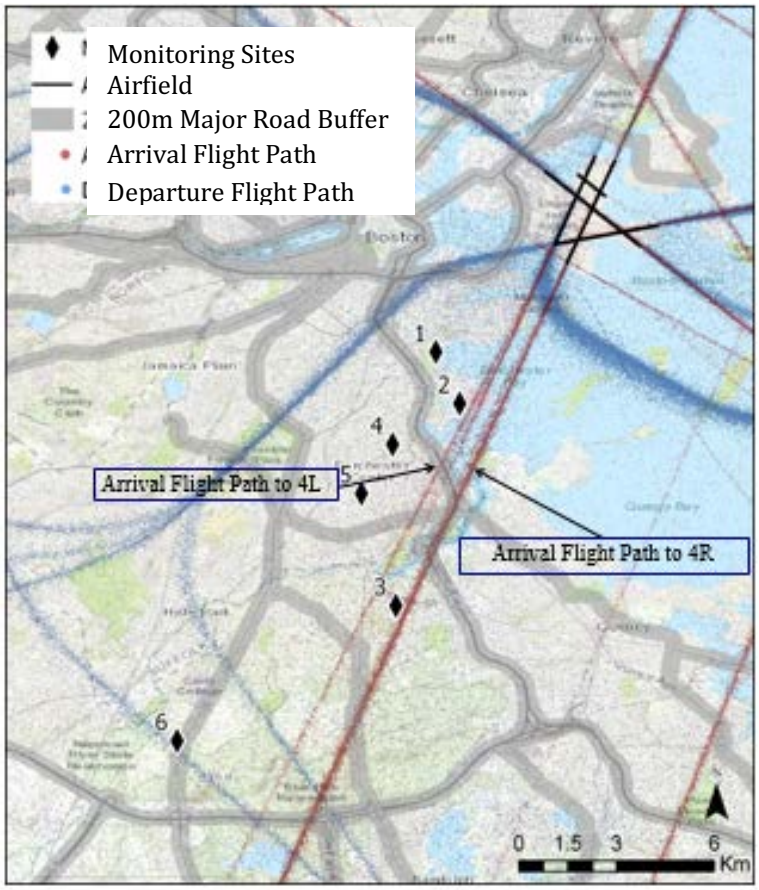


Figure P.1. Monitoring sites and runway 4R flight path.



Conservation and Recreation (DCR) Boston MA; Site 2 = University of Massachusetts (UMASS) Boston campus; Site 3 = Fonte Bonne Academy; Site 4 = Boston Community Development Corporation office (CDC); Site 5 = Community member residence; Site 6 = Blue Hills. Sites were selected through a systematic process, considering varying distances from the airport and laterally from the 4R flight path, and excluding locations close to major roadways or other significant sources of combustion. These sites were chosen specifically to isolate the contributions of arrival aircraft on runway 4R, which is important for the flight activity source attribution task.

Task 1- Construct Regression Models to Determine the Contributions of Aircraft Arrivals to UFP and BC Concentrations Measured During our 2017 Monitoring Campaign

Boston University School of Public Health

Objective(s)

Under Task 1 we developing regression models to examine contributions from arriving aircraft to ambient air pollution in a near-airport setting. The objective of this task was to address the question of whether aircraft emissions, and in particular in-flight arrival and departure emissions, can contribute significantly to ground-level ultrafine particulate matter (UFP) concentrations at appreciable distances from the airport.

Research Approach

Utilizing the air pollution data collected during the 2017 monitoring campaign, we examined average UFP concentrations on the days when the 4R runway was in use and wasn't in use under all wind conditions, to examine the overall impact of arrival aircraft on ambient UFP concentrations at the study sites. We also examined the correlations of simultaneously measured UFPs from multiple study sites to examine the similarities and variations of aircraft impact at different monitoring sites under different meteorological and flight activity levels. Prior to constructing regression models we examine space-time plots of our data identified distinct patterns of plume movement and potential time lag differences between the sites under specific meteorological conditions. Results from these descriptive analyses were used to inform the regression model development process.

For the regression models, we developed multivariate regression models to examine the prediction pattern of UFP, using covariates that included meteorology, PDARS flight activity, and other ground source contributions such as localized traffic. Each study site was modeled individually to look at location-specific impact of aircraft arrivals along with meteorological and other local environmental conditions. We also have explored novel statistical approaches elastic nets and random forest modeling to identify the importance of key covariates at different temporal and distributional scales of analysis.

Milestone(s)

The core milestones for Task 1 included:

- Finish QA/QC of 2017 UFP monitoring data and develop analytical dataset.
- Complete regression modeling of UFP and associated manuscript development.

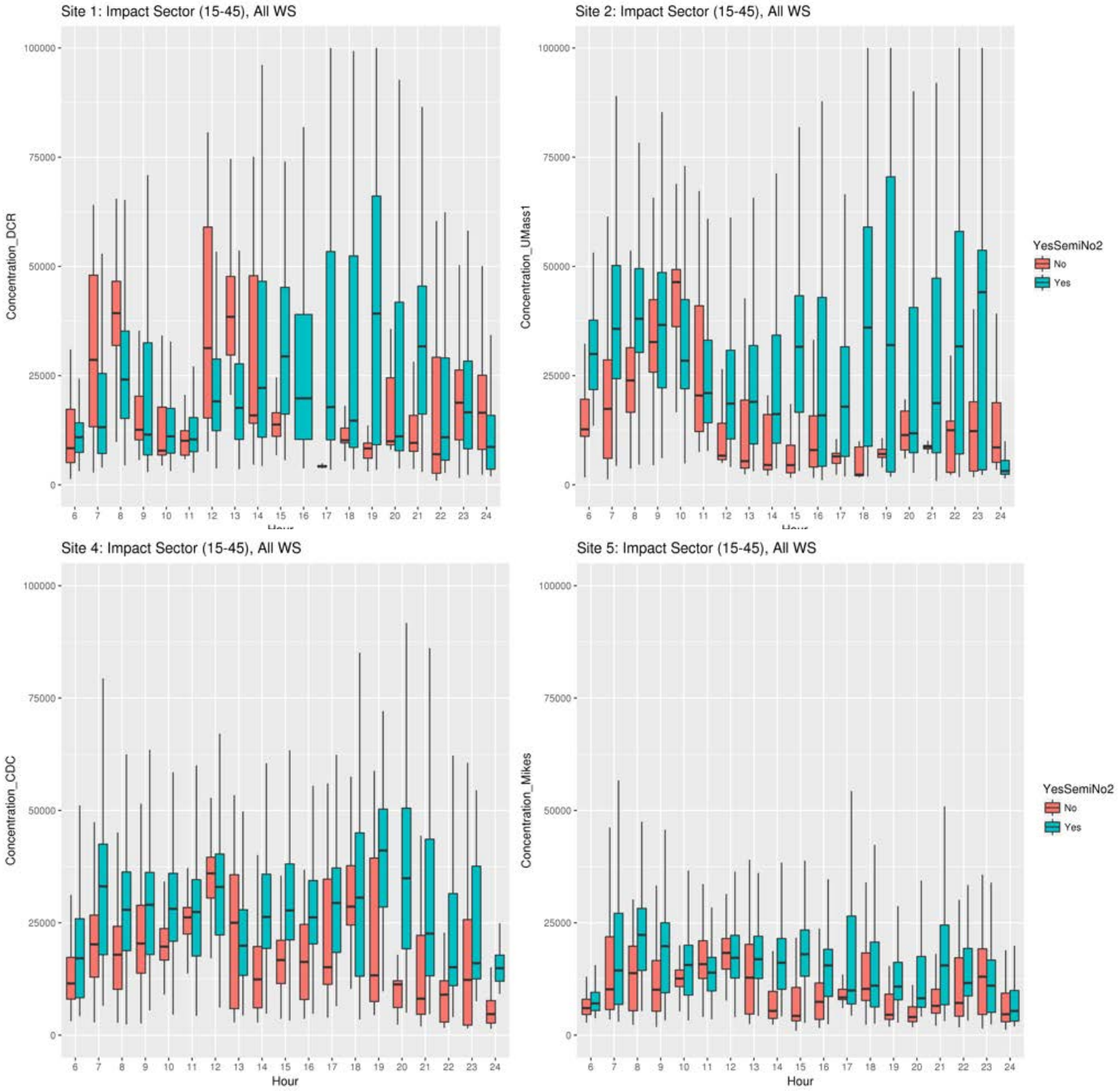
We successfully completed the QA/QC and data linkages with UFP monitor data. There was an unanticipated delay in regression model development as PDARS data for 2017 was being processed and was unavailable to use until spring 2018. Regression model development is being finalized and manuscripts are in preparation for submission to peer-reviewed literature.

Major Accomplishments

Descriptive Maps and PNC Wind Rose Plots

Statistical analysis for project 18 has expanded to improve our understanding on wind direction, wind speed, flight activity and aircraft engine type on ground-based PNC measures. The following sets of figures explain the patterns we observed in the 2017 data sampling period. Figures 1.1a and 1.1b are boxplots of hourly PNC during two different wind conditions at all airport sites when the 4R runway was fully or semi-operational. Wind direction is based upon the weather station at each monitoring site. Ideal wind conditions (15-45 degrees) had elevated concentrations at near-source sites compared to when

the monitors were upwind of the arriving aircraft (45-145). Wind direction had less impact on background site concentrations. We are also exploring relative wind direction as well as sub-categorization of the operational flight activity further to identify periods when arrivals into 4L were occurring instead of 4R during the non-operational time periods. These results identified the potential interactions that might be occurring between meteorology and flight activity that appear to be site-specific when informing on ground-level PNC source attribution.



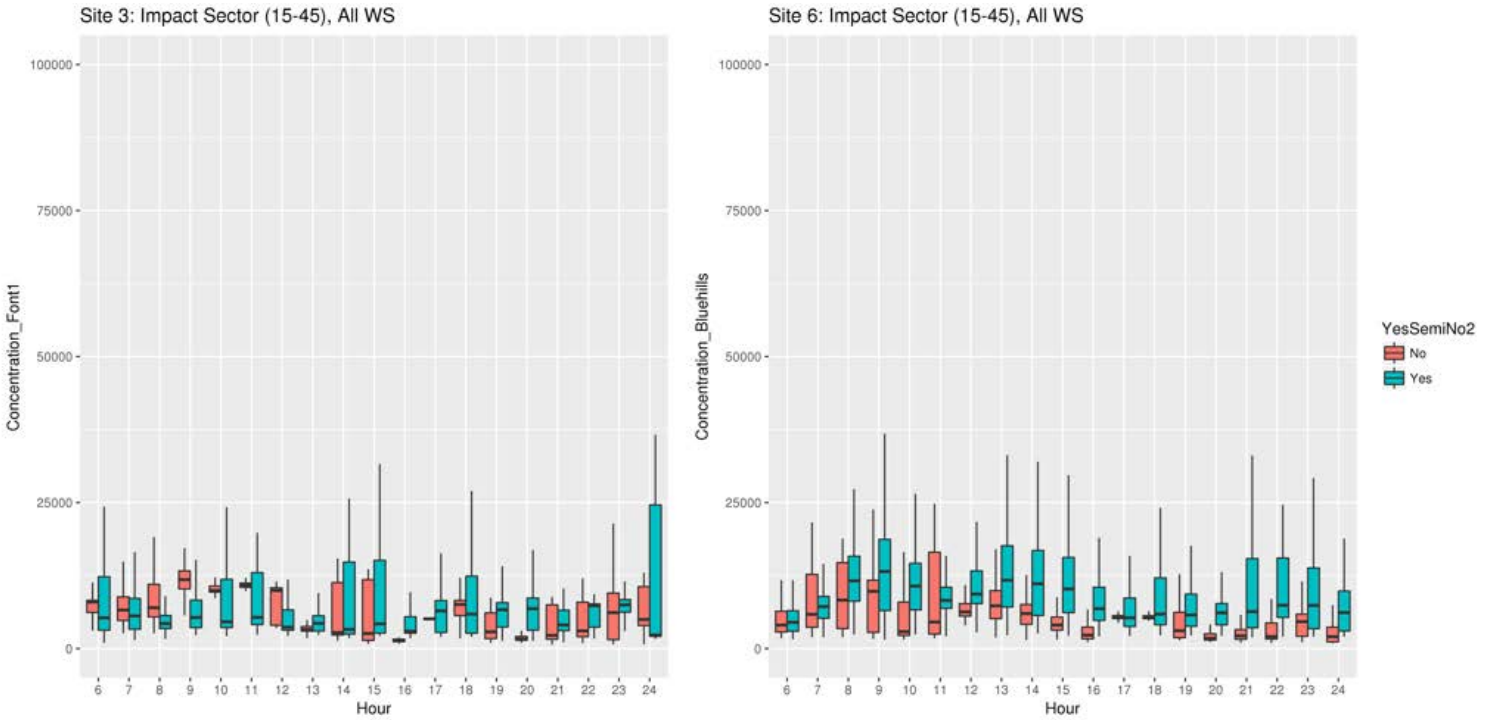
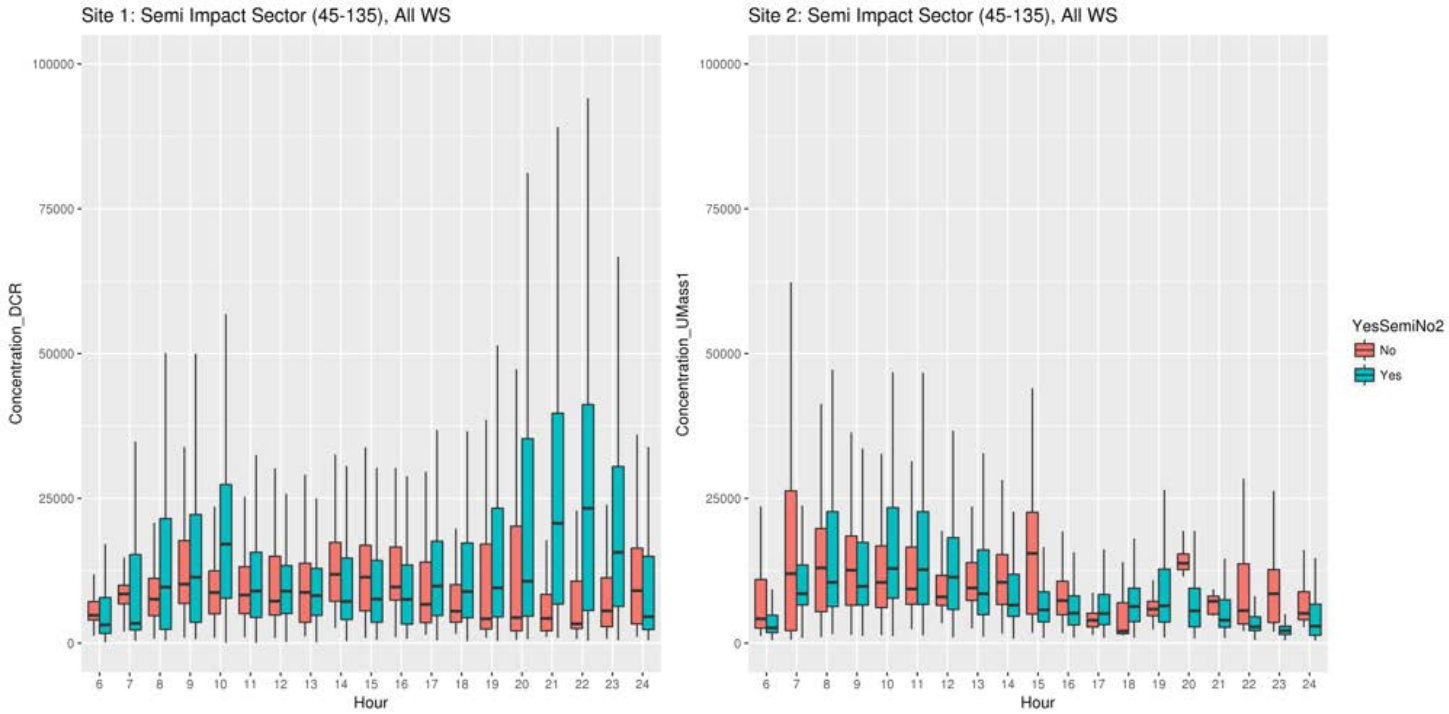


Figure 1.1a. Particle number concentration (PNC) under impact sector wind direction and flight activity at 4R monitoring sites for the 2017 monitoring period.



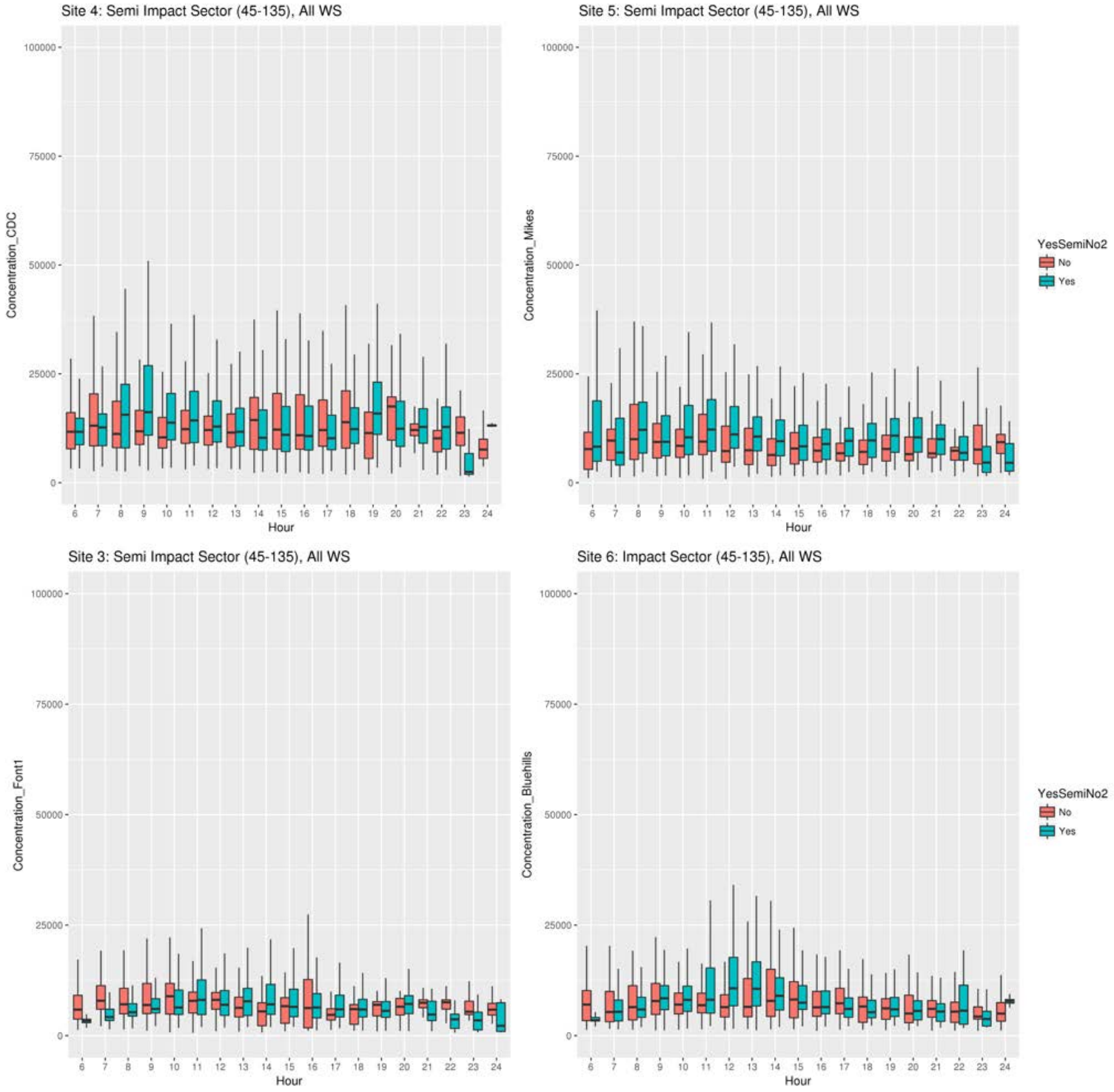


Figure 1.1b. Particle number concentration (PNC) under semi-impact sector wind direction and flight activity at 4R monitoring sites for the 2017 monitoring period.

Additional analysis is being conducted to examine PNC at different temporal resolutions below 1-hour. Previous studies have focused on analyzing the median or mean hourly concentrations, but the intermittent nature of flights could mean that we should be looking at more finely resolved times below 1-hour and potential peak exposures in the 95th and 99th percentile. We have started to plot and analyze the 1-second PNC data with corresponding meteorology to understand the simultaneous relationship between wind direction, wind speed, flight activity and PNC at each monitoring site. With this in mind we created wind rose PNC plots to identify hotspots under different meteorological conditions at each site (Figure 1.2).

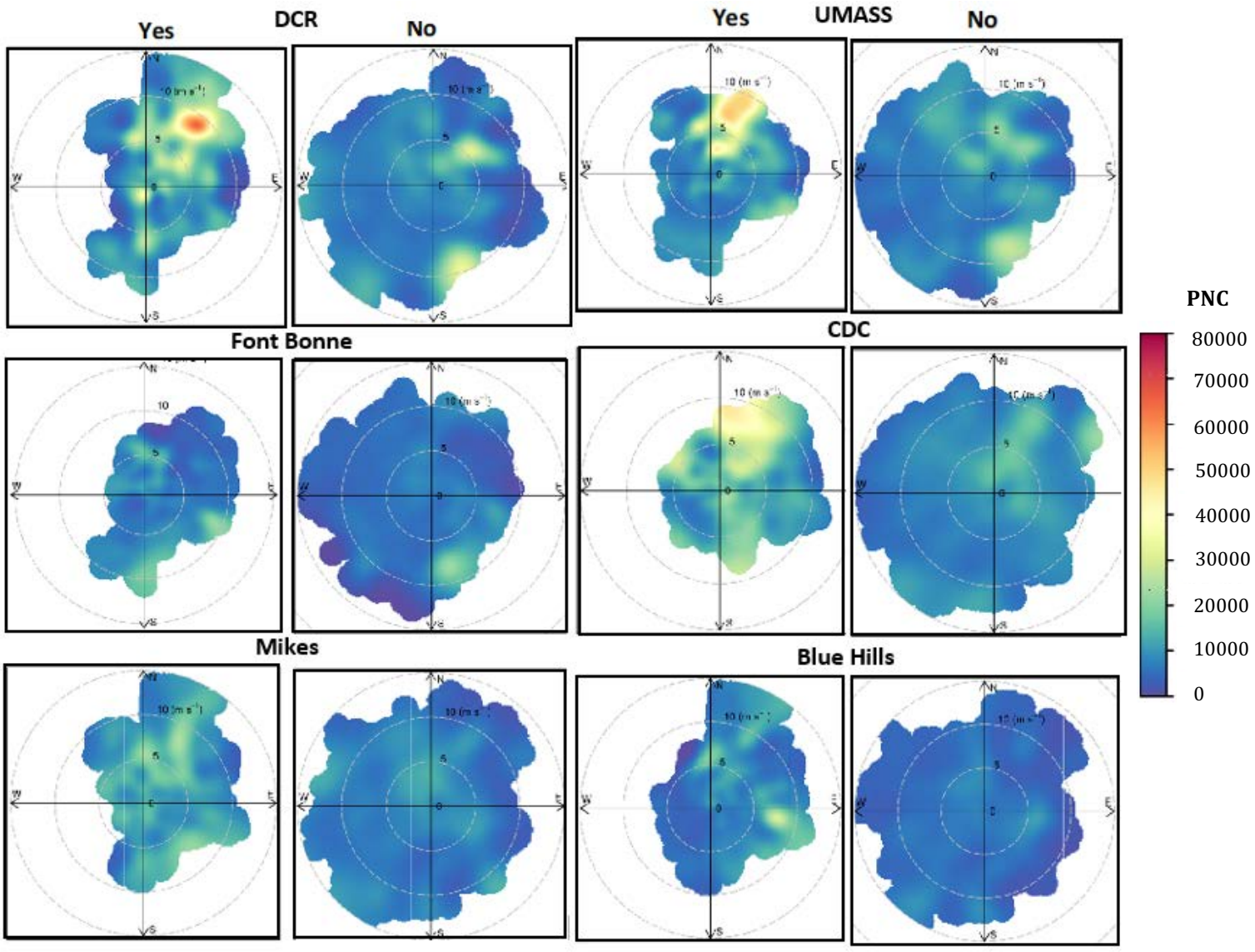


Figure 1.2. Particle number concentration (PNC) wind rose plots for each monitoring site by flight activity on 4R and 4L (Yes = 1 or more flights per hour; No = zero flights per hour).). The monitoring sites correspond to the map P.1. with Site 1 = Office of Department of Conservation and Recreation (DCR) Boston MA; Site 2 = University of Massachusetts (UMASS) Boston campus; Site 3 = Fonte Bonne Academy; Site 4 = Boston Community Development Corporation office (CDC); Site 5 = Community member residence; Site 6 = Blue Hills.

Each plot above can be interpreted as the monitoring site-specific wind rose, centered on each monitor GPS location, with airport located to northeast of each site. Each quadrant represents the direction in which the wind is blowing from, while the dashed circular lines indicate the wind speed in miles per hour. The color represents the ranges in PNC level. From the plots there are several key points that we can infer and use to explore further:

- When flights are occurring, there are higher PNC levels compared to when no flights are occurring.
- Closer sites have elevated PNC hotspots, specifically DCR and UMASS which are closer to the airport have higher levels than all other sites.
- Hotspots are more clearly shown when the wind is coming from the airport direction at DCR and UMASS under the Yes flight activity scenario compared to the No scenario.
- Background sites at Blue Hills and Fonte Bonne have more hotspots of PNCs under the 'Yes' flight activity then 'No' flight activity hours.

Overall, there is an elevated level of PNC when wind is coming from the airport direction and aircraft are flying at lower altitudes such as at the UMASS and DCR sites. An arriving aircraft into Logan that is overhead of a monitoring site location further away at our background sites does not produce a similar detectable PNC level under the ideal wind conditions which may be due to these aircrafts being at a higher altitude.

PNC Regression Modelling

The descriptive analyses above have informed regression modelling efforts, presented below. PNC has a non-normal distribution and is commonly examined as the natural log (LN) of PNC. Covariates included in this regression model have been found to have a significant univariate relationship with LN PNC. The multivariable linear regression model provides an initial examination of the relationship between spatial-temporal meteorological, flight activity, and other potential ground contributions from traffic sources on the association with natural log of hourly PNC. Results from this model should be considered as development to assist in refinement as the current model is being expanded to include additional covariate contributions as well as interactions between predictive factors. Our initial regression models have been developed for each monitoring site to compare the total model R^2. Additionally, covariates have been kept the same for all models to examine the explanatory power of each variable between sites to better understand the relative contributions on flight activity, meteorology and other local contributions such as traffic for source attribution of ground-measured PNC.

In Table 1.1 we present preliminary regression model results for hourly LN PNC at two near source sites 1 and 2 and a background site 3. Each model includes meteorological variables (wind direction, wind speed and temperature), temporal (weekend/ weekday and time of day) and flight activity on runway 4R/4L (categorized as no flights, low [1-10 arriving flights/hour] and high [>10 arriving flights/hour]). Using this preliminary model we can begin to formulate new hypotheses and identify potential interactions to explore further. The initial models support our hypotheses and descriptive analyses regarding the importance of wind direction with northeasterly winds being the impact sector winds for each of our near airport monitoring sites 1 and 2. Additionally, hourly number of flights was important at both near and background sites, but had a substantially larger association with LN PNC at sites 1 and 2 than site 3. We are currently integrating additional meteorological variables (i.e. mixing height and apparent monitor wind direction) as well as flight activity data from PDARS (i.e. flights by weight class per hour).



Table 1.1. Spatial-temporal model for hourly natural log (LN) of particle number concentration (PNC) at monitoring sites 1, 2 and 3. The monitoring sites correspond to the map P.1. with Site 1 = Office of Department of Conservation and Recreation (DCR) Boston MA; Site 2 = University of Massachusetts (UMASS) Boston campus; Site 3 = Fonte Bonne Academy.

		DCR (Site 1) R^2 = 0.31		UMASS (Site 2) R^2 = 0.31		Fontebonne (Site 3) R^2 = 0.17	
Variable Grouping	**Covariates**	**Coefficient**	**P-val**	**Coefficient**	**P-val**	**Coefficient**	**P-val**
Wind Direction (REF = West, W)	E	0.85	**	0.63	***	0.83	**
	EN	0.85	***	0.66	***	0.62	***
	ES	0.85	*	0.82	**	0.89	*
	N	1.08	0.34	1.64	**	1.2	0.34
	NE	2.04	***	1.71	***	0.77	***
	NW	1.2	*	1.26	**	1.18	*
	S	0.94	***	0.79	***	0.82	***
	SE	0.83	**	0.69	***	0.85	**
	SW	0.96	0.14	0.97	0.44	0.94	0.14
	WN	1.29	0.43	1.17	**	1.04	0.43
	WS	0.94	0.23	0.93	0.16	1.06	0.23
Arrival Flight Activity (REF = No Activity; 0 flights in hour)	Semi	1.21	***	1.26	***	1.21	***
	Yes	1.37	***	1.3	***	1.2	***
Temperature	1°Farenheit	0.99	***	0.98	***	0.99	***
Rush Hour (Ref = Overnight 12:00am - 5:00am)	Morning Rush Hour (5-10am)	1.63	***	1.78	***	1.45	***
	Daytime (10-3pm)	1.84	***	2.06	***	1.64	***
	Afternoon Rush Hour (3-6pm)	1.63	***	1.31	***	1.38	***
	Evening time (6pm-12am	1.52	***	1.38	***	1.23	***
Weekend vs. weekday	Weekend	0.89	***	0.7	***	0.86	***
Wind Speed	1 MPH	0.96	***	0.97	***	0.86	***

P-val *** ≤ 0.001; P-val ** ≤ 0.01; P-val *** ≤ 0.05.

In addition to linear regression modelling we have explored the use of machine learning regression approaches to identify key covariates and optimize prediction of PNC at each site. This research has focused on application to the UMASS site and uses a random forest approach which is a decision tree-based machine learning algorithm. Each tree is grown by a bootstrap sample, and a random subset of predictors is selected at each split. Predictions are obtained by averaging results of different trees. We developed three models to predict PNC using the random forest model approach to predict PNC at different hourly scales; 1) hourly median PNC, hourly 95th PNC, and hourly 99th PNC. Figure 1.3 provides the relative contributions of covariates to predict PNC measured as the mean square error.

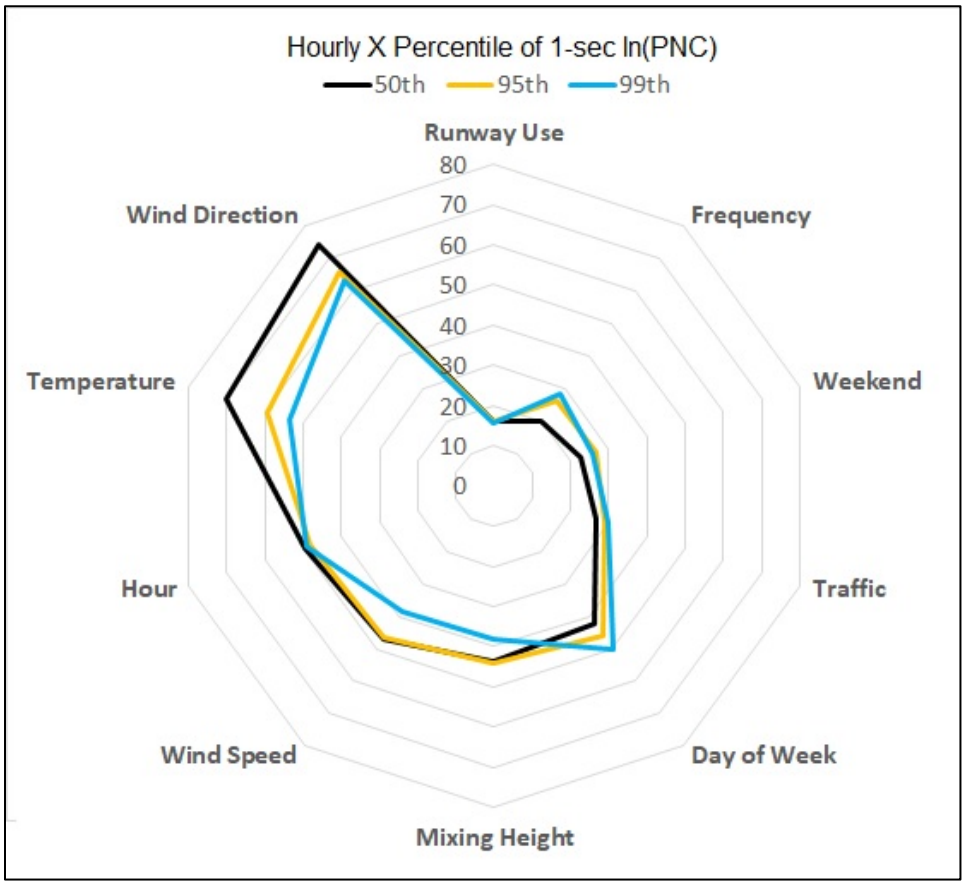


Figure 1.3. Spider plot showing the importance of each variable in the random forest model based on the mean decrease in model accuracy (as measured by mean square error).

The median model regression performance measured as R^2 improved prediction by over 20% using the random forest approach (R^2 = 0.56), compared to the linear regression modelling approach (R^2 = 0.31; see Table 1.1). As hourly PNC is predicted at higher percentiles (95th and 99th; see Figure 1.3), meteorological variables decreased in importance while variables related to flight activity such as schedules or frequency of flights arriving on 4R/4L gained importance. Flight frequency has the largest percent gain in model importance when comparing 95th and 99th percentile models to the 50th percentile. Additionally, the overall random forest model performance increased variance prediction with the 50th percentile variance explained = 55.7%; 95th percentile model variance explained = 59.7%; and 99th percentile model variance explained = 60.2%. The random forest modelling approach is being used in tandem with generalized linear regression modelling to identify the best prediction of PNC at each site, but also provide interpretable results.

Publications

None

Outreach Efforts

Dr. Kevin Lane presented an update of the Project 18 field monitoring and descriptive data analysis at the ASCENT Spring 2018 meeting.

Dr. Kevin Lane presented on “Ultrafine Particulate Matter Monitoring and Source Apportionment”, at the Aviation Emissions Characterization Meeting. National Academy of Sciences, DC, USA.



Dr. Kevin Lane Presented and sat on a panel on "Monitoring and modeling aviation-related ultrafine particles from background concentrations", at the Aviation Emissions Characterization Meeting. National Academy of Sciences, DC, USA.

Doctoral student Chloe Seyoung Kim presented an oral presentation on a portion of the major accomplishments of Project 18 at the International Society for Exposure Science annual meeting in October 2017.

PostDoc Dr. Matthew Simon presented an update of the Project 18 field monitoring and statistical analysis at the ASCENT Fall 2018 meeting.

Awards

Doctoral Student Chloe Kim was the DOT FAA Centers of Excellence Joseph A Hartman Student Paper Competition Winner for her work on "Spatial and temporal patterns of ambient ultrafine particulate matter (UFP) in communities along an arrival aircraft pathway".

Student Involvement

Chloe Seyoung Kim, a doctoral student at BUSPH, was involved with the descriptive analysis and regression modelling of 2017 PNC data. Claire Schoallert, a master's student at BUSPH has been involved with descriptive analysis of the 2018 sampling data. Sijia Li, a master's student at BU statistical department has been involved with machine learning regression modelling applications.

Plans for Next Period

Task(s) proposed over the next study period (10/1/18-9/30/19):
Construct UFP regression models using the 2017–2018 data and the flight activity data and covariates to determine the contributions of aviation sources to UFP and BC concentrations measured under multiple landing and take-off pathways.

Task 2- Conduct Site Selection for our 2018 Monitoring Campaign by Analyzing our 2017 Measurements and by Considering Optimal Sites to Determine Multiple Types of Aviation Source Contributions

Boston University School of Public Health

Objective(s)

Task 2 for the 2017-2018 funding cycle focused on designing and implementing an air pollution monitoring study that would allow us to determine contributions from arriving aircraft to ambient air pollution in a near-airport setting. The objective of this task was to address the question of whether aircraft emissions, and in particular in-flight arrival and departure emissions, can contribute significantly to ground-level ultrafine particulate matter (UFP) concentrations at appreciable distances from the airport.

Research Approach

An air pollution monitoring campaign was conducted at five sites at varying distances from the airport and arrival departure flight paths for Boston Logan Airport (Figure 2.1). Sites were selected through a systematic process, considering varying distances from the airport and laterally from each flight path, excluding locations close to major roadways or other significant sources of combustion. These sites were chosen specifically to isolate the contributions of in-flight aircraft, which is important for the flight activity source attribution task.

Particle number concentration (PNC, a proxy for UFP) monitoring instruments were established at each monitoring site in a pre-selected scheme to allow for multiple levels of comparison (e.g., sites underneath vs. not underneath flight paths given prevailing winds, sites at varying distances from the airport, sites at varying lateral distances underneath flight paths). PNC was measured with TSI Condensation Particle Counters (Model 3783). In addition, black carbon was measured using AethLabs Microaethalometers (Model AE51), and meteorological data at each site were collected using Davis Vantage Pro2 weather stations.



Milestone(s)

The core milestones for Task 2 included:

- Review 2017 monitoring data and identify optimal sites for follow-up field campaign to select candidate monitoring sites and obtain permission to monitor at those sites
- Update field monitoring and site location protocol.

We conducted a review of the 2017 monitoring data and identified sites for the 2018 field campaign, as planned using a rollout phase allowing for immediate sampling to occur throughout the fall and winter while new monitoring site location agreements and permission was sought. At each new monitoring site we conducted a rapid 2- week sampling and review of the data to validate suitable sampling conditions. Selection of monitoring sites was successful, and we obtained permission to sample at five sites including a continued sampling at the UMASS site from 2017 allowing for a multi-year site. Also through collaborations with Tufts University we were able to include long-term sampling data from the Chelsea site. We began collecting field data following our complete protocols in November 2017 with comprehensive data capture throughout the spring and summer, meeting our data collection milestone.

Major Accomplishments

We successfully identified five long-term monitoring sites, received authorization from the site owners and built sampling boxes to house all monitoring equipment that would allow for sampling in both winter and summer.

Publications

None

Outreach Efforts

None

Awards

None

Student Involvement

Chloe Kim, a doctoral student at BUSPH, has been involved with identifying new optimal site during the selection process. Claire Schoallert, a master's student at BUSPH has been involved with field site visits to determine feasibility of sampling protocol.

Plans for Next Period

Task(s) proposed over the next study period (10/1/18-9/30/19):
Conduct mobile monitoring in selected communities near Logan Airport to determine spatial and short-term temporal variation in aviation emissions contributions to concentrations at ground level.



Figure 2.1. Monitoring sites for the 2017-2018 sampling campaign around Boston Logan Airport. Site list corresponds to Table 3.1

Task 3- Measure UFP and Other Air Pollutants at Sites Near Boston Logan International Airport Selected Under Task 2

Boston University School of Public Health

Objective(s)

Given the sites chosen under Task 2, we conducted a monitoring campaign in 2018 to inform an aviation source attribution analysis to expand upon Task 1 regression model development. Our instrumentation and protocol was similar to the 2017 monitoring campaign, but with some key enhancements to improve insights regarding aviation source contributions.

Research Approach

At the sites chosen under Task 2, we conducted a monitoring campaign in 2018 to inform ground-contributions from inflight aviation sources underneath multiple landing and take-off runways at various distances from the airport and flight path. The Instrumentation and protocol used was the same as the 2017 monitoring campaign, but with some key enhancements to improve insights regarding aviation source contributions to NO/NO_2. Monitoring instruments included the TSI Model 3783 water-based CPC for UFP, our primary measure of interest, which was used in the 2017 monitoring campaign. The 3783 is intended for long-term deployment and can record 1-second average concentrations, valuable time resolution for capturing short-term concentration spikes. Of note, as the Model 3783 CPC is temperature-sensitive, we developed and deployed instrumentation in a temperature conditioned space to protect against extreme heat and cold, allowing for long-term deployment.

In addition, the AethLabs model AE51 microaethalometer will be used to measure BC. We also deployed the Alphasense NO/NO_2 sensor that gives high-fidelity outputs and could be used in future studies with simultaneous real-time measurements at numerous sites. This also provides an additional pollutant for any future comparisons with atmospheric dispersion model outputs, which could help isolate factors that influence predictions of particulate matter vs. gas-phase pollutants. The local Davis Vantage Pro2 weather stations was used to capture real-time wind speed/direction and other meteorological conditions at each sampling site.

Similar to 2017, obtaining flight activity data from FAA for the time periods of sampling will be essential for future regression model development, which will include location of each flight as well as basic aircraft characteristics, which could be linked with AEDT to determine aircraft-specific attributes that may be predictive of emissions and corresponding concentrations.

Milestone(s)

- Obtained permission to resample and/or sample new locations, and develop sampling schedule.
- Obtained new monitoring equipment and completed annual manufacturer cleaning and calibration of CPCs.
- Implemented air pollution monitoring protocols, including measurements of meteorological conditions and collection of flight activity data to be used in statistical analyses.
- Completed 2018 field sampling, prepare for air pollution regression modeling.

Major Accomplishments

As described above, the 2018 air pollution field monitoring campaign was conducted from November 2017 – September 2018 at five sites at varying distances from the airport under multiple arrival and take-off flight paths into Logan Airport (Figure 2.1). This met all targets for sample size and data capture, providing a strong foundation for future statistical analyses.



Table 3.1. Distribution of PNC at the five monitoring sites

	UMASS	Chelsea	East Boston	South Boston	Winthrop
Sample Size (days)	264	250	167	123	43
Location	Ground Level	Roof 4th Floor	2nd Floor Window	Roof 5th Floor	Ground Level
Other Samplers	BC, meteorology, NO, NO2	BC, meteorology, NO, NO2	BC, NO, NO2	BC, meteorology, NO, NO2	BC, meteorology
0.1st percentile	169	863	172	471	521
1st percentile	379	1750	904	1160	676
5th percentile	975	3270	2020	2610	1400
50th percentile	7440	11900	10800	8260	8680
95th percentile	24500	43700	65000	36300	47000
99th percentile	47200	87800	124000	66300	70300
99.9th percentile	76900	152000	229000	100000	111000

The summary statistics presented in Table 3.1 cannot provide definitive insight about aviation contributions to measured PNC, but are helpful for hypothesis generation and to inform future modeling efforts. For example, note that Chelsea and East Boston have the highest concentrations of all sites through the 95th and 99th percentiles of the distribution, consistent with their locations closest to the airport and with planes at an elevation that would be closer than at locations further away such as UMASS. This indicates that there could be a more rapid decline in PNC with regard to distance from the airport than observed in the 2017 sampling campaign that focused on only a single arrival pathway. There were consistent patterns observed by seasons at three monitor sites with data from winter, spring and summer.

Table 3.2. Seasonal Distribution of PNC at three monitoring sites.

	UMASS			Chelsea			East Boston		
Sample Size (days)	80	79	93	64	75	105	20	85	54
Season	Winter	Spring	Summer	Winter	Spring	Summer	Winter	Spring	Summer
0.1st percentile	493	309	139	1460	1090	552	879	137	862
1st percentile	1040	496	262	2460	1660	1610	1260	564	1300
5th percentile	3250	1640	547	4350	3210	2950	3290	1810	2230
50th percentile	10100	5970	6390	14100	11200	11100	13800	10600	9920
95th percentile	28600	20200	22800	42200	42100	46000	60100	65400	66100
99th percentile	50500	44800	45300	79900	92200	90300	172000	127000	113000

Winter consistently had elevated median PNC levels at all three sites with greater variation at the 95th and 99th percentile of PNC. It should be noted that East Boston did not have the same amount of sampling days within the winter season. In Table 3.2 East Boston and Chelsea have an elevated PNC at the median and 95th percentile for Chelsea and East Boston compared to UMASS sites across all seasons. Additionally, summer was observed to have the lower PNC levels than winter and/or spring across all three sites. Further analysis is currently being conducted to compare 2018 descriptive statistics between seasons by flight activity and meteorology.



Preliminary hypotheses generated from descriptive analysis of Tables 3.1 and 3.2 are being analyzed currently with aircraft activity data from the National Offload Program (NOP) data, and present us with insight on more formal analyses similar to that conducted under Task 1 once we receive the 2018 PDARS flight activity data.

Publications
None

Outreach Efforts
Dr. Kevin Lane presented on "Ultrafine Particulate Matter Monitoring and Source Apportionment", at the Aviation Emissions Characterization Meeting. National Academy of Sciences, DC, USA.

Dr. Kevin Lane Presented and sat on a panel on "Monitoring and modeling aviation-related ultrafine particles from background concentrations", at the Aviation Emissions Characterization Meeting. National Academy of Sciences, DC, USA.

PostDoc Dr. Matthew Simon presented an update of the Project 18 field monitoring and statistical analysis at the ASCENT Fall 2018 meeting.

Awards
None

Student Involvement
Claire Schoallert, a master's student at BUSPH, Bethany Haley, a doctoral student at BUSPH and Sijia Li, a master student at BU department of statistics has been involved with field monitoring of the 2018 sampling data.

Plans for Next Period
Task(s) proposed over the next study period (10/1/18-9/30/19):
- Continue long-term monitoring of air pollution at both new and existing stationary sites to assess temporal variation in aviation source contributions in greater Boston area communities.
- Incorporate particle size distribution on a rotational basis with each of our monitoring sites to inform our understanding of inflight contributions to community UFP relative to background sources.
- Conduct mobile monitoring in selected communities near Logan Airport to determine spatial and short-term temporal variation in aviation emissions contributions to concentrations at ground level.

Task 4- Develop Platforms that Would Allow for Comparisons Between Atmospheric Dispersion Models Implemented by Collaborators on ASCENT Project 19 and Monitored Pollutant Concentrations from Project 18
Boston University School of Public Health

Objective(s)
While the primary objective of Tasks 1-3 informed aviation source attribution using ambient pollution measurements, the insights from the monitoring data and models could be connected with atmospheric dispersion models applied at the same location and dates. Within Project 19, UNC researchers are implementing SCICHEM to examine the air quality implications of emissions of various air pollutants from aviation, with a current focus on modeling UFP. If in the future Project 19 applies atmospheric dispersion modeling tools focused on locations near Boston Logan International Airport, this would allow for future comparative analyses (modelling and monitoring). The purpose of this task is to develop data processing systems that would allow for these comparative analyses to be conducted.

Research Approach
To aid the efforts of Project 19, we developed two output files under Task 4. First, the UFP measurements collected during the 2017 monitoring campaign were processed and provided in a format requested by Project 19. These measurements reflect the contributions from both aviation and other sources, and are being directly compared with all-source dispersion models such as SCICHEM. In the second phase, regression models being developed under Task 1, development of an



analogous database with the aviation-attributable UFP concentrations has been processed and outputs are being compared with the dispersion models

Milestone(s)

The core milestones for task 4 included:

- Develop analytical dataset estimating aviation source contributions from the 2017 monitoring campaign and share with UNC to inform potential collaborative manuscript.

The monitoring dataset was completed and shared with Project 19. SCICHEM is being used to model PNC using the data provided by Project 18 and we are conducting a comparison between dispersion and regression model outputs.

Major Accomplishments

UFP data from the Project 18 2017 field campaign was cleaned, joined with flight activity and meteorology and shared with Project 19. During this time we have collaborated through teleconferences on dispersion modelling efforts conducted by Project 19 resulting in an abstract submission acceptance to the CMAS conference on modelling PNC.

Publications

None

Outreach Efforts

Dr. Moniruzzaman Chowdury from Project 19 presented on “An integrated modeled and measurement-based assessment of particle number concentrations from a major US airport”, at the CMAS conference.

Awards

None

Student Involvement

Chloe Seyoung Kim, a doctoral student at BUSPH, was involved with preparation of data to be shared with project 19 and comparison of regression model with dispersion model outputs.

Plans for Next Period

Four tasks are proposed over the next study period (10/1/18-9/30/19):

- Compile from FAA essential flight activity covariates needed for regression modelling under Project 18 and dispersion modelling under Project 19 for a data-sharing platform that would allow for comparisons between atmospheric dispersion models implemented by collaborators on ASCENT Project 19 and monitored pollutant concentrations and related regression models from Project 18.



Project 019 Development of Aviation Air Quality Tools for Airshed-Specific Impact Assessment: Air Quality Modeling

University of North Carolina at Chapel Hill

Project Lead Investigator

Saravanan Arunachalam, Ph.D.
Research Professor
Institute for the Environment
University of North Carolina at Chapel Hill
100 Europa Drive, Suite 490
Chapel Hill, NC 27517
919-966-2126
sarav@email.unc.edu

University Participants

University of North Carolina at Chapel Hill

- PI: Saravanan Arunachalam, Research Professor and Deputy Director
- FAA Award Number: 13-C-AJFE-UNC Amendments 1 - 9
- Period of Performance: October 1, 2017 – September 30, 2018
- Task(s):
  - Perform NAS-wide impact assessment for 2011 and 2015
  - Perform airport-by-airport assessment using CMAQ-DDM
  - Perform measurement-modeling assessment of air quality at Boston Logan

Project Funding Level

$200,390 from the FAA

Matching Cost-share provided by the National Aviation University of Ukraine

Investigation Team

Prof. Saravanan Arunachalam (UNC) (Principal Investigator) [Tasks 1,2,3]
Dr. Moniruzzaman Chowdhury (Co-Investigator) [Task 1,3]
Dr. Jiaoyan Huang (UNC) (Co-Investigator) [Task 1]
Mr. Calvin Arter (UNC) (Graduate Research Assistant) [Task 1,2,3]

Project Overview

With aviation forecasted to grow steadily in upcoming years,[1] a variety of aviation environmental policies will be required to meet emissions reduction goals in aviation-related air quality and health impacts. Tools will be needed to rapidly assess the implications of alternative policies in the context of an evolving population and atmosphere. In the context of the International Civil Aviation Organization (ICAO)'s Committee on Aviation Environmental Protection (CAEP), additional tools are required to understand the implications of global aviation emissions.

The overall objective of this project is to continue to develop and implement tools, both domestically and internationally, to allow for assessment of year-over-year changes in significant health outcomes. These tools will be acceptable to FAA (in the context of Destination 2025) and/or to other decision-makers. They will provide outputs quickly enough to allow for a

[1] Boeing Commercial Airplane Market Analysis, 2010.



variety of "what if" analyses and other investigations. While the tools for use within and outside the US (for CAEP) need not be identical, a number of attributes would be ideal to include in both:

- Enable the assessment of premature mortality and morbidity risk due to aviation-attributable $PM_{2.5}$, ozone, and any other pollutants determined to contribute to significant health impacts from aviation emissions;
- Capture airport-specific health impacts at a regional and local scale;
- Account for the impact of non-LTO and LTO emissions, including separation of effects;
- Allow for the assessment of a wide range of aircraft emissions scenarios, including differential growth rates and emissions indices;
- Account for changes in non-aviation emissions and allow for assessing sensitivity to meteorology;
- Provide domestic and global results;
- Have quantified uncertainties and quantified differences from EPA practices, which are to be minimized where scientifically appropriate; and
- Be computationally efficient such that tools can be used in time-sensitive rapid turnaround contexts and for uncertainty quantification.

The overall scope of work is being conducted amongst three collaborating universities – Boston University (BU), Massachusetts Institute of Technology (MIT), and the University of North Carolina at Chapel Hill (UNC). The project is performed as a coordinated effort with extensive interactions among the three institutions and will be evident in the reporting to the three separate projects (ASCENT 18, 19 and 20) by each collaborating university.

The components led by the University of North Carolina at Chapel Hill's Institute for the Environment (UNC-IE) included detailed modeling of air quality using the Community Multiscale Air Quality (CMAQ) model. UNC-IE is collaborating with BU to develop health risk estimates on a national scale using CMAQ outputs and with MIT for inter-comparing against nested GEOS-Chem model applications within the US and to further compare/contrast the forward sensitivity versus the inverse sensitivity (such as adjoint) techniques for source attribution. Our efforts for this project build on previous efforts within Project 16 of PARTNER. This includes detailed air quality modeling and analyses using CMAQ at multiple scales for multiple current and future year scenarios, health risk projection work that successfully characterizes the influence of time-varying emissions, background concentrations, and population patterns on the public health impacts of aviation emissions under a notional future emissions scenario for 2025. Under Project 16, we started to develop a new state-of-the-art base year modeling platform for the US using the latest version of models (CMAQ, WRF, SMOKE) and emissions datasets (AEDT, NEI), and tools (MERRA-2-WRF, CAM-2-CMAQ) to downscale from GCMs being used in Aviation Climate Change Research Initiative (ACCRI). We are continuing to adapt and refine the tools developed from that platform as part of ongoing work in this phase of the project.

In this project, the UNC-IE team is performing research on multiple fronts during the stated period of performance, and we describe them in detail below.

1. Perform NAS-wide impact assessment for 2011 and 2015
2. Perform airport-by-airport assessment using CMAQ-DDM
3. Perform measurement-modeling assessment of air quality at Boston Logan

Task 1- Perform NAS-wide Impact Assessment for 2011 and 2015

University of North Carolina at Chapel Hill

Objective(s)

Model $PM_{2.5}$ and O_3 concentration increases due to LTO aircraft emissions utilizing an up-to-date modeling platform (WRF-SMOKE-CMAQv5x-AEDT) for three years' worth of AEDT LTO emission inventory data: 2005, 2011, and 2015.

Research Approach

Introduction

The current modeling platform we use to model the aviation-attributable $PM_{2.5}$ from NAS-wide LTO aircraft emissions has evolved over the past few years to accommodate the state-of-the-science models present at the time. For instance, 2005



LTO aircraft emissions were modeled a few years back using CMAQv5.0.1 with CB05 chemical mechanism, 2011 has been modeled using CMAQv5.1 with CB05 chemical mechanism, and 2015 has been modeled using CMAQv5.2.1 with CB6 chemical mechanism. Each iteration of the CMAQ model has updated chemistry and physical mechanisms to reflect the current understanding of the field. These model differences yield slight differences in concentration outputs and it is necessary to examine the model version effects on the results.

There are also differences with regard to the modeling domain. For the 2005 simulation, we used a coarser grid cell resolution spanning the continental U.S. of 36km. For the 2011 and 2015 simulations, we used a finer grid cell resolution of 12km. In prior work under PARTNER and ASCENT, Arunachalam et al. (2011) and Woody et al. (2013) investigated secondary organic aerosols contributions from Atlanta airport (ATL) using CMAQ with three different resolutions (4, 12, and 36km). They concluded that different resolutions lead to different behaviors of organic chemistry related to aerosol formation.

Finally, there are slight differences in the way the AEDT inventories were constructed for each year. The 2005 AEDT LTO inventory was created with an older version of AEDT (AEDT 2a); while 2011 and 2015 were constructed with a newer version (AEDT 2d).

Methodology

Meteorology data (from the Modern Era Retrospective Analysis for Research and Applications (MERRA) downscaled with WRF v3.8.1):

The initial and boundary condition data for the main meteorology variables (except soil moisture and temperature, sea-surface temperature (SST) and snow height and snow-water equivalent) have been taken from NASA's MERRA data (Reienecker et al., 2011) which has 0.5 x 0.67 degree horizontal resolution with 72 vertical layers from surface to 0.01 hPa. The MERRA was chosen because it is a high resolution 3rd generation reanalysis dataset that includes high vertical and spatial resolution with 6-hourly data for entire globe which can be used in beyond CONUS domain such as northern hemispheric domain. MERRA does not provide soil data required for Weather Research Forecast (WRF) model (Skamarock et al., 2008) simulation. Soil moisture and temperature data for initial and boundary conditions were taken from National Centers for Environmental Prediction (NCEP) FNL (Final) Operational Global Analysis dataset which has 1x1 degree horizontal resolution with 6 hourly data. The sea-surface temperature data for WRF have been taken from the NCEP Environmental Modeling Center (EMC) real-time global SST dataset which has 0.5 x 0.5 degree resolution (Thiébaux et al., 2003). The snow height and snow water equivalent data have been taken from North American Mesoscale (NAM) model analyses datasets that were developed by the NCEP and obtained from the National Center for Environmental Information (NCEI) formerly known as National Climatic Data Center (NCDC). The model configurations for meteorology has been described in Table1.1. The 2011 and 2015 annual simulations were performed using 3 months spin-up time.

Background Emission data (from the National Emissions Inventories [NEI] 2011/2015 processed through SMOKE v3.7/v4.5):

We applied the Sparse Matrix Operator Kernel Emissions (SMOKE) v3.7/v4.5 to estimate background emissions. We processed 19 emission sectors within 3 emission categories, including point, on-road, and area emissions to generate 2011 and 2015 background emissions for the Continental United States (CONUS) 12km x 12km data. Biogenic emissions and wind-blown dust are not generated using SMOKE. They are calculated in CMAQ using inline modules.

Aircraft Emission data (from the FAA's Aviation Environmental Design Tool (AEDT) processed through AEDTProc v1)

AEDTProc was used to process segmented aircraft emissions from the FAA's Aviation Environmental Design Tool (AEDT). AEDTProc has been used extensively in prior ASCENT work by UNC for the production of regional scale modeling emission inputs like those needed for CMAQ. Table 1.1 shows the annual LTO aircraft emissions for the three AEDT inventory years used in the current platform, and the % values indicate the contribution of aircraft emissions to total emissions from all sources.



Table 1.1 – Annual LTO aircraft emission inventory from the current platform (kilometric tons yr^{-1}) † Current platform values reported as NO + NO_2; ‡ TOG pertains to only compounds that are directly emitted from aircraft (i.e. does not include species like isoprene)

Species	2005 % of total emissions Total Emissions	2011 % change from 2005 % of total emissions Total Emissions	2015 % change from 2005 % of total emissions Total Emissions
$NO_X^{\dagger}$	83.6 1.1% 7600	70.1 -16% 1.3% 5392	82.8 -1% 1.6% 5175
SO_2	7.4 0.04% 18500	6.0 -19% 0.07% 8571	6.8 -8% 0.12% 5667
PEC	0.28 0.04% 700	0.18 -36% 0.03% 600	0.20 -29% 0.03% 667
TOG‡	14.3 0.03% 47667	10.1 -29% 0.06% 16833	13.5 -6% 0.05% 27000

For a better understanding of what is happening at the airport level, we selected 10 relatively large airports that represent some of the more unique geographic areas of the country to analyze. The list of airports include: Atlanta Hartsfield-Jackson (ATL), Boston Logan (BOS), Charlotte Douglas (CLT), Denver (DEN), Dallas Fort Worth (DFW), John F. Kennedy (JFK), Los Angeles (LAX), Chicago O'Hare (ORD), Seattle-Tacoma (SEA), and San Francisco (SFO). Figure 1.1 shows the LTO gas-phase (top row) and primary PM (bottom row) emissions in the airport-containing grid cells. Airport-specific trends over the three years follow NAS-wide trends (Table 1.1), in that 2005 LTO emissions were higher than the proceeding years. Figure 1.2 shows the LTO emissions in the airport-containing grid cell as a percentage of the total emissions in that grid cell. The large increase from 2005 to 2011/2015 is due to the finer grid cell resolution (12km in 2011/2015 versus 36km in 2005).

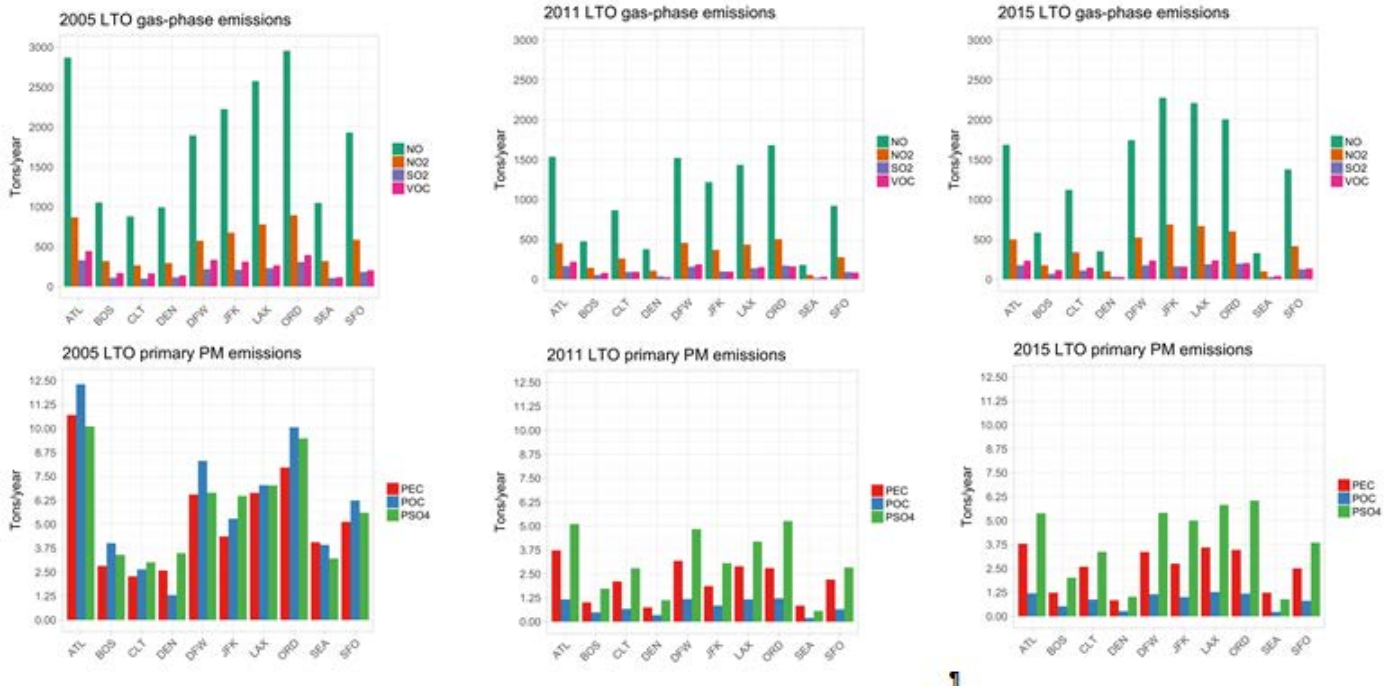


Figure 1.1. Airport specific LTO emissions at the airport-containing grid cell

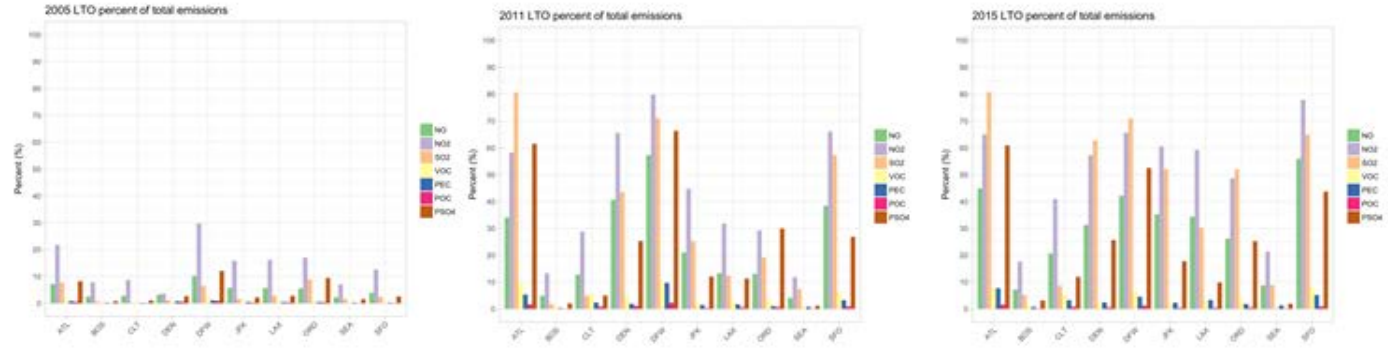


Figure 1.2. Percentage of airport-specific LTO emissions as compared to all emissions in airport-containing grid cell

Table 1.2 – CMAQ Model Configuration for Modeled Years

CMAQ Model Settings		Year		
Option	Description	2005	2011	2015
Model Version		5.0.1	5.1	5.2.1
Chemical Mechanism		cb05tump_ae6_aq	CB05e51_ae6_aq	cb6r3_ae6_aq
Domain		CONUS	CONUS	CONUS
Grid Resolution		36km	12km	12km
Boundary Conditions	Downscaled from the larger domain model runs	CAMChem	GEOS-chem	CMAQ-Hemispheric
CTM_WB_DUST	Use inline wind-blown dust estimations		Y(v5.2)	Y
CTM_LTNG_NO_x	Turn on hourly lightning NO_x	Y	Hourly	N
CTM_BIOGEMIS	Calculate inline biogenic emissions		Y	Y

The base CMAQ scenario discussed below includes non-aircraft emissions and the sensitivity scenario includes non-aircraft and aircraft emissions. Aircraft-attributable ambient $PM_{2.5}$ concentrations were calculated by subtracting sensitivity scenario model output from base scenario model output.

Results

Air Quality Results

Figure 1.3 shows the annual aviation-attributable $PM_{2.5}$ domain-wide for 2005, 2011, and 2015. The annual average was 0.0023, 0.0026, and 0.0027 μg/m^3 making up 0.03%, 0.05%, and 0.04% of total $PM_{2.5}$ for 2005, 2011, and 2015, respectively. Spatial analyses indicate an overall reduction in LTO emission impact in the Midwest but an increased impact in the Southeast and central valley of California over the three years. Figure 1.4 shows the aviation-attributable $PM_{2.5}$ at the airport-containing grid cell for a select few large airports. Airport level results vary across the years and are indicative of the differences in models used for each year.

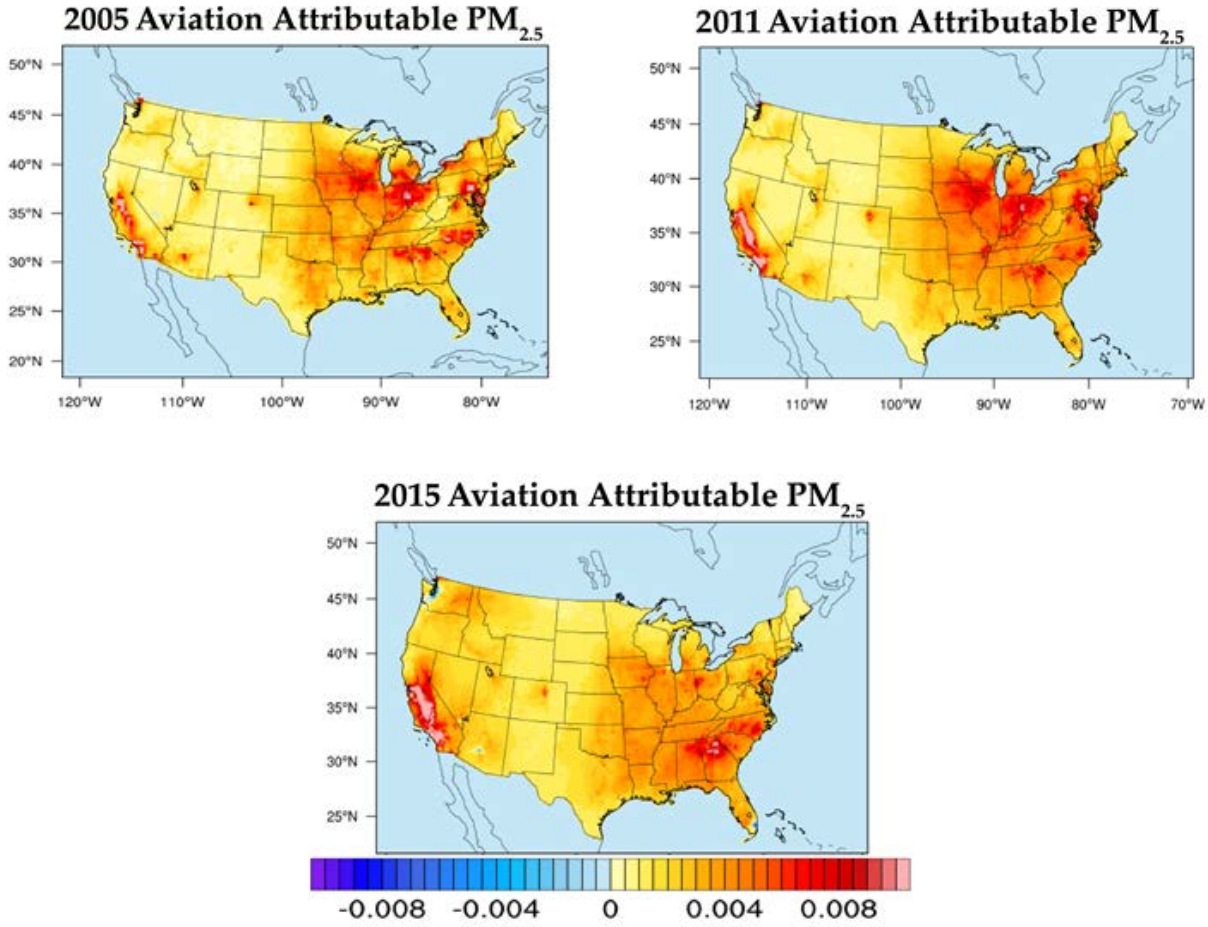


Figure 1.3. Domain-wide aviation attributable $PM_{2.5}$ for the years 2005, 2011, and 2015

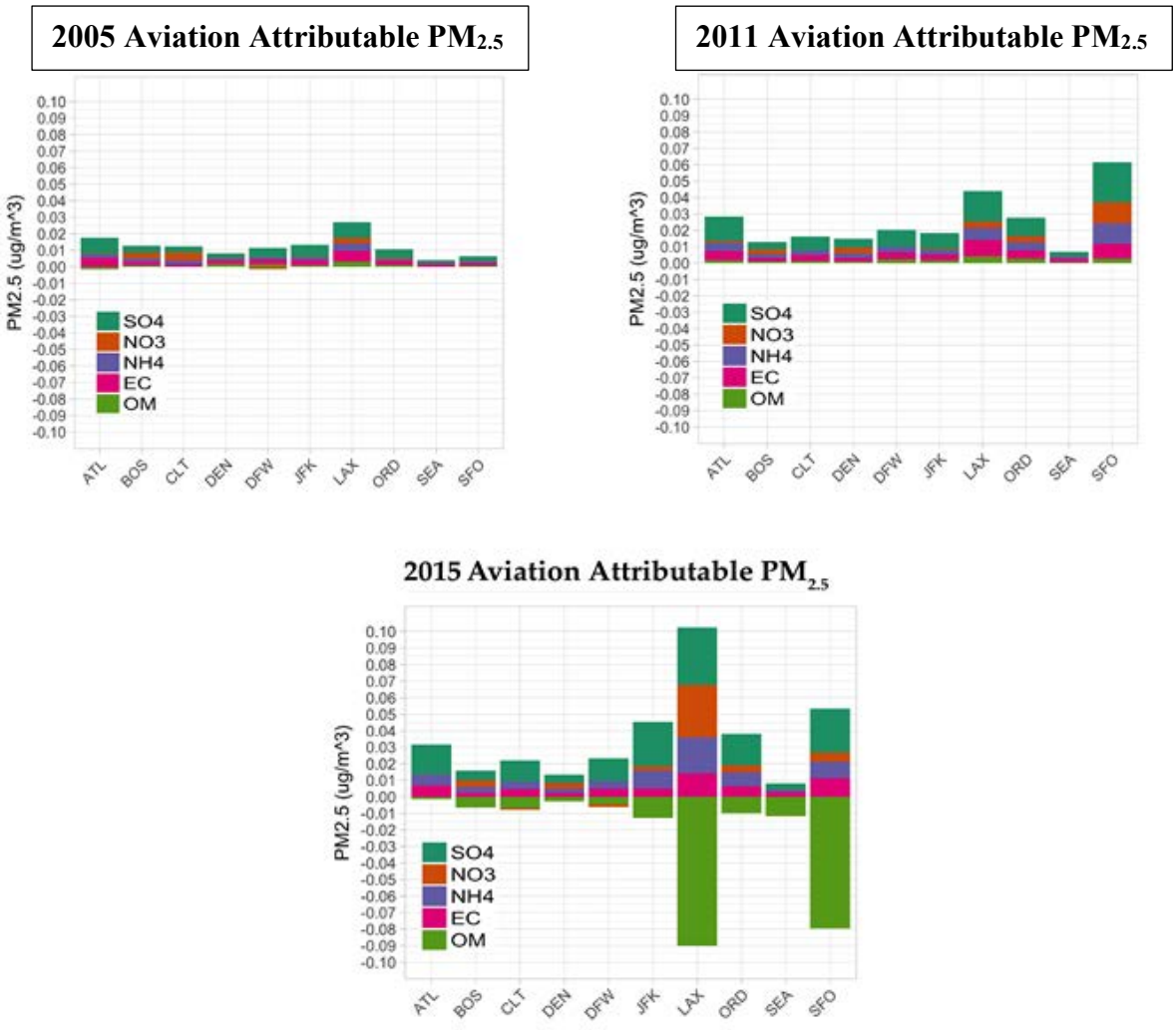


Figure 1.4. Airport-specific aviation attributable $PM_{2.5}$ for the years 2005, 2011, and 2015

We see differences at the airport-containing grid cell level between the 2005 and 2011 simulations due to the grid cell resolution effects as discussed in Woody et al. 2013 as well as the model updates from CMAQv5.0.1 to CMAQv5.1. Although the same gas-phase chemical mechanism was used in the 2005 and 2011 simulations, the updates to the treatment of aerosols in CMAQv5.1 will contribute to some of the differences seen between the two years. Along those same lines, the differences in aerosol concentrations at the airport grid cells are even larger when looking at the years 2011 and 2015. Although we have the same grid cell resolution for these two years, the large differences seen at the airport-grid cells are almost entirely due to the change in gas-phase chemical mechanism (CB05 to CB6) and a drastic shift in the way primary organic aerosols are treated in CMAQv5.2.1 versus CMAQv5.1. In CMAQv5.2.1, primary organic aerosols are speciated into semi-volatile organic gases that are then able to partition into the aerosol phase if the conditions to do so are met. In CMAQv5.1 (and all prior versions), primary organic aerosols remain in the particle phase and positively contribute to ambient $PM_{2.5}$ concentrations. We can see that for the 2015 case in which CMAQv5.2.1 was used, at the airport-containing grid cell there is a large disbenefit (reduction) in ambient $PM_{2.5}$ from the organic aerosols. This is because the directly emitted organic aerosols from aircraft in the immediate vicinity of the airport are no longer positively contributing to the organic aerosol budget since they are treated as semi-volatile and may not partition into the aerosol phase. Figure 1.5 shows the aviation-attributable primary organic aerosols for 2011 and 2015 simulations. The blue regions immediately surrounding the airport locations across the U.S. in the 2011 case indicate aircraft emissions positively contributing to the ambient $PM_{2.5}$ concentrations in the form of primary organic carbon; while the red regions surrounding the same locations in the 2015 case indicate that the semi-volatile primary organic gases are not partitioning

into the aerosol phase, thus negatively contributing to the ambient $PM_{2.5}$ concentrations. We can attribute this lack of partitioning into the aerosol phase to the aircrafts' NO_x emissions which suppress the yield of organic aerosol formed from anthropogenic aromatic hydrocarbons; and for the case of LAX, SFO, and SEA which reside in entirely different chemical regimes than airports on the east coast and southeast, this effect is exacerbated such that aircraft emissions from these airports greatly suppress the organic aerosol yield in the vicinity of the airport. Figure 1.6 shows the aircraft-attributable anthropogenic-VOC derived organic aerosol for the years 2011 and 2015. We see an even greater impact from aircraft NO_x emissions with regards to suppressed anthropogenic-VOC derived organic aerosol yield in the 2015 CMAQv5.2.1 case than the 2011 CMAQv5.1 case.

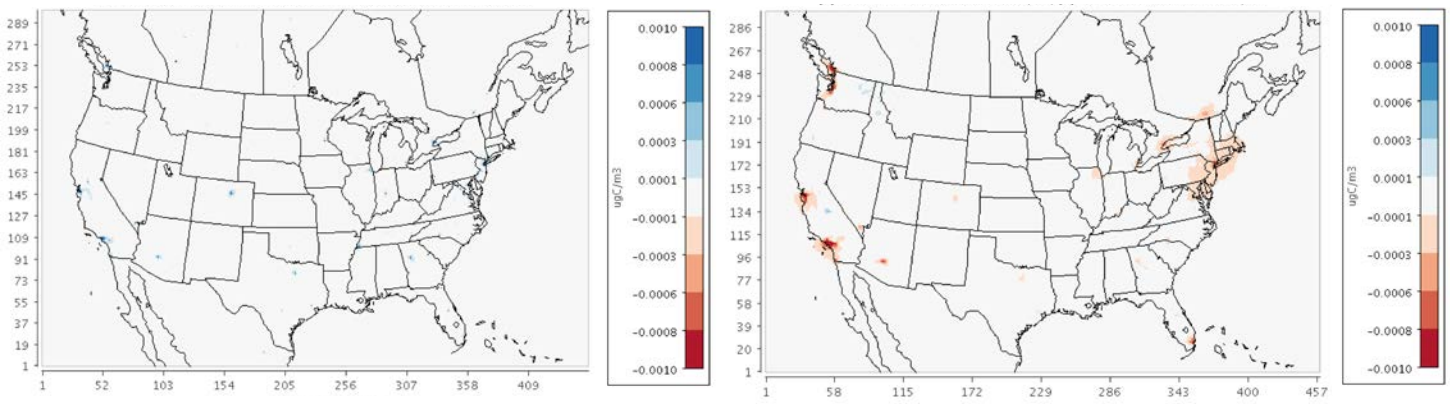


Figure 1.5. Aircraft-attributable primary organic aerosol for 2011 (left) and 2015 (right)

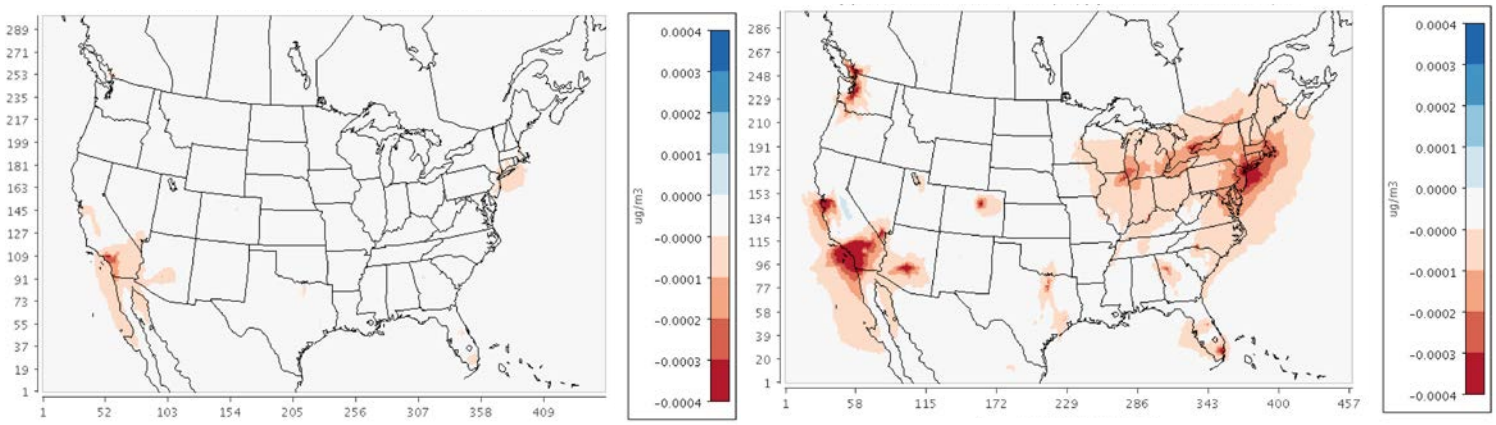


Figure 1.6. Aircraft-attributable anthropogenic-VOC derived organic aerosol for 2011 (left) and 2015 (right)

Figure 1.7 shows the aircraft-attributable O_3 for the years 2005, 2011, and 2015 and figure 1.8 shows the same at the airport-specific grid-cell. The impact of LTO aircraft emissions on O_3 is negatively correlated in the immediately vicinity of the airport due to the NO_X titration effect in a VOC-limited photochemical regime and positively correlated downwind of the airport due to a shift in photochemical regime outside of the urban area containing the airport. Over the three years, we see an overall increase in aircraft-attributable O_3 with the greatest amount of increase occurring in the central valley of California.

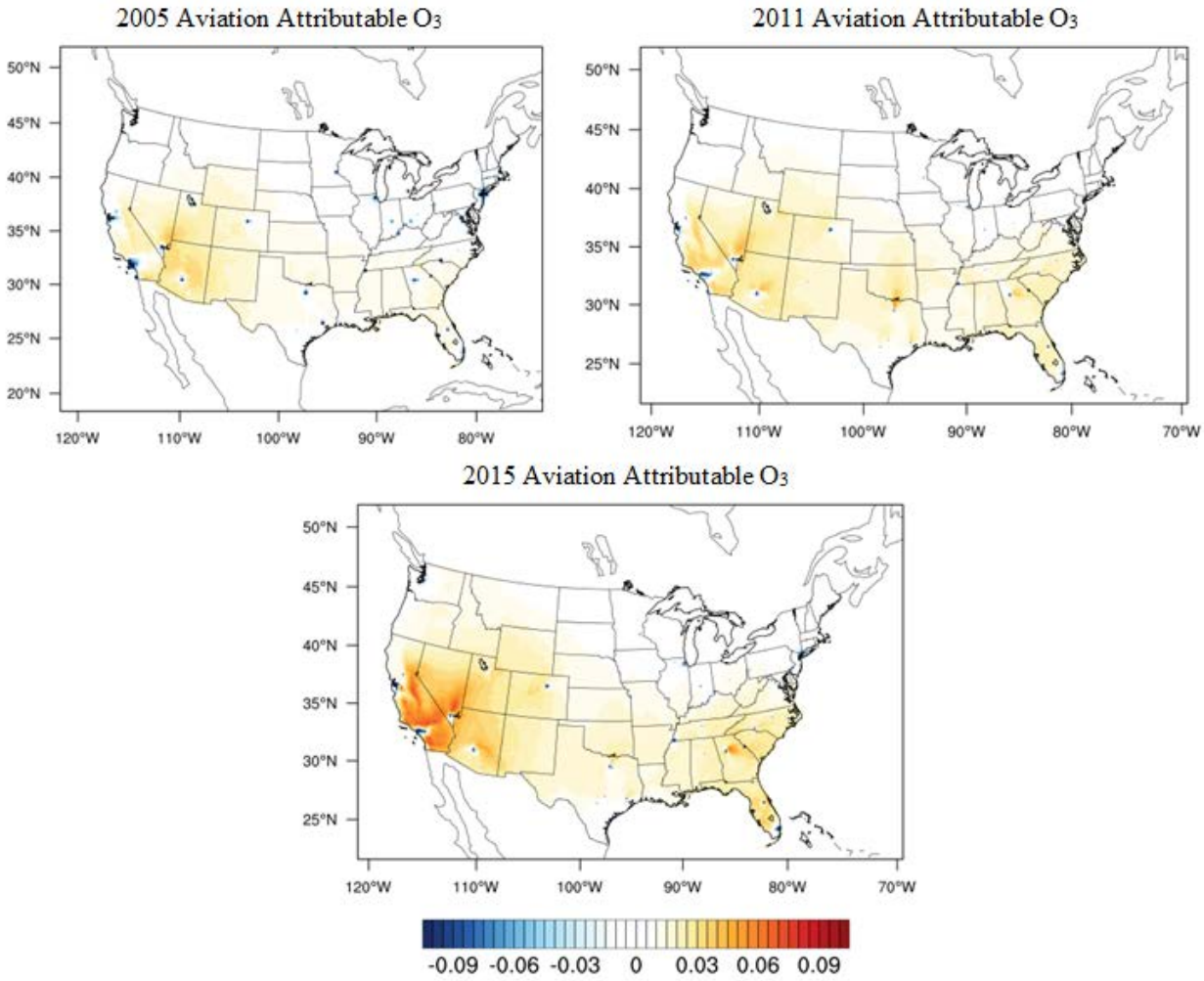


Figure 1.7. Domain-wide aviation attributable O_3 for the years 2005, 2011, and 2015

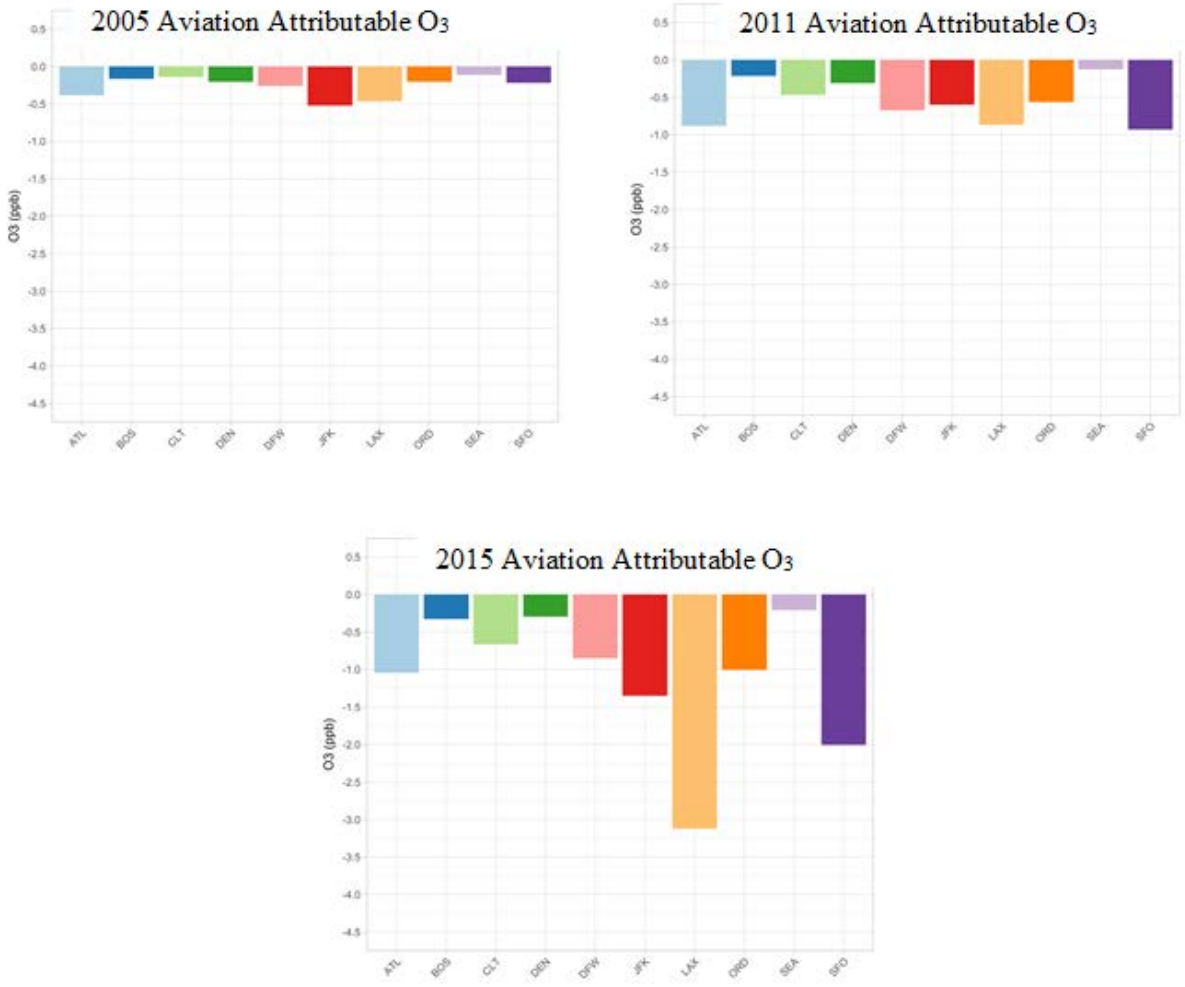


Figure 1.8. Airport-specific aviation attributable O_3 for the years 2005, 2011, and 2015

Milestone(s)

Completed simulating 2015 base and sensitivity scenarios with CMAQ for LTO aircraft emissions
Completed assessment of LTO aircraft-attributable impacts on O_3 and $PM_{2.5}$

Major Accomplishments

Quantified surface $PM_{2.5}$ and O_3 concentrations contributed by NAS-wide LTO emissions for 2005, 2011, and 2015.
Quantified health burden due to NAS-wide LTO emissions due to additional $PM_{2.5}$ formed.

Publications

Poster presentation at annual CMAS conference (October 2018)

Outreach Efforts

Presentation at semi-annual ASCENT stakeholder meetings in Spring and Fall 2018, Alexandria, VA.

Awards

None



Student Involvement

Calvin Arter, Ph.D. student, performed the CMAQ simulations for 2015 and the dynamic evaluation. Pradeepa Vennam, who graduated with her Ph.D. earlier performed the CMAQ simulations for 2005.

Plans for Next Period

Finalize analyses and develop manuscript.

References

Appel, K. W., Napelenok, S. L., Foley, K. M., Pye, H. O. T., Hogrefe, C., Luecken, D. J., Bash, J. O., Roselle, S. J., Pleim, J. E., Foroutan, H., Hutzell, W. T., Pouliot, G. A., Sarwar, G., Fahey, K. M., Gantt, B., Gilliam, R. C., Heath, N. K., Kang, D., Mathur, R., Schwede, D. B., Spero, T. L., Wong, D. C. and Young, J. O., 2017. Description and evaluation of the Community Multiscale Air Quality (CMAQ) modeling system version 5.1, Geoscientific Model Development, Volume 10, pp.1703-1732

Arunachalam, S., Wang, B., Davis, N., Baek, B.H., Levy, JI, (2011). Effect of Chemistry-Transport Model Scale and Resolution on Population Exposure to $PM_{2.5}$ from Aircraft Emissions during Landing and Takeoff, *Atmos. Environ.*, 45(19):3294-3300.

Huang, J., Vennam, L. P., Benjamin N. Murphy, B. N., Binkowski, F., and Arunachalam, S., in preparation. A Nation-wide Assessment of Particle Number Concentrations from Commercial Aircraft Emissions in the United States.

Iacono, M.J., Delamere, J.S., Mlawer, E. J., Shepherd, M.W., Clough, S.A., and Collins, W.D., 2008. Radiative forcing by long-lived greenhouse gases: Calculations with AER radiative transfer models. Journal of Geophysical Research, Volume 113, D13103.

Krewski, D., Jerrett, M., Burnett, R., Ma, R., Hughes, E., Shi, Y., Turner, C., Pope, C.A., Thurston, G., Calle, E.E., Thunt, M.J., 2009. Extended follow-up and spatial analysis of the American Cancer Society study linking particulate air pollution and mortality. HEI Research Report

Laden, F., Schwartz, F., Speizer, F., Dockery, D.W., 2006. Reduction in fine particulate air pollution and mortality: Extended follow-up of the Harvard Six Cities Study. American Journal of Respiratory and Critical Care Medicine, Volume 173, pp. 667-672

Levy, J., Woody, M., Baek, B.H., Shankar, U., Arunachalam, S., 2012. Current and Future Particulate-Matter-Related Mortalitiy Risks in the United States from Aviation Emissions During Landing and Takeoff. Risk Analysis, Volume 32, pp. 237-249

Ma, L-M, and Zhe-Min Tan, Z-M., 2009. Improving the behavior of the cumulus parameterization for tropical cyclone prediction: Convection trigger. Atmospheric Research, Volume 92, pp. 190–211.

Mitchell, K. E., and Coauthors, 2001: The Community Noah Land Surface Model (LSM)—user's guide (v2.2). [Available online at http://www.emc.ncep.noaa.gov/mmb/gcp/noahlsm/README_2.2.htm.]

Morrison, H., Thompson, G., and Tatarskii, V., 2009. Impact of Cloud Microphysics on the Development of Trailing Statiform Precipitation in a Simulated Squall Line: Comparison of One- and Two-Moment Schemes. Monthly Weather Review, Volume 137, pp. 991-1007.

Moore, T., 2014. Three-State Air Quality Modeling Study (3SAQS) -- Weather Research Forecast 2011 Meteorological Model Application/Evaluation, Report of Western Regional Air --Partnership c/o CIRA, Colorado State University 1375 Campus Delivery Fort Collins, CO 80523-1375.

National Land Cover Database 2011, http://www.mrlc.gov/nlcd2011.php

Pleim, J. E., 2007. A Combined Local and Nonlocal Closure Model for the Atmospheric Boundary Layer. Part I: Model Description and Testing. Journal of Applied Meteorology and Climatology, Volume 46, pp. 1383–1395.

Rienecker, M. M., Suarez, M. J., Gelaro, R., Todling, R., Bacmeister, J., Liu, E., Woollen, J., 2011. MERRA: NASA's modern-era retrospective analysis for research and applications. Journal of Climate, 24(14), 3624–3648. http://doi.org/10.1175/JCLI-D-11-00015.1.



Skamarock, W.C. and Klemp, J.B., 2008. A time-split nonhydrostatic atmospheric model for weather research and forecasting applications. Journal of Computation Physics, Volume 227, pp. 3465-3485.

Thiébaux, J., Rogers, E., Wang, W., and Katz, B., 2003: A New High-Resolution Blended Real-Time Global Sea Surface Temperature Analysis. Bull. Amer. Meteor. Soc., 84, 645–656, https://doi.org/10.1175/BAMS-84-5-645.

Woody, M.; Haeng, B.; Adelman, Z.; Omary, M.; Fat, Y.; West, J. J.; Arunachalam, S. 2011. An assessment of Aviation' s contribution to current and future fine particulate matter in the United States. Atmos. Environ. Volume 45, pp. 3424–3433.

Woody, M. C.; Arunachalam, S. 2013. Secondary organic aerosol produced from aircraft emissions at the Atlanta Airport: An advanced diagnostic investigation using process analysis. Atmos. Environ. Volume 79, pp. 101–109.

Task 2- Perform Airport-by-Airport Assessment Using CMAQ-DDM

University of North Carolina at Chapel Hill

Objective(s)

Using the modeling platform that we developed during the previous year, use CMAQ v5.1 enhanced with the Decoupled Direct Method in Three Dimensions (DDM-3D), an advanced sensitivity tool to expand from seasonal to annual simulations. We will focus on the use of 1st and 2nd order sensitivities, and further explore issues related to aircraft emissions and non-attainment of the U.S. National Ambient Air Quality Standards (NAAQS) at various locations in the U.S.

Research Approach

Introduction

Sensitivity analysis tools are often used within the air quality modeling framework to evaluate impacts due to changing input parameters in the model such as emission rates, initial conditions, or boundary conditions. These become important for utilizing models as a way to guide emission reduction policies. Sensitivity tools have been limited to finite difference and regression-based methods that often become computationally intractable and are often unable to describe *ad hoc* analyses. Furthermore, to calculate pollutant concentration sensitivities to LTO emissions we use the Decoupled Direct Method (DDM) in CMAQ. DDM methods calculate sensitivity coefficients in a single model run (Russell, 2005; Zhang et al., 2012) allowing for *ad hoc* analyses from changing multiple input parameters at a time. Most importantly, the use of DDM allows for the inline calculation of both first and higher order sensitivity coefficients, which become important for pollutant species that may not be linearly dependent on certain precursors. First order sensitivity calculations will yield information about the change in species concentrations with respect to varying one input parameter. In our case, these calculations will only describe linear changes of concentrations with respect to increasing or decreasing emissions from aircraft. However, some changes in species, such as secondary organic aerosols, do not linearly change with increasing or decreasing precursor emissions and higher order sensitivity coefficients can capture the non-linear change in species concentrations.

Methodology

Higher order DDM was implemented in CMAQ version 5.0.2. DDM becomes an ideal choice for describing aircraft (airport) emissions because the relatively small quantity of emissions emitted by each source can lead to numerical noise with other sensitivity methods that require multiple model runs for each varied parameter (Napelenok, Cohan, Hu, & Russell, 2006).

CMAQ-DDM simulations instrumented to compute first and second order sensitivities were performed for ten airports for the months of January and July, 2005. Of these 10 airports, we chose five [Hartsfield-Jackson Atlanta (ATL), Charlotte Douglas (CLT), John F. Kennedy (JFK), and Los Angeles (LAX) and Chicago O'Hare (ORD)] that are in current non-attainment areas for O_3 and/or $PM_{2.5}$, and five [Boston Logan (BOS), Kansas City (MCI), Raleigh Durham (RDU), Seattle-Tacoma (SEA), and Tucson (TUS)] that are in current attainment areas. Ten day spin-up simulations were performed prior to the start of each month (December and June, respectively). Six precursor species groups (NO_x, SO_2, VOCs, PSO_4, PEC and POC) were designated as sensitivity input parameters. First and second order sensitivities of O_3 and $PM_{2.5}$ to the emissions of these six precursors were calculated. First order sensitivities were of the form:



$$S^{1}_{i,j} = \frac{\partial C_i}{\partial E_j}$$

Eq. 2.1

While second order sensitivities were consisting of two forms:

$$S^{2}_{i,j} = \frac{\partial^2 C_i}{\partial {E_j}^2}$$

Eq. 2.2

$$S^{2}_{i,j,k} = \frac{\partial^2 C_i}{\partial E_j \partial E_k}$$

Eq. 2.3

Eq. 2.2 represents second order sensitivities to one emission species, while Eq. 2.3 represents second order cross sensitivities to two emission species (e.g., NOx and SO2).

Flight segment data from AEDT (Roof & Fleming, 2007; Wilkerson et al., 2010) were processed into gridded emission rate files using AEDTProc (Baek, B.H., Arunachalam, S., Woody, M., Vennam, L.P., Omary, M., Binkowski, F., Fleming, 2012). Landing and takeoff operations were considered by capping full-flight aircraft emissions at 3,000 feet. Our domain covered the continental United States with 36 x 36 km horizontal grid resolution and thirty-four time-varying pressure based vertical layers (LTO constrained to the first 17 layers around 3,000 feet or 914 meters). Sensitivities were calculated in the first model layer alone, to reflect where people live and are exposed to air pollution.

Other background anthropogenic emission sources were obtained from EPA's National Emissions Inventories (NEI-2005) and 2005 boundary conditions were derived from global CAM-Chem simulations (Lamarque et al., 2012). Meteorology conditions for 2005 were obtained from the Weather Research and Forecasting model (WRF) (Skamarock et al., 2008) with outputs downscaled from NASA's Modern-Era Retrospective Analysis for Research and Applications data (MERRA) (Rienecker et al., 2011).

Results

The O_3-precursor system is made up of tropospheric O_3 concentrations and the availability of NO_x and VOCs. Tropospheric O_3 is formed through the reactions of NO_x and VOCs with the OH radical. And since NO_x and VOCs compete for available OH in the atmosphere, the O_3 formation pathways can vary based on the emissions of VOCs or NO_x in a region. Regions with high NO_x emissions leading to O_3 formation are deemed NO_x -inhibited (VOC-limited) and are often highly localized to urban regions. Regions where available VOCs are comparable to available NO_x are deemed NO_x-limited and tend to categorize most suburban to rural areas. Due to the nonlinearity of O_3 production pathways, emission control strategies for reducing O_3 differ based on which chemical regime one may be in. Chemical regimes will be indicated by how O_3 either increases or decreases with respect to increasing or decreasing NO_x and VOC emissions. Figure 2.1 shows the first order sensitivities of O_3 to NO_x and VOC at LAX, for a zoomed-in portion of the entire modeling domain.

The negative first order sensitivity seen in Los Angeles county containing LAX indicates a NO_x -inhibited (VOC-limited) chemical regime. A clear boundary of negative NO_x first order sensitivities to positive first order sensitivities can be seen (indicated by the shift from blue to orange) which signifies the shift from a NO_x -inhibited (VOC-limited) to a NO_x-limited regime. Near the airport, VOC emission controls will govern the O_3 concentration response; and downwind of the airport, approximately 150 km, we see a shift to positive first order NO_x sensitivities indicating where NO_x emission controls will govern the O_3 concentration response. First order VOC sensitivities at the airport are positive across the domain and larger in the NO_x -inhibited (VOC-limited) regime. Our LAX findings indicating tropospheric O_3 NO_x -inhibited (VOC-limited) regimes near the airport fall in line with other studies on chemical regimes for major U.S. cities -inhibited (VOC-limited) chemical regime.

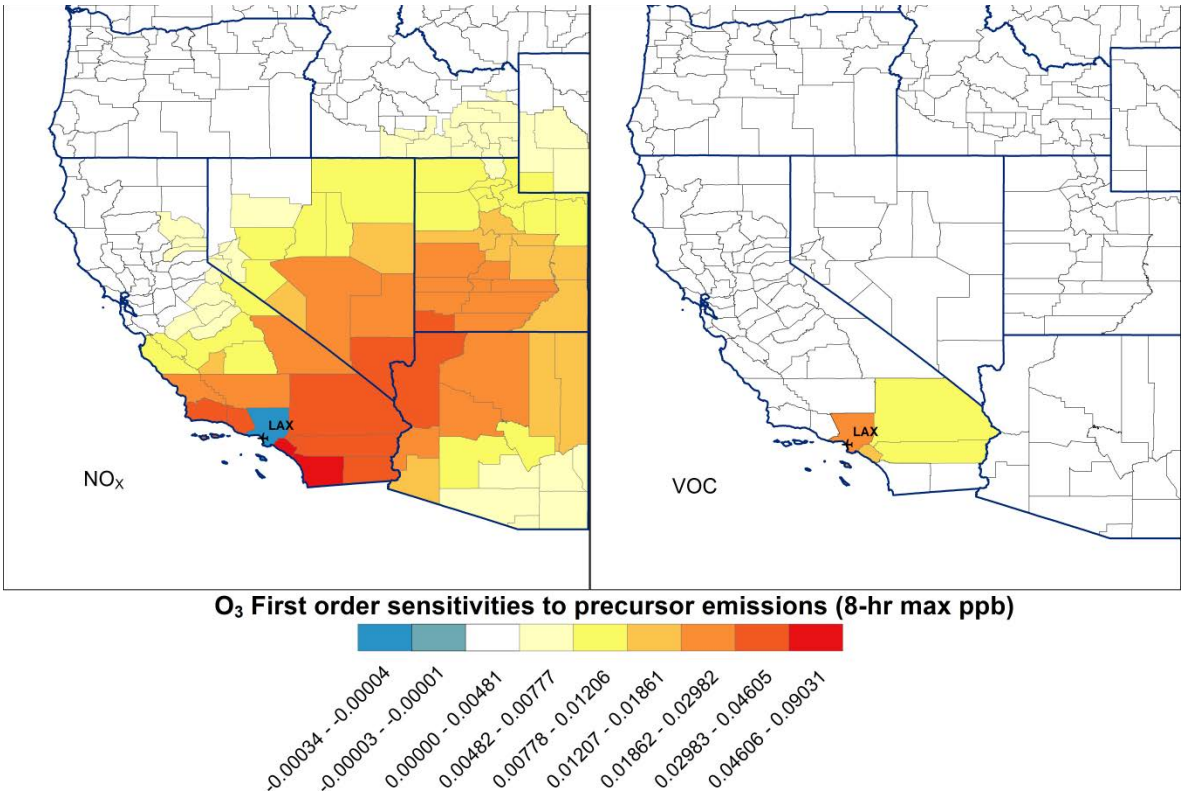


Figure 2.1. O_3 first order sensitivity coefficients with respect to LTO NO_x emissions (left) and VOC emissions (right) at LAX

Figure 2.2 shows the second order sensitivities of O_3 to LTO aircraft emissions of NO_x and VOC at LAX. While first order sensitivities tell us how changes in LTO emissions will linearly increase or decrease O_3 concentrations, non-zero second order sensitivities indicate that the concentration response to changes in LTO emissions is nonlinear. Matching signs (positive first order and positive second order for e.g.) indicate a convex concentration response while unmatched signs indicate a concave concentration response. Tropospheric O_3 production is a nonlinear system with formation being governed by the chemical regime and subsequent availability of NO_x and VOCs. This makes second order sensitivities critical in understanding how certain emission sectors will impact O_3 formation and constructing emission control strategies.

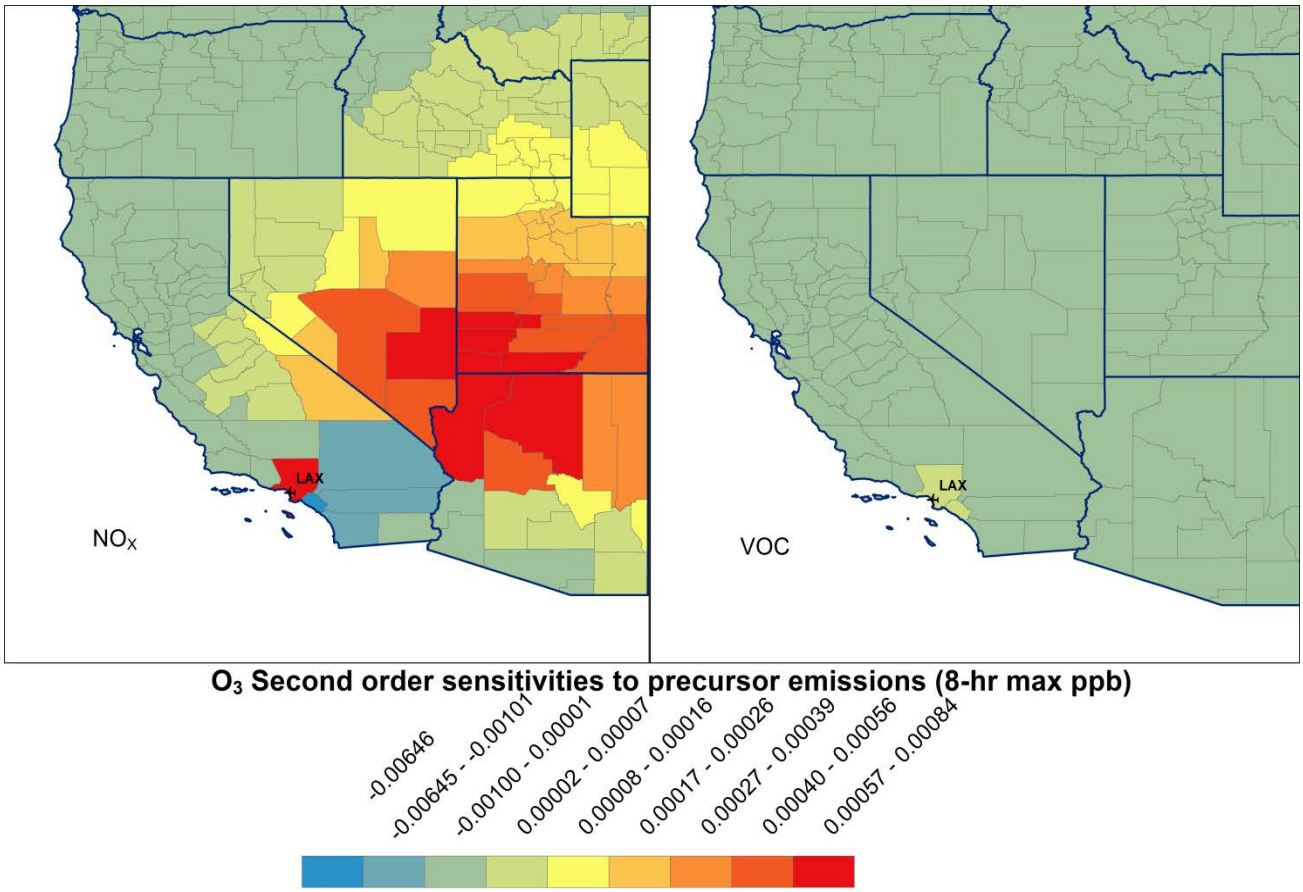


Figure 2.2. O_3 second order sensitivity coefficients with respect to LTO NO_x emissions (left) and VOC emissions (right) at LAX

We can see that NO_x emissions are responsible for most of the nonlinearity with defined regions of positive and negative second order sensitivity coefficients. At LAX, we see that positive second order sensitivities are present in the NO_x – inhibited (VOC-limited) regime indicating a negative concave O_3 concentration response as we would expect from a typical ozone isopleth describing a highly polluted urban area.



Figure 2.3 shows the first, second, and second order cross sensitivities calculated in the model grid cell containing each of our ten airports for O_3. While we lose some of the impacts of chemical processes leading to secondary products downwind of the airport, we are able to see how the magnitudes of different sensitivities change with respect to aircraft emissions at the grid-cell containing the airport. It is clear that for all airports, both first and second order sensitivities are heavily impacted by LTO NO_x emissions rather than VOC emissions. This is especially true for second order sensitivities with respect to NO_x indicating nonlinear effects (in this case concave response curves due to the positive second order sensitivities) from NO_x emissions will greatly outweigh nonlinear effects from VOC emissions. It should be noted however that the second order sensitivities are still approximately an order of magnitude smaller than first order sensitivities. Second order cross sensitivities indicate the interaction among precursors and can indicate how emission control strategy results may differ simply summing the results from reducing individual emission precursors. While second order cross sensitivities are smaller than second order sensitivities, not including the interaction term could result in an under prediction (in the case of positive second order cross sensitivities) or an over prediction (in the case of negative second order cross sensitivities) when assessing the contribution of each precursor independently to O_3 formed. In the case of O_3 first order sensitivities, O_3 sensitivities to NO_x are positive at RDU, TUS, ATL, and CLT while they are negative for the remaining airports. Table 2.1 below presents the actual sensitivity values, corresponding to the bar charts in Figure 2.3.

Table 2.1. O_3 first, second, and second order cross sensitivity coefficients disaggregated by precursor species at grid cell containing airport.

	O_3 Sensitivities (ppb)				
	First Order		Second Order		Second Order Cross
	NO_X	VOC	NO_X	VOC	$NO_X \times$ VOC
ATL	5.165×10^{-2}	3.114×10^{-2}	8.669×10^{-2}	5.012×10^{-5}	1.395×10^{-3}
BOS	-4.606×10^{-2}	8.981×10^{-3}	1.134×10^{-3}	5.549×10^{-6}	4.297×10^{-4}
CLT	3.185×10^{-2}	1.590×10^{-2}	1.122×10^{-3}	4.754×10^{-6}	8.740×10^{-5}
JFK	-2.157×10^{-1}	1.276×10^{-1}	9.968×10^{-2}	3.750×10^{-4}	-1.212×10^{-4}
LAX	-4.053×10^{-1}	4.165×10^{-2}	4.789×10^{-2}	3.206×10^{-4}	5.810×10^{-5}
MCI	-1.572×10^{-2}	5.469×10^{-3}	6.429×10^{-4}	2.704×10^{-6}	1.650×10^{-5}
ORD	-1.687×10^{-1}	2.164×10^{-2}	1.144×10^{-2}	1.725×10^{-5}	2.110×10^{-4}
RDU	2.484×10^{-2}	4.687×10^{-3}	3.743×10^{-4}	8.422×10^{-7}	3.920×10^{-5}
SEA	-1.015×10^{-1}	5.414×10^{-3}	1.748×10^{-3}	2.252×10^{-6}	3.290×10^{-5}
TUS	1.311×10^{-2}	1.237×10^{-3}	1.616×10^{-5}	1.021×10^{-7}	4.250×10^{-6}

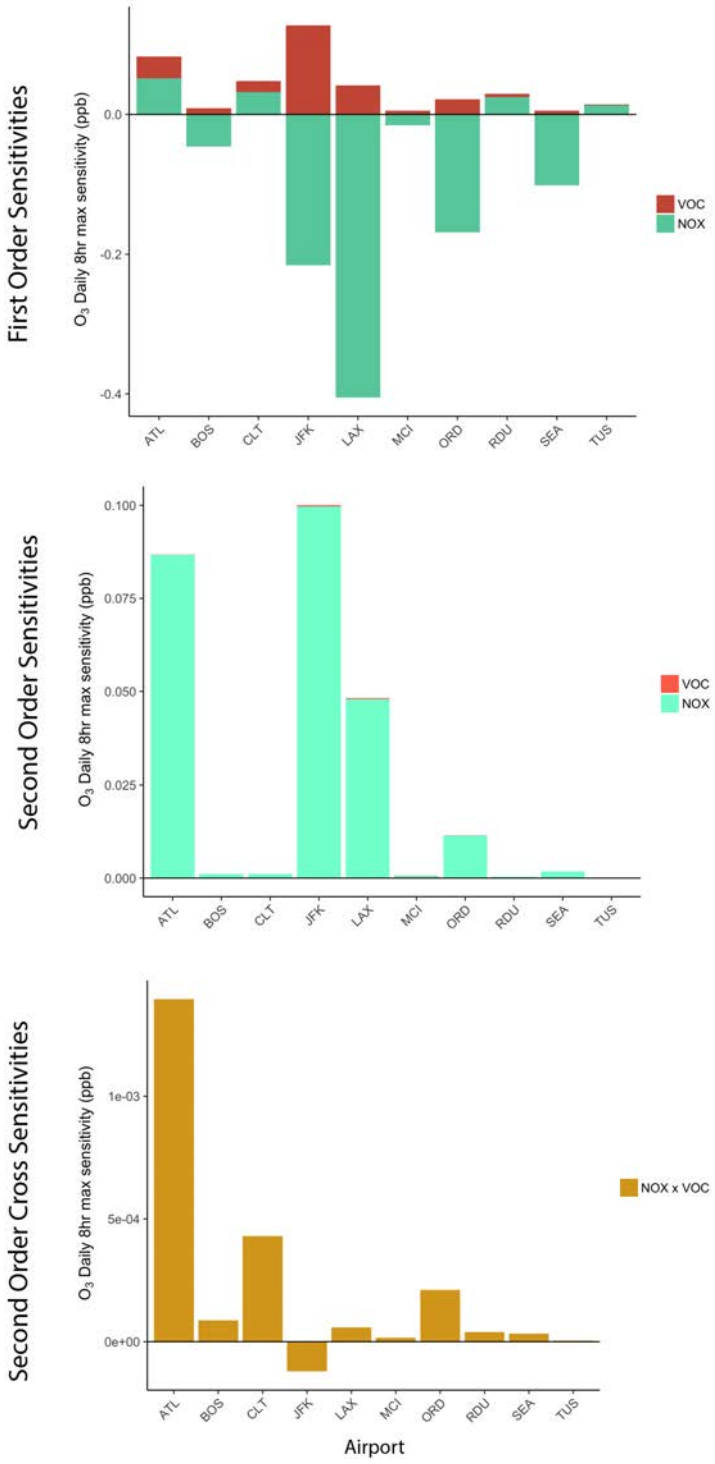


Figure 2.3. O_3 first, second, and second order cross sensitivity coefficients disaggregated by precursor species at grid cell containing airport



Figure 2.4 shows the first order sensitivities of $PM_{2.5}$ to LTO emissions of NO_x, VOC, SO_2, POC, PEC, and PSO_4 at ORD. Values shown are the monthly averages of the 24-hour averages of each day of the simulation. The impact of the particle-phase precursors is highly localized to the airport for both summer and winter months while the impact of the gas-phase precursors extends further downwind of the airport, and in the case of NO_x emissions, we can see a reduction in $PM_{2.5}$. $PM_{2.5}$ formation near the airport due to the particle-phase precursor emissions can be considered primary while the formation downwind can be considered secondary.

Seasonal differences are indicative of the meteorological and chemical regime differences that affect PM formation. Secondary $PM_{2.5}$ formation is highly dependent on available gas-phase precursors and meteorological conditions. Not only will NO_x-/VOC-limited regimes become important for determining the formation of secondarily formed $PM_{2.5}$, but also the availability of background (not directly emitted from aircraft) ammonia emissions (NH_3). Studies have characterized the importance of NH_3-rich versus NH_3-poor regimes on the formation of secondarily formed PM and one study in particular has looked at how important NH_3 is in the context of secondarily formed $PM_{2.5}$ from aircraft emissions (Woody et al. 2011).

Figure 2.5 shows the second order sensitivities of $PM_{2.5}$ to LTO aircraft emissions of NO_x, VOC, SO_2, POC, PEC, and PSO_4 at ORD. Like what we saw with O_3 sensitivities, NO_x emissions are almost entirely responsible for any nonlinearity in the $PM_{2.5}$-precursor system with positive and negative second order sensitivity coefficients. Second order NO_x in January near ORD seem to show a convex $PM_{2.5}$ response curve to negative first order NO_x sensitivities near the airport where free NH_3 competition occurs and a concave $PM_{2.5}$ response curve to positive first order NO_x sensitivities further west where free NH_3 is abundant. The same can be seen in July near ORD for the highly localized negative first order NO_x sensitivities near the airport and the large hot spot of free NH_3 directly west of ORD where we have the only contribution of NO_x emissions to aerosol nitrate formation in July.

In the case of $PM_{2.5}$ sensitivities at the airport grid cells, first order sensitivities to all precursors are positive except for NO_x emissions. We attribute this disbenefit (reduction) to either competition with SO_2 emissions near the airport for available free NH_3 to form secondary inorganic aerosols or LTO NO_x emissions' impacts on scavenging available SOA precursors. Second order sensitivities vary greatly depending on season, with second order impacts in July being much higher than January. Like we previously saw with O_3, second order sensitivities to NO_x emissions greatly outweigh second order sensitivities to all other precursors. NO_x emissions also play the greatest impact with regards to second order cross sensitivities. Second order cross sensitivities between NO_x and VOCs, and NO_x and SO_2 emissions indicate the most interaction between these precursor species and by not including these terms in a potential emission-control strategy, $PM_{2.5}$ reduction would be over predicted when only considering the reduction of independent precursors.

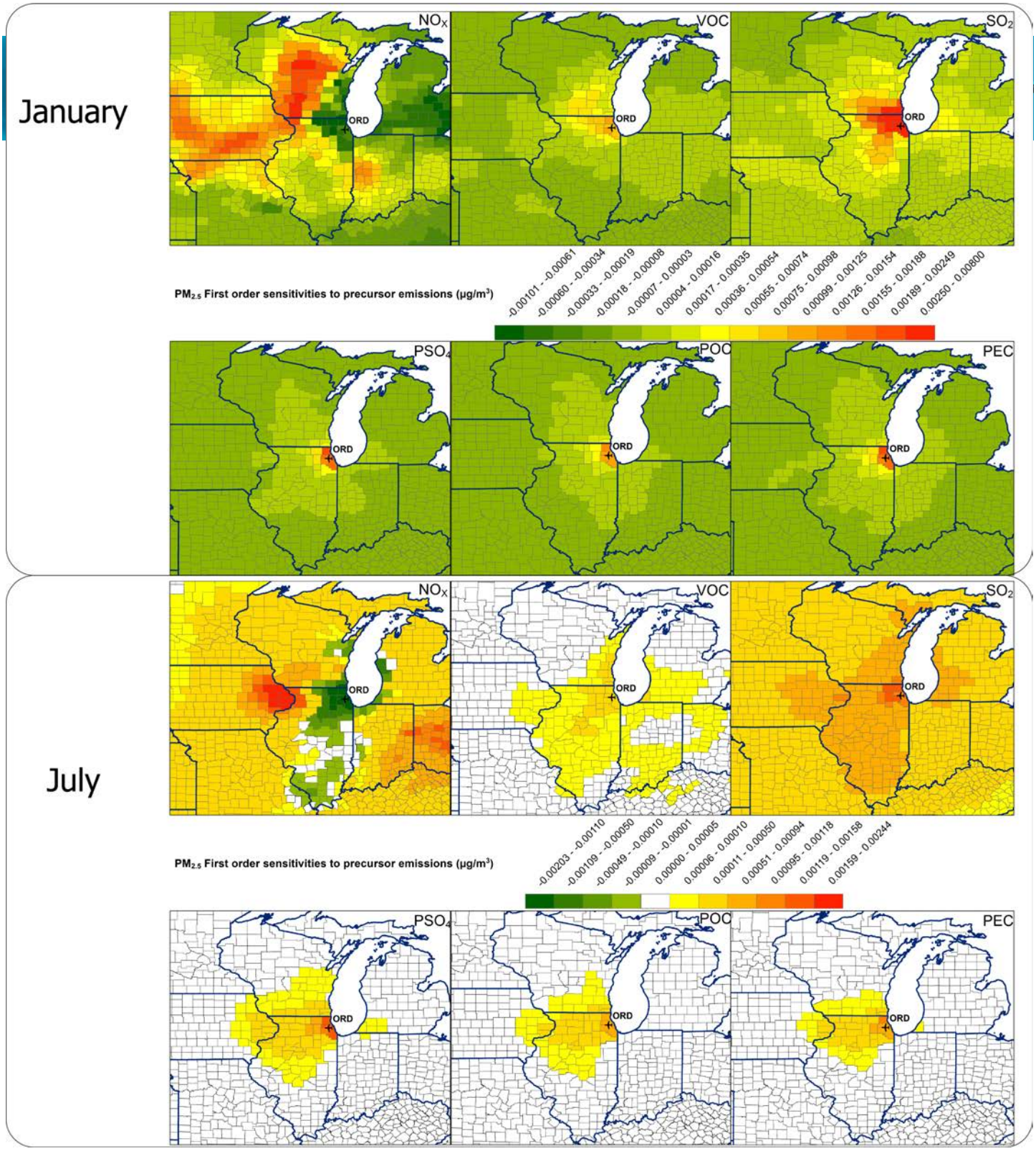


Figure 2.4. $PM_{2.5}$ first order sensitivity coefficients with respect to LTO gas-phase precursor emissions and particle-phase precursor emissions for the months of January (top) and July (bottom) at ORD

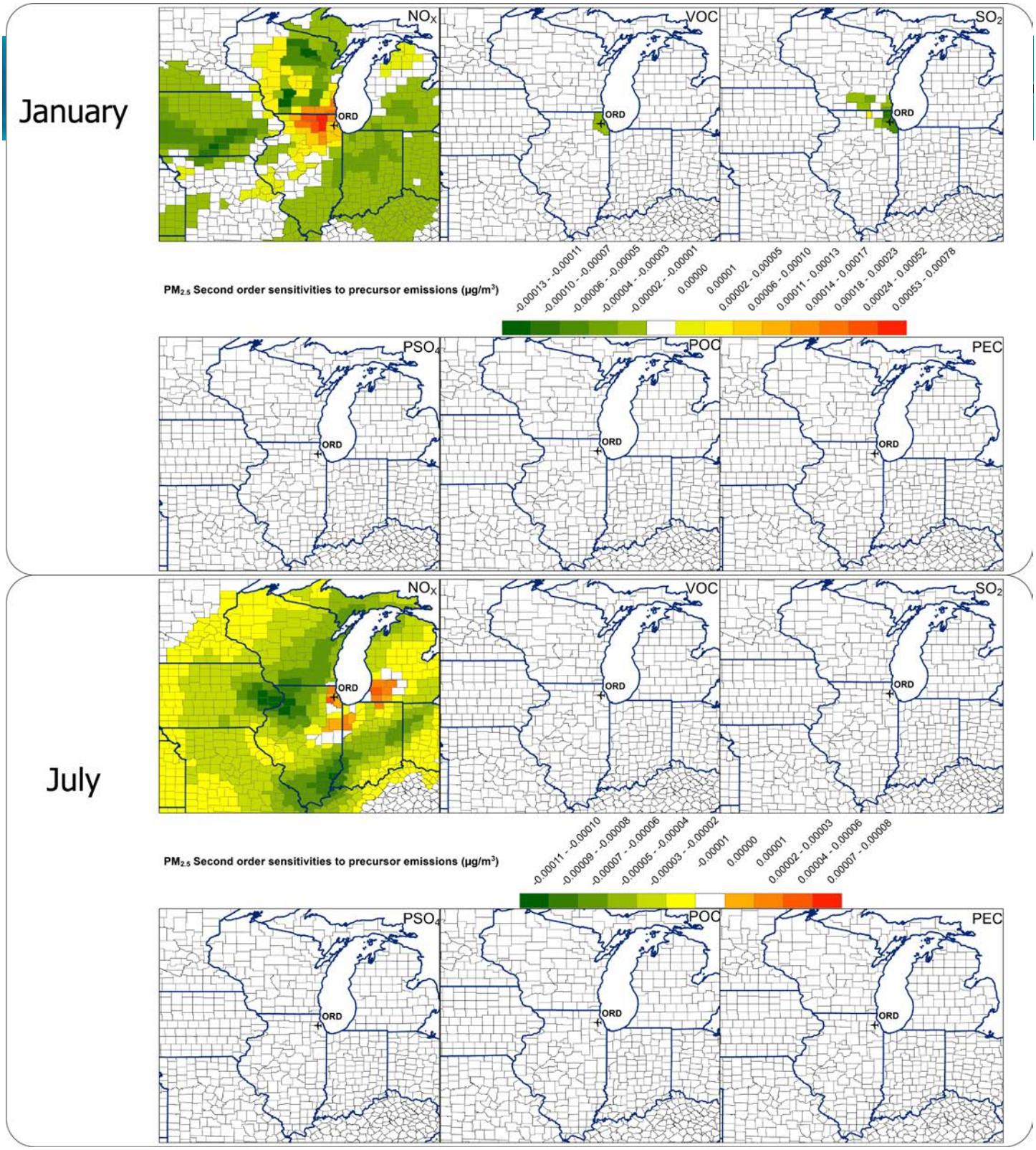


Figure 2.5. $PM_{2.5}$ second order sensitivity coefficients with respect to LTO gas-phase precursor emissions and particle-phase precursor emissions for the months of January (top) and July (bottom) at ORD

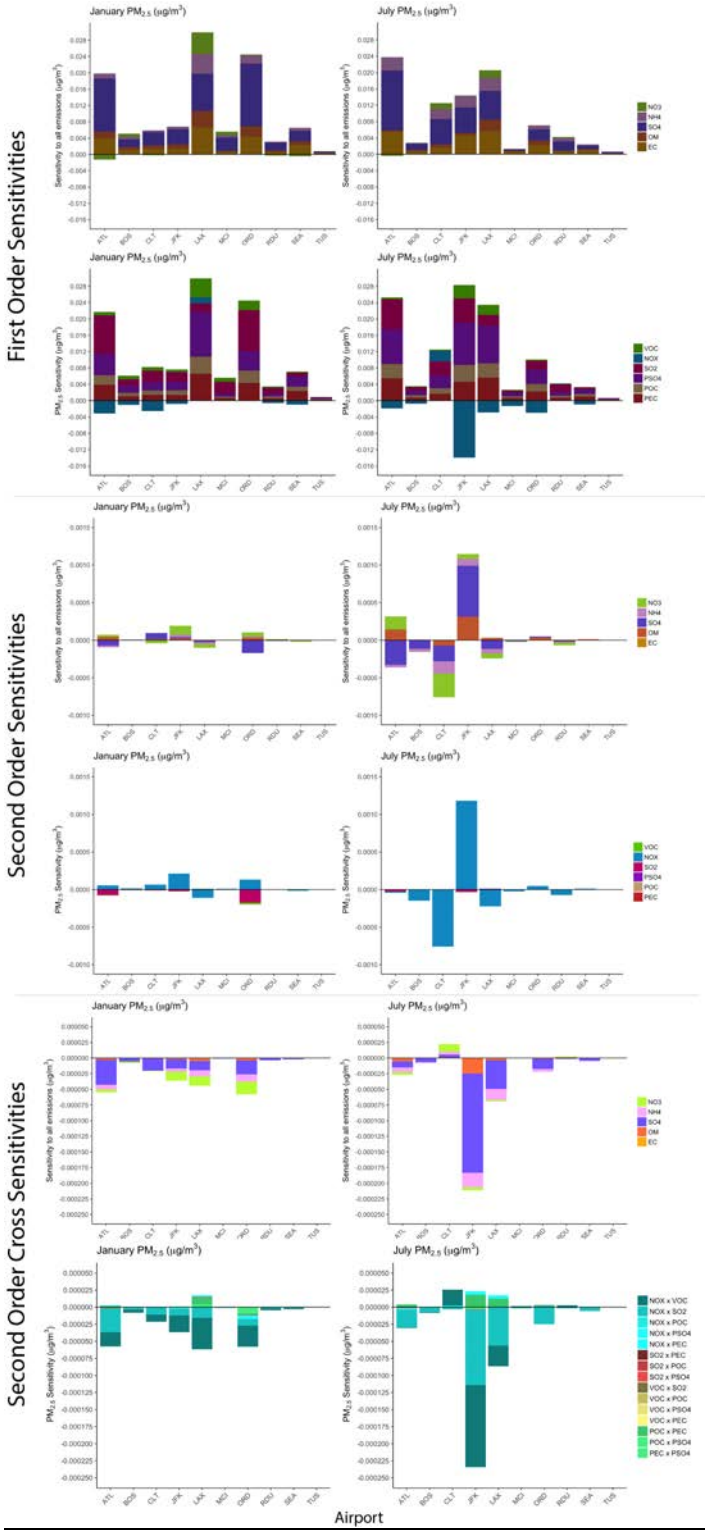


Figure 2.6. $PM_{2.5}$ first, second, and second order cross sensitivities disaggregated by precursor species at grid cell containing airport

From the prior sections, it is abundantly clear that LTO NO_x emissions are responsible for the most degree of nonlinearity in both our O_3-precursor and PM-precursor systems. Second order sensitivities to LTO NO_x represent the only significant second order sensitivities among any of our precursors. We make use of the nonlinearity ratio (Cohan et al. 2005 and Wang et al. 2011) to show how nonlinear an area may be based off of the magnitudes of the O_3-NO_x or PM-NO_x first order and second order sensitivities. This knowledge allows for a comprehensive understanding of where it would be necessary to include second order impacts when constructing emission-control strategies that rely on HDDM results and Taylor series approximations of concentration responses. Figure 2.7 shows the nonlinearity ratio for the O_3-NO_x system of LAX (left) and the $PM_{2.5}$-NO_x system of ORD (right). Higher nonlinearity ratios in the immediate vicinity of the airport indicate a nonlinear response due to NO_x emissions in the O_3-NO_x system while lower nonlinearity ratios downwind of the airport indicate a more linear response. In the case of ORD in January, a region of higher nonlinearity ratios directly west of ORD corresponds to a transition regime; going from an NH_3-poor regime to an NH_3-rich regime. Nonlinearity and the importance of second order impacts can indicate a transition regime with regards to the $PM_{2.5}$ concentration response to LTO NO_x emissions.

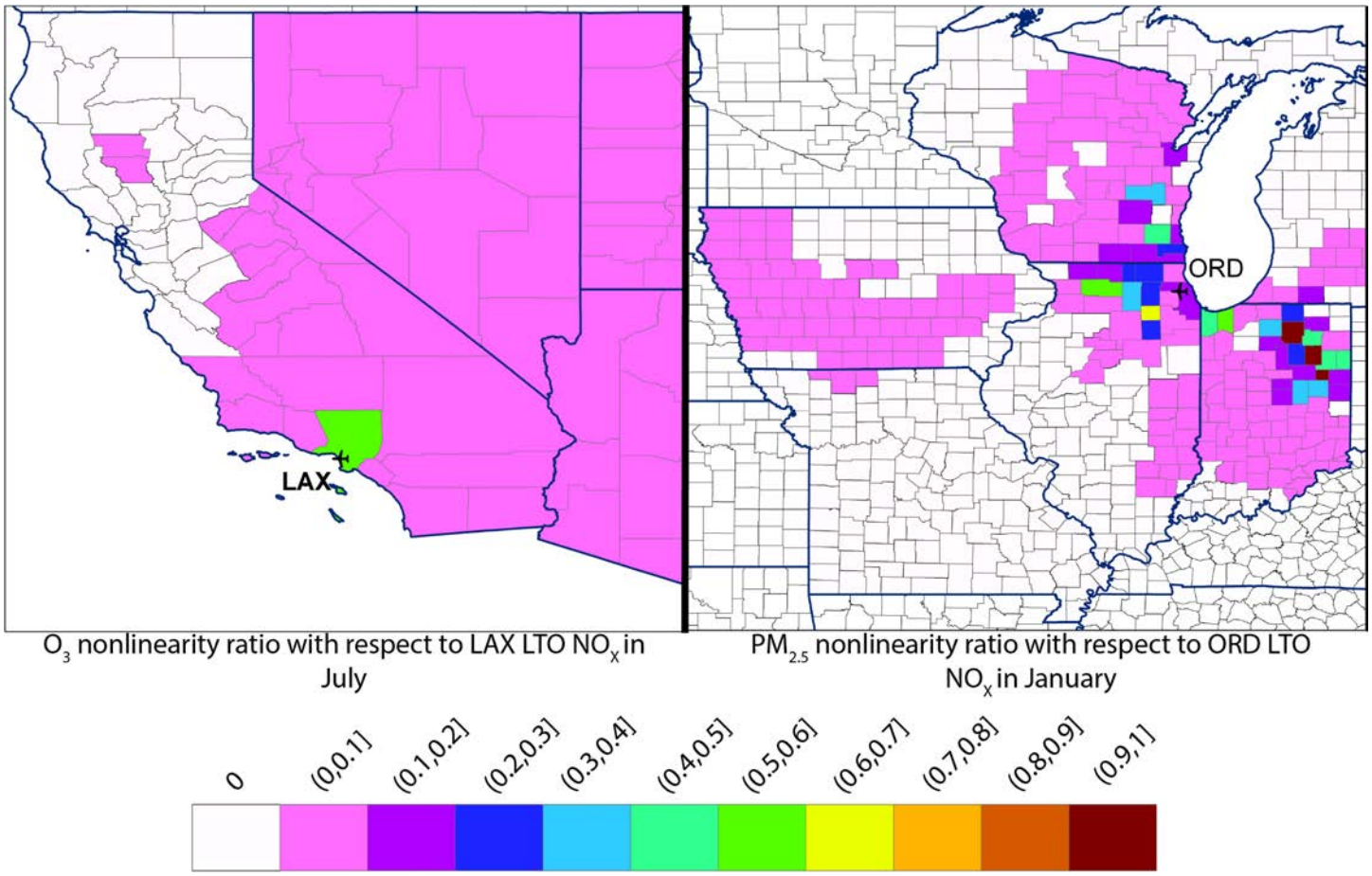


Figure 2.7. Nonlinearity ratios of O_3 to LTO NO_x at LAX (left) and $PM_{2.5}$ to LTO NOx at ORD (right) respectively

As an example of how HDDM sensitivities can be utilized for constructing emission control strategies, we present an analysis in which we calculate the total emission reductions/increases needed at each airport at the grid-cell level to decrease/increase O_3 by 1 ppb and $PM_{2.5}$ by 0.1 $\mu g/m^3$ for airports in non-attainment/attainment areas. By distinguishing



between airports in attainment versus non-attainment of O_3 and PM NAAQS, we can quantify the impacts of large airports on already polluted areas by determining the LTO emission reduction amounts to decrease ambient concentrations of O_3 and $PM_{2.5}$ and the impacts of moderate-large airports on relatively clean areas by determining the LTO emission increases to increase ambient concentrations of O_3 and $PM_{2.5}$. As our measure, we have chosen relatively small incremental values for O_3 and $PM_{2.5}$ since impacts from LTO aviation are modest (~1%) as compared to other emission sectors.

We utilize Taylor series expansions for calculating emission reductions/increases using only first order sensitivities and using first and second order sensitivities. By summing sensitivities, we are able to quantify reduction/increases amounts in terms of total LTO emissions. We then are able to relate the total emission reduction/increases amount to total fuel burn reduction/increases needed by relating the total amount of SO_2 emitted in each airport's grid cell to the amount of fuel burned in each grid cell.

Figure 2.8 shows the total fuel burn reductions/increases needed at our airports located in areas of non-attainment/attainment to decrease/increase O_3 by 1 ppb. Values reported on the y-axis indicate a scaled amount increased or decreased and should be thought of as a 'times' increase or decrease of fuel burned from what was originally burned (no perturbation in emissions); for example, if we look at the values for ATL in January in figure 2.9, about 6 times less fuel burn than what is currently being burned at the airport-containing grid cell is required to reduce $PM_{2.5}$ by 0.1 $\mu g/m^3$. The listed number above each bar is the actual amount of fuel burned (in tons) that would be needed to accomplish the reduction or increase in pollutant ambient concentration. The first thing that stands out is that the opposite trend of what is expected to either decrease or increase is observed at most airports (i.e., decreasing O_3 actually requires an increase in total fuel burned). As we saw when examining both the spatial distribution and the grid-based results for O_3 sensitivities, LTO NO_x emissions govern the concentration response and depending on the photochemical regime an airport may be located in, a disbenefit can occur with regards to LTO emissions impacting O_3 formation. This is readily apparent for LAX, JFK, and ORD where an increase in total fuel burned is needed to decrease O_3 by 1 ppb in the airport's grid cell. And for MCI, BOS, and SEA, a decrease in total fuel burned is needed to increase O_3 by 1 ppb. This trend occurs for estimating O_3 concentration response using both first and first and second order sensitivities. For airports that do not have negative first order sensitivities of O_3 to NO_x emissions, possibly indicating that they are in a NO_x-limited photochemical regime; using only first order sensitivities to estimate a concentration response will show a different trend than using both first and second order sensitivities, as seen at ATL, CLT, RDU, and TUS.

Figure 2.9 shows the total fuel burn reductions/increases needed at our airports located in areas of non-attainment/attainment to decrease/increase $PM_{2.5}$ by 0.1 $\mu g/m^3$. Although we saw some disbenefit due to LTO NO_x emissions on $PM_{2.5}$ formation at the airport grid cell, it was not enough to cause total LTO emission impacts to inversely impact $PM_{2.5}$ formation. For airports in regions of non-attainment, a decrease in total fuel burn is needed to decrease ambient $PM_{2.5}$ concentrations while airports in regions of attainment need an increase in total fuel burn to increase ambient $PM_{2.5}$. Unlike O_3 concentration response, nonlinear impacts are not as large in the grid cell containing the airport. We can see that by looking at the difference between using only first order and using both first and second order sensitivities in the Taylor series expansions.

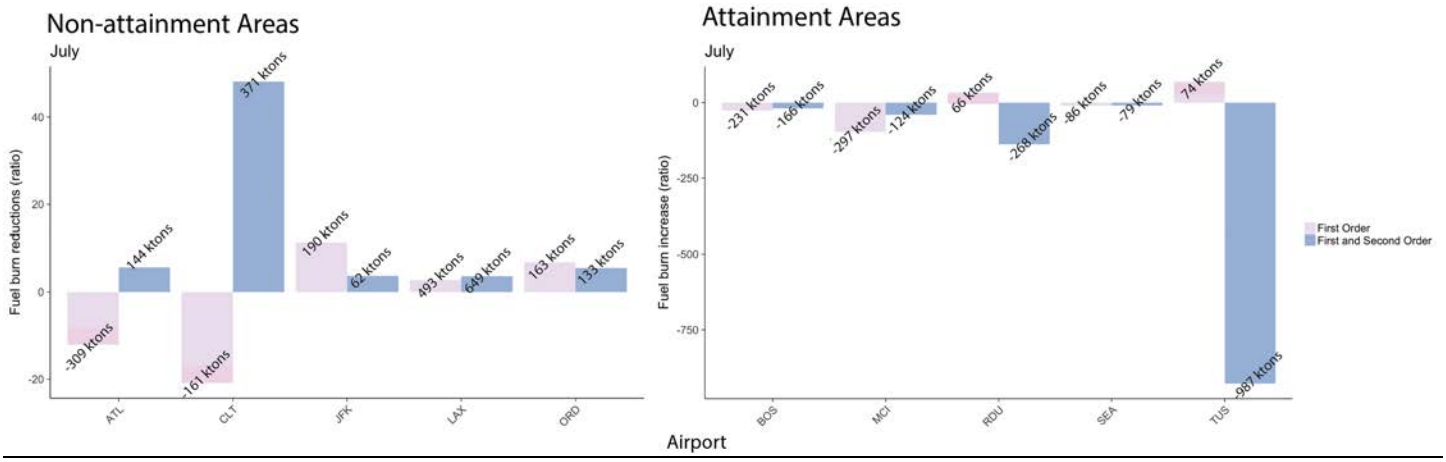


Figure 2.8. Fuel burn reductions/increases needed at airports in non-attainment/attainment areas to decrease/increase ambient maximum daily 8-hour O_3 by 1 ppb

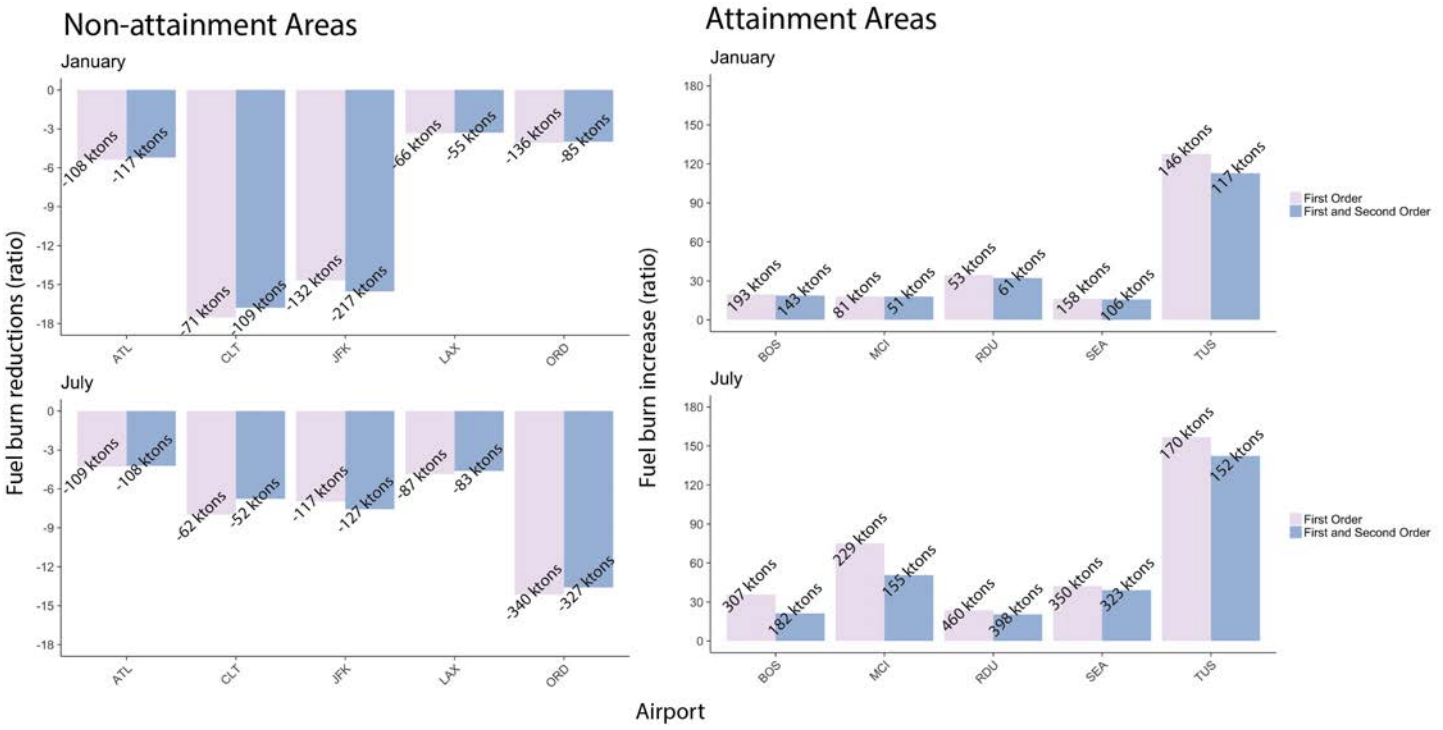


Figure 2.9. Fuel burn reductions/increases needed at airports in non-attainment/attainment areas to decrease/increase $PM_{2.5}$ by 0.1µg/m³

We have just finished preliminary testing with an updated CMAQv5.2 DDM modeling platform with inputs exactly similar to the 2015 modeling simulation platform as described in Task 1. We will begin modeling first order sensitivities of O_3 and $PM_{2.5}$ with respect to NAS-wide 2015 LTO aircraft emissions for the months of January and July.



Milestone(s)
We modeled first and second order sensitivities of O_3 and $PM_{2.5}$ with respect to LTO aircraft emissions from five airports located in regions of non-attainment and five in regions of attainment

Major Accomplishments
Calculated fuel burn reductions/increases needed to decrease/increase O_3 and $PM_{2.5}$ for airports located in regions of non-attainment/attainment, thus providing a novel approach that can be used to assess the overall contributions of small/large airports to potential attainment designations.

Publications
Poster Presentation at 2018 annual North Carolina BREATHE Conference (Raleigh, NC)
Poster Presentation at 2018 International Technical Meeting on Air Pollution Modeling and its Application (Ottawa, Canada)

Outreach Efforts
Presentation at semi-annual ASCENT stakeholder meetings in Spring and Fall 2018, Alexandria, VA.

Awards
None

Student Involvement
All of the work in the task has been performed by 3rd year PhD student, Calvin Arter

Plans for Next Period
Utilize the updated modeling platform used in Task 1 for 2015 to run CMAQv5.2 DDM for NAS-wide LTO emissions
Finalize analyses and develop manuscript.

References
Baek, B.H., Arunachalam, S., Woody, M., Vennam, L.P., Omary, M., Binkowski, F., Fleming, G. (2012). A New Interface to Model Global Commercial Aircraft Emissions from the FAA Aviation Environmental Design Tool (AEDT) in Air Quality Models.

Boone, S., & Arunachalam, S. (2014). Calculation of sensitivity coefficients for individual airport emissions in the continental U.S. using CMAQ-DDM/PM. In *ACM International Conference Proceeding Series*. [10] Association for Computing Machinery. 10.1145/2616498.2616504

Lamarque, J. F., Emmons, L. K., Hess, P. G., Kinnison, D. E., Tilmes, S., Vitt, F., … Tyndall, G. K. (2012). CAM-chem: Description and evaluation of interactive atmospheric chemistry in the Community Earth System Model. *Geoscientific Model Development*, *5*(2), 369–411. http://doi.org/10.5194/gmd-5-369-2012

Napelenok, S. L., Cohan, D. S., Hu, Y., & Russell, A. G. (2006). Decoupled direct 3D sensitivity analysis for particulate matter (DDM-3D / PM), *40*, 6112–6121. http://doi.org/10.1016/j.atmosenv.2006.05.039

Rienecker, M. M., Suarez, M. J., Gelaro, R., Todling, R., Bacmeister, J., Liu, E., … Woollen, J. (2011). MERRA: NASA's modern-era retrospective analysis for research and applications. *Journal of Climate*, *24*(14), 3624–3648. http://doi.org/10.1175/JCLI-D-11-00015.1

Roof, C., & Fleming, G. G. (2007). Aviation Environmental Design Tool (AEDT). *22nd Annual UC Symposium on Aviation Noise and Air Quality*, (March), 1–30.

Russell, A. G. (2005). Nonlinear Response of Ozone to Emissions : Source Apportionment and Sensitivity Analysis, *39*(17), 6739–6748.

Skamarock, W. C., Klemp, J. B., Dudhi, J., Gill, D. O., Barker, D. M., Duda, M. G., … Powers, J. G. (2008). A Description of the Advanced Research WRF Version 3. *Technical Report*, (June), 113. http://doi.org/10.5065/D6DZ069T

Wilkerson, J. T., Jacobson, M. Z., Malwitz, A., Balasubramanian, S., Wayson, R., Fleming, G., … Lele, S. K. (2010). Analysis of emission data from global commercial aviation: 2004 and 2006. *Atmospheric Chemistry and Physics*, *10*(13), 6391–6408. http://doi.org/10.5194/acp-10-6391-2010



Zhang, W., Capps, S. L., Hu, Y., Nenes, A., Napelenok, S. L., & Russell, A. G. (2012). Model Development Development of the high-order decoupled direct method in three dimensions for particulate matter : enabling advanced sensitivity analysis in air quality models, 355–368. http://doi.org/10.5194/gmd-5-355-2012

X. Wang, Y. Zhang, Y. Hu, W. Zhou, L. Zeng, M. Hu, D. S. Cohan, and A. G. Russell, Decoupled direct sensitivity analysis of regional ozone pollution over the Pearl River Delta during the PRIDE- PRD2004 campaign, Atmos. Environ. **45**, 4941 (2011).

M.C. Woody, H.-W. Wong, J.J. West, S. Arunachalam, Multiscale predictions of aviation-attributable PM2.5 for U.S. airports modeled using CMAQ with plume-in-grid and an aircraft-specific 1-D emission model, In Atmospheric Environment, Volume 147, 2016, Pages 384-394, ISSN 1352-2310, https://doi.org/10.1016/j.atmosenv.2016.10.016.

U.S. Federal Aviation Administration. List of Commercial Service Airports in the United States and their Nonattainment and Maintenance Status, 2016

Task 3- Develop Measurement – Modeling Assessment of Air Quality for Boston Logan Airport

University of North Carolina at Chapel Hill

Objective(s)

In this task, we will collaborate with ASCENT18 investigators at Boston University with a specific focus on modeling the Boston Logan airport at multiple spatial scales, and perform intercomparison of the measurement and modeling with a focus on fine particulate matter – mass and number concentrations due to aircraft emissions. Using airport-specific inventories that FAA will provide, we will explore the use of two modeling approaches – CMAQ and SCICHEM. Since SCICHEM uses the same aerosol treatment as CMAQ, but is able to characterize aircraft impacts at very fine scales around the airport, a key project outcome is the ability to improve aircraft-attributable PM on prior estimates, with a focus on particle number concentrations.

Research Approach

The UNC team has extensive experience to use SCICHEM to model aircraft emissions. Rissman et al (2013a,b) first used SCICHEM embedded in CMAQ to study aircraft emissions from the Hartsfield-Jackson International Airport in Atlanta. Subsequently, Woody et al (2016) used the same multi-scale modeling framework for a nation-wide study to assess sub-grid scale impacts of aircraft emissions from the top 99 U.S. airports. And, more recently Arunachalam et al (2017) completed an ACRP project study to develop guidance for airport operators to apply dispersion models for assessing local air quality at airports. In this study, four different dispersion models including SCICHEM were applied in a stand-alone basis for modeling airport emissions at the Los Angeles International (LAX) Airport. We used this experience to develop a SCICHEM application for the Boston Logan Airport (BOS), and specifically instrument the model to capture UFP impacts from the airport at very fine scales in the vicinity of the airport.

During Spring and Summer of 2017, the ASCENT18 investigators made multiple measurements of UFP and BC at various locations South and West of the Boston Logan airport. We collaborated with BU to obtain these measurements to perform inter-comparison against model outputs. Our specific focus was to look for potential discrepancies between modeled and measured values to help identify potential new locations where monitoring needs to be conducted during a follow-on campaign during the upcoming year.

To support this modeling study, we explored the use of obtaining Boston Logan specific airport-level emissions inventories from AEDT for the year 2017 from Massachusetts Port Authority (Massport), the public authority that manages the Boston Logan Airport. However, since we weren't able to obtain any data from Massport, we resorted to using aircraft emissions from FAA's EDMS from a prior study that UNC was involved in, and as described in Woody et al (2011). As part of this former study, UNC had access to a single day's airport-level emissions inventories from the year 2015 (as EDMS/AERMOD files) for BOS, modeled as area sources, and we decided to use them for SCICHEM. The number of emission source points at the BOS airport were 2194 for all the emissions within LTO height (1 km). In the next phase of this task during a follow-on year, we will explore developing detailed airport-level inventories for Boston Logan that matches the measurement campaign periods for an explicit and more robust measurement-modeling assessment of UFP from Boston Logan.



Methodology

We obtained the latest version of SCICHEM (Version 3.1) from the developers and configured a SCICHEM modeling domain that covers 120 km north-south direction and 166 km east-west direction having Boston Airport and its LTO path inside the domain shown in Figure 4.1. One of the goals of this study is to compare model simulated particle number concentration (PNC) with BU measurements. BU measurement stations are at south west direction from Boston Airport shown in Figure 4-1, and North-easterly winds bring plume to BU measurement stations. We analyzed the meteorological data from Boston airport, and chose July 13, 2017 because it has north-easterly and northerly wind over Boston airport as shown in Figure 4.2. Two receptor domains, where the output concentration of species at 15 min frequency are stored, were chosen in the simulations. These are:

1) 13x13 grids at 2x2-km resolution, and
2) 13x13 grids at 250x250-m resolution, as shown in Figure 4.1, along the wind direction path from Boston Logan Airport for the simulation day.

The input meteorology data were taken from National Climatic Data Center (NCDC). Most PNC are expected to be in the Aitken mode (0<Dp<100nm) because of their smaller sizes. Hence, concentration of Aitken mode particles (APMI), which is assumed to be the sum of the 3 EDMS emission inventory species in the Aitken mode: ASO4I, AORGI, AECI, are simulated in the SCICEHM without chemistry and aerosol microphysics. The particle number concentration is then approximated by the equation 4.1 given below. The PNC can be simulated using two methods discussed here. The first method was used to estimate the PNC presented in this report shown in Figures 4.4 and 4.5. The second detailed method will be used in the next step of this study.

Modeling PNC in SCICHEM by simple method

Neglecting nucleation and coagulation, PNC of the i^{th} mode can be approximated using the volume (mass) concentration of aerosol species in the post process by this equation (Binkowski 2003):

$$N_i = \frac{M_{3,i}}{D_{g,i}^3 \exp\left(\frac{9}{2} ln^2 \sigma_{g,i}\right)} \qquad \text{Eq. (4.1)}$$

Where:

- N_i = Particle number concentration of i^{th} mode (#/cm^3)
- $M_{3,i}$=3rd Aerosol moment (Total volume concentration) of i^{th} mode (cm^3/cm^3)
- $D_{g,i}$=Geometric mean diameter of i^{th} mode (cm)
- $\sigma_{g,i}$=Geometric standard deviation of i^{th} mode

The $D_{g,i}$ and $\sigma_{g,i}$ were used in Equation 4.1 based on the near source observation (Whitby, 1978)

Table 4.1. Geometric mean diameter and standard deviation for 3 aerosol modes based on near source observations (Whitby 1978).

	Aitken	Accumulation	Coarse
$D_{g,i}$ (μm)	0.03	0.3	6
$\sigma_{g,i}$	1.7	2	2.2

SCICHEM's single component run gave $M_{3,i}$ which were then used to estimate N_i by the above Equation (4.1).

Modeling PNC in SCICHEM by detailed moment model

Particles are assumed to follow a log-normal size distribution having 3 modes (Binkowski 2003): Aitken mode (particle diameter from 0 to 0.1 μm), Accumulation mode (particle diameter from 0.1 μm to 2.5 μm) and Coarse mode (particle diameter greater than 2.5 μm). The Moment-based algorithm of Binkowski and Roselle (2003) will be used in SCICHEM model to estimate PNC in the next step. SCICHEM will track the 0^{th} (number concentration), 2^{nd} (surface area concentration), and 3^{rd} (volume concentration) moments of all three distinct population modes (Aitken, Accumulation and Coarse modes).

The SCICHEM run cases:

The following 4 cases were run for the 2194 segmented area sources for all emissions within LTO height (1 km altitude):

- **Case 1**: Single component run for CO for receptor domain 1 (13x13 at 2x2km)
- **Case 2**: Single component run for CO for receptor domain 2 (13x13 at 250x250m)
- **Case 3**: Single component run for Aitken mode (0<Dp<100nm) particles (APMI which is sum of 3 Aitken mode FAA-EDMS emission inventory species: ASO4I, AORGI, AECI) for the receptor domain 1
- **Case 4**: Single component run for Aitken mode (0<Dp<100nm) particles (APMI) for the receptor domain 2

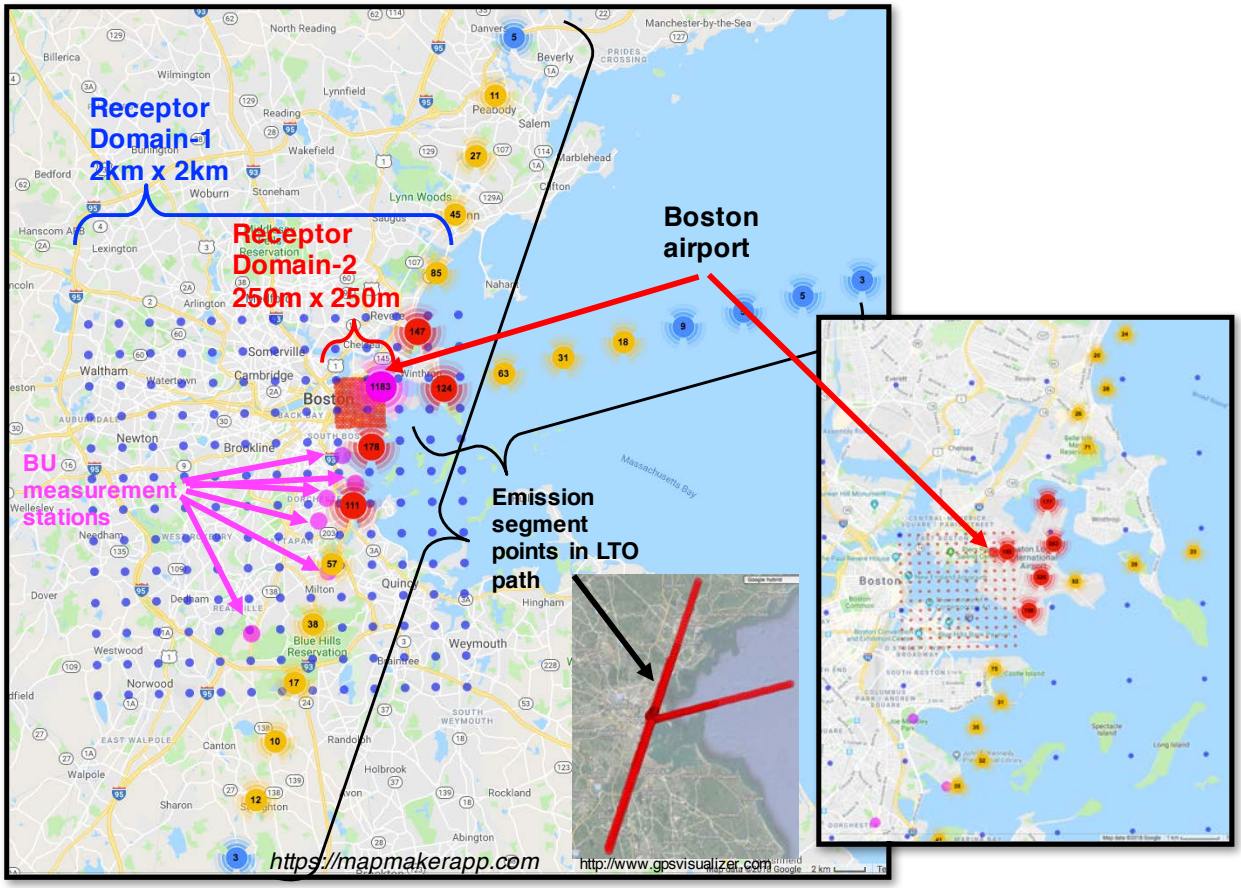


Figure 4.1. SCICHEM modeling domains 1 and 2, and emission sources for dispersion modeling of air pollutions from Boston Logan International Airport (BOS) (BU = Boston University, LTO = Landing and Take-off).

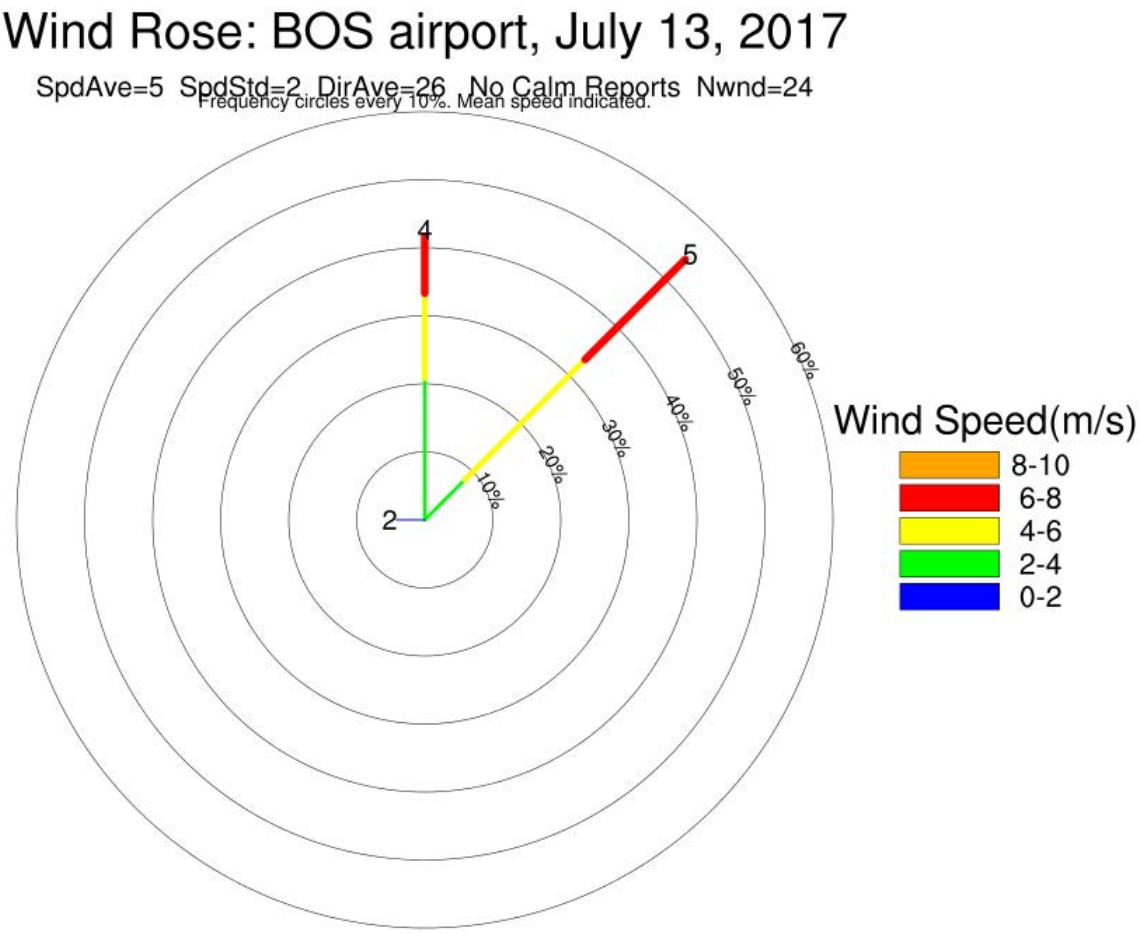


Figure 4.2. Wind profile at Boston Logan International Airport (BOS) on simulation day: July 13, 2017 (wind data taken from National Climatic Data Center (NCDC)).

Results

Figure 4.3 shows the emission profile from the Boston Logan International Airport. Most of the CO emission occurs at the terminal. The emission rates in the LTO paths were orders of magnitude less than that at the terminal shown in Figure 4.3. Hence, most of the pollutants are expected to originate from the terminal and to travel along the wind.

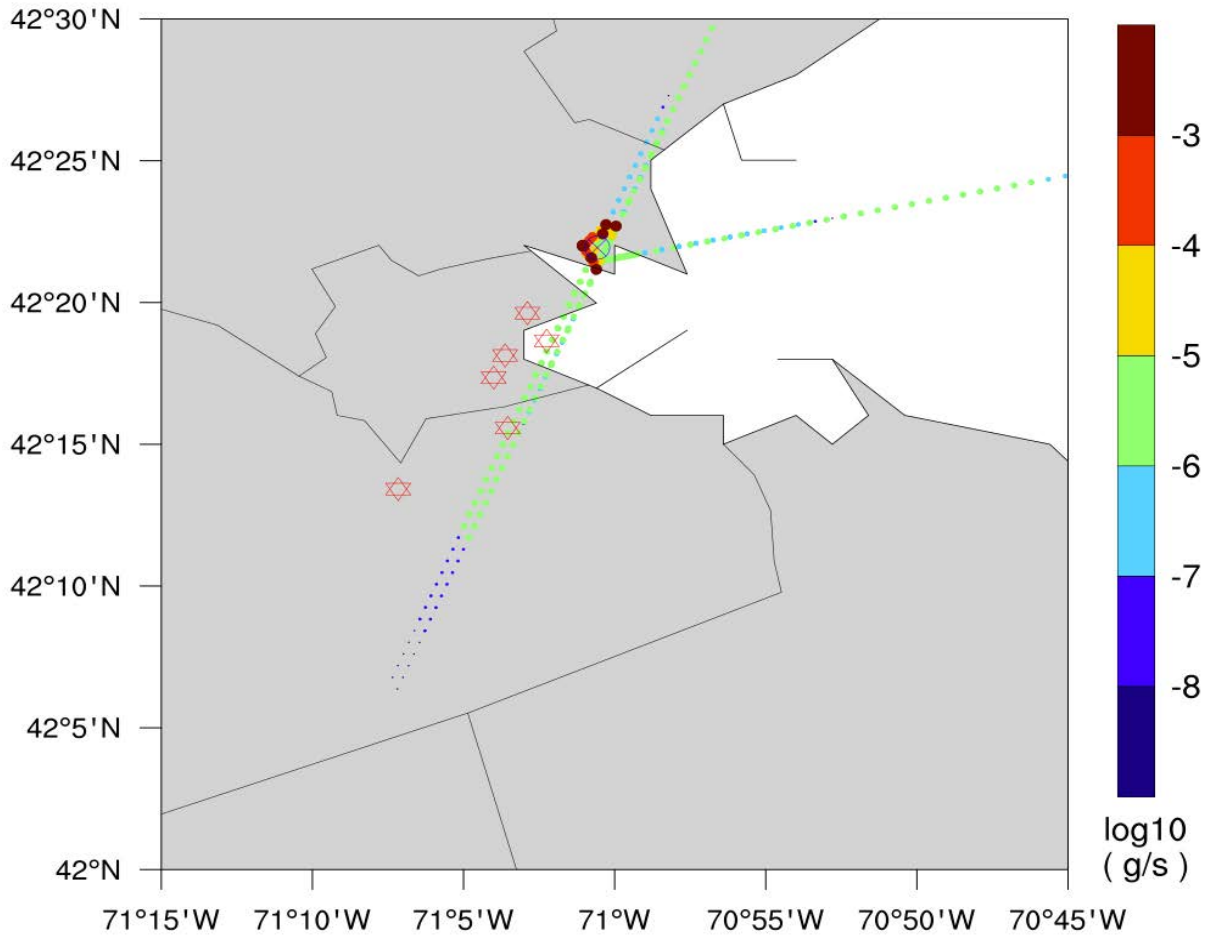


Figure 4.3. CO emissions from segmented points at landing and take-off (LTO) paths of Boston Logan International Airport (BOS) at 0090 EST, Feb 19, 2015 (Emission data processed from FAA's EDMS data, and Feb 19, 2015 emission rates data were time-shifted to simulation date July 13, 2017 for these test simulations).

The aircraft's LTO attributable hourly average CO concentration can be seen on the map shown in Figure 4.4a-j. Figure 4.4a-e shows that the plume travels along the wind (north-easterly and northerly wind shown in Figure 4.2). The model simulation captures the diurnal variation of CO which is the highest in the morning at 8 to 10 am shown in Figure 4.4d-e, when emission rates were higher at the terminal shown in Figure 4.4n-o. Figure 4.4 also shows the importance of high resolution simulation where CO concentration are found to be significantly higher in the high-resolution receptor domain (250m x 250m grids) shown in Figure 4.4f-j than that in the low-resolution receptor domain (2km x 2km grids) shown in Figure 4.4a-d. The high-resolution simulation, shown in Figure 4.4i-j, reveals the multiple hot spots for multiple emission sources which were not visible in the low spatial resolution simulation shown in Figure 4.4-d-e.

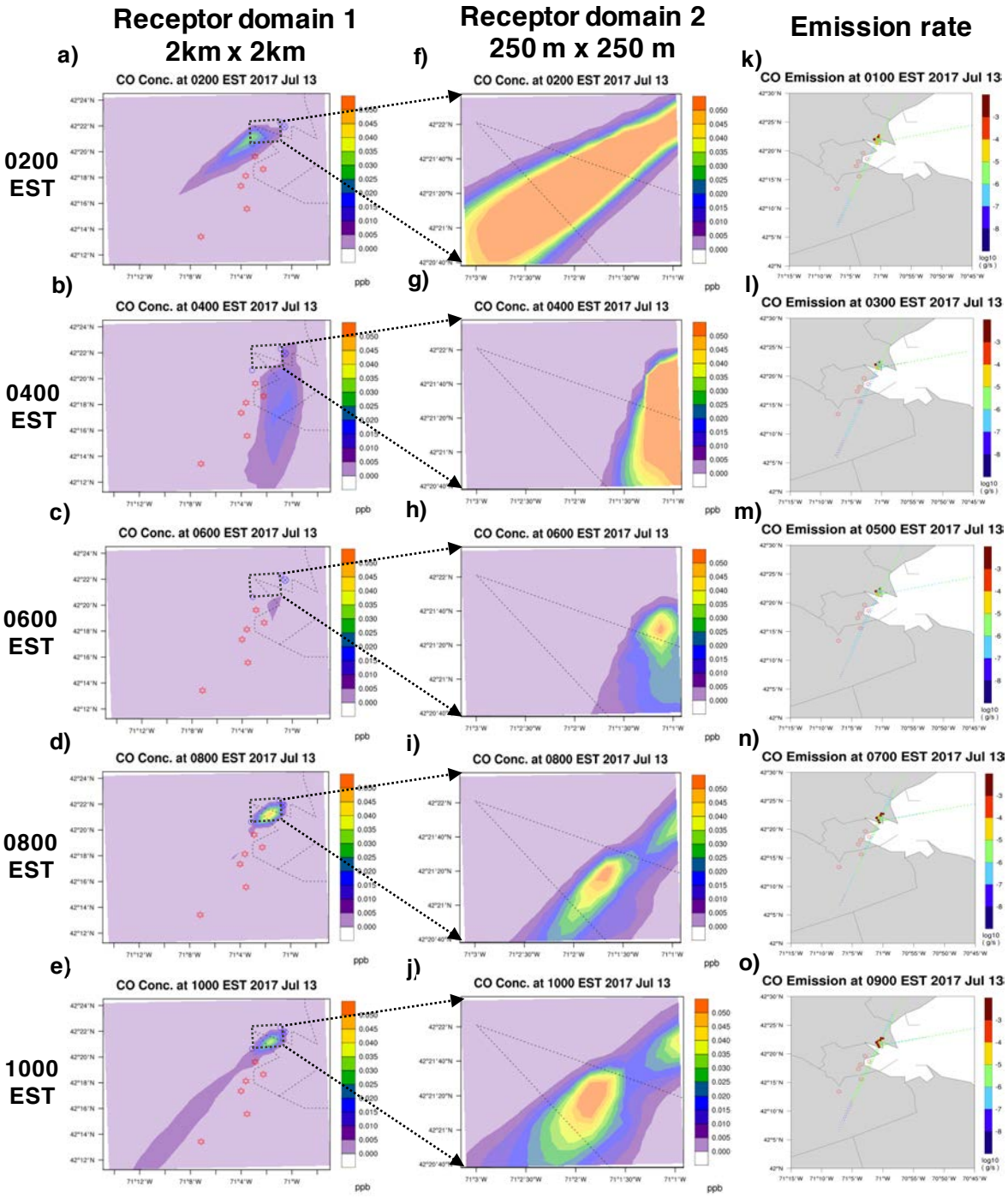


Figure 4.4. Aircraft attributable hourly average concentration of CO at a-e) in 2km x 2km receptor domain, f-j) in 250m x 250m receptor domain and k-o) hourly emission rates of CO in first 10 hours of July 13, 2017 (emission rates data were time-shifted from original Feb 19, 2015 to simulation date July 13, 2017).



We used method #1 described earlier to compute PNC due to BOS LTO emissions. The LTO-attributable Aitken mode (0<Dp<100 nm) particle (APMI's) mass and number concentration can be seen in 2 receptor domains, shown in Figure 4.5. Note APMI = AECI + AORGI + ASO4I. The model simulation captures the diurnal variation of APMI which is higher in the morning at 10 am shown in Figure 5.5e, when emission was higher at the terminal shown in Figure 4.4o for CO's emission (The APMI emission map is not presented here, but it follows the same trend of CO emission map shown in Figure 4.4k-o). Figure 4.5 also shows the importance of high-resolution simulation where both APMI's mass concentration (shown in Figure 5.5f-j) and number concentration (shown in Figure 5.5p-t) were higher in receptor domain 2 (250m x 250m grids) that in receptor domain 1 (2km x 2km) shown in Figures 5.5a-d and 5.5k-o respectively. The high-resolution simulation shown in Figure 5.5j for mass concentration and 5.5t for number concentration reveals the multiple hot spots for multiple emission sources which were not visible in the low spatial resolution simulation shown in Figure 5.5d for mass and Figure 5.5o for number concentration.

Maximum aircraft attributable PNC in the plume were ~100 #/cm3 for the low-resolution receptors shown in Figure 5.5o and ~500 #/cm3 for high resolution receptors shown in Figure 5.5t at 10 am. The present simulation neglected the aerosol microphysics and inclusion of the nucleation in the aerosol microphysics will increase the PNC through secondary particle formation.

Computation time

The SCICHEM simulation is computationally demanding which needs about 8 hours computation time for 1-hour simulation because of the 2194 emission source points at the airport used in the simulation. This issue was already documented in previous SCICHEM applications by our group and cited earlier, and we are exploring ways to optimize the computing burden or source representation in the model.

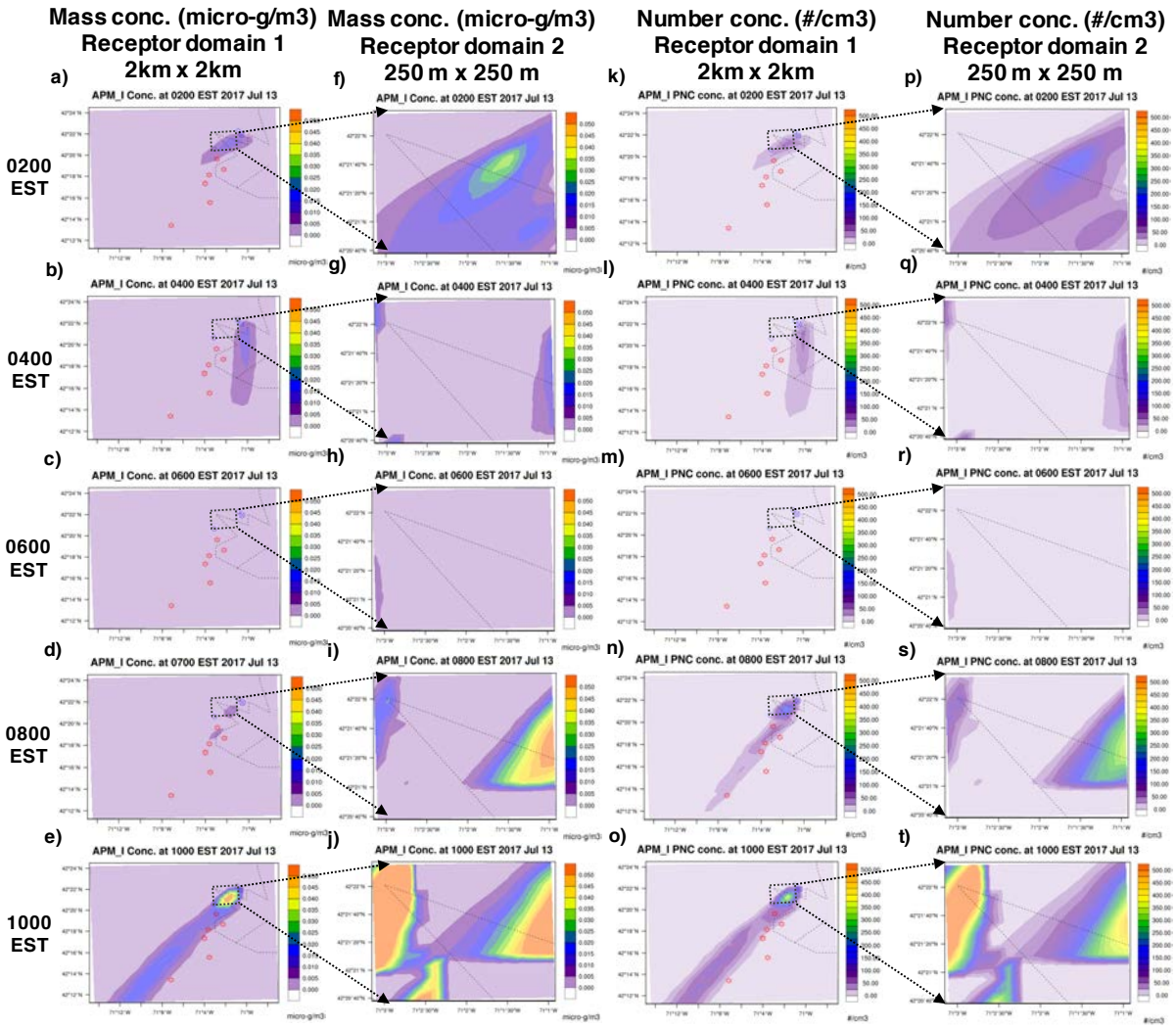


Figure 4.5. Aircraft attributable hourly average concentration of Aitken mode (particle having diameter 0 to 0.1 micron) particles (sum of 3 Aitken mode aerosol species: sulfate (ASO4I), organics (AORGI), elemental carbon (AECI)): a-e) mass concentration (μg/m^3) in 2km x 2km receptor domain, f-j) mass concentration (μg/m^3) in 250m x 250m receptor domain, k-o) number concentration (#/cm^3) in 2km x 2km receptor domain and l-t) number concentration (#/cm^3) in 250m x 250m receptor domain in first 10 hours of July 13, 2017.

Milestone(s)

SCICHEM model were run for the single-component without chemistry for CO and Aitken mode particles for Boston airport's emission at high spatial resolution domains (in 2km x 2km domain and in 250m x 250m domain) for 10-hour period for a single day.

Aircraft attributable particle number concentration for Aitken mode (0<Dp<100 nm) particles were estimated in two high spatial resolution domains (in 2km x 2km domain and in 250m x 250m domain) for 10-hour period of 1 day. SCICHEM was also run for multi-component with chemistry for gas species, and we are analyzing these results.



Major Accomplishments

Aircraft attributable particle number concentration from Boston Logan Internal Airport has been estimated at high spatial resolution domains (in 2km x 2km domain and in 250m x 250m domain) for 10-hour period of 1 day for the first time.
The simulation found that most of the PNC comes from the terminal where emissions are the highest.
Model simulation found that PNC is sensitive to modeled spatial resolution.

Publications

Moniruzzaman, C. G. & Arunachalam, S. (2018). *An integrated modeled and measurement-based assessment of particle number concentrations from a major US airport.* Oral presentation, Presented at the 2018 Annual CMAS Conference, Chapel Hill, NC.

Outreach Efforts

Presentation at semi-annual ASCENT stakeholder meetings in the Spring and Fall 2018, Alexandria, VA.
Presentation and collaborative discussion during monthly meetings with ASCENT18 team at Boston University.

Awards

None

Student Involvement

None

Plans for Next Period

- The next step for this project is to estimate the PNC by running SCICHEM with detailed aerosol microphysics (nucleation and coagulation) and multi-component chemistry. Then the source-based dispersion model's results of PNC will be compared with BU's regression model that will be developed for PNC from BOS.
- Enhance point source treatment in SCICHEM.

References

Arunachalam, S., A. Valencia, M. Woody, M. Snyder, J. Huang, J. Weil, P. Soucacos and S. Webb (2017). Dispersion Modeling Guidance for Airports Addressing Local Air Quality Concerns. Transportation Research Board Airport Cooperative Research Program (ACRP) Research Report 179, Washington, D.C. Available from: http://nap.edu/24881

Binkowski, F. S. and Roselle, S. J.: Models-3 Community Multi- scale Air Quality (CMAQ) model aerosol component. 1. Model description, *J. Geophys. Res.,* 108, 4183–4201, 2003.

Chowdhury, B. P., Karamchandani, P. K., Sykes, R. I., Henn, D. S., Knipping, E., Reactive puff model SCICHEM: Model enhancements and performance studies, *Atmos. Environ.*, 117, 242–258, 2015.

Rissman, J., Arunachalam, S., Woody, M., West, J. J., BenDor, T., and Binkowski, F. S. (2013). A plume-in-grid approach to characterize air quality impacts of aircraft emissions at the Hartsfield-Jackson Atlanta International Airport, *Atmos. Chem. Phys*., 13, 9285-9302.

Rissman, J., S. Arunachalam, T. Bendor and J.J. West (2013). Equity and Health Impacts of Aircraft Emissions at the Hartsfield-Jackson Atlanta International Airport, *Landscape and Urban Planning,* 120, 234-247.

Whitby, K. T., The physical characteristics of sulfur aerosols, *Atmos. Environ.*, 12, 135–159, 1978.

Woody, M., H.-W. Wong, J.J. West, S. Arunachalam, (2016). Multiscale predictions of aviation-attributable PM2.5 for U.S. airports modeled using CMAQ with plume-in-grid and an aircraft-specific 1-D emission model, *Atmos. Environ.*, 147, 384 – 394. http://dx.doi.org/10.1016/j.atmosenv.2016.10.016.



Project 020 Development of NAS wide and Global Rapid Aviation Air Quality Tools

Massachusetts Institute of Technology (MIT)

Project Lead Investigator

Prof. Steven R.H. Barrett
Associate Professor of Aeronautics and Astronautics
Department of Aeronautics & Astronautics
Massachusetts Institute of Technology
77 Massachusetts Ave.
Cambridge, MA 02139
(617) 452-2550
sbarrett@mit.edu

University Participants

Massachusetts Institute of Technology

- P.I.: Steven R. H. Barrett
- FAA Award Number: 13-C-AJFE-MIT, Amendment Nos. 007, 018, 025, 032, and 041
- Period of Performance: Aug. 19, 2014 to Aug. 31, 2020
- Tasks:
  - Provide surface air quality analysis and quantify the impacts of aviation on surface air quality
  - Continue work on the development of nested domains and provide tool validation
  - Incorporate the nested domains into a single user-friendly framework
  - Support and assist the nvPM standard team on consistency-checking input data and interpreting results
  - Finalize and project uncertainty in ammonia emissions onto aviation impact sensitivities
  - Perform scoping of work for developing a multi-scale adjoint tool

Project Funding Level

$800,000 FAA funding + $50,000 Transport Canada funding = $850,000 total sponsored funds, with just $800,000 matching funds required. Sources of match are that same $50,000 Transport Canada funding (it constitutes both matching funds itself, as well as being sponsored funds that do not need to be matched), plus approximately $215,000 from MIT, and 3rd party in-kind contributions of $114,000 from Byogy Renewables, Inc. and $421,000 from Oliver Wyman Group.

Investigation Team (all MIT)

Principal Investigator: Prof. Steven Barrett
Co-Principal Investigator: Dr. Raymond L. Speth
Co-Investigator: Dr. Florian Allroggen
Research Scientist: Dr. Sebastian Eastham
Graduate students: Guillaume Chossière, Kingshuk Dasadhikari, Irene Dedoussi,

Project Overview

The aim of this project is to develop tools that enable the rapid assessment of the health impacts of aviation emissions. The focus of the project is on aviation-attributable $PM_{2.5}$ and ozone at the NAS-wide and global scales. These tools should allow for rapid policy analysis and scenario comparison. The adjoint method, which the tools are based on, provides a computationally efficient way of calculating the sensitivities of an objective function with respect to multiple model inputs. The project enhances the existing tools in terms of the domains and impacts covered, and in terms of uncertainty quantification. The enhanced tools support the FAA in its strategic vision to reduce the health impacts of aviation emissions, and allow for detailed and quantified policy analyses.



Tasks for Current and Next Period

Current Period (AY2017-2018)

- **Task 1:** Quantify surface air quality impacts of aviation
- **Task 2:** Continue work on the development of nested domains and provide tool validation
- **Task 3:** Operationalize the rapid assessment tool for internal use by the FAA
- **Task 4:** Support and assist the nvPM standard team (ASCENT 48) on consistency-checking input data and interpreting results
- **Task 5:** Finalize and project uncertainty in ammonia emissions onto aviation impact sensitivities
- **Take 6:** Perform scoping of work for developing a multi-scale adjoint tool

Next Period (AY2018-2020)

- **Task 1:** Extend the ASCENT 20 air quality assessment tool to account for high altitude aviation, including supersonic emissions
- **Task 2:** Quantify the impact of uncertainty in non-aviation emissions on calculated aviation emissions impacts
- **Task 3:** Extend operationalized MATLAB tools to account for the effect of non-aviation emissions uncertainty, and to include updated sensitivity matrices
- **Task 4:** Enable European regional simulations

Objectives

The aim of the project during this performance period is to enhance the capabilities of the existing rapid assessment tool. The main objectives of this cycle are aligned with the aforementioned tasks. Specifically:

1. Continue to work on the development of nested domains and provide tool validation. This will include code development and testing in order to develop a high-resolution simulation for Europe,
2. Operationalize tools and transition them to the FAA. The various model updates and the additions of the new nested domains with be packaged and wrapped with a user-friendly MATLAB script and will be passed to the FAA with a brief guidance document, similarly to the way the global and nested North American sensitivities were done,
3. Support and assist PM standard team in ensuring upstream input consistency (e.g. gridded emissions data) and results interpretation,
4. Quantify how uncertainties in the ammonia emissions propagate into the calculations of the adjoint sensitivities and how these affect the aviation attributable air quality impacts,
5. Perform scoping of work for developing a multi-scale adjoint tool that will enable the calculation of impacts from emissions occurring outside of the current nested domains, at the global scale. Perform comparison of aviation AQ impacts estimated using the global grid with the fine/nested grids' corresponding calculations.

Research Approach

As documented in previous reports, the central tool for this project is the GEOS-Chem adjoint. This reporting period has been dedicated to further extending the tool's capabilities as well as its validation. Significant work has also been invested in making the results of this project available for internal FAA use. This has allowed to us to produce and deliver to the FAA updated sensitivity maps for health impacts calculations and to provide insights into second-order sensitivity with respect to ammonia, which quantify the degree to which calculated aviation-impacts very with non-aviation ammonia emissions.

Quantification of the surface air quality impacts of aviation

In line with the main objectives of the ASCENT 20 project, our work for this period of performance has produced updated estimates of the impacts of national and global aviation on the surface air quality and has derived their associated health outcomes. The AEDT inventory for aviation year 2015 was used to produce these estimates, as well as the sensitivities derived from the GEOS-Chem adjoint. Below are some example results for calculating the health impacts surface air quality attributable to aviation NO_x emissions. Ozone impact calculations are a recent development for this project, and those calculated here are based on the Turner et al 2015 concentration response function (see Technical Guidance Document). This results in significantly greater mortality impacts than calculated previously using the older Jerrett et al 2010 concentration response function. Impacts due to $PM_{2.5}$ are also calculated using the Burnett et al 2014 integrated exposure response function, which finds lower impacts than the functions previously used for $PM_{2.5}$ impacts.

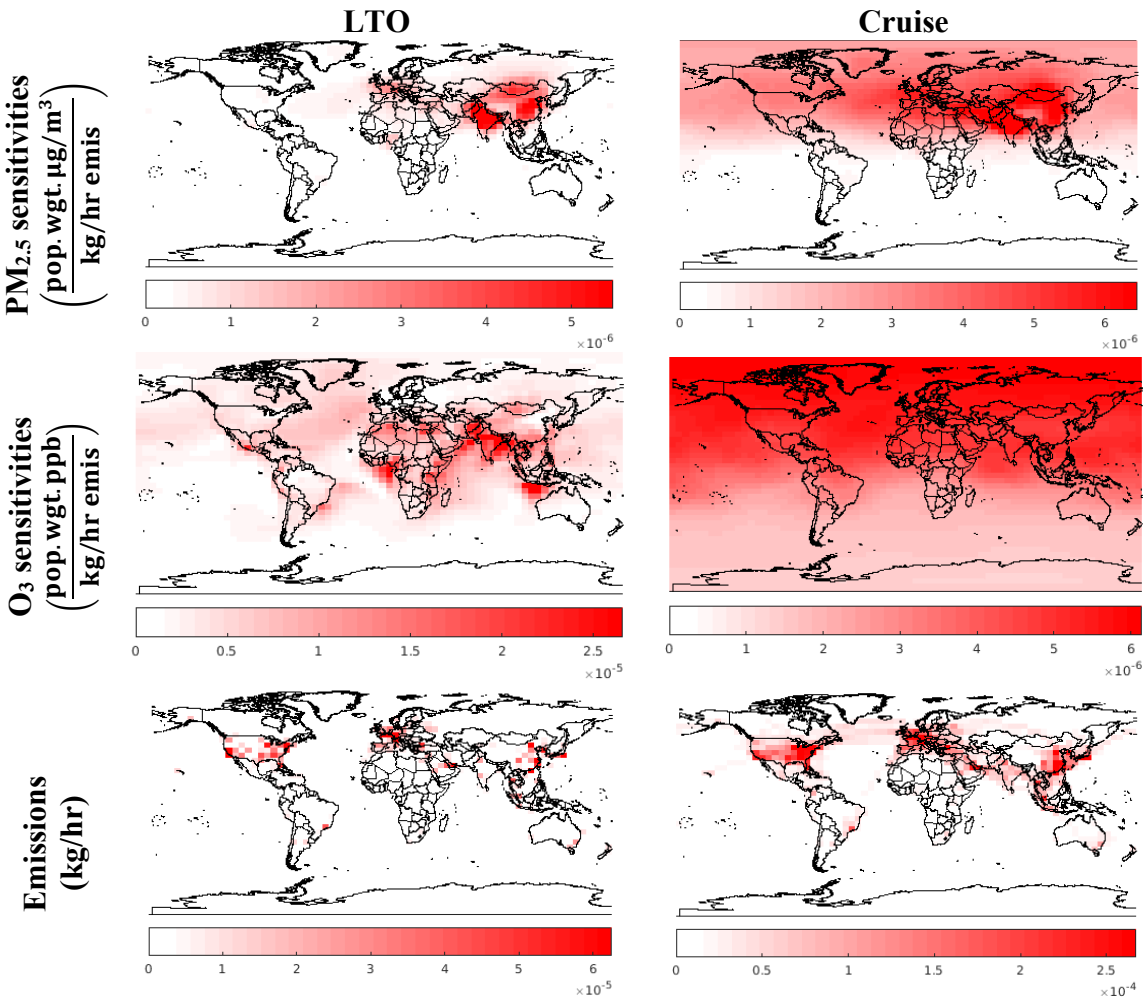


Figure 1. Global sensitivity to and aviation NO_x emissions in 2015. Color scales differ between panels to allow geographical distributions to be more easily resolved. Sensitivities show the annual average response.

Multiplying the emissions matrix for each species emitted by aviation element-wise by the corresponding sensitivity matrix and summing the products (the Technical Guidance document contains further details on these operations) allows us to compute the total health impacts of aviation 2015 emissions in each region. We find that uncertainties in the health-response function yields a 95% confidence interval of about (-49%, +50%).

Extension of the spatial capabilities of the tools and tool validation

Previous investigations using the North American nested domain have revealed that there are significant advantages to higher-resolution simulation over smaller domains. Capture of near-airport impacts is challenging with the coarse (~400 km) resolution at which the global model is run, while the finer (~50 km) resolution of the nested model is sufficient to isolate chemical and dynamical non-linearity associated with urban and coastal regions. This is complemented by further studies, such as Barrett et al (2010) and Eastham et al (2016), which show that the greatest impacts of aviation on surface air quality are incurred not in North America but rather in Western Europe and South Asia.

Accordingly, two additional nested domains were identified for use with the GEOS-Chem adjoint. The first is the South-East Asia nested domain. This domain, modeled at a resolution of 0.5˚×0.667˚, allows impacts of aviation to be finely resolved throughout India, China, Indonesia, and the rest of the South-East Asian domain. The domain is plotted in Figure 2. A similar grid is being developed and implemented for Europe.

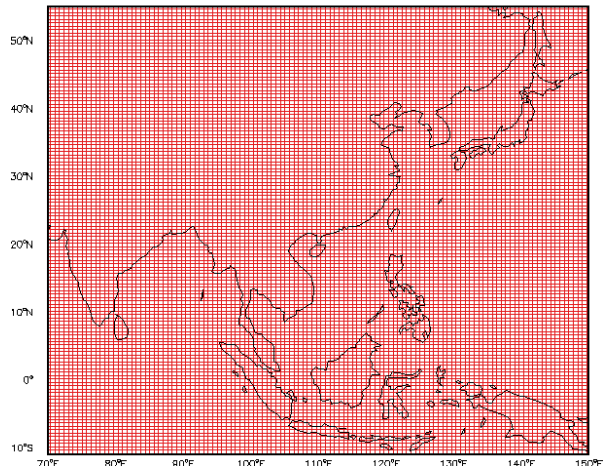


Figure 2. Fine-resolution domain covering Asia

Example sensitivity maps to aviation NO_x emissions for the nested Asia domain are shown in Figure 3. Beside committing work to capability extension, the project team has, during this past period of performance, conducted a validation of the tool by comparing the calculated health impacts attributable to aviation and due to exposure to $PM_{2.5}$ and ozone to the results obtained by modeling the impacts of aviation emissions on ground-level population exposure to $PM_{2.5}$ and ozone obtained from the forward model of GEOS-Chem. In both cases, the total health impacts were calculated using the gridded FAA AEDT-2015 aviation emissions. The comparisons between forward and adjoint results are presented in the Technical Guidance document delivered to the FAA along with the most up-to-date sensitivity data (see "Tool operationalization" section below). The error between the impacts computed using the forward and adjoint methods vary from 1% to 31%, with the highest error observed for the MDA-8 O_3 impacts for the Canadian receptor region. These errors are within the expected bounds for adjoint-based results.

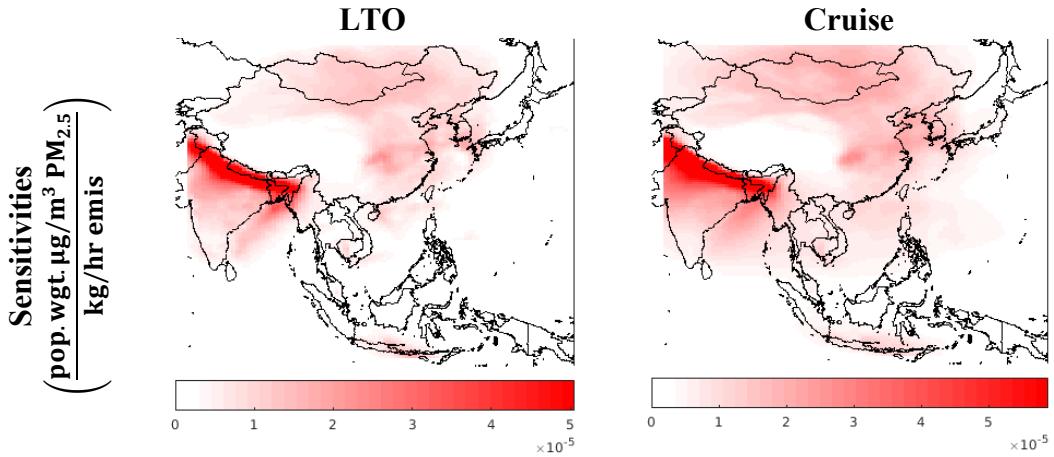


Figure 3. Example maps of the sensitivity of population-weighted $PM_{2.5}$ concentrations to aviation NO_x emissions during LTO (left) and at cruise altitude (right).

Tool operationalization

In this period of performance, the different model updates and the addition of the latest nested domains (namely Canada and Southeast Asia) have been packaged and wrapped in a MATLAB script to be delivered to the FAA along with the underlying data and supporting documentation on how the sensitivities were calculated and how to use them for practical health impacts calculations. This piece of software will be updated in the future as new domains become operational and as the air quality

impacts assessment tool gets updated. Uncertainty analysis will also be included in this piece of software in the future. Please refer to the Technical Guidance document for further details on this part of this period of performance.

Support to PM standard (ASCENT Project 48)
This part of our objectives consisted mainly in assisting the PM standard team and ensuring data consistency in their inputs such as gridded emissions data. We also provided them with support in the interpretation of their results.

Ammonia uncertainty
Following a literature review and feasibility analysis, a key (and, as yet, unquantified) source of uncertainty is the potential impact of uncertainty in ammonia emissions on the sensitivity of air quality to aviation emissions. The rate of near-surface $PM_{2.5}$ formation is highly sensitive to local concentrations of ammonia, which acts to neutralize acidic aerosol and thereby increase the total aerosol mass. However, no study has yet incorporated the known high uncertainty in ammonia emissions into their estimates of health impacts from aviation.

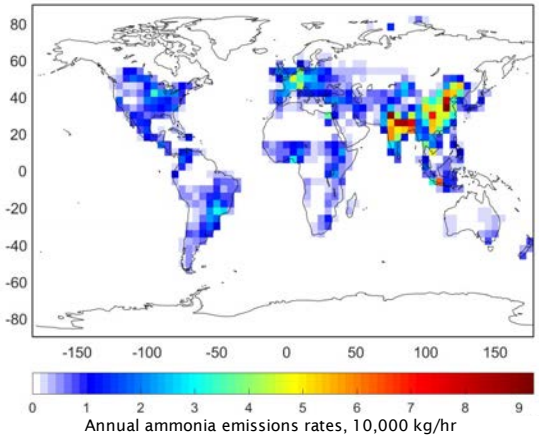


Figure 4. Baseline global ammonia emissions. Data are taken from the EDGAR v4.3.1 inventory.

A new strategy has been developed to estimate the impact of uncertainty in ammonia emissions on the sensitivity of average surface-level air quality to aviation emissions. This constitutes an application of the second-order sensitivity of aviation's impacts with respect to both aviation emissions and ammonia emissions, making use of the combined power of adjoint sensitivity calculation and forward differencing. We provide more details about this method and its application to project ASCENT 20 below. The global emissions that are currently used in the tool are plotted in Figure 4 at a resolution of 4˚×5˚. These emissions are taken from the EDGAR v4.3.1 inventory (Crippa et al. 2016), distributed as shown in Table 1.

Table 1. Baseline estimate of ammonia emissions by region

Region	Emission Total (Tg/Year)
Global	55.06 (*100%*)
China	14.02 (*25.5%*)
Other Asia	17.81 (*32.3%*)
Europe	5.65 (*10.3%*)
USA	4.17 (*7.57%*)
Other North America	2.11 (*3.83%*)
Other	11.24 (*20.4%*)



A key task performed during this period of performance was to estimate, from a literature review, the uncertainty associated with these regional ammonia inventories. The results are shown in Table 2. The column "Applied to" refers to the region to which the uncertainty was applied.

Table 2. Regionalized uncertainty in ammonia emissions

Region	Relative uncertainty	Applied to	Source
Global	(−18.75 %, +18.75 %)	Other	Beusen et al. (2008)
China	(−43 %, +50 %)	China, Other Asia	Zheng et al. (2012)
Europe	(−30 %, +30 %)	Europe	EMEP (2009)
USA	(−36 %, +36 %)	USA, Other NA	Zhu et al. (2012)

To compute the impact of these uncertainties in ammonia emissions on aviation-attributable health impacts, we first compute the first-order sensitivities of the desired health impacts to NH_3 emissions with and without aviation emissions. By multiplying the difference of these two matrices (whose values are expressed in units of $\frac{\mu g(PM_{2.5})/m^3}{kg(NH_3)/hr}$) by the uncertainty in ammonia emissions (in $\frac{kg\,(NH_3)}{hr}$), we compute, in each grid cell, the share of the uncertainty in the calculated total aviation-attributable impacts that can be traced back to uncertainties in ammonia emissions. The application of this method yielded the results shown in Table 3.

Table 3. Uncertainty in aviation impacts due to uncertainty in ammonia emissions

Summary	
Aviation-attributable, population-weighted $PM_{2.5}$	59.6 ng/m³ (*baseline*)
NH_3-driven uncertainty	(−24.0, +27.0) ng/m³ *(−40.2%, +45.5%)*
Regional Contributions to NH_3-Driven Uncertainty	**China:** (−11.9, +13.8) ng/m³ (*−43.9%, +51.1%*) **Other Asia:** (−6.6, +7.7) ng/m³ (*−24.5%, +28.5%*) **Europe:** ± 4.0 ng/m³ (*± 6.7%*) **USA:** ± 1.1 ng/m³ (*± 1.8%*) **Other NA:** ± 0.1 ng/m³ (*± 0.4%*) **Other:** ± 0.2 ng/m³ (*± 0.7%*)

Multi-scale adjoint tool

The development of a multiscale sensitivity analysis framework would combine the advantages of low-resolution global modeling for cruise sensitivity analysis with the advantages of high-resolution local modeling for resolving surface-level variations. Based on the work completed in this period of performance, a potential solution has been identified which would require to implement substantial modifications of the adjoint tool.

The proposed solution would involve re-engineering the adjoint to directly include sensitivity to changes in boundary conditions, supported by a finite-difference forward simulation to evaluate how the boundary conditions are affected by aviation. This effort would be supported by a multi-tier forward analysis to evaluate the difference in calculated impacts between the forward global, adjoint global, forward nested, and adjoint nested simulations.



Milestones

- *Surface air quality impacts of aviation*: Updated sensitivity to aviation emissions have been produced and used along with the AEDT 2015 inventory of aviation emissions to produce updated estimates of the health impacts of aviation emissions in different regions.
- *Nested domains and tool validation:* Work has continued on extending the capabilities of the tool to include high resolution modeling over various key regions. The tool was fully validated against the forward version of the GEOS-Chem model over all the operational domains.
- *Operationalize tools*: The various model updates and the additions of the new nested domains were packaged and wrapped into a user-friendly Matlab script that we passed to the FAA along with a brief guidance document.
- *Support PM standard analysis*: Support and assistance to the PM standard analysis team have continued, ensuring data consistency and providing help in result interpretation.
- *Ammonia uncertainty:* A full uncertainty quantification has estimated the share of the uncertainty in aviation-attributable health impacts that can be traced back to uncertainties in inventories of ammonia emissions.
- *Multi-scale adjoint modeling*: Scoping work was conducted for developing a multi-scale adjoint tool that will enable the calculation of impacts from emissions occurring outside of the current nested domains, at the global scale.

Major Accomplishments

During this period of performance, a validation of the tool in all of the operational geographical domain was performed. The tool was compared to calculations using the forward model of the global Chemical Transport Model GEOS-Chem. In addition, work has continued to enable higher resolution modeling over the European domain. Another key accomplishment during this period of performance was the quantification of the uncertainty in aviation-attributable health impacts that be linked to uncertainties in regional ammonia inventories. Finally, the tool was operationalized and packaged in a user-friendly MATLAB script, allowing the FAA to conduct air quality impacts analysis using up-to-date outputs from the air quality assessment tool.

Outreach Efforts

Results were presented at the 2018 ASCENT Spring and Fall meetings.

Student Involvement

Graduate students involved in this project are: Irene Dedoussi and Guillaume Chossière, PhD candidates in the Department of Aeronautics and Astronautics at MIT, and Kingshuk Dasidhakari, Masters student in the Department of Aeronautics and Astronautics at MIT.

Plans for Next Period

Over the next period of performance, we aim to improve our global impact assessment capabilities while quantifying key uncertainties in aviation's impacts on surface air quality. This includes novel applications of existing capabilities and the development of new capabilities, in order to both better characterize known uncertainties and to provide initial assessments of previously unquantified uncertainties. Data and model updated developed during the next period of performance will be packaged at the end of the year and passed to the FAA as updates to the MATLAB-based scripts provided during this period of performance. It will provide the FAA the ability to rapidly assess multiple aviation emissions scenarios in the context of uncertainties both internal and external to the aviation sector, as quantified by the work in this proposal. Following these overall objectives, we anticipate three major tasks to be undertaken by the ASCENT Project 20 team during the 2018/19 and 2019/2020 years.

Task 1 concerns the extension of the ASCENT 20 air quality assessment tool to account for high altitude aviation, including supersonic emissions. The adjoint model currently used for ASCENT project 20 to estimate sensitivity of population exposure to aviation was designed to capture the impacts of emissions within the troposphere and lower stratosphere. It is not yet capable of capturing impacts due to aviation at higher altitudes, particularly in the mid- or upper stratosphere, where supersonic aircraft would be expected to operate. The MIT Laboratory for Aviation and the Environment (LAE) has successfully extended the GEOS-Chem forward model, on which the adjoint is based, to simulate stratospheric chemistry and physics through the GEOS-Chem Unified Chemistry eXtension (UCX) (Eastham et al 2014). In order to accomplish this task, we will conduct a two-stage study to assess the impacts of projected supersonic aviation scenarios on surface air quality, including the differences in spatial pattern and in the timescale required to resolve the impacts. The first stage of the study will focus on single-case impact estimation using the validated forward model. The second stage of Task 1 will adapt and validate the adjointed version of the GEOS-Chem UCX model, which is currently under development at LAE for climate assessment purposes, to capture the sensitivity of air quality with respect to supersonic aviation.



Task 2 is an in-depth evaluation of the degree to which uncertainty in specific emissions related to non-aviation activities might affect the calculated impact of aviation. An initial estimate of the impact of uncertainty in ammonia emissions has revealed spatially heterogeneous relationships between ammonia emissions uncertainty and aviation emissions impacts. This pilot analysis has established a template for a broader assessment of these cross-sector second-order sensitivities, which are mathematically similar but functionally distinct from existing single-sector ("self") second-order sensitivities. In this task, we will use a combination of global and regional modeling to establish the degree of uncertainty which is propagated from background inventories of both anthropogenic ammonia, established during the previous project years as a key source of uncertainty in aviation's impacts, and in anthropogenic NO_x. This will require a thorough review of national- and regional-level uncertainties in emissions inventories for NO_x beyond the review for ammonia already underway.

For Task 3 we intend to package the sensitivity results from this year's and the previous years' efforts, to provide intuitive and consistent sensitivity matrices suitable for use in policy assessment. This includes not only the raw data but also MATLAB-based packages capable of accepting specific emissions scenarios and returning the expected air quality impacts. A central objective of this year's work would be to add multi-dimensional uncertainty quantification to the tool, including uncertainties in aviation emissions, uncertainty in background emissions of both ammonia and NO_x, and the impact functions themselves. This multi-dimensional assessment will be interpreted using a Monte Carlo analysis framework, which will provide the ability for any uncertainties already quantified through ASCENT project 20 to be propagated to the final impact estimate. Concurrent with this, we will provide an update to MIT's previous overview of the APMT-I Air Quality functionality in order to better reflect the latest air-quality-related functionalities. Ongoing work to enable European regional simulations, expected to be completed within the 2018-2020 period of performance, is included in this task.

References

Barrett, S. R. H., Britter, R. E., & Waitz, I. A. (2010). Global mortality attributable to aircraft cruise emissions. Environmental Science & Technology, 44(19), 7736–7742.

Beusen, A., Bouwman, A., Heuberger, P., Van Drecht, G., Van Der Hoek, K. (2008). Bottom-up uncertainty estimates of global ammonia emissions from global agricultural production systems. Atmos. Environ., 42 (2008), pp. 6067-6077

Eastham, S. D., D. K. Weisenstein, and S. R. H. Barrett (2014), Development and evaluation of the unified tropospheric-stratospheric chemistry extension (UCX) for the global chemistry-transport model GEOS-Chem, Atmos. Environ., 89, 52–63, doi:http://dx.doi.org/10.1016/j.atmosenv.2014.02.001

Eastham, S. D., & Barrett, S. R. H. (2016). Aviation-attributable ozone as a driver for changes in mortality related to air quality and skin cancer. Atmospheric Environment. https://doi.org/10.1016/j.atmosenv.2016.08.040

European Commission Joint Research Centre (JRC) and Netherlands Environmental Assessment Agency (PBL). (2014). Emission Database for Global Atmospheric Research (EDGAR), release EDGARv4.2 FT2012 [Data set]. Retrieved from http://edgar.jrc.ec.europa.eu

European Monitoring and Evaluation Program Centre on Emission Inventories and Projections (EMEP). WebDab Emissions Database. http://www.ceip.at/ms/ceip_home1/ceip_home/webdab_emepdatabase/reported_emissiondata/

Zhang, Q., Streets, D. G., Carmichael, G. R., He, K. B., Huo, H., Kannari, A., ... Yao, Z. L. (2009). Asian emissions in 2006 for the NASA INTEX-B mission. Atmospheric Chemistry and Physics, 9(14), 5131–5153.

Zheng, J.Y., Yin, S.S., Kang, D.W., Che, W.W., Zhong, L.J. (2012). Development and uncertainty analysis of a high-resolution NH_3 emissions inventory and its implications with precipitation over the Pearl River Delta region, China. Atmos. Chem. Phys., 12 pp. 7041-7058

Zhu, L., D. K. Henze, K. E. Cady-Pereira, M. W. Shephard, M. Luo, R. W. Pinder, J. O. Bash, and G.-R. Jeong (2013), Constraining U.S. ammonia emissions using TES remote sensing observations and the GEOS-Chem adjoint model, J. Geophys. Res. Atmos., 118, 3355–3368, doi: 10.1002/jgrd.50166.

Project 021 Improving Climate Policy Analysis Tools

Massachusetts Institute of Technology

Project Lead Investigator

PI: Steven R. H. Barrett
Raymond L. Bisplinghoff Professor of Aeronautics and Astronautics
Department of Aeronautics and Astronautics
Massachusetts Institute of Technology
77 Massachusetts Avenue, 33-316
Cambridge, MA 02139
+1 (617) 452-2550
sbarrett@mit.edu

co-PI: Florian Allroggen
Research Scientist
Department of Aeronautics and Astronautics
Massachusetts Institute of Technology
77 Massachusetts Avenue, 33-115A
Cambridge, MA 02139
+1 (617) 715-4472
fallrogg@mit.edu

University Participants

Massachusetts Institute of Technology

- P.I.: Steven R. H. Barrett, Florian Allroggen (co-PI)
- FAA Award Number: 13-C-AJFE-MIT, Amendment Nos. 004, 017, 024, 037, and 042
- Period of Performance: Aug. 1, 2014 to Aug. 31, 2020
- Tasks:
    1. Modeling the life-cycle impacts of methane and nitrous oxide;
    2. Enhance the spatial resolution of damages and benefits in APMT-IC;
    3. Analyze approaches for modeling physical impacts at increased spatial resolution in APMT-IC;
    4. Investigate state-of-the-art and reduced-order approaches for contrail and contrail-cirrus modeling;
    5. Support knowledge transfer.

Project Funding Level

$600,000 FAA funding and $600,000 matching funds. Sources of match are approximately $162,000 from MIT, plus 3rd party in-kind contributions of $114,000 from Byogy Renewables, Inc. and $324,000 from Oliver Wyman Group.

Investigation Team

Prof. Steven R. H. Barrett, Principal Investigator
Dr. Florian Allroggen, co-PI
Dr. Raymond Speth, co-I
Dr. Mark Staples, co-I
Dr. Sebastian Eastham
Carla Grobler (Ph.D. Student)



Project Overview

The objective of ASCENT Project 21 is to facilitate continued development of climate policy analysis tools that will enable impact assessments for different policy scenarios at global, zonal and regional scales and will enable FAA to address its strategic vision on sustainable aviation growth. Following this overall objective, the particular objectives of ASCENT 21 are (1) to continue the development of a reduced-order climate model for policy analysis consistent with the latest scientific understanding; and (2) to support FAA analyses of national and global policies as they relate to long-term atmospheric and environmental impacts.

In the current reporting period, these objectives have been addressed by: (i) extending the capabilities of the Aviation environmental Portfolio Management Tool – Impacts Climate (APMT-IC), specifically to assess the aviation fuel life-cycle impacts associated with life-cycle emissions of N_2O and CH_4; (ii) enhancing the spatial resolution of reported damages in the model; (iii) performing research investigating the regionalization of the physical atmospheric impacts; (iv) summarizing ongoing contrail research and propose a plan for development of a reduced-order contrail model; (v) facilitating knowledge transfer to FAA-AEE and other researchers.

Task 1 – Modeling the Life-cycle Impacts of Methane and Nitrous Oxide

Massachusetts Institute of Technology

Objective(s)

The objective of this task is to enhance the capabilities of APMT-IC in modeling the life-cycle impacts of alternative aviation fuels through adding emissions-to-impact pathways for methane and nitrous oxide (Stratton et al. 2011, Seber et al. 2014, Suresh 2016, Bond et al. 2014, Staples et al. 2014). The latest release of APMT-IC, version 24, already includes a simplified assessment module, which quantifies the life-cycle impacts in terms of 100-year global warming potential (GWP) CO_2 equivalents. Under this task, a more detailed model is developed and implemented which improves the accuracy of APMT-IC, particularly with regard to the magnitude and timescales of life-cycle emissions scenarios. As a result, the new version of APMT-IC does not only capture the long-term atmospheric and environmental impacts of in-flight emissions, but can also be applied to evaluate life cycle-related ground-level emissions. The flexibility of this modeling method also enables APMT-IC to model non-aviation methane, nitrous oxide, and carbon dioxide emissions scenarios.

Research Approach and Accomplishments

The new modeling capabilities were developed by leveraging recent work on the atmospheric response to methane and nitrous oxide (Meinshausen et al., 2011; Myhre et al., 2013). On the basis of this work, the impacts of the two climate forcers are modeled in APMT-IC through deriving atmospheric concentrations for all years under investigation using perturbation lifetimes (Myhre et al., 2013). More specifically, both the concentration due to the life-cycle emissions and background concentrations are quantified, with background concentrations being taken from Representative Concentration Pathway (RCP) scenarios.

To derive the radiative forcing impacts from both methane and nitrous oxide, the model implemented in APMT-IC now considers that both forcers lead to a direct radiative warming impact, with overlaps in radiative bands for methane, nitrous oxide, and carbon dioxide. As such, interaction effects are captured by using the radiative transfer function by Etminan et al. (2016). In addition, the indirect warming impacts of methane are computed using the methods described in Meinshausen et al. (2011). These methods capture the impacts resulting from increases in tropospheric ozone concentrations, additional stratospheric water vapor, and CO_2 impacts.

The results obtained from the newly implemented model were verified through comparisons to the literature. More specifically, impact magnitude and time responses were compared to results from the Model for Greenhouse Gas Induced Climate Change (MAGICC6) (Meinshausen et al., 2011), and the global warming potential was compared to results published in the IPCC Fifth Assessment Report (Myhre et al. 2013) and Cherubini et al. (2013). In both cases the implemented model was found to align with results in the literature.

These additional capabilities enable APMT-IC to not only evaluate aviation life-cycle emissions scenarios, but also to evaluate non-aviation emissions scenarios for ground emissions of methane, nitrous oxide, and carbon dioxide. In addition, while the previous life-cycle modeling capability in APMT-IC was capable of capturing life-cycle impacts in



accurate time scales, the current method is capable of capturing the impacts on their characteristic time scales. These new capabilities have already been applied in a paper accepted for publication in GCB Bioenergy. The paper illustrates the importance of capturing the emissions time scales, especially with regard to land use change emissions.

The code documentation was updated to include these new capabilities, which will be considered to be incorporated in a potential next release of APMT-IC (version 25).

Milestone(s)

Under this task, the team successfully implemented the new capabilities into APMT-IC, and presented the methods to the FAA. In addition, the novel modeling capabilities were used in a publication. As such, Task 1 was completed.

Publications

A paper titled *Using relative climate impact curves to quantify the climate impact of bioenergy production systems over time* was accepted to the journal GCB Bioenergy. The authors are Sierk de Jong, Mark Staples, Carla Grobler, Vassilis Daioglou, Robert Malina, Steven Barrett, Ric Hoefnagels, André Faaij, Martin Junginger. FAA support under ASCENT Project 1 and ASCENT Project 21 was acknowledged.

Outreach Efforts

The modeling approach was presented at ASCENT advisory board meetings (Spring 2018 and Fall 2018).

Student Involvement

The updates, validation and verification were completed by Carla Grobler (Ph.D. Student, MIT).

Plans for Next Period

During the next period, the literature will be surveyed continuously for updated methods and data.

References

Bond, J; Upadhye, A; Olcay, H; Tompsett, G; Jae, J; Xing, R; Alonso, D; Wang, D; Zhang, T; Kumar, R; Foster, A; Sen, S; Maravelias, C; Malina, R; Barrett, S; Lobo, R; Wyman, C; Dumesic, J; Huber, G. (2014). Production of renewable jet fuel range alkanes and commodity chemicals from integrated catalytic processing of biomass. *Energy & Environmental Science* 7(4), 1500-1523.

Cherubini, F., Bright, R.M. and Strømman, A.H., 2013. Global climate impacts of forest bioenergy: what, when and how to measure? *Environmental Research Letters* 8(1), p.014049.

Etminan, M. et al. (2016). Radiative forcing of carbon dioxide, methane, and nitrous oxide: A significant revision of the methane radiative forcing. *Geophysical Research Letters* 43(24), pp. 614–623. doi: 10.1002/2016GL071930.

Meinshausen, M., Raper, S. C. B. and Wigley, T. M. L. (2011). Emulating coupled atmosphere-ocean and carbon cycle models with a simpler model, MAGICC6 - Part 1: Model description and calibration. *Atmospheric Chemistry and Physics* 11(4), pp. 1417–1456. doi: 10.5194/acp-11-1417-2011.

Myhre, G. et al. (2013). Anthropogenic and Natural Radiative Forcing. In: Climate Change 2013: The Physical Science Basis. Contribution of Working Group I', in Stocker, T. F. et al. (eds) *Climate Change 2013: The Physical Science Basis. Contribution of Working Group I to the Fifth Assessment Report of the Intergovernmental Panel on Climate Change*. Cambridge, United Kingdom and New York, NY, USA: Cambridge University Press.

Seber, G., Malina, R., Pearlson, M. N., Olcay, H., Hileman, J. I., & Barrett, S. R. (2014). Environmental and economic assessment of producing hydroprocessed jet and diesel fuel from waste oils and tallow. *Biomass and Bioenergy* 67, 108-118.

Staples, M. D., Malina, R., Olcay, H., Pearlson, M. N., Hileman, J. I., Boies, A., & Barrett, S. R. (2014). Lifecycle greenhouse gas footprint and minimum selling price of renewable diesel and jet fuel from fermentation and advanced fermentation production technologies. *Energy & Environmental Science* 7(5), 1545-1554.

Stratton, R. W., Wong, H. M., & Hileman, J. I. (2011). Quantifying variability in life cycle greenhouse gas inventories of alternative middle distillate transportation fuels. *Environmental Science & Technology* 45(10), 4637-4644.

Suresh, P. (2016). Environmental and economic assessment of transportation fuels from municipal solid waste. SM Thesis, Massachusetts Institute of Technology.

Task 2 – Enhance the Spatial Resolution of Damages and Benefits in APMT-IC

Massachusetts Institute of Technology

Objective(s)

As shown by previous work, regional differences in global climate impacts can result from heterogeneities in current conditions, atmospheric responses and economic conditions, among others. For example, Tol (2009) shows that warm equatorial countries are projected to suffer the highest losses (measured as a percentage of their GDP) from climate change, while colder regions, such as eastern Europe or the former Soviet Union, might even benefit. The objective of this task is (i) to assess if there is consensus in the literature on how to derive the spatial distribution of benefits and damages; and (ii) if a suitable approach can be identified to amend APMT-IC for quantifying the distribution of global impacts.

Research Approach and Accomplishments

The Interagency Working Group on Social Cost of Greenhouse Gases used three models to quantify the global benefits and damages of a changing climate:

1. Dynamic Integrated Model of Climate and the Economy (DICE) (William Nordhaus)
2. Policy Analysis of the Greenhouse Effect (PAGE) (Chris Hope with John Anderson, Paul Wenman, and Erica Plambeck)
3. Climate Framework for Uncertainty, Negotiation and Distribution (FUND) (David Anthoff and Richard Tol)

Each of these models provide a regional break-down of benefits and damages. However, upon further investigation, no transparent documentation of the methods and assumptions for the regionalized models could be found, which is in line with the conclusions of the National Academies of Sciences (2017). Beyond that, Nordhaus (2017) compared the results of the regionalized benefit and damage models, and found little agreement in their results. As such, the project team concluded that there is currently insufficient scientific consensus on these top-down quantification approaches. In turn, regionalized benefit and damage models are not recommended for implementation into APMT-IC at this point.

However, recent work by Hsiang et al. (2017) quantified the US-based damages due to global mean surface temperature increases. The study uses a bottom-up approach where global mean surface temperature is translated to county-level changes in precipitation and temperature. The resulting benefits and damages are then quantified considering both market and non-market costs or benefits in agriculture yields, mortality, energy expenditure, labor changes, coastal damages, and crime. By computing the benefits and damages for different levels of global mean surface temperature changes, a US-based damage function is then derived. This damage function reasonably corresponds to the shape of the DICE damage function, although different approaches were followed to derive them.

Given reasonable similarity to DICE, the US-based damage function by Hsiang et al. (2017) was implemented into APMT-IC alongside the global damage model. As such, APMT-IC now outputs both global and U.S.-based benefits and damages.

To calculate the US-based benefits and damages, the temperature anomaly between preindustrial and the reference time period used by Hsiang et al. (2017) is determined. Using this data, temperature change as modeled in APMT-IC can be translated to temperature change for use in the US damage function and US damages can be estimated. Uncertainty at all levels of mean surface temperature is quantified by fitting continuous uncertainty distributions to the uncertainty estimates presented by Hsiang et al. for specific temperature changes. Finally, the US GDP Shared Socioeconomic pathway scenarios were incorporated into APMT-IC in an effort to infer total US-based benefits and damages.

Using this approach, we find a US-based social cost of carbon of $3 and $1 (per tonne of CO_2, 2007 USD) for aviation emissions in 2015 and for a 3% and 7% discount rate, respectively. According to our results, these US-based social cost of carbon values increase to $6 and $1.8 for aviation emissions in 2050. We note that due to differences in approaches between the global and the US-based model, these results should not be used to derive US damages as a fraction of global damages. In addition, the US-based damage function does not capture indirect economic impacts, e.g, from reduced trade, migration, and conflict.

The documentation of APMT-IC was updated to include this capability and underlying assumptions. The new capabilities will be considered for being incorporated in a potential next release of APMT-IC (version 25).



Milestone(s)
Modeling capabilities to compute the US benefits and damages were implemented into APMT-IC. The approach and results were presented to the FAA. As such, Task 2 is completed.

Outreach Efforts
The new modeling capability was presented at an ASCENT advisory board meeting (Fall 2018).

Student Involvement
The additional feature, and its verification and documentation were completed by Carla Grobler (Ph.D. Student, MIT).

Plans for Next Period
Continue to monitor new literature which attempts to provide a regionalized breakdown of global damage functions. As such, work on extensions of Task 2 is ongoing.

References
Hsiang, S. M. et al. (2017). Estimating economic damage from climate change in the United States. *Science* 356(6345), pp. 1362–1369. doi: 10.1126/science.aal4369.

National Academies of Sciences, Engineering, and Medicine. (2017). Valuing Climate Damages: Updating Estimation of the Social Cost of Carbon Dioxide. Washington, DC: The National Academies Press. doi: 10.17226/24651.

Nordhaus, W. D. (2017). Revisiting the social cost of carbon. *Proceedings of the National Academy of Sciences*, 114(7), pp. 1518–1523. doi: 10.1073/pnas.1609244114.

Tol, R. S. (2009). The economic effects of climate change. *The Journal of Economic Perspectives* 23(2), 29-51.

Task 3 – Analyze Approaches for Modeling Physical Impacts at Increased Spatial Resolution in APMT-IC
Massachusetts Institute of Technology

Objective(s)
The objective of this task is to study potential approaches for increasing the spatial resolution of radiative forcing impacts associated with aviation emissions in APMT-IC. Since APMT-IC is currently set up as a global model, global emissions are used as an input and globally averaged results are the model's main output. While this approach leads to reliable results for current-year assessments, it potentially biases results for future scenarios, which assume significantly changed aircraft technologies and/or traffic patterns. More specifically, biases due to changing traffic patterns can result from heterogeneities in atmospheric sensitivities. For example, NO_x emissions have been estimated to result in 4-5 times more tropospheric ozone formation per unit NO_x over the Pacific as compared to a unit of NO_x emissions over Europe or North America (Gilmore et al. 2013).

The objective of this task is to lay the groundwork for modeling the global impact due to changes in emissions region, and furthermore modeling regionalized temperature changes, and their impacts. This task should investigate literature on regionalized emissions-to-impacts pathways, and if sufficient scientific consensus is found, outline a concept for a regionalized version of APMT-IC.

Research Approach and Accomplishments
In a literature study, the ASCENT 21 team investigated the state-of-the-art for analyzing regional heterogeneities in the radiative forcing impacts associated with aviation emissions. For this purpose, two studies were found to provide particularly relevant insights. First, Fuglestvedt et al. (2010) present a review of regionalized physical impacts and find little agreement between the regionalized temperature responses. Second, more recent work by Lund et al. (2017) analyzes regionalized global warming potential and regionalized temperature potential of aviation emissions. They find global warming and global temperature potential vary by a factor of 2-4 between different source regions.



The global warming potentials by source region presented in Lund et al. (2017) can be used to derive an emissions region weighted global radiative forcing, which could, in turn be used to compute globally averaged temperature change. Because the resulting model would only be based on a single study, it is currently not being implemented in APMT-IC.

While studying potential implementation approaches for APMT-IC, the project team found that there is currently no conclusive evidence in the literature which could support reduced-order modeling of regionalized damages from regionalized temperature change. In turn, analyses of regionalized temperature change would currently be of little value within APMT-IC. As such, a model for regionalizing the temperature change impacts of aviation was not recommended for implementation at this point.

Milestone(s)
The literature study and model conception were completed.

Student Involvement
This preliminary research was completed by Carla Grobler (Ph.D. Student, MIT).

Plans for Next Period
Continue to follow current research which aims to model regional heterogeneities in atmospheric responses to aviation emissions. Additionally, continue to follow research to identify when regionalized damage functions become available that can translate regionalized temperature change to damages.

References
Fuglestvedt, J. S. et al. (2010). Transport impacts on atmosphere and climate: Metrics. *Atmospheric Environment* 44(37), pp. 4648–4677. doi: 10.1016/j.atmosenv.2009.04.044.

Lund, M. T. et al. (2017). Emission metrics for quantifying regional climate impacts of aviation. *Earth System Dynamics*, 8(3), pp. 547–563. doi: 10.5194/esd-8-547-2017.

Task 4 – Investigate State-of-the-Art and Reduced-order Approaches for Contrail and Contrail-Cirrus Simulations
Massachusetts Institute of Technology

Objective(s)
APMT-IC currently quantifies the radiative forcing impacts associated with contrails by scaling the overall impact derived in the ACCRI Phase 2 project (Brasseur et al., 2016) with fuel burn. This approach is consistent with other approaches in the literature (Fuglestvedt et al., 2010, Lund et al., 2016), but disregards a number of factors affecting contrail formation and persistence, including (i) differing geographical, diurnal, or seasonal distributions of flights, (ii) improved engine or fuel technologies, (iii) non-linearities between traffic growth and contrail formation; and (iv) changing climate conditions. As a result, if future emissions patterns differ from present day emissions, the contrail impacts will likely change without necessarily changing fuel burn numbers. The computational cost and complexity of detailed contrail models, which could consider these impacts, render such models infeasible to be included in a tool designed for informing decision-making like APMT-IC. Therefore, the objective of this task is to summarize the current state of contrail research, specifically at the MIT Laboratory for Aviation and the Environment (LAE), and to outline a plan for developing a reduced-order contrail model suitable for implementation in APMT-IC.

Research Approach and Accomplishments
Aircraft condensation trails, often referred to as contrails, are line-shaped ice clouds that form in the exhaust of aircraft engines. If linear contrails persist for several hours, they can grow and evolve into large, diffuse clouds called contrail-induced cirrus or contrail cirrus clouds. Overall, contrail and contrail-cirrus are potentially the largest component of the total radiative forcing (RF) from aviation (Lee et al. 2009).

LAE conducts research to model and understand contrail properties, and to quantify their global radiative forcing impact. Modeling contrail impacts through simulation involves scales ranging from the micron level for ice crystal microphysics to



the kilometer level for atmospheric bulk motion. In addition, LAE undertakes research to validate the model results by using satellite imagery to estimate contrail coverage.

A report summarizing contrail research at LAE was compiled. In addition, the factors which affect contrail properties were identified and a proposed plan for development of a reduce order contrail model was outlined.

Milestone(s)
A report outlining contrail research and a proposed approach to develop a reduced-order contrail model was finalized and handed over to the FAA. As such, Task 4 as proposed for the current period of performance was completed.

Publications
Internal report covering current state of contrail research and proposed plan for development of a reduced-order contrail model was compiled and made available to the FAA.

Student Involvement
The report was prepared by Carla Grobler with support from other members of LAE.

Plans for Next Period
If additional funding was provided, research could be pursued to develop a reduced-order contrail model as outlined in the report.

References
Brasseur, G.P., Gupta, M., Anderson, B.E., Balasubramanian, S., Barrett, S., Duda, D., Fleming, G., Forster, P.M., Fuglestvedt, J., Gettelman, A. and Halthore, R.N., 2016. Impact of aviation on climate: FAA's aviation climate change research initiative (ACCRI) phase ii. *Bulletin of the American Meteorological Society* 97(4), pp.561-583.

Fuglestvedt, J.S., Shine, K.P., Berntsen, T., Cook, J., Lee, D.S., Stenke, A., Skeie, R.B., Velders, G.J.M. and Waitz, I.A., 2010. Transport impacts on atmosphere and climate: Metrics. *Atmospheric Environment* 44(37), pp.4648-4677.

Lund, M. T. et al. (2017). Emission metrics for quantifying regional climate impacts of aviation. *Earth System Dynamics* 8(3), pp. 547–563. doi: 10.5194/esd-8-547-2017.

Task 5 – Support Knowledge Transfer
Massachusetts Institute of Technology

Objective(s)
The objective of this task is to support FAA analyses of national and global policies as they relate to long-term atmospheric impacts. APMT-IC version 24 builds upon the tool that was used to assess international aircraft and engine stringencies at CAEP 8, 9 and 10. Under ASCENT 21 (together with its predecessor, PARTNER 46), the ASCENT 21 team was directly involved in the analysis of all three standards. ICAO CAEP is currently considering the introduction of an nvPM-emission standard for international aviation, for which air quality impacts will be a driver of the cost-benefit-ratio, and for which trade-offs or co-benefits in climate are expected. While the analyses of the nvPM standard are conducted by a dedicated project team (ASCENT Project 48), the ASCENT 21 team was tasked to assist the ASCENT 48 team with the application of APMT-IC in order to ensure that inputs and outputs are handled correctly, assumptions are clearly stated, and outputs are correctly interpreted.

Furthermore, validation and verification of APMT-IC was performed by the ASCENT 22 project team during this reporting period. The objective under this task was to communicate all assumptions, methods, and to support the ASCENT 22 project team in using APMT-IC for validation and verification.

Research Approach and Accomplishments
APMT-IC and documentation were transferred to the ASCENT 22 team, and training was provided regarding the use of the model. Furthermore, regular meetings were held with members of the ASCENT 48 team to ensure APMT-IC is applied correctly.



Milestone(s)

Training has been provided to researchers as needed, including tools training for UIUC to review climate code capabilities, and for the ASCENT 48 team. As such, Task 5 as defined for this period of performance was completed.

Student Involvement

Carla Grobler (Ph.D. Student, MIT), who has been responsible for updating APMT-Impacts Climate to version 24 during the previous reporting period, provided training to a student UIUC, and has continued to provide support to the ASCENT 48 team.

Plans for Next Period

The ASCENT 21 team will continue to provide training and guidance on APMT-Impacts Climate as necessary.



Project 022 Evaluation of FAA Climate Tools: APMT

University of Illinois at Urbana-Champaign

Project Lead Investigator

Dr. Donald Wuebbles
Dept. of Atmospheric Sciences
University of Illinois
105 S. Gregory Street
Urbana, IL 61801
Tel: 217-244-1568
Fax: 217-244-4393
Email: wuebbles@illinois.edu

University Participants

University of Illinois at Urbana-Champaign
P.I.(s): Dr. Donald Wuebbles

- Period of Performance: October 16, 2017 to October 15, 2018
- Task(s):
    1. Evaluate version 24 of APMT
    2. Using the CESM global chemistry-climate model, update our earlier analyses of regional effects from aviation based on latitude bands and regions

Project Funding Level

Support from the FAA over this time period was $75,000 with an additional $75,000 in matching support, including about $10,000 from the University of Illinois, but also as in-kind support from Reading University.

Investigation Team

Dr. Donald Wuebbles: project oversight
Jun Zhang (graduate student): analyses of APMT and 3-D atmospheric climate-chemistry modeling analyses

Project Overview

The primary objective of this project was to evaluate the capabilities of the APMT-I model, particularly the Climate module, to ensure this FAA policy analysis tool uses the current state of climate science. Regional climate impacts of aviation were also evaluated using the 3D atmospheric climate-chemistry model. Findings from these studies were reported at several meetings and in special reports to the FAA.

Task 1- APMT-I Climate Evaluation and Review of Requirements Document

University of Illinois at Urbana-Champaign

Objective(s)

In this project, we act as a resource to FAA for analyses relating to metrics and to model development and evaluation of FAA modeling tools and datasets, with special emphasis on testing the Aviation Environmental Portfolio Tool (APMT) model and the further development and evaluation of its climate component to ensure that the underlying physics of the model is addressed properly. A specific focus of this project is on analyses of zonal and regional effects of aviation on climate and testing the resulting incorporation of such effects within APMT. As such, we want to make sure the APMT linking of aviation emissions with climate impacts and the representation of the various components of the cause-effect chain (i.e., from emissions to climate effect) properly represents the state-of-the-science.



Research Approach

We have evaluated APMT version 24 and provided the FAA with feedback and improvement for the future development. We have assessed the APMT v24 by looking into the entire emissions-to-impact pathways to ensure APMT represents each module correctly and then focused on the modules where the improvements can be made to enhance the whole model performance of APMT. The carbon module and temperature module are tested by looking at the response of aviation effect on the CO2 concentration, the radiative forcing on climate, and the change in temperature to an emission pulse and sustained emissions under low, mid and high future scenarios. The short-lived gas emissions effects module and the NOx-related effects have also been analyzed to ensure all aviation emissions are represented correctly based on the most recent findings, e.g., such as those from the FAA ACCRI program. We also are evaluating the APMT model following the cause-effect chain from aviation emissions to the resulting effects on climate. The project evaluates the APMT components relative to state-of-the-art modeling that fully considers the physics and chemistry important to the various processes. Our aim is to ensure that the physics and chemistry underlying the treatments in APMT are addressed properly based on our and others published modeling studies.

Milestone(s)

Evaluated the newly developed APMT v24 and sent report to FAA.

Major Accomplishments

Most relevant to this project is the evaluation we provided on APMT v24. We found some additional changes need to be made to improve the performance of this simplified climate model. We recommend that the water vapor be revised to separate the indirect from the direct effects to consider the longer lifetime of the indirect water vapor emission. Furthermore, the radiative forcing of NOx-related effects (O3-short, O3-long and CH4) in APMT should be updated to represent the most recent literature. As a result of making these changes, APMT should be better able to link the various components of aviation emissions with climate impacts relative to the findings from ACCRI. All in all, APMT v24 made significant progress compared to v23.

Publications

Zhang and Wuebbles, Evaluation of FAA Climate Tools: APMT. Report for the FAA, March 2018

Outreach Efforts

American Geophysical Union Fall Meeting – December 11-15, 2017 (Presentation)
ASCENT Advisory Committee Meeting – April 3-4, 2018 (Presentation)
ASCENT Advisory Committee Meeting – October 9-10, 2018 (Presentation)
Bi-weekly meeting with project manager Daniel Jacob

Awards

None

Student Involvement

Graduate Student: Jun Zhang
Ms. Zhang is responsible for the analyses and modeling studies within the project and leading the initial preparation of the project reports.

Task 2- Three-dimensional Atmospheric Climate-Chemistry Modeling Studies for Aviation Regional Effects on Climate

University of Illinois at Urbana-Champaign

Objective(s)

The aim in this work was to have a better understanding of the climate impacts from aviation emissions on a zonal and regional basis. Since the aviation emissions have significant spatial variability in the sign and magnitude of response, the strength of regional effects is highly likely hidden due to the global averaging of climate change. Thus, it can be important to look at the impact of aviation emission on climate on a regional scale as well as on the global scale. We continue to use a state-of-the-art three-dimensional chemistry-climate model to further our understanding of the chemistry and climate



effects from aviation emissions and to do our regional analysis and compare our results with the earlier findings. As part of this effort, we used CAM5-Chem and will now be using the new CAM6-Chem model, the atmospheric component of the Community Earth System Model (CESM). We plan to conduct a series of studies to evaluate aviation impact on climate both in 2006 and 2050. The ultimate goal of this project is to estimate the temperature change over specific regions of interest (e.g., the United States, Europe, and East Asia) resulting from aircraft emissions in 2006 and 2050.

Research Approach

In this study, the newest version of the NCAR chemistry-climate model Community Atmosphere Model (CAM-chem6) is being used to examine the regional climate effects based on 4 different latitude bands (90°S- 28°S, 28°S-28°N, 28°S-28°N, 60°N-90°N) and regions (contiguous United States, Europe and East Asia). We have also used existing CESM model results to derive the relationship between surface temperature change and radiative forcing change both on global and regional scale. Then this relationship will be applied to aviation emissions to calculate the regional temperature change using the regional radiative forcing simulated from CESM model. We are undergoing the development of the temperature and radiative forcing relationship.

Milestone(s)

We recently made the transition from CAM-chem5 to the new CAM-chem6 model (NCAR considers this model to be a major upgrade over previous versions of the global atmospheric model) to conduct high resolution one degree in latitude and longitude experiments. We will then derive temperature and radiative forcing change relationships based on the modeling studies. We already are laying out the exact plans for these analyses so that we go from emissions to regional temperature effects for aviation. A presentation of findings and discussion of progress is held with representatives from the FAA every two weeks.

Major Accomplishments

This project is currently on going. We have started to set up simulations on the newly released CAM-chem6 (the state-of-the-art climate-chemistry model) and at the same time we are develping the realtionships between the temperature change and radiative forcing using the exsiting CESM model results. Interim results (Figure 1) shows the annual surface temperature anomaly for both observation and model data in a 40 year period from 1975 to 2015. The dashed lines are the linear fit for observation and model data. Figure 1 indicates that the linear fit for observation and model data are very close both in global scale and regional scale, especially when you account for model noise and nature variability. The model has a good performance on simulating surface temperature change – we can now continue to develop the relationship between the surface temperature and radiative forcing change both globally and regionally.

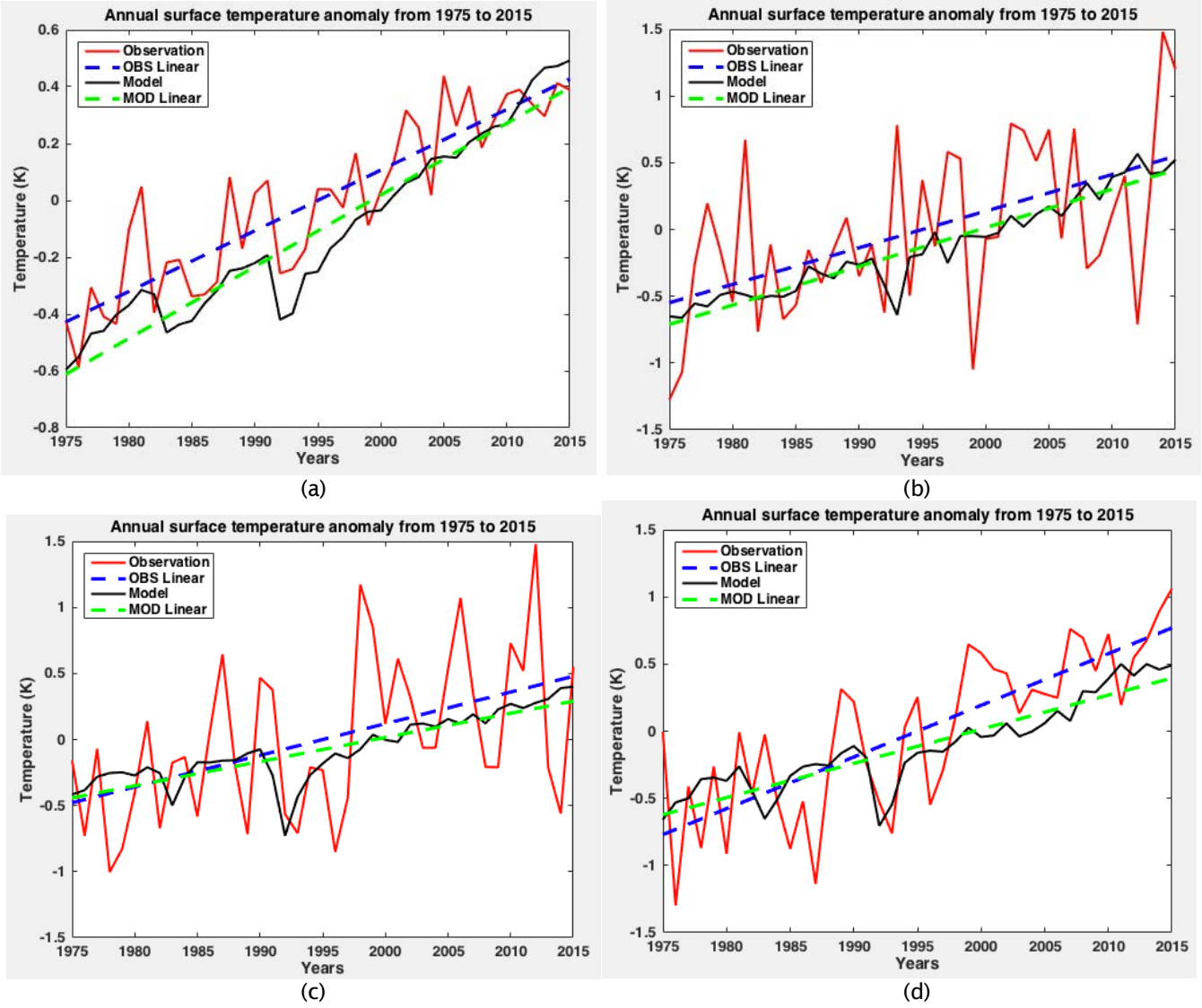
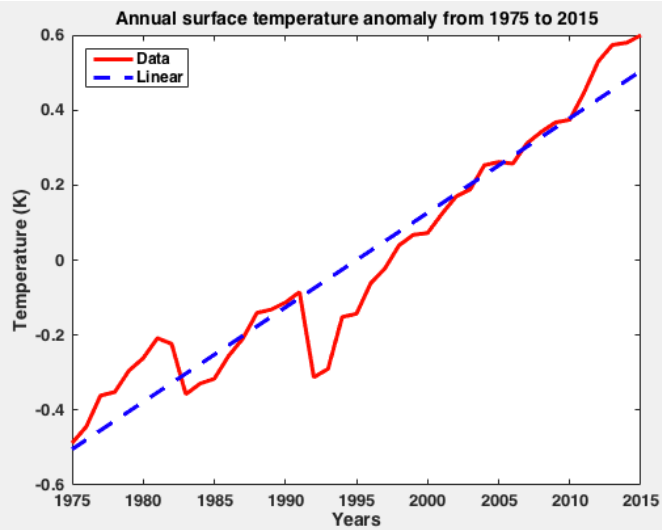
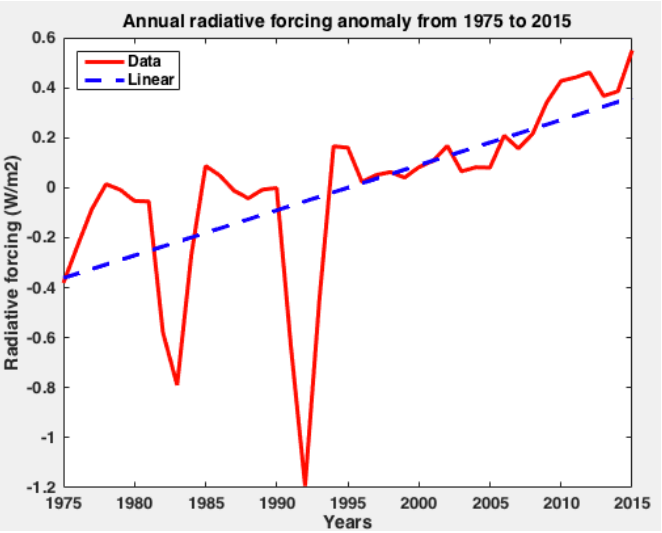


Figure 1. Annual surface temperature anomaly (degrees K) from 1975 to 2015 for (a) the global average; (b) Europe; (c) East Asia; (d) United States, respectively. The red and black lines are the observation data and model data, respectively; and the blue and green dash lines are the corresponding linear trend for observation and model data.

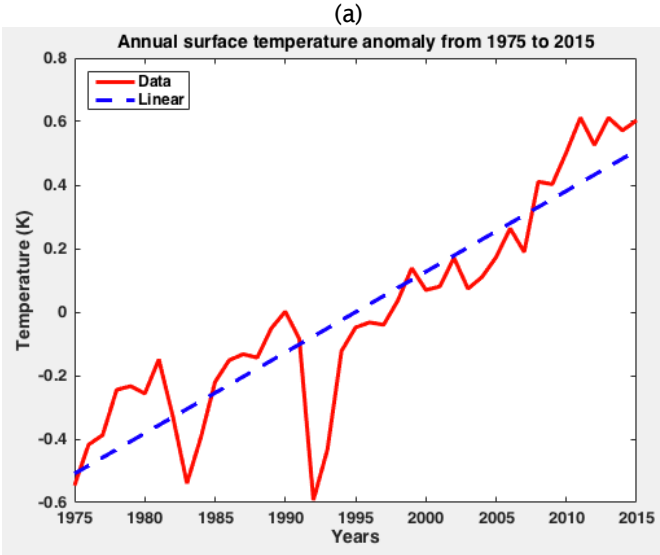
The annual surface temperature and radiative forcing anomaly from 1975 to 2015 is presented in Figure 2. The linear trend for surface temperature and radiative forcing anomaly for globe, United States and Europe (Figure (a), (b); (c), (d), (g). (h)) is both monotonic increase but at a different rate, which indicates that the surface temperature and radiative forcing change has positive relationship. As radiative forcing increase in time, the surface temperature will also increase. However, for East Asia (Figure 2 (e), (f)), as the radiative forcing decrease, the surface temperature increase, which shows an inverse relationship. This is due the large amount of aerosol emissions in East Asia region during 1975 to 2015 time period – the particles (not all but most) reflect solar radiation to cause cooling effect. However, reflection of sunlight by particles only happens during the day time, during the night time the greenhouse gases warming effects is dominant which results in the increase of the surface temperature. This will be accounted for in our analyses.


Annual surface temperature anomaly from 1975 to 2015
Data
Linear
Temperature (K)
Years

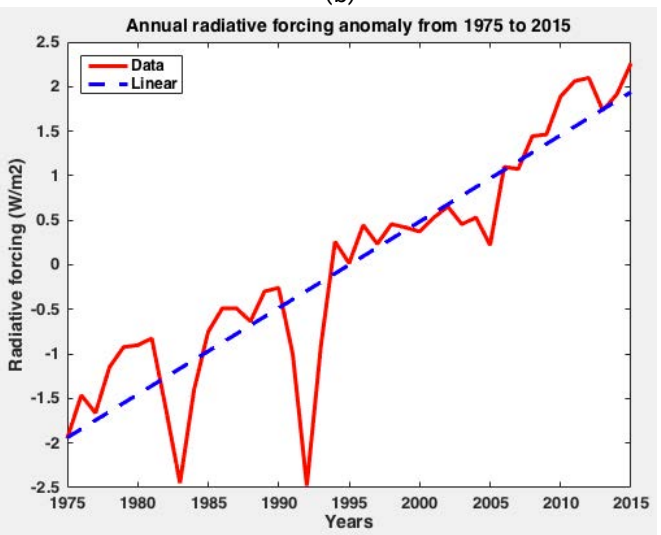
(a)


Annual radiative forcing anomaly from 1975 to 2015
Data
Linear
Radiative forcing (W/m2)
Years

(b)


Annual surface temperature anomaly from 1975 to 2015
Data
Linear
Temperature (K)
Years

(c)


Annual radiative forcing anomaly from 1975 to 2015
Data
Linear
Radiative forcing (W/m2)
Years

(d)

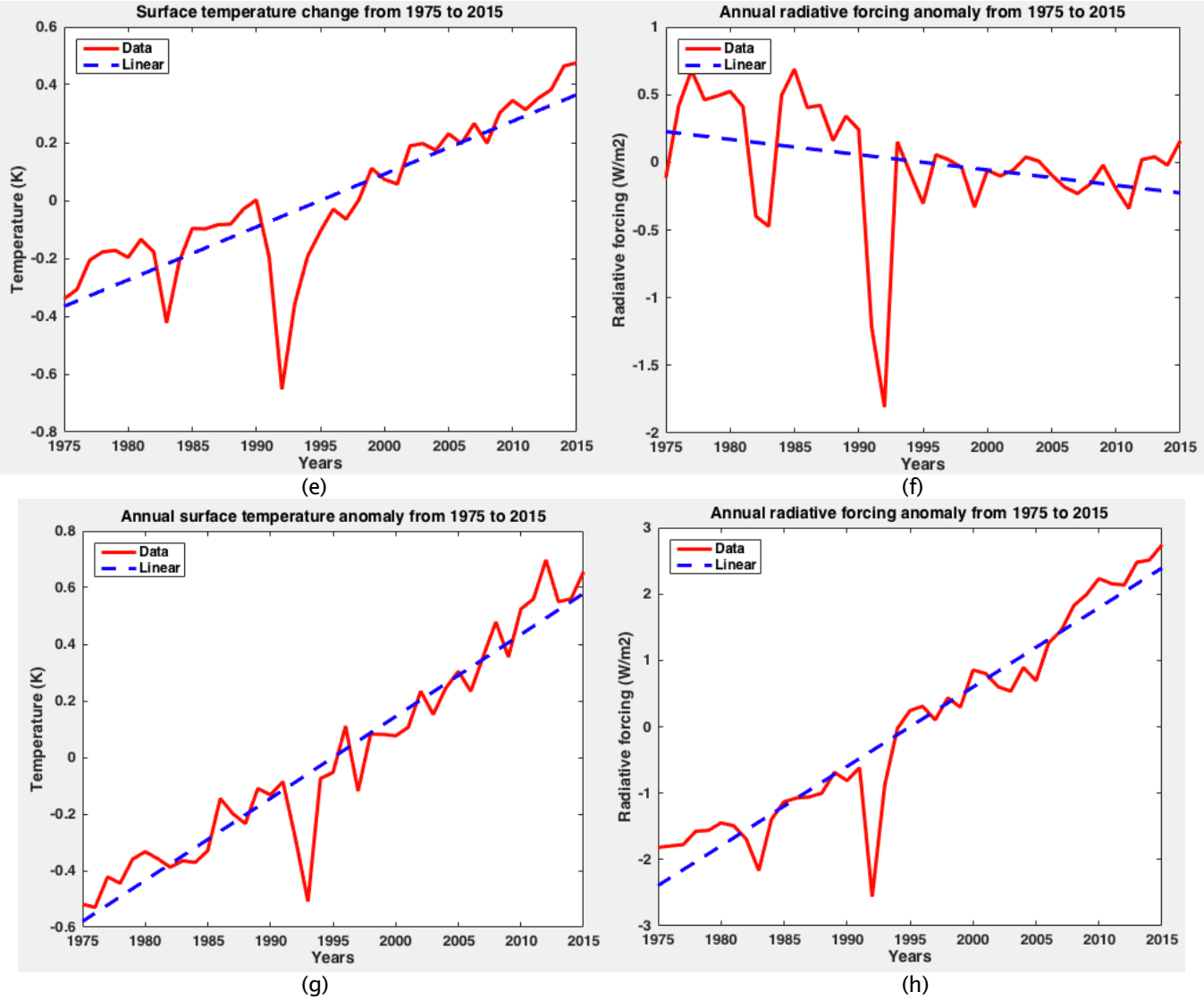


Figure 2. Annual surface temperature anomaly (degrees K) from 1975 to 2015 for (a) global average; (c) United States; (e) East Asia; (g) Europe. Annual radiative forcing anomaly from 1975 to 2015 for (b) global average; (d) United States; (f) East Asia; (h) Europe respectively. Red solid line is the model data; blue dash line is a linear fit.

Publications

Zhang, J., and D. Wuebbles, Report to the FAA on analyses of APMT v24. University of Illinois, 2018

Outreach Efforts

Results presented at several ASCENT meetings. Journal paper to expected from the regional aviation analyses.
Dr. Wuebbles made a special invited presentation on the history of the understanding of environmental effects from supersonic aircraft at a FAA sponsored meeting in spring 2018.

Awards

None



Student Involvement

Graduate student Jun Zhang is responsible for the analyses and modeling studies within the project and leading the initial preparation of the project reports.

Plans for Next Period

Continue doing regional analysis. The following aspects will be focused on in the next period:

1) Continue developing the relationship between surface temperature and radiative forcing change using the existing CESM model data – determine the appropriate approach to represent the radiative forcing change over East Asia;
2) Conducting model simulations to calculate the induced radiative forcing for aviation gases and particle emissions using the CAM-chem6 model;
3) Apply the developed relationship to aircraft emissions to obtain the aviation induced surface temperature change for both global and regional scales. The calculated aviation induced temperature change over four latitude bands will be compared with the temperature change calculated from CICERO approach, to evaluate the findings as a test of their and our methodologies;
4) Using the evaluated relationships, determine the change in temperature from aviation emissions (current and future projections) over various regions.
5) Prepare and submit report to the FAA and a corresponding journal paper.



Project 023 Analytical Approach for Quantifying Noise from Advanced Operational Procedures

Massachusetts Institute of Technology

Project Lead Investigator

R. John Hansman
T. Wilson Professor of Aeronautics & Astronautics
Department of Aeronautics & Astronautics
Massachusetts Institute of Technology
Room 33-303
77 Massachusetts Ave
Cambridge, MA 02139
617-253-2271
rjhans@mit.edu

University Participants

Massachusetts Institute of Technology

- P.I.(s): R. John Hansman
- FAA Award Number: 13-C-AJFE-MIT, Amendment Nos. 008, 015, 022, and 031
- Period of Performance: Oct. 28, 2014 to Aug. 31, 2018
- Task(s):
    1. Evaluate the noise impacts of flight track concentration or dispersion associated with PBN arrival and departure procedures
    2. Identify the key constraints and opportunities for procedure design and implementation of noise-minimizing advanced operational procedures
    3. Develop concepts for arrival and departure procedures that consider noise impacts in addition to operational feasibility constraints
    4. Analyze location specific approach and departure design procedures in partnership with impacted industry stakeholders
    5. Develop and propose a demonstration plan for new procedure designs through modeling and/or flight testing

Project Funding Level

Project Funding Level: $610,000 FAA funding and $610,000 matching funds. Sources of match are approximately $80,000 from MIT and $530,000 from Massachusetts Port Authority.

Investigation Team

Prof R. John Hansman (PI)
Greg O'Neill (Post Doctoral Researcher)
Luke Jensen (Graduate Student)
Jacqueline Thomas (Graduate Student)
Alison Yu (Graduate Student)



Project Overview

This project will evaluate the noise reduction potential from advanced operational procedures in the terminal (arrival and departure) phases of flight. The noise impact from these procedures is not well understood, or modeled in current environmental analysis tools, presenting an opportunity for further research to facilitate Air Traffic Management (ATM) system modernization. This project will leverage a noise analysis framework developed at MIT under ASCENT Project 23 to evaluate a variety of sample procedures. In conjunction, the project will contribute to the Memorandum of Understanding between the FAA and Massport to identify, analyze, and recommend procedure modifications at Boston Logan Airport.

Task 1- Evaluate the Noise Impacts of Flight Track Concentration or Dispersion Associated with PBN Arrival and Departure Procedures

Massachusetts Institute of Technology

Objective(s

This task evaluates the impact of flight track concentration arising from Performance-Based Navigation (PBN) procedure implementation and the potential noise mitigation impact of track dispersion. The effects of track concentration due to PBN procedure implementation have not been fully explored. While the potential benefits of PBN for flight efficiency and predictability are well understood, the resulting environmental impact has caused increased community awareness and concern over the procedure design process. Current methods and noise metrics do not provide adequate information to inform the policy decisions relating to noise concentration or dispersion due to PBN implementation.

In this task, models were used to evaluate noise concentration scenarios using a variety of metrics and procedure design techniques. Noise data from Massport was used to support the simulation effort. The impact of track dispersion was compared to potential community noise reduction through noise-optimal RNP procedure designs that avoid noise-sensitive areas and use background noise masking where possible.

Research Approach

- Evaluate the impact of noise dispersion directly through modeling of a dispersed set of flight tracks in AEDT
- Analyze population exposure impact using multiple metrics, including DNL and N_{above}
- Validate which metrics best capture the impacts of noise concentration and dispersion

Major Accomplishments

- Determined best metrics for analyzing noise impacts due to dispersion by evaluating which metrics best capture at least 80% of noise complaints from multiple airports and runways.
- Completed dispersion modeling method for multiple flight tracks from a single centerline route.
- Modeled and evaluated the impacts of dispersion in for several departure and arrival scenario examples at Boston Logan using the identified metrics that best captured noise complaints.

Task 2- Identify the Key Constraints and Opportunities for Procedure Design and Implementation of Noise-Minimizing Advanced Operational Procedures

Massachusetts Institute of Technology

Objective(s)

Arrival and departure procedure design is subject to physical, regulatory, and workload constraints. Procedures must be flyable by transport-category aircraft using normal, stabilized maneuvers and avionics. The procedures must comply with Terminal Instrument Procedures (TERPS) guidelines for obstacle clearance, climb gradients, and other limitations. The procedures must be chartable and work within the limitations of current Flight Management Systems. Advanced operational procedures must also be compatible with airport and air traffic control operations, avoiding workload saturation for air traffic controllers and pilots.



This task involved evaluating the key constraints impacting advanced operational procedures and opportunities to improve noise performance, identifying those that may impact design and implementation. This process involved collaboration with pilots, air traffic controllers, procedure designers, and community members. The task also considered current research and evidence on physical, psychological and social impacts of aircraft noise as well as emerging issues such as community perceptions of equity and the impact of overflight frequency on noise perception.

Research Approach

- Meet with key stakeholders in the implementation pathway to understand procedure development processes, timeline, and constraints.
- Research documentation on regulations and operational standards influencing new flight procedure development.
- Consult with stakeholders during candidate advanced operational procedure development to identify potential implementation obstacles.

Major Accomplishments

- Met with airport operators and airline technical pilots to discuss potential concepts for advanced operational procedures.
- Conducted follow-up meetings with ATC, Massport, FAA representatives, communities, and airline technical pilots to discuss initial procedure concepts.

Task 3- Develop Concepts for Arrival and Departure Procedures that Consider Noise Impacts in Addition to Operational Feasibility Constraints

Massachusetts Institute of Technology

Objective(s)

This task applied the findings from Task 2 to identify a set of generic constraints and procedures for designing feasible and flyable advanced operational procedures to minimize noise perception as measured by traditional metrics (e.g. 65 dB DNL) and alternate metrics that address noise concentration concerns introduced by PBN procedures and emerging equity issues. Given an understanding of technology capabilities and operational constraints, this task developed potential operational concepts and identified potential implementation pathways for both specific locations and generalizable operational concepts. Some of the approaches considered were;

- Lateral Track Management Approaches (e.g. Dispersion, Parallel Offsets, Equivalent Lateral Spacing Operations, Multiple Transition Points, Vectoring, High Background Noise Tracks, Critical Point Avoidance Tracks, etc.)
- Vertical/Speed Thrust Approaches (e.g. Thrust Tailoring, Steep Approaches, Delayed Deceleration Approaches, etc.)

In addition, procedures were identified and categorized for the noise reduction effort at Boston Logan Airport. These included “Block 1” procedures, which were characterized by clear predicted noise benefits, limited operational/technical barriers and a lack of equity issues, and “Block 2” procedures, which exhibited greater complexity due to potential operational and technical barriers as well as equity issues (defined as noise redistribution between communities).

Research Approach

- Use feedback from Task 2 to identify procedures with noise reduction potential
- Model procedures using AEDT and ANOPP for generic runways to evaluate noise impacts for candidate procedures on a single event and/or integrated basis
- Determine noise impacts based on multiple metrics that are location-agnostic (i.e. contour area) as well as location-specific (i.e. population exposure at specific runways)

Major Accomplishments

- Developed a set of generic approach and departure modifications using PBN and other techniques to take advantage of noise benefits from advanced procedures



- Identified key constraints for lateral, vertical, and speed profile redesign based on ATC operational guidelines and FAA procedure design criteria
- Modeled and showed the impacts of candidate vertical/speed thrust approaches that were within FAA procedure design criteria
- Identified and made recommendations for Block 1 procedures for assessment by the FAA for implementation at Boston Logan Airport
- Identified candidate Block 2 procedures for noise reduction at Boston Logan Airport

Task 4- Analyze Location Specific Approach and Departure Design Procedures in Partnership with Impacted Industry Stakeholders

Massachusetts Institute of Technology

Objective(s)

Advanced operational procedures may be particularly applicable for specific airports based on local geography, population density, operational characteristics, fleet mix, and local support for procedure modernization (among other factors). Specific procedures will be evaluated at a series of representative airports around the U.S. It is anticipated that this task will involve collaboration with multiple airports and air carriers on potential opportunities at locations which would benefit from advanced PBN procedures.

For the Boston Logan Airport noise reduction project, this task also involves collaboration with the FAA 7100.41 PBN working group, which is the initial operation evaluation group for new procedure design concepts.

Research Approach

- Coordinate with a specific airport operator to evaluate procedure design opportunities with noise reduction potential
- Work closely and communicate with impacted stakeholders throughout the procedure evaluation, design, and analysis process to ensure that key constraints and objectives are appropriate for the selected location on a procedure-by-procedure basis

Major Accomplishments

- Continued regular meetings and collaboration with Massport to finalize Block 1 procedure recommendations and to develop Block 2 arrival and departure procedures for analysis at Boston Logan Airport
- Performed detailed noise analysis for Block 1 and preliminary Block 2 arrival and departure procedure concepts that addressed community concerns, including population impact estimation based on 2010 census data and re-gridding methodology developed for this research
- Assisted with community outreach meetings about noise in the Boston area
- Presented at and collaborated with stakeholders during the FAA 7100.41 PBN working group meeting for evaluation of the Block 1 procedure concepts at Boston Logan Airport
- Modeled and assessed the noise impacts of adjusted Block 1 procedures that satisfied lateral position criteria as identified by the FAA 7100.41PBN working group meeting

Task 5- Develop and Propose a Demonstration Plan for New Procedure Designs Through Modeling and/or Flight Testing

Massachusetts Institute of Technology

Objective(s)

The noise impact of advanced operating procedures must be validated in terms of operational acceptability (crew workload, safety, precision, controller workload, etc.) and noise impact. This task involved the generation of a testing plan for high value candidate advanced operational procedures developed in Task 4. Test plans considered included flight simulator studies, noise modeling, initial discussions of flight testing, and noise monitoring plans for newly-implemented procedures.



Research Approach

- Document procedure recommendations thoroughly and unambiguously so that simulator or flight trials are possible
- Meet with airline technical pilots and representatives from aircraft manufacturers to discuss operational constraints and test opportunities
- Develop test plans and protocols for potential flight trials
- Develop test plans and protocols for potential noise measurement campaigns
    - Specific flight test locations
    - Operational field measurements

Major Accomplishments

- Coordinated with airlines, Massport, and a major aircraft manufacturer to discuss objectives and potential strategies for possible noise measurement campaigns for reduced-speed departure procedures
- Published Block 1 procedure recommendations for specific flight procedures at Boston Logan that could be implemented for noise reduction as a result of feedback from several stakeholders

Publications

- "Block 1 Procedure Recommendations for Logan Airport Community Noise Reduction," 2017. Link: http://hdl.handle.net/1721.1/114038
- "Framework for Analyzing Aircraft Community Noise Impacts of Advanced Operational Flight Procedures," *Submitted for Review, Journal of Aircraft*, 2018.

Outreach Efforts

9/27/2017: Poster to ASCENT Advisory Board
12/05/2017: Call with Boeing to Discuss Procedure Noise Impact Validity
03/16/2018: Discussion with MSP Airport About Metrics
4/04/2018: Poster to ASCENT Advisory Board
05/07/2018: Presentation to FAA 7100.41 PBN Working Group
06/24/2018: Discussion with Air Traffic Controllers about Dispersion Concepts
7/23/2018: Briefing to FAA Joint University Program research update meeting
10/09/2018: Poster to ASCENT Advisory Board
11/08/2018: Presentation to Airline Industry Consortium
Numerous community meetings
Numerous briefings to politicians representing Eastern Massachusetts (local, state, and federal)
Briefing to FAA Management Advisory Council
In-person outreach and collaboration with Massport, operator of Boston Logan Airport and ASCENT Advisory Board member

Awards

None

Student Involvement

Graduate students have been involved in all aspects of this research in terms of analysis, documentation, and presentation.

Plans for Next Period

The next phase of this project will involve continued outreach to stakeholders impacted by implementation of advanced operational procedures, including airlines, airports, air traffic controllers, the FAA, and communities. Specific procedures that have significant operational or equity challenges such as steep approaches, delayed gear approaches, and flight track dispersion will continue to be evaluated in a generic sense as well as at specific airports of interest, including Boston Logan Airport and any other locations agreed upon by the project team and FAA program managers. For the Boston Logan Airport noise reduction project, this will also include the finalization and publication of Block 2 procedure concepts. This procedure evaluation process is expected to inform recommendations to airport operators, airlines, and the FAA to develop noise-mitigating advanced operational procedures at specified locations in the NAS.



Project 024(B) PM Emission Database Compilation, Analysis and Predictive Assessment

The Pennsylvania State University, GE U.S. Aviation

Project Lead Investigator

Randy L. Vander Wal
Professor, Energy and Mineral Engineering, Materials Science and Engineering
John and Willie Leone Family Dept. of Energy and Mineral Engineering
Penn State University 104 Hosler Bldg.
814-865-5813
ruv12@psu.edu

University Participants

The Pennsylvania State University

- P.I.(s): Randy L. Vander Wal, Professor, Energy and Mineral Engineering, Materials Science and Engineering
- FAA Award Number: Grant 12148585, Amendment No. 13-C-AJFE-PSU-019
- Period of Performance: Aug. 1st, 2016, July 31st, 2017
- Task(s):
    1. Test for improved accuracy by separating the temperatures associated with nvPM formation and oxidation. Presently the ImFOX kinetic expression uses one temperature at the exit of the combustor as representing the global temperature. The accuracy of T4 is confirmed by GE cycle deck calculations and consistent with the Brayton thermodynamic cycle for the engine. Yet for RQL style combustors soot formation necessarily occurs near an estimated $\varphi \sim 2$ while oxidation occurs under lean conditions, $\varphi \sim 0.9$. Such differences suggest different temperatures as better representing nvPM formation and oxidation regions.
    2. Assess ACCESS II test procedure upon engine conditions at cruise. A key difference between ground and cruise altitude is the ram effect at cruise and lower (external) pressure. These conditions alter the air-to- fuel ratio and hence while the form of the ImFOX relation is uniform between ground and cruise, different AFR relations may be necessary to capture these effects. With guidance from GE Aviation and their cycle calculations one can assess whether two separate or one unified AFR relations is sufficient – the latter then simplifying ImFOX use.
    3. Evaluate ASAF as the global scaling factor in the ImFOX relation. The ASAF relation was formulated by MIT as an empirical correlation of nvPM across all available engine emissions data. It is based upon aromatic content as the driving parameter for carbon aerosol emission. The MIT consensus is that the ASAF serve as global scaling factor for the ImFOX relation. This will be evaluated by comparison to measured nvPM from JP-8 and blends between conventional and alternative fuels.
    4. Investigate alternative representations to capture fuel composition effects for alternative fuels. Given the limitation of the present ASAF relation a more encompassing metric to capture fuel compositional effects is required. Alternative fuels do not have aromatic content but do have considerable and varying proportions of cyclic and normal paraffins. This introduces a hydrogen variation as well as C/H variation. Blended fuels will contain aromatics as carry-over from the original petroleum component. However, naphthalene is currently considered to contribute disproportionately to soot formation with current FAA interest being to remove it from fuels. Such twists necessitate a more encompassing relation than ASAF to represent the different and varying fuel component classes. The fuels used in AAFEX I: JP-8, coal and natural gas based FT fuels and 50:50 blends with JP-8 encompass a range of aromatic and hydrogen contents for which EI(BC) plots are linear in semi-log format. Such data suggests that either or both of these fuel factors may be incorporated into the ImFOX relation in the formation pre-factor. These alternative fuel dependencies will be tested against the field campaign data and compared to the ASAF relation across engine thrusts.
    5. Evaluate the ImFOX relation against the ACCESS II flight data from NASA for nvPM. Presently ground based emission levels are scaled by the Doppelheuer and Lecht (DL) relation to estimate cruise EI(BC). This approach imposes redundancy as the DL relation is a kinetic based expression that then duplicates the kinetic rates



explicit in the ImFOX relation. Our remedy is to avoid this scaling step by developing a direct predictive relation that does not require scaling or correction factors between ground and cruise. Using cycle deck data from GE Aviation, accurate engine conditions of AFR and Tfl are identified and relationships with thrust can be developed. This then permits true evaluation of the ImFOX relation – without skew by inaccuracies in engine operating conditions – an aspect that has plagued and limited prior such efforts.

6. Validate the ImFOX for other engines in the CFM class. As shown by our prior work, with guidance from cycle deck calculations, engine conditions may be accurately modeled known and hence comparison of ImFOX to measured nvPM provides a true assessment of the ImFOX predictive ability. Comparison to the CFM56-3B engine is planned given presently available test data for this engine and with cycle deck calculations provided by our GE partners.

Project Funding Level

FAA funding: $75,000

GE Aviation is the Industrial Partner supplying matching funds, level $75,000, from an original commitment of $1,724895 available to the FAA COE AJFE ASCENT program, administered through Washington State University.

Investigation Team

Professor Randy L. Vander Wal, Penn State EME Dept., with responsibilities for project management, reports, interfacing with FAA program manager, and mentoring the graduate student supported on this project.
Mr. Joseph P. Abrahamson, graduate student. Responsibilities include data assembly, analysis and predictive relation assessment, as integral towards completion of a Ph.D. program.

Project Overview

The recently developed FOX method removes the need for and hence uncertainty associated with (SNs), instead relying upon engine conditions in order to predict BC mass. Using the true engine operating conditions an improved FOX (ImFOX) predictive relation was developed. Necessary for its implementation are its development and validation to estimate cruise emissions and account for the use of alternative jet fuels with reduced aromatic content. Refinement by incorporating separate, independent temperatures for fuel-rich and fuel-lean regions of the combustor will be evaluated against another CFM engine. Comparison to measured nvPM at cruise, to EI(BC) from conventional and alternative fuels across thrust will critically test the ImFOX tool predictive ability with positive results then aiding its adoption for EI(BC) estimates at ground and cruise with varied fuel compositions.

Tasks

1. Test for Improved Accuracy by Separating the Temperatures Associated with nvPM Formation and Oxidation
2. Assess ACCESS II Test Procedure Upon Engine Conditions at Cruise
3. Evaluate ASAF as the Global Scaling Factor in the ImFOX Relation
4. Investigate Alternative Representations to Capture Fuel Composition Effects for Alternative Fuels
5. Evaluate the ImFOX Relation Against the ACCESS II Flight Data from NASA for nvPM
6. Validate the ImFOX for Other Engines in the CFM Class

Objective(s)

1. Develop a predictive relation for nvPM at ground.
2. Develop a predictive relation for nvPM at cruise.
3. Include fuel composition effects for alternative fuels (absent aromatics and naphthalenic compounds) and their



blends with conventional fuels.
4. Incorporate thrust dependence into the predictive tool.

Research Approach

Jet engine aircraft exhaust contains combustion byproducts and particulate matter in the form of non-volatile particulate matter (nvPM). Black carbon (BC) is used synonymously for nvPM throughout this paper. Aircraft cruise emissions are the only direct source of anthropogenic BC particles at altitudes above the tropopause.[1] Black carbon aerosols are strong solar radiation absorbers and have long atmospheric lifetimes.[2] Therefore, BC results in positive radiative forcing and is believed to be the second largest contributor to climate change.[3] Additionally, upper troposphere and lower stratosphere BC particles contribute to climate forcing indirectly by acting as ice nucleation sites and cloud activators.[4-6] With regard to human health, a link between cardiopulmonary diseases and carbonaceous black particulate matter has recently been suggested.[7] As concern for human health risks and environmental impacts caused by aviation BC emissions increases, emission reduction strategies will need to be implemented. Predictive tools capable of accurately estimating BC emissions from the current in-service fleet will be needed for the next decades to quantify atmospheric BC inventory from aviation.

Current models do not accurately predict BC emissions. The First Oder Approximation-3 (FOA3) methodology is used worldwide for estimating BC emissions within the vicinity of airports.[8] The FOA3 was endorsed by the (ICAO)[9] in February 2007 and relies on a measured SN to predict BC emission. Black carbon is most often reported as an emission index of black carbon (EI_{BC}), reported as milligrams of BC emitted per kilogram of fuel combusted. Due to inaccuracies in measuring low SNs produced by modern high bypass ratio engines, the FOA3 and its modifications are unreliable. Recently a kinetic model based on formation and oxidation rates termed the FOX method was reported.[10] The FOX does not require input of a SN, instead the input variables are engine conditions. Hence, the FOX avoids the measurement error built into the FOA3. However, the FOX is fuel independent and cannot be applied to predict EI_{BC} from alternative fuels and alternative fuels blended with conventional jet fuels. Recently, a relation, the Approximation for Soot from Alternative Fuels (ASAF) has been developed to predict BC from alternative fuels relative to conventional fuel BC emissions.[11] Both the FOA3 and the FOX methods are designed to predict EI_{BC} at ground level, which is important for assessing human health concerns at and in the vicinity of airports, however, it is the cruise EI_{BC} that is of the most importance in determining the role aviation BC plays on the Earth's radiative balance. The current practice to arrive at a predicted cruise EI_{BC} is to scale ground values with an additional kinetic type expression, the Dopelheuer and Lecht relation.[12] At the time the Döpelheuer and Lecht relation was developed there were limited cruise BC emission measurements. The available data was not representative of real aviation emissions because the aircraft operated at reduced weight and velocities compared to regular operation.[13]

In our prior work, current predictive methods were evaluated for accuracy by comparison to over a decade's worth of field campaign data collected by the National Aeronautics and Space Administration's (NASA) Langley Aerosol Research Group with inclusion of cruise data.[14] An improved semi-empirical method was developed. Accurate engine condition relations were developed based on proprietary engine cycle data for a common rich-quench-lean (RQL) style combustor. In the forthcoming work predictive relations will be developed for alternative fuels and fuel blends as well as a direct cruise prediction. The intent is to provide an improved method to calculate EI_{BC} reductions from the use of alternative fuels.

References

Peck, J.; Oluwayemisi, O; Wong, H; Miake-Lye, R. An algorithm to estimate cruise black carbon emissions for use in developing a cruise emissions inventory. J. Air Waste Manage. Assoc. 2013, 63, 367-375.

Lee, D. S.; Fahey, D. W.; Forster, P. M.; Newton, P. J.; Wit, R. C. N.; Lim, L. L.; Owen, B.; Sausen, R. Aviation and global climate change in the 21st century. Atmos. Environ. 2009, 43, 3520-3537.

Bond, T.; Doherty, S.; Fahey, D.; Forster, P.; Berntsen, T.; DeAngelo, B.; Flanner, M.; Ghan, S.; Karcher, B.; Koch, D.; Kinne, S.; Kondo, Y.; Quinn, P.; Sarofim, M.; Schultz, M.; Schulz, M.; Venkataraman, C.; Zhang, H.; Zhang, S.; Bellouin, N.; Guttikunda, S.; Hopke, P.; Jacobson, M.; Kaiser, J.; Klimont, Z.; Lohmann, U.; Schwarz, J.; Shindell, D.; Storelvmo, T.; Warren, S.; Zender, C. Bounding the role of black carbon in the climate system: A scientific assessment. J. Geophys. Res.: Atmos. 2013, 118, 5380-5552.

Haywood, J. M.; Shine, K. P. The Effect of Anthropogenic Sulfate and Soot Aerosol on the Clear-Sky Planetary Radiation Budget. Geophys. Res. Lett. 1995, 22, 603-606.

Karcher, B.; Peter, T.; Biermann, U. M. Schumann, U. The Initial Composition of Jet Condensation Trails. J. Atmos. Sci.1996, 53, 3066-3083.

Heymslield, A. J.; Lawson, R. P.; Sachse, G. W. Growth of Ice Crystals in Precipitating Contrail. Geophys. Res. Lett. 1998, 25, 1335-1338.

Pope, C. A.; Dockery, D. W. Health effects of fine particulate air pollution: Lines that connect. J. Air Waste Manage. Assoc. 2006, 56, 709-742.
Wayson, R. L.; Fleming, G. G.; Lovinelli, R. Methodology to estimate particulate matter emissions from certified commercial aircraft engines. J. Air Waste Manage. Assoc. 2009, 59, 91-100.
ICAO. Airport Air Quality Guidance Manual; International Civil Aviation Organization: Montreal, Canada, 2011.
Stettler, M. E. J.; Boise, A. M.; Petzold, A.; Barrett, S. R. H. Global civil aviation black carbon emissions. Environ. Sci. Technol. 2013a, 47, 10397-10404.
Speth, R. L.; Rojo, C.; Malina, R.; Barrett, S. R. H. Black carbon emissions reductions form combustion of alternative fuels. Atmos. Environ. 2015, 105, 37-42.
Döpelheuer, A.; Lecht, M. Influence of engine performance on emission characteristics. In RTO AVT Symposium on Gas Turbine Engine Combustion Emissions and Alternative Fuels; Lisbon, Portugal, 1998; p. RTO MP-14.
Schumann, U.; Arnold, F.; Busen, R.; Curtius, J.; Karcher, B.; Kiendler, A.; Petzold, A.; Schlager, H.; Schröder, F.; Wohlfrom, H. Influence of fuel sulfur on the composition of aircraft exhaust plumes: The experiments SULFUR 1-7. J. Geophys. Res. 2002, 107, 4247.
Moore, R.; Shook, M.; Beyersdorf, A.; Corr, C.; Herndon, S.; Knighton, W.; Miake-Lye, R.; Winstead, S.; Yu, Z.; Ziemba, L.; Anderson, B. Influence of Jet Fuel Composition on Aircraft Engine Emissions: A synthesis of aerosol emissions data from the NASA APEX, AAFEX, and ACCESS missions. Energy Fuels 2015, 29, 2591-2600.

Milestone(s)

Milestone	Planned Due Date
1. Comparison of ImFOX predictions for nvPM at cruise altitude and engine operating conditions to measured values from ACCESS II.	Sept. 30th, 2016
2. Develop a predictive relation for nvPM at cruise.	Dec. 30th, 2016
3. Include fuel composition effects for alternative fuels (absent aromatics and naphthalenic compounds) and their blends with conventional fuels.	March 30th, 2017
4. Incorporate thrust dependence into the predictive tool.	June 30th, 2017
5. Final report	July 30th, 2017

Major Accomplishments

Overview

Aviation black carbon (BC) emissions impact climate and health. Inventory estimates are essential to quantify these effects. These in turn require a means of estimating BC emission indices from jet aircraft. The first order approximation (FOA3) currently employed to estimate BC mass emissions under predicts BC emissions due to inaccuracies in measuring low smoke numbers (SNs) produced by modern high bypass ratio engines. The recently developed Formation and Oxidation (FOX) method removes the need for and hence uncertainty associated with (SNs), instead relying upon engine conditions in order to predict BC mass. Using the true engine operating conditions from proprietary engine cycle data an improved FOX (ImFOX) predictive relation is developed. Still, the current methods are not optimized to estimate cruise emissions or account for the use of alternative jet fuels with reduced aromatic content. Here improved correlations are developed to predict engine conditions and BC mass emissions at ground and cruise altitude. This new ImFOX is paired with a newly developed hydrogen relation to predict emissions from alternative fuels and fuel blends. The ImFOX is designed for rich-quench-lean style combustor technologies employed predominately in the current aviation fleet.

Preface to Task Progress

Given the dependence of task 5 upon the combustor temperature (task 1), AFR, (task 2), evaluation of the ASAF as a global factor for fuel effects (task 3) and evaluation of alternative measures of fuel composition, e.g. C/H ratio (task 4), tasks are reported in order as initial tasks represent key engine condition whose values must be determined prior to assessing the ASAF and C/H ratio methods for incorporating fuel dependence. Last, task 6 is then reported for comparison of ImFOX predictions to nvPM (EI_{BC}) from another RQL style combustor to evaluate the transferability and applicability of the predictive tool for other combustors in the current fleet.



Rationale for a Singular Predictive Tool for EI_{BC} from RQL style combustors – Improved Engine Condition Relations
In this section engine conditions required as inputs for the improved FOX (ImFOX) expression are more accurately provided in the form of predictive relations based on proprietary cycle deck calculations for a common RQL combustor. Aerosol emissions from the NASA campaigns: Aircraft Particle Emissions eXperiments (APEX-I)[1,2]. Alternative Aviation Fuel Experiments I and II (AAFEX-1, AAFEX-II)[3,4]. Alternative-Fuel Effects on Contrails & Cruise EmiSSions I and II (ACCESS-I, ACCESS-II)[5], are from a Douglas DC-8 aircraft equipped with four CFM56-2C turbo fan engines. Although, this engine is an older design it is a high-bypass engine and serves as the basis for the whole engine family employed by thousands of commercial and military aircraft worldwide. The EI curves from five of the six RQL style combustors tested during APEX-III [6-8] followed a common distorted U-shaped curve[9], with upturns both at low (idle) and high (take-off) thrust levels. (The exception was the Rolls-Royce engine RB211-535E4-B with 40,100 lbs. maximum thrust, which has a BC emission profile peaking at 65% of the maximum thrust and deceased emissions thereafter.) Therefore, it appears the relationships developed here are considered applicable for a majority of rich-burn, quick-quench, lean-burn (RQL) style combustors. Only a select few engine conditions are addressed in this section. This is intentional as the goal is to simplify the calculations needed to predict EI_{BC}. For the relations developed here, the only needed input is the fuel flow rate from which all other engine conditions as input for the ImFOX expression can be calculated.

Task 1- Test for Improved Accuracy by Separating the Temperatures Associated with nvPM Formation and Oxidation

The Pennsylvania State University

Flame Temperature, T_{fl}. Flame temperature is arguably the most important variable as it appears in both exponential terms in both the FOX and the Döpelheuer and Lecht scaling relation. Several T_{fl} predictive methods have been developed in addition to the one currently used for the FOX expression, Equation-7. The common practice is to predict a T_{fl} using a linear relationship to T_3. Whereas Equation-7 assumes that 90% of the incoming sensible heat from the hot air leaving the compressor, T_3, adds to a stoichiometric adiabatic flame temperature of 2120 K. A common alternative flame temperature predictor for an RQL style combustor based on T_3 is given in Equation-1.[10]

$$T_{fl}[K] = 0.6T_3 + 1800 \quad [1]$$

This method assumes that 60% of the initial air temperature is converted to flame temperature and that the flame temperature without this addition is that of a fuel rich flame at 1800 K. Considering that the primary zone of an RQL combustor runs fuel rich for flame stabilization, Equation-1 is a more realistic flame temperature predictor to determine the primary zone flame temperature. However, the only variable in either flame temperature predictor is T_3 and since the AFR is a function of thrust the second term should also be variable with relation to AFR, and hence thrust (given flame temperature dependence upon stoichiometry, or AFR). However, since this localized AFR as a function of thrust is proprietary and not readily determined we have elected to use the flame temperature at the back of the combustor (T_4) in place of primary zone flame temperature. Using T_4 for the flame temperature is logical considering that the AFR being used is also from the back of the combustor as a global average of the processes occurring in the formation and oxidation regions of the combustor. Additionally, T_4 is readily calculated by the engine cycle deck, yielding Equation-2.

$$T_4[K] = 490 + 42{,}266FAR \quad [2]$$

There is a strong correlation between T_3 and T_4, the Pearson r correlation value is 0.966. However, it was not selected in the T_4 relation because there is a much stronger correlation between T_4 and fuel-air-ratio (FAR), Pearson r value of 0.995, but more importantly for the fact that an explicit AFR dependence accounts for the expected dependence of T_{fl} upon stoichiometry. Additionally, T_3 is an engine specific parameter that may not be readily available in all cases. Equation-2 accurately predicts T_4 at both ground and cruise. Given the success of this semi-empirical T_4 calculation based on FAR, a thermodynamic basis was evaluated. The thermodynamic Air Standard Brayton Cycle is applied to a jet engine in the SI. Two equations are required to define this cycle. The first is the definition of the polytropic compressor efficiency that is currently used to find combustor inlet temperature, T_3, and the second equation reveals that T_4 is equivalent to exhaust gas temperature (EGT) squared divided by temperature ambient. The NASA campaigns (APEX I-III, AAFEX I & II, and ACCESS I & II) documented both EGT and ambient temperature. Values of T_4 found using the Brayton Cycle compared to values predicted using Equation-2 were slightly higher (~5%), likely because the Brayton Cycle is treated as an idealized adiabatic system. Either relation can be used to find T_4, the benefit of Equation-2 is that only the FAR is needed and Equations-3 and 4 below provide accurate FAR relations.



Task 2- Assess ACCESS II Test Procedure upon Engine Conditions at Cruise

The Pennsylvania State University

Air-to-Fuel Ratio, AFR. The first condition investigated is AFR, it should be mentioned that AFRs found here are those at the back of the combustor, typically referred to as plane-4, and are not the AFRs in the primary zone or the quench zone. The current method, Equation-5, has been widely accepted. This is partially because an engine manufacture had released nominal AFR values at 7, 30, 85, and 100 thrust settings.11 Those values were linearly fit to derive the current predictive AFR expression. However, after comparing values using this relation to engine cycle deck data it was evident that the current method results in over prediction of AFR. Two separate equations are needed to accurately calculate AFR. One for ground and another for cruise, equations 3 and 4 respectively.

$$AFR_{grd} = 71 - 35.8\left(\frac{\dot{m}_f}{\dot{m}_{f,max}}\right) \quad [3]$$

$$AFR_{cru} = 55.4 - 30.8\left(\frac{\dot{m}_f}{\dot{m}_{f,max}}\right) \quad [4]$$

As seen from the two AFR equations, at a matching thrust level AFR will be lower at cruise than at ground. This is sensible considering the decreased air density at altitude. However, the cruise cycle deck calculations were case matched to the ACCESS-II campaign and ACCESS-II conditions do not exactly match real conditions. During ACCESS-II the outboard engines were significantly throttled back to maintain an aircraft Mach number of 0.6. This was done so the chase plane could keep up. Therefore, the inboard engines from which the emissions were measured, were burning fuel at a rate typical of a Mach speed of 0.75, the DC-8's nominal cruising speed. It is likely that the AFR would be increased from the ram effect at a higher Mach number, therefore, it is possible that a singular relation (Equation-3) may adequately predict AFR at both ground and cruise.

Task 3- Evaluate ASAF as the gGlobal Scaling Factor in the ImFOX Relation

The Pennsylvania State University

ASAF inclusion. Black carbon emissions from turbo fan jet engines are significantly reduced when conventionally produced (i.e., from petroleum) Jet-A or JP-8 are blended with low aromatic content synthetic blending components as demonstrated in recent measurement campaigns.[5,12-14] Efforts to relate BC emissions from gas turbines to fuel chemistry is a research focus of long-standing interest. A prime motivator is that a decrease in aromatic content results in reduced BC emissions. The ASAF is the first analytical approximation to estimate the BC emission reduction associated with using alternative fuels as compared to conventional jet fuel BC emissions.[15]

$$B = 1 - (1-\lambda\frac{\dot{m}_f}{\dot{m}_{f,max}})(1-\hat{A}) \quad [5]$$

Where B is the relative BC emission reduction, λ is a fitting parameter, and Â is the normalized aromatic content and equal to aromatic content of the fuel over aromatic content of a reference conventional fuel.

The model we have developed uses the FOX16 as the starting point. The FOX is a kinetically balanced relation predicting EI_{BC} by subtracting the rate of soot formation from the rate of soot oxidation. Each global process is represented by a single-step Arrhenius rate. The activation energy (E_a) value in the oxidation step is the well accepted value first proposed by Lee et al.[17] Given the success of this value, no modification to the oxidation step was made, outside of correcting AFR and substituting T_{fl} with T_4. The formation activation energy is that reported by Hall et al.[18] and is their inception E_a based on the formation of polyaromatic hydrocarbons (PAHs). The pre-exponential frequency factor is a function of two and three member PAHs concentration, which in turn is a function of PAH building block molecules; acetylene and benzene. Since there is no practical way to determine these molecular concentrations this pre-exponential factor (also referred to as a formation constant) is fit to C_{BC} data. Using a formation constant value of 356 Settler et al.[16] achieve a coefficient of determination, R^2 , value of 0.8 when fitting to the APEX campaign data. The limitation of this approach is that it does not account for alternative fuels. A different formation constant would be necessary for each fuel composition. A solution encompassing alternative fuels follows.



By combining the ImFOX with the ASAF relation developed by Speth et al.[15] determination of BC emissions from alternative fuels is possible.

$$C_{BC}[\frac{mg}{m^3}] = \dot{m}_f \times B\,(A_{form} \times e^{(-6390/T_4)} - A_{ox} \times AFR \times e^{(-19778/T_4)}) \quad [6]$$

Where B in Equation-6 is the ASAF value found using Equation-5. The fitting parameter λ was found to vary between neat (i.e., 100%) alternative fuel blend components ($\lambda_{alt\text{-}neat}$) and alternative fuel blends ($\lambda_{alt\text{-}blend}$) as follows:

$$\lambda_{alt\text{-}neat} = -0.058 + 0.105(\frac{\dot{m}f}{\dot{m}f,max}) \quad [7]$$

$$\lambda_{alt\text{-}blend} = -5.3 + 9.6(\frac{\dot{m}f}{\dot{m}f,max}) - 4.7(\frac{\dot{m}f}{\dot{m}f,max})^2 \quad [8]$$

Since the ASAF provides the relative EI_{BC} reduction due to decreased aromatic content, it is ideal as a global correction factor located outside of the ImFOX expression. However, ASAF does not consider naphthenic compounds known to have a higher sooting index[19,20] than that of paraffinic compounds found predominantly in alternative fuels and fuel composition effects more logically belong in the formation constant, rather than as a global correction factor for the ImFOX. Therefore, an alternative approach was developed using hydrogen content in the form of fuel carbon-to-hydrogen (C/H) ratios to determine the formation constants for alternative fuels.

The current version of the FOX over predicts measured values, as displayed in Figure-1. However, the method is promising considering the clear trend between EI_{BC} and thrust.

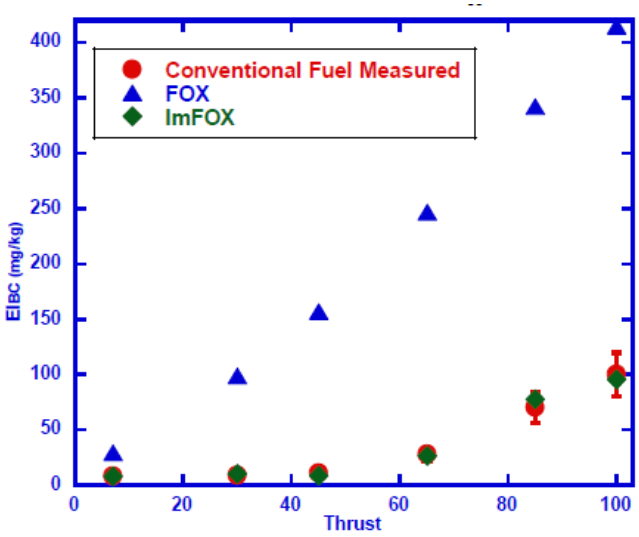


Figure 1. Measured conventional fuel black carbon emission from AAFEX-I (red circles) Shown for comparison are predicted EI_{BC} values from the FOX (blue triangles) and the ImFOX (green diamonds).

As seen in Figure-1 the ImFOX method accurately captures the emissions trend across a full range of thrust settings. The ImFOX method developed subsequently utilizes improved engine condition relations and a thrust dependent formation constant to accurately predict BC emissions from petroleum-based fuel combustion. The agreement represents a vast improvement from the current FOX method given the mean variance is reduced from 400% to less than 10%.

Task 4- Investigate Alternative Representations to Capture Fuel Composition Effects for Alternative Fuels

The Pennsylvania State University

C/H-ImFOX. An alternative approach was developed using hydrogen content in the form of fuel carbon-to-hydrogen (C/H) ratios to determine the formation constants for alternative fuels. This revised expression is Equation 6 without the ASAF correction (B) and the addition of a variable A_{from} constant. The formation constants have units of (mg×s/kg-fuel×m^3). The formation constant relation, analogous to the ASAF fitting factor (λ), needs to vary between neat alternative fuels ($A_{form,alt-neat}$) and alternative fuel blends ($A_{form,alt-blend}$) as given here:

$$A_{form,alt-neat} = \left(\frac{C}{H} - 0.342\right)T \quad [9]$$

$$A_{form,alt-blend} = \left(\frac{C}{H} - 0.212\right)T \quad [10]$$

Equations 9 and 10 go a step beyond just correcting for C/H ratio, as they relate the formation constant to thrust. The term T, a third order expression, captures the thrust dependent relation and is equal to:

$$T = 1013 - 4802\left(\frac{\dot{m}f}{\dot{m}f,max}\right) + 7730\left(\frac{\dot{m}f}{\dot{m}f,max}\right)^2 - 3776\left(\frac{\dot{m}f}{\dot{m}f,max}\right)^3 \quad [11]$$

For conventional fuels T is the formation constant, without a C/H correction. EI_{BC} was not found to vary between conventional fuels with varying aromatic contents tested during APEX-I, however, the hydrogen content of the fuels tested were nearly equivalent. As part of the Aircraft Particulate Regulatory Instrumentation Demonstration Experiment (A-PRIDE) 7, it was demonstrated by Brem et al.[21] that BC emissions from conventional fuels may vary due to a range of aromatic content and emissions are best predicted based on hydrogen mass content. Therefore, the addition of a C/H term in equation 11 to account for the varying hydrogen content in available conventional fuels may prove to make the relation applicable to a wider range of conventional fuels. However, Equation 11 based on the available NASA data should capture EI_{BC} from the majority of conventional jet fuels. The complex relation between thrust and the formation constant is also evident in the ASAF-ImFOX relation as the λ values already contain thrust terms and are multiplied by an additional thrust term in the ASAF relation, Equation 9. This is sensible considering that PAH building block molecule concentrations will vary with thrust. High-resolution transmission electron microscopy and X-ray photoelectron spectroscopy have been used to demonstrate how the macro, micro, and nano-structure of BC from commercial aircraft vary across thrust settings.[9, 22] Black carbon nanostructure can reflect the species concentrations available for BC formation and growth.[9] As reported by Vander Wal et al.[9] BC emissions vary from amorphous at low power (idle) to graphitic at high power (take off). This observation supports the need for the formation constant to have a complex dependence on thrust.

The C/H dependent fuel effect developed here based on ground data applies equally well at cruise as the emission trend with C/H ratio is the same at both ground and cruise altitude. However, EI_{BC} measured at cruise during the recent ACCESS-II campaign was 264 % higher than ground based measurements when averaged across all observed powers. This is likely due to the decreased AFR at cruise brought on by the reduced air density. The lower AFR or higher equivalence ratio at cruise will give rise to more fuel rich pockets and higher concentrations of BC precursor molecular species. Therefore, the A_{form} needs to be unique between ground and cruise to account for this. During cruise operation thrust settings are typically higher than 30 %, therefore, cruise EI_{BC} emission profiles do not possess the common curve, with upturns both at low (idle) and high (take-off) thrust levels as measured from ground campaigns. From the limited cruise altitude BC measurements, the EI_{BC} increases linearly with thrust, hence complex formation constants, like derived for ground based emissions, are not necessary. A constant formation constant of 295 captures the observed linear trend of increasing EI_{BC} with increased thrust at cruise.

To capture the emission reductions from the use of alternative fuels two variations of the ImFOX were compared: the ASAF-ImFOX and the C/H-ImFOX. Black carbon emissions from a FT fuel measured during AAFEX-I are plotted in Figure 2 with the calculated values from the two versions of the ImFOX expression.

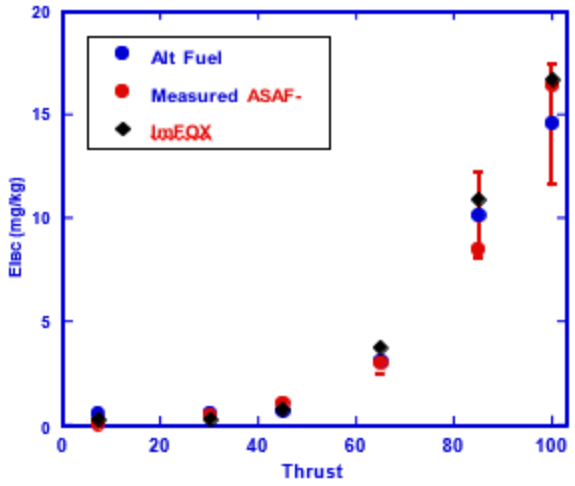


Figure 2. Neat Fischer-Tropsch blend component BC emissions measured during the AAFEX-I campaign. Comparison of the ASAF-ImFOX and C/H-ImFOX methods used for EI_{BC} predictions.

As displayed in Figure 3 both the ASAF-ImFOX and C/H-ImFOX methods capture the emission reductions from the use of a neat Fischer-Tropsch synthetic paraffinic kerosene (SPK) blend component. Due to fuel performance requirements including mass density and wetted-material compatibility SPKs such as the Fischer-Tropsch depicted in this work are approved as alternative fuels only when blended up to a maximum of 50% blend ratio with conventional fuel. Regardless, the SPKs blended up to this limit are still an attractive solution for reducing BC emissions. The ASAF-ImFOX and C/H-ImFOX calculated values are compared to measured BC in Figure 3 for a FT-JP-8 50/50 blend that is within the alternative fuel specification requirements.

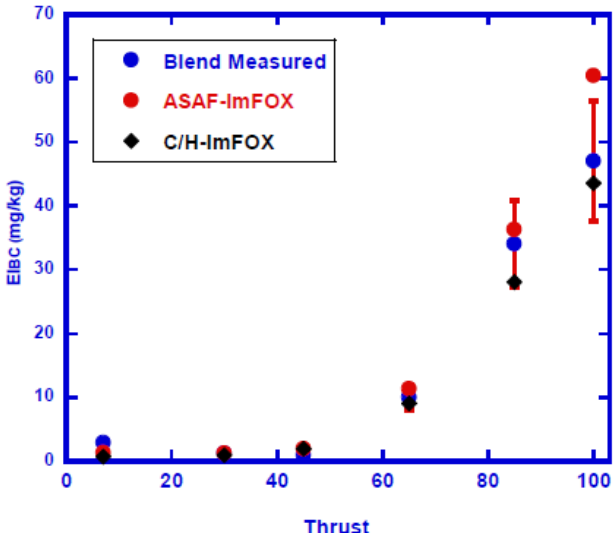


Figure 3. EI_{BC} from a 50/50 blend of Fischer-Tropsch and JP-8 measured during the AAFEX-I campaign. Also shown is a comparison of the ASAF-ImFOX and C/H-ImFOX methods for EI_{BC} predictions of the alternative fuel blend.

As demonstrated in Figure 3 alternative fuel blend emissions are accurately calculated with both expressions except for the ASAF-ImFOX slightly over predicting EI_{BC} at 100% thrust level. This demonstrates that EI_{BC} reductions from alternative fuels can be predicted by correlating the ImFOX with an aromatic or C/H reduction term.



Task 5- Evaluate the ImFOX Relation Against the ACCESS II Flight Data from NASA for nvPM

The Pennsylvania State University

H-ImFOX. As previously mentioned, the pre-exponential frequency factor is a function of two and three member PAH concentration, which in turn is a function of PAH building block molecule concentrations; acetylene, benzene, phenyl radical, and hydrogen. Since there is no practical way to determine these molecular concentrations this pre-exponential factor (also referred to as a formation constant) is fit to C data and given in equation 12.

$$A_{form} = 1013 - 4802\left(\frac{\dot{m}f}{\dot{m}f,max}\right) + 7730\left(\frac{\dot{m}f}{\dot{m}f,max}\right)^2 - 3776\left(\frac{\dot{m}f}{\dot{m}f,max}\right)^3 \quad [12]$$

This 3rd order dependence of the formation constant upon thrust is sensible considering that PAH building block molecule concentrations will vary with thrust. High-resolution transmission electron microscopy and X-ray photoelectron spectroscopy have been used to demonstrate how the macro, micro, and nano-structure of BC from commercial aircraft vary across thrust settings.[9, 22] Black carbon nanostructure can reflect the formation conditions, i.e. species and temperature, of BC.[9] As reported by Vander Wal et al.[35] BC emissions vary from amorphous at low power (idle) to graphitic at high power (take off). This observation supports the need for the formation constant to have a complex dependence on thrust. Black carbon is not an equilibrium product of combustion.[10] Thus, it is difficult to predict its rate of formation and final concentration from kinetics or thermodynamics alone. In practice, the rate of soot formation is strongly impacted by the physical processes of atomization and fuel-air mixing as these processes control the equivalence ratio and resulting flame temperature.[10] This variable, thrust dependent fuel air mixing may be the origin of the complex dependence of A_{from} upon thrust, as expressed in equation 12. This mixing effect would apply across all fuels: conventional, blended, and neat SPK. Therefore, equation 12 developed here for conventional fuel can be used to represent the mixing (combustor) effect across all fuels with a separate fuel term then added explicitly for fuel composition, specifically decreasing EI_{BC} with increasing hydrogen mass content. The new predictive expression is accordingly termed the H-ImFOX, and given in equation 13.

$$C_{BC}\left[\frac{mg}{m^3}\right] = \dot{m}_f \times e^{(13.6-H)}\left(A_{form} \times e^{(-6390/T_4)} - A_{ox} \times AFR \times e^{(-19778/T_4)}\right) \quad [13]$$

The “H” in equation 13 represents hydrogen mass percent and as seen in equation 15 BC emission decays exponentially with increasing hydrogen content. This trend was observed across the previously mentioned NASA campaigns.9 The H-ImFOX will hereafter be referred to as just the ImFOX as the new hydrogen fuel term is universally applied across all fuels and therefore, equation 13 is the ImFOX. A strong correlation between hydrogen content and BC reduction was recently observed during the Aircraft Particulate Regulatory Instrumentation Demonstration Experiment (A-PRIDE) 7. Brem et al.21 found BC emissions from conventional fuels to vary due to a range of aromatic content and concluded that emissions are best predicted based on hydrogen mass content. Additionally, Lobo et al.23 recently reported similar findings by varying the ratio of SPK blending components with conventional fuel.

The hydrogen dependent fuel effect developed here based on ground data applies equally well at cruise as the BC emission trend with hydrogen content is the same at both ground and cruise altitude. However, EI_{BC} measured at cruise during the recent ACCESS-II campaign was 264% higher than ground based measurements when averaged across all observed powers. This is likely due to the decreased AFR at cruise brought on by the reduced air density. The lower AFR or higher equivalence ratio at cruise will give rise to more fuel rich pockets and higher concentrations of BC precursor molecular species. Accordingly, different A_{form} relations are necessary for ground and cruise to account for these differences in mixing. During cruise operation thrust settings are typically higher than 30%, therefore, cruise EI_{BC} emission profiles do not possess the commonly observed emission curve with upturns both at low (idle) and high (take-off) thrust levels as measured in ground campaigns. From the limited cruise altitude BC measurements, the EI_{BC} increases approximately linearly with thrust, hence complex formation constants, like derived for ground based emissions, are not necessary. Although a complex expression for cruise A_{form} may ultimately be needed, however, the limited range of thrust values at cruise presently do not provide justification for such, instead the simplest expression (a constant) was chosen and found

adequate by quality of fit. A A_{form} increased cruise value of 295 captures the observed linear trend of increasing EI_{BC} with increased thrust at cruise.

ImFOX Direct Cruise Prediction.

The litmus test of the ImFOX formalism is whether it captures the range of cruise EI_{BC} values. The ImFOX predictive tool only requires the combustor conditions, AFR and T_4, as input values. If these can be known or otherwise accurately predicted at cruise, then the ImFOX should accurately predict EI_{BC}. Predicted values are compared to measurements made at cruise altitudes during the ACCESS-II campaign for both conventional fuel and an alternative fuel blend, displayed in Figure-4.

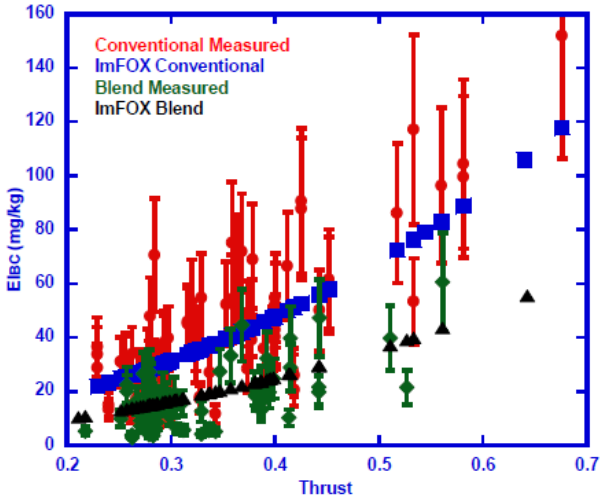


Figure 4. Measured EI_{BC} at cruise altitude burning Jet-A (red circles) and 50/50 blend of Hydrotreated Esters and Fatty Acids (HEFA-SPK) and Jet-A (green diamonds). Shown for comparison are ImFOX predicted values for conventional (blue squares) and blended alternative (black triangles) fuels.

This demonstrates that the ImFOX can be applied to directly predict EI_{BC} values at cruise and will yield accurate results if combustor conditions are known. Predicted values were found using a constant formation constant of 295 and the hydrogen dependent fuel term as described above.

Task 6- Validate the ImFOX for Other Engines in the CFM Class

The Pennsylvania State University

CFM56-3B. If the form of the ImFOX is correct, it should accurately estimate nvPM emissions from other RQL style combustors. When engine cycle data is not available, the above AFR and T_4 relations can be used. Comparison of the 2C to the 3B is interesting as both are RQL technology and have the same maximum fuel flow rate. Thus, predicted AFR will be the same as dependence is on fuel flow rate with respect to maximum ground fuel flow rate. Predicated T_4 will also be the same as it is dependent on AFR. The ImFOX therefore predicts equivalent emission from the two engines. Evaluating the ImFOX against the 3B is essentially boiled down to comparing emission from the 2C with the expectation of equivalent emissions. Measured nvPM emissions from the NASA APEX campaigns for both engines are provided in Fig. 5. As seen the emission profiles are within the measurement standard deviation. Although within measurement uncertainty, the average emission from three repeated measurements is higher from the 3B as compared to the 2C at higher fuel flow rates. The key difference between these engines is the shape, the 3B has a less rounded bottom by design so it could readily fit under the 737. In doing so, it cut 8 inches off of the front fan blade. Since this was a design restriction and not an engine optimization it may have resulted in a less efficient engine as compared to the 2C. The 2C has a higher pressure ratio and higher maximum thrust. This subtle difference between these two similar engines and the potentially higher emissions from the 3B shows how sensitive emissions are to engine design.

Emission trends from newer combustor technology like the dual staged CFM56-5 and lean burn CFM56-7 are of interest. This is a potential area of collaboration between Penn State and Georgia Institute of Technology as Georgia can provide engine calculations for these engines.

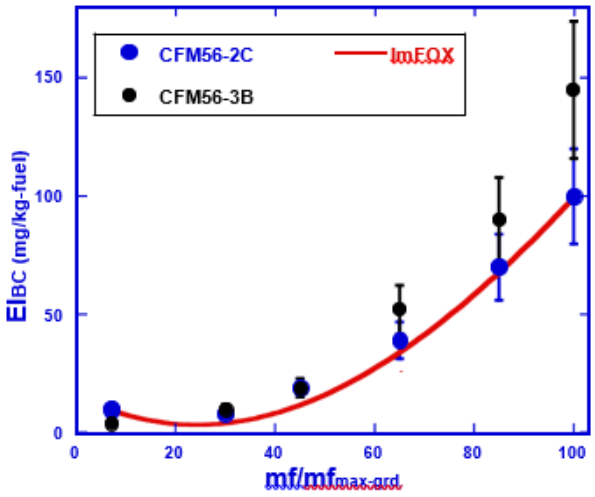


Figure 5. EI_{BC} curves for CFM56- 2C and 3B. Predicted ImFOX values shown for comparison.

Publications and Presentations

Publication

Abrahamson, J. P., Zelina, J., Andac, M. G., & Vander Wal, R. L. (2016). Predictive Model Development for Aviation Black Carbon Mass Emissions from Alternative and Conventional Fuels at Ground and Cruise. Environmental Science & Technology, 50(21), 12048-12055.

Presentations

Vander Wal, R. L. Abrahamson, J. P., ASCENT Project No. 24B, Emissions data analysis for CLEEN, ACCESS and other tests. FAA Center of excellence for alternative jet fuels and environment. Contractor's workshop. Alexandria, VA. Sept. 27th–28th, 2016.

Abrahamson, J. P., Vander Wal, R. L., PM Emissions Analysis and Predictive Assessment: Update on nvPM predictive modeling from conventional and alternative jet fuels. Aviation Emissions Council (AEC) WEBEX seminar. Feb. 23rd, 2017.

Vander Wal, R. L., Abrahamson, J. P., nvPM Emissions Analysis and Predictive Summary. Poster Presentation. Project 24B Report. FAA Center of Excellence for Alternative Jet Fuels & Environment (FAA COE AJFE). Alexandria, VA April 18th - 19th, 2017.

Abrahamson, J. P., Vander Wal, R. L., (2017). Gas turbine nvPM formation and oxidation semi-empirical model for commercial aviation. Paper 2E19. Topic: Gas Turbine Combustion. 10th US National Meeting of the Combustion Institute, The University of Maryland, College Park, MD April 23rd - 26th, 2017.

Conference Paper

Abrahamson, J. P., Vander Wal, R. L., (2017). Gas turbine nvPM formation and oxidation semi-empirical model for commercial aviation. Paper 2E19. Topic: Gas Turbine Combustion. 10th US National Meeting of the Combustion Institute, The University of Maryland, College Pak, MD April 23rd - 26th, 2017.

Outreach Efforts
Informal discussions with the US EPA regarding variations in nvPM structure and composition dependent upon source.

Awards
None

Student Involvement
The current graduate student, Joseph P. Abrahamson, is conducting data assembly, analysis and predictive relation assessment, towards partial fulfillment of his Ph.D. program in EME, with Fuel Science option.

Plans for Next Period
Options offered:

Possible tasks for this coming year could include,

1. Evaluation of the ImFOX against newer, lean burn engines.
2. Formulation and evaluation of T3, P3 scaling relationships for nvPM (EIbc) between ground and cruise.
3. Testing for correlation between YSI (a lab-based measurement for fuel sooting tendency) and measured EIbc (from jet engines) for JP-8, synthetic fuels and their blends.
4. Develop a number-based predictive relation, including fuel dependence, given forthcoming regulations.

These are described in more detail in the white paper, which was shared with James Hileman and Ralph Iovinelli in April of 2017.

Based on the AEC Roadmap meeting of June 13-15 2017, other needs may be:

1. In our petroleum engineering program, and fuel science courses, we use HYSYS. Aspen HYSYS is the energy industry's leading process simulation software that's used by top oil and gas producers, refineries and engineering companies for process optimization in design and operations. Aspen HYSYS is a process simulation software for the optimization of conceptual design and operations including multiphase flow modeling, gas processing, refining and distillation. We could evaluate necessary refinery operations.
2. Based on Dr. Bruce Anderson's overview of their upcoming contrail/plume measurements this coming year, he stated that extra sampling ports were available on the NASA DC-8, and that other measurements could be accommodated. This would truly be a unique opportunity to collect in situ particulate samples for microscopic analyses, SEM, TEM to benchmark what other aerosol instrumentation is actually measuring, (and insights into the aerosol processing within the plume.)

References
Wey, C. C.; Anderson, B. E.; Hudgins, C.; Wey, C.; Li-Jones, X.; Winstead, E.; Thornhill, L. K.; Lobo, P.; Hagen, D.; Whitefield, P.; Yevington, P. E.; Herndon, S. C.; Onasch, T. B.; Miake-Lye, P. C.; Wormhoudt, J.; Knighton, W. B.; Howard, R.; Bryant, D.; Corporan, E.; Moses, C.; Holve, D.; Dodds, D. Aircraft Particle Emissions eXperiment (APEX); ARL-TR-3903; NASA Langley Research Center: Hampton, VA, 2006

Wey, C. C.; Anderson, B. E.; Wey, C.; Miake-Lye, R. C.; Whitefield, P.; Howard, R. Overview of aircraft particle emissions experiment. J. Propul. Power 2007, 23, 898-905.

Anderson, B.; Beyersdorf, A.; Hudgins, C.; Plant, J.; Thornhill, K.; Winstead, E.; Ziemba, L.; Howard, R.; Corporan, E.; Miake-Lye, R. Alternative aviation fuel experiment (AAFEX); NASA Langley Research Center: Hampton, VA, 2011

Beyersdorf, A. J.; Timko, M. T.; Ziemba, L. D.; Bulzan, D.; Corporan, E.; Herndon, S. C.; Howard, R.; Miake-Lye, R.; Thornhill, K. L.; Winstead, E.; Wey, C.; Yu, Z.; Anderson, B. E. Reductions in aircraft particulate emissions due to the use of Fischer-Tropsch fuels. Atmos. Chem. Phys. 2014, 14, 11-23.

Moore, R.; Shook, M.; Beyersdorf, A.; Corr, C.; Herndon, S.; Knighton, W.; Miake-Lye, R.; Winstead, S.; Yu, Z.; Ziemba, L.; Anderson, B. Influence of Jet Fuel Composition on Aircraft Engine Emissions: A synthesis of aerosol emissions data from the NASA APEX, AAFEX, and ACCESS missions. Energy Fuels 2015, 29, 2591-2600.

Kinsey, J. S. Characterization of emissions from commercial aircraft engines during the Aircraft Particle Emissions eXperiment (APEX) 1 to 3; EPA-600/R-09/130; Environmental Protection Agency: Washington DC, 2009.

Kinsey, J. S.; Dong, Y.; Williams, D. C.; Logan, R. Physical characterization of the fine particle Emissions form commercial aircraft engines during the Aircraft Particle Emissions eXperiment (APEX) 1-3. Atmos. Environ.2010, 44, 2147-256.



Dong, Y.; Williams, D. C.; Logan, R. Chemical characterization of the fine particle emissions form commercial aircraft engines during the Aircraft Particle Emissions eXperiment (APEX) 1 to 3. Environ. Sci. Technol. 2011, 45, 3415-3421.

Vander Wal, R. L.; Bryg, V. M.; Huang, C.-H. Aircraft engine particulate matter: Macro- mico- and nanostructure by HRTEM and chemistry by XPS. Combust. Flame 2014, 161, 602-611.

Arthur H. Lefebvre; Dilip R. Ballal Gas Turbine Combustion: Alternative Fuels and Emissions; 3rd ed.; CRC Press, 2010; p. 72.

Wayson, R. L.; Fleming, G. G.; Lovinelli, R. Methodology to estimate particulate matter emissions from certified commercial aircraft engines. J. Air Waste Manage. Assoc. 2009, 59, 91-100.

Timko, M. T.; Herndon, S. C.; Blanco, E. R.; Wood, E. C.; Yu, Z.; Miake-Lye, R. C.; Knighton, W. B.; Shafer, L.; DeWitt, M. J.; Corporan, E. Combustion products of petroleum jet fuel, a Fischer–Tropsch synthetic fuel, and a biomass fatty acid methyl ester fuel for a gas turbine engine. Combust. Sci. Technol. 2011, 183, 1039-1068.

Corporan, E.; Dewitt, M. J.; Belovich, V.; Pawlik, R.; Lynch, A. C.; Gord J. R.; Meyer, T. R. Emissions characteristics of a turbine engine and research combustor burning a Fischer–Tropsch jet fuel. Energy Fuels 2007, 21, 2615–2626.

Cain, J.; DeWitt, M.J.; Blunck, D.; Corporan, E.; Striebich, R.; Anneken, D.; Klingshirn, C.; Roquemore, W.; Vander Wal, R. Characterization of gaseous and particulate emissions from a turboshaft engine burning conventional, alternative, and surrogate fuels. Energy Fuels 2013, 27, 2290-2302.

Speth, R. L.; Rojo, C.; Malina, R.; Barrett, S. R. H. Black carbon emissions reductions form combustion of alternative fuels. Atmos. Environ. 2015, 105, 37-42.

Stettler, M. E. J.; Boise, A. M.; Petzold, A.; Barrett, S. R. H. Global civil aviation black carbon emissions. Environ. Sci. Technol. 2013a, 47, 10397-10404.

Lee, K.B; Thring, M.W; Beer, J.M. On the rate of combustion of soot in a laminar soot flame. Combust. Flame 1962, 6, 137–145.

R.J. Hall, M.D. Smooke, M.B. Colket, in Physical and Chemical Aspects of Combustion: A Tribute to Irvine Glassman, F.L. Dryer and R.F. Sawyer (Ed.), Gordon & Breach, 1997, p. 201.

Mensch, A.; Santoro, R. J.; Litzinger, T. A.; Lee, Y.-Y. Sooting characteristics of surrogates for jet fuel. Combust. Flame 2010, 157, 1097-1105.

Yang, Y.; Boehman, A. L.; Santoro, R. J. A study of jet fuel sooting tendency using the threshold sooting index (TSI) model. Combust. Flame 2007, 149 (1−2), 191−205.

Brem, B. T.; Durdina, L.; Siegerist, F.; Beyerle, P.; Bruderer, K.; Rindlisbacher, T.; Rocci-Denis, S.; Andac, M. G.; Zelina, J.; Penanhoat, O.; Wang, J. Effects of fuel aromatic content on nonvolatile particulate emissions of an in-production aircraft gas turbine. Environ. Sci. Technol. 2015, 49, 13149-13157.

Huang, C.-H.; Vander Wal, R. L. Effect of soot structure evolution from commercial jet engine burning petroleum based JP-8 and synthetic HRJ and FT fuels. Energy Fuels 2013, 27, 4946-4958.

Lobo, P.; Christie, S.; Khandelwal, B.; Blakey, S. G.; Raper, D. W. Evaluation of Non-volatile Particulate Matter Emission Characteristics of an Aircraft Auxiliary Power Unit with Varying Alternative Jet Fuel Blend Ratios. Energy Fuels 2015, 29, 7705-7711.

Project 025 Shock Tube Studies of the Kinetics of Jet Fuels

Stanford University

Project Lead Investigator

Ronald K Hanson
Woodard Professor
Mechanical Engineering Department
Stanford University
452 Escondido Mall
650-723-6850
rkhanson@stanford.edu

University Participants

Stanford University

- P.I.s: Prof. Ronald K Hanson
- FAA Award Number: 13-C-AJFE-SU-008
- Period of Performance: 10/01/2016 to 09/30/2017
- Task: Area #1 – Chemical Kinetics Combustion Experiments

Project Funding Level

$200,000 from FAA with 1-1 matching funding of $200,000 from Stanford University.

Investigation Team

Prof. Ronald K Hanson, Principal Investigator, Research Direction
Dr. David F Davidson, Senior Research Engineer, Research Management
Jiankun Shao, Graduate Student, Research Assistant
Yu Wang, Graduate Student, Research Assistant
Nicolas Pinkowski, Graduate Student, Research Assistant

Project Overview

Provide shock tube/laser absorption experiments for a fundamental kinetics database for jet fuels. Experiments are expected to continue to reveal the sensitivity of combustion properties to fuel composition for the ultimate use in simplifying the alternative fuel certification process.

Task 1A- Chemical Kinetics Combustion Experiments

Stanford University

Objective(s)

Experiments provide an extensive fundamental kinetics data for selected jet fuels. These data are used as critical input for Area #2 that seeks to develop a new hybrid and detailed kinetics model for jet fuels (HyChem). These experiments continue to reveal the sensitivity of combustion properties to variations in fuel composition for ultimate use in simplifying the alternative fuel certification process. The team works in close collaboration with Professor Hai Wang, also of Stanford University, the PI for Area #2, who uses the data acquired in our experiments. The data provided will also ensure that the combustion models developed in Area #4 - Combustion Model Development and Validation to model the extinction and ignition processes controlling lean blowout, cold ignition and high altitude relight, are chemically accurate.

Research Approach

The development, refinement and validation of detailed reaction mechanisms describing the pyrolysis and oxidation of fuels require experimental data as targets for kinetics models. Experimentally, the best way to provide these targets at high temperatures and pressures is with shock tube/laser absorption experiments, conducted over a wide range of pressure, temperature, and fuel and oxidizer composition.

Reflected shock wave experiments provide a test environment that does not introduce additional fluid mechanics, turbulence, or heat transfer effects to the target phenomena. This allows isolation of the target phenomena (ignition delay times and species concentration time-histories) in a quiescent high-temperature, high-pressure environment that is very well characterized and hence amenable to modeling. Recent work in our laboratory to develop the Constrained Reaction Volume (CRV) methodology provides an additional tool to provide shock tube data under constant-pressure constraints when needed, to significantly simplify the gasdynamic/thermodymamic models needed to properly simulate reactive reflected shock wave data.

The strength in the Stanford shock tube approach comes with the implementation of laser diagnostics that enable the simultaneous measurement of species time-histories. Using laser absorption, we are able to provide quantitative time-histories during fuel pyrolysis and oxidation of the fuel, including transient radicals (e.g., OH, CH3), stable intermediates (e.g., CH4, C2H4, iso-butene and aromatics), combustion products (including CO, CO2, and H2O), and temperature.

Measurements of the pyrolysis and oxidation systems of real fuels, rather than of surrogates or solvent surrogates, provide a direct link to actual fuel behavior. The combination of high-quality shock tube and flow reactor measurements combined with the HyChem kinetic model based on real fuel decomposition products proposed by Professor Hai Wang is meeting the FAA program objectives.

An important goal of the current research is to investigate the possibility of characterizing fuel composition and combustion behavior based on the jet fuel infrared absorption (FTIR) spectra. As the shock tube/spectroscopic research has progressed under FAA support, a large database of kinetic and spectroscopic measurements for a variety of jet fuels has been acquired. Using this database, we have developed correlations between the spectroscopic properties of neat jet fuel with fuel composition and with important combustion parameters such as DCN, LBO and C2H4 pyrolysis yields.

Experimental Studies

Stanford has the largest and best-equipped shock tube laboratory in the U.S., perhaps in the world, with five shock tubes: three large-diameter (10, 14 and 15 cm I.D.) high-purity shock tubes (see Fig. 1a); one heated high-pressure shock tube (5 cm I.D., capable of achieving 500+ atm); and 10 cm I.D. expansion tube for generating supersonic flows. Additionally, we have unique capability for species measurements using laser absorption (see Fig. 1b) developed over the past 30 years. In these experiments, temperatures from below 500 K to above 3000 K, and pressure from sub-atmospheric (0.2 atm) to 10-500+ atmospheres can be achieved in different carrier gases, such as argon or air, with demonstrated test times up to and exceeding 50 ms at low temperatures.

The primary shock tube experiments are species concentration time-history measurements obtained during fuel pyrolysis. These data are used to place strong constraints on the reaction mechanism and the individual reaction rates and pathways. Laser absorption techniques, many pioneered at Stanford, are used to measure these species time-histories. The following species time-histories measurements have been acquired and used in the development of the HyChem model: fuel at a wavelength of 3.39 or 3.41 microns, and the stable fuel decomposition products: ethylene, methane, propene, and iso-butene, at wavelengths of 10.53, 3.1754, 10.96, and 11.3 microns, respectively. We also are able to measure the transient radical OH (in the UV at 306 nm), the combustion products CO, CO2 and H2O (in the IR at 2.7, 4.6 and 2.5 microns, respectively) as well as other product species.

Representative data acquired using these methods are shown in Figures 2a and 2b along with preliminary HyChem model results. These measurements of the major jet fuel decomposition products during Cat C4 fuel pyrolysis (fuel, ethylene, propene, and isobutene time-histories) were directly applicable to the development of the HyChem Jet Fuel model by Prof. Hai Wang.

FTIR spectra for Jet A (Cat A2 fuel) and average FTIR spectra for the major molecular classes of fuel components are shown in Figures 3a and 3b. FTIR measurements of the jet fuel can be used to characterize the fuel component composition by spectrally decomposing the jet fuel FTIR spectra using the major molecular class FTIR spectral basis set.

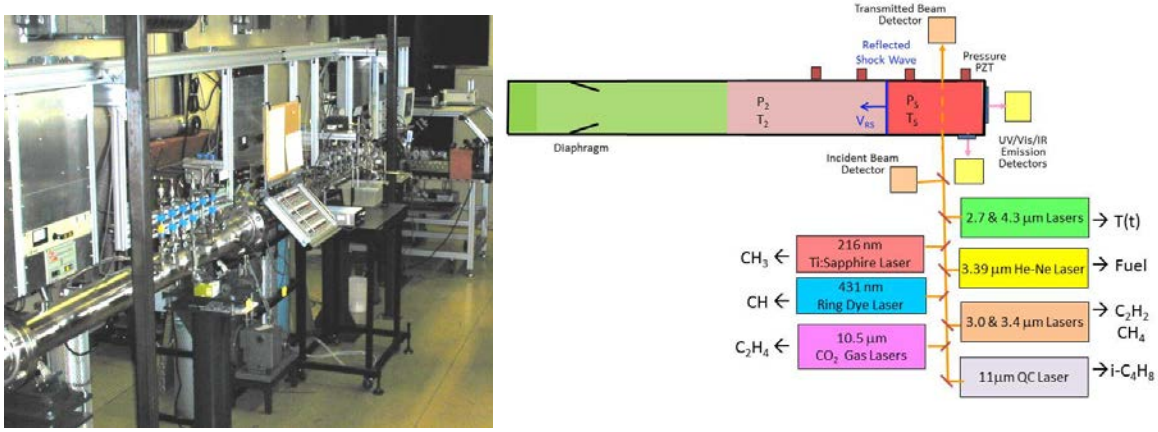


Figure 1a. Stanford 15 cm diameter shock tube. **Figure 1b.** Schematic of shock tube/laser absorption setup. Simultaneous measurement of multiple species time-histories and temperature with microsecond time resolution are enabled using this arrangement. Only a partial list of accessible species is indicated.

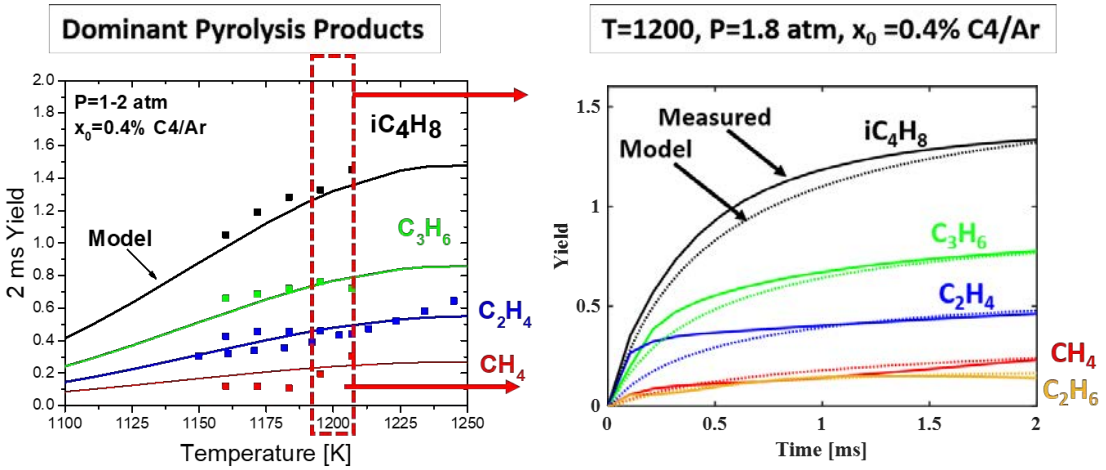


Figure 2a. Variation of the CH4, C2H4, C2H6, C3H6 and iC4H8 pyrolysis yields acquired during the pyrolysis of C4 fuel as a function of temperature and comparison with a preliminary HyChem model. **Figure 2b.** Representative measurements and preliminary modeling of C4 pyrolysis at 1200K, 1.8 atm.

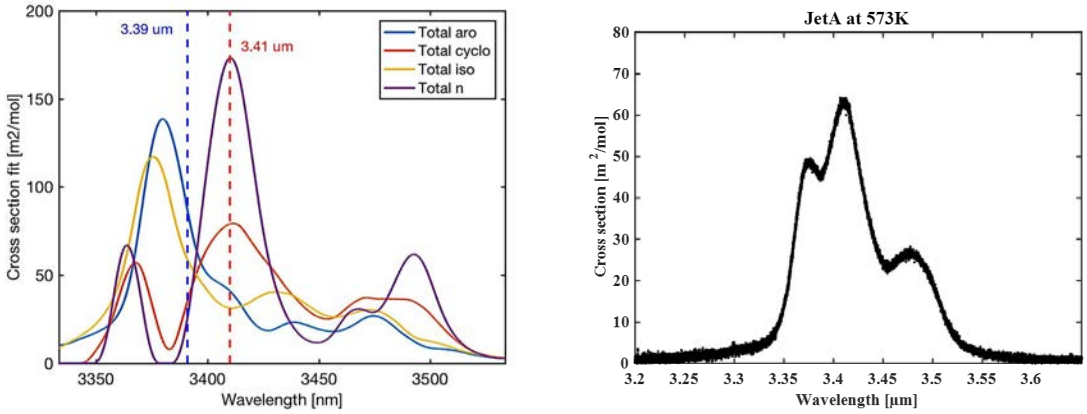


Figure 3a. Average FTIR spectra for alkane (n-, iso-, & cyclo-) and aromatic molecular classes of jet fuel components. Primary wavelengths (3.39 and 3.41 microns) used to measure fuel loading are also indicated. **Figure 3b:**.FTIR spectra for Jet A fuel (Cat A2). Strong absorption is seen at the n-alkane peak near 3.41 microns.

Milestones

Major milestones included regular reporting of experimental results and analysis at monthly meetings for both the Kinetics Working Group and the Steering Working Group, as well as reporting at FAA Quarterly and ASCENT annual meetings.

Major Accomplishments

During this fourth year of this program, we made advances in several areas.

We have developed or refined infrared laser diagnostics schemes for ethane at 3.35 microns and for aromatics at 3.28 microns. These diagnostics provide quantitative, sensitive, low-noise detection of key species involved in the combustion of jet fuels.

Using these new diagnostics schemes and our existing systems for ethylene, methane and isobutene, we have acquired refined multi-species data for the decomposition of the important jet fuel pyrolysis product i-butene and for Cat C4 fuel using a nine-IR-wavelength strategy.

In the analysis of this multi-species/multi-wavelength approach we have also assessed the role of minor interfering species (e.g. 1-butene, 2-butene, and allene) on the measured iso-butene and propene pyrolysis yields.

We have acquired FTIR spectra near 3.4 microns for the majority of the FAA Cat A and Cat C fuels as well as verifying the published spectra for single fuel components.

We have developed correlations that relates the measured IR absorption ratio at 3.41 and 3.39 microns to C2H4 pyrolysis yield, fuel DCN value, LBO (lean blow out) and IDT (ignition delay times).

We have investigated, and continue to investigate, the link between FTIR spectra measurements and fuel functional groups, combustion properties and HyChem.

Publications

Peer-reviewed journal publications

Archival Publications

S. Wang, T. Parise, S.E. Johnson, D.F. Davidson, R.K. Hanson, "A New Diagnostic for Hydrocarbon Fuels using 3.41-micron Diode Laser Absorption," Combustion and Flame 186 129-139 (2017)

T. Parise, D.F. Davidson, R.K. Hanson, "Shock Tube/Laser Absorption Measurements of the Pyrolysis of a Bimodal Test Fuel," Proceedings of the Combustion Institute 36 281-288 (2017)



H. Wang, R. Xu, K. Wang, C.T. Bowman, R.K. Hanson, D.F. Davidson, K. Brezinsky, F.N. Egolfopoulos, "A Physics-based approach to modeling real-fuel combustion chemistry - I. Evidence from experiments, and thermodynamic, chemical kinetic and statistical considerations," Combustion and Flame 193 502-519 (2018)

R. Xu, K. Wang, S. Banerjee, J. Shao, T. Parise, Y. Zhu, S. Wang, A. Movaghar, D.J. Lee, R. Zhao, X. Han, Y. Gao, T. Lu, K. Brezinsky, F.N. Egolfopoulos, D.F. Davidson, R.K. Hanson, C.T. Bowman, H. Wang, "A physics-based approach to modeling real-fuel combustion chemistry - II. Reaction kinetic models of jet and rocket fuels," Combustion and Flame 193 520-537 (2018)

J. Shao, Y. Zhu, S. Wang, D. F. Davidson, R. K. Hanson, "A shock tube study of jet fuel pyrolysis and ignition at elevated pressures and temperatures, Fuel 226 338-344 (2018)

N. Pinkowski, T. Parise, Y. Ding, S. Johnson, Y. Wang, D. F. Davidson, R. K. Hanson, "High-temperature infrared absorption cross-sections to facilitate the study of hydrocarbon pyrolysis," submitted to Journal of Quantitative Spectroscopy and Radiative Transfer, August 2018

Y. Wang, D. F. Davidson, R. K. Hanson, "A new method of predicting derived cetane number for hydrocarbon fuels," submitted to Fuel, September 2018

N. Pinkowski, "Jet fuel chemical kinetics: shock tubes, laser diagnostics, and machine learning methods," ASCENT Program Student Paper Competition 2018

Outreach Efforts

FTIR spectral analysis of a series of jet fuels with varying cetane number from the Army Research Laboratory (ARL) providing fuel characterization data of use to both the FAA and the ARL.

FTIR spectral analysis of a series of jet fuels from geographically varying locations from the Air Force/Wright Patterson Airbase providing fuel characterization data of use to both the FAA and the AFOSR.

Awards

None

Student Involvement

Graduate students are actively involved in the acquisition and analysis of all experimental data. Tom C. Parise successfully defended his Ph.D. thesis that was based on work performed under this contract. Nicolas Pinkowski won an FAA ASCENT Program Student Paper Competition for his paper "Jet fuel chemical kinetics: shock tubes, laser diagnostics, and machine learning methods."

Plans for Next Period

In the next period we plan to:

1. Acquire IDT & speciation data base for SHELL IH2 fuel and develop a HyChem model for this fuel.
2. Complete the kinetics and HyChem section of the AIAA volume entitled *Fuel Effects on Operability of Aircraft Gas Turbine Combustors*.
3. Finalize HyChem model for Cat C4 fuel.
4. Continue development of correlations between IR fuel absorption, pyrolysis yields & combustion properties.
5. Continue exploration of IR absorption as a fuel screening tool and potential fuel specification.
6. Extend correlations of IR absorption to physical properties (e.g., viscosity, surface tension, etc.).



Project 027A National Jet Fuels Combustion Program – Area #3: Advanced Combustion Tests

Tim Lieuwen[1], Jerry Seitzman[1], Wenting Sun[1], David Blunk[2], Tonghun Lee[3],

Georgia Institute of Technology[1], Oregon State University[2], University of Illinois[3]

*this report covers portion of University of Illinois

Project Lead Investigator

Tonghun Lee
Associate Professor
Mechanical Science & Engineering
University of Illinois at Urbana-Champaign
1206 W. Green St.
Urbana IL 61801
517-290-8005
tonghun@illinois.edu

University Participants

University of Illinois at Urbana-Champaign

- P.I.(s): Tonghun Lee, Associate Professor
- FAA Award Number: 13-C-AJFE-UI-004
- Period of Performance: 12/1/2014 to 12/31/2017
- Task(s):
    1. Optimize and apply laser diagnostics for application in the advanced combustion tests at GA Tech.
    2. Optimize and apply laser diagnostics for application in the Referee Combustor.
    3. Optimize and apply laser diagnostics for ignition experiments at Georgia Tech.
    4. Conduct high altitude relight ignition probability measurements in the modified sector rig at ARL.
    5. Conduct ignition delay measurements of the targeted cetane number fuels in the RCM at UIUC.

Project Funding Level

FAA Funding Level: $360,000
Cost Share: In-kind academic time of the PI, Lab Renovation Cost by Department for Diagnostics Work, cost share provided by software support from Convergent Sciences, Inc.

Investigation Team

- Eric Mayhew (Graduate Student, University of Illinois at Urbana-Champaign): Execution of laser and optical diagnostics at ARL.
- Kyungwook Min (Graduate Student, University of Illinois at Urbana-Champaign): Rapid Compression Machine testing of fuels.
- Brendan McGann (Graduate Student, University of Illinois at Urbana-Champaign): Execution of laser and optical diagnostics at ARL.
- Constandinos Mitsingas (Graduate Student, University of Illinois at Urbana-Champaign): Execution of laser and optical diagnostics at ARL.
- Stephen Hammack (Graduate Student, University of Illinois at Urbana-Champaign): Execution of laser and optical diagnostics at GATech.

Project Overview

The goal of this study is to develop, conduct, and analyze advanced laser and optical measurements in the experimental combustors developed under ASCENT National Fuel Combustion Program to measure sensitivity to fuel properties. We conducted advanced spatially resolved high-speed planar imaging, high-speed Schlieren imaging, high-speed OH* chemiluminescence imaging, 2D phase Doppler anemometry, and other advanced diagnostics to provide insight into the physicochemical response of the combustion process for various alternative fuels. Moreover, the results provided data for development of new predictive combustion models in ASCENT. Once fully characterized, the standard referee combustor rig can streamline and simplify fuel certification procedures outlined in the ASTM D4054 (Standard Practice for Qualification and Approval of New Aviation Turbine Fuels and Fuel Additives) through minimization of full-scale engine testing.

Task 1 – Optimize and Apply Laser and Optical Diagnostics for Application in the Referee Combustor

University of Illinois at Urbana-Champaign

Objective(s)

The main objectives of the work in this proposal are to work with UDRI and AFRL in carrying out diagnostics measurements for the referee combustor. The following tasks will guide this collaboration:

- Identify the operating conditions and key parameters for detection in the referee combustor
- Evaluate and modify the referee combustor at AFRL for laser and optical diagnostics
- Design laser and optical diagnostics setup and assist in the fuel screening process
- Analyze data and pass on data to modeling groups in combustion program.

Research Approach

The main effort in year 1 was the assembly of the laser system around the test rig at GATech and completion of simultaneous stereo PIV and two camera PLIF. A picture of the experimental setup, with the four high-speed cameras positioned around test rig, is shown in Figure 1.

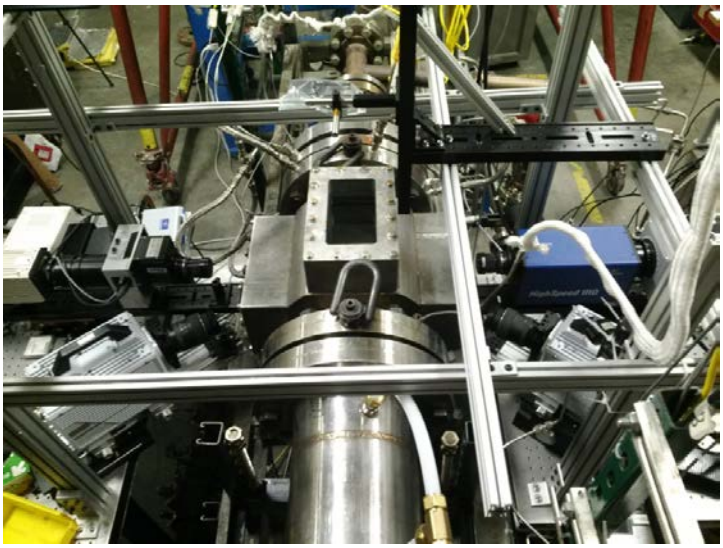


Figure 1. Diagnostics Setup at GATech with Stereo PIV and 2 Camera PLIF (4 high speed cameras + 2 lasers)

The laser system, which is composed of a high speed Nd:YAG pumping a tunable high-speed dye laser is situated in the adjacent room and the beam is routed to the experimental setup. Prior to reaching the test rig, the beam is expanded into a sheet using a custom set of optics and is routed into the test rig from the top. The beam is about 4 inches in width and about 100μm in thickness. The combustor itself is fully accessible through the top port and two side windows on either side. Prior to the measurements, the Illinois calibration burner is inserted into the chamber and imaging is done with the exact same setup to ensure wavelength position of the laser as well as the intensity of the OH LIF signal, which can later be fully quantified using a spectroscopic model. The laser is tuned to the A-X (1,0) transition of OH at 283nm. For the shakedown of the rig, an air pressure atomizer was used while for the actual tests in August, an air blast atomizer was mainly utilized.

The two cameras on either side at the top are the PLIF detection cameras, which are both intensified. The bottom two cameras at a slight angle are the PIF cameras which are mounted in a scheimpflug setup so as to ensure clear focus across the entire imaging plane. The entire system is synchronized at 5 kHz, which is an adequate repetition rate considering the turbulent intensity of the required flow conditions. The setup was installed and tested in May 2015 and the actual full-scale measurements of A2, C5 fuels were conducted in August.

In addition to the quantification issue of the LIF signal, it became obvious during the May campaign that fuel PLIF was a major interference source in our measurements. In order to resolve this issue and to isolate the OH PLIF signal, a two camera PLIF setup was utilized with two differing spectral bandpass filters. The difference in the optical bandpass allows the ratio of OH and fuel PLIF to be varied and the strategy is to use one set of images to correct for the fuel PLIF in the other image. An example of this is shown in Figure ***2***.

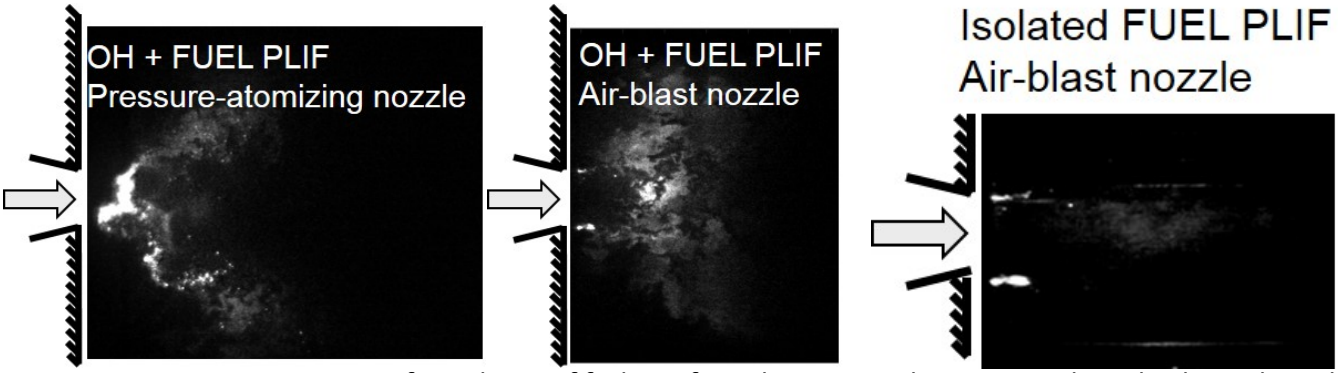


Figure 2. Two camera OH PLIF setup for isolation of fuel PLIF from the images. The image on the right shows the isolation of the fuel PLIF using the added camera with a wide band-pass filter and suppression of OH PLIF

Task 2 – Optimize and Apply Laser and Optical Diagnostics to Characterize Fuel Spray in Advanced Combustor Tests at the Referee Combustor

University of Illinois at Urbana-Champaign

Objective(s)

The objectives in this proposal are to work with AFRL in their referee rig experiments and achieve the following goals:

- Design and set up laser diagnostic and optical diagnostics for referee rig measurements.
- Implement phase Doppler anemometry to determine fuel spray characteristics, including droplet diameters and velocities.

Diagnostics Optimization and Setup

A 2D PDPA system was used to characterize the fuel droplets during combustion, measuring diameter and two components of velocity. The 2D PDPA (Dantec 112mm fiber PDPA) measures the frequency of the Doppler burst signal to determine velocity (one component from each pair of beam wavelengths) and the phase difference between two Doppler bursts to calculate the droplet diameter. An argon-ion laser (Ion Laser Technology), which produces a continuous laser beam with wavelengths ranging from 457 nm to 514.5 nm, is directed into a transmitter where the beam is split up by wavelength and coupled into optical fibers. Four beams, two at 488 nm and two at 514.5 nm (about 4 mW of power per beam), are focused by a 500mm focal length lens on the PDPA transmitter head and directed into the combustion chamber. The transmitter head and receiver head, with an 800mm focal length lens, are mounted on traverses placed on either side of the combustor. The traverses, fitted with encoders, are linked and controlled via a LabVIEW code. Data is collected using BSA Flow Software, and the data is written to text files.



Fuel Droplet Characterization

Droplet axial and radial velocity distributions, SMD distributions, and data collection rates for the fuels studied are presented. For A-2 at ϕ = 0.096, data collection rate is shown in Figure 1 as a function of y-position at various axial locations. The origin is taken to be the intersection of the centerline of the injector and the downstream face of the heat shield. Positive z-position is taken to be positive downstream (flowing out of the combustor) and y-position is taken to be positive up (towards the top of the combustor). The axes and basic referee rig geometry is shown in Figure 4 for reference. The data rate is a good indicator of where the spray is located and can be used to calculate and report spray angles. The low data collection rate near the centerline verifies that the fuel injection is a hollow cone.

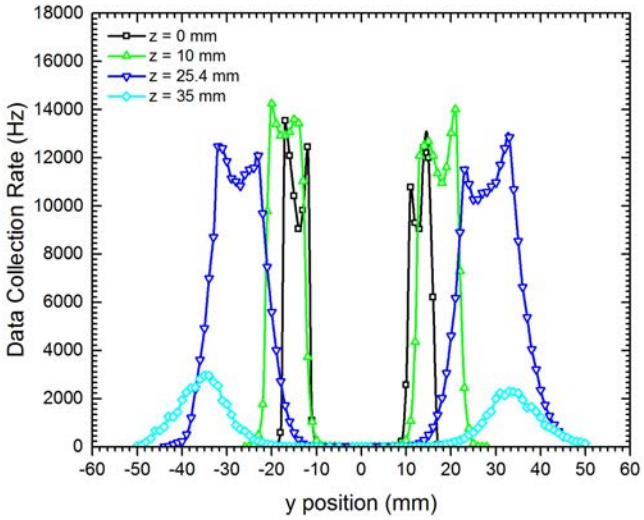


Figure 3. A-2 data collection rate. Data collection rate versus y-position at various axial locations for A-2 at ϕ=0.096

It is unsurprising that the width of each side of the spray increases with increasing distance downstream, and the overall width of the spray increases until it spans nearly the full height of the combustor (109 mm) by 35 mm downstream. At 35 mm downstream, the data collection rates are greatly diminished, which can be explained by further spread of the spray as well as evaporation due to combustion.

A. Comparison of Fuel Droplet Diameters

SMD is calculated at each position where diameter data is collected, and Figure 5a shows the SMD versus y-position 0 mm, 5 mm, and 10 mm downstream of the deflector plate for each fuel tested. SMDs are only reported at locations where more than 1000 droplets were measured. Figure 5b, 5c, and 5d show normalized histograms of the droplet diameters 10 mm, 15 mm, and 20 mm above the centerline at each axial location shown. The differences in SMD between the fuels are seen in the diameter histograms as a larger fraction of large droplets. As seen in Figure 5a, just downstream of the deflector plate (z = 0 mm), C-1 has a higher SMD than either A-2 or C-5, between 10 and 35 microns greater at y positions more than 12 mm above the centerline. This can be seen in Figure 5b, as C-1 has relatively few droplets with a diameter less than 20 microns compared with A-2 and C-5 at the same y positions. This seems to indicate that C-1 is either still undergoing fuel droplet breakup or that C-1 experiences less upstream evaporation compared to A-2 and C-5. At 5 mm downstream of the deflector plate, the A-2 and C-5 fuels have very similar SMDs at all measurement points where enough droplets were collected.

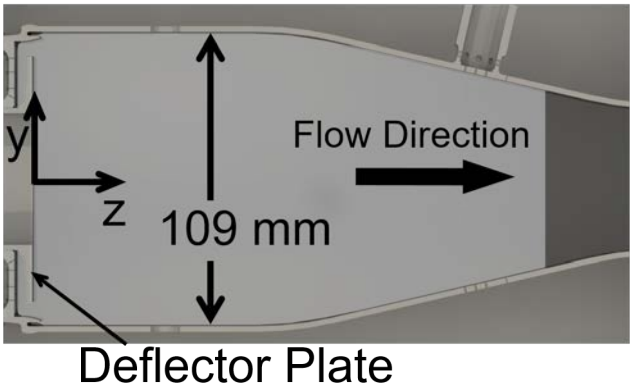


Figure 4. Cutaway of the single cup referee combustor. The origin is taken to be at the intersection of centerline of the combustor with the front plane of the deflector plate as marked.

The maximum difference between the SMDs for those two fuels is about 8 microns, occurring at y = 15 mm. The histograms in Figure 5c and 5d explain this difference; about 65 percent of the A-2 fuel droplets have diameters smaller than 20 microns while less than 50 percent of C-5 fuel droplets have diameters smaller than 20 microns. A-2 also has fewer than 4 percent of droplets with diameters larger than 40 microns while C-5 has about 10 percent of droplets with diameters larger than 40 microns. The C-1 fuel droplets have similar SMDs to A-2 and C-5 at y positions greater than 12 mm above the centerline, but below 12 mm, the SMDs of C-1 are 10 to 15 microns smaller than those of A-2 or C-5. It is also notable that the maximum C-1 SMD has dropped by about 25 microns, bringing it in line with the SMDs of A-2 and C-5.

At 10 mm downstream of the deflector plate, C-1 and A-2 have similar SMD profiles, with a maximum difference of about 11 microns from y = 10 mm up to 22 mm. The profiles diverge at y positions above 22 mm, with the A-2 SMDs increasing slightly, while the C-1 SMDs slowly decrease with increasing y position until it hits a minimum of 20 microns at 27 mm above

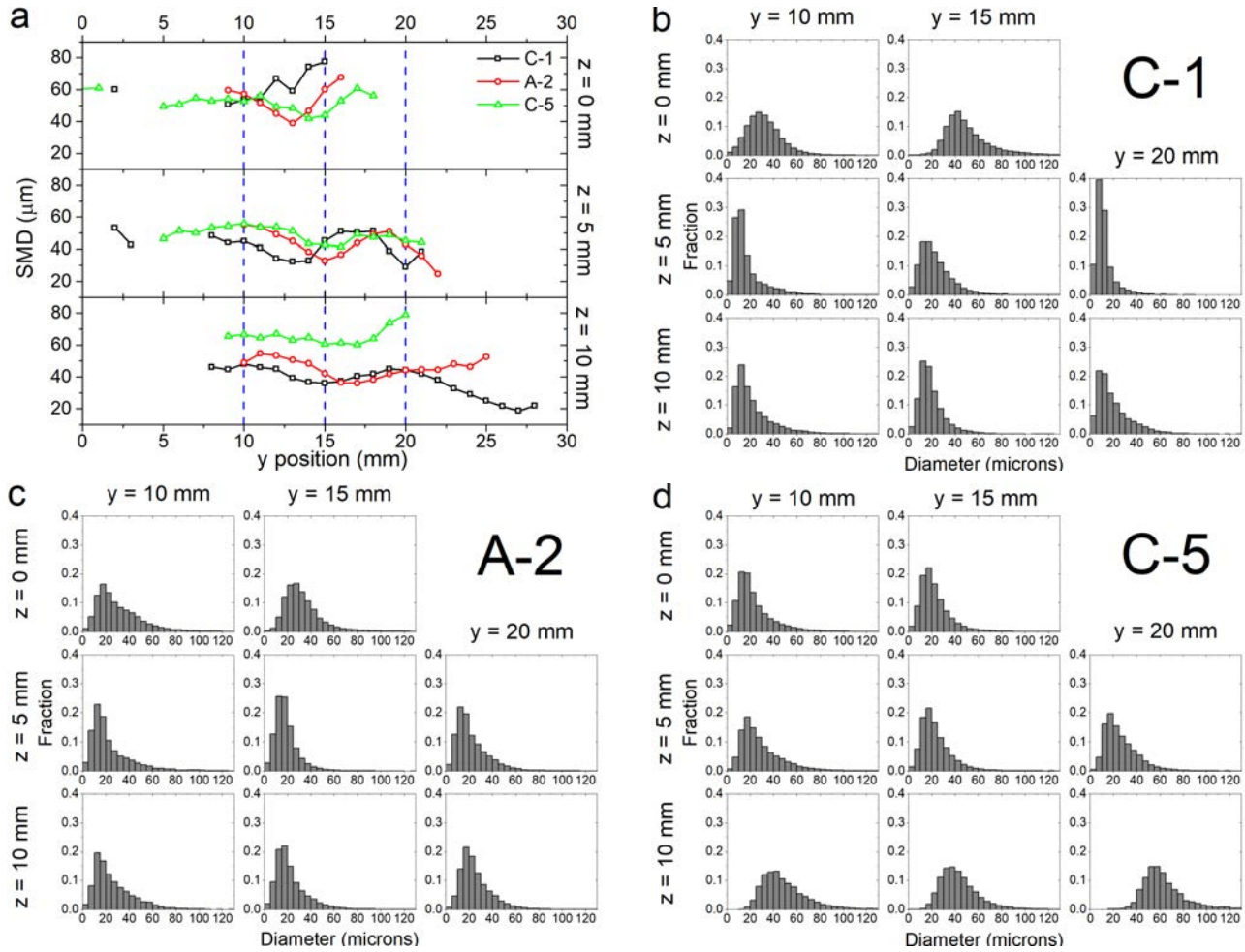


Figure 5. Sauter mean diameter and representative diameter histograms a) Sauter mean diameter plotted versus y position for each fuel 0 mm, 5 mm, and 10 mm downstream of the deflector plate for comparison with b) C-1 diameter histograms, c) A-2 diameter histograms, and d) C-5 diameter histograms

the combustor centerline. The C-5 fuel droplets at 10 mm downstream of the deflector plate show a marked decrease in the fraction of droplets smaller than 20 microns in diameter as seen in the last row of Figure 5b. Less than 3 percent of C-5 fuel droplets measured 10 mm downstream of the deflector plate (at y = 5, 10, 15 mm) have diameter smaller than 20 microns. At those same locations, at least 40 percent of A-2 and at least 57 percent of C-1 fuel droplets are smaller than 20 microns in diameter. The result of this absence of small C-5 fuel droplets is an SMD that is 12 to 37 microns greater than the corresponding C-1 or A-2 SMD. This indicates that small C-5 fuel droplets have almost completely evaporated between 5 mm and 10 mm downstream of the deflector plate. The small droplets are expected to evaporate first because they have a larger surface area to volume ratio than larger droplets. The evaporation of the small C-5 droplets before those of C-1 and A-2 is consistent with C-5's flat boiling curve (0 to 95 percent distillation between 155˚C and 165˚C). The C-1 (0 to 95 percent distillation between 175˚C and 246˚C) and A-2 (0 to 95 percent distillation between 160˚C and 255˚C) fuels boil over a much wider range of temperatures.

B. Droplet Velocities

Figure 6 shows the A-2 fuel droplet mean axial and radial velocity distributions versus y-position at various axial locations. Both the axial and radial velocity distributions are symmetric about the centerline, and the distributions broaden with increasing downstream location. One interesting feature present in both the axial and radial velocity distributions is the near zero or slightly negative velocities along the centerline. This indicates the presence of an inner recirculation zone, but very few droplets are present in the center as indicated by the low data collection rates near the centerline. As seen in Figure 6, the mean radial velocity profiles at 0 mm, 5 mm, and 10 mm downstream of the deflector plate are very similar to each other. At 25 mm and 35 mm downstream of the deflector plate, the radial velocity profiles broaden and the maximum droplet velocities decrease. The axial velocity profiles at 5 mm and 10 mm for A-2 exhibit a sharp peak that roughly corresponds with the center of the spray as marked by the data collection rate. As with the radial velocity, the axial velocity profiles broaden and have a lower maximum value further downstream (25 mm and 35 mm).

A comparison of fuel droplet radial velocity for the different fuels is shown on the left in Figure 7 at 0 mm, 5 mm, and 10 mm downstream of the deflector plate, and a comparison of fuel droplet axial velocity at 5mm is shown on the right in Figure 7. The radial velocity profiles for each fuel have a great deal of similarity across the fuels at each downstream position shown. Figure 7 also shows the axial velocity profile 5 mm downstream of the deflector plate. The C-1 axial velocity profile is slightly different from C-5 and A-2, reaching its peak about 2 mm inside of the peaks for C-5 and A-2.

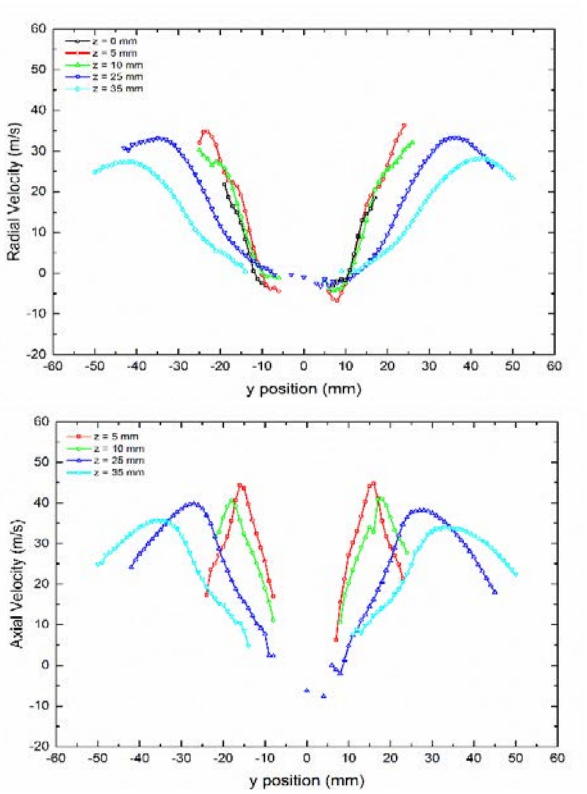


Figure 6. A-2 fuel droplet mean radial and axial velocity. Mean radial velocity plotted against y position (top) and mean axial velocity plotted against y position (bottom) at various distances

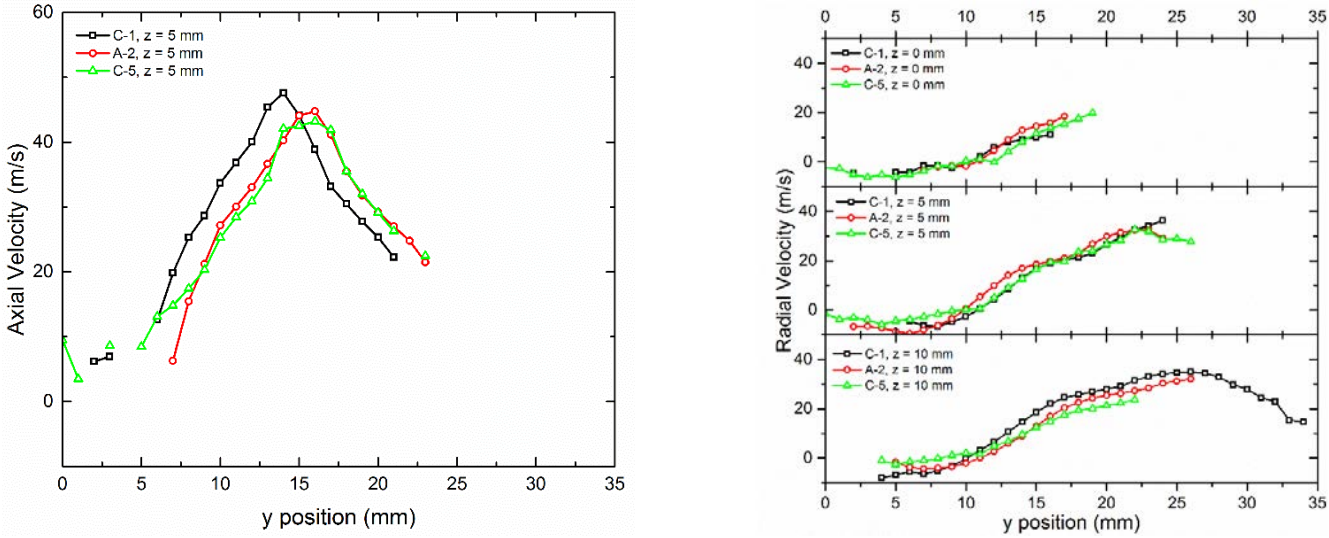


Figure 7. Axial and radial velocity profiles. a) Axial velocity plotted versus y position for each fuel 5 mm downstream of the deflector plate and b) radial velocity plotted as a function of y position at 0 mm, 5 mm, and 10 mm downstream of the deflector plate for each of the tested fuels.

Comparison to OH* Chemiluminescence

The imaging of OH* chemiluminescence is conducted using a LaVision High-Speed IRO and Photron FASTCAM SA-Z with a Semrock Brightline 320/40 bandpass filter in front of a Cerco, 100 mm, f/2.8 UV lens. Images are taken at 20 kHz with a 1000 ns gate and 60 percent gain. The spatial resolution for the imaging is approximately 0.29 mm per pixel, and a total of 3000 images are used for each average image. Excited OH* is a good indicator of heat release rate from the flame zone, which makes it useful for visualizing flame structure. The OH* chemiluminescence signal is normalized by the maximum possible intensity to yield the reported image.

Average OH* chemiluminescence images show significant differences in the flame structures of the different fuels as seen in Figure 8. The averaged chemiluminescence images are normalized by the maximum intensity in each averaged image. The C-1 flame has straight top and bottom edges, suggesting that the flame is stabilized on the spray edges, while the A-2 and C-5 flame have more rounded top and bottom edges. The flames for all three fuels demonstrate some amount of asymmetry; gravitational effects likely play some role in this asymmetry. However, the A-2 flame has significantly more OH* emission in the lower half of the combustor than in the top half. A proposed explanation for C-1's lower deviation from axisymmetry is that, because of its lower cetane number, the flame anchors more closely to the spray zone where equivalence ratio will be highest, resulting in flame emission that largely follows the spray cone. A proposed explanation for C-5's reduced deviation from axisymmetry is that low-temperature vaporization results in the fuel droplets rapidly evaporating, creating a fuel vapor cloud that is negligibly affected by gravity. A-2 has neither of these fuels' extreme properties, allowing gravitational effects on the A-2 fuel droplets to play a larger role, resulting in more lower half OH* emission.

Figure 8 shows the SMD distribution superimposed on the average OH* image with marker size corresponding to the SMD. The C-1 droplet SMD profile at 10 mm downstream (the closest SMD profile to the start of the C-1 flame) shows a decrease in SMD at y-positions greater than 19 mm, corresponding to an absence of OH* emission at these locations. This indicates that outside of the main body of the flame, the smallest droplets do not evaporate as rapidly. A comparison of the SMD profile and diameter histograms for C-5 at 10 mm downstream of the deflector plate show that the smallest droplets have already evaporated before reaching the body of the flame, which starts at about 15 mm downstream. The local minimum in the SMD distribution at z = 10 mm, corresponding to a y position of 17 mm for A-2 and C-5 and 15 mm for C-1 spatially correlates with outer edge of flame structure, indicating that the flame is stabilizing on the interior of the spray cone. The observable differences in flame structure, as marked by the averaged OH* emission, combined with the SMD distributions provides valuable insight into the complex spray combustion processes near LBO.

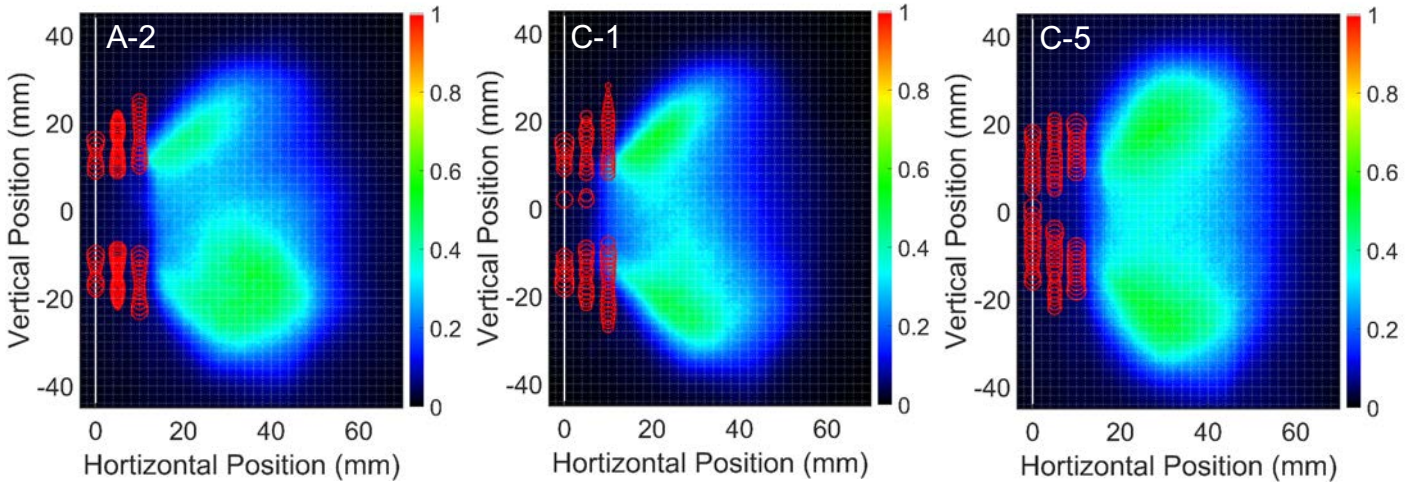


Figure 8. Average OH* chemiluminescence images. SMD distributions are superimposed on the average normalized OH* image with the marker size corresponding to the SMD calculated at each point.

Task 3 – Optimize and Apply Laser and Optical Diagnostics for Application in the Advanced Ignition Tests at Georgia Institute of Technology and Army Research Laboratory

University of Illinois at Urbana-Champaign

Objective(s)

The objectives in this proposal are to work with Georgia Tech in their advanced ignition experiments and achieve the following two goals:

- Evaluate the experimental ignition testing setup and operating conditions for laser and optical diagnostics
- Design and set up laser and optical diagnostics for use in ignition experiments at Georgia Institute of Technology

Research Approach

Diagnostics Optimization and Setup on Georgia Tech Atmospheric Ignition Rig

The main goal is the development of 2D diagnostics using Planar Laser Induced Fluorescence (PLIF), Schlieren, and OH* chemiluminescence to understand the ignition development at the boundaries and flame dynamics in the GATech atmospheric ignition rig. The goal is to apply simultaneous measurements from high speed PLIF, Schlieren, and chemiluminescence. For each of the imaging sets, we will look to obtain spatially resolved data. We will configure and set up the laser and optical diagnostics equipment around the ignition rig at GATech. For the high speed PLIF measurements, we pumped a high speed dye laser (Credo, Sirah) with a high speed diode pumped Nd:YAG (Edgewave) for generation of the UV light. The PLIF, Schlieren, and chemiluminescence imaging will be 10 kHz. Energy per laser pulse at these conditions may be small (200 µJ/pulse) and light collection from the PLIF will be enhanced using a f/2.8 UV lens.

Georgia Tech Ignition Experiments

The primary effort on the ignition experiments was transporting the Edgewave Nd:YAG high repetition rate laser to Georgia Tech. The laser was coupled to the Sirah Credo Dye Laser, as shown in Figure 9 (left), and both lasers were tuned to optimize laser power and beam profile. Optics to form and steer the laser sheet in through the top of the combustor, as shown in Figure 9 (right). The primary ignition testing campaign was carried out by Georgia Tech personnel.

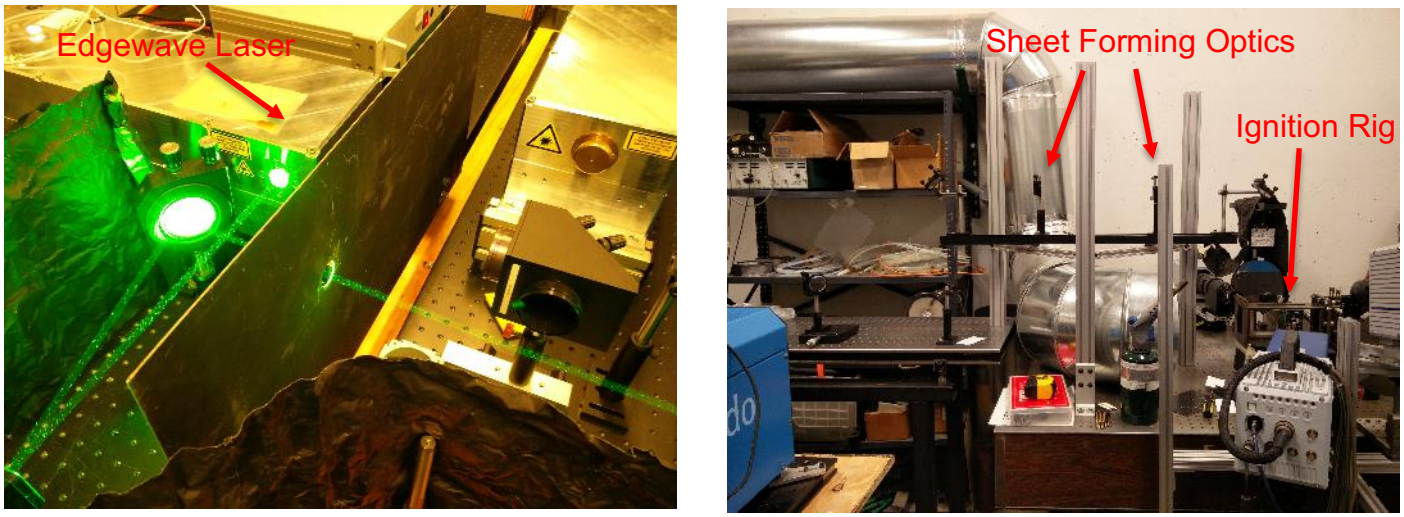


Figure 9. Edgewave pump laser (left) and dye laser with sheet forming optics, and the ignition rig

Task 4 – Measure Ignition Probability for Various Fuels at High Altitude Conditions and Implement High-Speed Imaging to Visualize Ignition Process

University of Illinois at Urbana-Champaign

Objective(s)

The objectives in this proposal are to work with ARL in the design, setup, and implementation of ignition experiments in the high-altitude chamber at Army Research Laboratory at Aberdeen Proving Ground:

- Design and set up sector rig in high altitude chamber at Army Research Laboratory at Aberdeen Proving Ground.
- Conduct measurements of ignition probability at high altitude conditions (low temperature, low pressure).
- Implement high-repetition rate broadband and OH* imaging to visualize ignition kernel and flame kernel propagation.

Research Approach

The process of developing and approving new jet fuels derived from alternative feedstocks requires certifying that those fuels, whether neat or blended with conventional fuels, can be used in current engines without hardware modification. Understanding how these new fuels perform in extreme combustion regimes is important to ensuring that the fuels can be used as drop-in replacements. One regime in which it is essential that new fuels perform as well as conventional fuels is in a scenario where an engine needs to be relit at high altitude. The lower temperatures and pressures seen at high altitudes result in a lower probability of spark kernel ignition and flame stabilization when compared to sea level conditions. A few of the causes of this reduced probability include slower chemistry, poorer atomization due to the higher fuel viscosity, slower evaporation due to the reduced vapor pressure of the fuel, and shorter spark kernel lifetime due to the entrainment of the lower temperature air. To study the effects of fuel differences in this high altitude relight scenario, a gas turbine combustor sector rig was designed and built. The sector rig is operated inside of a high-altitude chamber with the chamber conditions varying as shown in Table 1, with 30,000 ft being the highest altitude that the chamber is capable of simulating.

Table 1. Chamber air temperature and pressure as a function of altitude

Altitude (ft)	T_{air} (K)	P_{air} (kPa)
0	288	101.3
10,000	268	69.6
20,000	249	46.6
25,000	239	37.7
30,000	229	30.2

Ignition probabilities for alternative and conventional jet fuels are measured in a gas turbine sector rig inside of a high-altitude chamber as shown in Figure 10. Experiments are designed to simulate combustor relight at high altitude conditions. Initial relight experiments were conducted at conditions representative of ambient air at 10,000 feet with an air mass flow rate of 0.3lbm/s. This air flow mass flow rate resulted in a pressure drop across the swirler of 3.87%. The fuel is chilled by placing the fuel holding vessel in the inlet air flow path, resulting in an average fuel injection temperature of -15°C. The equivalence ratio is varied by changing the inlet fuel pressure, and fuel flow rates could be varied to achieve equivalence ratios from 0.6 and 1.0. This range of equivalence ratios was sufficient to span from no ignition to always igniting.

A single test begins with the opening of a solenoid valve just upstream of the nozzle, allowing fuel flow at the desired equivalence ratio. After two seconds in which the fuel flow rate is allowed to stabilize, a 24 VDC voltage is supplied to an ignition exciter (Champion CH305050), which supplies high voltage to an igniter from a General Electric T700 at a frequency of 3.7 Hz. The igniter is allowed to spark for 10 seconds, after which the voltage and fuel supply are stopped. The sparks and flame are monitored with a photo diode as well as a high-speed camera (Photron SA-Z) coupled to a high-speed intensifier (LaVision IRO), fitted with a bandpass filter centered at 320 nm, with a full-width, half-max of 20 nm. A sample photodiode trace is shown in Figure 12. The spark emission events are shown as the sharp peaks, and the flame is observed as the slight increase in photodiode signal above the baseline between the sharp peaks.

A total of 5 fuels were tested, all from the National Jet Fuel Combustion Program. Three conventional fuels, designated A-1 (JP-8), A-2 (Jet A), and A-3 (JP-5), represent current petroleum-derived fuels that are used in modern aircraft engines. Two category C fuels were tested as well, designated C-1 and C-3. The C-1 fuel is Gevo alcohol-to-jet; its notable properties are a low derived cetane number (~16) and a relatively low temperature boiling curve. C-3 is notable for its high viscosity, a parameter that is particularly important for atomization at these low temperatures.



Figure 10. High altitude chamber at the Army Research Laboratory at Aberdeen Proving Ground

For each test, a photo diode trace is obtained, like the one shown in Figure 12 (Task 5). A flame is considered to have stabilized when the ratio of the absolute value of the integrated negative signal to the integrated positive signal is less than 1% for two consecutive periods between sparks. The number of sparks that do not result in a stable flame are counted along with the one spark that resulted in the stable flame. The ignition probability for a single equivalence ratio for a single fuel is the number of successful sparks divided by the total number of sparks. The ignition probability for all of the fuels and equivalence ratios tested are shown in Figure 10 as well as the binomial regression fits calculated from the ignition probabilities. Defining the 'best' fuel case as the fuel that has the highest ignition probability for each equivalence ratio, the preliminary analysis yielded a fuel ordering, from best to worst of: A-1, C-1, A-2 and A-3 about equal, and then C-3. More complete analysis of the images and ignition probabilities is ongoing; however, the parameters that appear to be most important in determining ignition probability are viscosity and vapor pressure at the temperatures measured in the rig. Further analysis of the video will provide a better qualitative understanding of the process in which a spark kernel leads to a flame kernel, eventually resulting in stabilization of the flame in the combustor. Further testing is required and planned to obtain lower uncertainties in the probability curves as well as to obtain data for more fuels and at more altitudes.

Task 5 – Measure Ignition Delay at Low Temperature Conditions for Fuels with Targeted Cetane Numbers

University of Illinois at Urbana-Champaign

Objective(s)

The objectives in this proposal are to make measurements of ignition delay of targeted cetane number fuels developed by ARL cetane number has shown a strong correlation to lean blow out equivalence ratio.



Varied Cetane Number Army Research Fuels

Six different fuels have been tested to measure the ignition delay time in the RCM. These fuels are blended to match a targeted cetane number between 30 and 55. CN 50 appears to be the base fuel used prior to the inclusion of cetane inhibitors /improvers. Isododecane (pentamethylheptane) is used as the cetane inhibitor, as well as naphthalene in the CN 30. Inclusion of higher n-alkanes (C14 - C16) is used as the cetane improver for CN 55. Navy Fuel Composition and Screening Tool (FCAST) have been used to classify detailed chemical group composition of the fuels as in Table 2. Contents of isoalkanes and aromatics are higher for low cetane number fuels, whereas higher cetane number fuels tend to contain more normal alkanes.

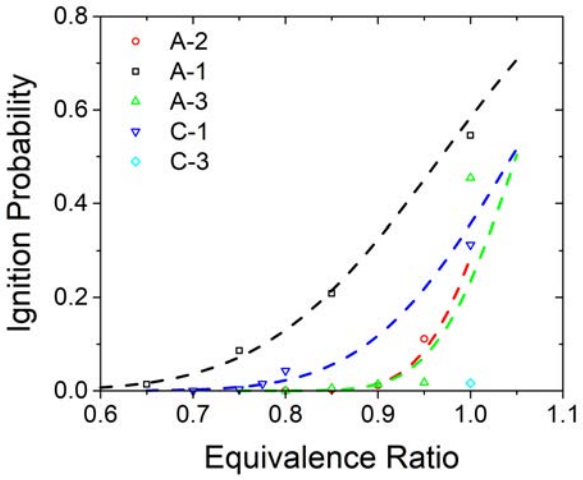


Figure 11. Ignition Probability versus equivalence ratio for the 3 category A fuels and 2 category C fuels at 10,000 ft.

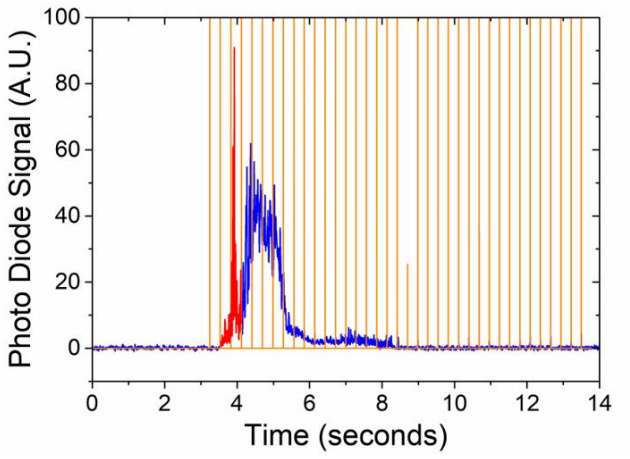


Figure 12. Example photodiode trace of sparks and a successful ignition

Table 2. Composition of the Army research fuels tested

mass %	Jet A-30CN	Jet A-35CN	Jet A-40CN	Jet A-45CN	Jet A-50CN	Jet A-55CN
Normal Alkanes	16.02	16.48	21.83	19.54	36.50	54.10
Isoalkanes	54.80	58.22	41.41	48.14	34.14	28.33
Cyclocalkanes	3.85	1.21	3.22	10.94	12.18	6.08
Aromatics	25.32	24.08	33.53	21.41	17.18	11.46

Ignition Delay of Varied Cetane Number Fuels

Ignition delay time measurements have been conducted for compressed pressures of P_c=20 bar, at equivalence ratios (φ) of 1.0, 0.5, and 0.25. Compressed temperature T_c varies by compression ratio: 615K to 725K. Figure 14 shows measured ignition delay time at P_c=20 bar.

As expected, fuel with lower cetane number results in longer ignition delay, and the tendency is more prominent at leaner conditions. In the φ=1 case, some of the ignition delay time results do not exactly follow the cetane number ordering. No negative temperature coefficient (NTC) behavior is observed in these tests. Further analysis of the φ=0.25 case is illustrated in Figure 13, where dotted lines are separated first stage ignition delay time. The difference in first stage ignition delay time by fuels are much less than difference in overall ignition delay time. In other words, the second stage ignition delay constitutes nearly all of the differences in the overall delay time. Additional ignition delay time measurements will be conducted at lower compressed pressure, P_c=10 bar. Further analysis on multistage ignition will be investigated using CHEMKIN, chemical kinetics simulation results.

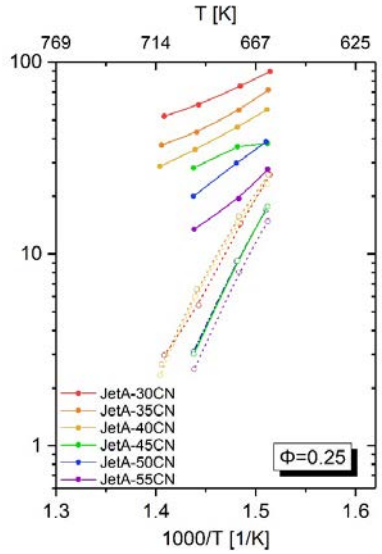


Figure 14. First and overall ignition delay time results at φ=0.25

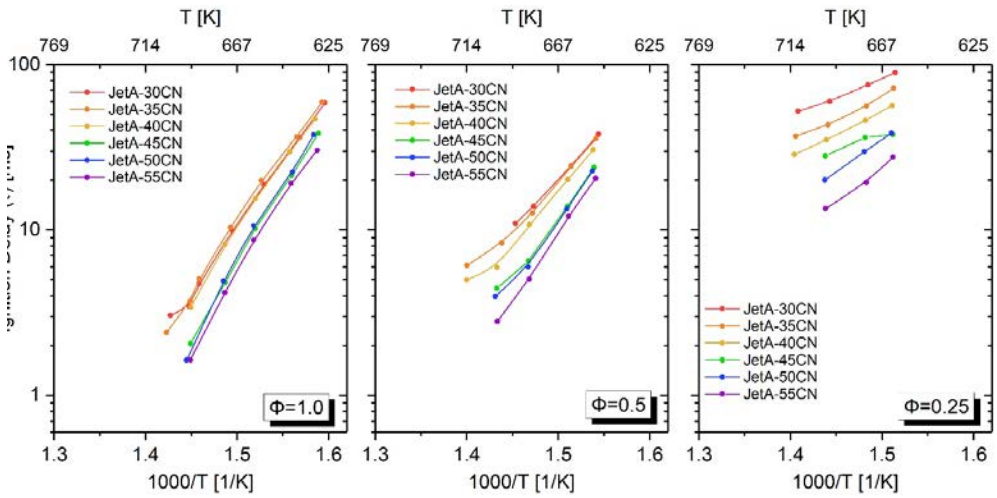


Figure 13. Ignition delay times of Jet A fuels with varied cetane numbers at Pc=20 bar, varied temperatures, and equivalence ratios

Milestone(s)

Milestones from each period

Year I

Proposed (3 Month): At the 3-month mark, we will conclude the analysis of the experimental setup and should be close to finishing the design of the laser and diagnostics setup.
Achieved: Design of the laser setup complete and fabrication of calibration torch started.

Proposed (6 Month): At the 6-month mark, we should be finalizing the experimental setup and getting ready to deploy measurements described in Task 1 of the proposal. Fuel screening will be conducted during this phase.
Achieved: Most of experimental setup was completed. Calibration torch completed and initial quantification of radicals complete.

Proposed (9 Month): At the 9-month mark, we should be almost complete with the initial shakedown of the tests in Task 1 and making changes to optimize the experimental setup. Send preliminary test guidelines and results of the fuel screening studies (sensitivity to fuel characteristics) to the modeling groups.
Achieved: First test run at GATech for simultaneous PLIF and PIV successfully completed and results analyzed. Laser and optical setup successfully implemented and tested. Identified key problems such as fuel PLIF. Main measurement campaign set for last quarter.

Proposed (12 Month): At the 12-month mark, we should have completed an initial set of data for tasks outlined in the proposal. We should be planning for additional measurements in the next phase of the combustion program.
Achieved: Major three-week campaign completed at GATech for two of the test fuels. Experiments included two camera PLIF and stereo PLIF over a wide range of test conditions. Data analysis started. Fuel PLIF isolated using two camera PLIF setup with differing detection bandwidth.

Year II

Proposed (3 Month): At the 3-month mark, we will have identified the key features that are important in the design of the rig. Preliminary designs will have been shared with the OEMs for feedback.
Achieved: Two rounds of preliminary designs have been completed and key features have been identified.

Proposed (6 Month): At the 6-month mark, we should be have finalized the design and sent the drawings to the machine



shop for construction.
Achieved: The designs have been finalized and drawings sent to the machine shop. Materials for the rig have been ordered.

Proposed (9 Month): At the 9-month mark, we should have the main body of the high altitude relight rig constructed and windows for the rig purchased.
Achieved: The main body of the rig has been machined and assembled.

Proposed (12 Month): At the-12 month mark, we should have obtained the swirler and injector and made any modifications to the rig to ensure that they fit into the main body.
Achieved: The swirler and injector have been retrieved from Wright-Patterson Air Force Base. Preparations have been made to transport the rig to ARL.

Year III
Proposed (3 Month): At the 3-month mark, we should have shipped the sector rig to ARL to begin setting it up in the high altitude chamber.
Achieved: Army Research Combustor-L1 shipped to ARL, and preparations for high altitude relight campaign have begun.

Proposed (6 Month): At the 6-month mark, we should have purchased peripheral components for the high altitude relight campaign, and a test matrix should have been decided.
Achieved: The designs have been finalized and drawings sent to the machine shop. Materials for the rig have been ordered.

Proposed (9 Month): At the 9-month mark, we should have completed the high altitude ignition probability test matrix set out in the previous period. The ignition delay measurements in the RCM should have been completed.
Achieved: High altitude relight measurements at 10,000 ft, and hardware upgrades for future campaigns have been planned. Ignition delay measurements have been completed.

Proposed (12 Month): At the 12-month mark, we should have finished analyzing the ignition probability data and RCM ignition delay data.
Achieved: Preliminary analysis of the ignition probability data and RCM data has been completed.

Major Accomplishments

High-Speed OH PLIF and Stereo-PIV imaging in the Georgia Tech Gas Turbine Rig
Laser and camera systems for the high-speed OH PLIF and stereo-PIV were set up and implemented at Georgia Tech on the advanced gas turbine rig. One observed issue was the presence of significant fuel PLIF, which was mitigated using a two camera PLIF setup with two differing spectral bandpass filters. The difference in the optical bandpass allows the ratio of OH and fuel PLIF to be varied; one set of images is used to correct for the fuel PLIF in the other image set. Quantification of the OH PLIF signal was also conducted using a flat-flame calibration burner developed at UIUC.

Fuel Spray and Flame Characterization in the Referee Combustor
A 2D PDA system is used to make measurements of fuel droplet diameters and velocities for Jet-A and two alternative jet fuels under the ASCENT's NJFCP. Average OH* chemiluminescence images are used to determine flame structure to correlate spray characteristics with flame location. The axial and radial velocity profiles show great similarity between the fuels with near identical radial velocity profiles and only small differences in the axial velocity profiles. The OH* emission reveals some distinct differences in the flame structure for each of the fuels. The observed differences in SMD profiles and mean velocity distributions do not seem sufficient to explain the differences in LBO equivalence ratio.

Georgia Tech Atmospheric Ignition Experiments
We transported and setup the laser system around the ignition rig at GATech for the execution of simultaneous PLIF, Schlieren, and OH chemiluminescence imaging. Imaging and measurements of ignition probability in a stratified flow of pre-vaporized fuel and air were conducted.

High Altitude Relight Combustor
Design and fabrication of a high altitude relight rig, replicating the key geometry and flow features of the referee rig has been completed. The sector rig was set up in the high-altitude chamber, and modifications to the chamber and fuel delivery system were made. Measurements of ignition probability for 5 fuels across a range of equivalence ratios at

ambient pressure and temperature conditions that correspond to 10,000 ft. Further data is needed at higher altitudes to gain a better understanding of the fuel properties that drive ignition behavior at these conditions.

Target Cetane Number Ignition Delays
Ignition delay measurements for targeted cetane number fuels, with cetane numbers varying from 30 to 55, were made in a rapid compression machine at the University of Illinois at Urbana-Champaign. Higher cetane number correlated strongly with shorter ignition delay at low temperature. The results warrant further investigation into the targeted cetane number fuels in the NTC region to gain a better understanding of how the cetane number drives autoignition delay time in this regime.

Publications

Chterev II, Rock NN, Ek HH, et al. Reacting Pressurized Spray Combustor Dynamics: Part 2 — High Speed Planar Measurements. ASME. Turbo Expo: Power for Land, Sea, and Air, Volume 4A: Combustion, Fuels and Emissions ():V04AT04A020. doi:10.1115/GT2016-56345.

E. Mayhew, C. Mitsingas, B. McGann, T. Lee, T. Hendershott, S. Stouffer, P. Wrzesinski, A. Caswell, Spray Characteristics and Flame Structure of Jet A and Alternative Jet Fuels, AIAA SciTech, AIAA-2017-0148, 2017

I. Chterev, N. Rock, H. Ek, B. Emerson, J. Seitzman, T. Lieuwen, D. Noble, E. Mayhew, T. Lee, Simultaneous High Speed (5 kHz) Fuel-PLIE, OH-PLIF and Stereo PIV Imaging of Pressurized Swirl-Stabilized Flames using Liquid Fuels, AIAA SciTech, AIAA-2017-0152, 2017

Outreach Efforts

None

Awards

I. Chterev, N. Rock, H. Ek, B. Emerson, J. Seitzman, T. Lieuwen, D. Noble, E. Mayhew, T. Lee, Simultaneous High Speed (5 kHz) Fuel-PLIE, OH-PLIF and Stereo PIV Imaging of Pressurized Swirl-Stabilized Flames using Liquid Fuels, AIAA SciTech, AIAA-2017-0152, 2017
(winner of the ***The Walter R. Lempert Student Paper Award in Diagnostics for Fluid Mechanics, Plasma Physics, and Energy Transfer***)

Student Involvement

Five graduate students (listed above) have participated in this project on a rotational basis to address various aspects of the project. Rajavasanth designed and fabricated the calibration burner used at GATech, and conducted experiments to determine the actual concentration of radical concentrations in the flame. Two other students (Stephen Hammack and Eric Mayhew) made trips to GATech to make test measurements in the high shear combustor. This included assisting in the setup of the laser and optics as well as participating in the actual measurements. The calibration torch as well as other optical and imaging equipment was taken down to GATech for testing.

Two students (Brendan McGann and Eric Mayhew) set up and executed the PDPA measurements outlined in Task 1and they (Brendan McGann and Eric Mayhew) traveled to GATech to transport and couple the Edgewave Nd:YAG pump laser to the dye laser for use in the PLIF imaging. In addition, they assisted in the setup of the optics and participated in the initial phase of the measurements. The Edgewave and other optical and imaging equipment was taken down to GATech for testing. Rajavasanth designed and fabricated the high altitude relight chamber.

Brendan McGann and Eric Mayhew also made trips to ARL to deliver and set up the Army Research Combustor-L1 in preparation for the high altitude experiments. Three students (Brendan McGann, Constandinos Mitsingas, and Eric Mayhew) set up and executed the high altitude relight experiments outlined in Task 1. Kyungwook Min conducted the ignition delay measurements in RCM at UIUC.

Plans for Next Period

As of this report, all tasks have been completed but if required we will continue to participate in the NJFCP program to gather more high altitude data at the Army Research Laboratory.

Project 027B Advanced Combustion (Area #3)

Georgia Institute of Technology
Oregon State University

Project Lead Investigator

Tim Lieuwen
Professor
Aerospace Engineering
Georgia Institute of Technology
270 Ferst Drive, G3363 (M/C 0150)
Atlanta, GA 30332-0150
404-894-3041
tim.lieuwen@ae.gatech.edu

University Participants

Georgia Institute of Technology

- P.I.(s):
  - Professor Tim Lieuwen
  - Professor Jerry Seitzman
  - Professor Wenting Sun
- FAA Award Number: 13-C-AJFE-GIT-008
- Period of Performance: 12/1/2017 to 11/30/2018
- Task(s):
  - Lean Blowout. This task measures the lean blowout characteristics of alternative jet fuels and compares them to the lean blowout characteristics of jet A.
  - Ignition. This task measures the ignition probabilities of alternative jet fuels and compares them to the ignition probabilities of jet A.

Oregon State University

- P.I.(s): David Blunck
- FAA Award Number: 13-C-AJFE-OSU-02
- Period of Performance: 12/1/2017 to 11/30/2018
- Tasks:
  - Turbulent Flame Speed. This task measures the turbulent flame speeds of alternative jet fuels and compares them to the turbulent flame speeds of jet A.

Project Funding Level

Georgia Institute of Technology
FAA Funding: $206,000
Cost Share: $206,000 provided by Georgia Institute of Technology

Oregon State University
FAA Funding: $59,000
Cost Share: $59,000 provided by Oregon State University



Investigation Team

Tim Lieuwen (Georgia Institute of Technology): Principal Investigator. Professor Lieuwen is the PI overseeing all tasks, and is manager of Task 1.
Jerry Seitzman (Georgia Institute of Technology): Co-Principal Investigator. Professor Seitzman is the manager of Task 2.
David Blunck (Oregon State University): Co-Principal Investigator. Professor Blunck is the manager of Task 3.
Wenting Sun (Georgia Institute of Technology): Co-Principal Investigator. Professor Sun is acting as an internal expert consultant on kinetic mechanisms
Tonghun Lee (University of Illinois at Urbana-Champaign): Co-Principal Investigator. Professor Lee is the lead diagnostic expert.
Benjamin Emerson (Georgia Institute of Technology): Research Engineer. Dr. Emerson is responsible for designing and maintaining experimental facilities, experimental operations and management & safety of graduate students. He is also acting as the administrative coordinator for all three tasks.
David Wu (Georgia Institute of Technology): Research Engineer. Mr. Wu is responsible for designing and maintaining experimental facilities, experimental operations and management & safety of graduate students.
Glenda Duncan (Georgia Institute of Technology): Administrative Staff. Mrs. Duncan provides administrative support.
Tiwanna Williams (Georgia Institute of Technology): Administrative Staff. Mrs. Williams provides administrative support.
Seth Hutchins (Georgia Institute of Technology): Lab Coordinator. Mr. Hutchins maintains the core lab facilities and provides technician services.
Machine Shop Staff (Georgia Institute of Technology). The Aerospace Engineering machine shop provides machining services for experimental facility maintenance/construction
Nick Rock (Georgia Institute of Technology): Graduate Student. Mr. Rock is leading the lean blowout task.
Hanna Ek (Georgia Institute of Technology): Graduate Student. Ms. Ek is the lead data analyst for the lean blowout task.
Sheng Wei (Georgia Institute of Technology): Graduate Student. Mr. Wei currently leads the ignition task.
Jonathan Bonebrake (Oregon State University): Graduate Student. Mr. Bonebrake was the lead grad student experimentalist on the turbulent flame speed task.
Nathan Schorn (Oregon State University): Graduate Student. Mr. Schorn recently started and has transitioned to leading the effort to operate the burner and collect and analyze data
Eric Mayhew (Graduate Student, University of Illinois at Urbana-Champaign): Graduate Student. Mr. Mayhew leads the execution of laser and optical diagnostics at ARFL.

Project Overview

The objective of this project was to provide advanced combustion testing of alternative jet fuels. We performed this advanced combustion testing to accomplish two goals. The first goal was to rank the lean blowout boundaries, ignition probabilities, and turbulent flame speeds of alternative fuels relative to conventional Jet A. The second goal was to produce data that could support the modeling and simulation tasks of other teams. For the second goal, data were measured as needed and as requested by the other teams. These data typically consisted of velocity field measurements, high speed flame images, and test rig boundary conditions.

During this program we tested twenty total fuel mixtures. Sixteen of the fuels have been pure (un-blended) fuels, known to the program as: A1, A2, A3, C1, C2, C3, C4, C5, S1, S2, S3, high TSI, C7, C8, C9, and n-dodecane. The A1, A2, and A3 fuels represent the range of conventional jet-A fuels. The other fuels have different physical and/or chemical properties. We have also tested three different sets of blends: A2/C1 blends, A2/C5 blends, a C1/n-heptane blend, and a C1/n-dodecane blend. These fuels have been tested under three different tasks, which are summarized next and which are detailed in the rest of this report.

(1) The first task consisted of lean blowout (LBO) measurements. The highest priority lean blowout measurement was fuel screening, where the blowout boundaries of various fuels were compared to the blowout boundary of jet A. This task also included measurements of the combustor velocity field, the spatio-temporal evolution of the flame position, and several thermodynamic rig boundary conditions. Thermodynamic boundary conditions included measurements such as air flow rates, surface temperatures, gas temperatures, and gas pressures.

(2) The second task consisted of forced ignition measurements. Like the blowout task, the highest priority forced ignition measurement was fuel screening. In the case of the forced ignition task, the fuel screening activity measured the ignition probabilities of various fuels and compared them to the ignition probability of Jet A. Ignition probability is a common measure of combustor ignitability. It was measured by sparking the igniter hundreds of times and measuring the fraction of spark events that successfully ignited the combustor. This task included a modeling



component which began to develop predictive capability for ignition probability. Such a predictive capability would take combustor conditions (pressure, temperature, and fuel-air ratio), in addition to key fuel properties (vaporization and chemical kinetic properties), as inputs and would produce an ignition probability as the output. To support this modeling effort, the forced ignition task produced measurements of detailed ignition physics. These detailed measurements captured fuel spray images, ignition kernel images, and flame images.

(3): The third task consisted of turbulent flame speed measurements. Like the other two tasks, the high priority measurement was fuel screening. For this task, fuel screening compared the turbulent flame speeds of various fuels to the turbulent flame speed of Jet A. This task additionally had a significant rig development aspect. The rig development added sub-atmospheric pressure capability.

These tasks were designed to address critical needs of the larger program. These needs are the rapid screening of alternative fuels and detailed measurements to support the modeling teams. The rest of this report details the specific activities that have been conducted under each of these tasks to address these important needs.

Task 1- Lean Blowout

Performance site: Georgia Institute of Technology

Objective(s)

The objective of this task was to obtain two types of measurements-fuel screening and detailed diagnostics- in a combustor rig operating near lean blowout. The objective of the fuel screening was to rank the blowout boundaries of each fuel relative to the blowout boundary of jet-A. The objective of the detailed diagnostics was to produce data that could support the modeling teams by providing physical insight and important simulation boundary conditions.

Research Approach

This task was performed with the combustor rig, shown in Figure 1. The rig is a high pressure, swirl-stabilized spray combustor with OEM-relevant hardware. The combustor was configured similarly to the referee rig at the Air Force Research Lab. The difference between the Georgia Tech rig and the referee rig is their dome and liner cooling arrangements. The referee rig has a greater level of complexity of these components, providing a closer simulation of a real combustor. However, the reduced complexity of the Georgia Tech rig enabled a greater rate of data generation. The reduced complexity of the Georgia Tech rig also enabled laser-based diagnostics that were not possible in the referee rig.

The research approach consisted of four major activities. The first of these activities was to collaboratively select the test conditions. This activity was conducted through the LBO working group. Thus, test condition selection included input from the OEMS and other stakeholders such as the referee rig team and the modeling teams. Together, the teams selected one combustor pressure and three air preheat temperatures for lean blowout testing. These were designed to simulate idle and altitude conditions where lean blowout poses the greatest risk. The selected combustor pressure was 3 atmospheres and the selected air preheat temperatures were 300 K, 450 K, and 550 K.

The second activity was to acquire screening data. This was accomplished by outfitting the combustor test rig with an advanced fuel cart. The fuel cart had ten different fuel tanks, each of which could hold a different fuel. The cart could rapidly switch between these fuels, which enabled the lean blowout testing of ten different fuels in a single sitting. The testing of many fuels in one sitting was advantageous because it promoted repeatability by eliminating the potential for uncontrolled variations in test conditions between test days. Fuel screening was conducted by igniting the combustor and intentionally leaning it to the lean blowout limit. Conditions where the combustor blew out were recorded, and the process was repeated until the first fuel tank was empty. This repetition process typically produced 20-30 blowout points for a single fuel. This was then repeated for the fuels in the other nine tanks.

The third activity was detailed data acquisition. This activity produced data to support the modeling groups, and it also produced data to improve the program's understanding of the physics of lean blowout. In support of the modeling groups, the lean blowout team performed detailed laser-based measurements. These measurements were delivered to the modeling groups to help them refine and validate their simulations. The measurements incorporated several different laser-based techniques that were synchronized together at 5,000 frames per second. These diagnostics included:

- Stereoscopic particle image velocimetry (s-PIV) to obtain planar measurements of the three-component velocity field
- Planar laser-induced fluorescence of the OH molecule (OH PLIF) to obtain measurements of the flame position

- Planar laser-induced fluorescence of the liquid fuel (fuel PLIF) to obtain measurements of the liquid fuel spray location

The third activity also produced high speed chemiluminescence images. These measurements were easier to perform and analyze than the laser-based diagnostics outlined above. Therefore, the advantage of the chemiluminescence imaging was that it was faster to implement. Because it was faster to implement, it was applied for more fuels and test conditions than the laser-based techniques. The chemiluminescence images helped reveal the qualitative burning characteristics near lean blowout. The chemiluminescence images also produced data to help the program determine the roles of ignition and extinction in the lean blowout process. National Jet Fuel Combustion Program Area 3 and Area 7 have both been analyzing these data to try to make such a determination. In addition to these optical measurements, the third activity also produced measurements of combustor boundary conditions. The measured boundary conditions included air flow rates, air and fuel temperatures, combustor pressure, and surface temperatures.

The fourth activity was data analysis. This activity was very important because it converted the raw measured data into useful data. In the case of screening data, analysis was performed on the combustor operational data to identify lean blowout events and their associated operating points. Analysis of screening data also included uncertainty analysis. The uncertainty analysis was necessary to determine the statistical significance of the results, and in some cases it motivated the lean blowout group to take additional data in order to tighten the uncertainty. In the case of detailed data, analysis was performed in two steps: pre-processing and post-processing. Pre-processing was applied to the velocity field measurements, and consisted of an intensive cross-correlation algorithm to convert raw images into velocity fields. This was extremely time consuming and was the most difficult data analysis step. Post-processing was conducted to produce the time-averaged velocity field, to produce the rms velocity field, and to extract key vortical flow features. These post-processed data were the deliverable to the modeling teams.

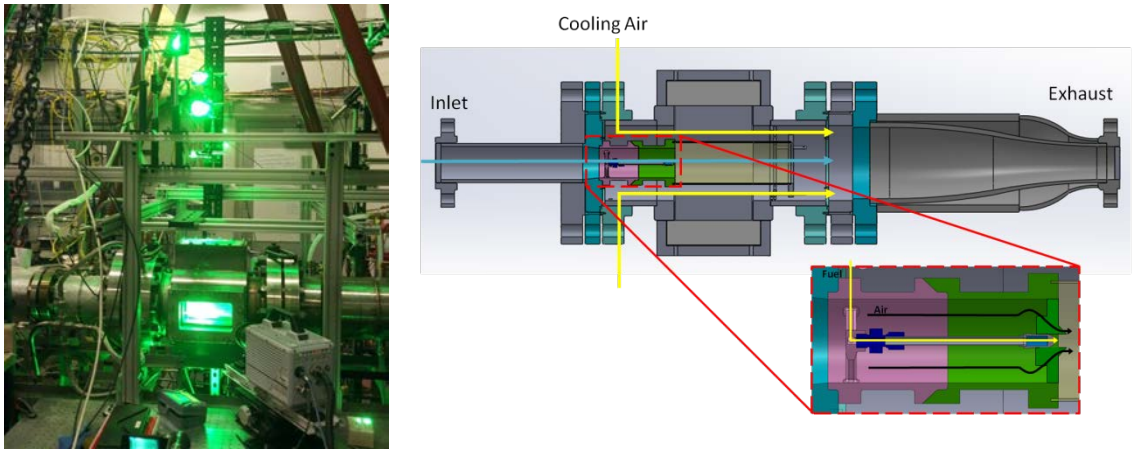


Figure 1. High shear swirl combustor, showing a) pressure vessel instrumented for high speed stereo PIV and OH PLIF, and b) a cross section with generic swirler holder/injector for illustrative purposes

Milestone(s)

1. Boundary condition measurements. All requested boundary condition measurements have been produced and delivered to modeling teams.
2. Detailed diagnostic measurements. All detailed diagnostic imaging that was planned for year 4 has been completed and is currently being analyzed to extract physical insight.
3. Screening data. This has been completed for all planned cases in year 4 and is being analyzed and has been disseminated to all project participants.
4. Analysis. Substantial data analysis has been completed this year and has delivered insight into the importance of the cetane number as well as the dynamics of lean blowout. These findings have been presented at the mid-year and monthly meetings.

Major Accomplishments

1. To date, we have expanded our screening dataset which consists of several thousand lean blowout measurements. We have added data for three new fuels in year 4: S3, C-1/n-heptane, and C-1/n-dodecane.
2. We have shown supporting evidence of the preferential vaporization theory that has been hypothesized to this program by Sang Hee Won of the University of South Carolina.
3. We have further demonstrated that the cetane number nicely captures the lean blowout risk of a given fuel (see Figure 2), especially at higher temperatures.
4. During year 4 we have characterized the intermittent burning stage that we identified during year 3. Identification of the intermittent burning stage provides an important qualitative picture for blowout simulations (see
5. Figure **3** for a sample chemiluminescence image from this diagnostic). Characterization of this phenomenon provides quantitative statistics that could be used for assessment of models and simulations. An example of these statistics is presented in
6. Figure 4, which shows distributions of flame leading point velocity. The leading point velocity is a physically relevant flame feature which is easily extracted from both experimental and CFD data.

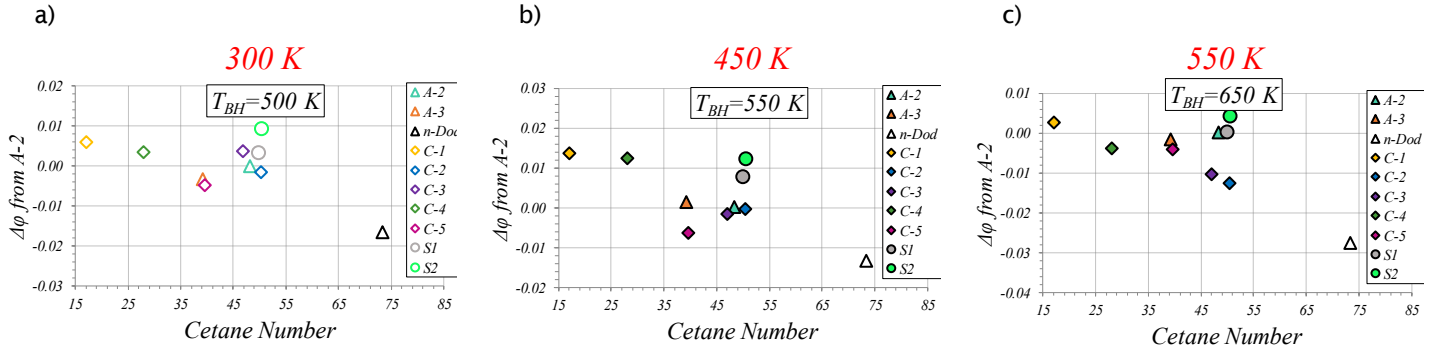


Figure 2. Sample of year 3 screening data at three different preheat temperatures and three different bulkhead temperatures, demonstrating the strong correlation of lean blowout with the cetane number



Figure 3. Sample flame chemiluminescence image from n-dodecane burning at 300 K air preheat temperature.

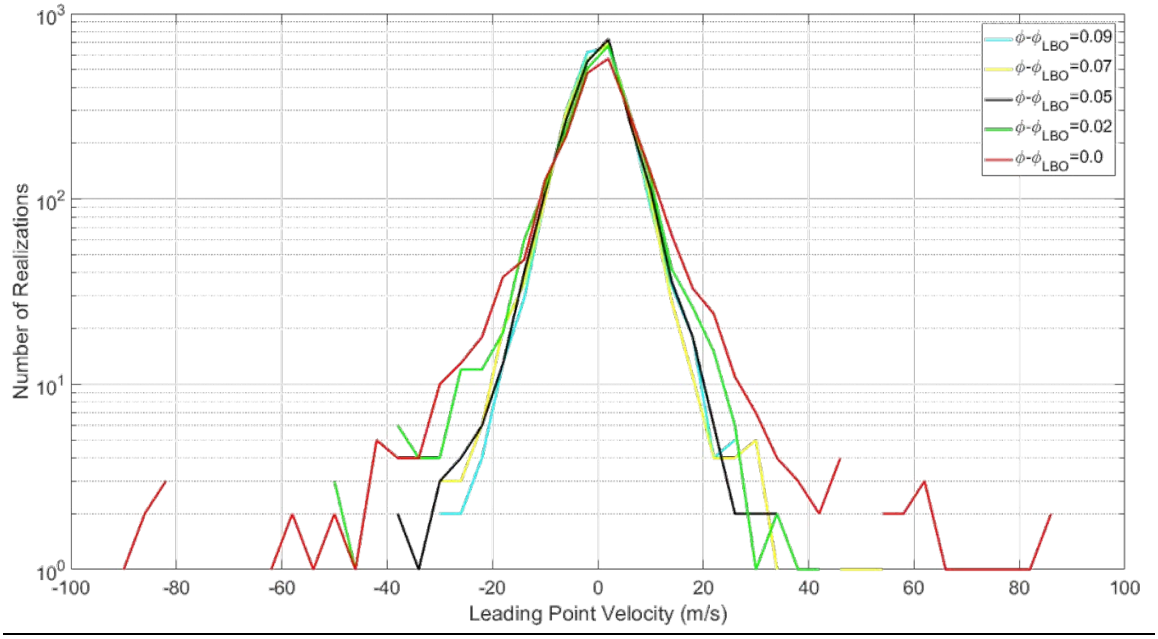


Figure 4. Flame leading point velocity statistics at five different equivalence ratios

Publications

Chterev, I., Rock, N., Ek, H., Emerson, B.L., Seitzman, J.M., Lieuwen, T.C., Noble, D.R., Mayhew, E. and Lee, T., 2017. Simultaneous High Speed (5 kHz) Fuel-PLIE, OH-PLIF and Stereo PIV Imaging of Pressurized Swirl-Stabilized Flames using Liquid Fuels. In 55th AIAA Aerospace Sciences Meeting (p. 0152).

Chterev, I., Rock, N., Ek, H., Emerson B., Seitzman J., Jiang, N., Roy, S., Lee, T., Gord, T., and Lieuwen, T. 2017. Simultaneous Imaging of Fuel, OH, and Three Component Velocity Fields in High Pressure, Liquid Fueled, Swirl Stabilized Flames at 5 kHz. Combustion and Flame. 186, pp. 150-165.

Chterev, I., Rock, N., Ek, H., Smith, T., Emerson, B., Noble, D.R., Mayhew, E., Lee, T., Jiang, N., Roy, S. and Seitzman, J.M., 2016, June. Reacting Pressurized Spray Combustor Dynamics: Part 2—High Speed Planar Measurements. In *ASME Turbo Expo 2016: Turbomachinery Technical Conference and Exposition* (pp. V04AT04A020-V04AT04A020). American Society of Mechanical Engineers.

Ek H., Chterev I., Rock N., Emerson B., Seitzman J., Jiang N., Proscia W., Lieuwen T., Feature Extraction from Time Resolved Reacting Flow Data Sets, Proceedings of the ASME Turbo Expo, Paper #GT2018-77051, 2018.

Emerson, B., and Ozogul, H. 2018. Experimental Characterization of Liquid-gas Slip in High Pressure, Swirl Stabilized, Liquid-fueled Combustors, in Western States Section of the Combustion Institute – Spring 2018 Meeting.

Rock, N., Chterev, I., Emerson, B., Seitzman, J. and Lieuwen, T., 2017, June. Blowout Sensitivities in a Liquid Fueled Combustor: Fuel Composition and Preheat Temperature Effects. In ASME Turbo Expo 2017: Turbomachinery Technical Conference and Exposition (pp. V04AT04A022-V04AT04A022). American Society of Mechanical Engineers.

Rock, N., Chterev, I., Smith, T., Ek, H., Emerson, B., Noble, D., Seitzman, J. and Lieuwen, T., 2016, June. Reacting Pressurized Spray Combustor Dynamics: Part 1—Fuel Sensitivities and Blowoff Characterization. In *ASME Turbo Expo 2016: Turbomachinery Technical Conference and Exposition* (pp. V04AT04A021-V04AT04A021). American Society of Mechanical Engineers.



Outreach Efforts

We have provided research opportunities to undergraduate students and a high school student with this program. We have submitted a paper for the 2019 AIAA Scitech conference which will give a graduate student the opportunity to attend the conference.

Awards

Graduate student Nick Rock was awarded ASCENT student of the year in April 2017.

Student Involvement

- Nick Rock has been actively involved in the lean blowout experimental effort for all years. Nick was the PhD student responsible for operating the experimental facility. He led the screening measurements and operated the facility for the detailed diagnostic efforts, and has also performed the analysis of the screening data.
- Hanna Ek was involved in the lean blowout effort as a data analysist. Hanna has been responsible for processing and analyzing the large volume of detailed data produced by the PIV, PLIF, and Mie scattering measurements.
- Ianko Chterev was also actively involved in the lean blowout experimental effort. His primary responsibility was the design of experimental procedures and support of detailed diagnostic measurements. Ianko has now graduated with his Ph.D.

Plans for Next Period

Three activities have been planned for the next period and are related to the close of the program. The activities are:

- Support the LBO chapter of the AIAA book that is being produced from this program.
- Complete the data analysis activity that characterizes flame leading point velocity statistics.
- Use the screening data from year 4 to assess the preferential vaporization hypothesis from the University of South Carolina.

These three activities will require no new measurements. The first task will compile the data and the results from the first four years of the program into part of the blowout chapter of the AIAA alternative fuels book. In addition, this activity will detail the experimental facility and test procedures for the book chapter.

The second activity will complete the analysis of flame leading point velocity statistics. This is a promising data analysis technique which could use experimental data to help validate models and simulations. It also provides additional physical insight into fuel effects. The methodology to produce these statistics from experimental data is still under development at the end of year 4, and will be completed during year 5.

The third activity will use screening data from year 4 to assess the preferential vaporization hypothesis. This hypothesis entered late in the program, and could explain some of the scatter in the test data that is observed across all experimental teams. Georgia Tech produced blowout data for three new fuels during the fourth year: S3, C-1/n-heptane, and C-1/n-dodecane. These fuels were selected for their unique preferential vaporization characteristics. Therefore, the fifth year will examine these test data in order to further support (or bust) the preferential vaporization hypothesis.

Task 2- Ignition

Performance site: Georgia Institute of Technology

Objective(s)

There were four objectives for this year's ignition task.

1. Expand the database of room temperature ignition probability measurements.
2. Acquire and analyze ignition probabilities for chilled fuels.
3. Characterize the droplet size distribution in the liquid spray.
4. Couple liquid droplet heating and vaporization physics to the previously developed Perfectly Stirred Reactor (PSR) model. This enhanced model would simulate the spark kernel development process to show the relative effect of chemical reactions, dilution cooling, and droplet heating and vaporization on the ignition process.

Research Approach

The first activity in year 2018 was to test ignition probabilities of liquid sprays for room temperature and chilled fuels. This began with modification of the test facility. The fuel delivery system was modified to provide liquid sprays rather than pre-vaporized fuels. The most important fuel system modifications were the installation of a solid cone pressure atomizer (a fuel injector) near the entrance to the test section and the addition of a fuel chiller. Also, the splitter plate was removed from the test rig to provide a single pure air stream. The fuel injector location was selected to produce ignition probabilities in the range of 1-10%. The injector location was also fine-tuned to prevent fuel droplet impingement on the igniter. Scattering of a HeNe laser from the liquid droplets was used to monitor the fuel spray trajectory. The schematic of the fuel delivery system is shown in Figure 5.

Liquid fuel testing was conducted with a crossflow air velocity of 10 m/s and an equivalence ratio of φ=0.55. The crossflow air temperature was 80˚F and its pressure was 1 atmosphere. For room temperature fuel sprays, ignition probabilities were measured for A2, A3, C1, C2, C3, C5, C7, C8, and C9. For chilled fuel, ignition probabilities were measured for A1, A2, A3, C1, C3, C4, C5, C7, and C8. Some fuels could not be chilled in this system as they would freeze. The ignition probabilities of each fuel relative to A2 are shown in Figure 6. For comparison, the figure also includes the results from earlier testing of pre-vaporized fuels. There are several noteworthy differences between the ignition probabilities of liquid versus pre-vaporized fuels. One of these noteworthy differences is a change in the ranking of ignition probabilities. For example, the ignition probabilities of A3, C2, and C3 are reduced relative to the other fuels when tested as liquid sprays. Another noteworthy difference is the range in probabilities is larger for chilled fuel sprays than for room temperature fuel sprays.

The differences in the ignition probabilities of liquid sprays versus pre-vaporized fuels provide some important insight. For example, the rate-limiting properties of pre-vaporized fuels should be the chemical properties. This is because the physical properties govern the vaporization process, which has been bypassed by pre-vaporization. However, the rate-limiting properties for liquid sprays may include physical properties in addition to chemical properties. Therefore, the differences in ignition probability demonstrate the important role of physical properties (such as viscosity, boiling points, etc.) for ignition of liquid fuel sprays. Special attention has been paid to properties that govern vaporization (recovery temperature, vapor pressure) and atomization (viscosity). The correlations to the viscosities and the 10% recovery temperatures for the fuel sprays are shown in Figure 7 and Figure 8.

The third activity in the ignition task was to measure the droplet distribution with PDPA. In aviation gas turbine combustors, jet fuels are injected as liquid sprays. These liquid sprays transition to gaseous fuel vapors before they burn. The droplet sizes can play an important role in the phase transition process by affecting the droplet heat transfer process. Therefore, PDPA measurement of droplet size and velocity distribution for an array of fuels was acquired. Normalized size distribution data for fuel C3 (high viscosity), A2 (middle viscosity), and C5 (low viscosity) at ~ 5 mm above the igniter center are presented in Figure 9. Significant differences in droplet size distributions were observed. The C3 fuel has more droplets at the larger size range (above 30 μm), and the C5 fuel only has a small percentage of droplets in that size range. The PDPA data can be used for more advanced CFD simulation.

Lastly, a reduced order model was enhanced to study the physics of forced ignition in liquid fuel spray. The conceptual model construction is shown in Figure 10. An example case study simulates forced ignition in a spray of 5 μm single size droplets uniformly distributed with an equivalence ratio of 1. The heat release, the dilution cooling, and the droplet heating and vaporization rates are shown in Figure 11. The initial results show that the energy required to heat and vaporize a droplet is 10 times smaller than the heat release rate and the dilution cooling. Therefore, droplet during ignition heating is not expected to substantially affect the ignition kernel's temperature. Thus, the time delay that is observed before chemical heat release occurs is likely due the heating of the droplets. If this time is too long, the kernel will be cooled significantly by dilution and ignition will not occur.

Milestone(s)

- Produced high quality, repeatable ignition probability data for room temperature liquid fuel sprays
- Produced high quality, repeatable ignition probability data for chilled liquid fuel sprays
- Acquired droplet size and velocity distribution data for several fuels.
- Enhanced a reduced order ignition model that includes droplet heating and vaporization processes

Major Accomplishments

- Fuel spray ignition probabilities correlate to properties that controls droplet sizes and vaporization.
- The acquired droplet distribution data is useful for CFD modelers.

- The reduced order ignition model shows the magnitude of the droplet cooling effect is small compared to those of the chemical heat release and the dilution cooling.

Publications

Wei, S., Sforzo, B., and Seitzman, J., 2018, "Fuel Composition Effects on Forced Ignition of Liquid Fuel Sprays," *ASME Turbo Expo 2018: Turbomachinery Technical Conference and Exposition*, Oslo, Norway

Outreach Efforts

Conference presentation at ASME Turbo Expo 2018, Oslo, Norway

Awards

None

Student Involvement

- Sheng Wei was the lead student on all of the ignition task objectives.
- Daniel Cox was involved in data analysis.
- Sabrina Noor helped analyzed results for pre-vaporized ignition simulation.
- Vedant Mehta conducted a parametric study on droplet ignition.
- John Ryu helped with the multi-size droplet ignition study.

Plans for Next Period

As the program is concluding for Georgia Tech ignition, we are planning on using the available data and model analysis to write journal papers. At the moment, we have three journal papers in mind. The first paper will use the pre-vaporized ignition data and the reduced order model to study ignition fuel chemistry. The second paper will use the ignition data in fuel spray to develop new insight into droplet ignition processes. The third paper will use the droplet ignition model to better parameterize droplet ignition processes.

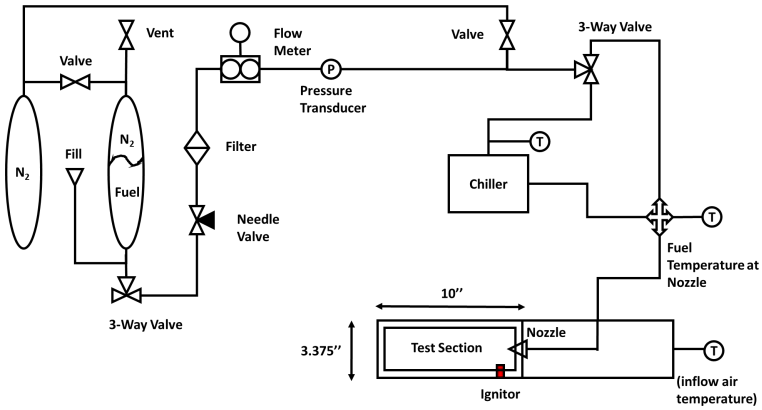


Figure 5. Schematic of the liquid fuel delivery system

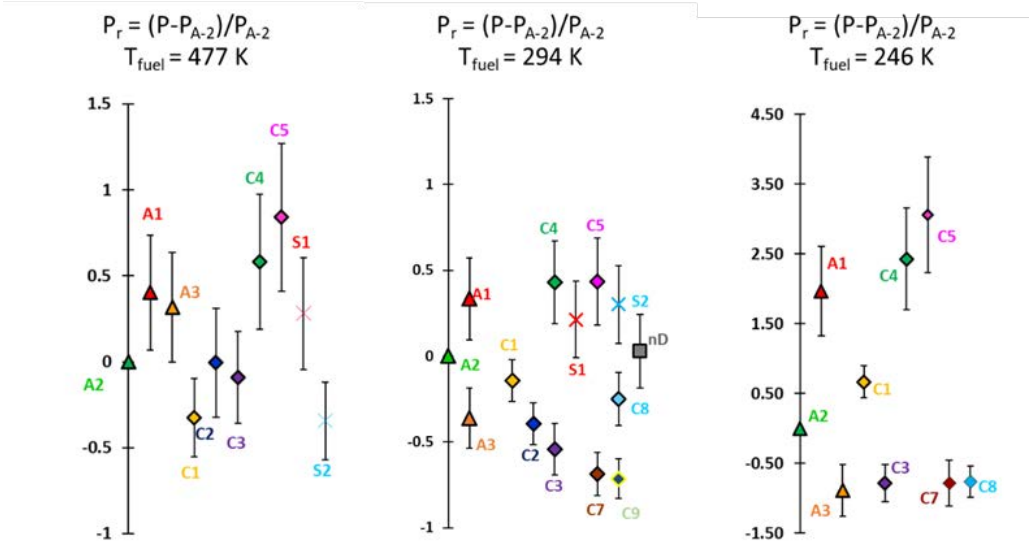


Figure 6. Ignition probability rankings, scaled with respect to A2 probability. Error bars show 68% uncertainty. Left: pre-vaporized fuel/air mixture; Middle: room temperature Liquid fuel spray; right: chilled liquid fuel spray

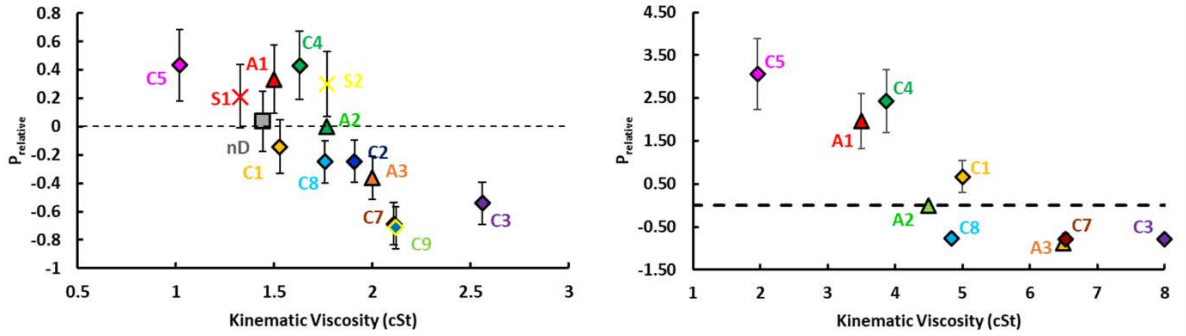


Figure 7. Relative probabilities versus relative viscosity for room temperature fuel Left: Probability results for room temperature fuel spray; right: probability results for chilled fuel sprays

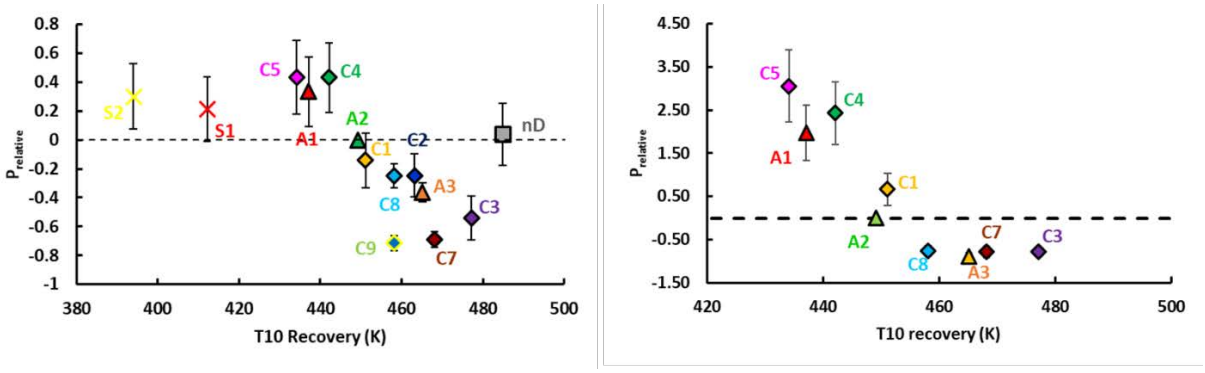


Figure 8. Relative probabilities versus 10% recovery temperature. Left: Probability results for room temperature fuel spray; right: probability results for chilled fuel sprays

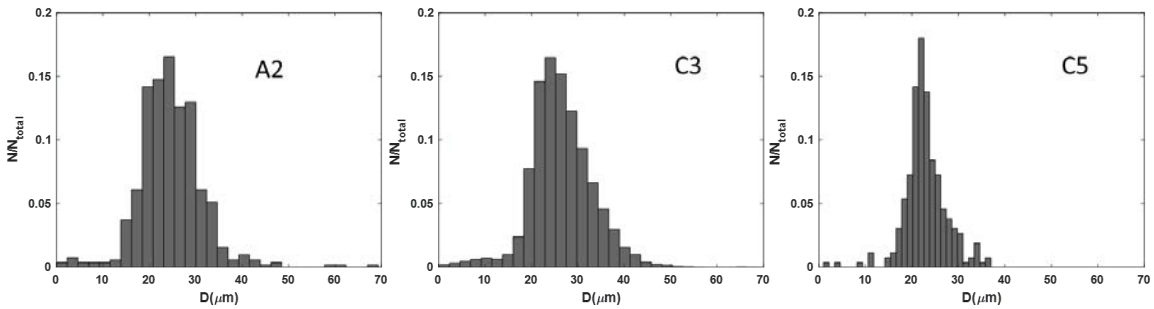


Figure 9. Normalized size distribution at 5 mm above the igniter center

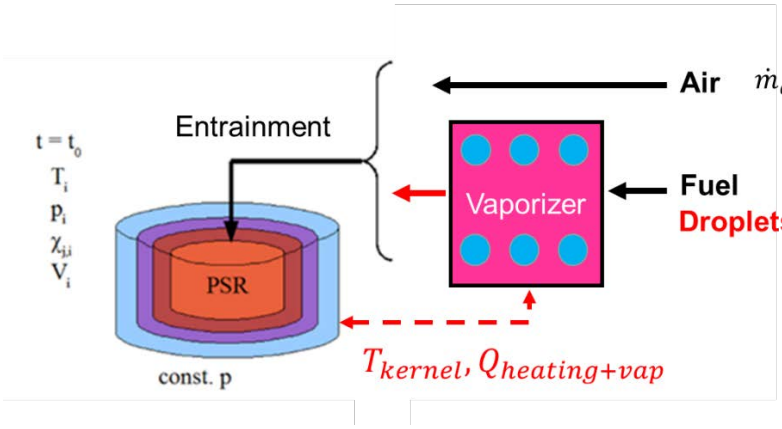


Figure 10. Conceptual model PSR modeling with droplet vaporization

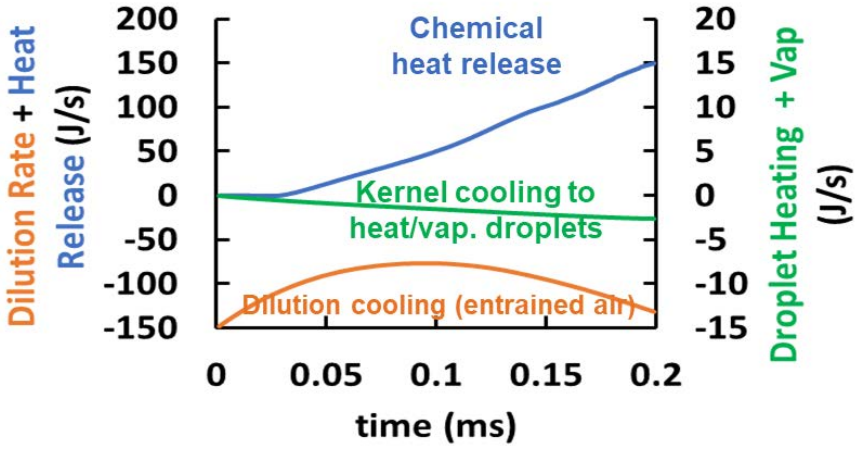


Figure 11. Chemical heat release, dilution cooling, and droplet heating/vaporization rates for a successful ignition of 5 μm droplets at an equivalence ratio of 1

Task 3- Turbulent Flame Speed

Performance site: Oregon State University

Objective(s)

This task had three objectives:

1. Measure and identify the sensitivity of the turbulent flame speed to fuel composition. This objective spanned a range of jet fuels and test conditions (including atmospheric and sub-atmospheric pressures).
2. Build a database of turbulent flame speeds for pre-vaporized jet fuels. This year we initiated a collaboration with Suresh Menon (GT) who is performing simulations of the turbulent flames anchored to the burner.
3. Measure the sensitivity of turbulent flames to local extinction.

Research Approach

Testing was conducting using a laboratory test rig that produced turbulent flames. The rig featured a pre-vaporizer based on designs developed by the Air Force Research Laboratory and a burner based on designs developed by Lieuwen and colleagues. The experimental arrangement consisted of fuel and air metering systems that delivered pre-vaporized jet fuel and air to the burner. Fuel was vaporized using a series of heaters, and elevated to a temperature near 200ºC. The air/fuel mixture flowed through an adjustable turbulence generator which produced turbulence intensities (TI) ranging from 10% to 20% of the bulk flow velocity. The TI is independent of bulk flow velocity. A premixed methane pilot flame was used for ignition and to stabilize the Bunsen burner flame.

Data was collected for three fuels (A2, C1 and C5). Test conditions included two pressures (1 and 0.7 atm), Reynolds numbers near 10,000, a range of equivalence ratios ($0.75 \leq \Phi \leq 1.0$), and turbulence intensities near 20%. The test data consisted of chemiluminescence imaging for all conditions and high speed imaging for a subset of the tests. Chemiluminescence imaging was conducted using a 16-bit intensified charge-coupled device (ICCD) camera with a 1024 x 1024 pixel resolution and a 25 mm f/4.0 UV camera lens. For each flow condition (Re, Φ, and TI), data were typically collected over a 3 minute period at 2 Hz.

The most important accomplishment of this activity was sub-atmospheric pressure testing (i.e., objective 1). Such measurements are relevant to relight conditions in engines at high altitudes. Figure 12 shows a photograph of the burner operating at sub-atmospheric conditions. Figure 13 (left panel) shows measured turbulent consumption speeds for C1, C5 and A2 at 1 and 0.7 atm. The right hand panel shows normalized turbulent consumption speeds. Note that the flame speeds increase as the pressure is reduced, and a fuel sensitivity is observed between C1, C5, and A2. This observation indicates that the relight characteristics between C1, C5 and A2 may be different when an aircraft is at altitude. More testing of practical systems are required to verify this postulate. It is noted that while the turbulent consumption speed increases with decreasing pressure, the mass consumption rate of the fuel decreases with decreases in pressure (see Figure 14). The latter trend is consistent with literature.

The second objective was partially addressed by initiating a collaboration with Suresh Menon (GT). His team has simulated the cold-flow conditions through the burner and has plans to simulate the reacting flow. It is anticipated that this collaborate will serve as a baseline for evaluating the chemistry models created as part of the NJFCP program.

The third activity (i.e., objective 3) was evaluating a methodology to detect the onset of local extinction events in the flame brush. Earlier in this program a fuel sensitivity to the onset of instabilities of the flame was detected based on large changes in the apparent turbulent flame speed. However, using this technique to evaluate fuels was quite time consuming and it was difficult to link the physics of flame speed measurements to local extinction. This year efforts were made to develop a better method to more readily determine breaks in the flame front. High speed images were collected of flames and analysis tools were developed to quantify the turbulent statistics of emissions from the flames. Figure 15 provides a representative image of a turbulent statistic (i.e., integral length scale) that was evaluated to determine if it could be used as a metric of the onset of breaks in the flame front. Our current approach is to use the shape of the radial distribution of intensity as a marker of flame tip opening. Further testing is required to verify that this approach is valid.

Milestone(s)

- A method for evaluating the onset of local extinction events is 80% complete. Additional testing is required to verify that the proposed method is consistent for different fuels and operating conditions.



- Collaboration with Suresh Menon (GT) was initiated. Suresh is modeling the turbulent Bunsen burner flame to evaluate if the model can capture fuel sensitivities. Data and boundary conditions have been shared.
- A portion of the introduction to the lean blowout chapter in the forthcoming AIAA book has been drafted.

Major Accomplishments

- Turbulent flame speeds at atmospheric and sub-atmospheric conditions were measured. A fuel sensitivity is evident.
- Observation was made that flame extinction is sensitive to fuel composition. This will be important for the program's lean blowout tasks, which aim to understand how ignition and extinction influence the lean blowout process.



Figure 12. Picture of flame operating in pressure vessel at sub-atmospheric conditions

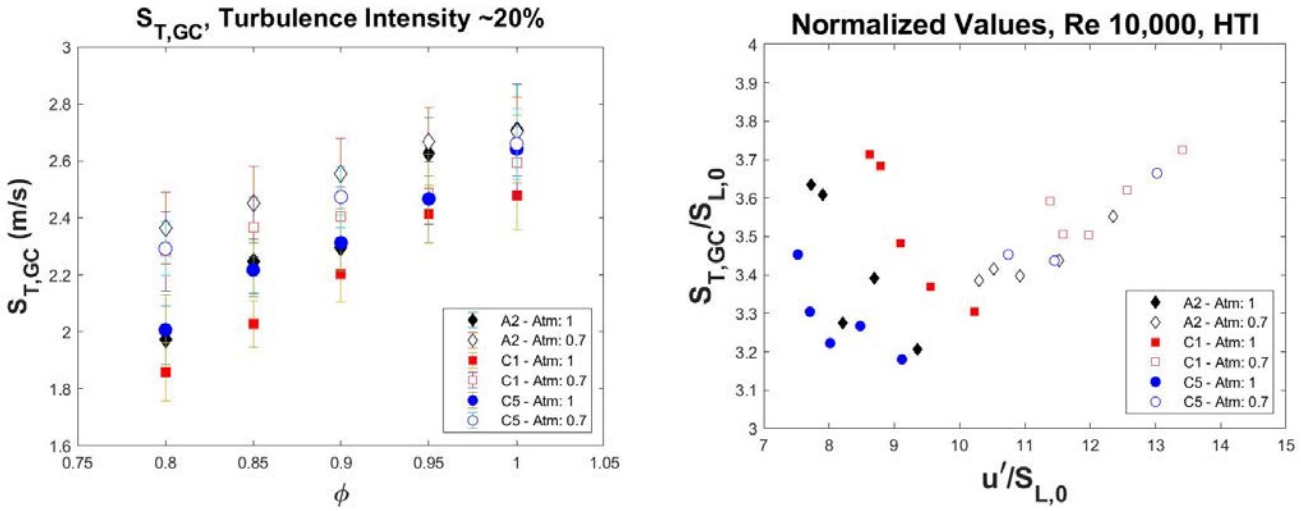


Figure 13. Turbulent consumption speeds (left panel) and normalized turbulent consumption speeds (right panel) for A2, C1, and C5 when tested at 1 and 0.7 atm

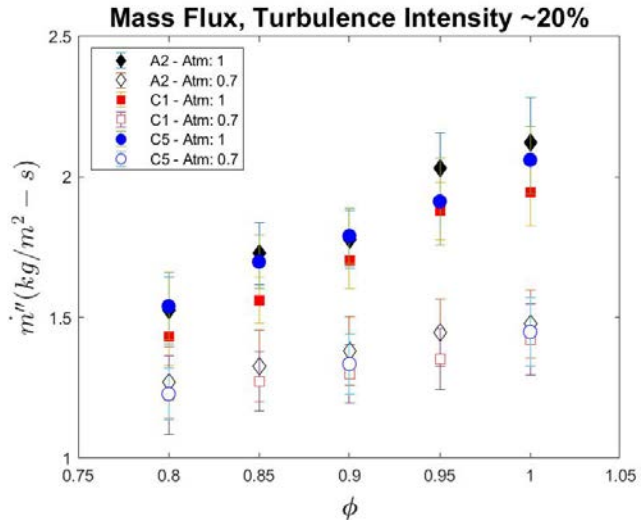


Figure 14. Mass consumption speeds of jet fuels for 1 and 0.7 atm

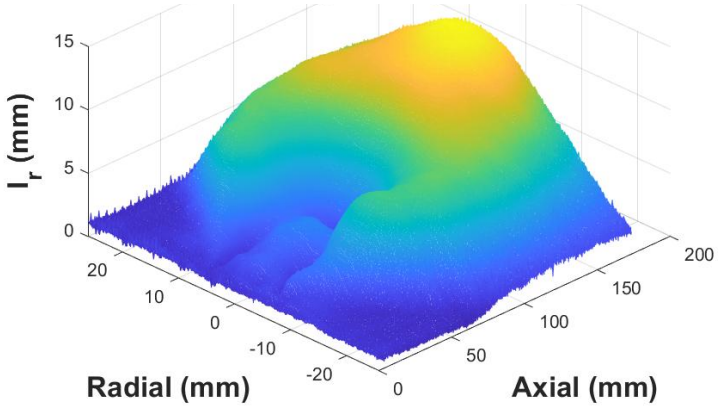


Figure 15. Radial integral length scale of visible light emissions from turbulent Bunsen burner flame burning A2 fuel. Such statistics have been considering as a marker of the onset of openings of the flame brush.

Publications

N. Schorn, **D. Blunck**, "Flame Stability of Turbulent Premixed Jet Flames of Large Hydrocarbon Fuels," *Western States Section of the Combustion Institute Meeting*, Laramie, WY (2017).

A. Fillo, J. Bonebrake, **D. Blunck**, "Impact of Fuel Chemistry and Stretch Rate on the Global Consumption Speed of Large Hydrocarbon Fuel/Air Flames," *10th US Combustion Meeting,* College Park, ME (2017).

Fillo, Aaron, M.S., Thesis, "The Global Consumption Speeds of Premixed Large- Hydrocarbon Fuel/Air Turbulent Bunsen Flames," Oregon State University.

Outreach Efforts

None



Awards

Fillo, Aaron, M.S., Thesis, "The Global Consumption Speeds of Premixed Large- Hydrocarbon Fuel/Air Turbulent Bunsen Flames," received a 2017 OSU Distinguished Master's Thesis Award.

Student Involvement

- Jonathan Bonebrake, a PhD student, has helped to collect and analyze data. He also designed and built the sub-atmospheric pressure vessel and vacuum system.
- Aaron Fillo, a PhD student, has worked tangentially on this project to analyze results and further investigate scientific phenomena.
- Nathan Schorn, a MS student, has taken over responsibility of the project is now collecting and analyzing data.
- Multiple undergraduate students, including underrepresented students have worked with the graduate students to operate the burner and collect data. This has provided a significant opportunity for the students to experience research.

Plans for Next Period

Three activities are planned to complete this project. The first activity is to complete measuring the turbulent flame speeds of the jet fuels at sub-atmospheric pressures. This activity will focus on the fuels that the program determines to be of interest. The second activity will be completing analysis of the flame extinction observations for different fuels. It is hypothesized that local extinction events observed on this burner coincide with the onset of extinction for other burners. The results of this activity can be used to help determine if turbulent flame speed testing can provide insight into the risk of lean blowout for practical systems. The third activity is an on-going collaboration with Suresh Menon at GT who is simulating the turbulent Bunsen burner flames. It is expected that data collected using this burner can be used to evaluate turbulent chemistry models. If successful, this evaluation can serve as an intermediate step between testing using shock tubes and three-dimensional simulations of practical combustors.

Project 28 National Jet Fuels Combustion Program Area #4- Combustion Model Development and Evaluation

Georgia Institute of Technology

Project Lead Investigator

Suresh Menon
Professor
School of Aerospace Engineering
Georgia Institute of Technology
270 Ferst Drive, Atlanta, GA 30332-0150
(404)-894-9126
suresh.menon@ae.gatech.edu

University Participants

Georgia Institute of Technology

- P.I.(s): Suresh Menon, Professor; Wenting Sun, Associate Professor
- FAA Award Number:13-C-AJFE-GIT-018
- Period of Performance: Dec. 1, 2014-Dec. 31, 2017
- Task(s):
    1. Travel to NJFCP meeting. Funds only for travel for years 2 and 3 (S. Menon, PI)
    2. Development of dynamic adaptive chemistry solver and demonstrate the algorithm in different flame configurations, travel to meeting (W. Sun)

University of Connecticut

- P.I.(s): Tianfeng Lu, Associate Professor
- FAA Award Number: 13-C-AJFE-GIT-018
- Period of Performance: Dec. 1, 2014-Dec. 31, 2018
    3. The task of UCONN in the NJFCP program is to develop reduced chemical kinetic models for jet fuels that can be employed in efficient large eddy simulations.
    4. The technical aspects of the UCONN task is to cover the travel expenses of the UCONN team to present the results from the NJFCP program in the conferences and program review meetings.

Project Funding Level

$350K from FAA and $350K cost share for year 1.
Subsequent years were funded primarily for travel to attend meetings twice a year. All research was funded by NASA under a separate NRA.

The Georgia Tech award is $6000 for S. Menon (PI), FY 2017 for travel
The Georgia Tech award is $39,999 for W. Sun, FY 2017 for travel and partial student support.
The UCONN subaward is $5000 for FY2017 for travel support

Investigation Team

The Georgia Tech team includes: Suresh Menon (PI) (travel funds only),
Wenting Sun (co-PI), Suo Yang (graduate student), Xiang Gao (graduate student)
Tianfeng Lu (co-PI, UCONN), Yang Gao (graduate student), and Ji-Woong Park (graduate student)

The investigation team with specific tasks is as follows:

1. **Task 1:**
    - **Title:** Development of reduced kinetics for NJFCP Fuels



- **Lead:** Professor Tiangfeng Lu
- **Post Docs & Students:** Y. Gao, B. Majda, Y. Liu
- **University Affiliation:** University of Connecticut

2. **Task 2:**
   - **Title:** Network modeling and kinetics acceleration
   - **Lead:** Professor Wenting Sun
   - **Post Docs & Students:** S. Yang, X. Gao
   - **University Affiliation:** Georgia Institute of Technology
3. **Task 3:**
   - **Title:** LES of spray combustion in NJFCP test facilities
   - **Lead:** Professor Suresh Menon
   - **Post Docs & Students:** Dr. R. Ranjan, A. Panchal
   - **University Affiliation:** Georgia Institute of Technology

Project Overview

The overall objective of this activity is to establish a predictive capability to evaluate new aviation fuels in combustors for ASTM D4054 at operating conditions including lean blowout, cold start or altitude relights. The key objectives of this project are as follows:

- Establish a simulation strategy using Large-Eddy Simulations (LES) to capture fuel sensitivity in experimental screenings
- Collaborate with Area 2 to develop, optimize and evaluate efficient reduced chemical kinetics for use in LES
- Collaborate with Areas 3, 5 and 6 to perform LES investigation of the experimental rig for stable and LBO conditions

Task 1 – Development of Reduced Kinetics for NJFCP Fuels

University of Connecticut

Objective(s)

The objective of this research activity is to develop, optimize and evaluate reduced chemical kinetics models for use in LES of spray combustion in NJFCP test facilities. Additionally, for FY 16-18 only travel funds are provided to attend NJFCP program reviews in May and December. All research is funded by a NASA NRA.

Research Approach

Model Reduction for Cat A & C fuels

Skeletal and reduced models for Cat A and C fuels, including Cat A2 (POSF10325), C1 (POS11498, beta version) and C5 (POSF12345) have been developed based on the detailed HyChem models from Area 2 of the NJFCP program. The reduced models are validated over a wide range of parameters for ignition, extinction and flame propagation. The hybrid modeling approach with lumped fuel cracking reactions assumes that the intermediates of the fuel cracking are in quasi-steady state as demonstrated in [1, 2], resulting in highly compact detailed-lumped models for high-temperature real fuel oxidation. The detailed-lumped models consist of more than 100 species while the reduced models consist of less than about 30 species.

Procedurally, the DRG-based methods, including DRG [3-6] and DRG-aided sensitivity (DRGASA) [7, 8], are first employed to remove unimportant species and reactions based on reaction states sampled from auto-ignition and perfectly stirred reactors (PSR). The H radical is selected as the starting species in the graph searching in DRG. After the skeletal reduction of DRG, the skeletal mechanism is further reduced by using DRGASA with ignition delay and extinction residence time of PSRs being the target parameters. The skeletal models are then reduced using the linearized quasi steady state approximations (LQSSA) [9]. Global QSS species are identified and approximated with algebraic equations, which are analytically solved using a graph-based method to ensure high accuracy and robustness [9].

The reduction covered a wide range of parameters: pressure from 0.5 to 30 atm, initial temperature from 1000 K to 1600 K for auto-ignition, inlet temperature 300 K for PSR, and equivalence ratio from 0.5 to 1.5. A worst-case error tolerance of 20% was set for the target parameters in DRGASA. The sizes of the detailed-lumped, skeletal and reduced models are summarized in Table 1. The performance of the reduced models is demonstrated with Cat A2 in Fig. 1 for ignition delay, laminar flame



speed, and extinction of premixed and non-premixed counterflow flames for different flame conditions. Similar performances were observed for the reduced models for Cat C1 and C5.

Extended validation was further performed for Cat A2 for PSR at both lean and rich extinction conditions as shown in Fig. 2. The important reaction pathways controlling lean blow-out (LBO) are identified using bifurcation analysis [10] as shown in Fig. 3. It was found that LBO at the investigated conditions is primarily controlled by reactions involving small molecules, such as H, OH, CO and HCO. These reaction rates need to be accurately computed for accurate prediction of LBO.

High-Performance Model-Specific Solvers for Jet Fuels

Analytic Jacobian was developed for Cat A2, C1 and C5 for efficient time integration of chemistry using implicit ODE solvers, for which the Jacobian evaluation and factorization are typically the most time-consuming components. Analytic chemical Jacobian evaluation can reduce the computational cost to a level comparable to that for a single rate evaluation. As such the computational efficiency of implicit solvers can be significantly improved. The strategy to couple implicit solvers with the analytic Jacobian is applicable for simulations with arbitrarily large integration time steps.

Dynamic adaptive hybrid integration (AHI) [11] was further developed in addition to the analytic Jacobian technique by only solving the fast species and reactions implicitly, while treating the slow variables and source terms explicitly. The size of the implicit core to be solved in AHI can thereby be significantly reduced and the computational efficiency can be improved.

For simulations with integration time steps smaller than about 20 ns, non-stiff reduced models based on the dynamic chemical stiffness removal [12] are developed for Cat A2, C1 and C5, such that explicit solvers for time integration can be employed to achieve high efficient in high-fidelity DNS and LES of compressible flows.

The performances of implicit solvers with analytic Jacobian, AHI, and explicit solvers with dynamic chemical stiffness removal are compared in Fig. 4 for mechanisms of different sizes, including the skeletal and reduced Cat A2 models. Speedup factors close to or larger than an order of magnitude are achieved using analytic Jacobian, AHI and dynamic chemical stiffness removal.

Table 1. Size of the detailed-lumped, skeletal and reduced models for Cat A2, C1 and C5.

	A2		C1 (beta)		C5	
	Species	Reactions	Species	Reactions	Species	Reactions
Detailed	112	790	112	794	112	790
Skeletal	38	185	37	210	38	185
Reduced	29		27		29	

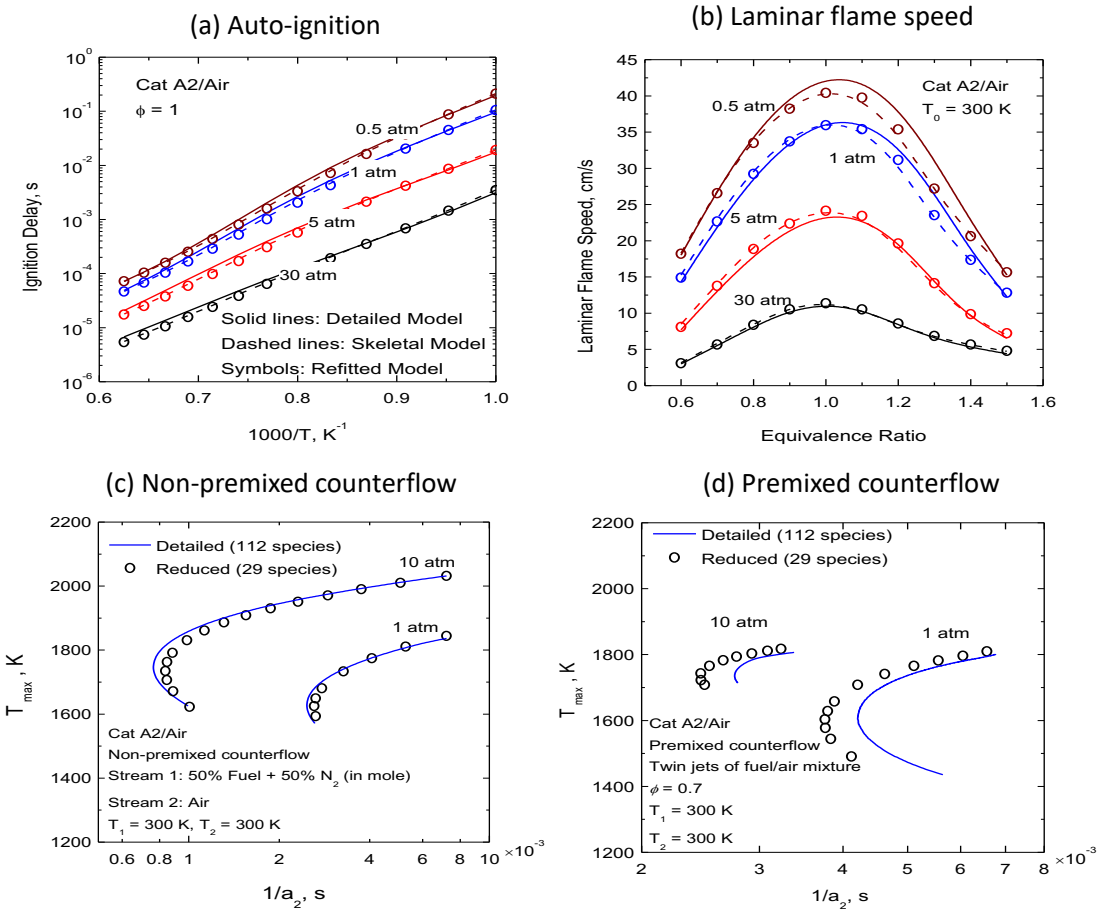


Figure 1. Validation of the reduced model against the detailed model for Cat A2 for a) ignition delay, b) laminar flame speed, c) extinction of non-premixed counterflow flames, and d) extinction of premixed counterflow flames.

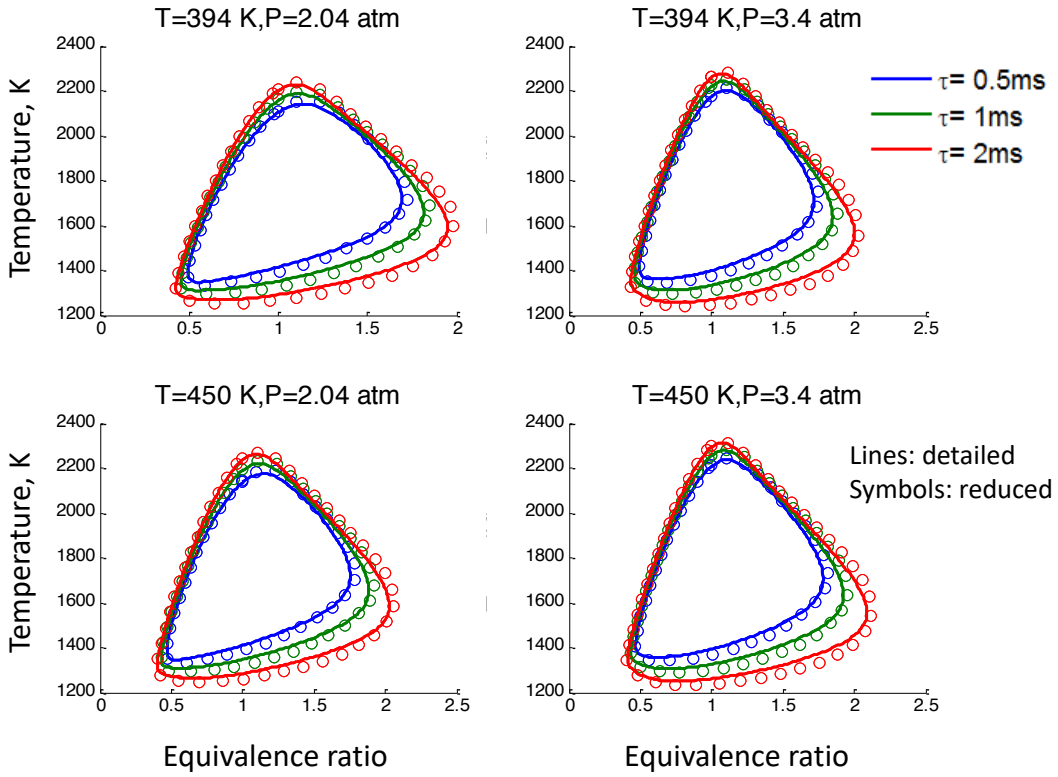


Figure 2. Extinction of Cat A2/air in PSR at different inlet temperatures, pressures and residence time.

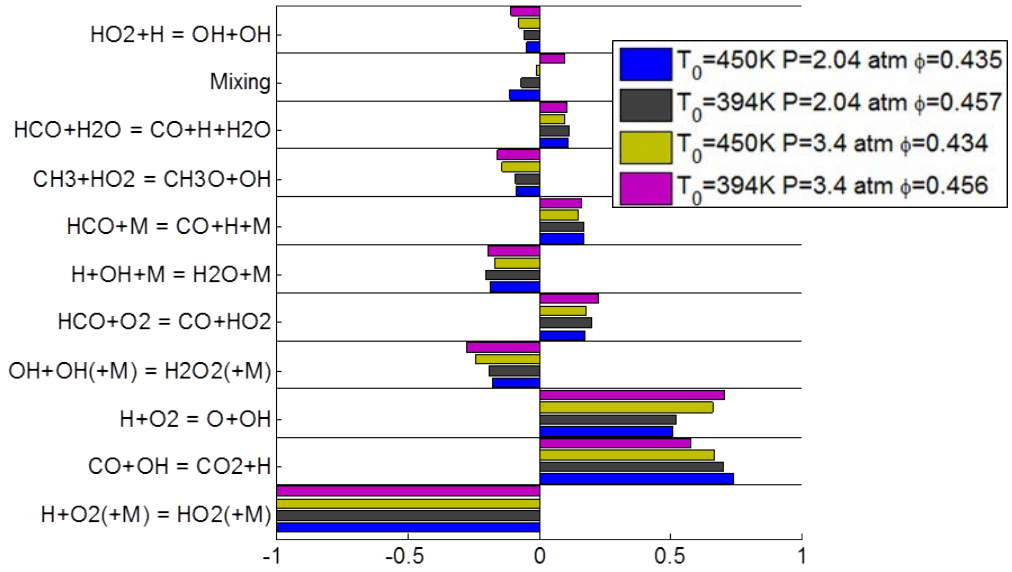


Figure 3. Controlling reactions identified using bifurcation analysis at the lean blow-out conditions in Figure 2.

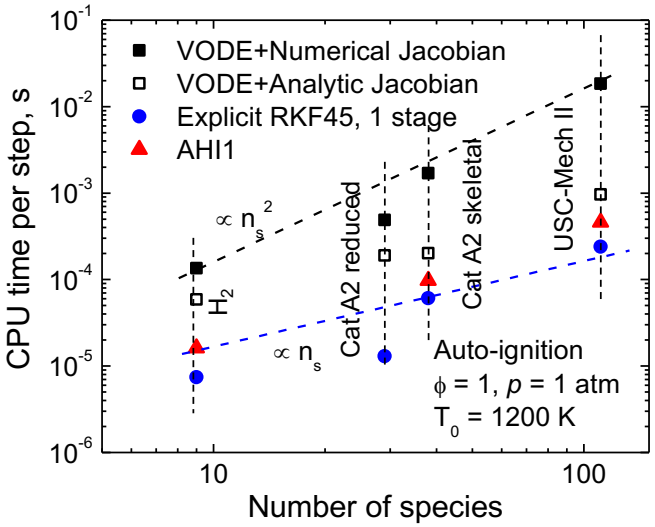


Figure 4. Averaged computational cost per integration time step in auto-ignition using different solvers and mechanisms of different sizes.

Milestone(s)

None

Major Accomplishments

The accomplishments of the current year's research activity with their impact on the rest of the project are as follows:

- **Development of reduced chemical kinetics models for Cat A2 and C5:** Based on the detailed-lumped models from Area 2, we developed a 38 species skeletal and 29 species reduced kinetics, which were used in the LES of spray combustion under Task 3 for stable and LBO conditions.
- **Comprehensive validation of the newly developed reduced models:** We performed a comprehensive validation of the new models by considering variety of combustion physics such as auto-ignition, perfectly stirred reactors (PSR), flame speed, extinction of premixed and non-premixed counter-flow flames, etc. The developed models are accurate enough to capture wide variety of combustion physics of interest such as LBO, cold restart, altitude re-lightning etc. Additionally, these models can capture the effects of fuel sensitivity, which is an essential element of the current research effort.
- **Development of efficient approaches for handling chemical kinetics in LES:** In LES with finite-rate chemical kinetics, use of a skeletal or reduced chemical kinetics lead to excessive computational cost associated with the chemical kinetics. Therefore, novel approaches have been developed to alleviate this excessive computational cost. This has been achieved by developing analytical Jacobian and non-stiff routines, which can be used for LES under Task 3. Additionally, having a mixture-averaged transport in a LES is also expensive, when the number of species is large. Therefore, reduced transport models of 15 species group has been generated, which can be used in LES instead of the expensive 29-species based transport for the reduced models, with a similar level of accuracy. The efficient approaches developed in this research effort will reduce the cost of large-scale LES and they will allow OES to simulate these problems without sacrificing the accuracy.

Publications

Yang Gao, "Model Reduction and Dynamic Adaptive Hybrid Integration for Efficient Combustion Simulations," Ph.D thesis, University of Connecticut, 2017.

Outreach Efforts

None

Awards

None



Student Involvement

- Y. Gao
- B. Magda
- Y. Liu

Plans for Next Period

None

References

1. X. You, F. N. Egolfopoulos, and H. Wang, "Detailed and simplified kinetic models of n-dodecane oxidation: The role of fuel cracking in aliphatic hydrocarbon combustion," *Proceedings of the Combustion Institute*. 32, 403-410 (2009).
2. E. D. B. Sirjean, D. A. Sheen, H. Wang, *JetSurF 1.0-l: Simplified chemical kinetic models for high-temperature oxidation of C1 to C12 nalkanes*, in *6th U.S. National Combustion Meeting*. 2009, Paper 23.F1: Ann Arbor, Michigan.
3. T. F. Lu and C. K. Law, "A directed relation graph method for mechanism reduction," *Proceedings of the Combustion Institute*. 30, 1333-1341 (2005).
4. T. F. Lu and C. K. Law, "Linear time reduction of large kinetic mechanisms with directed relation graph: n-Heptane and iso-octane," *Combustion and Flame*. 144, 24-36 (2006).
5. T. F. Lu and C. K. Law, "Toward accommodating realistic fuel chemistry in large-scale computations," *Progress in Energy and Combustion Science*. 35, 192-215 (2009).
6. T. Lu and C. K. Law, "On the applicability of directed relation graphs to the reduction of reaction mechanisms," *Combustion and Flame*. 146, 472-483 (2006).
7. X. L. Zheng, T. F. Lu, and C. K. Law, "Experimental counterflow ignition temperatures and reaction mechanisms of 1,3-butadiene," *Proceedings of the Combustion Institute*. 31, 367-375 (2007).
8. R. Sankaran, E. R. HawkeS, J. H. Chen, T. F. Lu, and C. K. Law, "Structure of a spatially developing turbulent lean methane-air Bunsen flame," *Proceedings of the Combustion Institute*. 31, 1291-1298 (2007).
9. T. F. Lu and C. K. Law, "Systematic approach to obtain analytic solutions of quasi steady state species in reduced mechanisms," *Journal of Physical Chemistry A*. 110, 13202-13208 (2006).
10. R. Shan and T. Lu, "Ignition and Extinction in Perfectly Stirred Reactors with Detailed Chemistry," *Combustion and Flame*. 159, 2069–2076 (2012).
11. Y. Gao, Y. Liu, Z. Ren, and T. Lu, "A dynamic adaptive method for hybrid integration of stiff chemistry," *Combustion and Flame*. 162, 287-295 (2015).
12. T. F. Lu, C. K. Law, C. S. Yoo, and J. H. Chen, "Dynamic stiffness removal for direct numerical simulations," *Combustion and Flame*. 156, 1542-1551 (2009).

Task 2 – Network Modeling and Kinetics Acceleration

Georgia Institute of Technology

Objective(s)

The objectives of this research activity are as follows:

- **Develop a dynamic mechanism reduction approach for LES Modeling:** The focus of this research effort was to develop a novel approach to perform a dynamic mechanism reduction for LES by identifying the reactor models such as mixing zone, flame zone etc., so that efficient computation of the chemical kinetics can be performed while using a chemical kinetics with large number of species.
- Travel funds are provided to attend NJFCP program reviews in May and December for FY 16 and 17. Some additional funds provided for student support in FY17.

Research Approach

Dynamic Adaptive Chemistry for LES Modeling

The developed algorithm CoDAC last year was further successfully implemented into a turbulent jet flame (Sandia Flame E). Detailed results were obtained for Sandia Flame E. Figure 1 below shows the snapshots of the spatial distribution of number of active species and number of active reactions, generated from the local PFA mechanism reduction (threshold=2%) of CoDAC method. Outside the jet brush, only 2 species (preselected seed species: fuel and oxidizer) and none of the reactions



are selected, because no chemical reactions occur there. Near the highly distributed turbulent partially premixed flame, a large number of species and reactions are selected, which is close to the full mechanism (20 species and 84 reactions). There is a large buffer zone between above two regions, which has intermediate number of selected species and reactions. The reduction of number of species and reactions in most spatial locations is responsible for the acceleration of chemistry calculation from the DAC method. Due to the highly efficient correlation techniques, the PFA mechanism reduction time is more than 500 times smaller than the chemistry calculation time, and only occupies 0.135% of the total computation time. Therefore, the computational overhead of CoDAC is negligible.

The computation time distribution is shown in Figure 2. The Frozen case (multi-species transport equations without chemical kinetics source terms) serves as the theoretical upper limit for the computation speed of all FRC models. From FPV case to Frozen case, the number of equations rises from 7 to 24 by a factor of 3.4. For this reason, the total computation time increases by a factor of 2.7, which is even better than the ideal linear computational complexity. The time for preconditioning matrix inversion increases by a factor of 11.2≈3.42, which is much better than the theoretical cubic computational complexity. This super-scaling maybe due to the relatively small size of chemical kinetics mechanism used in this study. The chemistry calculation is very expensive and dominates the total computation time. With respect to the conventional FRC model using DVODE, the new FRC model using ODEPIM and CoDAC significantly accelerates the chemistry calculation by a factor of 8.6 and reduces the total computation by a factor of 6.4. The chemistry time, however, still occupying 70% of the computation time in the new FRC model, which is the largest portion of the total computation time. In contrast, preconditioning matrix inversion only accounts for 7.4% of the total computational time. Therefore, the reduction of computational time in this part is not a high priority. In summary, the computation time of the new FRC model is within 3 times of that of the Frozen model without chemistry, within 8 times of that of the FPV model, and 6.4 times faster than the conventional FRC model.

Figure 3 below shows the time-averaged temperature distributions of Sandia Flame D and E, calculated by FRC-LES and FPV-LES approaches. Both flames have relatively simple flow characteristics, and the chemical reactions interlink to the local strain in both inner and outer shear layers. At approximately x/d = 40, intense flame regions can be observed in both flames, where the mixing and combustion are close to complete such that peak temperatures are achieved there. Due to the higher flow velocity in Sandia Flame E, the flame is either pushed further downstream (FPV) or detached from the centerline (FRC). So, the topologies of the results from the two models become different for Sandia Flame E. Besides this difference, both FRC and FPV models present a similar simple diffusion flame, and agree with Nd:YAG laser beam images.

In contrast to time-averaged temperature distributions, the instantaneous temperature distributions of the two models are much more different, as shown in Figure 4. The topology difference between the results from the two models are much more obvious now: FRC predicts no flame near the center line, but FPV still predicts strong flame regions across the center line. In addition, FRC predicts intense flames wrapping around the vortices in the upstream region, which is not predicted by FPV. Particularly, results from FPV-LES approach agree with those from previous FPV studies. It is not obvious which one is closer to the experiment here, because a quantitative experimental measurement of instantaneous temperature distribution is not available. Therefore, even though both models could predict similar time-averaged statistics or spatial distributions, the prediction of unsteady/un-stationary evolution between FRC-LES and FPV-LES approaches could still be significantly different from each other. In view of the unsteady/un-stationary phenomena (e.g. ignition, extinction, combustion instability), such magnification of deviation between the two models becomes an important issue.

Both models predict very dynamic jet flow and flame structures and some levels of local extinction. Near the inlet, the broad pilot flame enhances the stability of the flame and results in minimal local extinction. In addition, turbulence intensity is very low in this region, and the flow field is close to laminar. This means that multi-species differential diffusion effect should be important, which cannot be captured by the FPV-LES approach if unity Lewis number assumption is enforced. For FRC, the piloted flame can survive further downstream to wrap around the vortices generated by shear layers. For FPV, however, the piloted flame distinguished much more upstream. In the downstream region, the outer co-flow and the inner fuel jet interact with each other in the high temperature region of the shear layer, which results more local extinction. In this region, the FPV-LES approach predicts relatively smaller regions with high temperature than the FRC-LES approach, and a completely different topology. Unlike Sandia Flame D, the large deviations between the two models are in both upstream and downstream regions. To better understand the deviations between the two models, detailed species distributions are investigated. Figure 5 compares the distributions of OH radical predicted by the two models. In the upstream region, FRC-LES predicts significantly more OH than FPV-LES. On the contrary, in the downstream region, FPV-LES predicts more regions with high OH concentration, although it is more distributed. However, in the downstream, FPV-LES actually predicts less

regions with high temperature. This contradicts with the general understanding that higher radical levels will result in a stronger heat release and a higher temperature.

To explain this observation, distributions of CO from the two models are compared in Figure 6. FPV-LES predicts both smaller peak CO level and smaller regions with high CO levels, in both upstream and downstream regions. $CO+OH=CO_2+H$ is one of the primary heat release reactions for methane flame. For this reason, CO oxidation becomes the rate-controlling step for the heat release in FPV-LES model, which also explains why it predicts significantly smaller regions with high temperature and partially explains its over-prediction of OH in the downstream region. The comparison of concentrations of major products (CO_2 and H_2O) between the two models (not show here for succinct) indicates that the FPV-LES approach predicts both lower peak product level and smaller regions with high product levels in the downstream region, which further confirms the above conclusion.

On the other hand, FPV-LES predicts smaller regions with high level of CH_4. Therefore, in the prediction of FPV-LES, part of the carbon element must be stuck at some intermediate species between CH_4 and CO, which mainly includes CH_2O and HCO. The conversion from HCO to CO is very fast, thus, only very low level of HCO can be accumulated in the flames (up to mass fractions of 10-5 level in this problem). In the generation of FPV table using 1D steady counter-flow configurations, the flame temperature is higher than the real unsteady conditions in turbulent combustion, thus $CH_2O+OH=HCO+H_2O$ tends to dominate the conversion from CH_2O to HCO. However, there are many holes in the intense flame regions with lower temperature of ~1200 K, in which $CH_2O+O_2=HCO+HO_2$ should dominate the conversion from CH_2O to HCO. With this intermediate-temperature, $CH_2O+O_2=HCO+HO_2$ is more likely to occur during the unsteady evolution. However, the steady FPV table cannot capture the flow unsteady evolution history of the flame, thus could easily overlook this important reaction. As a result, in those holes, carbon element in FPV case is partially stuck at CH2O and has difficulty to convert into HCO and CO. In this problem, CH_2O is accumulated up to mass fractions of 10-3 level.
The discrepancies between the two models could come from the different transport models, the FPV library, the unsteady evolution of filtered mixture fraction and progress variable in the FPV-LES approach, or some combinations of them. For this reason, in the following sections, predictions from the two models will be compared to experimental data in terms of (1) axial and radial distribution of both mixture fraction and progress variable, and (2) the conditional statistics in mixture fraction space.

Figures

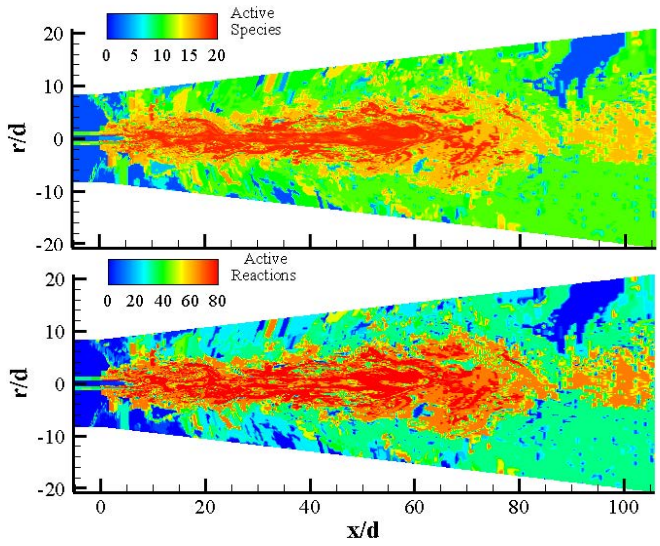


Figure 1. Instantons spatial distribution of numbers of active species (upper) and reactions (lower), generated from the CoDAC method with the FRC-LES approach

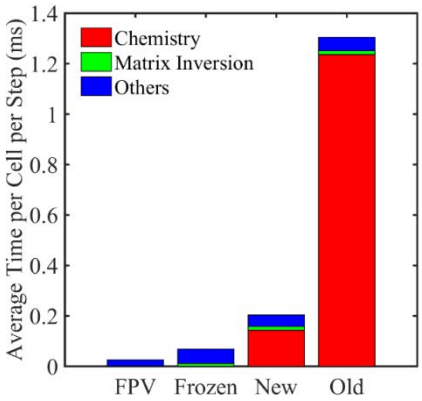


Figure 2. Average computation time distribution of the four models: FPV, Frozen (multi-species transport equations without chemical kinetics source terms), New (new FRC model using ODEPIM and CoDAC), Old (conventional FRC model using DVODE)

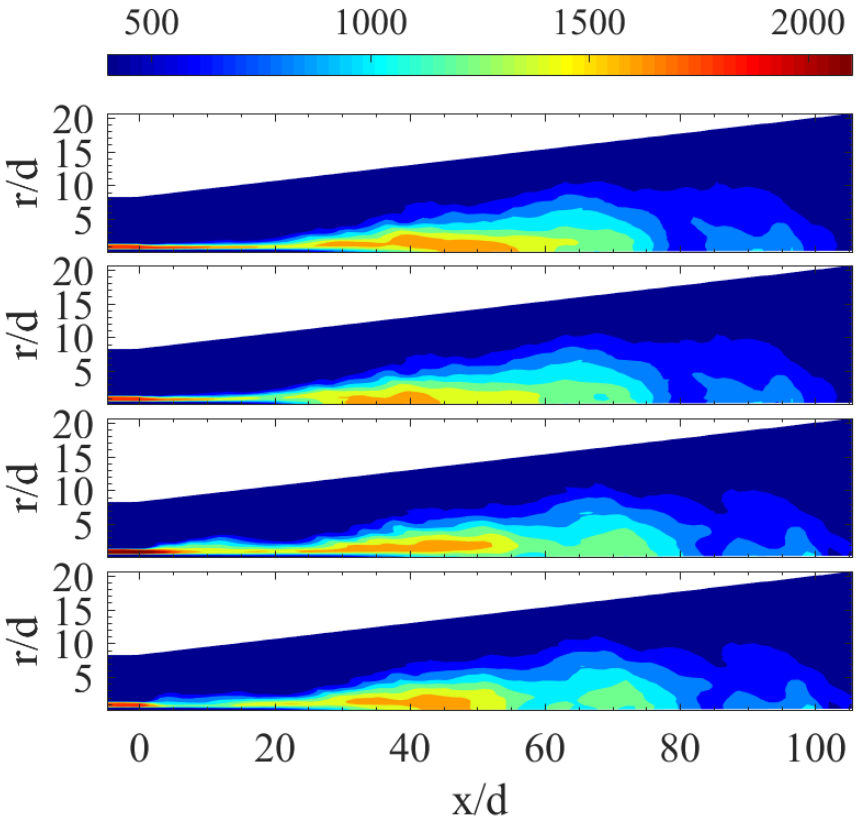


Figure 3. Time-averaged temperature distributions. From upper to lower: Sandia Flame D from FRC-LES; Sandia Flame D from FPV-LES; Sandia Flame E from FRC-LES; Sandia Flame E from FPV-LES

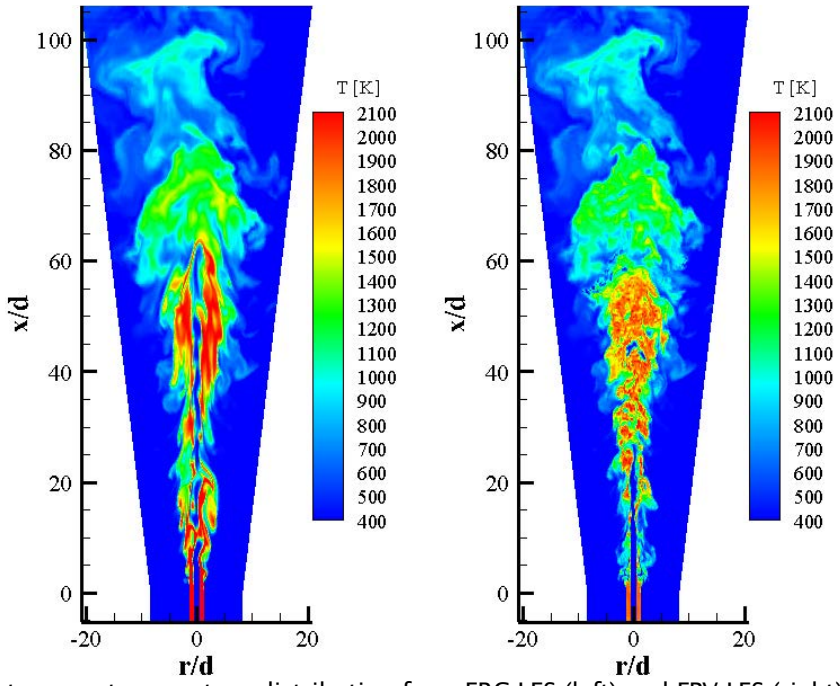


Figure 4. Instantaneous temperature distribution from FRC-LES (left) and FPV-LES (right) at a same time

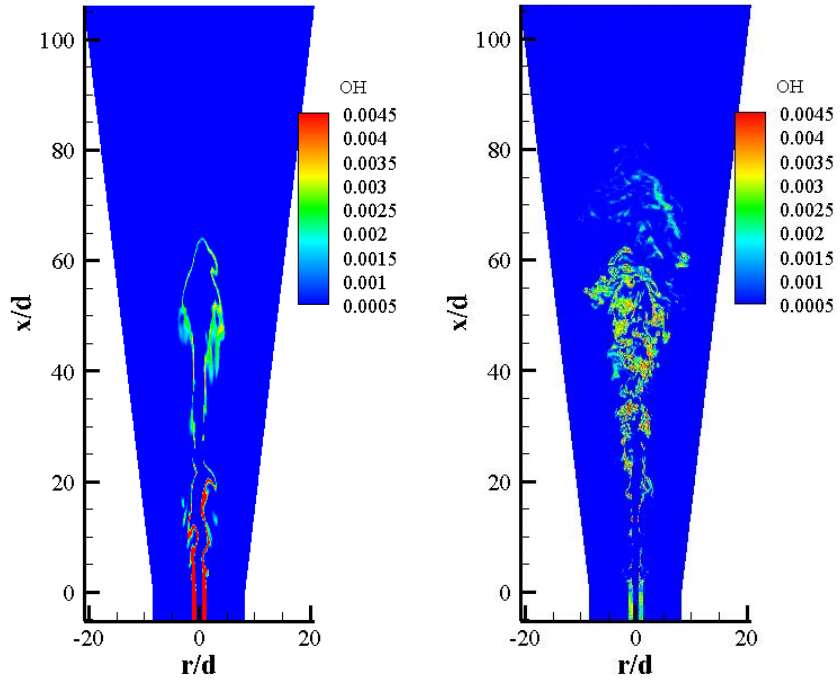


Figure 5. Instantaneous YOH distribution from the FRC-LES (left) and the FPV-LES (right) at a same time

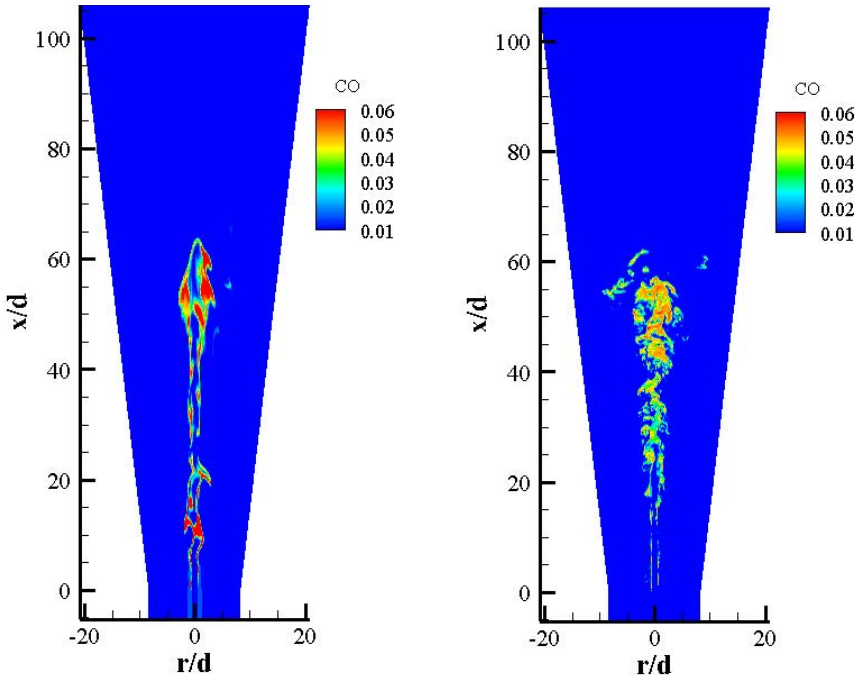


Figure 6. Instantaneous YCO distribution from the FRC-LES (left) and the FPV-LES (right) at a same time

Milestone(s)
Project completed

Major Accomplishments
The accomplishments of the current year's research effort with the impact on the rest of the project are as follows:

- Detailed analysis of Sandia Flame E results were conducted to evaluate the performance of the algorithm in terms of computation time. Simulation results were also compared with results without using DAC to assess the accuracy of the DAC algorithm for both major species and minor species.

Publications
Suo Yang, "Effects of detailed finite rate chemistry in turbulent combustion," Ph.D thesis, Georgia Institute of Technology, 2017

Outreach Efforts
None

Awards
None

Student Involvement
Suo Yang, Xiang Gao

Plans for Next Period
Project is complete



References

1. Sun, W., Chen, Z., Gou, X., Ju, Y., (2010). A path flux analysis method for the reduction of detailed chemical kinetic mechanisms. *Combustion and Flame*, *157*(2), 1298–1307
2. Sun, W., Gou, X., El-Asrag, H. A., Chen, Z., and Ju, Y., (2015). Multi-timescale and correlated dynamic adaptive chemistry modeling of ignition and flame propagation using a real jet fuel surrogate model. *Combustion and Flame*, *162*(4), 1530–1539
3. Yang, S., Yang, V., Sun, W., Nagaraja, S., Sun, W., Ju, Y., (2015) Parallel On-the-fly Adaptive Kinetics for Non-equilibrium Plasma Discharges of C2H4/O2/Ar Mixture. *AIAA SciTech 2015*, *(submitted)*

Task 3 – LES of Spray Combustion in NJFCP Test Facilities

Georgia Institute of Technology

Objective(s)

The objective of this research activity is to establish a simulation strategy using LES to capture fuel sensitivity in experimental test facilities. In particular, the focus of the current year's effort is to perform a baseline validation of the numerical framework for two of the NJFCP fuels, namely Cat A2 and Cat C5 by matching experimentally stable conditions and to demonstrate that the method can predict lean blowout and can capture fuel sensitivity.

Simulations were conducted initially for Area 6 and Area 3 rigs during Year 1 but subsequent work was funded by NASA and FAA support during FY16 and FY17 was focused on travel funds to attend the FAA meetings. Results reported below were obtained during Year 1 effort funded by FAA and current results are substantially different but are reported under NASA funding separately.

Research Approach

Numerical Methodology

We use the well-established Eulerian-Lagrangian (EL) formulation [1] to perform LES of spray combustion in NJFCP test facilities. In the EL method, a Lagrangian tracking of the dispersed phase is performed and the gas phase is modeled using the conventional Eulerian framework [2]. The coupling between the dispersed phase and the gas phase is specified through inter-phase exchange source terms that appear in the mass, momentum and energy transport equations. A detailed description of the governing equations, turbulence closure and numerical method is provided elsewhere [1, 3]. Here, we briefly summarize the numerical method used in this study.

The gas phase is simulated using a second-order accurate (in both space and time) finite-volume solver for the unsteady Favre-filtered, multi-species, compressible Navier-Stokes equations [3]. A hybrid scheme, which dynamically switches between a second-order-accurate central scheme and a third-order-accurate MUSCL (Monotone Upstream-centered Schemes for Conservation Laws) scheme [3] is used in this study. The subgrid-scale (SGS) momentum and energy fluxes are closed using a subgrid eddy viscosity model, which is obtained using the local grid filter Δ and the subgrid kinetic energy k_{sgs}, for which an additional transport equation is solved [4]. The dispersed phase is simulated using the Lagrangian tracking method [5], which solves for the individual droplet evolution in space and time within the gas phase. The time advancement of the Lagrangian equations are performed through a fourth-order-accurate explicit Runge-Kutta scheme [1]. The closure of the subgrid-scale turbulence chemistry interaction is attained through the quasi-laminar formulation.

LES of Area 3 Rig

The simulation parameters for the Area 3 rig for the gas and spray phase are summarized in Table 1 and Table 2, respectively. The focus of this research effort was to perform a validation of the numerical methodology by simulating the Area 3 rig matching the experimental test conditions corresponding to the stable combustion configuration. Afterward, the same configuration and numerical methodology is used to study fuel sensitivity and LBO. Here, we describe the results for the stable combustion with two different fuels, namely Cat A2 and Cat C5. The experimental data is only available for Cat A2 fuel.

Figure 1 shows the instanteneous contours of the temperature field for in the central and axial planes of the combustor. We can observe a high temperature region in the core of the vortex bubble. This central recirculating region with high temperature products and radicals acts an aerodynamic flame holder leading to stable flame on the periphery of the vortex



bubble in its updstream part. Figure 2 shows the instanteneous OH mass fraction on the same planes. Note that OH mass fraction is typically considered as an indicator of the flame location. We can observe that simiar to the temperature contours, the OH radical is present in the core region with flame anchoring occurring on the periphery of the central vortex bubble. Figure 3 shows the spray droplets colored by their temperature along with the flame identified by the temperature iso-surface (T 1800 K). We can clearly observe lower temperature particles near the location where they are being injected in the domain and the higher temperature particles near the flame where they eventually get evaportated.

Figure 4 shows comparison of the time averaged velocity components with the experiments. Overall the results show a reasonable agreement with the experiments, and the trends appear to be captured by the simulations. Note that the experimental profiles shown in this figure are only available for Cat A2 stable configurations. In addition to Cat A2 simulation results, Figure 4 also includes results for Cat C5 cases (A3-$C5_1^S$ and A3-$C5_2^S$) for stable conditions. Here, Case A3-$C5_1^S$ uses chemical kinetics for C5 with A2 as the liquid fuel, whereas Case A3-$C5_2^S$ uses chemical kinetics and fuel corresponding to C5. These cases were considered to demostrate sensitivity of the fuel on the results. We can observe that the results for the velocity components only show minor sensitivity. However, the radial profiles of the temperature shown in Figure 5, show differences among the three cases, where the central core appears to be colder in the case employing C5 as the liquid fuel.

Based on the results presented here, we can conclude that the LES framework employed in this research effort is adequate to capture the dynamics of unsteady spray-flame-trubulence interaction, which is essential to study the combustion physics such as LBO, cold restart and altitude relightning for the present NJFCP program.

Tables

Table1. Gas phase simulation parameters for the Area 3 rig.

Parameter	Value	Source
Outlet/reference pressure	50 Psi	Experiment
Inlet mass flow rate	53 g/s	Experiment
Inlet temperature	350 F	Experiment
Bulkhead temperature (Isothermal walls)	530 F	Experiment

Table 2. Details of the spray parameters for the Area 3 rig.

Injector type	Pressure blast	Experiment
Pressure drop across nozzle	40 Psi	Experiment
SMD	27 μm	Rizk scaling
Mass flow rate (stable)	1.3 g/s	Experiment
Mass flow rate (LBO)	1.14 g/s	Experiment
Injection temperature	100 F	Experiment
Particles distribution	Log normal	Simulation
Injection	Hollow cone with cone angles 50° and 90°	Estimated from number density obtained from experiments

Table 3. List of LES cases indicating their current status.

Case	Fuel	Kinetics	Condition	Rig	Status
A3-A2^{S}	Cat A2	Cat A2	Stable	Area 3	Complete
A3-C5$_1^{S}$	Cat A2	Cat C5	Stable	Area 3	Complete
A3-C5$_2^{S}$	Cat C5	Cat C5	Stable	Area 3	Complete
A3-A2^{B}	Cat A2	Cat A2	LBO	Area 3	Underway
A3-C5^{B}	Cat C5	Cat C5	LBO	Area 3	Underway
A6-A2^{S}	Cat A2	Cat A2	Stable	Area 6	Underway
A6-C5^{S}	Cat C5	Cat C5	Stable	Area 6	Future work
A6-A2^{B}	Cat A2	Cat A2	LBO	Area 6	Future work
A6-C5^{B}	Cat C5	Cat C5	LBO	Area 6	Future work

Figures

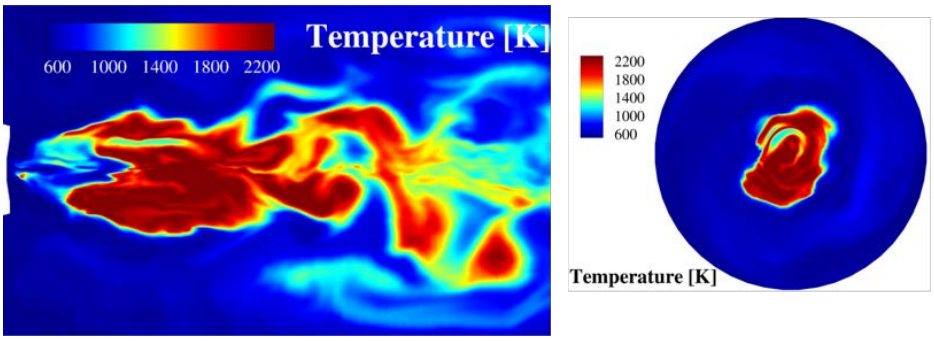


Figure 1. Temperature contours for LES of experimentally stable configuration with CatA2 kinetics.

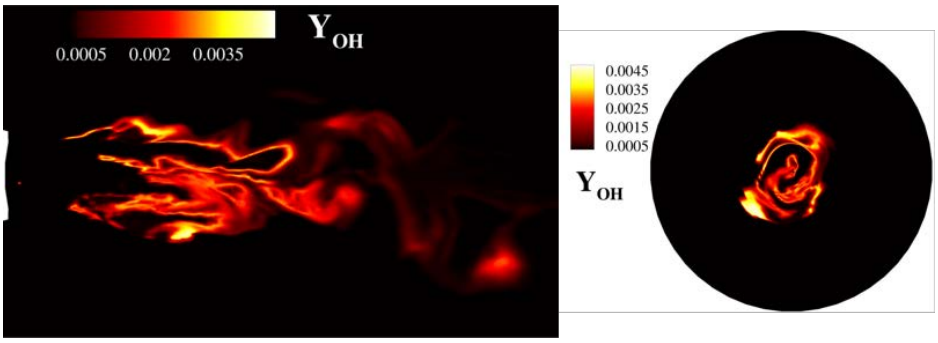


Figure 2. OH mass fraction contours for LES of experimentally stable configuration with CatA2 kinetics.

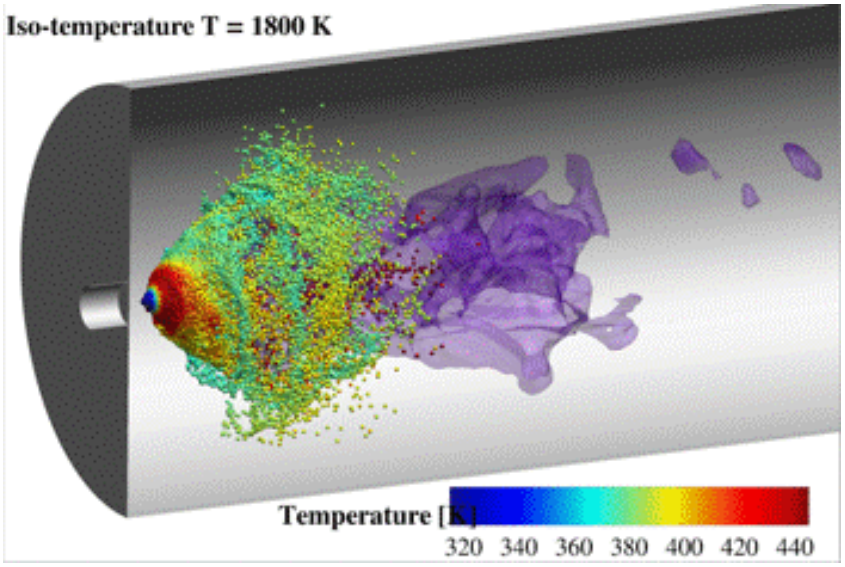


Figure 3. Spray particles (colored by temperature) and flame (identified by temperature iso-surface) visualization in LES of experimentally stable configuration with CatA2 kinetics.

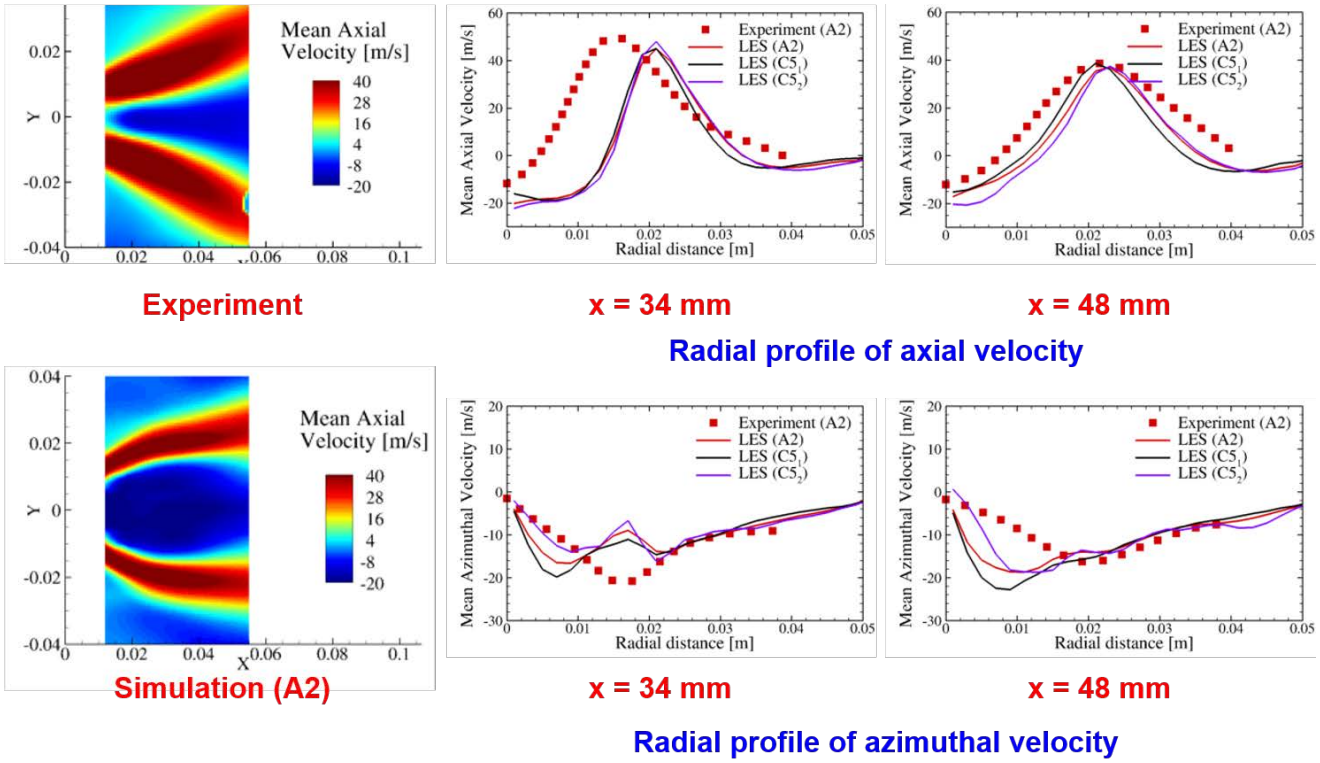


Figure 4. Comparison of time averaged velocity components obtained from LES (A3-A2^S, A3-C5$_1^S$ and A3-C5$_2^S$) and experiment (A3-A2^S).

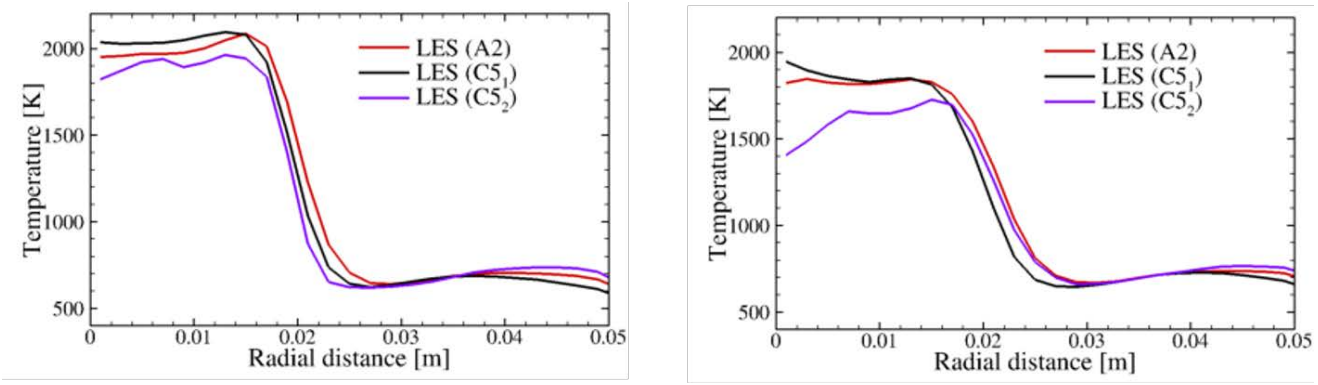


Figure 5. Comparison of the time temperature obtained from LES of different cases illustrating fuel sensitivity.

Milestone(s)

Project completed

Major Accomplishments

The accomplishments of the current year's research effort with the impact on the rest of the project are as follows:

- **Simulation of the Area 3 rig with Cat A2 fuel**: The simulation has been performed matching the experimentally stable conditions to validate the numerical methodology. It used the reduced chemical kinetics model developed under Task 1. The spray condition was partly estimated from the experiment and additional condition was prescribed through the Rizk's scaling law. Overall, the results show a reasonable agreement thus establishing the suitability of the numerical framework employed in this investigation.
- **Simulation of the Area 3 rig with Cat C5 fuel:** The simulation was conducted by keeping the same configuration as mentioned above and only changing the fuel. The change in the fuel was done in two sub-steps leading to two cases. In the first case, only the chemical kinetics was modified whereas in the second case both the liquid fuel and the chemical kinetics corresponded to the Cat C5 fuel. The results obtained from Cat A2 and C5 cases show fuel sensitivity, which is an essential element of the NJFCP program.
- **Simulation of the Area 3 rig under LBO conditions:** Additional set of simulations corresponding to LBO conditions is currently underway.
- **Simulation of the Area 6 referee rig:** The simulation of the Area 6 referee rig with effusion cooling holes and Cat A2 fuel is also currently underway.

Publications

[1] Yang, S., Ranjan, R., Yang, V., Menon, S., Sun, W., "Sensitivity of Predictions to Chemical Kinetics Models in a Temporally Evolving Turbulent Non-premixed Flame," Combustion and Flame, Vol. 183, 224-241, 2017.
[2] Yang, S., Ranjan, R., Yang, V., Menon, S., Sun, W., "Parallel on-the-fly Adaptive Kinetics in Direct Numerical Simulation of Turbulent Premixed Flame," Proceedings of the Combustion Institute, Vol. 36, Vol. 2, 2025-2032, 2017.
[3] Yang, S., Ranjan, R., Sun, W., Yang, V., and Menon, S., "Sensitivity to Chemical Kinetics Models in Time Evolving Turbulent Non-Premixed Flames," 10th U.S. National Combustion Meeting, College Park, MD, April 23-26, 2017.
[4] Rieth, M., Ranjan, R., Kempf, A., and Menon, S., "On the Comparison of Finite-rate Kinetics and Flamelet Based Subgrid Models for LES of Turbulent Premixed Flames," 10th U.S. National Combustion Meeting, College Park, MD, April 23-26, 2017.

[5] Milan, P., Ranjan, R., Panchal, A., and Menon, S., "Flame Dynamics Sensitivity to Turbulent Combustion Models in a Swirl Spray Combustor," AIAA-2017-5079, 53rd AIAA/SAE/ASEE Joint Propulsion Conference, Atlanta, GA, 10-12 July 2017.
[6] Ranjan, R., Panchal, A., Hannebique, G., and Menon, S., "Towards Numerical Prediction of Jet Fuels Sensitivity of Flame Dynamics in a Swirl Spray Combustion System," AIAA-2016-4895, 52nd AIAA/SAE/ASEE Joint Propulsion Conference, Salt Lake City, UT, July 25-27, 2016.

Outreach Efforts
None

Awards
None

Student Involvement
- A. Panchal

Plans for Next Period
There are no more plans for this project. For the following two years FY 16 and FY 17 all research was done under NASA funding and FAA provided only travel funds to attend appropriate meetings twice a year.

References
1. Patel, Nayan, and Suresh Menon. "Simulation of spray–turbulence–flame interactions in a lean direct injection combustor." Combustion and Flame 153.1 (2008): 228-257.
2. Elghobashi, S. "Particle-laden turbulent flows: direct simulation and closure models." Applied Scientific Research 48.3-4 (1991): 301-314.
3. Génin, Franklin, and Suresh Menon. "Simulation of turbulent mixing behind a strut injector in supersonic flow." AIAA journal 48.3 (2010): 526-539.
4. Kim, Won-Wook, and Suresh Menon. "An unsteady incompressible Navier–Stokes solver for large eddy simulation of turbulent flows." International Journal for Numerical Methods in Fluids 31.6 (1999): 983-1017.
5. Faeth, Gerard M. "Mixing, transport and combustion in sprays." Progress in Energy and Combustion Science 13.4 (1987): 293-345.



Project 029(A) National Jet Fuels Combustion Program – Area #5: Atomization Test and Models

Purdue University

Project Lead Investigator

Robert P. Lucht
Ralph and Bettye Bailey Distinguished Professor of Combustion
School of Mechanical Engineering
Purdue University
West Lafayette, IN 47907-2088
765-714-6020 (Cell)
Lucht@purdue.edu

University Participants

Purdue University

- P.I.(s): Robert P. Lucht, Jay P. Gore, Paul E. Sojka, and Scott E. Meyer
- FAA Award Number: COE-2014-29A , 401321
- Period of Performance: 10/1/2017-9/30/2018
- Tasks:
  1. Obtain PDA data across one plane in the VAPS test rig operated with the Referee Rig nozzle and for numerous fuels at near-lean blowout (LBO) conditions and for cold fuel/cold air flow conditions approximating ground light off (GLO) and high-altitude relight (HAR) conditions
  2. Extend PDA measurements to obtain data across multiple planes for evaluation of Detailed Combustor Simulations (DeCS) by Suresh Menon, Vaidya Sankaran, and Matthias Ihme,
  3. Obtain PDA and/or Malvern measurements for selected operating conditions either in the VAPS test rig to provide data for the spray correlation analysis of Nader Rizk,
  4. Perform PDA measurements for fuel blends including Fuel X and/or another blend designed for testing differences in atomization characteristics to examine the sensitivity of correlations and computations to changes in fuel properties,
  5. Ensure quality of data with repetition tests at Purdue and comparisons with spray measurements at P&W, UDRI/AFRL, and UIUC.

Project Funding Level

The funding level from the FAA was $150,000 for Year 4. Purdue University provided cost sharing funds in the amount of $150,000.

Investigation Team

PI Dr. Robert Lucht, Bailey Distinguished Professor of Mechanical Engineering is responsible for the oversight of the entire project here at Purdue University. He is also responsible for mentoring one of the graduate students, coordinating activities with Stanford and will work with all parties for appropriate results and reporting as required.

Co-PI Dr. Jay Gore, Reilly Professor of Mechanical works closely with the PI for all deliverables of Purdue University, and oversees the work performed by one of the graduate students that he is mentoring. He is also responsible for interacting with the CFD groups to suggest comparisons with experiments and with results of an adaptive grid solver.

Co-PI Dr. Paul Sojka, Professor of Mechanical Engineering is responsible for mentoring one of the graduate students and is responsible for supervising the PDPA measurements.

Co-PI Scott Meyer, Managing Director of the Maurice J. Zucrow Laboratories is responsible for coordinating facility upgrades and for facility design reviews.



Senior Research Scientist Dr. Sameer V. Naik is responsible for direct supervision of two graduate students involved in the experimental portion of the project.

Graduate students Andrew Bokhart and Daniel Shin are responsible for performing the PDPA measurements and for modifying the RTS test rig for operation at near-lean-blow-out (LBO) and cold start conditions.

Project Overview

The objectives of this task as stated in the Invitation for ASCENT COE Notice of Intent (COE-2014-29) are to "measure the spray characteristics of the nozzles used in the Referee Combustor used in Area 6 tests and to develop models for characterizing the atomization and vaporization of the reference fuels." We are the experimental part of a joint experimental and modeling effort to achieve these objectives. The experimental tasks will be performed at Purdue University and the modeling tasks will be performed by Prof. Matthias Ihme's group at Stanford University, Prof. Suresh Menon's group at Georgia Tech, and by Vaidya Sankaran at UTRC. Nader Rizk will also develop spray correlations based on our measurements.

Purdue University has very capable test rig facilities for measuring spray characteristics over very wide ranges of pressure, inlet air temperature, and fuel temperature. The experimental diagnostics that are applied include both phase Doppler anemometry (PDA) as well as high-frame-rate shadowgraphy. The atomization and spray dynamics for multiple reference and candidate alternative fuels have been characterized for the referee rig nozzle operated at near lean blowout (LBO) conditions. In the future these same sorts of measurements will be performed for many of these same fuels at operating conditions characteristic of high-altitude relight (HAR). A new fuel, IH2, has been added to the test matrix and will be investigated at LBO and cold start conditions.

Task 1- Measurement of Spray Characteristics at Near Lean Blowout and Chilled Fuel Conditions

Purdue University

Objective(s)

The objectives of this research program are to visualize and measure the characteristics including drop size distributions, axial velocity components of the sprays generated by a nozzle being used in the Referee combustor rig in the Area 6 tests. The resulting data will be used for the development of spray correlations by consultant Nader Rizk and for the purpose of submodel development for detailed computer simulations being performed by Matthias Ihme (Stanford University), Suresh Menon (Georgia Tech), and Vaidya Sankaran (UTRC). The experimental tasks are performed at Purdue University and the resulting data will be shared with FAA team members developing modeling, simulations, and engineering correlation based tools.

The upgraded Variable Ambient Pressure Spray (VAPS) test rig at Purdue University is used for measuring spray characteristics over the ranges of pressure, atomizing gas temperature, and fuel temperature. Our work during the first year allowed us to identify the challenges associated with making reliable and repeatable spray measurements while keeping the windows of the rig clean. Phase Doppler Anemometry (PDA) has emerged as a technique of choice for obtaining fundamental drop size distribution and axial and radial velocity data for comparison with numerical simulations. The VAPS facility has been upgraded to allow us to test over the entire range of fuel and air temperatures and air pressures of interest. We will be able to directly compare reacting and non-reacting spray data by collaborating with the UIUC/UDRI/AFRL Area 6 team.

The experimental data will support continued development and evaluation of engineering spray correlations including the dependence of Sauter Mean Diameter (SMD), spray cone angle, and particle number density per unit volume on the fuel properties at fuel and air temperatures of interest. The experimental data will provide detailed statistical measurements for comparisons with high-fidelity numerical simulations of mixing and combustion processes. The prediction of the spatial distribution of the liquid fuel and resulting vapor and breakdown components from the liquid fuels critically affects the ignition, flame-stabilization, and pollutant formation processes.

The project objectives are summarized as:

(a) Obtain PDA data across one plane in the VAPS test rig operated with the Referee Rig nozzle and for numerous fuels at near-lean blowout (LBO) conditions and for cold fuel/cold air flow conditions approximating ground light off (GLO) and high-altitude relight (HAR) conditions



(b) Extend PDA measurements to obtain data across multiple planes for evaluation of Detailed Combustor Simulations (DeCS) by Suresh Menon, Vaidya Sankaran, and Matthias Ihme,
(c) Obtain PDA measurements for selected operating conditions either in the VAPS test rig to provide data for the spray correlation analysis of Nader Rizk,
(d) Perform PDA measurements for fuel blends including Fuel X and/or another blend designed for testing differences in atomization characteristics to examine the sensitivity of correlations and computations to changes in fuel properties,
(e) Ensure quality of data with repetition tests at Purdue and comparisons with spray measurements at P&W, UDRI/AFRL, and UIUC.

Research Approach

The Purdue University test rig facilities are designed for measuring spray characteristics over very wide ranges of pressure, atomizing gas temperature, and fuel temperature. An atmospheric pressure spray test rig facility was extensively used in year 1 of the project to establish the differences in spray properties of the different fuels at multiple fuel temperatures, fuel pressures, and swirler pressure drops. The second facility is the VAPS test rig which allows measurements under high and low pressure conditions relevant to the aviation applications and was being reactivated during the last part of year 1 activities and the first part of year 2 activities.

The operating system for the atmospheric pressure spray facility and the instrument positioning and atomization systems have been upgraded over the first year to allow high repeatability for PDA drop size and velocity measurements. The PDA system itself was repaired and refurbished near the end of Year 2, beginning of Year 3. A high speed camera with backlighting has yielded significant insights into the structure of the liquid fuels flowing out of the nozzle with and without the swirling co-flow through the injector. An optical patternator was also used for rapid analysis of spray distribution patterns.

Liquid fuels can be supplied to the test rigs by multiple systems. A facility-integrated system draws fuel from one of two certified flame-shield fuel containments for testing standard aviation fuels as well as other alternative blends. A mobile fuel system, developed under the combustion rules and tools (CRATCAF) program and redeployed during the first year of the NJFCP program is being utilized for further control of additional injector circuits or for running alternative fuel blends. Both systems were designed with two independently controlled and metered circuits to supply fuel to pilot and main injector channels of the test injector. The mass flow rates of both supplies are measured with Micro Motion Elite® Coriolis flow meters. A nitrogen sparge and blanket ullage system is used to reduce the dissolved oxygen content of the fuel, which is monitored with a sensor just upstream of the fuel control circuits. High pressure gear pumps provide fuel at up to 30 kg/hr, supplied to the control circuits at a 10 MPa regulated line pressure. The mobile fuel system was built with two onboard heat exchangers and a chilling unit controls the temperature of the fuel over a range of 193 K to 263 K (-80 ºC to -10 ˚C).

Milestone(s)

The tasks that were performed in FY2018 are listed below:

Quarter 1

1. Performed PDA measurements for chilled fuel/nitrogen conditions for A2, A3, and C3 fuels after installation of system to inject liquid nitrogen into the gaseous nitrogen airbox flow. Measurements were performed for A2, A3, and C3 fuels at -30F fuel temperature and -30F nitrogen airbox temperature.
2. Performed PDA measurements for chilled fuel/nitrogen conditions for A1, A2, A3, C1 and C7 fuels after Installation of system to inject liquid nitrogen into the gaseous nitrogen airbox flow. The test matrix was provided by the Area 6 group based on their ignition measurements. The conditions provided were conditions where the probability of ignition was 5%.
3. Developed computational methodology based on CONVERGE code for LBO predictions in referee combustor for a given fuel. CFD model utilizes the on fly automatic mesh generation and adaptive mesh refinement techniques. All tiny effusion holes on the liners are resolved and gridded in this methodology.
4. Performed non reacting RANS and LES simulations to estimate the flow splits for swirler passages (radial, inner axial, outer axial and swirler cooling slot), primary and secondary dilution holes, and effusion holes. Both and RANS and LES results compared with experimental data.
5. Reacting LES Simulations were performed using finite rate chemistry solver (laminar closure for sub-grid scale turbulent chemistry interactions) and compact kinetic models for A-2 and C-1 fuels.
6. PhD student Veeraraghava Raju Hasti presented two papers at the 2018 SciTech meeting (1. Assessment of turbulent combustion models with automatic meshing and AMR for Volvo bluff body flame 2. Evaluation



of LES methodology based on automatic meshing and AMR for capturing the turbulent flame structures with CO2 addition (0%, 5% and 10%)).

Quarter 2

1. Performed PDA measurements for high ambient pressure conditions for A2. Measurements were performed for A2 fuel at 45 F fuel temperature and 45 F nitrogen airbox temperature at vessel pressure of 1, 2, 5, and 7 bar.
2. Began the process of moving the VAPS test rig and PDA system to a test cell in the new High Pressure Combustion Laboratory.
3. Began the process of designing a new stand for the VAPS rig system in the new facility.
4. MS students Andrew Bokhart and Daniel Shin co-authored a paper for the 2018 AIAA SciTech Meeting. Daniel Shin presented the work at 2018 AIAA SciTech.
5. Reacting LES Simulations were performed using finite rate chemistry solver (laminar closure for sub-grid scale turbulent chemistry interactions) and HyChem mechanisms (detailed, skeletal and reduced version) for A-2 and C-1 fuels. Skeletal mechanism showed the correct trends for both fuels where as detailed and reduced mechanisms showed opposite trends with multi-zone finite rate chemistry model.
5. PhD student Veeraraghava Raju Hasti drafted 3 AIAA JPC papers – 1. Non reacting flow-splits 2. LBO computation with Compact kinetic models 3. Flame structure evaluation and key markers identification during LBO for both A-2 and C-1 fuels.

Quarter 3

1. A new stand design for the VAPS rig system was developed to accommodate to the new facility. A new stand frame that will support the pressure vessel was redesigned. A Linos structure for PDA system was designed for the VAPS test rig. This structure will also allow other measurement techniques such as SLIPI, holography, etc.
2. Began the process of expanding the data acquisition and control system (DACS) in new test facility for VAPS test rig. Working in progress counting channels, cables, instrumentations, hardware, etc.
3. Worked on editing and revising AIAA book chapter describing the NJFCP program.
4. Graduate students Daniel Shin and Andrew Bokhart co-authored a paper for the ICLASS 2018 and submitted the abstract for 2019 AIAA Sci-Tech. Daniel Shin presented the measurements at Cold Start Condition in the ICLASS 2018 conference.
5. Collected spray boundary conditions for cold start ignition LES simulations
6. Graduate student Veeraraghava Raju Hasti presented 3 papers at the AIAA JPC meeting and also delivered training on LBO computation using CONVERGE CFD tool organized by the Convergent Science for OEMs and Gas turbine community at the JPC 2018.
7. Developed a conjugate heat transfer methodology based LES simulations to account for heat losses through liner walls on the flame structure and LBO limits for referee combustor
8. Abstract on LBO mechanism submitted and accepted for presentation at the 71st APS division of fluid dynamics annual meeting.

Quarter 4

1. New stand design for VAPS test rig has been developed and fabricated. Frames were welded/assembled together and moved in a new test cell.
2. Expansion on data acquisition & control system (DACS) for the VAPS test rig in a new test cell has been initiated. Assembling and installing parts for additional DACS components in a new test cell is still in progress.
3. Previous fuel line design on a mobile fuel system damaged the flowmeter. Modification on fuel line on a mobile fuel system has been done, and a new flowmeter will be installed.
4. Facility fluid supply lines for the atomizing flow, vessel flow, purge, and pilot in a new test cell have been specified and are under modification.
5. AIAA Sci-Tech 2019 abstract for the cold start condition measurement has been accepted.
6. Attended and presented the work at NJFCP mid-year meeting hosted by GE at Cincinnati, Ohio.
7. Graduate student Hasti Veeraraghava Raju edited the 3 JPC papers for submission to AIAA journal and AIAA Journal of Propulsion and Power

8. Evaluated the Flamelet Generated Manifold combustion model with diffusion flamelet for C-1 fuel with compact kinetic mechanism to compute the LBO. This model show blow-out for C-1 fuel at global equivalence ratio of 0.084 and experimentally measured global equivalence ratio at the blow-out is 0.0869.
9. Implemented Partially Stirred Reactor (PaSR) combustion model in CONVERGE code to account for sub-grid scale turbulence-chemistry interactions for LBO simulations.
10. LBO mechanism identified based on LES simulations and presented this work at the 71st APS division of fluid dynamics annual meeting in Atlanta, Georgia, USA.

Major Accomplishments

Experimental Contribution

The work described in this section is a part of the Purdue contributions to the larger FAA-funded effort, the National Jet Fuels Combustion Program (NJFCP). The major objective of the work at Purdue is to perform measurements of spray properties (droplet size, droplet velocity, spray cone angle) for a variety of jet fuels and candidate jet fuels under a wide range of conditions, including lean blowout (LBO), Ground Lift Off (GLO), and high altitude relight (HAR). Representative measurements of spray characteristics at cold start conditions are presented in the rest of this section. The Purdue Variable Ambient Pressure Spray (VAPS) test rig is discussed along with modifications needed for the cold start measurements. A generic hybrid airblast pressure-swirl injector is used and we have investigated the spray characteristics of three different fuels. The spray data was provided to Dr. Nadar Rizk for developing correlations as well as to modelers for computational models of the combustion process in a Referee rig developed by the NJFCP team.

Experimental Systems

Purdue Variable Ambient Pressure Spray (VAPS) rig is consisted of two major components: the airbox assembly and the pressure vessel. The airbox is a length of pipe on which the hybrid airblast pressure-swirl atomizer was mounted. The airbox is placed within the pressure vessel. This allows a pressurized atomizing gaseous flow through the airbox to be isolated from the vessel to create a pressure difference across the gas swirler. Nitrogen is used for all gaseous flows in this investigation to prevent the formation of combustible mixtures. A liquid nitrogen flow is injected into the gaseous nitrogen airbox flow to chill the atomizing gas flow to 239 K for cold start condition measurements. The airbox assembly was capable of vertical translation allowing measurements at multiple locations downstream of the injector. A diagram of the VAPS rig with all the fuel/gas flows is shown in Figure 1.

The pressure vessel houses the airbox and injector assemblies and allows the variation of different ambient pressure into which the fuel is being injected. The vessel is rated to withstand 4.14 MPa (600 psi) at 648.9°C (1200°F). The pressure within the vessel is controlled by a butterfly valve downstream of the test section which can be partially closed to increase pressure and opened to vent pressure or operate at ambient pressures. For this study, the vessel pressure remained at approximately standard atmospheric pressure. The vessel has four windows in the same horizontal plane, which allow laser diagnostic measurements to be performed within the test section. Two windows have a diameter of 127 mm (5 inches) and the other two windows have a diameter of 76.2 mm (3 inches). The 76.2 mm windows are both at a 60° angle from one of the 127 mm windows, with one of the 76.2 mm windows located on either side of the 127 mm window. Two heated nitrogen flows enters the vessel to mitigate fuel recirculation and collection of fuel drops on the windows: the sweeping flow and the window purge flow. These two flow are also used to build pressure within the vessel. A diagram depicting these two nitrogen flows as well as the airbox co-flow is shown in Figure 1(a) and a picture of the VAPS vessel is shown in Figure 1(b).

The mobile fuel system uses an IMO CIG Lip Seal and Weep Hole Design gear pump, which is used to supply pressurized fuel to the injector mounted on the airbox. The mobile fuel system also uses a chiller unit with two heat exchangers to chill the fuel to the desired fuel temperature. The fuel supply line passes through two heat exchangers and travels along a jacketed fuel line in which the heat transfer fluid is circulated. The chiller unit can chill the heat transfer fluid to a temperature within the range of -80 °C to -10 °C with ±0.1 °C control stability.

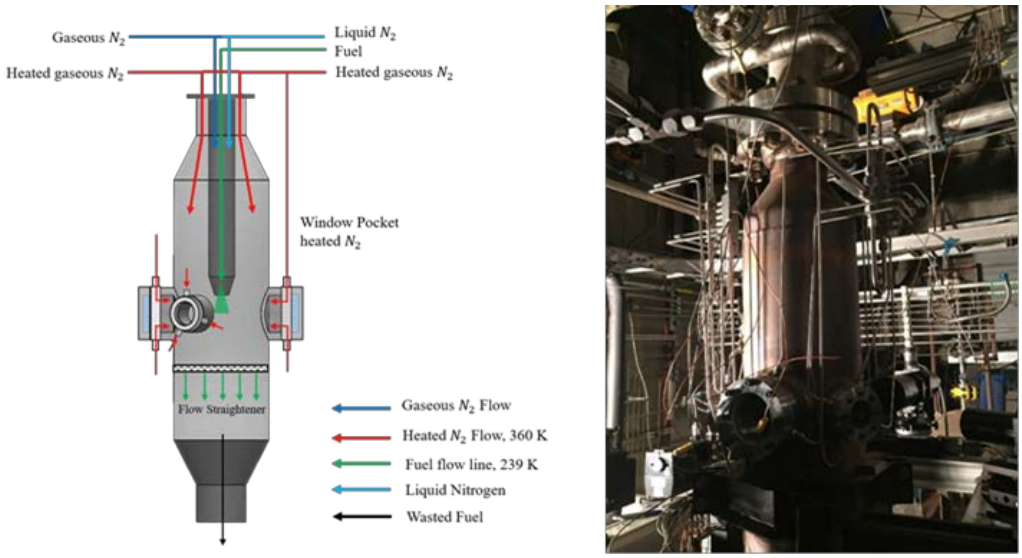


Figure 1. Schematic diagram and photograph of the Variable Ambient Pressure Spray (VAPS) test rig.

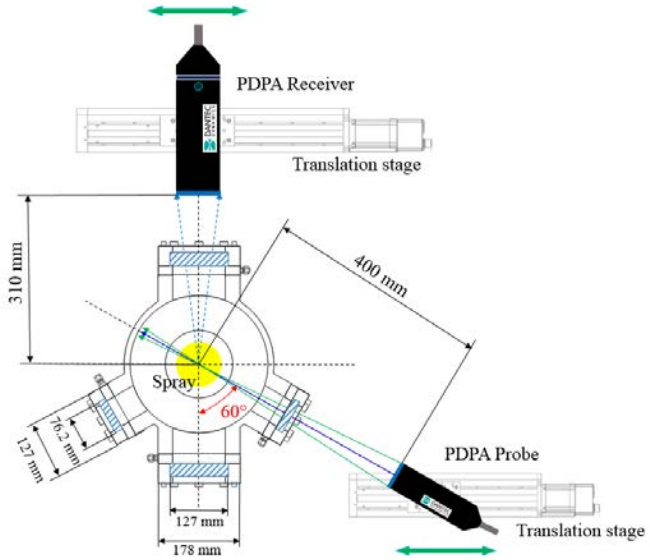


Figure 2. PDA measurement system for the VAPS test rig.

There are two independently controlled and metered fuel lines, which are used to supply fuel to the pilot and main orifices on a hybrid airblast pressure-swirl atomizer. The schematic of this hybrid airblast pressure-swirl atomizer is provided in 3. The atomizer consists of two parts: the fuel injector and gas swirler. The atomizer is assembled such that the fuel injector is housed within the gas swirler. The fuel injector has two types of injection orifices that can be operated separately: the pilot and the main. The pilot orifice is comprised of a single orifice at the centerline of the injector and performs as a pressure swirler of the hybrid design. The main is comprised of multiple orifices that injects fuel tangentially onto a prefilming surface on the interior of the gas swirler. The resulted spray of this hybrid atomizer is a hollow cone spray.

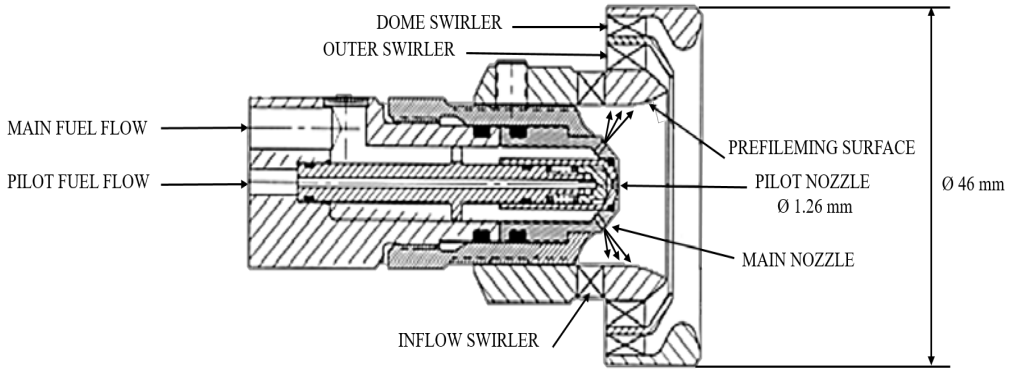


Figure 3. Schematic of the hybrid airblast pressure-swirl atomizer

The fuel sprays are characterized using a DANTEC Dynamics phase Doppler anemometry (PDA) system which measured a variety of mean diameter statistics and a component of drop velocity. The receiving probe and the transmitter probe are aligned at a scattering angle of 60˚ due to the orientation of the windows on the vessel. The alignment of the PDA system relative to the VAPS vessel is shown in Figure2. The PDA probe and receiver optics are mounted on Zaber translation stages to move the system to measurement locations throughout the spray along the horizontal axis. The center of the spray on the horizontal axis is defined as the zero location for the radial locations. Measurements are taken between ±30 mm from the center of the spray with increments of 5 mm and 20,000 samples at each radial location.

Experimental Results: PDA Measurements

Spray measurements at cold start operating conditions have been performed in the VAPS rig for three different fuels: A-2, A-3, and C-3. The cold start operating conditions are at an ambient pressure of 1 bar (15.4 psia), an air box nitrogen temperature of 239 K (-30^{0}F), a pilot fuel temperature of 239 K (-30^{0}F), a pilot fuel mass flow rate of 9.22 kg/hr (20 lb/hr), and a pressure drop (ΔP/P) of 2, 3, and 4 % across the swirler. All three fuels were investigated at three different axial distance downstream from the exit of swirler: 12.7 mm (0.5 inch), 25.4 mm (1 inch), and 38.1 mm (1.5 inch). Figure 4 shows the D_{32} and U_z measurements for C-3 fuel at 25.4 mm measurement plane. The distribution shows that the symmetry of the spray produced by the hybrid atomizer for this study is preserved at cold start conditions, similar to the previous lean blowout (LBO) investigation using the same injector.

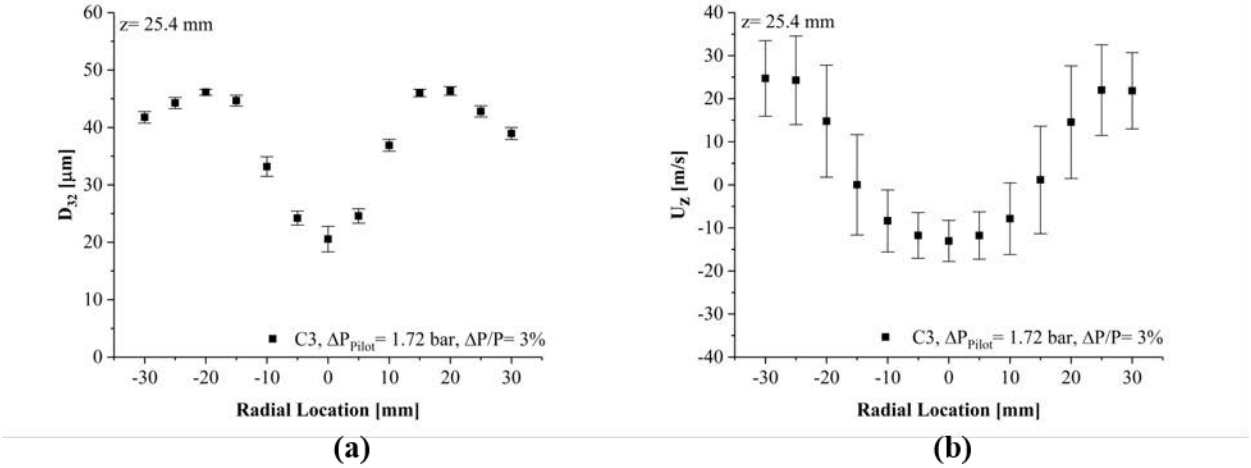


Figure 4. D_{32} and U_z distributions for C-3 with ΔP/P =3 %, T_{fuel} = 238 K, T_{gas} = 238 K at 25.4 mm measurement plane. Vertical bars on velocity represent RMS.

The D_{32} and U_z distributions for C-3 at 12.7 mm, 25.4 mm, and 38.1 mm measurement planes are shown in Figure 5. The minimum values of all of these distributions remained at the center of the spray (r = 0 mm) for all three planes investigated, but the peaks of the distributions shifted away from the center of the spray toward the edge of the spray as the axial distance from the injector increased. These observations demonstrated that as the spray travels downstream from the injector the largest drops continued to maintain their trajectories and spread radially outward.

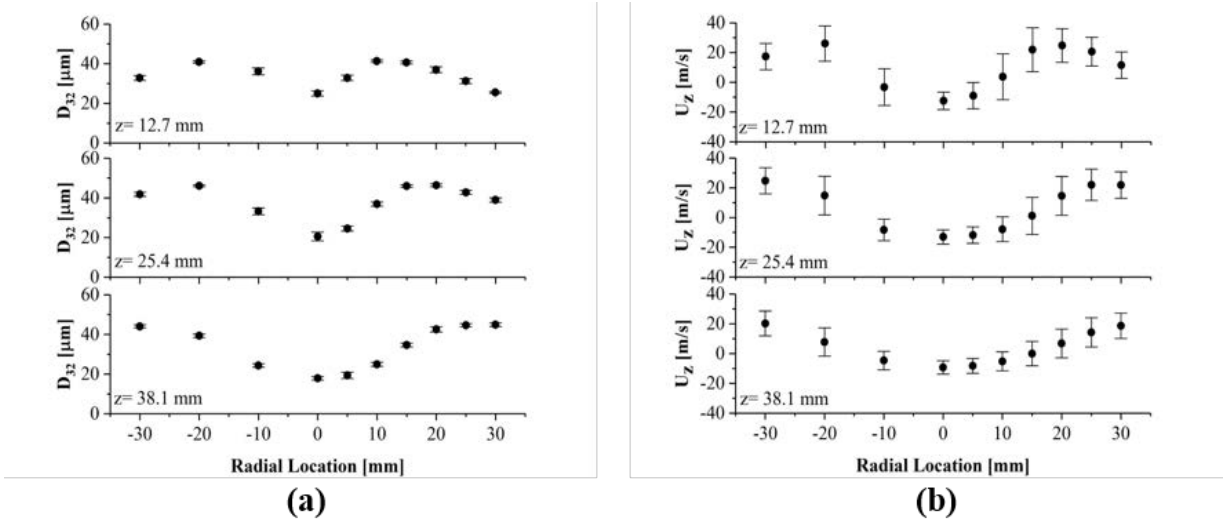


Figure 5. Comparisons of D_{32} and U_z distributions for C-3 at different measurement planes at ΔP/P =3 %, T_{fuel} = 238 K, T_{gas} = 238 K at 25.4 mm measurement plane. Vertical bars on velocity represent RMS.

The effect of pressure drop across the swirler (ΔP/P) on the D_{32} and U_z was observed to be significant for the A-2, A-3, and C-3 fuels. Figures 6 to 8 show the comparisons of D_{32} and U_z distributions at three different pressure drops of 2, 3, and 4% for A-2, A-3, and C-3. It was observed that a decrease in D_{32} with increases in ΔP/P at all radial locations. The U_z comparisons at different ΔP/P values for the A-2 fuel are shown in Figure 6(b). The magnitude of drop velocities increased as ΔP/P increased due to the larger inertia imparted by the greater gas flow.

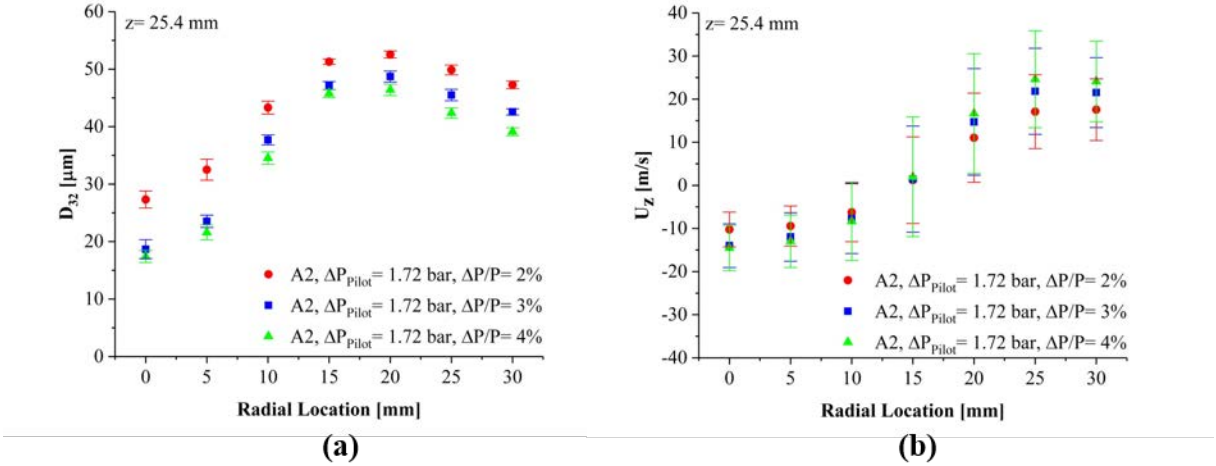


Figure 6. Comparisons of D_{32} and U_z distributions for A-2 when ΔP/P = 2, 3, 4 %, T_{fuel} = 238 K, and T_{gas} = 238 K at 25.4 mm measurement plane. Vertical bars on velocity represent RMS.

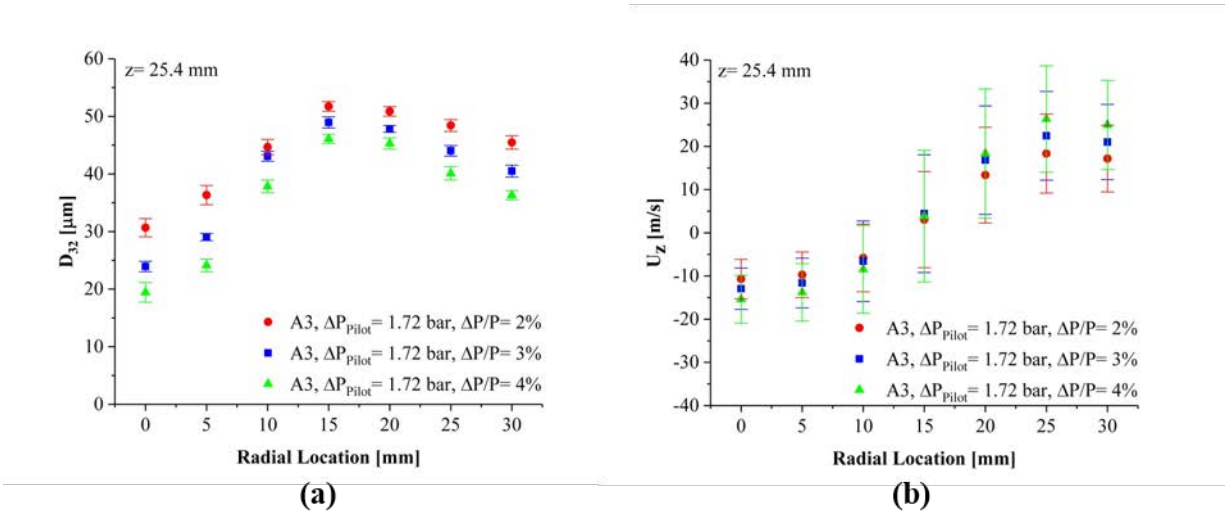


Figure 7. Comparisons of D_{32} and U_z distributions for A-3 when ΔP/P = 2, 3, 4 %, T_{fuel} = 238 K, and T_{gas} = 238 K at 25.4 mm measurement plane. Vertical bars on velocity represent RMS.

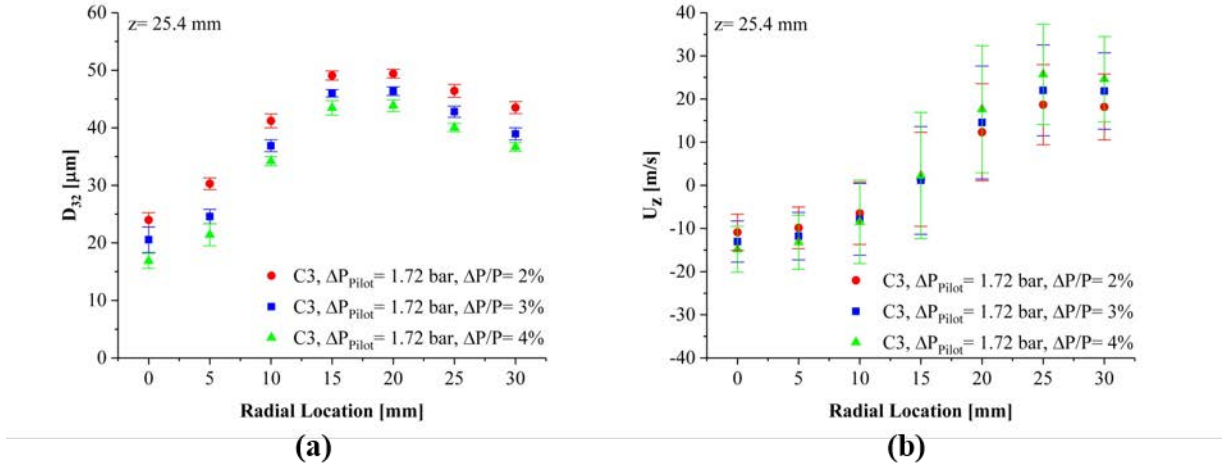


Figure 8. Comparisons of D_{32} and U_z distributions for C-3 when ΔP/P = 2, 3, 4 %, T_{fuel} = 238 K, and T_{gas} = 238 K at 25.4 mm measurement plane. Vertical bars on velocity represent RMS.

The effect of fuel type on D_{32} and U_z was investigated at the cold start conditions on the 25.4 mm measurement plane. The comparisons of D_{32} and U_z for A-2, A-3, and C-3 are shown in Figure 9. The D_{32} comparison showed that A-3 fuel formed the highest D_{32} within the recirculation zone. The U_z measurements showed no significant variations among the fuels. The fuel properties at the cold start conditions did not provide any definitive conclusions regarding observations made about the effect of fuel type.

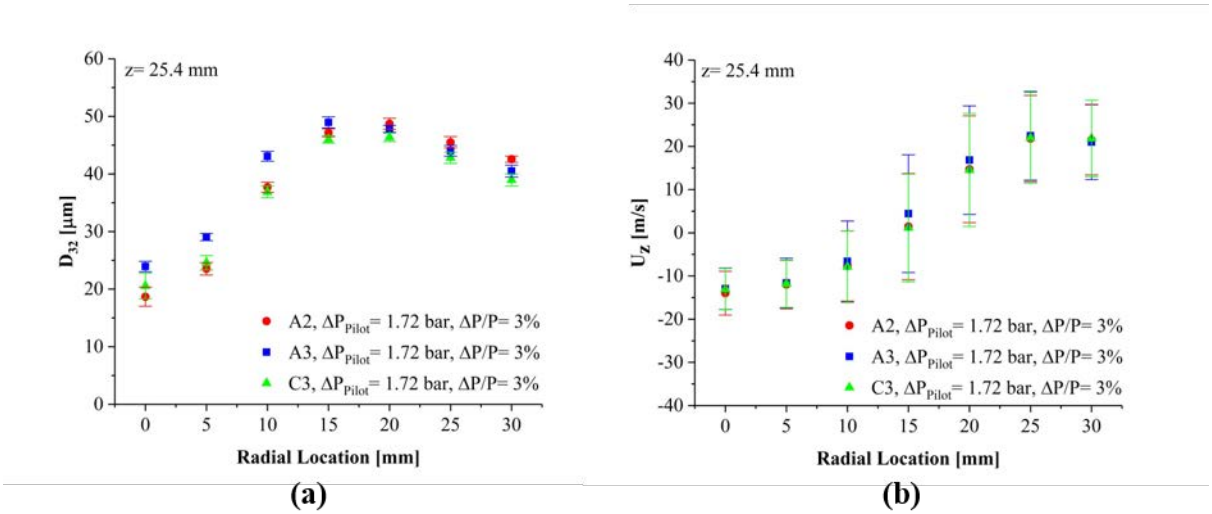


Figure 9. Comparisons of D_{32} and U_z for A-2, A-3, and C-3 when ΔP/P = 2, 3, 4 %, T_{fuel} = 238 K, and T_{gas} = 238 K at 25.4 mm measurement plane. Vertical bars on velocity represent RMS.

The effect of ambient pressure on spray characteristics was also investigated with A-2 fuel in VAPS test rig. The operating conditions for this investigation were ΔP/P =2 %, ΔP_{pilot} = 1.72 bar, T_{fuel} = 278 K, and T_{gas} = 259 K. The ambient pressure was varied to values of 1, 2, 5, and 7 bar, and the measurements were taken at 25.4 mm downstream from the swirler exit. Figure 10 shows the comparisons of D_{32} and U_z for A-2 at different ambient pressures. The observation shows that a decrease in D_{32} with increases in ambient pressures. However, the effect of ambient pressure on the drop size diminished with continuous increase in ambient pressure. The U_z comparison shows that the the drop velocity was not affected significantly by the ambient pressure variation.

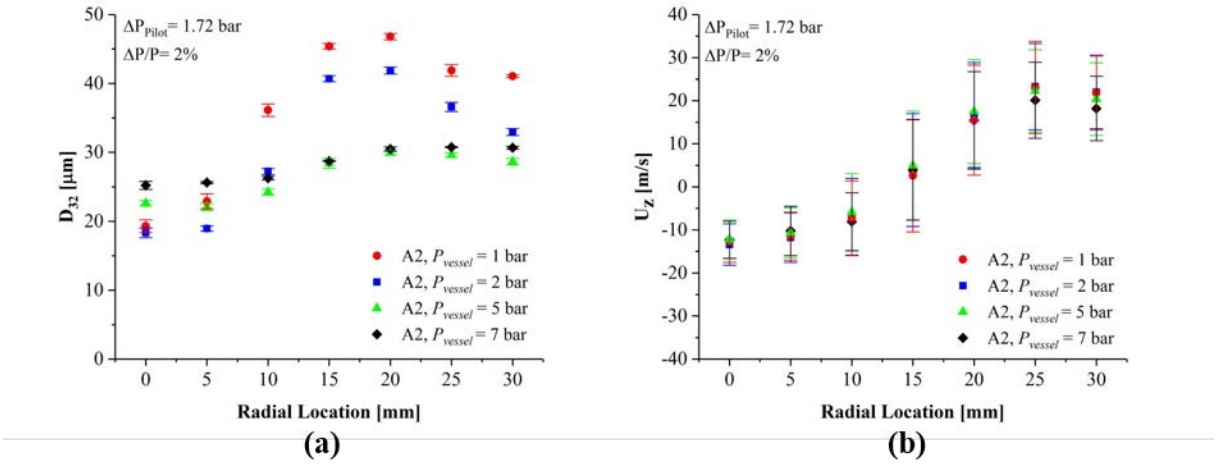


Figure 10. Comparisons of D_{32} and U_z for A-2 at ambient pressure of 1, 2, 5, and 7 bar when ΔP/P = 2 %, T_{fuel} = 278 K, and T_{gas} = 259 K at 25.4 mm measurement plane. Vertical bars on velocity represent RMS.

Computational Contribution

The following section describes the computational efforts for predicting the fuel sensitivity to LBO in referee combustor. The CFD model developed for LBO calculations is shown in Figure 11. Flow through all passages including tiny effusion holes on the liners is resolved in this CFD model. The computational grid for flow simulations with all passages open is shown in



Figure 11. The grid is locally refined in the regions with the steepest gradients in the domain while leaving the grid relatively coarse in sections with weaker gradients using adaptive mesh refinement (AMR).

Non-reacting simulations are carried out first for flow rate comparison with experimental data for swirler component-wise passages and all passages in the referee combustor. Reacting flow LES simulations are carried out for referee combustor using a finite volume based compressible flow solver CONVERGE and detailed finite-rate chemistry. The gas phase equations are described with the Eulerian approach and the liquid spray is modeled with discrete injections of droplets in a Lagrangian frame to simulate the liquid fuel spray. The compressible form of the Favre-averaged Navier-Stokes equations after LES decomposition is solved on a non-staggered, collocated computational grid along with the species transport equations, energy equation and the equation of state in the present study. The sub-grid stress tensor, $\tau_{ij} = \bar{\rho}\left(\widetilde{u_i u_j} - \tilde{u}_i \tilde{u}_j\right)$ in the momentum equation is modeled using a non-viscosity based one-equation sub-grid scale model to obtain the closure. The filtered reaction rate in the species transport equation is estimated using the Arrhenius law and assumed well-stirred reactor model for sub-grid level turbulence-chemistry interactions.

The spray boundary conditions (droplet diameter, average velocity, and cone angle) specified at 2 mm from the nozzle exit are obtained from the PDPA measurements (provided details on these measurements in our experimental contribution section) at 25.4 mm from the deflector plate. An ensemble of six ring injectors, each with its own droplet size and velocity distributions, represents the nozzle. Taylor Analogy Secondary Breakup and the dynamic drag models are employed to estimate the secondary breakup and resulting spray droplet dynamics. A droplet dispersion model is used to include the effects of the sub-grid-scale flow field on the discrete parcels. The drop evaporation rates are calculated using the Frossling correlation based on the laminar mass diffusivity of the fuel vapor, a mass transfer number, and a Sherwood number. The prescribed fuel properties are as determined for A-2 and C-1 fuels.

Parts of this work were carried out at Argonne National Laboratory.

CFD Model:

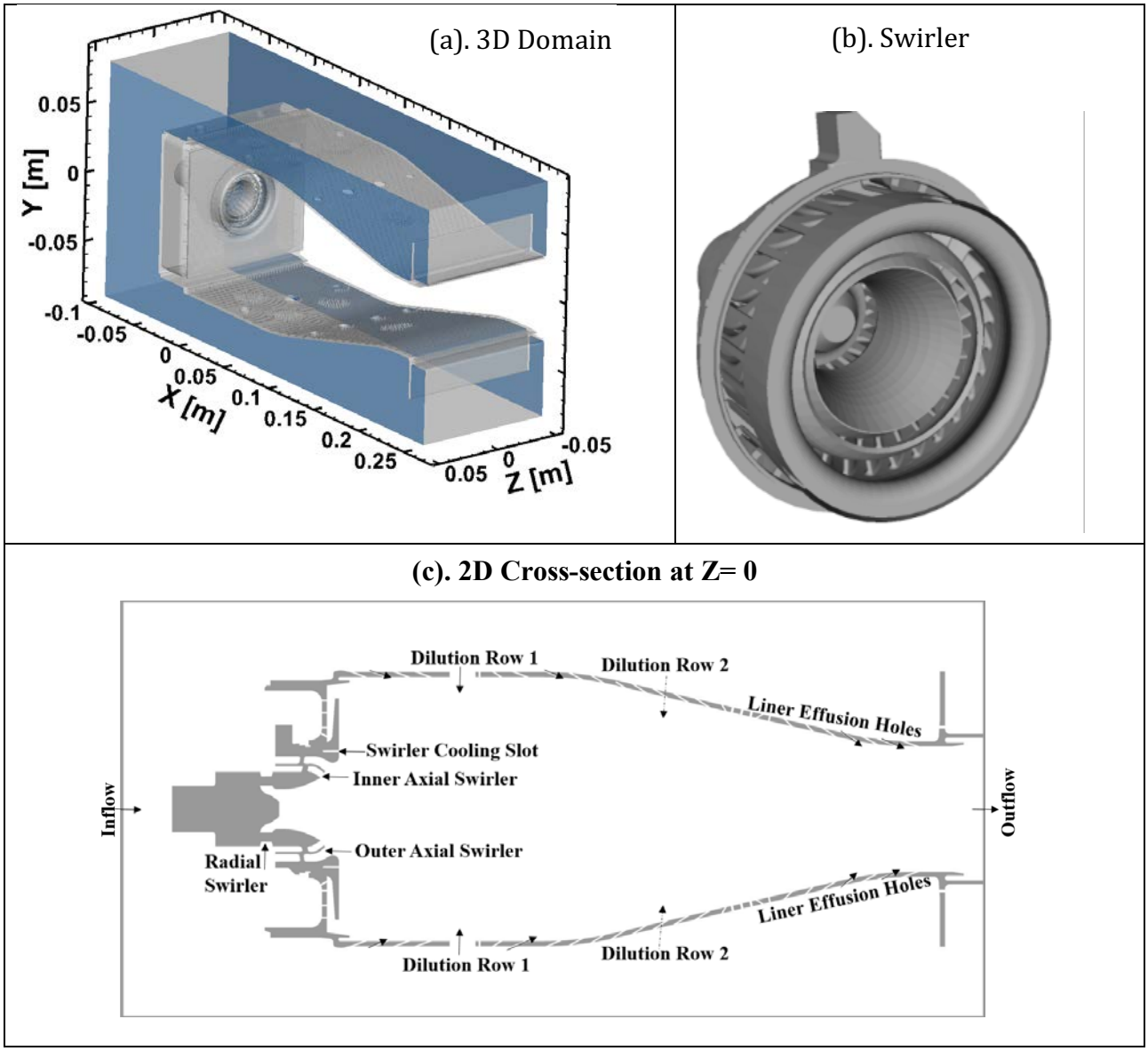


Figure 11. (a) 3D Computational domain (b) magnified view of the 3D swirler (c) magnified the view of the 2D cross-section at Z=0 (mid-plane).

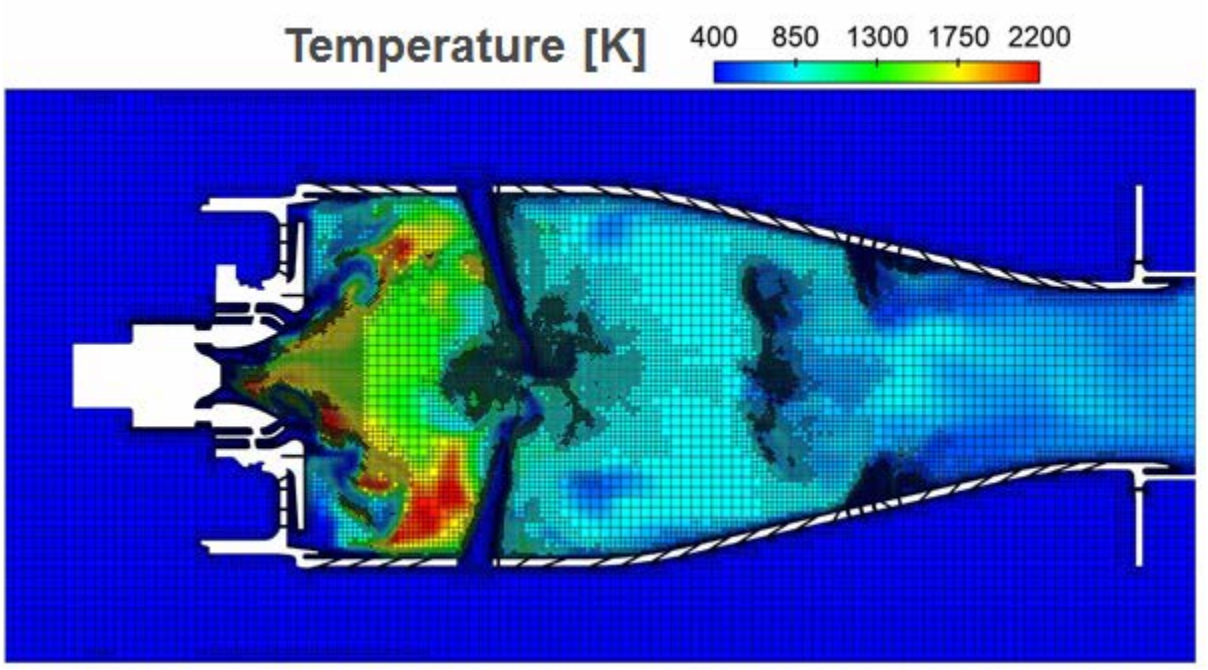


Figure 12. Computational grid with AMR on mid-plane of the referee combustor for a reacting case and colored with temperature contours

Non-reacting swirler component-wise flow splits study (one passage open at a time)

For the component-wise flow split study, a comparison between the experimental and computed results is shown in Figure 13. Computed results are in excellent agreement with experimental data for outer axial, inner axial and radial swirlers. Both RANS and LES underestimate (by about 22%) the order of magnitude smaller swirler cooling flow. However, both computational models capture the flow splits contributing to over 95% of the total flow accurately.

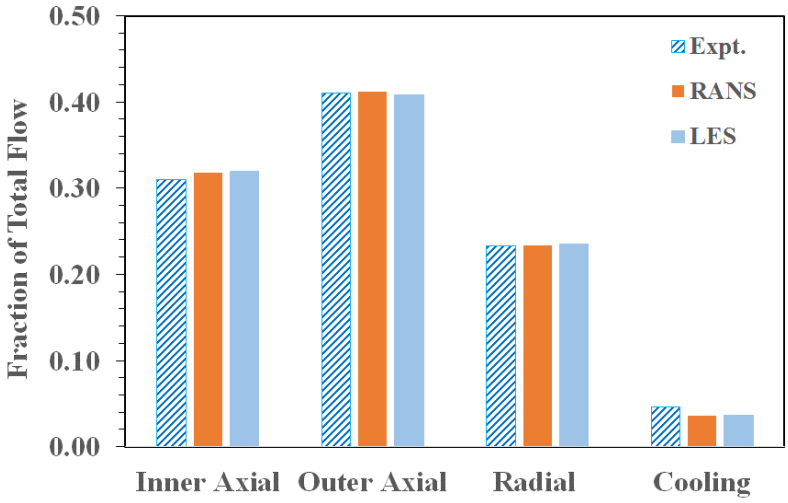


Figure 13. Comparison of component-wise flow splits for swirler passages for 10 million cells.



Non-reacting flow with all combustor passages open at the same time

RANS model is evaluated for a total cell count of 10 million with a maximum cell size 3 mm and a minimum cell size of 0.375 mm. The LES model is evaluated for a total cell count of 10 million and a total cell count of 21 million. The LES results for the two different meshes show grid convergence for flow splits. Both RANS and LES estimate similar flow splits for total swirler, total dilution and total effusion flow and comparison with experimental data and previous literature is shown in Table 4 and bar chart in Figure 14. Total swirler flow is overestimated by 19% with the coarse mesh and by 17.6% with the fine mesh; total dilution flow is overestimated by 14% with the coarse mesh and 9% with the fine mesh, and total effusion flow underestimated by 11.7% with coarse mesh and 10.6% with fine mesh. The differences between experiments and computations can be attributed to the interactions between the flows from multiple passages, numerical errors

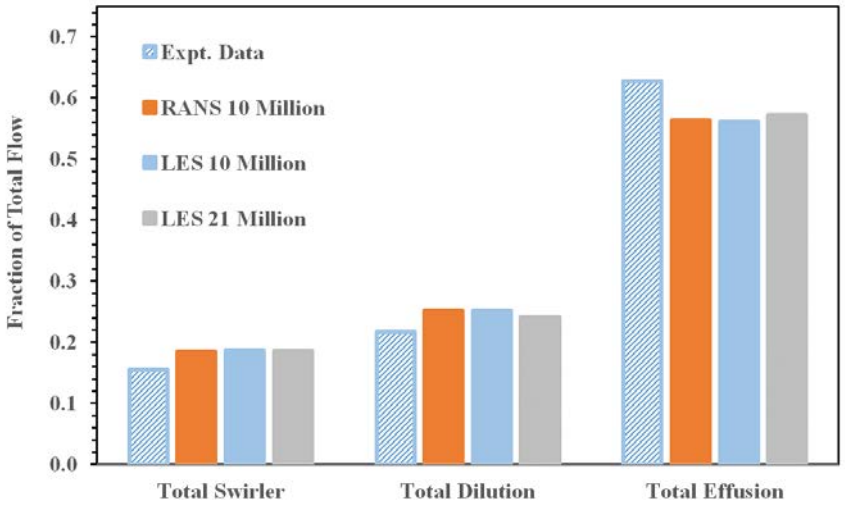


Figure 14. Comparison of combustor flow splits.

Non-reacting primary zone flow field

The mean velocity magnitudes on the XY-plane at Z=0 are shown in Figure 15. Air flows through all swirler passages interact resulting in a radially outward airflow entering the combustor. The primary dilution holes result in the highest velocities and their impingement leads to local flow reversals in this cross section. Bending of the cross jets in the stream wise direction is observed. However, the dilution jets have a high enough momentum to impinge upon each other. A relatively low velocity region exists beyond the cross flow jets and the primary zone. Flow is accelerated as it passes through the convergent section. The flows from the effusion holes form a film on the liner walls and pass along the wall. While the overall flow field seen in Figure 8 is highly symmetric around the X-axis, small dis-symmetries observed in the experiments are also captured in the results of the simulations. For example, the measured angles of the cross-jets are 13 and 14 degrees while the computed angles of the cross-jets are 12 and 13 degrees, respectively. While these comparisons are encouraging, more quantitative measurements of velocities and other detailed flow features are awaited for comparison with the LES results.

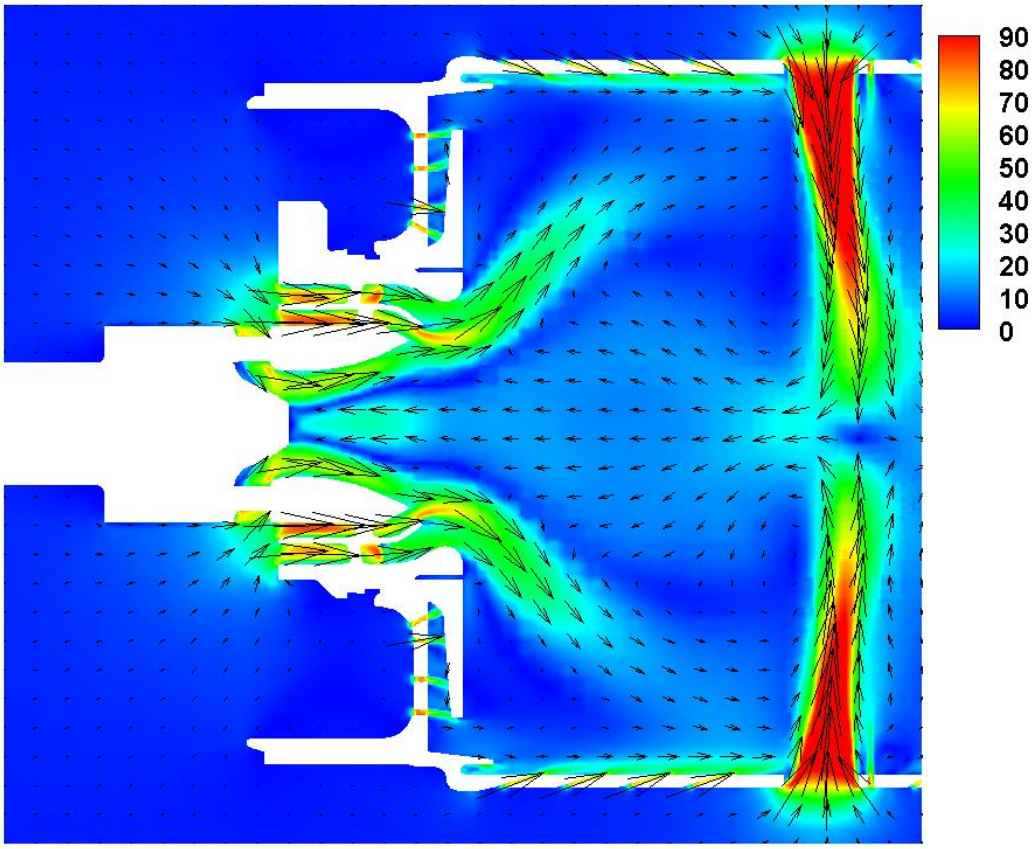


Figure 15. LES time-averaged velocity magnitude (m/s) on mid-plane with velocity vectors for 10 million cells (all passages open).

LBO LES Simulations

LBO Approach

LES simulations are carried out at a global equivalence ratio of 0.096, which was experimentally found to produce stable combustion. From this condition, the fuel flow rate is reduced in a gradual stepwise manner with larger time steps first and progressively reduced flow rate reduction steps as evidence of impending blowout behavior is approached as shown in Figure 16. The simulations are run with a fixed global equivalence ratio for at least two flow-through times, estimated to be approximately 30 ms. The fixed equivalence ratio is maintained beyond 30 ms, if a quasi-steady heat release rate is not reached during either of those limits. Heat release rate is used as a criterion for identifying the lean blowout. The global equivalence ratio steps resulting from this process are plotted as a function of time in Figure 16 for fuel A-2 on the left-hand side and fuel C-1 on the right-hand side. Experimental data shown as red filled circles indicate that the C-1 fuel shown on the right-hand frame blows out at higher equivalence ratio than for the A-1 fuel (left-hand frame).

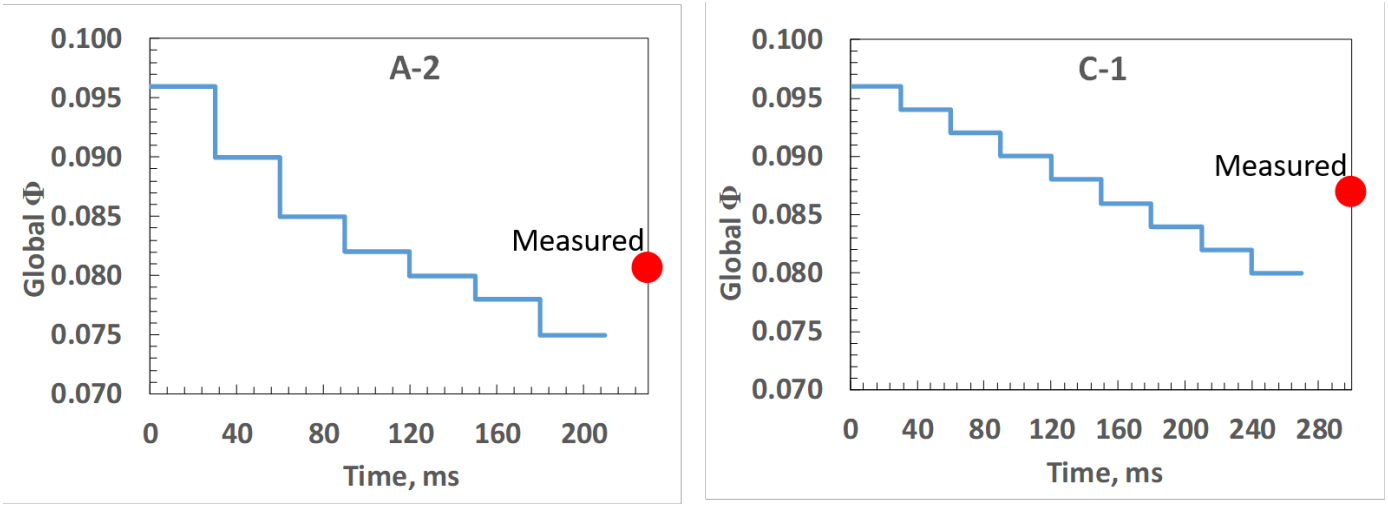


Figure 16. Staged fuel ramp down approach for LBO prediction. The red dot represents the measured lean blowout global equivalence ratio

Reacting spray comparison

Spray statistics were collected using LES calculations at a stable operating point are over a period equal to two flow-through times. The averaging process over two flow-through times is started after the flame and heat release rate reached a quasi-steady state. Figure 17 shows the experimental and predicted statistics of droplets at four axial stations as a function of radial distance. The fuel spray exhibits a pattern with smaller diameter droplets near the hollow cone surface 10mm downstream of the nozzle exit. This distribution widens in the radial direction as we go towards the downstream locations with larger droplets towards the center and vice-versa. The model is able to satisfactorily capture this trend for both the fuels. Better agreement with experiments is observed for the downstream locations. Axial and radial velocities increase away from the center and then decrease again with increasing spray cone angle. These trends are accurately captured for the near-nozzle regions as well as in downstream regions for both fuels. Overall, the Lagrangian spray setup is able to accurately capture the spray breakup and evaporation.

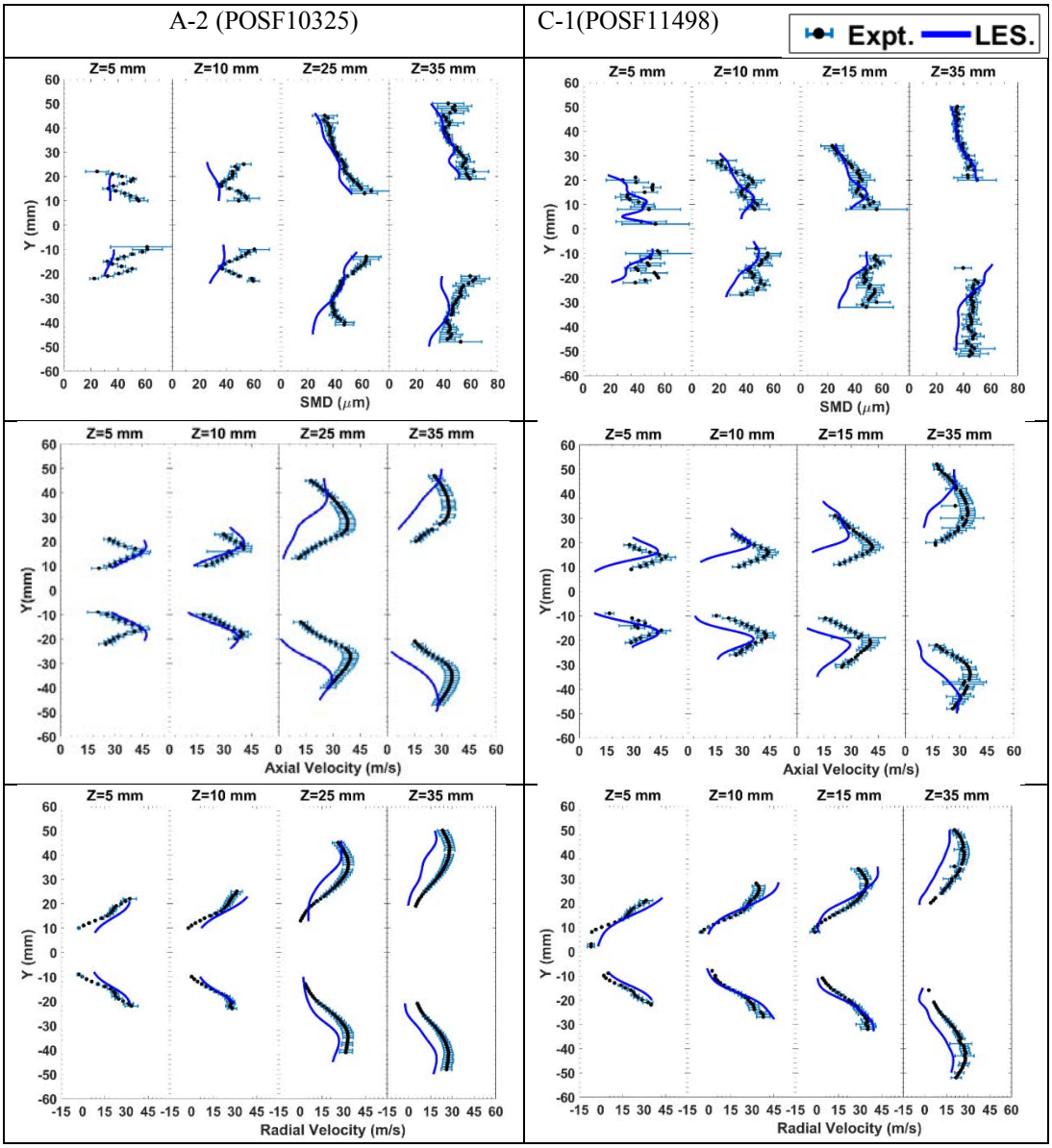


Figure 17. Spray statistics comparison with PDPA data[9] for a stable flame case at $\phi = 0.096$

Flame shape comparison

The OH* chemiluminescence data from UIUC experiments is utilized to compare the line of sight averaged OH mass fraction from LES simulations. They are reported for detailed, skeletal, reduced and compact mechanisms in Figure 18 alongside experimentally observed OH* chemiluminescence. The results from the detailed, the skeletal and the reduced mechanisms are qualitatively similar. The experimental data (OH* chemiluminescence) and the results of the detailed mechanism calculations (OH) show a similar spread in radial and axial directions. It must be noted these comparisons are qualitative in nature. The experimental images are based on false color and do not indicate a quantitative measurement of the OH field. The horizontal position of 0 mm corresponds to the deflector plate. OH formation marks the high temperature heat release regions, which extends 50 mm downstream of the deflector plate and also corresponds to the downstream location of first

row of dilution holes. This is the flame stabilization region of the swirl-stabilized flame. It exhibits a truncated cone shape with high regions of OH/heat release corresponding to the cone angle of the hollow spray cone. This indicates strong burning and heat release near the spray cone surface downstream of the swirl cup. The A-2 fuel exhibits a higher degree of asymmetry in OH* for this configuration and measurements. These regions of intense heat release are captured qualitatively by all the four chemistry mechanisms.

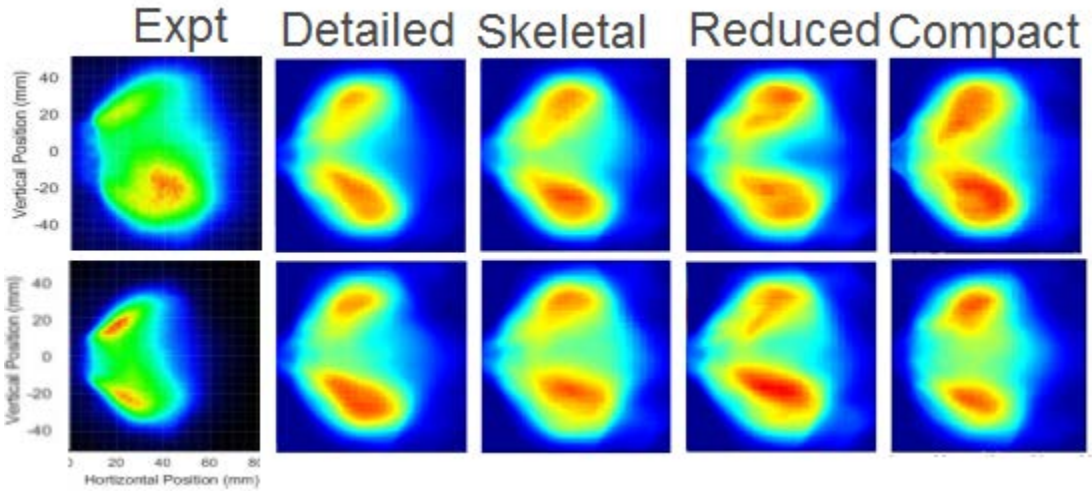


Figure 18. Line of Sight averaged mass fraction of OH from LES compared with experimental OH* from chemiluminescence.

Heat release rate

The evolution of heat release rates for each equivalence ratio and the two different fuels with compact and HyChem skeletal mechanism shown in Figure 19. The flame is observed to be stable for the first couple of milliseconds; this is followed by a steady decrease and eventually by a sharp drop in heat release rate for both A-2 and C-1 fuels. The heat release rates are allowed to reach a steady state before the next step down.

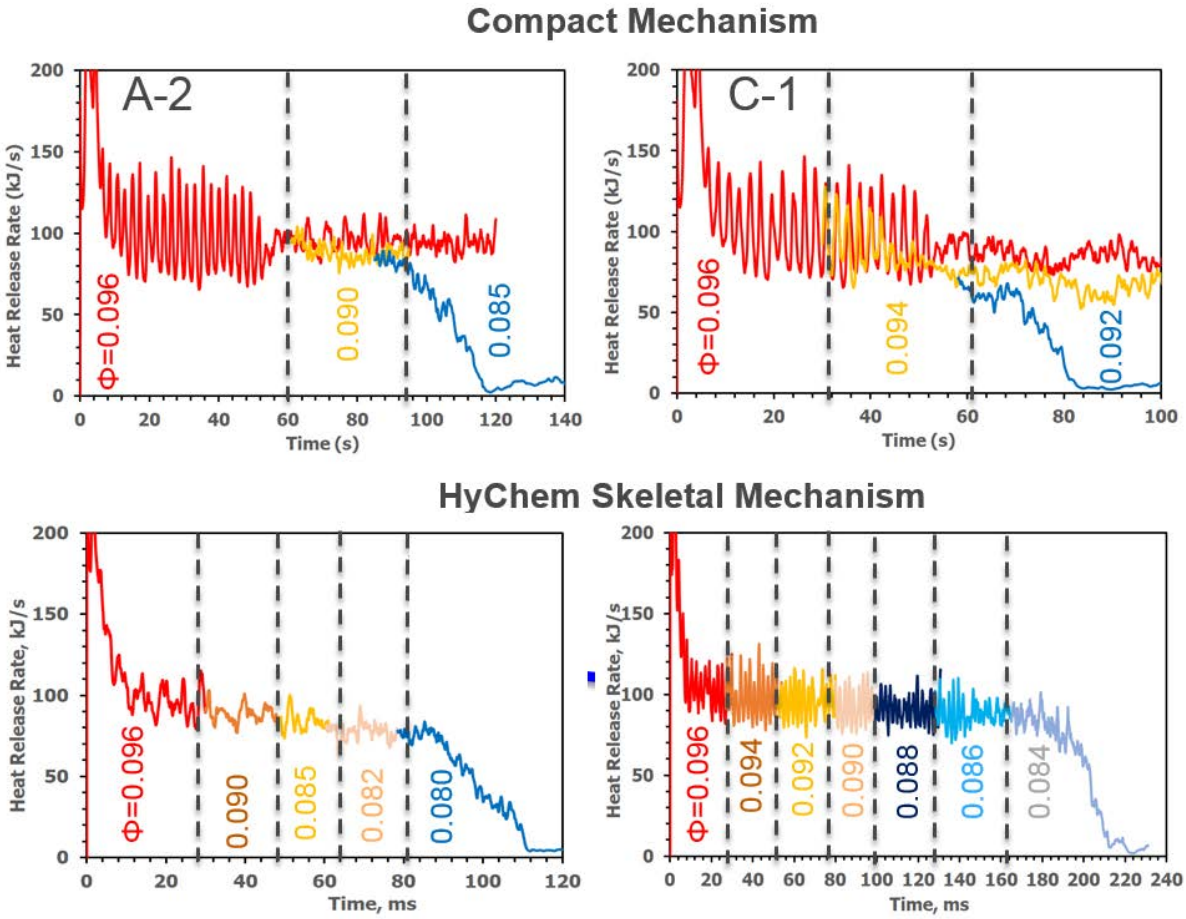


Figure 19. Heat release rate

Lean blowout equivalence ratio comparison

The LBO trends for both fuels are summarized and compared against experiments in Figure 20. C-1 blows-out at a significantly higher equivalence ratio compared to A-2 in the experiments. This LBO dependence on the fuel physical and chemical properties is very complex. The simulations are able to capture qualitatively the trend in LBO for each fuel as well as their relative behaviors with compact and HyChem skeletal mechanism.

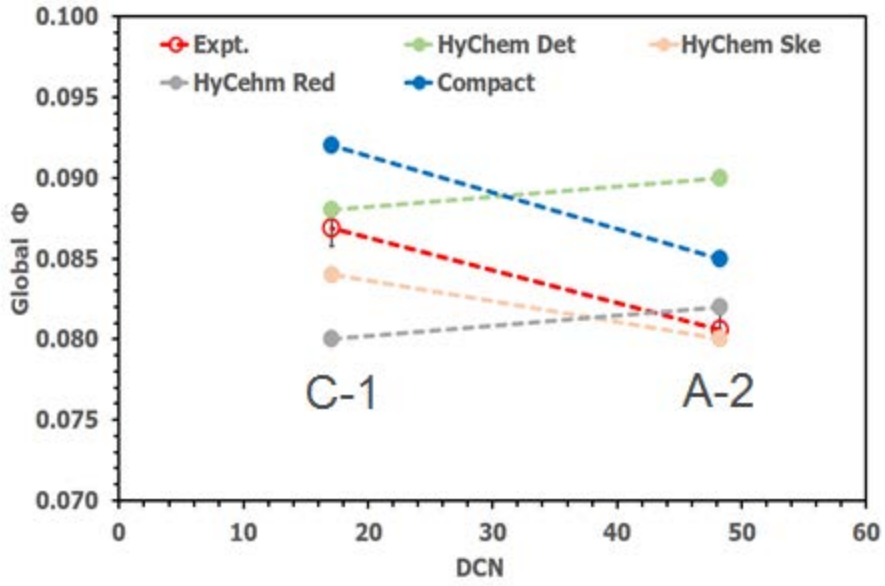


Figure 20. LBO Equivalence ratio comparison between LES and experiments

Flame structure during LBO

LES results from the HyChem skeletal mechanism are chosen for understanding the flame extinction process during the LBO for both A-2 and C-1 fuels. A qualitative analysis of the flame during LBO is presented in Figure 21. Instantaneous temperature contour plots at the combustor mid-plane are shown on the left for both fuels and corresponding formaldehyde mass fractions are shown on the right. The primary recirculation zone corresponds to the region of intense heat release rate. These regions correspond to the high OH formation regions described in the previous section. For A-2 fuel, after the final step-down, at an equivalence ratio of 0.080, a lifted flame is observed to stabilize inside the swirler cup region between the 0 to 5 ms window. Formaldehyde is observed to form very close to the nozzle tip and follows the spray regions. It gets oxidized to form the high-temperature regions. As time progresses, the flame stabilization point starts to move in the axial direction and a remarkable shift in the CH_2O regions is observed away from the nozzle tip. Finally, by 15 ms, the heat release in the primary recirculation region decreases considerably with a considerable shift of CH_2O formation in the downstream regions. Finally, the flame is observed to blowout by 25 ms. A similar trend is observed for the C-1 fuel, however, at a much higher global equivalence ratio of 0.084. The C-1 fuel has significantly higher CH_2O formation even at 0 ms and this will be analyzed further in the next section. From these plots, it can be summarized that overall the flame is observed to shift downstream as we approach LBO along with a downstream movement of intermediate species. The reduction of heat release rates and overall temperatures lead to a partial oxidation of these intermediate species which shows up as a corresponding downstream shift in the contour plots.

To understand the flame stabilization and key factors governing LBO limits, species formation in the mixture fraction space analyzed in the primary zone of the combustor. These are reported in Figure 22. The aim is to identify key markers or events that are universal in nature, with respect to different fuels.

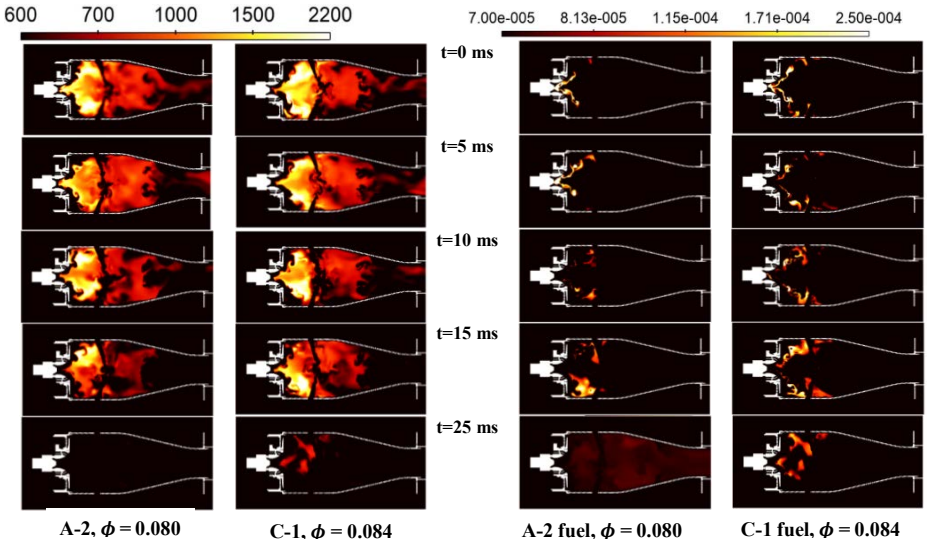


Figure 21. Instantaneous temperature [K] contour plots (left) at the combustor mid-plane and formaldehyde mass fractions (right) for A-2 and C-1 fuel during LBO.

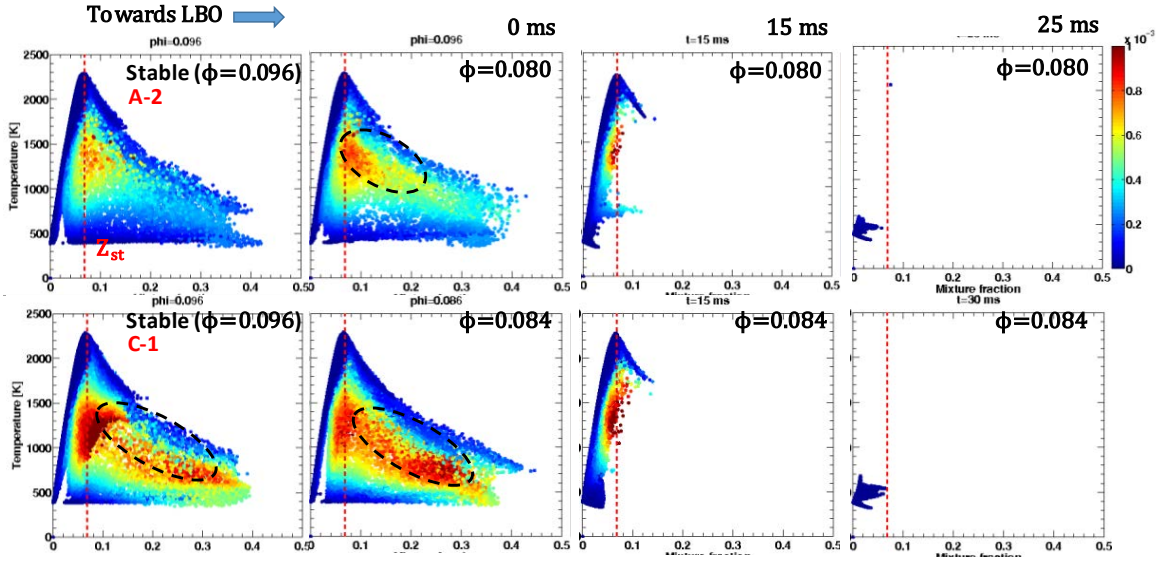


Figure 22. Temperature versus mixture fraction scatterplots for A-2 fuel (top) and C-1 fuel (bottom) sampled from the primary zone. Colored with CH2O mass fraction

The intermediate radical OH is formed in the high-temperature stoichiometric regions and does not shift with lower global equivalence ratios as shown in Figure 23. This study showed that the trend of increasing concentrations of intermediate species in rich regions is an important marker during the LBO process.

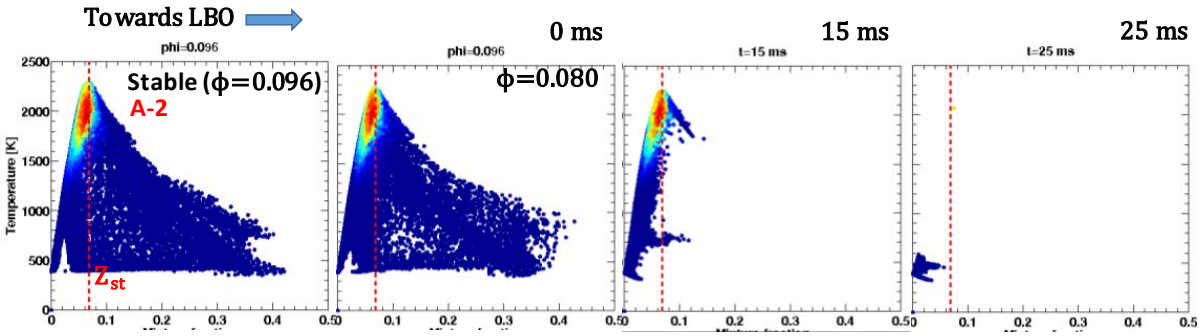


Figure 23. Temperature versus mixture fraction scatterplots for A-2 fuel sampled from the primary zone. Colored with OH mass fraction.

Temperatures from the primary zone (upstream of the primary dilution holes) are isolated from the 3-D CFD domain and further filtered based on their axial velocities. The computational cells that have axial velocities in the negative direction are selected for analysis. As this is a non-uniform grid, these points are weighted with their respective cell volumes. These set of points represent the recirculating fluid that flows from the high temperature regions towards the base of the flame. Statistical analysis is carried out by generating a probability density function of the temperature distribution of these points. The temperature distribution of the recirculation zone shows a non-uniform, multi-modal distribution with a peak in the 500 K zone and major part of the distribution spread in the range of 1500 K – 2300 K. This indicates that high temperatures are a major part of the recirculation zone and these play a significant role in stabilizing the flame. The reduced fuel flow rates corresponding to stable operation condition also exhibit a similar distribution; however, the distributions show more bias towards the low temperatures. At the blowout equivalence ratio, the distribution is observed to have shifted significantly. The second peak of the bimodal distribution corresponding to the high temperature region is now at a significantly lower temperature compared to the previous equivalence ratios. As the flame finally approaches LBO, we observe that this distribution shifts towards the low temperature region and merges into a delta PDF type of distribution. Thus, it is observed that, as the flame blows out, the recirculation zone cools down due to the decrease in overall heat release rates. This causes lower evaporation rates and further triggers a reduction in heat release leading to a cyclic process. This weakening of the recirculation zone is a key marker of flame stability. A significant shift in the PDF distribution of temperatures of the recirculating fluid can be marker for the start of LBO. This is demonstrated for both fuels A-2 and C-1 in Figure 24.

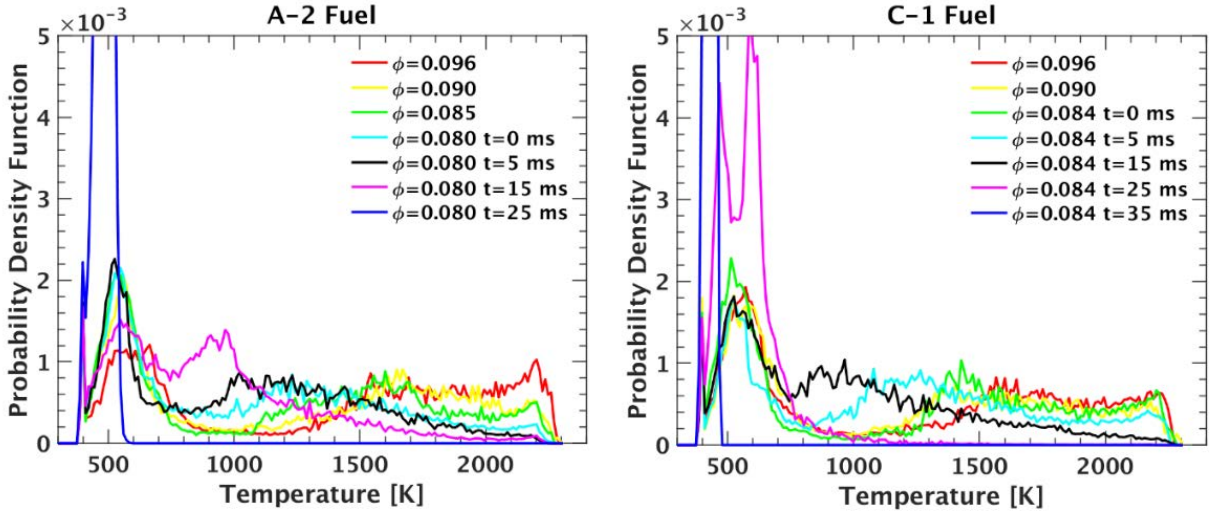


Figure 24. Probability density function of the temperatures of the recirculating gases in the primary zone for A-2 fuel (left) and C-1 fuel (right).



Mesh resolution sensitivity to LBO computations

We have carried out a study to understand the effect of mesh resolution on the computed LBO equivalence ratio for C-1 fuel with Won-Dryer compact mechanism.

Table 1. Details of the minimum mesh resolution for establishing a mesh independent solution with a base size of 3 mm

Total Cells (Millions)	10	25
Adaptive Mesh Refinement Level	3	4
Min.Cell Size, mm	0.375	0.1875

Volume integrated heat release rate is compared for different mesh resolutions in Figure 25. We noticed stable heat release rate for both mesh resolutions at the near LBO condition showing stable flame corresponding to global equivalence ratio of 0.094 and then decrease in heat release rate due to flame extinction at 0.092 for both mesh resolutions. It is noted from this study that minimum mesh resolution of 0.375 mm and 0.1875 mm considered in this study yielded the same LBO global equivalence ratio.

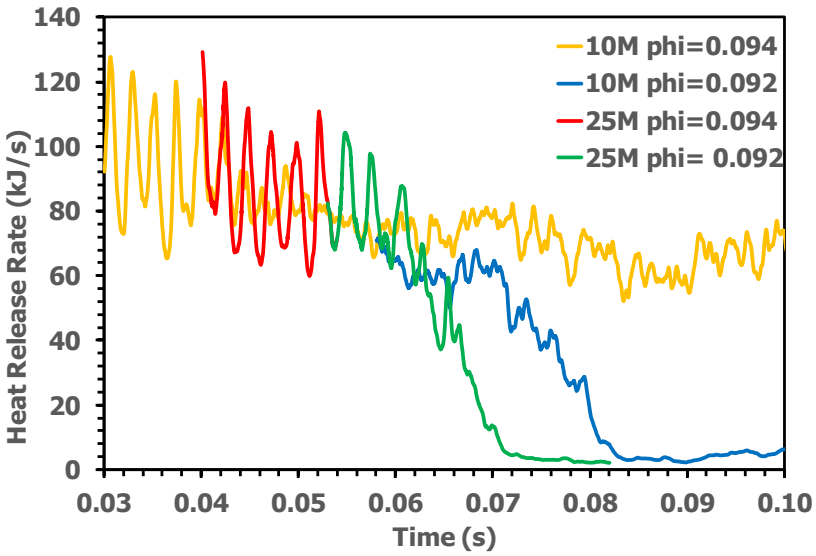


Figure 25. Heat release rate for the LBO study with two different mesh resolution (C1 fuel with compact mechanism)

Implementation of sub-grid scale combustion model in CONVERGE CFD code to account for sub-grid scale turbulence chemistry interactions for Referee rig LBO simulations. Work in progress

The LBO simulations done so far, for A-2 and C-1 fuels with different kinetic models (detailed, skeletal and reduced) and Won-Dryer compact mechanism used laminar chemistry model and ignored the sub-grid scale interactions between combustion and turbulence. We have made efforts during the reporting period to include these SGS TCI using Partially Stirred Reactor (PaSR) model. Many researchers, for treating the SGS TCI with Finite Rate Chemistry approach successfully, use this model.

Favre filtered species transport equation:

$$\frac{\partial \bar{\rho}\,\widetilde{Y_m}}{\partial t} + \frac{\partial \bar{\rho}\tilde{u}_j\widetilde{Y_m}}{\partial x_j} = \frac{\partial}{\partial x_j}\left(\bar{\rho}(D + D_t)\frac{\partial \widetilde{Y_m}}{\partial x_j}\right) + \bar{\dot{\omega}}_m\,, \quad m = 1,2,3\ldots\ldots,n \qquad (3)$$



In laminar chemistry model, the filtered reaction rate $\overline{\dot{\omega}}_m$ in the above equation is computed using the Arrhenius law and resolved flow field. In PaSR model, the filtered reaction rate term computed using Arrhenius law is scaled to account for sub-grid scale turbulence chemistry interactions by computing the chemical and mixing time scales.

$$\overline{\dot{\omega}_i\,(\rho,\, Y_i,\, T)} \;\approx k\;\dot{\omega}_i\,(\bar{\rho},\, \widetilde{Y}_i,\, \tilde{T})$$

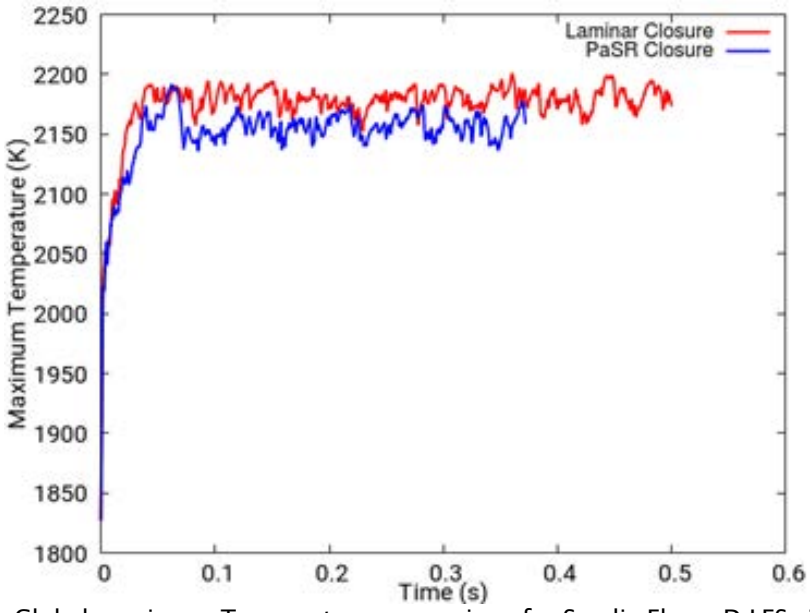


Figure 26. Global maximum Temperature comparison for Sandia Flame D LES simulations

Where k is known as reacting volume fraction and is computed as $k = \frac{\tau_c}{\tau_m + \tau_c}$, τ_c is chemical time scale and τ_m is mixing time scale. More details on this model can be found in the literature [1-7].

This model implementation is tested for Sandia flame D, computed global maximum temperature with, and without SGS TCI effect with LES turbulence model is shown in Figure 26.

Conjugate Heat Transfer model developed for Referee combustor to study the effect of heat losses across the combustor liners on flame structure and LBO. Work in progress. Conjugate heat transfer model developed for a realistic gas turbine combustor (Referee) under reacting conditions in order to understand the effect of heat loss through liners walls on the flame stabilization and lean blowout (LBO) as shown in Figure 27.

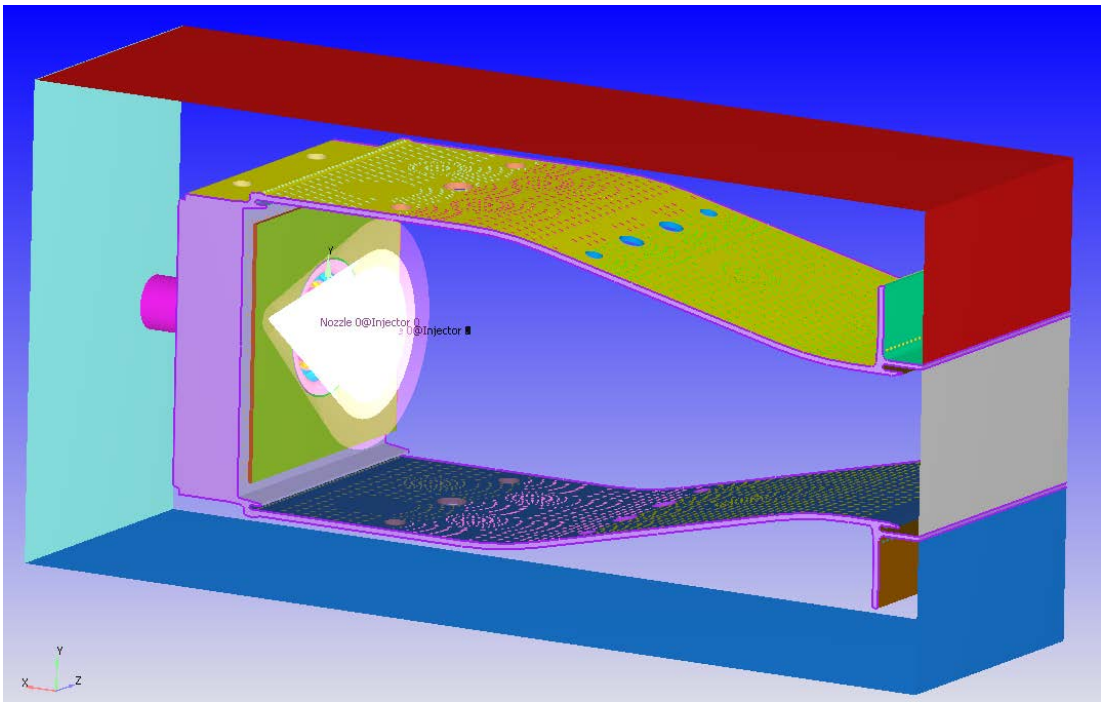


Figure 27. Fluid-solid domain of referee combustor for conjugate heat transfer analysis

Gas turbine combustors under engine relevant high-pressure conditions have high rate of heat transfer to the liner walls through convection and radiation. Combustor liner walls are heated through radiation and convection from the flame on the hot side and are cooled through convection to the cold air in the annulus and radiation to the outer casing. Thermal conduction along the liner wall also contributes to the distribution of heat flux and wall temperature. Transient three dimensional solid-fluid fully coupled numerical simulations will be performed to account for the effects of spatio-temporal variations of temperature of hot gases in the combustor on the rate of heat transfer to the combustor liner. The coupled simulations facilitate an accurate estimation of liner temperature distribution and heat losses and the subsequent effect on the flame stabilization and lean blowout process. The computational domain consists of a combustor fitted with a hybrid airblast swirler, dilution holes and a large number of liner effusion cooling holes. Automatic mesh generation with fixed embedding and adaptive mesh refinement are employed to generate an optimized mesh distribution on the fly for accurately resolving the flow field along with a reduction in computational time. The dynamic structure sub-grid scale turbulence model is utilized for LES computation. Combustion is modeled using finite rate detailed chemistry using the HyChem skeletal mechanism consisting of 41 species and 202 reactions for a conventional petroleum derived fuel (denoted as A-2). Flame radiation is not considered in the present study. The computed LBO equivalence ratio for A-2 fuel with wall temperature predicted using the conjugate heat transfer model without radiation model will be compared with that assessed using an adiabatic wall condition. The computed liner temperature distribution with conjugate transfer model will also be compared against the experimental data at near-blowout but stable flame condition. Conjugate heat transfer methodology developed for practical combustors in the present work can contribute to improvements in component life by optimizing liner-cooling schemes. Future work will involve incorporating the flame radiation in the calculations.

Assessment of Flamelet approach with adaptive mesh refinement for LBO calculations. Work in progress

Flamelet Generated Manifold approach under adaptive mesh refinement framework is currently being assessed for LBO predictions. C-1 fuel with Won-Dryer compact mechanism is chosen for this study. Currently simulations are in progress for global equivalence ratio of 0.086 with stable flame at this condition. Experimental data for C-1 fuel show LBO at 0.087.The finite rate chemistry model with Won-Dryer mechanism computed LBO at 0.092. We will continue to decrease the fuel flow rate with FGM model to assess its capability to capture flame extinction processes.



Publications

1. "Effect of Aviation Fuel Type and Fuel Injection Conditions on Non-Reacting Spray Characteristics of Hybrid Air Blast Fuel Injector," Timo Buschhagen, Robert Z. Zhang, Sameer V. Naik, Carson D. Slabaugh, Scott E. Meyer, Jay P. Gore, and Robert P. Lucht, presented at the 2016 AIAA SciTech Meeting, San Diego, CA, 4-8 January 2016, Paper Number AIAA 2016-1154.
2. "Large-Eddy Simulations of Fuel Injection and Atomization of a Hybrid Air-Blast Atomizer," P. C. May, M. B. Nik, S. E. Carbajal, S. Naik, J. P. Gore, R. P. Lucht, and M. Ihme, presented at the 2016 AIAA SciTech Meeting, San Diego, CA, 4-8 January 2016, Paper Number AIAA 2016-1393.
3. "Spray Measurements at Elevated Pressures and Temperatures Using Phase Doppler Anemometry," A. J. Bokhart, D. Shin, R. Gejji, T. Buschhagen, S. V. Naik, R. P. Lucht, J. P. Gore, P. E. Sojka, and S. E. Meyer, presented at the 2017 AIAA SciTech Meeting, Grapevine, TX, 8-13 January 2017, Paper Number AIAA-2017-0828,.
4. "Spray Characteristics at Lean Blowout and Cold Start Conditions using Phase Doppler Anemometry," A. J. Bokhart, D. Shin, N. Rodrigues, S. V. Naik, R. P. Lucht, J. P. Gore, P. E. Sojka, and S. E. Meyer, presented at the 2018 AIAA SciTech Meeting, Kissimmee, Florida, 8-12 January 2018.
5. "Spray Characteristics of a Hybrid Airblast Pressure-Swirl Atomizer at Cold Start Conditions using Phase Doppler Anemometry," Dongyun Shin, D. Shin, A. J. Bokhart, N. Rodrigues, S. V. Naik, R. P. Lucht, J. P. Gore, P. E. Sojka, and S. E. Meyer, presented at ICLASS 2018 14th Triennial International Conference on Liquid Atomization and Spray Systems, Chicago, Illinois, 22-26 July 2018.
6. Veeraraghava Raju Hasti, Prithwish Kundu, Gaurav Kumar, Scott A. Drennan, Sibendu Som, and Jay P. Gore. "A Computational Study of Flame Characteristics in Referee Combustor during Lean Blow-Out", Under preparation for AIAA Journal of Propulsion and Power
7. Veeraraghava Raju Hasti, Prithwish Kundu, Gaurav Kumar, Scott A. Drennan, Sibendu Som, Sang Hee Won, Frederick L. Dryer, and Jay P. Gore. " Computation of Fuel Sensitivity to Lean Blow-Out in a Gas Turbine Combustor", Under preparation for AIAA Journal
8. Veeraraghava Raju Hasti, Prithwish Kundu, Gaurav Kumar, Scott A. Drennan, Sibendu Som, and Jay P. Gore. " Numerical Simulations of Gas Turbine Combustor Flows using Adaptive Mesh Refinement", Under preparation for AIAA Journal of Propulsion and Power
9. Veeraraghava Raju Hasti, Prithwish Kundu, Gaurav Kumar, Scott A. Drennan, Sibendu Som, and Jay P. Gore. "A Numerical Study of Flame Characteristics during Lean Blow-Out in a Gas Turbine Combustor", 2018 Joint Propulsion Conference, AIAA Propulsion and Energy Forum, (AIAA 2018-4955)
10. Veeraraghava Raju Hasti, Prithwish Kundu, Gaurav Kumar, Scott A. Drennan, Sibendu Som, Sang Hee Won, Frederick L. Dryer, and Jay P. Gore. "Lean blow-out (LBO) computations in a gas turbine combustor", 2018 Joint Propulsion Conference, AIAA Propulsion and Energy Forum, (AIAA 2018-4958)
11. Veeraraghava Raju Hasti, Prithwish Kundu, Gaurav Kumar, Scott A. Drennan, Sibendu Som, and Jay P. Gore. "Numerical Simulation of Flow Distribution in a Realistic Gas Turbine Combustor", 2018 Joint Propulsion Conference, AIAA Propulsion and Energy Forum, (AIAA 2018-4956)
12. Veeraraghava Raju Hasti, Gaurav Kumar, Shuaishuai Liu, Robert P Lucht and Jay P Gore "A Computational Study on H2 Piloted Turbulent Methane / Air Premixed Flame with CO2 Dilution",2018 Spring Technical Meeting, Central States Section of the Combustion Institute, Minneapolis, MN 55455 USA
13. Veeraraghava Raju Hasti, Shuaishuai Liu, Gaurav Kumar, and Jay P. Gore. "Comparison of Premixed Flamelet Generated Manifold Model and Thickened Flame Model for Bluff Body Stabilized Turbulent Premixed Flame", 2018 AIAA Aerospace Sciences Meeting, AIAA SciTech Forum, (AIAA 2018-0150)
14. Veeraraghava Raju Hasti, Gaurav Kumar, Shuaishuai Liu, Robert P. Lucht, and Jay P. Gore. "Large Eddy Simulation of Pilot Stabilized Turbulent Premixed CH4+Air Jet Flames", 2018 AIAA Aerospace Sciences Meeting, AIAA SciTech Forum, (AIAA 2018-0675)
15. Dong Han, Veeraraghava Raju Hasti, Jay P. Gore and Robert P Lucht, "An Experimental and Computational Study of Turbulent Lean Premixed Flames", Propellants and Combustion Session, AIAA Propulsion and Energy 2015 Conference, Orlando, Florida, USA
16. Vikrant Goyal, Veeraraghava Raju Hasti, Jay P. Gore, Hukam C. Mongia, "Detached eddy simulation of turbulent swirl-stabilized flame" 9th U.S. National Combustion Meeting, Central States Section of the Combustion Institute, May 17-20, 2015, Cincinnati, Ohio, USA



Outreach Efforts

1. "Effect of Aviation Fuel Type and Fuel Injection Conditions on Non-Reacting Spray Characteristics of Hybrid Air Blast Fuel Injector," Timo Buschhagen, Robert Z. Zhang, Sameer V. Naik, Carson D. Slabaugh, Scott E. Meyer, Jay P. Gore, and Robert P. Lucht, presented at the 2017 AIAA SciTech Meeting, San Diego, CA, 4-8 January 2016
2. "Large-Eddy Simulations of Fuel Injection and Atomization of a Hybrid Air-Blast Atomizer," P. C. May, M. B. Nik, S. E. Carbajal, S. Naik, J. P. Gore, R. P. Lucht, and M. Ihme, presented at the 2016 AIAA SciTech Meeting, San Diego, CA, 4-8 January 2016.
3. "Spray Measurements at Elevated Pressures and Temperatures Using Phase Doppler Anemometry," A. J. Bokhart, D. Shin, R. Gejji, T. Buschhagen, S. V. Naik, R. P. Lucht, J. P. Gore, P. E. Sojka, and S. E. Meyer, presented at the 2017 AIAA SciTech Meeting, Grapevine, TX, 8-13 January 2017, Paper Number AIAA-2017-0828,
4. "Spray Characteristics at Lean Blowout and Cold Start Conditions using Phase Doppler Anemometry," A. J. Bokhart, D. Shin, N. Rodrigues, S. V. Naik, R. P. Lucht, J. P. Gore, P. E. Sojka, and S. E. Meyer, presented at the 2018 AIAA SciTech Meeting, Kissimmee, Florida, 8-12 January 2018.
5. "Spray Characteristics of a Hybrid Airblast Pressure-Swirl Atomizer at Cold Start Conditions using Phase Doppler Anemometry," Dongyun Shin, D. Shin, A. J. Bokhart, N. Rodrigues, S. V. Naik, R. P. Lucht, J. P. Gore, P. E. Sojka, and S. E. Meyer, presented at ICLASS 2018 14th Triennial International Conference on Liquid Atomization and Spray Systems, Chicago, Illinois, 22-26 July 2018.
6. Veeraraghava Raju Hasti, Prithwish Kundu, Sibendu Som, Robert P. Lucht and Jay P. Gore, "Lean blow-out mechanism in a swirl-stabilized turbulent spray combustion in a realistic gas turbine combustor, Presented at the 71st Annual Meeting of the APS Division of Fluid Dynamics, Sunday–Tuesday, November 18–20, 2018; Atlanta, Georgia, USA
7. Veeraraghava Raju Hasti, Prithwish Kundu, Gaurav Kumar, Scott A Drennan, Sibendu Som and Jay P. Gore, "A computational investigation of lean blow-out in a realistic gas turbine combustor", Poster Presentation, 37th International Symposium on Combustion, 29th July – 3rd August 2018, Dublin, Ireland
8. Veeraraghava Raju Hasti, Gaurav Kumar, Shuaishuai Liu, Robert P. Lucht and Jay P. Gore, "A computational study on turbulent premixed flames with CO2 dilution", Poster Presentation, 37th International Symposium on Combustion, 29th July – 3rd August 2018, Dublin, Ireland
9. Veeraraghava Raju Hasti presented the work on "Computational modeling of fuel effects on engine combustion" at the 2018 Spring Reception Meeting, Office of Interdisciplinary Graduate Programs, Purdue University, West Lafayette, IN, USA
10. Veeraraghava Raju Hasti, Prithwish Kundu, Gaurav Kumar, Scott A. Drennan, Sibendu Som, and Jay P. Gore. "A Numerical Study of Flame Characteristics during Lean Blow-Out in a Gas Turbine Combustor", Presented at the 2018 Joint Propulsion Conference, AIAA Propulsion and Energy Forum, (AIAA 2018-4955)
11. Veeraraghava Raju Hasti, Prithwish Kundu, Gaurav Kumar, Scott A. Drennan, Sibendu Som, Sang Hee Won, Frederick L. Dryer, and Jay P. Gore. "Lean blow-out (LBO) computations in a gas turbine combustor", Presented at the 2018 Joint Propulsion Conference, AIAA Propulsion and Energy Forum, (AIAA 2018-4958)
12. Veeraraghava Raju Hasti, Prithwish Kundu, Gaurav Kumar, Scott A. Drennan, Sibendu Som, and Jay P. Gore. "Numerical Simulation of Flow Distribution in a Realistic Gas Turbine Combustor", Presented at the 2018 Joint Propulsion Conference, AIAA Propulsion and Energy Forum, (AIAA 2018-4956)
13. Veeraraghava Raju Hasti, Shuaishuai Liu, Gaurav Kumar, and Jay P. Gore. "Comparison of Premixed Flamelet Generated Manifold Model and Thickened Flame Model for Bluff Body Stabilized Turbulent Premixed Flame", Presented at the 2018 AIAA Aerospace Sciences Meeting, AIAA SciTech Forum, (AIAA 2018-0150)
14. Veeraraghava Raju Hasti, Gaurav Kumar, Shuaishuai Liu, Robert P. Lucht, and Jay P. Gore. "Large Eddy Simulation of Pilot Stabilized Turbulent Premixed CH4+Air Jet Flames", Presented at the 2018 AIAA Aerospace Sciences Meeting, AIAA SciTech Forum, (AIAA 2018-0675)
15. Dong Han, Veeraraghava Raju Hasti, Jay P. Gore and Robert P Lucht, "An Experimental and Computational Study of Turbulent Lean Premixed Flames", Presented at the Propellants and Combustion Session, AIAA Propulsion and Energy 2015 Conference, Orlando, Florida, USA
16. Vikrant Goyal, Veeraraghava Raju Hasti, Jay P. Gore, Hukam C. Mongia, "Detached eddy simulation of turbulent swirl-stabilized flame" Presented at the 9th U.S. National Combustion Meeting, Central States Section of the Combustion Institute, May 17-20, 2015, Cincinnati, Ohio, USA

Awards

Ph.D. student Veeraraghava Raju Hasti received Research Aide (Jan – Aug 2018) from Argonne National Laboratory, Department of Energy and carried out part of this work at the DOE laboratory.



Student Involvement

Ph.D. student Daniel Shin is primarily responsible for performing the PDA measurements at LBO, HAR/GLO conditions and for upgrading VAPS test rig in a new test cell. PhD students Neil Rodrigues and postdoctoral research associate Rohan Gejji assist with the project when their expertise is required.
Ph.D. student Veeraraghava Raju Hasti is primarily responsible for developing and performing the LES simulations.

Plans for Next Period

The proposed deliverables and tasks for FY2019 are listed below:

Year 5 Deliverables

The Year 5 deliverables for Area #5, Project 29A are as follows:

1. Bring the variable ambient pressure sprays (VAPS) test rig up to operation.
2. Install the ejector on the test rig to verify sub atmospheric operation for the VAPS test rig.
3. Begin measurements with chilled fuel (-30F)/chilled nitrogen (-30F) measurements at sub atmospheric ambient pressure (down to 4 psia), coordinate with Nader Rizk and Area 6 on exact operating conditions to investigate.
4. Begin measurements for a new candidate fuel, IH2, at near lean blowout conditions.
5. Collaborate with Andrew Corber at NRC on SLIPI imaging measurements in the VAPS test rig.
6. Continue interactions with the three CFD groups (Ihme, Vaidya and Menon).
7. Investigate spray structure for sprays with very low levels of pressure drop across the swirler or with the swirler removed.
8. Investigate the structure with the pilot+main spray and/or the main without pilot spray.
9. Computational methodology with sub-grid scale turbulent combustion model to predict fuel sensitivity to LBO
10. Effect of NOx chemistry on LBO mechanism
11. Assessment of flamelet based models for LBO prediction with adaptive mesh refinement
12. Conjugate heat transfer CFD model to study the effect of heat losses through liners on flame structure and LBO
13. Spray boundary condition sensitivity to LBO prediction in the LES computational methodology

The tasks to be performed for FY2019 are listed below:

Quarter 1 FY2019

1. Bring the VAPS test rig back to operational status. Conduct preliminary test to verify that repeatable data can be obtained.
2. Collaborate with Area 4 and Area 6 members, and with the spray subcommittee, for development of experimental test matrix for the remainder of Year 4.
3. Make measurements at near-lean blowout conditions with a new fuel, IH2.
4. Share boundary, initial, and operating conditions and resulting experimental data with correlations and modeling team (Rizk, Ihme, Menon, and Sankaran).
5. Perform LBO LES simulations for A-2 and C-1 fuel with PaSR combustion model with compact kinetic model.
6. Write a journal paper (Fuel) on the LBO mechanism based on the LES simulations with sub-grid combustion model.

Quarter 2 FY2019

1. Collaborate with Area 4 and Area 6 members, and with the spray subcommittee, for development of experimental test matrix for Year 5.
2. Continue extensive characterization of sprays of the new fuel, IH2, with chilled fuel and chilled N_2.
3. Share boundary, initial, and operating conditions and resulting experimental data with correlations and modeling team (Rizk, Ihme, Menon, and Sankaran).
4. Study the effect of NOx chemistry in the compact kinetic model on the flame structure and LBO.
6. Write a journal paper (Combustion and Flame) on the effect of NOx chemistry on the flame structure and LBO.

Quarter 3 FY2019

1. Make the ejector operational on the VAPS test rig for subatmospheric condition test.
2. Perform measurements with chilled fuel and chilled N_2 at subatmospheric pressure.



3. Share boundary, initial, and operating conditions and resulting experimental data with correlations and modeling team (Rizk, Ihme, Menon, and Sankaran).
4. Evaluate and improve the flamelet generated manifold model having the flamelets for the upper burning branch of the S-curve and all the flamelets for the entire S-curve on the LBO predictions.
5. Write a journal paper (Fuel) on the FGM LES based methodology for LBO prediction.

Quarter 4 FY2019

1. Collaborate with Andrew Corber at NRC on SLIPI imaging measurements in the VAPS test rig.
2. Continue extensive investigation on sprays at subatmospheric conditions.
3. Share boundary, initial, and operating conditions and resulting experimental data with correlations and modeling team (Rizk, Ihme, Menon, and Sankaran).
4. Perform LES simulations with conjugate heat transfer (CHT) model and sub-grid combustion model to study the effect of wall boundary condition on the flame structure and LBO.
6. Write a journal paper (International Journal of Heat and Mass Transfer) on the CHT LES based methodology for LBO prediction in a realistic combustor.

Quarter 1 FY2020

1. Investigate spray structure for sprays with very low levels of pressure drop across the swirler or with the swirler removed.
2. Investigate the structure with the pilot+main spray and/or the main without pilot spray.
3. Share boundary, initial, and operating conditions and resulting experimental data with correlations and modeling team (Rizk, Ihme, Menon, and Sankaran).
4. Spray boundary condition sensitivity to LBO prediction in the LES methodology (Collaboration with Vaidya Sankaran, UTRC)
5. Write a journal paper (International Journal of Spray and Combustion Dynamics) on importance of having accurate spray boundary conditions for computational models
6. Identify the gaps if any in the data for detailed spray model validation and work with experimentalists for both non-reacting and reacting spray measurements.



Project 31(A) Alternative Jet Fuel Test and Evaluation

University of Dayton Research Institute

Project Lead Investigator

Steven Zabarnick, Ph.D.
Division Head
Fuels and Combustion Division
University of Dayton Research Institute
300 College Park, Dayton, OH 45469-0043
937-255-3549
Steven.Zabarnick@udri.udayton.edu

University Participants

University of Dayton Research Institute

- P.I.(s): Steven Zabarnick, Division Head
- FAA Award Number: 13-C-AJFE-UD
- Overall Period of Performance: April 8, 2015 to August 31, 2019
- Period of Performance: April 8, 2015 to March 14, 2016 – Amendment No. 006
  1. Evaluate candidate alternative fuels for their performance via the ASTM D4054 approval process
- Period of Performance: August 13, 2015 to August 31, 2016 – Amendment No. 007
  2. Evaluate candidate alternative fuels for their performance via the ASTM D4054 approval process
- Period of Performance: August 5, 2016 to August 31, 2017 – Amendment No. 012
  3. Management of Evaluation and Testing of Candidate Alternative Fuels
- Period of Performance: July 31, 2017 to August 31, 2019 – Amendment No. 016
  4. Management of Evaluation and Testing of Candidate Alternative Fuels
- Period of Performance: August 30, 2018 to August 31, 2019 – Amendment No. 021
  5. Management of Evaluation and Testing of Candidate Alternative Fuels

Project Funding Level

Amendment No. 006	$309,885
Amendment No. 007	$ 99,739
Amendment No. 012	$693,928
Amendment No. 016	$999,512
Amendment No. 021	$199,966

In-kind cost share has been obtained from:

LanzaTech	$ 55,801 (2015)
LanzaTech	$ 381,451 (2016)
Neste	$ 327,000 (2017)
Boeing	$2,365,338 (2017)

Investigation Team

Steven Zabarnick, PI, New candidate fuel qualification and certification
Richard Striebich, Researcher, Fuel chemical analysis and composition
Linda Shafer, Researcher, Fuel chemical analysis and composition
John Graham, Researcher, Fuel seal swell and materials compatibility
Zachary West, Researcher, Fuel property evaluations



Project Overview

Alternative jet fuels offer potential benefits of reducing global environmental impacts, achieving national energy security, and stabilizing fuel costs for the aviation industry. The Federal Aviation Administration is committed to the advancement of "drop in" alternative fuels and has set the aspirational goal of enabling the use of 1 billion gallons annually by 2018. Successful adoption of alternative fuels requires approval for use of the fuel by the aviation community followed by large scale production of a fuel that is cost competitive and meets safety standards of conventional jet fuel. Alternative jet fuels must undergo rigorous testing to become qualified for use and be incorporated into ASTM International Specifications.

Cost effective and coordinated performance testing capability (in accordance with ASTM D4054) to support evaluation of promising alternative jet fuels is needed. The objective of this project is to provide capability to conduct the necessary work to support alternative jet fuel evaluation of either a) to-be-determined fuel(s) that will be selected in coordination with the FAA or b) a fuel test and evaluation project with a specific fuel(s) in mind.
The proposed program should provide the following capabilities:

- Identify alternative jet fuels (which may include blends with conventional jet fuel) to be tested and that have the potential to be economically viable and support FAA's NextGen environmental goals.
- Perform engine, component, rig, or laboratory tests, or any combination thereof, to evaluate the performance of an alternative jet fuel in accordance with ASTM International standard practice D4054.
- Identify and conduct unique testing, beyond that defined in ASTM International standard practice D4054, necessary to support evaluation of alternative jet fuels for inclusion in ASTM International jet fuel specifications.
- Obtain data for baseline and alternative jet fuels to demonstrate any effects of the alternative jet fuel on aircraft performance, maintenance requirements, and reliability.
- Coordinate effort with activities sponsored by Department of Defense and/or other government parties that may be supporting relevant work.
- Report relevant performance data of the alternative fuels tested including a quantification of the effects of the alternative fuel on aircraft and/or engine performance and on air quality emissions relative to conventional jet fuel. Reported data will be shared with both the FAA (NJFCP) and the broader community (e.g., ASTM International) and with ASCENT COE Program 33 "Alternative Fuels Test Database Library."

Tasks 1 and 2- Evaluate Candidate Alternative Fuels for their Performance via the ASTM D4054 Approval Process and Management of Evaluation and Testing of Candidate Alternative Fuels

University of Dayton Research Institute

Objective(s)

Cost effective and coordinated performance testing capability (in accordance with ASTM D4054) to support evaluation of promising alternative jet fuels is needed. The objective of this project is to provide capability to conduct the necessary work to support alternative jet fuel evaluation of either a) to-be-determined fuel(s) that will be selected in coordination with the FAA or b) a fuel test and evaluation project with a specific fuel(s) in mind.

Research Approach

The intent of this program is to provide the capability of performing specification and fit-for-purpose (FFP) evaluations of candidate alternative fuels toward providing a pathway forward through the ASTM D4054 approval process. The UDRI team possesses the capability of performing a large of number of these evaluations and we are prepared to work with other organizations such as SwRI and engine OEM's, as needed, for their unique test capabilities. These include additional engine, APU, component, and rig evaluations. The UDRI testing capabilities cover our efforts at the laboratories of the Fuels Branch of AFRL and at our campus laboratory facilities.

The following are examples of the evaluations that UDRI is able to provide:
Tier I
1. Thermal Stability (Quartz Crystal Microbalance)
2. Freeze Point (ASTM D5972)
3. Distillation (ASTM D86)
4. Hydrocarbon Range (ASTM D6379 & D2425)



5. Heat of Combustion (ASTM D4809)
6. Density, API Gravity (ASTM D4052)
7. Flash Point (ASTM D93)
8. Aromatics (ASTM D1319)

Tier II

1. Color, Saybolt (ASTM D156 or D6045)
2. Total acid number (ASTM D3242)
3. Aromatics, (ASTM D1319 & ASTM D6379)
4. Sulfur (ASTM D 2622)
5. Sulfur mercaptan (ASTM D3227)
6. Distillation temperature (ASTM D86)
7. Flash point (ASTM D56, D93, or D3828)
8. Density (ASTM D1298 or D4052)
9. Freezing point (ASTM D2386, D5972, D7153, or D7154)
10. Viscosity, at -20˚C, (ASTM D445)
11. Net heat of combustion (ASTM D4809)
12. Hydrogen content (ASTM D3343 or D3701)
13. Smoke point (ASTM D1322)
14. Naphthalenes (ASTM D1840)
15. Calculated cetane index (ASTM D976 or D4737)
16. Copper strip corrosion (ASTM D130)
17. Existent gum (ASTM D381)
18. Particulate matter (ASTM D2276 or D5452)
19. Filtration time (MIL-DTL-83133F Appendix B)
20. Water reaction interface rating (ASTM D1094)
21. Electrical conductivity (ASTM D624)
22. Standard Test Method for Thermal Oxidation Stability of Aviation Turbine Fuels (ASTMD3241)

Extended Physical and Chemical Characterization

1. Lubricity Evaluation- BOCLE test (ASTM D5001)
2. Low Temperature Properties – Scanning Brookfield Viscosity
3. Detect, quantify, and/or identify polar species - Analyze as necessary
4. Detect, quantify and/or identify dissolved metals - Analyze as necessary
5. Initial Material Compatibility Evaluation – Perform optical dilatometry and Partition Coefficient Measurements to determine the fuel-effected swell and the fuel solvency in 3 O-ring materials (nitrile, fluorosilicone and fluorocarbon) and up to 2 additional fuel system materials
6. Experimental Thermal Stability Evaluation – Quartz Crystal Microbalance – Measure thermal deposit tendencies and oxidation profile at elevated temperatures
7. Viscosity versus Temperature – (ASTM D445) determination of the fuels viscosity at 40˚C and -40˚C to assess the fuel's viscosity's variation with temperature

In addition to the above physical and chemical fuel evaluation capabilities, UDRI has extensive experience in evaluation of microbial growth in petroleum-derived and alternative fuels. These evaluations include standard lab culturing and colony counting methods, and advanced techniques such as quantitative polymerase chain reaction (QPCR) and metagenomic sequencing. These methods allow the quantitative measurement of microbial growth rates in candidate alternative fuels in comparison with petroleum fuels.

UDRI also has extensive experience in evaluation of elastomer degradation upon exposure to candidate alternative fuels. Various methods are used to evaluate seal swell and o-ring fixture leakage, including: optical dilatometry, measurement of sealing pressure, fuel partitioning into elastomer, and a pressurized temperature controlled o-ring test device.

UDRI is also able to perform fuel-material compatibility testing using the D4054 procedures for fuel soak testing, post-exposure non-metallic and metal materials tests, and surface and microstructural evaluation. Testing of both 68 "short-list" materials and the complete 255 materials list can be performed.



Milestone(s)
The schedule for this project is dependent upon receipt of alternative fuel candidates for testing. As candidate fuels are received a schedule of testing will be coordinated with the FAA and collaborators. Our existing relationships with these organizations will help expedite this process.

Major Accomplishments
The Phase I Research Report for the LanzaTech/PNNL Ethanol-to-Jet (LT/PNNL ATJ) Synthetic Paraffinic Kerosene Fuels and Blends has been completed and submitted to the OEM's for approval. The Boeing/Neste HFP-HEFA research report has been completed and is in the process of Phase I review by the OEM's. We are awaiting arrival of the Shell IH2 and IHI Bb Oil fuels for Phase 1 evaluations.

Publications
"Evaluation of LanzaTech/PNNL Ethanol-to-Jet (LT/PNNL ATJ) Synthetic Paraffinic Kerosene Fuels and Blends Phase 1 Research Report," 2016.

"Evaluation of High Freeze Point HEFA as Blending Component for Aviation Jet Fuels," ASTM Research Report Version 1.1, 2017.

Outreach Efforts
Presentations were given at the April and Sept 2017 ASCENT meeting and meetings were held with European D4054 Clearinghouse initiators at the Rome IASH meeting in September. Meetings were held in Dayton with IHI, a Japanese company interested in entering their algae fuel in the D4054 process. We also continue to speak with Shell on their soon to be submitted IH2 fuel.

Awards
None

Student Involvement
None

Plans for Next Period
We plan to attend the ASTM December meeting in Houston and hold an OEM meeting with fuel producers in a separate session prior to the main ASTM meeting as in the past. We expect to receive the first shipment of the Shell IH2 fuel and begin the process of testing the fuel for Tier 1 and 2 evaluations. We expect to receive the first shipment of the IHI Bb oil algae fuel near the end of 2018.

Tasks 3 and 4- Management of Evaluation and Testing of Candidate Alternative Fuels
University of Dayton Research Institute

Objective(s)
The objective of this work is to manage the evaluation and testing of candidate alternative jet fuels conducted in accordance with ASTM International standard practice D4054 (see Figure 1).

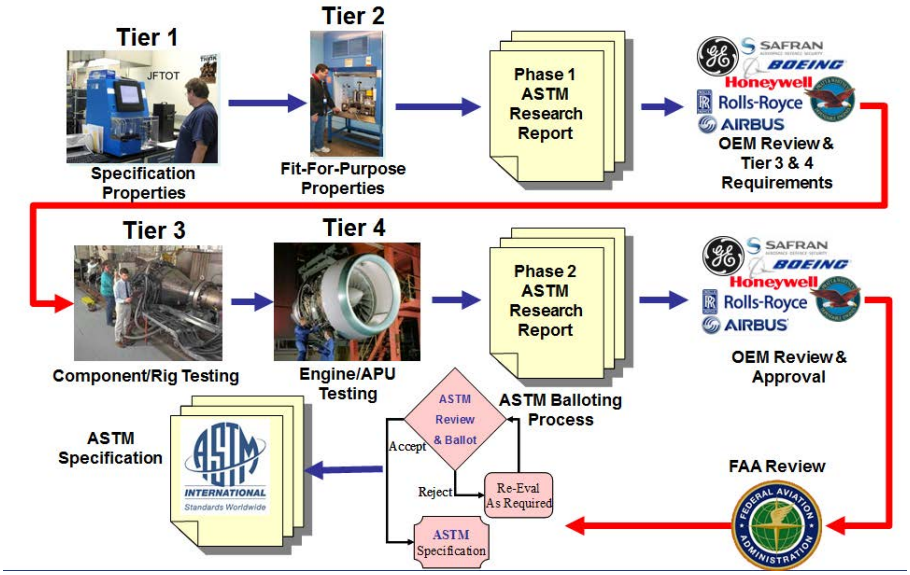


Figure 1. ASTM D4054 Qualification Process

Research Approach

UDRI will subcontract with other research organizations and/or test laboratories or OEMs to carry out the following tasks in support of evaluation and ASTM specification development for AJFs. The purpose of the project is to manage and coordinate the D4054 evaluation process shown in Figure 2 in order to facilitate transition of alternative fuels to commercial use.

Subtask 1: General Support

- Develop and make available a D4054 process guide that describes logistics procedures for handling of test fuels, documentation requirements, test report issuance and delivery, and contact information. This is intended to provide clear instructions to candidate fuel producers for entering into the ASTM D4054 process.

Subtask 2: Phase 1 Support

- Coordinate the handling of the Phase 1 candidate test fuel samples for Tier 1 and 2 testing.
- Review process description provided by the fuel producer for acceptability for incorporation into the Phase 1 research report.
- Review test data from Tier 1 and 2 testing for acceptability for incorporation into the Phase 1 research report.
- Issue and deliver a Phase 1 research report to the OEMs.
- In conjunction with the fuel producer, review and respond to comments to Phase 1 Research Report submitted by the OEMs.
- Conduct additional Tier 1 or 2 testing in response to OEM comments, as required.
- Review and consolidate OEM requirements for D4054 Tier 3 and 4 testing submitted by the OEMs.
- Deliver consolidated D4054 Tier 3 and 4 testing requirements to the fuel producer.

Subtask 3: Phase 2 Support

- Coordinate the funding and scheduling of D4054 Tier 3 and 4 testing with OEMs and other test facilities.
- Coordinate the handling of the Phase 2 candidate test fuel samples for Tier 3 and 4 testing.
- Review test data from Tier 3 and 4 testing for acceptability for incorporation into the Phase 2 research report.
- Issue and deliver the Phase 2 research report to the OEMs.
- In conjunction with the fuel producer, review and respond to comments to the Phase 2 Research Report submitted by the OEMs.
- Conduct additional Tier 3 or 4 testing in response to OEM comments as required.
- Issue and deliver Phase 2 research report addendums reporting the additional Tier 3 or 4 test results, as required.

Subtask 4: OEM Review Meetings

- Schedule periodic OEM Review Meetings to review the status of testing and research report review.
- Identify suitable meeting venues and support equipment.
- Develop agendas and coordinate with attendees for participating in the meeting.
- Record meeting minutes, including agreements, commitments, and other action items.
- Issue and distribute the meeting minutes to all attendees.

Subtask 5: Single Laboratory GCxGC Method Documentation

- Document UDRI GCxGC methodology for hydrocarbon type analysis.
- Develop reference materials for creation of GCxGC hydrocarbon type templates.
- Measure single laboratory precision of the GCxGC methods.
-

Subtask 6: Multi-Laboratory GCxGC Method Documentation

- Validate precision of the methods over multiple laboratories and GCxGC methods.
- Identify alternative GCxGC methods, including column selection and order, and modulation techniques.
- Perform correlation study to determine agreement between laboratories, methods, and hardware choices.

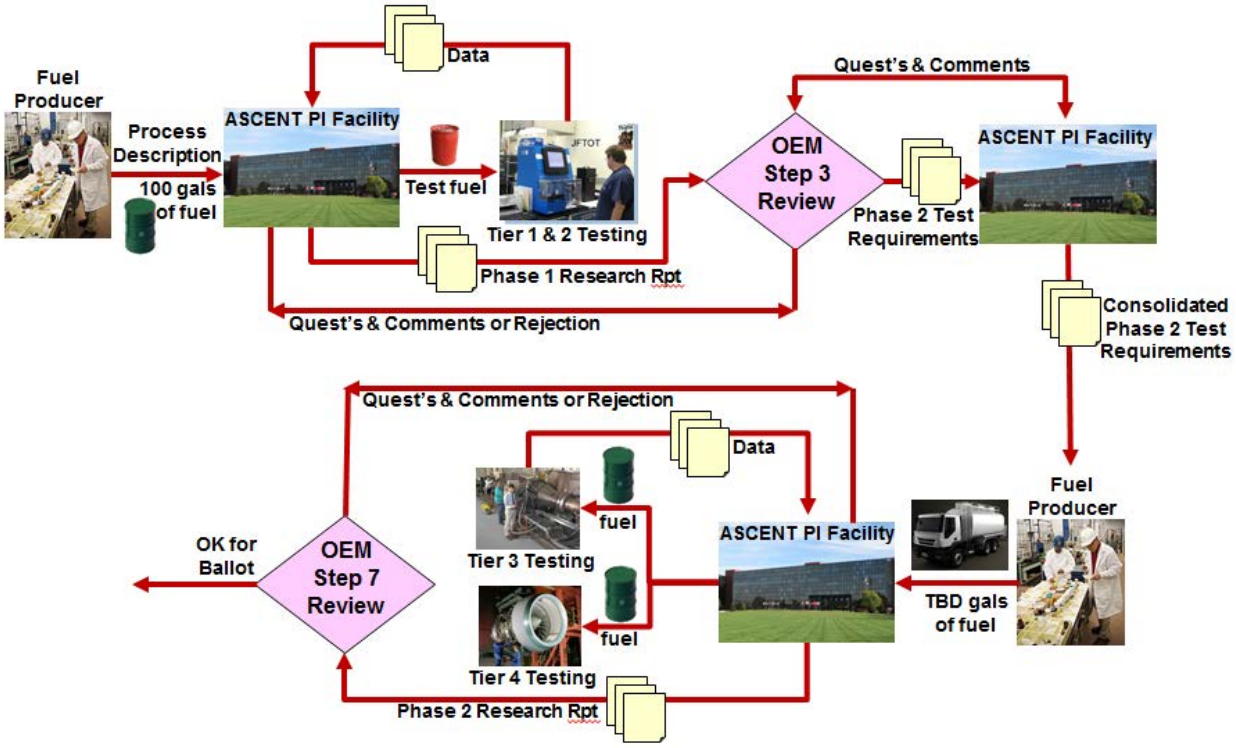


Figure 2. D4054 Evaluation Process

Milestone(s)

The schedule for this project is dependent upon receipt of alternative fuel candidates for testing. As candidate fuels are received a schedule of testing will be coordinated with the FAA and collaborators. Our existing relationships with these organizations will help expedite this process. Figure 3 shows a Gantt chart schedule for the testing and approval of candidate fuels that are in the process of being evaluated and/or about to the enter the process.

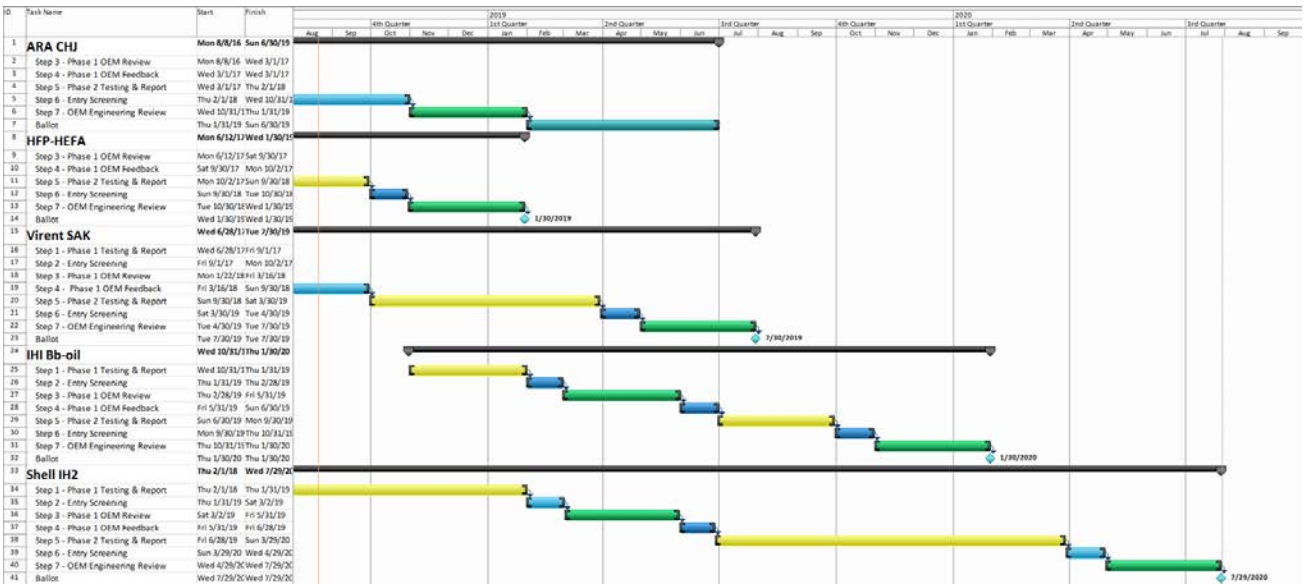


Figure 3. Schedule for Fuel Evaluations

Major Accomplishments

A major accomplishment of this project is the approval of the LanzaTech Ethanol-to-Jet Synthetic Paraffinic Kerosene Fuel and inclusion into Annex A5 of ASTM D7566 in March 2018. The Boeing/Neste HFP-HEFA research report has been completed and is in the process of Phase I review by the OEM's. The Virent SAK fuel Phase 1 research report is completed and awaiting evaluation by the OEM committee. The ARA CHJ fuel report is in the hands of the supplier after OEM feedback. UDRI performed initial testing of the Shell IH2 fuel and provided feedback and guidance to the supplier for methods which will improve the quality and stability of a future sample submission. We are awaiting the imminent arrival of this second Shell IH2 sample and an initial sample of the IHI Bb Oil fuel for Phase 1 evaluations. We held OEM meetings on the fuel approval process at the December 2017 ASTM D02 meeting in Houston and the March 2018 UK MoD Aviation Fuels Committee meeting in London.

We began support of the development of a generic annex for a more rapid approval of fuels to D7566. The generic annex concept was abandoned in the spring of 2018 as the OEMs wanted to continue to have approval authority for new production processes and feedstocks (the generic annex did not require OEM approval). A new concept was developed, called the "fast track annex," which would provide (via D4054) a rapid approval pathway for new fuels that meet a set of strict composition and performance criteria. This fast track annex is being viewed positively and was submitted for ASTM balloting in October 2018.

We evaluated an oxygen measurement instrument (the Elementar Oxycube with IR detector) for measurement of low concentrations of oxygenate contaminants in candidate fuels. The OEM committee is concerned that current chemical analysis techniques may not be able to detect all of the species. Via a catalytic partial reduction, the instrument converts all O atoms in a sample to CO followed by IR detection. We evaluated the instrument using multiple sample injection methods for its ability to measure down to 10 ppm oxygen. Unfortunately, background oxygen molecules and dissolved water interfere with the measurement. Working closely with the instrument company we determined that the instrument was unable to provide the required detection limit, repeatability, and reproducibility needed for measuring low levels of oxygenate contaminants in candidate fuel samples.



We continue to provide feedback to fuel suppliers and the OEM committee on the candidate fuel evaluation schedule via the Gantt chart shown in Figure 3. The chart is updated frequently as testing and evaluation is accomplished and schedule changes occur.

We have held biweekly meetings with the Shell IH2 team on the status of the fuel submission and the planned testing. We have also held monthly meetings with the IHI Bb Oil team on their fuel submission.

We attended the ASTM OEM meeting (December 2017 in Houston) with engine and airframe OEMs to review progress on ASTM research report reviews. We gave a presentation on the chemical analysis of heteroatomic polars for development of a generic annex for alternative fuel certification. We presented a project overview at the ASCENT April 2018 ASCENT meeting in Cambridge, MA. We also attended the March 2018 AFC meeting in London and discussed alternative fuel qualification and certification with the FAA and OEMs. Discussions with alternative fuel candidate producers also occurred at each of these meetings.

Publications

"Evaluation of High Freeze Point HEFA as Blending Component for Aviation Jet Fuels," ASTM Research Report Version 1.1, 2017.

UDRI Method FC-M-101, "Flow Modulation GCxGC for Hydrocarbon Type Analysis of Conventional and Alternative Aviation Fuels," UDR-TR-2018-40.

UDRI Method FC-M-102, "Identification and Quantification of Polar Species in Conventional and Alternative Aviation Fuel Using SPE-GCxGC," UDR-TR-2018-41

Outreach Efforts

Presentations on Project 31a were given at the April (Boston) and October (Alexandria) 2018 ASCENT meetings. Meetings were held with the OEM team, FAA, and others at the December 2017 ASTM D02 Committee Meeting in Houston TX and the March 2018 UK MoD Aviation Fuels Committee meeting in London UK. Monthly meetings were held in Dayton with IHI, a Japanese company interested in entering their algae fuel in the D4054 process. We also continue to have biweekly teleconferences with Shell on their soon to be submitted IH2 fuel.

Awards

None

Student Involvement

Amanda Arts, University of Kentucky Co-op Student

Plans for Next Period

We plan to attend the ASTM December meeting in Atlanta and hold an OEM meeting with fuel producers in a separate session prior to the main ASTM meeting as in the past. We expect to receive the first shipment of the Shell IH2 fuel and begin the process of testing the fuel for Tier 1 and 2 evaluations. We expect to receive the first shipment of the IHI Bb oil algae fuel near the end of 2018 and will begin testing at that time.

Project 033 Alternative Fuels Test Database Library (Year IV)

University of Illinois Urbana-Champaign, University of Dayton Research Institute

*this report covers portion of University of Illinois

Project Lead Investigator

Tonghun Lee
Mechanical Science & Engineering
University of Illinois at Urbana-Champaign
1206 W. Green St.
Urbana IL 61801
517-290-8005
tonghun@illinois.edu

University Participants

University of Illinois at Urbana-Champaign

- P.I.(s): Tonghun Lee, Associate Professor
- FAA Award Number: 13-C-AJFE-UI-022
- Period of Performance: 8/15/2017 to 8/14/2018
- Task(s):
    1. Conversion of Database into Non-Relational Format
    2. Inclusion of Additional Data: GC x GC, Metron, PQIS

Project Funding Level

Funding Level: $140K ($165K total, $25K contracted to UDRI)
Cost Share: Software license support from Reaction Design (ANSYS)

Investigation Team

- Anna Oldani (Graduate Student, University of Illinois at Urbana-Champaign): Compilation of fuel test data and development of database.
- Siddhartha Jahorie (Graduate Student, University of Illinois at Urbana-Champaign): Compilation of fuel test data.

Project Overview

This study seeks to create a comprehensive, foundational database of current and emerging alternative jet fuels by integrating relevant pre-existing jet fuel data into a common archive that can provide guidelines for design and certification of new jet fuels in our future, as well as aid federal work including fuel certification. The effort has focused on the integration and analysis of pre-existing jet fuel data from various government agencies and individual research groups with oversight from the Federal Aviation Administration (FAA). In this year, we are making a significant transition of data into a non-relational format, allowing for real time analysis of all the data and also enabling our database to link with a similar effort in Europe (JETSCREEN). We hope that the database will one day serve as 'the comprehensive and centralized knowledgebase' shared by the academic, government, and industrial communities in fuels research and policy, possibly facilitated on a cyber-based infrastructure. With ongoing prolific diversification of new jet fuels, this effort to integrate dispersed information is critical in providing the FAA with an overview of the latest developments and to support many other tangential fields of research in government, industry, and academia impacted by integration of new alternative jet fuels.

Task 1 – Conversion of Database into Non-Relational Format

University of Illinois at Urbana-Champaign

Objective(s)

The main objective of this project is to establish a foundational database current and emerging alternative jet fuels (AJFs) and fuel blends by compiling relevant data and storing this data in a centralized location for easy retrieval and analysis. The format for storing data should be consistent for all fuels and easily accessible by some common programming languages. The focus this year was coming up with a digital non-relational database structure what could be linked with other databases and readily analyzed. The intention of creating this database is to facilitate the large-scale analysis of AJF data and ease the creation of statistical correlations and surrogate models for AJFs. The goals of this project are:

- Select a suitable database for optimal storage and retrieval of jet fuel data
- Design a centralized data structure for compiling data
- Conversion of AFRL data to JSON format
- Preliminary analysis of AFRL fuel data using database resources.

Research Approach

Development Strategy of a Successful Fuels Test Database (Long Term Plan)

Database selection

The selection of a database service was a key aspect of this project. The first step involves a choice of relational (SQL) or non-relational (NoSQL) database. The major differences between these databases are summarized in Figure 1. A NoSQL database was considered more appropriate for two major reasons. First, documents and reports gathered for fuels had different formats and varying amounts of data. For example, data for one fuel may include viscosity, density and heat of combustion, while data for another fuel may only include density. Furthermore, multiple tests may be performed for a single fuel property. Data for one fuel may include five (5) measurements of viscosity, while data for another may only include one. Due to these considerations, a flexible schema was considered to be of primary importance when selecting a database service. SQL databases require that data fit into predefined tables, which could be problematic. Second, one of the goals of this initiative included collaboration with the European Agency, JETSCREEN (JET fuel SCREENing and optimization), which also studies AJFs. JETSCREEN's AJF data is already hosted by MongoDB, a NoSQL database service. Since MongoDB uses an unstructured schema, interfacing with a SQL database using a fixed schema would impose greater complexity compared to interfacing with a NoSQL database. The acid and base properties mentioned in Figure 1 describe consistency models used by the different databases. The BASE model used by NoSQL databases is a much weaker consistency model that the ACID model. However, a flexible schema cannot be used within the confines of the ACID consistency model. Therefore, NoSQL databases sacrifice consistency for flexibility. JOIN operations accommodate the merging of SQL tables to compare data across different tables. By exploiting the flexible schema of NoSQL databases, one can eliminate the need for JOIN operations.

Non-Relational (NoSQL)	*Relational (SQL)*
Highly scalable	**Less scalable**
Flexible schema - data can be inserted/altered anytime without issue	**Structured schema** - data has to fit into predefined tables
Does not support JOIN operations	Supports JOIN operations
BASE properties	ACID properties
Does not use SQL as query language	Mainly uses SQL as query language

Figure 1. Comparison of relational and non-relational databases

Once it was decided to use a NoSQL database, the next choice is to decide on a NoSQL service. While using MongoDB would be the most convenient choice to interface with JETSCREEN, DynomoDB was selected for several logistical reasons. Using university resources, DynamoDB was the easiest NoSQL database service to use. The University of Illinois has an agreement with Amazon AWS, which provides the DynamoDB service. As such, Amazon AWS representatives are present on campus to assist in the setup of the database and handle any potential problems. Because the IT services at the university do not have any staff experienced with NoSQL databases, implementation of any other NoSQL database would have to be done in-house or arranged with an external organization. MongoDB is notoriously difficult to setup and therefore it was decided to avoid doing this in-house. Using an external organization would also involve additional challenges as such an organization would need the right clearances to work with government data. This was not an issue with DynamoDB due to their partnership with the University of Illinois. Since DynamoDB and MongoDB both store data in the JSON (JavaScript Object Notation) format, interfacing between the two services is not expected to be difficult.

Data Schema

Both MongoDB and DynamoDB stores data using the JSON (JavaScript Object Notation) format. Therefore, the next step involved converting data to the JSON format. The JSON format stores data using key, value pairs. Values can also be keys pointing to other values resulting is a complex schema with nested keys. This is often the most appropriate way to store data. In order to access data, these specific keys are required. Since JETSREEN already had a schema in place, our schema was created by modifying JETSCREEN's schema to account for additional data that we collected. Since the same keys are used, integrating and sharing data would be fairly straightforward.

Conversion of AFRL data to JSON format

Data received from AFRL mostly included fuel lab reports from the Air Force Petroleum Office (AFPET). These reports were in pdf form and had to be converted to a format that is easily accessible by code. The Able2Extract software was used to convert AFPET lab reports to suitable excel tables. Since many reports, particularly old reports, were scanned pdfs, these tables were also manually checked for errors and the ensure consistency in formatting. After converting AFPET reports to excel tables, scripts were written in python 3 to extract the data from these excel tables and create JSON files. The scripts mapped key phrases in the names of fuel tests to specific keys defined in the data schema. The process of converting AFRL data to a JSON format is illustrated in Figure 2. It should be noted that a single JSON file was created for each POSF number. Because there were multiple AFPET lab reports for a single POSF number, these were combined into a single JSON file.

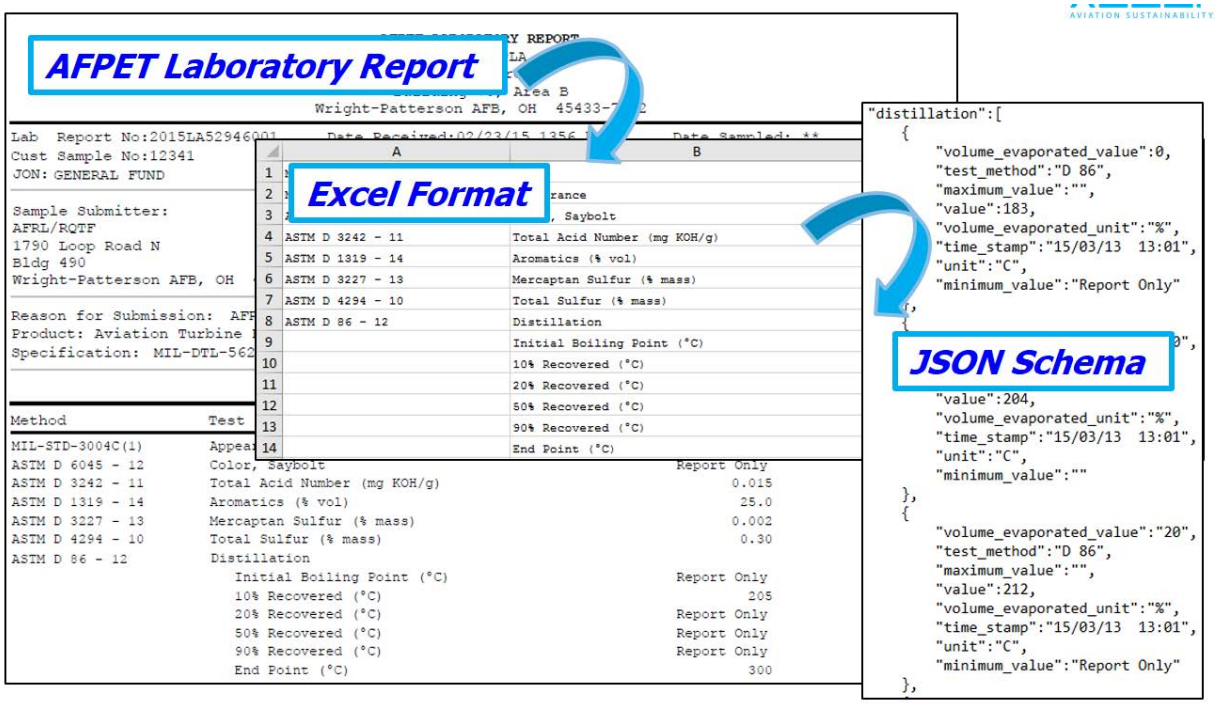


Figure 2. Conversion of AFRL Laboratory Reports from pdf files to excel tables to serialized JSON files

Preliminary analysis of data

Once data for AFRL fuels were stored in JSON files, scripts could be easily created in most programming languages to access this data and perform numerical analysis. Uploading the data to DynamoDB allows the data to be shared by other collaborators. In the future, we hope to use the capabilities of DynamoDB to interface with the AJFTD site to allow users to easily sort, filter and perform simple analysis on fuels.

Figures 3 and 4 demonstrate some of the analysis that can be performed using the database. Figure 3 shows the distillation curves for Category A and C fuels and the average distillation profile of all AFRL fuels. The unusual boiling curve of C-1, the asymmetric boiling curve of C-2 and the flat boiling curve of C-5 can be easily observed from this plot. The effect of farnesane on the boiling range of a fuel can be observed by comparing the distillation curve for C-3, which is composed of 64% A-3 and 36% farnesane, and A-3. The distillation temperatures for C-3 is higher than A-3 up to about 90% recovered, and from 90%-100% recovered the distillation temperatures are quite similar. This occurs since farnesane is a C15 hydrocarbon and lower carbon number components generally evaporate first. The average distillation distribution is very close to that of A-2, further demonstrating the suitability of A-2 as a nominal fuel.

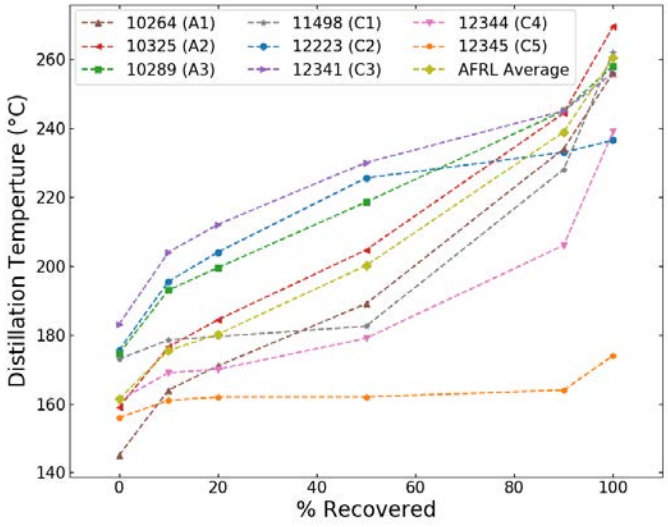


Figure 3. Distillation temperature for AFRL fuels

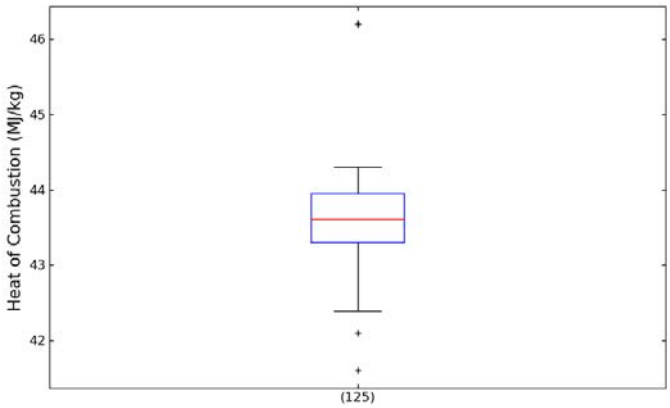


Figure 4. Boxplot showing range of heat of combustion values for AFRL fuels

Figure 4 shows a boxplot of the heat of combustion values for AFRL fuels. The range of values can be easily observed in such a plot. Outliers and erroneous data can also be easily identified. In the future, by integrating DynamoDB with the AJFTD site, it may be possible to plot data for new fuels against a range of existing data to determine if the data is within the expected range, or if it may be a possible outlier.

The analysis shown here is just a demonstration of the flexibility offered by turning the entire database into a non-relational format. The analysis enabled by this database is now only limited on the programming and can be easily extended to new data which is added to the database. The current version was carried out with customized PYTHON codes based on the output for which we were aiming. As stated above, it is anticipated that in year V, we will be integrating the functionality to the website so that other users can log in and conduct basic functions using the data. More importantly, we anticipate that this type of structure will allow the current database to be linked with other databases including the JETSCREEN database in Europe. In order to accomplish this, the format in the JSON schema were based on the existing architecture of the JETSCREEN database with minor modifications. These minor modifications were mainly required to address US specific data terms and add other testing information such as the GC x GC (will be addressed below).

Task 2 – Inclusion of Addition Data: GC x GC, Metron, PQIS

University of Illinois at Urbana-Champaign

Objective(s)

The main objective of this project is to augment the existing data by adding GCxGC data and collecting data from additional sources, with a focus on fuels in use. As more data is added to the database, more meaningful analysis can be performed. The major goals of this project are as follows:

- Collect GCxGC data and integrate into JSON schema
- Convert Metron Aviation data to JSON format
- Convert PQIS data to JSON format
- Preliminary analysis of GCxGC, Metron Aviation and PQIS data

Research Approach

Development Strategy of a Successful Fuels Test Database (Long Term Plan)

Integration of GCxGC data to JSON Schema

Gas chromatography is a technique for separating complex mixtures based on differences in boiling point/vapor pressure and polarity. Two-dimensional gas chromatography (GCxGC) subjects a sample to two dimensions of separation. The first separation is based on volatility as seen in GCMS, and the second separation is a very fast separation based on polarity. This allows identification of different hydrocarbon types and carbon numbers.

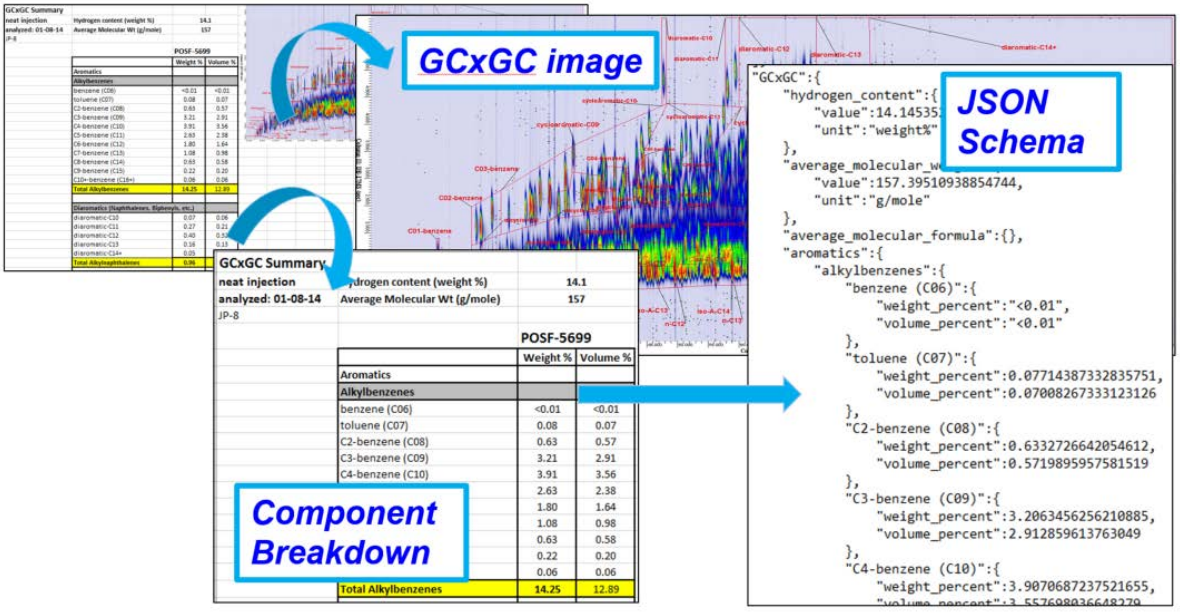


Figure 5. Conversion of GCxGC data to JSON format

The GCxGC technique provides important information for understanding fuel properties. The carbon number provides information on fuel volatility, which also affects flash point and freeze point. For example, lighter fuel fractions (with lower carbon numbers) are more reactive and lower the flash point of the fuel. Heavier fuel fractions (with higher carbon numbers) raise the freezing point of the fuel. Due to flash point and freezing point constraints, jet fuels typically do not contain significant amounts of hydrocarbons below C8 and above C17. Hydrocarbon type also imparts particular properties to fuels. For example, normal paraffins are the most reactive hydrocarbon group. Isoparaffins have the same chemical formula as

normal paraffins but are less reactive and have much lower freezing points. Cycloparaffins have lower freezing points and higher densities than both normal and isoparaffins of the same carbon number. Single-ring aromatics (alkylbenzene) are important for elastomer (O-ring) swell and have high energy density per unit volume, while multi-ring aromatics contribute to soot formation. It is worth noting that GCxGC is weak in differentiating the level of branching in iso-paraffins and side chains in aromatics and cycloparaffins. The level of branching in these molecules can impact the cetane number and hence ignition delay of fuels

GCxGC data was collected for several AFRL fuels and converted to the JSON format as shown in Figure 5. The GCxGC schema includes data on average molecular weight, hydrogen content and four major hydrocarbon types (n-alkanes, iso-alkanes, cycloalkanes and aromatics), including a carbon number breakdown.

Conversion of Metron Aviation and PQIS Data to JSON format

Additional fuel data was received from Metron Aviation and Petroleum Quality Information Systems (PQIS). Metron Aviation collected 14,823 fuel samples from 11 airports across the United States. PQIS, which is managed by the Defense Logistics Agency (DLA) has provided information on 9,201 conventional and alternative fuels used by DLA customers. These data are particularly interesting to study since they contain data of fuels in use. One downside of the Metron Aviation data is that very little identifying information if available for fuels. Therefore, we do not know what type of fuel is used or if the fuel is blended with an alternative fuel. On the other hand, PQIS fuel data can be categorized into alternative fuels, Air Force kerosene, Air Force gas and Air Force diesel. Furthermore, the alternative fuels can be categorized as hydroprocessed reformed jet (HRJ), alcohol-to-jet (ATJ), direct sugar to hydrocarbon (DSHC) or hydroprocessed depolymerized cellulosic diesel (HDCD) fuels. Data from both of these sources were received in formats that are easily accessed by code. There scripts were written to directly convert the data into JSON files.

Preliminary Analysis of GCxGC, Metron and PQIS data

This section again demonstrates the utility of the database by showing some of the analyses which can be performed with relative ease. Distillation data collected from Metron Aviation, averaged over airport locations, is shown in Figure 6. While the reporting units for distillation temperatures are supposed to be in degrees Fahrenheit, it appears that the data collected at Portland airport (PDX) were reported in degrees Celsius. The distillation temperatures for PDX, seen in Figure 6(a) appears to be too low for a kerosene range fuel. Figure 6(b) was produced by assuming that these values were in Celsius and converting them to Fahrenheit. The graphs with the converted values fit much better with the traditional boiling ranges for kerosene range fuels.

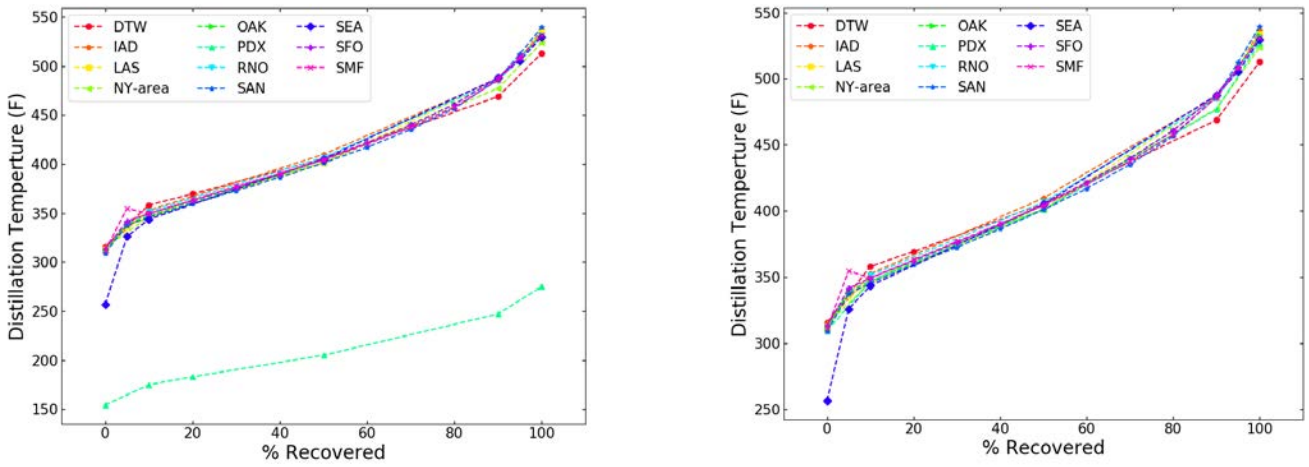


Figure 6. Metron Aviation Distillation Curves

Figure 7(a) shows the composition of category A and category C fuels that were reconstructed from the GCxGC data. The red bar represent category A fuels and the green bars represent category C fuels. Only the four major hydrocarbon groups, n-paraffins, iso-paraffins, cycloparaffins and aromatics, are shown, because the amounts of other hydrocarbon types are negligible. While an even spread of hydrocarbons can be observed for category A (conventional) fuels, the predominance of iso-paraffins is observed in category C fuels. Figure 7(b) shows the average GCxGC composition of six different types of neat alternative fuels and compares this with conventional fuels and fuel blends. Again, the predominance of iso-paraffins is observed in most alternative fuels with the exception of HDO-SK (Hydro DeOxygenated Synthetic Kerosene)/HDO-SAK (Hydro DeOxygenated Synthetic Aromatic Kerosene) and HDCJ (Hydroprocessed Depolymerized Cellulosic Jet) fuels. HDO-SAK fuels are intentionally produced to have a high aromatic content, while the cellulosic feedstock of HDCJ fuel usually produce fuels that predominantly composed of cycloparaffins and aromatics. It is interesting to note that the alternative fuels which have low iso-paraffins content are the ones which have not been approved for use as drop-in fuels when blended with conventional fuels, while the alternative fuels with high iso-paraffin content have all been approved.

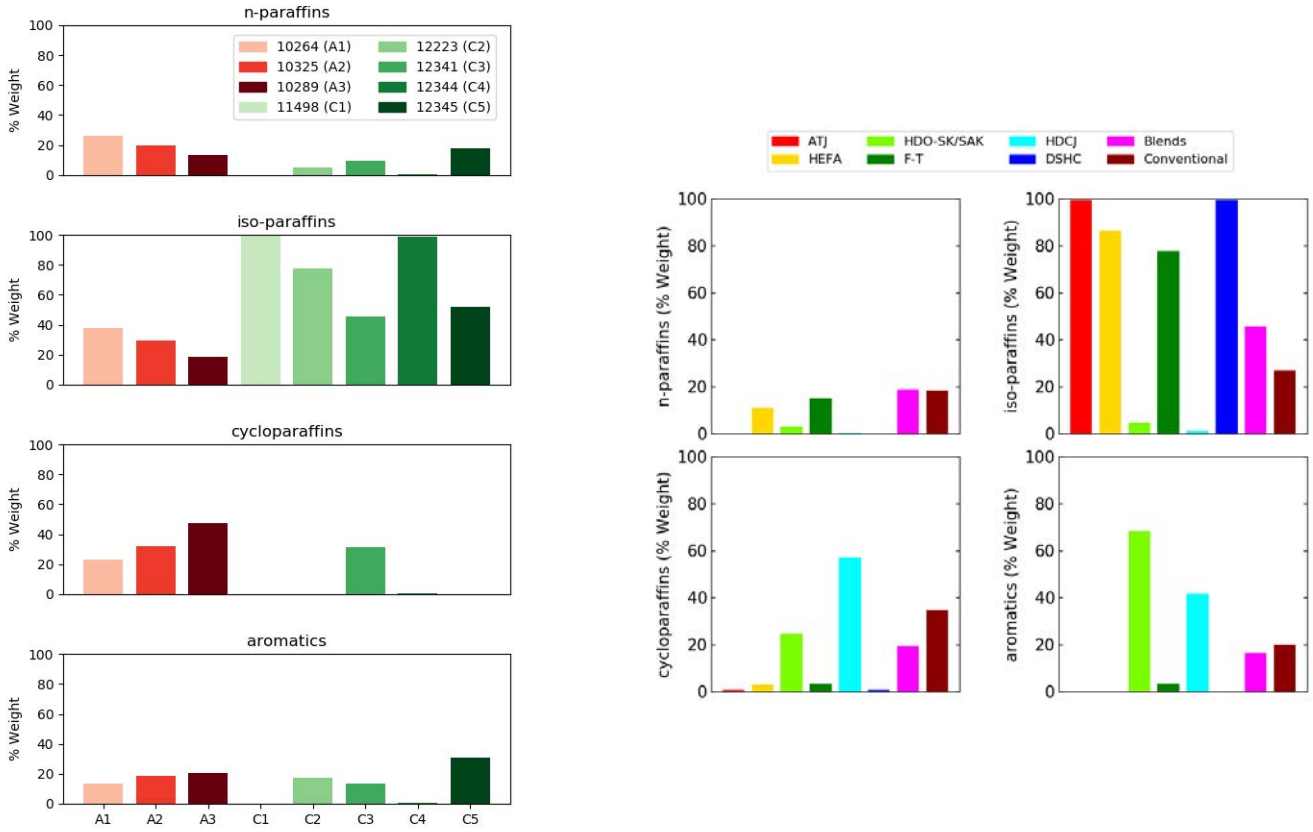


Figure 7. GCxGC graphs showing the hydrocarbon content of various fuels

In an attempt to develop a procedure for shortlisting viable candidates for drop-in fuels, Won et al. proposed the formulation of a surrogate model for predicting global combustion properties. The model would be based on a multivariate linear regression (MLR) analysis of certain combustion property targets (CPTs). Some of the suggested CPTs were derived cetane number (DCN), molecular weight (MW), hydrogen to carbon ratio (H/C ratio) and smoke point (SP). In order to perform an MLR analysis, it must be verified that the selected CPTs are independent. Figure 8 shows a correlational analysis of these CPTs using both the data provided by this paper and data from the database. The number in parenthesis are the Pearson correlation coefficients of the Won et al. data, while the number above (without parenthesis) are the Pearson correlation

coefficients for data from the database. The high correlation coefficient values for smoke point and H/C ratio suggests that these CPTs cannot be considered independent. Therefore, any meaningful MLR analysis will have to be performed with only one of these.

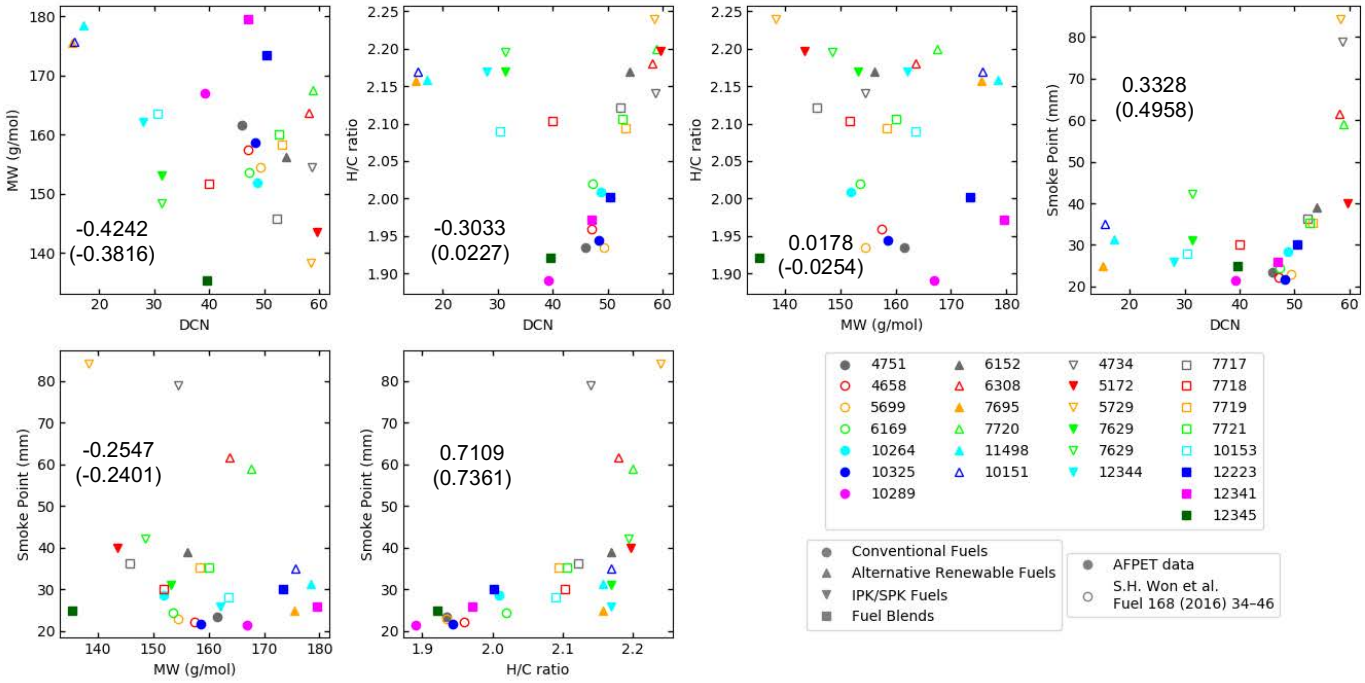


Figure 8. MLR Analysis

Milestone(s)

Proposed (3 Month): At the 3 month mark, we should have decided on a standard non-relational data format in collaboration with the JETSCREEN program in Europe. Plans should be underway to convert database structure into a non-relational format.
Achieved: A JSON format for integrating all data was selected (in discussion with JETSCREEN) and the conversion of all of the data in the database was initiated. Special routines were programmed using an assortment of codes (mostly in PYTHON) to facilitate the transition.

Proposed (6 Month): At the 6 month mark, data conversion to the JSON format should be well underway. We should also have started the integration process of additional GCxGC data from AFRL as well as airport data from Metron.
Achieved: All the data was gathered from AFRL and Metron and specialized routines were set up for conversion of all this data to JSON format. We also decided on a DynamoDB framework supported by Amazon to host the non-relational data.

Proposed (9 Month): At the 9 month mark, conversion of all data to JSON format should be nearing completion and preliminary analysis of data using the JSON format should be conducted.
Achieved: Nearly all of the data (>85%) was converted to the JSON format at this point and preliminary analysis of data was initiated using PYTHON codes. Correction of errant data from METRON and AFRL was also completed.

Proposed (12 Month): At the 12 month mark, all data to date should be converted to JSON format. Discussions with the School's IT office should be underway for integration of JSON format data into the DynamoDB framework and integration of this into the database website.
Achieved: All data conversion to was JSON completed. Discussions with school IT office of integrating the database analysis into the website were initiated.



Major Accomplishments

Conversion of Data to JSON format (non-relational digital format)
A total of 24,386 fuel records have been converted to the JSON format, which can easily be accessed by most programming language. GCxGC data have been obtained for 87 AFRL fuels and added to the JSON schema. This is the first step in the establishing a foundational fuel database that would enable researchers to more easily analyze surrogate models and statistical correlations for alternative jet fuels. This format will also allow us to link the database with others including JETSCREEN.

Integration of New Data
We have included a number of new data into the database in year IV including the GCxGC data from AFRL, actual airport data from Metron Aviation, and the PQIS database. All the data integrated into the database has been converted into JSON format for full analysis.

Preliminary Analysis
Analysis of fuel data have demonstrated the efficacy of the database in identifying erroneous data and outliers. Insightful compositions graphs and distillations plots highlight the most salient features of alternative and conventional fuels were also produced. As more fuel data is obtained and added to the database, more meaningful and statistically significant analysis would be possible.

Publications

(In Progress) Oldani, Anna. "Alternative Jet Fuel Variation and Certification Considerations." 2018.

Outreach Efforts

None

Awards

Anna Oldani (Graduate Student): DOT Student of the Year Award
Anna Oldani (Graduate Student): Society of Women in Engineering (SWE) Award for Research Excellence

Student Involvement

Two graduate students (listed above) have participated in this project on a rotational basis to address various aspects of the project. They have surveyed the data, interacted with the data sources and created strategies to integrate the data into the database. They developed the web-based portal for the actual implementation of the web interface. They have also conducted a statistical analysis of the available data to evaluate property variance. They continue efforts to update the database with relevant alternative jet fuel test data as it is made available.

Plans for Next Period: Start of Analysis and Integration of Database

Year V for the database project will see the full extended evaluation activities of the data using the new non-relational structure. We anticipate that a publication or report will result from the full analysis.

- Evaluation and analysis of all GC x GC, Metron, PQIS data
- Full integration of the JSON format into the DynamoDB infrastructure
- Integration of the database structure (DynamoDB) to a web interface on aljetfuels.illinois.edu for public access.
- Inclusion of NJFCP data: continued integration of the NJFCP data to the website for fuel certification activities
- Integration of efforts with European JETSCREEN program to collaborate fuel screening and property evaluation under NJFCP program (Meeting Scheduled in December of 2018)

Project 034 Overall Integration and Coordination

University of Dayton

Project Lead Investigator

Joshua Heyne
Assistant Professor
Mechanical Engineering
University of Dayton
300 College Park
Dayton, OH 45458
937 229-5319
Jheyne1@udayton.edu

University Participants

University of Dayton

- P.I.(s): Joshua Heyne and Scott Stouffer
- FAA Award Number: 13-C-AJFE-UD (Amendment Nos. 9, 10, 13, 17, & 18)
- Period of Performance: September 18, 2015 to December 31, 2018
- Task(s):
    1. Overall NJFCP integration and coordination
    2. Chemical effects in Toroidal Jet Stirred Reactor
    3. Preferential vaporization effects on LBO of the Referee Rig
    4. Cross-experiment analysis
    5. Common format routine software and model development
    6. Spray modeling of Area 3 (GT P&W pressure atomizer)
    7. Cold ignition experiments in the Referee Rig of alternative fuel blends

Project Funding Level

Amendment No. 9: $134,999.00 (September 18, 2015 to February 28, 2017)
Amendment No. 10: $249,330.00 (July 7, 2016 to December 31, 2017)
Amendment No. 13: $386,035.00 (August 30, 2016 to December 31, 2017)
Amendment No. 17: $192,997.00 (August 3, 2017 to September 30, 2018)
Amendment No. 18: $374,978.00 (December 7, 2017 to December 31, 2018)

Cost share is provided by GE Aviation ($135,000.00), DLR Germany ($3,113,564.00), United Technologies Research Center ($150,000.00), ANSYS/FLUENT ($175,000.00), and the University of Dayton ($53,887.00) in to form of in-kind research at GE Aviation, DLR Germany, and United Technologies, direct financial support at the University of Dayton, and reduced software license fees at ANSYS/FLUENT.

Investigation Team

- Joshua Heyne (University of Dayton) is the Project Lead Investigator for coordinating all NJFCP teams (both ASCENT and non-ASCENT efforts), Well-Stirred Reactor experiments, procuring additional geometrical configurations, and leading studies across experimental platforms within the NJFCP.
- Scott Stouffer (University of Dayton Research Institute) is the P.I. conducting ignition testing of NJFCP fuels in the Referee Rig.
- Alejandro Briones (University of Dayton Research Institute) is the P.I. responsible for leading the common format routine software development.
- Vaidya Sankaran (UTRC) is sub-contracted to conduct the spray modeling of the Area 3 pressure atomizing spray injector.



- Bob Olding (University of Dayton Research Institute) is part of the team managed by Alejandro Briones to develop the common format routine software. Mr. Olding's main task is on Scheme GUI/TUI programing for later use by OEM CFD teams.
- Mike Hanchak (University of Dayton Research Institute) is part of the team managed by Alejandro Briones to develop the common format routine software. Mr. Hanchak's main task is on CFD and combustion programing for later use by OEM CFD teams.
- Tyler Hendershott (University of Dayton Research Institute) is part of the team working on the ignition of conventional and alternative jet fuels in the Referee Rig.
- Jeffery Monfort (University of Dayton Research Institute) is part of the team working on the ignition of conventional and alternative jet fuels in the Referee Rig.
- Robert Stachler (University of Dayton) is a Ph.D. student conducting the Lean Blowout and emissions measurements in the Well-Stirred Reactor.
- Erin Peiffer (University of Dayton) is a Master's student linking experimental results across ASCENT and non-ASCENT teams.
- Sherri Alexander (University of Dayton) is an administrative assistant aiding in the compilation of meeting minutes and setting up teleconference times.
- Katherine Opacich (University of Dayton) is an undergraduate research assistant working to document NJFCP activities and analyze ignition data across NJFCP teams.
- Shane Kosir (University of Dayton) is an undergraduate research assistant working to analyze LBO data.
- Zhibin (Harrison) Yang (University of Dayton) is a graduate student research assistant working to develop physical surrogates
- Jen Colborn (University of Dayton) is an undergraduate research student assistant aiding in the testing of fuels on the Referee Rig.
- David Bell (University of Dayton) is a graduate student research assistant working to develop physical surrogates.

Project Overview

The NJFCP is composed of more than two dozen member institutions contributing information and data as diverse as expert advice from gas turbine Original Equipment Manufacturers (OEMs), federal agencies, other ASCENT universities and corroborating experiments at DLR Germany, NRC Canada and other international partners. The project is tasked to: coordinate and integrate among these diverse program stakeholders and academic Principle Investigators (PIs); cross-analyze results from other NJFCP areas; collect data for modeling and fuel comparison purposes in a Well-Stirred Reactor (WSR); conduct Large Eddy Simulations (LES) of sprays for the Area 3 High Sheer Rig; procure additional swirler geometries for the NJFCP Areas and Allied Partners while developing interface of NJFCP modeling capabilities with OEM requirements. Work under this program consists of, but is not limited to:

- conduct meetings with member institutions to facilitate the consistency of testing and modeling,
- coordinate timely completion of program milestones,
- document results and procedures,
- create documents critical for program process (e.g. fuel down selection criteria)
- solicit and incorporate program feedback from OEMs,
- report and present on behalf of the NJFCP at meetings and technical conferences,
- integrate the state-of-the-art combustion and spray models into user-defined-functions (UDFs),
- WSR testing of NJFCP Category A, Category C, and Surrogate fuels,
- LES of sprays for A2, C1, and C5 fuels using the Area 3 High Sheer Rig Pratt & Whitney swirler and air blast atomizer,
- facilitate travel for University of Cape Town student,
- advise the program Steering Committee.

Task 1- Integration and Coordination of NJFCP Teams

University of Dayton

Objective(s)

The objective of this task is to integrate and coordinate all ASCENT and non-ASCENT team efforts via facilitation of meetings, summarizing results, presenting results external to the NJFCP, communicating on a regular basis with the Steering Committee, and other related activities.



Research Approach

The NJFCP is integrated and coordinated via two main techniques: 1) the structural lumping of various teams into six Topic areas and 2) routine meetings and discussion both internal and external to individual Topic areas. The Topic areas are distinguished by the dominant physics associated with them (Topics I and IV), the culmination of all relevant combustion physics (Topics II, III, V), and wrapping all work into a singular OEM GUI package (Topic VI). These six Topic areas are:

Topic I. Chemical Kinetics: Foundational to any combustion model is a chemical kinetic model and the validation data anchoring modeling predictions.
Topic II. Lean Blow Out (LBO): This Topic covers data, screening, and validation at relevant conditions to statistically and theoretically anticipate fuel property effects on this Figure of Merit (FOM).
Topic III. Ignition: Similar to the LBO topic, the focus here is experimental screening and validation data for statistical and theoretical predictions.
Topic IV. Sprays: Historically, the dominant effect of fuel FOM behavior has been the spray character of the fuel relative to others. Experimentalists in this Topic area focus on measuring the fuel property effects on spray behavior. In analogy to Topic I, the spray behavior is not a FOM like Topic II and III, although it is critical to bound the physical property effects on combustion behavior relative to other processes, i.e. chemical kinetics.
Topic V. Computational Fluid Dynamics (CFD) Modeling: Complementary to the empirical Topics II, III, and IV, the CFD Modeling Topic focuses on the theoretical prediction of measured data and facilitates the development of theoretical modeling approaches.
Topic VI. User Defined Function (UDF) Development: Once the theoretical modeling approaches matured in Topic V are validated. UDFs are developed for OEM evaluation of fuel performance in proprietary rigs.

These topic area teams meet and coordinate on a regular basis. At minimum, NJFCP wide meetings are held monthly with Topic area meetings occurring typically every 2-3 weeks.

Milestone(s)

NJFCP Mid-Year Meeting 2018

Major Accomplishments

Invited NJFCP Related Presentations

- Colket, Heyne, Lee, "NJFCP Update: Properties and Modeling to FOM Predictions," JetScreen Meeting, Paris, FR, December 2018.
- Heyne, Colket, Lee, "An overview of ASCENT research efforts to improve our understanding of how fuel composition and characteristics determine performance," CAAFI Biennial General Meeting, December 2018.
- Heyne, J., Edwards, T., "What makes a Great Jet Fuel?," Keynote, Tri-Lateral US-Mexico-Canada Bio-Jet Workshop, Pacific Northwest National Laboratories, May 2018.
- Heyne, Colket, "Overview and Results from the National Jet Fuels Combustion Program," CAAFI SOAP-Jet Webinar, Jan. 2018.
- Med Colket, Sang Hee Won, Stephen, Dooley, Bill Pitz, Charlie Westbrook, Josh Heyne, Fred Dryer, Steve Zeppieri, "Surrogates for Practical Fuels: Historical Perspective, Palettes, Selection, Use and Modeling," 2018 MACCCR Meeting, Sandia National Laboratories, Livermore, CA, 2018.
- Colket, Heyne, "NJFCP Update," JET SCREEN Meeting, Rome, October 2017.

Publications

Peer-Reviewed Journal Publications

None

Published conference proceedings

Heyne, J., Peiffer, E., Colket, M., Moder, J., Edwards, J. T., Roquemore, W. M., Shaw, C., Li, C., Rumizen, M., and Gupta, M., "Year 3 of the National Jet Fuels Combustion Program: Practical and Scientific Impacts," 56th AIAA Aerospace Sciences Meeting, Kissimmee, FL: 2018, https://doi.org/10.2514/6.2018-1667

Stachler, R., Peiffer, E., Kosir, S., Heyne, J., and Stouffer, S., "A Study into the Chemical Timescale for a Toroidal Jet-Stirred Reactor (TJSR)," Central States Section of The Combustion Institute, Minneapolis: 2018, https://doi.org/10.2514/6.2018-4914

Bell, D. C., Heyne, J. S., Won, S. H., and Dryer, F. L., "The Impact of Preferential Vaporization on Lean Blowout in a Referee Combustor at Figure of Merit Conditions," ASME 2018 Power and Energy Conference, Lake Buena Vista: 2018, https://doi.org/10.1115/POWER2018-7432
Peiffer, E., Heyne, J.S., Colket, M., "Characteristic Timescales for Lean Blowout of Alternative Jet Fuels in Four Combustor Rigs," Joint Propulsion Conference, Cincinnati, OH: 2018, https://doi.org/10.2514/6.2018-4914

Outreach Efforts
Presentations at CRC Aviation Meeting, AIAA SciTech Meeting Paper and Presentation, ASCENT Spring and Fall presentations 2017, and DESS ASME conference.

Awards
None

Student Involvement
Erin Peiffer, Graduate Research Assistant, June 2017 - present.
Harrison, Graduate Research Assistant, August 2018 - present.

Katherine Opacich, Undergraduate Research Assistant, November 2017 – present.
Shane Kosir, Undergraduate Research Assistant, January 2018 – present.

Plans for Next Period
Continue to perform all relevant coordination and integration related tasks.

Overall NJFCP Summary Coordination
As it was reported previously[1,2], alternative jet fuels (AJFs) are identified as a means to mitigate climate change and pollution, potentially reduce costs and underlying volatility, and diversify the energy supply for national security. One of the key requirements of these new fuels is that they are "drop-in-ready," i.e., require no augmentation of engine, air frame components or ground-based and aircraft on-board infrastructure. Historically, this requirement for new alternative fuels necessitates extensive testing ranging from fit-for-purpose to full-scale engine testing, resulting in high costs and longtime scales for certification. Thus, the National Jet Fuels Combustion Program (NJFCP) was initiated[1] to reduce and streamline this extensive testing process, with a sole focus on the combustion operability of these fuels, i.e., Lean Blowout (LBO) and Ignition at cold start and altitude relight conditions. Fuel certification of alternative fuels requires consideration of a broad range of other practical issues and will not be reviewed here. The last two years we reported an extensive description of the NJFCP structure, historical context, key contributors, programmatic shifts, and key technical findings[1,2]. This year we are reporting on the results of the previous year from the perspective of key strategic technical findings as well as potential impacts in evaluating fuels via experiments and models.

The certification of an AJF largely focuses on three performance metrics, Figures of Merit (FOM), which largely bound a fuel's use for safe flight operations: i) LBO, ii) cold start, and iii) altitude relight, see Figure 1 for pertinent operating conditions. The performance of a fuel for these FOM relative to conventional fuels establishes a minimum criteria for fuel approval. Following this logic, the NJFCP early in the program defined three conventional jet fuels to quantify an expected 'best,' 'average,' and 'worst' case performance of conventional jet fuels, referred to herein as 'category A' or 'A' fuels [3]. Correspondingly, a series of AJF-like blends are defined to bound and explore the potential effects of AJFs, referred to herein as 'category C' or 'C' test fuels[3]. The performance comparisons of these A and C fuels for various experiments, models, and conditions establish the basis of the NJFCP.

The certification of AJFs typically involves a range of testing of the fuels in laboratory experiments to full scale engines. The later tests in turn contribute largely to the significant costs of the certification process, with the NJFCP's experimental platforms are a proof of concept that can reduce size and cost experiments while capturing the same effects as the larger, more costly full engine tests. Correspondingly, experimental platforms are paired in the NJFCP with a modeling complement. The experimental platforms and modeling complements are lumped into 6 major Working Groups which largely categorize the goals of the NJFCP to bound AJF FOM performance characteristics, and then create and deliver useful tools to the OEMs for AJF evaluation. These Working Groups are summarized below as well as a brief description of previous accomplishments:



- The *LBO Working Group* is focused on understanding the effects of fuel on the lean blowout limits in a combustor. Efforts include: a) screening category C fuels, NJFCP AJFs, with respect to the category A fuels, b) providing validation data to the CFD Working Group, and c) experimentally probing some more fundamental physical features of the results. Previous years of the NJFCP have reported combined statistical plots on LBO screening of A and C fuels. Here we report the most comprehensive statistical analysis of LBO behavior across 9 rigs in the NJFCP as well as referencing additional more fundamental physical effects of fuels effects on LBO.
- The *Ignition Working Group* is focused on fuel effects on ignition and altitude relight. It is similarly tasked with screening, providing validation data, and probing more fundamental physical effects of AJFs on FOM behavior. Previous years have resulted in screening for prevaporized fuels and Auxiliary Power Unit (APU) testing at Honeywell. Additionally, significant effort has been allocated to facility development to achieve the relevant low-pressure and low-temperature conditions in the lower right hand corner of Figure 1. These newly developed experimental capabilities are currently being utilized for screening with possibly additional validation data and probing of physical effects.
- The *Spray Working Group* is tasked with characterizing spray behavior at relevant conditions for the ignition and LBO conditions. These spray characterizations are used to determine the effect of spray on FOM performance, the effect of fuel properties on spray characterizations, and the validation of computational spray results. Over the last year, additional detailed phase Doppler particle anemometry (PDPA) measurements have been taken at LBO and cold ignition conditions. Moderate spray differences are observed at the LBO conditions, while initial results showing greater spray differences across the fuels are observed at chilled conditions.
- The *Computational Fluid Dynamics (CFD) Working Group* is currently focused on predicting the correct trends for the fuel sensitivity of lean blow in the Area 6 referee rig. Large-Eddy reacting spray simulations begin at an experimentally-demonstrated stable flame condition near lean blowout (LBO). Approach to LBO in CFD simulations proceeds through a series of step reductions in fuel mass flow rate since the approach to lean blowout over tens of seconds in the experimental procedure is not practical for CFD large-eddy reacting spray simulations, even using thousands of processors. Lean blowout predictions have been completed, but the correct trend in the fuel sensitivity of LBO is still being pursued with a consistent set of boundary conditions and spray injection conditions. Initial CFD simulations for prevaporized forced ignition have also begun.
- The *Kinetics Working Group* is focused on understanding the effects of fuel chemistry on the FOMs. Major accomplishments over the past year include the development and demonstration of new capabilities for measurements on the evolution of species during fuel decomposition; new ignition delay data that show variability in the hot ignition region with DCN; refinement and documentation of the HyChem modeling approach; and exploration of alternate methods for reduction of chemical kinetic mechanisms.
- The *Common Format (CFR) Working Group* develops tools from academic research that Original Equipment Manufacturers (OEMs) can use to evaluate potential fuel effects in proprietary combustor configurations. In this way, OEMs can utilize the most recent research advances to evaluate fuel property effects in geometries not typically available in research institutions. During the past year of the NJFCP the CFR Working Group has developed and delivered a GUI which can tabulate Flamelet prolongation of the intrinsic low-dimensional manifold (FPI) and Flamelet progress variable (FPV).

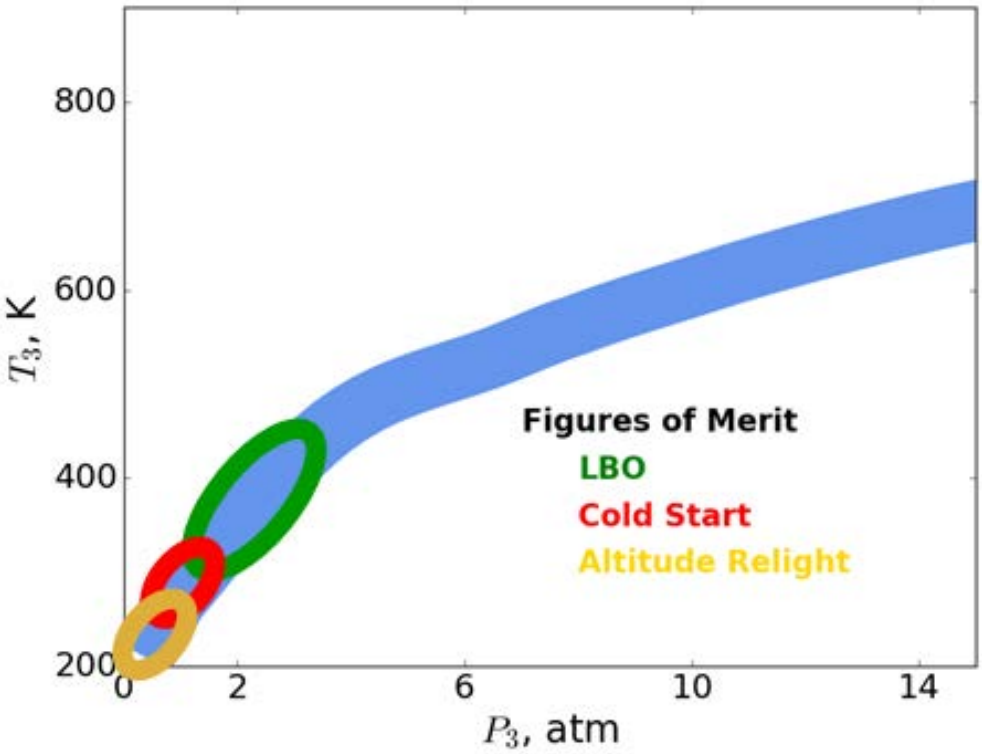


Figure 1. T_3-P_3 conditions, which are the temperature and pressure at the inlet to the combustor, for measuring the Figure of Merit (FOM) behavior. Targeted Lean Blowout (LBO), Cold Start, and High Altitude Ignition conditions are given as 2-4 atm and 400-450 K, 1 atm and 255-350 K, and >0.25 atm and >230 K for each FOM respectively. Initial experimental capabilities allowed for experiments at LBO conditions vs. the other FOM.

Summary of Technical Results

Fuels

As described in previous papers[1,3–5], three conventional (petroleum-derived) fuels and various test fuels, with components from or representing molecules present in alternative fuels, have been identified to span the range of conventional and extreme alternative fuel combustion behavior. Brief descriptions and illustrations of key properties of these fuels are provided in Table 1 and Figure 2. In this way, the three conventional fuels are intended to exhibit 'best,' 'average,' and 'worst' case combustion behavior based on their relative aromatic content, flash point, and viscosity. Further, the various alternative test or 'designed' fuels represent a range of fuel properties and compositions expected from alternative fuel processes. Seven additional test fuels in three groups became available in 2017. The first group (C-7, C-8, C-9) were designed to explore new regions of composition/property space as shown in Table 1. Three other test fuels were original developed by Haltermann for the Army Research Laboratory (ARL), and were designed to have relatively constant physical properties (such as viscosity, flash point, etc.) but widely varying derived cetane numbers (31, 45, 54) as shown in Table 2. These fuels are designed to be used to verify cetane number effects since the C-1 fuel has too many varying properties, other than low cetane. The last test fuel is a new "surrogate" fuel that is enabled by recent acquisition of "*iso*-dodecane", which replaces *iso*-octane in the first two surrogates. i*so*-Octane significantly impacts flash point and initial boiling point, which can have uncertain effects on combustion behavior.



Table 1. NJFCP category A and C fuels targeted to be tested in as many rigs as possible. The Category A fuels represent the range of petroleum-derived fuels currently in use today. A-1 was recommended as the 'best' fuel with low flash point, viscosity, and aromatics, A-2 as the 'nominal' jet fuel, and A-3 as the 'worst' with high flash point, viscosity, and aromatics. The Category C fuels represent alternative jet fuels that have normal to extreme properties.

Fuel/Solvent Mixture	POSF Number	Composition, % volume	Description
A-1	10264	Petroleum JP-8 (w/high flash point and low viscosity and aromatics)	Low flash, viscosity, and aromatics
A-2	10325	Petroleum Jet A	Nominal jet fuel
A-3	10289	Petroleum JP-5	High flash, viscosity, and aromatics
C-1	11498, 12368, 12384	Gevo ATJ, Highly branched C12 and C16 paraffins	Low DCN, unusual boiling range
C-2	11813, 12223	16% *tri*-methylbenzene + 84% C14 *iso*-paraffins	Chemically-asymmetric boiling range
C-3	12341, 12363	64% A-3 + 36% farnesane	High viscosity fuel, at viscosity limit for jet fuel at -20°C
C-4	12344, 12489	60% C9-12 *iso*-paraffins, 40% C-1	Low DCN, conventional, wide boiling range
C-5	12345, 12713, 12789, 12816	73% C10 *iso*-paraffins, 17% *tri*-methylbenzene	Flat boiling range
C-6		High cycloalkane content	High *cyclo*-paraffins
C-7	12925	75% RP-2, 23% A-3, 2% decalin	High *cyclo*-alkanes
C-8	12923	Jet A + Exxon aromatic blend	High (maximum allowable) aromatics
C-9	12933	80% R-8 HEFA, 20% *n*-C12	High DCN

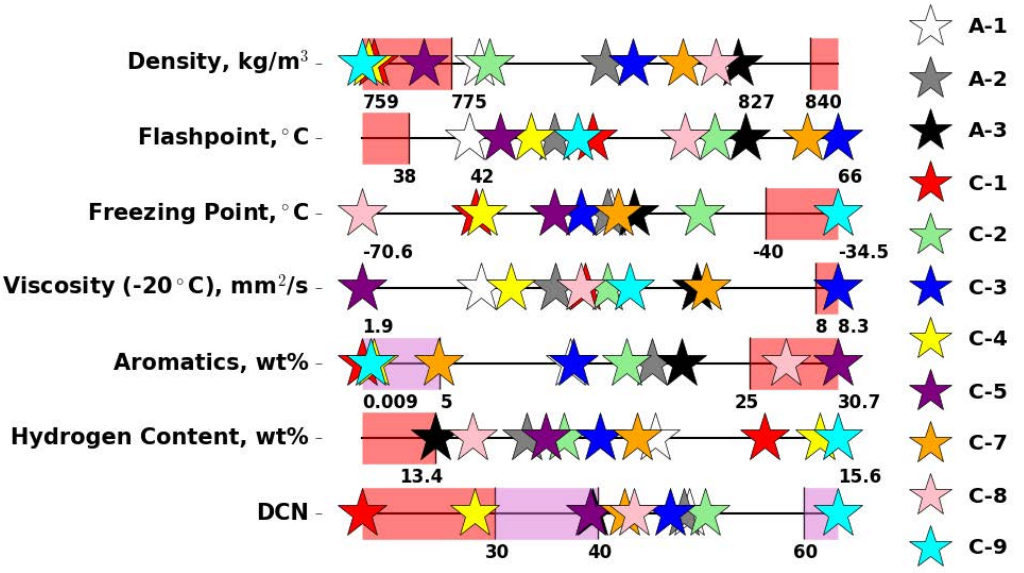


Figure 2. Category A and C range of fuel properties. Red regions represent established limits while purple areas represent proposed limits or areas to explore further. Category A fuels set the bounds of what is currently being used compared to the alternative jet fuel property ranges represented by the Category C fuels.



Table 2. Fuels blended to target specific fuel effects in experiments. These fuels were made to stress specific fuel characteristics at the key FOM. 'F' fuels are defined as blends of other NJFCP category 'A' and 'C' fuels. 'S' fuels are surrogate fuels blended to match certain combustion performance characteristics of A-2.

F-1	80/20 A-2/C-2	Blends
F-2	50/50 A-2/C-1	Blends
F-3	20/80 A-2/C-1	Blends
F-4	80/20 A-2/C-5	Blends
n-C12	n-C12	High DCN
n-C12/n-C16 mix	71.6% *n*-C12, 28.4% *n*-C16	High molecular weight blend
n-C12/M-xylene mix	75% *n*-C12, 25% *m*-xylene	Aromatic
n-C7	*n*-C7	High DCN, low molecular weight
n-C7/n-C12 mix	31.2% *n*-C7, 68.8% *n*-C12	Normal paraffin
n-C12/MCH mix	71.6% *n*-C12, 28.4% MCH	*Cyclo*-paraffin
n-C7/n-C16 mix	73.5% *n*-C7, 26.5% *n*-C16	Wide boiling range
Sasol (IPK)	~88% *iso*-alkanes, 12% cycloalkanes, 0.4% aromatic	Highly branched, low DCN
n-C12/i-C8 mix	69.1% *n*-C12, 30.9% *i*-C8	Branched paraffin
S-1	59.3/18.4/22.2 vol% *n*-dodecane/ *iso*-octane/ 1,3,5-*tri*-methylbenzene	Similar to A-2, lower density and average molecular weight
S-2	52.6/25.1/22.2 vol % *n*-hexadecane/ *iso*-octane/ 1,3,5-*tri*-methylbenzene	Similar to A-2, higher density and average molecular weight
S-3	34.3/17.4/26.7/21.5 vol% *n*-C12, *n*-hexadecane, PMH-*iso*-C10 (*penta*-methyl heptane), *tri*-methyl benzene	Similar to other surrogate fuels with less desirable initial boiling point and flash point properties
HTSI	53.7/17.6/28.8 vol% HRJ Camelina (POSF 10301), NORPAR 13 Solvent, Aromatics 100 (POSF12364)	High TSI, otherwise similar to A-2
Jet A – 55 CN	Nearly constant fuel properties with varying cetane numbers	High cetane (54)
Jet A 45 CN		Medium cetane (44)
Low Cetane Jet A 30 – 32		Low cetane (31)

In Figure 3 we report the total variation in category A and C fuels, and the correlation of properties amongst each other. The relative chemical composition and viscosity of the fuels varies the most across the category A and C fuels in terms of relative variation to A-2. Heats of combustion (both volumetric and mass), density, and surface tension vary the least across category A and C fuels. Perhaps a result of the jet fuel specifications, properties that are required to be within specific limits vary the least across category A and C fuels, while properties not specified in the specification vary the most with the exceptions of viscosity and aromatics.

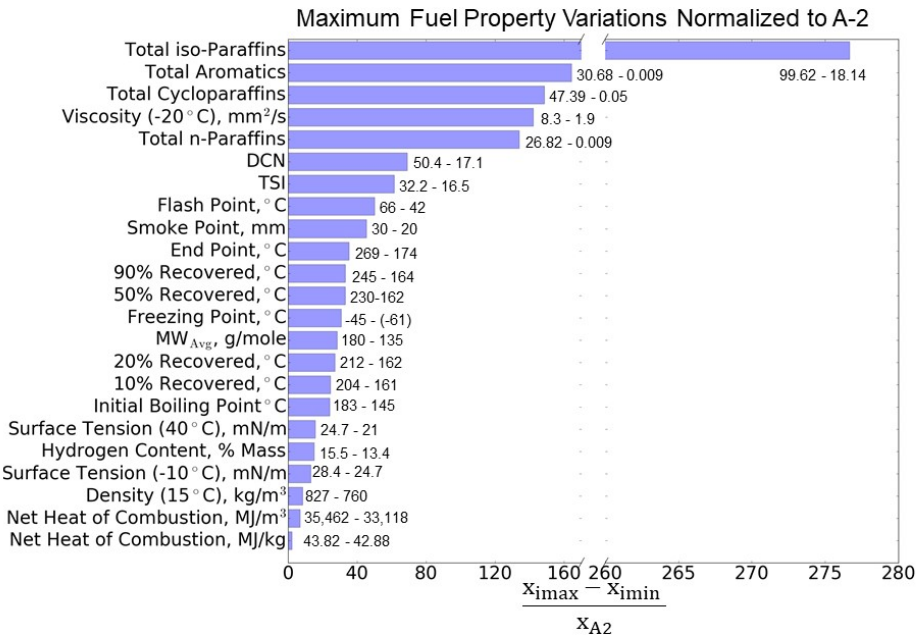


Figure 3. The maximum fuel property variations for Category A and C-1 through C-5 fuels. X_i represents a specific fuel property for a fuel while x_{A2} represents the fuel property for A-2. Chemical properties such as total *iso*-paraffins have the most relative variation while net heat of combustion for the fuels has the least. Knowing which properties vary the greatest can help when considering the bounds for new fuel blends to stress key combustion properties.

Properties are correlated across category A and C fuels via Pearson Correlation coefficients in Figure 4. Properties that are strongly positively/negatively correlated are represented with a large blue/red colored circle, with larger circles expressing more correlation and the absence of a circle expressing no correlation. These properties can be categorized correspondingly as volatility, physical properties, and chemical properties. The volatility properties relate to the distillate properties of the fuel which related to vaporization potential. The physical properties here refer to the viscosity, density, freeze point, average molecular weight, and surface tension. The physical properties most strongly impact the spray character and droplet breakup of a fuel. Finally, the chemical properties here refer to the chemical composition, DCN, H/C ratio, and the heat of combustion. In the subsequent random forest regression analysis, the cross correlation of properties can convolute interpretations of the regressions. Broadly, Figure 4 results show:

- all volatility-volatility properties (e.g. distillation fractions and flash point) are positively correlated;
- physical-volatility property correlations, with the minor exception of freezing point and initial distillation point, are positively correlated;
- the physical-physical properties of viscosity-molecular weight and surface tension-density are correlated;
- chemical-volatility and chemical-physical properties are largely uncorrelated except for DCN-freeze point and *n*-paraffins-freeze point; and
- several chemical-chemical properties are most strongly correlated with H/C ratio which is correlated with H_C, aromatics, and *iso*-paraffins respectively.

These correlations are important later in the paper while interpreting the Random Forest Regression plots which express the relative importance in predicting a FOM performance characteristic with a given fuel property.

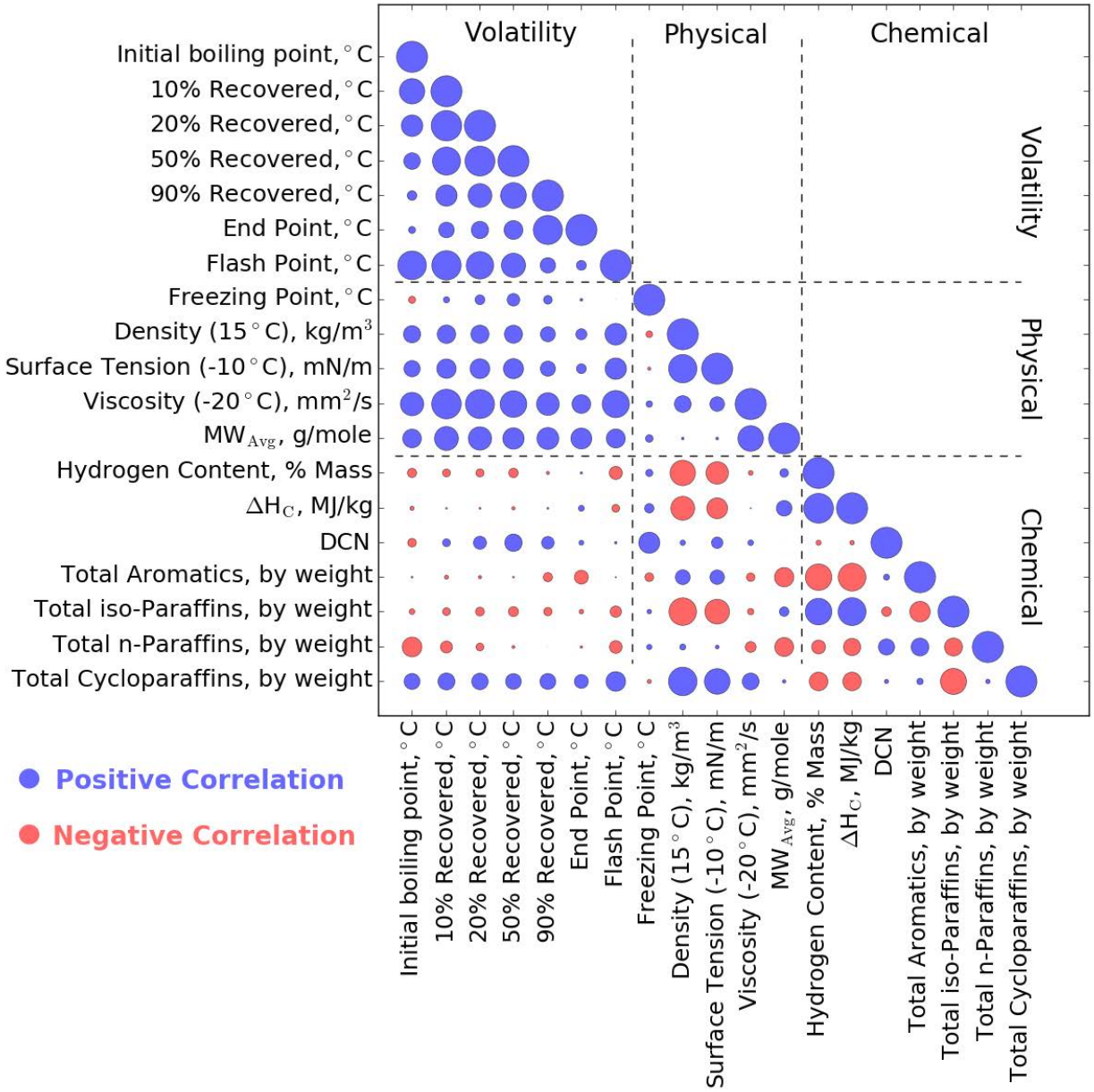


Figure 4. Pearson Correlation of Category A and C fuel properties. Marker size scales with the absolute Pearson Correlation between fuel properties, from zero to one. Positive correlations are marked in blue while negative correlations are marked in red. The properties are further broken down into volatility (distillate), physical, and chemical properties.

Lean Blowout (LBO)

LBO historically has been studied by Lefebvre and Mellor[6,7]. Lefebvre compared the relative LBO limits of a fuel based on the relative properties of a fuel to JP-4[6], which culminated in Eq. (1).

$$FAR_{LBO} = \underset{(i)}{\left[\frac{A}{V_{pz}}\right]} \quad \underset{(ii)}{\left[\frac{\dot{m}_A}{P_3^{1.3} e^{(T_3/300)}}\right]} \quad \underset{(iii)}{\left[\frac{D_r^2}{\lambda_r H_r}\right]} \tag{1}$$

Eq. (1) can be considered as three separate terms each nominally representing orthogonal effects that lead to LBO. The first term, (*i*), captures the relative effect that a combustor geometry can have on the relative LBO with A being an empirical fit and V_{pz} representing the primary combustion zone of the combustor. The second term, (*ii*), represents the effect that the mass flow rate ($\dot{m}_A$) which effects the fluid dynamics of the combustion chamber, the pressure in the combustion chamber (P_3), and the inlet temperature to the combustion chamber (T_3) which effects the chemical kinetic rates. The final term, (*iii*), represents the effect of fuel properties with D_r being the relative droplet size to JP-4, λ_r being the relative mass transfer coefficient of the fuel versus JP-4, and H_r being the relative heat of combustion as compared to JP-4. Combine these properties have been shown to reproduce experimental data fairly well for historical conventional fuels.

Work reported by Plee and Mellor focused on evaluating the relative time scales for various processes. The work of Burger[8] more recently showed the relative effect of chemical and evaporative time scales with the chemical kinetic time scale of autoignition dominating the LBO stability limit at high loading parameters. Conversely, at low loading parameters the evaporative time scales dominated the stability limit. Similarly, last year we reported the stability limit for numerous NJFCP rigs at FOM conditions were dominated by the DCN, a property of a fuel's autoignition chemistry[2]. Hence, analysis reported last year, and more so this year, focuses on fuel chemistry effects that are not incorporated into Eq (1). This equation was derived following results of historical conventional fuels which have much less chemical variations as compared to the variations we currently have in the NJFCP. The result of these previous studies can be illustrated phenomenologically as Figure 5.

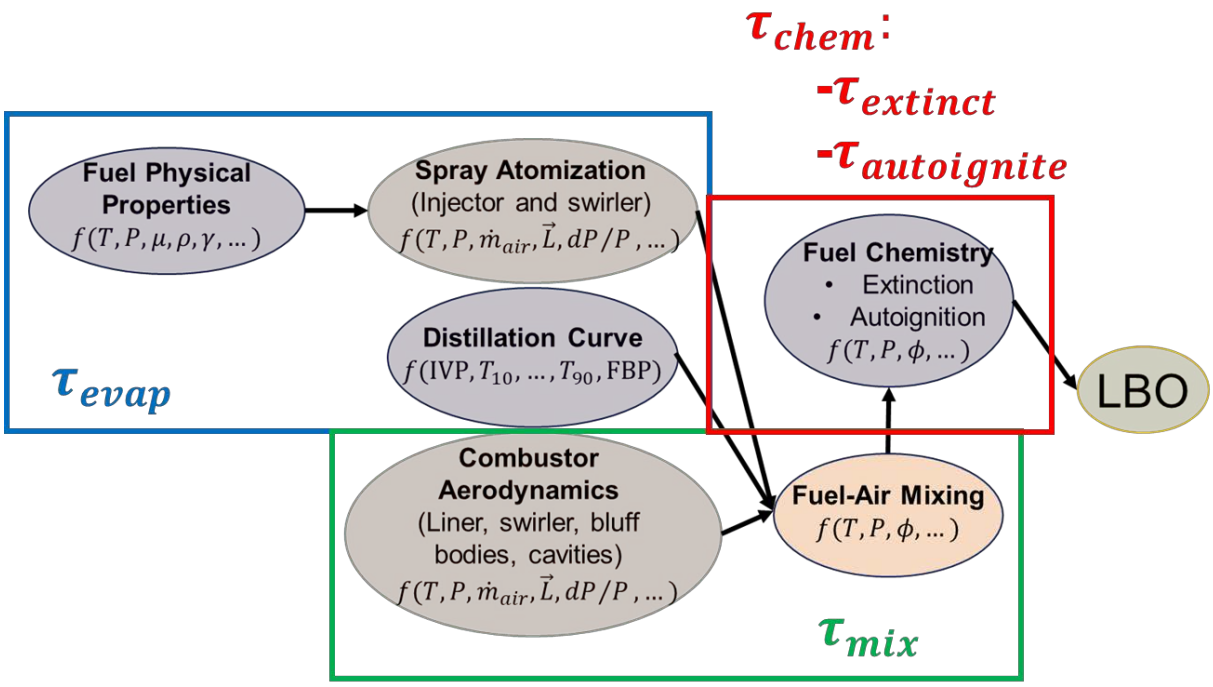


Figure 5. Phenomenological illustration of possible paths to LBO. Three generic time scales define stability with the limit determined by the longest time scale. The orange ovals are more associated with non-fuel property effects. The purple ovals are phenomena associated with fuel effects.



LBO thus scales with the inverse sum of each of the time scales boxed in Figure 5, see Eq. (2).

$$\boldsymbol{\phi_{LBO_i}} \backsim \left[\left(\frac{1}{\tau_{evap_i}} + \frac{1}{\tau_{mix_i}} + \frac{1}{\tau_{chem_i}}\right)\right]^{-1} \quad (2)$$

Here τ_{evap_i} is the time scale associated with fuel *i*'s droplets evaporating which is affected by thermodynamic, spray atomization and distillation curve properties of the combustor. The τ_{mix} time scale is the characteristic time to mix the fuel and air mixtures. This time scale is again dependent on thermodynamic parameters (T and P),, geometries ($\vec{L}$), equivalence ratios (ϕ), and the pressure drop (dP/P) across the swirler and liner. Finally, the chemical time scale can be interpreted as at least two characteristic time scales: an autoignition ($\tau_{autoignite}$) and extinction ($\tau_{extinct}$) time scale, dependent on the fuel and the local equivalence ratio (ϕ). The autoignition time scale here refers to the time needed to time needed to raise the temperature locally from a temperature below the critical H+O_2 chain branching temperature to above it in the absence of sufficient heat or mass transfer to initiate or propagate a flame. Finally, it should also be noted that in reality there could be layered or nested timescales within each of these broadly defined time scales.

A brief description of the rigs to study such phenomena and results are detailed in other publications[8–17], listed in Table 3 and Table 4, and test conditions are illustrated in Figure 6. Eight of the ten rigs in the NJFCP are able to determine LBO limit by reducing flowrates until combustor extinction. The other NJFCP rigs used to study LBO measure emissions as LBO is approached and measure incipient extinction – and not LBO – in the case of the NASA LDI rig and the Oregon State turbulent flame speed rig, respectively.

This year we report the culmination of data from 10 rigs associated with the NJFCP. Figure 7 reports LBO data as a Box and Whisker Plot for NJFCP fuels at conditions near those identified in Figure 1. Φ on the y-axis of the figure is the percent difference of a given fuel relative to the mean $\phi(LBO)$ of A-2, and is defined mathematically as:

$$\boldsymbol{\Phi} = \frac{\boldsymbol{\phi(LBO_i)} - \bar{\boldsymbol{\phi}}\boldsymbol{(LBO_{A2})}}{\bar{\boldsymbol{\phi}}\boldsymbol{(LBO_{A2})}} \quad (3)$$

where $\phi(LBO_i)$ is a single LBO event for fuel *i* and $\bar{\phi}(LBO_{A2})$ is the mean LBO ϕ for A-2. This normalization accounts for variations across rigs in dilution air and other combustor design characteristics. The symbols represent individual LBO observations, the whiskers of the plot represent the upper and lower 99.1% confidence intervals, the lower and upper limits of the shaded rectangles are the 25 and 75 percentiles respectively, data points outside the whiskers are outliers, and median is represented by the horizontal line in the rectangle for the percent difference relative to the nominal jet fuel (A-2). Values of $\Phi > 0$, for a given fuel, are LBO events with a $\phi(LBO_i)$ greater than the mean LBO ϕ of A-2. Thus, the stability of the fuel is worse than A-2. Inversely, $\Phi < 0$ is considered more stable LBO behavior as the fuel was able to stabilize in the rig at a lower equivalence ratio. This plot shows statistically the variation in the conventional (category A) fuels versus the observations with the alternative (category C) fuels. Statistically, only C-1 and C-4 are outside the LBO performance of all the category A fuels for the Referee Rig as the upper whiskers of the category A fuels do not overlap the lower whiskers of C-1 and C-4. Similarly, C-1 is observed to have distinguishable LBO performance for the GT rigs and the WSR. The Honeywell APU, however, does not exhibit this behavior with no category C fuels performing worse than the conventional fuels.

Analysis of these rigs suggests that the Derived Cetane Number (DCN) is the best predictor for combustor stability, see Figure 8. Eight of 9 rigs that measure LBO or the onset of it show strong correlations with DCN. Seven of the 8 rigs that can directly measure LBO also show this trend. In the case of several rigs, an $R^2 > 0.9$ is achieved by a simple one dimensional regression versus LBO. Further, Random Forest Analysis combining measured fuel properties with LBO data corroborates the dependency of LBO on DCN, see Figure 9. Additional Random Forest Analysis regressions are reported in the Task 4 Appendix. While to first order the LBO trends well with DCN, Random Forest Regressions show deviations across rigs and devices. Collectively, these results strongly corroborate our previous results and those more recently reported by Burger, and that the chemical time scale for autoignition is the limitation for combustor stability. More detailed studies have been performed at Georgia Tech to investigate the potential effect of autoignition[9]. This work focused on measuring the chemiluminescence in the rig near blow out. Movies of these diagnostics appear to show the approach to LBO being a two stage process, the first stage being the transition of a local signal to the absence of one, local extinction. Local extinction then begins to dominate the frame as fuel flow is sequentially reduced. During the progression of increasing local extinction, local autoignition appears in regions with no initial signal at earlier times. Thus,



the limit of the rig sustaining any combustion is when autoignition ceases to occur. The Georgia Tech team also reported that at a given ϕ above the LBO limit an indefinite series of autoignition-extinction events could be observed.

Additional regression parameters are observed to be important such as the relative atomizer and rig geometry as illustrated in Figure 9. These parameters and the subsequent Random Forest regressions in the Task 4 Appendix show that, while DCN is shown to be a common parameter determining the LBO limit, the regressions between two rigs can be drastically different. This is partially illustrated in Figure 10 which compares the slope of the lines in Figure 8 for various rigs. The most sensitive rig to LBO is the Sheffield rig, and the least sensitive rig to LBO is the prevaporized and premixed WSR.

Finally, the Honeywell rig, which showed no correlation between DCN and LBO, has shown to have different geometrical characteristics. The Honeywell rig has an Axillary Power Unit (APU) combustor geometry. Thus, the size is overall smaller than the other rigs which represent a more main engine size and configuration. The smaller size in turn means there is no swirler to generate a primary recirculation zone as in the Referee Rig, and the flow number of the nozzle is smaller than the corresponding Referee Rig. These features combine to make physical properties of the fuel drastically more important, see Figure 23 located in the Appendix to this section.

Table 3. Summary of LBO rigs and test conditions. LBO results for each rig are detailed in these papers[8-18].

Rig Name	Geometry type (injector/swirler)	T_{air}	T_{fuel}	P	Institution
PA-GT	Pressure atomizer/ Pratt & Whitney Swirler	550, 450, 300 K	445-460 K	3.4 atm	Georgia Tech
AA-GT	Air blast atomizer/ Pratt & Whitney Swirler	450 K	445-460 K	3.4 atm	Georgia Tech
PA-HON	Pressure atomizer/ toroidal	324, 525, 557, 562, 394 K	288 K	1, 1.3, 1.4, 3.3, 5.7, 2 atm	Honeywell
PA-RR	Pressure atomizer/ High-Swirl (P03)	400 K	320 K	2 atm	AFRL/UDRI
PV-WSR	Prevaporized/ toroidal	450 K	450 K	1 atm	AFRL/UDRI
LDI-NASA	Lean Direct Injection/ swirl stabilized	575, 645, 730, 830 K		6.8, 10.9, 17 atm	NASA
AA-SH	Airblast atomizer/ swirler stabilized/Rolls-Royce Tay Combustor	323, 373, 423 K		1atm	Sheffield
PA-OSU	Pressure atomizer/ swirl stabilized	470 K		1 atm	Oregon State
PA-CAM	Pressure in bluff-body/	340 K	300 K	1 atm	Cambridge
PA - UTRC	Pressure atomizer/ Pratt & Whitney Swirler	555, 494 K		8.64, 5.6 atm	UTRC
PA-DLR	Pressure atomizer/ swirl stabilized	323, 373 K		1 atm	DLR Germany

*Future analysis of GT data is only for the 450 K testing.



Table 4. LBO rigs and fuels tested. Bolded fuels were tested in the last year for Sheffield and Cambridge. Non-NJFCP fuels tested at UTRC and DLR Germany are listed in the table as well and included in some of the LBO results presented in this paper.

	A-1	A-2	A-3	C-1	C-2	C-3	C-4	C-5	F-1	F-2	F-3	F-4	S-1	S-2	nC12
GT	X	X	X	X	X	X	X	X	X	X	X		X	X	X
Honeywell	X	X	X	X	X			X							
Referee Rig	X	X	X	X	X	X	X	X	X	X	X	X	X	X	X
WSR		X	X	X			X	X							X
NASA		X		X		X									
Sheffield	**X**	**X**	**X**	**X**		**X**	**X**	**X**							
Oregon State		X		X				X							
Cambridge		**X**		**X**				**X**							
UTRC	**Sasol IPK, F-76, L-210, JP-5, Jet-A, L-142, HRJ JP-5, Linpar 1416**														
DLR	**Crude-derived Jet A-1,Jet A-1 + 50% n-dodecane, FSJF (certification), FSJF (commercial), FSJF (commercial) + 1.5% HCPP, Experimental GTL kerosene, Synthetic paraffinic kerosene (SPK), Heavy naphtha refinery stream**														

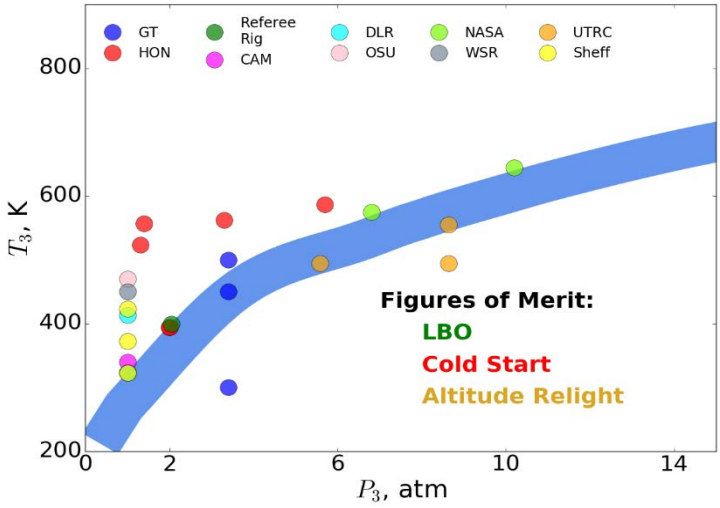


Figure 6. P_3-T_3 figure displaying the rig conditions tested to measure LBO, one of the Figures of Merit (FOM), for Georgia Tech (GT), Honeywell (HON), Referee Rig, Cambridge (CAM), DLR Germany (DLR), Oregon State University (OSU), NASA, the Well-Stirred Reactor (WSR), United Technologies Research Center (UTRC), and the University of Sheffield (Sheff). LBO test conditions fall within 2-4 atm and 400-450 K for main engines. APU LBO conditions can vary as evident from the elevated T3s and lower P3s tested here.

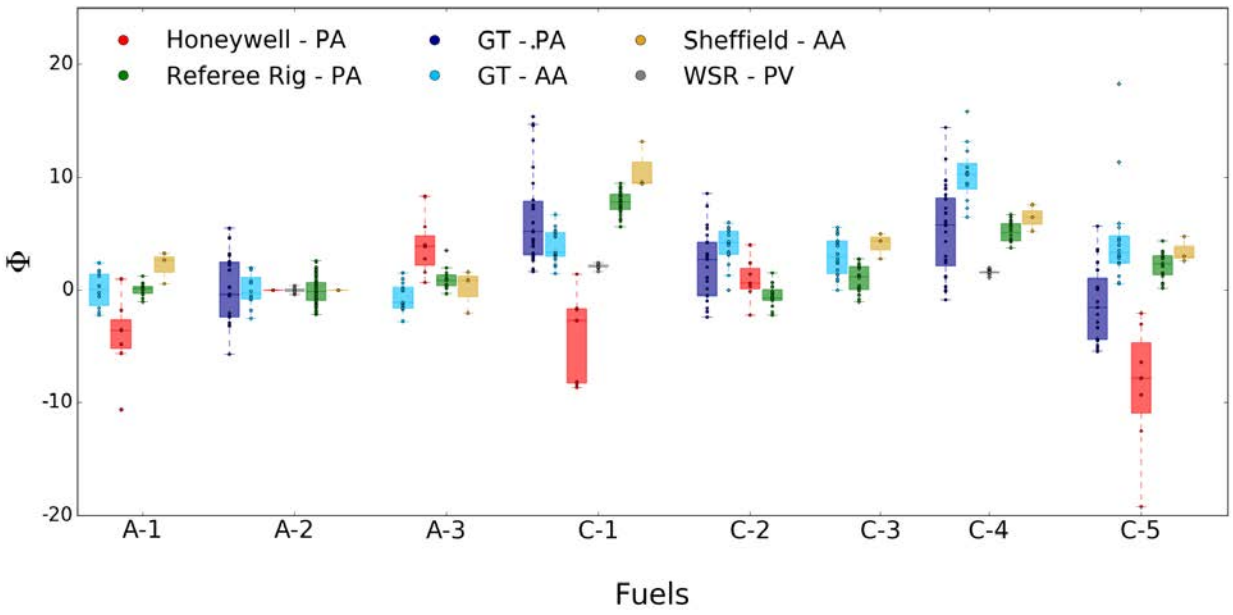


Figure 7. Box plot of LBO percent differences for NJFCP fuels across various rigs. PA (pressure atomized), AA (airblast atomized), PV (pre-vaporized), refers to the vaporizing mechanism used in the respective rigs. Honeywell, Referee Rig, GT (Georgia Tech), Sheffield (University if Sheffield), and WSR (Well-Stirred Reactor) refer to the respective institutions and/or rig at which the fuels where tested. The scatter for LBO percent difference can be observed for each rig for the category A and category C fuels where the circles represent individual data points and the box represents the lower and upper quartiles along with the median. Data that falls outside of the box and lines represents outliers. While C-1 and C-4 have the overall highest LBO equivalence ratio, variability among tests are still largely greater than the LBO differences observed among the fuels.

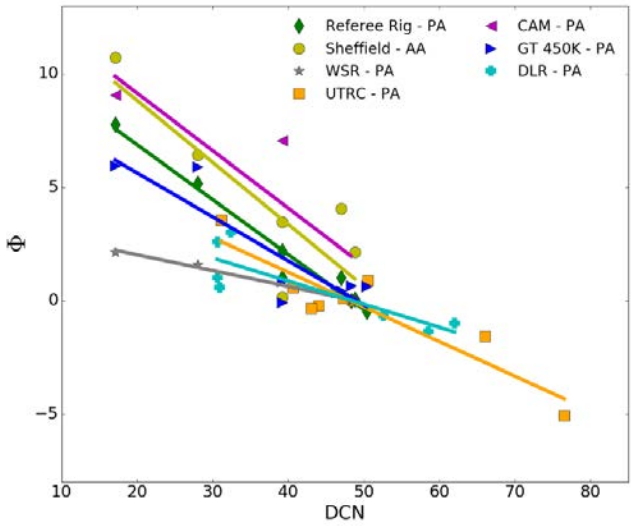


Figure 8. Relative LBO rig sensitivity to DCN. Currently, 7 of the 8 rigs that directly measure LBO show first order sensitivity to DCN. The Honeywell rig is the only one that is not stabilized with a swirler and has a low flow number injector. It does not show the sensitivity to DCN and is not plotted here.

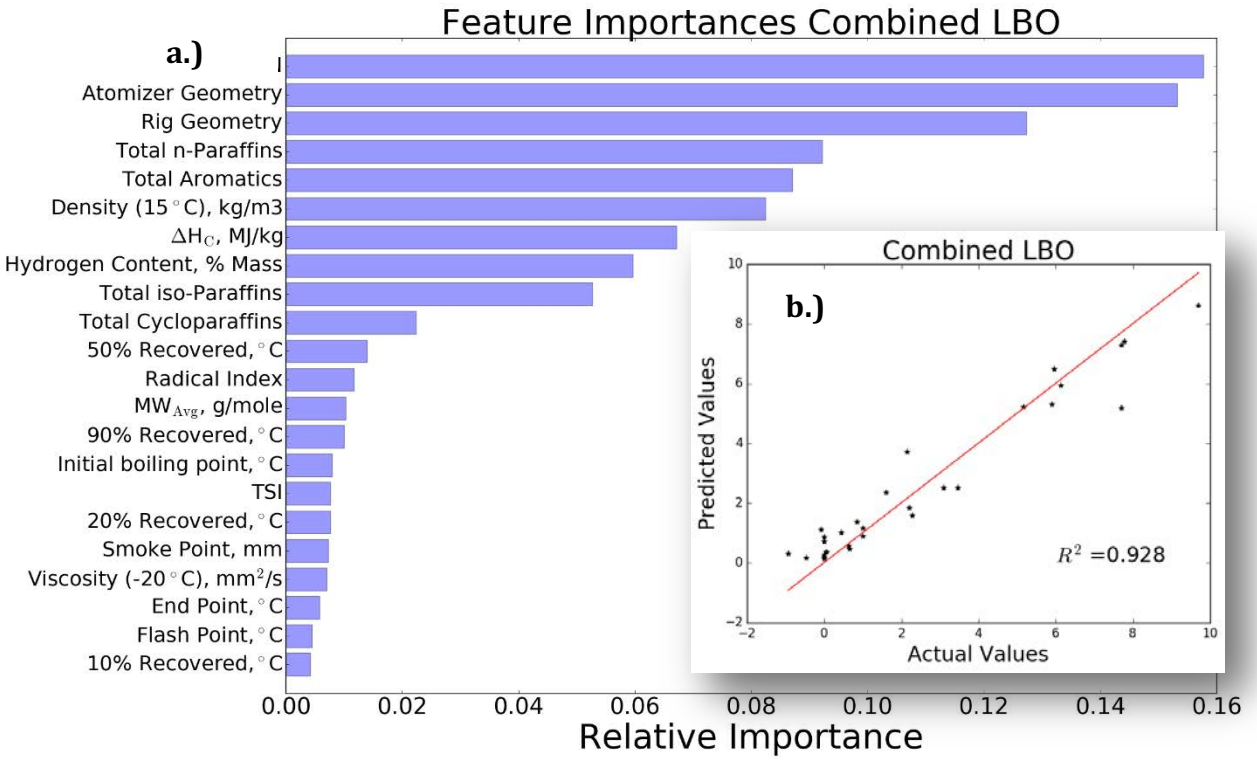


Figure 9. Random Forest regression feature importance and fit for combined LBO. a.) DCN is the most important factor in determining LBO when looking at the combined results from the Referee Rig, Georgia Tech, University of Sheffield, Oregon State and the Well-Stirred Reactor. b.) The predicted versus measured (actual) values for combined LBO for the five rigs included.

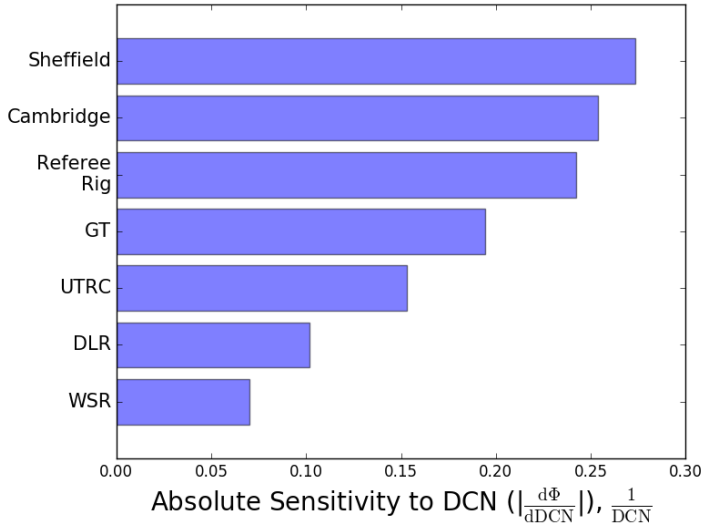


Figure 10. Absolute rig sensitivity to DCN for LBO. Comparing sensitivities across rigs, Sheffield shows the highest sensitivity to DCN while the Well-Stirred Reactor (WSR) shows the least sensitivity.



Ignition

Ignition is a critical performance metric for alternative fuel certification as the consequences of an unsuccessful relight in flight could be catastrophic. Thus, similar to LBO, the ignition performance of an alternative fuel undergoing certification must be equivalent or, preferably, better than typical conventional fuels. Historically, the certification of previous alternative fuels and experience has yielded the criteria that a fuel must have a viscosity less than 12 cSt at -40 ^{0}F. This criteria is required to enable sufficient spray performance to ignite. Not only do these cold conditions deleteriously effect the spray character, they also can inhibit the ability of a fuel to form a combustible mixture with air as the vapor pressure of the fuel is lower at lower temperatures. Testing fuels at the appropriate conditions is essential to mapping laboratory performance to real engines and the certification process. Year 2 of the NJFCP has largely been devoted to capacity development for these cold air and fuel at sub-atmospheric conditions. Table 5 and Table 6 report conditions, brief descriptions of rigs, and fuels tested in rigs associated with the NJFCP. Nominally, rigs are designed with the intention of matching the FOM conditions in Figure 1. Data from the Referee Rig and Cambridge ignition studies are still in process and will not be reported here, although a recent paper details the Referee Rig progress on ignition[19]. Figure 11 reports the air temperatures and pressures of experiments on the T_3-P_3 plot reported earlier. Figure 12 reports the fuel temperatures the individual rigs are capable of testing at. Here we present nominal ignition results and their analysis from 4 different rigs: 2 combustor rigs and 2 more fundamental configuration.

Combustor rig test comparisons at Honeywell (APU combustor)[11] and NRC Canada (TRS18 engine)[20] are reported in Figure 13. These rigs are compared on the basis of minimum equivalence ratios for ignition as Box and Whisker plots. Unlike the previous LBO plot which illustrated results at a given condition, these results are for multiple conditions, see Figure 11, and the normalization of Φ for each point is at similar conditions. Fuels with minimum equivalence ratios (Φs) greater than zero once again have deleterious performance characteristics relative to A-2. Category C fuels with lower whiskers above the highest whisker of category A fuels are statistically distinct. The Honeywell rig did not observe any category C fuels that performed worse that the worst category A fuel (A-3). However, the C-3 results from NRC Canada did produce worse ignition performance than any of the tested category A fuels. It should be noted that NRC Canada did not test A-3 which is considered the 'worst' conventional fuel in the NJFCP, and the C-3 fuel was not tested at Honeywell. Random Forest regressions of the NRC Canada and Honeywell data (Figure 14) suggest that the properties most effecting minimum ignition equivalence ratios are viscosity and volatility/distillate properties. C-3 is a blend containing 64% of A-3 and 36% farnesane, suggesting that the results between the two rigs are largely consistent.

Figure 15 reports relative ignition probabilities for several NJFCP fuels at a fixed equivalence ratio[21,22] at atmospheric pressure and at air temperatures of 478 K and 300 K for the prevaporized and liquid spray tests, respectively. The prevaporized fuel temperatures were around 450 K while the liquid spray was injected at 295 K. The probabilities as reported here are the single spark ignition probabilities determined from multiple ignition attempts. Two types of experiments are reported with one experimental configuration being prevaporized and partially premixed, while the other configuration employed a liquid spray jet. The deleterious fuel effects in this plot are associated with negative values on the y-axis. Interpretations from the spray configuration are preliminary and may change upon further analysis. Interestingly, A-3 is observed to perform better than all the category A and C fuels for the spray experiments. The prevaporized and partially premixed ignition experiments (GT PV) in Figure 15 show little fuel effect influence.

Additional cold fuel and air experiments at or below one atmosphere are being analyzed for two Referee Rig type geometries at AFRL/UDRI and ARL/UIUC. Preliminary analysis of these data sets suggest general consistencies with the Honeywell and NRC Canada results. Spray quality and fuel volatility via viscosity and distillation curve, respectively, determine the relative ignitability of a fuel. The implications for the fuel certification process is that alternative fuels preferably exhibit lower viscosities and higher volatilities to ensure safe and functional operability during altitude relight and cold start.

Table 5. Summary of ignition rigs and conditions tested. Ignition results for each rig are detailed in these papers[10,11,18-22].

Rig Name	Rig Description	Ignition Source	T_{air}	T_{fuel}	P	Institution
NRC-CAN	Pressure atomizer in a small gas turbine engine (TRS-18)	Discharge	254 to 268 K	254 to 268 K	10-17 kft	NRC-CAN
Honeywell	Pressure Atomizer in APU	Discharge	230 to 317 K	236 and 288 K	0.2 to 1.1 atm	Honeywell
Cambridge	Partially Prevaporized flow Rig	Laser (YAG)	323 to 373 K		1 atm	Cambridge
GT – PV	Prevaporized fuel/air flow split from air coflow	Discharge	478 K	450 K	0.96 atm	Georgia Tech
Referee Rig	Pressure atomizer, high swirl	APU Igniter	394 and 233 K	322 and 233 K	2 atm	AFRL/UDRI
GT – Spray	Pressure atomizer injected into air coflow	Discharge	300 K	244 and 295 K	0.96 atm	Georgia Tech

Table 6. Ignition rigs and fuels tested. Bolded fuels for the Referee Rig and Georgia Tech Spray are new fuels tested since last year.

	A-2	A-1	A-3	C-1	C-2	C-3	C-4	C-5
NRC-CAN	X			X		X		X
Honeywell	X	X	X	X	X			X
Cambridge	X			X				
GT – PV	X	X	X	X	X	X	X	X
Referee Rig	**X**	**X**	**X**	**X**				
GT – Spray	**X**	**X**	**X**	**X**	**X**	**X**	**X**	**X**

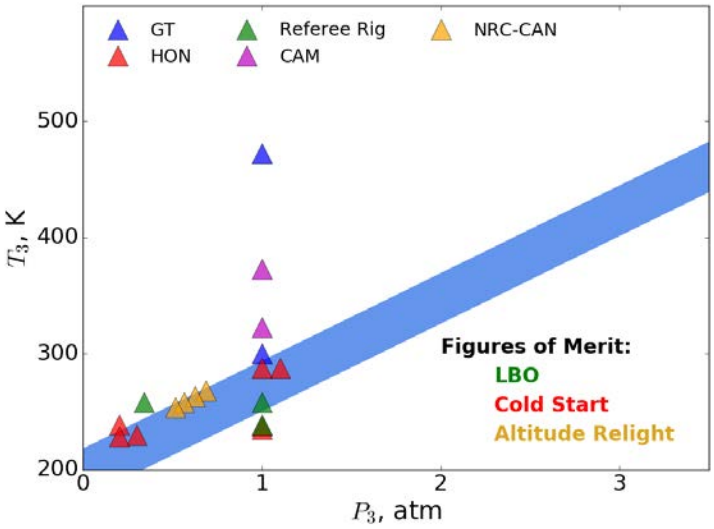


Figure 11. P_3-T_3 figure displaying the rig conditions tested to measure the Figures of Merit (FOM), specifically for the cold start ignition and altitude relight tests for Georgia Tech (GT), Honeywell (HON), Referee Rig, Cambridge (CAM), and NRC-Canada (NRC-CAN). Cold start and altitude relight conditions occur at 1 atm and 225-350 K, and >0.25 atm and >230 K, respectively.

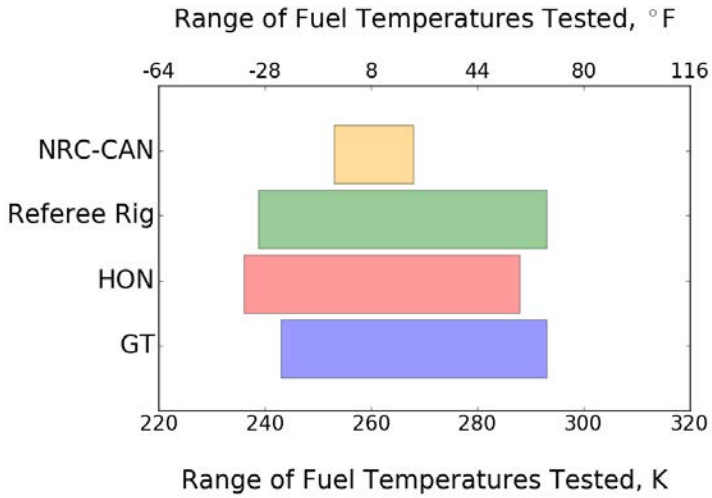


Figure 12. Range of fuel temperatures that were used in ignition testing from NRC Canada (NRC-CAN), Referee Rig, Honeywell (HON), and Georgia Tech (GT). Fuel temperatures heavily impact ignition performance as they change viscosity, surface tension, and density of the fuel making ignition more difficult at lower temperatures.

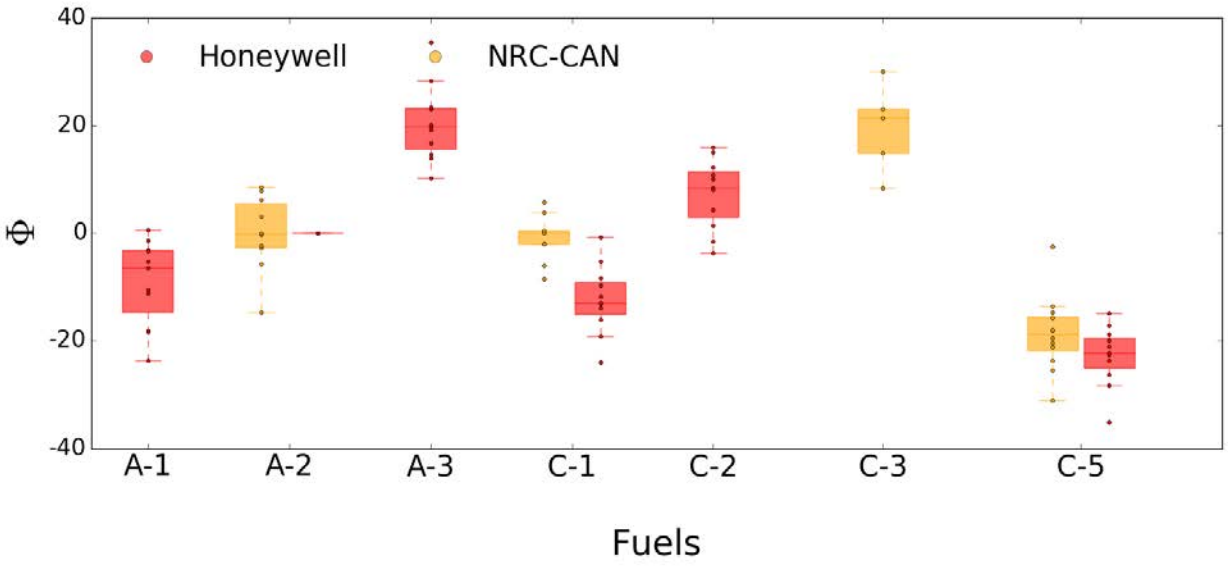


Figure 13. Honeywell and NRC Canada (NRC-CAN) ignition box plot of minimum normalized equivalence ratios for ignition. The circles represent individual data points while the box represents the median and lower and upper quartiles. Points that fall outside the box and line range are outliers. The Honeywell ignition data was collected at two different fuel temperatures (15˚C and -37˚C) at seven different inlet temperatures and pressures and was normalized to A-2 for each test condition. The NRC-Canada ignition data was collected at four different altitude conditions with a constant fuel temperature around -13˚C and was normalized to A-2 for each altitude condition. Of the seven fuels tested, A-3 and C-3 performed the worst, while C-5 performed the best for both Honeywell and NRC-Canada.

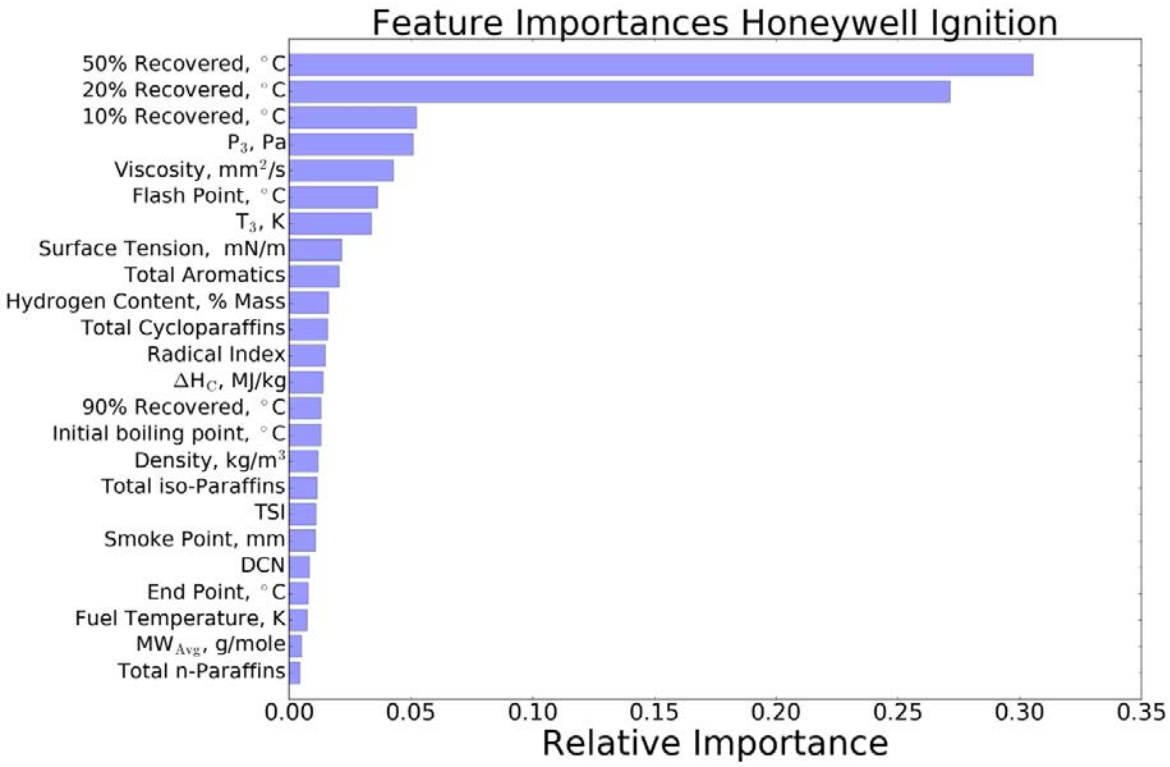


Figure 14. Random Forest regression feature importance and fit for minimum ignition FAR in a Honeywell APU. The physical properties, such as the distillation curve and viscosity, of the fuel dominate the relative ignition performance of a fuel in addition to the inlet pressure and temperature. The viscosity, surface tension, and density values used are based off of the temperature of the fuel tested. NOTE: Units have been intentionally renormalized such that these numbers are not relevant to actual operating limits.

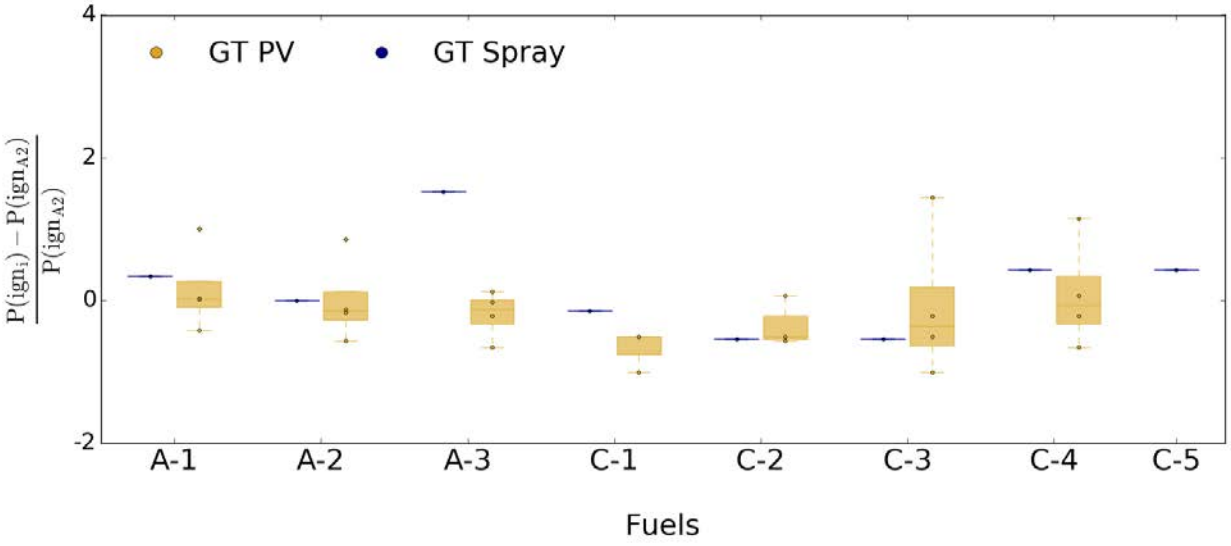


Figure 15. Georgia Tech Prevaporized (GT PV) and Georgia Tech Spray (GT Spray) ignition box plot of normalized probability of ignition. The circles represent individual data points while the box represents the median and low and upper quartiles. Points that fall outside of the box and line range are outliers. Instead of measuring ignition performance using minimum equivalence ratio to ignite, a fixed equivalence ratio for each test was used and the probability of ignition was measured. The Georgia Tech prevaporized ignition data included here was run at an equivalence ratio of 1.5-1.57 with an average test section temperature of 480 K and fuel vapor temperatures around 450 K. The Georgia Tech spray ignition data was run at an equivalence ratio of 0.55 with an air temperature of 300 K and fuel temperature of 295 K.

Computational Fluid Dynamics

Computational Fluid Dynamic (CFD) simulations of the combustion experiments conducted under this program were performed at several locations including Stanford University, Georgia Institute of Technology (GT), and United Technologies Research Center (UTRC). Current CFD simulations are focused on LBO predictions in the Area 6 referee rig for the NJFCP test fuels A-2, C-1 and C-5. Predictions of LBO fuel sensitivity were completed by Stanford using a Flamelet/progress-variable approach and spray injection based on Rosin-Rammler drop size distribution with secondary breakup included in the spray evolution[23]; these simulations predicted the LBO fuel trend for A-2 versus C-5 in agreement with experiments, but predicted the opposite LBO fuel trend for A-2 versus C-1 compared to experiments. Since January 2017, the three CFD teams have agreed on a consistent set of spray injection conditions for A-2, C-1 and C-5 based on non-reacting spray measurements conducted at Purdue University and provided by the Spray Working Group. PDPA data measured at 25mm downstream of the injector cup exit is projected upstream into six concentric rings at a location 2mm from the fuel nozzle exit and the experimental drop size distribution is randomly sampled in each ring in the CFD simulations. Spray velocity magnitude and direction at several radial locations based on the PDPA data are also used in the spray injection conditions for the CFD simulations. No secondary spray breakup is used in current simulations of approach to LBO. PDPA measurements at the near LBO condition in the referee rig are available to compare with CFD simulations. Chemistry models for the A-2, C-1 and C-5 test fuels employed in the CFD simulations are the full HyChem models, reduced models based on HyChem, or a set one-step mechanisms tuned to match HyChem predicted laminar flame speeds over a range of equivalence ratios.

Approach to LBO simulations for the Area 6 referee rig begin at the experimental near LBO condition (an equivalence ratio ϕ=0.096, or slightly higher if required to obtain a stable flame) for the A-2, C-1 and C-5 test fuels. Step reductions in fuel mass flow rate on the order of a 4% change in ϕ are performed after confirming that a stable flame exists at each new ϕ. Flame stability is evaluated in terms of time histories of integrated heat release rate (such as shown in Figure 16) and total evaporation rate oscillating about an essentially constant average value after an initial transient, as well as by inspection of contour plots of temperature and species concentration variables in cut planes through the center of the combustor

indicating a significant flame is still present in the combustor. All three teams have established stable flames at the near LBO condition using the new spray injection conditions. Improvements were seen in CFD predicted drop sizes and velocities compared to PDPA data at the near LBO condition using the new spray injection conditions. Simulations of approach to LBO are underway for the A-2 and C-1 test fuels. Also, while CFD work is currently focused on LBO predictions, initial simulations have begun on the forced ignition experiments in the Georgia Tech Prevaporized (GT PV) rig experiments[21] which track the evolution of ignition kernels (but not the establishment of a stable flame).

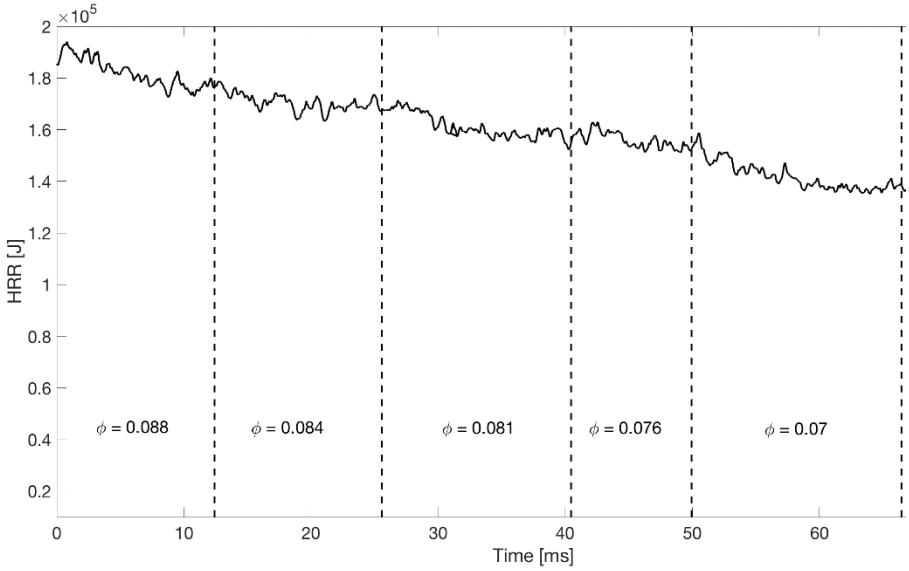


Figure 16. Time history of integrated heat release rate over entire CFD grid during approach to LBO simulations using step reductions in fuel mass flow rate for the A-2 fuel[24].

Common Format Routine

The performance evaluation of an alternative fuel has historically utilized OEM experimental hardware, which is costly. These tests are essential due to FOM dependency on rig geometries and otherwise proprietary information. And the proprietary information is critical to the proper comparison of an alternative jet fuel to conventional fuels. The CFD Working Group is iterating towards FOM evaluation methods using academic codes. Unfortunately, the CFD codes as written by the academic teams are not conducive to OEM usage. The codes maybe written in languages not standard in OEM workflows, and if they are, the formatting and communication between other engineering standard work by OEMs. A need is identified in the NJFCP to bridge this chasm between the latest CFD theory and codes and OEM standard work. For this reason, the Common Format Routine (CFR) Working Group was established to reformulate and package codes into software that can innately mesh with OEM modeling methods.

The current (CFD) evaluation of a jet fuel by the NJFCP involves many methods, models, and codes to represent essential chemistries, sprays, fluid dynamics, and other physics. Each of these physical models has its own impact on the evaluation of relative fuel performance. Year 2 of the NJFCP identified a critical need to develop a CFR for the development of two of these models: a flamelet prolongation of the intrinsic low-dimensional manifold (FPI) model, used for premixed combustion, and a flamelet progress variable (FPV) model, utilized for nonpremixed combustion[25]. These models previously did not exist for OEM standard work and provided an opportunity for more robust fuel evaluation of OEM hardware by OEMs.

Figure 17 displays the results of four model predictions (lines) and experimental values (red symbols) for the Sandia D flame. Blue lines represent the CFR models developed as part of the NJFCP for k-ϵ and k-ω RANS simulations, and black lines are those of the default FLUENT capabilities. The CFR model reproduced experimental data as well or better than the default FLUENT code, particularly for the k-ω simulations.

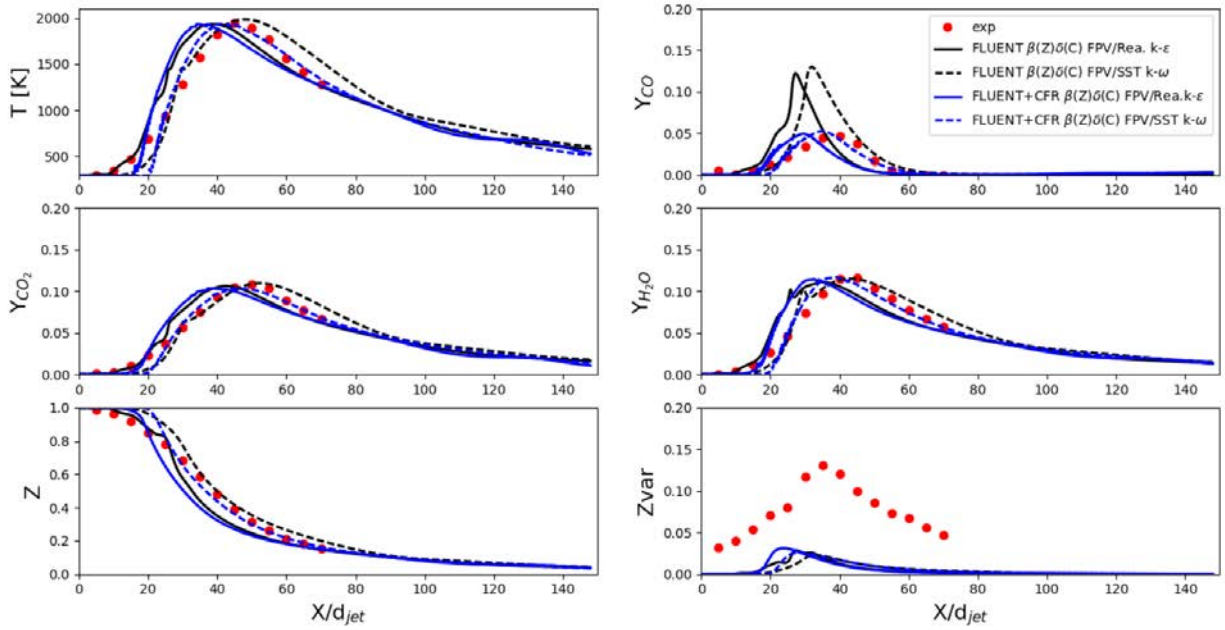


Figure 17. Centerline comparison between experiments and RANS simulations of the Sandia D turbulent flame. Reproduced from an anticipated publication[25].

In addition to model development, the CFR Working Group has packaged these codes into a Graphical User Interface (GUI) / Text-based User Interface (TUI) which removed the requirement that OEMs communicate with the software in a potentially non-native language.

Chemical Kinetics

Major accomplishments in the tracking of the chemical kinetics of fuels over the past year include:

1. Development of new capabilities for (nearly) simultaneous measurements for the evolution of species as a function of time in the shock tube
2. Collection of new speciation data, for more fuels, in the shock tube and in a new reactor facility
3. New ignition delay data showing variability in the hot ignition region with DCN
4. Refinement and documentation of the HyChem modeling approach, and
5. Exploration of alternate methods for mechanism reduction following strong pull from the CFD modeling teams for smaller, yet still reliable, mechanisms.

The next several paragraphs provide more details on the progress.

New optical diagnostic capabilities at Stanford have been developed this past year, using multiple infrared absorption lines that allow for the simultaneous determination of the evolution of olefinic species during pyrolysis of the parent fuel. In addition, infrared absorption characteristics of aromatic species have been explored to estimate the concentration of the aromatic species, specifically those of benzene and toluene. Along with the olefinic species and methane, the tracking of (limited) aromatics allows for the recovery of nearly 90% of the carbon contained in the pyrolytic products of the parent fuel molecules.

New shock tube data on the pyrolysis of the NJFCP fuels at Stanford have been collected. In addition, new pyrolytic data has been collected at AFRL by partially decomposing fuels under high temperature, high pressure conditions flowing through a long narrow reactor tube. Products at AFRL are being analyzed via an on-line FTIR. Similar to previous plots generated by Stanford showing a correlation between ethylene product yield and DCN, correlations were made for product species vs. the lean blow-off limit (LBO) as observed in the referee rig (described in the LBO section of this manuscript). Since LBO has been shown to correlate with DCN the AFRL results have similar trends to the Stanford results. The AFRL correlations, however, extend Stanford's results, since AFRL has found nearly all of the species data correlate with LBO (not



just ethylene) and that some species (e.g., isobutene and methane) are anti-correlated. This contrary dependence is consistent with the general understanding in chemical kinetics regarding the relative ease of combustion of ethylene and other straight chain olefins vs. slower combustion rates for methane and isobutene.

In addition to the speciation data under pyrolytic conditions, Stanford has also measured ignition delay times (IDT) above 1100K in the 'hot ignition regime' for a series of fuels with varying DCN values, ranging from about 17 to 55. Previously, it had been well established that IDT vary with DCN in the negative temperature coefficient region, typically lower that 1000 K. But the newly obtained results clearly show a consistent trend of increasing IDT with decreasing DCN above 1200 K.

The HyChem modeling approach for simulating the combustion kinetics of real fuels has been reviewed and is being documented in two companion articles to be submitted for publication[26,27]. The first article reviews the theory behind the model construction. The second applies the method to several 'real' fuels that are approved for application. The model is based on the experimental data on pyrolytic products and then validated against the ignition delay, flame speed, and flame extinction data. Once this documentation is complete, the method will be re-applied to the Category C fuels.

Reduction methods of the chemical kinetic models have been successfully developed and applied by the University of Connecticut to the NJFCP fuels to reduce the reaction models down to about 35 species. While this reduction is a significant achievement with minimal loss of fidelity in replicating kinetic predictions, there is a desire to reduce further the models to facilitate detailed simulations using computational fluid dynamics (CFD). Pre-processed Flamelet solutions can be used to capture the characteristics of the detailed mechanisms, but does not guarantee accurate simulation of the interaction of the turbulence and the chemistry near limit behavior at flame extinction or re-ignition. The University of Connecticut, together with Georgia Institute of Technology, are now exploring Chemical Explosive Mode Analysis (CEMA) to see whether smaller reduced mechanisms can be developed using a few critical chemical targets.

Sprays

The spray performance of a jet fuel can enable or debilitate stable combustion near LBO, and prohibit the ability of a fuel to ignite with this performance nominally decreasing with decreasing temperature or low fuel flow rate, such as at reduced combustor pressures. Spray performance of a jet fuel is characterized by droplet size, droplet size distribution as a probability distribution function (PDF), and spray location. Sprays with large/small Sauter Mean Diameters (SMDs), which is the diameter (d) of a droplet with the same surface to volume ratio of the spray, are considered deleterious/advantageous for combustor performance. The PDF of a droplet distribution describes the relative distribution of the droplets in a spray, as the SMD only describes nominal distributions. PDFs with large/small deviations can be considered deleterious/advantageous because large deviations in the PDF leads to a disproportionate fraction of liquid volume/mass existing in the largest spray droplets which could lead to incomplete combustion. The final spray metric discussed here, spray location, can refer to a spray cone angle or other metric that describes where the maximum flux of fuel volume/mass exists in a spray. Here we report some combine spray results from various teams associated with the NFJCP and how the various fuel properties effect the aforementioned spray performance metrics.

Spray work in the NJFCP has involved the support of 4 rigs, only three rigs[28–30,23] are discussed at present with the fourth being UTRC, which studied the performance of a different fuel injector. A brief description of the rigs, diagnostics, and test conditions are reported in Table 8. All spray data presented here used the same nozzle and swirler as reported in the LBO studies for the Referee Rig. Corresponding documentation of the fuels tested in the rigs are presented in Table 7. The tested conditions are also plotted on the T_3- P_3 plot, Figure 18. Temperatures and pressures above ambient conditions are targeting LBO conditions, while experiments are sub ambient temperatures and pressures are aimed to inform ignition phenomena. Similar to the ignition studies, Year 4 of the program will focus on spray performance at sub ambient temperatures and pressures.

Figure 19 presents a Bar and Whisker plot for the Purdue and Referee Rig using PDPA data at LBO conditions. The Purdue data was collected under non-reacting conditions. The data presented from the Referee Rig is under a stable burning condition just above the LBO limit. SMD values with a significant spread suggest that the fuel SMD varies significantly versus various radial and axial locations. Values greater/less than the maximum/minimum category A fuels are associated with poorer/better spray performance as larger SMDs are associated with longer τ_{evap} time scales for LBO. The SMDs for each of the fuels in the Purdue rig are statistically similar, and the SMDs for A-2 and C-1 are also similar. A-2, C-1, and C-5 SMDs in the Referee Rig are shown to be greater than the SMDs in the Purdue rig for these PDPA measurements, which is likely due to the evaporation of smaller droplets relative to the larger droplets. The favorable vaporization of the small



droplets then could bias the SMD to larger droplets which evaporate on longer time scales and require additional energy/heat transfer to evaporate. Interestingly, C-5 in the Referee Rig is observed to have significantly higher SMDs relative to the C-5 fuel in the Purdue rig. This observation is likely explained by the much lower final boiling point of C-5 relative to the A-2 and C-1. C-5 has been reported to have a very flat and relatively low boiling point (174 ^{0}C for C-5 versus 263/269 ^{0}C for C-1/A-2) which implies a significantly increased vaporization potential for C-5[3].

Figure 20 is a Box and Whiskers plot for chilled conditions at NRC Canada and Purdue for various NJFCP fuels, all under non-reacting conditions. It is important to note that the diagnostics at NRC Canada are different than the diagnostics used at Purdue. Purdue used a PDPA system while NRC Canada used a Malvern system. PDPA measurements are reported at specific locations, and Malvern measurements are reported as line of sight. The Purdue results for A-2, A-3, and C-3 are shown to deviate very little relative to the fuels tested implying very little viscosity effects. The relative ordering of the NRC Canada category A fuels is consistent with prior expectations as SMD_{A1} is less than SMD_{A2} and SMD_{A2} is observed to be less than the SMD_{A3}. The nominally smaller SMDs of C-1 relative to A-1 is consistent with the preliminary ignition work at cold conditions for the Referee Rig, which shows slightly better ignition behavior for C-1 vs. A-2.

Chilled versus heated SMD results are reported in Figure 21. The SMD of A-2 is observed to increase significantly between the heated and chilled conditions, and the relative SMD across fuels is not observed to deviate significantly. These results suggest that the relative ignition differences between fuels is not due to their relative droplet sizes when comparing SMD. There could, however, be additional spray performance characteristics that explain the observed ignitability differences, or the experimental temperatures and pressures were not sufficiently low enough to measure SMD differences here. Figure 22 reports PDF confidence intervals of 25%, 50%, and 75% as well as SMD for one chilled plane and 3 heated LBO planes. The 25% confidence interval determines the limit where 25% of the measured droplets are smaller, and 75% of droplets are larger. Interestingly, the SMD values are all larger than the 75% confidence interval. The SMD is thus biased by perhaps only a small number of relatively large droplets. These larger droplets in turn contain substantially more mass than a smaller droplet. The relative impact of these confidence intervals will be an ongoing area of investigation as the NFJCP proceeds into Year 4 as the pointed impact of sprays on FOM performance is yet to be determined.

Table 7. Rig descriptions and test conditions for spray. Spray results for the individual rigs can be found in these papers[28-30,23,31].

Rig Name	Description	T_{air}	T_{fuel}	P	ΔP/P	Ppilot	Institution
Purdue	PDPA	280 and 394 K	240 and 322 K	15 and 30 psia	2,3,4,6 %	25,35,45, 50,75 psi	NRC-CAN
Referee Rig	Pressure atomizer/ 2D PDA	394 K	236 and 288 K	30 psia	3%		AFRL/UDRI
NRC-CAN	Malvern	295 K		14.7 psia	2,4,6 %	25, 50, 75 psid	NRC-CAN

Table 8. Rigs and fuels tested for spray.

	A-1	A-2	A-3	C-1	C-2	C-3	C-4	C-5	C-7	C-8	C-9
Purdue		X	X	X		X		X	X	X	X
Referee Rig		X		X				X			
NRC-CAN	X	X	X	X			X				

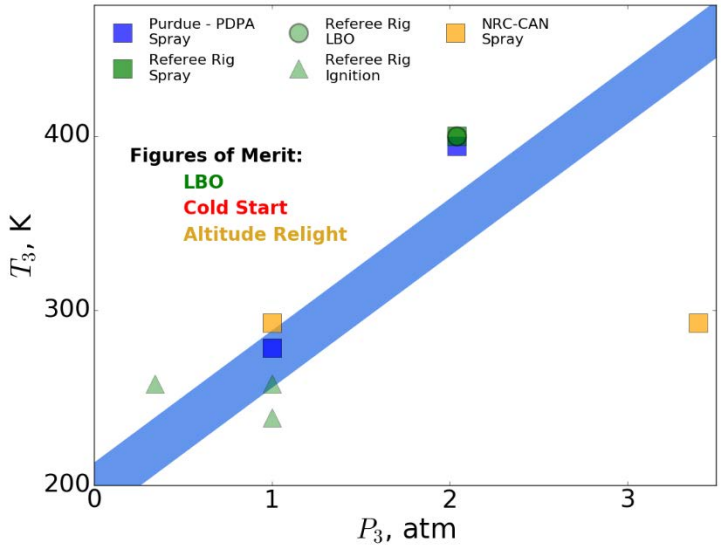


Figure 18. P_3-T_3 figure displaying the rig conditions tested to measure the Figures of Merit (FOM), specifically for the spray tests for Purdue, Referee Rig, and NRC-Canada (NRC). Referee Rig LBO and Ignition test conditions are included on this plot for reference. LBO, cold start, and altitude relight conditions occur at 2-4 atm and 400-450 K, 1 atm and 225-350 K, and >0.25 atm and >230 K, respectively.

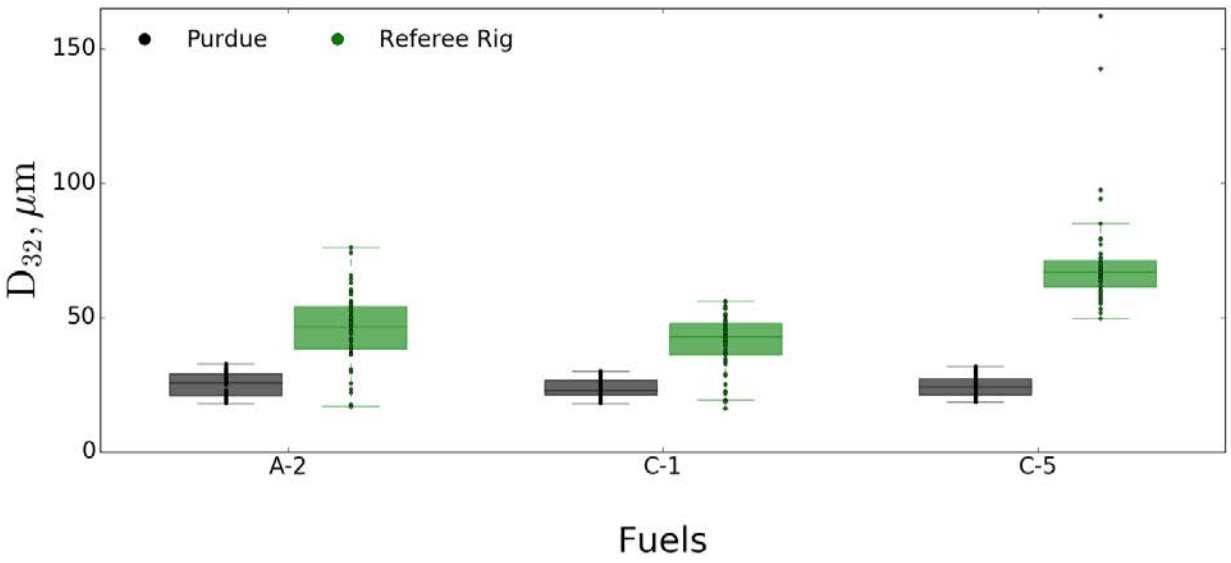


Figure 19. Spray box plot comparison of SMD (D_{32}) for Referee Rig and Purdue PDPA LBO test conditions. Data was taken at the 10 mm and 12.7 mm plane for the Referee Rig and Purdue PDPA, respectively. Radial locations span from -30 mm to 30 mm with a pressure drop of 3% and 25 psi pilot for Purdue. Each SMD point was normalized to A-2. Fuel C-5 is observed to have the largest SMD at this plane for the range of radial locations.

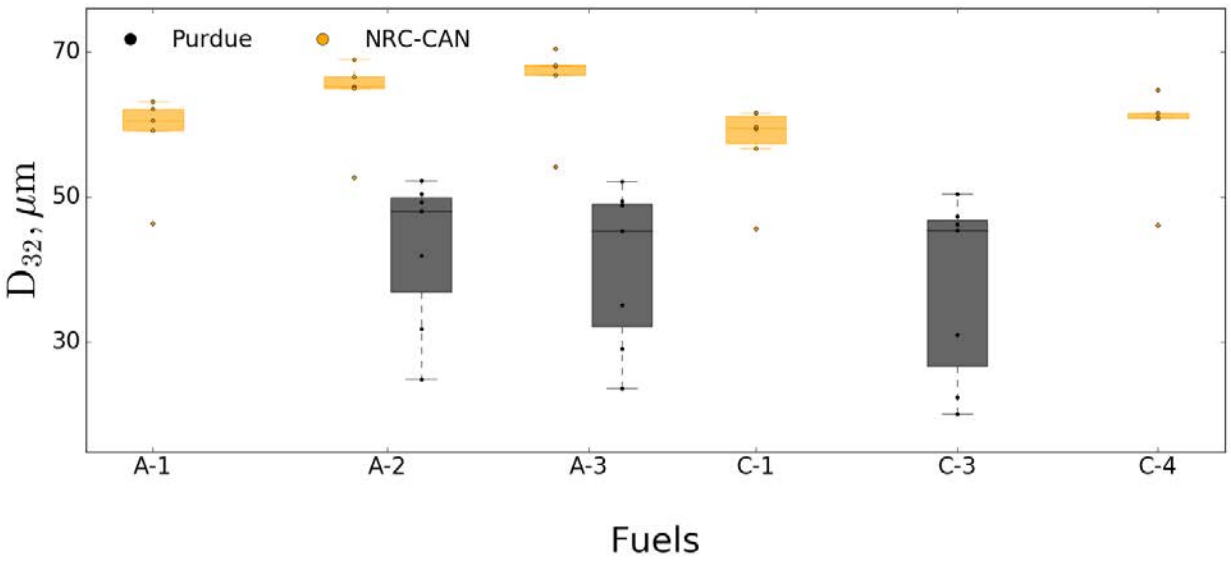


Figure 20. Spray box plot comparison of SMD (D_{32}) for NRC Canada (NRC-CAN) and Purdue PDPA for cold start test conditions using Malvern and PDPA measurement methods respectively. Data was taken at the 1 inch plane with radial locations from 0 mm to 30 mm. The pressure drop was 2% with a pilot pressure of 25 psi, all normalized to A-2. Purdue's fuel temperature was chilled to 238 K while NRC Canada's fuel was 292 K. A-1, C-1, and C-4 all had better SMDs relative to A-2 for NRC Canada while Purdue, at colder fuel temperatures had a large spread for C-3 and saw some improvement from A-2 for the A-3 fuel.

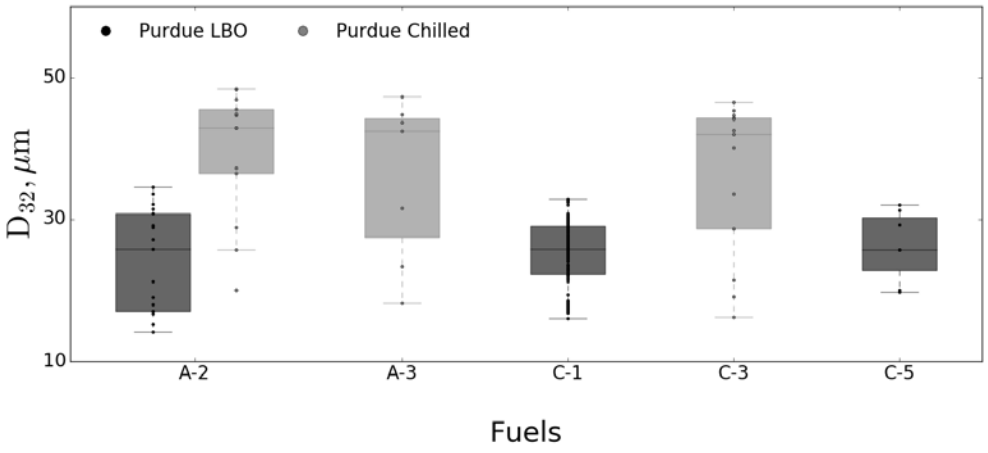


Figure 21. Spray box plot comparison of SMD (D_{32}) for chilled and heated fuels using PDPA diagnostics at Purdue. These data are reported previously in Figure 19 and Figure 20. This plot compares the effect of decreased temperatures on SMD. The SMD of A-2 is observed to increase significantly as test temperatures are reduced.

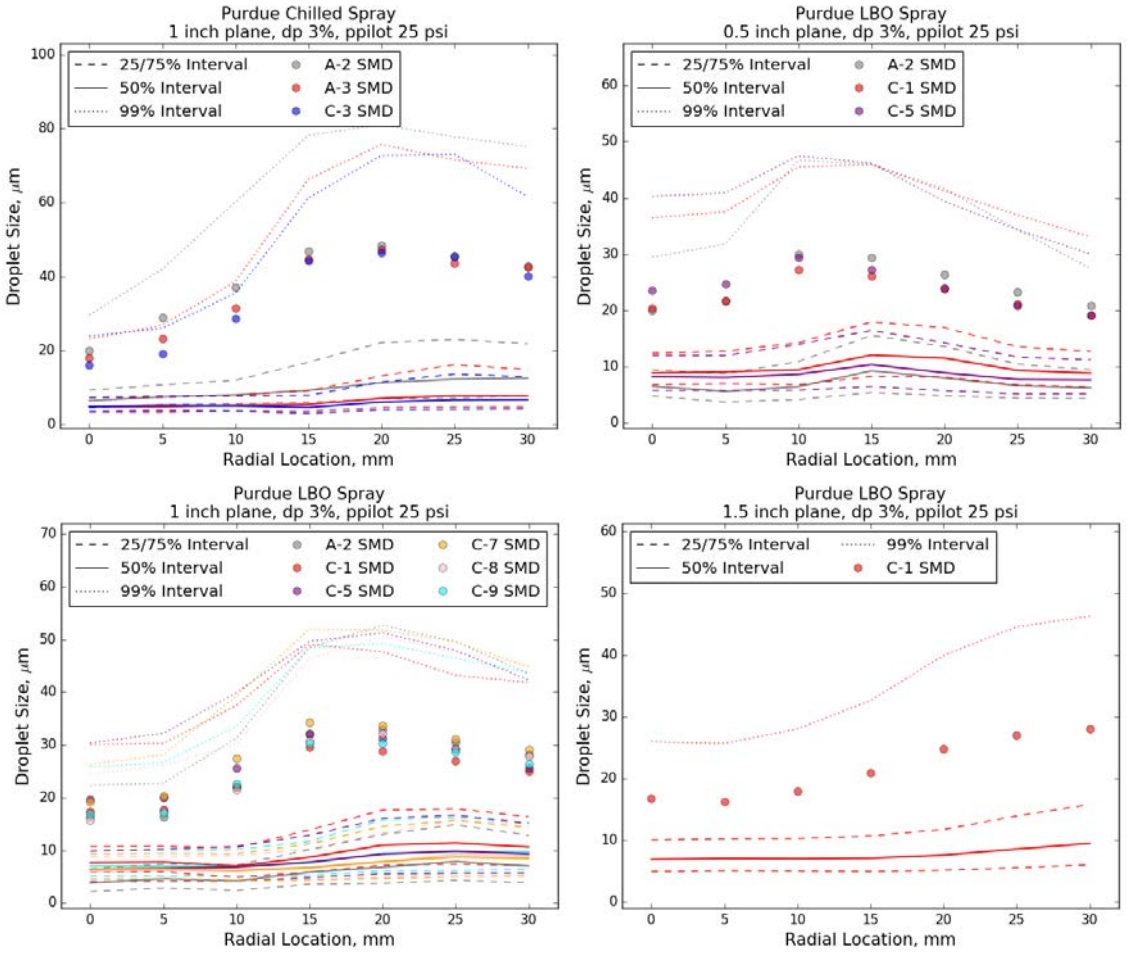


Figure 22. Confidence intervals for droplet size distribution and SMD for Purdue. All data taken with a pressure drop of 3% and pilot pressure of 25 psi. Top Left: Chilled spray at the 1 inch plane. A-2 has a larger droplet size distribution for all of the confidence intervals and SMD. Top Right: LBO spray at the 0.5 inch plane, droplet size peaks between the 10 and 15 mm radial location. Bottom Left: LBO spray at the 1 inch plane, droplet size peaks between the 15 and 20 mm radial location. Bottom Right: LBO spray at the 1.5 inch plane, droplet size peaks at the 30 mm radial location.

Summary and Conclusions

Year 3 of the NJFCP has been highlighted by multiple scientific and capacity developments. Significant gains have been made in combining the various LBO results from across the NJFCP and other rigs that have studied LBO. DCN has been shown to be a "least-common-denominator" predictor for combustion stability across 9 of the 10 rigs reported here. Other properties have been shown to have greater predictive fidelity for a given rig and conditions. Progress towards understanding the potential impact on ignition by AJFs has been accomplished by facility development and initial experimental data that suggests fuel spray and volatility characteristics determine AJF performance.

Additional gains have been made in the NJFCP in regards to models, kinetics rate measurements, and the development of these models for AJF evaluation by OEMs in OEM proprietary hardware. Various CFD models have been aligned, consistent boundary conditions and gridding where appropriate, to iterate towards predicting consistent and LBO predictions. The chemical kinetic modeling approach, HyChem, has submitted several publications detailing their modeling approach and results for several NJFCP fuels, which detailed laser diagnostic methods have been developed to balance carbon in shock tube experiments up to 85%. Finally, CFRs have been developed to enable OEM usage of the latest Flamelet modeling methods.



Year 4 of the NJFCP will entail experimental measurements that are yet to be determined to provide the maximum impact of the NJFCP and iterative improvements on current modeling paths. Some examples of identified experimental options are LBO and ignition studies with:

- additional geometries to access the relative impact on FOM performance by AJFs,
- different thermodynamic and loading parameters to access the relative importance of T3, P3, and τ_{mix} on FOM performance, and
- the use of additional fuels to stress test aforementioned hypotheses governing FOM behavior with respect to fuel properties.

These experimental directions will be determined in the coming weeks weighing the desires of Federal Sponsors and OEMs as to which test campaigns will yield the greatest impact on streamlining the certification process.

Milestone(s)

Presentation at the NJFCP Year-End Meeting. Contributing to the upcoming AIAA book.

Major Accomplishments

We have shown strong evidence that LBO is most strongly predicted by the chemical property DCN across four experimental platforms in the NJFCP. This could potentially aid in developing blending rules for fuels to proceed through the ASTM approval process.

Publications

Peer-reviewed Publications:

None

Conference Proceedings:

Peiffer, Erin, Heyne, Joshua, Colket, Meredith. 2018. "Characteristic Timescales for Lean Blowout of Alternative Jet Fuels." Joint Propulsion Conference. Cincinnati, Ohio: AIAA.

Joshua S. Heyne, Erin Peiffer, Meredith B. Colket, Aniel Jardines, Cecilia Shaw, Jeffrey P. Moder, William M. Roquemore, James T. Edwards, Chiping Li, Mark Rumizen, and Mohan Gupta. "Year 3 of the National Jet Fuels Combustion Program: Practical and Scientific Impacts of Alternative Jet Fuel Research", 2018 AIAA Aerospace Sciences Meeting, AIAA SciTech Forum, (AIAA 2018-1667)

Outreach Efforts

Oral presentations:

Peiffer, Erin, Heyne, Joshua. 2018. "Combustor Rig Sensitivity to Derived Cetane Number for Lean Blowout and Ignition Results from Year Three of the National Jet Fuels Combustion Program." Dayton-Cincinnati Aerospace Sciences Symposium. Dayton, Ohio: ASME.

Peiffer, Erin, Heyne, Joshua, Colket, Meredith. 2018. "Characteristic Timescales for Lean Blowout of Alternative Jet Fuels." Joint Propulsion Conference. Cincinnati, Ohio: AIAA.

Joshua S. Heyne, Erin Peiffer, Meredith B. Colket, Aniel Jardines, Cecilia Shaw, Jeffrey P. Moder, William M. Roquemore, James T. Edwards, Chiping Li, Mark Rumizen, and Mohan Gupta. "Year 3 of the National Jet Fuels Combustion Program: Practical and Scientific Impacts of Alternative Jet Fuel Research", 2018 AIAA Aerospace Sciences Meeting, AIAA SciTech Forum, (AIAA 2018-1667)

Awards

None

Student Involvement

Erin Peiffer, Graduate Research Assistant, June 2017 - present.

Jennifer Colborn, Undergraduate Research Assistant, August 2016 – August 2017, now at UDRI.
Katherine Opacich, Undergraduate Research Assistant, November – 2017 – present.



Plans for Next Period

We plan to continue our current research technique incorporating greater depth into our results and incorporating additional data into our work.

References

[1] Colket, M. B., Heyne, J., Rumizen, M., Edwards, J. T., Gupta, M., Roquemore, W. M., Moder, J. P., Tishkoff, J. M., and Li, C., "An Overview of the National Jet Fuels Combustion Program," *54th AIAA Aerospace Sciences Meeting*, 2016, pp. 1–24.

[2] Heyne, J. S., Colket, M. B., Gupta, M., Jardines, A., Moder, J. P., Edwards, J. T., Roquemore, M., Li, C., and Rumizen, M., "Year 2 of the National Jet Fuels Combustion Program: Towards a Streamlined Alternative Jet Fuels Certification Process," *55th AIAA Aerospace Sciences Meeting*, 2017, p. 145.

[3] Edwards, J. T., "Reference Jet Fuels for Combustion Testing," *Submitted to the 55th AIAA Aerospace Sciences Meeting*, Grapevine: American Institute of Aeronautics and Astronautics, 2017.

[4] Colket, M. B., Heyne, J. S., Rumizen, M., Edwards, J. T., Gupta, M., Roquemore, W. M., Moder, J. P., Tishkoff, J. M., and Li, C., "An Overview of the National Jet Fuels Combustion Program," *AIAA Journal*, Jan. 2017.

[5] Edwards, T., Moses, C., and Dryer, F. L., "Evaluation of Combustion Performance of Alternative Aviation Fuels," *46th AIAA/ASME/SAE/ASEE Joint Propulsion Conference & Exhibit*, Nashville, TN: .

[6] Lefebvre, A., and Ballal, D., *Gas Turbine Combustion Alternative Fuels and Emissions*, Boca Raton: Taylor and Francis Group, 2010.

[7] Plee, S. L., and Mellor, A. M., "Characteristic time correlation for lean blowoff of bluff-body-stabilized flames," *Combustion and Flame*, vol. 35, 1979, pp. 61–80.

[8] Burger, V., "The Influence of Fuel Properties on Threshold Combustion in Aviation Gas Turbine Engines," 2017.

[9] Chtev, I., Rock, N., Ek, H., Smith, T., Emerson, B., Nobel, D. R., Seitzman, J., Lieuwen, T., Mayhew, E., Lee, T., Jiang, N., and Roy, S., "Simultaneous High Speed (5 kHz) Fuel-PLIE, OH-PLIF and Stereo PIV Imaging of Pressurized Swirl-Stabilized Flames using Liquid Fuels," *Submitted to the 55th AIAA Aerospace Sciences Meeting*, Grapevine: American Institute of Aeronautics and Astronautics, 2017.

[10] Stouffer, S., Hendershott, T., Monfort, J. R., Diemer, J., Corporan, E., Wrzesinski, P., and Caswell, A. W., "Lean Blowout and Ignition Characteristics of Conventional and Surrogate Fuels Measured in a Swirl Stabilized Combustor," *55th AIAA Aerospace Sciences Meeting*, 2017, pp. 1–14.

[11] Culbertson, B., and Williams, R., *ALTERNATIVE AVIATION FUELS FOR USE IN MILITARY APUS AND ENGINES VERSATILE AFFORDABLE ADVANCED TURBINE ENGINE (VAATE), PHASE II AND III*, AFRL-RQ-WP-TR-2017-0047: 2017.

[12] Stachler, R. D., Heyne, J. S., Stouffer, S. D., Miller, J. D., and Roquemore, W. M., "Investigation of Combustion Emissions from Conventional and Alternative Aviation Fuels in a Well-Stirred Reactor," *Submitted to the 55th AIAA Aerospace Sciences Meeting*, Grapevine: American Institute of Aeronautics and Astronautics, 2017.

[13] Podboy, D. P., Chang, C., and Moder, J. P., "Lean Blowout Fuel Sensitivity for a Lean Direction Injection Combustor," *55th AIAA Aerospace Sciences Meeting*, Grapevine, TX: American Institute of Aeronautics and Astronautics, 2017.

[14] Khandelwal, B., and Ahmed, I., "Research Report on Lean Blowout Limit The University of Sheffield Department of Mechanical Engineering," 2017.

[15] Jonathan, B., Nathan, S., Fillo, A., and David, B., "Effect of Sub-Atmospheric Pressures on the Turbulent Flame Speed of Jet Fuel," *Submitted to 56th AIAA Aerospace Sciences Meeting*, Kissimmee, FL: American Institute of Aeronautics and Astronautics, 2018.

[16] Sidney, J. A. M., Allison, P. M., and Mastorakos, E., "The effect of fuel composition on swirling kerosene flames," *55th AIAA Aerospace Sciences Meeting*, Grapevine, TX: American Institute of Aeronautics and Astronautics, 2017.

[17] Colket, M., Zeppieri, S., Dai, Z., and Hautman, D., "Fuel Research at UTRC," *In Multi-Agency Coordinating Council for Combustion Research 5th Annual Fuel Research Meeting*, 2012.

[18] Allison, P. M., Sidney, J. A. M., and Mastorakos, E., "Forced Response of Kerosene Flames in a Bluff-body Stabilised Combustor," *55th AIAA Aerospace Sciences Meeting*, Grapevine, TX: American Institute of Aeronautics and Astronautics, 2017.

[19] Hendershott, T. H., Stouffer, S. D., Monfort, J. R., Diemer, J., Corporan, E., Wrzesinski, P., and Caswell, A. W., "Ignition of Conventional and Alternative Fuel at Low Temperatures in a Sing-Cup Swirl-Stabilized Combustor," *56th AIAA Aerospace Sciences Meeting*, Kissimmee, FL: American Institute of Aeronautics and Astronautics, 2018.

[20] Canteenwalla, P., and Chishty, W. A., "Investigation of Engine Performance at Altitude Using Selected Alternative Fuels for the National Jet Fuels Combustion Program," *55th AIAA Aerospace Sciences Meeting*, Grapevine, TX: American Institute of Aeronautics and Astronautics, 2017.

[21] Sforzo, B., Wei, S., and Seitzman, J., "Non-premixed Ignition of Alternative Jet Fuels," *55th AIAA Aerospace Sciences*

Meeting, Grapevine, TX: American Institute of Aeronautics and Astronautics, 2017.

[22] Wei, S., Sforzo, B., and Seitzman, J., "Fuel Composition Effects on Forced Ignition of Liquid Fuel Sprays," *ASME/IGTI Turbo Expo: Power for Land, Sea and Air*.

[23] Corber, A., Rizk, N., and Chishty, W. A., "Experimental and Analytical Characterization of Alternative Aviation Fuel Sprays Under Realistic Operating Conditions," *ASME Turbo Expo*.

[24] Esclapez, L., Ma, P. C., Mayhew, E., Xu, R., Stouffer, S. D., Lee, T., Wang, H., and Ihme, M., "Large-Eddy Simulations of Fuel Effect on Gas Turbine Lean Blow-out," *55th AIAA Aerospace Sciences Meeting*, Grapevine, TX: American Institute of Aeronautics and Astronautics, 2017.

[25] Briones, A. M., Olding, R., Sykes, J. P., Rankin, B. A., McDevitt, K., and Heyne, J. S., "COMBUSTION MODELING SOFTWARE DEVELOPMENT, VERIFICATION AND VALIDATION," *Proceedings of the ASME Power and Energy Conference*, 2018.

[26] Wang, H., Xu, R., K, W., Bowman, C. T., Hanson, R. K., Davidson, D. F., Brezinsky, K., and Egolfopoulos, F. N., "A Physics-based approach to modeling real-fuel combustion chemistry - I. Evidence from experiments, and thermodynamic, chemical kinetic and statistical considerations," *Combustion and Flame*.

[27] Xu, R., Wang, K., Banerjee, S., Shao, J., Parise, T., Zhu, Y., Wang, S., Movaghar, A., Lee, D. J., Zhao, R., Han, X., Gao, Y., Lu, T., Brezinsky, K., Egolfopoulos, F. N., Davidson, D. F., Hanson, R. K., and Bowman, C. T., "A Physics-based approach to modeling real-fuel combustion chemistry - II. Reaction kinetic models of jet and rocket fuels," *Combustion and Flame*.

[28] Mayhew, E., Mitsingas, C., Mcgann, B., Hendershott, T. H., and Stouffer, S. D., "Spray Characteristics and Flame Structure of Jet A and Alternative Jet Fuels," *55th AIAA Aerospace Sciences Meeting*, American Institute of Aeronautics and Astronautics, 2017.

[29] Bokhart, A. J., Shin, D., Gejji, R., Buschhagen, T., Naik, S. V, Sojka, P. E., Gore, J. P., and Lucht, R. P., "Spray Measurements at Elevated Pressures and Temperatures Using Phase Doppler Anemometry," *Submitted to the 55th AIAA Aerospace Sciences Meeting*, Grapevine: American Institute of Aeronautics and Astronautics, 2017.

[30] Bokhart, A. J., Shin, D., Rodrigues, N., Sojka, P., Gore, J., and Lucht, R. P., "Spray Characteristics at Lean Blowout and Cold Start Conditions using Phase Doppler Anemometry," *56th AIAA Aerospace Sciences Meeting*, Kissimmee, FL: American Institute of Aeronautics and Astronautics, 2018.

[31] Esclapez, L., Ma, P. C., Mayhew, E., Xu, R., Stouffer, S. D., Lee, T., Wang, H., and Ihme, M., "Large-Eddy Simulations of Fuel Effect on Gas Turbine Lean Blow-out," *Submitted to the 55th AIAA Aerospace Sciences Meeting*, Grapevine: American Institute of Aeronautics and Astronautics, 2017.

[32] Hastie, Trevor, Tibshirani, Robert, Friedman, J., *The Elements of Statistical Learning The Elements of Statistical LearningData Mining, Inference, and Prediction, Second Edition*, 2009.

Appendix

Random Forest Regression Documentation for Individual Rig Results

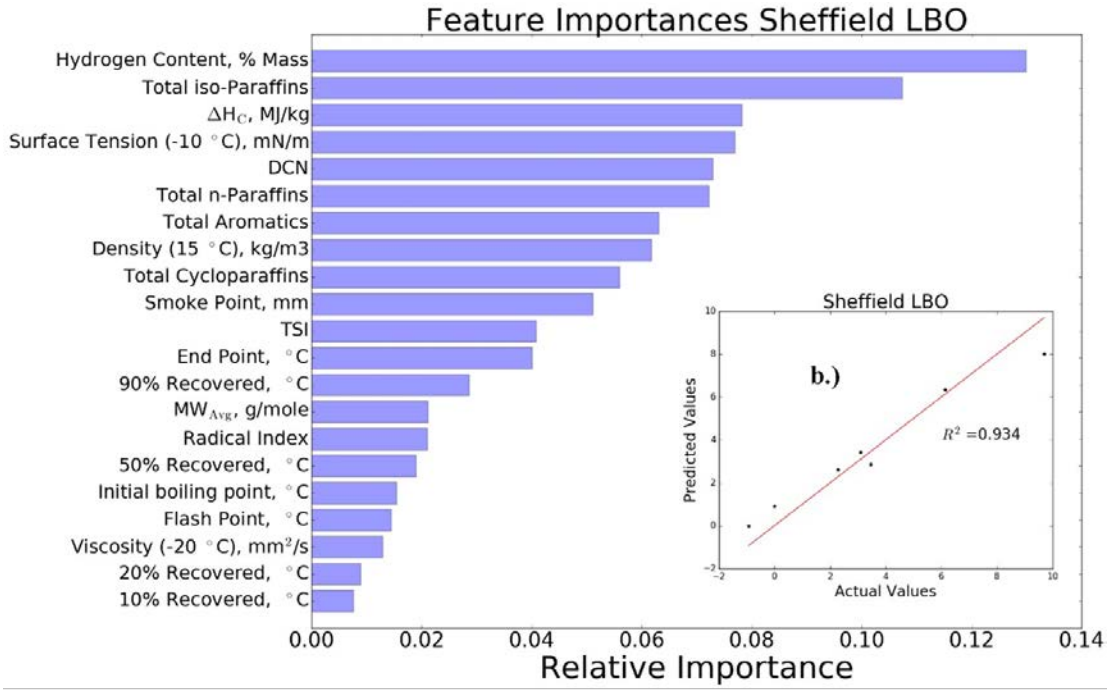


Figure 23. Random Forest regression feature importance and fit for Honeywell LBO. a.) Distillate properties and test conditions were the most important features in predicting LBO for the Honeywell rig, the one nonswirl stabilized rig in the program. Surface tension, density, and viscosity values are at the fuel temperatures. b.) the predicted versus measured (actual) values for Honeywell LBO. NOTE: Units have been intentionally renormalized such that these numbers are not relevant to actual operating limits.

Task 2- Chemical Effects in a Toroidal Jet Stirred Reactor

University of Dayton

Objective(s)

Measure the Lean Blowout (LBO) limit and emissions/speciation characteristics for NJFCP fuels within the program.

Research Approach

Introduction

Due to increasing global concern about climate change resulting from anthropocentric carbon emissions, the aviation sector has identified alternative jet fuels (AJFs) to have major potential for carbon mitigation. As alternative modes of transportation are seeking the usage of alternative fuel sources for the near and long term (e.g., fuel cells, batteries), power density is critical for the aviation sector resulting in hydrocarbon dependencies for years to come. Additionally, fuel costs for commercial airliners is large, accounting for roughly 27% of operating expenses with slight increases in the crude oil price resulting in millions of dollars of additional expenses [1,2]. Jet fuel made from alternative feedstocks has the opportunity to increase national security by reducing country dependence on foreign oil, reduce impacts of oil industry cost fluctuations, and create jobs. [1]. Use of bioderived jet fuels requires alternative pathways into the market as large capital cost paired with other economic and technological barriers exist in transition promising AJFs to market.

The National Jet Fuels Combustion Program (NJFCP) was created to streamline certification pathways of AJFs by minimizing the barrier of increased cost and testing in full scale combustor testing rigs [3]. Fuel properties to be studied against Combustor Figures of Merit (FOMs) include high altitude relight, cold start ignition, and lean blowout (LBO) [3,4]. Tests on these FOMs provide a scope of fuel performance among a variety of aviation gas turbine engine operating conditions.

LBO occurs when the flame extinguishes, which requires re-ignition of the given combustor cups or cans, during operation presenting potential safety concerns [3]. Chemical effects are shown to yield importance as lean flammability limits are being approached signifying the relevance of LBO as a FOM [3]. Target conditions for temperature and pressure, referenced to the inlet of the combustor, are 400-450 K and 2-4 atm., respectively [3]. Prior experiments with the Referee Rig and Toroidal Jet-Stirred Reactor (TJSR) have shown a first order correlation with derived cetane number (DCN) and LBO, assessed via equivalence ratio [3,5–7]. Identification of DCN, a metric seldom considered in initial fuel screening processes, illuminates the importance of fuel autoignition capabilities in these combustors near LBO.

Lefebvre, Mellor, and later Burger developed a phenomenological explanation of LBO behavior, relating it to the evaporation, chemical and mixing timescales shown in Equation 1 and Figure 1 [8–11]. Burger was able to integrate the use of non-conventional fuels into this timescale analysis to describe the competition between chemistry and evaporation in the fuels as it pertains to combustor performance. The time associated with fuel atomization and evaporation correlates to the evaporative timescale. Mixing timescales are primarily a function of combustor design, and effects of pressure, temperature, air flow rate, and recirculation within the device. Chemical timescales are influenced by the fuel, at the supplied temperature and pressure. The recent findings concerning LBO and DCN imply that the chemical timescales largely correspond to autoignition timescales. A common measure of autoignition timescales is ignition delay, which is indirectly how DCN is calculated per ASTM D6890, which will be leveraged in the subsequent analysis [12].

$$\phi(LBO) \sim \left(\frac{1}{\tau_{chem}} + \frac{1}{\tau_{evap}} + \frac{1}{\tau_{mix}} \right)^{-1} \quad (1)$$

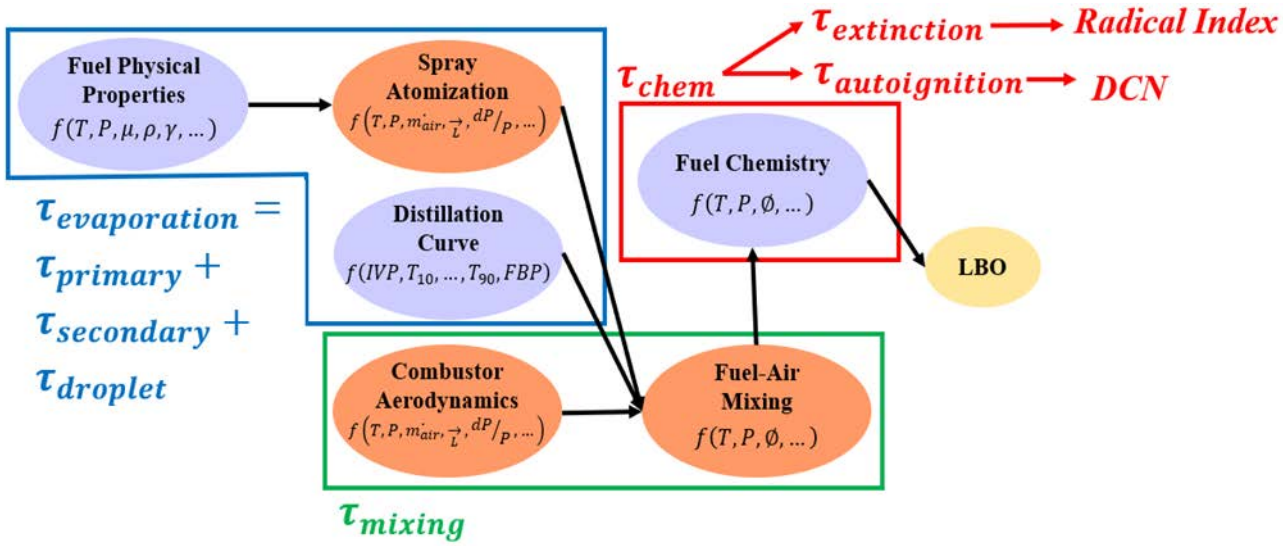


Figure 1. Relevant timescales driving LBO performance and the parameters influencing those associated timescales. Purple circles correspond to the fuel effects whereas orange circles are influenced by the combustor design.

A previous random forest regression analysis for the TJSR LBO data, including physical and chemical properties commonly measured for jet fuel performance, suggests radical index is a key predictor for LBO. Radical index (RI), a value used to measure the role of kinetics in extinction strain rate for counterflow diffusion flames, could effectively describe the effects of extinction within the TJSR [13]. Both DCN and RI are metrics that can lead to the fundamental timescales associated with autoignition and extinction, respectively. The relevant pathways to understand the competition between these timescales as they relate to the chemical timescale are shown below:



$$\tau_{extinction} \rightarrow Radical\ Index \rightarrow Extinction\ Strain\ Rate\ (a_e)$$

$$\tau_{autoignition} \rightarrow DCN \rightarrow Ignition\ Delay$$

The TJSR, an applied combustion device, has been previously used to investigate soot inception, emissions, and lean/rich blowout stability limits while operating in the well-stirred regime [14–20]. This well-stirred regime allows for reduced order physics to a 0-D system, synonymous to a perfectly-stirred reactor (PSR) with modeling efforts, where concentration, temperature, and flow fields are homogeneous with space and steady state. Minimal gradient effects exist near the wall of the TJSR, but temperature and species concentrations have yielded near constant profiles in prior experiments [15]. Using a premixed, prevaporized fuel-air mixture allows for assessment of fuels on a gas phase basis allowing for isolation of exclusively the chemical effects, as opposed to other combustion devices which study LBO in a multiphase environment where physical and chemical effects are coupled represented, in addition, by the evaporative timescale. Atomized fuel and air near the primary recirculation zone has been modeled previously as a PSR or an array of PSRs due to the 0-D nature in space and time with the reduced conservation equations associated to them. Development and implementation of a device operating near a well-stirred regime allows for the observation of chemistry effects of alternative fuels to be studied in an environment similar to that of typical gas turbine combustors, where a device to assess performance in this regime does not exist. The TJSR uses multiple jets injecting premixed, prevaporized fuel and air into the 250-mL reactor volume at temperatures and pressures near 458 K and 1 atm, respectively, and bulk fluid residence times of around 6-7 ms. LBO performance vs fuel type was assessed at high temperatures using fused silica (Rescor 750) reactor hemispheres with an Inconel jet-ring manifold and an absence of dilution. Experimental conditions for the TJSR are relatively similar to that of typical gas turbine combustors [3,18]. The influence of the chemical timescale will be discussed relative to the competition of extinction timescales and autoignition timescales.

Methods/ Experimental

TJSR Information and Instrumentation

LBO testing was performed in the TJSR where lean, premixed, prevaporized fuel and air enter the reactor via jets located on the outer diameter of the toroid. Fuel is vaporized and mixed with air upstream of the reactor, where it is then exhausted through exhaust ports located within the center of the toroid. Diagrams and additional reactor information are in Stachler, et. al., 2017 [7].

Four diagnostic ports are located within the bottom hemisphere of the TJSR. A linear tracking, bare, type B thermocouple (0.2 mm diameter, platinum – 6% rhodium, platinum – 30% rhodium) surrounded by alumina was used to measure the temperature within the reactor. Measurements were assessed approximately 0.25" from the bottom of the reactor and were not corrected for radiation and other heat losses. A custom igniter which was located flush with the reactor wall. Pressure fluctuations within the TJSR were measured using a high speed 0-5 psid pressure transducer, and it was found that pressure fluctuations were limited to +/- 5.5 kPa. Exhaust gas samples were extracted within the reactor using a 1.4 mm OD oil-cooled (420 K) probe. Measurements were taken as the probe rested approximately 5 mm from the lower wall of the toroid, situated 90 degrees relative to the thermocouple.

Fuels Tested

Various fuel/solvent mixtures were used for assessment of LBO in the TJSR that span a wide range of chemical and physical properties. These fuels are shown in Table 1, where additional fuel property information can be found in Edwards, 2017 [4]. DCN, a chemical property of fuels which is measured using ASTM D6890, varied from 17 to 74, outside of the 40 to 60 range that current aviation fuels exhibit [5,12]. RI values were estimated for A-2, C-1, and C-4 using previously published results, whereas the radical indices of the 1-3 species mixtures (nC12, S-1, and J-1) were calculated using the sum of mole fractions of the fuel multiplied by their respective radical index value [13].

A-2 is the nominal jet fuel, containing average values in flash point, viscosity, and aromatic content among the Jet-A fuels. C-1 and C-4 fuels have lower DCN values than that of conventional jet fuels and have an unusual and broad boiling range, respectively [3,4]. S-1, a surrogate fuel, was formulated to stress key combustion properties including DCN, molecular weight, H/C ratio, and threshold sooting index while emulating Jet-A fuel performance in prevaporized fuel-air environments [4,21]. The single species *n*-dodecane is a common fuel surrogate utilized for the contribution of n-alkanes in petroleum derived jet fuels [7,21]. Lastly, J-1, which has a similar DCN to C-1, was designed to stress the importance of RI to gain understanding of the kinetic influence in the progress to LBO. This 2-species fuel mixture contains a high mole fraction of aromatics to effectively lower RI without the presence of any *iso*-paraffins.



Table 1. Fuels tested within the TJSR for LBO testing. Additional fuel properties for A-2, C-1, C-4, and S-1 are in Edwards, 2017 [4]. Other 1-3 component fuel / solvent mixtures values were estimated using traditional blending methods [22,23].

Fuel / Solvent Mixture Nomenclature	Composition (% vol)	Fuel / Solvent Mixture Chemical Composition C_mH_n	Derived Cetane Number (DCN)	Radical Index (RI)
nC12	*n*-dodecane	$C_{12}H_{26}$	74.0	1.000
A-2	Petroleum Jet A	$C_{11.4}H_{22.1}$	48.3	0.750
S-1	59.3% *n*-dodecane, 18.4% *iso*-octane, 22.2% 1,3,5-*tri*-methylbenzene	$C_{10.3}H_{20.1}$	50.4	0.745
C-4	60% C9-12 *iso*-paraffins, 40% C-1	$C_{11.4}H_{24.8}$	28.0	0.720
C-1	Highly branched C12 & C16 paraffins	$C_{12.6}H_{27.2}$	19.08	0.700
J-1	75.5% 1,3,5-*tri*-methylbenzene, 24.5% *n*-dodecane	$C_{9.5}H_{14.3}$	17.01	0.466

Operating Conditions and Procedure

Liquid fuel is delivered using two syringe pumps (Teledyne Isco 500 D), where the fuel passes a swirler and heat exchanger to elevate the temperature to 473 K prior to being introduced in the vaporizer. Uncertainty in the liquid flow measurement with calibration is estimated to be +/-1.4%, where the piston flow meter accuracy is +/- 0.5%. The heated fuel is introduced with 10-20% of the air flow in the beginning of the vaporizer via an air-swirled atomizer and air at 400 K. The remainder of air is introduced coaxially throughout the length of the vaporizer at 489 K. The air lines are filtered, monitored, and controlled upstream of the vaporizer using mass flow controllers (Brooks Instruments 5851i and 5853). Uncertainty for the mass flow controllers is +/- 1.5% FSO. PID-controlled electric heaters were used to establish consistent temperatures in the heated fuel and air streams. Total air flow rate was held constant at around 600 g/min, adjusting fuel flow rate to attain the desired equivalence ratio. The constant air flow rates establish a near constant residence time and constant turbulence intensities.

Measurements of pressure, temperature, and fuel and air mass flow rates were monitored and controlled via LABVIEW software. Calculations for other relevant parameters (equivalence ratio, bulk residence time, mass flow) were performed in real time with this software as well. Global residence time for the experiment was around 6-7 ms and varied slightly with temperature differences and reduction in overall mass flow due to fuel flow rate [15]. Inlet temperatures were held constant around 458K and were measured prior the fuel-air mixture to the jet ring manifold.

Initial operation of the TJSR uses a gaseous fuel (ethylene) to allow the initial warmup of the reactor and jet ring to avoid condensation of low volatility fuels in the small passages of the jet ring. Once operational temperatures are established, and the reactor is thermally stable, fuel usage was transitioned to the liquid fuel. Thermal conditions are stabilized again before LBO testing. The ethylene was controlled using a series of pressure regulators and a mass flow controller (MKS Instruments M100B).

Each LBO test was initiated at an equivalence ratio (ϕ) of 0.48, where temperatures within the reactor were below the maximum allowable temperature for the fused silica reactor. Equivalence ratios were reduced by reducing fuel flow rate until LBO. This limiting condition occurs when the heat loss becomes large enough to where combustion becomes unstable and is not sustained. A change in operating noise and a sharp decrease in reactor temperature correspond to LBO [15]. The

fuel flow rate was automated to decrease at approximately 0.05 mL/min (ϕ ~ 0.001) every 4 seconds to LBO conditions to minimize hysteresis effects of the LBO values, e.g. hotter temperatures sustaining LBO to leaner conditions. Automation of decreasing fuel flow rate is similar to the methodology presented for the Referee Rig and their subsequent LBO testing [6]. This ramp rate for fuel flow provides for use of a singular fuel pump throughout the duration of the LBO test and minimizes transitional effects between operation of the two syringe pumps. To minimize fuel contamination between LBO testing of different fuels and dead volume associated with the syringe pumps, the pumps were flushed out with the new fuel approximately 4 times prior to the liquid fuel being introduced for testing. Also, as the WSR was approaching stable thermal conditions, the fuel lines experienced proper flushing of previous fuel to minimize contamination. Once LBO occurs, reignition of the fuel and air mixture occurs, where thermal equilibrium is achieved at ϕ = 0.48 and LBO process begins again. Thirteen (13) LBO points were taken for all fuels except nC12. Only five LBO points were taken for nC12.

Computational Methods

Ignition delay estimations were calculated using Cantera and a constant volume ideal gas reactor [24]. Initial temperatures and pressures of 700-1500 K and 1 atm, respectively, were selected to emulate the TJSR experimental conditions. Simulations stepped through time using internal stepping to minimize gradients and increase computational efficiency. A 965-species model from Dooley, et. al. was employed as the mechanism in this work as it consisted of models for the species components in the fuels tested [25]. The time at which OH concentration reached a maximum was interpreted in this work is the ignition delay time.

Perfectly stirred reactor (PSR) modeling with Cantera was also explored using an ideal gas reactor, introducing mass flow aligning with the experimental conditions at a volume of 250 mL and a bulk residence time of 7.1 ms. Mass fractions of the fuel-air mixture and temperature were extracted at steady state conditions and at equivalence ratios at LBO. Equilibrium temperatures were also calculated using the experimental conditions (T=458K, P=1atm, ϕ=ϕ_{LBO}).

Results and Discussion

Lean blowout was measured using six fuels in the TJSR, which span a wide DCN range, to investigate the first-order dependence on DCN in a premixed, prevaporized configuration. Fuel flow rate was lowered, lowering the reactor temperature, until a large drop (> 20 K) in temperature occurred, at LBO. Figure 2 illuminates this trend as the different fuels blowout at different equivalence ratios, as shown in the larger symbols. Points beyond LBO are included to illustrate the rapid decrease in temperature that occurs once LBO is experienced

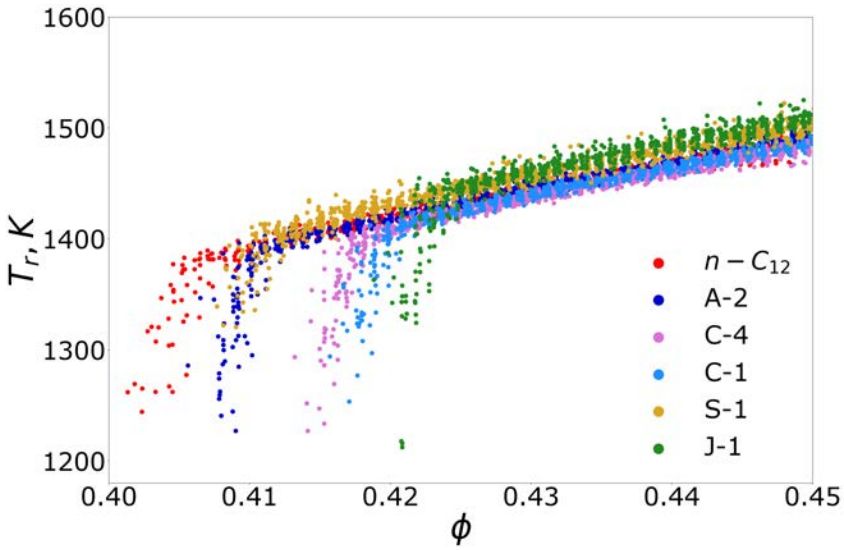


Figure 2. Reactor Temperature (K) as a function of ϕ in the TJSR. TJSR experimental conditions: P=~1atm, T_o=458K, τ = 6-7 ms.

The LBO values were then normalized relative to the LBO values of A-2, where a random forest regression analysis was utilized. This analysis, shown in Figure 3, provides a method to assess the relative important factors from the ranging physical and chemical properties among the different fuels and fuel mixtures. DCN and RI are among the top feature



importances of the data set. Normalized fuel property regression results yield the same top feature importances, but to a lesser degree than the results shown in Figure 3. Chemical properties, like iso-paraffins and n-paraffins, correlate with the next important factors, being DCN and RI. The importance of DCN and RI are both fuel property values that can influence the timescales of autoignition and extinction within the TJSR.

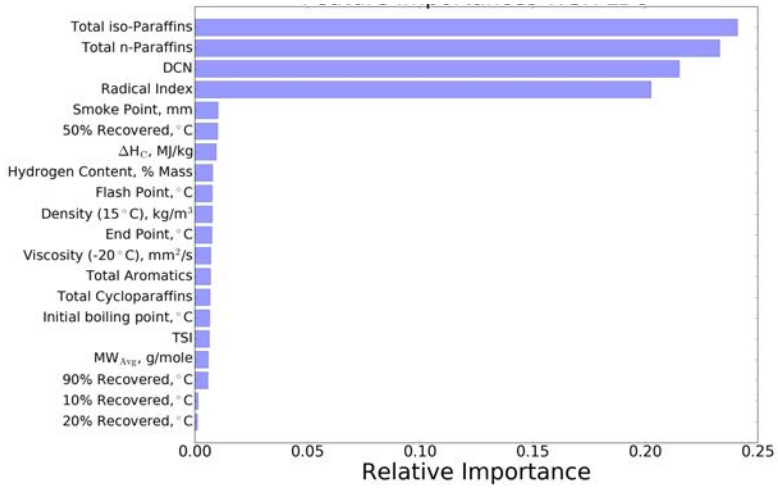


Figure 3. Relative feature importances using random forest regression analysis on the TJSR LBO data.

Figure 4 illuminates a first order correlation to LBO recorded using the TJSR. Although the LBO values are narrow with ~4% between max and min values, the statistical uncertainty with the testing performed still show a relative performance difference among the fuels and contains a moderate R^2 value. LBO for A-2 and S-1 yield consistent results in a premixed, prevaporized fuel-air environment, as with other experiments [6,21]. C-1 also exhibited an extended stability limit compared to J-1, although the fuels had similar DCN values (17.1 v. 19.08). It is also shown that the highest radical index value - 1 for nC12 - has the most resistance to LBO. Moderate radical index fuels span the gap between the two extremes of LBO performance. Figure 4 also shows the relative competition between DCN and RI, which have associated timescales corresponding to autoignition and extinction, respectively, within the chemical timescale category.

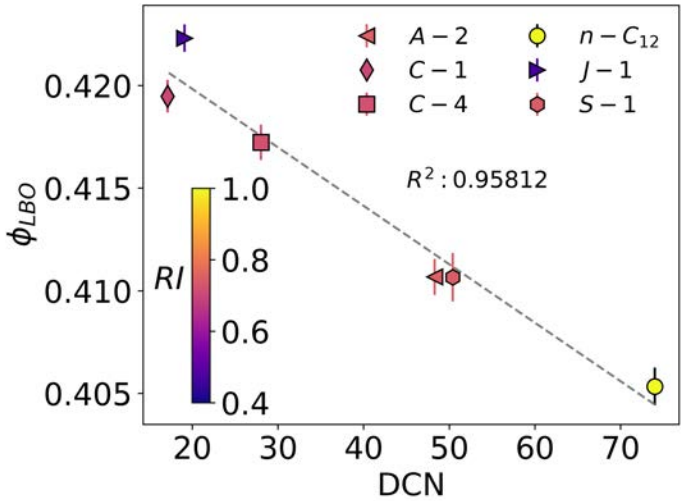


Figure 4. ϕ_{LBO} as a function of DCN in a TJSR. TJSR experimental conditions: P=~1atm, T_o=458K, τ = 6-7 ms. Error bars correspond to 1σ of the statistical uncertainty between measured LBO. RI values are included in figure as colors, indicated via the color bar. Gray dotted lines correspond to the line of best fit, with the given R^2 value provided in the figure.



Radical index aids in estimation of extinction strain rate values and toward an extinction timescale. Extinction strain rate values were calculated using the equation provided in Figure 5 from S.H. Won, et. al., 2012 [13], which is shown below for brevity. Fuel concentration represented by [Fuel] was estimated given the equivalence ratio at LBO. ΔH_c corresponds to the heat of combustion of the given fuel, where MW_{fuel} and $MW_{nitrogen}$ correspond to the molecular weights of the fuel and nitrogen, respectively.

$$a_e\left[\frac{1}{s}\right] = 230\ RI\ [Fuel]\Delta H_c\left(\frac{MW_{fuel}}{MW_{nitrogen}}\right)^{-\frac{1}{2}} - 54 \quad (2)$$

Previous counterflow diffusion flame efforts were made to study the kinetic effect of extinction strain rate for varying fuel species and components. A correlation was established, collapsing the experimental and simulated data on a line. This was accomplished via RI and transport weighted enthalpy [13]. Values of RI, fuel used, and equivalence ratio allowed for relative comparison amongst the fuels and their LBO values. Figure 5 displays LBO as a function of the calculated extinction strain rate. Fuels with large n-alkane content show increased extinction had high strain rate values whereas the lower DCN fuels had smaller strain rate values. Surrogate mixtures with large amounts of aromatics tend to have lower extinction strain rates as the radical indices are smaller than that of the other components. A linear trend of increased strain rate to decreased LBO is additionally seen in the figure with a lower R^2 value than that of Figure 4. Inverses of strain rate yields values in the 1.5-2 ms range. However, it is not determined if an inverse of the strain rate, with a unit of time, is adequate as the higher extinction strain rate values result in lower time values.

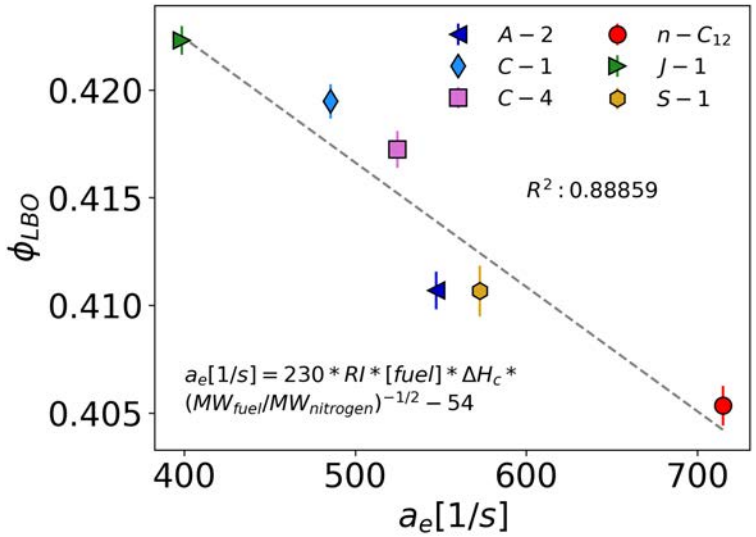


Figure 5. ϕ_{LBO} as a function of extinction strain rate (a_e) in a TJSR. TJSR experimental conditions: P=~1atm, T_o=458K, τ=6-7 ms. Error bars correspond to 1σ of the statistical uncertainty between measured LBO. Gray dotted lines correspond to the line of best fit, with the given R^2 value provided in the figure.

Correlations with DCN and the TJSR indicate autoignition as an important characteristic when approaching LBO conditions. Ignition delay allows for investigation in the effect of autoignition and comparison of those timescales relative to other timescales that may exist. In Figure 6, ignition delay was estimated via simulation with Cantera using *n*-dodecane and *iso*-octane, the latter of which is utilized in this effort because the DCN value is very similar to that of C-1[26]. Because of this assumption, the experimental temperature in the plot where *iso*-octane is located is the temperature at which LBO occurred for C-1. To illuminate the effects of recirculation of burned exhaust products to fresh reactants, burned mass fractions of products, expressed as a percentage, were incorporated into the lines provided in the figures. The remaining percentage was multiplied by the respective mass fractions of fresh reactants at the given equivalence ratio. Burned mass fractions were extracted using a PSR simulation at the given LBO value. Figure 6 displays ignition delay for different percentages of burned products incorporated within the overall mixture. A green line on both figures indicates the bulk residence time. Toward the reactor temperature limits, ignition delay is roughly two orders of magnitude less than that of the bulk residence time, but

drastically approaches the bulk residence time around ~ 1111 K. Even among the two fuels presented in the figure, these small differences between *n*-dodecane and *iso*-octane impact the ability to autoignite in adequate time for a given gas turbine combustor.

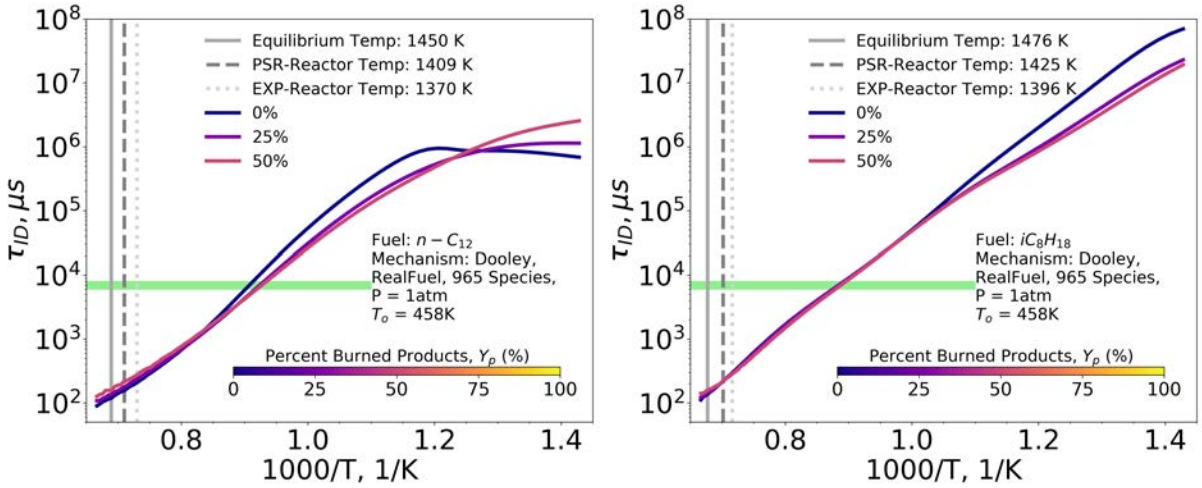


Figure 6. Ignition delay plots for *n*-dodecane and *iso*-octane for various mass percentages of burned products introduced in initial conditions. Equilibrium, PSR, and experimental temperatures are plotted in gray with the values provided in the legend. The experimental temperature for C-1 was assumed as the experimental value for *iso*-octane. The green bar on the plot signifies the order of magnitude of the bulk residence time relative to the other ignition delay times estimated from the simulation.

Conclusions

Lean blowout (LBO), a common combustor performance metric to assess alternative fuels, was assessed in a toroidal jet-stirred reactor (TJSR) with a variety of fuels spanning derived cetane numbers (DCN). This device operates in a premixed, prevaporized environment, under relevant gas turbine combustor conditions, where other combustor devices offer limited insight into experiments near perfectly stirred reactor environments. Key findings of this work include:

- LBO contains a first-order effect with DCN, which is additionally elucidated in other practical and applied combustor experiments.
- Radical index was identified as a feature importance in predicting LBO in this experimental configuration, emphasizing extinction timescales as a driving factor for LBO in a TJSR, which can be investigated using extinction strain rate.
- A competition between autoignition and extinction timescales exists on the approach to LBO, and this affects the overall chemical timescale as it relates to the bulk residence time of the reactor.

References

[1] Alternative Aviation Fuels: Overview of Challenges, Opportunities, and Next Steps, US DOE, 2016.
[2] W-C. Wang, L. Tao, J. Markham, Y. Zhang, E. Tan, L. Batan, E. Warner, M. Biddy. Review of Biojet Fuel Conversion Technologies, Report No TP-5100-66291, NREL, 2016.
[3] M. Colket, J. Heyne, M. Rumizen, M. Gupta, T. Edwards, W.M. Roquemore, G. Andac, R. Boehm, J. Lovett, R. Williams, J. Condevaux, D. Turner, N. Rizk, J. Tishkoff, C. Li, J. Moder, D. Friend, V. Sankaran, AIAA J. 55 (2017) 1087–1104.
[4] J.T. Edwards, Reference Jet Fuels for Combustion Testing. 55th AIAA Aerosp. Sci. Meet., AIAA, 2017.
[5] J. Heyne, E. Peiffer, M. Colket, J. Moder, J.T. Edwards, W.M. Roquemore, C. Shaw, C. Li, M. Rumizen, M. Gupta, Year 3 of the National Jet Fuels Combustion Program: Practical and Scientific Impacts, 2018 AIAA Aerosp. Sci. Meet., AIAA, 2018.
[6] S. Stouffer, T. Hendershott, J. Monfort, J. Diemer, E. Corporan, P. Wrzesinski, A. Caswell, Lean Blowout and Ignition Characteristics of Conventional and Surrogate Fuels Measured in a Swirl Stabilized Combustor, 55th AIAA Aerosp. Sci. Meet., AIAA, 2017.
[7] R.D. Stachler, J.S. Heyne, S. Stouffer, J.D. Miller, W.M. Roquemore, Investigation of Combustion Emissions from Conventional and Alternative Aviation Fuels in a Well-Stirred Reactor, 55th AIAA Aerosp. Sci. Meet., AIAA, 2017.

[8] A.H. Lefebvre, D.R. Ballal. Gas Turbine Combustion: Alternative Fuels and Emissions. 3rd ed. CRC Press, Boca Raton, FL, USA, 2010.
[9] A.H. Lefebvre, Int. J. Heat Fluid Flow 107 (1985) 24-37.
[10] S.L. Plee, A.M. Mellor, Combust. Flame. 31 (1979) 61–80.
[11] V. Burger, The Influence of Fuel Properties on Threshold Combustion in Aviation Gas Turbine Engines. 2017.
[12] A Standard Test Method for Determination of Ignition Delay and Derived Cetane Number (DCN) of Diesel Fuel Oils by Combustion in a Constant Volume Chamber, D6890-16e1, ASTM Int., 2016.
[13] S.H. Won, S. Dooley, F.L. Dryer, Y. Ju, Combust. Flame 159 (2012) 541–551.
[14] S.D. Stouffer, D.R. Ballal, J. Zelina, D.T. Shouse, R.D. Hancock, H.C. Mongia. Development and Combustion Performance of High Pressure WSR and TAPS Combustor. 43rd AIAA Aerosp. Sci. Meet. Exhib., AIAA, 2005.
[15] S. Stouffer, R. Pawlik, G. Justinger, J. Heyne, J. Zelina, D. Ballal, Combustion Performance and Emissions Characteristics for a Well Stirred Reactor for Low Volatility Hydrocarbon Fuels. 43rd AIAA/ASME/SAE/ASEE Jt. Propuls. Conf. Exhib., AIAA, 2007.
[16] D. Blunck, J. Cain, R.C. Striebich, S.Z. Vijlee, S.D. Stouffer, W.M. Roquemore, Fuel-rich Combustion Products from a Well-Stirred Reactor Operated using Traditional and Alternative Fuels. Cent. States Combust. Meet., The Combustion Institute, 2012.
[17] S.Z. Vijlee, Effects of Fuel Composition on Combustion Stability and NOX Emissions for Traditional and Alternative Jet Fuels. University of Washington, 2014.
[18] J. Zelina, D.R. Ballal, J. Eng. Gas Turbines Power 119 (1997) 70–75.
[19] A. Briones, B. Sekar, J. Zelina, R. Pawlik, S. Stouffer, Numerical Modeling of Combustion Performance for a Well-Stirred Reactor for Aviation Hydrocarbon Fuels, 44th AIAA/ASME/SAE/ASEE Jt. Propuls. Conf. Exhib., AIAA, 2008.
[20] J.E. Nenniger, A. Kridiotis, J. Chomiak, J.P. Longwell JP, A.F. Sarofim, Proc. Comb. Inst. 20 (1984) 473–479.
[21] S.H. Won, F.M. Haas, S. Dooley, T. Edwards, F.L. Dryer, Combust. Flame 183 (2017) 39–49.
[22] S. McAllister, J-Y. Chen, A.C. Fernandez-Pello, Fundamentals of Combustion Processes. Springer New York, New York, NY, 2011.
[23] B.E. Poling, J.M. Prausnitz, J.P. O'Connell, The Properties of Gases & Liquids. vol. 1. 5th ed. The McGraw-Hill Companies, Inc., 2001.
[24] D.G. Goodwin, H.K. Moffat, R.L. Speth, Cantera: An Object-oriented Software Toolkit for Chemical Kinetics, Thermodynamics, and Transport Processes, 2017.
[25] S. Dooley, F. Dryer, S.H. Won, T. Farouk, Reduced Kinetic Models for the Combustion of Jet Propulsion Fuels, 51st AIAA Aerosp. Sci. Meet. Incl. New Horizons Forum Aerosp. Expo, AIAA, 2013.
[26] J. Yanowitz, M.A. Ratcliff, R.L. Mccormick, J.D. Taylor, M.J. Murphy. Compendium of Experimental Cetane Numbers, Report No. TP-5400-67585, NREL, 2017.

Milestone(s)

- Measured LBO, a Figure of Merit in the NJFCP, for four fuels. Results are consistent with the more complicated Area 6 Referee Rig. LBO trends with both DCN and Radical Index, chemical properties that correspond to autoignition and extinction phenomena, respectively.
- Emissions were additionally recorded, and trends for a surrogate fuel, S-1, are similar to that of A-2, a conventional jet fuel.

Major Accomplishments

Reporting LBO equivalence ratios for four NJFCP fuels.

Publications

Peer-reviewed Publications

None. (One publication is in preparation.)

Conference Proceedings

Stachler, R., Peiffer, E., Kosir, S., Heyne, J., and Stouffer, S., "A Study into the Chemical Timescale for a Toroidal Jet-Stirred Reactor (TJSR)," Central States Section of The Combustion Institute, Minneapolis: 2018, https://doi.org/10.2514/6.2018-4914

Outreach Efforts

Conference presentations

Stachler, R., Peiffer, E., Kosir, S., Heyne, J., and Stouffer, S., "A Study into the Chemical Timescale for a Toroidal Jet-Stirred Reactor (TJSR)," Central States Section of The Combustion Institute, Minneapolis: 2018, https://doi.org/10.2514/6.2018-4914

Awards
Outstanding Research Award – Mechanical Engineering - Robert Stachler, Ph.D. student (Awarded at University of Dayton April 2018)

Student Involvement
Robert Stachler, Ph.D. student, leads this effort.

Plans for Next Period
Finalize the publication in progress and for Robert Stachler to finish his PhD.

Task 3- Preferential Vaporization Effects on LBO in the Referee Rig
University of Dayton

Objective(s)
Explain Lean blowout (LBO) results from the Referee Rig, including NJFCP and non-NJFCP fuels. Some of these fuels exhibited non-monotomic behavior at LBO.

Research Approach
The certification process for non-conventional jet fuels historically has required significant time and financial resources, as full-scale engine tests for multiple engine geometries have been used in the past to evaluate fuel effects. (These large-scale tests then jeopardize the plausibility of a new fuel's implementation.) Not only does this restrict the development and deployment of biotechnological research and results, but also it fosters a non-sustainable, longer term dependence on fossil fuels which are contributing to climate change. Jet fuel certification rightfully errs to the side of caution as system failure in flight will likely result in catastrophic results. For non-conventional fuels this caution is amplified, as these fuels often contain unique molecular compositions resulting in different chemical and physical properties from conventional fuel sources. Thus, paramount to the decarbonization of aviation transportation and the certification of alternative jet fuels is the mapping of unique chemical and physical properties to the fit-forpurpose performance and safety criteria for conventional fuels.

The National Jet Fuels Combustion Program (NJFCP) was formulated with the mission of reducing the costs and time of the jet fuel certification process [1,2]. The NJFCP's method for accomplishing this task is to map the performance of extreme alternative fuel properties to three so called Figures of Merit: cold start ignition, altitude relight, and lean blowout (LBO). These areas were selected because of their implications on safety and because of their sensitivity to fuel properties [2]. In the context of the NJFCP, significant progress has been made toward the evaluation of alternative fuel effects on LBO, with significant progress toward ignition sensitivity only occurring very recently [3]. The NJFCP tests a wide variety of fuels on multiple different experimental rigs with different geometries to evaluate Figure of Merit performance in diverse geometries [4].

A keystone of the experimental NJFCP work is the development of a combustor rig capable of capturing fuel sensitivity typical of a swirl stabilized rich-quench-lean geometry with effusion cooling. This combustor rig, in theory, would be able to capture fuel effects in an aircraft main engine by screening the fuel, which would either reduce or eliminate subsequent and costly large-scale tests. The motivation to develop this rig has led to the development of the Referee Rig at AFRL/UDRI. Previous LBO work reported on the Referee Rig has shown that fuels with conventional fuel properties exhibit an LBO first order dependency on the fuel DCN. That is, fuels with a higher DCN exhibited greater stability limits than fuels with a lower DCN. These results, and detailed measurements reported by Chtev et al.[5] , suggest that the LBO limit of a fuel in a swirl stabilized rig is limited to first order by the ability of a fuel to autoignite, which has only very recently been suggested [2,4,6,7].

Fundamentally, LBO behavior will scale with evaporative, mixing, and chemical time scales. Both fuel properties and combustor design will have impacts on the significance of each of these relative time scales with LBO being limited by the longest relative time scale. A phenomenological description of LBO, based on these time scales, was developed by Mellor,



where he hypothesized LBO will occur when combustion efficiency drops below a certain threshold [8,9]. The time scale behavior described is shown in Equation 1.

$$\eta_c = f\left((air\ flow\ rate)^{-1}\left(\frac{1}{\tau_{evap}}+\frac{1}{\tau_{mix}}+\frac{1}{\tau_{chem}}\right)^{-1}\right) \qquad (1)$$

The evaporative time scales will be determined by droplet spray and atomization behavior as well as by the volatility of the fuel. The mixing timescales will primarily be driven by combustor fluid dynamic properties. In turbulent combustion, mixing will be dominated by convection; combustor flow behavior will determine mixing time scales. The correlation found between LBO and DCN in the Referee Rig suggests the chemical time scales are at least in part determined by autoignition time scales as indicated by DCN. As DCN is a property describing a fuel's propensity to autoignite, the chemical time scales could be effectively ignition delay times. Regardless, the chemical timescales will also be a function of temperature, pressure, and concentrations of the fuel and oxidizer. As the individual time scales increase in magnitude, the overall time scale of the process increases correspondingly. When the overall process exceeds the time available in the combustor, LBO will occur. Therefore, reducing any of these time scales will improve overall combustion stability.

Historically, fuel property effects on combustor performance have been studied by Lefebvre, Mellor, and more recently by Burger, whose work was initiated with altitude LBO experiments as part of the certification of a Fully-Synthetic-Jet-Fuel (FSJF) [7–11]. Lefebvre and Mellor's work focused on the variation of properties associated with conventional fuels and did not include as significant of variations of alternative fuel property effects as those within the NJFCP. Conventional fuels chemical properties do not vary significantly between fuels, obscuring the impact of chemical effects as they relate to LBO. Burger did consider the inclusion of non-conventional fuels in his work and leveraged Mellor's time scale analysis to explain the various trends in LBO data by the competing time scales for chemistry and evaporation. The inclusion of non-conventional fuels increased the range of chemical properties tested, highlighting the effects of the chemical time scales.

While much of the Referee Rig LBO data are consistent with the propensity of a fuel to autoignite, some of the data appear anomalous. This could be a result of second order effects from other time scales interfering with the autoignition correlation. Lefebvre and Mellor showed physical properties dominating fuel performance effects, and correspondingly their results have served as the primary fuel guidelines for certification. The identification of autoignition as a property of interest will also serve as important guidelines for new fuel certification. With added fuel property requirements, there will be more clarity on how future alternative fuels must be composed. New fuels will be able to be screened for certification/qualification using relatively inexpensive, small volume fuel property tests as opposed to expensive full-scale combustor tests.

The fuels tested for LBO on the Referee Rig are intentionally diverse in nature. With the goal to understand fuel effects on performance, fuels with diverse chemical and physical properties are utilized. Physical property variations will affect droplet atomization and vaporization, while chemical variations will affect combustion behavior. The fuels include conventional fuels, alternative fuels and fuel blends [12]. Real fuels used in applications generally contain many different species of diverse properties. Multi-species fuels vaporize differently from single species fuels [13–18]. Because future alternative fuels are expected to be multi-species in nature, understanding multi-species effects on combustion is of particular interest.

Here we propose three potential hypotheses explaining the previously reported anomalous Referee Rig LBO data by coupling droplet theory, distillation curve properties, and reactivity (via DCN). The possible explanations suggested here are: preferential vaporization (τ_{evap} and τ_{chem} coupling), extended droplet lifetimes (τ_{evap}), and local thermal quenching (τ_{evap} dilation via distillation and droplet time scale coupling). No single hypothesis is shown to explain all observed LBO behavior. Finally, fuel blends to test preferential vaporization are suggested for future work.

Methodology

Time Scale Approach to LBO Modeling

Similar to the previously reported work by Mellor and Burger, time scales can be assigned to the various competing phenomena and related to the three hypothesized criteria for deviation from DCN-LBO correlations. LBO thus can be interpreted to scale with the inverse sum of evaporative (τ_{evap}), chemical (τ_{chem}), and mixing (τ_{mix}) time scales.

$$\phi(LBO) \sim \left(\frac{1}{\tau_{chem}}+\frac{1}{\tau_{evap}}+\frac{1}{\tau_{mix}}\right)^{-1} \qquad (2)$$



Evaporative times scales are associated with the relative spray and evaporation time scales of a fuel. Mixing time scales are associated with the fluid dynamic primary recirculation time scales. Chemical time scales are best characterized by an autoignition time scale. Nominally, one can interpret the time scales to be independent, as in the prevaporized premixed toroidal jet-stirred reactor which could be considered a two time scale device (chemical and mixing) [6]. Results from the toroid stirred reactor were found to be largely consistent with the Referee Rig results with greater agreement with subtle variations that are still being investigated.

The agreement between the Referee Rig and the toroidal jet stirred reactor suggest the chemical time scales are a function DCN and equivalence ratio, ϕ, and not heat of combustion as implied with Lefebrve's correlation. DCN is a measure of the fuels autoignition propensity; this is consistent with the observation of the simultaneous extinction and ignition events as blowout is approached [19]. Although DCN is a measure of autoignition in the negative temperature coefficient regime, DCN correlates accurately with ignition delays at high temperatures, which is the case in LBO [20]. From this, the significant chemical time scale could be proposed to be the ignition delay time. Regardless, the chemical time scale of significance can be described as,

$$\tau_{chem} = \tau_{chem}(DCN, \phi, T)$$

with the DCN being a function of the local (net species evolved/evaporated since droplet inception) or global (sum of total reactivity of the fuel.

Evaporation time scales can be interpreted as the algebraic sum of primary and secondary atomization (τ_{atom}) and droplet evaporation time ($\tau_{droplet}$) scales. Spray experiments on the same geometry and conditions as the Referee Rig have shown nominally similar Sauter Mean Diameters in the primary combustion region for fuels with significantly different fuel properties associated with primary and secondary atomization such as viscosity and surface tension[21]. These results imply similar primary and secondary atomization time scales.

$$\Rightarrow \tau_{atom} = \text{constant}$$

Droplet evaporation time scales ($\tau_{droplet}$) conventionally have been described by the d^2-law for a droplet of SMD [22]. The d^2-law assumes single species vaporization of a spherically symmetric, isolated droplet at steady state in a quiescent environment [23]. In the highly turbulent, multi-species vaporization of a spray, most of these assumptions are not met [24]; however the d^2-law is still generally used as an indicator of relative droplet evaporation times [25].

Initial droplet size, d_0, is a function of atomizer and physical properties of the fuel. Spray measurement experiments with the atomizer used in the Referee Rig have been made showing little variation in droplet distribution amongst fuels with variation amongst properties associated with spray quality [21].

The vaporization rate constant expression in the classic d^2-law, K_v, is a function of thermal conductivity, specific heat, heat of vaporization, fuel density, heat of combustion, air inlet temperatures and droplet surface temperature. All of these properties except for droplet surface temperature are approximately constant across fuels [12]. Droplet surface temperature will change throughout the vaporization process and is analogous to distillation temperatures in combustion applications.

Two fuels which with extreme distillate properties were tested, C-3 and C-5. C-3 distills between 183-256 ˚C and C-5 distills between 156-173 ˚C[12,26], with $\tau_{droplet}(\text{C5}) < \tau_{droplet}(\text{C3})$. Neither of these fuels performed abnormally according the LBO vs. DCN trend suggesting the absolute distillate temperatures didn't result in measurable differences. The surface temperature term in K_v does not have a significant impact on the overall value because the term is included as a temperature difference from the surrounding temperature; because the surrounding temperature is much greater than the vaporization temperatures, K_v is relatively insensitive to it. The coupling of the relatively constant droplet distribution and the relative vaporization rate constant suggest overall absolute evaporative time scales are either relatively constant or small as compared to the other timescales. And droplet time scales that followed the DCN-Law correlation follow the following relationship.



$$\tau_{droplet} \ll \tau_{mix} \text{ and/or } \tau_{chem}$$
$$\Rightarrow \quad \forall \text{ fuels with } \tau_{droplet} < \tau_{droplet} \text{(C3)}$$

In a swirl stabilized combustor like the Referee Rig, mixing is primarily driven by convection (as opposed to diffusion). Because all of the fuels were tested in the same geometry with the same conditions, it is assumed mixing time scales are constant across all fuels.

$$\tau_{mix} \cong \text{constant}$$

Given these results, the divergence in the DCN-Law suggest performance variation could be explained by the eclipsing of chemical time scales by droplet time scales or a coupling of the chemical and droplet timescales. In the latter case, the time scales cannot be viewed as independent characteristics, but rather co-dependent as they progress simultaneously. In these LBO results, chemical time scales are to first order DCN dependent with droplet time scales being described with a d^2-law accounting for distillation properties. The two hypothesized explanations both examine how the fuel vaporization could impact the chemical time scales and thus affect the stability of the fuel. Both explanations will assume vaporization and combustion follow the batch distillation limit. Each of these theories describe the vaporization of the entire spray as the vaporization of a single droplet.

Fuels

The fuel data considered in this study have been reported previously [4,12,27] and are for fuels that have been widely tested at a number of experimental facilities within the NJFCP. This suite of fuels is composed of three conventional fuels (a 'best,' average, and worse case jet fuel), five alternative fuels with fuel properties near those of jet fuel specifications, four conventional-alternative fuel blends, 2 single species fuels, and 9 blends of pure components. Two of the blended pure component (S-1 and S-2) surrogates were designed to mimic the fully prevaporized chemical combustion property targets of A-2, but have significantly differing physical properties than A-2. A full list of all fuels and their properties can be found in Table 1 and are detailed further by Edwards [12].

The listed fuel properties can be related to relative time scale estimates for each fuel. The evaporative time scale is most closely related to the distillation curve of a fuel and the fuel's effect on the spray/droplet character. High relative T_{10}, T_{50}, and T_{90} distillation properties are associated with lower vapor pressures, flash points, and increased heat transfer to the droplet surface to maintain a constant hydrocarbon vapor pressure. Higher relative viscosities, densities, and surface tensions are associated with poorer spray character as these properties inhibit atomization and mixing.

At the LBO conditions referenced here, negligible spray effects have been observed for fuels with varying properties associated with spray quality [21]. Thus, deviations in evaporative time scales are likely due to the relative distillation differences rather than spray effects based on these spray data. Additional support for this claim has been documented in reacting versus non-reacting spray data at AFRL/UDRI and Purdue respectively. These data show that for the non-reacting case very little variation is seen in the A-2 and C-5 fuels. However, very few small droplets were measured in the C-5 reacting case versus A-2 as C-5 has much lower distillation temperatures relative to A-2. The chemical time scales can be associated with the relative DCN of the fuels. A very wide range of DCNs for the fuels have been reported previously.

LBO Data Analyzed

Data used in this paper is reported in previously published literature, see [26,27]. Nominally, the LBO of a fuel is measured at a constant air mass flow rate (0.392 kg/sec), $\Delta P/P$ (3%), T (394/322 K air/fuel), and P (2 atm), with the LBO of a fuel being determined as the fuel mass flow rate limit in which extinction is global within the rig. The LBO conditions of these data are typical where LBO events at altitude occur. The LBO point as reported here is determined from multiple LBO events with uncertainties of the LBO point of approximately $+/-1.5\%$ the reported value. LBO data from 23 fuels are used in the reported analysis, see a description of these fuel in Table 1. Three conventional fuels associated with 'best' (A-1), 'average' (A-2), and 'worse' (A-3) combustion properties are used to determine stability limits of conventional fuels. While, 20 additional alternative fuels, alternative-conventional fuel blends, and solvent blends are used to approximate the 'best' and 'worse' case alternative fuel behavior for LBO by significantly varying their associated properties [4]. Fuels distinguished with a 'C' are fuels studied extensively in the NJFCP.



Table 1. Fuels tested for LBO on the Referee Rig. The fuels have diverse chemical, physical and distillate properties. The 2/3 species blends are shown in bold.

Fuel/Solvent Mixture	Composition, % volume
A-1	Petroleum JP-8 (w/high flash point and low viscosity and aromatics)
A-2	Petroleum Jet A
A-3	Petroleum JP-5
C-1	Highly branched C12 and C16 paraffins
C-2	16% *tri*-methylbenzene + 84% C14 *iso*-paraffins
C-3	64% A-3 + 36% farnesane
C-4	60% C9-12 *iso*-paraffins, 40% C-1
C-5	73% C10 *iso*-paraffins, 17% *tri*-methylbenzene
F-1	80/20 A-2/C-2
F-2	50/50 A-2/C-1
F-3	20/80 A-2/C-1
F-4	80/20 A-2/C-5
n-C12	*n*-C12
n-C12/n-C16 mix	**71.6% n-C12, 28.4% n-C16**
n-C12/M-xylene mix	**75% n-C12, 25% m-xylene**
n-C7	*n*-C7
n-C7/n-C12 mix	**31.2% n-C7, 68.8% n-C12**
n-C12/MCH mix	**71.6% n-C12, 28.4% MCH**
n-C7/n-C16 mix	**73.5% n-C7, 26.5% n-C16**
Sasol (IPK)	~88% *iso*-alkanes, 12% cycloalkanes, 0.4% aromatic
n-C12/i-C8 mix	**69.1% n-C12, 30.9% i-C8**
S-1	**59.3/18.4/22.2 *n*-dodecane/ *iso*-octane/ 1,3,5-*tri*-methylbenzene**
S-2	**52.6/25.1/22.2 *n*-hexadecane/ *iso*-octane/ 1,3,5-*tri*-methylbenzene**

LBO for these fuels are reported in Figure 1. The LBO points are plotted relative to the fuel's respective DCN. Blue symbols are fuels that do not include fuels composed of only 2/3 species, and the dashed line is a regression of $\phi(LBO)$ versus DCN for fuels excluding 2/3 species blends. All LBO measurements are found to be in agreement with the reported regression within their statistical uncertainty. Red symbols are fuels that are composed of only 2/3 species, and the solid black line is a DCN regression for all fuels plotted. Strong agreement between the non-2/3 species blends and the DCN was observed. There is a strong correlation of LBOs with DCN when the 2/3 species blends are excluded. Their correlation for all fuels is much weaker, especially in terms of correlative results for only the 2/3 species blends. Of particular note is the disparity of the S-2 fuel LBO (labeled with red text) from the strong correlation results, while the LBO data for A-2 lie very near the correlation. Recall that the S-2 mixture was derived by matching the fully prevaporized combustion property targets of A-2. Regression analysis, considering all fuel properties, continues to demonstrate that the DCN is still the leading order predictor for LBO behavior in the Referee Rig and 8 other rig geometries [4].

Fuels are distinguished by their apparent ability to stress the following three criteria:

- A lag in the relative mass evaporation rate of a droplet leading to local *thermal quenching*. Again, fuels with significant quantities of a light front distillate fraction and a heavy back distillate fraction, such as *n*-cetane, could

lead to lower mass evaporation rates after the light end of the droplet evaporates and before the heavy end of the droplet begins.

- The *relative lifetime of a droplet* (τ_{evap}) evaporating in the rig is substantially longer than other droplets. The longer droplet lifetime leads to incomplete combustion and, again, poorer stability limits at LBO. High concentrations of *n*-cetane, for example, could extend the lifetime of a droplet significantly, leading to lower combustion efficiencies that are associated with the onset of LBO [6].
- The ability of a droplet to have locally varying autoignition propensities as a function of evaporated droplet mass fraction, referred to as *preferential vaporization*. Fuels with non-reactive light components and highly reactive heavy components, such as S-2, could exhibit less stability as LBO is approached than a fuel of similar DCN but no evaporation-reactivity sensitivity [28].

Fuels composed of 2 or 3 components meet one or more of the above criteria and are distinguished as such in **Figure 1. It should be additionally noted that all the 2 and 3 component blends investigated here exhibited poorer stability than their corresponding DCN would predict.**

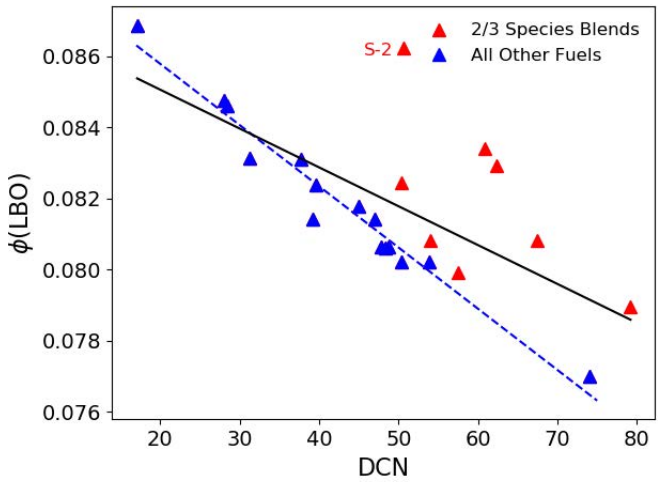


Figure 1. Experimental lean blowout as a function of DCN. The correlation is weak (R^2=0.40) until the 2 and 3 species blends are removed (R^2=0.97). The correlation with the 2 and 3 species blends removed represents the 'DCN-law.' "S-2" is labeled as it represents the greatest deviation from the d^2-law and is used as the representative fuel.

Results and Discussion

Thermal Quenching

The first explanation is the multi-species nature of the blends alone is causing the change in behavior. The explanation would support the theory of a 'DCN trend'. Each species has a unique volatility. If the species have significantly different volatilities, the species could vaporize in multiple phases divided by a heating phase in between. This concept has been observed experimentally in a heptane/cetane mixture [29]. Conventional fuels have a wide array of species and therefore volatilities. The distribution of volatilities causes the vaporization and by extension the combustion to occur at a relatively constant rate. Figure 2 shows how fuels with conventional distillation curves, like Jet A (A-2), have relatively constant vaporization rates similar to the d^2-law.

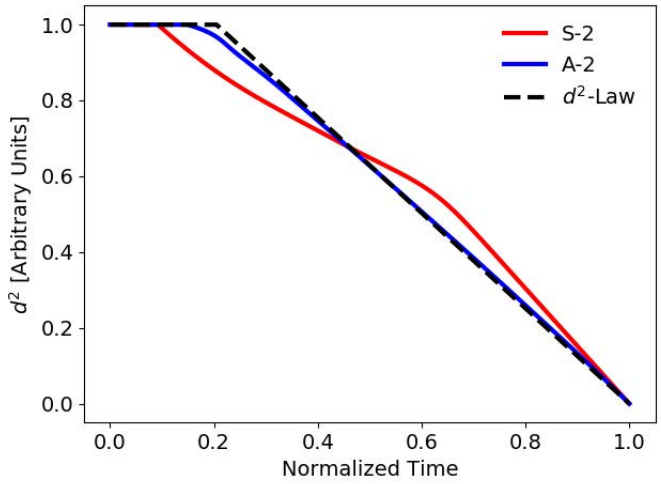


Figure 2. The relative normalized vaporization rates of a 3 species blend with bi-modal vaporization behavior, a conventional fuel, and the d^2-law. Conventional fuels with many species have a constant volatility distribution which causes them to follow similar behavior to the d^2-law.

It is unclear how multispecies blends would affect LBO behavior, however, there are multiple theories as to why this behavior could affect lean blowout. The first explanation is a concept called *thermal quenching*. Thermal quenching refers to the change in heat transfer behavior during the transition phase between the highly volatile and less volatile component. During the transition period, heat transfer continues to enter the droplet, but significantly less vapor is created per unit energy. Extinction and ignition phenomena are both highly temperature sensitive events. If at any point in the vaporization and combustion process extinction without reignition occurs, then blowout will occur. At each limit there is a balance of heat loss and energy generation which describes their limit. If during the transition phase, the heat entering into the droplet is viewed as heat loss, extinction and, correspondingly, lack of ignition could be described by the Semenov criterion. The Semenov criterion states that reactions will continue as long as heat generation exceeds heat losses. If heat generation is constant, then the increase in instantaneous heat losses could cause this limit to be reached.

Following the same assumption, during the transition phase the gaseous temperatures will decrease. Reduced gaseous temperatures will decrease flame speed which will lead to increased extinction probability. Simultaneously, reduction of the temperature of the vapor will have non-linear effects on ignition delay. If reignition is attempted at lower temperatures, it is highly unlikely it would occur and correspondingly no combustion would occur, signifying blowout.

The heat transfer into the droplet will be driven by the temperature of the flame and products. When these temperatures are high, increased amounts of heat are consequently lost to the walls and non-reacting air. If during the volatility transition this temperature decreases because of less mass combusting, the heat transfer into the droplet would decrease. Subsequently, a decrease in heat transfer would lead to further decrease in mass transfer, resulting in a negative feedback loop concluding with extinction.

Similar to thermal quenching, another theory is the volatility transition period has an effect on specifically mass transfer. During the transition, the reduction in mass vaporization rate would have an impact on instantaneous localized equivalence ratio. Chemical time scales will be significantly affected by reduced mass concentrations. Due to the turbulent environment, combustion occurs at fuel-to-air ratios other than stoichiometric. Because chemical time scales have been described as functions of equivalence ratio, potentially, the reduction in mass vaporization rate could have an impact on effective chemical time scales.

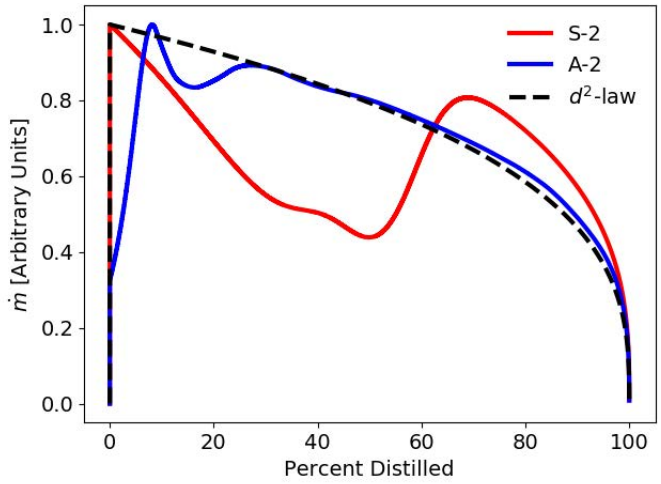


Figure 3. Mass vaporization/combustion rate as a function of volume combusted. Again, real fuels follow a similar trajectory to idealized fuels, but 2 and 3 species blends do not. Vaporization rates significantly slow down during the transition period.

During blowout testing, it was qualitatively observed that while testing S-2, unburned liquid particles were escaping the combustor [30]. This did not occur for other fuels. This supports the theory that the discontinuous volatility distribution of 2 and 3 species blends is causing the issue. Each of the explanations proposed suggest there is difficulty in advancing past the transition period to the less volatile component. Other fuels tested with comparably high final boiling points didn't show this behavior.

To stress test this theory, more 2/3 species blends need to be tested. The blends should be constructed of species with highly different volatilities. Ideally the concentrations of each species are close to equal as possible; this would maximize the distinctness between the different phases of distillation and highlight the effects.

Relative Lifetime of Droplets

The second explanation for the unique behavior of some of the fuels is that the time scale of vaporization is lower for the blends. Three of the greatest outliers include nC_{16} as a blending component. This molecule is among the least volatile molecules typically found in jet fuel. Inherently this increases vaporization time to some degree. If the more volatile component vaporizes first, the remaining non-volatile nC_{16} will be left with less surface area for heat transfer into the droplet, enhancing the effect of the high distillation temperatures. This is strongly influenced by the observation of liquid fuel escaping the combustor for the tests of the fuel S-2 [30]. This effect does not explain all of the outliers but could contribute to moving these points closer to the DCN trend line.

Preferential Vaporization

The third explanation of the unique behavior of the 2 and 3 species blends is preferential vaporization. Each of the 2 and 3 species blends tested were a blend of a more reactive, less volatile species with a less reactive volatile species. Preferential vaporization suggests that the species concentrations vaporizing as a function of time changes which, by extension, impacts combustion behavior. Preferential vaporization has been shown to occur in droplet vaporization [13,29]. Preferential vaporization has been shown to have an effect in both ignition and extinction experiments [31,32]. If this behavior is occurring in the Referee Rig, the bulk DCN may not be the chemical property of significance, but rather some intermediate DCN partially through the distillation process.

The more volatile species will be the first to vaporize. Once vaporized they will be present throughout the process either in the form their original molecule, intermediate species, or products with their corresponding heat. The species with the most time in vapor form have the most potential to impact combustion. If preferential vaporization is the behavior driving the



performance deviation between the 2 and 3 species blends from the DCN-law, then it would be possible to have a fuel that outperforms the DCN-law.

To validate a preferential vaporization model, the instantaneous property, in this case DCN, needs to be numerically estimated throughout the distillation process. Because of the variety of fuels tested to be compared, three different approximations are used: 1) a constant DCN throughout the distillation process, 2) a linear by volume blending rule of DCN and 3) a Quantitative Structure-Property Relation (QSPR) regression approximation. A constant DCN was approximated throughout the distillation process for fuels that were never blended before testing. This approximation is used for the conventional fuels. Although it is possible these fuels have variation in properties throughout the distillation process, these variations are approximated as negligible because of the relatively normal distribution of the different species types throughout the molecular weight (MW) distribution [12]. A linear by volume blending rule, in conjunction with an approximated blend distillation method, is used to approximate fuels which are blends of fuels with known properties [33,34]. QSPR regression combined with the Antoine Equation and vapor-liquid equilibrium is used to estimate DCN throughout the distillation of the fuels with known species and concentrations [28]. The methods used for each fuel is shown in Table 2

Table 2. The method used to estimate DCN as a function of percent distilled for each fuel. *=Methyl-cyclohexane could not be used in QSPR because it does not yet include cyclo-paraffin behavior.

Constant DCN	Linear by Volume	QSPR Regression
A-1, A-2, A-3, Sasol IPK	C-2, C-3, C-4, C-5, A-2/C-1 blends, A-2/C-5 blend, nC_{12}/MCH*	C-1, nC_{12}, nC_7, nC_{12}/M-Xylene, nC_{12}/iC_8, nC_{12}/nC_{16}, nC_7/nC_{12}, S-1, S-2

Using the methods described above, the DCNs throughout the distillation curve are calculated and power law regressions of LBO, as a function of the instantaneous DCN, are run to identify the optimal predictive value. In Figure 4, the R^2's of the regressions of LBO, with the calculated instantaneous DCN as the only indicator, are shown. The ideal predicator is found to be the DCN through 34% of the distillation process with a corresponding R^2 of 0.824. This result suggests that for the Referee Rig the first 34% of the fuel to vaporize are the species which will drive when blowout will occur. For different combustor designs, the physical time scales would vary and would thus have a different ideal predictive indicator. The predicted LBO will follow the regression shown in equation 4.

$$\frac{\phi(LBO_i)}{\phi(LBO_{A2})} = \left(\frac{DCN34_i}{DCN34_{A2}}\right)^{-0.069} \quad (4)$$

This analysis shows DCN through 34% of the distillation process is a better indicator than the overall DCN of a fuel, however the current data only contains fuels with more reactive, 'second halves' of the distillation process. Although this parameter does not predict the overall combustion perfectly, the predicted results from the chemistry alone are unbiased. Figure 5 shows the absence of bias between predicted and experimental results. The resulting error could potentially be explained by other chemical and physical properties.

None of the fuels tested have 'beat' the limiting 'DCN trend.' To show preferential vaporization has an effect, it needs to be shown preferential vaporization can be leveraged to improve a fuels performance and not only make it perform worse. The goal is to produce a fuel that will land in below the DCN-law line. If the partially vaporized DCN value appropriately captures the chemical-physical interaction in describing lean blowout, then designing a fuel to beat this trend should be possible.

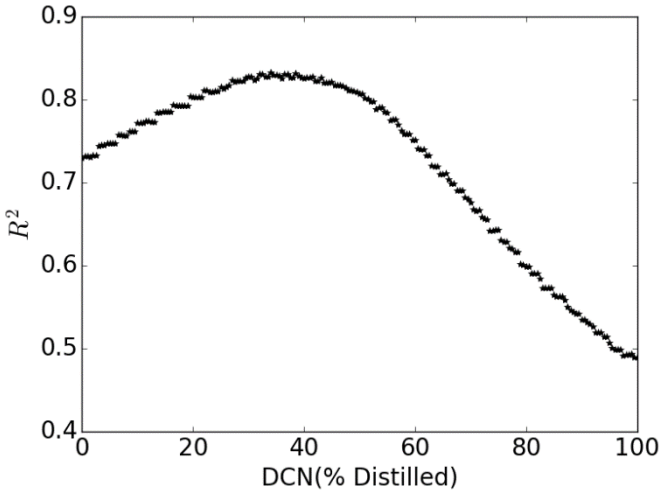


Figure 4. The R^2 of LBO vs instantaneous DCN, where DCN is a function of percent distilled. This result shows the optimal predictor of LBO for this experiment is the DCN at 34% distilled (R^2 = 0.824).

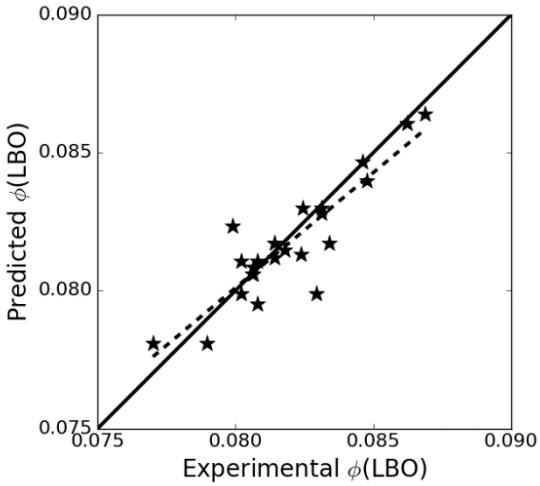


Figure 5. Predicted $\boldsymbol{\phi(LBO)}$ vs. Experimental $\boldsymbol{\phi(LBO)}$ for fuels reported in Table 1. The error associated with a prediction using Equation 4 is the distance from the solid line (R^2=0.824). The dashed line is a fit showing that there is consistency between experimental and predicted values.

Proposed Fuels

A fuel that will land below the DCN-law line needs to have a higher DCN at 34% vaporized than its overall DCN. To accomplish this, a fuel with high DCN and low molecular weight (MW), which corresponds with lower volatility, needs to be blended with a fuel with low DCN and high MW. Normal paraffins have the highest DCN among the different general molecular structures. Unfortunately, the normal paraffins with the highest DCN are the molecules with the highest MW. A range of *n*-paraffins are considered for use as the high DCN, low MW component in the blend. Low DCN, high MW fuels include large aromatics and large highly branched *iso*-paraffins. Highly branched *iso*-paraffins are preferred as the primary blending component because high concentrations of aromatics could have unforeseen effects as they less mimic previously tested fuels.

Fuel availability constraints lead us to a fuel which has already been tested, C-1. C-1 is a mix of almost exclusively *iso*-paraffins ranging from 5 to 20 carbons. It is heavily weighted towards highly branched *iso*-dodecane and *iso*-cetane [12]. For the purposes of this research, C-1 is approximated to be exclusively 80% by mole *iso*-dodecane and 20% by mole *iso*-cetane. *iso*-Cetane would be a near perfect candidate for the less reactive blending component due to its high MW and low DCN. In conventional jet fuels, there are very few molecules larger than 16 carbons, thus *iso*-cetane represents the upper bound for MW. *iso*-Cetane blends are considered as they represent an upper bound for maximizing preferential vaporization behavior.

The final fuel blend is selected as the blend that produces the highest difference between predicted LBOs by the DCN trend and the new 34% vaporized DCN regression in equation [2] (Figure 6). *n*-Paraffins between 7 carbons and 10 carbons are considered and blended with both C-1 and *iso*-cetane. Figure 7 shows the potential fuel blends and their respective differences between their predicted LBOs. The C-1 blended with *n*-heptane (nC_7) is the best option among C-1 blends offering a predicted difference of about 0.0022 in equivalence ratio at blowout with concentrations of 21% nC_7 and 79% C-1 by moles. The blend showing the greatest improvement with *iso*-cetane occurs similarly with *n*-octane (nC8) and *n*-nonane (nC9) offering a difference of about 0.0026 in equivalence ratio at blowout from the DCN-law line. This difference is achieved with 17% nC_8 and 83% *iso*-cetane as well as with 17% nC_9 and 83% *iso*-cetane.

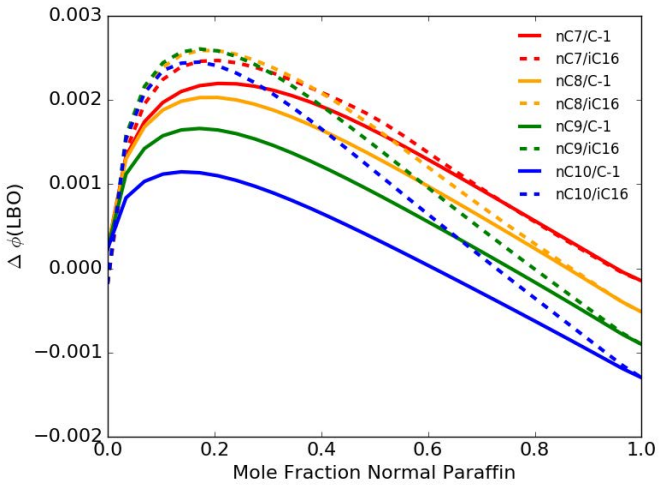


Figure 6. The difference between LBO predictions using DCN vs DCN through 34% of distillation. The difference is plotted for different blending ratios of *n*-paraffins mixed with C1 and Distilled C1. The peaks represent the ideal blending ratio for each blending combination.

The new blends as they are expected to perform are shown in Figure 8. Both the points for the generated fuels are in the target region, but not to the degree of the surrogates on the opposite side of the line. This is caused by physical limitations in the chemistry as low molecular weight species cannot have as high of DCN's as large molecular weight fuels. Each of the blends is shown as to their performance relative to the DCN trend line. Unfortunately, the predicted improvement below the DCN-law line is very close to the bounds of experimental error.

Both of the explanations for the outlier experimental results described above could be tested with one fuel. A 2-species blend fuel designed to test preferential vaporization would illuminate the impact of both effects if they are present. If the proposed fuels perform significantly worse than the DCN law line, then it would suggest it is not a chemical effect but rather a characteristic of 2 species blends. If the proposed fuels perform better than the DCN trend line, then it would be further evidence of preferential vaporization and its corresponding impact on chemistry, having an effect.

The Referee Rig, similar to other gas turbine combustors, requires a minimum amount of aromatics present in fuel to facilitate o-ring swelling. A large aromatic in relatively low concentrations can be added to the fuel and it should not significantly affect performance.

In theory, the effect of both of the described phenomenon would be enhanced in a low-pressure experiment. At lower pressures, individual species vaporize more ordinarily. Figure 8 shows the preferential distillation DCN values of S-2 at three different pressures. At 20 atm, the nC_{16} has higher relative partial vapor pressures resulting in higher molar concentrations to vaporize early in the process. This causes the partially distilled DCN to be higher at lower volumes distilled. At low pressures, a local minimum can be seen around 45% distilled. This is caused by the vaporization of the 1,3,5 TMB. At each of the pressures the final ~30% distilled is all nC_{16} vaporizing, resulting in similar paths.

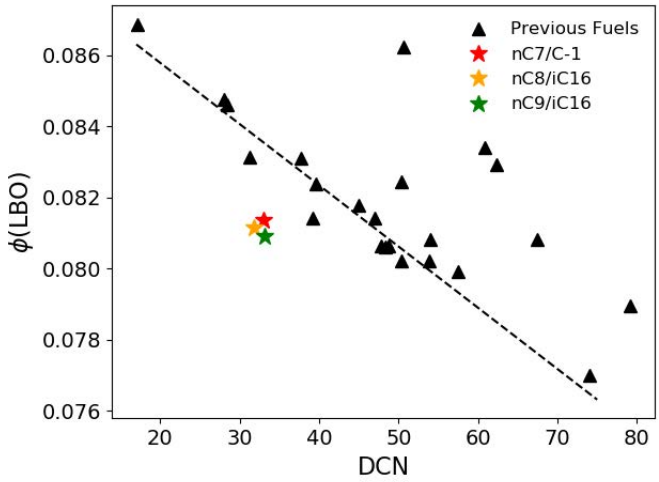


Figure 7. Shows the predicted LBO using preferential vaporization of the newly generated fuels. The new fuels would land below the current limiting bound.

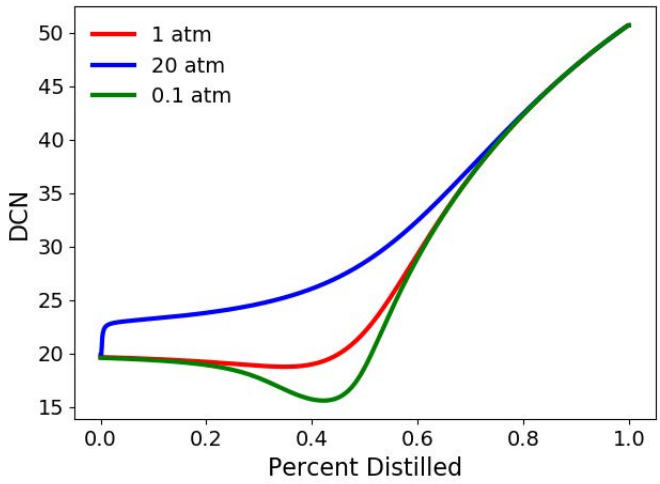


Figure 8. The DCN as a function of percent distilled of S-2 at various pressures. At high pressures, the species vaporize less ordinally. At 0.1 atm the decrease in DCN seen is the vaporization of 1,3,5 TMB. To maximize preferential distillation behavior, a low-pressure experiment is preferred.

It should be noted, tests at different pressures will significantly affect boiling points and correspondingly vaporization rates. This could have unanticipated impact on the overall behavior near lean blowout.



Conclusions

The time scales of evaporative, chemical, and chemical-evaporative have been discussed and developed into several hypothesis to explain LBO events anomalous to the previously reported DCN trend. This time scale analysis has been applied to LBO data reported on the Referee Rig at AFRL/UDRI. These analyses suggest that no single time scale analysis or coupling is sufficient to explain all the observation in the Referee Rig. Numerical analysis suggests that one developed hypothesis, preferential vaporization, has the possibility to explain much of the observed discrepancies versus the DCN trend. Additionally, fuel blend and compositions to test this hypothesis have been suggested to confirm or discredit this hypothesis (21% by mole *n*-heptane and 79% Gevo ATJ (C-1)). Finally, additional work is needed to explore in greater depth the quantitative effects of the other two hypothesis listed and discussed (thermal quenching and relative lifetime of a droplet).

References

[1] Colket, M. B., Heyne, J., Rumizen, M., Edwards, J. T., Gupta, M., Roquemore, W. M., Moder, J. P., Tishkoff, J. M., and Li, C., 2016, "An Overview of the National Jet Fuels Combustion Program," 54th AIAA Aerosp. Sci. Meet., (Jan), pp. 1–24.

[2] Heyne, J. S., Colket, M. B., Gupta, M., Jardines, A., Moder, J. P., Edwards, J. T., Roquemore, M., Li, C., and Rumizen, M., 2017, "Year 2 of the National Jet Fuels Combustion Program: Towards a Streamlined Alternative Jet Fuels Certification Process," *55th AIAA Aerospace Sciences Meeting*, p. 145.

[3] Hendershott, T. H., Stouffer, S. D., Monfort, J. R., Diemer, J., Corporan, E., Wrzesinski, P., and Caswell, A. W., 2018, "Ignition of Conventional and Alternative Fuel at Low Temperatures in a Single-Cup Swirl-Stabilized Combustor," *56th AIAA Aerospace Sciences Meeting*, American Institute of Aeronautics and Astronautics, Kissimmee, FL.

[4] Heyne, J. S., Peiffer, E., Colket, M., Shaw, C., Jardines, A., Moder, J., Edwards, J. T., Roquemore, W. M., Li, C., Rumizen, M., and Gupta, M., 2018, "Year 3 of the National Jet Fuels CombustionProgram: PRactical and Scientific Impacts of Alternative Jet Fuel Research," *56th AIAA Aerospace Sciences Meeting*.

[5] Chtev, I., Rock, N., Ek, H., Smith, T., Emerson, B., Nobel, D. R., Seitzman, J., Lieuwen, T., Mayhew, E., Lee, T., Jiang, N., and Roy, S., 2017, "Simultaneous High Speed (5 kHz) Fuel-PLIE, OH-PLIF and Stereo PIV Imaging of Pressurized Swirl-Stabilized Flames Using Liquid Fuels," *Submitted to the 55th AIAA Aerospace Sciences Meeting*, American Institute of Aeronautics and Astronautics, Grapevine.

[6] Stachler, R. D., Heyne, J. S., Stouffer, S. D., Miller, J. D., and Roquemore, W. M., 2017, "Investigation of Combustion Emissions from Conventional and Alternative Aviation Fuels in a Well-Stirred Reactor," *Submitted to the 55th AIAA Aerospace Sciences Meeting*, Grapevine, TX.

[7] Burger, V., 2017, "The Influence of Fuel Properties on Threshold Combustion in Aviation Gas Turbine Engines," (Feb).

[8] Plee, S. L., and Mellor, A. M., 1979, "Characteristic Time Correlation for Lean Blowoff of Bluff-Body-Stabilized Flames," Combust. Flame, **35**(C), pp. 61–80.

[9] Mellor, A. M., 1980, "Semi-Empirical Correlations for Gas Turbine Emissions, Ignition, and Flame Stabilization," Prog. Energy Combust. Sci., **6**(4), pp. 347–358.

[10] Lefebvre, A. H., and Ballal, D. R., 2010, "Gas Turbine Combustion," Book, **Third Edit**.

[11] Lefebvre, A. H., *Influence of Fuel Properties on Gas Turbine Combustion Performance*, West Lafayette, IN.

[12] Edwards, J. T., 2017, "Reference Jet Fuels for Combustion Testing," *Submitted to the 55th AIAA Aerospace Sciences Meeting*, American Institute of Aeronautics and Astronautics, Grapevine.

[13] Law, C. K., Prakesh, S., and Sirignano, W. A., 1981, "Theory of Transient Multicomponent Droplet Vaporization in a Convective Field," Symp. Combust., **18**(1), pp. 1365–1374.

[14] Yang, S., Ra, Y., and Reitz, R. D., 2010, "A Vaporization Model for Realistic Multi-Component Fuels," *Proceedings of the 22nd Annual Conference on on Liquid Atomization and Spray Systems*.

[15] Sirignano, W. A., 1983, "Fuel Droplet Vaporization and Spray Combustion Theory," Prog. Energy Combust. Sci., **9**(4), pp. 291–322.

[16] Clercq, P. Le, and Dou, N., 2009, "Validation of a Multicomponent-Fuel Model for Spray Computations ∗," 47th AIAA Aerosp. Sci. Meet., (January), p. 2009.

[17] Rauch, B., Le Clercq, P., Aigner, M., Rachner, M., Calabria, R., and Massoli, P., 2011, "Jet A-1 Fuel Spray Evaporation in a Turbulent Flow : Experimental Investigations and Validation of Numerical Models," *49th AIAA Aerospace Sciences Meeting*, Orlando, FL, pp. 1–13.

[18] Liu, Y. C., Savas, A. J., and Avedisian, C. T., 2012, "Surrogate Fuel Development Based on Droplet Combustion : Comparison of Multi-Component Mixtures with an Aviation Fuel," *50th AIAA Aerospace Sciences Meeting Including the New Horizons Forum and Aerospace Exposition*, Nashville, TN, pp. 1–8.

[19] Emerson, B., Lieuwen, T., and Juniper, M. P., 2017, "Local Stability Analysis and Eigenvalue Sensitivity of Reacting Bluff-Body Wakes," J. Fluid Mech, **788**, pp. 549–575.

[20] Hanson, R. K., "Personal Communication," December 2017.

[21] Bokhart, A. J., Shin, D., Rodrigues, N., Sojka, P., Gore, J., and Lucht, R. P., 2018, "Spray Characteristics at Lean Blowout and Cold Start Conditions Using Phase Doppler Anemometry," *56th AIAA Aerospace Sciences Meeting*, Kissimmee, FL.
[22] Law, C. K., 2006, *Combustion Physics*, Cambridge University Press, New York.
[23] Law, C. K., 1982, "Recent Advances in Droplet Vaporization and Combustion," Prog. Energy Combust. Sci., **8**(3), pp. 171–201.
[24] Marti, F., Martinez, O., Mazo, D., Garman, J., and Dunn-Rankin, D., 2017, "Evaporation of a Droplet Larger than the Kolmogorov Length Scale Immersed in a Relative Mean Flow," Int. J. Multiph. Flow, **88**, pp. 63–68.
[25] Law, C. K., and Law, H. K., 1982, "A d2-Law for Multicomponent Droplet Vaporization and Combustion," AIAA J., **20**(4), pp. 522–527.
[26] Stouffer, S., Hendershott, T., Monfort, J. R., Diemer, J., Corporan, E., Wrzesinski, P., and Caswell, A. W., 2017, "Lean Blowout and Ignition Characteristics of Conventional and Surrogate Fuels Measured in a Swirl Stabilized Combustor," *55th AIAA Aerospace Sciences Meeting*, Grapevine, TX, pp. 1–14.
[27] Corporan, E., Edwards, J. T., Stouffer, S., DeWitt, M., West, Z., Klingshirn, C., and Bruening, C., 2017, "Impacts of Fuel Properties on Combustor Performance, Operability and Emissions Characteristics," *55th AIAA Aerospace Sciences Meeting*, pp. 1–19.
[28] Won, S. H., Haas, F. M., Dooley, S., Edwards, T., and Dryer, F. L., 2017, "Reconstruction of Chemical Structure of Real Fuel by Surrogate Formulation Based upon Combustion Property Targets," Combust. Flame, **183**, pp. 39–49.
[29] Wang, C. H., Liu, X. Q., and Law, C. K., 1984, "Combustion and Microexplosion of Freely Falling Multicomponent Droplets," Combust. Flame, **56**(2), pp. 175–197.
[30] Stouffer, S. D., "Personal Communication," Novemb. 2017.
[31] Stagni, A., Esclapez, L., Govindaraju, P., Cuoci, A., Faravelli, T., and Ihme, M., 2017, "The Role of Preferential Evaporation on the Ignition of Multicomponent Fuels in a Homogeneous Spray/air Mixture," Proc. Combust. Inst., **36**(2), pp. 2483–2491.
[32] Yi, F., and Axelbaum, R. L., 2014, "Utilizing Preferential Vaporization to Enhance the Stability of Spray Combustion for High Water Content Fuels," Combust. Flame, **161**(8), pp. 2008–2014.
[33] Bell, D., Heyne, J. S., Won, S. H., Dryer, F. L., Haas, F. M., and Dooley, S., 2017, "On the Development of General Surrogate Composition Calculations for Chemical and Physical Properties," *55th AIAA Aerospace Sciences Meeting*, American Institute of Aeronautics and Astronautics, Grapevine, TX.
[34] Lefkowitz, J. A., and Haas, F. M., 2017, "Distillation-Resolved Evolution of Key Combustion Properties," *10th U.S. National Combustion Meeting*, College Park, Maryland.

Milestone(s)

- ASME Power Expo Convergence Publication

Major Accomplishments

- Explained the anomalous non-monotomic LBO behavior previously

Publications

Peer-reviewed Publications:
None

Conference Proceedings:
Bell DC, Heyne JS, Won S, Dryer FL. The Impact of Preferential Vaporization on Lean Blowout in a Referee Combustor at Figure of Merit Conditions. ASME. ASME Power Conference, *Volume 1: Fuels, Combustion, and Material Handling; Combustion Turbines Combined Cycles; Boilers and Heat Recovery Steam Generators; Virtual Plant and Cyber-Physical Systems; Plant Development and Construction; Renewable Energy Systems* ():V001T01A011. doi:10.1115/POWER2018-7432.

Outreach Efforts

Conference presentations:
Bell DC, Heyne JS, Won S, Dryer FL. The Impact of Preferential Vaporization on Lean Blowout in a Referee Combustor at Figure of Merit Conditions. ASME. ASME Power Conference, *Volume 1: Fuels, Combustion, and Material Handling; Combustion Turbines Combined Cycles; Boilers and Heat Recovery Steam Generators; Virtual Plant and Cyber-Physical Systems; Plant Development and Construction; Renewable Energy Systems* ():V001T01A011. doi:10.1115/POWER2018-7432.

Awards
David Bell, 2018 Young Engineer of the Year- ASME Dayton Section Award

Student Involvement
David Bell is lead for this project.

Plans for Next Period
Continue with additional LBO tests for the remaining NJFCP fuels (i.e., the remaining category A and C fuels as well as the fuel blends and surrogate blends). This paper will also proceed to publication once the foundational data for the analysis is published.

Task 4- Cross-Experiment Analysis
University of Dayton

Objective(s)
The objective of this task is to link low cost fundamental experiments to larger cost more complicated experiments internal to the NJFCP.

Research Approach
Methodology
The combustor rigs in the NJFCP aim to capture combustor variations found in actual gas turbine engines. In testing in the different combustors, rig sensitivity to fuel properties can be more fully realized. The Referee Rig, Georgia Tech, Sheffield, Cambridge, UTRC, and DLR rigs are all variations of traditional Rich-Quench-Lean combustors. The Honeywell rig is an Auxiliary Power Unit, a combustor that is used to start the main engines and provide emergency backup for electrical systems in the case of engine failure during flight. As such, this combustor is smaller than the other rigs in the program. The last rig in the program, the Well Stirred Reactor (WSR), is premixed and prevaporized. Although not currently used in gas turbine engines, the WSR is a useful research tool to evaluate the chemical fuel property effects on combustion. Table 1 provides a breakdown of the combustor rigs in the NJFCP including atomizer geometry and the operating conditions tested. An additional column, “Random Forest”, was included to indicate the rigs that were used in the random forest regression results presented later.

The results discussed in this paper include conventional (Category A) and test (Category C) fuels, with the latter representing a large range of physical, volatile, and chemical properties. Category A fuels are conventional petroleum-derived fuels in use today that characterize the ‘best’ to ‘worst’ range of fuel properties while Category C fuels represent alternative jet fuels having extreme properties.

Figure 2 shows how the Category C fuel properties compare to the conventional Category A fuels. Notably, many of the Category C fuels fall outside the range of current experience, as depicted in the red regions on the plot, allowing for insight into how these fuels impact the key FOM.

Tables 2 and 3 provide a summary of the fuels tested and included in the results for this paper. In addition to the A and C fuels included in Table 2, there are F fuels which are blends of the A and C fuels, and there are the surrogate (S) fuels which were designed to stress specific fuel properties. Detailed properties of the Category A and C fuels are provided by Edwards[13] and properties for other mixtures and blends were estimated using standard (linear) mixing rules. Radical indexes, a scaled determination of a fuels reactivity at strained extinction, for the A and C fuels were obtained from previously published literature[14] while surrogate values were calculated by the summation of mole fractions multiplied by their corresponding radical index[15].



Table 1. NJFCP combustor rig descriptions and LBO test conditions for each institution. The DCN Slope column records the LBO vs DCN slope representing rig sensitivity to DCN. Rig data used in future Random Forest results are indicated here.

Rig Name	Geometry type (injector/swirler)	Secondary air jets	T_{air}, K	T_{fuel}, K	P, atm	DCN Slope	Institution	Random Forest
PA-GT	Pressure atomizer/ Pratt & Whitney Swirler	No	550, 450, 300	445-460	3.4	-0.194	Georgia Tech	
PA-HON	Pressure atomizer/ toroidal	No	324, 525, 557, 562, 394	288	1, 1.3, 1.4, 2, 3.3, 5.7	NA*	Honeywell	X
PA-RR	Pressure atomizer/ High-Swirl (P03)	Yes	239, 258, 400	239, 258, 320	2	-0.242	AFRL/ UDRI	X
PV-WSR	Prevaporized/ toroidal	No	450	450	1	-0.070	AFRL/UDRI	X
AA-SH	Airblast atomizer/ swirler stabilized/Rolls-Royce Tay Combustor	Yes	323, 373, 423		1	-0.273	Sheffield	X
PA-CAM	Pressure in bluff-body/	Yes	340	300	1	-0.254	Cambridge	
PA - UTRC	Pressure atomizer/ Pratt & Whitney Swirler	No	555, 494		8.64, 5.6	-0.153	UTRC	
PA-DLR	Pressure atomizer/ swirl stabilized	No	323, 373		1	-0.102	DLR Germany	

***HON data renormalized to protect proprietary rig information**

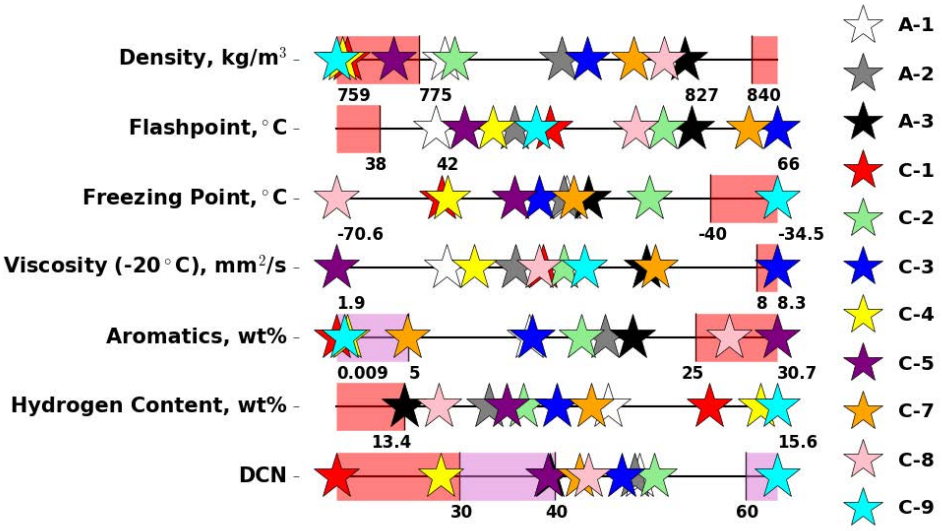


Figure 2. Category A and C range of fuel properties. The red regions represent current specification limits while the purple regions represent areas of interest to explore.

Table 2. NJFCP category A and C fuels representing petroleum-derived and alternative fuels, respectively. The F fuels are blends consisting of both the A and C fuels. The S fuels are surrogates that were designed to stress certain fuel properties.

Fuel/Solvent Mixture	POSF Number	Composition, % volume	Description
A-1	10264	Petroleum JP-8	Low flash, viscosity, and aromatics
A-2	10325	Petroleum Jet A	Nominal jet fuel
A-3	10289	Petroleum JP-5	High flash, viscosity, and aromatics
C-1	11498, 12368, 12384	Gevo ATJ, Highly branched C12 and C16 paraffins	Low DCN, unusual boiling range
C-2	11813, 12223	16% *tri*-methylbenzene + 84% C14 *iso*-paraffins	Chemically-asymmetric boiling range
C-3	12341, 12363	64% A-3 + 36% farnesane	High viscosity fuel, at viscosity limit for jet fuel at -20˚C
C-4	12344, 12489	60% C9-12 *iso*-paraffins, 40% C-1	Low DCN, conventional, wide boiling range
C-5	12345, 12713, 12789, 12816	73% C10 *iso*-paraffins, 17% *tri*-methylbenzene	Flat boiling range
C-6		High cycloalkane content	High *cyclo*-paraffins
C-7	12925	75% RP-2, 23% A-3, 2% decalin	High *cyclo*-alkanes
C-8	12923	Jet A + Exxon aromatic blend	High (maximum allowable) aromatics
C-9	12933	80% R-8 HEFA, 20% *n*-C12	High DCN
F-1	NA	80/20 A-2/C-2	Blends
F-2	NA	50/50 A-2/C-1	Blends
F-3	NA	20/80 A-2/C-1	Blends
F-4	NA	80/20 A-2/C-5	Blends



J-1	NA	75.5% 1,3,5-tri-methylbenzene, 24.5% n-dodecane	Similar DCN to C-1 with low Radical Index
n-C12	NA	n-C12	High DCN
S-1	12765	59.3/18.4/22.2 vol% *n*-dodecane/ *iso*-octane/ 1,3,5-*tri*-methylbenzene	Similar to A-2, lower density and average molecular weight
S-2	12785	52.6/25.1/22.2 vol % *n*-hexadecane/ *iso*-octane/1,3,5-*tri*-methylbenzene	Similar to A-2, higher density and average molecular weight

Table 3. Fuels tested for LBO in each of the NJFCP rigs.

	A-1	A-2	A-3	C-1	C-2	C-3	C-4	C-5	F-1	F-2	F-3	F-4	S-1	S-2	nC12
GT	X	X	X	X	X	X	X	X	X	X	X		X	X	X
Honeywell	X	X	X	X	X			X							
Referee Rig	X	X	X	X	X	X	X	X	X	X	X	X	X	X	X
WSR		X	X	X			X								X
Sheffield	X	X	X	X		X	X	X							
Cambridge		X		X				X							
UTRC	Sasol IPK, F-76, L-210, JP-5, Jet-A, L-142, HRJ JP-5, Linpar 1416														
DLR	Crude-derived Jet A-1 Jet A-1 + 50% n-dodecane, FSJF (certification), FSJF (commercial), FSJF (commercial) + 1.5% HCPP, Experimental GTL kerosene, Synthetic paraffinic kerosene (SPK), Heavy naphtha refinery stream														

A methodological approach was taken to examine the observed differences in rig sensitivities, starting first with a statistical analysis of the LBO data from each rig using random forest regressions, as seen in Figure 4- Figure 7. Random forests, a machine learning technique, utilize a "forest" of decision trees to model complex sets of data without overfitting. A "forest" of regression trees, 500 in this case, is formed from the original data set by random sampling with replacement, also called bagging, which helps to de-correlate the trees and reduce bias. Each regression tree is then grown using Equation 2 where j is the splitting variable, s is the split point, R is the region, and c is the average y_i in the region. Trees are then modeled using Equation 3 where c_m is the average of $y_i|x_i \in Rm$.

$$\min_{j,s}\left[\min_{c_1}\sum_{x_i\in R_1(j,s)}(y_i-c_1)^2+\min_{c_2}\sum_{x_i\in R_2(j,s)}(y_i-c_2)^2\right] \tag{2}$$

$$f(x)=\sum_{}^{M}c_m I(x\in R_m) \tag{3}$$

For the regression, an additional level of randomness is added by randomly selecting m variables from p total variables at each node. The random forest predictor is then calculated using Equation 4 where B is the number of trees, $\{T(x;\Theta_b)\}_1^B$ is the actual trees in which Θ_b describes the bth tree in terms of split variables, cut points, and terminal-node values. In this case, the tree continues to grow until the number of samples left at a given node is two.

$$\hat{f}_{rf}^{B}(x)=\frac{1}{B}\sum_{b=1}^{B}T(x;\,\Theta_b) \tag{4}$$

From the random forest predictor, features from the regression can be identified based on their importance to the model. These feature importance plots were used to understand the properties most impactful in LBO for each rig. For the LBO random forest regressions, the equivalence ratios (ϕ) at blowout for each fuel were normalized to A-2 to allow for equivalent comparison across rigs in combined regressions. This normalized phi value was used as the output of the regression while all other fuel characteristics, including volatile, physical, and chemical properties, along with test conditions (when relevant) were used as the predictors.

To better illuminate the importance of the characteristic timescales resulting in LBO, one fuel property was chosen to represent each of the timescales. The properties chosen in an attempt to maintain orthogonality, that is the variables (properties) are not correlated or covariate of each other. Twenty percent (20%) recovered, one measure of a fuel's volatility, was chosen to represent droplet evaporation. Viscosity was considered to represent the primary and secondary droplet breakup, but due to its high correlation with the distillate properties, density was chosen instead to characterize droplet break-up times.[16] Although DCN and radical index are highly correlated for fuels with high aromatic or n-alkane content, fuels with high *iso*-alkane content, such as C-1, break this correlation as seen in Figure 3. Additionally, the J-1 fuel was designed to have a DCN similar to C-1 with a lower radical index to stress the difference in the two fuel properties as explore by Stachler, et. al.[15] As such, DCN was used to represent the autoignition timescale while radical index was used to characterize the extinction timescale. Table 4 shows the breakdown of fuel property and corresponding timescale.

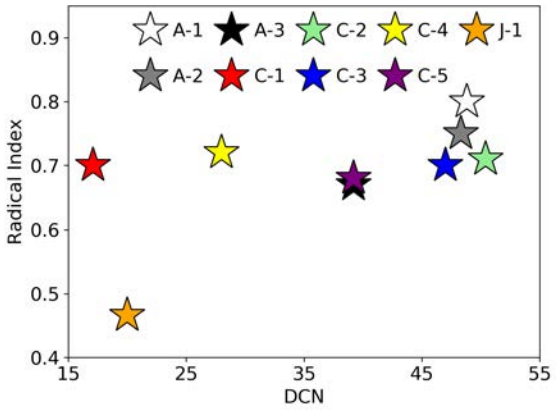


Figure 3. DCN versus Radical Index for the A and C fuels shows how high *iso*-octane fuels such as C-1 stress their correlation. The J-1 fuel was designed to further explore the importance of Radical Index relative to DCN.

Table 4. Fuel properties were chosen to characterize each of the different timescales on the progression to LBO to orthogonalize the random forest results.

Fuel Property	Timescale
DCN	Autoignition
20% Recovered	Droplet Evaporation
Density	Primary and Secondary Droplet Breakup
Radical index	Extinction

Results

The results presented here focus on individual rig regressions as it was found that combined regressions were limited by the geometrically known properties of each rig. Of the nine rigs mentioned, only four are discussed here to show the range of rig physical property effects, where the WSR and Honeywell APU rig represent the extreme ends, and the Referee Rig and Sheffield rig represent real main engine effects. For the combined regressions to capture more variability in the data adequately, more detailed rig descriptions are needed. While past combined random forest regression results showed DCN as being the most important feature, interestingly, individual rig regressions show a wide range of results with additional fuel properties and test conditions appearing to have significant influence. As shown in Figure 4 the individual regression for the Referee Rig, when considering only the timescale representative fuel properties, shows DCN, or the autoignition timescale, as being the dominating timescale followed by droplet evaporation and droplet breakup. The extinction timescale, represented by radical index, was the least important timescale for this rig. The WSR, as seen in Figure 5 shows both the autoignition and extinction strain rate chemical timescales as being the most important in determining LBO, supporting past reported results. In contrast, for example to the WSR regression, the random forest regression for Honeywell shows DCN and radical index as the least important fuel properties in determining LBO while volatile and physical properties dominate, as seen in Figure 6[17]. Honeywell was able to test for LBO at a variety of inlet temperature and pressures unlike the other rigs discussed here, and as expected, these inlet conditions were among the top features important in determining LBO. Lastly, Sheffield, in Figure 7, showed droplet breakup and the autoignition timescales to be of near equal importance in the progression to LBO followed by droplet evaporation and extinction. Interestingly, using only four fuel properties representative of the various timescales in the progression to LBO yielded R-squared values comparable to the random forest regressions in which all fuel properties were included.

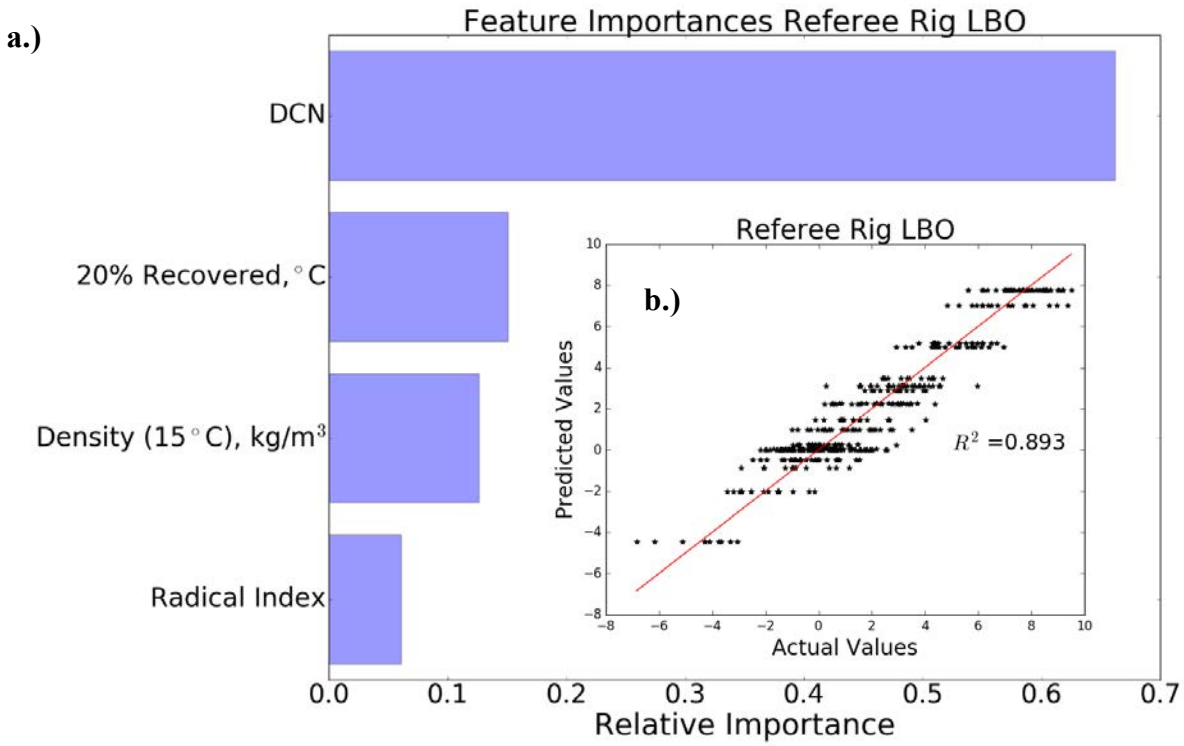


Figure 4. a.) Feature importances from the random forest regression for the Referee Rig show DCN as the most important fuel property representative of the autoignition timescale. **b.)** The predicted versus actual LBO data points are presented here.

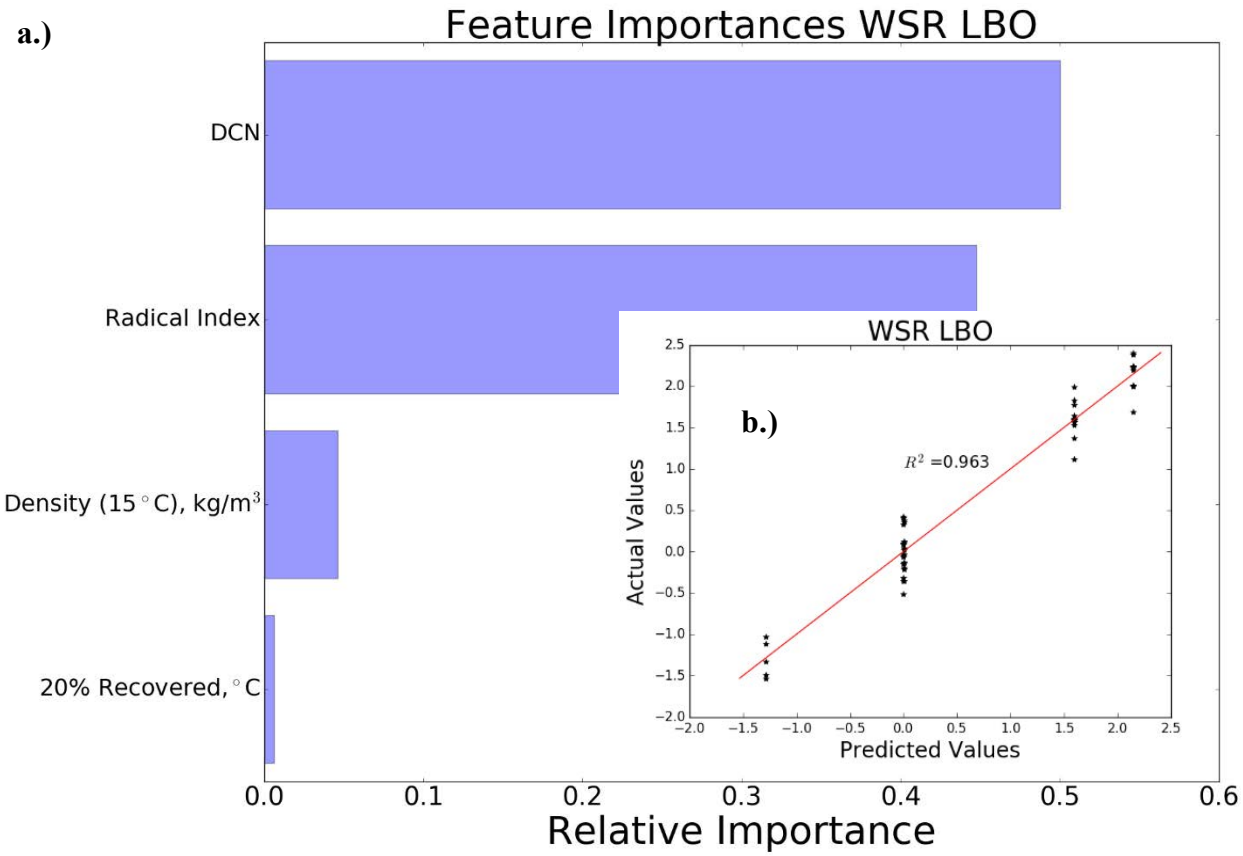


Figure 5. a.) Feature importances from the random forest regression for the Well-Stirred Reactor show the chemical timescales represented by DCN and radical index as being the most important features in determining LBO. Other properties such as distillate and physical properties show almost no statistical significance in the regression. **b.)** The predicted versus actual normalized LBO points are shown here.

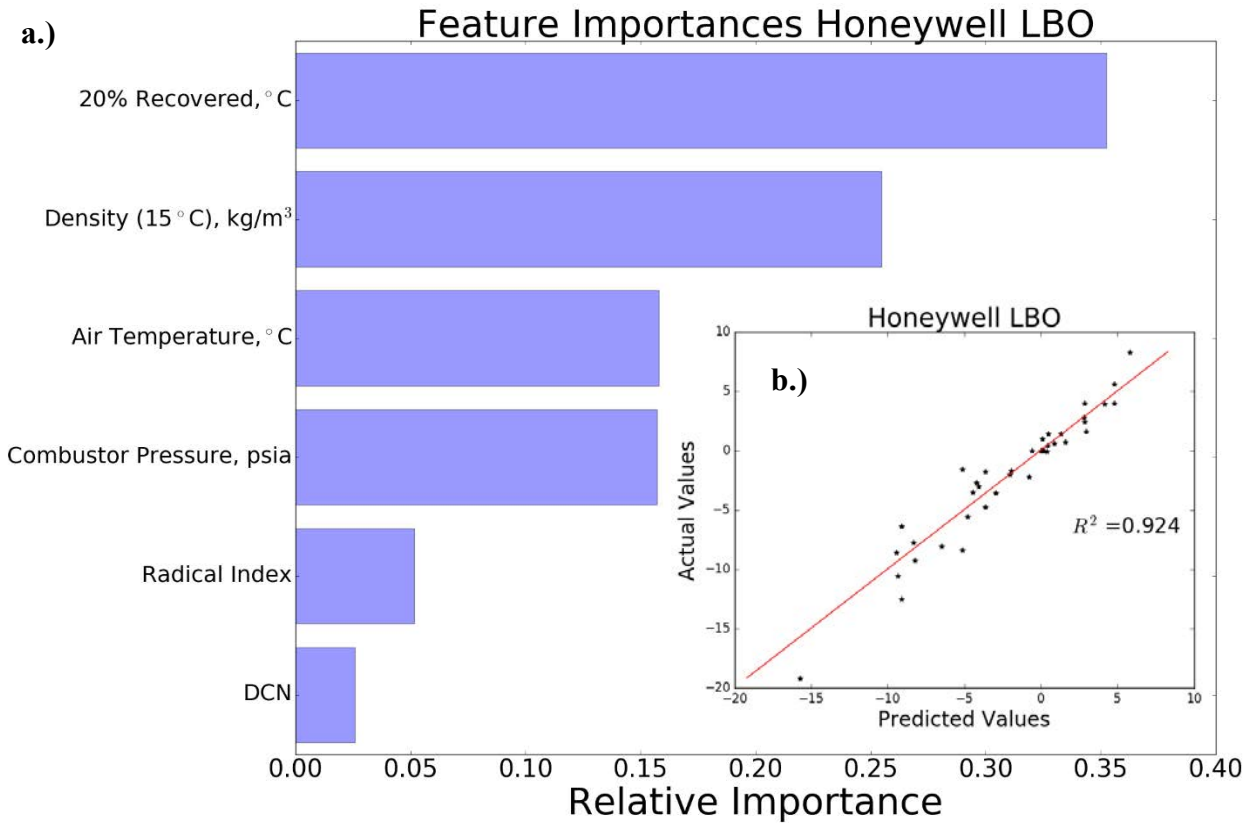


Figure 6. a.) Feature importances from the random forest regression for the Honeywell APU rig, the only rig in the NJFCP that does not show a dependency on DCN for predicting LBO. Distillate and density fuel properties, representative of droplet evaporation and breakup size, respectively, along with inlet temperature and pressure conditions were identified as the most import features for LBO for this rig. **b.)** Please note that the actual versus predicted values have been intentionally renormalized to protect proprietary information. Without the air temperature and combustor pressure parameters, the random forest regression only captures 61% of the variability in the data compared to the 92% presented here.

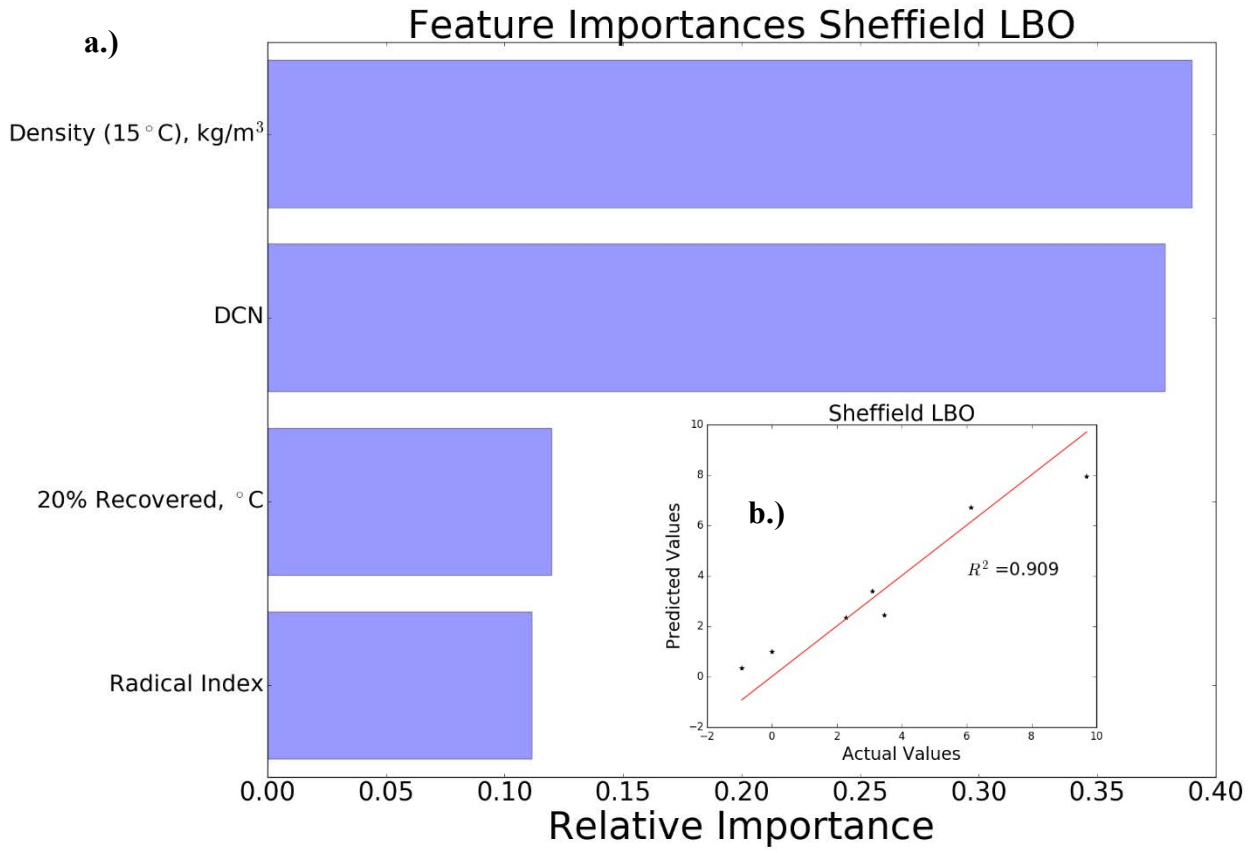


Figure 7. a.) Feature importances for the Sheffield rig show density, representative of droplet breakup, and DCN, representative of the autoignition timescale, as being of equal importance. b.) The predicted versus actual normalized LBO points are shown here.

Discussion

Although each rig expressed a different sensitivity to DCN, here we elaborate on a previously reported theory tying the observed sensitivity to experimental configuration of various rigs. Previously, a timescale analysis was suggested to account for preferential vaporization[18], spray-chemical reactivity timescales[4], and historical explanations of relative physical process times[3]. Figure 8 illustrates LBO as conceptual flow chart, beginning with fuel atomization and terminating with chemistry. LBO occurs when any of the six broad independent variables perturbe the system sufficiently that chemical heat release effectively terminates. Three of these broad physical variables revolve around fuel properties, and three physical variables revolve around geometrical and flow rate variables. Purple ovals represent fuel properties that can perturb stabile burning and coral ovals represent geometrical biases to the system. Fuel properties, purple ovals, are incorporated in the each of the previously reported random forest regressions. Geometrical variations across rigs, coral ovals, are only captured in combined random forest regressions, not reported here, through atomizer and rig geometry distinctions.

The six broad independent variable sets that can lead to LBO can additionally be described as three dependent times scales- referred to as evaporative, mixing, and chemical timescales. These timescales, therefore, are a combination of relevant fuel properties, geometrical biases, thermodynamic conditions, and rig flow rates. LBO occurs when a geometrically biased fuel property dependent timescale exceeds some other critical rig dependent timescale, such as primary recirculation or bulk rig residence times. Here the three dependent timescales are further explored and estimated to explain the relative fuel sensitivity differences across rigs.

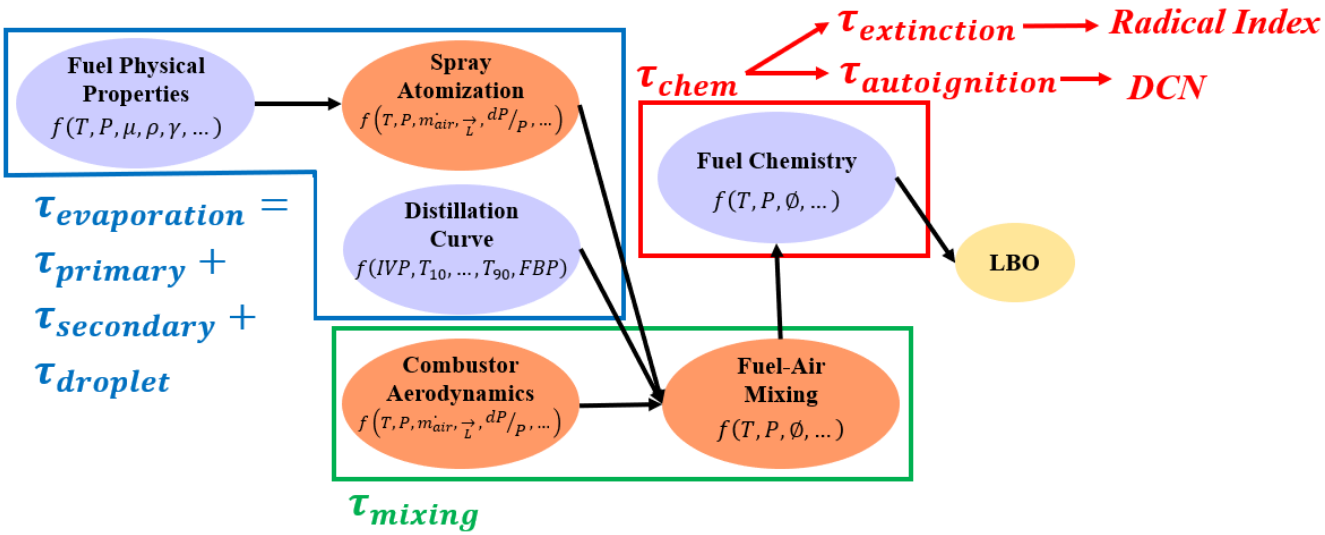


Figure 8. The pathways to LBO can be broken down into a conceptual flowchart. The purple ovals represent fuel properties while the orange ovals represent combustor characteristics. These pathways can be grouped to illustrate the evaporative, mixing, and chemical timescales that are factors in affecting blowout.

The evaporation timescale is a function of fuel physical properties, distillate properties, and atomizer characteristics for a given set of conditions. It can be approximated as the algebraic sum of primary atomization, secondary atomization, and droplet timescales. Primary and secondary atomization timescales increase with increasing fuel density, surface tension, and viscosity. Larger atomization timescales then result in larger droplets and longer evaporation times, and it should be noted that the atomization method has a significant effect on the primary and secondary atomization timescales. The droplet timescale of a fuel can be estimated with fuel volatility, as expressed through the distillation curve. Increases in the relative distillation temperatures of a fuel result in longer droplet timescales via larger characteristic heat capacities and lower vapor pressures. While all of the distillate properties are highly correlated, the 20% recovered temperature has been found to be the most influential in predicting LBO of the volatile properties for the rigs discussed here and thus was used in the earlier regressions.

The mixing timescale includes both combustor aerodynamics and fuel-air mixing, no fuel properties. Combustor aerodynamics is a function of combustor geometry ($\vec{L}$), temperature (T), pressure (P), mass flowrates of fuel and air ($\dot{m}$), relative pressure drop $\left(\frac{dP}{P}\right)$, along with other combustor operating conditions. The combustor timescale for mixing is assumed to be constant for a given rig at a given set of conditions.

Finally, the chemical timescale is a function of the fuel chemical properties and, similar to perfectly stirred reactor (PSR) theory, can be described as two timescales. PSR theory predicts an extinction and ignition timescale. Similarly, extinction and autoignition timescales have been observed[6] and speculated[15] from various NJFCP rigs reported here. Autoignition timescales are estimated from the DCN of a fuel, and extinction timescales can be approximated using radical indexes and extinction strain rates[15]. The relative concentrations of aromatics, *iso*-paraffins, *n*-paraffins, and cyclo-paraffins result in a fuel's radical index and DCN, which are derived directly from a fuel's chemical reaction pathways, specific energy [MJ/kg], and diffusivity [molecular weight, gm/mol]. Interestingly, autoignition timescales can be derived from both zero dimensional simulations and measurements, but extinction timescales have been best approximated by one dimensional experiments.

Combined, these timescales can be used to illuminate dominate/controlling timescales/physics in each of the aforementioned rigs, which can be used to inform the ASTM alternative jet fuel evaluation and approval process. Figure 9 illustrates estimated (relative) timescale differences between the four rigs with the total time normalized to the same value. Evaporation timescale (blue) and chemical timescale (red) are estimated from the random forest regressions while the mixing timescale (green) is currently unquantified between the rigs (but is nearly constant for a rig across the fuels tested).



Collectively, the four rigs show chemical and evaporative dominated results as well as a rig with a competition between chemical and evaporative timescales.

Chemical timescales dominate for the Referee Rig and the WSR. The observed results for the WSR corroborate expectations, as the rig introduces prevaporized and premixed fuel into the reacting region. In the absence of any two phase flow in the reactor, the evaporative timescale influence is anticipated to be zero. Similarly, Stachler et al. have shown in more detail that extinction strain rates (via radical indexes) are likely the controlling timescale for extinction strain rates. From the above regressions and past results, the WSR has demonstrated a dependence on DCN for predicting LBO. Alternatively, it can be argued that pure extinction is playing a much larger and limiting role than in the other combustor designs with strong recirculation.

The swirler and wide nozzle spray angle of the Referee Rig are anticipated to be the root causes for chemical timescale dominance in the Referee Rig. It is hypothesized that the strong recirculation zone, caused by the swirler, of the Referee Rig relative to the Honeywell APU elevates the probability of a reignition event in the region of primary recirculation. Additionally, the wide spray angle of the Referee Rig causes wetting on the surface of the swirler[7]. This wetting in turn enables an additional mechanism for atomization and spray break-up. Combined, it is hypothesized that the swirler and wide spray angle diminish the sensitivity of LBO to evaporative timescales.

Evaporative timescales are observed to dominate in the Honeywell APU, with chemical-evaporative timescales appearing to be in equilibrium in the Sheffield rig. Honeywell, in complete contrast to the WSR, showed almost no dependence on the chemical properties encompassing the chemical timescale in the progression to LBO[16]. Instead the droplet breakup and evaporation are the dominating timescales. The Honeywell rig, in contrast to the WSR and Referee Rig, does not have a swirler, nor does it prevaporize or premix the fuel. Additionally, the Honeywell rig has a considerably smaller pressure atomizer. Pressure atomizers are known to more sensitive to atomization properties relative to air blast atomizers, with smaller pressure atomizers known to be even more sensitive to physical properties than larger pressure atomizers. This analysis, again, is consistent with existing/historical conceptual understandings of fuel spray effects.

The Sheffield rig shows an even split between the droplet breakup and autoignition timescale on the progression to LBO. As the Sheffield rig utilizes an airblast atomizer in contrast to the other pressure and prevaporized rigs, the larger dependence on density and other droplet breakup properties is well explained, although further analysis is needed to explain the autoignition timescale importance. The evaporative timescale and extinction timescale were found to be of lesser significance on the progression to LBO.

Of the seven rigs, the three most sensitive to DCN have secondary air jets which act to strengthen the primary recirculation zone. This would help to explain past results showing the DLR rig[4], a rig similar to the Referee Rig except without secondary air jets, having a much smaller sensitivity to DCN. This hypothesis could be confirmed through the acquisition of swirl numbers, a property than can be used to describe a combustors primary recirculation zone strength. Additionally, continued LBO tests with varying secondary air jet configurations/strengths could confirm this hypothesis as well.

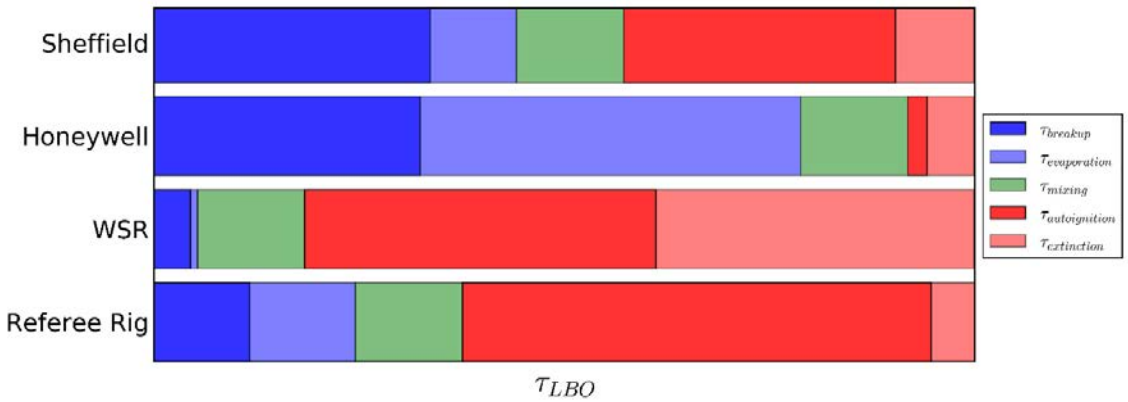


Figure 9. The LBO timescale, a summation of the evaporative (blue), mixing (green), and chemical (red) timescales, for the Referee Rig, Well-Stirred Reactor (WSR), and Honeywell based on feature importances from the random forest regressions. The mixing timescale was not captured in the regressions and thus the relative size of its timescale is unknown, represented here by two areas that suggest the true value could be larger or smaller than what is shown here.

Conclusion

The sensitivity of a combustor to fuel effects at LBO will remain a hurdle towards the certification of alternative jet fuel. This paper has sought to explain the differences in rig sensitivity at LBO for four down selected fuel properties. These down selected fuel properties are proposed to represent four fuel property dependent timescales near LBO. Random forest regressions with these four properties over four rigs were able to explain nearly 90% or better of all variance across all fuels considered. This analysis was extended to describe the relative timescales in each rig as LBO is approached.

Two rigs were shown to have chemical timescales dominate near LBO. Chemical timescales were dominate in the event of minimal spray importance via swirler recirculation, prevaporization, and rapid atomization as in the WSR and Referee Rig. The Honeywell APU, with its small pressure atomizer and lack of swirler, was shown to be dominated by evaporative timescales. The Sheffield rig was observed to have nearly equal evaporative and chemical timescale importance. Additional investigation into this rig is needed to fully explain the relative fuel effects in this rig. Future work will involve quantifying each timescale through modelling.

References

[1] Friedrich, C., and Robertson, P. A., "Hybrid-Electric Propulsion for Aircraft," *Journal of Aircraft*, vol. 52, 2015, pp. 176–189.
[2] Plee, S. L., and Mellor, A. M., "Characteristic time correlation for lean blowoff of bluff-body-stabilized flames," *Combustion and Flame*, vol. 35, 1979, pp. 61–80.
[3] Mellor, A. M., "Semi-empirical correlations for gas turbine emissions, ignition, and flame stabilization," *Progress in Energy and Combustion Science*, vol. 6, 1980, pp. 347–358.
[4] Burger, V., "The Influence of Fuel Properties on Threshold Combustion in Aviation Gas Turbine Engines," 2017.
[5] Heyne, J., Peiffer, E., Colket, M., Moder, J., Edwards, J. T., Roquemore, W. M., Shaw, C., Li, C., Rumizen, M., and Gupta, M., "Year 3 of the National Jet Fuels Combustion Program: Practical and Scientific Impacts," *56th AIAA Aerospace Sciences Meeting*, Kissimmee, FL: 2018.
[6] Chtev, I., Rock, N., Ek, H., Smith, T., Emerson, B., Nobel, D. R., Seitzman, J., Lieuwen, T., Mayhew, E., Lee, T., Jiang, N., and Roy, S., "Simultaneous High Speed (5 kHz) Fuel-PLIE, OH-PLIF and Stereo PIV Imaging of Pressurized Swirl-Stabilized Flames using Liquid Fuels," *Submitted to the 55th AIAA Aerospace Sciences Meeting*, Grapevine, TX: American Institute of Aeronautics and Astronautics, 2017.
[7] Stouffer, S., Hendershott, T., Monfort, J. R., Diemer, J., Corporan, E., Wrzesinski, P., and Caswell, A. W., "Lean Blowout and Ignition Characteristics of Conventional and Surrogate Fuels Measured in a Swirl Stabilized Combustor," *55th AIAA Aerospace Sciences Meeting*, 2017, pp. 1–14.
[8] Stachler, R. D., Heyne, J. S., Stouffer, S. D., Miller, J. D., and Roquemore, W. M., "Investigation of Combustion Emissions from Conventional and Alternative Aviation Fuels in a Well-Stirred Reactor," *Submitted to the 55th AIAA Aerospace*

Sciences Meeting, Grapevine, TX: American Institute of Aeronautics and Astronautics, 2017.
[9] Khandelwal, B., and Ahmed, I., "Research Report on Lean Blowout Limit The University of Sheffield Department of Mechanical Engineering," 2017.
[10] Allison, P. M., Sidney, J. A. M., and Mastorakos, E., "Forced Response of Kerosene Flames in a Bluff-body Stabilised Combustor," *55th AIAA Aerospace Sciences Meeting*, Grapevine, TX: American Institute of Aeronautics and Astronautics, 2017.
[11] Sidney, J. A. M., Allison, P. M., and Mastorakos, E., "The effect of fuel composition on swirling kerosene flames," *55th AIAA Aerospace Sciences Meeting*, Grapevine, TX: American Institute of Aeronautics and Astronautics, 2017.
[12] Colket, M., Zeppieri, S., Dai, Z., and Hautman, D., "Fuel Research at UTRC," *In Multi-Agency Coordinating Council for Combustion Research 5th Annual Fuel Research Meeting*, 2012.
[13] Edwards, T., "Reference Jet Fuels for Combustion Testing," *55th AIAA Aerospace Sciences Meeting*, Grapevine: American Institute of Aeronautics and Astronautics, 2017.
[14] Won, S. H., Dooley, S., Dryer, F. L., and Ju, Y., "A radical index for the determination of the chemical kinetic contribution to diffusion flame extinction of large hydrocarbon fuels," *Combustion and Flame*, vol. 159, Feb. 2012, pp. 541–551.
[15] Stachler, R., Peiffer, E., Kosir, S., Heyne, J., and Stouffer, S., "A Study into the Chemical Timescale for a Toroidal Jet-Stirred Reactor (TJSR)," *Central States Section of The Combustion Institute*, Minneapolis: 2018.
[16] Heyne, J. S., Peiffer, E., Colket, M. B., Jardines, A., Shaw, C., Moder, J. P., Roquemore, W. M., Edwards, J. T., Li, C., Rumizen, M., and Gupta, M., "Year 3 of the National Jet Fuels Combustion Program: Practical and Scientific Impacts of Alternative Jet Fuel Research," *2018 AIAA Aerospace Sciences Meeting*, Reston, Virginia: American Institute of Aeronautics and Astronautics, 2018.
[17] Culbertson, B., and Williams, R., *ALTERNATIVE AVIATION FUELS FOR USE IN MILITARY APUS AND ENGINES VERSATILE AFFORDABLE ADVANCED TURBINE ENGINE (VAATE), PHASE II AND III*, AFRL-RQ-WP-TR-2017-0047: 2017.
[18] Bell, D. C., Heyne, J. S., Won, S. H., and Dryer, F. L., "The Impact of Preferential Vaporization on Lean Blowout in a Referee Combustor at Figure of Merit Conditions," *ASME 2018 Power and Energy Conference*, Lake Buena Vista: 2018.

Task 5- Common Format Routine Software Development

University of Dayton Research Institute

Objective(s)

We aim to develop a software package in which the OEMs can utilize the state of the art models being developed by the other NJFCP modeling teams.

Research Approach

This work is motivated for the imperative necessity of expediting combustor rig evaluation process for ASTM D4054 through improved combustion modeling capabilities. This fuel certification entails three main figures of merit, lean blowout, ignition, and cold relight. Current fuel certification requires expensive and time-consuming experimental testing in gas turbine engines. State-of-the-art combustion models that could expedite this process are not readily available for original engine manufacturers (OEMs). The main objective of this work is to bridge the gap between state-of-the-art academic combustion models and industrial software. The second aspect of this project is to speed up the academic codes for reaching industrial grade software category. The third aspect of this project involves verification and validation of this common format routine (CFR) software.

Modeling and simulation of complex fuels in gas turbine combustors is not trivial. Gas turbine combustors are intricate devices with characteristic length scales varying from the sub-millimeter laminar flamelet thickness to the large centimeter-size dilution holes. Therefore, the mesh resolution for gas turbines combustors is in the order of millions to even hundreds of million cells. The time scales associated with combustion and turbulence in the combustor vary from microseconds for the Kolmogorov turbulent length scales and species reaction rates to milliseconds associated with the flow through-time of the combustor. The time steps and mesh requirements for modeling and simulating a combustor are nearly prohibitive. In order to mitigate some of the challenges associated with modeling and simulation of gas turbine combustors, the lower-dimensional manifold combustion (LDMC) models decouple the chemistry and chemistry-turbulence interaction from the complex turbulence computational fluid dynamics (CFD) calculations. The chemistry is computed *a priori* from one-dimensional stagnation flow equations and/or equilibrium calculation. The chemistry-turbulence interaction is computed by presuming probability density functions (PDFs). Transport equations for the moments of the



mixture fraction (Z) and progress variable (C) are solved in the physical space. These values are then used to interpolate and to extract the thermo-chemical and transport information of the pre-tabulated table.

Commercial software such as Fluent [1,2] and Star-CCM+ already have built-in LDMC models. However, there are always limitations in terms of implementation. For instance, Fluent [1,2] pre-tabulates the table in a mixture fraction space directly. Hence, it does not solve for the one-dimensional equations. On the other hand, the CFR software presented in this paper uses a modified Cantera 2.3 [1] package. The CFR pre-tabulates chemical-turbulence interaction in the one-dimensional physical space. This allows the user to vary the transport coefficient formulation and investigated such effects on numerical predictions. Another difference between Fluent [1,2] and the CFR is that the latter can compute the three branches of the combustion phenomenon. The CFR is also more flexible because molecular properties are directly interpolated from the table. Fluent [1,2] does not offer this capability. However, other commercial software package such as Chemkin [1] offers flamelet calculations that include the three branches of combustion. This software is very robust, but does not offer the turbulence-chemistry convolution capability needed for computing turbulent flames. To the best of our knowledge there is no standalone software that offers the capability of performing turbulence-chemistry convolution of a flamelet library. In addition, the CFR software is designed in a manner that more modules and capability can be easily annexed providing more flexibility to the user.

The purpose of this paper are to document the development of the CFR as well as to prove that such software has been verified and validated. Subsequently, the software is introduced. Important definitions are formulations are illustrated and discussed. The verification and validation tests are then presented.

Common Format Routine (CFR) Software

In short, the CFR software can be sub-divided into two components, the pretabulator and the flamelet-based software, which is illustrated in Appendix Figure 1. The pretabulator is capable of tabulating thermo-chemical and transport data for laminar and turbulent flames. The pretabulator is based on a modified version of Cantera 2.3 [3]. Cantera is written in C++ and Python wrappers/codes were developed in order to include new capabilities in Cantera. This Python codes also interact with a C# GUI. This can currently tabulate flamelet prolongation of the intrinsic low-dimensional manifold (FPI) and flamelet progress variable (FPV). The flamelet-based software can attach the pretabulated turbulence-chemistry interaction table to a CFD code. In this case the flamelet-based software was attached to Fluent [1,2]. The flamelet-based software machinery can perform bilinear, trilinear and tetralinear interpolation of this thermochemical table. This software is written in C and its GUI is written using C#. Now detailed description of the software is provided next.

A. Mixture Fraction Definition

Mixture fraction is a conserved scalar. This means that mixture fraction cannot be created or destroyed. Because atomic elements and enthalpy cannot be created or destroyed, mixture fractions is typically defined in this context. Here the mixture fraction is defined in terms of atomic elements and any combination of atomic elements is valid. However, the atomic composition needs to be chosen so that mixture fraction varies between zero and unity.

$$\mathrm{Z} = \sum_{i=1}^{N_{atomic\ selection}} \sum_{n=1}^{N_{species}} \frac{MW_i}{MW_n} Y_n \qquad (1)$$

The user selection of the mixture fraction definition is given by Appendix Figure 2.

B. Progress Variable Definition

The progress variable provides quantitative information of the combustion efficiency. The latter is equal to zero when the flame blows out and combustion efficiency is zero. The maximum value of the progress variable is a real number less than unity. The progress variable is defined in terms of species mass fractions. The equation below indicates that the mixture fraction is the summation of species mass fractions. Typically in the literature CO and CO_2 are selected to indicate the level of completeness of the combustion process. In addition, CO, CO_2, H_2 and H_2O are also chosen species to indicate the combustion efficiency (or completeness of the combustion process).

$$\mathrm{C} = \sum_{n=1}^{N_{species\ selected}} Y_n \qquad (2)$$

The user selection of the mixture fraction definition is given by Appendix Figure 3.



C. Progress Parameter Definition

For premixed and diffusion flamelets, the progress variable defined by Eq. (2) varies in the spatial direction. For a premixed flamelet C increases monotonically from the unburned reactants from zero to a maximum value downstream the flame front. For diffusion flamelets the behavior is non-monotonic and the maximum value of C occurs near stoichiometry and then its value decreases to zero towards the reactant inlets. Therefore, the progress variable definition is a function of mixture fraction, i.e. $C = \mathrm{C}(\mathrm{Z})$. Thereby, the progress parameter Λ is defined as a bijective, unique identifier that can be used to sort each flamelet. This definition is given below.

$$\Lambda = f(C, Z) \tag{3}$$

This definition is particularly useful for modeling diffusion flamelets and has been implemented in the current software. In the CFR this conversion can be enable or disable.

D. Convoluted Thermochemical and Transport Variables

Once state relationships have been computed between thermochemical and transport properties and the lower dimensional manifold variables (i.e., Z andϕ) these quantities need to be convoluted for the turbulence-chemistry interaction using the equation below. The probability density functions (PDF) in this equation reads as "the probability density function of Z as a function of $\tilde{Z}$ and $\widetilde{Z''^2}$." Then, all thermochemical and transport properties (ϕ) such as density (ρ), molecular weight (MW), temperature (T), specific heat capacity (c_p), dynamic viscosity (μ), thermal conductivity (k), species mass fractions (Y_i) and species reaction rates ($\dot{\omega}_i$) are a function of the transported lower-dimensional manifold variables ($\tilde{Z}, \widetilde{Z''^2}, \tilde{\Lambda}$ and $\widetilde{\Lambda''^2}$).

$$\widetilde{\phi}(\tilde{Z}, \widetilde{Z''^2}, \tilde{\Lambda}, \widetilde{\Lambda''^2}) = \int_0^1 \int_0^1 \phi(Z, \frac{\Lambda}{\Lambda_{max}})\, PDF(Z; \tilde{Z}, \widetilde{Z''^2}) PDF(\frac{\Lambda}{\Lambda_{max}}; \tilde{\Lambda}, \widetilde{\Lambda''^2})\, dZ d\Lambda \tag{4}$$

Importantly to note is that the above equation, the progress parameter requires normalization before integration.

E. Lower Dimensional Manifold Transported Variables For Laminar Flows

Equations (5) and (6) are mixture fraction (Z) and progress variable (C) transported equations. When solving for laminar flows convolutions such as that represented by (4) are not necessary. Both equations here contain a transient, a convective and a diffusive term. However, the progress variable in addition contains a source term $\dot{\Omega}_C$.

$$\frac{\partial(\rho Z)}{\partial t} + \frac{\partial(\rho Z u_j)}{\partial x_j} = \frac{\partial}{\partial x_j}\left(\frac{\lambda}{c_p}\frac{\partial Z}{\partial x_j}\right) \tag{5}$$

$$\frac{\partial(\rho C)}{\partial t} + \frac{\partial(\rho C u_j)}{\partial x_j} = \frac{\partial}{\partial x_j}\left(\frac{\lambda}{c_p}\frac{\partial C}{\partial x_j}\right) + \dot{\Omega}_C \tag{6}$$

The source term ($\dot{\Omega}_C$) is computed as follows,

$$\dot{\Omega}_C = \sum_{i=1}^{N_{species\ selected}} \dot{\Omega}_i \tag{7}$$

Hence, the definition of Eq. (7) has to be consistent with the definition of Eq. (2). Then, all thermochemical and transport properties such as density (ρ), molecular weight (MW), temperature (T), specific heat capacity (c_p), dynamic viscosity (μ), thermal conductivity (k), species mass fractions (Y_i) and species reaction rates ($\dot{\omega}_i$) are a function of the transported lower-dimensional manifold variables. The progress parameter can be obtained via Eq. (3).

F. Lower Dimensional Manifold Transported Variables For Turbulent Flows

The transport equations for the lower-dimensional manifold variables (i.e., mixture fraction ($\tilde{Z}$), mixture fraction variance ($\widetilde{Z''^2}$), and progress variable ($\tilde{C}$) are illustrated by equations (8)-(10)) in tensor notation (and in conservative form) in the context of either the unsteady Reynolds-Averaged Navier Stokes (URANS) or Large-eddy simulation (LES) turbulence model formulations. For the former formulation the dependent variable represents the Favre-weighted time-averaged variable whereas for the latter the dependent variable represents the Favre-weighted filtered variable. Equations (8) through (10), respectively, correspond to the mixture fraction ($\tilde{Z}$), mixture fraction variance ($\widetilde{Z''^2}$), and progress variable ($\tilde{C}$).



1. Transport Equations

The transported equations of the lower-dimensional manifold variables contain at least three terms, transient, convection and diffusion. The mixture fraction variance in addition contains a destruction and production of $\widetilde{Z''^2}$ represented by the last two terms of Eq. (9), respectively. The progress variable transport equation also contains a source term represented by the last term of Eq. (10).

$$\frac{\partial(\bar{\rho}\tilde{Z})}{\partial t}+\frac{\partial(\bar{\rho}\tilde{Z}\tilde{u}_j)}{\partial x_j}=\frac{\partial}{\partial x_j}\left(\left(\frac{\lambda}{c_p}+D_t\right)\frac{\partial\tilde{Z}}{\partial x_j}\right) \tag{8}$$

$$\frac{\partial\left(\bar{\rho}\widetilde{Z''^2}\right)}{\partial t}+\frac{\partial\left(\bar{\rho}\widetilde{Z''^2}\tilde{u}_j\right)}{\partial x_j}=\frac{\partial}{\partial x_j}\left(\left(\frac{\lambda}{c_p}+D_t\right)\frac{\partial\widetilde{Z''^2}}{\partial x_j}\right)-\bar{\rho}\widetilde{\chi_Z}+2\bar{\rho}D_t\left(\frac{\partial\tilde{Z}}{\partial x_j}\right)^2 \tag{9}$$

$$\frac{\partial(\bar{\rho}\tilde{C})}{\partial t}+\frac{\partial(\bar{\rho}\tilde{C}\tilde{u}_j)}{\partial x_j}=\frac{\partial}{\partial x_j}\left(\left(\frac{\lambda}{c_p}+D_t\right)\frac{\partial\tilde{C}}{\partial x_j}\right)+\bar{\rho}\widetilde{\dot{\omega}_C} \tag{10}$$

2. Closure Models

For RANS, SAS, DES and LES models the scalar dissipation rate associated with the progress variable (C) is as computed as follows [5].

$$\widetilde{\chi_C}=\gamma_C\frac{\widetilde{Z''^2}}{\widetilde{C''^2}}\widetilde{\chi_Z} \tag{11}$$

The closure models for the RANS-based lower-dimensional manifold transported variable equations are given by the following equations [5].

$$D_t=\frac{\mu_t}{Sc_t} \tag{12}$$

$$\widetilde{\chi_Z}=2.0\frac{\varepsilon}{k}\widetilde{Z''^2} \tag{13}$$

The turbulent Schmidt number (Sc_t) is a constant that is typically chosen to be equal to 0.9. The closure models for the LES-based lower-dimensional manifold transported variable equations are given by the following equations [5].

$$D_t=C_\phi\Delta^2|S| \tag{14}$$

$$\widetilde{\chi_Z}=2.0\frac{\mu_t}{Sc_t}\frac{1}{\Delta^2}\widetilde{Z''^2} \tag{15}$$

The constant C_ϕ is typically chosen to be equal to 0.4.

G. Low-Dimensional Manifold Combustion Models

The flamelet prolongation of ILDM (FPI) and the flamelet/progress variable (FPV) model utilize the one-dimensional stagnation flow equations for computing freely-propagating premixed flames and counterflow diffusion flames, respectively. The freely-propagating premixed flamelets of the FPI model are computed in the physical space and each flamelet is converted to the progress variable space (C) using Eq. (2). In turn, each premixed flamelet correspond to a mixture fraction (Z), which is directly related to an equivalence ratio. On the other hand, FPV model invokes the calculation of multiple diffusion flames. Each flame is computed in the physical space as well. The physical space can be converted to a mixture fraction state relationship (Z) following Eq. (1). Each flamelet correspond to a progress parameter (Λ). Therefore, calculations of multiple premixed and diffusion flamelets lead to a tabulation of thermochemical and transport properties as a function of mixture fraction (Z) and progress variable (C).

1. Transport Equations

The one-dimensional stagnation flow equations are presented above from Eqs. (16)-(21). In ascending order these equations represent the continuity, radial momentum, pressure curvature or strain rate eigenvalue, energy, species and a one-point or two-point dummy differential equation. The equations on the left of the table represent the original equations in Cantera 2.3 [3] for which the pressure curvature is the eigenvalue. The equations on the right represent the optional equations in a modified Cantera 2.3 in which strain rate (a) replaces the pressure curvature as the eigenvalue. The species

Table 1. Original and modified Cantera governing equations.

Equation	Cantera	Modified Cantera	
Continuity	$\frac{\partial \rho u}{\partial z} + 2\rho V = 0,\ V = \frac{v}{r}$	$\frac{\partial \rho u}{\partial z} + a\rho V = 0\ ,\ V = \frac{v}{v_e}$	(16)
Radial Momentum	$\rho u \frac{\partial V}{\partial z} + \rho V^2 = -\Xi + \frac{\partial}{\partial z}\left(\mu \frac{\partial V}{\partial z}\right)$	$\rho u \frac{\partial V}{\partial z} = \frac{\partial}{\partial z}\left(\mu \frac{\partial V}{\partial z}\right) + \Xi(\rho_F - \rho V^2)$	(17)
Pressure Curvature/Strain Rate	$\frac{d\Xi}{dz} = 0,\ \Xi = \frac{1}{r}\frac{\mathrm{dP}}{dr}$	$\frac{d\Xi}{dz} = 0,\ \Xi = a$	(18)
Energy	$\rho u c_p \frac{\partial T}{\partial z} = \frac{\partial}{\partial z}\left(\lambda \frac{\partial T}{\partial z}\right) - \sum_k j_k c_{p,k} \frac{\partial T}{\partial z} - \sum_k h_k W_k \dot{\omega}_k$		(19)
Species	$\rho u \frac{\partial Y_k}{\partial z} = -\frac{\partial j_k}{\partial z} + W_k \dot{\omega}_k$		(20)
One- or Two-point Control	$\frac{du_O}{dz} = 0$		(21)

and temperature equations are not modified. However, an additional dummy Eq. () was added to the governing equations for when the flame control methods are activated.

2. Flamelet Prolongation of ILDM (FPI)

The FPI model computes premixed flamelets for each mixture fraction (Z). When the calculations do not converge because either the flamelets have exceeded the flammability limits or because the maximum temperature of the flamelet is higher than that of equilibrium, equilibrium calculations replace the freely-propagating premixed flamelets. The transport equations for the freely-propagating flamelets are given by Eqs. (22) – (26). The boundary conditions associated with the freely-propagating flamelets are shown in Table 2.

Table 2. Premixed flame boundary conditions.

Equation	Fuel Inlet	Oxidizer Inlet	
Continuity	-----	$\rho u = (\rho u)_O$	(22)
Radial Momentum	$V = V_F$	$V = V_O$	(23)
Pressure Curvature/ Strain Rate	$\rho u = (\rho u)_F$	-----	(24)
Energy	$T = T_F$	$T = T_O$	(25)
Species	$\rho u Y_k + \rho Y_k V_k = (\rho u Y_k)_F$	$\rho u Y_k + \rho Y_k V_k = (\rho u Y_k)_O$	(26)

Table 3. Nonpremixed flamelet boundary conditions.

Equation	Inlet B.C.	Internal B.C.	Outflow B.C.	
Continuity	-----	$T_{j=specified} = T_{fixed,specified}$	------	(27)
Radial Momentum	$V = V_0$	--------	$\frac{dV}{dz} = 0$	(28)
Pressure Curvature/ Strain Rate	$\Xi = 0$	--------	-----	(29)
Energy	$T = T_0$	--------	$\frac{dT}{dz} = 0$	(30)
Species	$\rho u Y_k + \rho Y_k V_k = (\rho u Y_k)_0$	--------	$\frac{dY_k}{dz} = 0$	(31)

3. Flamelet Progress/Variable

The FPV model computes diffusion flamelets for each progress parameter (Λ) along the S-curve. Multiple diffusion flamelets are necessary to build a table of thermochemical and transport properties. The first flamelet is computed at $\Lambda_{max}|Z$ and



then the strain rate is increased by either increasing the inlet velocities, reducing the distance between the opposing jets, or by either the one-point or two point continuation. The computation of diffusion flamelets as a function of strain rates leads to the calculation of the S-curve containing two stable branches (strong and weak) and one unstable (middle) branch. Special continuations techniques are needed to compute the S-curve associated with the diffusion flamelets. This will be discussed in subsequent chapters. The boundary conditions associated with the counterflow flamelets are shown in Table 3.

H. Continuation Methods

Continuation techniques are now presented, zero-order, scaling rules, arc-length, and one- and two-point continuation techniques are presented. The zero-order continuation technique is used for FPI, whereas hybrid continuation techniques of zero-order, scaling rules, some features of arc-length continuation, and one- and two-point continuation techniques are used for the FPV model. The arc-length continuation technique was, however, fully utilized for perfectly-stirred reactors (PSRs) in order to progressively attain the now-used continuation technique for the FPV model. The arc-length continuation for PSR is only available in Python scripts and not through the GUI.

1. Zero Order Continuation

Zero-order continuation techniques can be applied to any flamelets. This technique only supposes that the previous solution is the initial solution to the current solution. This can be represented as $\boldsymbol{x}^* = \boldsymbol{x_0}$, where $\boldsymbol{x}$ refer to a vector solution with M grids points times N equations. This continuation methods can be applied to both FPI and FPV methods. For the former this is the only method available for continuation. For the latter the number of zero-order continuation can be selected from the Flame Control tab as illustrated in the Task 5 Appendix, Figure 4.

2. Scaling Rules

The scaling rules are ideal for computing the upper branch of S-curve. The scale factor proposed by Fiala and Sattelmayer [2] are suitable for the FPV model. These scaling factors are $u{\sim}a^{-1/2}$, $V{\sim}a$, $\dot{m}''{\sim}a^{1/2}$, and $\Lambda{\sim}a^2$. The strain factor, which is the ratio of two sequential flame strain rates, can be entered by the user as illustrated in Appendix Figure 4.

3. Arc-Length Continuation

The system of nonlinear ODEs is represented by $\boldsymbol{F}(\boldsymbol{x}) = 0$. The solution is given by the vector $\boldsymbol{x}$. The results of these equations depend on the parameter λ. The extended solution is represented by $\boldsymbol{F}(\boldsymbol{x}(\lambda), \lambda) = 0$. The arc-length continuation [3] is a predictor-corrector continuation technique.

1. Predictor:

One such predictor is the forward Euler predictor given by:

$$\boldsymbol{x}^* = \boldsymbol{x_0} + \frac{\boldsymbol{dx}}{\boldsymbol{ds}} ds \qquad (32)$$

The gradient $\boldsymbol{dx/dF}$ can be either a tangent or a secant gradient. Here the former is used. The predicted solution $\boldsymbol{x}^*$ is the initial guess for computing the new flame. The solution vector $\boldsymbol{x}$ that lies on the path depends on the parameter λ and this, in turn, depends on arclength s.

2. *Corrector:*

The plane equation parameterized as a function of arclength, s, needs to correct the initial guess $\boldsymbol{x}^*$.

$$N\left(\boldsymbol{x}(\lambda(s)), \lambda(s)\right) \equiv \left\|\frac{\partial \boldsymbol{x}}{\partial s}\right\|_2^2 + \left(\frac{\partial \lambda}{\partial s}\right)^2 - 1 = 0 \qquad (33)$$

Now the augmented systems of equations is given by:



$$\begin{vmatrix} \boldsymbol{F}\left(\boldsymbol{x}(\lambda(s)),\lambda(s)\right) \\ N\left(\boldsymbol{x}(\lambda(s)),\lambda(s)\right) \end{vmatrix} = \begin{vmatrix} 0 \\ 0 \end{vmatrix} \quad (34)$$

This new vector can also be written as $\mathrm{G}(\mathrm{F}(\mathrm{y}),\mathrm{N}(\mathrm{y})) = 0$. The augmented solution vector is given by $\mathrm{y} = \left(\mathrm{x}(\lambda(\mathrm{s})),\lambda(\mathrm{s})\right)$. The Jacobian matrix for the augmented system is represented by the following equation.

$$\boldsymbol{J} = \begin{vmatrix} \frac{\partial F}{\partial x} & \frac{\partial F}{\partial \lambda} \\ \frac{\partial N}{\partial x} & \frac{\partial N}{\partial \lambda} \end{vmatrix} \quad (35)$$

The partial derivative of the plane equations needs to be determined from the plane equation:

$$N\left(\boldsymbol{x}(\lambda(s)),\lambda(s)\right) \equiv \left\|\frac{\partial \boldsymbol{x}}{\partial s}\right\| d\boldsymbol{x} + \frac{\partial \lambda}{\partial s} d\lambda - ds = 0 \quad (36)$$

$$\frac{\partial N}{\partial x} = \left|\frac{\partial \boldsymbol{x}}{\partial s}\right|^T \quad (37)$$

$$\frac{\partial N}{\partial \lambda} = \frac{\partial \lambda}{\partial s} \quad (38)$$

After substituting the equations above into the Jacobian, the augmented Jacobian is now given by:

$$\boldsymbol{J} = \begin{vmatrix} \frac{\partial F}{\partial x} & \frac{\partial F}{\partial \lambda} \\ \left|\frac{\partial \boldsymbol{x}}{\partial s}\right|^T & \frac{\partial \lambda}{\partial s} \end{vmatrix} \quad (39)$$

The augmented Jacobian and the residual equations are used in a Newton-Raphson type solver. The previous k solution is used to compute the new solution k+1.

$$\boldsymbol{y_{k+1}} = \boldsymbol{y_k} - \boldsymbol{J^{-1}G} \quad (40)$$

The Newton-Raphson solver proceeds in this way. It computes the new change in the solution vector, $\Delta \boldsymbol{y_k}$. This change is added to the solution vector of the previous iteration. Note that k=0 the values of $y_0[0{:}N_{eqs}-2]$ are equal to the values of $\boldsymbol{x}^*$.

$$\boldsymbol{J}\Delta \boldsymbol{y_k} = -\boldsymbol{G} \quad (41)$$

$$\boldsymbol{y_{k+1}} = \boldsymbol{y_k} + \Delta \boldsymbol{y_k} \quad (42)$$

$$if\ \Delta \boldsymbol{y_k} < \varepsilon \rightarrow \boldsymbol{y_n} = \boldsymbol{y_{k+1}} \quad (43)$$

3. *Step-size Control:*

The user specifies an initial step size ds that is very large at first and the simulation proceeds. Near the turning points (bifurcations) the step size needs to become smaller in order to resolve the curve and avoid divergence of the Newton solver. Once the solution has passed the turning point the step size ds needs to increase again towards the other turning point. This is accomplished using the following step size control method.

$$\delta = N_{opt}/i_{Newton} \quad (44)$$

$$if\ \delta < 0.5 \rightarrow \delta = 0.5 \quad (45)$$

$$if\ \delta > 2.0 \rightarrow \delta = 2.0 \quad (46)$$

$$ds = \delta \cdot ds \quad (47)$$



This step size control technique works by allowing the user to specify the optimum number of Newton iterations, N_{opt}. If the number of Newton iterations i_{Newton} is below or above the N_{opt} the step size will increase or decrease, respectively. The multiplication factor δ is bounded between 0.5 and 2.0 in order to avoid very small step size or very large step sizes that would either get the simulation stagnant or diverging. The step size control can be accessed through the Flame Control tab.

Some verification calculations are shown in Figure 1 through Figure 3 with numerical results available in the literature. There is nearly perfect match between previously computed S-curve for perfectly-stirred reactors (PSRs) and those computed here. This demonstrates that homotopic calculations and step size control are appropriately programmed for later used in the FPV tabulation procedure.

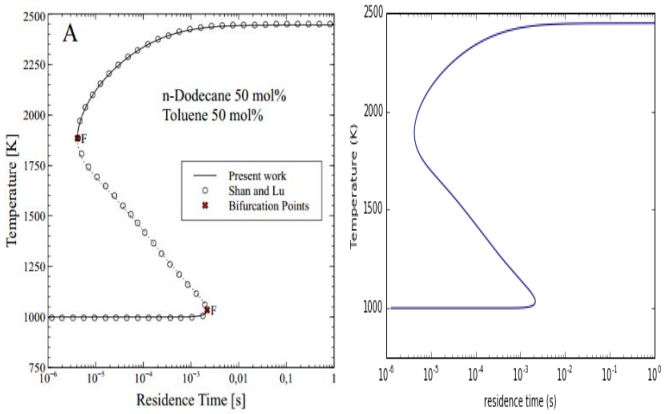


Figure 1. Comparison between Acampora and Marra [7] and in-house arc-length continuation for perfectly-stirred reactor (PSR). The inlet mass flow rate is the independent variable. Both temperature and residence time are output of the PSR. Reprinted from Computers and Chemical Engineering, 85, Acampora, L., Marra, F.S., A general study of counterflow diffusion flames at subcritical and supercritical conditions: Oxygen/hydrogen mixtures, with Permission from Elsevier



4. Flame Control Methods: One- and Two-Point

When the zero-order continuation and the scaling rules fail a flame control can be used to continue the bifurcation path of the S-curve. In the CFR this is automatically activated. The one- and two-point boundary conditions are based on the work of Nishioka et al. [8]. The boundary conditions for the pressure curvature or strain rate eigenvalue (Eq. (24)) is removed and replaced with an internal boundary condition (Eq. (48)) for the one-point continuation method. For the two-point continuation method the continuity equation boundary condition (Eq. (22)) is removed and a new internal boundary condition is added (Eq. (49)). For the one-point control method the oxidizer flux is specified as well as a fixed temperature on the fuel side. For the two-point control method neither the fuel nor the oxidizer flux are specified, but instead two fixed temperature location for the consecutive flamelet calculation at each side of the stagnation plane are prescribed.

Table 4. One- and two-point control boundary conditions.

Equation	Fuel Inlet	Internal B.C.	Internal B.C.	Oxid Inlet	
Pressure Curvature/ Strain Rate	-----	$T(j_{F,specified}) = T_{F,specified}$	-----	-----	(48)
Two-Point Control	------	-----	$T(j_{O,specified}) = T_{o,specified}$		(49)

Figure 4 shows the calculation of the S-curve for a more practical fuel used in gas turbine combustors.

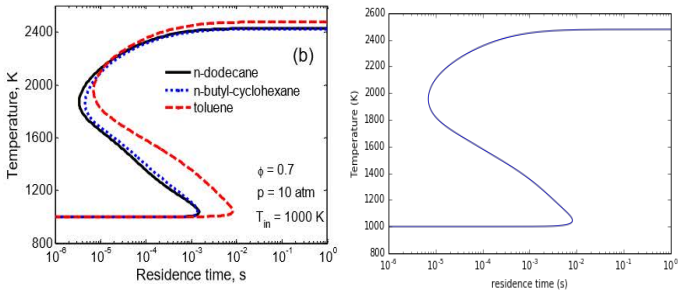


Figure 2. Comparison between Shan and Lu [1] and in-house arc-length continuation for perfectly-stirred reactor (PSR) burning Toluene. The inlet mixture temperature is the independent variable.

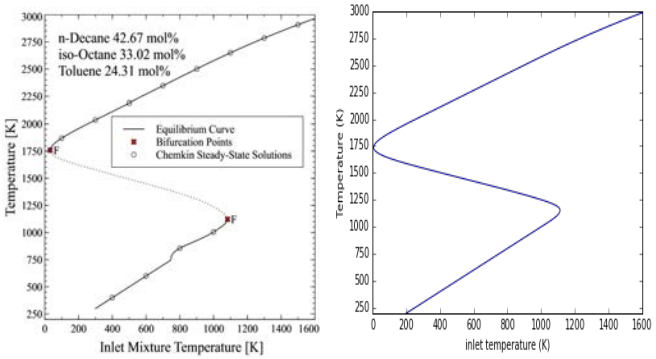


Figure 3. Comparison between Acampora and Marra [8] and in-house arc-length continuation for perfectly-stirred reactor (PSR). The inlet mixture temperature is the independent variable. Reprinted from Computers and Chemical Engineering, 85, Acampora, L., Marra, F.S., A general study of counterflow diffusion flames at subcritical and supercritical conditions: Oxygen/hydrogen mixtures, with Permission from Elsevier.

Figure 5 clearly shows that upper and middle branches can be successfully calculated with the CFR at low and high pressure conditions. Figure 5 illustrates the effect of transport model on the S-curve. There is a slight change on the S-curve for hydrogen-oxygen combustion. This is important because it suggests that the inexpensive unity Lewis number computation is sufficient for PSR without having to invoke more computationally-expensive calculations such as mixture-averaged diffusivity. Figure 7 demonstrates that effect of varying the detailed chemistry. The same fuel-air composition is used with two different chemistry sets, but there is substantial change in the extinction strain rate.

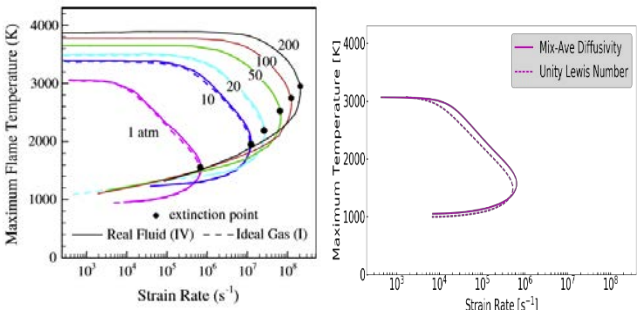


Figure 4. Comparison between mixture-averaged diffusivity and unity Lewis number. The mechanism used here is that of Burke et al. [13] Reprinted from Combustion and Flame, 161, Huo, H., Wang, X., Yang, V., A general study of counterflow diffusion flames at subcritical and supercritical conditions: Oxygen/hydrogen mixtures, with Permission from Elsevier**.**

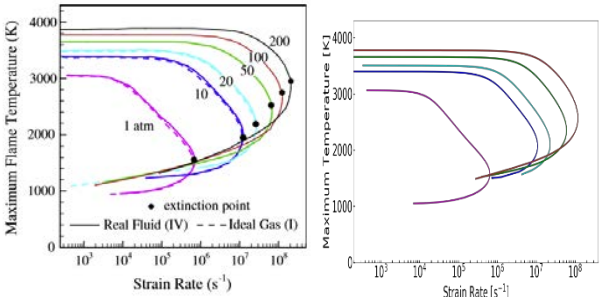


Figure 5. Comparison of strain rate vs. maximum flame temperature between Wang et al. [11] (left) and the in-house model (right). Wang et al. uses Li et al. [12] mechanism, whereas the in-house model uses Burke et al. [13] *Reprinted from Combustion and Flame, 161, Huo, H., Wang, X., Yang, V., A general study of counterflow diffusion flames at subcritical and supercritical conditions: Oxygen/hydrogen mixtures, with Permission from Elsevier.*

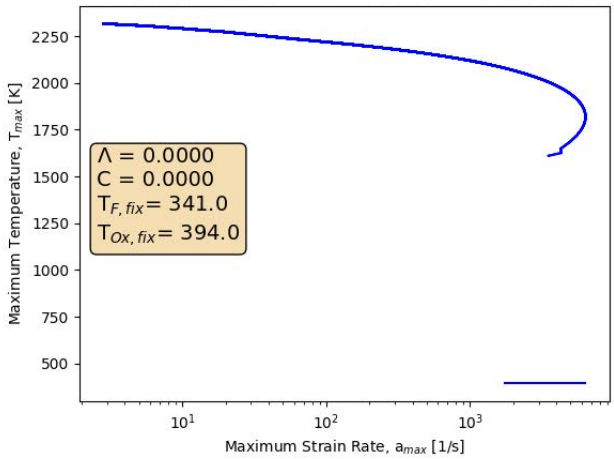


Figure 6. POSF10325-air diffusion flame s-curve.

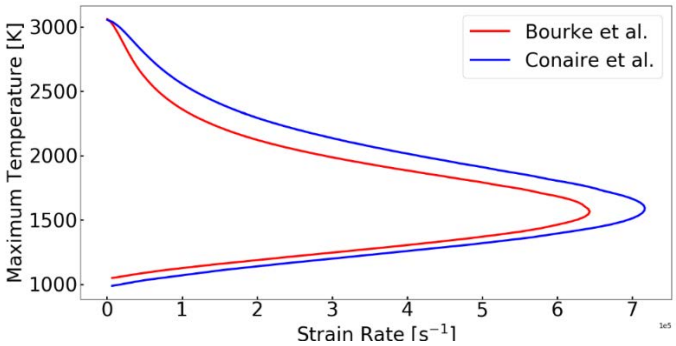


Figure 7. Comparison between Bourke et al. and Conaire et al. mechanisms for the H_2-O_2 flame at 1 atm and inlet temperatures of 300K.

I. Probability Density Functions

Here the Dirac-delta and Beta probability density functions (PDFs) are discussed here. These PDFs could be applied to either the lower-dimensional manifold variables. However, it has been proven that the Beta PDF is more suitable for mixture fraction (Z), whereas Dirac-delta or Beta PDF can be used for progress parameter (Λ).

1. Dirac Delta

The Dirac-delta probability density function is given by the equation below. Dirac-delta could be used for the progress parameter. Hence the x in the equation can be substituted by Λ.

$$\delta(x - x_0) = \begin{cases} 0, & x \neq x_0 \\ 1, & x = x_0 \end{cases} \tag{50}$$

2. Beta

The Beta probability density function is given by the equations below. The probability density function is appropriate for the mixture fraction (Z). Hence, the x in the equation can be substituted for the Z. This PDF could also be utilized to model the progress parameter and the x below would be substituted by Λ.

$$\beta\left(x;\tilde{x},\widetilde{x''^2}\right)=\frac{\Gamma(a+b)}{\Gamma(a)\Gamma(b)}x^{a-1}(1-x)^{b-1} \quad (51)$$

$$a=\frac{\tilde{x}\left(\tilde{x}-\tilde{x}^2-\widetilde{x''^2}\right)}{\widetilde{x''^2}} \quad (52)$$

$$b=\frac{(1-\tilde{x})\left(\tilde{x}-\tilde{x}^2-\widetilde{x''^2}\right)}{\widetilde{x''^2}} \quad (53)$$

The demonstration of these convolutions are shown in Figure 8. The images correspond to a convoluted methane-air diffusion flame. Dirac-delta PDF was used for the progress variable. Note that the effect of turbulence-chemistry interaction represented by the variance of the mixture fraction (in this case) is to weaken the flame by lowering the peak temperature from ~2050 K to ~1750K. Similar the peak progress variable source term drops from ~500 to ~100 ks/m^{3}s^{-1}.

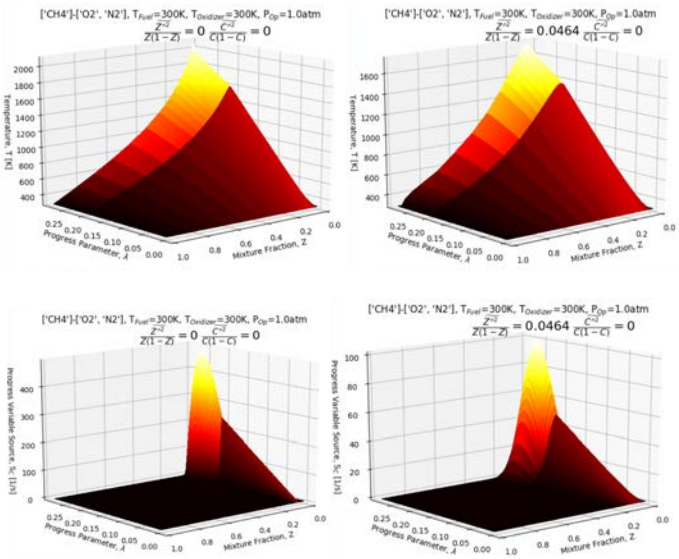


Figure 8. Sample images of a tabulated thermochemical transport tables for a CH_4-air diffusion flame. The top and bottom images illustrate temperature and progress variable source, respectively. The left images show the tabulated variables when both mixture fraction and progress variables are zero. The right images show the tabulated variables when the mixture fraction variance is non-zero.

J. Verification Tests

There are several verification and validation tests. A canonical laminar triple flame was computed using FPI or FPV models. The Sandia D piloted flame was also simulated using RANS/FPV and LES/FPV model. Finally, a single cup combustor rig was simulated using the LES/FPV model.

A. Simulations of a Canonical Triple Flame

Here is the verification test for the laminar formulation for the FPI model. Figure 9 indicates that both calculations are very similar in terms of temperature and CO mass fraction contours. Subtle difference can be attributed to the fact that Wu et al. [9] used FlameMaster solver [10], which computes the flamelets in mixture fraction space directly.

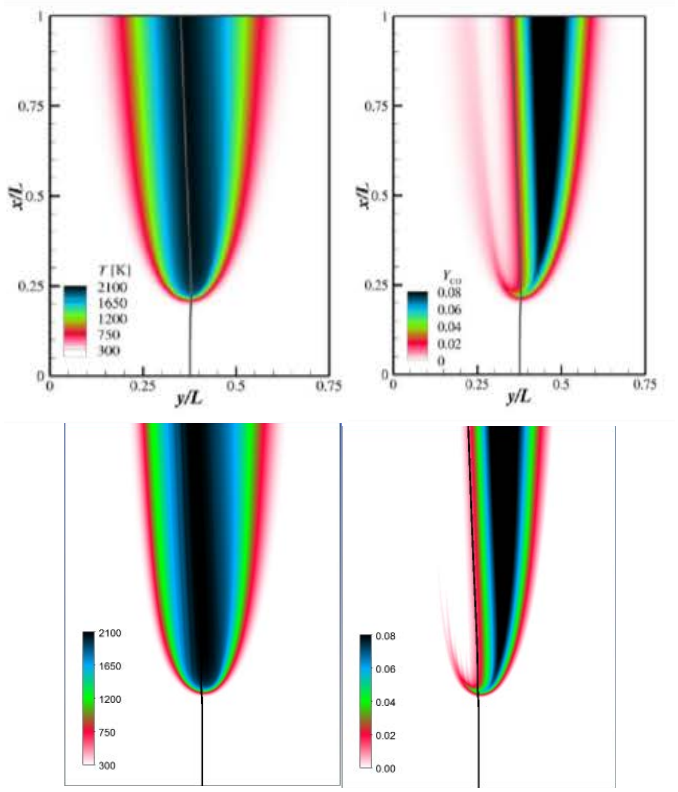


Figure 9. Comparison between (top) Wu et al. [15] and (bottom) CFR results of a laminar triple flame using FPI in terms of (left) temperature and (right) CO mass fractions.

B. Laminar Fpv Simulations For A Canonical Triple Flame

Here is the verification test for the laminar formulation for the FPV model. Figure 10 illustrates the verification step for computing the laminar version of the FPV combustion model of the CFR software.

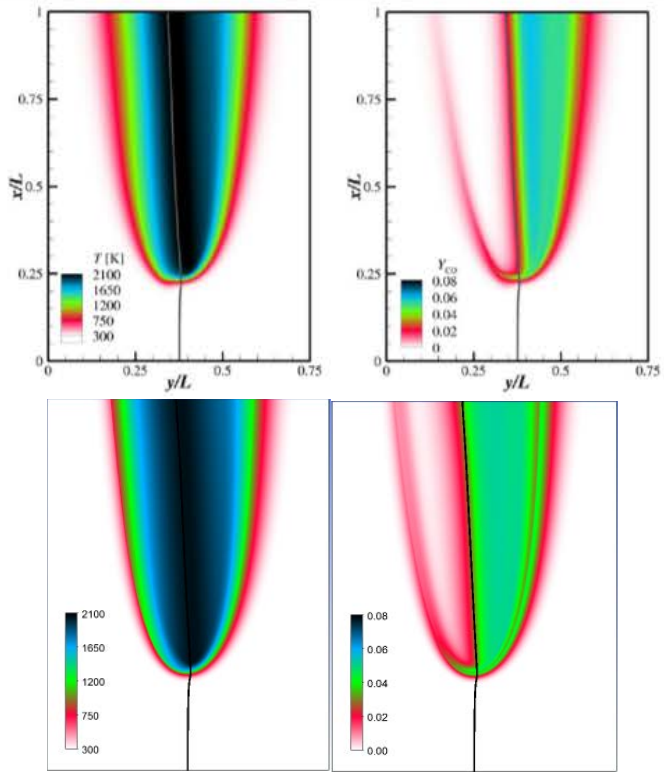


Figure 10. Comparison between (top) Wu et al. [15] and (bottom) CFR results of a laminar triple flame using FPV in terms of (left) temperature and (right) CO mass fractions.

C. Turbulent Simulations of Sandia D Flame

Here are the verification and validation tests for turbulent formulation of the FPV model. Figure 11 presents the experimental measurements against numerical predictions. Numerical simulations were performed only with Fluent [1,2] and with Fluent+CFR software. The k-ε and k-ω RANS version of FPV model were utilized. The Beta PDF is used for mixture fraction and Dirac-delta is used for progress variable. Generally, both the Fluent and Fluent+CFR results compared well with the experimental measurements in terms of temperature and species mass fractions. However, the Fluent+CFR outperforms the Fluent results, specifically, in terms of CO mass fraction. Both Fluent and Fluent+CFR results, nonetheless, underpredict the mixture fraction variance. In terms of RANS model, the k-ω better approximates the measurements.

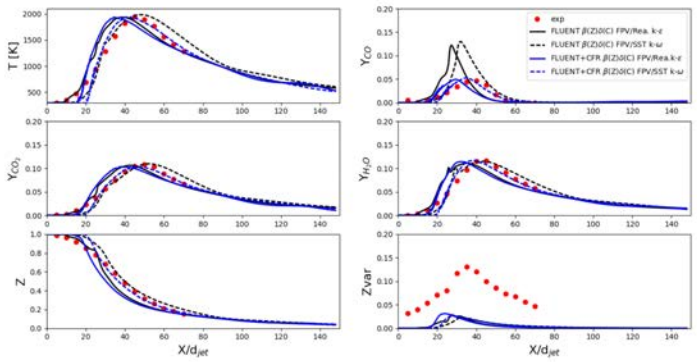


Figure 11. Centerline comparison between experiments and RANS simulations of the Sandia D turbulent flame.

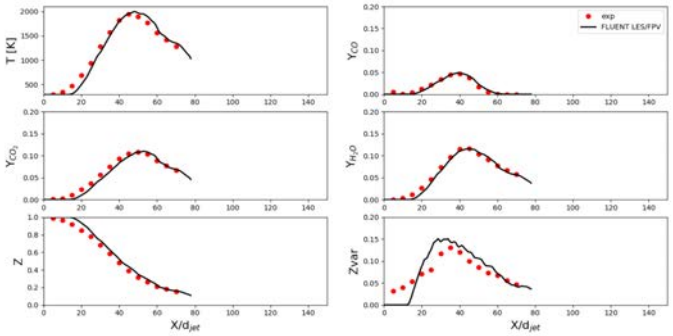


Figure 12. Centerline comparison between experiments and LES simulations of the Sandia D turbulent flame.

Conclusions

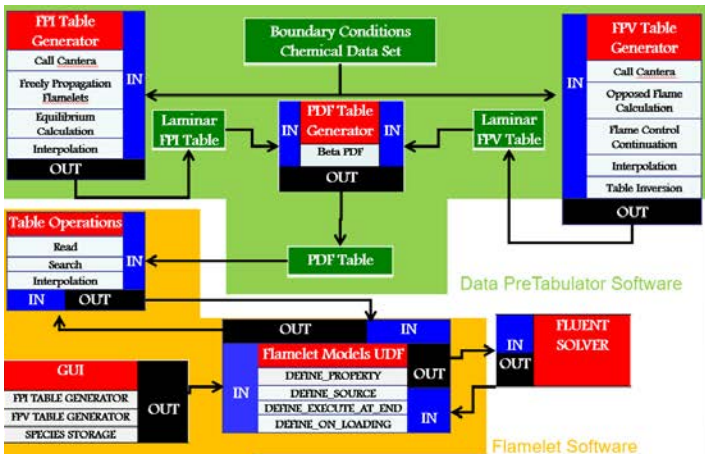
A common format routine (CFR) software for modeling combustion problems have been developed. This software is sub-divided into a thermochemical transport property pretabulator software and a flamelet-based software. The former can be used to create flamelet prolongation of the ILDM (FPI) or flamelet/progress variable (FPV) tables for either laminar or turbulent flames. The pretabulator allows for turbulence-chemistry interaction through either Beta or Dirac-delta probability density function (PDF) of the independent variables. The flamelet-based software can read, search and interpolate the table to extract thermochemical and transport composition based on lower-dimensional manifold transport variables (i.e., mixture fraction, mixture fraction variance and progress parameter). The k-□ and k-□ RANS, SAS, DES and LES turbulence model were coupled with the flamelet-based combustion models. A multiphase spray model successfully couples with the gas phase by exchanging mass. The CFR software was positively compared against laminar and turbulent flames in canonical configurations as well as in more practical single-swirler combustor rig. The developed software is reliable for modeling and simulation of complex combustion phenomena.

References

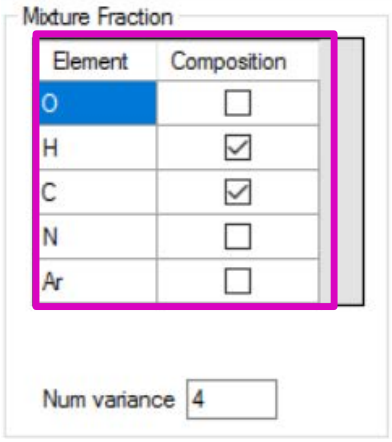
1. Ansys Inc., Fluent User's Guide, v18.0.
2. Ansys Inc., Fluent Theory Guide, v18.0.
3. Goodwin, D.G., Moffat, H.K., Speth, R.L., Cantera: An object – oriented software toolkit for chemical kinetics, thermodynamics, and transport properties," http://www.cantera.org, 2017, Version 2.3.0. doi:10.5281/zenodo.170284
4. ANSYS 18.0, Chemkin-Pro Theory Manual, ANSYS, Inc.: San Diego, 2017.
5. Ihme, M., Pitsch, H., "Prediction of extinction and reignition in nonpremixed turbulent flames using flamelet/progress variable model: 2. Application in LES of Sandia flames D and E," Combustion and Flame, 155, (1-2), pp. 90-107, 2008.
6. Fiala, T., Sattelmayer, T., "Nonpremixed Counterflow Flames: Scaling Rules for Batch Simulations," Journal of Combustion, 2014, 484372.
7. H. B. Keller, in Applications of bifurcation Theory, P. Rabinowithz, Ed. (Academic Press, New York, 1977).

8. Luigi Acampora and Francesco S. Marra, "Numerical Strategies for the Bifurcation Analysis of Perfectly Stirred Reactors with Detailed Combustion Mechanisms," Computers and Chemical Engineering 82 (2015) 273-282.
9. Ruiqin Shan, Tianfeng Lu, Effects of Surrogate Jet-Fuel Composition on Ignition and Extinction in High Temperature Applications, 8th U. S. National Combustion Meeting Organized by the Western States Section of the Combustion Institute and hosted by the University of Utah May 19-22, 2013.
10. Nishioka, M., Law, C., Takeno, T., "A flame controlling continuation method for generating S-curve responses with detailed chemistry," Combust. Flame 104 (3):328-342
11. Huo, H., Wang, X., Yang, V., "A general study of counterflow diffusion flames at subcritical and supercritical conditions: Oxygen/hydrogen mixtures," Combustion and Flames, 161, 2014.
12. J. Li, Z. Zhao, A. Kazakov, F.L. Dryer, "An updated comprehensive kinetic model of hydrogen combustion," Int. J. Chem. Kinetics, 36, 2004, 566-575.
13. Burke, M.P., Chaos, M., Ju, Y., Dryer, F.L., Klippenstein, S.J., "Comprehensive H2/O2 Kinetic Model for High-Pressure Combustion," Int. J. Chem. Kinet. (2011).
14. Connaire, M. O., Curran, H J., Simmie, J. M., Pitz, W. J. and Westbrook, C.K., "A Comprehensive Modeling Study of Hydrogen Oxidation", International Journal of Chemical Kinetics, 36:603-622, 2004.
15. Wu, H., See, Y.C., Wang, Q., and Ihme, M., "A Pareto-efficient combustion framework with submodel assignment for predicting complex flame configurations," 162(1), 2015, 4208-4230
16. Pitsch, H., FlameMaster v3.1, "A C++ computer program for 0D combustion and 1D laminar flame calculations," 1998.

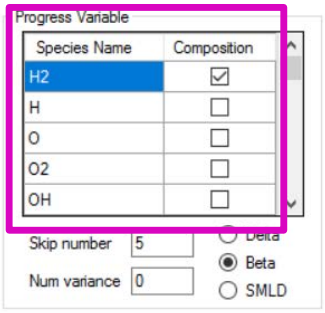
TASK 5- APPENDIX



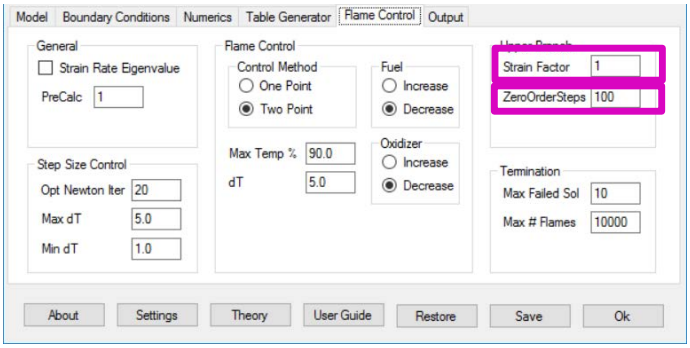
Appendix Figure 1. Schematic of the Common Format Routine (CFR) software. All the components with the green background correspond to the thermochemical and transport data pretabulator. All the components with the amber background corresponds to the flamelet-based software.



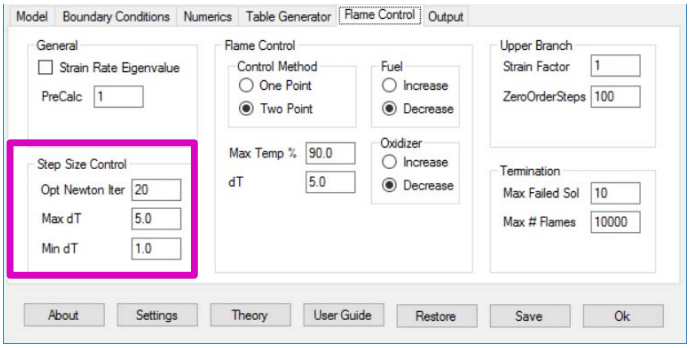
Appendix Figure 2. Pretabulator software selection of user's mixture fraction definition is indicated within the magenta-line box.



Appendix Figure 3. Pretabulator software selection of user's progress variable definition is indicated within the magenta line box.



Appendix Figure 4. Pretabulator software selection of zero order continuation steps and strain factor are indicated in the magenta boxes.



Appendix Figure 5. Pretabulator software selection of step size control is indicated in the magenta box.

Task 6- Spray Modeling of Area 3 Pressure Atomized Spray Injector

UTRC (Sub-contract)

Objective(s)

The objective of this task is to simulate the Area 3 High Sheer Rig pressure blast spray atomizer. Simulations of NJFCP experiments in the Area 3 High Sheer Rig will be done to explore the relative performance of simulations versus experiments and the relative spray and combustor character between the A-2, C-1, and C-5 fuels. These computational results will also illuminate the relative impact of a Pratt & Whitney swirler-injector geometry as compared to the other geometries in the program.

Research Approach

Research & Development Final Report 2018 Executive Summary

The objective of this effort is to develop, enhance and apply computational fluid dynamics-based models to simulate stable combustion and lean blowout behavior in a high shear rig combustor that was also experimentally studied at Georgia Institute of Technology. The goal is to understand if the models can predict the dependence of lean blowout (LBO) phenomena on fuel physical and chemical properties of the alternative jet fuels. A Large Eddy Simulation (LES) based modeling is employed to simulate the unsteady combustion phenomena for the stable and LBO conditions. Several sub-models for unsteady flow simulation, spray injection boundary conditions, spray evaporation models, wall heat flux boundary conditions and turbulent combustion models are required to correctly simulate the physical processes. Detailed description of the different submodels, along with validation or verification where possible, is presented as a part of this work. Simulation of lean blowout were performed upon completing the reacting LES for the two fuels at near blowout but stable conditions. To simulate lean blowout, fuel flow rate is reduced in discrete steps 6% (instantaneously instead of gradually) for three different values of fuel-flow rates. Each flow rate was held constant for 100 mill-seconds for the combustor to respond to the flow rate change and stabilize at the new condition. Overall, the two fuels show differences in evaporation rate and also commensurate differences in heat release rates. Both the simulation show reduction in heat release rate as the flow rate is reduced but C1 seems to be dropping faster relatively compared to A2. C1 fuels also shows increased evaporation rates compared to A2, however this leads to quick build of fuel vapor in a concentrated region and if the flow conditions in that region is not conducive in terms of residence time to complete the reaction, it contributes to even more accumulation of fuel vapor from the incomplete combustion. In the case of C1 fuel, this is hypothesized to be the mechanism for earlier flame blow out compared to the A2 fuel. Long combustor dimension coupled with very small time steps to resolve the flame structure, leads to excessive computational time at each flow rate for the combustion to reach a quasi-steady state. As a result, it was not possible to reduce the flow-rate all the way to the lean blowout value to demonstrate the lean blowout behavior. However the qualitative trend observed from the three simulate fuel flow rate conditions seems to indicate that the models employed in this study have the ability to discriminate between the different fuel physical properties and its impact on the lean blow out behavior.

Research in Support of FAA-ASCENT Program & National Jet Fuels Combustion Program LES of High Shear Rig Combustor – Area 3 support

Introduction

Fuel cost, availability and environmental impact are main concerns that drive the search and use of alternative fuels (petroleum and non-petroleum derived) in commercial and military aviation. By understanding and establishing the properties of fuel and their impact on engine (combustor) performance, it may be possible to broaden the fuel specification and, in turn, broaden the available choice of economical and eco-friendly fuels for aviation engines. However, the introduction of fuels from alternative sources presents potential risks to aircraft engine operability, emissions and durability and hence requires a comprehensive understanding of the fuel properties and their potential impact on the systems and their performance. For instance, flame blowouts can occur during transient events in the flight envelope during rapid throttle movements. For example, during flight decent when the fuel flow-rates are typically low, the combustor fuel-air ratio may approach lean flammability limits that may result in a flame-out. This is typically known as the Lean Blow Out (LBO) and has obvious safety implications. During such highly transient events, fuel property variations have a large effect on the combustion processes. Since the fuel flow rates are low, physical properties of the fuel can alter the fuel spray atomization and vaporization processes, leading to a strong effect on combustion. In addition, fuel chemistry effects are presumed to be strongest at lean conditions, where chemical reaction rates are lowest and can therefore be coupled with the combustor aerodynamic stabilization processes. For these reasons, LBO is considered one of the most important operability metrics for evaluating alternative fuel effects. Other combustor performance metrics such as ignition at ground (cold start) and altitude conditions, gaseous and particulate emissions, liner temperature, radiation and durability, pattern/profile factor and combustion efficiency are all linked intimately to different physical and chemical properties of the fuel such as viscosity, surface tension, heating values, specific heats, boiling point distribution, vapor pressure, Cetane number etc. In general, there is some understanding of the impact of physical fuel properties on selective combustion behavior. However, the collective impact due to all or multiple properties (chemical and physical) is not well understood. Because the next-generation of combustors will be operating closer to stability limits they are more likely to exhibit stronger fuel sensitivity which warrants research to better understand the potential impacts of the new fuels on engines.

One of the important objectives of this research program is to develop modeling tools for predicting the performance of gas turbine combustors when using future alternative fuels. The success would enable a significant reduction in cost and effort when qualifying new fuels for use in aircraft engines. Computational Fluid Dynamics (CFD) simulations of the High Shear Combustor are being performed to develop and assess the ability of models to capture the impact of fuel properties on Lean Blow Out phenomena.

Experimental Facility

The high shear rig combustor is a canonical representation of an aviation combustor which was experimentally characterized by the teams at Georgia Institute of Technology. This rig was designed with optical access to enable non-intrusive diagnostics and for visualization of the combustion. Data obtained include non-reacting and reacting PIV for the velocity fields at an equivalence ratio close to LBO where a stable flame configuration can be realized. PDPA measurements of the spray under non-reacting conditions close to the swirler/nozzle exit were also obtained in this configuration at UTRC. Temperature measurements at the combustor bulk-head were also obtained to characterize / quantify lean blowout phenomena.

Figure 1 shows the key components of this rig such as preconditioning air flow path, fuel supply, the optically accessible pressure vessel and liner and exhaust section. Compressed air at pressures up to 20 atm is heated to temperatures from 350 to 750 K. Following the heating process, a portion of the air is sent to the test section and the remainder is cooled to approximately 320 K in a heat exchanger. The secondary air flows around the liner and keeps the pressure vessel structure and windows cool. Hot combustion products mix with the cooling air downstream of the test section and exit through a water cooled exhaust. A choked orifice plug of variable size is installed at the exhaust exit to maintain elevated pressure in the combustion chamber. Air mass flow rates and the air temperature were measured upstream of the dump plane and its value was continuously recorded during measurements.

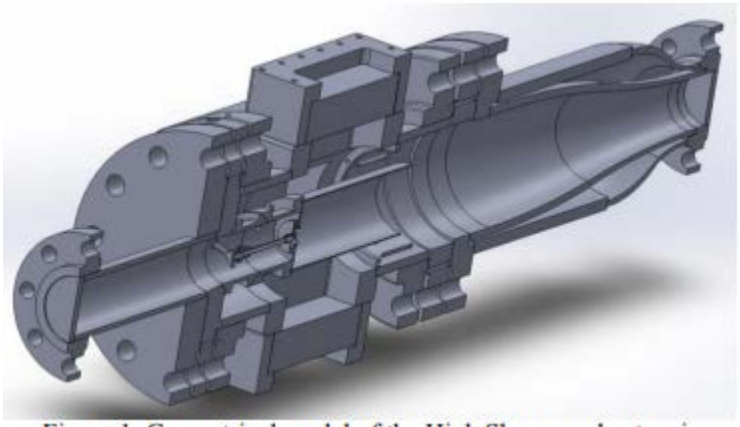


Figure 1. Geometrical model of the High Shear combustor rig

The combustor liner consists of a 30.5 cm long, 105 mm inner diameter quartz section. The front end of the combustor, called the bulkhead, is a stainless steel wall without secondary cooling passages. This bulkhead face contains four thermocouples situated flush with the surface for monitoring bulkhead temperature, a static pressure transducer, and an ignitor. The pressure vessel that houses the liner has optical access on all four sides and four quartz windows (Figure 1). The fuel nozzle uses a Pratt & Whitney proprietary swirler geometry, through which the pressurized preheated air passes through prior to entering the test section. The pressure atomizer is a commercially available McMaster-Carr misting nozzle (part number 3178K45) with a 0.51 mm orifice diameter and a flow number of 2.3.

Computational Models and Setup

The experimental setup of the high shear combustor rig was simulated using Large Eddy Simulations. Figure 2 shows a simple schematic diagram of the combustor. The simulation domain has an upstream plenum or air preconditioning flow path, from where the air enters the domain. Air mass flow rate is specified at the inflow boundary along with correct air temperature. This air passes through the swirler to enter into the combustor. A part of this air also flows on the outside of the combustor wall and enters the convergent section on the aft of the combustor to cool the hot gases that leave the cylindrical combustion chamber. Cooling air is specified at a surface near the exit of the combustion chamber using measured cooling mass flow that enters the convergent section.

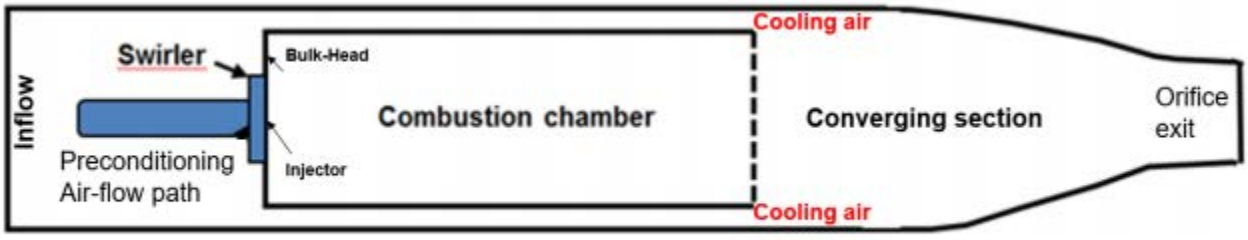


Figure 2. Schematic diagram of the High Shear combustor rig simulated using LES

The long computational domain is needed to setup the correct exit boundary conditions even though it makes the simulation run time longer to obtain statistically steady solutions. Measurements of the wall temperatures on the bulkhead and secondary flow path were used to setup isothermal boundary conditions on these boundaries to simulate the heat transfer that happens at these walls. Before we present the results from this work, a brief summary of the CFD models are being provided here. LES solver used for this work is the fully compressible finite-volume based code LESLIE. It is a block-structured solver that uses a predictor-corrector scheme which is 2nd accurate in time and employs 2nd/4th order accurate spatial integration schemes. More details of the submodels are provided in the Table 1. Computational domain was resolved with hexahedral cells with finest mesh of 0.1 mm near the swirler walls and a coarsest mesh of 3mm in some plenum locations. Fine meshes were used in the vicinity of the swirler in the front end of the combustor to resolve the



turbulent flow structures, swirling flow and the flame anchoring in this region. The combustor region is resolved with nearly uniform sized cells to avoid dissipation errors. The total mesh count is little over 6 million cells.

Table 1. A comprehensive list of all the sub-models used in the current study

	Sub-Models
Solver Name	LESLIE
Spray Flame Modeling Approach	**Eulerian-Lagrangian (EL),**
Governing Equations	**Compressible multi-species Navier-Stokes with spray**
Grid Type	**Multi-block structured**
Solver Type	**Finite volume**
Spatial Discretization	**$2^{nd}/4^{th}$ order MacCormack,**
Time Integration	2^{nd} order explicit predictor-corrector **$2^{nd}/4^{th}$ order explicit Runge-Kutta for spray equations**
Boundary Conditions	**Characteristic boundary conditions**
Thermodynamics	Thermally perfect gas
Transport	Sutherland,
Chemical Kinetics	**Finite-rate (reduced/skeletal/detailed)**
Momentum Flux Closure	Boussinesq hypothesis, **Constant coefficient k^{sgs},**
Energy Flux Closure	**Gradient diffusion hypothesis**
Species Flux Closure	**Gradient diffusion hypothesis**
Reaction Rate Closure	**Quasi-laminar (QL),**
Dispersed Phase Physics	**Polydisperse with Evaporation**

Results and Discussion

Validation of non-reacting aerodynamic flow-fields

A series of step-by-step validation for the various sub-models used in this study was completed before performing the Lean Blowout simulations. As a first step, cold-flow validations were conducted to ensure the grids, boundary conditions and subgrid momentum closure models are adequate to simulate the non-reacting conditions.

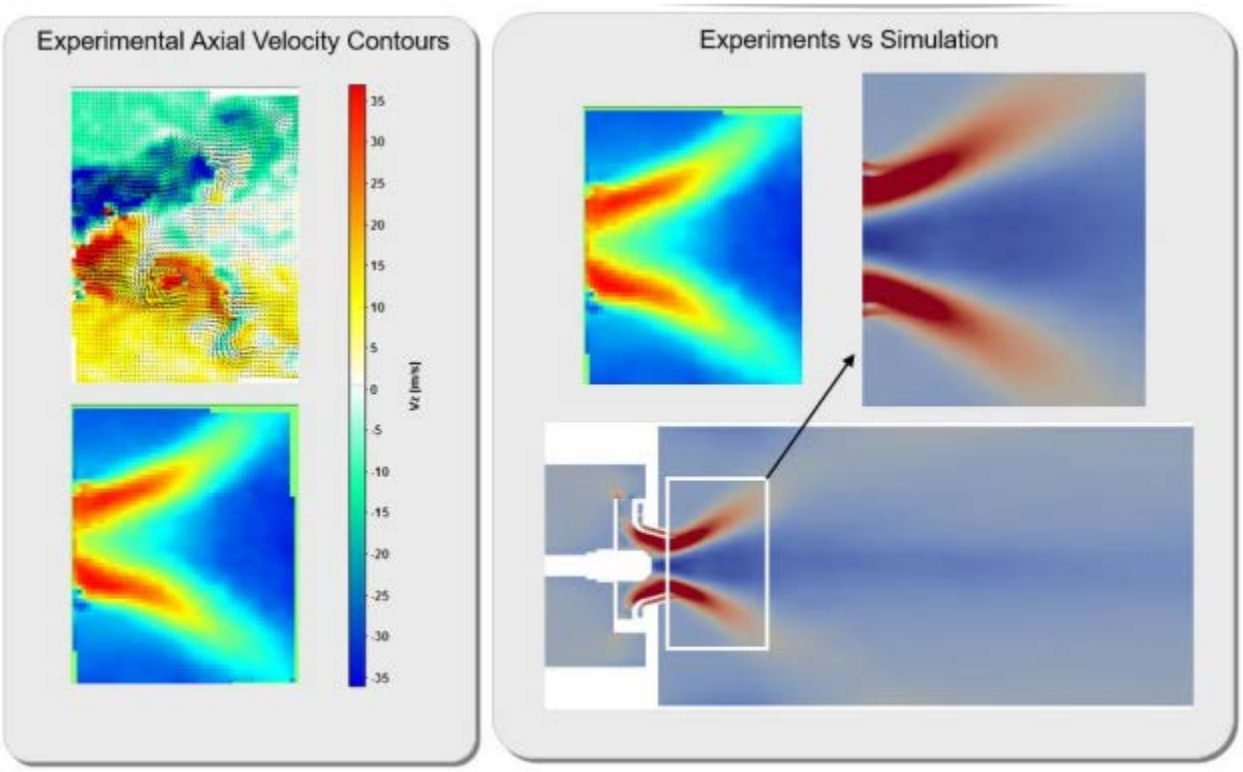


Figure 3. Time averaged contours of axial velocity from experiments (left panel) compared to simulations (right panel) from the central cross-sectional plane at non-reacting conditions in the High Shear Rig

Figure 3 shows the time-averaged contours of instantaneous and mean axial velocity obtained from PIV measurements on the left panel in the central cross-sectional plane of the combustor for non-reacting conditions. Flow through the radial and axial swirlers are clearly visible in this plot. As the flow enters the confining passages of the swirler from the preconditioning flow path, area reduction and continuity accelerates the flow significantly causing a high velocity annular jet to emanate out of the swirler. The tangential flow trajectory pushes the flow away from the center line of the swirler and hence a region of negative axial velocity or recirculation zones are created in the central sections of the combustor near the swirler exit. This recirculation region is intended for flame stabilization. Large velocity gradients near the swirler are also intended to help with better spray atomization. Overall, all the flow features are captured well in the simulation and are qualitatively in good agreement with the data. The spread angle, velocity magnitudes and the extent of the central recirculation regions were compared to be in good agreement with the measurements.

Figure 4 shows the time-averaged axial velocity field from the non-reacting experiments compared to non-reacting simulations in the high shear rig. Measurement data was obtained using stereo PIV. Overall there is a reasonable agreement even though some particular discrepancies can be noticed. Simulations are over predicting the shear layer width especially in the near-field of the swirler. This could be attributed the subgrid momentum closure models and the grid resolution. The mesh resolution near the solid wall in the swirler passages is usually inadequate as it would be prohibitively expensive to resolve the fine scales in the turbulent boundary layer. It is typical to use some specialized wall models or hybrid RANS-LES models to account for the lack of resolution near the wall. However, in this study no such models have been used. On the other hand the measurements also report errors related to the inability of the stereo PIV technique to distinguish between the spray droplets and the PIV tracer particles. This can lead to systemic errors in the measurement data. Moreover, the measurements near the periphery of the optical windows have increased errors due to reflections and other issues related to light intensity. The swirling motion also causes flow perpendicular to the optical plane which also would introduce measurement errors. Considering all this, the overall qualitative and quantitative

agreement between the experiments and the simulation is reasonable to provide confidence in the mesh, subgrid momentum closure models and other boundary conditions used for nonreacting flow simulations.

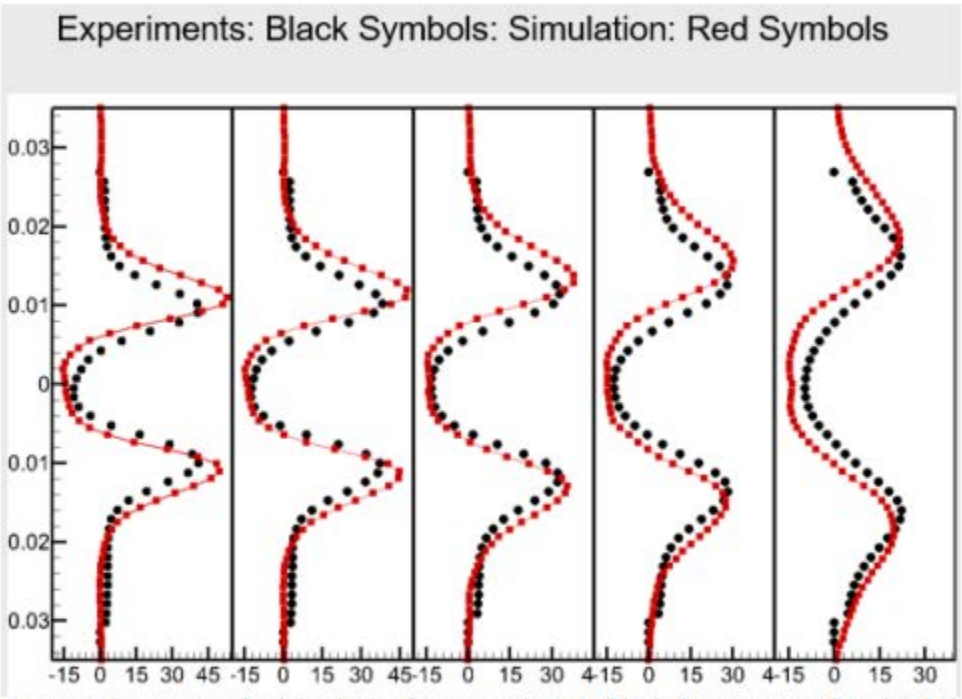


Figure 4. Time averaged contours of axial velocity from experiments (black dots) compared to simulations (red dots) at five axial stations showing the variation in radial directions for non-reacting conditions in the High Shear Rig

Validation of non-reacting spray boundary conditions and transport

Parametric study conducted for the spray initial conditions revealed that the spray evolution downstream and the flame location depends very strongly on the spray inlet boundary conditions such as the initial size distribution, position and velocity. Typically spray formation processes are not modeled in the reacting LES, due to the excessive modeling complexities and the computational cost required for simulating the atomization processes. Known empirical spray size distributions are prescribed as initial conditions (ignoring the primary break-up process). Log-normal and Rosin-Rammler are two popular spray size distributions that match experimentally measured spray size distributions for different injectors and flow conditions. But these correlations assume the same size distribution is valid across the entire fuel nozzle cross-section, which is known to be incorrect. Droplet velocity information is also not specified by these correlations and hence all droplets (regardless of their size) are assumed to be injected at the same velocity which can be another source of major error in the simulations. PDPA based measurement data can provide correlated spray size-position-velocity information, however, it is difficult to obtain such data very close to the injector and data is available only some distance downstream of the fuel injector. For this particular fuel injector and swirler configuration, UTRC conducted a testing campaign to obtain detailed PDPA data to simultaneously measure spray position, size and velocity for three different fuels at several flow conditions. Modeling team devised an approach to utilize the spray PDPA data measured downstream and specify boundary conditions close to the fuel injector. A snapshot image of the spray dispersing out of the fuel nozzle geometry is shown in Figure 5 below.

Our approach is based on geometric projection of the measured data, from the actual measurement plane to a plane close to the injector called the CFD injection plane. In the Figure 5, the dashed red line shows the location of the measurement plane. Because the measurement planes are reasonably close to the swirler exit, it was assumed here that no significant evaporation would have occurred and that the droplet size obtained in the measurement is the result of atomization only. Based on this, we defined annular concentric strips at an arbitrary injection plane close to the injector face, as shown by the image in the middle of the panel in Figure 5. The number of strips corresponds to the number of radial location at

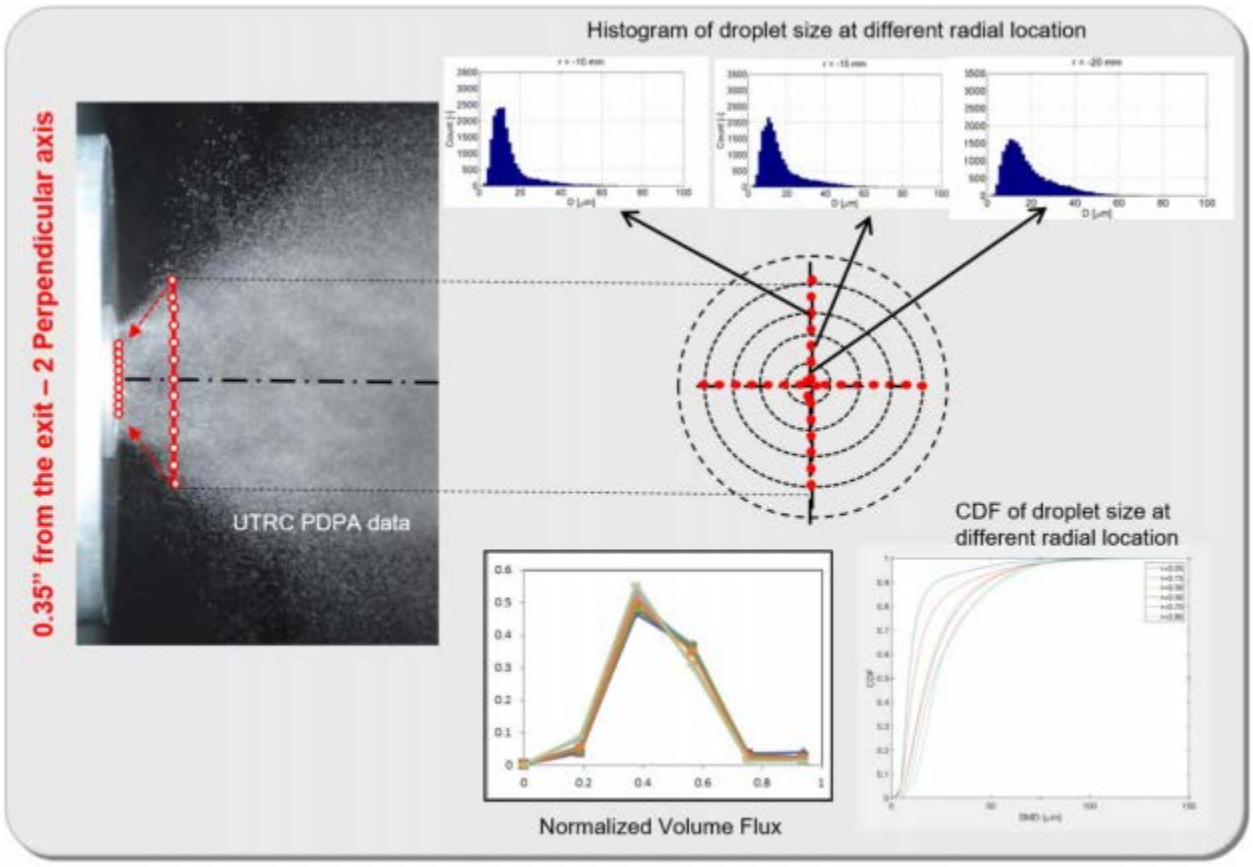


Figure 5. A snapshot of the spray injected out of the fuel nozzle and a conceptual image of the spray boundary conditions employed in the current work

Because PDPA gives correlated droplet size and velocity, one could also use the measured droplet size directly from the measurement as well. If all three components of the velocity are known from the measurement, then there is no need to specify spray cone angle. In the absence of a component data, one could use the spray cone angle to obtain an estimate of the velocity components that is not available from the measurements. The key advantage of this approach is that joint PDF of drop-size-velocity and position can be specified in CFD. Droplets at different location disperse to different positions based on their size and hence it is important to preserve the correlation between position, size and velocity to obtain the correct droplet dispersion. This would ensure that the correct size droplets disperse to the correct location which in turn would yield correct flame location and structure. Another major advantage of this approach comes from the use of measured data that is far enough from the injector face where secondary breakup and other atomization processes are nearly complete. By using such a data, one could avoid the need for secondary break-up models which further saves computational time. The major drawback of this approach is the implicit assumption that the droplet trajectories follow the geometrical projection from the injection plane to the measurement plane and that the evaporation between the CFD injection plane and the actual measurement plane is minimal. So validation of this approach is required to ensure that such approximations do not introduce unacceptable errors in the reacting flow simulation.

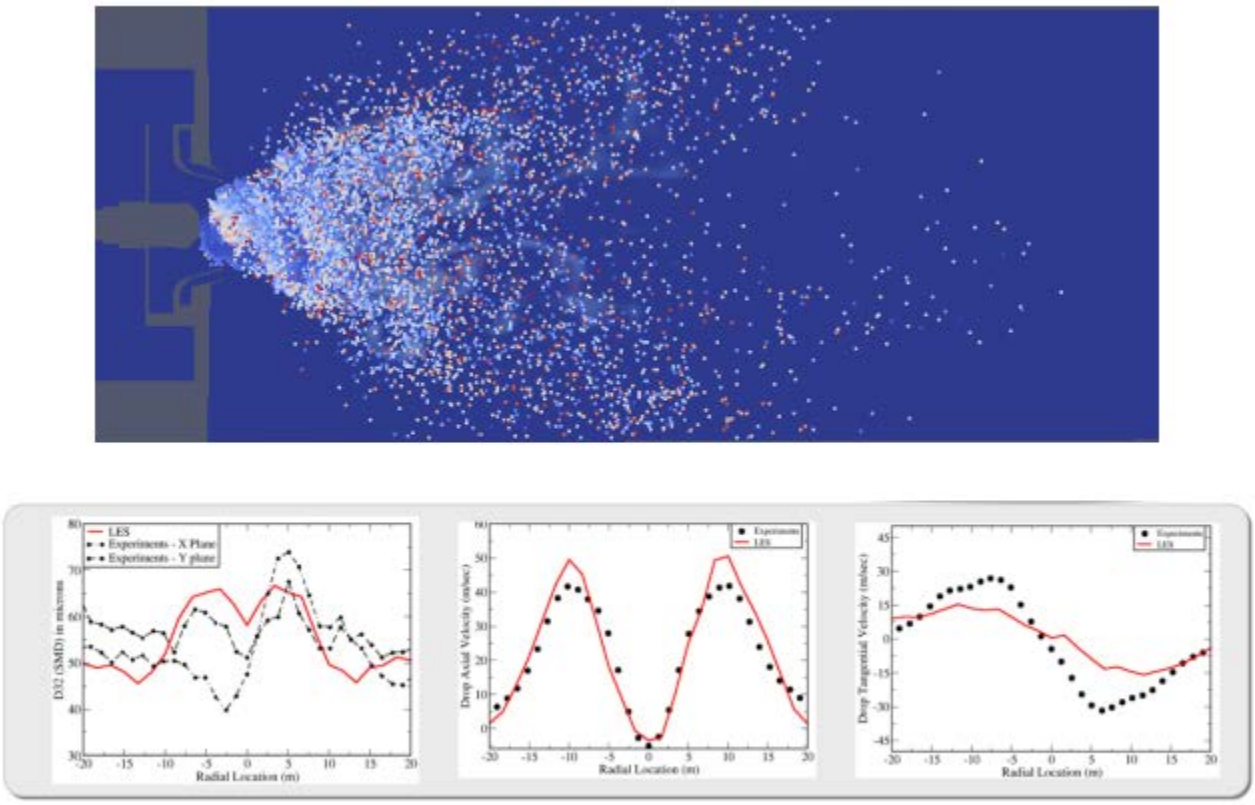


Figure 6. Top: Snapshot of spray dispersion in the high shear rig combustor (bottom) comparison of spray SMD, droplet axial and tangential velocity profiles between experiments (black dots) and simulations (red line).

Figure 6 (top image) shows the spray dispersion pattern from the spray boundary conditions described in this section. Experimental images and animations confirmed that the swirling air flow disperses the smaller sized drops in a swirling pattern and the simulated swirling spray pattern is in line with the expectation. In figure 6, (bottom image) compares the measured PDPA data with simulations. The image on the left-most side compares the Sauter mean diameter (D32) and the comparison is reasonable with differences less than 5 microns. The image in the middle of the panel compares the drop axial velocity and the agreement is excellent validating the supposition that the spray parcels follow the flow as assumed in the injection boundary conditions model. The image on the right hand side of the panel compares the droplet tangential velocity with data. The differences seen here are attributed to the lack of specification of tangential velocity boundary conditions for the droplets. Even though it is possible to specify the tangential component of droplet velocity, it was not used here intentionally due to the supposition that the swirling carrier gas flow would impart the momentum to the droplets and enable the droplets to achieve the correct velocity. As it can be observed from the simulation data that the droplets have picked up a tangential component and this can be further improved by specifying the tangential component of droplet velocity. Overall, the agreement in spray size, velocity and position demonstrates the potential of the proposed boundary conditions and also serves as a validation of this relatively easier and affordable methodology.

Multi-component evaporation models

Jet fuels are multi-component in nature with 100s of species. Liquid fuel vaporization depends on many thermo-physical properties such as its density, heat capacity, latent heat of evaporation, vapor pressure etc. Since these properties are functions of local temperature, pressure and composition, a good evaporation model is important to capture the correct evaporation behavior and the correct spatial distribution of fuel-air mixture which in turn impacts flame-stabilization and



blowout. UTRC developed a multi-component evaporation model based on the distillation curve (under a different contract in NJFCP) and validated with partial data from the AFRL. This model provides all thermo-physical properties for the liquid fuel based on a surrogate representation of the liquid that matches the distillation curve constrained by liquid-vapor thermodynamic equilibrium. An ab initio equilibrium calculator (SuperTrapp) from NIST that uses the corresponding state theory (the cubic equations of state which take into account the molecular potential energy interaction between different hydrocarbons) was utilized to compute the equilibrium fluid properties of the mixture. The distillation curve calculator was derived from the equilibrium library of SuperTrapp to simulate the ASTM distillation process. This method is designed to track the changes in the composition in the liquid (and gas) during the evaporation process. The distillation curve computed for a given surrogate fuel is then compared with the experimentally obtained distillation curve, overall molecular weight, and density and other fuel properties, such as viscosity, surface tension etc. The surrogate model is adjusted until it provides a good match to available data and meeting other constraints such as the overall C to H ratio and average molecular weight. This process of adjustment is based on the properties of each component; for example, increasing the composition of a cyclic compound while decreasing an aliphatic compound of the same carbon number will change the density of the mixture while keeping all other properties constant. The surrogate model thus found was then utilized to predict all fuel properties during the evaporation process. This way, we are basically deriving fuel properties from first principles using a representative set of hydrocarbons found in a specific fuel sample with fuel physical properties that are valid for a wide range of temperature and pressure. This model assumes that as a droplet evaporates, it follows the distillation curve and hence the volume recovery fraction is a one-to-one function of temperature. This way one can construct a look-up table for all fluid properties using temperature as the independent variable. For temperatures below the starting temperature of the distillation curve, we evaluate the liquid properties along the curve defined by the loci of the bubble point.

Figure 7 shows the distillation curves and liquid density variation as a function of temperature predicted by the surrogate model of JetA, JP8 and JP5 fuel at 1Bar. The modeling results compared with experimental data (from AFRL) show very good agreement and is also in good agreement with Jet A distillation curve data found in the CRC handbook.

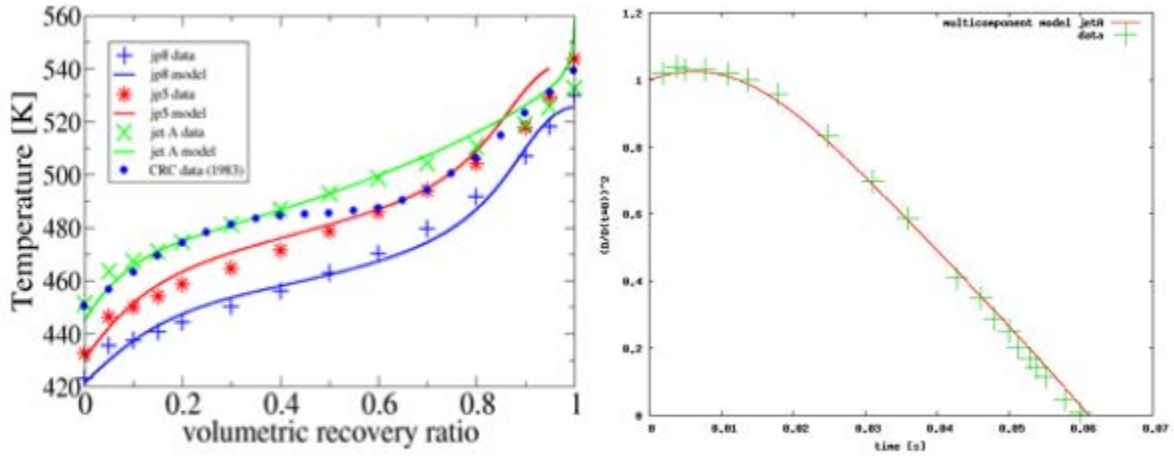


Figure 7: (left) Comparison of distillation curve predicted using data from AFRL and UTRC multicomponent evaporation model (right) comparison of single droplet evaporation time using the evaporation model

The properties needed for droplet evaporation simulation, computed using our surrogate models, are all tabulated and implemented into the reacting LES CFD code. Standard equations for droplet momentum, heat and mass transport equations are solved with classical correlations for drag and other inter-phase exchange terms. Another validation of the model was performed by simulating a single droplet evaporation. An isolated droplet of size 100 microns at an initial liquid fuel temperature of 300K embedded in ambient conditions of 1 bar and 800K was simulated for the Jet A fuel. Figure 7 (right) compares the D2 variation with time for Jet A as a function of time at 1 bar pressure and compares with the results from Burger et al exhibiting a very good level of agreement. Figure 8 shows the fuel physical properties for a range of temperatures and for 3 different pressures. Data at 1 atm is used for comparison with the models and data at 2 atm and

3 atm are used for LES simulations of referee rig (which operates at 2 atm) and high shear combustor rig (which operates at 3 atm), respectively. Overall the model captures the physical property variation for a wide range of conditions.

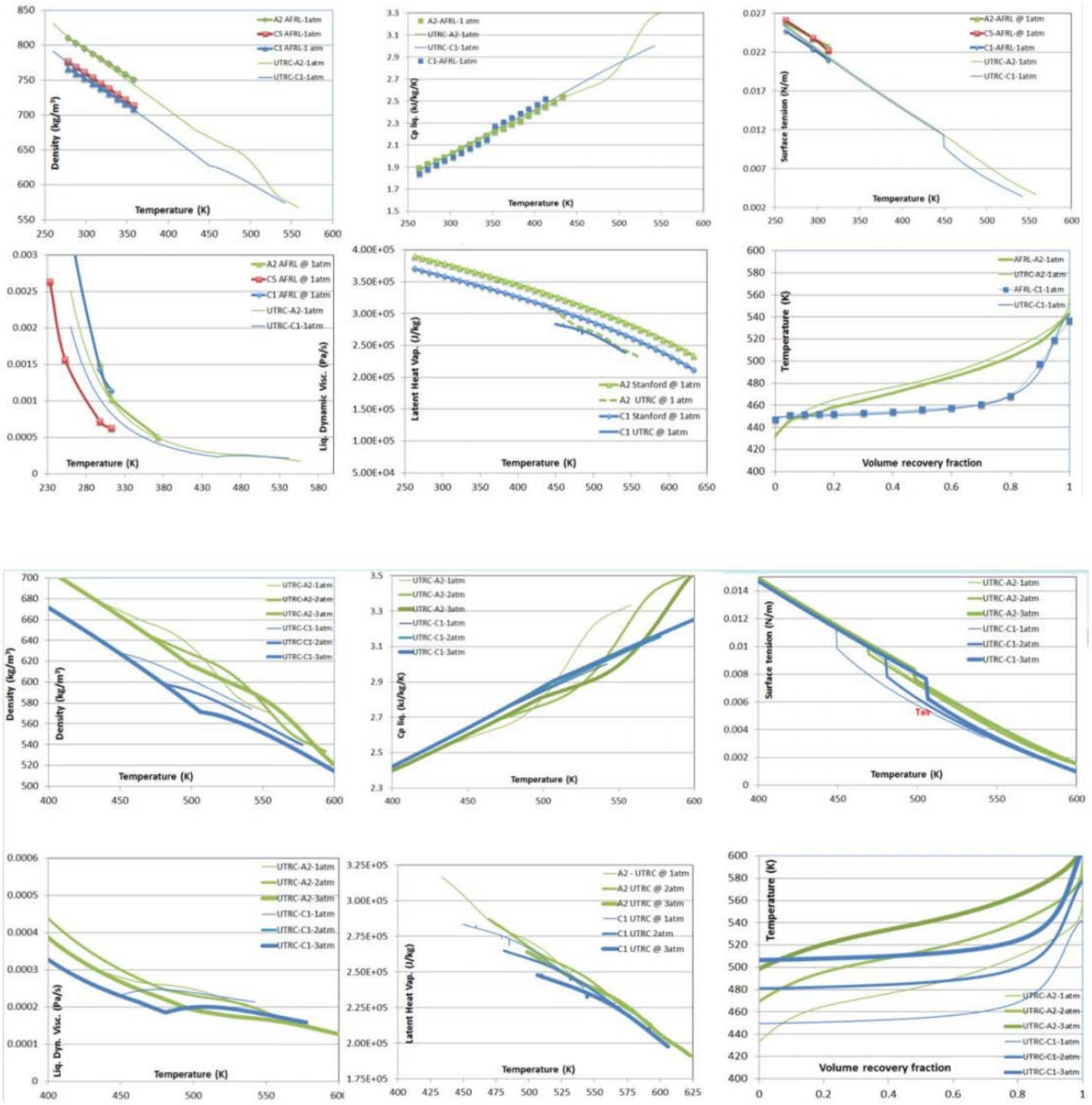


Figure 8: Prediction of fuel physical properties from the multi-component evaporation model. The top two rows (six figures) show comparison of density, specific heat surface tension, viscosity, vapor pressure and distillation curve at 1 atm and comparison to available data from AFRL. The bottom two rows of six figures shows the same properties at three different pressures.



Combustion Chemistry Mechanisms

As a part of the National Jet Fuels Combustion Program (NJFCP) teams from Stanford University developed a version of HyChem model for combustion chemistry or chemical kinetic mechanisms for A2, C1 and C5 fuels. The detailed chemical mechanism was calibrated and validated using species yields measured from flow reactor experiments. Research teams from the University of Connecticut developed skeletal and reduced mechanisms using Directed Graph Approach and verified these mechanisms by matching with combustion target properties like flame- speed, ignition delay, extinction strain rate, etc. These mechanisms consists of over 30 species and 100s of reaction steps and hence would be expensive to use in reacting LES of high shear rig combustor. As a compromise, we devised a single step chemistry with 5 species as shown below:

$$C_cH_h + \left(c + \frac{h}{4}\right)(O_2 + 3.76N_2) \rightarrow cCO_2 + \left(\frac{h}{2}\right)H_2O + \left(c + \frac{h}{4}\right)3.76N_2$$

The reaction rate expression was chosen to mimic the Westbrook and Dryer single step chemistry and an empirical Pre-exponential factor (AFAC in the expression shown below) was introduced to account for the changes in the reaction rate as the local equivalence ratio varies in an evaporating spray combustion environment.

$$\mathrm{k} = AFAC * 5.1e^{11} \exp\left(-\frac{15098}{T}\right) Fuel^{0.25} O_2^{1.5}$$

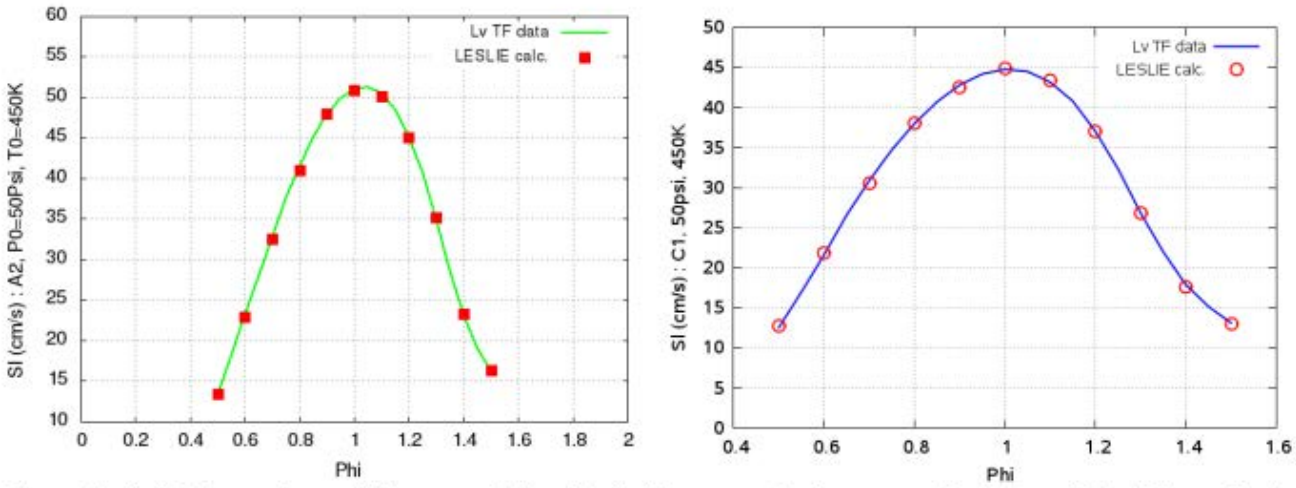


Figure 9: (left) Comparison of flame-speed for A2 fuel between single-step mechanism and detailed mechanism based on HyChem V2 chemistry model. (Right) Comparison of flame-speed for C1 fuel between current single-step mechanism and detailed mechanism based on HyChem V2 chemistry model

We simulated a one-dimensional freely-propagating premixed flame for different values of equivalence ratio (ϕ). For each value of ϕ, the AFAC term was changed until the mechanism yielded the correct flame-speed compared to the detailed mechanisms. By repeating this exercise for different values of ϕ, a correlation for AFAC as a function of ϕ was obtained that would be used in the reacting LES simulation of the high shear rig. Figure 9 shows the comparison of flame-speed obtained from the single-step mechanism for A2 and C1 fuels at inlet temperature and pressure corresponding to the high shear rig experiments. Overall an excellent agreement is obtained using this simple but empirical approach for deriving combustion chemistry models for complex LES simulations

Turbulent Combustion Models

The final sub-model that is needed for performing reacting LES is a turbulent combustion model. Even though different turbulent combustion models are available in the current CFD solver, a simple direct laminar closure model was used in this study. This model assumes that most of the turbulent mixing is resolved by the grid and hence the subgrid turbulent mixing can be ignored. As a result, the resolved species mass fractions, temperature, density and pressure can be used directly in the reaction rate expressions. The validity of the model is a function of how well the fine scale turbulent mixing is resolved by the underlying computational meshes used in this study.

In the next section, results from the simulations of high shear rig at near blow out but stable conditions will be presented for A2 and C1 fuels. Qualitative and quantitative comparisons of the contours and line plots will be presented to highlight any similarities and differences in the flow-field and flame structure for the two different fuels used here.

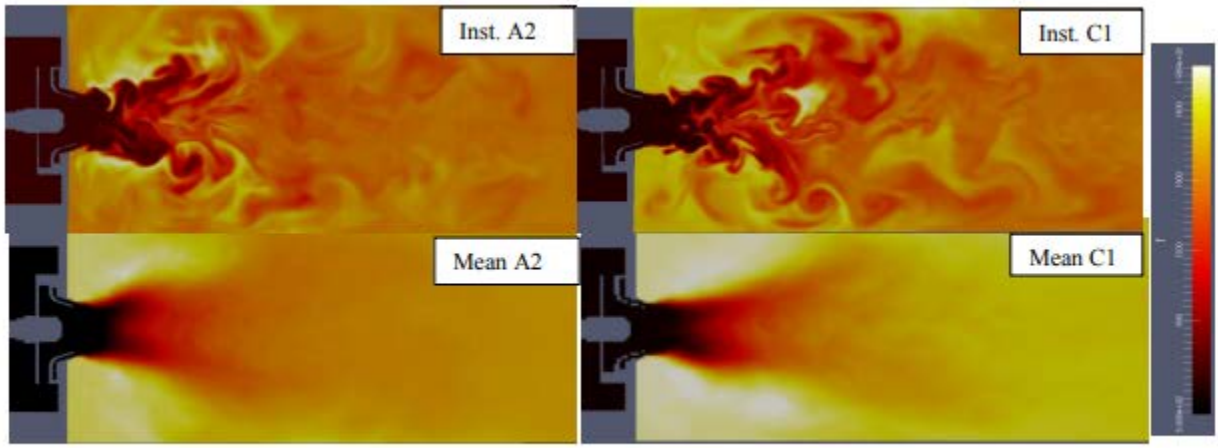


Figure 10: Contours of temperature from reacting LES of high shear rig combustor (top row) Instantaneous temperature contours (bottom row) mean or time-averaged temperature contours in central plane

Figure 10 shows the contours of temperature from the reacting simulations using the A2 and C1 fuels at near blowout (but stable) condition. The top row shows an instantaneous snapshot of the temperature contours at a particular instant and the bottom row shows time-averaged temperature contours for the same setup. Simulations were run for approximately 100 milli-seconds before averaging. To obtain mean or time-averaged data, simulation results were run for another 100 milli-seconds due to the lengthy combustor dimension. Darker regions near the swirler indicate colder air and it appears like a lifted flame is realized in this setup. The outer or corner recirculation zones bring in partially burnt hot products and mix them with the fresh air and evaporating fuel spray near the shear layers at the swirler exit. This creates a lifted flame that is stabilized between the shear layers and the central recirculation zones. It should be noted however that neither the instantaneous images nor time-averaged images show any visually significant differences for the two fuels simulated in this study.

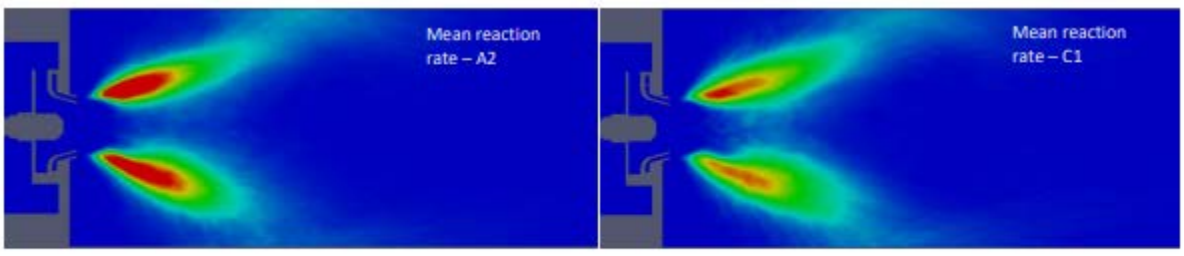


Figure 11: Contours of time-averaged fuel reaction rate obtained from reacting LES of high shear rig combustor (left) for A2 fuel (right) for C1 fuel

Figure 11 shows the contours of time-averaged fuel species reaction rate from the simulations of the stable conditions using A2 and C1 fuels. It can be observed that the flame structure, flame angle, anchoring locations are very similar for the two fuels. However, the magnitudes are noticeably different. A2 flame seems to have higher values of time-averaged reaction rates compared to C1 which is an indication that the A2 flames more robust and stable compared to the C1 flames, even though the C1 fuel has higher volatility compared to A2 fuels. This counterintuitive behavior is associated with the fact that all liquid fuel components in C1 fuel evaporate nearly at the same boiling temperature and hence in a very small region. Locally the mixture can be rich and has very little time for premixing. On the other hand the distillation curve for A2 fuel is gradual (see fig. 7) and different liquid fuel component evaporate at different boiling temperature. Hence, all the fuel vapor are not dumped in a small region but instead smoothly spread over a wide area which gives it time for premixing and combustion. This observation is consistent with the experimental observation under stable and lean blow out conditions.

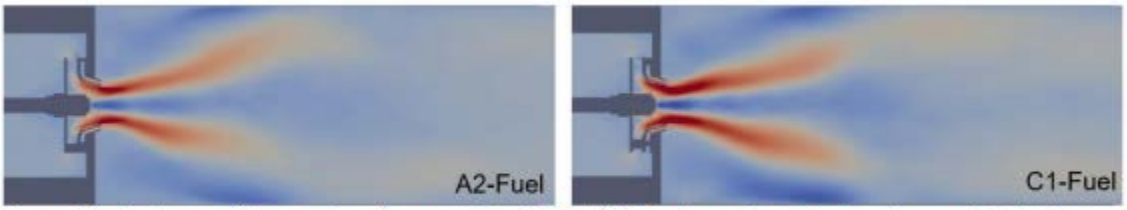


Figure 12: Contours of temperature from reacting LES of high shear rig combustor (top row) Instantaneous temperature contours (bottom row) mean or time-averaged temperature contours in central plane

Figure 12 shows contours of time-averaged axial velocity fields obtained from the reacting simulations using A2 and C1 fuels in the high shear rig. Consistent with the temperature contours, very little differences can be observed in the velocity fields. However, notable differences can be seen in comparison to the non-reacting velocity fields (Figure. 3). The angle of the annular swirling jet that comes out of the swirler in the reacting flow is shallower than the non-reacting flow field. This is an indication of a reduction in swirling or tangential component of the velocity due to combustion related flow acceleration in the axial direction. The magnitude of the axial velocity was also higher than the non-reacting flow field. The combined effect of the reduction in angle and increase in velocity leads to a more coherent or lengthy annular jet which will have an impact on the flame stabilization.

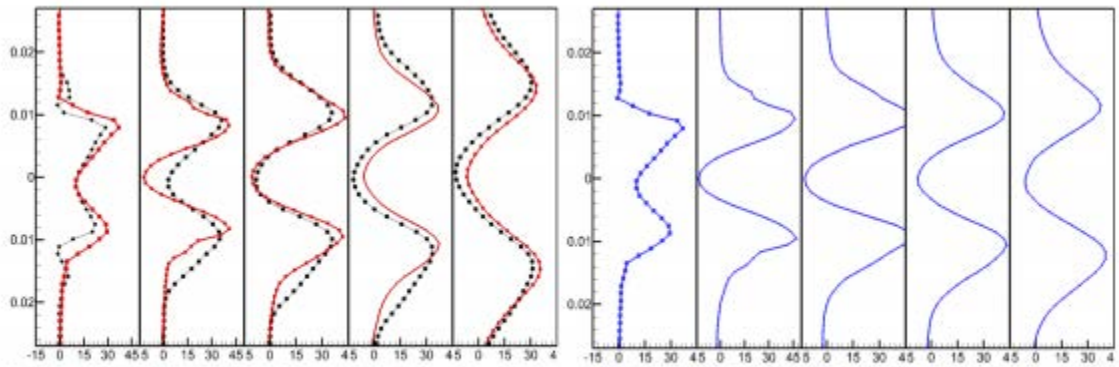


Figure 13: Radial profiles of axial velocity at five different axial stations for the A2 fuel (left) and for the C1 fuel (right). For the A2 fuel black dots represent the measurements and the red lines are from the simulation. For the C1 fuel measurements are not shown due to unavailability of the data at the time of comparison

Figure 13 shows the radial profiles of axial velocity at five different axial stations from the reacting simulations using A2 and C1 fuel. For the A2 fuel, comparison is also shown with measured data. For C1, fuel measurement data were not available for comparison with simulations. While some differences can be seen relative to the measurements, the agreement is still reasonable. As before, no significant differences can be observed between the two cases for these conditions. The lack of differences in the velocity fields between the two fuels indicate that the flames see/encounter

similar level of turbulence and mixing and any notable differences in the lean blow out behavior would be due to evaporation and or chemistry effects.

Lean Blow Out Simulations

Upon completion of the reacting LES for the two fuels at near blowout but stable condition, simulations were performed to understand the capability of the tools to predict observed lean blow out trends for the two fuels considered in this study. Starting from the near blowout simulations, fuel flow rate was reduced in steps of 6% and held constant for 100 milli seconds before reducing the fuel flow rate again. This was continued until the flame blow-out was observed. It was empirically determined based on the simulation that it takes approximately 100 milliseconds for the combustor to respond to the flow rate change and stabilize at the new condition. Based on the experiments, the near blowout fuel flow rate was set at 11.40 pph. Figure 14 shows the variation of liquid fuel evaporation rate as a function of time that was observed in the simulations for A2 and C1 fuels. It can be observed that for the A2 fuel, it takes approximately 100 milli-seconds (black line) to reach ~94% evaporation efficiency (defined as evaporation rate/injected fuel flow rate). It is hypothesized that the isothermal heat transfer boundary condition employed in this study does not accurately reflect the true heat transfer magnitudes and location from the experiments and therefore, could be over-predicting the heat loss, which in turn reduces the evaporation efficiency in the simulations. However, in the absence of accurate wall temperature measurements from the tests, this approximate boundary conditions is a compromise between the accuracy and simulation cost. It is also possible if the simulations were continued further, the evaporation efficiency may increase and reach 100%. However in the interest of getting to the lean blow out conditions, it was empirically assumed to be the steady state and the fuel flow rate was reduced at this point. At this stage, the fuel flow rate was reduced instantaneously to 10.72 pph (6% lower than the near blowout condition), and the simulation was continued for another 100 milli-seconds (red line). With the fuel flow rate reduction, a slight increase in evaporation rate was observed for a brief period before it begins to reduce and approach a mean steady value of ~10.3 pph. Again this is approximately 93-94% of the liquid fuel flow rate and similar to the previous flow rate complete evaporation was not achieved. At this state, the fuel flow rate was further reduced instantaneously to 10 pph (green line) and the simulations were continued for another 100 milliseconds. The evaporation rate further decreased and appears to reach a steady state for which ~95% evaporation efficiency was predicted. Figure 14 (right image) shows the evaporation rate for C1 fuel. At a flow rate of 11.40 pph (black line) an improved evaporation rate for C1 compared to A2 fuel. Approximately 98% of the fuel evaporates after 100 mil-seconds. This is in in line with the expected better vaporization characteristics of the C1 fuel. As the fuel flow rate was further reduced to 10.72 pph, the evaporation rate decreased after a brief period and reaches a near stable state evaporating 98% of the injected fuel. As the flow rate was reduced to 10 pph, initially the evaporation rate decreased to ~88% and then it increases and reaches a near steady value of 96%. This is an indication of some unsteadiness as the fuel flow is approaches the lean blowout range (~9 pph) but not a conclusive evidence of the tool's ability to discriminate the effect of fuel property on the LBO behavior.

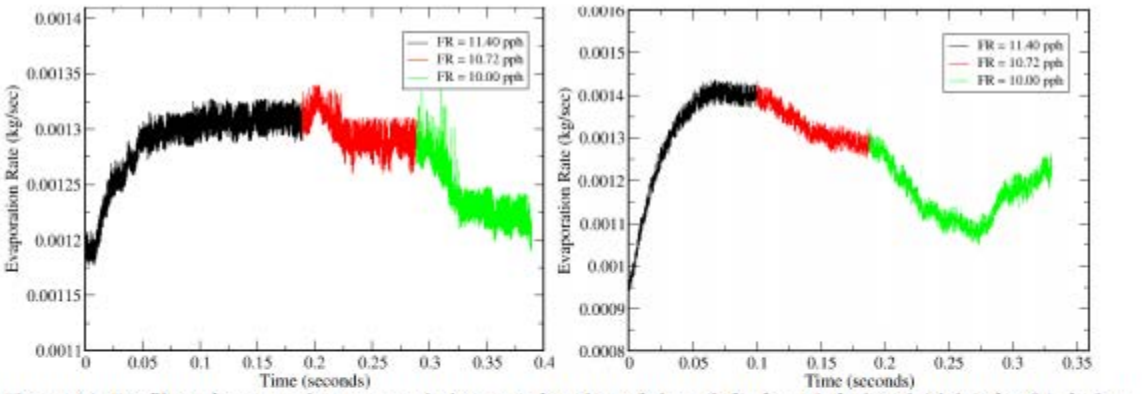


Figure 14: Profiles of evaporation rate evolution as a function of time (left) for A2 fuel and (right) for C1 fuel at three different flow rate conditions identified in the legend box

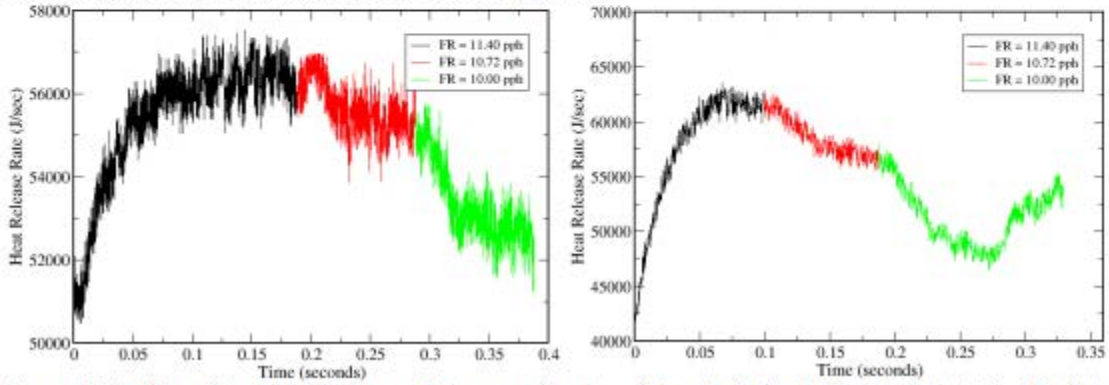


Figure 15: Profiles of heat release rate evolution as a function of time (left) for A2 fuel and (right) for C1 fuel at three different flow rate conditions identified in the legend box

Figure 15 shows corresponding profiles of heat release rate for the two fuels as the fuel flow rate was decreased systematically from the near blow out condition. Similar to the evaporation rate profiles, the heat release rate also decreases as the flow rate is reduced. In alignment with evaporation rate, heat release also shows relatively higher fluctuation levels for A2 fuel compared to C1 fuel. While the lower heating values of the two fuels are nearly the same (~43 MJ/kg) slightly lower levels of evaporation observed in the A2 fuel simulation leads to a slightly lower values of heat release rates predicted for A2 fuel. Overall, the two fuels show differences in evaporation rate and also commensurate differences in heat release rates. Both the simulations show reduction in heat release rate as the flow rate is reduced but C1 seems to be dropping faster relatively compared to A2. The experimental work indicates that the blowout for both the fuels was a sharper event unlike the referee rig combustor. Even though the current simulations show reduction in evaporation rate and heat-release rate, it is hard to infer the propensity of one fuel to blowout compared to the other unless the simulations were continued to fuel flow rates lower than the experimentally observed LBO flow rates. Unfortunately, these simulations take significantly long execution times due to small time-step, and long combustor length. For instance, each 100 mill-seconds of simulation requires 2.5 million steps of calculation and assuming discrete steps of fuel flow rate reduction, it requires 15 million time-step simulation for each fuel. The steady state at near blowout was run for significantly longer times. As a result of this long simulation times, we could only simulate three different flow rate reduction and use the results to extrapolate the model behavior.

Figures 16 and 17 shows the contours of temperature and fuel mass fraction contours for the simulations using A2 fuel at five different time instants during the simulation. Qualitative behavior of the flame can be inferred from such snap-shots and are usually helpful in providing insights about the driving mechanisms responsible for a particular physics. It can be observed from the temperature plots that the outer recirculation zones near the bulkhead are effective in mixing the hot products and the incoming fresh mixture of fuel vapor and air. Due to the increased residence time available in this area, the gas temperature in these locations are always hotter. Also, due to good turbulent mixing at shear layer, the flame

anchors in this location. As the flow moves downstream, the mixing and chemistry gets enough time for combustion and relatively higher temperatures can be observed. At lower fuel flow rates, with a globally lean mixture, the temperatures go down. Relatively cooler combustion products get pulled into the corner recirculation zones and the temperature in these locations begin to reduce as seen by darker contours of temperature. At the lowest flow rate simulated, much cooler temperatures were observed downstream to the exit of the combustors. Even though the global equivalence ratio reduces, the local equivalence ratio may not be as lean and hence in regions around the shear layers, robust flame structure can still be seen as one moves from one flow rate to the other. It is hypothesized here that the corner recirculation zone controls the lean blow out in this combustor. Reduction of fuel flow rate reduces the overall temperature of the hot products in the corner recirculation zone, which will be further reduced by the incoming cold air at the shear layers. If the resulting temperature is below the ignition temperature, then chemical reaction cannot be completed on time and it would be blown away. On occasion, local hot pocket from the corner recirculation zone may successfully burn a local fuel vapor-air mixture and hence re-ignition events may be possible in this combustor as observed in the experiments. A2 fuel having a wide distillation range, would be able to provide a spatially smoother fuel vapor distribution and hence has a better chance to reignite or sustain combustion for a longer time. Figure 17 shows the fuel vapor mass fraction contours at the corresponding time instants and it can be seen that higher values of fuel vapor (purple color) can be seen in the corner recirculation zone as the fuel flow rate is reduced due to the decrease in temperature and decrease in reaction rates which results in incomplete combustion of the reactants.

Figures 18 and 19 show the contours of temperature and fuel mass fraction contours for the simulations using C1 fuel at five different time instants during the simulation. Even though the same physics of shear layer mixing of reactants with hot products from the corner-recirculation zone applies in this scenario, evaporation rates are different for these two fuels. As a result increased values of fuel mass fraction is seen both near the injector and also inside the combustor. While increased vaporization rates are beneficial, it also leads to quick build of fuel vapor in a concentrated region and if the flow conditions in that region is not conducive in terms of residence time for completing the reaction, then it would result in even more accumulation of fuel vapor from the incomplete combustion. In the case of C1 fuel, this is hypothesized to be the mechanism for earlier flame blow out compared to the A2 fuel. While our simulations do not conclusively shows this, the qualitative trend seems to indicate that the models have the ability to discriminate between the different fuel physical properties and its impact on the lean blow out behavior.

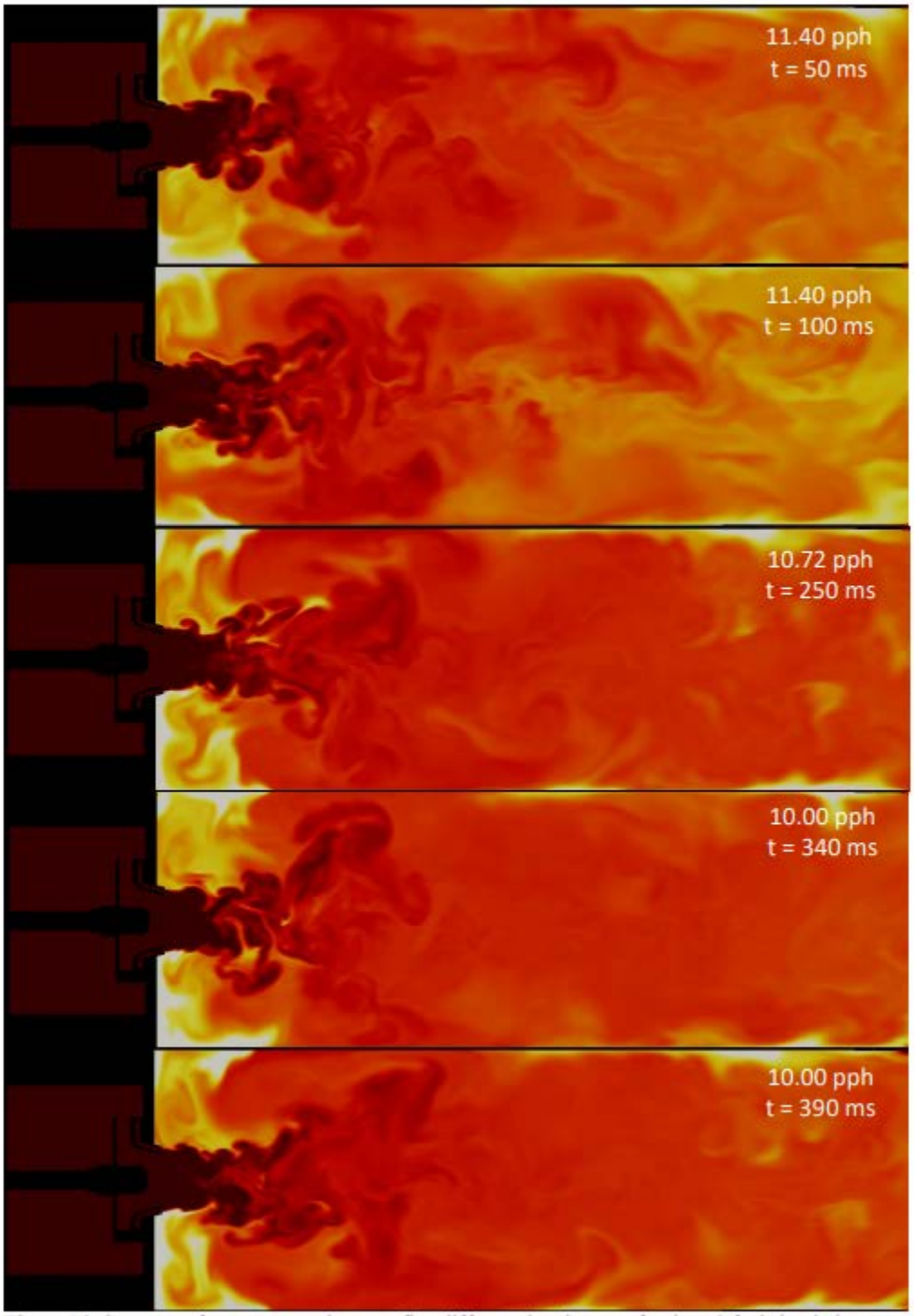


Figure 16: Contours of temperature shown at five different time instants for the A2 fuel simulation

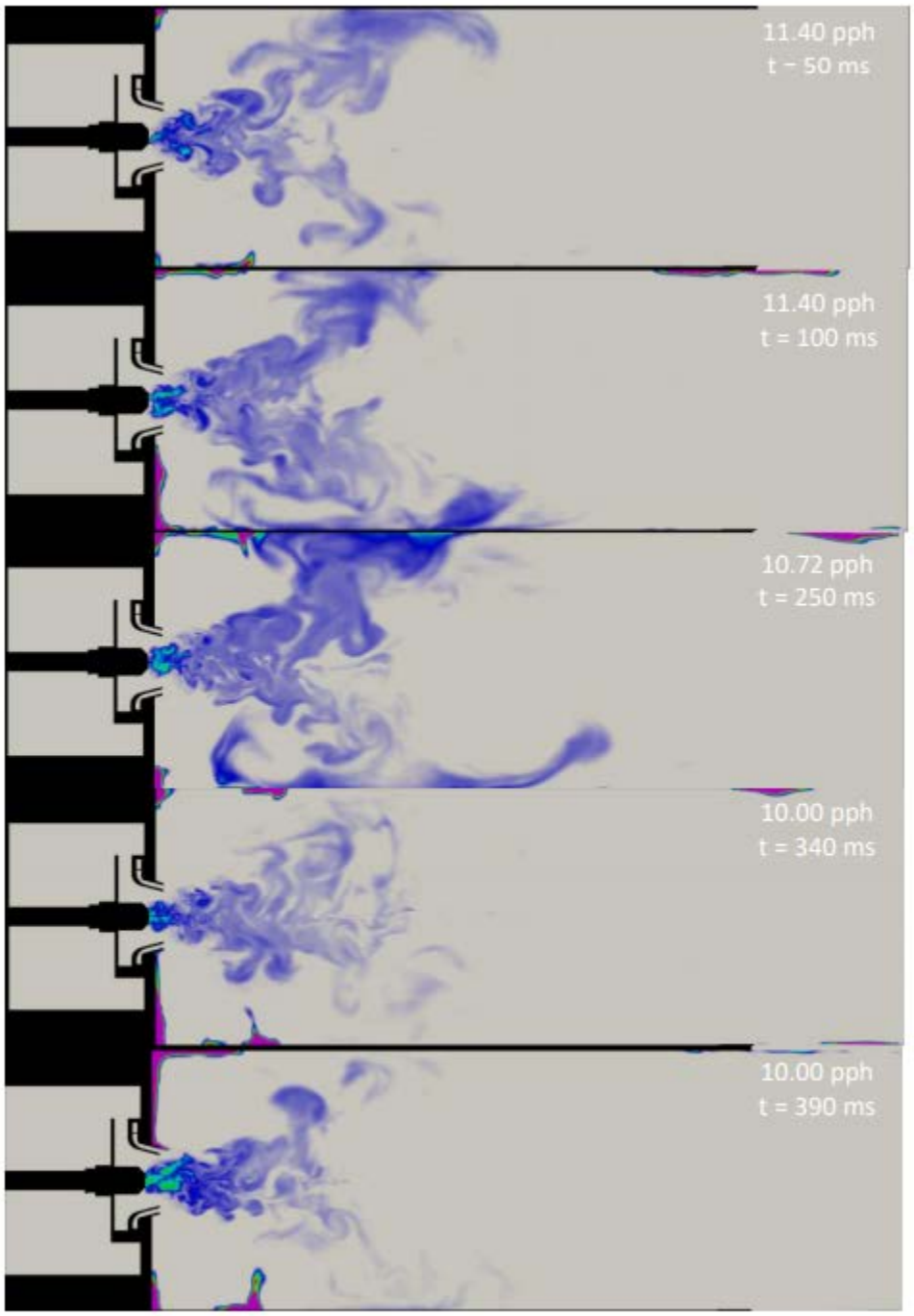


Figure 17: Contours of fuel mas fraction shown at five different time instants for the A2 fuel simulation

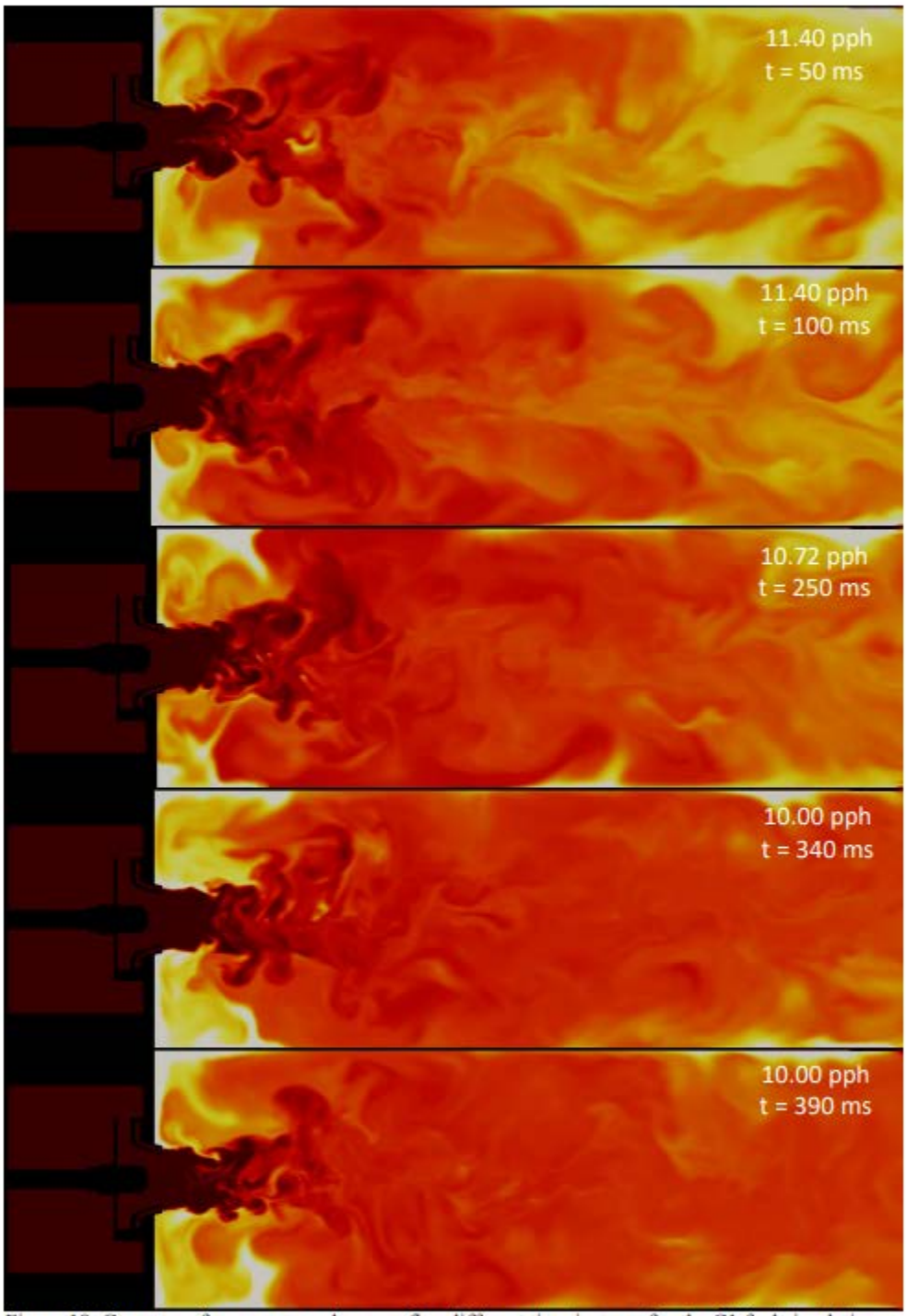


Figure 18: Contours of temperature shown at five different time instants for the C1 fuel simulation

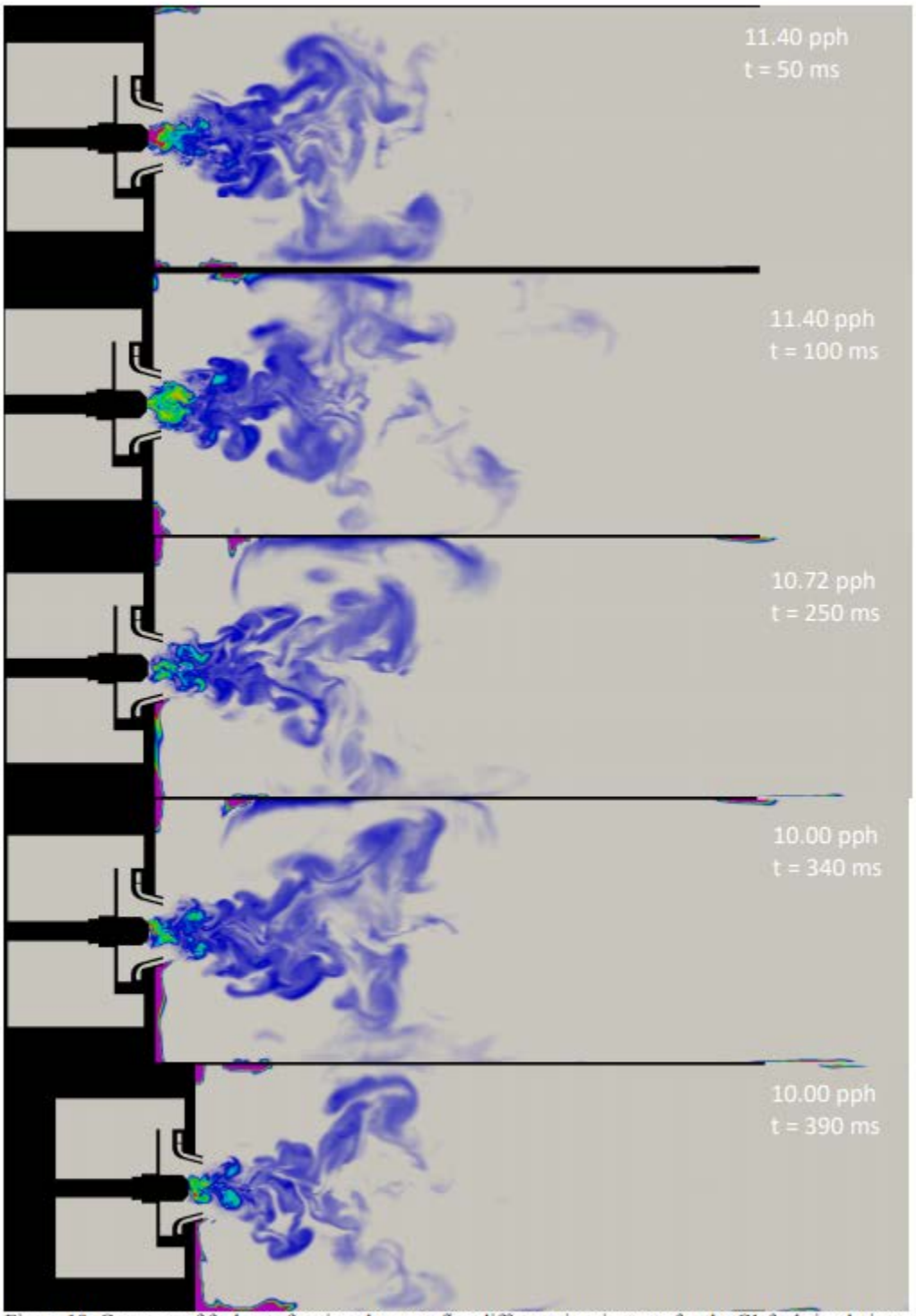


Figure 19: Contours of fuel mas fraction shown at five different time instants for the C1 fuel simulation



Conclusions
A Large Eddy Simulation-based analysis of the high shear rig combustor that was experimentally studied at Georgia Institute of Technology was performed in this study. The objective of this effort is to develop, enhance and apply computational fluid dynamics-based models to simulate stable combustion and lean blowout behavior in a high shear rig combustor. The goal is to understand if the models can predict the dependence of lean blowout phenomena on the physical and chemical properties of the alternative jet fuels. Several sub-models for unsteady flow simulation, spray injection boundary conditions, spray evaporation models, wall heat flux boundary conditions and turbulent combustion models are required to correctly simulate the physical processes. In this report we presented a description of different sub models, along with validation or verification where possible. Upon completion of the reacting LES for the two fuels at near blo out but stable condition, simulations of the lean blowout were performed by instantaneously reducing the fuel flow rate in steps of 6% for three different values of fuel-flow rates. Each flow rate was held constant for 100 mill-seconds for the combustor to respond to the flow rate change and stabilize at the new condition. Overall, the two fuels show differences in evaporation rate and also commensurate differences in heat release rates. Both the simulation show reduction in heat release rate as the flow rate is reduced but C1 seems to be dropping faster relatively compared to A2. C1 fuels also shows increase evaporation rates compared to A2, however this leads to quick build of fuel vapor in a concentrated region and if the flow conditions in that region is not conducive in terms of residence time to complete the reaction, it contributes to even more accumulation of fuel vapor from the incomplete combustion. In the case of C1 fuel, this is hypothesized to be the mechanism for earlier flame blow out compared to the A2 fuel. Long combustor dimension coupled with very small time steps to resolve the flame structure, leads to excessive computational time at each flow rate for the combustion to reach a quasi-steady state. As a result, it was not possible to reduce the flow-rate all the way to the lean blow out value to demonstrate the lean blow out behavior. However, the qualitative trend observed from the three simulate fuel flow rate conditions seems to indicate that the models employed in this study have the ability to discriminate between the different fuel physical properties and its impact on the lean blow out behavior.

Other Efforts
As a part of this contract UTRC also participated in working group meetings to provide and receive updates on the progress of different areas of research and also travelled to mid-year and yearly review meetings.

Milestone(s)

- Execution of sub-contract.
- Simulation of multiple fuels for the swirler and nozzle configuration at Georgia Tech.

Major Accomplishments

Completion of sub-contract period of performance.

Publications

None

Outreach Efforts

None

Awards

Joshua Heyne – SOCHE Faculty Excellence Award, 2016.

Student Involvement

None

Plans for Next Period

LBO simulations are being conducted to assess the impact of fuel on the LBO phenomena. UTRC to deliver final report on Area 3 spray simulations in Spring 2019.

Task 7- Ignition and LBO Testing of Conventional and Alternative Jet Fuels

University of Dayton Research Institute

Research Approach

A. Atmospheric Cold Start

A study of atmospheric cold start ignition was completed for nine NJFCP fuels in the Referee Combustor Rig. The conditions for the study near atmospheric pressure, in the combustor, and fuel and air temperatures ranging from 239K to 258K (-30 to +5 ℉) with a pressure drop across the dome of 2 or 3.5%. For all of the experiments, the fuel temperature was controlled to match the air temperature.

The controlled cooling of the fuel and air temperatures was accomplished using a system designed around two recirculating fluid process chillers and five heat exchangers. A schematic and image of the cooling system are shown in Figure 1. The air is cooled in two stages, via four heat exchangers, with the heat transfer fluid supplied from two different chillers. To achieve air temperatures of -30 ℉, the air first passes through two parallel heat exchangers to cool the air down to -10 ℉. The air then flows through a second stage of heat exchangers, also arranged in parallel, cooled by the fluid circulated by a second chiller, to finish the cooling process and supply air at target temperature at the combustor. Control of the air temperature was accomplished by PID control of the temperature from both chillers and by controlling the fraction of coolant from the lower temperature chiller that was supplied to the air heat exchangers.

For all of the ignition experiments, the igniter current and voltage were measured and computed a delivered energy (to the igniter plug). The measurements of the spark energy provided a check on the consistency of the delivered energy for each spark as well as an early detector of excessive igniter plug erosion. The combustor pressure before ignition for the cold experiments was approximately 1 atm and the fuel and air were controlled to the same temperature ($T_{air} = T_{fuel}$ = -30 ℉ or 5 ℉). For each combination of fuel type and flow conditions (ΔP, P_{cmb}, T_{air}, T_{fuel}) at least five volume flow rates were selected which resulted in between high and low ignition probabilities, at each fuel flow rate there were ten ignition attempts which consisted up to 40 sparks occurring at a frequency of ~3.5 Hz. After a successful ignition attempt was confirmed by video of the combustor, the spark sequence was stopped, and the fuel flow was stopped to end the ignition attempt. If ignition did not occur with 40 sparks the ignition attempt was halted for safety to avoid filling the downstream rig exhaust with large quantities of unlit fuel.

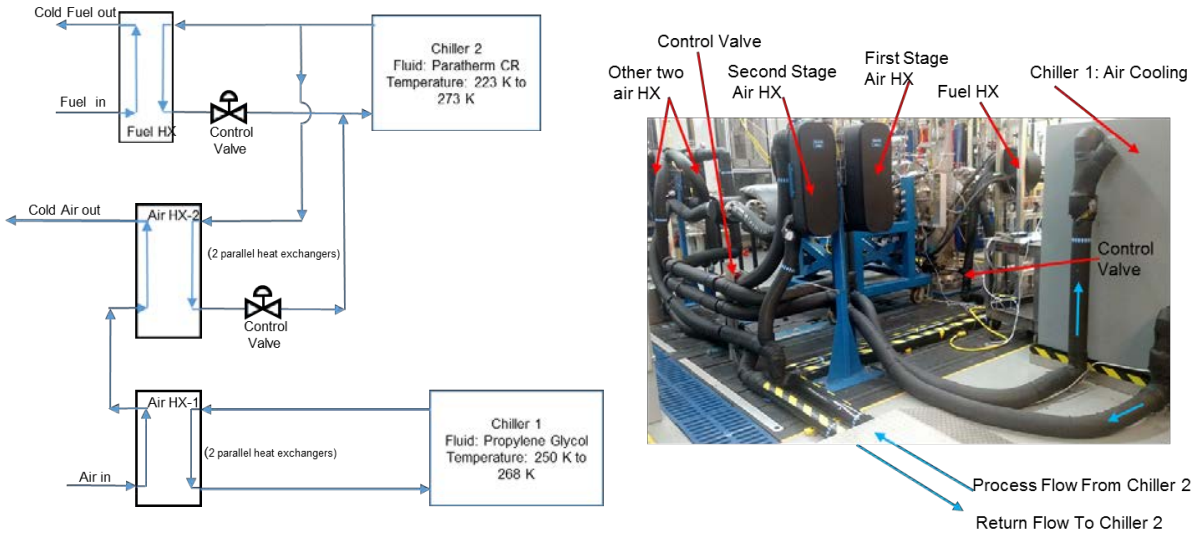


Figure 1. Schematic and Image of the Air and Fuel Cooling System

Each individual spark resulted in either a successful ignition, determined by spreading of the visible flame upstream of the spark ignitor and across the combustor, or an ignition failure. The successful ignition was determined from the

photodiode traces as a continuous elevated signal above the threshold extending in time past the next spark. Figure 2 shows a bar chart for each set of combustor conditions noting the number of successful and unsuccessful sparks for each fuel. A total of 23,548 sparks were attempted, resulting in 1438 successful ignitions.

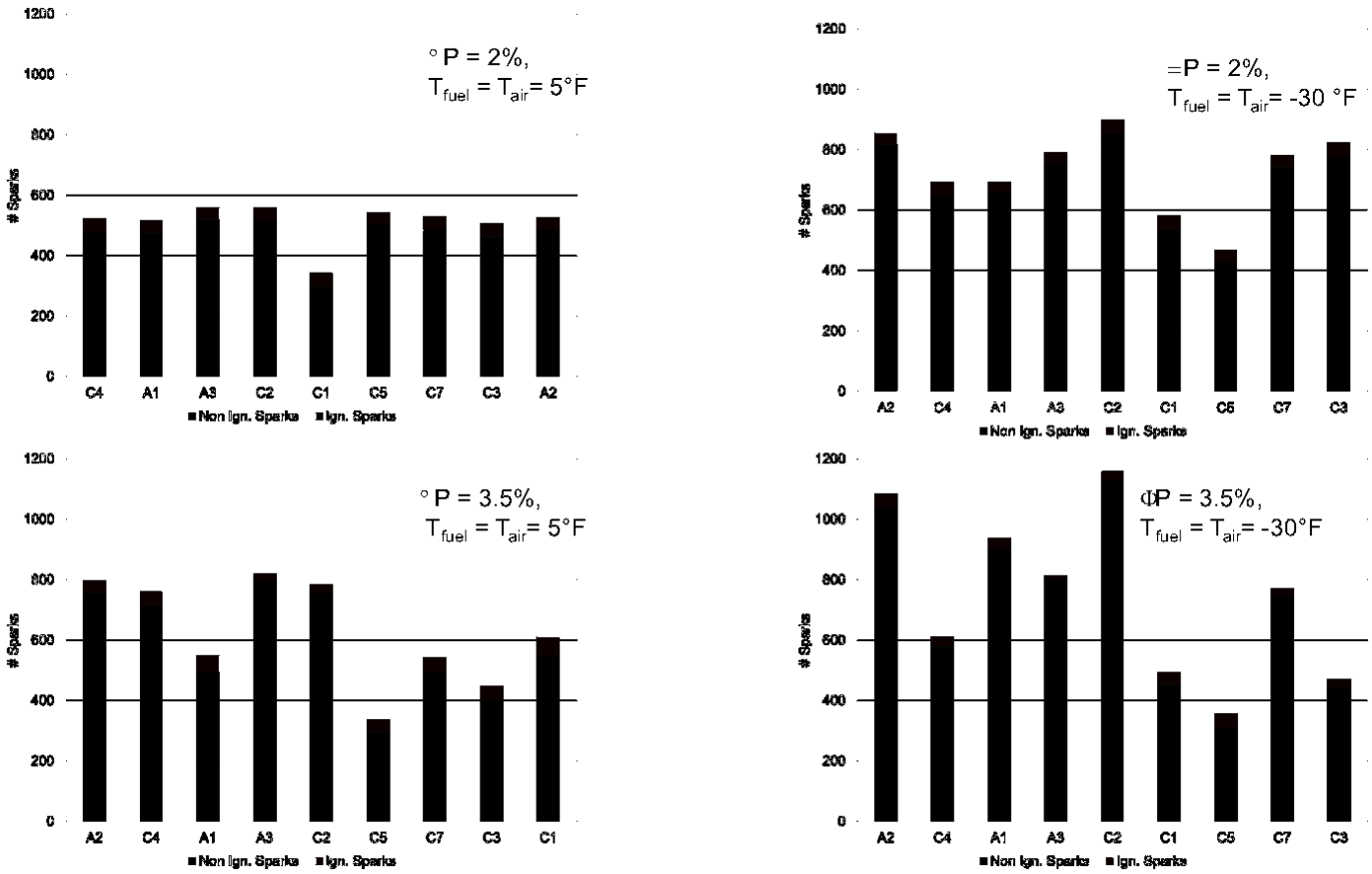
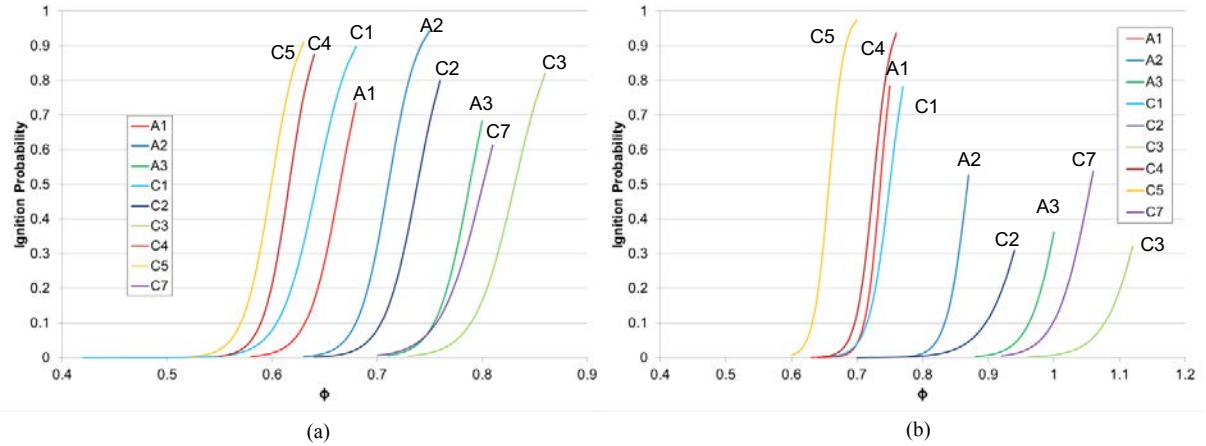


Figure 2. Summary of Sparks Resulting in Ignition and Non-Ignition for the Atmospheric Ignition Experiment. 23548 Sparks total, 1438 Successful Ignitions

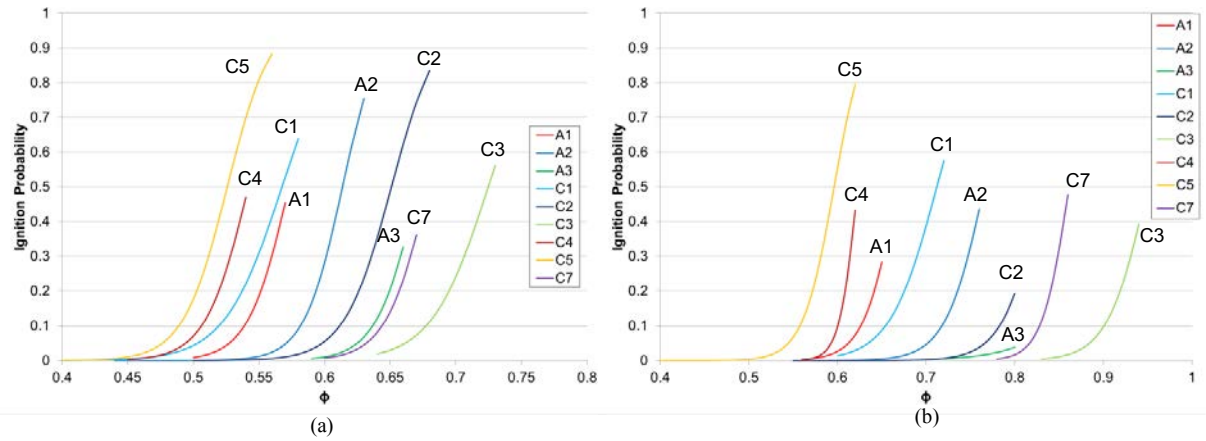
The results from each spark were used to calculate ignition probabilities, with the sparks counted using the photodiode and characterized as either a 1 for ignition or a 0 for non-ignition. At low values of equivalence ratio the probability of ignition is essentially zero, whereas at higher equivalence ratios the probability approaches one. In between these two extremes there is a region where the successful and non-successful ignition results overlap. Binomial logistic regression was used with the logistic function to reduce the 0's and 1's into a probability curve vs the equivalence ratio.

Ignition probability curves are plotted in Figure 3 and Figure 4 for 3.5% ΔP cases. The data is shown as a regression line for each case and fuel plotted up to the maximum equivalence ratio ϕ tested. Each curve increases in ignition probability as ϕ increases. For all fuels and pressure drop conditions, raising the temperature increased the ignition probability at a given ϕ. The rankings of the ignition performance for all of the fuels remained consistent as the imposed external conditions (T_{fuel}, T_{air} and ΔP) changed, with the only exception being the performance of C1 and A1 relative to each other.



(a) (b)

Figure 3. Ignition Probability vs ϕ for cases with ΔP = 2%, Pcomb = 1 atm. (a) $T_{air} = T_{fuel} = 5^{\circ}F$, (b) Tair = $T_{fuel} = -30^{\circ}F$



(a) (b)

Figure 4. Ignition Probability vs ϕ for cases with ΔP = 3.5%, P_{comb} = 1 atm. (a) $T_{air} = T_{fuel} = 5^{\circ}F$, (b) $T_{air} = T_{fuel} = -30^{\circ}F$

The effect of the physical properties on the ignition performance of the fuels was considered and partial results are shown in Figure 5 - Figure 7. Strong correlations are shown with the atomization, surface tension, & viscosity, and distillation properties (T10, and T 20). Further efforts are underway to better understand the relationship to of ignition to properties through advanced regression analysis. Further details from the cold start ignition experiments were presented at the AIAA SCITECH conference [1].

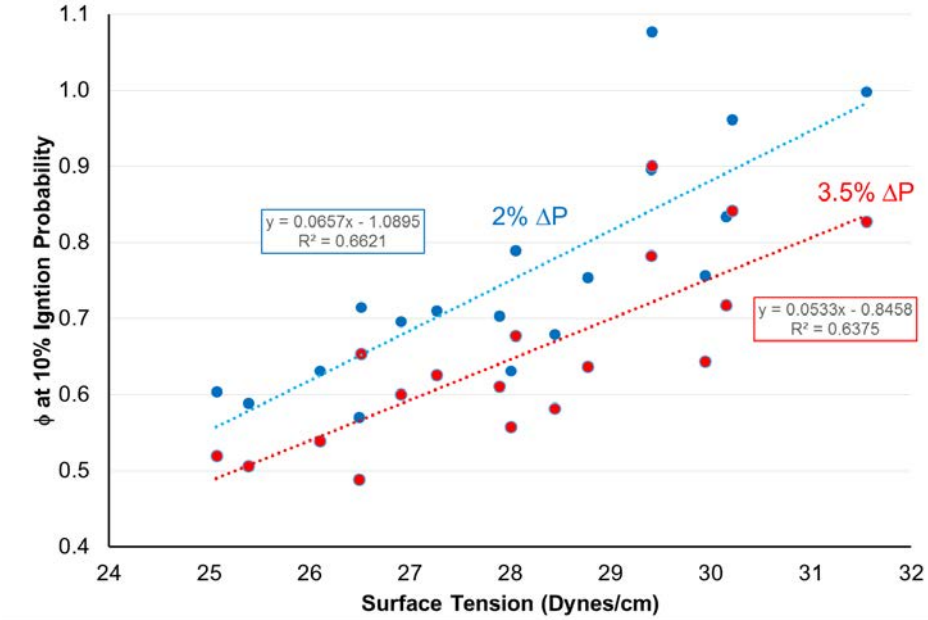


Figure 5. Equivalence Ratio at 10% probability vs Surface Tension for Atmospheric Cold Start Tests

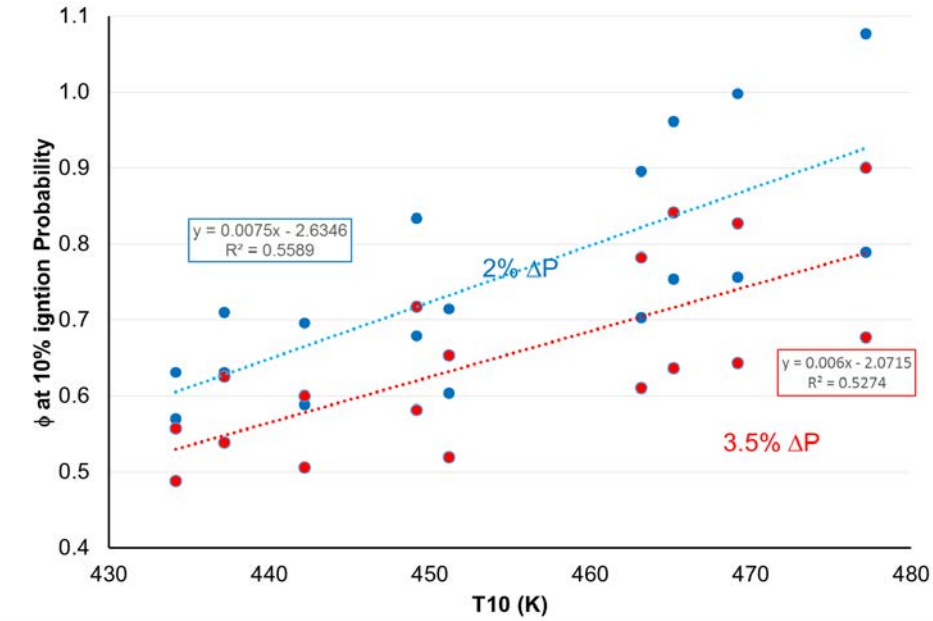


Figure 6. Equivalence Ratio at 10% probability vs T10 for Atmospheric Cold Start Tests

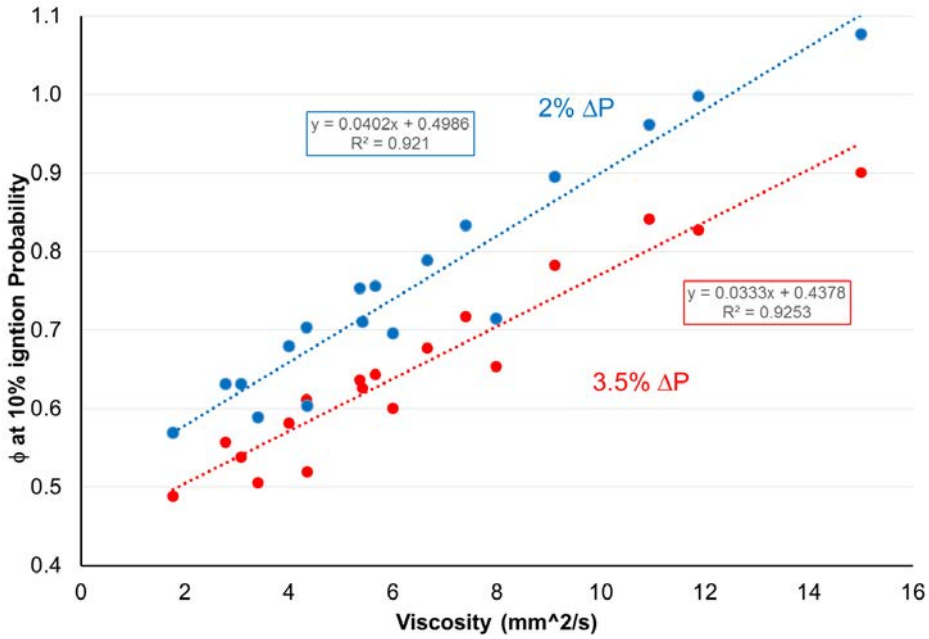


Figure 7. Equivalence Ratio at 10% probability vs Viscosity for Atmospheric Cold Start Tests

B. Cold Lean Blowout Experiments

Lean Blowout data was also obtained from form a subset of the tests cold start tests. The conditions represented during the LBO are not strictly conditions that show up in operation of the normal operation but represent a stressed, low pressure, low temperature condition. The motivation for this test came from the OEM committee involved with the project, with the rationale of "as long as we are lighting the combustor we may as well get data during blowout."

Several practical testing issues made these tests challenging and time consuming. The normal LBO experiments, conducted previously at high temperatures and pressures, were conducted over a time period of ~5 minutes per LBO attempt, and the hardware downstream of the combustor was water-cooled. The cold flow experiments precluded the use of water cooling because of the difficulties of using water as a coolant at air temperatures 25 to 65 ℉ below the freezing temperature of the water. Therefore, the experimental method used was a quick LBO approach in which the ramp rate was greatly increased to allow LBO to occur within 20 seconds of light off, and rely on heat sink to cool the rig. This compromise approach worked, but required an additional 7-10 minutes, with the internal flow of cold air to cool the combustor back down to the baseline temperature, between ignition attempts.

Results for the cold LBO experiments taken at combustor pressures of ~1 atm are shown in Figure 8 along with previous results at 2 atm and T_{air} =250˚F. It can be seen that the decrease in temperature decreases the magnitude of the phi at LBO. Previous results for LBO at high temperatures showed that the LBO results correlated strongly with Derived Cetane Number (DCN), and showed little correlation with atomization and evaporation parameters (Density, surface tension, viscosity) implying that the chemistry is important for LBO at normal conditions seen during LBO. For the cold LBO tests the opposite was observed. DCN showed little correlation to the LBO results and the LBO correlated best with viscosity and T50. Linear correlations of the LBO ϕ normalized by the LBO ϕ for A2 with viscosity and T50 are shown in Figure 9.

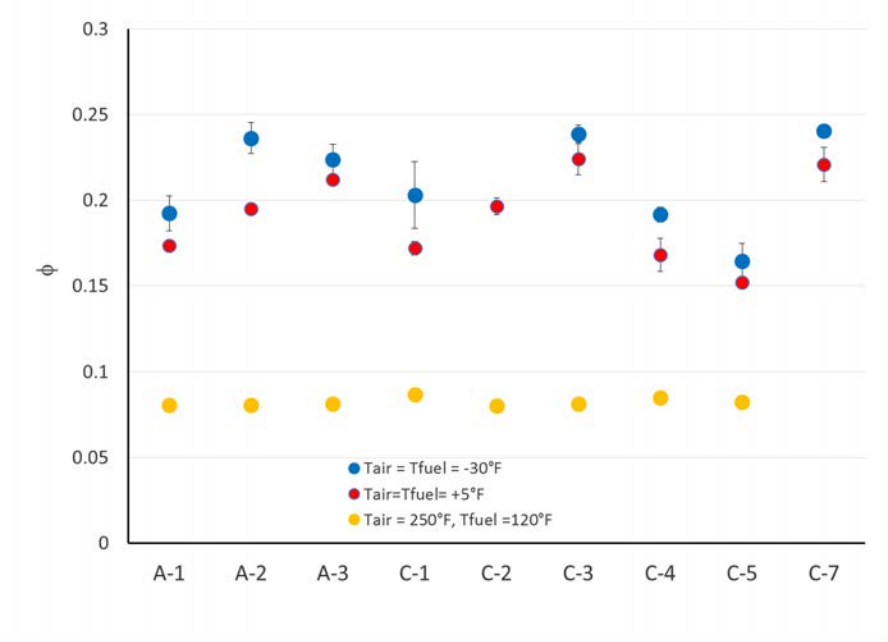


Figure 8. ϕ at LBO for Hot and Cold Experiments

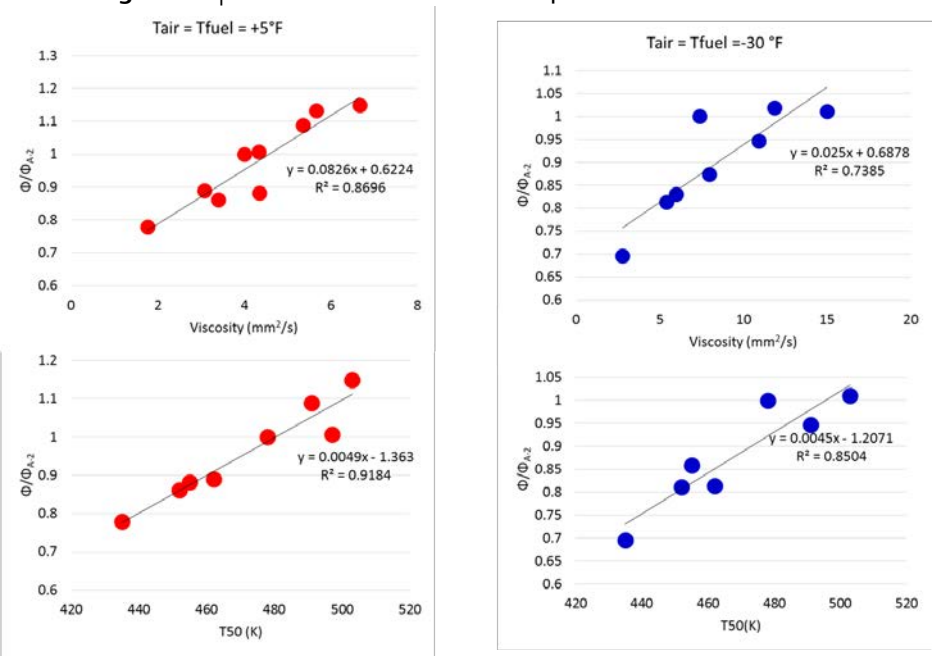


Figure 9. LBO Equivalence Ratio Relative to the LBO Equivalence Ratio for the Baseline A2 Fuel plotted vs T50 and Viscosity

C. Configuration for High Altitude Relight

The Referee Rig was modified in the past year to facilitate high altitude relight experiments. The ability to conduct altitude relight experiments at sub-atmospheric pressures was added to the facility by the addition of an air ejector and associated subsystems to the rig. The ejector was installed in the downstream side of the rig as shown in Figure 10. The control of the combustor back pressure for ignition experiment was set by maintaining a steady pressure at the ejector motive flow port. The pressure within the combustor was then controlled control valves to bleed room air at atmospheric pressure into

the duct upstream of the suction port of the ejector. The hazard of unburnt fuel downstream of the combustor was eliminated by sucking fuel through several ports on the exhaust stack, while the pressure on the exhaust was temporarily increased by stalling the ejector with air from additional ball valves.

In general, the altitude relight experiments required much more effort and time than the atmospheric cold start due to the low mass fuel mass flows which led to excessive heat gain between ignition attempts. Most of the sub-atmospheric experiments were conducted at a temperature of -30°F and a combustor pressure of 5.45 psia (0.37 atm) which corresponds to the pressure at 25,000 ft. Initial experiments attempted to use the same nozzle that was used for the atmospheric experiments, however it was not possible to ignite either A2 or C5 fuel at the desired conditions at equivalence ratios up to 1.3. It should be noted that the low air flow rates at high altitude resulted in low fuel flows which, in turn, resulted in low fuel pressures resulting in poor atomization. After the initial experiments with the larger flow number nozzle, a small flow number nozzle, was selected for the rest of the studies. With the low flow number (higher pressure drop) nozzle it was possible to ignite all of the fuels at the imposed temperatures and air flow rates.

Figure 11 shows a bar chart of the sub atmospheric ignition experiments over 5880 sparks leading to 456 successful ignitions. Figure 12 shows the regression curves reduced from all of the data points for the altitude relight experiments. The rankings of the fuels were similar to those at atmospheric pressure, shown in Figure 3a above, with the same fuel and air temperature (-30°F) with the exception of C5 and C1. At atmospheric pressures the C1 performed better than the A1 and A2, however, for the altitude case the C1 was shifted to the right (worse performance) of the A2 fuel. The C5 fuel which was the easiest to light under all conditions explored in the atmospheric cold start experiments exhibited odd ignition characteristics. At altitude C5 was the easiest to light at low ignition probabilities. However, the ignition probability curve for C5 crossed that for the other fuels leading to lower performance (higher ignition ϕ) at higher ignition probabilities. In addition, the confidence intervals for the C5 fuel were much wider than the other fuels. The reasons for these differences is under examination.

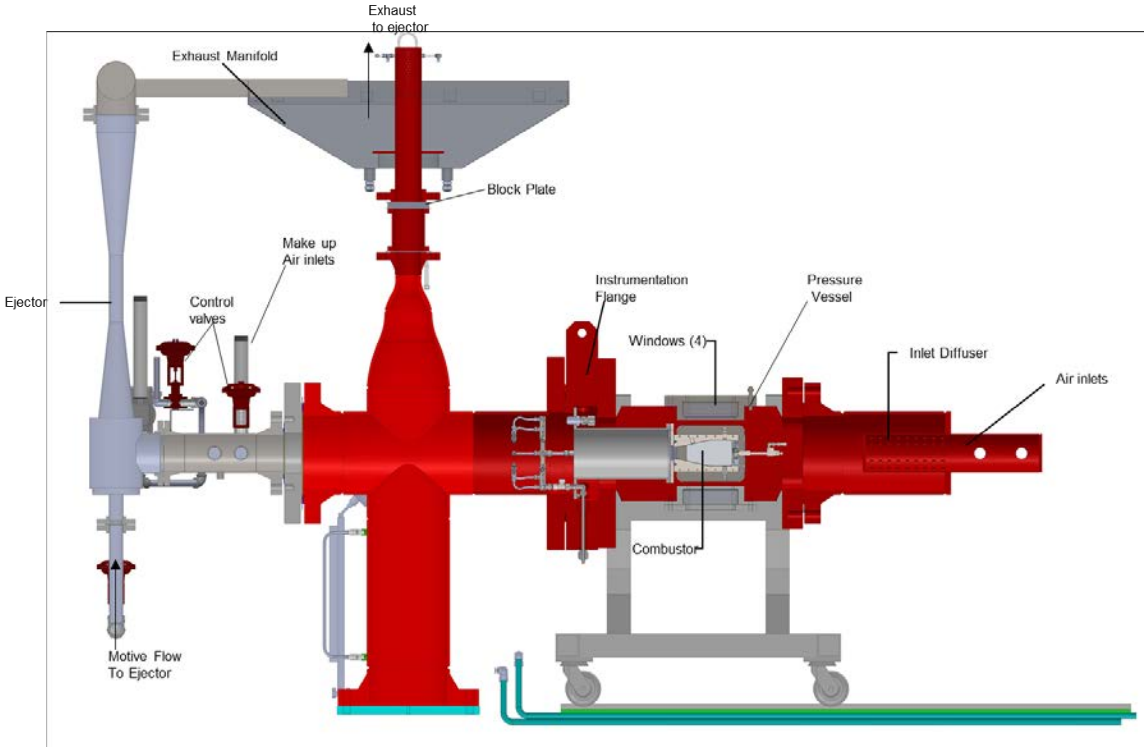


Figure 10. Referee Rig Configured for High Altitude Relight Studies

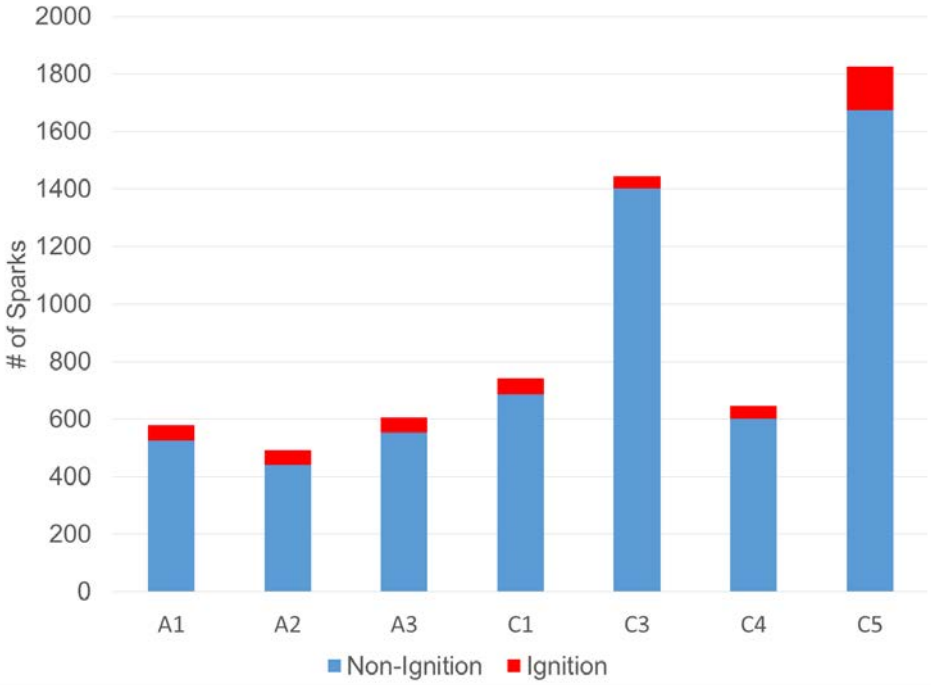


Figure 11. Summary of Sparks Resulting in Ignition and Non-Ignition for the High Altitude Ignition Experiment. 5881 Sparks total, 456 Successful Ignitions

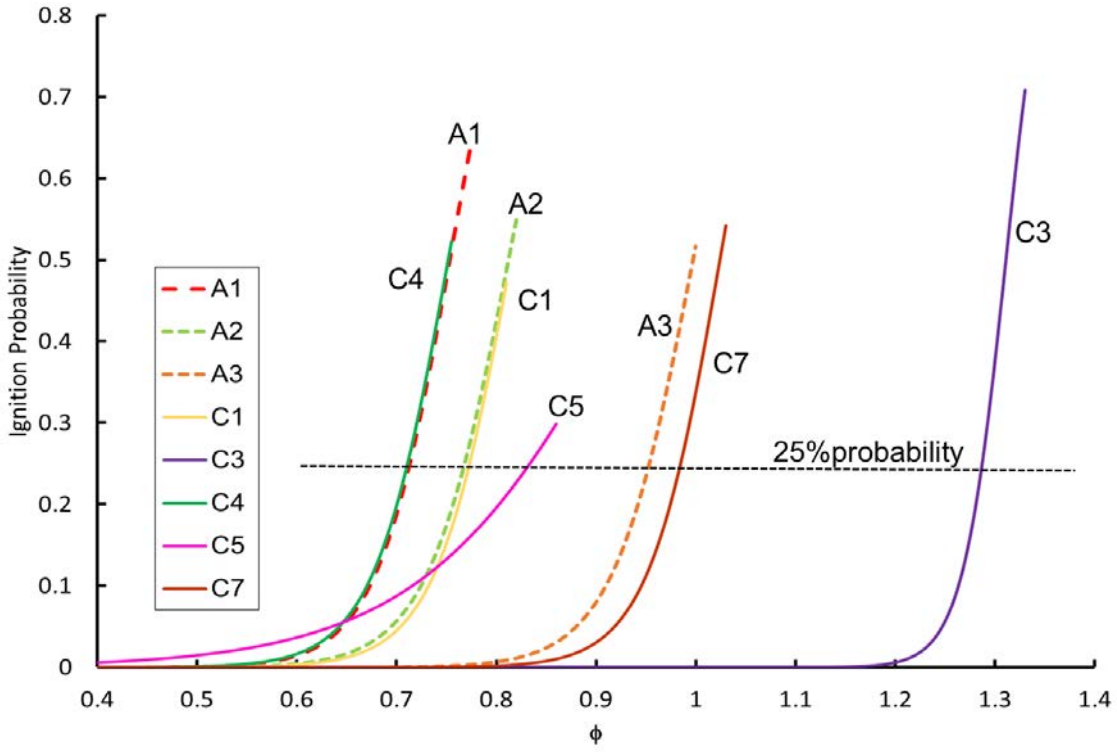


Figure 12. Ignition Probability Curves for Pcmb =5.45 psi, ΔP = 2%, T = -30˚F.

The effect of the various physical properties vs the equivalence ratio at 25% ignition probability is examined in Figure 13 - Figure 14. The best correlations were found with the viscosity and the distillation properties. The ignition performance showed poor correlation with DCN and vapor pressure. It was noted that the C3 fuel, which had the lowest viscosity, showed high sensitivity to temperature change. Figure 15 shows the ignition probability at different fuel and air temperatures for C3 fuel. The viscosity curve for the C3 is also plotted. The results were obtained by 10 separate ignition attempts of up to 40 sparks at each temperature. The results show a large drop in ignition performance between -18 and -30 ℉. This range is also the range in which the viscosity exceeds 12 cSt.

After noting that fuel viscosity seemed to be a major driver of ignition performance, an experiment was conducted to determine if three fuels of the same viscosity (created by heating the more viscous fuels to higher temperatures) would have the same ignition performance. Figure 16 shows the results for C1 at -30 ℉, A3 at -16 ℉ and C3 at 4 ℉. For reference, the 25% probability line is shown along with the crossing points marked by x's. It can be seen that increasing the temperature shifted the curves for the C3 and A3 to the left (improved performance) however, the effect was not enough to overlap the curves showing that the viscosity, while important, is not the only driver of ignition performance.

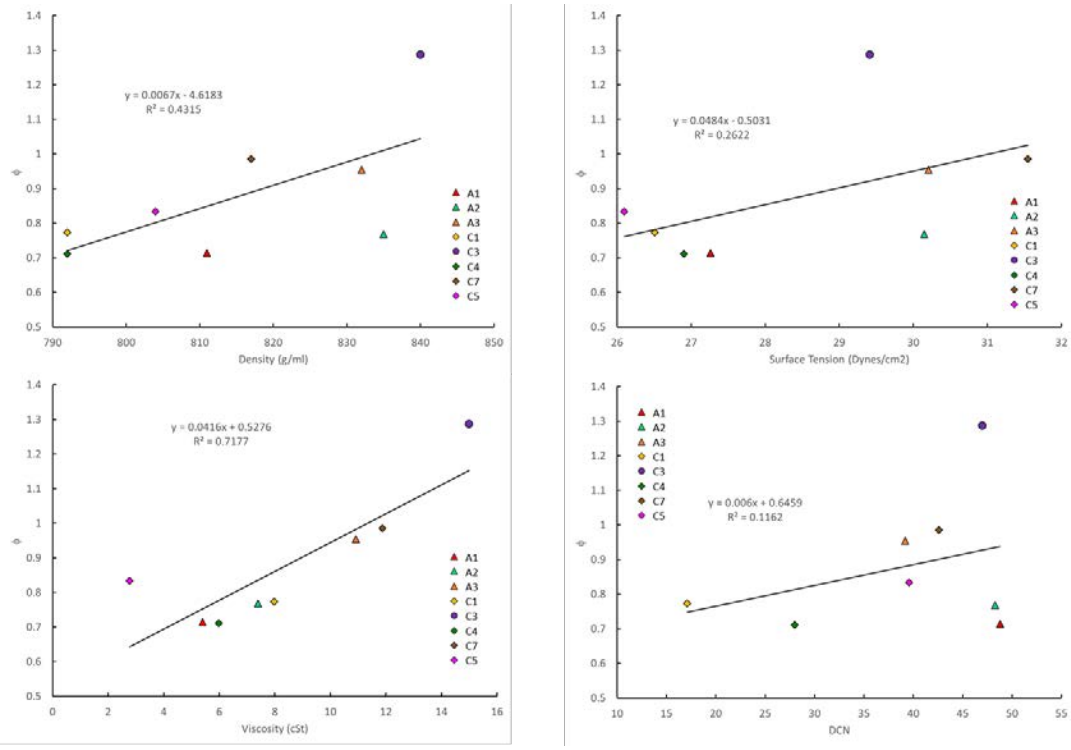


Figure 13. ϕ at 25% ignition Probability vs Atomization and Chemical Properties

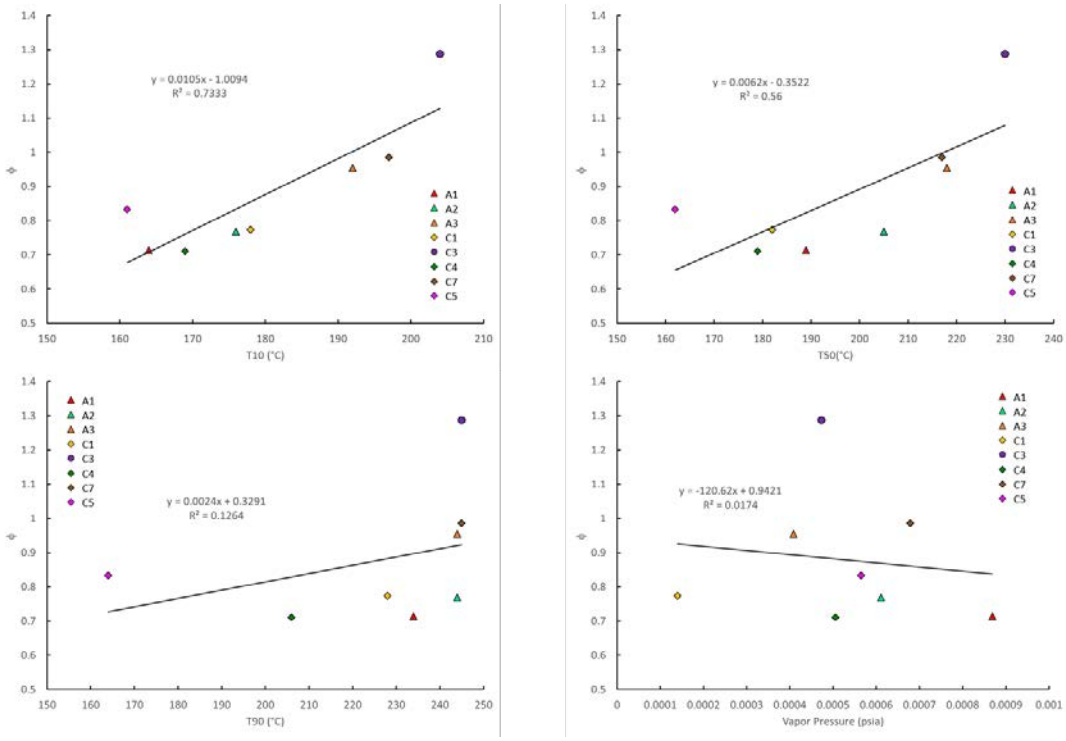


Figure 14. ϕ at 25% ignition Probability vs Atomization Properties

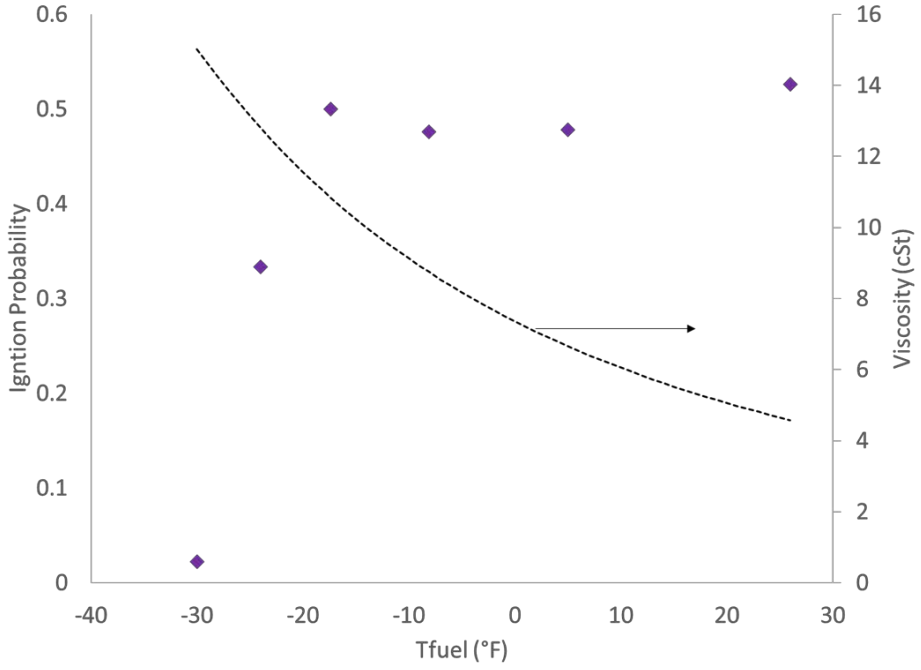


Figure 15. Ignition probability of C3 at Various Fuel and Air Temperatures ΔP =2%, Pcmb=5.45 psia.

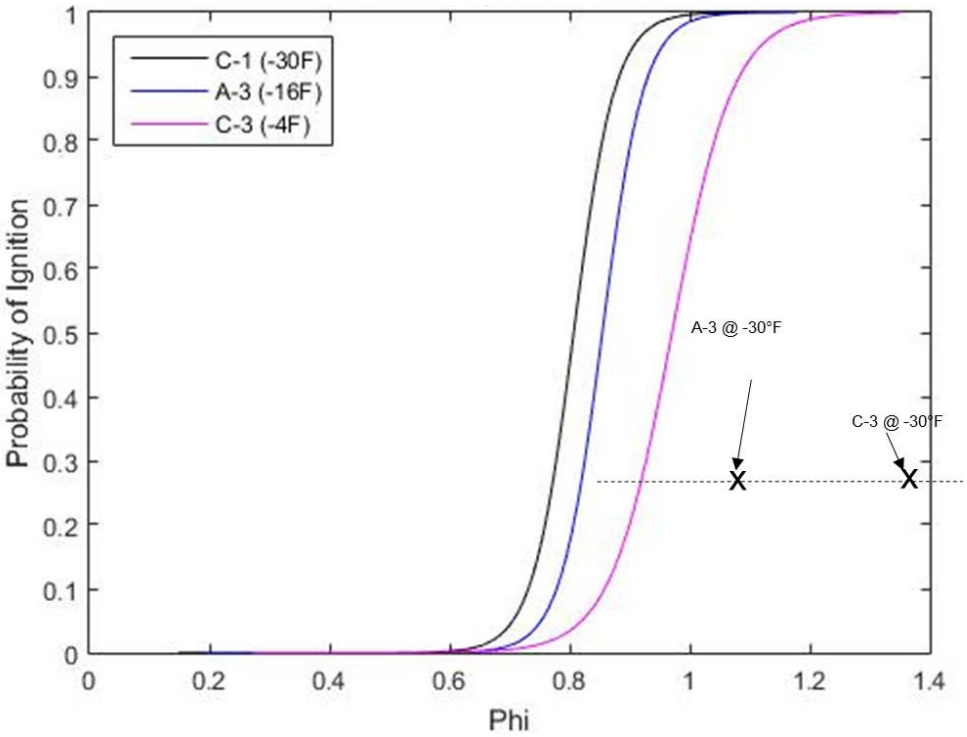


Figure 16. Ignition Probability Curves for Three Fuels at the Same Viscosity

The results from these experiments are under further analysis and will be presented at an upcoming AIAA meeting [2].

Near Term Activities
After completing experiments in cold conditions the focus for the experiments in the referee rig are being shifted to LBO at elevated pressures and temperatures. This requires several major hardware changes. The timeline for starting LBO experiments again is in November 2018. We are also working on further analysis of the data which will allow us to publish the results in archival journals. In addition, we are working with others to present the results in a coordinated way in an AIAA book on alternative fuels.

Milestone(s)
The generation of cumulative distribution functions for the various conventional and alternative jet fuels in the Referee Rig at cold conditions for ignition.

Major Accomplishments
Demonstrating significant fuel sensitivity in ignition probability for various fuels.

Publications
None

Outreach Efforts
Presentation and poster at ASCENT meetings in 2018.

Awards
None

Student Involvement
Jennifer Colborn, Undergraduate Research Assistant.



Plans for Next Period

1. Additional LBO measurements.
2. Testing of the Shell IH^2 fuel when it arrives.
3. Additional cold ignition tests once appropriate fuels are identified and LBO testing is over.
4. Writing up the results in a conference and journal publication.

References

[1] T. H. Hendershott, S. Stouffer, J. R. Monfort, J. Diemer, K. Busby, E. Corporan, P. Wrzesinski and A. W. Caswell, "Ignition of Conventional and Alternative Fuel at Low Temperatures in a Single-Cup Swirl-Stabilized Combustor," in *2018 AIAA Aerospace Sciences Meeting*, 2018.

[2] Stouffer, S.D., Hendershott, Colborn, J.T.H.,Monfort, J.R., Corporan, E., Wrzesinski, P., Caswell, A.W., “Altitude Relight Performance of Conventional and Alternative Fuels”, paper under preparation to be presented at SCITECH 2019, Jan 2019.



Project 036 Parametric Uncertainty Assessment for Aviation Environmental Design Tool (AEDT)

Georgia Institute of Technology

Project Lead Investigator

Principal Investigator:
Professor Dimitri N. Mavris
Director
Aerospace Systems Design Laboratory
School of Aerospace Engineering
Georgia Institute of Technology
Phone: (404) 894-1557
Fax: (404) 894-6596
Email: dimitri.mavris@ae.gatech.edu

Co-Principal Investigator:
Dr. Dongwook Lim
Chief, Air Transportation Economics Branch Aerospace Systems Design Laboratory
School of Aerospace Engineering
Georgia Institute of Technology
Phone: (404) 894-7509
Fax: (404) 894-6596
Email: dongwook.lim@ae.gatech.edu

Co-Principal Investigator:
Dr. Yongchang Li
Chief, Environmental & Policy Programs Brach Aerospace Systems Design Laboratory
School of Aerospace Engineering
Georgia Institute of Technology
Phone: (404) 385-2776
Fax: (404) 894-6596
Email: yongchang.li@ae.gatech.edu

- FAA Award Number: 13-C-AJFE-GIT, Amendment 019, 29, and 30
- Period of Performance: January 1, 2017 – August 31, 2018
- Task(s):
    1. Development and Test of New Profiles with Reduced Thrust and Alternative Weight
    2. Validation and Verification of BADA4 Implementation
    3. Capability Demonstration and Validation of AEDT 2d and 2e Functionality

Project Funding Level

According to the original project plan, the funding from the FAA is $175,000 for 12 months. The Georgia Institute of Technology has agreed to a total of $175,000 in matching funds. The project was augmented for the period for 12/1/2016 to 3/31/2017 to add additional tasks. The augmented funding from the FAA is $80,000 for 4 months. The Georgia Institute of Technology has agreed to additional $80,000 in matching funds. The latest augmentation was for $300,000 for the period of performance of 4/1/2017 to 8/31/2018. The Georgia Institute of Technology has agreed to additional $300,000 in matching funds.



Investigation Team

Prof. Dimitri Mavris, Dr. Michelle Kirby, Dr. Dongwook Lim, Dr. Yongchang Li, Dr. Matthew Levine, Yee Chan Jin (Graduate student), Ameya Behere (Graduate student), Junghyun Kim (Graduate student), and Zhenyu Gao (Graduate student), with consultation/support by research staff Dr. Holger Pfaender.

Project Overview

The Federal Aviation Administration's Office of Environment and Energy (FAA/AEE) has developed a comprehensive suite of software tools that allow for a thorough assessment of the environmental effects of aviation, in particular the ability to assess the interdependencies between aviation-related noise and emissions, performance, and cost. At the heart of this tool suite is the high fidelity Aviation Environmental Design Tool (AEDT). AEDT is a software system that models aircraft performance in space and time to estimate fuel consumption, emissions, noise, and air quality consequences. This software has been developed by the FAA Office of Environment and Energy for public release. It is the next generation FAA environmental consequence tool. AEDT satisfies the need to consider the interdependencies between aircraft-related fuel consumption, emissions, and noise. AEDT 2 has been released in four phases. The first version, AEDT 2a, was released in March 2012 [1, 2]. The second version of AEDT 2b was released in May 2015 [3], the third version of AEDT 2c was released in September 2016, and the fourth version of AEDT 2d was released in September 2017. A new series AEDT 3a will be released in December 2018 which have major updates including Base of Aircraft Data 4 (BADA4) performance model for fuel consumption, emissions and noise, reduced thrust profiles, and implementation of ASCENT Project 45 findings.

This uncertainty quantification comprehensively assesses the accuracy, functionality, and capabilities of AEDT during the development process. The major purposes of this effort are to:

- Contribute to the external understanding of AEDT
- Build confidence in AEDT's capability and fidelity (ability to represent reality)
- Help users of AEDT to understand the sensitivities of output response to the variation of input parameters/assumptions
- Identify gaps in functionality
- Identify high-priority areas for further research and development

The uncertainty quantification consists of verification and validation, capability demonstrations, and parametric uncertainty/sensitivity analysis.

Task 1-Development and Test of New Profiles with Reduced Thrust and Alternative Weight

Georgia Institute of Technology

Objective(s)

Under ASCENT Project 45, new reduced thrust and alternative weight profiles were developed for major aircraft and implemented in AEDT 3a [4]. The new profiles allow the aircraft to takeoff at reduced thrust and alternative weight to better represent the real-world departure operations. There are three reduced takeoff thrust levels: 5%, 10% and 15% reduction on full takeoff thrust. In addition, the profiles with 10% and 15% takeoff thrust reduction also have a 10% climb thrust reduction. The alternative weight is a simple average of the current stage length weight and the weight of the immediate higher stage length. In the new profiles, the rate of climb for the acceleration step was converted to energy share percentage which can provide the same climb rate and be used for different reduced thrust levels.

The implementation of the reduced thrust and alternative weight profiles is a big change to AEDT, thus, uncertainty quantification analysis needs to be conducted to make sure these profiles were implemented correctly. In this task, the study focused on thoroughly testing the newly developed profiles to verify if they are working properly for different aircraft at different stage length, airport, weather profiles, and comparing the environmental impacts of the new profiles including fuel burn, emission and noise.

Research Approach

New departure profiles for AEDT were created for 90 aircraft. These profiles were based on the STANDARD procedural profiles. A total of 7 sets of profiles were created for each aircraft, 4 for the alternate weights and 4 for original AEDT weight. These 2 subgroups both contain profiles with full thrust takeoffs and reduced thrust takeoffs with 5%, 10% and 15% thrust reduction. The creation of these new profiles involved the use of SQL data tables. New thrust types were implemented for reduced thrust capabilities, this was done by applying the reduction percentage to the relevant thrust equation coefficients. High temperature thrust types were not modified. Alternate weight profiles were created by creating new profiles and assigning them the appropriate weight. The weight assigned to such profiles was taken to be the average of the current and the next stage length weight. The final stage length weight was not modified. Finally, the procedural profile steps were implemented for the new profiles by converting the accelerated climb steps to energy share percentage climb steps. The new thrust type codes were also assigned as appropriate. In total, across 90 aircraft, an additional 524 thrust settings and 3143 profiles were created involving an additional 13636 procedural steps.

To test the new profiles with reduced thrust and alternative, AEDT studies were created with the new profiles for different scenarios. Each metric results in AEDT was run with both ANP and BADA4, and the fuel burn, emissions and noise results will be compared between ANP and BADA4 for different scenarios.

ANP and BADA4 Case Study with New Profiles

The purpose of this study is to fully test the new profiles by comparing the fuel burn, NOx, CO, and noise between Aircraft Noise and Performance (ANP) model and BADA4 model using a fleet study consisting of 41 available BADA4 aircraft. This could then help understand the difference in the environmental impacts between ANP and BADA4 and identify the outliers for each of these parameters. The study consisted of a total of 2214 cases, which is the combinations of 41 aircraft, 2 operation types, 3 airports, 1 runway (shortest at the airport), 2 temperature profiles (modeling normal and hot day), 1 stage length (maximum stage length of the aircraft), and 8 profiles including the 7 new profiles for each aircraft, as shown in Figure 1. And in the name of profiles RT stands for reduced thrust and AW stands for alternative weight. The process of generating, running, extracting, and analyzing the large sum of cases can be seen in the depiction Figure 2.

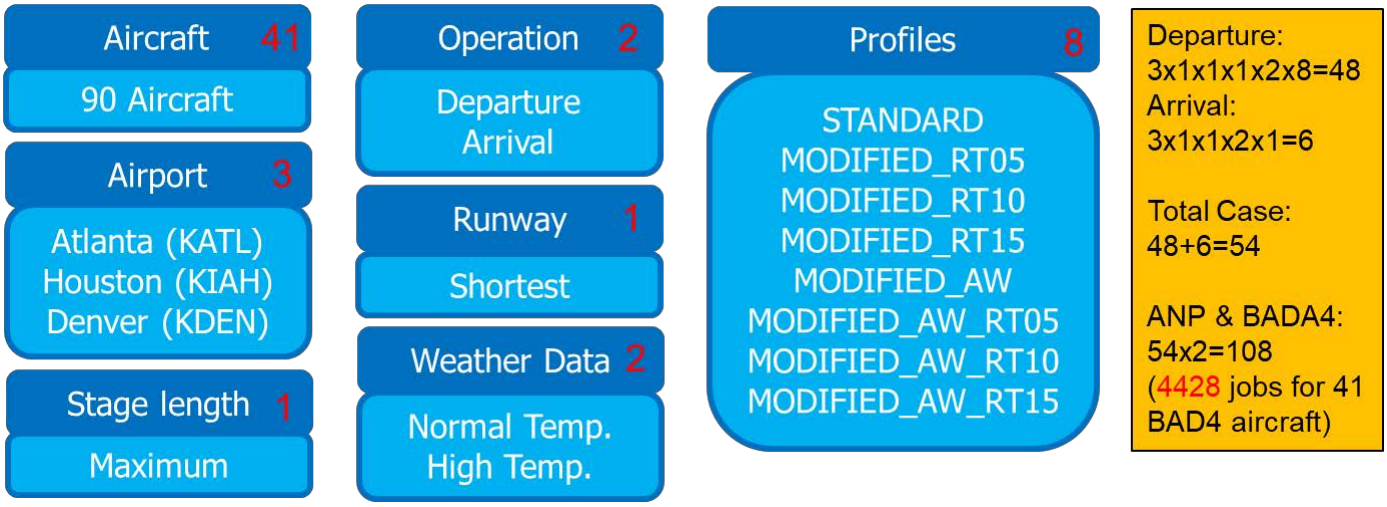


Figure 1. Combination of settings for the 41 BADA4 aircraft case study

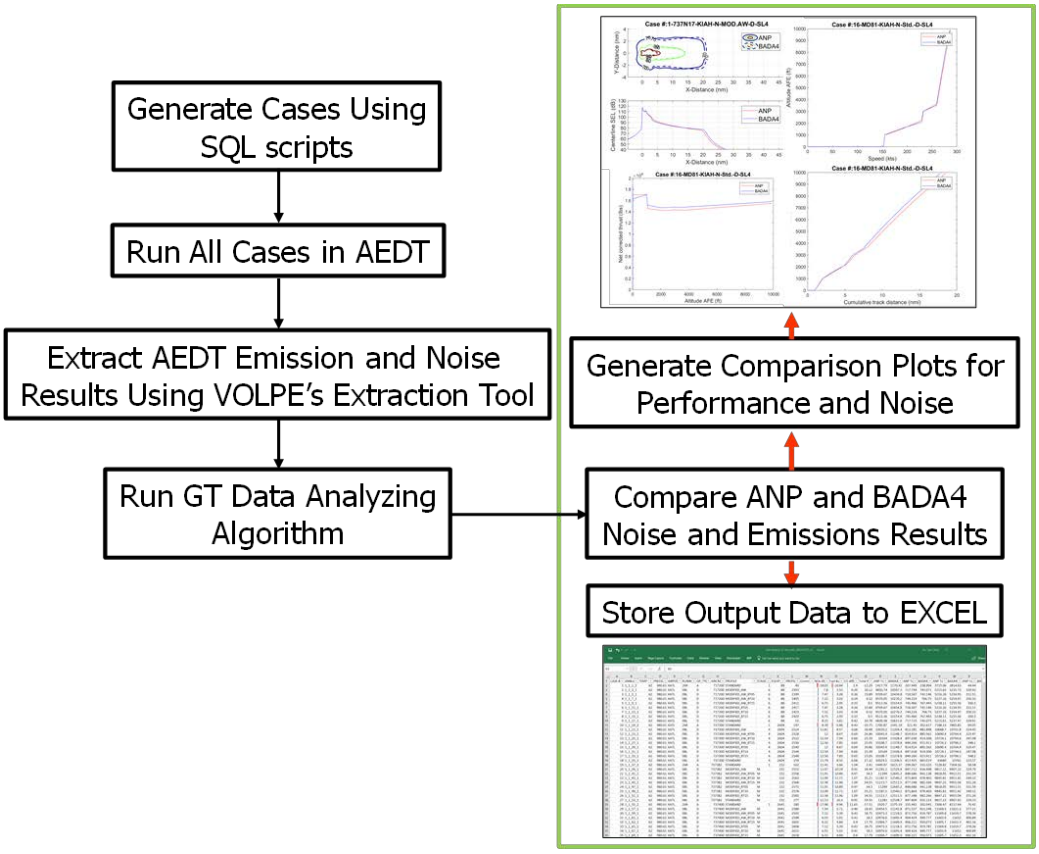


Figure 2. The processing cycle of the 41 BADA4 Case Study

The 2,214 cases were generated using a SQL script that automatically created the cases in AEDT by ANP and BADA4 (thus a total case study of 4,428 cases). Once the cases were generated and the study was run in AEDT. It was observed that 27 of 4428 jobs failed which is only 0.6% of total cases and they all happened at Denver airport. After the AEDT study was run, a batch mode tool developed by Volpe can be used to extract the performance, fuel burn, emissions and noise results. Then the fuel burn, emission and noise data were analyzed using a tool created by the Georgia Tech (GT) team. The tool could directly extract the necessary data from SQL or from relevant AEDT output files and generate a datasheet of input parameters, ANP versus BADA4 performance plots, noise contours, centerline plots, noise contour area differences, and emission comparisons. Essentially, the tool can generate all the relevant ANP and BADA4 comparison data, regardless of the case study size and complexity.

Figure 3 shows the fuel burn statistical comparison for departure and arrival operations of the 41 aircraft between ANP and BADA4. It can be seen that BADA4 departure fuel burn is greater by 12.6% on average than ANP. This is expected since BADA4 used the Mean Seal Level (MSL) based profile, that is, the 250 knot Calibrated Air Speed (CAS) at 10,000 ft above MSL rule is implemented in BADA, while ANP uses 250 knot CAS at 10,000 ft Above Field Elevation (AFE). This implementation results in differences in the performance, fuel burn, emissions and noise results between ANP and BADA4, especially for operations at airport with high altitude. This also leads to that BADA4 has much longer trajectories before reach 10,000 ft AFE, and thus produces more fuel. Since BADA4 follows the 250kt/10000ft MSL Federal Aviation Regulation (FAR) rule, its results are closer to the real aircraft operation and more accurate than ANP. It is also can be seen from Figure 3 that fuel burn produced by BADA4 is 7.6% less on average than ANP, which mainly is due to different approach modeling between ANP and BADA4. Readers can refer to the section Idle Descent where the difference in approach modeling was discussed and it was indicated that BADA4's results are more accurate.

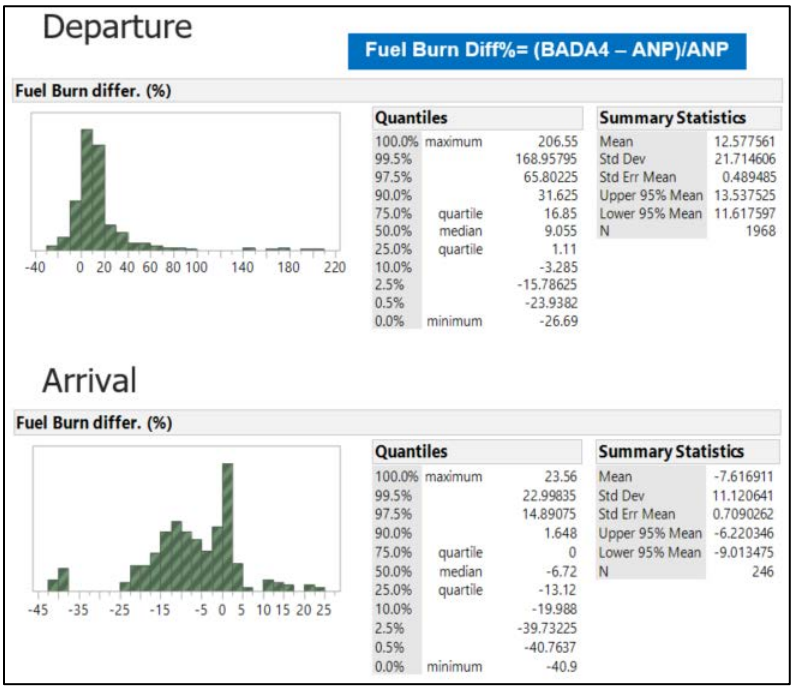


Figure 3. Fuel Burn Comparison between ANP and BADA4

Figure 4 to Figure 5 show the ANP versus BADA4 emission comparisons for NOx, fuel burn, and CO by airport and profile type for all profiles, with labels showing the outlier aircraft models. The airport specific plot has also been divided into departure and arrival procedures. The figures show a grouping of outliers for KDEN departure procedures, which is further explained in the outlier analysis section, and very little, to no outliers in the other two airports. Furthermore, the F10062 and several Embraer aircraft can be seen showing up as outliers throughout different profile types for all emission types; however, it was decided to rather draw concern on outliers that were either Airbus or Boeing aircraft since these are the more prevalent models. Consequently, the outlier plots show the A340-642 and B737-N17 as consistent outliers for departure operation throughout various profile types for all the emission types. The A340-642 was then selected for further investigation to narrow down the source of the large emission differences between ANP and BADA4.

In the airport-specific study for departure cases, the gap between the first and third quartile (except for KDEN) is extremely small around 2-10%. This means that for KIAH and KATL departure cases, the emission results comparison between APN and BADA4 are quite similar regardless of the aircraft type. Additionally, only a handful of aircraft showed up as outliers under these settings. This is not the case for departure cases at KDEN where the maximum differences in emission reach up to 200%. This is four to five times larger than the maximum emission differences from each of the corresponding airports. The difference in first to third quartile for KDEN departure is also around 20%, which is at least twice that of the other airports. Further looking into arrival procedures, there is a similar trend in CO results as KDEN shows a much larger quartile difference of 20% compared to that of the other two airports of 10%. Nevertheless, the arrival cases show relatively uniform emission result plots across the different airports compared to that of departure cases. It was found that many of the outliers occurred for departure cases at KDEN.

Looking at the emission results by profile type in general, the modified profiles (which are all departure procedures since arrival procedures do not have modified profiles) had mean emission values (for CO, fuel burn, and NOx) that were above zero. Fortunately, the quartile differences for CO and fuel burn were less than 10%; however, the quartile differences for NOx were relative high at 20% for all modified profiles. The outliers for all the modified profiles were found to be consistent throughout the profiles with F10062 and Embraer showing up with the largest emission differences between ANP and BADA4. For the standard profiles, which included arrival procedures, shows similar trends to that of the modified profiles. The profile-specific study shows how the outliers are not necessarily dependent on profile types (since they are equally spread out over all the profiles), but rather dependent on airport type and aircraft model.

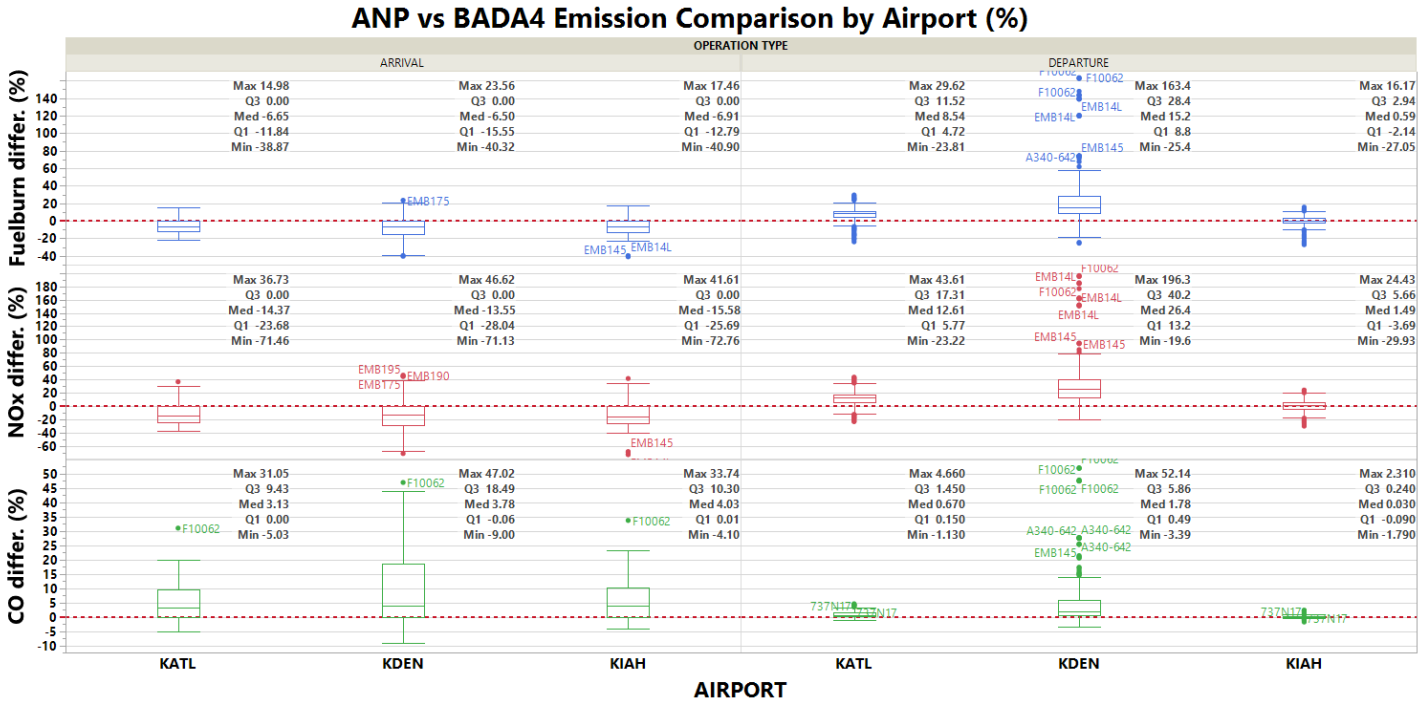


Figure 4. ANP vs. BADA4 Emission Comparison by Airport

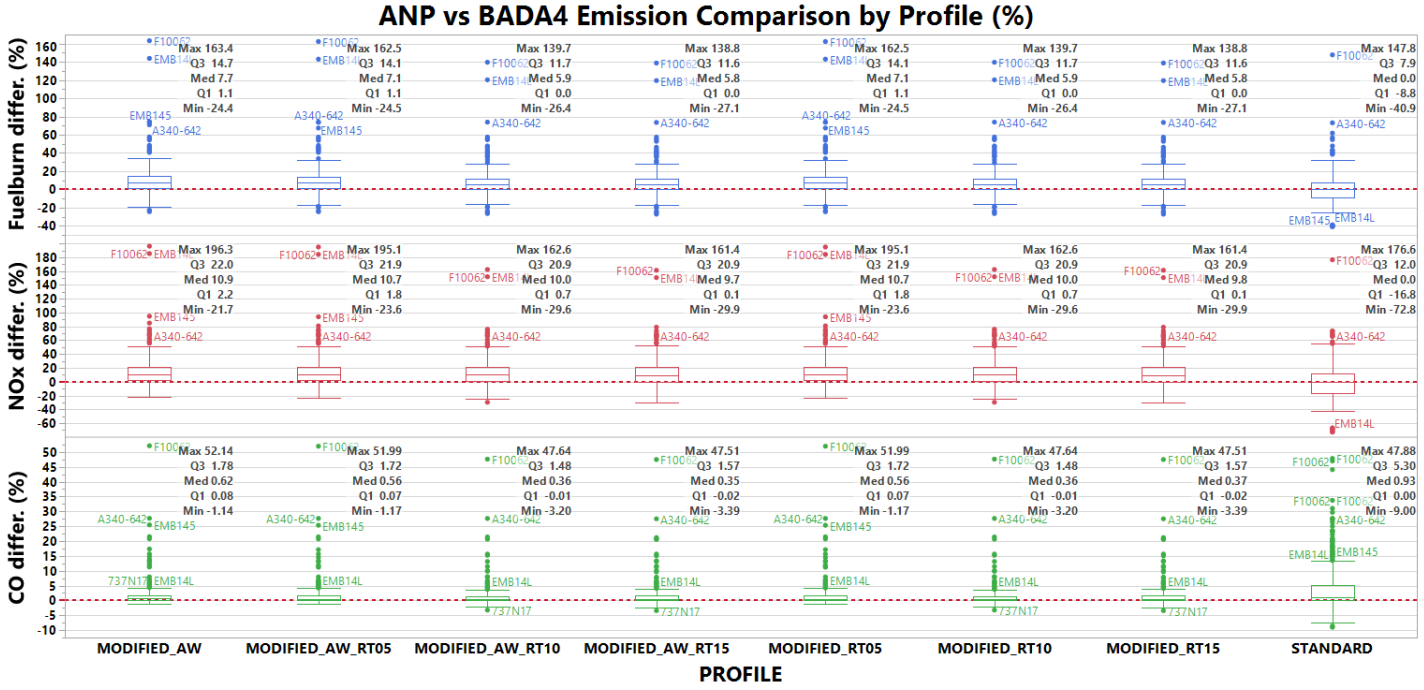


Figure 5. ANP vs. BADA4 Emission Comparison by Profile Type

Subsequently, Figure 6 to Figure 7 show the noise comparison between ANP and BADA4 by airport and profile type. The noise levels are categorized by SEL, from 70 dB to 90 dB with the airport specific plot also split into departure and arrival procedures. As mentioned in the emission outlier study, the majority of the outliers seem to occur around the KDEN airport, which will be further explained in the analysis section, but is primarily due to the airport's high elevation. Congruent to that of the emission study, the F10062 and several Embraer aircraft have been identified as outliers throughout the selected SEL range for all three airports. Furthermore, the MD82 had emerged as a consistent outlier in the noise study, but no further investigation was performed by GT as it was selected by the FAA for further data updates. Looking through the different profiles, besides the outliers already identified through the emission study, some new outliers were found to be A321-232 and the B747-20B which occurred during standard profiles. Since these aircraft are either Boeing or Airbus, they were selected for further study.

Similar to the emission study, the airport-specific plots show a very small quartile difference throughout all the airports but show a cluster of outliers at KDEN airport. And further looking at the profile-specific study, it shows how the MD82 and Embraer aircraft are strong outliers throughout all profile types with no other specific clusters easily noticeable throughout the profiles. It is, however, important to note that the standard profiles experience a larger difference in ANP and BADA4 noise levels from outliers than that of modified profiles with maximum differences occurring at over 170%. Hence, from the noise study it was found that the majority of the noise outliers occurred around KDEN for standard profiles.

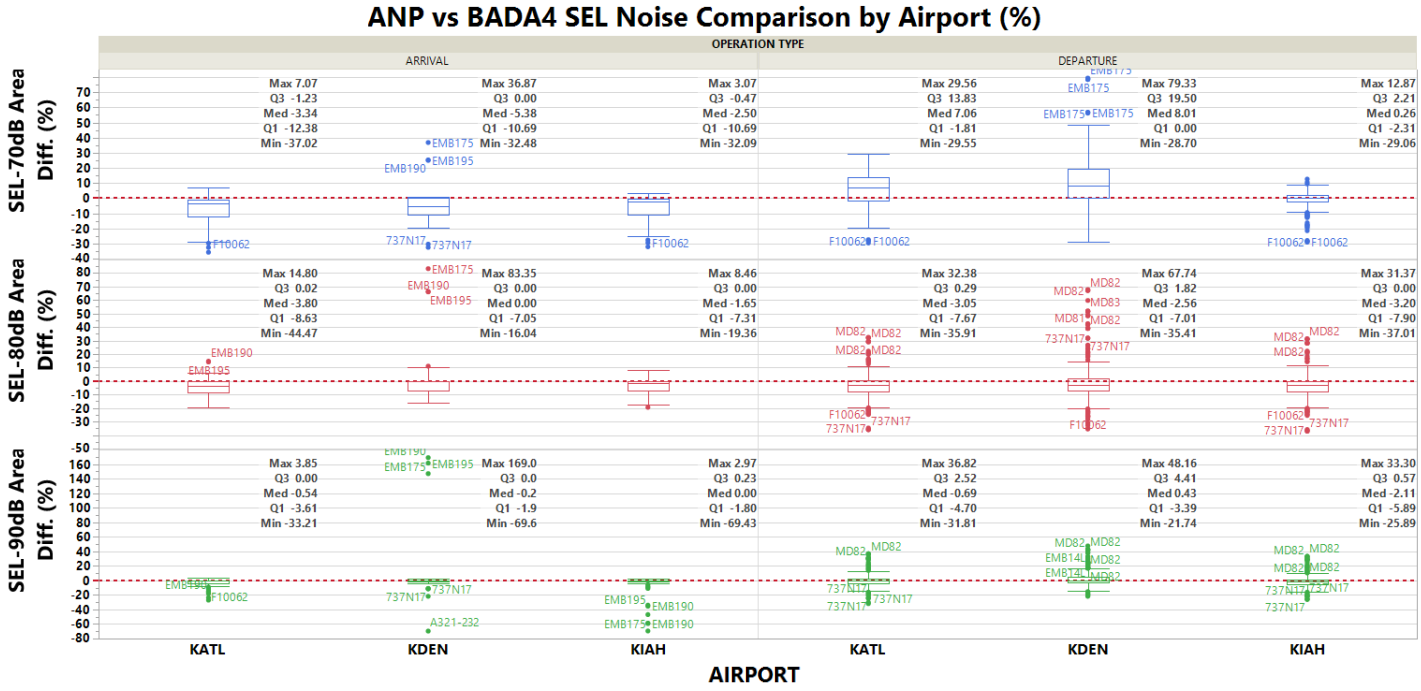


Figure 6. ANP vs. BADA4 SEL Noise Comparison by Airport

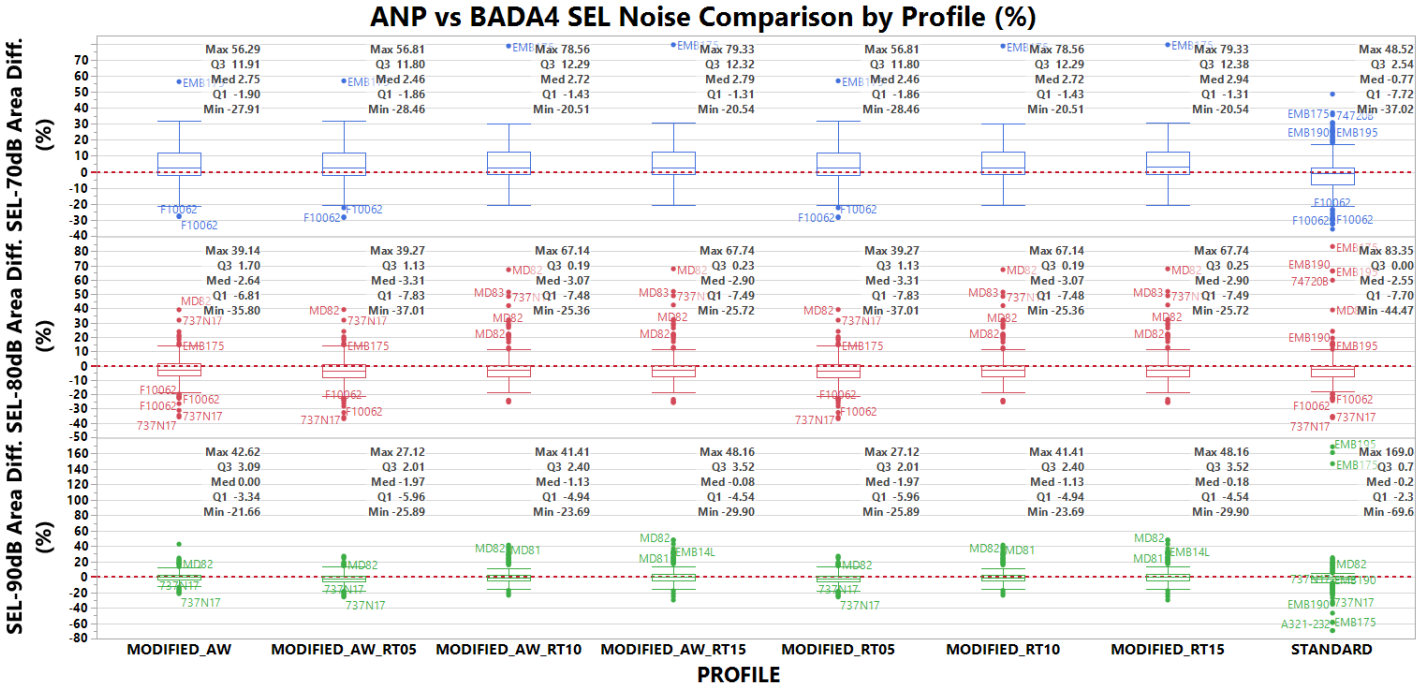


Figure 7. ANP vs. BADA4 SEL Noise Comparison by Profile Type

Outlier Analysis

In addition, the study shows that the outlier aircraft were MD82, F10062, A340-642, B737-N17, B747-20B, and several Embraer aircraft. Most of the outlier cases occurred at Denver International Airport (KDEN). The primary reason for much of the outliers being present in KDEN is due to the airport's high elevation (around 5,000 ft MSL) since BADA4 uses the 250 knot speed limit based on 10,000 ft MSL instead of 10,000 ft AFE which is used by ANP. Thus, the KDEN departure and arrival cases would have a relatively large difference in emission and noise results. An example of the trajectory differences for KDEN can be seen in Figure 8. The figure shows how the trajectories deviate away from each other around 5,000 ft AFE at KDEN, which is 10,000 ft MSL.

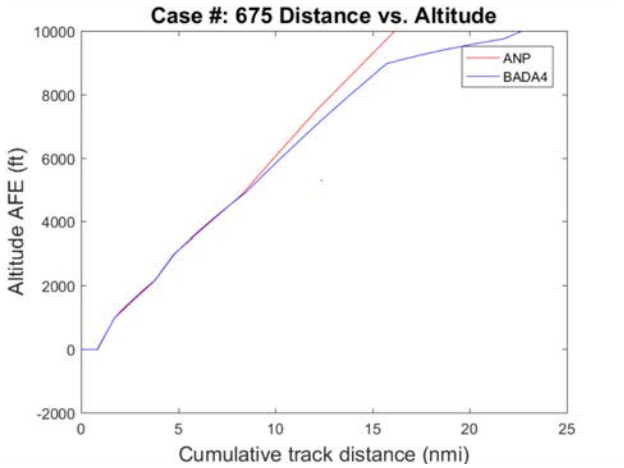


Figure 8. Differences in Trajectory between ANP and BADA4 for High-Elevation Airports

The figure shows that above 5,000 ft AFE, ANP maintains a constant climb rate while BADA4 will accelerate out and cover more distance. Consequently, this will lead to a higher fuel burn for BADA4 compared to that of ANP. For the KDEN outliers, the trajectory difference directly impacted the performance results. As an example, Figure 9 shows the net thrust, speed, and trajectory differences between ANP and BADA4 for the A340-642 during a standard departure at KDEN under average airport weather. At around 5,000 ft AFE, where ANP and BADA4 start to have different trajectories, the BADA4 shows a drastic increase in speed.

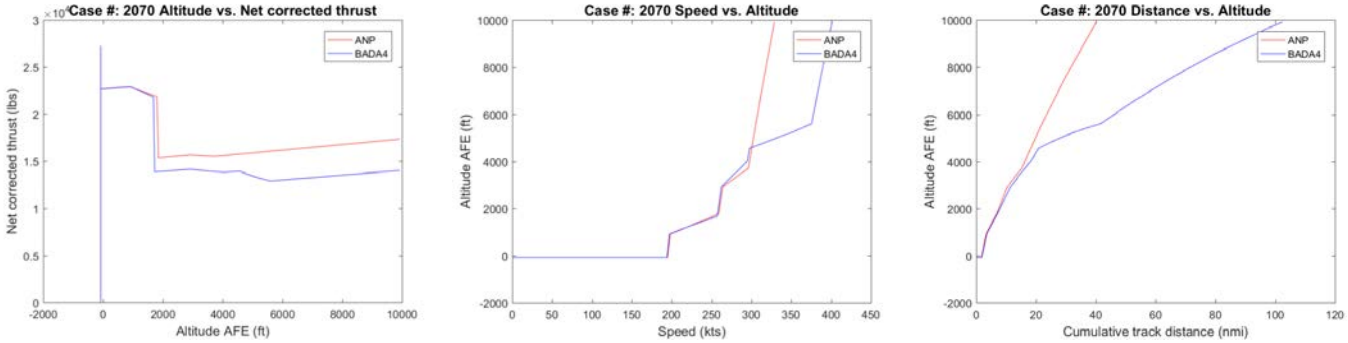


Figure 9. Net Corrected Thrust, Speed, and Trajectory Differences between ANP and BADA4 for the A340-642

Additionally, the subsequent noise contour plots and centerline plots are from the B737-N17 and the MD81 aircraft during departure at KIAH with 15% reduced thrust settings (the MD aircraft and B737-N17 are under further investigation). The contour plots show how the ANP runs generated a noise level of 70dB over a longer X-direction than that of BADA4. The centerline plot also shows the large differences in noise levels for ANP and BADA4, which is why these two aircraft were identified as outliers during the noise outlier study. Since this large noise difference for these aircraft occurred at KIAH (whose elevation is close to sea-level), it was an obvious choice for further investigations.

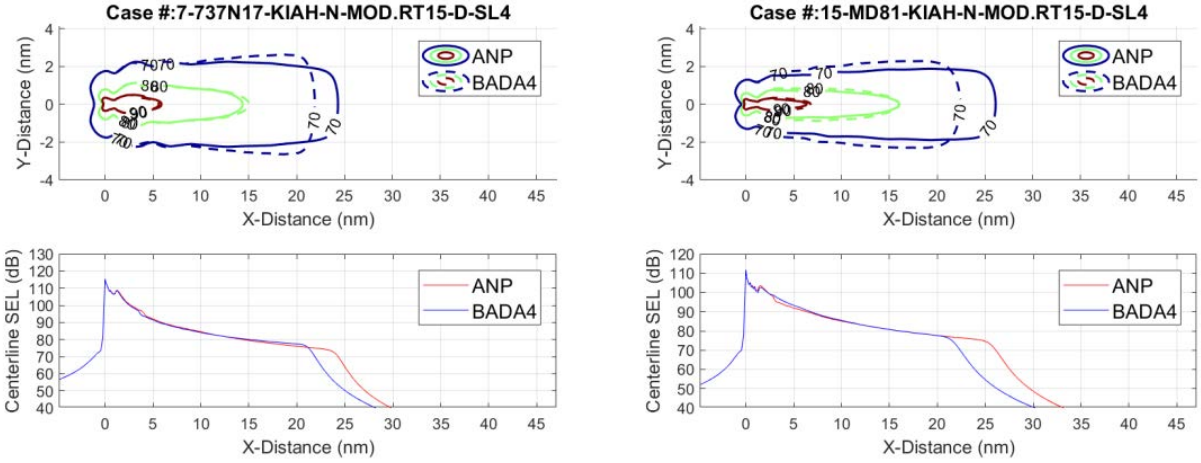


Figure 10. Noise Contour Plot and Centerline Plot of B737-N17 (left) and MD81 during 15% reduced thrust departure at KIAH

For outliers that appeared for airports besides KDEN, specifically the MD aircraft and the B737-N17, further investigation is underway to determine the source of the large differences in emission and noise (except the F10062 and Embraer; these were not pursued).

Task 2-Validation and Verification of BADA4 Implementation

Georgia Institute of Technology

Objective(s)

The FAA has incorporated BADA4 as part of the AEDT Fleet DB. This task focuses on a fleet wide environmental V&V effort to assess the implications of BADA4 from the historical Fleet DB. GT will ensure that the BADA4 algorithm and associated data are properly incorporated into AEDT by performing investigation at flight segment, entire flight, and airport level tests. The BADA4 performance results will be compared to the results using ANP model for terminal area operations. The environmental impacts that are fuel burn, emission, and noise results, using BADA4 will be compared to the results from using ANP.

Research Approach

Performance and Environmental Impact Comparisons between ANP and BADA4

Base of Aircraft Data Family 3 (BADA3) method has been widely used for aircraft performance and fuel consumption modeling in AEDT. Although BADA3 works well in the cruise region, it is known that BADA3 is not optimized for terminal area operations. For this reason, AEDT uses BADA3 for aircraft performance modeling at altitude above 10,000 feet and uses Aircraft Noise and Performance (ANP) method for aircraft performance modeling at altitude below 10,000 feet. In order to address the drawbacks of BADA3 in the terminal area, the high fidelity Base of Aircraft Data Family 4 (BADA4) has been developed. The BADA4 model had only been used for sensor-path flights, which are based on trajectory-driven flight performance. Since the AEDT development team has added procedure-based flight performance using BADA 4, the research team investigated the BADA4 model with a procedure-based performance by comparing with ANP model.

As a system testing plan, the research team considered harmonizing a variety of scenarios with a testing matrix as shown in Figure 11 which consists of two aircraft, three airports, two operation types, two temperature profiles. In this example, the research team compared the performance results generated by BADA4 and ANP models for each case defined in the test matrix.



Figure 11. Testing matrix for BADA4 vs. ANP comparison

Since there were a lot of test cases, in order to avoid repeating work, the Python code was written to automate the generation and visualization of the detailed metric results. The general process includes the following steps: 1) Run AEDT; 2) Parse all results from SQL server; 3) Specify data-frames for both ANP and BADA4; 4) Plot performance comparison between ANP and BADA4 for each case; 5) Plot emission comparison between ANP and BADA4 for each case; 6) Modify the noise data-frame to calculate noise contour area; 7) Calculate ANP and BADA4 noise contour areas; and 8) Plot noise receptors. The algorithm overview is shown in the Figure 12. For a verification and validation purpose, the Python code was validated against AEDT results with respect to noise contour area. For instance, the difference in noise contour area between AEDT and the Python code were only approximately 0.01%.

Using the Python code, the research team was able to generate all comparison plots between ANP and BADA4 within approximately 6 seconds for one case comparison. After running all possible combinations from the testing matrix, the Python code was used to generate all metrics for all test cases. The results for all cases are summarized in the Table 1.

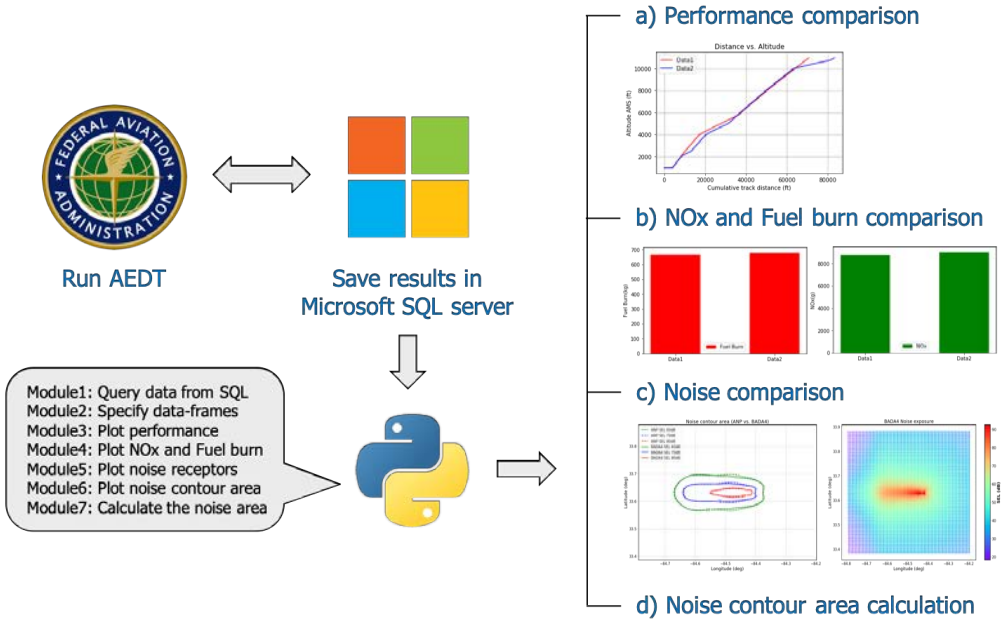


Figure 12. Overview of the Python code for AEDT post-processing

Table 1. Test results for all cases (BADA4 vs. ANP comparison)

Case #	Airport	Temperature	Weather data	Aircraft	Operation	NOx differ. (%)	Fuel Burn differ. (%)	BADA4 is working?
1	KATL	Normal	Airport average	B737-700	Departure	9.19	5.84	Yes
2	KATL	Normal	Airport average	EMB-190LR	Departure	7.25	3.98	Yes
3	KATL	Normal	Airport average	B737-700	Arrival	-16.27	-11.27	Yes
4	KATL	Normal	Airport average	EMB-190LR	Arrival	-2.64	-0.28	Yes
5	KSAN	Normal	Airport average	B737-700	Departure	0.78	1.72	Yes
6	KSAN	Normal	Airport average	EMB-190LR	Departure	-0.4	0.71	Yes
7	KSAN	Normal	Airport average	B737-700	Arrival	0	0	APM Fallback
8	KSAN	Normal	Airport average	EMB-190LR	Arrival	0	0	APM Fallback
9	KDEN	Normal	Airport average	B737-700	Departure	15.89	13.54	Yes
10	KDEN	Normal	Airport average	EMB-190LR	Departure	17.92	8.34	Yes
11	KDEN	Normal	Airport average	B737-700	Arrival	-19.83	-13.67	Yes
12	KDEN	Normal	Airport average	EMB-190LR	Arrival	22.27	12.18	Yes
13	KATL	Hot	Airport average	B737-700	Departure	13.35	8.62	Yes
14	KATL	Hot	Airport average	EMB-190LR	Departure	18.15	11.41	Yes
15	KATL	Hot	Airport average	B737-700	Arrival	-18.51	-11.84	Yes
16	KATL	Hot	Airport average	EMB-190LR	Arrival	8.92	4.63	Yes
17	KSAN	Hot	Airport average	B737-700	Departure	2.89	3.92	Yes
18	KSAN	Hot	Airport average	EMB-190LR	Departure	7.59	7.16	Yes
19	KSAN	Hot	Airport average	B737-700	Arrival	0	0	APM Fallback
20	KSAN	Hot	Airport average	EMB-190LR	Arrival	0	0	APM Fallback
21	KDEN	Hot	Airport average	B737-700	Departure	25.71	24.15	Yes
22	KDEN	Hot	Airport average	EMB-190LR	Departure	42.49	36.86	Yes
23	KDEN	Hot	Airport average	B737-800	Arrival	-22.6	-14.52	Yes
24	KDEN	Hot	Airport average	EMB-190LR	Arrival	51.51	23.91	Yes

As can be seen in the Table 1, some of cases had a small difference between ANP and BADA4 with respect to fuel burn and emission. Figure 13 and Figure 14 also show the performance and noise comparison for such cases with small difference between ANP and BADA4 at San-Diego airport. Although ANP and BADA4 were almost identical for most of the test cases, it was found that some of the cases produced a big difference in emission and fuel burn results. The research team conducted an airport elevation test for ANP and BADA4 performance comparison using the same aircraft, operation,

temperature, and weather. As a result, it was observed that there is a big difference between ANP and BADA4 performance at high elevation airport as shown in the Figure 15. The research team investigated the reason that leads to the huge difference at high elevation airport; and concluded that the difference was due to MSL/AFE based procedure used by BADA4 and ANP BADA4 model respectively. To be more specific, at low elevation airport such as San-Diego, the performance profiles between ANP and BADA4 are very close; however, at high elevation airport such as Denver (field elevation 5,434ft), the performance results produced by ANP and BADA4 are very different. This is because BADA4 model calculates the performance based on Mean Sea-Level; whereas, ANP model is based on Above Field Elevation. Since the Denver airport has 5,434ft elevation, the performance calculation would be quite different between them. As discussed earlier, since BADA4 follows the 250kt/10000ft MSL FAR rule, its results are closer to the real aircraft operation and more accurate than ANP. In addition, the research team also investigated the other outlier cases such as the B737-700 arrival case with normal temperature at KATL airport. The results show that both fuel burn and emissions produced by ANP and BADA4 were different which is again due to the fact that they use different profile resulting different trajectory and thrust results. The results are shown in Figure 16.

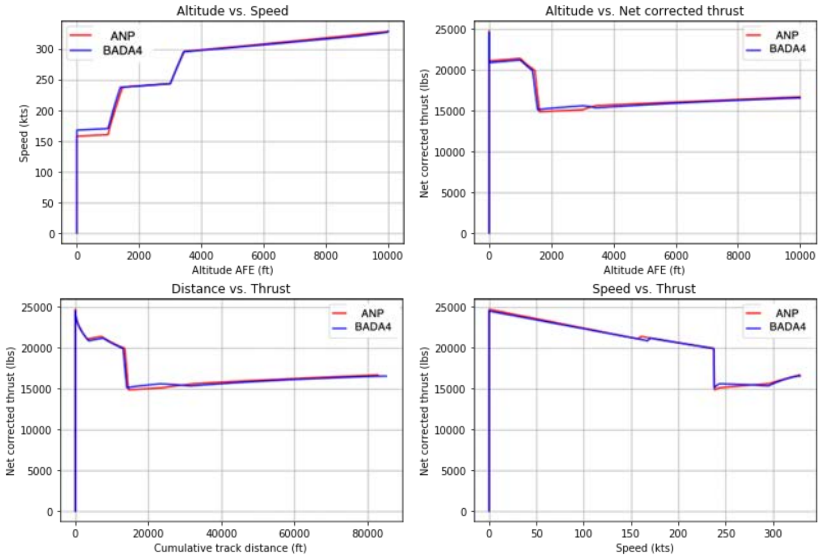


Figure 13. Performance comparison between ANP and BADA4

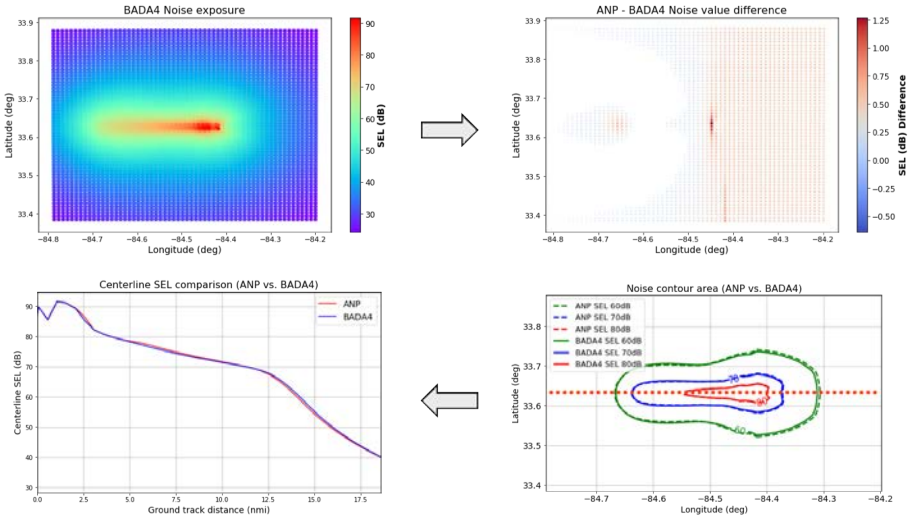


Figure 14. Noise contour and Centerline SEL comparison between ANP and BADA4

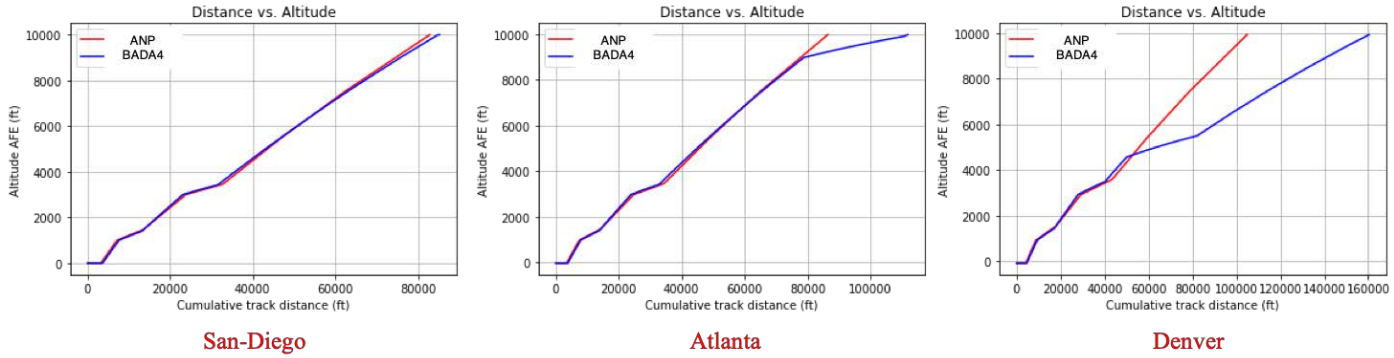


Figure 15. ANP vs. BADA4 comparison by airport with different elevations

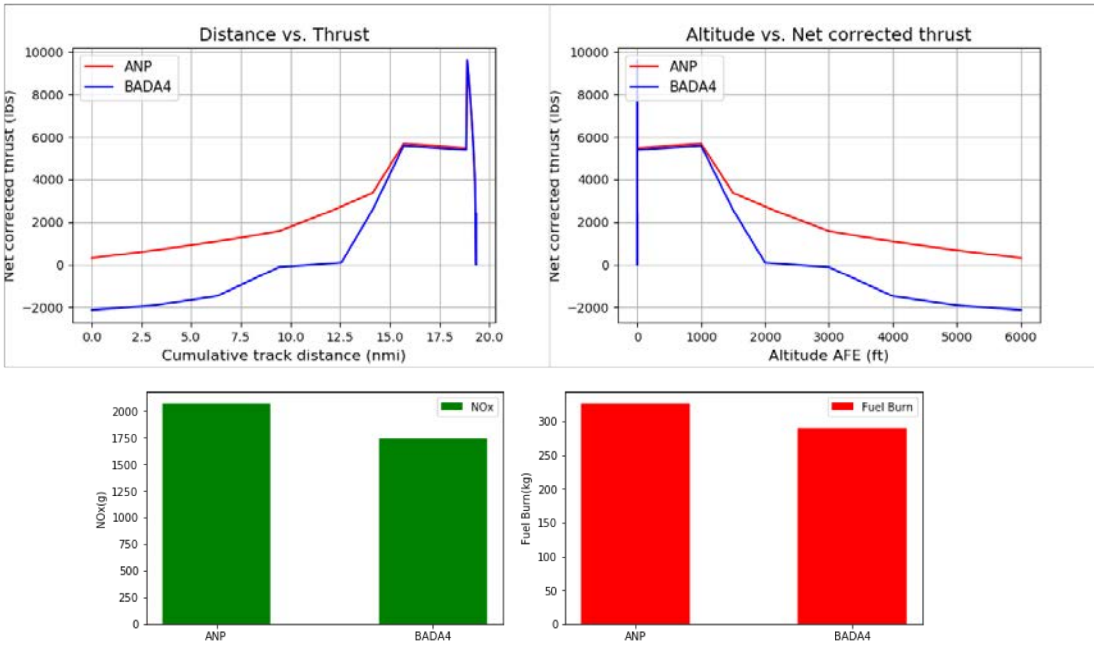


Figure 16. ANP vs. BADA4 comparison for the outlier arrival case at ATL

Task 3- Capability Demonstration and Validation of AEDT 2d and 2e Functionality

Georgia Institute of Technology

Objective(s)

For AEDT 2d and 2e, the scope of the UQ effort identifying the key changes to the AEDT versions from the previous releases was formulated. Depending on the type of updates incorporated, it would be necessary to identify the key sources of uncertainties and the best approach to conduct V&V and parametric uncertainty analysis. Depending on the analysis scope of the V&V, Parametric UQ can be optional. The outcome of this task is the definition of analysis scope, required tools, required data, V&V method, Parametric UQ method, and a list of input parameters to vary and their uncertainty bounds. Due to the dynamic nature of the agile AEDT development process, it is important that the research team remains



flexible in the choice of the V&V approach and the work scope. The best available methods and data will be used in order to ensure accuracy and functionalities of future AEDT versions based on the discussion with the FAA/AEE.

A V&V and capability demonstration was conducted of the newly released AEDT versions. The analysis in this task can take a couple of different approaches depending on the type of updates and data availability. In the past UQ efforts, one of the most important methods of ensuring confidence in the tool capability was to conduct a use case(s) using both legacy tools and the new AEDT release and compare the results. This method would be the most appropriate way whenever a legacy tool has the same or similar functionalities and a validated use case has been modeled in that legacy tool. When the new functionality of AEDT does not exist in the legacy tools, the V&V exercise should use direct comparisons to the results generated by the mathematical algorithms behind the newly added functionality and/or real world data whichever available.

Research Approach

In order to provide the best possible environmental impacts modeling capabilities, the FAA/AEE continues to develop AEDT by improving existing modeling methods and data and adding new functionalities. The AEDT development team led by Volpe has been exercising the agile development process, as shown in Figure 17, where minor updates are released in a new Sprint version every three weeks. Major updates and/or new functionalities are incorporated as new service packs or feature packs in about a three months cycles as shown in Figure 17. An AEDT development cycle includes rigorous testing of all levels of software functionality from the individual modules to the overall system. However, the FAA/AEE seeks a robust uncertainty quantification effort in addition to this test program.

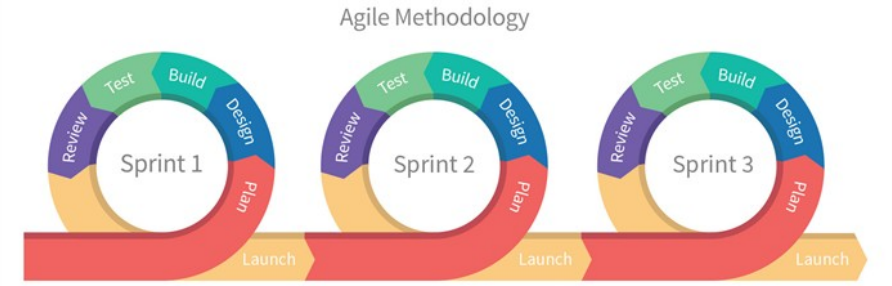


Figure 17. The Agile Methodology [Source: http://www.screenmedia.co.uk]

Table 2: AEDT Development and Public Release Schedule

Dates	Milestones
Sep. 2017	AEDT 2d Release
Dec. 2018	AEDT 3a Release

For each of the AEDT version and service pack releases, GT reviewed the AEDT requirement documents and AEDT release notes to identify the key features and functionalities that need to be tested. During the period of December 2017 to October 2018, two public version of AEDT were released – including AEDT 2d SP1, and AEDT 2e, as listed in Table 2.

The main features/capabilities that were added to AEDT during the period include the following:

- BADA4 Features
  - BADA4 implementation of procedural departures and arrivals
  - Encryption of BADA 4 data
  - BADA4 with reduced thrust and alternative weight departure procedures
  - BADA4 implementation for sensor-path



    - Climb thrust taper
- Emissions Analysis Features
    - Enhanced nvPM methods for CAEP nvPM Standard
    - Roadway network designer in AEDT GUI
    - Emission concentration display for non-closing contours
- Noise Analysis Features
    - Dynamic grid for non-dB metrics
    - Bulk creation of operations
    - Detailed noise results report
- Other Features
    - Non-closing contours
    - Fixed terminal area wind directions

The V&V and capability demonstration of the new features listed above are either completed or in progress. Starting from December 2017, all the new AEDT sprint releases including Sprints from 95 to 111 have been tested. Seventeen sprint releases of AEDT focusing on new features and capabilities added have also been tested. Some of the new features/capabilities were minor updates to the GUI, bug fixes or data updates. Major updates included BADA4 implementation of procedural departures and arrivals, BADA4 with reduced thrust and alternative weight departure procedures, enhanced nvPM, Idle descent, climb thrust tamper, NOx calculation.

In order to understand the background of new AEDT features, the relevant documents were reviewed including the software requirement documents, Database Design Documents (DDD), AEDT sprint release notes, updated technical manual [5, 6], user manual [7, 8], and research papers/reports [9-12]. Basic testing of all the new AEDT versions to confirm its functionality have been performed. While some of the tests are in progress, the next subsections discuss the current progress and findings in more details.

Investigation of Idle Descent

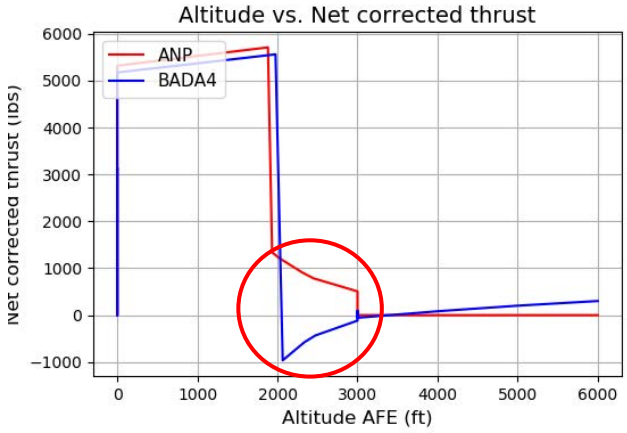
The purpose of this investigation is to determine the cause of large net thrust differences in ANP and BADA4 during approach procedures. AEDT may utilize different descent types during the approach procedure. Table 3 shows the different types of descent as well as their corresponding thrust equations for ANP.

Table 3. ANP Thrust Equations for Different Types of Descent

Step Type	Given	Calculate	Thrust Equation	Note
Descend	Initial and final speed and altitude Descent angle	thrust and horizontal distance	$\left(\frac{F_n}{\delta}\right)_2 = \frac{\left(\frac{W}{\delta_2}\right)\cdot\left(R_f - \frac{\sin\gamma}{1.03}\right)}{N}$	Neglect deceleration effects
Descend-decel	Initial and final speed and altitude Descent angle	thrust and horizontal distance	$\frac{F_n}{\delta} = \frac{W}{N\cdot\delta}\left(R\cdot\cos\gamma - \sin\gamma + \frac{a}{g}\right)$	SAE-AIR-1845 equation A15 with an additional acceleration term
Descend-idle	Initial and final speed and altitude Descent angle	horizontal distance Idle thrust is a rated thrust specification	$\frac{F_n}{\delta} = E + F\cdot v + G_A\cdot h + G_B\cdot h^2 + H\cdot T_C$	Preserves the acceleration value implied by its inputs

One of the reasons for net thrust differences to occur between ANP and BADA4 is because some ANP approach cases use step types that do not take deceleration into account (this is the case when “descend” is utilized for ANP) while BADA4 does take deceleration into account. Therefore, BADA4 would result in a more accurate representation of the approach procedure compared to that of ANP.

Besides the cases with deceleration affecting the net thrust differences between ANP and BADA4, large net thrust differences primarily occurred during the idle-descent segments of approach.



Step Number	Step Type	Altitude AFE (ft)
1	Idle Thrust Descend	6000
2	Idle Thrust Level	3000
3	Idle Thrust Level	3000
4	Idle Thrust Descend	3000
5	Idle Thrust Descend	2471
6	Idle Thrust Descend	2336
7	Idle Thrust Descend	2066
8	Descend	1976
9	Descend	50
10	Land	
11	Landing Decelerate	
12	Landing Decelerate	

Figure 18. Image Showing Region of Largest Net Thrust Difference Between ANP and BADA4 is During Idle-descent

Figure 18 shows the standard approach procedure for A340-642 at KATL under average airport weather conditions. Between 2,000 ft AFE and 3,000 ft AFE, the net thrust difference between ANP and BADA4 is largest as shown on the left image. The corresponding region is shown to be where the aircraft is flying under "idle thrust descend" conditions (shown on right). Further investigations into how ANP and BADA4 calculated net thrust during idle descent was conducted. It was found that both ANP utilized regression coefficients that depended on engine power states given by Equation (1).

$$\frac{F_n}{\delta} = E + Fv + G_A h + G_B h^2 + HT_c \tag{1}$$

Where

$\frac{F_n}{\delta}$ is corrected net thrust per engine (lbf)
v is the equivalent/calibrated airspeed (kt)
h is the pressure altitude MSL (ft)
T_c is the temperature at altitude (°C)
E, F, G_A, G_B, H are the regression coefficients that depend on the engine power states and temperature state

Furthermore, the BADA4 idle thrust is calculated using a thrust coefficient.

$$Th = \delta W_{mref} C_T \tag{2}$$

$$C_T = ti_1\delta^{-1} + ti_2 + ti_3\delta + ti_4\delta^2 + (ti_5\delta^{-1} + ti_6 + ti_7\delta + ti_8\delta^2)\cdot M + (ti_9\delta^{-1} + ti_{10} + ti_{11}\delta + ti_{12}\delta^2)\cdot M^2 \tag{3}$$

Where

δ is the pressure ratio
m_{ref} is the reference mass (kg)
W_{mref} is the weight force at m_{ref} (N)
C_T is the thrust coefficient
M is the Mach number
ti_1 to ti_{12} are the idle rating thrust coefficients

The ANP and BADA4 idle thrusts were plotted against a variation of Mach number and altitude to visualize the thrust curves of both models, as shown in Figure 19. It was found that the ANP thrust curve closely resembled a typical thrust curve; however, the BADA4 thrust curves showed erratic behavior.

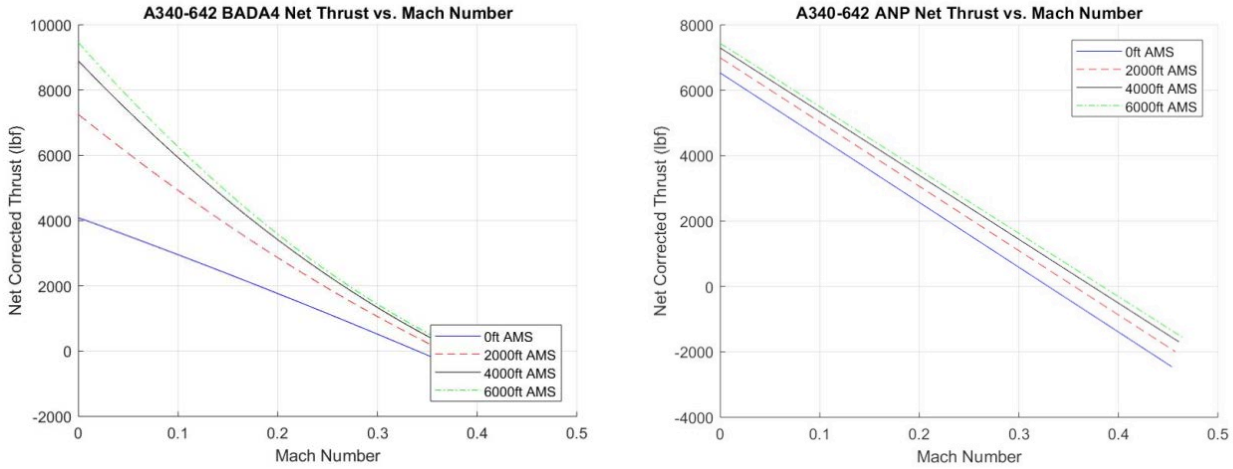
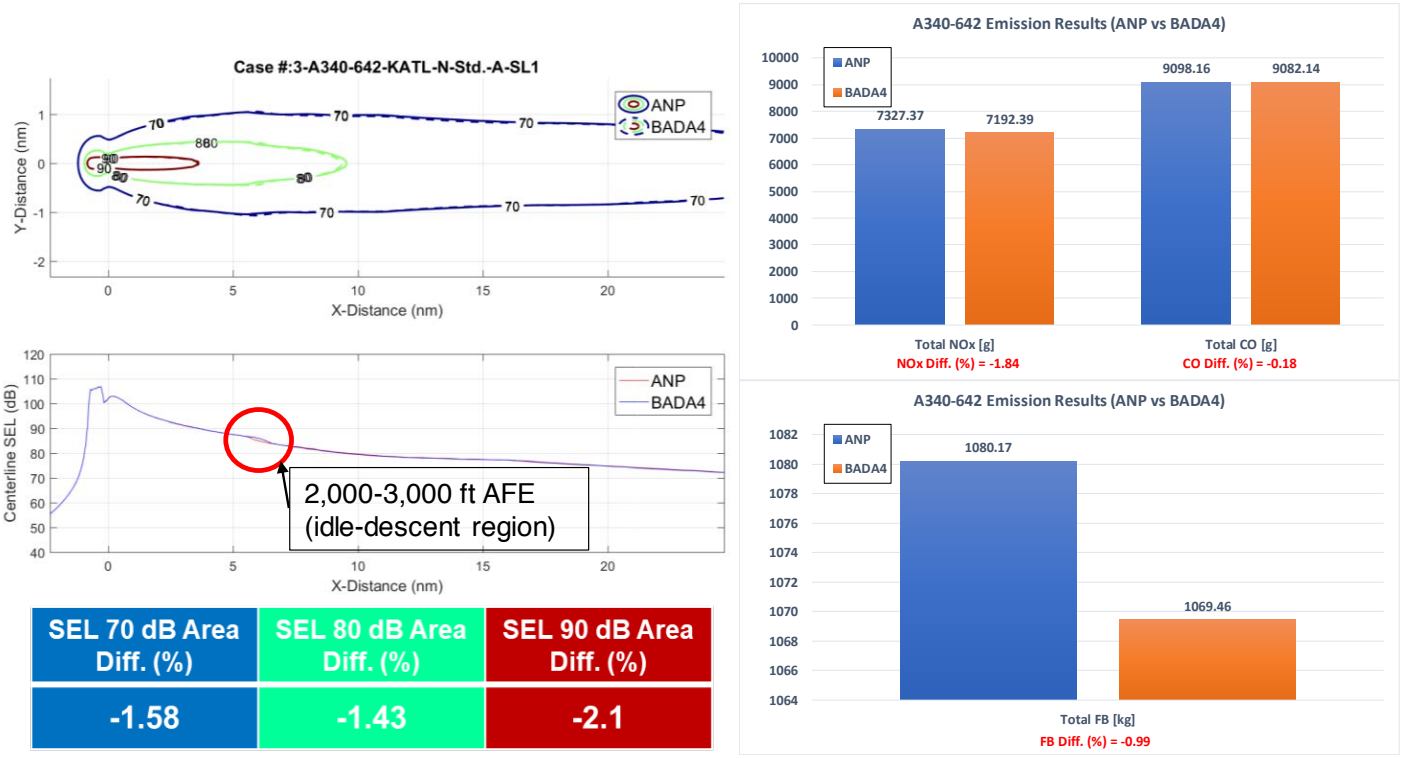


Figure 19. Image of ANP and BADA4 Thrust Curves for a Variety of Altitudes

The ANP thrust curve shows a gradual shift to the right as the altitude is increased with a reduction in net thrust as the Mach number is increased. The ANP thrust curve also shows the linear relationship between net thrust and Mach number, unlike BADA4. The BADA4 model shows a congruent behavior to that of ANP when increasing altitude and Mach number. However, it clearly shows that the net thrust, and Mach number do not necessarily behave linearly with each other.

Despite the large difference in thrust curves, ANP and BADA4 do not show a proportional difference for noise and emissions results. The following tables and figures show the noise contour, centerline plots, and emission results for the particular case above mentioned.



SEL 70 dB Area Diff. (%)	SEL 80 dB Area Diff. (%)	SEL 90 dB Area Diff. (%)
-1.58	-1.43	-2.1

Figure 20. Images of Noise Contours, Centerline Plots, and Emission Results for the A340-642 during KATL Approach

Figure 20 shows that despite the large differences in net thrust during idle-descent segments, the difference is not propagated to noise and emission results. The largest noise contour area difference is only around 2% with the slight difference in centerline plot depicting the idle-descent segment (circled in red). The largest emission difference is from NOx emission, which comes to around -1.84%. This concludes the investigation with the notion that ANP and BADA4 idle thrust curves may have relatively different thrust curves. But the utilization of the thrust curves in the correct regions of Mach number and altitude have allowed the models to reflect similar noise and emission results between ANP and BADA4.

NOx Calculation

Through the idle-descent investigation, it was discovered that the NOx differences between ANP and BADA4 were relatively large compared to other emission results. Additionally, from the routine analysis at conducted to test all combinations of stage lengths and profiles using KIAH airport, it was found that there are several outliers for NOx calculations as shown in Figure 21. As can be seen in the figure, the Boeing 737 Max 8 aircraft was a prominent outlier for the reduced thrust cases. This aircraft was selected for further investigation into NOx calculations.

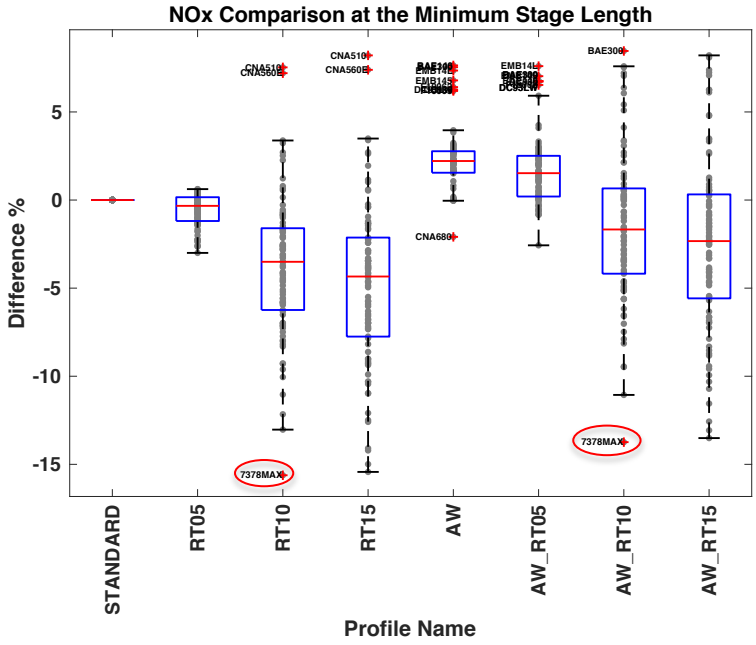


Figure 21. Outlier analysis for NOx calculations

A preliminary analysis revealed that the trend of reduction in NOx emissions is dependent only on whether reduced thrust was implemented. However, this reduction of NOx itself is not consistent with the change in fuel burn. As can be seen in Figure 22, for reduced thrust profiles, the fuel consumption increases by about 4 to 8% however, the NOx emissions decrease by about 12 to 15%. This anomaly is observed across all stage lengths and does not seem to be affected by the added weight profiles. Further, the amount of thrust reduction itself does not seem to affect the trend, rather it is driven by whether thrust reduction was applied or not. This preliminary analysis motivates the need to compare reduced thrust profiles to the others on a more detailed level.

7378MAX	Fuel/NOx Difference 5%													
Profile	SL 1		SL2		SL 3		SL 4		SL 5		SL 6		SL 7	
Fuel/NOx	Fuel	NOx	Fuel	NOx	Fuel	NOx	Fuel	NOx	Fuel	NOx	Fuel	NOx	Fuel	NOx
STANDARD	0	0	0	0	0	0	0	0	0	0	0	0	0	0
MODIFIED_RT05	0:34	0:55	0:37	0:58	0:37	0:61	0:42	0:67	0:51	0:8	0:54	0:84	0:61	0:91
MODIFIED_RT10	4:15	-15.6	4:46	-15.4	4:78	-15	5:56	-14.6	6:68	-13.8	7:02	-13.6	7:76	-13
MODIFIED_RT15	4:63	-15	4:98	-14.7	5:35	-14.3	6:21	-13.7	7:48	-12.7	7:86	-12.4	8:69	-11.7
MODIFIED_AW	1:65	2:27	1:8	2:43	3:48	4:66	4:37	5:68	1:15	1:48	2:46	3:11	0	0:02
MODIFIED_AW_RT05	2	2:81	2:17	3:01	3:9	5:31	4:85	6:42	1:69	2:29	3:05	3:97	0:61	0:91
MODIFIED_AW_RT10	6:01	-13.7	6:51	-13.3	8:84	-11.1	10:8	-9:66	8:1	-12.5	10:1	-10.8	7:76	-13
MODIFIED_AW_RT15	6:51	-13.1	7:05	-12.6	9:45	-10.2	11:5	-8:65	8:91	-11.4	10:9	-9:54	8:69	-11.7

Figure 22. Comparison of NOx emissions and fuel burn across stage lengths

For detailed analysis, the performance and emissions tables from AEDT were analyzed. These tables break down the entire operation into segments (about 30, in this case). A typical performance table is shown in Figure 23. The segments for the RT05, RT10 and RT15 profiles were compared to the corresponding segments of the STANDARD profiles. In particular the percent change of segment fuel burn was compared to the percent change of segment NOx emission. It was observed that



these match exactly, all the way up to segment 21, which approximately corresponded to about 1500 ft altitude. Beyond this segment, there was a high deviation in these two percentages. Further, this deviation was only observed for RT10 and RT15 profiles; the RT profile segment percent comparisons continued to be in agreement until the top of climb. These two observations seem to point towards the reduction in climb thrust as being the root cause of the problem.

	A	B	C	D	E	F	G	H	I	J	K	L	M	N	O
1	RESULT_ID	AIR_OP_ID	SEGMENT_	TRACK_LE	CUM_TRA	THRUST_C	SPEED_CH	FUELFLOW	FUELBURN	DURATION	LENGTH	OP_MODE	TRAJ_MOI	MACH_NU	TIME
2	15379	451	0	0	0	0	0	0.095	247.57	21:43.0	0	100000	0	0	00:00.0
3	15380	451	1	25	0	-42.2758	12.46514	1.307171	7.149963	00:02.7	25	1	1	0.009886	00:00.0
4	15381	451	2	75	25	-42.2758	12.46514	1.306757	7.147696	00:02.7	75	1	1	0.01212	00:02.7
5	15382	451	3	262.6527	100	-708.449	22.54556	1.293085	12.79269	00:04.9	262.6527	1	1	0.019663	00:05.5
6	15383	451	4	426.2204	362.6527	-708.449	22.54556	1.267669	12.54126	00:04.9	426.2204	1	1	0.035052	00:10.4
7	15384	451	5	589.788	788.873	-708.449	22.54556	1.247002	12.33679	00:04.9	589.788	1	1	0.057749	00:15.4
8	15385	451	6	753.3557	1378.661	-708.449	22.54556	1.230582	12.17435	00:04.9	753.3557	1	1	0.087754	00:20.3
9	15386	451	7	916.9234	2132.017	-708.449	22.54556	1.217911	12.04899	00:04.9	916.9234	1	1	0.125067	00:25.3
10	15387	451	8	1080.491	3048.94	-708.449	22.54556	1.208489	11.95577	00:04.9	1080.491	1	1	0.169688	00:30.2
11	15388	451	9	1244.059	4129.431	-708.449	22.54556	1.201816	11.88976	00:04.9	1244.059	1	1	0.221617	00:35.1
12	15389	451	10	384.2789	5373.49	4.264154	0.159766	1.197739	3.469769	00:01.4	388.4053	1	2	0.249537	00:40.1
13	15390	451	11	458.6554	5757.769	5.084603	0.190506	1.195485	4.129589	00:01.7	463.5806	1	2	0.249819	00:41.5
14	15391	451	12	545.4281	6216.424	6.039678	0.22629	1.192804	4.894276	00:02.1	551.285	1	2	0.250155	00:43.3
15	15392	451	13	687.9832	6761.853	7.607614	0.285036	1.189516	6.147866	00:02.6	695.3708	1	2	0.250567	00:45.3
16	15393	451	14	923.5089	7449.836	10.19349	0.381922	1.185229	8.20788	00:03.5	933.4257	1	2	0.251107	00:47.9
17	15394	451	15	1369.768	8373.345	15.08036	0.56502	1.179146	12.0805	00:05.1	1384.477	1	2	0.251876	00:51.4
18	15395	451	16	2435.832	9743.113	26.70368	1.000514	1.169095	21.20932	00:09.1	2461.989	1	2	0.253154	00:56.5
19	15396	451	17	1711.343	12178.95	-299.566	11.98027	1.156926	14.11255	00:06.1	1713.483	1	2	0.261669	01:05.6
20	15397	451	18	1818.378	13890.29	-299.566	11.98027	1.145401	13.97196	00:06.1	1820.652	1	2	0.27755	01:11.7
21	15398	451	19	2734.614	15708.67	-432.069	17.52626	1.130631	19.34117	00:08.6	2738.3	1	2	0.29692	01:17.8
22	15399	451	20	2954.181	18443.28	-432.069	17.52626	1.112569	19.03219	00:08.6	2958.163	1	2	0.320208	01:26.3
23	15400	451	21	1000	21397.46	-2504.3	0.373956	1.027496	5.753085	00:02.8	1004.985	1	3	0.332616	01:34.9

Figure 23: Sample AEDT metric result performance table, partially shown

Additionally, several plots were made to visualize these differences. Through several iteration of plots, it was concluded that time based plots seemed to be the best suited for these visualizations. Most notably, the segment level data allowed the calculation of the emissions index (EI) that AEDT was using to calculate the NOx emissions. Such a plot is shown in Figure 24. It is clearly seen that there is a large difference between the emissions indices for the RT10 and RT15 profiles when compared to the STANDARD or RT05 profile.

It was eventually deemed necessary to try to replicate the NOx calculations as done by AEDT. AEDT utilizes the Boeing Fuel Flow Method 2 (BFFM2) for calculating the NOx emission and a further investigation was conducted to verify that AEDT was correctly implementing the BFFM2 in its NOx calculations. In order to do so, an independent tool was created that could replicate the NOx results generated by AEDT. The tool would follow the steps of the BFFM2 while utilizing parameters generated in AEDT (i.e. temperature, pressure, Mach number, etc.).

After several iterations of the independent BFFM2 tool, the results from the tool matched with AEDT to an error of about 0.1 %. It was concluded that AEDT has a correct implementation of the method, albeit with a few ambiguities and an inconsequential deviation from the BFFM2 recommendations. These are explained in detail towards the end of this section.

The design of the independent tool helped better understand AEDT's implementation which was not always evident from the Technical Manual. With this new knowledge, the presence of the Boeing 737 Max 8 aircraft as an outlier in Figure 21 could finally be explained. As we know from Figure 24, the EI difference results from a change in the climb thrust. We know this because RT10 and RT05 profiles implement a derated climb thrust, whereas STANDARD and RT05 profiles use full climb thrust. In order to relate this 10% reduction in climb thrust to the ~30% reduction in NOx EI, a segment level comparison was performed. The comparisons were made for the final segment in the performance table and key metrics at different steps of

the BFFM2 were compared. A summary of the comparisons is provided in Table 4. This table along with Figure 25 explains the large change in NOx EI that results from the reduction in climb thrust.

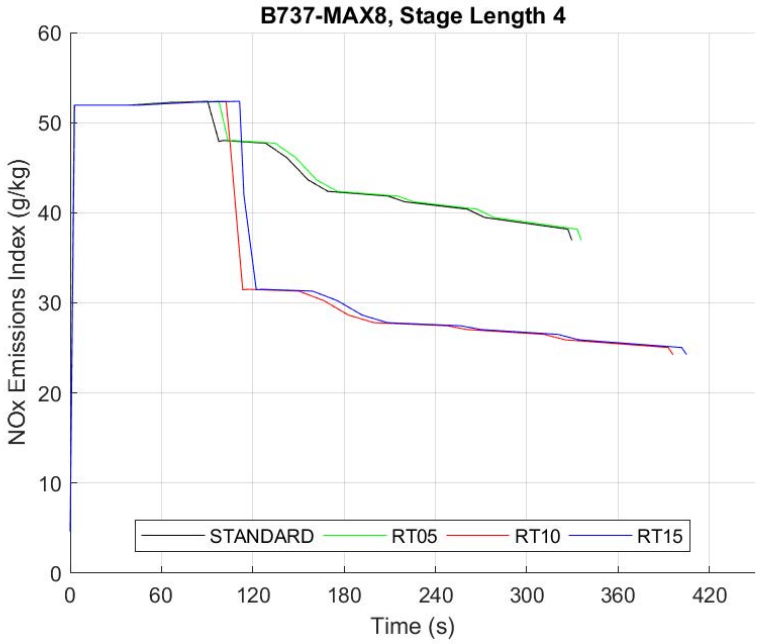


Figure 24. Emissions Indices comparison

Table 4. Key comparisons of BFFM2 steps, final segment, B737Max8, RT05 v/s RT10

Final segment performance metrics	Full Climb Thrust	Derated Climb Thrust	Difference (%)
Thrust	17561 lbs	15829 lbs	-9.86 %
Non-Reference Fuel Flow	0.800 kg/s	0.720 kg/s	-10.00 %
Reference Fuel Flow	0.9247	0.8322	-10.00 %
Log Reference NOx EI	1.5707	1.3877	-11.65 %
Reference NOx EI	37.22 g/kg	24.42 g/kg	-34.39 %
Non-Reference NOx EI	36.97 g/kg	24.26 g/kg	-34.27 %

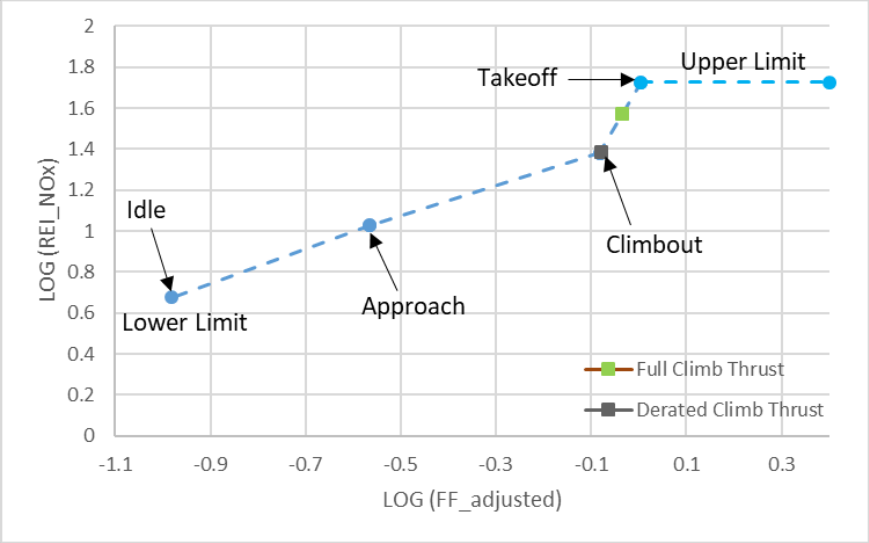


Figure 25. Reference NOx EI calculation, B737Max8

First, the thrust values are compared and is found to be around 10% as is expected. Note that the reduction is not exactly 10% as the aircraft flying these two profiles have different trajectories. The thrust, which depends on both speed and altitude is therefore not reduced by exactly 10%. Next, fuel flow values are compared. Non-reference values are the values provided by the AEDT performance calculations. Reference values are obtained from these using conversion formulas, these are explained in detail in the subsequent paragraphs. The BFFM2 method uses reference values to calculate the EIs. Both the fuel flows are also different by 10%. Next, from the Reference Emissions Index is found as shown in Figure 25. This figure gives us the logarithm (base 10) of the Reference EI. Finally, when this value is converted to the actual value, and the Reference EI to the non-Reference EI, the large difference of ~34% appears. By doing this step by step analysis, the exact step of the difference was isolated.

From the observation of the reference NOx EI values, it is seen that the change from the Takeoff point to the Climbout point is rather steep (noting that the axes are not of the same scale). Further, these differences are on a logarithmic scale, and the difference is amplified when the anti-log is taken. Thus, was concluded that the Boeing 737 Max 8 being an outlier for the reduced climb thrust profiles is a result of aircraft's reference Emissions Indices and not due to an incorrect implementation of the Boeing Fuel Flow Method 2 in AEDT.

The subsequent steps outline the BFFM2:
- Step 1: Using the four ICAO reference fuel flows provided in SQL (specific for each engine), multiply them by a modal-specific adjustment factor to account for installation effects. These modes reflect the four types of engine power settings.

Table 5:.Adjustment Factors for Installation Effects

Mode	Power Setting (%)	Adjustment Factor
Takeoff	100	1.010
Climbout	85	1.013
Approach	30	1.020
Idle	7	1.100

- Step 2: Using the adjusted fuel flows from step 1 and the reference emission index (REI) values from the FLEET database (there is one REI value for each mode and emission parameter), develop a log-log relationship between the REI and fuel flow values. An example of this point-to-point relationship is found in Figure 26.

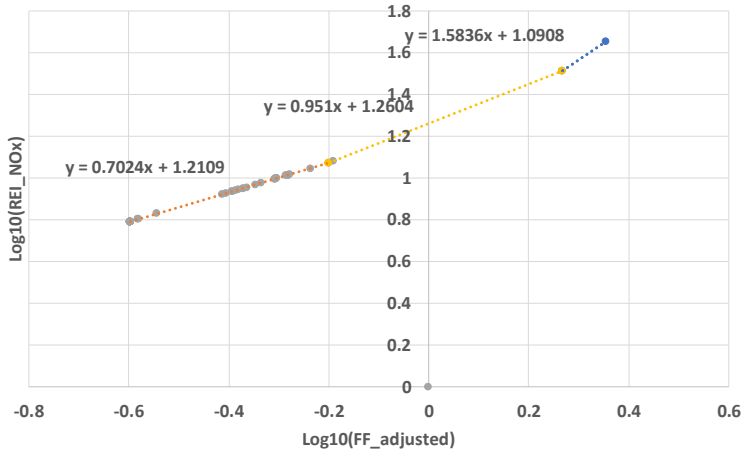


Figure 26. Example of a Log-Log Relationship between the REI Values and the Adjusted Fuel Flows

- Step 3: Obtain the non-reference fuel flow values calculated from AEDT case runs. These results can be found in the SQL database under dbo.RSLT_EMISSIONS_RESULTS after a case has been run.

- Step 4: Convert non-reference fuel flow from step 3 to reference conditions, to take into account the influence of fuel flow for different altitudes, using the following equation.

$$RWf = \frac{Wf}{\delta}\theta^{3.8}e^{0.2M^2} \tag{4}$$

Where
RWf is the fuel flow at reference conditions (kg/s)
Wf is the fuel flow at non-reference conditions (kg/s)
δ is the pressure ratio
θ is the temperature ratio
M is the Mach number

- Step 5: Using the reference fuel flow from step 4, find the corresponding REI values using the log-log plot from step 2. The corresponding REI values may not be outside the scope of the provided REI range (from idle REI to takeoff REI).

- Step 6: Convert the reference REI values to non-reference conditions using the following equation.

$$NO_xEI = NO_xREIe^{H}\left[\frac{\delta^{1.02}}{\theta^{3.3}}\right]^{0.5} \tag{5}$$

$$H = -19[\frac{0.62197058\phi P_v}{P-\phi P_v} - (6.34 * 10^{-3})] \tag{6}$$

Where
NO_xEI at non-reference conditions (g/kg)
NO_xREI at reference conditions (g/kg)
H is the humidity coefficient
ϕ is the relative humidity
P is the ambient pressure (psi)
P_v is the saturation vapor pressure (psi)
δ is the pressure ratio
θ is the temperature ratio
M is the Mach number



- Step 7: Lastly, multiply the obtained NO_xEI values from step 6 by the corresponding fuel burn (generated by AEDT) to get the NOx emission results for each segment. Combining all the segments would provide the total NOx emission.

Using the outlined BFFM2 process, a tool was created to replicate the NOx results obtained from AEDT, which was designed from the knowledge obtained from the AEDT manual and the AEDT source code. A tool that could successfully replicate the NOx results from AEDT could help verify that AEDT was implementing the BFFM2 correctly in calculating NOx emissions, as shown in Figure 27. Albeit some minor setbacks along the way, where the AEDT manual failed to explicitly define certain terms in its BFFM2 process and had to be resolved through analyzing the AEDT source code, the replication tool was completed. The image below shows the NOx results generated by AEDT compared to the NOx results obtained from the replication tool. The 0.01 difference found in the BADA4 results between AEDT and the tool is from the difference in significant figures during calculations.

	AEDT Gen. Nox Values	Replicated Nox BFFM2
ANP	7327.37	7327.37
BADA4	7192.39	7192.38
Diff. (%)	-1.84	-1.84

Figure 27. NOx Result Comparisons between the AEDT Generated Results and the Replication Tool Results

After successfully replicating the NOx results from AEDT, some ambiguous terms defined in the AEDT manual for the BFFM2 process were clarified. For example, the temperature ratios and pressure ratios used in AEDT's BFFM2 process were not defined as ratios under static conditions, which is the condition required for the BFFM2 process. To avoid future confusion, these terms were reported and will be updated in the manual for the upcoming AEDT 3a release.

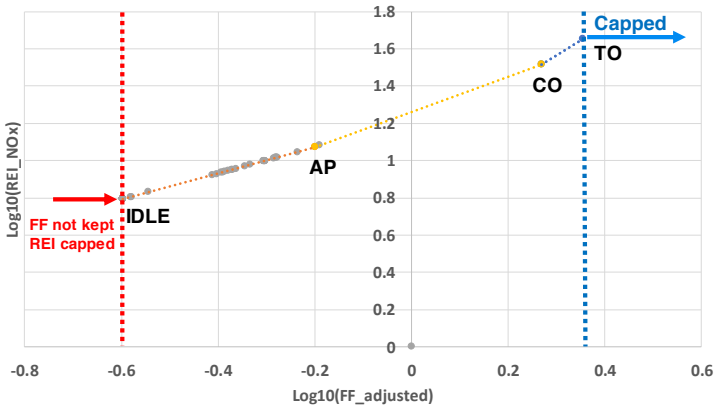


Figure 28. AEDT's bounds for the Log-Log relationship between REI and Fuel Flow

Other concerns were raised when it was discovered that the AEDT BFFM2 replaced reference fuel flow values that were found to be below the idle reference fuel flow value (depicted in Figure 28). It would set the reference fuel flow values equal to the idle reference fuel flow value while the emission index values would also be capped to the emission index value of idle. This could lead to loss of information and accuracy during approach and idle flight conditions. Further investigations are underway to resolve these events. For fuel flow values exceeding that of takeoff, the emission index would be capped to the emission index value of takeoff with the fuel flow values retained.

Thrust Taper

The purpose of this study is to evaluate the new capability of thrust taper, which was introduced in AEDT 3a, for BADA4 operations. The capability could only be utilized for cases with reduced thrust departure settings. This option would allow the engine to gradually change the thrust (starting from 10,000 ft Above Mean Sea Level (AMS)) from the reduced thrust setting to the full-power BADA4 climb setting at a user-defined taper upper limit (default set to 12,000 ft AMS). Hence, the rate at which the aircraft would transition from the reduced thrust setting to the full-power setting during departure could be varied.

The thrust during the reduced thrust to full-power transition is given as

$$k_{taper} = \begin{cases} 0, & h < H_1 \\ \frac{h - H_1}{H_2 - H_1}, & H_1 \leq h \leq H_2 \\ 1, & h > H_2 \end{cases} \quad (7)$$

$$F_{flat,taper} = [k_{reduced} + (1 - k_{reduced}) \cdot k_{taper}] \cdot F_{flat} \quad (8)$$

Where

k_{taper} is the taper coefficient
h is the current altitude (AMS)
H_1 is the transition starting altitude (10,000 ft AMS)
H_2 is the upper taper limit altitude (user-defined)
$F_{flat,taper}$ is the thrust during transition
$k_{reduced}$ is the reduced thrust coefficient
F_{flat} is the thrust at full power

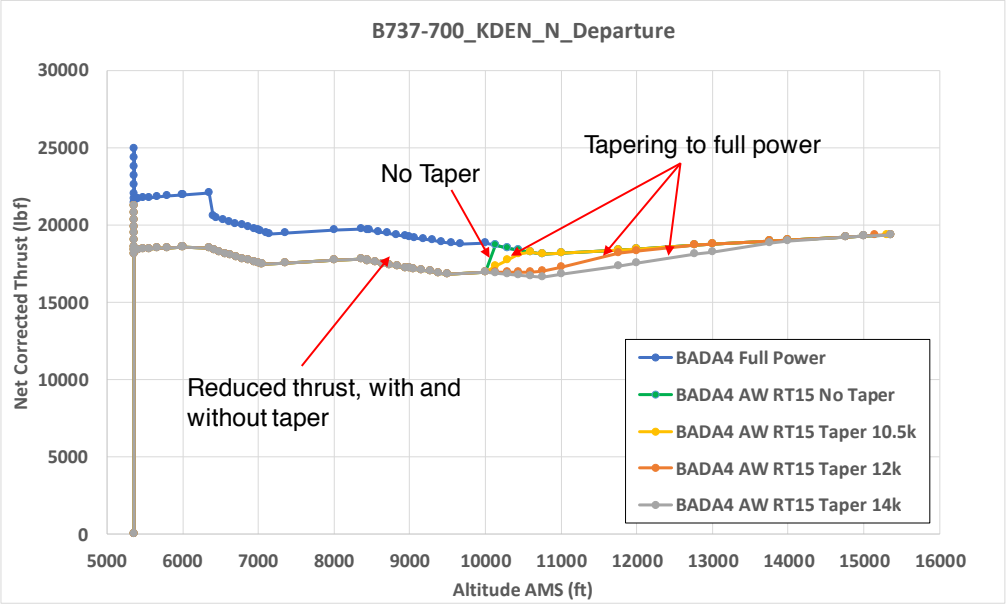


Figure 29. Reduced Thrust to Full-power Transitions for Different Thrust Taper Settings

This shows that the slope of the transition curve is primarily dependent on the full-power thrust curve since the taper coefficient increases linearly from 0 to 1 as h goes from H_1 to H_2 and the reduced thrust coefficient is a constant value (dependent on level of reduced thrust).

The thrust taper capability was tested on the B737-700 for departure at Denver International Airport (KDEN). Figure 29 shows how an upper taper limit setting of 14,000 ft AMS allows the engine to transition from reduced thrust to full-power at a slower rate than a upper taper limit setting of 10,500 ft AMS. Since the upper taper limit would define the final altitude at which the thrust must reach full-power, this outcome is expected. With no thrust taper setting, the thrust would simply jump from reduced thrust to full-power at 10,000 ft AMS.

Track control

AEDT has two different types of flight performance: 1) Procedure-Driven and 2) Trajectory-Driven flight. In the trajectory-driven flight, there are two types of flight performance: 1) Sensor path and 2) Track control flight. The track control flight

consists of altitude and speed control. In particular, the track control flight is useful when the profiles do not represent actual routes. The diagram of flight performance modeling options in AEDT is shown in the Figure 30.

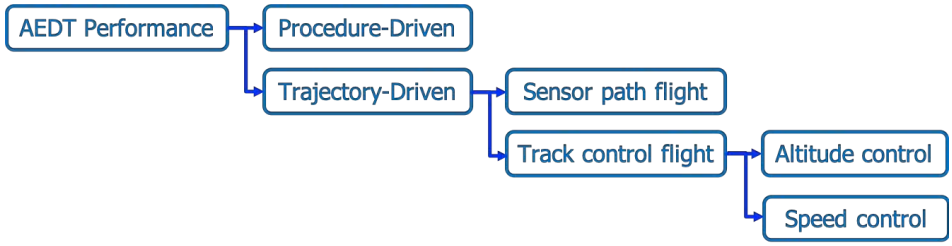


Figure 30. AEDT Flight Performance Diagram

A track control flight defines what aircraft's altitude must be as it passes over a particular track point. In AEDT, it provides three types of altitude/speed restrictions. For example, there are three different types of altitude control as shown in the Figure as below. First, "At" restricts the aircraft from being more than 300 ft from the target altitude when passing over the track point. Second, "At or Above" restricts the aircraft from being more than 300 ft below the target speed when passing over the track point. Third, "At or Below" restricts the aircraft from being more than 300 ft above the target speed when passing over the track point. This is described in the Figure 31.

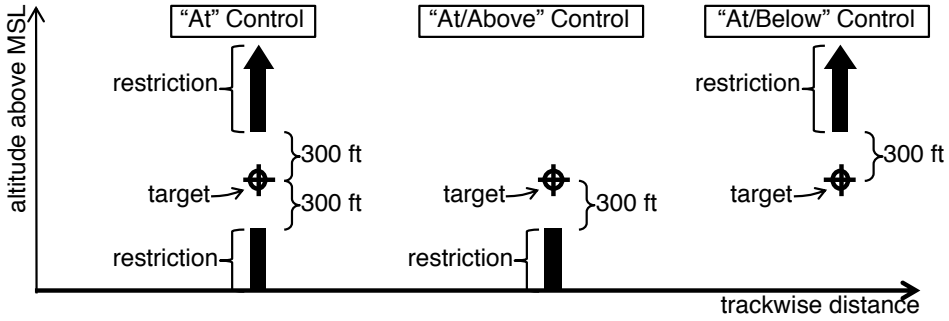
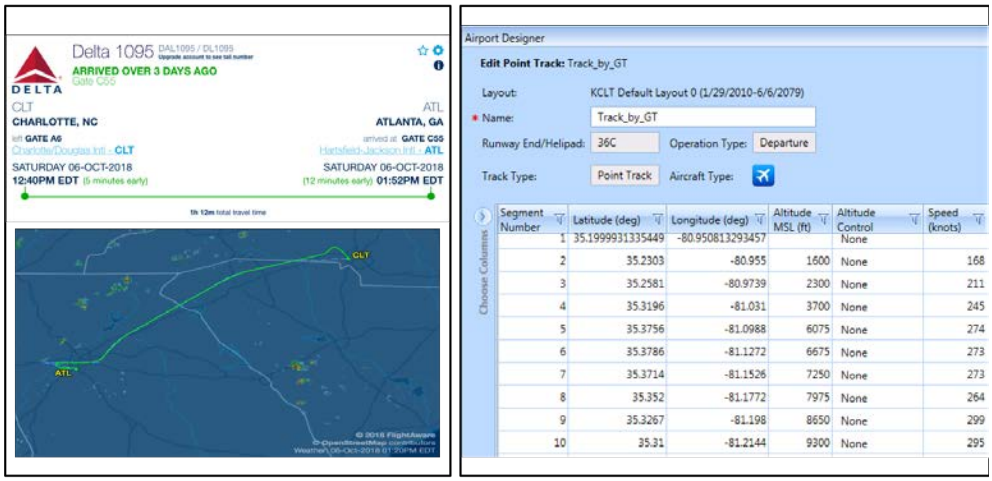


Figure 31. Options for altitude control in AEDT

The objective of this section is to demonstrate the functionality of track control flight.
In order to test a functionality of altitude/speed control, the research team created a new point track with real flight data from FlightAware, which is a global aviation software and data service platform. In FlightAware, they offer free flight tracking data information of world-wide commercial Air Transportation Network (ATN). Its comprehensive dataset contains time, speed, altitude, latitude, longitude, direction, rate of climb, etc. with accompanying information such as origin, destination, airline, flight number, operating aircraft. The case study used for this test is shown in the Figure 32.



Real Flight Data

AEDT Airport Designer – Point Track

Figure 32. Compiling flight data information and modeling point track with the information

To test all the combinations with ANP, BADA4, Altitude control, and Speed control, the research team created a test matrix as shown in the Table 5.

Table 5. Test matrix for track control flight in AEDT

Case #	Performance Model	Altitude Control	Speed Control
1	ANP	on	off
2	ANP	off	on
3	ANP	on	on
4	BADA4	on	off
5	BADA4	off	on
6	BADA4	on	on

When the altitude control was only turned on at the particular point with both ANP and BADA4 cases, it was observed that the track control functionality worked well as shown in the Figure 33 and Figure 34. (Note that only one point was controlled)

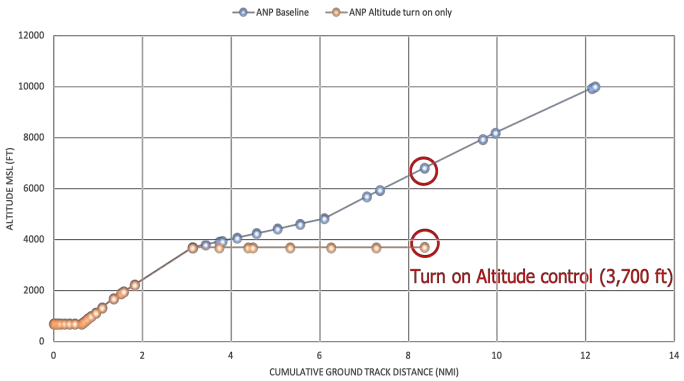


Figure 33. Altitude control only for ANP case

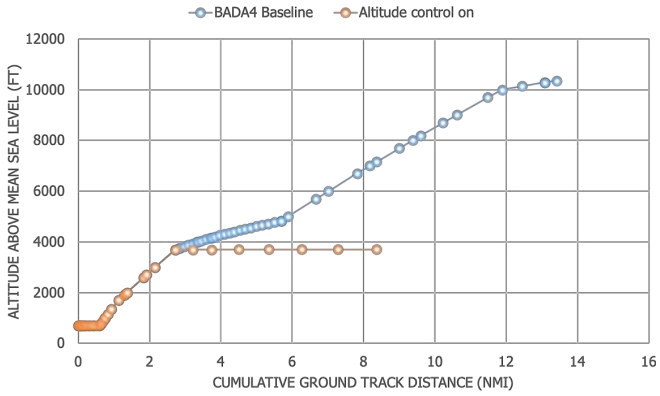


Figure 34. Altitude control only for BADA4 case

When the speed control was only turned on at the particular point with both ANP and BADA4 cases, it was observed that the track control functionality did not work. This was because the speed control should be implemented with the altitude control simultaneously regardless of the performance model in AEDT. For this reason, the research team conducted the test case with both speed and altitude control. They were turned on with Match option at the particular point in order to test the functionality for both ANP and BADA4. The test results are shown in the Figure 35 and Figure 36.

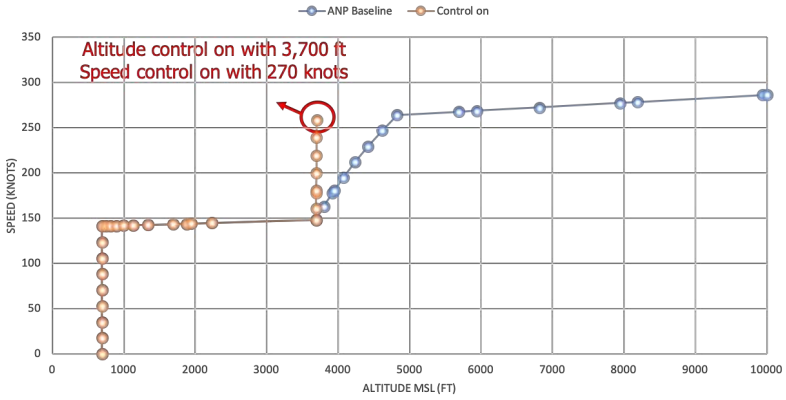


Figure 35. Speed and altitude control for ANP case

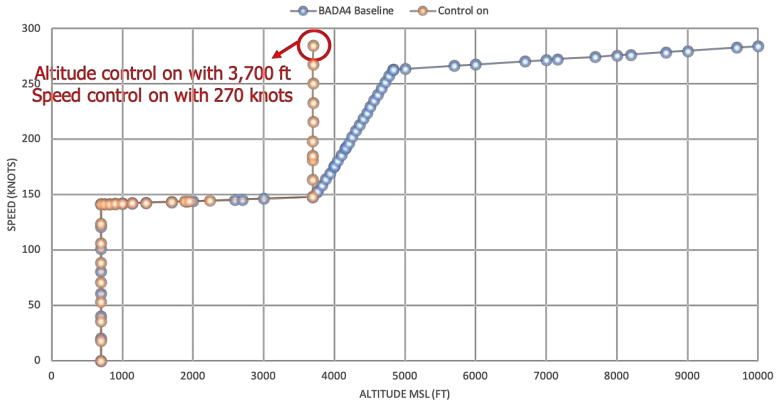


Figure 36. Speed and altitude control for BADA4 case

In summary, it was concluded that:

1) An altitude control for both ANP and BADA4 can be used without a speed control for track control flight in AEDT.
2) A speed control should be managed with an altitude control simultaneously for both ANP and BADA4.
3) Controls of both altitude and speed at the same time work for both ANP and BADA4.

According to the technical manual, there are a few control input requirements when users want to use track control flight in AEDT. The requirements are shown in the Table 6.

Table 6. Control input requirements in AEDT

Case	AEDT3a Technical manual (August 2018)
1	Controls specifying altitudes below 500 ft AFE are ignored by AEDT.
2	Controls on the first point in a departure track are ignored by AEDT.
3	Controls on the last two points in an approach track are ignored by AEDT.
4	An aircraft must have procedural standard profiles to be used with a track that includes altitude controls.
5	Overflight tracks containing altitude controls must have a minimum of two altitude controls above 500 ft AFE.
6	Approach tracks cannot have sequentially ascending altitude control targets.
7	Departure tracks cannot have sequentially descending altitude control targets.
8	BADA4 analysis of flight on controlled tracks requires observed controls of both altitude and speed.

The research team tested all the control input requirements in order to demonstrate the track control flight functionalities in AEDT. As a result, it was found that all the requirements are true except for case 3 and 5. For example, the research team tested the case shown in the Figure 37 and found that controls specifying altitudes below 500ft AFE should be an error in AEDT. For example, if the altitude control was turned at 852ft AFE, it worked well. However, if the altitude control was turned on at 250ft AFE, it was unable to process flight because the altitude control must exist above 500ft AFE.

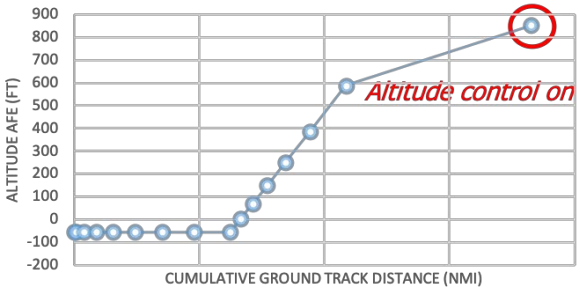


Figure 37. Control Input Requirement 1 - Test

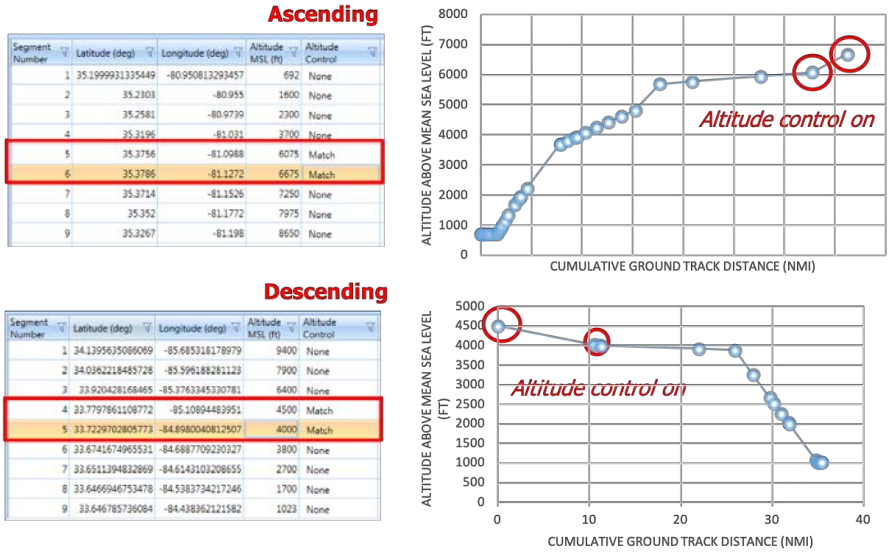


Figure 38. Control input requirement 6 and 7 - Test

In a similar way, in order to test the control input requirement 6, the research team defined the sequentially ascending for a departure operation and descending for an approach operation altitude control targets. As a result, it was observed that approach tracks cannot have sequentially ascending altitude control targets. Furthermore, departure tracks cannot have sequentially descending altitude control targets. The results are shown in the Figure 38.

In order to test the control requirement 3, the research team specified two altitude control points at the last two points in an arrival track. Based on the technical manual, the controls on the last two points in an approach track should be ignored. However, it was observed that controls on the last point in an approach track are ignored but controls on the point before ground are not ignored as shown in the Figure 39.

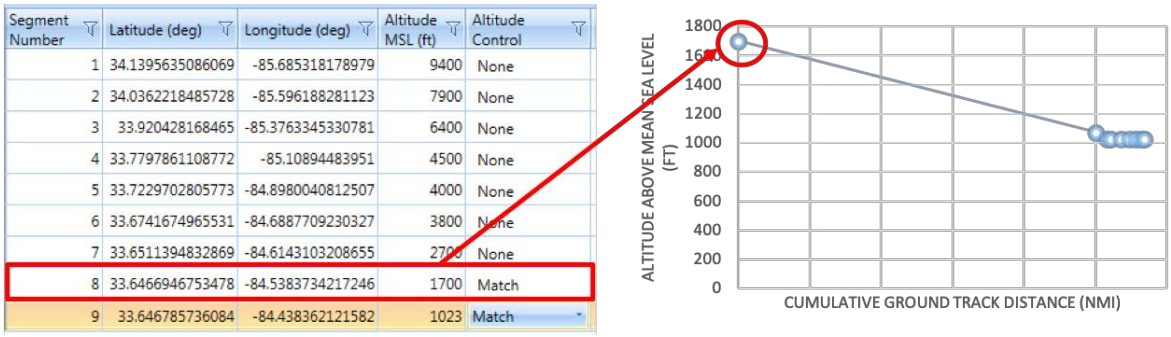


Figure 39. Control input requirement 3 - Test

Milestone(s)

Milestone	Due Date	Estimated Date of Completion	Actual Completion Date	Status	Comments (Problems & Brief Resolution Plan)
A36 Kickoff Meeting	5/3/2016	5/3/2016	5/3/2016	Completed	
Quarterly Report (Aug)	7/31/2016	7/31/2016	7/31/2016	Completed	



ASCENT Meeting	9/27-28/2016	9/27-28/2016	9/27-28/2016	Completed	
Quarterly Report (Nov)	10/31/2016	10/31/2016	10/31/2016	Completed	
Annual Report	1/18/2017	1/18/2017	1/13/2017	Completed	
Quarterly Report (Jan)	1/31/2017	1/31/2017	1/27/2017	Completed	
Quarterly Report (March)	3/31/2017	3/31/2017	3/31/2017	Completed	
ASCENT Meeting	4/18/2017	4/18/2017	4/18/2017	Completed	
Quarterly Report (June)	6/30/2017	6/30/2017	6/30/2017	Completed	
ASCENT Meeting	9/26/2017	9/26/2017	9/26/2017	Completed	
Quarterly Report (Oct)	10/30/2017	10/30/2017	10/30/2017	Completed	
Annual Report	11/30/2017	11/30/2017	11/30/2017	Completed	
Quarterly Report (Jan)	1/31/2018	1/31/2018	1/31/2018	Completed	
Quarterly Report (March)	3/31/2018	3/31/2018	3/31/2018	Completed	
ASCENT Meeting	4/3 - 4/2018	4/3 - 4/2018	4/3 - 4/2018	Completed	
Quarterly Report (June)	6/30/2018	6/30/2018	6/30/2018	Completed	
ASCENT Meeting	10/9 - 10/2018	10/9 - 10/2018	10/9 - 10/2018	Completed	
Quarterly Report (Oct)	10/30/2018	10/30/2018	10/30/2018	Completed	
Annual Report	11/30/2018	11/30/2018	11/30/2018	In Progress	

Major Accomplishments

Starting from December 2017, all the new AEDT sprint releases including Sprints from 95 to 111 have been tested. Seventeen Sprints of AEDT have been tested focusing on new features and capabilities added. Some of the new features/capabilities were minor updates to the GUI, bug fixes, or data updates. Major updates included enhanced nvPM, VALE reporting with MOVES, runup operation of military aircraft, open contour, vector track, track dispersion, contour combination, dynamic grid, detailed noise and bulk operation creation. In order to understand the background of new AEDT features, all the relevant documents were reviewed including the software requirement documents, Database Design Document, AEDT sprint release notes, updated technical manual, user manual, and research papers/reports. Basic testing of all the new AEDT versions and service packs was completed to confirm its functionality and a number of minor and major bugs and reported them to the FAA and the development team via bi-weekly ASCENT project telecons and weekly AEDT development-leads calls. Through the on-line system named Team Foundation Server (TFS), identified issues and follow-up actions taken by the developers were documented and shared. The TFS also allows for reporting any potential areas of improvements in AEDT algorithms and user-friendliness.

Finally, additional tests were conducted to investigate the environmental impact of new profiles with reduced thrust and alternative weight. Comprehensive analysis were carried out to compare the fuel burn, emissions and noise results produce by ANP and BADA4 for different scenarios with new profiles. It was concluded BADA4 has better performance modeling capability and can generate environmental results closer to real world data. Further studies were designed and performed to test new features, and findings and recommendations were reported.



Publications

Yongchang Li, Dongwook Lim, Michelle Kirby, Dimitri Mavris, George Noel, Uncertainty Quantification Analysis of the Aviation Environmental Design Tool in Emission Inventory and Air Quality Modeling, AVIATION 2018 conference, June 17 – 21, 2018.

Dongwook Lim, Yongchang Li, Matthew J Levine, Michelle R Kirby, Dimitri, Mavris, Parametric Uncertainty Quantification of Aviation Environmental Design Tool, AVIATION 2018 conference, June 17 – 21, 2018.

Jung-Hyun Kim, Kisun Song and Seulki Kim, Yongchang Li, Dimitri Mavris, Aircraft Mission Analysis Enhancement by using Data Science and Machine Learning Techniques, Submitted to AVIATION 2019 conference

Outreach Efforts

None

Awards

None

Student Involvement

Yee Chan Jin is a first year Master student who started in fall 2018. Mr. Jin has conducted a literature review on UQ methods, and performed tests for newly release AEDT features. Mr. Jin is being trained on related tools such as INM, AEDT Tester, AEDT2c and AEDT 2d.

Ameya Behere is a third year PhD student who started in fall 2016. Mr. Behere has conducted a literature review on UQ methods, and performed tests for newly release AEDT features. Mr. Behere is being trained on related tools such as INM, AEDT Tester, AEDT2c and AEDT 2d.

Junghyun (Andy) Kim is a third year Master student who started in fall 2015. Mr. Kim has conducted a literature review on UQ methods, and performed tests for newly release AEDT features. Mr. Kim is being trained on related tools such as INM, AEDT Tester, AEDT2c and AEDT 2d.

Zhenyu Gao is a third year Ph.D student who started in fall 2016. Mr. Gao has conducted a literature review on UQ methods, and performed tests for newly release AEDT features. Mr. Gao is being trained on related tools such as INM, AEDT Tester, AEDT2c and AEDT 2d.

Plans for Next Period

GT will continue uncertainty quantification tasks for new AEDT 2e AEDT 3a is planned to be released in December 2018. GT will perform the validation and verification tasks for the preliminary versions of AEDT 3a to identify any issues that need to be addressed by the development team.

Task 1. Proper Definition of AEDT Input Parameter Uncertainty

The first step in the UQ effort is to properly define the problem. For each of the AEDT service pack releases, GT will define the scope of the UQ effort identifying the key changes to the AEDT versions from the previous releases. Depending on the type of updates incorporated, it would be required to identify the key sources of uncertainties and properly define the uncertainties for the input parameters if it is necessary.

Task 2. Verification and Validation plus Capability Demonstrations

GT will continue to conduct V&V and capability demonstrations of the newly released AEDT versions. The V&V analysis can take a couple of different approaches depending on the type of updates and data availability. In the past UQ efforts, one of the most important methods of ensuring confidence in the tool capability was to conduct a use case(s) using both legacy tools and the new AEDT release and compare the results. This method would be the most appropriate way whenever a legacy tool has the same or similar functionalities and a validated use case has been modeled in that legacy tool. When the new functionality of AEDT does not exist in the legacy tools, the V&V exercise should use direct comparisons to the results generated by the mathematical algorithms behind the newly added functionality and/or real world data whichever available.



Task 3. Identification of Important Output to Input Relationships (Optional)
This optional task may not be performed for every AEDT service pack releases. Instead, this task will be performed when a major feature is added to the AEDT, and if potential sources of uncertainties remain through the analysis of previous two tasks. The outcome of this task will be the identification of the key input drivers across multiple vehicle types to multiple AEDT metric outputs. This can provide a comprehensive insight to the uncertainty associated with AEDT outputs and the joint-distribution of Fleet DB coefficients. Various uncertainty quantification techniques will be used depending on the metric of interest. This may include, but not limited to the following techniques: Analysis of Variance (ANOVA), Multivariate Analysis of Variance (MANOVA), Monte Carlo Simulation, Copula Techniques, or Global Sensitivity Analysis. The specific techniques will be proposed by GT and reviewed by the FAA for concurrence.[i]

Task 4. Guidelines for Future Tool Research
In this task, each of the prior tasks will culminate into a summary document of the data assumptions, techniques utilized, the resulting observations and findings to help guide the FAA to further research the areas of AEDT development to improve its supporting data structure and algorithms. In addition, the document will build confidence in AEDT's capability and fidelity and help users to understand the sensitivities of output response to the variation of input parameters/assumptions.

References

[1] US FAA, AEDT 2a UQ Report, 2014

[2] US FAA, AEDT 2a SP2 UQ Supplemental Report, 2014

[3] US FAA, AEDT 2b UQ Report, 2016

[4] US FAA, Annual Report ASCENT Project 45, 2017

[5] US FAA, AEDT 2c User Manual, 2016

[6] US FAA, AEDT 2d Technical Manual, 2017

[7] US FAA, AEDT 2c Technical Manual, 2016

[8] US FAA, AEDT 2d User Manual, 2017

[9] Noel, George, "AEDT Uncertainty Quantification", presented in FAA/AEE Tools Review, December 2010

[10] Willcox, "Tools Uncertainty Quantification", presented in FAA/AEE Tools Colloquium, December 2010

[11] Allaire and Willcox, "Surrogate Modeling for Uncertainty Assessment with Application to Aviation Environmental System Models", AIAA Journal, 2010

[12] EUROCONTROL, Base of Aircraft Data (BADA) Aircraft Performance Modeling Report, EEC Technical/Scientific Report No. 2009-009, March 2009



Project 037 CLEEN II System Level Assessment

Georgia Institute of Technology

Project Lead Investigator

Dimitri Mavris (PI)
Regents Professor
School of Aerospace Engineering
Georgia Institute of Technology
Mail Stop 0150
Atlanta, GA 30332-0150
Phone: 404-894-1557
Email: dimitri.mavris@ae.gatech.edu

University Participants

Georgia Institute of Technology

P.I.(s): Dr. Dimitri Mavris (PI), Dr. Jimmy Tai (Co-PI)
FAA Award Number: 13-C-AJFE-GIT-013
Period of Performance: August 31, 2017 – August 31, 2018

Project Funding Level

FAA funding was distributed at the following levels.

- Georgia Institute of Technology ($170,000).

The Georgia Institute of Technology has agreed to a total of $170,000 in matching funds. This total includes salaries for the project director, research engineers, graduate research assistants and computing, financial and administrative support, including meeting arrangements. The institute has also agreed to provide tuition remission for any students paid for by state funds.

Investigation Team

Georgia Institute of Technology
Principal Investigator: Dimitri Mavris
Co-Investigators: Christopher Perullo, Jimmy Tai
Fleet Modeling Technical Lead: Holger Pfaender

Project Overview

The objective of this research project is to support the FAA by independently modeling and assessing the technologies that will be developed under the CLEEN II program. This will involve direct coordination and data sharing with companies developing technologies under CLEEN II, in order to accurately model the environmental benefits of these technologies at the vehicle and fleet levels.

Georgia Tech (GT) was previously selected to perform all of the system level assessments for the CLEEN program under PARTNER Project 36 and ASCENT Project 10. As a result, Georgia Tech has a unique position from both a technical and programmatic standpoint to continue the system level assessments for CLEEN II. From a technical perspective, GT has significantly enhanced the Environmental Design Space (EDS) over the last 5 years to incorporate advanced, adaptive, and operational technologies targeting fuel burn, noise, and emissions. EDS was successfully applied to all CLEEN I contractor technologies including: GE open rotor, TAPS II combustor, FMS-Engine and FMS-Airframe; Pratt & Whitney geared fan; Boeing adaptive trailing edge and CMC nozzle; Honeywell hot section cooling and materials; and Rolls-Royce turbine cooling technologies. GT also gained significant experience in communicating system level modeling requirements to industry engineers and translating the impacts to fleet level fuel burn, noise, and emissions assessments. This broad



technical knowledge-base covering both detailed aircraft and engine design and high level benefits assessments puts GT in a unique position to assess CLEEN II technologies.

As the ultimate goal of this work is to conduct fleet level assessments for aircraft representative of future 'in-service' systems, GT will need to create system level EDS models using a combination of both CLEEN II and other public domain N+1 and N+2 technologies. The outcomes of the technology and fleet assumptions setting workshops conducted under ASCENT Project 10 will be heavily leveraged for this effort. Non-CLEEN II technologies for consideration along with potential future fleet scenarios will help to bound the impact of CLEEN II on future fleet fuel burn, emissions, and noise. In the first year, non-disclosure agreements have already been signed with all of the CLEEN II contractors.

Since the FAA will also be performing a portion of the EDS technology modeling work, EDS training has been provided to the FAA in 2016 under the ASCENT Project 10. The training has provided the requisite skill set required to use EDS.
In the prior year of this project, Georgia Tech began modeling activities with Aurora, Pratt and Whitney, and GE. This modeling process included validation of underlying EDS models, information and data exchange necessary to model the individual technologies, and related EDS modeling activities. In addition, Georgia Tech has assisted the FAA with in-house modeling of Delta/MDS and GE combustion technologies. This process has increased the FAA's use of FAA personnel for EDS system level assessment modeling.

This year has focused on modeling the GE MESTANG, Boeing Compact Nacelle, GE TAPS III, Boeing Structurally Efficient Wing, Honeywell Blade Outer Air Seal (BOAS) and UTAS zoned liner technologies.

Major Accomplishments

- GT has signed non-disclosure agreements with all CLEEN II contractors.
- The Delta/MDS modeling is complete.
- The Aurora modeling is complete.
- The modeling for GE FMS is completed, pending further updates to technology.
- The modeling for GE TAPS III is completed.
- The modeling framework for GE MESTANG is complete.
- The modeling for Boeing Compact Nacelle is complete.
- The data exchange and assumptions were defined for Honeywell Blade Outer Air Seal and Combustor.
- The discussions on the modeling process were held with all contractors.
- The modeling assumptions and framework were defined for UTAS zoned liner technology.

Publications

None

Outreach Efforts

None

Awards

None

Student Involvement

Siyuan Wu is a graduate student who has been assisting with modeling of UTAS noise technologies.

Plans for Next Period

Future work will focus on completing technology modeling and conducting preliminary fleet analysis assessments for presentation at the May 2019 Consortium.

This work will also support attendance at CLEEN consortium meetings and contractor preliminary and detailed design reviews to identify any updates required to technology models developed in prior years.

References

None



Project 038 Rotorcraft Noise Abatement Procedures Development

The Pennsylvania State University/Continuum Dynamics, Inc.

Project Lead Investigator

Kenneth S. Brentner
Professor of Aerospace Engineering]
Department of Aerospace Engineering
The Pennsylvania State University
233 Hammond Building, University Park, PA
(814)865-6433
ksbrentner@psu.edu

University Participants

The Pennsylvania State University

- P.I.: Kenneth S. Brentner, Professor of Aerospace Engineering
- FAA Award Number: 13-C_AJFE-PSU-038, Amendment No. 37
- Period of Performance: September 2017 to August 2018
- Task(s): (during this period)
  9. Analyze noise abatement procedures flown in flight test program
  10. Compare flight test noise results with predicted results
  11. Assist in the initial evaluation of flight test data to determine effectiveness of noise abatement procedures

Project Funding Level

FAA: $150,000; In-Kind Match: (Continuum Dynamics, Inc.: $150,000)

Investigation Team

Kenneth S. Brentner, PI, The Pennsylvania State University; acoustics predictions lead on all tasks.
Joseph F. Horn, Co-PI, The Pennsylvania State University; flight simulation lead supporting all tasks
Daniel A Wachspress, Co-PI, Continuum Dynamics, Inc.; responsible for rotor loads and wake integration, and CHARM coupling.
Mrunali Botre, Graduate Research Assistant, The Pennsylvania State University; primary responsibility for setting up new aircraft models, developing simulations with new helicopter types, acoustic predictions and development of flight abatement procedures, involved in all tasks.

Project Overview

Rotorcraft noise consists of several components including rotor noise, engine noise, gearbox and transmission noise, etc. Rotor noise is typically the dominant component of rotorcraft noise that is heard by the community upon takeoff, landing, and along the flight path of the helicopter. Rotor noise consists of several different noise sources including thickness noise and loading noise (together typically referred to as rotational noise), blade-vortex-interaction (BVI) noise, high-speed-impulsive (HSI) noise, and broadband noise – with each noise source having its own unique directivity pattern around the helicopter. Furthermore, any aerodynamic interaction between rotors, interaction of the airframe wake and a rotor, or unsteady, time-dependent loading generated during maneuvers typically results in significant increases in loading noise. The combination of all the potential rotor noise sources makes prediction of rotorcraft noise quite complex, even though not all of the noise sources are present at any given time in the flight (e.g., BVI noise usually occurs during descent and HSI noise only occurs in high-speed forward flight).



In ASCENT Project 6, "Rotorcraft Noise Abatement Operating Conditions Modeling", the project team coupled a MatLab - based flight simulation code with CHARM and PSU-WOPWOP to preform rotorcraft noise predictions. This noise prediction system was used for developing noise abatement procedures through computational and analytical modeling. Although this noise prediction system does not contain engine noise or HSI noise prediction capability, it was thoroughly validated by comparing predicted noise levels for a Bell 430 aircraft with flight test data (Ref. 19) for several observer positions and operating conditions.

In the previous work in ASCENT Project 38, representative helicopters for noise abatement procedure development were recommended. These helicopters were selected to determine if it is feasible to develop noise abatement procedures for categories of helicopters, (i.e., 2 blade light, 4 blade light, 2 blade medium, etc.) or if aircraft specific design considerations will be required in the development of noise abatement procedures. Aircraft models were set up for the following aircraft: Bell 430, Sikorsky S-76C+ and S-76D, Bell 407 and 206L, Airbus EC130 and AS350, and Robinson R-66 and R44 aircraft. Predictions were made before the FAA/NASA noise abatement flight test to provide guidance for the flight test.

Objectives

The objective of the continuing project is to utilize computational and analytical modeling to develop noise abatement procedures for various helicopters for various phases of flight. The extension of the project also includes prediction to support analysis of previous flight test data and planning for a potential new noise abatement procedure flight test. Comparison of predictions with flight test data provides further validation of the noise prediction system and deeper understanding of the impact of noise abatement procedures on the noise directivity and amplitude. Comparisons have been made using various noise metrics (SEL, DNL, EPNL, etc.) along with the acoustic pressure time history and acoustic spectrum plots.

Task 9- Analyze Noise Abatement Procedures Flown in Flight Test Program.

The Pennsylvania State University

Objective(s)

The objective of this task is to analyze noise abatement procedures performed in the FAA/NASA noise abatement flight test program. Comparison of predictions and measured data will be used to assess the importance of each flight procedure in the flight test plan. This task will also continue to assess the fidelity of input data required for accurate noise predictions.

Research Approach

The noise prediction system developed in ASCENT Projects 6 and 38 will be used and updated as necessary. The PSU-WOPWOP code will be used for noise prediction and will be coupled with a MatLab flight simulator and CHARM (Comprehensive Hierarchical Aeromechanics Rotorcraft Model) to form a rotorcraft noise prediction system. Limited validation of the system through comparison with the NASA/Bell flight test has demonstrated that the system is reasonably accurate with very reasonable computational cost. By comparing the predictions with flight test data of different aircraft, deficiencies of the noise predictions can be determined. The noise abatement procedures will be compared to standard procedures through comparison of several different acoustic metrics. Finally, the noise from the various flight procedures can be analyzed more thoroughly by investigating the physics in the noise prediction.

Milestone(s)

The milestones for this task include: 1) analysis of noise abatement procedures performed in the flight test for the flight test aircraft; 2) begin comparison of the predicted data and flight test data to evaluate; and 3) further validate the noise abatement procedures and the noise prediction system. This task will also provide any needed support for the pre- and post-flight test planning and analysis.

Major Accomplishments

Through comparing the noise predictions and flight test data (L_A vs. time plots and SEL contours), it was discovered that there was an underprediction in the noise when broadband noise was a major contributor to the SEL values, but in cases where the loading noise was comparable or higher than broadband noise the SEL underprediction was not as evident. This is underprediction was related to the fact that the broadband noise model in PSU-WOWPOP did not include ground reflection. All the other noise components were increased due to reflection from a hard ground.

Once this deficiency was understood, the PSU-WOPWOP code was modified to change the way in which the reflections were computed – to include broadband noise reflection. Two representative comparisons are shown in Figure 9.1 for a 80 kts, level flight case. On the left in the figure is the SEL contour data for the Robinson R66 and on the right is data for Bell 407. The top figure in each column is the measured data, the middle figures are the predicted SEL contours without the broadband noise reflection from the ground plane, and the bottom figures in each column are the SEL contours when the broadband noise is properly reflected by the ground plane. The particular cases shown here are chosen because for the Robinson R66 broadband noise is a dominant component of the SEL (higher than loading noise), but for the Bell 407, loading noise and broadband noise contribute approximately equally to the SEL values. Notice that the prediction with broadband noise reflection is significantly closer to the measured data for the Robinson R66 than for the Bell 407. This is due to the fact that the SEL values in the Bell 407 case are set largely by loading noise, but for the R66 the SEL values are set by broadband noise. The corrected broadband noise values for the Bell 407 are slightly overpredicted and the Robinson R66 was slightly underpredicted – but much less so than without broadband noise reflection.

Similar predictions and comparisons with measured data were made for all of the flight test aircraft and for several different flight conditions. The results are very similar to this. This example demonstrates how the comparisons can be used to determine that one component of the noise is more important relative to the others by examining the noise predictions. The example also shows that the predictions can be improved by understanding the differences between the prediction and the data. In this case the direct and reflected broadband noise signals were assumed to be incoherent, which is typically the case for random noise sources. Actually, for a microphone on a ground board – like was used in the experiments – the two broadband noise signals should be coherent and the broadband noise levels would be raised even higher. More work needs to be done to investigate if the broadband noise prediction model consistent overpredicts the broadband noise (and hence, may need to be modified).

Publications

None

Outreach Efforts

None

Awards

None

Student Involvement

Mrunali Botre, graduate assistant currently working toward her Ph.D. at Penn State, performed the acoustic predictions and worked to develop and implement the broadband noise reflection capability in PSU-WOPWOP.

Plans for Next Period

Validation of the system with the FAA/NASA flight test data will be an ongoing process, that will be done in parallel to "understanding" what was likely the reasons for changes in noise in the flight tests. The flight test data does not have any details about blade loadings, specific BVI information, etc., but the predictions can suggest which noise components were dominant in different parts of the flyover and at different directivity angles. In particular, the broadband noise prediction model will be more thoroughly investigated and validated.

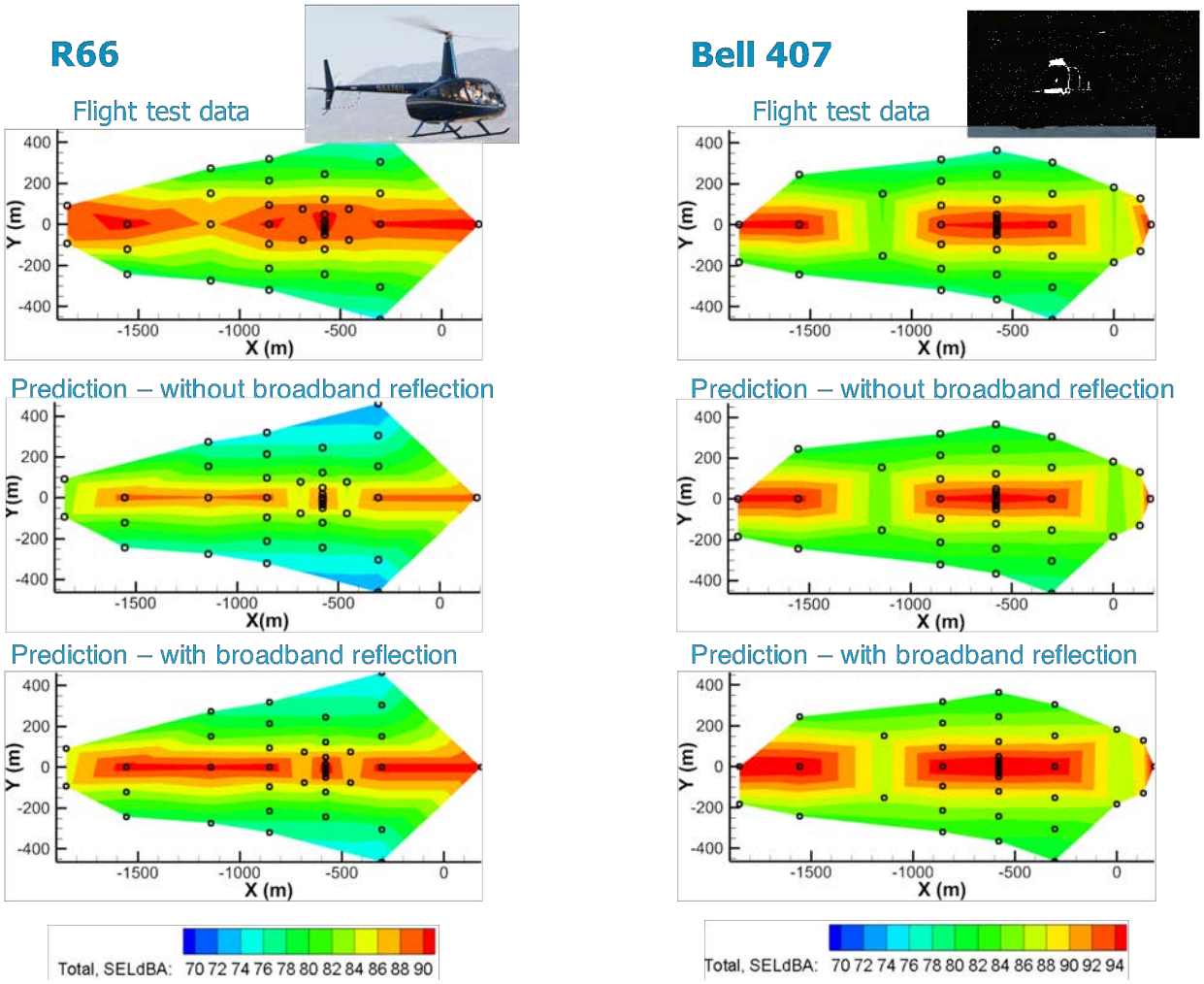


Figure 9.1. Comparison of measured data and predictions (with and without broadband noise ground reflection) for two aircraft; 80 kts, level flight.

Task 10- Compare Flight Test Noise Results with Predicted Results.

The Pennsylvania State University

Objective(s)

The objective of this task is to assess and validate the effectiveness of the prediction system, determine the significance of noise sources not currently modeled, and evaluate the effectiveness of noise abatement flight procedures performed in the FAA/NASA noise abatement flight test program.

Research Approach

For this effort, the noise prediction system developed in ASCENT Projects 6 and 38 will be used to perform the noise predictions and to process the acoustic pressure data from the FAA/NASA noise abatement flight test. This comparison will have two primary goals: 1) to assess and validate the effectiveness of the prediction system and to determine the significance of noise sources not currently modeled (i.e., engine noise); and 2) to evaluate and verify the effectiveness of noise abatement flight procedures. Validation of the predicted noise abatement is achieved by comparing the predicted

noise abatement to that measured in the flight test – for a range of helicopters. Incidentally, it will also be important to determine if the limited information about the helicopters we have (i.e., incomplete data with some estimates to fill in the gaps) is sufficient to agree with the flight test data, or if more detailed data is needed for accurate prediction (and what that data is).

Milestone(s)

The milestones for this task are: 1) analysis and validation of the predicted noise through comparison with flight test data; and 2) consideration of more complete/complex procedures than were possible in the flight test by combining segments of the flight test into more comprehensive results

Major Accomplishments

Noise predictions were made to compare with the FAA/NASA noise abatement flight test. First the flight test will be described, and then representative examples of the noise comparison will be presented.

The FAA and NASA performed a series of noise abatement flight tests for six different helicopters during the fall of 2017. The six helicopters tested were chosen for comparison of key features and availability. The first two aircraft, the Robinson R44 and R66, are aircraft with similar weight, but the R44 has a piston engine and the R66 has turbine engine. Both the R44 and R66 have two bladed main rotors and tail rotors, but the main rotor blade chord and twist are different. The next two aircraft, the Bell 206L and 407, are similar aircraft, but different generations. The 206L has a two bladed main rotor, while the newer 407 has a four bladed main rotor and is slightly heavier. The final two aircraft, the Airbus AS350 and Airbus EC130 are also very similar aircraft, but the EC130 is newer. The Airbus helicopters have three bladed main rotors that operate in the clockwise direction (instead of counterclockwise when viewed from above – like the other aircraft). The EC130 also uses a different antitorque device (a fenestron) as compared to the two bladed main rotor of the AS350.

Sound exposure level (SEL) predictions are compared to flight test data in Figure 10.1 for the six test aircraft. The acoustic pressure measured at the test microphones was processed with the PSU-WOPWOP code so that all the post processing is identical for the predictions and measurements (eliminating any uncertainty due to differences in acoustic post processing). The black dots represent the microphone locations in the flight test. Predictions were made at the same microphone locations that were available for each test condition – and if any data was missing during the test at a microphone location, the prediction data for that microphone location was also excluded (which is why some of the black dots are apparently missing). The predictions shown in Figure 10.1 are for an 80 kts, 6 deg. descent case, which is a strong BVI condition. It is apparent in the figure that the peak SEL values and the contour shapes agree within about 2 dBA or less for all of the aircraft, except for the EC130. This agreement is very good. In fact, the subtle changes in noise directivity found when comparing one aircraft to another are also predicted quite well (i.e., compare the R44 vs the R66 or the Bell 206L and the Bell 407). Notice that a subtle skew in the contours to the right (positive y values) is observed for the aircraft with counter-clockwise main rotor rotation. This skew shifts to the left (negative y values) for the two Airbus helicopters, which have clockwise main rotor rotation. The fact that such subtle changes are predicted is very encouraging and a good validation of the noise prediction system. The EC130 prediction is lower than the measured data by 5 to 6 dB. This is likely because the Fenestron duct/shroud is not modeled in the prediction. (Other predictions for previous research has shown that the shroud is expected to increase the noise levels, which is consistent with underprediction here.) Also note that while the engine noise is different for the R44 and R66, little difference is seen in the measure noise levels due to the engine - and the predictions do not include engine noise.

Publications

None

Outreach Efforts

None

Awards

None

Student Involvement

Mrunali Botre, graduate assistant currently working toward her Ph.D. at Penn State, performed the acoustic predictions for this task. She also post-processed the flight test data for the comparison.

Plans for Next Period

Validation of the system with the FAA/NASA flight test data will be an ongoing process, that will be done in parallel to "understanding" what was likely the reasons for differences between the predicted and measured noise. Comparisons will be made for more flight conditions that were performed in the flight test – especially time dependent maneuvers.

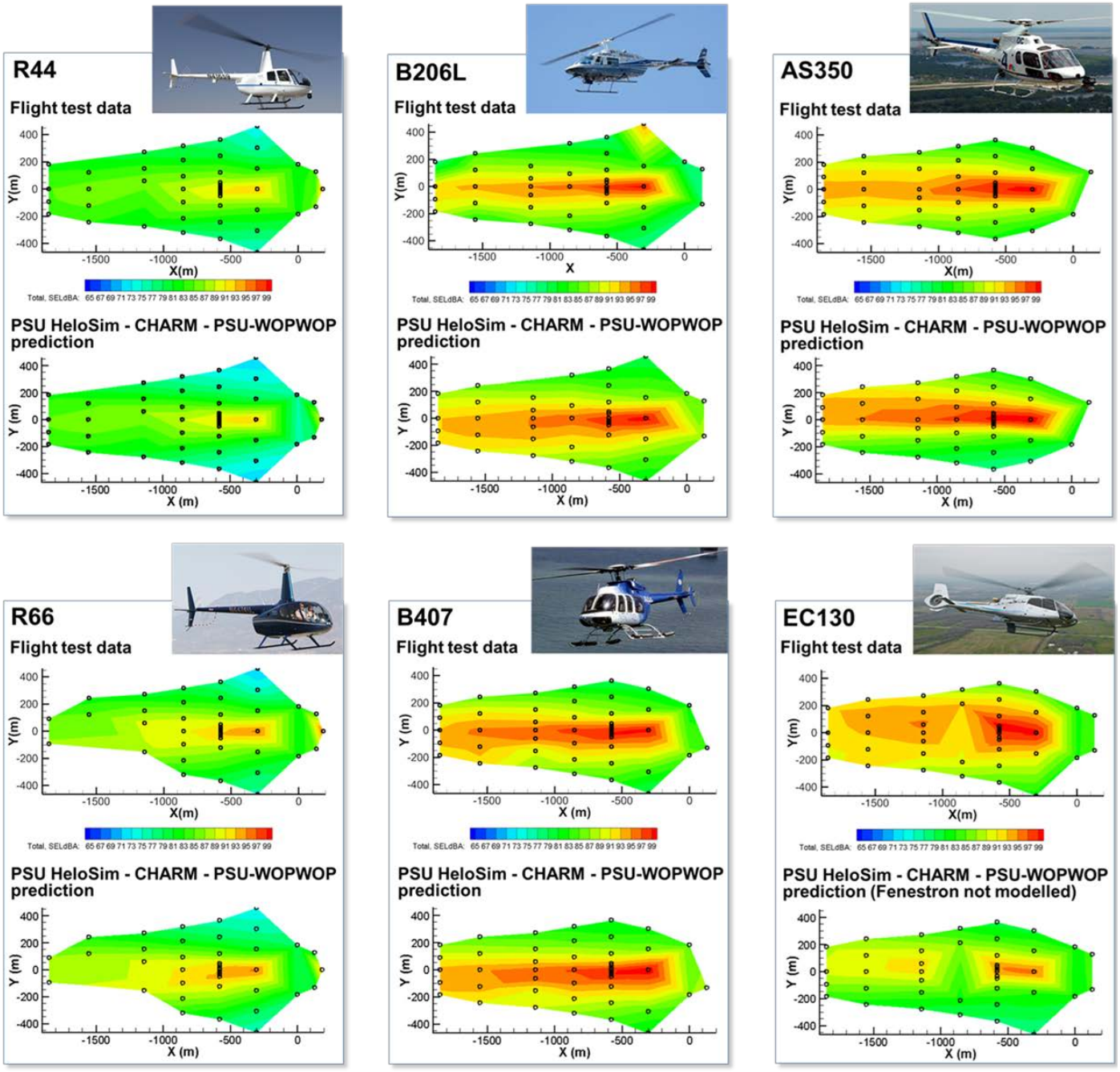


Figure 10.1 Comparison of measured and predicted Sound Exposure Level contours for 6 helicopters; 80 kts, 6 degree descent case (BVI noise condition). These comparisons are BEFORE broadband noise reflection was included.

Task 11- Assist in the Initial Evaluation of Flight Test Data to Determine Effectiveness of Noise Abatement Procedures.

The Pennsylvania State University

Objective(s)

The objective of this task is to provide assistance in the initial evaluation of the flight test data and the effectiveness of various noise abatement procedures.

Research Approach

In this task predictions are made to provide guidance for planning and executing the flight test and then evaluating the noise abatement procedures. This involves evaluation of the flight test data and examination and comparison of measured and predicted results to help explain any significant unexpected noise measurements. This evaluation can also identify which noise sources are the primary and secondary noise sources involved in a flight procedure and provide understanding about how the noise abatement was achieved (which can lead to generalizing the procedure to other helicopter categories, weights, etc.). Prediction of noise hemispheres in advance can also be used to develop the noise abatement procedures in that are proposed and test.

Milestone(s)

Provide a more thorough comparison of flight test noise data and predicted noise. Focus analysis on the effectiveness of various noise abatement procedures and interrogate the elements of the predicted airloads, flight dynamics, and noise to understand more completely the reason for noise reduction (or lack of noise reduction) during flight test procedures.

Major Accomplishments

Noise hemispheres were computed for each of the aircraft and all of the flight procedures planned in the FAA/NASA noise abatement flight test prior to the test. These hemispheres were provided to Volpe before the test so that they could evaluate potential noise abatement procedures. SEL contours on the ground plan were also computed prior to the flight test. Figure 11.1 shows an example of the ground contour data provided to Volpe and the flight test team. Then during the flight test, the preliminary data was compared to the PSU predictions. One example of this preliminary data comparison is shown in Table 11.1. This information was used in the noise abatement part of the flight test, which used predictions and prior days test data to develop some of the procedures during the flight test.

Noise predictions for the Sikorsky S-76C+ helicopter were made for a wide range of steady flight conditions for Juliet Page at Volpe to support a test/event where she worked with operators and pilots. The noise hemispheres were used as input for fly neighborly guidance, which was given to the pilots as they carried out typical operations flying to Long Island.

Table 11.1 Preliminary during the flight test

R-44 Day 227 Run #164 3deg 60 knots

Mic # **	Measured #164	Ideal Traj Std Meteo	Actual Traj Std Meteo	Ideal Traj Actual Meto*	Actual Traj Actual Meteo*
19	95.50	95.8	95.6	95.8	95.6
23	83.79	83.3	83.3	83.1	83.2
15	82.90	81.8	81.9	81.7	81.8

* No %RH or Press available from Meteo equipment yet.
** Actual Mics used to build the sphere are TBD.
All use Sphere #164; Ideal Trajectory vs. Actual Trajectory
Standard Meteo (US 76, 70% RH) vs. Actual Meteo (78 F, 80 %RH)
* Updated PSU runs (proper height of flight path, 9/18/2017)

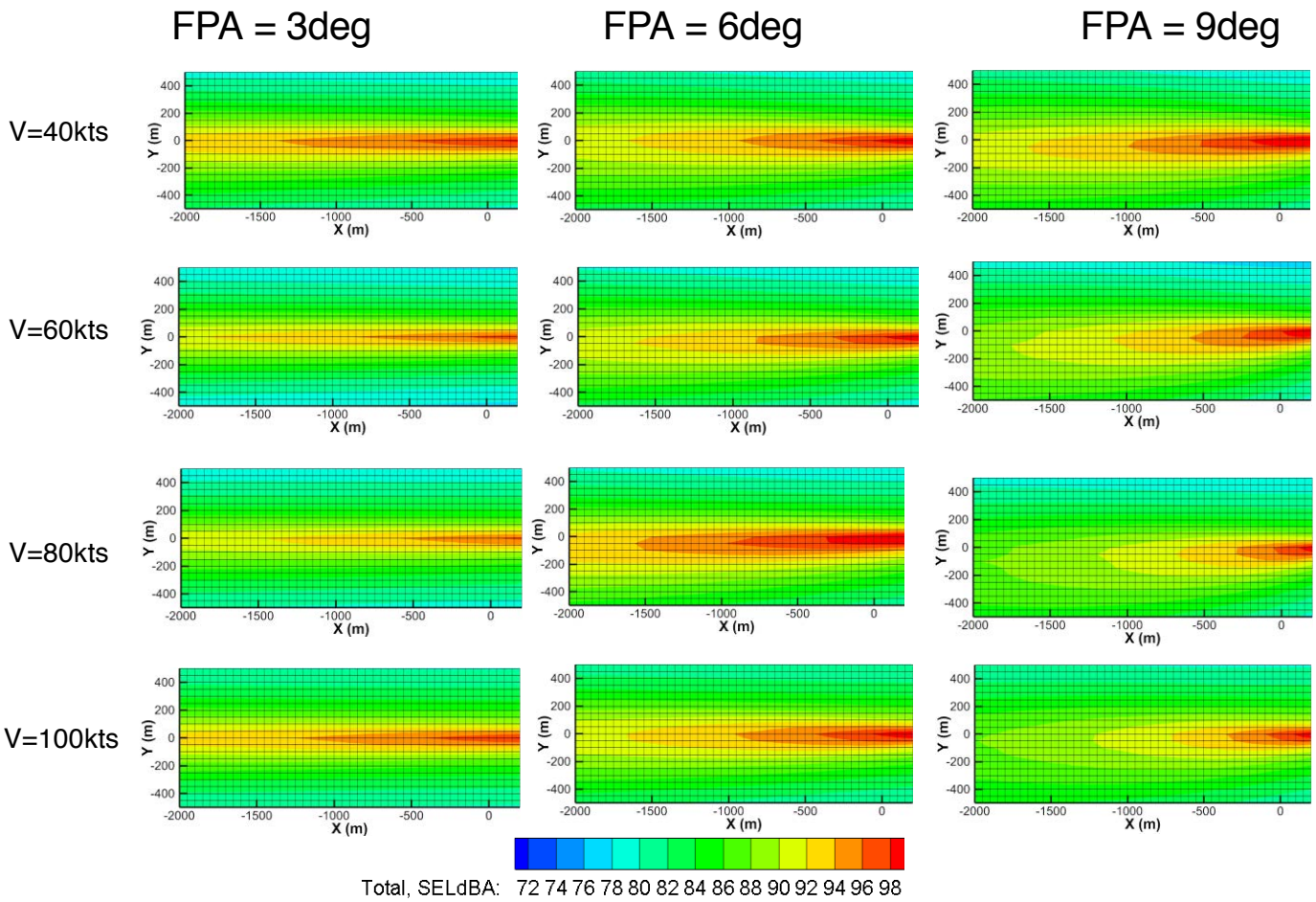


Figure 11.1. Sound exposure level ground contours for the Bell 407 aircraft. Note, when the aircraft is at $x = 0$, it is 200 ft AGL. (FPA is flight path angle)

Table 11.2 shows some key characteristics of the S-76C+ aircraft and Table 11.3 shows the matrix of flight test data provided to Volpe.

Table 11.2 Key characteristics of S-76C+ and S-76D aircraft.

	S76C+	S76D
Power (hP)	1844	2244
Weight (lb)(90 % of max takeoff weight)	10530	10688
Number of blades	4	4
Blade radius	22	22
Vtip	220	220



Table 11.3 Flight condition matrix for noise hemispheres provided to Volpe for S-76C+.

Speed	FPA								
	0.0	1.5	3.0	4.5	6.0	7.5	9.0	10.5	12
75	X	X	X	X	X	X	X	X	X
90	X	X	X	X	X	X	X		
105	X	X	X	X	X				
120	X	X	X						
135	X								
150	X								

Publications
None

Outreach Efforts
None

Awards
None

Student Involvement
Mrunali Botre, graduate assistant currently working toward her Ph.D. at Penn State, performed the acoustic predictions and worked with Volpe to provide the needed predictions and any explanation of the results.

Plans for Next Period
We will support efforts by Volpe, FAA, and NASA to evaluate the flight test data and provide more understanding of the noise abatement procedures. Efforts will also extend this understand to develop new procedures and use the validated noise prediction system to assess the effectiveness of the new procedures.



Project 039 Naphthalene Removal Assessment

Massachusetts Institute of Technology

Project Lead Investigator

Prof. Steven Barrett
Leonardo Associate Professor of Aeronautics and Astronautics
Department of Aeronautics and Astronautics
Massachusetts Institute of Technology
77 Massachusetts Avenue – Bldg. 33-316
Cambridge, MA 02139
(617)-452-2550
sbarrett@mit.edu

University Participants

Massachusetts Institute of Technology

- P.I.(s): Prof. Steven Barrett & Dr. Raymond Speth
- FAA Award Number: 13-C-AJFE-MIT, Amendment Nos. 026, 034, and 043
- Period of Performance: July 8, 2016 to Aug. 31, 2020 (With the exception of funding and cost share information, this report covers the period from October 1st, 2017 to September 30th, 2018)
- Task(s):
    1. Estimate capital and operating costs of naphthalene removal
    2. Explore relationship between PAH formation and aircraft PM emissions
    3. Compare kinetic model results to LFP/PIMS experimental data
    4. Calculate air quality and climate impacts of naphthalene removal
    5. Conduct integrated cost-benefit analysis of impacts of naphthalene removal in the U.S.

Project Funding Level

Project Funding Level: $490,000 FAA funding and $490,000 matching funds. Sources of match are approximately $129,000 from MIT, plus 3rd party in-kind contributions of $361,000 from Oliver Wyman Group.

Investigation Team

Prof. Steven Barrett (MIT) serves as principal investigator for the A39 project as head for the Laboratory for Aviation and the Environment. Prof. Barrett coordinates both internal research efforts and maintains communication between investigators in the various MIT research teams mentioned below.

Dr. Raymond Speth (MIT) serves as co-principal investigator for the A39 project. Dr. Speth directly advises student research in the Laboratory for Aviation and the Environment focused on assessment of naphthalene removal refinery options, climate and air quality modelling, and fuel alteration life-cycle analysis. Dr. Speth also coordinates communication with FAA counterparts.

Prof. William Green (MIT) serves as a co-investigator for the A39 project as a head of the Green Research Group. Prof. Green advises student work in the Green Research Group focused on computer-aided chemical kinetic modeling of PAH formation.

Mr. Randall Field (MIT) is the Executive Director of the MIT Energy Initiative, and a co-investigator of the A39 project. Drawing upon his experiences as a business consulting director at Aspen Technology Inc., Mr. Randall provides mentorship to student researchers in selection and assessment of naphthalene removal refining option, and process engineering at-large.



Mr. Drew Weibel (MIT) is a graduate student researcher in the Laboratory for Aviation and the Environment. Mr. Weibel is responsible for conducting selection and assessment of naphthalene removal refining options, calculation of refinery process requirements and fuel composition effects from selected processes, relating PAH formation to aircraft PM emissions, estimating capital and operating costs of naphthalene removal, air quality and climate modelling, and an integrated cost-benefit analysis.

Mr. Max Liu (MIT) is a Ph.D. candidate in the Green Research Group. Mr. Liu is responsible for development and analysis of a chemical kinetic model of PAH formation with fuel-composition effects.

Dr. Mica Smith (MIT) is a Postdoctoral associate in the Green Research Group. Ms. Smith is responsible for the experimental measurements which are being used for the validation of the chemical kinetic mechanisms.

Dr. Agnes Jocher (MIT) is a Postdoctoral associate in the Green Research Group. Ms. Jocher is responsible for evaluating microphysical models which link the presence of PAH molecules to the formation of soot particles and providing modeling expertise on combining these models with the kinetic models being developed.

Project Overview

Aircraft emissions impact the environment by perturbing the climate and reducing air quality, which leads to adverse health impacts, including increased risk of premature mortality. As a result, understanding how different fuel components can influence pollutant emissions, as well as the resulting impacts and damages to human health and the environment, is of importance to leading future research aims and policy. Recent emissions measurements have shown that removal of naphthalenes, while keeping total aromatic content unchanged, can dramatically reduce emissions of particulate matter (Brem *et al* 2015, Moore *et al* 2015). The objective of this research is to determine the benefits, costs, and feasibility of removing naphthalenes from jet fuel, in regards to the refiner, the public, air quality, and the environment. Specific goals of this research include:

- Assessment and selection of candidate refining processes for the removal of naphthalenes from conventional jet fuel, including details of required technology, steady-state public cost, and changing life-cycle emissions impacts at the refinery.
- Development of a chemical kinetics model to better understand the link between fuel aromatic composition resulting PM emissions due to jet fuel combustion.
- Assessment of the intrinsic climate and air quality impacts associated with naphthalene reduction and/or removal from jet fuel.
- Development of a succinct life-cycle analysis of the relative costs of removing naphthalene from jet fuel and the associated benefits due to avoided premature mortalities and climate damages for a range of possible scenarios.

Task 1- Estimate Capital and Operating Costs of Naphthalene Removal

Massachusetts Institute of Technology

Objective(s)

The objective of this task is to evaluate refinery technologies which can be used to remove naphthalene to determine their feasibility, costs, and effects on fuel composition. This includes calculating the costs of constructing new refinery unit processes, and determining additional utility and other operating costs associated with operating the process units responsible for naphthalene removal.

Research Approach

Naphthalene is present in varying levels in the straight-run crude oil distillation cuts used to produce jet fuel. For cuts which exceed the 3% volume limit on naphthalenes (ASTM D1655 2016), this exceedance can be resolved solely through blending, since the average naphthalene content of commercial Jet A is ~1.4% (DLA Energy 2013). Reducing the naphthalene content of jet fuel or eliminating it would therefore require the introduction of additional refinery processing. After reviewing several candidate refining processes in the previous year of this project, we have decided to further explore two in detail: selective hydrotreatment and extractive distillation. These processes are both used in industry for reduction or separation of aromatics and show promise in their ability to reduce and remove naphthalene from jet fuel. Selective



hydrotreatment reacts hydrogen with the feedstock and leads to removal of impurities and saturation of aromatics. Extractive distillation allows for the full separation of aromatics from the feedstock via polar solvents. The aromatics stream can then be processed to separate mono-aromatics and naphthalenes, with the former stream being returned to the jet fuel blending pool. These processes were chosen for their low added complexity and energy and because they have a minimal effect on the resultant fuel properties. It is, however, important to note that changes in fuel density, specific energy, fuel sulfur content, hydrogen content, and aromatic content will occur and are considered.

We have developed fundamental process models to estimate effects of fuel constituents and completed a literature search to collect data on process energy requirements, capital costs, and operating costs for both hydro-treatment and extractive distillation. In order to evaluate each candidate process, we leverage existing literature to estimate the utility (process fuel, electricity, hydrogen, etc.) requirements for each process, the effect on the composition of the resulting jet fuel, and the capital costs of new refinery equipment required, including the effects and costs of pre-processing and auxiliary process units that may be required. We then compare processes side-by-side in order to demonstrate the trade-offs associated with naphthalene removal at the refinery.

We consider the hypothetical adoption of a policy whereby jet fuel naphthalene content in the U.S. is reduced by 95% via either hydro-treatment or extractive distillation, at each of the 116 operational U.S. refineries with capacity of greater than 1000 barrels per day (BPD). We calculate costs using a stochastic discounted cash flow model of each refinery. Refinery capital costs are calculated using standard cost curve estimation methods, which relate process unit costs to capacity. Cost curves are used for both the primary naphthalene-removing process units (e.g. extractive distillation column or hydrotreater) as well as auxiliary process units (e.g. steam-methane reformer, CLAUS sulfur recovery unit, pressure-swing hydrogen recovery units, and steam generators). Direct operating costs include maintenance, local taxes, insurance, and supplies, calculated as a percentage of capital costs. Variable operating costs such as process water and chemicals are calculated based on the process unit utility requirements. The stochastic refinery model is used to determine the net present value (NPV) of each naphthalene removal process over its operating lifetime. The NPV can also be used to calculate the cost premium (i.e. cents per gallon) associated with the production of naphthalene-free fuel. Cost estimates are considered from two perspectives: that of the fuel market, and that of society. The market perspective computes cost premiums including all cash flows incurred by fuel producers, thus estimating the expected increase in the market price for naphthalene-free jet fuel. The societal cost estimate is computed from a resource-based perspective, placing it on the same basis as the monetization of potential benefits from improved air quality and potential climate impacts. In this perspective, redistribution of resources, e.g. taxes or loan payments, are disregarded, and the discount rate is assumed to be equivalent to society's long-term cost of capital.

Milestone(s)

The work completed for this task was documented in Deliverable 2-1, provided to the FAA on November 30, 2017.

Major Accomplishments

The resource-based (societal) cost premium and market cost premium estimate distributions for a policy in which all US produced jet fuel has its naphthalene content reduced by 95% (to 0.06 vol%) are shown in **Figure 1**, with cost data presented in 2016 USD. The mean societal cost premium of hydro-treating is found to be 2.4 cents/liter (95% confidence interval (CI): 2.3–2.5) and of extractive distillation is 1.7 cents/liter (95% CI: 1.6–1.8). This represents an annual NPV of $2.26 billion/year (95% CI: 2.17–2.35) and $1.65 billion/year (95% CI: 1.58–1.73), respectively.

The mean market cost premium of hydro-treating is 4.7 cents/liter (95% CI: 4.6–4.8) and of extractive distillation is 3.1 cents/liter (95% CI: 3.0–3.2). Given the average US Gulf Coast cost of jet fuel in 2016 was $0.33/liter, this represents a 14% and 9% increase in the cost of jet fuel for naphthalene removal via hydro-treatment and extractive distillation, respectively.

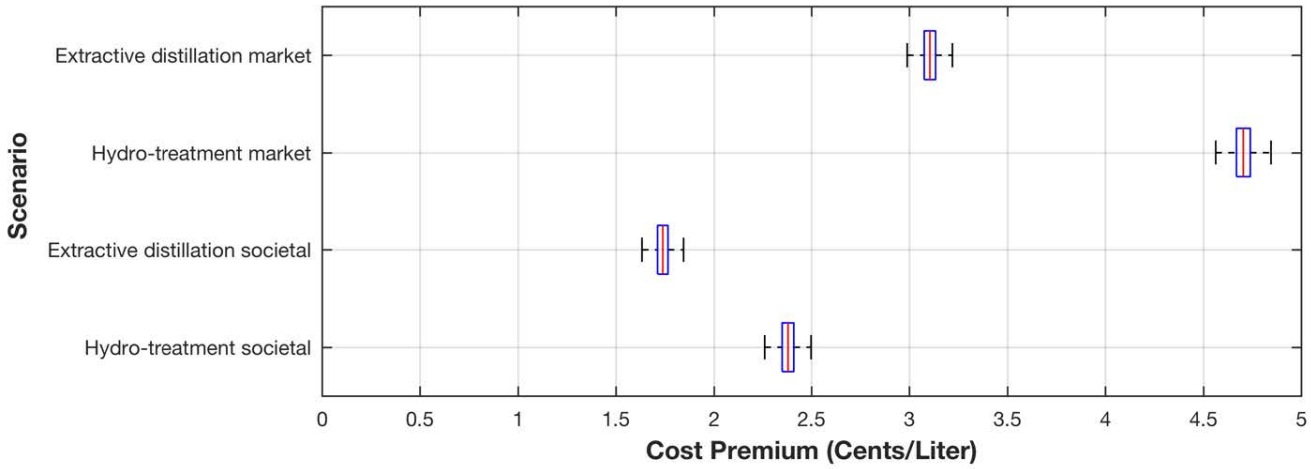


Figure 1. Boxplot for the societal and market cost premiums of hydro-treatment and extractive distillation. All values provided in cents/liter. Red markers represent the distribution means, blue boxes represents the first and third quartiles, and whiskers represent the 95% confidence interval.

Publications

This work is currently being prepared for publication as a paper entitled "Techno-economic Assessment of Removing Jet Fuel Naphthalene to Reduce Aviation-attributable Non-volatile Particulate Matter Emissions."

Outreach Efforts

Drew Weibel gave a presentation entitled "Naphthalene Removal Assessment: Cleaning up Jet Fuel for Reduced Environmental Impacts" at the CRC Aviation Meeting on May 3, 2018.

Student Involvement

This task was conducted primarily by Drew Weibel, working directly with Prof. Steven Barrett and Dr. Raymond Speth.

Plans for Next Period

This task has been completed.

Task 2- Explore Relationship Between PAH Formation and Aircraft PM Emissions

Massachusetts Institute of Technology

Objective(s)

The formation of black carbon (soot) from hydrocarbon fuels can be considered as taking place in two stages. First, fuel components and combustion intermediates react to form polycyclic aromatic hydrocarbons (PAHs). Large PAHs then act as soot nuclei, which grow as they absorb both PAH and other species, coagulate through collisions with other soot particles, carbonize, and partially oxidize (Richter and Howard 2000). The details of fuel composition mainly affect the first step of this process, the formation of PAHs. The objective of this task is to develop chemical kinetic mechanisms and combustor models which include the formation of PAH species from different fuel components and the conversion of these PAH species to soot particles (or nvPM emissions), in order to be able to evaluate the sensitivity of nvPM emissions to fuel composition.

Research Approach

The Reaction Mechanism Generator (RMG) was used to develop a detailed chemical kinetic mechanism for jet fuel combustion that includes the formation of PAH (Gao *et al* 2016). As part of this task, we have extended RMG to include recently-discovered PAH growth pathways, such as the phenyl addition pathway, cyclization via carbenes, and an aromatic-catalyzed intramolecular H-transfer mechanism. We then used this improved version of RMG to generate a higher-fidelity chemical kinetic model for the formation of PAHs in naphthalene-containing flames. This approach is being utilized to produce a chemical kinetic mechanism describing the first stage of soot particle production.

These mechanisms are then utilized within Cantera (Goodwin *et al* 2013), a combustion modelling framework, to compute PAH formation rates in fundamental combustion configurations. A schematic of the combustor model with the soot microphysical model is shown in Figure 2.

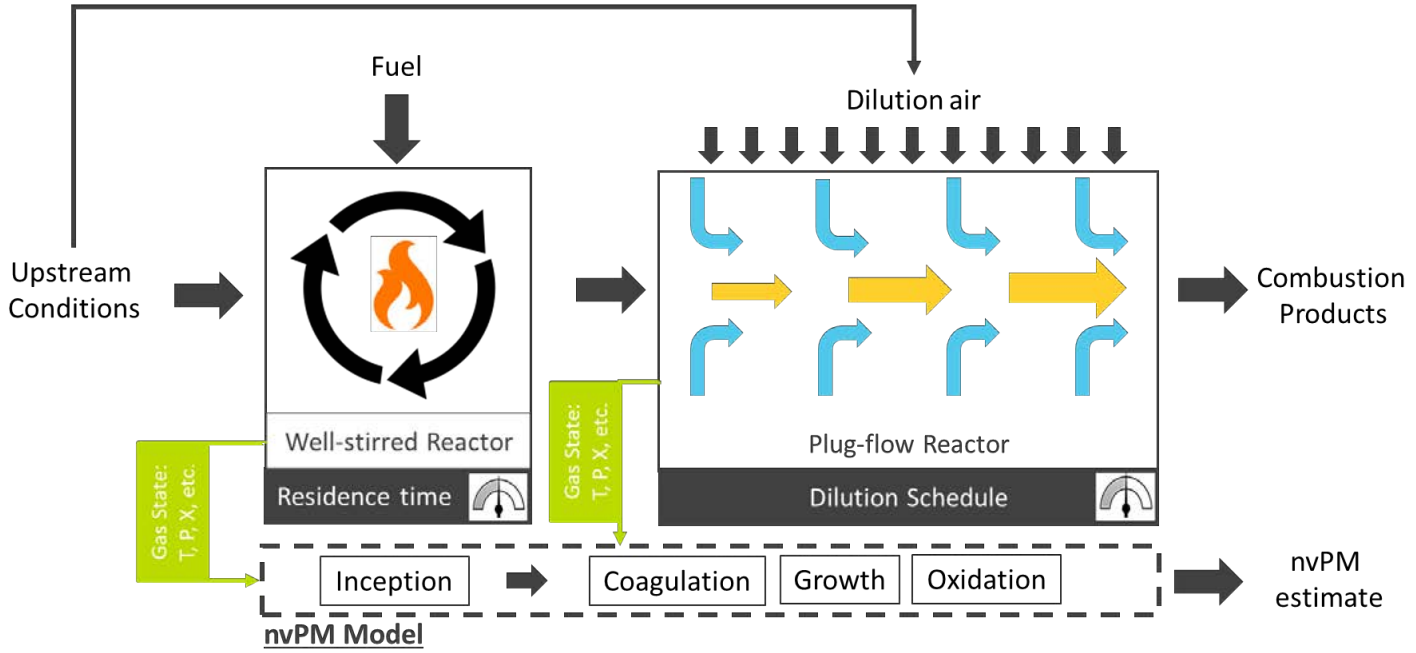


Figure 2. Schematic of a gas turbine combustor model including nvPM microphysical model

The second stage of soot formation is less well understood and more dependent on conditions within the combustor, such as fuel atomization and local temperature and pressure. In order to both capture differences between engines and avoid the uncertainties of modeling soot nucleation and growth processes, we have utilized existing analyses of PM emissions from aircraft engines to develop bounding scenarios describing the extent to which naphthalene removal results in decreases in expected PM emissions.

Milestone(s)

The work completed for this task was documented in Deliverable 2-2, provided to the FAA on February 28, 2018.

Major Accomplishments

The chemical kinetic mechanism and combustor model developed were used to calculate formation rates of PAH species over a range of engine relevant conditions. Figure 3 shows the evolution of several key aromatic species as the engine thrust setting is varied from near-idle to full power conditions for a representative surrogate fuel.

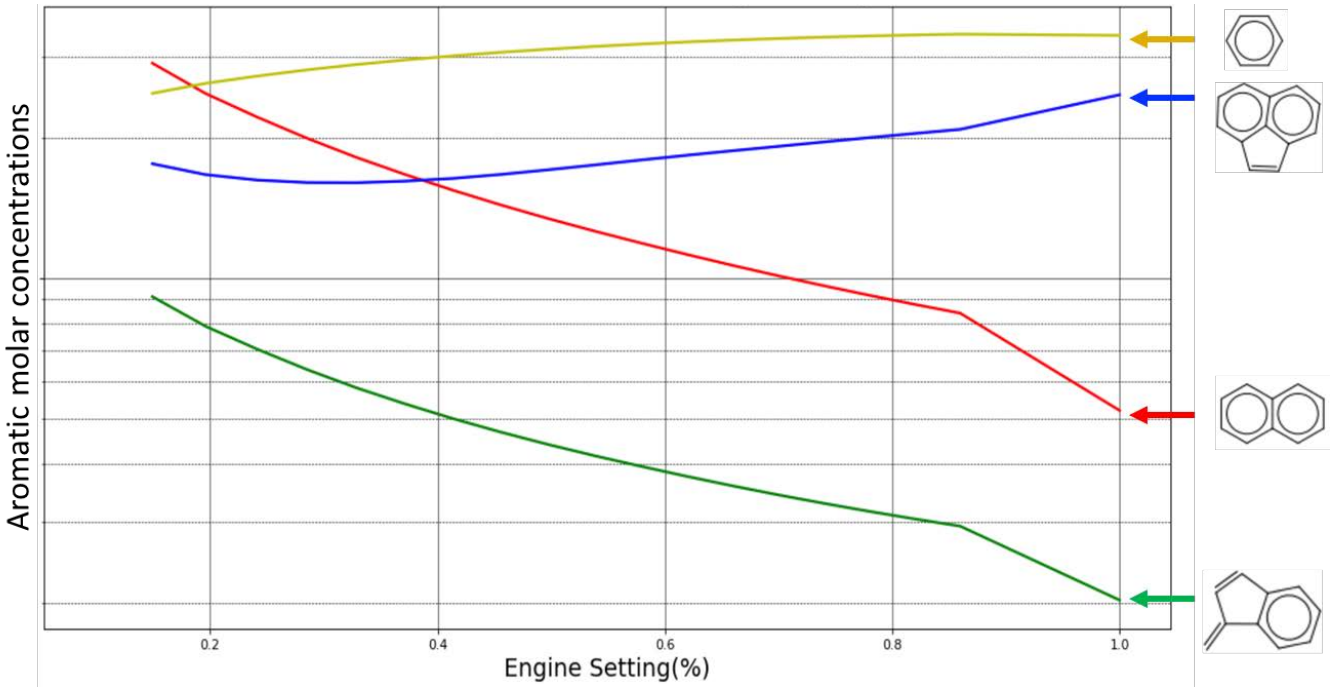


Figure 3. Evolution of selected aromatic species concentrations in the combustor primary zone as a function of engine setting.

Outreach Efforts

Raymond Speth gave a presentation with an overview of the project at the Aviation Emissions Characterization Roadmap Meeting on May 23, 2018.

Student Involvement

This task was conducted primarily by Drew Weibel, working directly with Prof. Steven Barrett and Dr. Raymond Speth.

Plans for Next Period

This task has been completed.

Task 3- Compare Kinetic Model Results to LFP/PIMS Experimental Data

Massachusetts Institute of Technology

Objective(s)

The growth of aromatic rings as part of PAH formation is controlled by radical reactions, especially the hydrogen abstraction – C_2H_2 addition (HACA) mechanism. The objective of this task is to produce experimental data which can be used to improve estimates of rate coefficients used in chemical kinetic models of PAH formation.

Research Approach

Laser flash-photolysis photoionization mass spectrometry (LFP/PIMS) is an experimental technique in which a photolysis laser pulse initiates controllable, quantifiable radicals in a temperature and pressure controlled reactor. The evolution of the chemical composition in the reactor is then monitored by ionization with VUV light and detection with a mass spectrometer. Experimental conditions are simulated using reactor modeling software, using rate coefficients estimated from the literature. Because these rate coefficients are often pressure dependent, quantum chemistry calculations are used to extrapolate from the low-pressure experimental values to the high pressures relevant to engine operations. Simulations

using RMG-generated mechanisms are compared with literature-based rates and the experimental results in order to improve important pathway parameters for aromatic growth.

For this task, two pathways were evaluated. The first is the addition of a vinyl radical (C_2H_3) to acetylene (C_2H_2), which is key step in a formation pathway for benzene (C_6H_6). Studying this system allows us to confirm that we can observe ring formation in our experiment, and measure the kinetics and branching ratios which describe C_4H_5/C_4H_4 formation and the yield of benzene, as shown in Figure 4.

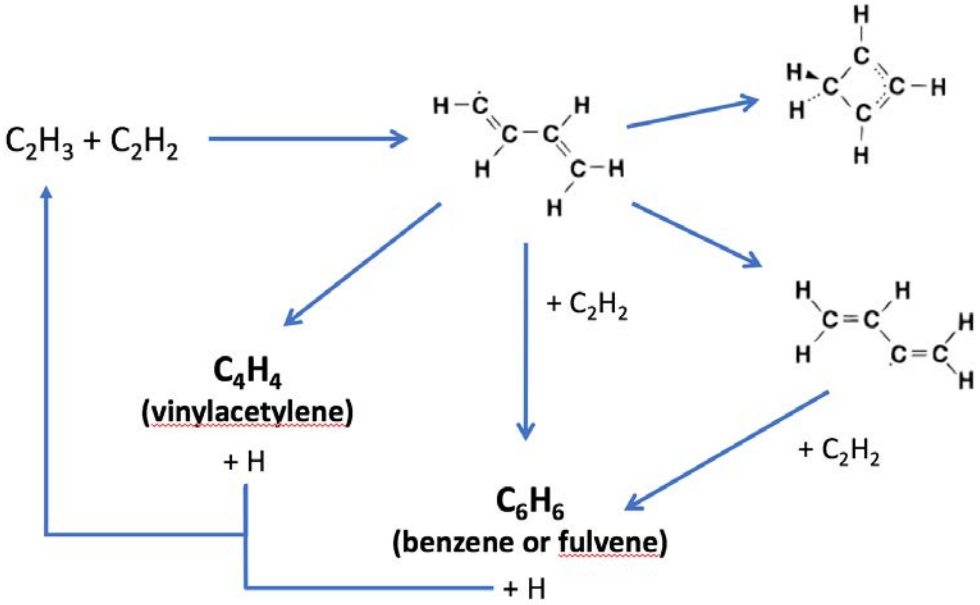


Figure 4. Formation pathways of benzene from vinyl radical and acetylene

The second pathway which was explored is acetylene addition to naphthyl radicals. While aromatic growth from naphthalene is thought to be dominate by the HACA mechanism, under experimental conditions, three-ring PAHs have generally not been observed. This leads to the question of what other pathways could exist that convert naphthalenes to PAHs, which can be explored using LFP-PIMS.

Milestone(s)

The work completed for this task was documented in Deliverable 2-3, provided to the FAA on April 30, 2018.

Major Accomplishments

Results for the vinyl radical – acetylene pathway, comparing experimental time profiles with simulations, are shown in Figure 5. Kinetics calculated from LFP-PIMS were found to generally agree with the results of the RMG-generated model over a range of temperatures. Preliminary experiments for 1-naphthyl addition to C_2H_2 revealed branching between stable $C_{12}H_8$ products (e.g. acenaphthalene) and $C_{12}H_9$ adducts, as shown in Figure 6. Work is ongoing to incorporate this finding into RMG.

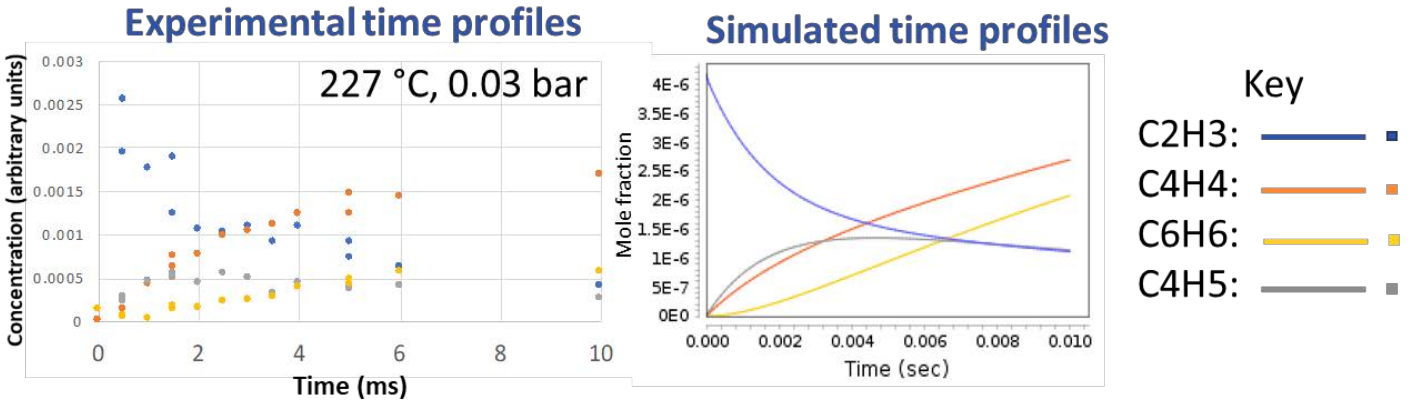


Figure 5. Comparison of experimental and simulated concentration profiles for reaction of vinyl radical and acetylene.

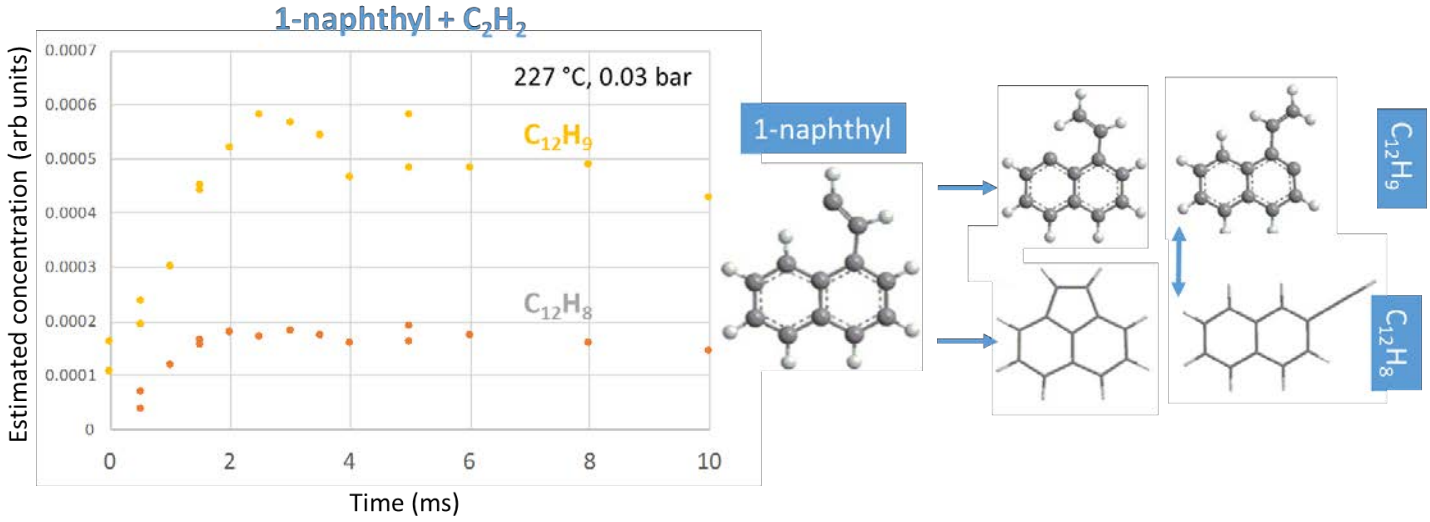


Figure 6. Experimentally-observed branching ratios between stable $C_{12}H_8$ species and $C_{12}H_9$ adducts formed by the reaction of 1-naphthyl radicals with acetylene.

Student Involvement

This work was conducted primarily by Dr. Mica Smith, a postdoctoral associate working under the supervision of Prof. William Green.

Plans for Next Period

This task has been completed.

Task 4- Calculate Air Quality and Climate Impacts of Naphthalene Removal

Massachusetts Institute of Technology

Objective(s)

The objective of this task is to calculate the air quality and climate impacts of a policy in which naphthalene is removed from jet fuel used in the United States.

Research Approach

The air quality effects of changes in aircraft PM emissions are evaluated using the GEOS-Chem adjoint model, which we have previously used for assessing health impacts of emissions (Dedoussi and Barrett 2014). The use of an adjoint model, which is a computationally-efficient approach to calculating sensitivities of an aggregate objective function (e.g. population exposure to $PM_{2.5}$), makes it possible to evaluate a range of scenarios in a single run, which allows incorporation of upstream uncertainty in the emissions indices for different species. The PM exposure calculated using GEOS-Chem includes both the effects of changes in black carbon emissions and changes due to sulfur reductions which accompany the removal of naphthalenes (in the case where hydrotreating is used to remove naphthalenes). The spatial pattern of emissions of nvPM, and sulfur compounds is taken from the 2015 inventory from the Aviation Environmental Design Tool (AEDT).

Climate impacts of naphthalene removal include contributions both at the fuel production and fuel consumption stages. The additional refinery processing required to reduce or remove naphthalene requires process fuel, steam, electricity, and, in the case of hydrotreating, hydrogen production. The greenhouse gas (GHG) emissions associated with each of these processes increase lifecycle jet fuel GHG emissions. Using the results calculated in Task 1, the GHG emissions associated with naphthalene removal were found to be 135 g CO_2e per kg fuel for hydro-treating and 144 g CO_2e per kg fuel for extractive distillation. Consumption of reduced-naphthalene fuel decreases radiative forcing from aviation black carbon, while reductions in sulfur reduce the cooling effect of sulfates (Mahashabde *et al* 2011). The combined climate impacts of these effects are evaluated using the APMT-Impacts Climate model, which is a policy-oriented rapid assessment tool that provides probabilistic estimates of climate impacts.

Milestone(s)

The work completed for this task was documented in Deliverable 2-4, provided to the FAA on May 31, 2018.

Major Accomplishments

Based on a literature review of nvPM emissions measurements from engines using fuels with varying levels of naphthalene (DeWitt *et al* 2008, Brem *et al* 2015), the potential range of reduction in nvPM emissions associated with 95% naphthalene removal was estimated to be 15–40%, or 5.0–12.5 mg nvPM per kg fuel. Monetized climate impacts for the different climate forcing pathways are summarized in Table 1, presented on a cents per gallon basis with both median values and a range indicating the 90% confidence interval. Monetized air quality impacts of naphthalene removal are similarly summarized in Table 2.

Table 1. Monetized climate benefits of naphthalene removal

Impact Pathway	Impact (¢/gallon)
BC radiative forcing (15% nvPM reduction)	0.09 (90% CI: 0.01 – 0.23)
BC radiative forcing (40% nvPM reduction)	0.23 (90% CI: 0.04 – 0.61)
Hydrotreating CO_2 emissions	-1.82 (90% CI: -0.30 – -4.70)
Extractive distillation CO_2 emissions	-1.89 (90% CI: -0.31 – -5.01)
Sulfate aerosol (hydrotreating only)	-4.17 (90% CI: -0.61 – -11.23)

Table 2. Monetized air quality benefits of naphthalene removal

Impact Pathway	Impact (¢/gallon)
nvPM emissions (15% nvPM reduction)	0.04 (90% CI: 0.02 – 0.06)
nvPM emissions (40% nvPM reduction)	0.11 (90% CI: 0.06 – 0.16)
Sulfur emissions (hydrotreating only)	1.92 (90% CI: 1.04 – 2.76)

Student Involvement

This task was conducted primarily by Drew Weibel, working directly with Prof. Steven Barrett and Dr. Raymond Speth.

Plans for Next Period

This task has been completed as originally planned. The current results do not include the effect that changes in nvPM emissions have on contrails, which are a significant component of aviation's climate impact. As such, additional work has been planned to estimate changes in contrail radiative forcing associated with the use of naphthalene-depleted fuels using the Contrail Evolution and Radiation Model (Caiazzo *et al* 2017). In addition, the air quality results are based on a regional atmospheric model, simulated at a resolution of 0.5˚ × 0.667˚, while nvPM impacts have been shown to be underestimated with lower-resolution models (Punger and West 2013). Additional work has been planned to provide better estimates of these impacts based on higher-resolution local modeling approaches.

Task 5- Conduct Integrated Cost-benefit Analysis of Impacts of Naphthalene Removal in the U.S.

Massachusetts Institute of Technology

Objective(s)

The objective of this task is to produce an integrated cost-benefit analysis of naphthalene removal in the United States, accounting for the additional refining cost as well as the air quality and climate impacts.

Research Approach

The overall cost benefit assessment of naphthalene removal includes fuel production costs, air quality benefits, and climate impacts from fuel production and fuel consumption. These effects are placed on a common monetized basis in order to compare different naphthalene removal scenarios. We consider uncertainties in the assessment of each component and use these uncertainties to compute the likelihood of a net benefit for different scenarios.

Milestone(s)

The work completed for this task was documented in Deliverable 2-5, provided to the FAA on July 31, 2018.

Major Accomplishments

The processing costs, air quality benefits, and climate impacts of naphthalene removal are converted to a common basis of cents per gallon, and presented in Table 3. The totals shown exclude contrail effects, which have not yet been quantified. In the absence of large impacts on contrail net radiative forcing, the current results suggest that the benefits of widespread naphthalene removal are outweighed by the costs of processing the fuel and the CO_2 emissions associated with that processing.

Table 3. Costs (positive) and benefits (negative) of naphthalene removal.

	Component	Hydrotreatment (¢/gallon)		Extractive Distillation (¢/gallon)	
Air quality	nvPM	-0.1	(-0.02 – -0.16)	-0.1	(-0.02 – -0.16)
	Fuel sulfur	-1.9	(-1.1 – -2.7)	0	
Climate	nvPM	-0.2	(-0.02 – -0.6)	-0.2	(-0.02 – -0.6)
	Fuel sulfur	4.1	(0.6 – 11.1)	0	
	Contrails	*unknown*		*unknown*	
	Refinery CO_2	1.9	(0.3 – 4.8)	1.9	(0.3 – 5.1)
Processing	Refinery	9.1	(8.7 – 9.5)	6.4	(6.1 – 6.8)
Total		**13.0**	**(9.0 – 20.7)**	**8.1**	**(6.5 – 11.4)**

For both naphthalene removal processes, the climate impacts of the refinery CO_2 emissions exceed the air quality and climate benefits of naphthalene removal, neglecting the potential for significant contrail effects. In addition, in the case of hydrotreatment, the net present value of the climate warming associated with sulfur removal is larger than the NPV of the reduced air-quality related damages. In addition to these environmental costs are the costs associated with processing jet



fuel in the refinery. These results suggest that, in the absence of a strong contrail effect, it is unlikely that naphthalene removal on a nationwide basis would be cost beneficial. However, naphthalene removal may still be beneficial under certain circumstances, e.g. if applied to fuels used at airports with particular air quality concerns.

Student Involvement

This task was conducted primarily by Drew Weibel, working directly with Prof. Steven Barrett and Dr. Raymond Speth.

Plans for Next Period

This task, as originally planned, has been completed. Future work includes incorporating estimates of the effect of naphthalene on contrail climate impacts, as well as the potential to evaluate scenarios where naphthalene is removed only at certain places or times in order to maximize the benefit, e.g. targeting fuel used at specific airports.

References

ASTM D1655 2016 *Standard Specification for Aviation Turbine Fuels* (West Conshohocken, PA: ASTM International) Online: https://doi.org/10.1520/D1655-16C

Brem B T, Durdina L, Siegerist F, Beyerle P, Bruderer K, Rindlisbacher T, Rocci-Denis S, Andac M G, Zelina J, Penanhoat O and Wang J 2015 Effects of Fuel Aromatic Content on Nonvolatile Particulate Emissions of an In-Production Aircraft Gas Turbine *Environ. Sci. Technol.* **49** 13149–57

Caiazzo F, Agarwal A, Speth R L and Barrett S R H 2017 Impact of biofuels on contrail warming *Environ. Res. Lett.* **12** 114013

Dedoussi I C and Barrett S R H 2014 Air pollution and early deaths in the United States. Part II: Attribution of PM2.5 exposure to emissions species, time, location and sector *Atmos. Environ.* **99** 610–7

DeWitt M J, Corporan E, Graham J and Minus D 2008 Effects of Aromatic Type and Concentration in Fischer−Tropsch Fuel on Emissions Production and Material Compatibility *Energy Fuels* **22** 2411–8

DLA Energy 2013 *Petroleum Quality Information System 2013 Annual Report*

Gao C W, Allen J W, Green W H and West R H 2016 Reaction Mechanism Generator: Automatic construction of chemical kinetic mechanisms *Comput. Phys. Commun.* Online: http://www.sciencedirect.com/science/article/pii/S0010465516300285

Goodwin D G, Moffat H K and Speth R L 2013 *Cantera: An object-oriented software toolkit for chemical kinetics, thermodynamics, and transport processes* (http://www.cantera.org)

Mahashabde A, Wolfe P, Ashok A, Dorbian C, He Q, Fan A, Lukachko S, Mozdzanowska A, Wollersheim C, Barrett S R H, Locke M and Waitz I A 2011 Assessing the environmental impacts of aircraft noise and emissions *Prog. Aerosp. Sci.* **47** 15–52

Moore R H, Shook M, Beyersdorf A, Corr C, Herndon S, Knighton W B, Miake-Lye R, Thornhill K L, Winstead E L, Yu Z, Ziemba L D and Anderson B E 2015 Influence of Jet Fuel Composition on Aircraft Engine Emissions: A Synthesis of Aerosol Emissions Data from the NASA APEX, AAFEX, and ACCESS Missions *Energy Fuels* **29** 2591–600

Punger E M and West J J 2013 The effect of grid resolution on estimates of the burden of ozone and fine particulate matter on premature mortality in the USA *Air Qual. Atmosphere Health* **6** 563–73

Richter H and Howard J B 2000 Formation of polycyclic aromatic hydrocarbons and their growth to soot—a review of chemical reaction pathways *Prog. Energy Combust. Sci.* **26** 565–608



Project 040 Quantifying Uncertainties in Predicting Aircraft Noise in Real-world Scenarios

The Pennsylvania State University
Purdue University

Project Lead Investigator

Victor W. Sparrow
Director and United Technologies Corporation Professor of Acoustics
Graduate Program in Acoustics
The Pennsylvania State University
201 Applied Science Bldg.
University Park, PA 16802
+1 (814) 865-6364
vws1@psu.edu

University Participants

Pennsylvania State University

- P.I.: Victor W. Sparrow, United Technologies Corporation Professor of Acoustics
- Co-PI: Philip J. Morris, Boeing/A.D. Welliver Professor of Aerospace Engineering
- FAA Award Number: 13-C-AJFE-PSU, Amendment 32
- Period of Performance: August 7, 2017 through December 31, 2018
- Task(s):
  Quantifying the effect of uncertainty in meteorological conditions on aircraft noise propagation using techniques demonstrated by Wilson et al. (2014)[1]

Purdue University

- P.I.(s): Kai Ming Li, Professor of Mechanical Engineering
- FAA Award Number: 13-C-AJFE-PU, Amendment 20
- Period of Performance: August 7, 2017 through December 31, 2018
- Task(s):
  1. Validate the noise model capabilities of AEDT by comparing numerical results with field data
  2. Quantify uncertainties of both model prediction and measurement in trying to predict aircraft noise (or pattern of change) in real world

Project Funding Level

FAA funding to Penn State in 2017-2018 is $110K. FAA funding to Purdue in 2017-2018 is $90K.

Cost sharing this year for ASCENT Project 40 was from ANOTEC Engineering, Motril, Spain regarding the BANOERAC data set. An in-kind cost share of $115K was provided to both Penn State and Purdue, for a cost share total of $230K. The point of contact for this cost sharing is Nico van Oosten, nico@anotecengineering.com.

Additional cost sharing from Airbus is in negotiation for next year in ASCENT Project 40 with respect to the SILENCE-R data set. The primary point of contact for that proposed cost sharing is Pierre Lempereur, pierre.lempereur@airbus.com, and the technical contact is Sasha Zaporozhets, zap@nau.edu.ua, of National Aviation University, Ukraine.

Investigation Team

Pennsylvania State University

Victor W. Sparrow (PI)

Philip J. Morris (Co-PI)
Graduate Research Assistant Harshal Patankar
Purdue University
Kai Ming Li (PI)
Graduate Research Assistant Yiming Wang

Project Overview

The purpose of this project is to understand the uncertainty in the prediction of noise of aircraft. Many ways of calculating aircraft noise are available. Also many experimental datasets have been obtained to assess aircraft noise. ASCENT Project 40 is developing methods that could later be used in FAA tools for predicting aircraft noise. There are three goals for the work of the current year:

(1) Extend the uncertainty methods of Wilson, et al. (2014) and other algorithms to realistic aircraft trajectories and meteorology in the atmosphere, and comparing the calculated results with field data already acquired in the Vancouver Airport Authority, BANOERAC, and SILENCE(R) databases (Penn State);
(2) Validate the noise model capabilities of AEDT by comparing numerical results with field data (Purdue);
(3) Quantify uncertainties of both model prediction and measurement in trying to predict aircraft noise in real world (Purdue).

In addition, a collaborative initiative with National Aviation University of Ukraine is continued and a new close cooperation with Georgia Tech on ASCENT Project 43 was initiated.

If successful, the ASCENT Project 40 research will develop methodologies that should be implemented in FAA tools for predicting aircraft noise in the presence of real world weather. By having more accurate and faster predictions and predictions that were verified with field data, the project will allow FAA to more accurately predict the potential noise impacts when making decisions regarding FAA federal actions, such as in the site-ing of new runways and implementing new landing approach and take-off patterns over populated areas.

This research aims to enhance the accuracy of AEDT through improved aircraft noise propagation modeling. This improvement is needed to support the evaluation and development of aircraft flight routes and procedures that could reduce community noise. These improvements will also facilitate the implementation of NextGen through improved characterization of the efficiency benefits it would deliver.

Task 1- Quantifying the Effect of Uncertainty in Meteorological Conditions on Aircraft Noise Propagation Using Techniques Demonstrated by Wilson et al. (2014)[1]

Pennsylvania State University

Objective(s)

This research seeks to not only to validate current FAA/Volpe noise modeling capabilities by comparing with measurement data, but also to quantify uncertainties of both model prediction and measurement in trying to predict aircraft noise (or patterns or changes) in real world situations, particularly when meteorological conditions over various different time periods may affect prediction output. The research will (1) review and analyze available field measurement data for patterns that are influenced by the (change of) meteorological conditions; (2) identify sets of field data for specific scenarios that contain proper parameters/quality input values to validate the enhanced modeling capabilities; (3) use the enhanced modeling capabilities to understand the patterns identified in the field measurement data that are influenced by the (change of) meteorological conditions and (4) quantify uncertainties in predicting aircraft noise in real-world situations. In addition, a new collaborative initiative on aircraft noise propagation model validation is continuing with National Aviation University, Kiev, Ukraine.

Research Approach

Introduction

Accurate prediction of aircraft noise is necessary for complying with noise regulations and for planning infrastructure around airports. To address these needs, sophisticated noise propagation models which account for the aircraft state, complexities in the propagation path and the ground condition are being developed. This necessitates addressing how the uncertainties in inputs for these high-fidelity models affect the predicted noise levels. The work presented here focuses on the effect of uncertainties in the meteorological conditions on the aircraft noise levels as received near the ground. Typically, simplified meteorological profiles, such as homogeneous or constant gradient, are used as inputs to the noise propagation models. The variation in meteorological profiles away from the mean values needs to be accounted for, to arrive at better estimates of the noise levels.

Wilson et al. (2014)[1] have demonstrated an approach to quantify the effect of uncertainties for near-ground outdoor sound propagation using the method of expected values and stochastic sampling techniques. These techniques have also been successfully employed recently[2] to address the variability in wind turbine noise which occurs because of the changes in wind velocity and direction. The work presented here extends the methodology to the geometry of aircraft noise propagation and addresses the effect of meteorological uncertainties on aircraft noise propagation.

Problem description (Assumed meteorological conditions and sound speed profile)

For this work, the profiles of temperature and wind are assumed to be range-independent. For simplicity, the relative humidity is assumed to be both height-independent and range-independent. A linear temperature profile is assumed as given by Eqn. (40.1) where L is the lapse rate and z is the height from the ground. A logarithmic wind speed profile is assumed to represent the eastward wind speed u(z) as given by Eqn. (40.3), where z_0 is the roughness length. The value of roughness length z_0 is set to 0.02 m which is a typical value for flat terrain covered with grass. The equivalent sound speed profile resulting from the assumed meteorological conditions is obtained by Eqn. (40.4) and Eqn. (40.5).

$$T(z) = T(z)|_{z=0} + Lz \tag{40.1}$$

$$c(z) = c_0\sqrt{\frac{273.15 + T(z)}{T_0}} \quad \text{where, } c_0 = 331\,\text{m/s and } T_0 = 273.15 \tag{40.2}$$

$$u(z) = b\ln\left(\frac{z}{z_0} + 1\right) \tag{40.3}$$

$$c_{\text{eff}}(z) = c(z) + u(z) \quad \text{(for eastward propagation)} \tag{40.4}$$

$$c_{\text{eff}}(z) = c(z) - u(z) \quad \text{(for westward propagation)} \tag{40.5}$$

Table 1. Gaussian uncertainty in the meteorological parameters.

Parameter	Units	Mean (μ)	Std. deviation (σ)
Temperature at the ground $T(z)\|_{z=0}$	°C	-3	3.7
Lapse rate L	°C/km	-4	1.5
Parameter b in the wind profile	m/s	1.1	0.6
Relative humidity r_h	%	85	4.5

Instead of expressing the parameters representing the meteorological profiles (e.g. the lapse rate L) by their mean values, they are expressed as probability density functions i.e. distributions of values with varying probability of occurrence. For simplicity, the Gaussian function is assumed to describe the uncertainties. The mean values and the standard deviations describing the probability density functions for the meteorological parameters are given in Table 1. These values are estimates based on the six-hourly data measured in January 2011 (State College, PA, USA). Figure 1 shows the effective sound speed profile obtained with Eqn. (40.4) and Eqn. (40.5) for the mean values of the meteorological parameters.

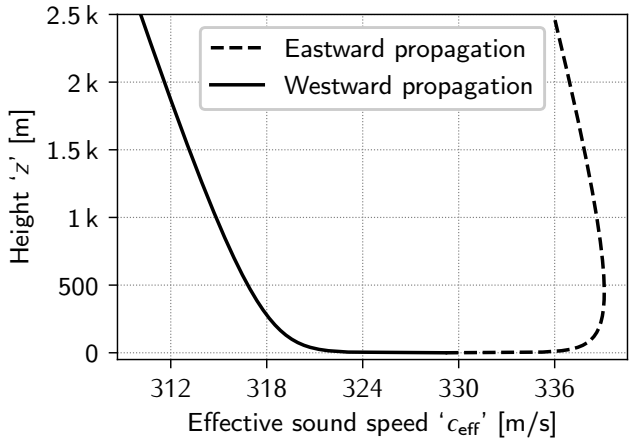


Figure 1. Effective sound speed profiles corresponding to the mean values of temperature and wind profiles.

Problem description (Source and receiver)

A retrofitted sound-power-level spectrum of a Boeing 777-300 (maximum thrust, departure setting)[3] is used to represent an omni-directional source. The spectral content between 50 Hz to 2000 Hz is considered for calculations since higher frequencies are attenuated by atmospheric absorption and don't contribute significantly to the overall sound pressure levels. The sound power spectrum for one-third octave bands is shown in Figure 2.

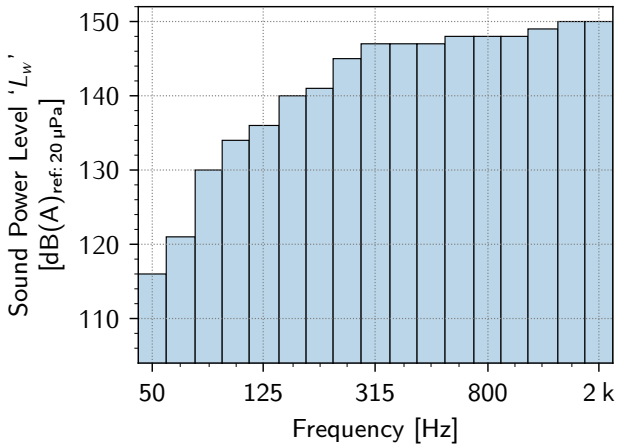


Figure 2. Retrofitted Boeing 777-300 sound power level spectrum (maximum thrust, departure setting)[3]

The receiver height z_r is set to 1.2 m and three different source heights z_s (1.0 km, 1.5 km, 2.0 km) are considered for the calculations. Propagation calculations are performed over a 10 km range (5 km each for eastward and westward propagation).

Problem description (Ground properties)

Attenborough's four-parameter model[4] is used to represent a soft ground with static flow resistivity σ = 200 kPa.s/m^2, the porosity Ω = 0.27, the grain shape factor g = 0.5 and the pore shape factor s_f = 0.75. The ground properties are assumed to be independent of the range.

Methodology (Approach for incorporating the effect of meteorological uncertainties)

Let R[x, z_r, f, ϕ_1, $\cdots$, ϕ_m] be the power spectral density [Pa^2/Hz] of the sound pressure level received at range x, receiver height z_r, the frequency f and for the meteorological variables ϕ_1, $\cdots$, ϕ_m (such as lapse rate, temperature at the ground). If



the mean values of the meteorological variables are used as a representation of the reality, then Eqn. (40.6) would give the overall sound pressure level (SPL) at the receiver.

$$\Pi(x,z_r)=\int_{f_{\min}}^{f_{\max}} R[x,z_r,f,\underbrace{\phi_1,\cdots,\phi_m}_{\text{mean values}}]\,df \tag{40.6}$$

The approach shown by Eqn. (40.6) neglects the deviations of meteorological variables from their mean values. It would be more realistic to use the expected value of the received SPL $\langle\Pi(x,z_r)\rangle$ which incorporates the effect of the uncertainties, as given by Eqn. (40.7).

$$\langle\Pi(x,z_r)\rangle=\int_{f_{\min}}^{f_{\max}}\int_{-\infty}^{\infty}\cdots\int R\left[x,z_r,f,\phi_1,\cdots,\phi_m\right]\,g_{\phi_1}(\phi_1)\cdots g_{\phi_m}(\phi_m)\,d\phi_1\cdots d\phi_m\,df \tag{40.7}$$

In Eqn. (40.7), '$g\phi_1(\phi_1), \cdots, g\phi_m(\phi_m)$' are the probability density functions (PDFs) for the uncertain variables $\phi_1, \cdots, \phi_m$ respectively. The uncertain variables are assumed to vary independently, hence their combined probability density function is equal to the product of the individual PDFs. It is clear from Eqn. (40.7) that adding more uncertain variables would imply more dimensions added to the integral for obtaining the expected SPL. An efficient approach to handle such multi-dimensional integrals is to use stochastic sampling techniques. To proceed with this approach, it is convenient to normalize the limits of integration. This is achieved by using normalized frequency ν as given by Eqn. (40.8) and cumulative density functions as given by Eqn. (40.9).

$$\nu=[\ln(f)-\ln(f_{\min})]/\Delta_f,\quad \text{where } \Delta_f=\ln(f_{\max})-\ln(f_{\min}) \tag{40.8}$$

$$G_{\phi_m}(\phi_m)=\int_{-\infty}^{\phi_m} g_{\phi_m}(\phi_m)\,d\phi_m \tag{40.9}$$

After the change of variables, Eqn. (40.7) changes to Eqn. (40.10). After this, stochastic sampling techniques can be used to draw N random samples from each dimension of the integral and the integral is approximated as given by Eqn. (40.11).

$$\langle\Pi(x,z_r)\rangle=\int_0^1\cdots\int R\left[x,z_r,f(\nu),\phi_1\left(G_{\phi_1}\right),\cdots,\phi_m\left(G_{\phi_m}\right)\right]f(\nu)\Delta_f\,dG_{\phi_1}\cdots dG_{\phi_m}\,d\nu \tag{40.10}$$

$$\langle\Pi(x,z_r)\rangle\simeq\frac{1}{N}\sum_{n=0}^{N-1} R\left[x,z_r,f(\nu_n),\phi_1\left(G_{\phi_1,n}\right),\cdots,\phi_m\left(G_{\phi_m,n}\right)\right]f(\nu_n)\Delta_f \tag{40.11}$$

It is important to note the interpretation of the presented mathematical procedure. Each random sample represents a set of values of all the uncertain variables and the frequency. The values for uncertain variables are drawn based on their cumulative density functions, which is an indirect way of applying the probability density functions. The advantage of this approach is that any method can be used for the propagation calculations.

Methodology (Wave propagation method)

In this work, a wide-angle Crank-Nicolson Parabolic Equation[4,5] (CNPE) method is used as the propagation method. This method is chosen because it solves the exact one-way wave equation (neglecting back-scattering) and is accurate even for the low frequencies. The only caveat is that the angle limitation of CNPE restricts the usable numerical grid to elevation angles less than 35° as illustrated in Figure 3.

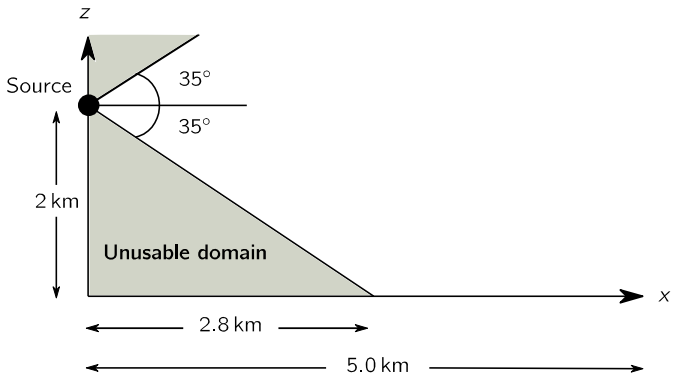


Figure 3. Angle limitation of CNPE method. Outside of the 35° elevation angle shown, the CNPE results are unreliable and such results are not included in the analysis.

Methodology (Atmospheric absorption)
This work assumes a rather simple approach to account for the attenuation due to atmospheric absorption. Attenuation due to atmospheric absorption is calculated using ISO 9613-1, based on (1) the value of relative humidity (which is allowed to vary), (2) the average temperature across the vertical profile (which varies with ground temperature and lapse rate), and (3) the geometric distance between the source and the receiver. For third-octave band calculations, the SAE-ARP-5534 method[6,7] is used to correctly account for the absorption.

Numerical experiments
Using the methodology explained in the previous section, numerical experiments are performed for three different aircraft heights (z_s = 1.0 km, 1.5 km, 2.0 km). For each aircraft height, four types of scenarios are considered i.e. (1) with no uncertainty in meteorological conditions (2) with uncertainty in temperature profile and relative humidity (3) with uncertainty in wind profile and (4) with uncertainty in temperature, wind profile and relative humidity. The results are shown in Figures.4 to 7.

Numerical experiments with no uncertainty in meteorological conditions are performed for 17 third-octave bands between 50 Hz and 2000 Hz. For numerical experiments which include the effect of uncertainties, 102 samples obtained using 'Latin Hypercube Sampling' (LHS) are used. The LHS method is chosen rather than the ordinary Monte-Carlo sampling since it has been shown1 to be more accurate when the uncertainties involved are reducible (as is the case for this work). In general, it is challenging to determine the number of samples required to obtain accurate estimates using stochastic sampling techniques. The number of samples required does not necessarily de- pend on the number of uncertainties (since all the uncertain variables are handled simultaneously). It does depend on the sensitivity of the propagation calculation to the uncertain variables.

One way to check the accuracy of the estimated SPLs is to rely on confidence intervals obtained using the Bootstrap sampling method[1]. But, the use of Bootstrap sampling requires large number of samples obtained using the ordinary Monte-Carlo sampling. Hence in this work, the accuracy of the estimated SPLs obtained using 102 LHS samples is checked by repeating the numerical experiments 10 times and calculating the RMS errors to see if they fall within acceptable limits (shown in Figure 7).

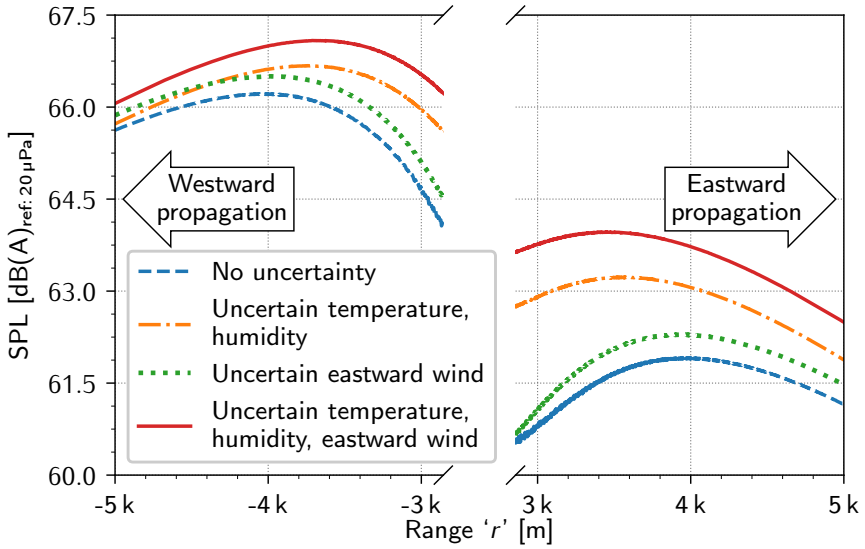


Figure 4. Effect of meteorological uncertainties on the received SPL for 2.0 km aircraft altitude. SPLs for eastward and westward propagation are shown on the right and left side of the plot respectively.

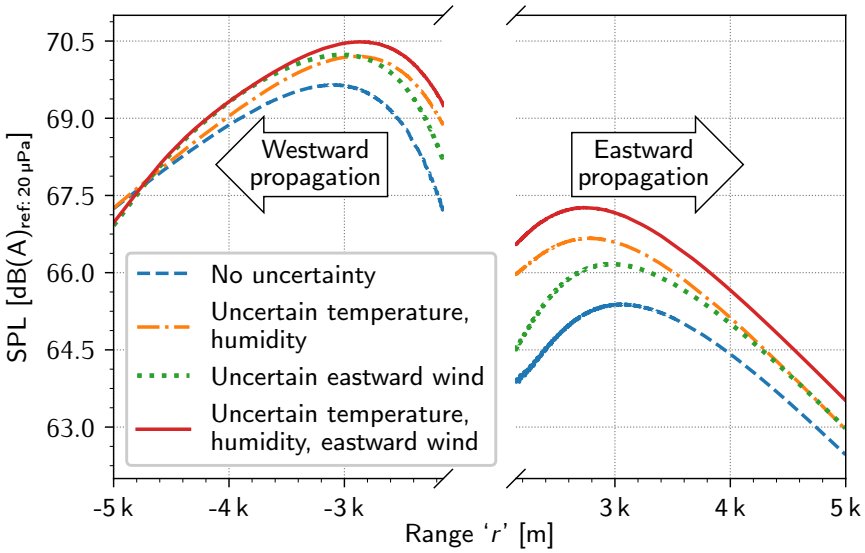


Figure 5. Effect of meteorological uncertainties on the received SPL for 1.5 km aircraft altitude. SPLs for eastward and westward propagation are shown on the right and left side of the plot respectively.

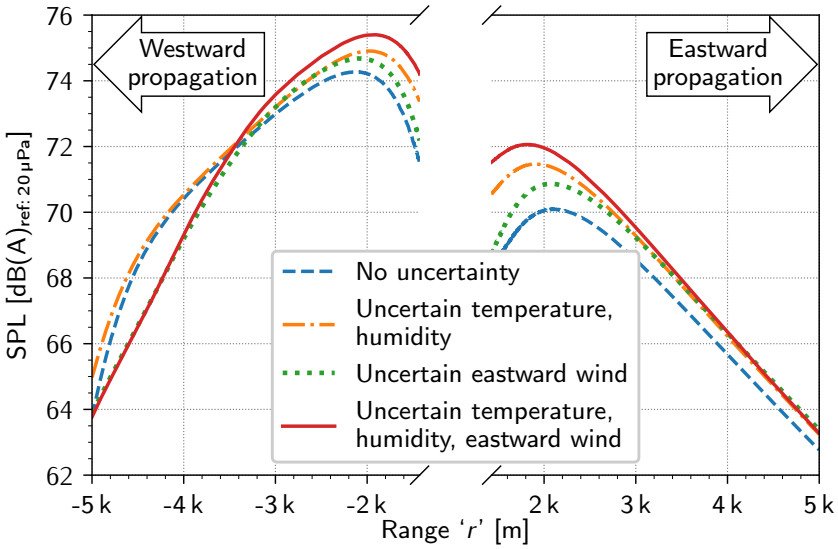


Figure 6. Effect of meteorological uncertainties on the received SPL for 1.0 km aircraft altitude. SPLs for eastward and westward propagation are shown on the right and left side of the plot respectively.

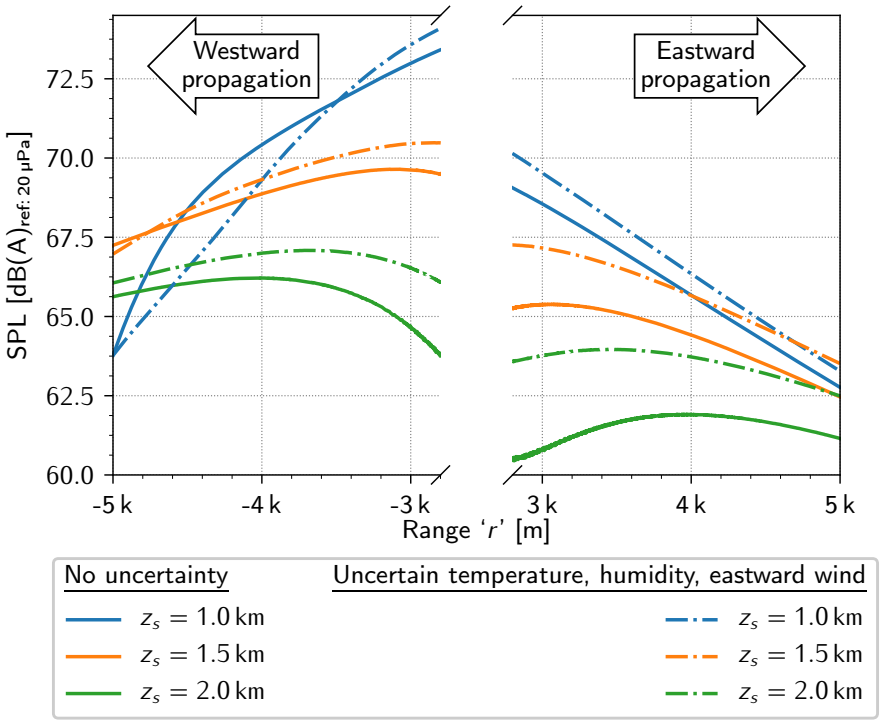


Figure 7. Effect of meteorological uncertainties on received SPLs for aircraft heights 1.0 km, 1.5 km, 2.0 km. Received SPLs for the no uncertainty cases are shown for comparison.

Results and discussion

1. Looking at Figures 4 to 6, for a fixed source height, the effect of meteorological uncertainties seems to fade away as the distance between the source and the receiver is increased. This might be attributed atmospheric absorption, which increases with propagation distance and dominates over the effect of uncertainties. An exception to this observation can be seen for the westward propagation scenario. In the case of westward propagation, the effect of temperature lapse and wind adds up resulting in stronger upward refraction (see Fig. (40.1)). When the source height is lowered, upward refraction starts to play a noticeable role (e.g. around 3.5 km westward propagation for aircraft height 1.0 km as seen in Fig. (40.6)).

2. Uncertainty in the wind profile alone seems to have a lesser effect on the received SPL when compared to the effect of uncertainty in temperature and humidity profile.

3. Figure 7 shows the comparison of results obtained for three different aircraft heights (1.0 km, 1.5 km, 2.0 km) when all the meteorological uncertainties are considered simultaneously. It is evident that the effect of meteorological uncertainties is more pronounced when the source height is increased. This makes intuitive sense because increased source height implies a longer propagation path which allows for more exposure to the uncertainties in meteorological profiles.

4. Figure 8 shows the RMS errors in the estimated SPLs (obtained by repeating the numerical experiments 10 times). It can be seen that the errors are less than 0.4 dB in all the cases. This implies that the estimations of the SPLs obtained using 102 LHS samples are reliable. The increase in RMS error for westward propagation in the case of z_s = 1.0 km can be attributed to the strong upward refraction (and its sensitivity to temperature and wind profile) as explained previously.

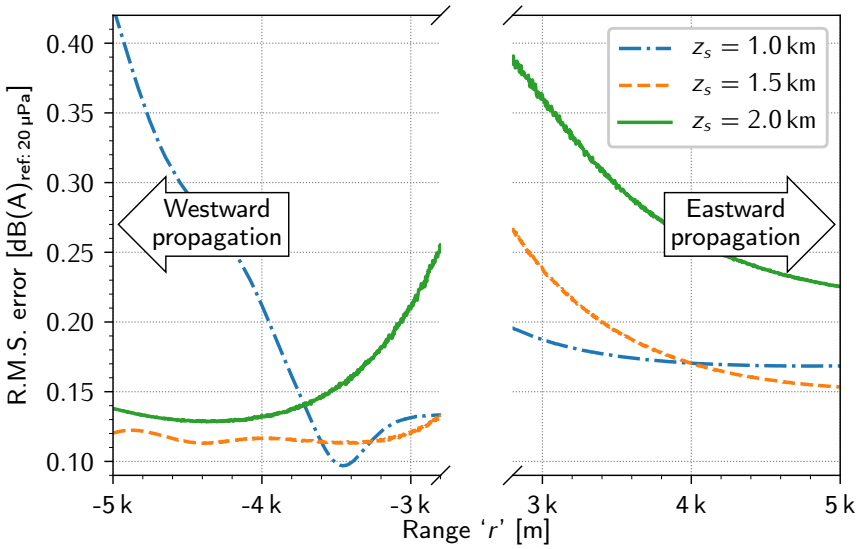


Figure 8. R.M.S. error in the estimation of SPL when uncertainties in temperature, humidity, wind are considered and 102 LHS samples are used. Since the RMS errors are below 0.4dB, the results obtained using 102 LHS samples are reliable.

Supporting investigations on source and directivity effects

Penn State also provided reviews and recommendations concerning the interpretation of the Discover A/Q acoustics data ongoing at Purdue University. In particular it was noted that the effects of source variation on the spiral flight paths could be minimized by taking data samples when the aircraft was travelling on a section of the flight path where it was normal to the observation station. If the source directivity is assumed to be symmetric about the aircraft, from port to starboard, then the differences in spectra, when allowance is made for the different propagation distances, should be dominated by propagation effects. Input was also provided on the likely directivity of a propeller-driven aircraft to assist in the choice of multipoles to be used in the source modeling.



Milestone(s)

The overall approach of Wilson et al. (2014)[1] has been shown to be adaptable for the aircraft noise prediction problem.

Major Accomplishments

One way of including uncertainty in aircraft noise sound level predictions has been successfully demonstrated. It is shown that the overall approach of Wilson et al. (2014)[1] is adaptable for the aircraft noise prediction problem. In the cases examined with the three uncertain variables of temperature profile, wind profile, and humidity, the expected values of sound pressure level change due to the uncertainty. The expected SPLs change since the variation around the mean input variables do not result in symmetric changes in the SPLs. Further, it was found that the uncertainty grows with increasing aircraft altitude, which is an expected result.

Publications

Patankar, H. P., and Sparrow, V. W. "Quantifying the effect of uncertainty in meteorological conditions on aircraft noise propagation." 47th International Congress and Exposition on Noise Control Engineering, INTER-NOISE 2018.

Outreach Efforts

None

Awards

None

Student Involvement

Graduate Research Assistant Harshal Patankar has been the primary person working on this task.

Plans for Next Period

1. In the work performed until now, the CNPE has been used for the propagation calculations. However, one can use any propagation method with the approach of Wilson et al. (2014)[1]. A logical next step would be to determine if ray tracing and/or integrated calculation methods give similar results to the CNPE results if uncertainty is similarly included (as has been shown in the work presented in this report).
2. In the work completed thus far, a simple meteorological model of temperature lapse and logarithmic wind profile is assumed which could be replaced by a custom function fitted to measured atmospheric profiles. For now, the uncertainties have been modeled using Gaussian distribution for simplicity. In a real-world situation, the uncertainties might not be symmetrically distributed around their mean values (as in the case of Gaussian function), hence it would be better to build a custom probability density function based on measured atmospheric profiles.
3. Advanced stochastic sampling techniques such as importance sampling and adaptive importance sampling[1] could be used to reduce the computation time.

References

1. D. K. Wilson, C. L. Pettit, V. E. Ostashev, and S. N. Vecherin, "Description and quantification of uncertainty in outdoor sound propagation calculations," The Journal of the Acoustical Society of America 136(3), 1013–1028 (2014).
2. K. Poulain, "Numerical propagation of aircraft en route noise," Master's thesis, The Pennsylvania State University (2011).
3. E. M. Salomons, Computational atmospheric acoustics (Springer Science and Business Media, 2012).
4. M. West, K. Gilbert, and R. Sack, "A tutorial on the parabolic equation (PE) model used for long range sound propagation in the atmosphere," Applied Acoustics 37(1), 31–49 (1992).
5. E. J. Rickley, G. G. Fleming, and C. J. Roof, "Simplified procedure for computing the absorption of sound by the atmosphere," Noise Control Engineering Journal 55(6), 482–494 (2007).
6. "Aerospace Recommended Practice 5534: Application of pure-tone atmospheric absorption losses to one-third octave-band data," SAE Technical Report, SAE International (Issued8/2013).
7. Patankar, H. P., and Sparrow, V. W. "Quantifying the effect of uncertainty in meteorological conditions on aircraft noise propagation." 47th International Congress and Exposition on Noise Control Engineering, INTER-NOISE 2018.

Task 1 – Validate the Noise Model Capabilities of AEDT by Comparing Numerical Results with Field Data

Task 2 – Quantify Uncertainties of Both Model Prediction and Measurement in Trying to Predict Aircraft Noise (or Pattern of Change) in Real World

Purdue University

Research Approach

Background

Predictions of noise generated by en-route aircraft have become increasingly important in the current regulations on civil aviation worldwide.[8-10] The propagation of airborne noise is influenced by many factors including the divergence effect, air absorption, acoustic impedance of the ground surfaces, effects of atmospheric refraction due to the presence of wind and temperature profiles, atmospheric turbulence and the aircraft's Doppler effect.[11] The Doppler effect perceived by a ground-borne receiver, which is caused by the motion of sound sources, will change two aspects of the aircraft noise. First, the received noise levels are augmented when an aircraft approaches and they are diminished for a receding aircraft. In the past, this effect has been studied extensively with theoretical modeling[12] and experimental measurements.[13] Secondly, the perceived sound frequency at the receiver location will be shifted due to the motion of the aircraft. This apparent change in frequency depends on the aircraft's speed and the relative positions between the source and receiver. Although it cannot change directly the sound pressure levels, this Dopplerized frequency changes the characteristics of the received noise spectrum affecting human's perceptions. Generally speaking, noise sources with low pitch components (below 250 Hz, say) has shown less effect on annoyance than those with higher frequency (above 1000 Hz) components.

Some of the previous studies exploited the Doppler effect for tracking of aircrafts[14], while other studies included it in their respective numerical models for synthesis of aircraft noise.[15,16] We examine the influence of the Doppler shift on predicting en-route aircraft noise. Particularly, we investigate into the impact of the Dopplerized frequencies on the prediction of A-weighted noise levels due to an aircraft mounted with (a) jet engines or (b) turboprop propulsion systems.

The ray model used that provides a framework for calculating the attenuations due to geometrical spreading, air absorption and Doppler effect. Numerical simulations are presented quantifying the possible errors if the Doppler effect is not included in the prediction of the A-weighted sound pressure levels. Based on the ray model, the sound exposure levels for 89 spectral classes of flight arrival and departure data (obtainable from Ref. 8 and 24) are calculated with and without the inclusion the Doppler effects. The errors for not including the Doppler effect in the ray model are summarized in a bar chart for ease of reference.

1. Numerical simulations for flyover events

Despite its well-known shortcomings,[22] A-weighted sound pressure level has become one of the internationally accepted metrics for evaluating aircraft noise. In this section, the ray model is applied to simulate the en-route aircraft noise. Specifically, the impact of the Doppler effect on the A-weighted noise levels is examined. Two distinct types of aircraft noise spectra are used in the numerical simulations:

(a) Test aircraft: Lockheed P3B Orion mounted with turboprop engines;[21]
(b) Reference aircraft: Lockheed Martin F22/A Raptors operating with the afterburners during the statics tests.[23]

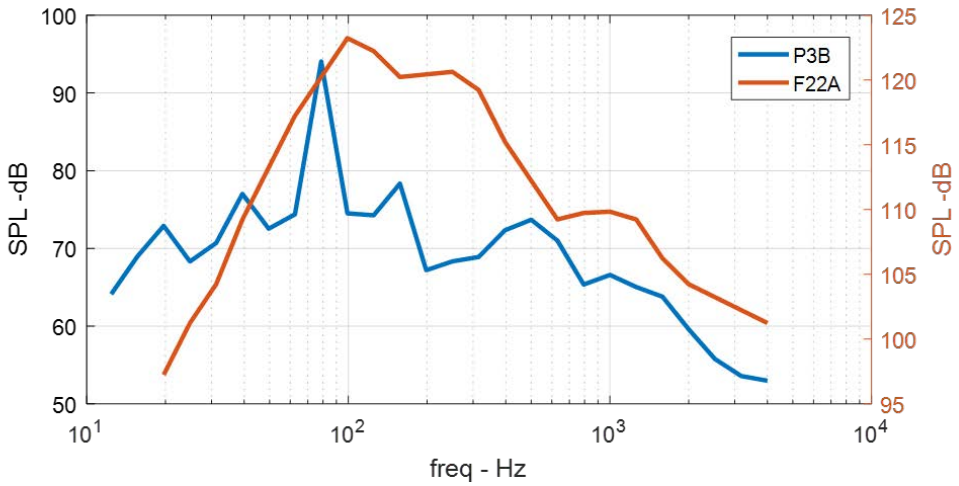


Figure 9. Measured spectra of sound pressure level (SPL) for Lockheed P3B Orion (blue) and Lockheed Raptor (red).

The scale of SPL for P3-B Orion is shown on the left vertical axis and Lockheed F22/A shown on the right axis. Here, the source directivity effects are not included in this study. Hence, one typical set of the source spectrum from each aircraft is used in our numerical simulations because the main objective of the present study is to examine the Doppler effect for a moving aircraft. In Figure 9, the spectrum of the P3-B Orion is shown in blue with the scale of the measured SPL displayed in the left vertical axis. For ease of comparison, the spectrum for the F22/A Raptor (with the scale of the measured SPL shown in the right axis) is plotted in the red line. As shown in Figure 9, the turboprop engine has a peak tonal component at about 70 Hz. On the other hand, the jet engine has demonstrated a broadband spectrum with the peak at about 100 Hz. The majority of the sound energy is concentrated between 50 and 500 Hz where the sound pressure levels dropped by 10 dB from about 123 dB at the peak to 113 dB at either sides of the limit. These two spectra are scaled in Figure 9 with the non-linear effects of jet engines ignored. These graphs represent the corresponding situations of obtaining the source spectra with each engine measured at 100 m from the source.

In the numerical analyses, the flyover of the P3-B Orion and the F22/A Raptor are simulated with the receiver located at 1 m above the ground. The numerical simulations are prepared with the aircraft traveling at a speed of approximately 100 m s^{-1} (Mach number of 0.3) at a constant height of 500 m above the ground. The flight path has no offset distance between the aircraft and the receiver, i.e. a direct overhead flight path. The spectrograms for these two distinct engines are presented in Figure 10 in order to illustrate the effects of spectral characteristics upon the predicted A-weighted noise levels.

An aircraft flyover event is one of the most common operations near airports. When an aircraft is approaching, a higher pitch sound is heard due to the Doppler effect. When an aircraft recedes, a lower pitch sound is experienced instead. As a result, the frequency of the received sound is not exactly the same as that emitted by the aircraft due to the effect of Doppler shift. This section compares the possible error made by the Dopplerized frequency by comparing the effect on two different types of aircrafts: the P3-B Orion and the F22/A Raptor.

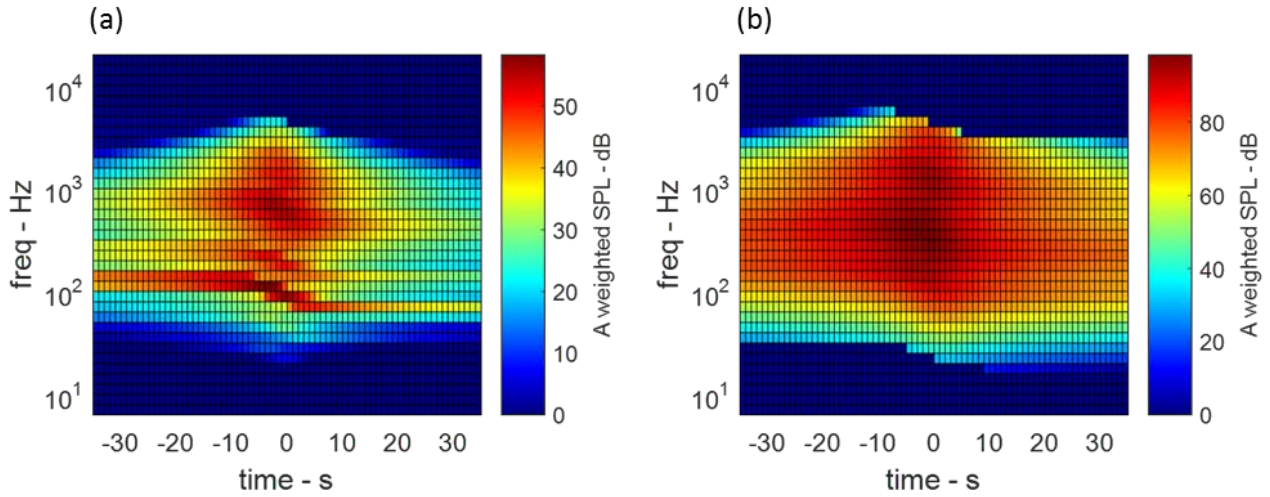


Figure 10. Predicted A-weighted spectrograms for (a) Lockheed P3-B Orion and (b) Lockheed Martin F22/A raptor (right). Flyover event with source height at 500 m and receiver height at 1 m, Mach number of 0.3 and sideline distance of 0 m.

As shown in Figure 9, the P3-B Orion has a clear tonal component around 70 Hz but the F22/A Raptor has a rather smooth broadband spectrum. The spectrograms in Figures 10 (a) and (b) show a clear Doppler effect especially for the P3-B Orion which has a dominant tonal component at 70 Hz. In the spectrograms, the one-third octave bands with the red/dark red colors have the highest sound pressure levels in the contour maps. When time is equal to zero, the aircraft is situated directly above the receiver. Increasing the time parameter from negative to zero (along the horizontal axis) indicates that the aircraft moves towards the receiver. The locations of the red color blocks moves towards the low frequency end as time increases in the spectrogram: this is mainly attributed to the effect of Doppler shift. Shifting in the frequency domain will cause the change in the predicted A-weighted SPL. A broadband and smooth source spectrum (such as that shown in the F22/A Raptor) has less noticeable frequency shift in the spectrogram, see Figure 10(b).

In Figure 11, the prediction of the A-weighted noise levels with and without the inclusion of the Doppler effect are compared. The predicted A weighted SPL with the Doppler effect is larger when the aircraft is approaching the receiver. This difference becomes zero when the aircraft is directly above the receiver and continue to decrease to negative value when it traverses away from the receiver. The comparisons between Figures 11 (a) and (b) show that the impact of the Doppler shift on the P3-B Orion is larger than that on the F22/A Raptor. The reason for this difference mainly lies in the fact that the spectral characteristics of these two types of aircraft are fundamentally different. The spectrum of the P3-B Orion has a dominant low-frequency tonal component at 70 Hz. When the Dopplerized peak frequency is shifted from 70 Hz to 110 Hz, the A-weighted correction factor will be changed by a factor of 6 dB. Hence, the sound source with the same unweighted sound pressure level will be increased by 6 dB because of a larger change in the correction factor as required by A-weighting of the sound levels. On the other hand, the smooth feature of the F22/A Raptor's spectrum makes the shift in Dopplerized frequency much gentler. For example, the frequency shift will have no effect to a broadband white noise because the sound pressure level is the same anywhere in the frequency domain.

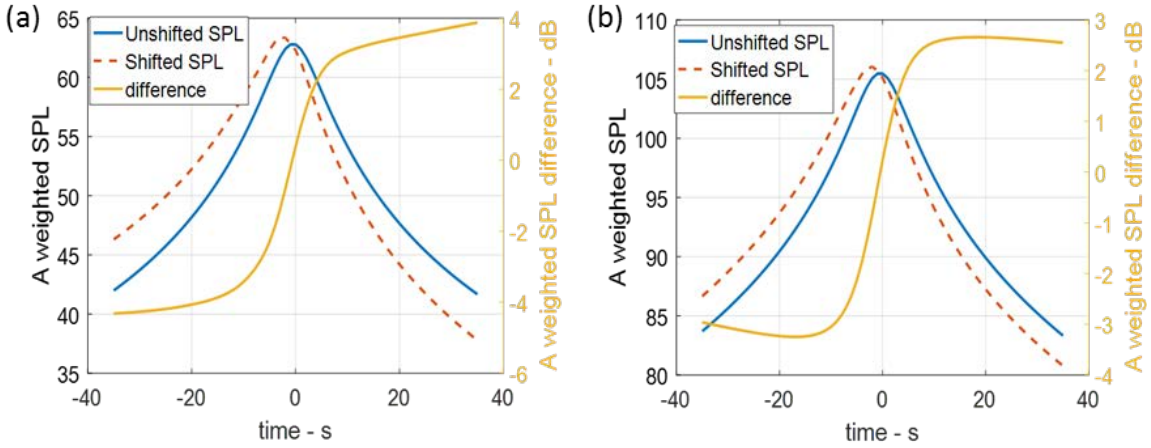


Figure 11. Predicted time histories of the overall A-weighted sound pressure levels (SPL). Blue line: Prediction without the Doppler effect. Red dashed line: Prediction with the Doppler effect. Yellow: Difference between these two predictions. (a) P3-B Orion; (b) F22/A Raptor.

Since the effect of the Doppler shift is decided by the spectral characteristics of the noise source, it is of interest to analyze this impact for different types of aircrafts with various spectral characteristics. In support of the current study, a dataset with 89 unique spectral classes have been used in Refs. 1 and 24 for assessing noise levels around airports.

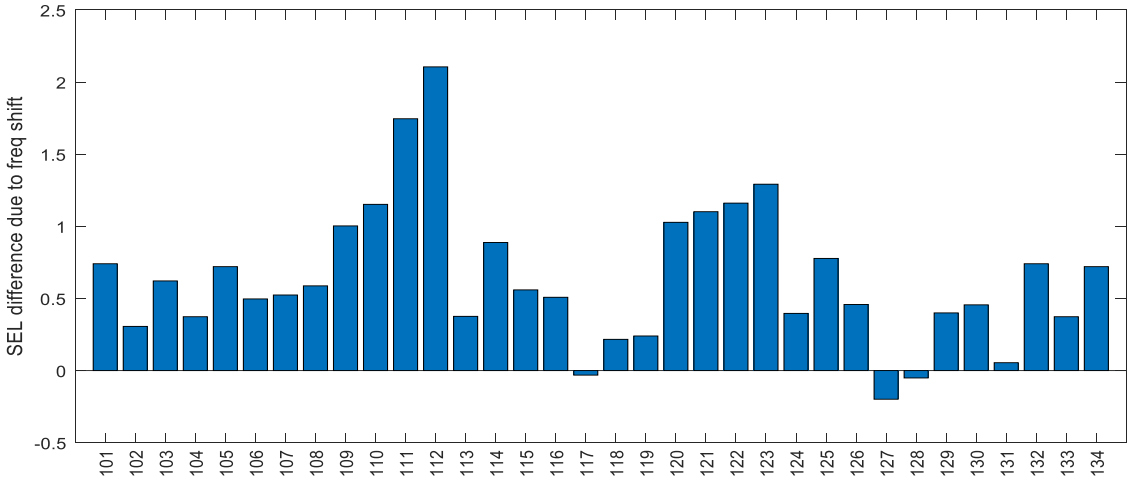


Figure 12. Difference in predicting A-weighted SEL with/without the inclusion of the frequency shift due to Doppler effect for the classes of flight departure.[1,22]

Sound exposure level (SEL) is a widely used metric to evaluate the overall noise impact of a single fly-over event. According to the earlier explanations, different spectral characteristics tend to produce different results after the application of the Doppler shift to the ray model. Each of the 89 spectral classes are used as the source spectra in the prediction of SEL. Influence of the Doppler effect is not very prominent if SEL is used as the indicator. It is because the Doppler effect increases the noise levels of an approaching aircraft but it decreases the noise levels for a receding aircraft. These two influences are additive which leads to a partial cancellation when approaching and receding events are combined during the integration process in calculating the total SEL for a fly-over event.

Nevertheless, these 89 spectral classes are grouped into three categories: departure, arrival and flyover. For example, the class 101 represents the departure event of civilian aircraft Boeing 737. The detailed information of these spectral classes



can be found in Ref. 24. Only the results for departure and arrival classes are shown in this study for succinctness, see Figures 12 and 13 for the calculated results.

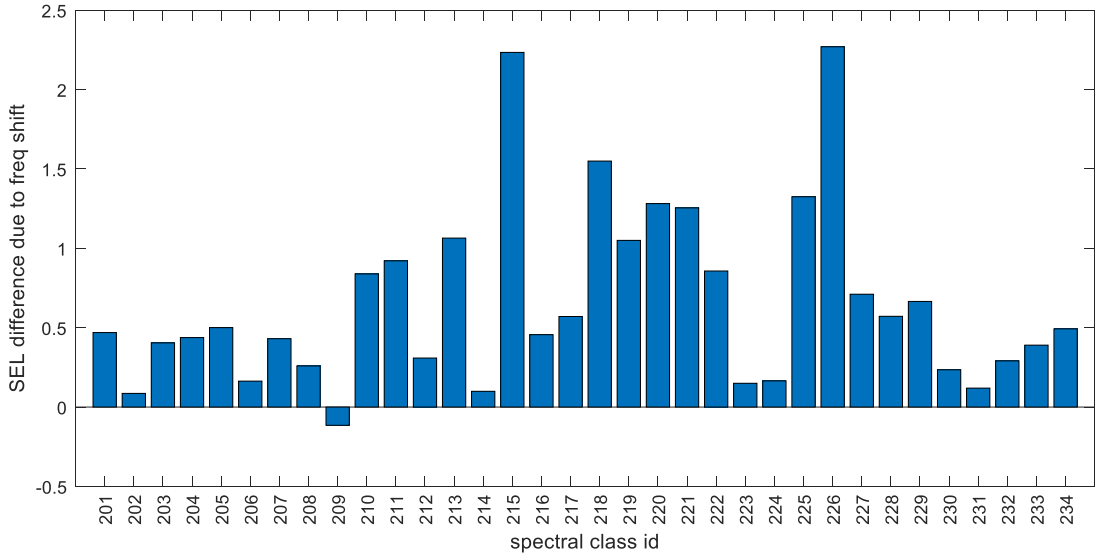


Figure 13. Difference in predicting A-weighted SEL with/without the inclusion of the frequency shift due to Doppler effect for the classes of flight arrival.[1,22]

For the results presented in Figures 12 and 13, each of the spectra is used as the noise source in the prediction of SEL for a flyover event where 200 s before and after the overhead point are used in the numerical integration. The source and receiver heights are set, respectively, as 1 km and 1 m above ground and the source Mach number is set to 0.5. For the calculation of air absorption, the air temperature is set as 15° C, relative humidity as 50% and the atmospheric pressure ratio as 0.77. Using the ray model, the predicted SEL with and without the inclusion of the Doppler effect are compared.

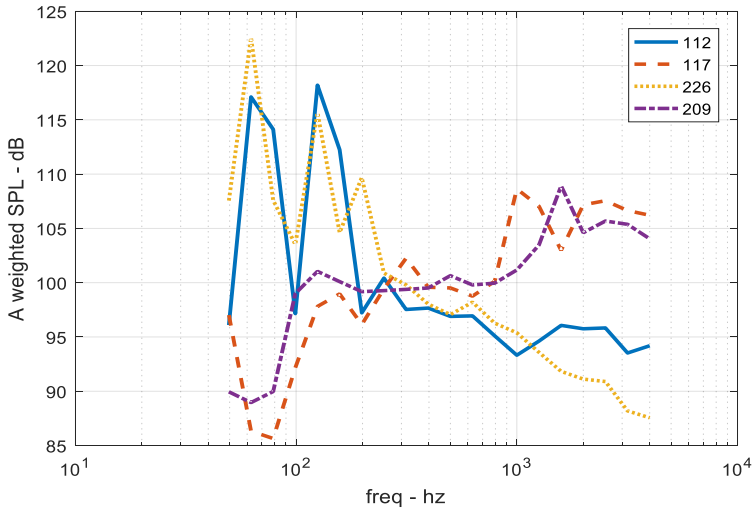


Figure 14. Source spectra for Classes 112, 117, 226 and 209.

With this set of calculations, the following conclusion can be drawn from the results shown in Figures 12 and 13. If the Doppler effect is not included in the SEL calculations, the possible 'error' varies between 0 and 2.2 dB for different classes of aircraft.



Among all spectra, classes 117 and 209 have the smallest influences caused by the effect of the Doppler shift. In contrast, classes 112 and 226 have the largest impacts. These 4 source spectra are organized and plotted in Figure 14 for illustration purposes. The two most influenced spectra have obvious tonal components with twin peaks at the spectral region around 100 Hz. The two least influenced spectra are relatively smooth. These 4 Spectral Classes confirm our observation in our earlier analyses for the P3-B Orion and the F22/A Raptor. A low-frequency tonal component can cause higher errors in the prediction of A-weighted sound pressure level if the Doppler effect is not included. On the other hand, an aircraft with a smooth spectral characteristic is less sensitive to the Doppler effect for accurate predictions of the A-weighted sound pressure levels.

Milestone(s) and Major Accomplishments

The Doppler effect on the prediction of the A-weighted sound pressure level is analyzed. The proposed ray model was validated with field data. The ray model was subsequently used to investigate the possible errors if the Doppler effect is not included in the prediction of A-weighted sound pressure levels. Numerical simulations were also conducted to calculate the sound exposure levels for 89 arrival and departure flight classes.[17] It is found that an error exits between 0 to 2.2 dB if the Doppler effect is not included in the ray model. However, it is worth noting that noise predictions by the FAA's tool, the Aviation Environmental Design Tool (AEDT) is based on the Noise Power Distance (NPD) curves.[1] The NPD curves are typically developed by the aircraft manufacturers from measurement data. To a certain extent, the effect of Doppler shift is therefore captured in the current AEDT calculations. It may be useful to extend the analysis here to evaluate to what degree the Doppler effect is included in the NPD data.

Publications

- ASA Fall 2017, Abstract
- INTERNOISE 2018 paper

Outreach Efforts

None

Awards

Graduate Research Assistant, Yiming Wang has been awarded with INCE Best Graduate Student Award, 2018

Student Involvement

Graduate Research Assistant, Yiming Wang, has been the primary student working on this project. A new Graduate Research Assistant, Jianxiong Feng, has been recruited as Yiming Wang will be expected to finish his PhD thesis in the Summer 2019.

Plans for Next Period

For the Purdue effort, there are 4 tasks listed below:

A. Assess the DISCIVER-AQ datasets for use in validating noise tools (propagation).
B. Assess the influence of source (aircraft) motion on the accuracy in predicting en-route aircraft noise (source).
C. Assess the impacts of geometric locations of source and receiver, the effective surface impedance and the ground topography on the accurate prediction of aircraft noise (receiver).
D. Assess the overall uncertainty in the noise prediction (propagation+source+receiver) of overflight aircraft.

Three of these 4 tasks are conducted in coordination with the PSU team. The Purdue team will also focus on the use of DISCOVER-AQ datasets to investigate the influence of ground effects on predicting aircraft noise (Task C). Other Purdue efforts include the investigation of the Doppler Effect on the measured noise contents (for the shift in frequency and the change in the noise levels) for the approaching and receding aircraft.

References

8. Aviation Environmental Design Tool (AEDT) Technical Manual, Version 2d, US Department of Transport, Federal Aviation Administration, (2017).
9. ECAC.CEAC. Report on standard method of computing noise contours around civil aviation airports, Technical Report, ECAC.CEAC (2005).



10. Y. Wang, S. Liu, Y. Dong, J. Cai, "Effects of acoustic characteristics on annoyance of aircraft flyover noise," Noise Control Engineering, Journal **63**, 279-286 (2015).
11. B. G. Ferguson, Doppler effect for sound emitted by a moving airborne source and received by acoustic sensors located above and below the sea surface," Journal of Acoustical Society of America **94**, 3244-3247 (1993).
12. K. Attenborough, K. M. Li, and K. Horoshenkov. Predicting outdoor sound. CRC Press, (2014).
13. J. Lighthill, Introduction, Ch. 27, Encyclopedia of Acoustics, Part III: Aeroacoustics and Atmospheric Sound, pp 283-299, Wiley Online Library (1997).
14. S. R. Martin, M. Genesca, J. Romeu, T. Pamies, "Aircraft by means of the acoustical Doppler effect," Aerospace Science and Technology **28**, 305-314 (2013).
15. S. A. Rizzi, A. R. Aumann, L. C. Lopes, C. L. Burley, "Auralization of hybrid wing body aircraft flyover noise from system noise predictions," Journal of Aircraft **51**, 1914-1926 (2014).
16. M. Arntzen, D. G. Simons, "Modeling and synthesis of aircraft flyover noise," Applied Acoustics, **84**, 99-106 (2014).
17. Y. Wang, K. M. Li and B. N. Tong "Sound field generated by a 3-dimensional moving monopole point source above a locally reacting surface," Noise-Con 2016, Providence, RI, Paper 179. (2016).
18. B. N. Tong and K. M. Li. "Atmospheric effects on noise propagation from an en-route aircraft," NOISE-CON 2014 nc-66594, Fort Lauderdale, Florida, September 8-10 (2014).
19. H. E. Bass et al, "Atmospheric absorption of sound: Further development." Journal of Acoustical Society of America **97**, 680-683, (1995).
20. International Standards Organization, "Acoustics - Attenuation of sound during propagation outdoors - Part 2: General method of calculation", International Organization for Standardization (1996).
21. E. Boeker et al, "DISCOVER-AQ Acoustics: Measurement and data report," DOT/FAA/AEE/2015-11 (2015).
22. Committee on Technology for a quieter America, National Academy of Sciences, "Technology for a quieter America," Ch. 3 Metrics for Assessing Environmental Noise. (2010) [see https://www.nap.edu/read/12928/chapter/1 (Last assessed 1 May 2018)].
23. K. L. Gee et al, "The role of non-linear effects in the propagation of noise from high-power jet aircraft," Journal of Acoustical Society of America, **123**, 4082-4093 (2008).
24. H. He et al, "Integrated Noise Model (INM) Version 7.0 User's Guide," FAA-AEE-07-04, pp. 369-386 (2007).



Project 041 Identification of Noise Acceptance Onset for Noise Certification Standards of Supersonic Airplanes

The Pennsylvania State University

University Members

Penn State Acoustics Program	Principal Investigator	Victor W. Sparrow
Penn State Applied Research Laboratory	Co-Principal Investigator	Kathleen K. Hodgdon

Advisory Committee Members

AERION: Jason Matisheck, Peter Sturdza, *et al.*
Boeing: Hao Shen, Bob Welge, *et al.*
Gulfstream: Robbie Cowart, Matthew Colmar, Brian Cook, Joe Gavin, *et al.*
Lockheed Martin: John Morgenstern, Tony Pilon, *et al.*
Volpe-The National Transportation Systems Center: Juliet Page, Bob Samiljan, et.al.
Wyle: Kevin Bradley, Chris Hobbs, *et al.*

Project Lead Investigator

Victor W. Sparrow
Director and United Technologies Corporation Professor of Acoustics
Graduate Program in Acoustics
The Pennsylvania State University
201 Applied Science Bldg.
University Park, PA 16802
+1 (814) 865-6364
vws1@psu.edu

University Participants

The Pennsylvania State University

- P.I.: Vic Sparrow, United Technologies Corporation Professor and Director, Graduate Program in Acoustics
- Researcher: Kathleen Hodgdon, Research Associate
- FAA Award No.: 13-C-AJFE-PSU Amendment 34
- Period of Performance: August 7, 2017 to December 31, 2018
- Task(s):
  1. Obtaining confidence in signatures, assessing metrics sensitivity, and adjusting for reference day conditions

The Pennsylvania State University Applied Research Laboratory

- P.I.: Kathleen Hodgdon Research Associate
- Researcher: John Morgan R&D Engineer
- FAA Award No.: 13-C-AJFE-PSU Amendments 35 and 39
- Period of Performance: August 7, 2017 to July 31, 2019
- Task(s):
  2. Community Instrumentation and Monitoring

Project Funding Level

This project supports the identification of noise acceptance onset for noise certification standards of supersonic airplanes through research conducted on multiple tasks at the Penn State University. The FAA funding to Penn State in 2017 -2018 was $221K comprised of $150K to Task 1 and $71K to Task 2. Matching funds are expected to meet cost share on both Tasks. Funds have not been received to support these tasks during 2018-2019 at the time of the writing of this report.



Investigation Team

For 2017-2018 the investigation team includes:

The Pennsylvania State University
Victor W. Sparrow (Co-PI) (Task 1)
Kathleen K. Hodgdon (Co-PI) (Task 2)
Researcher: John Morgan R&D Engineer (Task 2)
College of Engineering Graduate Research Assistants Janet Xu and Luke Wade (Task 1: Signatures and metrics investigation)
ARL Eric Walker Graduate Assistant: Annelise Hagedorn (Task 2: Community Monitoring)

Project Overview

FAA participation continues in International Civil Aviation Organization, Committee on Aviation Environmental Protection (ICAO CAEP) efforts to formulate a new civil, supersonic aircraft sonic boom (noise) certification standard. This research investigates elements related to the potential approval of supersonic flight over land for low boom aircraft. The efforts include investigating certification standards, assessment of community noise impact and methods to assess public acceptability of low boom signatures. The proposed research will support NASA in the collaborative planning and execution of human response studies that gather the data to correlate human annoyance with low level sonic boom noise. As the research progresses, this may involve the support of testing, data acquisition and analyses, of field demonstrations, laboratory experiments or theoretical studies.

Task 1- Obtaining Confidence in Signatures, Assessing Metrics Sensitivity, and Adjusting for Reference Day Conditions

The Pennsylvania State University

Objective

As national aviation authorities move forward to develop noise certification standards for low-boom supersonic airplanes, several research gaps exist in the areas of signature fidelity, metrics, metrics sensitivity to real-world atmospheric effects, adjustments for reference-conditions, etc. Research support is needed by FAA and international partners in these areas to progress toward standards.

The objective of this activity is to continue research at The Pennsylvania State University in the ASCENT COE to complement the sonic boom standards development ongoing within the Committee for Aviation Environmental Protection's (CAEP) Working Group 1 (Noise Technical), Supersonics Standards Task Group (SSTG). This research will ensure that the behavior of the sonic boom metrics considered in the SSTG discussions are well-understood, and account for sonic boom variability effects, to move forward with sonic boom noise certification standards development and consideration of subsequent rulemaking.

Task 1 in ASCENT Project 41 focuses on several, but not all, research initiatives needed to move forward toward the development of a low-boom supersonic en-route noise certification standard. In addition, this project supports the travel of V. Sparrow so that he can serve as co-rapporteur of the CAEP Impacts and Science Group (ISG).

Research Approach

Background

Previous work in the last few years of ASCENT Project 41 has focused on a number of different topics associated with developing approaches that could lead to the sonic boom noise certification of future supersonic aircraft. For example, the work described in the Project 41 annual report last year focused on the appropriate placement and number of microphones that could be used during certification. It was found that at least 10 microphones are required to minimize the confidence intervals. The authors are currently writing up those results for submission to a peer-reviewed journal.

One of the ongoing topics of discussion is to determine how one can remove the effects of atmospheric turbulence from sonic boom signatures (pressure versus time recordings). The term currently used for removing the turbulence is called deturbing and this concept had previously been discussed in Project 41. Since there has never been a thorough



investigation on methods for deturbing, this was the focus of the Project 41 Task 1 effort in 2017-2018. The work was primarily undertaken by Graduate Research Assistant Janet Xu, supplemented by project PI Dr. Victor Sparrow and Graduate Research Assistant Luke Wade. The detailed description has been prepared for submission to a peer-reviewed journal, and the following paragraphs provide an overview of some of the research development and initial results.

Categories of deturbing methods
Developed methods include those performed on individual sonic boom signatures to output the same number of deturbed signatures (individual deturbing), those performed on an ensemble of signatures to output one deturbed signature (group deturbing), and those based on matching the sonic boom signature to a database of known signatures (comparative deturbing). Work has primarily been carried out on the first two methods.

Individual deturbing methods
The two individual methods tested were low-pass filtering and turbulence subtraction. Low-pass filtering involves filtering around the shocks of the signature in order to retain the high-frequency shock features while removing turbulent noise. Turbulence subtraction is based on the fact that the back shock of an ideal N-wave behaves like a step function. Any difference from this idealized step function is subtracted off, giving an estimate for the turbulence present during the back shock. This estimated turbulence is then removed from the front and back shocks to give a deturbed waveform. Note that this method is only effective for N-wave-like signatures.

Group deturbing methods
Nearly every type of group deturbing ends with the ensemble of signatures being averaged. However, turbulence can cause each recorded signature to have a different shock width so that the signatures become misaligned. Thus, the key difference between each of the group deturbing methods is how they re-align the ensemble of signatures before they are averaged. One may choose not to align before averaging, or to individually deturb the signatures and average without aligning, but different methods of alignment were also explored. These include aligning by peak, aligning by maximum slope, and aligning by maximum cross-correlation. Aligning by peak determines the width of each signature by finding the time difference between the peak of the front shock and the peak of the back shock, then resampling ("time-stretching") the signature so that its width matches the width of the median width signature (i.e., their peaks align). Aligning by maximum slope determines the width by finding the time difference between the point of maximum slope in the front shock and the point of maximum slope in the back shock, then time-stretching the signature so that its width matches the width of the median width signature (i.e., their points of maximum slope align). Aligning by maximum cross-correlation does not assume features of the shocks. Rather, it aligns each signature to a reference signature by scaling and shifting the signature until maximum cross-correlation with the reference signature is achieved. All the signatures are then time-stretched to have the same width as the median width signature, where width is determined by maximum slopes as outlined above. A method known as dynamic time warping was also investigated. It involves pairing off and nonlinearly mapping signatures onto each other tournament-style until one composite signature remains.

Initial comparisons of the deturbing methods
The effectiveness of each deturbing method was determined by the closeness of the output deturbed signature to the original input signature, using both an objective metric (energy normalized mean-square error) and several subjective metrics (Stevens Mark VII Perceived Level, ISBAP, ASEL, and BSEL). Table 1 contains the mean square error for each deturbing method for different sonic boom datasets. Note that each dataset has two rows per deturbing method. This corresponds to using two separate methods to calculate points of maximum slope for a signature where applicable. The heatmap highlights the largest (red) and smallest (white) MSE for each set of two rows, and shades of red for the in-between values. It can be seen that averaging with time-stretching by maximum slope and low-pass filtering with averaging (LPF (group)) were the most effective in achieving a low MSE match. The former implies that the location of maximum slope in the pressure signature may be the feature most robust to noise, while the latter implies that low-pass filtering may improve the alignment of the average without the need for time-stretching.



Table 1. Normalized mean square error for each deturbing method for various sonic boom datasets. The heatmap displays where the PL is lower than in the original signature (blue) and higher (red)

		Individual		Group						
Data Set	None	LPF	Sub	None	Peak	Slope	Xcorr	DTW	LPF	Sub
Stout/SonicBAT	5.119	4.209	1.975	0.907	2.329	0.930	1.689	25.974	0.757	0.993
	x	x	1.829	0.925	x	0.924	1.689	24.554	0.788	0.996
Northrup	3.989	3.407	2.127	2.605	2.766	1.461	1.581	20.533	2.543	1.620
	x	x	2.074	2.474	x	1.400	1.581	20.314	2.503	1.616
SSBD	1.853	1.687	2.631	1.319	1.596	1.297	1.310	15.070	1.299	2.379
	x	x	3.139	1.340	x	1.420	1.301	16.785	1.288	2.724
L.Boom 1	2.379	2.198	2.813	0.429	0.388	0.301	0.626	15.171	0.412	0.920
	x	x	2.577	0.374	x	0.315	0.625	14.444	0.358	0.758
L.Boom 2	3.206	3.046	3.745	3.899	0.634	1.658	1.271	10.014	2.631	5.377
	x	x	3.715	0.452	x	0.436	1.273	7.947	0.466	1.815
L.Boom 3	2.119	1.924	2.901	1.148	1.097	0.266	0.896	12.485	0.534	1.448
	x	x	3.228	0.870	x	0.274	0.894	15.664	0.863	1.152
L.Boom 4	1.220	1.111	4.654	0.189	0.214	0.604	0.439	5.093	0.179	3.235
	x	x	4.821	0.187	x	0.573	0.440	4.145	0.177	3.343
L.Boom 5	1.026	0.967	11.682	0.131	0.339	0.139	0.322	16.101	0.123	10.819
	x	x	8.786	0.152	x	1.548	0.322	35.613	0.141	6.857

Table 2 contains the change in Stevens Mark VII Perceived Level (PL) for each deturbing method for different simulated sonic boom datasets. Note that each dataset has two rows per deturbing method. This corresponds to using two separate methods to calculate points of maximum slope for a signature where applicable. The heatmap displays where the PL is lower than in the original signature (blue) and higher (red). It can be seen that the smallest changes in PL occur for individual low-pass filtering (LPF), dynamic time warping (DTW), and averaging with time stretching by maximum slope (Slope). The DTW result may be misleading, however, as it has such a high MSE across the board (see Table 41.1).

Table 2. PL change for each deturbing method for various sonic boom datasets. Same heatmap as in Table 1.

			Individual		Group						
Data Set	Source	None	LPF	Sub	None	Peak	Slope	Xcorr	DTW	LPF	Sub
Stout/SonicBAT	99.4	-1.7	-2.1	1.4	-3.0	-5.4	-2.9	-4.0	-5.1	-3.6	-1.6
	x	x	x	2.2	-2.1	x	-2.3	-4.0	-5.5	-2.7	0.8
L.Boom 1	77.7	-1.8	-0.1	11.6	-4.9	-5.0	-2.8	-5.6	2.3	-4.0	7.4
	x	x	x	11.2	-4.4	x	-3.1	-5.6	2.2	-3.2	6.6
L.Boom 2	80.0	-2.1	-2.0	1.9	-5.9	-4.1	-5.9	-5.4	1.4	-5.4	-3.6
	x	x	x	2.7	-3.4	x	-3.2	-5.4	-0.8	-3.9	-3.4
L.Boom 3	74.2	-2.3	0.8	7.7	-7.5	-5.7	-2.7	-6.4	-1.0	-4.6	2.2
	x	x	x	8.3	-6.4	x	-3.7	-6.3	-1.3	-4.6	3.9
L.Boom 4	69.0	-1.6	-1.1	23.9	-6.6	-3.7	-1.8	-4.8	5.9	-6.7	20.8
	x	x	x	24.4	-6.2	x	-1.6	-4.8	6.4	-6.2	21.0
L.Boom 5	69.3	-2.0	1.4	18.8	-4.7	-6.8	-2.4	-7.0	0.4	-3.1	15.2
	x	x	x	17.4	-3.4	x	-3.3	-7.0	3.8	-2.0	14.3



As a result, it is suggested that individual low pass filtering, averaging with time stretching by maximum slope, low pass filtering before averaging, and averaging with time-stretching by cross correlation be used for deturbing if applied in sonic boom aircraft certification.

Milestone(s)

A number of different methods were assessed for removing the effects of atmospheric turbulence on recorded sonic boom signatures.

Major Accomplishments

ASCENT Project 41 Task 1 has now provided guidance to remove atmospheric turbulence from sonic boom signatures that could be used in sonic boom noise certification of supersonic aircraft.

Publications

J. Xu, V. Sparrow, "Investigation of deturbing methods for sonic boom signatures," J. Acoust. Soc. Am. **143**(3, Pt. 2) 1913 (2018), 7-11 May 2018 Acoustical Society of America presentation, Minneapolis, MN, USA.

Outreach Efforts

None

Awards

None

Student Involvement

Janet Xu was the Penn State graduate research assistant who worked on ASCENT Project 41 during the 2017-2018 academic year. She now has taken a job at Bose Corporation where she continues to work on the topics of acoustics and signal processing. Luke Wade also came on the project during the summer of 2018 and overlapped with Janet Xu for a few weeks.

Plans for Next Period

If funding arrives, the plan is to continue supporting CAEP's WG1, SSTG, and ISG in the area of supersonic certification.

References

[1]J. Xu, V. Sparrow, "Investigation of deturbing methods for sonic boom signatures," J. Acoust. Soc. Am. **143**(3, Pt. 2) 1913 (2018), 7-11 May 2018 Acoustical Society of America presentation, Minneapolis, MN, USA.
[2]D. Maglieri, *et al.*, *Sonic Boom: Six Decades of Research* (NASA SP-2014-622, 2014), pp. 51-52.

[3]M. Muller, Dynamic Time Warping, (Springer Berlin Heidelberg, Berlin, Heidelberg, 2007), doi: 10.1007/978-3-540-74048-3_4.

Task 2- Community Instrumentation and Monitoring

The Pennsylvania State University

Objective

This is part of a series of research efforts that were designed to devise scientific evidence to help answer the question: "What data is needed through a standard to reconsider 14 CFR part 91.817, which currently prohibits civil supersonic flight over land?" This effort supports research on the human perception of *low level* sonic booms and the exploration to enhance capabilities for the assessment of community impact by aviation noise field tests.

The research supports the standard development process and the identification of noise acceptance onset. The tasks were conducted in support of NASA in the development of protocols, methods and planning for execution of human response studies and community exposure testing.

Research Approach

This research encompassed several topics that were investigated in support of future field tests to assess community noise impact and public acceptability of low boom signatures. Community noise impact research requires gathering noise data as well as community response data. This effort is finalizing the design of low cost noise monitors (LCNM) that could be used as a rapid deploy monitor to augment the use of standard higher fidelity instrumentation to gather noise data. A review of the aviation noise literature is underway. The intent is to assess differences in perception between urban and rural environments to better understand the potential impact that background environmental noise has on community noise impact.

Milestone(s)

This research was conducted in support of future NASA sponsored low boom noise community field tests. The LCNM design is being finalized. PSU researchers are sharing the design with researchers from Volpe, The National Transportation Systems Center for further testing and development. The literature review of urban vs. rural aviation noise impact is ongoing to assess the role of environmental background noise.

Major Accomplishments

The Low Cost Noise Monitor design is being finalized. This task was conducted in support of efforts to gather objective measurements community noise tests. The literature review of the impact of environmental background noise on community noise impact is ongoing. The review of environmental masking was initiated to understand the potential impact that masking has on noise field test results for human impact. Accomplishments on each of these tasks follow.

Low Cost Noise Monitor (LCNM) Design

A report that provides an overview of the design for the Low Cost Noise Monitors (See Figure 1 and Table 1) is in development. The design will be shared with Volpe for further development and testing. The LCNM was designed as a prototype with the potential for project specific modifications when building future monitors.



Figure 1. LCNM prototype

Table 1. LCNM Components

LCNM Components
2 Microphones
GPS Sensor
Environmental Sensor
Accelerometer Sensor
Single Board Computer (SBC)

Several low cost options were explored, assessing the electrical power considerations, mechanical components, and the electrical data flow and data storage. Design selection was contingent on the availability of low cost parts for the monitor. The noise monitoring is provided through a single board computer, microphones, and batteries. The design includes two microphone channels that can be set with different dynamic ranges. This affords the ability to capture low level signals with integrity, and affords a second microphone channel set with a higher dynamic range. The monitor also includes temperature and humidity sensors as well as an accelerometer channel to provide greater applicability for a range of noise monitoring projects. The monitor will require the development of software to facilitate the ability to readily download the field data.

Environmental Masking (urban vs suburban/rural) Literature Review and Survey Development
This task includes a review of concepts and available literature of noise studies related to the role masking plays on the perception of noise. Masking is the extent that one noise source “covers” or masks another noise source. The low boom noise has been described as sounding like distant thunder, or two car door slams in quick succession. In urban areas, a car door slam may not be noticed, due to other noise sources. The same car door slam would be more clearly noticed in a quiet rural environment. The noise impact is measured by both objective noise metrics and subjective human response.



The task will initially review and compile information on urban vs. rural impact of aviation noise. While the preferred noise source to investigate is aviation noise, data gathered on analysis methods for other noise sources may also prove to be relevant. A review of noise impact and analysis methods for various noise sources and environments could further identify patterns in noise impact and response, and provide a more informed approach to illuminate those patterns in future data sets. An attempt is being made to include a range of publications such as The Journal of the Acoustical Society of America, Journal of Sound and Vibration, Journal of Environmental Psychology, and Environment and Behavior. The literature review is intended to further understanding of potential differences in noise impact between such communities that could inform future research efforts. The results of this study should provide insight into the influence of background noise on the annoyance rating of aviation noise pertaining to low sonic boom noise.

Publications

None

Outreach Efforts

This research task supports NASA activities on supersonics and low boom research. The team has provided information to the NASA sponsored Waveforms Sonicboom Perception and Response Risk Reduction (WSPRRR) team as warranted.

Awards

None

Student Involvement

Annelise Hagedorn started this effort as an Eric Walker Graduate student, looking at aviation environmental impacts on urban vs rural communities. She left the university this past year for an excellent job opportunity.

Plans for Next Period

The LCNM instrumentation task is being finalized. The outcome is the development of noise monitoring technology that can be used to supplement existing noise measurement methods for greater quantification of coverage at lower cost and complexity. Such technology could be used as intermediate measures among the standard higher fidelity instrumentation to confirm and interpolate data.

The literature review will be continued on noise studies related to the role masking plays on the potential low boom noise impact in differing background noise for urban, suburban or rural noise environments. The findings of the Environmental Masking literature review will facilitate interpreting noise field test results and masking due to environmental surrounding (community density), and the relevance masking has on low boom noise for such varying background environments.

References

Brambilla, G. & L. Maffei (2006) Responses to noise in urban parks and in rural quiet areas. Acta Acustica United with Acustica, 92, 881-886.

Brink, M., K. E. Wirth, C. Schierz, G. Thomann & G. Bauer (2008) Annoyance responses to stable and changing aircraft noise exposure. Journal of the Acoustical Society of America, 124, 2930-2941.

Fields, J. M. (1998) Reactions to environmental noise in an ambient noise context in residential areas. Journal of the Acoustical Society of America, 104, 2245-2260.

Maris, E., P. J. Stallen, R. Vermunt & H. Steensma (2007) Noise within the social context: Annoyance reduction through fair procedures. Journal of the Acoustical Society of America, 121, 2000-2010.

Miedema, H. M. E. & H. Vos (1999) Demographic and attitudinal factors that modify annoyance from transportation noise. Journal of the Acoustical Society of America, 105, 3336-3344.

Project 042 Acoustical Model of Mach Cut-off Flight

The Pennsylvania State University

Project Lead Investigator

Victor W. Sparrow
Director and Professor of Acoustics
Graduate Program in Acoustics
The Pennsylvania State University
201 Applied Science Bldg.
University Park, PA 16802
+1 (814) 865-6364
vws1@psu.edu

University Participants

Pennsylvania State University

- P.I.(s): Dr. Victor W. Sparrow (PI), Dr. Michelle C. Vigeant (Co-PI)
- FAA Award Number: 13-C-AJFE-PSU, Amendments 20, 33, and 42
- Period of Performance: June 28, 2016 - December 31, 2019
- Task(s):
    1. Assess and extend modeling capability for Mach Cut-off events (a.k.a. Task 1A)
    2. Study human perception of Mach Cut-off sounds

Project Funding Level

$150K for 2017-2018 and $170K for 2018-2019, The Pennsylvania State University

Aerion Corporation is providing cost-share in-kind matching funds to Penn State. Our point of contact at Aerion is Jason Matishek, jrmatisheck@aerioncorp.com. Aerion is providing the necessary near-field CFD data and other relevant information to help guide the project team make accurate predictions of the Mach cut-off sonic boom signatures that may be produced by Aerion's future supersonic aircraft.

Investigation Team

Pennsylvania State University
Principal Investigator: Victor W. Sparrow
Co-Investigator: Michelle C. Vigeant
Graduate Research Assistant Zhendong Huang (assessment and extension of Mach cut-off models)
Graduate Research Assistant Nick Ortega (human perception of Mach cut-off sounds)

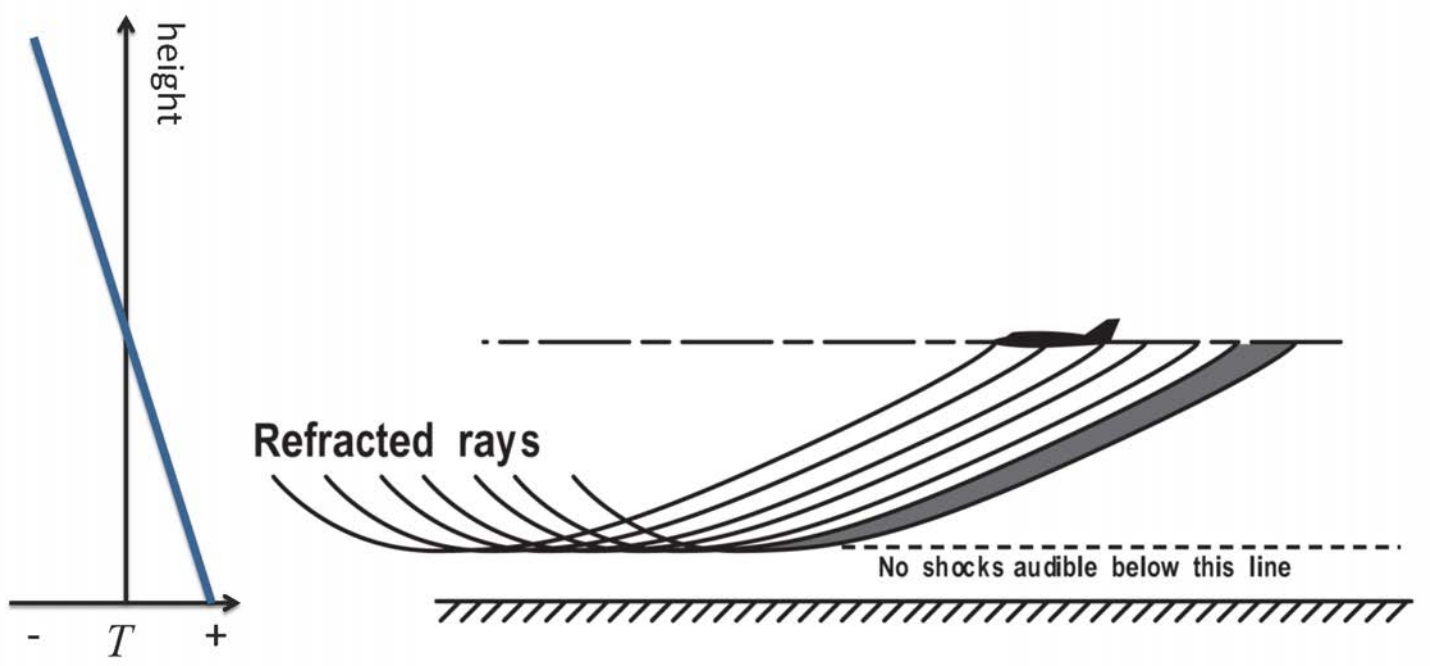
Project Overview

ASCENT Project 42 brings together resources to provide preliminary information to the FAA regarding the noise exposure of supersonic aircraft flying under Mach cut-off conditions. Studies in the 1970s showed that Mach cut-off supersonic flight was possible, but there is currently no data establishing the frequency and extent of noise exposures and no guidelines for managing such exposures. Penn State is shedding light on the Mach cut-off phenomena.

Aerion Corporation and many others believe that Mach cut-off supersonic flight is both viable [Plotkin, et al., 2008] and very likely to be acceptable to the public. But there is a lack of data to back up this assertion. Thus, research needs to be conducted to provide a technical basis for rulemaking regarding Mach cut-off operations.

The basic concept of Mach cut-off relies on the fact that the ambient temperature is substantially colder at flight altitudes than on the ground. Hence, the speed of sound is substantially slower at flight altitudes than at the ground. As illustrated

in the simplified graphic below, it is possible to fly in a range of Mach numbers (perhaps between Mach 1.0 and Mach 1.15) while having the sonic boom noise refract (bend) upwards such that the rays never reach the ground. However, the reader should be aware that this picture is over-simplified since the temperature profile in the atmosphere is never a smooth, linear function as depicted here. For higher Mach numbers, the sonic boom will impact the ground before refracting upward.



Simplified view of Mach cut-off where sonic boom noise does not reach the ground surface. Left: ambient temperature versus height. [Sparrow] Right: aircraft and ray diagram showing refraction of sonic boom [NASA].

Little is known about the noise impact of Mach cut-off operations for future supersonic aircraft. The concept of Mach cut-off was introduced by Lockheed engineers in the mid-1960s [Shurcliff, 1970]. NASA conducted some field experiments in the early 1970s, focusing on other speed regimes of flight, validating some of the Mach cut-off theory for some of the sound field. This research was conducted in Nevada with a 466 m (1,529 ft) tower [Haglund and Kane, 1973]. Then to more directly address the Mach cut-off issue, a theoretical and experimental study was conducted in the mid-1970s with FAA support. The studies estimated altitudes and Mach number regimes to ensure the focus boom does not reach the ground. That field campaign used fighter jets flying out of Langley AFB to a test area in the Atlantic Ocean off Wallops Island, Virginia [Perley, 1977]. Using the available instrumentation, the study concluded that Mach cut-off flight was feasible.

In none of those studies were any recordings made of sufficient quality to assess human response to the Mach cut-off noise. The theoretical studies estimating the altitude and Mach number restrictions for focus boom avoidance assumed a simple atmospheric model (linear sound speed profile), and did not include real-world atmospheric effects. Hence the 1960s-1970s work was very good, but is only a start to determining appropriate flight conditions for routine Mach cut-off supersonic flights over the continental United States.

Task 1A- Propagation Modeling with Enhanced Ray-tracing Capabilities

The Pennsylvania State University

Objective(s)

Research will be conducted to understand Mach cut-off operations and how often people would hear the unique Mach cut-off sounds. This includes estimating the flight altitude and Mach number restrictions for focus boom avoidance including real-world atmospheric effects and providing assessments of practical Mach cut-off flight.

Research Approach

Methodology

Mach cut-off depends on the upward refraction of the sound in the atmosphere due to the temperature and wind speed gradients. To examine this phenomenon, the original propagation theory [Nichols, 1971] was retraced for extensibility. Nichols' theory was used back in 1970s to assess Mach cut-off. In that theory, the atmosphere is assumed to have only vertical variations of temperature and horizontal wind. Based on one form of the refraction law specifying the normal direction of a wavefront, it was argued that for upward sound refraction, a direct sonic boom noise would not reach the ground as long as the acoustic wavefront normal becomes parallel to the ground aloft. The "safe" flight altitude and distance between the sonic boom caustic and the ground can then be determined.

One limitation of earlier Mach cut-off theories (including Nicholls') and existing tools (e.g. PCBoom) is that vertical winds are not included. In a realistic atmosphere, however, a noticeable vertical wind can sometime exist. A sea breeze is one example in which a wind is blowing from sea to land, which normally occurs along coasts during daytime which involves with ascending and descending motion of the air. As the vertical wind becomes non-negligible, both the launch angle of sound rays away from the aircraft and the altitude of the caustic will be affected, as shown in Figure 1. Thus, it's important to clarify the difference between the refraction law for a sound ray and that for the normal to a wavefront in a moving atmosphere [Ostashev, 2001].

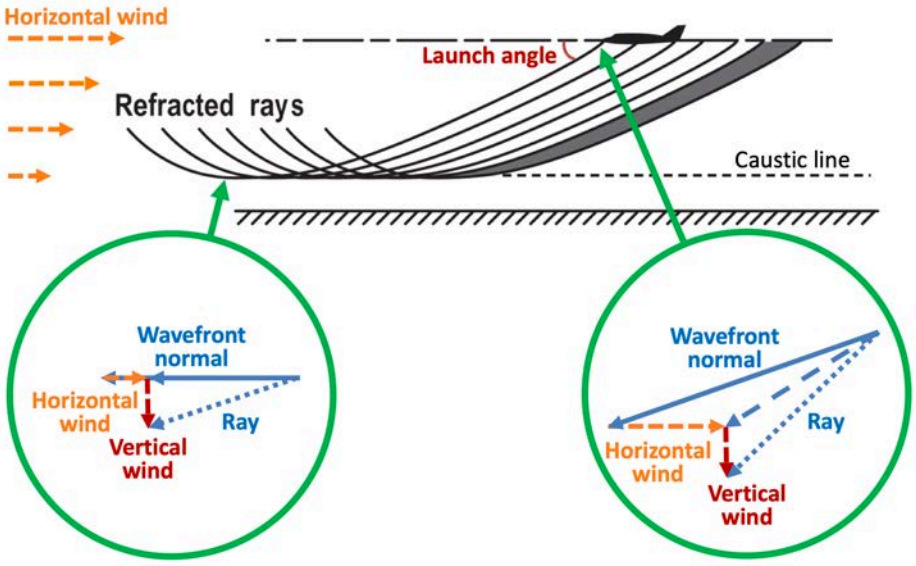


Figure 1. Contributions of a vertical wind to the difference between the wavefront normal and ray directions.

Another limitation in Nicholls' theory is, by calculating the cut-off Mach number based on the atmospheric conditions only at the flight and ground levels, the impact of realistic vertical atmospheric profiles in between those two levels on the sound propagation hasn't been included. For sonic boom propagation over a long horizontal distance, horizontal variations of the atmosphere can also be important for Mach cut-off.

In order to have an acoustical model that can lead to more accurate estimates of the safe cut-off altitude, flight Mach number and ground speed for Mach cut-off flight, 3-D ray tracing equations have been examined [Pierce, 1989]. Based on which, a 3-D 4th order Runge-Kutta integration ray tracing scheme has been developed, which can read-in realistic atmospheric data that includes arbitrary speed of sound variations as well as arbitrary three-dimensional winds including longitudinal, lateral and vertical wind components. It can be used to simulate sonic boom propagation through the 3-D atmosphere.

The data from Climate Forecast System version 2 (CFSv2) was used for the atmosphere [Saha, 2014]. CFSv2 provides an averaged and smoothed atmosphere globally at a horizontal resolution of 0.5 degree in both longitude and latitude, with 37 pressure levels up to an altitude of 40 km. The data is provided every 6 hours since January 1st, 2011 and updated on a daily basis that includes temperature, pressure, eastward and northward winds, vertical wind, and ground elevation that were used among other variables.

As shown in Figure 2, the horizontal resolution of the CFSv2 grid points corresponds to a distance of approximately 55 km over the ground. Since typical horizontal distances the sonic boom can travel before it reaches a cut-off point would be mostly in the range of 80 – 100 km, the CFSv2 grid point resolution is not good enough to provide information about the horizontal variation of the atmosphere in a local ray-tracing scale. Thus, the atmosphere is assumed to be vertically stratified in the computational domain of the simulation for each single case. On the other hand, in a global scale, the horizontal change of the atmosphere is included in our model. For each simulation, after the instantaneous location of the cruising aircraft along the flight path had been specified, this can be achieved by choosing the atmospheric data at the nearest CFSv2 grid point to represent the local atmospheric condition at the aircraft location.

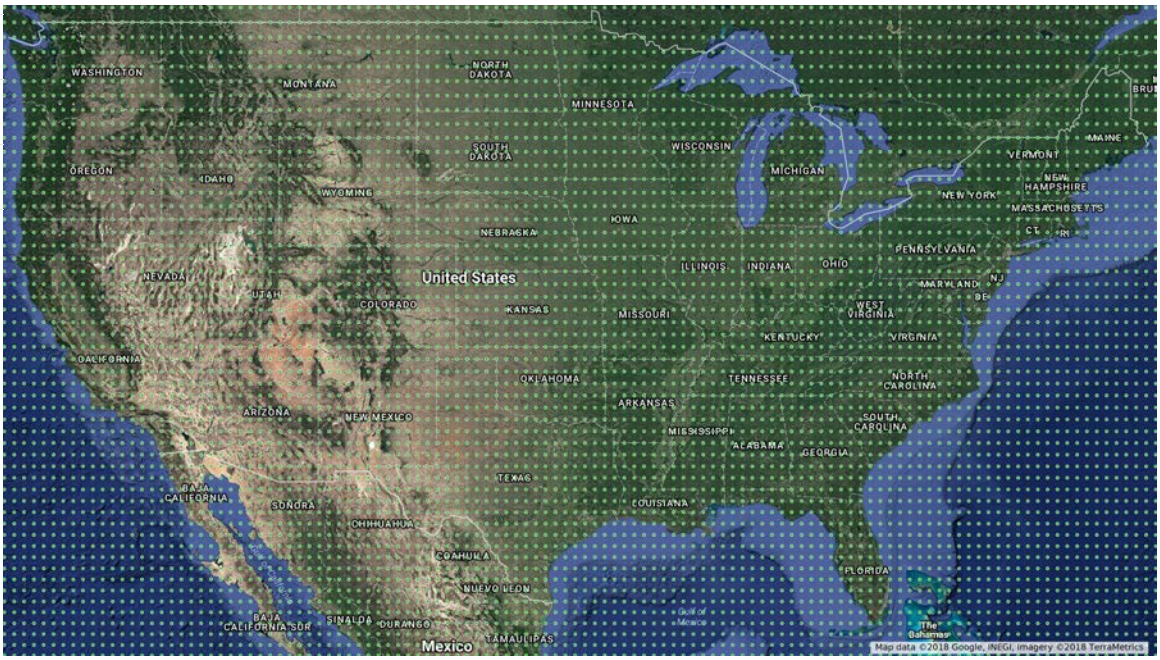


Figure 2. Contiguous United States map with grid points of the CFSv2 data.

With the input atmospheric data, the next step is to incorporate the Mach cut-off operational parameters proposed by Aerion Corporation. For this study, both a lower flight altitude of 12.5 km (41,010 ft) and a higher one of 15.24 km (50,000 ft) were adopted. The flight direction was inferred based on the location of the aircraft along the flight path.

When an aircraft is flying under the Mach cut-off condition, a focused boom is formed at the cut-off altitude, which corresponds to loud sound energy. Below that cut-off altitude, there is an evanescent wave decaying rapidly towards the ground, which typically covers a distance of a few hundred feet. To ensure the caustic never intercepts the ground, an adequate safety margin needs to be allowed [Plotkin, 2008]. So far, the cut-off Mach number was determined as the largest Mach number possible with at least a 500 m clearance of a caustic on the ground. The corresponding true air speed, aircraft

ground speed, and vertical distance between the caustic and ground were then calculated. This method was used to assess the viability of Mach cut-off operations for one of the busiest air routes in the U.S. at a particular time of a year.

Results

As an example, a preliminary 3-D ray-tracing result using CFSv2 data is given for an aircraft flying over Los Angeles under cruise condition at an altitude of 12.5 km (41,010 ft) at 12 PM UTC on Jan 1, 2017, with a flight direction of 21.6 degree north of east, as shown in Figure 3. The cut-off Mach number for this case is 1.09, and the corresponding aircraft ground speed is 747.83 mph.

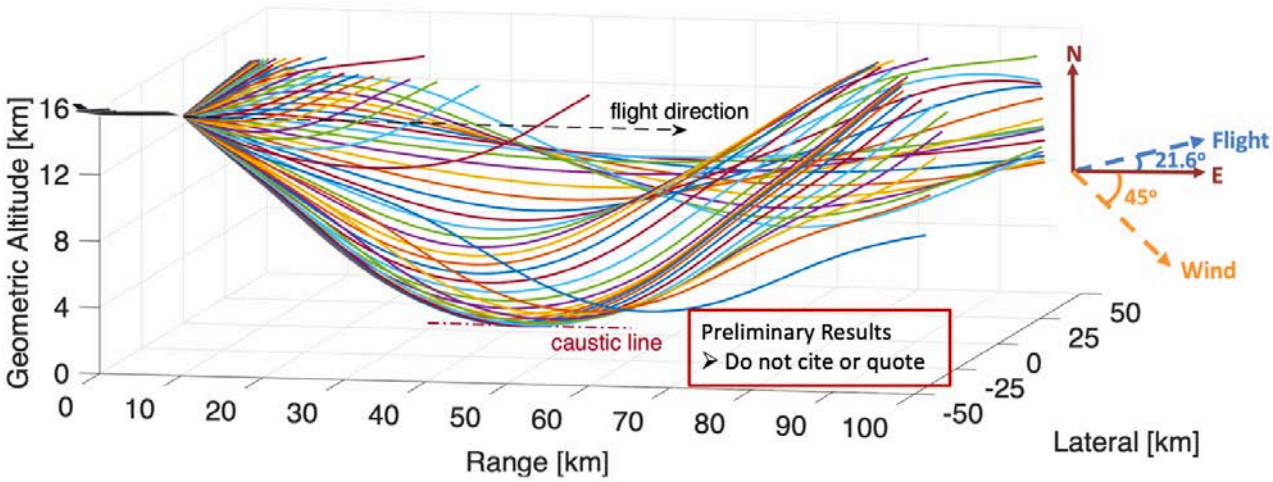


Figure 3. 3-D ray-tracing diagram, isometric view.

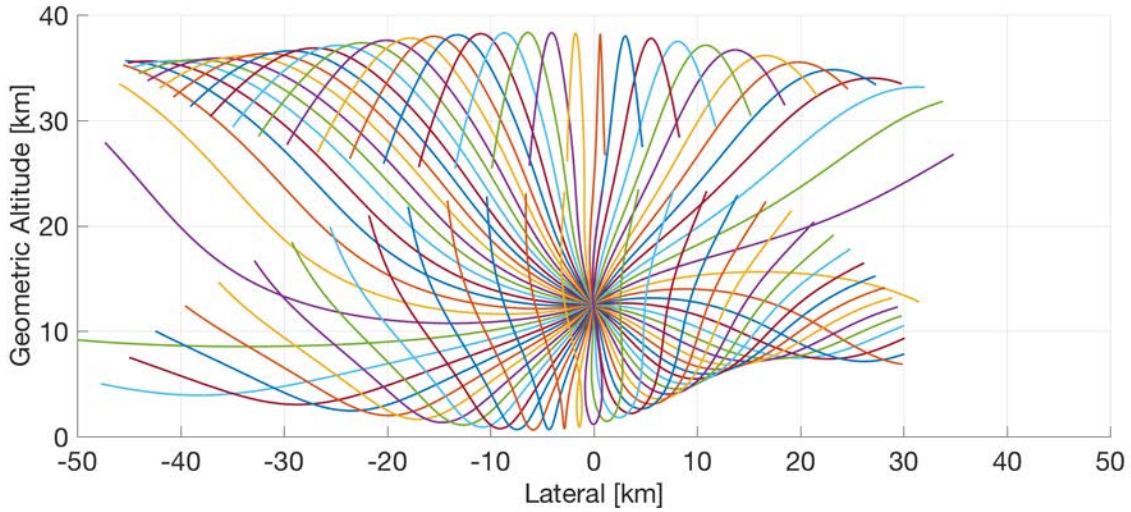


Figure 4. A side view of the 3-D diagram.

Figure 4 is a sideview of the 3-D diagram shown in Figure 3. In Figure 4, the flight direction is pointing perpendicularly out of the paper. It shows that the crosswind bends the sound rays toward the left side, and it's not necessarily the bottom ray (which has the deepest launch angle) that's the most likely one to reach the ground. Thus, it can be important to trace not only the bottom ray, but also the neighboring side rays.

Another example given below is to examine the impact of the vertical wind on the Mach cut-off altitude. In this example, the aircraft is flying at an altitude of 12.5 km northward. The CFSv2 atmospheric data for 12 PM UTC on September 10, 2017 in Miami, Florida is used. The atmospheric profiles are given in Figure 5.

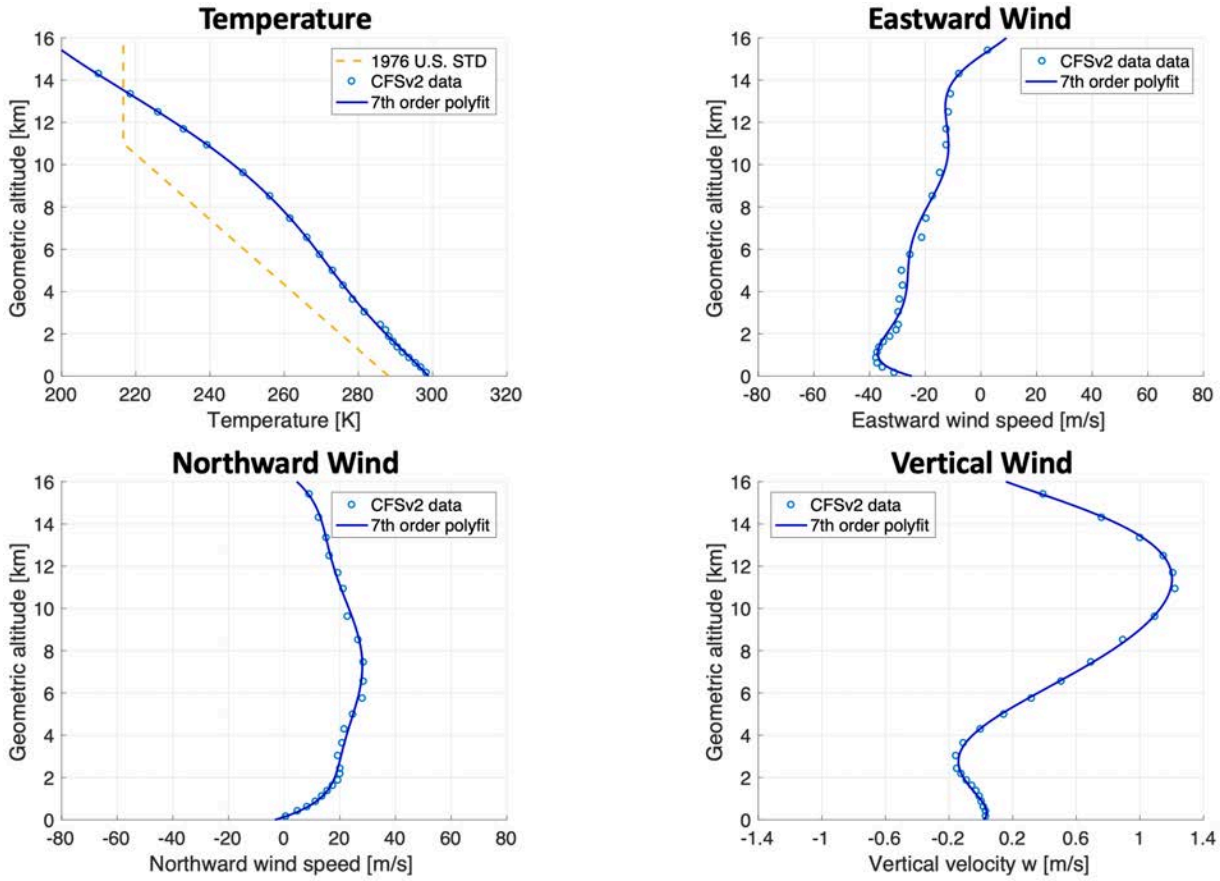


Figure 5. Atmospheric condition at 12 PM UTC on Sept. 10, 2017 in Miami, FL.

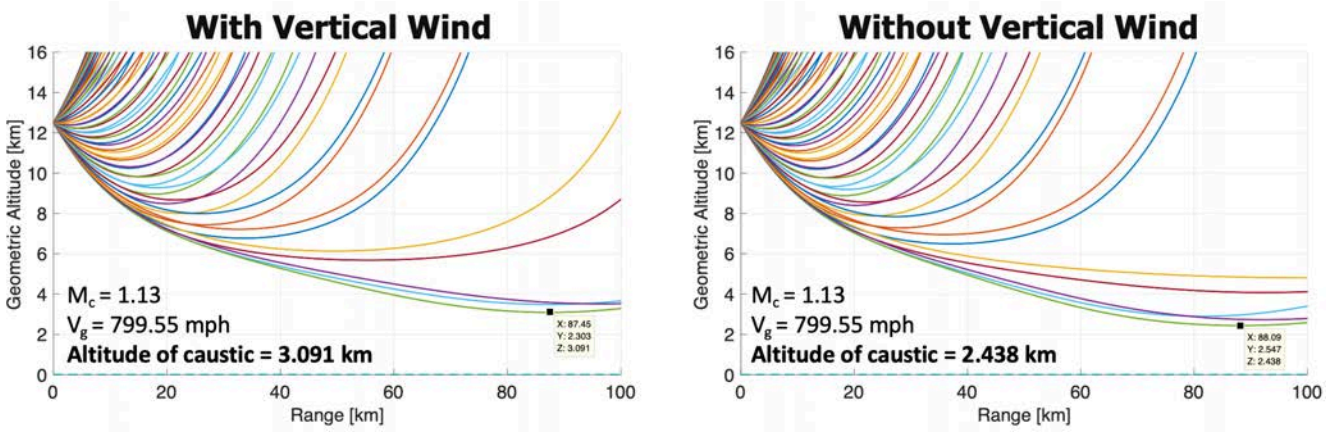


Figure 6. The impact of vertical wind on the Mach cut-off altitude.

In Figure 6, both of the two pictures are side views of the ray diagram. The only difference is, the vertical wind was included for the calculation shown in the left subfigure, while it was ignored for that shown on the right. A simple comparison shows

that including a vertical wind while keeping other atmospheric variables the same can contribute to a 653 m difference in the Mach cut-off altitude. This means, sometimes the vertical wind is an important factor. It should also be stated that this particular atmospheric event is an unusual one, corresponding to when hurricane Irma hit Florida.

In a last example, the safe altitudes and speeds for Mach cut-off flight for a hypothetical round trip between Los Angeles and New York (as shown is Figure 7) were investigated, in which two different flight altitudes were used. The cut-off Mach number was determined as the largest Mach number possible with at least a 500 m clearance of a caustic above the ground. The ray-tracing calculation results for the westbound and eastbound cases are given in Figures 8 and 9, respectively.

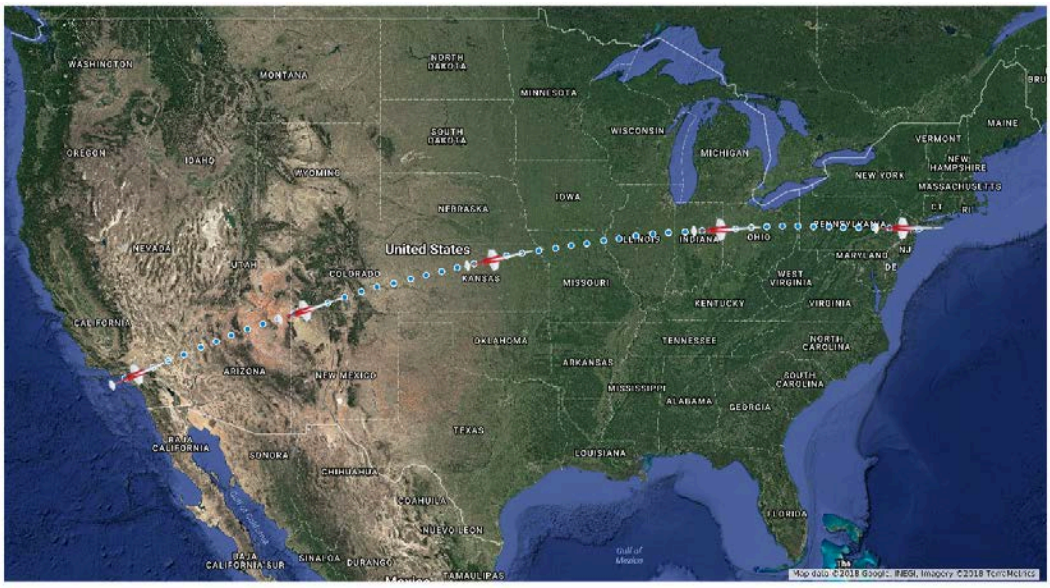


Figure 7. Air Route from LAX to JFK, Los Angeles to New York.

The top picture in Figure 8 provides the results for the westbound case. It shows when the aircraft was leaving the east coast, flying at a higher altitude didn't necessarily contribute to a higher cut-off Mach number. This is primarily because, the dominant eastward wind speed is decreasing with increasing altitude at altitudes above 10 km so that in the same region the effective sound speed (thermodynamic speed of sound plus wind speed) increases with increasing altitude. Thus, a higher cut-off Mach number can be achieved by flying at an altitude where the local effective sound speed is a minimum. However, a higher Mach number does not necessarily correspond to a higher aircraft ground speed unless we are talking about the same flight altitude, because the Mach number only represents a relative speed. In this case, we are comparing two different flight altitudes, since the temperature and wind speed at those two different altitudes are also different. Although sometimes a higher Mach number is achieved at a higher altitude, adjusting the flight altitude between 12.5 km and 15.24 km didn't gain significant benefit in the maximum aircraft ground speed.

Comparing Figures 8 and 9, it can be seen that, it's easier to implement Mach cut-off for a westbound flight than for an eastbound flight whenever the wind is mainly blowing eastward, which seems to be relatively common. In other words, it's easier to implement Mach cut-off when flying into a head wind than with a tail wind. When it's inevitable to fly with a tail wind, one should try to fly at an altitude where the local longitudinal wind speed is smaller. This is so that the local effective sound speed can be smaller, and this may help to achieve a higher Mach number that's well above Mach 1.0 if the temperature is not varying significantly in that region, even though by doing so one may not be able to increase the aircraft ground speed.

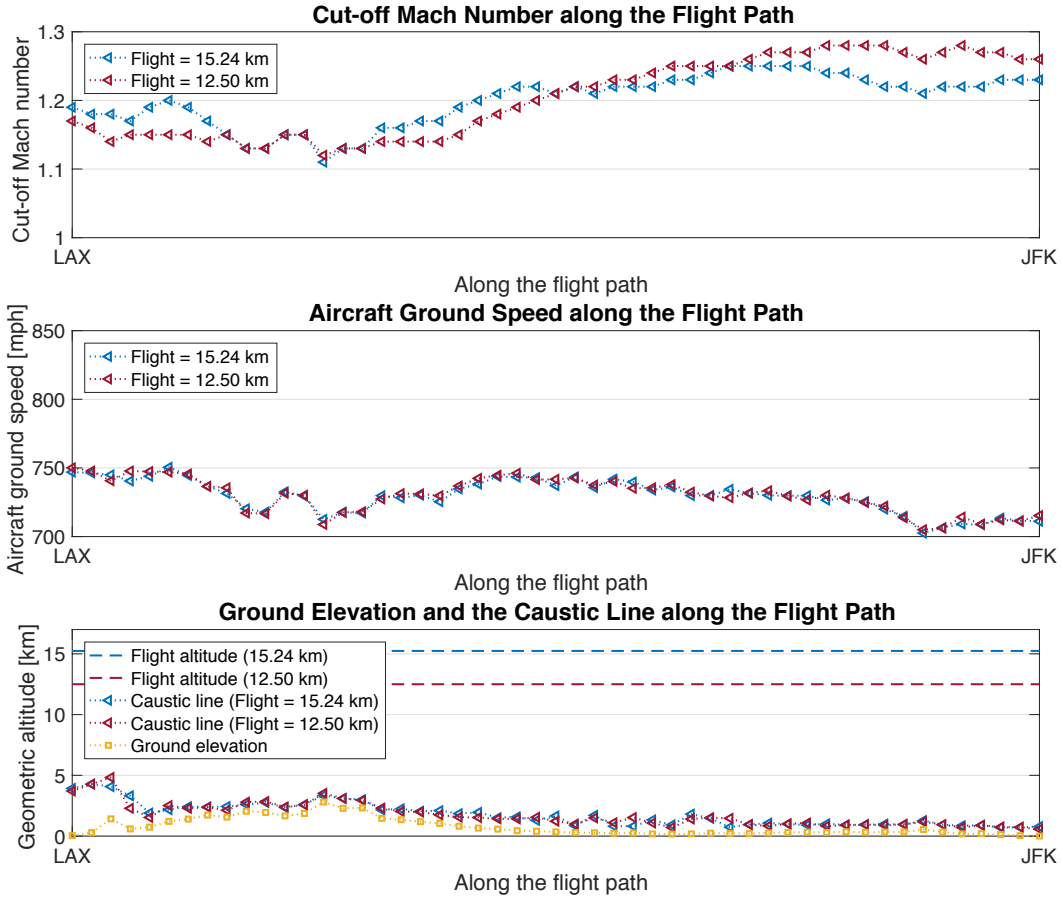


Figure 8. JFK to LAX air route (westbound into a headwind) on Jan 1 2017 at 12 PM UTC.

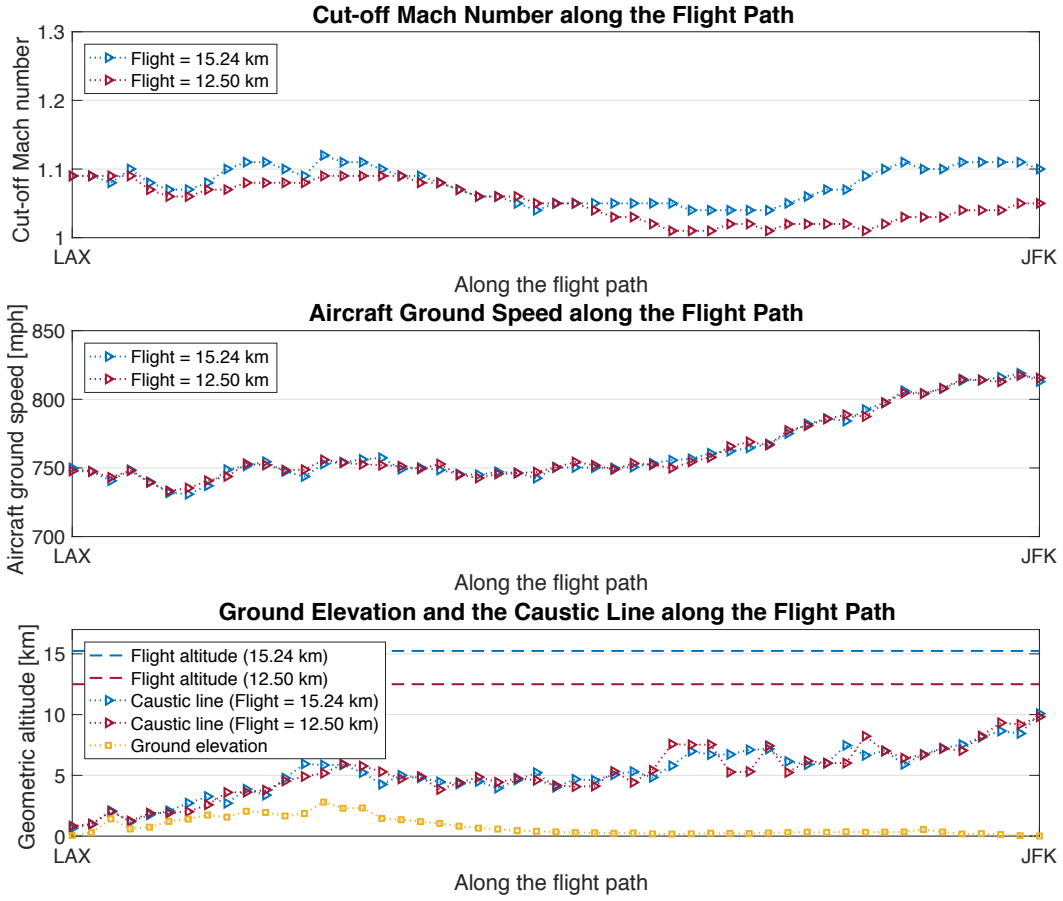


Figure 9. LAX to JFK air route (eastbound with a tailwind) on Jan 1 2017 at 12 PM UTC.

Milestone(s)

Milestone	Date
A 3-D ray-tracing algorithm had been developed, which showed vertical wind speed can be an important factor in the prediction of safe altitude.	January 31, 2018
The safe altitudes and speeds for Mach cut-off flight for a hypothetical trip from Los Angeles to New York was investigated.	March 31, 2018
Examine other atmospheric model datasets, which have better time and spatial resolution than the CFSv2 datasets	September 30, 2018



Major Accomplishments

In this research, a 3-D ray-tracing algorithm has been developed for the acoustical model of Mach cut-off flight, which can read-in realistic atmospheric data that includes arbitrary speed of sound variations as well as arbitrary three-dimensional winds. It is shown that vertical wind can be an important factor in the prediction of safe altitude. For certain wind profiles and aircraft headings a change in Mach number of 0.01 can send a focus boom down to the ground, even at a low Mach number such as 1.04. The safe altitudes and speeds for Mach cut-off flight for a hypothetical trip from Los Angeles to New York was investigated. Because of the persistent tailwind for such an eastward flight, Mach cut-off is much more challenging than for a westward flight.

Publications

Z. Huang and V. W. Sparrow, "An improved Mach cut-off model based on a 3-D ray tracing method and realistic atmospheric data," *J. Acoust. Soc. Am.*, **143**(3), 1913 (2018), invited presentation at 175th Meeting of the Acoustical Society of America, Minneapolis, MN, USA, May 07-11, 2018.

Outreach Efforts

Z. Huang and V. W. Sparrow, " An Improved Mach Cut-off Model Based on a 3-D Ray Tracing Method and Realistic Atmospheric Data," Poster for the Penn State Center for Acoustics and Vibration (CAV) Spring Workshop, University Park, PA, April 24-25, 2018.

Awards

None

Student Involvement

Zhendong Huang is the graduate research assistant supported by Project 42 at Penn State on this task. He is pursuing his Ph.D. in the Penn State Graduate Program in Acoustics.

Plans for Next Period

The project team is examining other atmospheric models with much better temporal and spatial resolutions than the CFSv2 datasets, so that it would be possible to include impact of temporal variations of the atmosphere along a flight path, as well as the contribution of horizontal variation of the atmosphere in a local scale, on the safe altitude and cut-off Mach number. This approach is based on excellent inputs from the Penn State Department of Meteorology on appropriate atmospheric datasets. A statistical analysis is underway which will help to answer the question that how often people could hear sounds from Mach cut-off operations.

References

G. Haglund and E. Kane, "Flight test measurements and analysis of sonic boom phenomena near the shock wave extremity," NASA Report CR-2167 (1973).

Z. Huang and V. W. Sparrow, "An improved Mach cut-off model based on a 3-D ray tracing method and realistic atmospheric data," *J. Acoust. Soc. Am.*, **143**(3), 1913 (2018), invited presentation at 175th Meeting of the Acoustical Society of America, Minneapolis, MN, USA, May 07-11, 2018.

J. Nicholls, "A note on the calculation of 'cut-off' Mach number, " Meteorological Mag. **100** 33-46 (1971).

V. E. Ostashev, D. Hohenwarter, K. Attenborough, P. Blanc-Benon, D. Juvé, & G. H. Goedecke, "On the refraction law for a sound ray in a moving medium, " Acta Acustica united with Acustica, **87**(3), 303-306 (2001).

A. Pierce, "Acoustics: An Introduction to its Physical Principles and Applications, " Acoustical Soc. Am., New York (1989).

K. Plotkin, J. Matisheck, and R. Tracy, "Sonic Boom Cutoff Across the United States," in 14th AIAA/CEAS Aeroacoustics Conference (29th AIAA Aeroacoustics Conference), AIAA Paper 3033 (2008).

S. Saha et al., "The NCEP Climate Forecast System Version 2," J. Clim., **27**(6), 2185–2208, Mar. (2014).

Task 2- Subjective Study on Annoyance, Metrics, and Descriptors

The Pennsylvania State University

Objective(s)

- Identify the key perceptual attributes of Mach-cutoff ground signatures.
- Determine how these attributes are correlated with annoyance ratings of these signals.
- Identify a metric appropriate for predicting annoyance due to Mach-cutoff ground signatures.

Research Approach

Introduction

This research will be the first major contribution to the body of literature on the perception of Mach cut-off. The ultimate goal of this work is to identify a metric that can be used to predicting annoyance due to Mach-cutoff flights. Subjective testing data will inform metric selection and corresponding values for possible use in certification. Mach-cutoff ground signatures are unique sounds and have not been part of the public's day-to-day experience, so the impact on community annoyance is difficult to predict. In addition, these signatures are perceptually different from N-shaped sonic booms. As such, new subjective tests are necessary to assess perception of these sounds and ultimately predict annoyance in communities.

The task is subdivided into three studies: (1) descriptor study, (2) annoyance factor study, and (3) absolute annoyance study. The descriptor study was nearing completion at the end of the last period and was used to identify a set of perceptual attributes that could be used to describe Mach-cutoff ground signatures for the second study, which is the annoyance factor study. This second study is nearing completion and will identify correlation between annoyance and various noise metrics. A secondary goal of this study is to evaluate any possible correlations between annoyance and the attributes identified in the first study. The third study, the absolute annoyance study, is still in the development stages. The purpose of this study is obtain annoyance ratings of the signatures relative to other common traffic noises, i.e. road, rail, and subsonic aircraft noise, and to further evaluate the proposed metric(s) from the second study to use for predicting community annoyance response to Mach-cutoff ground signatures.

Study 1 – Descriptor study

Data Collection

Study 1 was designed as an exploratory study to identify terms used to describe perceptual attributes associated with these signatures since no prior work exists on this topic. Several different subjective testing methods were considered to obtain this set of terms as described in the 2016-2017 annual report. The method of Free Choice Profiling (FCP) was selected since it allows participants complete freedom to identify attributes they associate with this type of sound without any influence from the test structure or administrator. Free Choice Profiling was developed by Williams and Langron [21,2] to study perception of foods, but it has been applied in the audio field [3-5]. The general procedure includes three steps: vocabulary generation, vocabulary refinement, and stimulus ratings.

A set of 24 stimuli was used in this study, which where a subset of Mach cutoff recordings obtained from NASA's Farfield Investigation of No-boom Thresholds (FaINT) recordings [6]. (The selection process was detailed in the 2016-2017 annual report and involved careful listening and categorization of the stimuli.) For the vocabulary generation step, the participants were required to listen to the stimuli in two groups of 12 to generate ideas of appropriate descriptors. Subjects were then instructed to enter up to 10 separate terms that they felt emphasized perceptual differences between the stimuli (see Figure 1 for the testing interface). Participants could listen to each individual stimulus as many times as they chose. The process was then repeated with the other half of the stimuli.

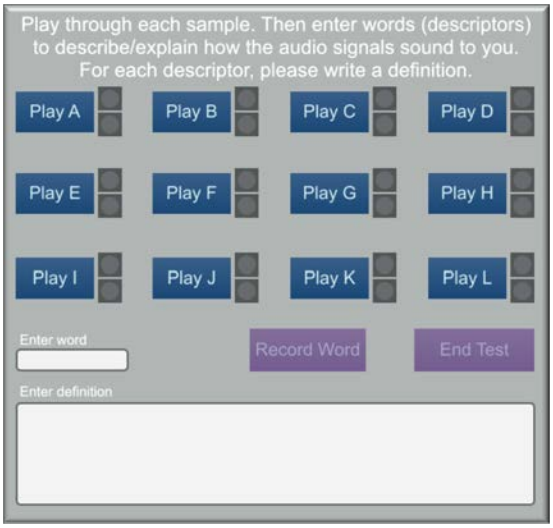


Figure 1. Study 1user interface for descriptor entry. This interface allowed test subjects to enter their own descriptors for Mach-cutoff stimuli along with accompanying definitions.

Once a subject had generated descriptors, the list was reduced to a maximum of 5 though an interview with the test administrator (Ortega). Interview questions included "Are any of the descriptors describing the same aspect of the sound as another descriptor?" and "Would it be difficult to rate stimuli on any of these descriptors?". Once the list was narrowed down to 3-5 attributes, subjects rated this set of attributes for each of the 24 stimuli using the interface shown in Figure 2. (The screen pictured was repeated for each stimulus, with each of the subject's descriptors appearing.) This process served as the final step of the FCP procedure. Note that the stimulus order was randomized for all sets for both listening tests in steps 1 and 3.

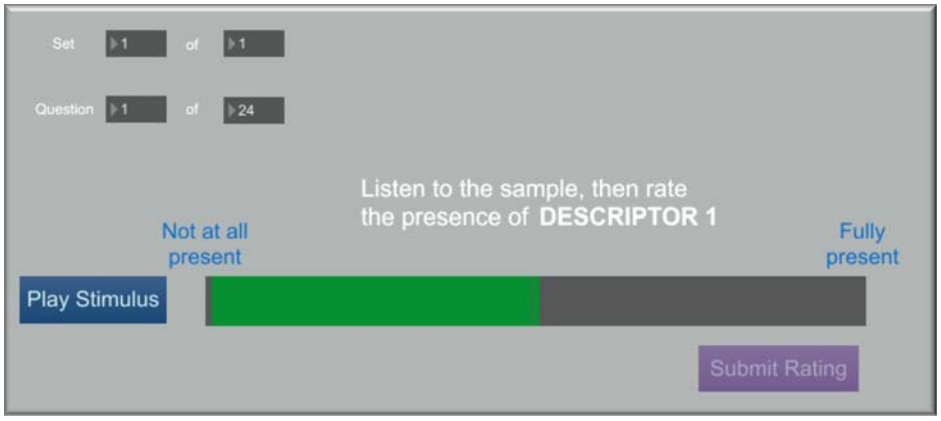


Figure 2. Study 1 user interface for stimulus rating. This interface allowed subjects to rate stimuli on their own descriptors. During testing, a subject's descriptor replaced the label "DESCRIPTOR 1".

Test participants were recruited from the State College community. Inclusion criteria were minimum age of 18 years old and normal hearing thresholds of 25 dB HL or lower for the 125 -4k Hz octave bands. In addition, since musicians have been shown to provide more reliable data in these types of tests with much less training than non-musicians [7], a target was set to have about 2/3rds of the participants be musicians and the remainder non-musicians. In this manner, it was hoped that any noise in the data would be reduced. Non-musicians, however, were explicitly also recruited so that it would be possible to evaluate how representative the terms used by the musicians were of the general population.

A total of 28 subjects participated in the study, where their ages ranged from 18 to 38 years of age, median age 22, with 14 males and 14 females. While this age range is low relative to the general population, this study was intended to be a preliminary study only, and a broader age range was used in the second study and will also be used in the third study. The target of having approximately 2/3rds of the participants was roughly achieved with a total of 19 musicians participating in the study.

Data Analysis

The first step of the analysis of Free Choice Profiling data is the Generalized Procrustes Analysis (GPA) method [8]. This analysis method unifies the rating sets of each subject in order to pool together the results of all participants. This step is necessary since the subjects rated the stimuli using their own individual terms with (potentially) different definitions even for the same terms. The first step of GPA is to scale each set of ratings by subtracting the mean ratings and multiplying each rating on all terms for one subject by one value. This process normalizes each subjects' ratings, adjusting for subjects that use more of the scale than others. Second, the normalized rating sets are rotated in the multi-dimensional space to align the ratings of each stimulus. If each subject "places" the stimuli in their own subjective space, with axes defined by their own descriptors, then GPA rotates all spaces until the stimuli in every space lie on top of each other, as much as possible. Third, GPA defines new axes through Principal Component Analysis (PCA). These axes define a "consensus space".

The average stimulus ratings plotted against the first two principal components in the consensus space are shown in Figure 3. Immediately apparent is that stimulus 23 appears to be an outlier and a separate analysis, described below, supported the decision to exclude the data from this stimulus. A clustering algorithm was run on the rest of the data to find groups of similar stimuli. Overall, the clustering analysis revealed that a single cluster best characterizes all of the stimuli. However, since this finding didn't allow for more specific groupings, the next possible number of clusters resulting from the analysis was three clusters, which led to interpretable results. The three clusters labeled 1, 2, and 3 in Figure 3 are characterized by softer sounds, more impulsive sounds, and more high frequency sounds, respectively.

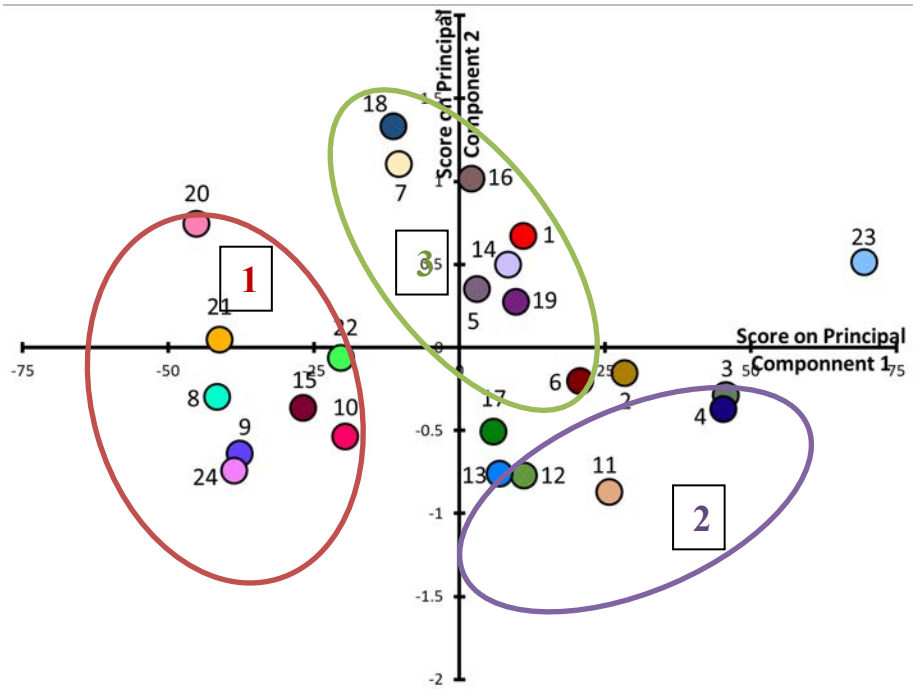


Figure 3. Average stimulus principal component scores after Generalized Procrustes Analysis. Circles show three main clusters. Note that the ratings of stimulus 23 were excluded from the remainder of the analysis as it was determined to be an outlier. Cluster 1 is characterized by softer sounds, 2 by more impulsive sounds, and 3 by more high frequency sounds

To further investigate if stimulus 23 was an outlier, the variance in the principal component scores for all stimuli were calculated. (Traditional statistical analyses can be run once the data has been transformed as described previously into the consensus space). As shown in Figure 4, the variance in the scores of stimulus 23 is nearly twice the average variance for the other stimuli. Therefore, based on both the visual inspection of the results shown in Figure 3 of stimulus 23 scores and the computation of the variance, stimulus 23 was omitted from all data analyses.

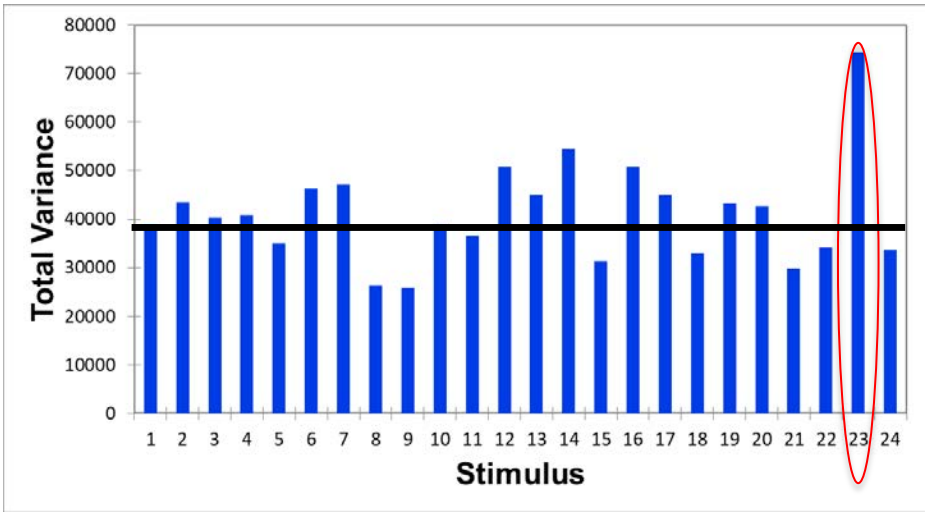


Figure 4. Total variance by stimulus. Note that the variance for stimulus 23 is nearly twice that of the average indicated by the black horizontal line.

In a similar manner to obtaining a set of scores for each principal component for each stimulus, a set of scores can be obtained for each attribute (descriptor) rated by each participant. These results can then be analyzed to determine the number of components (factors) that can explain the results for each individual attribute and the associated factor loading for each descriptor can be obtained. The results of this analysis for all rated terms are shown in Figure 6, where the results are plotted as a function of where each individual term falls on the scales (axes) of the two factors (components). This set of scores for each term can then be used to carry out a clustering analysis to determine how the terms may be grouped to ultimately identify a set of 2 to 4 perceptual attributes associated with Mach-cutoff ground signatures, which can then be used in follow-on studies to identify a metric to predict annoyance.

With the factor loadings obtained in the previous step, meaning can be given to the principal components. First, the terms were clustered using k-means clustering on the factor loadings. In Figure 6, these clusters are highlighted by the four circles. The largest cluster is on the positive end of the first axis and contains terms related to loud, impulsive sounds (example terms are “thunderous” and “powerful”). On the negative end is the next largest cluster, with terms related to soft sounds (e.g. “distance” and “soft”). These clusters show that the first principal component, Factor 1, is likely related to a sense of loudness. The second and third clusters place low frequency terms such as “rumble” on the negative end of the second axis and high frequency terms, such as “whistling” and “white noise”, on the positive end, showing that the second principal component, Factor 2, is likely related to pitch perception (frequency). This information was used to group the terms into clusters as shown. These clusters along with a fifth are broken down into the most common terms from each cluster in Table 1. The most commonly used terms were related to “Thunder” in the first cluster and the next most common term was “Rumble” in the third cluster. No obvious representative terms could be identified for the remaining three clusters. For the second and fourth clusters categorize as “soft” and “high frequency”, respectively, it was deemed unnecessary to identify representative terms, since those clusters appeared to have opposite meaning to “Thunder” and “Rumble”, respectively. For the final cluster, while no clear term emerged, it was decided that this perceptual feature may be worth further investigation. After a close review of the provided terms and definitions in this group, the word “Swoosh” was selected to represent this group, which was a term provided by a non-musician.

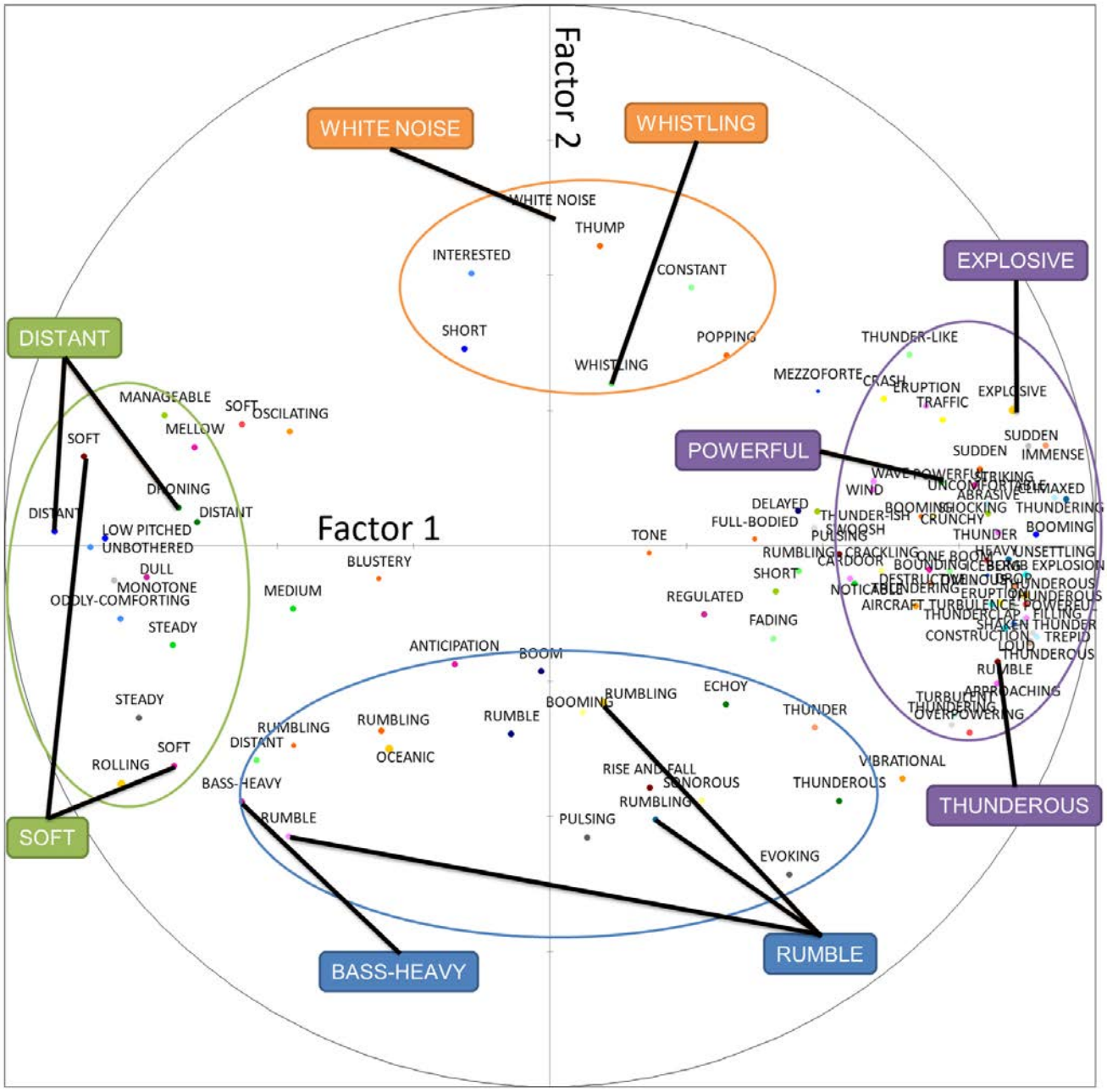


Figure 6. Descriptors plotted by loadings on first two principal components (Factor 1 and Factor 2). Key terms have been highlighted. Ovals show first four clusters of words.



Table 1. Descriptors grouped into clusters. "Thunder" was the most common term. Rumble was the most common term not related to thunder.

Loud		Soft		Low-f		High-f		Swell/Swoosh	
Thunder	13	Soft	3	Rumble	8	White noise	1	Ocean terms	3
Explosion/boom	10	Distant	3	Heavy bass	2	Whistling	1	Pulsing	2
Sudden	5	Steady	2			Short	1	Swoosh	1

Study 2: Annoyance factor study

Study Design

Having established terms linked to the perception of Mach-cutoff ground signatures in Study 1, the second study was designed to link these perceptual aspects to perceived annoyance and noise metrics. The three terms that were selected from the results of the first study were "thunderous", "rumbly" and "swooshing", where the first two each represented one of the two primary factors, and the third was selected as a possible third factor, although not strongly supported by the PCA results. The terms were defined as follows for the participants: "Thunderous indicates the degree to which the sound resembles the crack of nearby thunder (booming, explosive, etc.)"; "Rumbly is defined by an excess of low-frequency sound"; "Swooshing is defined as a sound that transitions from lower to higher pitch and from louder to quieter volume"; and finally for "annoyance", "Annoying describes how annoyed you feel by the sound".

In terms of the experimental design, it was now possible to carry out a more conventional subjective study using a common set of attributes for all participants to evaluate. The experimental method chosen was a combination of the paired comparison and rating scale methods, which has been shown to be an easier task for participants and yield more consistent responses over other test designs. However, this approach, relative to the one used in the first study where participants rated each stimulus individually, is much more time consuming to complete since paired comparison requires that participants evaluate all stimuli relative to all of the other stimuli in pairs. As a result, the number of test questions grows relatively quickly for a small number of stimuli, e.g. for a set of only 6 stimuli, there are 15 possible combinations for stimuli grouped in pairs. Due to testing time constraints to minimize participant fatigue, it was not possible to use all 24 of the stimuli from the first test. As a result, a subset of 6 stimuli was used in this study, where two stimuli from each of the three groups were selected as representative from each group respectively. An additional 3 simulated stimuli were included in the annoyance set, resulting in a total of 36 pairs for that set (further details are below). The overall test was subdivided into four sets, one for annoying and one for each of the three attributes.

The participants were presented a pair of stimuli and asked to select which stimulus had more of a given attribute, i.e. annoying, thunderous, rumbly, or swooshing. Subjects also had to rate the degree with which the one stimulus had more of a given attribute by using the scale shown in Figure 7. (Note that the different attributes ("THUNDEROUS", "RUMBLY", "SWOOSHING", or "ANNOYING") would replace the label "ATTRIBUTE" depending on which term the subject was rating. First, subjects would listen to both stimuli.) More details about the test procedure are provided in the next section.

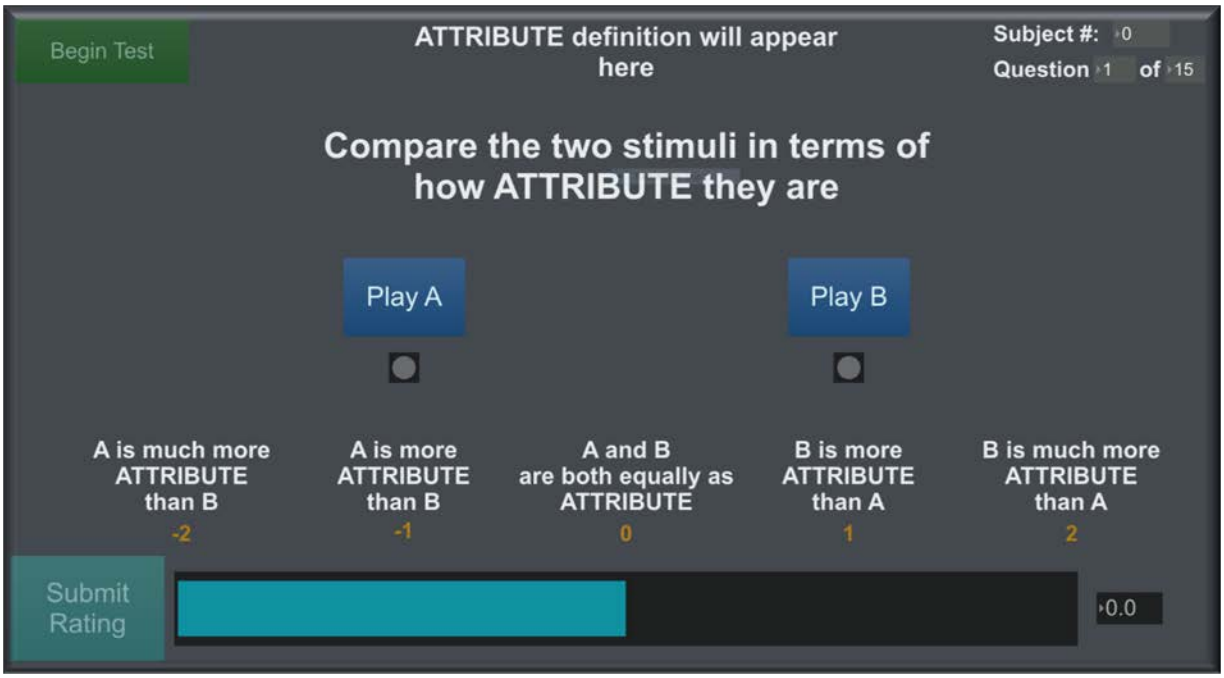


Figure 7. Study 2 rating interface. Subjects would click on the "Play A" and "Play B" buttons, decide which stimulus had more of the given attribute, i.e. annoying, thunderous, rumbly or swooshing, and rate how large that difference was using the slider bar.

The primary independent variable in Study 2 was different Mach cutoff signatures, the same as in the first study. However, for this second study, an additional independent variable was also of interest: the effect of the initial Mach-cutoff evanescent wave on perception, where this initial part of the signature was simulated from the work in Task 1. Three such signatures were synthesized for different elevations above the ground by modifying two input N-waves from glider recordings using a Hilbert Transform method. However, these signals lacked realism due to the lack of post-boom noise. As such, the simulation outputs were combined with a Mach-cutoff recording that had no audible evanescent shock noise and only post-boom noise, labelled "original" in Figure 8. This recording was selected from the set of 6 since it contained minimal background noise. The research team listened to the resulting waveforms and determined that they sounded realistic. The 3 resulting waveforms along with the original recording are plotted in Figure 8. Note that the signals only differed in the early part of the waveform, where the simulation was layered in. Due to testing time constraints, these stimuli were only included in the annoyance set.

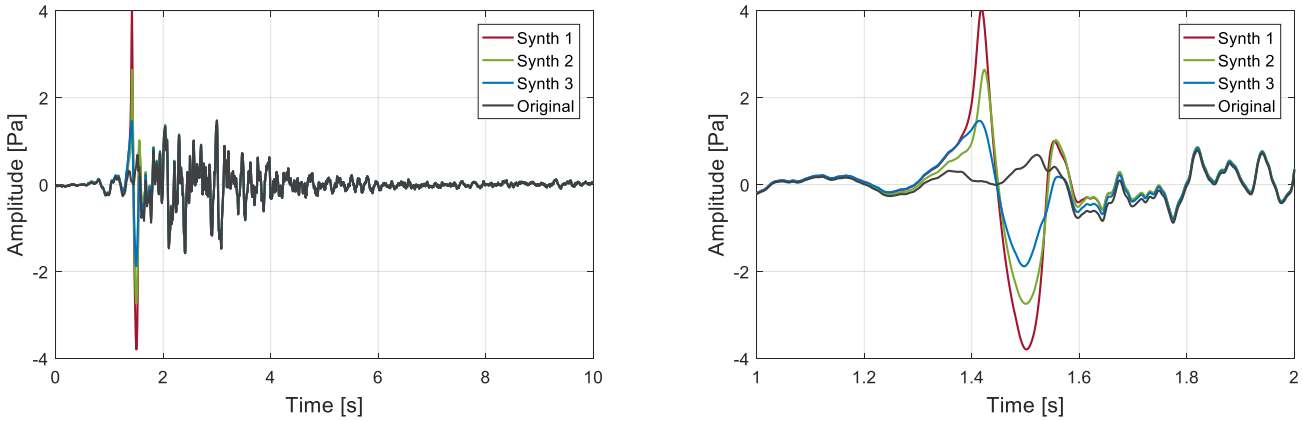


Figure 8. The three additional stimuli included in the annoyance rating set. The three simulated wave forms contain only the initial Mach-cutoff evanescent wave and not the remaining portion of a typical signature. As a result, the synthesized stimuli were combined with one of the six selected recordings to add post-boom noise. The full waveform is shown on left, while a detailed view is shown on right.

A final design element for this second study was to broaden the age of the participants to be more representative of the general population and not only college-aged students. Targets were set to collect 10 participants from each of the four age ranges: 18-29, 30-39, 40-49, and 50-60, with a goal of including 40 participants. To remove the possibility of gender effects on the results, a second target was to recruit an equal number of males and females.

Data Collection

The testing procedure for each subject was as follows. First, subjects would read and sign the informed consent form. Then, a hearing screening would be administered to ensure subjects had normal hearing in the range of interest (1000 Hz and below). Next, subjects would rate the stimuli on a paired comparison scale for each of the terms in four sets, one for each term. The first three sets were in a randomized order and used the terms “thunderous”, “rumbly”, and “swooshing”. As 6 stimuli were used for these sets, there were a total of 15 comparisons made for each of these terms. For the last set, subjects rated the 9 stimuli on the term “annoying” (36 comparisons). Before each set, tutorial slides were presented defining the attribute to be rated in that set (as defined above). Breaks were provided between each set, with a break in the middle of the “annoying” set. Afterwards, demographic and other information were collected through questionnaires. Average testing time was around 80 minutes per subject, with only 2 subjects taking longer than 90 minutes.

As of 5 November 2018, 42 subjects had participated in the study. Age and gender demographics are summarized in Figure 9. In general, there were fewer subjects in the highest age group, but overall the subjects’ ages were well distributed across the target age range. The gender ratio is skewed slightly towards female, with a 4:3 female to male ratio. It should also be noted that 7 of the 42 subjects met our criteria to be classified as a musician, though this was not a requirement for participation. Future analyses may evaluate the effect of musical training on the results.

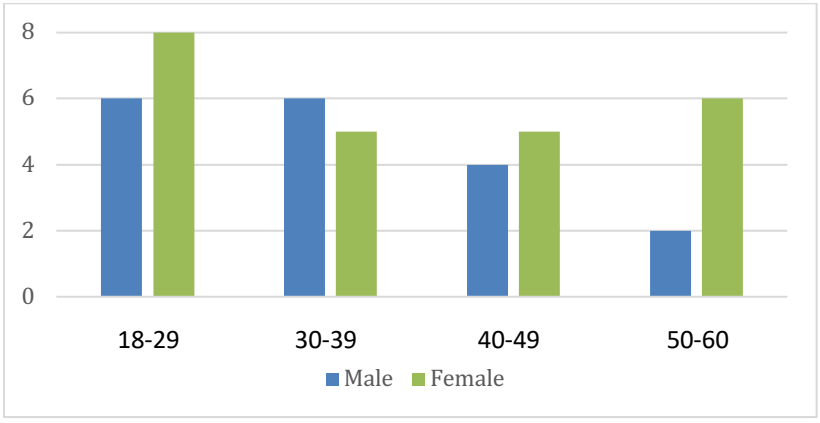


Figure 9. Demographic breakdown of Study 2 participants. Participants dropped off with age, and more females participated than males.

Data Analysis (Preliminary: 39 subjects)
The following analyses are **preliminary** and are based on the results from 39 out of the 42 subjects run (those run before 30 September 2018).

For all analysis, ratings on the paired comparison scale must be converted into ratings for individual stimuli on a relative scale. This conversion is achieved by summing across all pairs for a given stimulus. First, all stimuli are given an initial "rating" of zero. Then, for each pair, the stimulus rated as having more of the given attribute has the magnitude of the comparison rating added to the total rating for that stimulus. This process results in a single rating value for each stimulus for each participant. All the following analyses were run using these ratings.

The first statistical analysis looked at the effect of demographics on these ratings. A multivariate analysis of variance (MANOVA) was run with the ratings on each of the four attributes as the output variables and age category, gender, noise sensitivity, and Mach-cutoff signature (stimuli). A significant effect of ratings on individual stimuli was found ($p < 0.05$), but no statistically significant effects of age category or gender. The average annoyance ratings separated by demographic groups are shown in Figure 10. While there are some visible differences, these are not statistically significant and the overall shapes of the individual curves are similar, which means that the age of a participant did not influence their annoyance ratings. In other words, these findings suggest that future studies may not need to recruit as broad an age range which was done for this study. Finally, the effect of an individual's noise sensitivity was also not found to have a significant effect on the ratings.

The effect of the simulated boom on annoyance ratings was also investigated. For this analysis, ratings were calculated using only pairs including the three simulated booms and the original recording (4 stimuli, 6 pairs). This was done to directly compare the effect of the simulated boom. ANOVA was run with annoyance as the output variable and subject number and stimulus (now only 4 stimuli) as the input variables. While the effect of subject number was significant (at $p < 0.05$), the effect of stimulus was not significant (at $p < 0.05$). This result indicates that the simulated boom portion of the stimulus did not significantly affect the perception of annoyance and invites investigation into whether annoyance from Mach-cutoff ground signatures is due to the post-boom noise only.

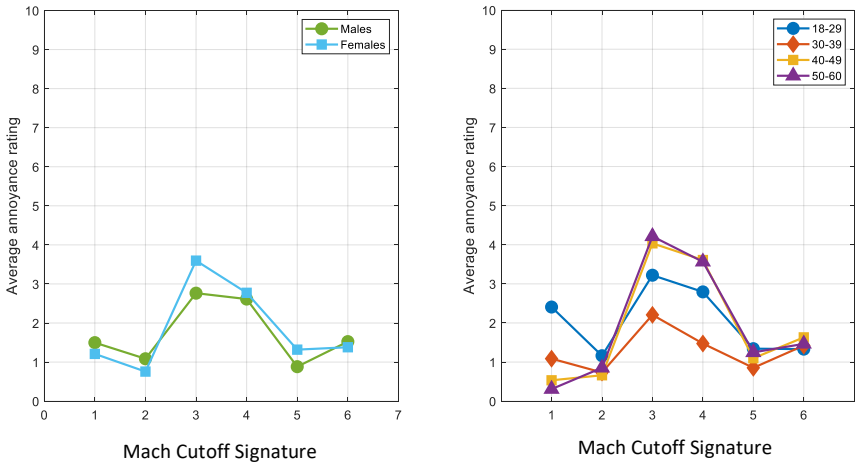


Figure 10. Annoyance ratings of the six Mach cutoff recorded signatures separated by gender (left) and age group (right). No statistically significant effects of either gender or age on ratings were found.

Annoyance ratings were also modeled using a linear regression of ratings of "thunderous", "rumbly", and "swooshing". To run this analysis, ratings on the three attributes were converted into factor scores through a varimax rotation. This process leads to orthogonal regressors, which is assumed in linear regression. The regression revealed a strong dependence of "annoying" ratings on "thunderous" ratings as shown in Table 2. While the dependence was significant for each factor, the slope estimate was strongest for the factor related to "thunderous" ratings, and metrics related to this factor will likely be the strongest predictors of annoyance. This finding will be further investigated in the next period.

Table 2. Linear regression results for dependence of annoyance on perceptual factors. While all factors had a significant effect on annoyance, the thunderous factor had the largest effect (slope).

Factor	p-value (slope ≠ 0)	Slope estimate	Standard error
Rumbly	<.0001	0.41	0.10
Swooshing	.0029	0.30	0.10
Thunderous	<.0001	0.79	0.10

Multiple metrics were calculated for each stimulus in order to investigate possible quantities that could be used to predict annoyance and the three perceptual attributes evaluated. Calculation procedures were written in MATLAB. Procedures were written to calculate weighted *sound exposure levels* (SEL) using A-, B-, C-, D-, and E- weighting (SEL_A, etc.). In addition, *perceived sound exposure level* (PL_SEL) was calculated according to the FaINT report [6], as was the sound quality metric *sharpness*.

The calculated metrics were used to evaluate the degree of correlation of these metrics with the rating data, as shown in Table 3. The highest correlations, which are indicated in **bold**, suggest that loudness-based metrics are somewhat correlated with the ratings on "annoying" and "thunderous". These metrics were also often correlated with the other perceptions of "rumbly" and "swooshing" as well, though to a lesser extent. It is apparent that loudness influences all the ratings, so a more complete analysis will be conducted in the next period to parse out which portion of the variance is explained by each metric.



Table 3. Correlations between calculated metrics and average ratings.

	SEL_A	SEL_B	SEL_C	SEL_D	SEL_E	PL_SEL	Sharpness	RC-based
Thunder	**0.92**	**0.95**	0.83	0.89	**0.97**	0. 88	0.61	0.39
Rumble	0.28	0.68	0.81	0.67	0.56	0. 30	0.06	0.62
Swoosh	0.86	**0.93**	0.76	0.82	**0.94**	0. 83	0.43	0.53
Annoy	0.79	**0.97**	**0.91**	**0.91**	**0.94**	0. 77	0.41	0.46

This preliminary analysis indicated that none of these metrics were highly correlated with "rumbly" ratings without also being correlated with thunderous ratings. A non-traditional aircraft noise annoyance metric was explored as a possible metric to predict this attributed. A new metric was developed based on Room Criteria Mark II (RC Mark-II). RC Mark-II was designed to analyze background noise in rooms due to heating, ventilation, and air conditioning (HVAC) systems. This metric was chosen since it includes an indicator for the perception of "rumble". In particular, the numerical quantity used in the RC Mark-II metric that predicts the perception of "rumble" was selected as the basis for this proposed "RC-based" metric. However, due to the lack of higher frequency content in these signatures, which would typically be present in HVAC noise, an early step in the calculation has been changed to be based on the mid- and low-frequency octave bands. The correlation analysis of this proposed RC-based metric and the perceptual ratings are shown in the last column of Table 3. As shown, the correlation values are relatively low for this proposed metric, however, further analyses are planned to evaluate if the variance due to loudness is reducing the predictive power of this metric.

Milestone(s)

Milestone	Planned Due Date	Status
Report on Mach cut-off descriptor subjective test	November 1, 2017	Complete
Report on experimental design of metric and annoyance study	February 1, 2017	Complete
Report on possible metrics that could be used to predict annoyance due to Mach cut-off sounds	July 31, 2018	In progress

Major Accomplishments

- Subjective testing for descriptor study (Study 1) was completed – 28 subjects participated in the study
- Study 1 data were analyzed – stimuli were characterized and the most significant terms were determined to be "Thunderous" and "Rumbly".
- Annoyance factor study (Study 2) was designed – paired comparison test designed to look at Annoyance along with perception of "Thunder", "Rumble", and "Swoosh".
- Study 2 data collection completed – 42 subjects participated in the full study (by Nov. 5).
- Multiple metric calculation procedures written for Study 2 data analysis – metric calculation procedures written for sharpness, sound exposure level (A-, B-, C-, D-, and E- weighting), Perceived Loudness, Perceived Sound Exposure Level, and an RC-based metric to possibly predict "Rumbly" ratings.
- Study 2 preliminary annoyance data analysis completed – annoyance deemed to be related to perception of thunder; ratings not likely affected by demographics of subjects.
- Further statistical analyses planned for Study 2 – in particular, a stepwise regression will be used to determine which metrics to include in the full analysis.

Publications

Acoustical Society of America Spring 2018 meeting abstract [9].

Outreach Efforts

CAV Workshop 2018 – Poster presentation: This consisted of one poster including the results from the descriptor study.

Awards

CAV Workshop 2018 student poster competition – 3rd place.

Student Involvement

Nicholas Ortega was primarily responsible for test design, stimulus selection, test preparations, statistical analyses, and presentation preparations for the first two studies. He also presented the poster at the CAV workshop and the talk at the ASA Conference.

Jonathan Broyles started in September 2018 and has been responsible for test design for Study 3. He will complete work on Study 3 during the following period.

Plans for Next Period

The major goals for the next period are to (1) complete the data analysis for Study 2 to propose a set of possible metrics to predict annoyance due to Mach cutoff ground signatures by January 2019 [Ortega] and (2) design and conduct a third subjective study to investigate the degree of annoyance due to Mach cutoff signatures relative to typical traffic noise [Broyles].

Based on the results of the second study wherein the inclusion of simulated stimuli did not have a significant effect on the annoyance ratings, it was decided that the third study will not include any simulated stimuli. The aims of the third study were further adjusted after meeting with AERION representatives in September 2018. From the discussions, it was determined that utilizing everyday traffic stimuli in context to the FaINT Mach-cutoff signatures based on annoyance would be beneficial in developing an annoyance metric. The everyday traffic stimuli of interest include road, rail, and subsonic air traffic noise. The proper authorities for each stimulus will be contacted to obtain permission to obtain recordings. Recording the stimuli will commence late November and be complete by December 2018. The experimental design will be developed in early 2019, data collection to take place in March – April 2019, and data analysis and final report by July 2019.

References

1. A. A. Williams; S. P. Langron, “The Use of Free-choice Profiling for the Evaluation of Commercial Ports”, J. Sci. Food Agri. **35** 558-568 (1984).
2. V. Dairou; J.-M. Sieffermann, “A Comparison of 14 Jams Characterized by Conventional Profile and a Quick Original Method, the Flash Profile”, J. of Food Sci. **67**(2) 826-834 (2002).
3. L. Gaëtan, “”Individual Vocabulary Profiling of Spatial Enhancement Systems for Stereo Headphone Reproduction”, Audio Engineering Society Convention 119, paper 6629 (2005).
4. T. Lokki; J. Pätynen; Antti Kuusinen, *et al.,* “Concert hall acoustics assessment with individually elicited attributes”, J. Acousti. Soc. Am. **130**(2) 835-849 (2011).
5. M. Gerzon, "Periphony: With-Height Sound Reproduction," J. Audio Eng. Soc. **21**(1) 2-10 (1973).
6. L. J. Cliatt II; M. A. Hill; E.A. Haering Jr., “Mach cutoff analysis and results from NASA’s Farfield Investigation of No-boom Thresholds”, 22nd AIAA/CEAS Aeroacoustics Conference, AIAA 2016-3011 (2016).
7. M. S. Lawless; M. C. Vigeant, “Effects of test method and participant musical training on preference ratings of stimuli with different reverberation times.” J. Acoust. Soc. Am. **142**(4) 2258-2272 (2017).
8. J. C. Gower, “Generalized Procrustes Analysis,” Psychometrika **40**(1) 33-51 (1974).
9. N. D. Ortega; M. C. Vigeant; V. W. Sparrow, “Perceptual characterization of Mach cut-off Sonic Booms,” J. Acoust. Soc. Am. **143** (3, Pt. 2) 1936 (2018). Presentation at ASA Spring 2018 in Minneapolis, MN, USA in May 2018.



Project 043 Noise Power Distance Re-Evaluation

Georgia Institute of Technology

Project Lead Investigator

Dimitri Mavris (PI)
Regents Professor
School of Aerospace Engineering
Georgia Institute of Technology
Mail Stop 0150
Atlanta, GA 30332-0150
Phone: 404-894-1557
Email: dimitri.mavris@ae.gatech.edu

University Participants

Georgia Institute of Technology
P.I.(s): Dr. Dimitri Mavris (PI), Mr. Christopher Perullo (Co-PI), Dr. Michelle Kirby (Co-I)
FAA Award Number: 13-C-AJFE-GIT-021
Period of Performance: June 28, 2016 – August 14, 2018

Project Funding Level

The project is funded at the following levels: Georgia Institute of Technology ($225,000). Cost share details are below:

The Georgia Institute of Technology has agreed to a total of $225,000 in matching funds. This total includes salaries for the project director, research engineers, graduate research assistants and computing, financial and administrative support, including meeting arrangements. The institute has also agreed to provide tuition remission for the students paid for by state funds.

Investigation Team

Georgia Institute of Technology
Principal Investigator: Dimitri Mavris
Co-Investigator: Christopher Perullo, Michelle Kirby
Research Faculty: Matthew LeVine, Greg Busch, Holger Pfaender
Students: Arturo Santa-Ruiz, Kenneth Decker, Sara Huelsman, Edan Baltman

Project Overview

The standard technique for evaluating fleet noise from flight procedures estimates source noise using Noise Power Distance (NPD) curves. Noise calculations within the Aviation Environmental Design Tool (AEDT) rely on NPD curves derived from aircraft certification data, provided by aircraft manufacturers. This dataset reflects representative aircraft families at set power levels and aircraft configurations. Noise levels are obtained as a function of observer distance via spherical spreading through a standard atmosphere. Other correction factors are applied to obtain the desired sound field metrics at the location of the receiver. The current NPD model does not take into account the aircraft configuration (e.g., flap settings) or alternative flight procedures being implemented. This is important as the noise characteristics of an aircraft depend on thrust, aircraft speed and airframe configuration, among other contributing factors such as ambient conditions. The outcome of this research is a suggested NPD + configuration (NPD+C) format that enables more accurate noise prediction due to aircraft configuration and speed changes.

Georgia Tech leveraged domain expertise in aircraft and engine design and analysis to evaluate gaps in the current NPD curve generation and subsequent prediction process as it relates to fleet noise prediction changes from aircraft



configuration and approach speed. The team used EDS physics based modeling capabilities to conduct a sensitivity analysis to identify additional parameters to be included in the NPD+C (NPD + Configuration) curve format.

This study assumes that the aircraft procedure is unchanged. The sensitivity studies provided are indicative of changes due solely to changes in the source noise characteristics and propagation effects due to use of the NPD+C. A coupled study of changes in trajectories using NPD+C vs. the traditional NPD is recommended as a follow on effort.

NPD and NPD+C Modeling and Prediction Overview

The current method used to obtain an airport (DNL) contour is outlined in Figure 1. First, the NPD data is obtained either through testing and certification or analytically. In this project, Georgia Tech used NASA's ANOPP software to predict aircraft source noise. A traditional NPD assumes limited variation in engine and airframe noise for a limited number of configurations. Typically an approach and departure NPD are generated, each of which assumes a fixed configuration as described later in Table 5. This data is currently acquired or calculated for a vehicle flying at a reference speed of a 160 kts. Noise prediction is then coupled with aircraft performance analysis to compute the SEL contour area for each stage length. DNL contours can then be generated using an assumed operations mix. For this study, only SEL contour areas were examined to simplify examination of the results. Historically, an 80 dB SEL contour area is representative of a 65 DNL contour area; therefore, the 80 db SEL is used in this study to calculate representative changes in contour area.

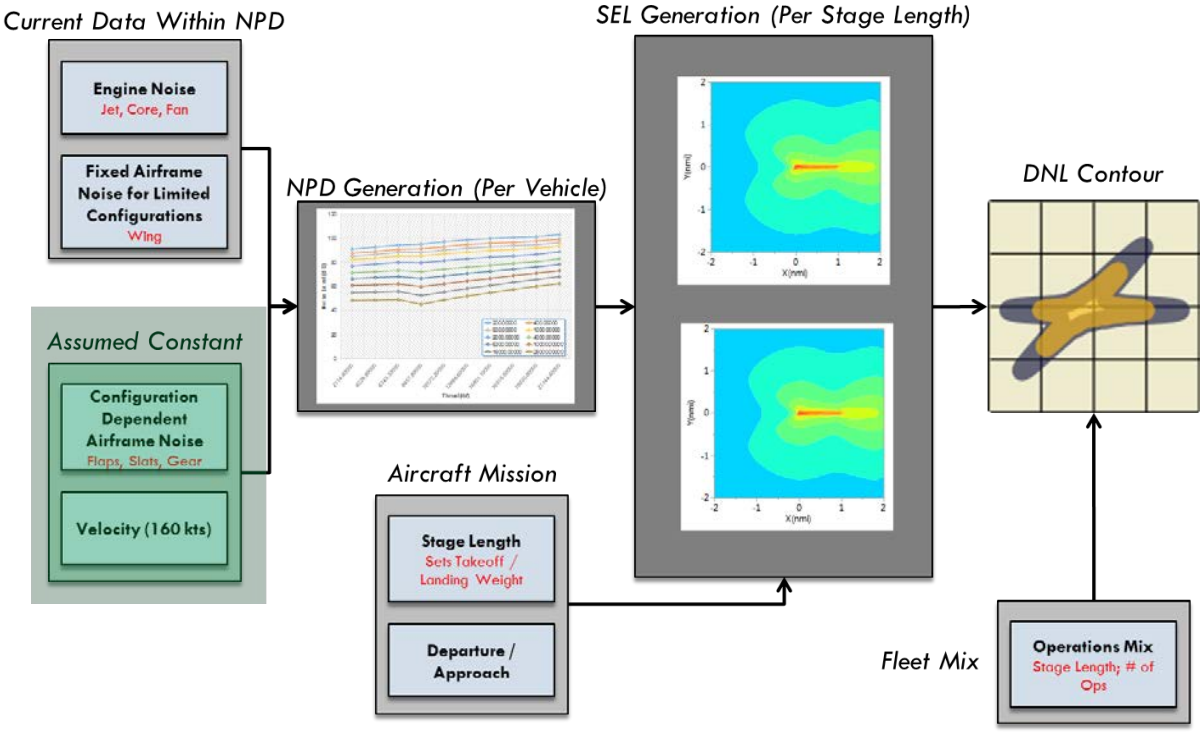


Figure 1. Noise contour analysis process

It is evident from the described approach that the final noise signature computed relies significantly on the physics based corrections present in the algorithm. Furthermore, a high-fidelity analysis of missions considerably deviating from the baseline procedures becomes strenuous. Consequently, the Georgia Tech team pursued two main objectives:

- Understand the sensitivity of including aircraft configuration changes and speed in NPDs, developing thus NPD+Cs on resulting noise contours
- Provide physics-based recommendations on format of NPD + Configuration (NPD+C) curves for use in AEDT.



The research is broken down into three distinct phases. First, a sensitivity study is performed on the generation of NPDs to understand the dimensions required to accurately assess each vehicle class. This step is detailed within the Task 1 section of the report. The second step is to generate the NPD+Cs (superset of 12 NPDs) and research the impact of including aircraft configuration (gear and flap-slat settings) at a range of reference velocities (130 – 190 kts) on the resulting 80 dB SEL noise contour. In order to perform this task, a thorough understanding of the acoustic computation process within AEDT is obtained. AEDT's relevant algorithm sections regarding procedures, performance and acoustic analyses were modified to properly assess the input XML vehicles. The Task 2 section of the report details the process, modifications of the adjustments to the source algorithm. The AEDT NPD+C studies section includes results and analyses. The last phase, the Task 3 section, highlights the steps taken to validate Georgia Tech's approach and confirm the reproducibility of results. Furthermore, the analysis provides an intuitive understanding of each segment's contribution to the total noise contour shape. Finally, Task 4 provides a summary of work performed to identify if a correction function could be used in combination with an existing NPD to estimate the noise changes of the NPD+C without the need to create a detailed model.

Task 1- Perform Sensitivity Study on NPD+C Curve Generation and Prediction

Georgia Institute of Technology

Objectives

The first task of this study is to determine which airframe configuration parameters to include in the subsequent sensitivity analysis. It is possible to consider contour area sensitivity with respect to gear setting (up or down), speed, flap angle, and slat angle. Statistical analysis is performed with respect to each of these parameters to determine the appropriate resolution required in each dimension when constructing the NPD+C. Reduction of resolution is desirable since this will be less computationally expensive and will ultimately require fewer experimental runs if this information is to be generated experimentally. In addition, each dimension (speed, flap angle, slat angle, gear up/down) will be analyzed to determine which parameters, if any, do not significantly contribute to the overall variability of the source noise characteristics.

Before sensitivity analyses can be performed, careful consideration must be given to determining appropriate methods for modeling the effects of configuration parameters on vehicle source noise. Typically, vehicle manufacturers experimentally generate Noise Power Distance (NPD) curves for each vehicle as part of the noise certification process. These NPD curves are then provided to AEDT to predict SEL contours. In this study, the effects of configuration parameters are modeled by extending traditional NPD data to include additional dimensions for configuration parameters. These expanded data sets will be referred to as Noise Power Distance plus Configuration (NPD+C) curves and will enable sensitivity analysis with respect to vehicle configuration. While NPD+Cs are a key enabler for noise power distance re-evaluation, manufacturers do not typically provide data in the form of an NPD+C. Due to the expense of experimental testing, limited experimental data is available beyond that which is required for official certification. Due to the absence of experimental or historical data, NPD+C data must be generated for this using physics-based computational modeling methods. NASA's ANOPP tool was used to generate configuration specific noise information. The specific procedures used to generate NPD+Cs in ANOPP are discussed in further detail in the following sections.

To accurately analyze a mission in AEDT, NPD+C information must be available for every point in the takeoff or landing trajectory. Whereas a normal NPD is applicable to all points in the departure or approach trajectories, since the configuration behind the NPD is fixed, the NPD+C is speed and configuration dependent. This means that there is conceivably a NPD+C unique to every segment in the trajectory. To generate these unique NPD+C signatures, it is possible to use ANOPP to generate NPD+C data for each point in the AEDT trajectory. While this method is more accurate when considering a few standard mission profiles, it lacks generality. Any time a new mission is considered, a new set of NPD+Cs would have to be generated for each segment, which can be time consuming and computationally expensive. Furthermore, the cost of experimentally obtaining enough NPD information to analyze any arbitrary mission profile may be cost prohibitive for manufacturers. Therefore, the NPD+Cs must be generated in a way that is general enough to be applicable to a variety of mission profiles while minimizing the information that must be obtained from either experimental data or modeling and simulation tools. To achieve this, NPD+Cs will be generated using a polynomial interpolate model with respect to each configuration dimension (flap/slat, gear setting, and speed). Once it is determined which of these dimensions are to be considered, a sensitivity analysis is conducted to determine the regression order to be used and the number of model fit points necessary to accurately predict noise levels with respect to each configuration dimension. AEDT is then modified to perform this interpolation prior to its analysis based on a superset of NPD+C data generated from ANOPP. This method is



advantageous because it can be applied to any mission profile or parameters so long as the settings lie within the ranges of data generated for the interpolate model. Moreover, by performing a sensitivity analysis to determine the appropriate polynomial orders and grid densities for each dimension, it is possible to minimize the number of model fit points that are required to generate the interpolate model, which will reduce computational cost and/or experimental effort.

Research Approach

ANOPP NPD Generation

The first phase of research for this task is to generate the vehicle-level NPD curves using non-standard configurations for various vehicle class models. Georgia Tech used NASA's Aircraft Noise Prediction Program (ANOPP) to simulate the noise generated by individual sources on board the aircraft. ANOPP has the capability to generate NPD tables (which can be plotted to produce NPD curves) for a specific aircraft model. NPD tables include four noise metrics (as a function of power setting and altitude): sound exposure level (SEL); effective perceived noise level (EPNL); maximum A-weighted sound pressure level (max SPL); and maximum tone-corrected perceived noise level (max PNLT). The input variables in the NPD prediction method include airframe geometry, engine geometry and performance, aerodynamic performance, flight path and configuration parameters.

AEDT currently requires specific standard settings for NPD generation. As a result, ANOPP's NPD prediction module has corresponding pre-set defaults for many of the flight path and configuration parameters. It is necessary to alter ANOPP to account for non-standard configuration settings. This includes flap deployment angle, slat deployment angle, landing gear setting, and flight velocity. Flap/slat deployment angles and landing gear settings are classified as configuration parameters while aircraft flight velocity is a flight path parameter. However, for the sake of simplicity, flight velocity will also be referred to as a configuration parameter in this report. This is required because as the flight velocity changes, the source noise levels will also change drastically. Once the parameters to be altered are identified in the ANOPP model, a new set of flight path library files must be generated for each configuration (using a separate ANOPP module). These flight path library files are then used by source prediction and propagation modules that comprise the rest of the ANOPP model to generate NPD curves for the aircraft. This process is repeated for each distinct configuration of the aircraft model used in the sensitivity analysis. The results of the sensitivity analysis will then determine the number of executions of ANOPP are necessary for the NPD superset generation for each vehicle class being assessed.

NPD Sensitivity Analysis

A sensitivity analysis was performed to determine the effect that each configuration parameter has on the sound exposure level (SEL) generated by the vehicle at a given distance and thrust setting. This study is repeated for EPNL and max PNLT, showing similar results. To perform the sensitivity analysis, ANOPP was used to generate NPD curves for the 150 passenger class (150pax) vehicle model by sweeping through a range of flap angles, slat angles and speeds for both the gear up and gear down configurations. The 150pax model is used as the baseline vehicle to indicate sensitivity to these factors because the model has gone through extensive calibration and verification in previous studies to emulate the performance a Boeing 737-800. It is important to note that a sensitivity analysis of each vehicle can be time consuming due to program set up and run times; however, the trends are expected to be similar across different vehicle size classes. These results will be used to infer sensitivity of SEL to configuration parameters for other vehicle size classes.

Ultimately, ANOPP data will be used to interpolate noise level with respect to configuration parameters. To avoid extrapolation, the maximum possible ranges of each configuration parameter are considered.

Table 1. Variable ranges for sensitivity analysis

Variable	Min	Baseline	Max	Units
Flap angle	0	15	30	deg
Slat angle	0	10	30	deg
Speed	130	160	200	kts



Table 2. NPD+C superset values for 150 passenger class

Run	Gear	Speed (kts)	Flap (deg)
1	Up	130	0
2	Up	130	15
3	Up	130	40
4	Up	190	0
5	Up	190	15
6	Up	190	40
7	Down	130	0
8	Down	130	15
9	Down	130	40
10	Down	190	0
11	Down	190	15
12	Down	190	40

Table 2 shows a breakdown of the 12 NPD simulations that must be run in ANOPP, compiled into an NPD+C, and then imported into AEDT. It is important to note that while particular values and ranges may change from vehicle to vehicle, it is expected that the same interpolation method should be valid for each vehicle in the fleet. The 150pax class model provides a valuable case study due to the availability of calibration and verification data from previous studies that can be used to validate the method. Now that the method has been validated, the next step is to apply it to all other vehicle size classes.

Task 2- NPD+C Generation, AEDT Modifications and SEL Sensitivity Study

Georgia Institute of Technology

Objectives

With the ANOPP NPD+C's superset-generation-procedure completed, the team at Georgia Tech used it and EDS to generate the input vehicles with the respective NPD+C curves for different aircraft size classes. Table 3 lists the EDS vehicles that have been used in the analysis. NPD+C curves are generated for vehicles in each size class to ensure the resulting format is appropriate and representative across the fleet. GT and the FAA coordinated on the appropriate vehicles of interest to carry forward in the research. EDS and ANOPP are used to parametrically vary vehicle low-speed configuration, speed, and ambient conditions. The outcome of this parametric study is a series of NPD curves that represent varying configurations, speeds, and ambient conditions. A sensitivity study is performed to identify the quantitative impact of changing vehicle characteristics on both the resulting NPD and on the resulting fleet noise. Finally, the results of the sensitivity study are used to recommend a format for the NPD+C tables. The format includes both the additional parameters that should be included (i.e., flap angle, gear setting, vehicle speed), and the number of additional conditions at which NPD data must be provided (e.g., 3 coupled flap/slat settings and 2 flight speeds). The outcome of Task 2 is a detailed comparison of differences in predicted noise when using the AEDT database NPDs, EDS baseline vehicle NPDs, and the NPD+C curves generated in this task.

To perform the analysis, a detailed research of AEDT acoustic process and source code was required. The Task 2 section synthesizes the solution modifications for NPD+C implementation. Several approaches were considered in integrating the capability to assess multidimensional noise power distance curves. This process is explained in the Task 2 section, which also contains more detail about the types of different analysis performed.



Table 3. Existing EDS baseline vehicles

AIRCRAFT SIZE	EDS REPRESENTATIVE AIRCRAFT
50 PAX	CRJ900
100 PAX	737-700
150 PAX	737-800
210 PAX	767-300ER
300 PAX	777-200ER
400 PAX	747-400

Research Approach

Including the vehicle's varying low-speed configuration and reference velocity for the complete flight will lead to differences in predicted contour area. In order to generate these contours to evaluate the impact of aircraft configuration on contour area, representative NPD+C curves are required. These curves are acquired through an interpolation of the NPD supersets, which are described in more detail in the Task 1 section of the report. For the first iteration, each superset contains a grid of NPDs for a combination of the three following parameters: coupled flap and slat setting (0°, 15°, & 40°); aircraft airspeed (133.35 knots & 190 knots); and gear setting (up & down). Furthermore, each individual NPD superset, from the 12 simulated in ANOPP, is composed of 12 NPD curves. A curve describes the uncorrected noise metric (SEL or LAmax) for a specified slant distance for increasing thrust settings. Figure 2 depicts a notional NPD supersets library. The NPD superset is collectively referred to as an NPD+C.

For the computation of an SEL grid, AEDT currently assumes a fixed reference speed of 160 knots and flight trajectory information that is discretized into segments. The segment's data can be expanded to include instantaneous reference speed and the vehicle's configuration. By increasing the data used in the acoustic computation algorithm, an interpolated NPD (NPD+C) is obtained corresponding to a higher fidelity description of the segmented vehicle parameters. This description is to be propagated in AEDT to appropriately obtain the noise characteristics for the complete flight envelope.

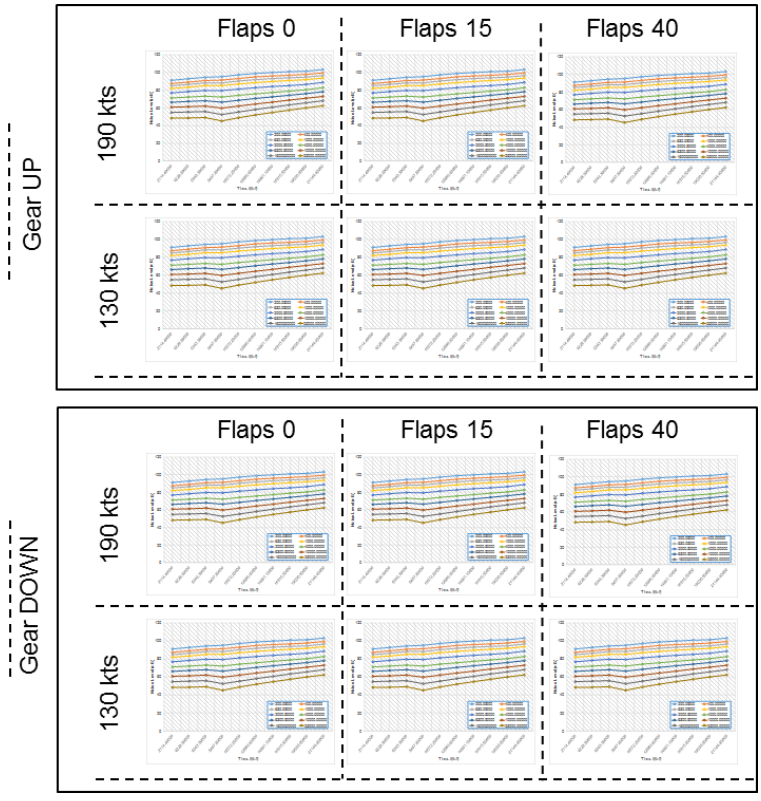


Figure 2. In-house developed NPD supersets library

NPD+C Integration Approaches with AEDT

In order to integrate the NPD+C supersets into AEDT, three approaches were initially considered. The first option involved running each NPD from the superset one-at-a-time through the AEDT algorithm in order to extract the custom noise metric results describing the flight procedure. This method was discarded due to the prohibitive computational expense incurred for a fleet of vehicles. Generating a full set of NPD+Cs for one aircraft in ANOPP takes approximately 2-3 hours of execution time within ANOPP. There are approximately 200 unique NPD noise identifiers within AEDT and upwards of 5000 equipment IDs. Furthermore, creating a new, calibrated ANOPP model for a given vehicle takes several weeks. A normal procedure result for a single aircraft is computed on the order of minutes. An analysis including 12 different combinations of a vehicle configuration and reference speed amounts for several hours in a fleet analysis. Furthermore, by following this process, a more intensive modification of the source code would be required because segment-to-segment information would need to be post-processed. The parameters required to properly assess the noise adjustments would complicate the procedure as each computation would include its native configurations and reference velocities.

A variation to this approach requiring the analysis of all the NPD supersets was deliberated as well. In this case, the custom SEL grid was to be used in the ANGIM tool available to Georgia Tech in order to superimpose the necessary segmented grids to portray the mission. This methodology suffered from the same weaknesses as the aforementioned practice.

Figure 3 further portrays the discarded methods. It is important to note that Figure 3 does not reflect the NPD's currently used. Slat angle and flap angle were found to be correlated in the algorithm and are considered in the same vehicle configuration.

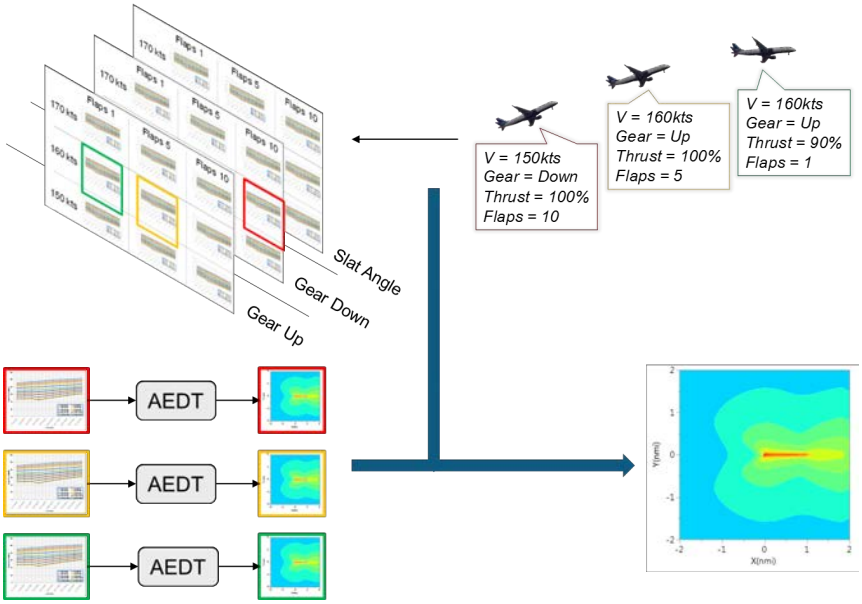


Figure 3. Discarded methods for the integration of the NPD library

The third, and subsequently selected, approach was to assemble a custom NPD+C representing the flight procedure input to AEDT. This is illustrated in Figure 4. This approach uses vehicle flight segment and trajectory information (velocity, configuration) to interpolate among the 12 NPD+C input curves. In this approach a single NPD is essentially created for each segment that contains a noise signature specific to the vehicle configuration and velocity at that segment. The segment-to-segment part of the acoustic computation process is then expanded to contain an interpolation algorithm for each specific point required within the 12 NPD supersets. The detailed process description is available upon request from the authors. Using this approach does not increase the computational expense as significantly as the two other solutions considered. The required alterations to AEDT's source code, even though significant, are considered to have less potential alterations and be more computationally efficient due to the potential inclusion of the interpolation algorithm within the segmented

information. The parameters describing the mission profile are available, and the NPD+C interpolation of the LAMAX and SEL metrics need to be computed only once through the profile (for the initial grid point considered) and are then utilized for the complete grid. Modifications were made within AEDT to read in the higher fidelity NPD+C data. A description of these modifications is available upon request from the authors.

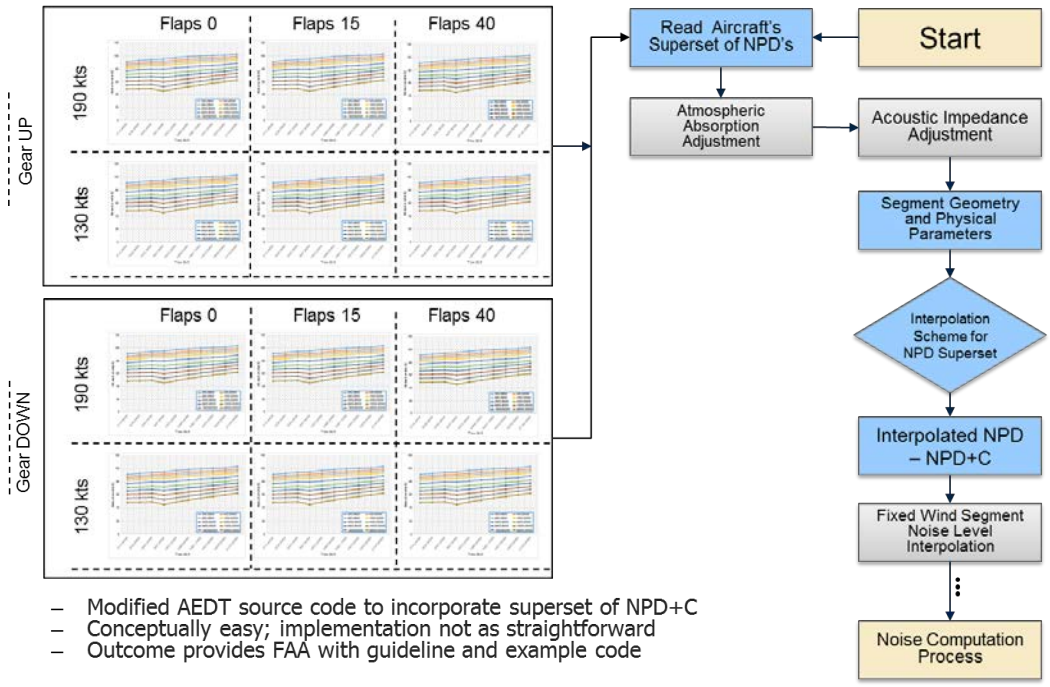


Figure 4: Selected NPD+C Integration with AEDT

AEDT NPD+C Studies

Dimension specific procedures

With the interpolation scheme implemented in AEDT and the superset of NPD+C data generated using ANOPP, the modified version of AEDT is used to analyze the effects of configuration on noise contours. For each vehicle, 80 dB SEL contours are generated and compared to those generated from the unmodified version of AEDT using the baseline vehicle configuration.

Table 4. Study I & II

Grouping	Study	Parameters
Baseline	0	Baseline NPD
Main Effects	I.A	Include only reference speed
	I.B	Include only flaps-slats setting
	I.C	Include only gear setting
Cross Terms	II.A	Speed + Gear
	II.B	Speed + Flaps
	II.C	Gear + Flaps
	II.D	Speed + Gear + Flaps

Table 4 outlines the sensitivity analyses to be performed in this study. Currently, NPD data only contains the ability to predict aircraft SEL as a function of engine power and aircraft distance. NPD+C data now adds the capability to predict aircraft noise as a function of flap angle, speed, and gear setting. Sensitivity analyses must be performed to determine which of these



configuration parameters has the most significant effect on contour area. This could influence future recommendations to OEMS about which dimensions should be included when gathering empirical data. In Study I, all aspects of the baseline vehicle are held constant except for NPD+C data in the dimension being studied. This allows the effect of each configuration parameter to be isolated and assessed. In Study II, multiple configuration parameters are allowed to vary in a single study. This is achieved by holding each aspect of the original baseline constant except for NPD+C data in the dimensions being studied. Study II is performed to reveal whether the interactions between multiple configuration dimensions are significant with respect to the main effects. Furthermore, by examining each possible combination of configuration parameters, it is possible to determine if any of the given parameters have a dominant effect on aircraft noise.

Table 5. Standard Configuration Parameters

Noise Curve Generation		*V_{ref}*	*Flaps/Slats*	*Gear Setting*
Baseline	Approach	160 kts	15	Down
	Departure	160kts	15	Up
NPD+C	Approach	130 - 190 kts	0 → 15	Up → Down
	Departure	130 - 190kts	5 → 1 → 0	Down → Up

Table 5 shows the configuration that is used for both the baseline vehicle and the NPD+C vehicle during standard approach and departure procedures. The 80 dB SEL contour for each sensitivity study is compared to the baseline to graphically show the effects that changes in NPD data have on contour size and shape. Furthermore, the area, length, and maximum width of the contours are computed and compared to quantify NPD+C effects. A standard mission profile is performed for each study. This eliminates variability in contour dimensions due to mission profile variations to isolate the effects of NPD data. The speed, distance, and flap angle of the vehicle at each segment is computed by AEDT based on standard approach and departure procedures. In this study, landing gear considered to be deployed when flaps are deployed and retracted when flaps are retracted.

Before generating contours accounting for variations in each configuration dimension, it is of interest to analyze the effect of each configuration dimension individually. Isolating each configuration parameter is important to determine the relative contribution each parameter makes to the overall variability of contour dimensions.

Table 6. Main Effect Study Parameters

Noise Curve Generation		*V_{ref}*	*Flap/Slat Setting*	*Gear Setting*
Speed Sensitivity	Approach	130-190 kts	15	Down
	Departure	130-190 kts	15	Up
Flap Sensitivity	Approach	160 kts	0 → 15	Down
	Departure	160 kts	5 → 1 → 0	Up
Gear Sensitivity	Approach	160 kts	15	Up → Down
	Departure	160 kts	15	Down → Up

Table 6 shows the vehicle configurations for the main effect sensitivity analyses. The goal of these studies is to isolate the effects of each configuration variable individually. In speed sensitivity study, NPD data is only changed as speed changes during the mission profile. NPD data is interpolated for speeds between 130 and 190 kts with zero velocity correction. For speeds above below 130 kts or above 190 kts, velocity corrections are applied as previously described. Flap and gear settings are kept identical to the baseline in the speed sensitivity. Likewise, in the flap sensitivity, NPD data is only allowed to change when flaps are deployed or retracted in the mission profile. NPD data is interpolated from ANOPP data at flaps 0, 15, and 40 as described previously. Speed and gear settings are kept identical to the baseline configuration in the flap sensitivity. Finally, in the gear setting, NPD data only changes when landing gears are deployed or retracted during the mission. Speed and flap settings are kept identical to the baseline configuration in the gear sensitivity.



Table 7. Cross-Effect Study Parameters

Noise Curve Generation		*V_{ref}*	*Flap/Slat Setting*	*Gear Setting*
Speed + Gear	Approach	130-190 kts	15	Up → Down
	Departure	130-190 kts	15	Down → Up
Speed + Flap	Approach	130-190 kts	0 → 15	Down
	Departure	130-190 kts	5 → 1 →0	Up
Flap + Gear	Approach	160 kts	0 → 15	Up → Down
	Departure	160 kts	5 → 1 →0	Down → Up
Speed + Flap + Gear	Approach	130-190 kts	0 → 15	Up → Down
	Departure	130-190 kts	5 → 1 →0	Down → Up

Once the main effect studies are performed, sensitivity analysis are conducted using each possible combination of variation using each of the three configuration parameters. Table 7 shows all combinations that are analyzed with the respective configuration parameter ranges. These cross-term studies are of particular interest since they allow the relative significance of each configuration parameter to be directly quantified. By comparing the results of the cross-term studies with the main effect studies, it is possible to identify which configuration variables make the most significant contribution to the overall variability of contour dimensions.

Finally, once sensitivity analyses are performed for each combination of configuration parameters, modifications are made to the flap/slat settings in the mission profile. Table 7 shows the modified flap/slat settings during the profile that are to be examined. It is important to note that no changes are made to aerodynamic performance in AEDT; only the noise related to flap/slat setting pertaining to source noise prediction is changed. This allows the mission profile to remain constant so that only changes in NPD data are considered. Changing the flap setting causes the modified version of AEDT to interpolate new NPDs based on ANOPP generated data, which does account for variations in flap lift coefficients as flap setting changes as described previously.

The following analysis is performed for each vehicle in each proposed study. Both approach and departure operations are considered. The process enables the build-up analysis of the given total SEL for the relevant segment and grid-point pair,

- Output graphs of ground track, velocity profile, trajectory, thrust profile, and 80 dB SEL segment contours (representative of 65 DNL contours) are obtained.
- SEL & LAMAX NPD curves are shown for both the baseline, and the NPD+C cases.
- Velocity correction, noise fraction, and interpolated SEL & LAMAX dB values are calculated for each segment, and each grid-point.
- Normalized noise power contribution of each segment to the relevant grid point is computed.

The contour shown is expanded upon, to clearly see the differences between the baseline and the main effect of speed for the case of Figure 5. Once the major differences in the contour are associated to the maximum contributing segment of the aircraft's flight procedure, Figure 6 is plotted. It is important to note that the representative figures shown for this section correspond to the analysis of including a range of speeds (130 kts – 190 kts) as a main effect, for the 100-passenger class vehicle. This example shows the complete procedure and analysis performed for each study and each specific aircraft. Any vehicle-study could have been chosen as an example (all the material shown in this section is available for all of the classes); however, the 100 PAX main effect analysis allows the reader to follow the effect with relative ease.

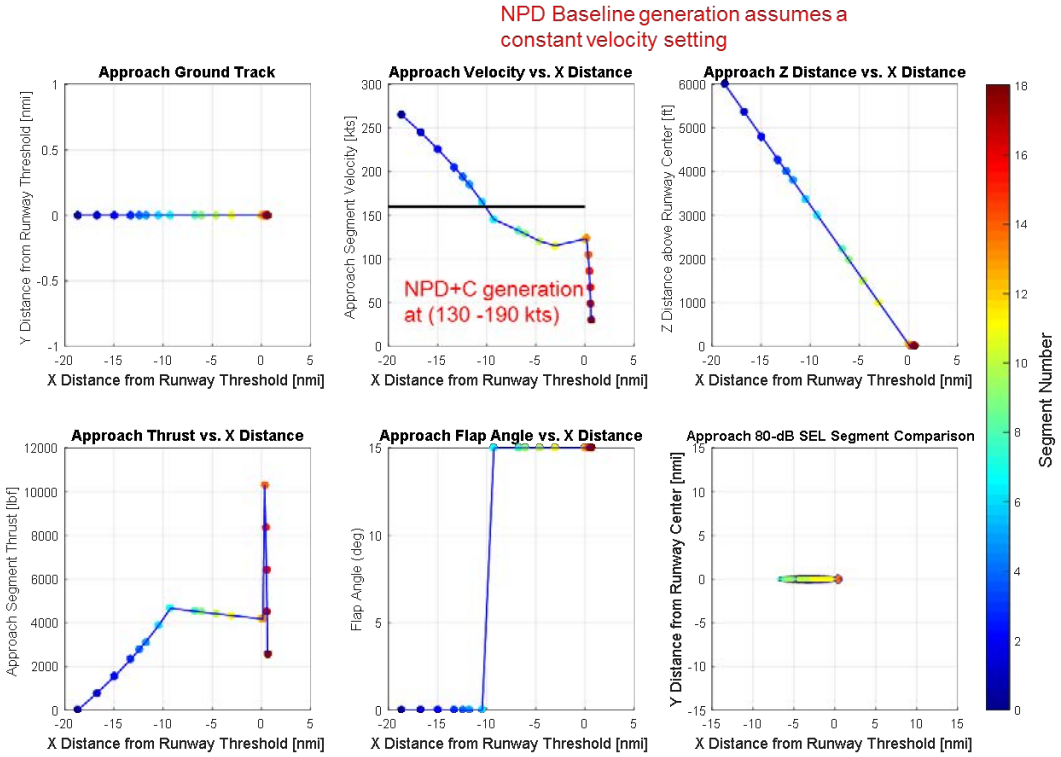


Figure 5. Vehicle specific analysis 100 PAX, I.A - 1

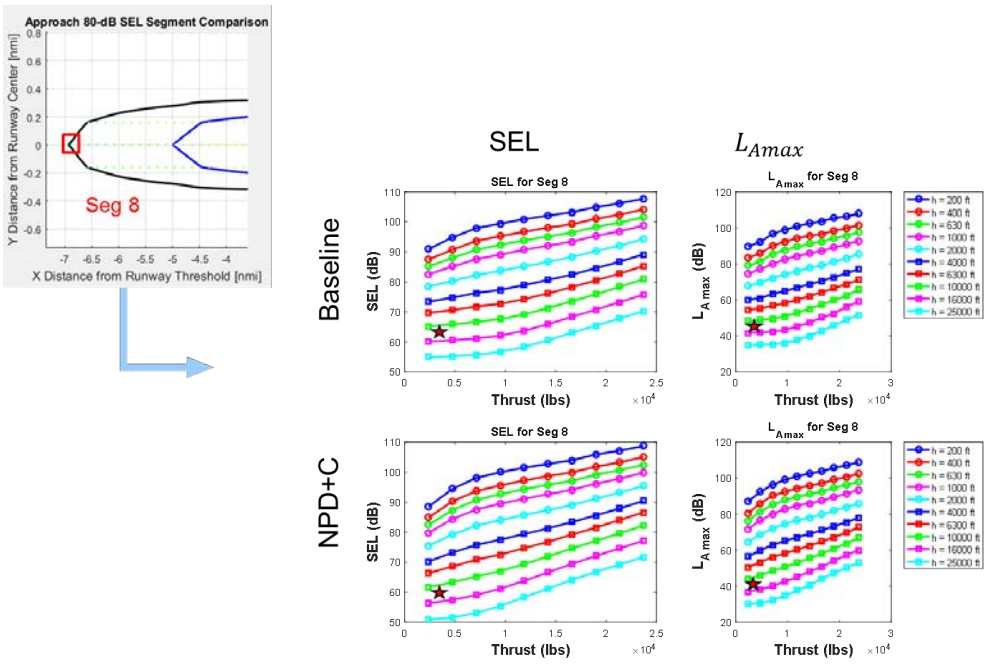


Figure 6. Vehicle specific analysis 100 PAX, I.A -2

With this information at hand, three grid points are studied for a higher fidelity analysis to understand the trends. Figure 7 depicts the contribution of the grid points located at the maximum difference between the baseline and the sensitivity contours. The ANOPP generated metrics, which are interpolated for both the NPD+C and the baseline, are tabulated with a corresponding velocity correction (duration adjustment) and noise fraction for the flown segment.

(X = -7.04 nmi, Y = 0 nmi, seg 8)

	Baseline	NPD+C
Distance (ft)	13842	13842
Thrust (lbs)	4651	4651
NPD Value (SEL dB)	62.2	59.2
LA max (dB)	44.1	40.6
Noise Fraction	0.787	0.828
Velocity Correction	0.6055	0
Contour Area (nmi^2)	4.0134	2.2715
Total SEL	79.88	77.76

(X = -6.88 nmi, Y = 0 nmi, seg 8)

	Baseline	NPD+C
Distance (ft)	14793	14793
Thrust (lbs)	4651	4651
NPD Value (SEL dB)	61.5	58.4
LA max (dB)	43.1	39.5
Noise Fraction	0.577	0.594
Velocity Correction	0.6055	0
Contour Area (nmi^2)	4.0134	2.2715
Total SEL	80.05	77.84

(X = -6.72 nmi, Y = 0 nmi, seg 9)

	Baseline	NPD+C
Distance (ft)	2292	2292
Thrust (lbs)	4527	4527
NPD Value (SEL dB)	79.1	77.3
LA max (dB)	67.7	66.2
Noise Fraction	0.646	0.709
Velocity Correction	0.8695	0
Contour Area (nmi^2)	4.0134	2.2715
Total SEL	80.31	77.98

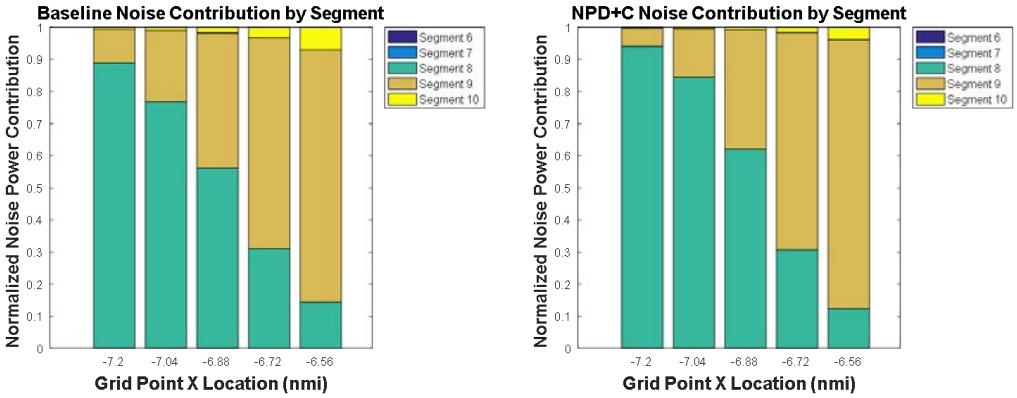


Figure 7. Vehicle Specific Analysis 100 PAX, I.A – 3

The method allows for a detailed research of the effects of including each dimension by itself (Study I), or a combination of expanded dimensions (Study II) and their combined impact on the noise contour created for the single runway analyzed.

A detailed research of the 100 PAX aircraft at an approach procedure, shows that the smaller contour generated by the AEDT NPD+C is explained by a combination of the velocity corrections and the noise metrics obtained at a lower reference velocity. The SEL and LAMAX values used for the interpolation correspond (in the case of the most contributing segment) to a velocity of 145.47 kts. It is evident that they will consequently yield lower noise results. Segment 7 for the specific case contributes to approximately 80% of the total SEL metric at the studied grid-points.

The aforementioned approach was taken for all vehicle sizes and studies. Figures 8 and 9 depict the result for a departure operation for the same representative vehicle (100 PAX). The AEDT NPD+C Studies section analyzes the full results.

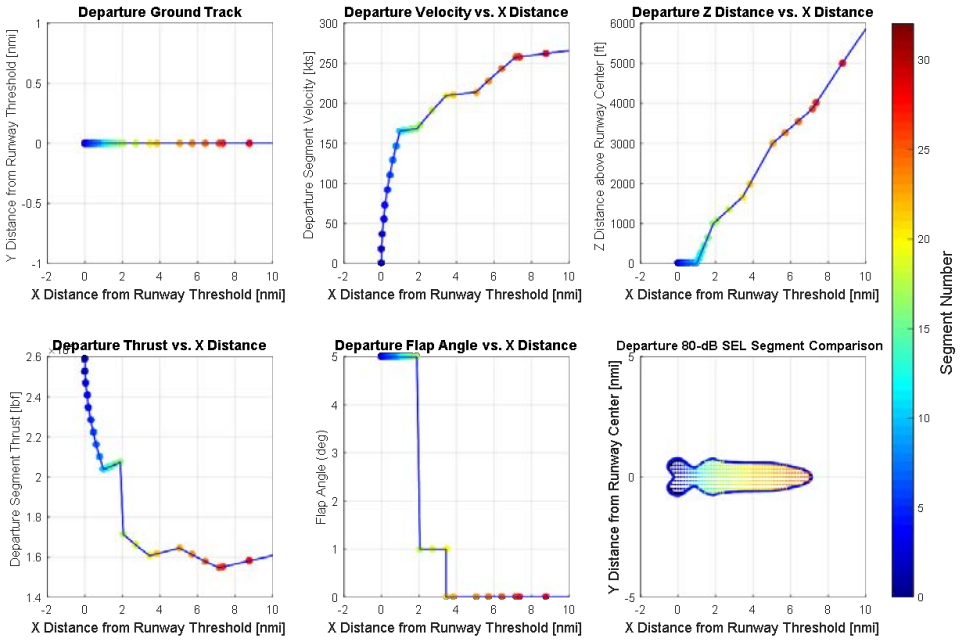


Figure 8. Departure trajectory - zoomed in

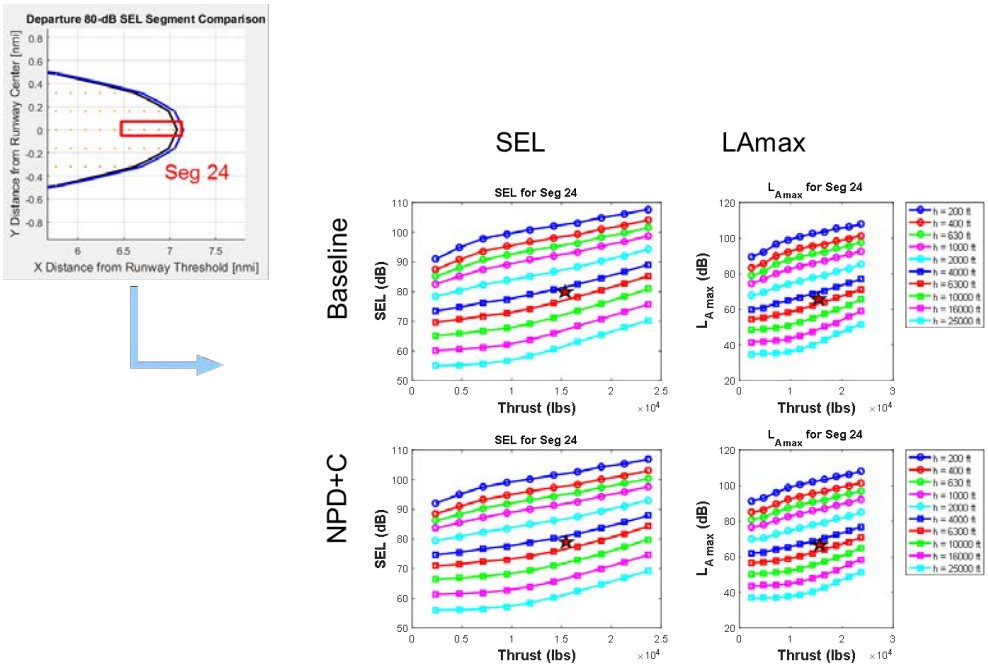


Figure 9. Segment NPD+C vs. NPD data

(X = 6.88 nmi, Y = 0 nmi)

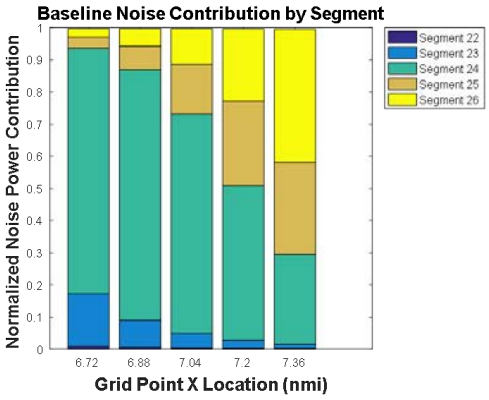
	Baseline	NPD+C
Distance (ft)	4610	4610
Thrust (lbs)	15793	15793
NPD Value (SEL dB)	80.5	79.9
LA max (dB)	68	67.9
Noise Fraction	0.777	0.760
Velocity Correction	-1.9436	-1.2065
Contour Area (nmi^2)	8.1854	8.5523
Total SEL	80.40	80.52

(X = 7.04 nmi, Y = 0 nmi)

	Baseline	NPD+C
Distance (ft)	5283	5283
Thrust (lbs)	15793	15793
NPD Value (SEL dB)	79.2	78.6
LA max (dB)	66.1	66
Noise Fraction	0.662	0.648
Velocity Correction	-1.9436	-1.2065
Contour Area (nmi^2)	8.1854	8.5523
Total SEL	80.08	80.20

(X = 7.20 nmi, Y = 0 nmi)

	Baseline	NPD+C
Distance (ft)	6038	6038
Thrust (lbs)	15793	15793
NPD Value (SEL dB)	78	77.4
LA max (dB)	64.2	64.1
Noise Fraction	0.452	0.450
Velocity Correction	-1.9436	-1.2065
Contour Area (nmi^2)	8.1854	8.5523
Total SEL	79.76	79.90



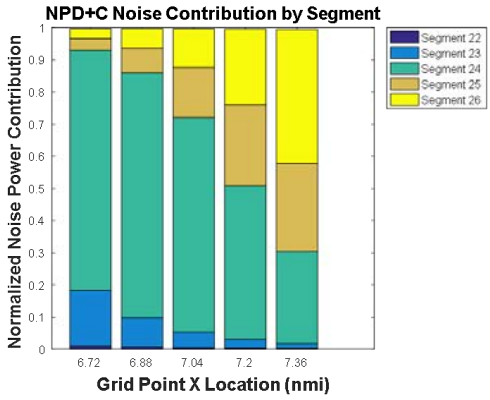


Figure 10. Analysis and noise contribution - 100 PAX I.A Departure

Main effects

Study I.A

As explained in the Dimension specific procedures section, the 100 PAX vehicle was chosen as an example because the reader is able to follow the analysis presented before encountering the effects of further increases in NPD dimensions. Any vehicle could have taken its place (the material, plots, and tables are available). For the case of the speed sensitivity analysis (I.A) presented in Table 4, the interpolated SEL & LAMAX NPD+C values are lower because of the lesser reference speed at which the aircraft noise metrics were acquired. Furthermore, the NPD baseline metrics generated at 160 kts are corrected (duration adjustment = +0.6049), while NPD+C generated metrics interpolated to the aircraft velocity of 145.47 kts at segment 7 have no correction applied. The velocity correction for this type of aircraft is found to have a significant contribution to the total SEL value differences. From the lower part of Figure 7, it is evident that the normalized noise contribution is larger for segment 7 in the NPD+C case, as the segment 8 noise metrics are obtained at a 132.93 kts reference velocity. For the 100 PAX in study I.A, it is concluded that the overall contour is smaller due to the effect of the velocity corrections and the lower noise metrics at the most contributing segments.

The contour area, length and width is plotted as a bar chart for the nominal results of the NPD+C case vs. the baseline outputs. With this information, the percent change is graphed for all of the case studies. Study I.A results -which researches the main effect of including speed as the expanded dimension for ranges 130 -190 kts- are depicted in Figure 16. Two interesting main trends are observed: first, the percent change in area is negative, then, there is a linear trend from the smaller sized vehicles to the largest.

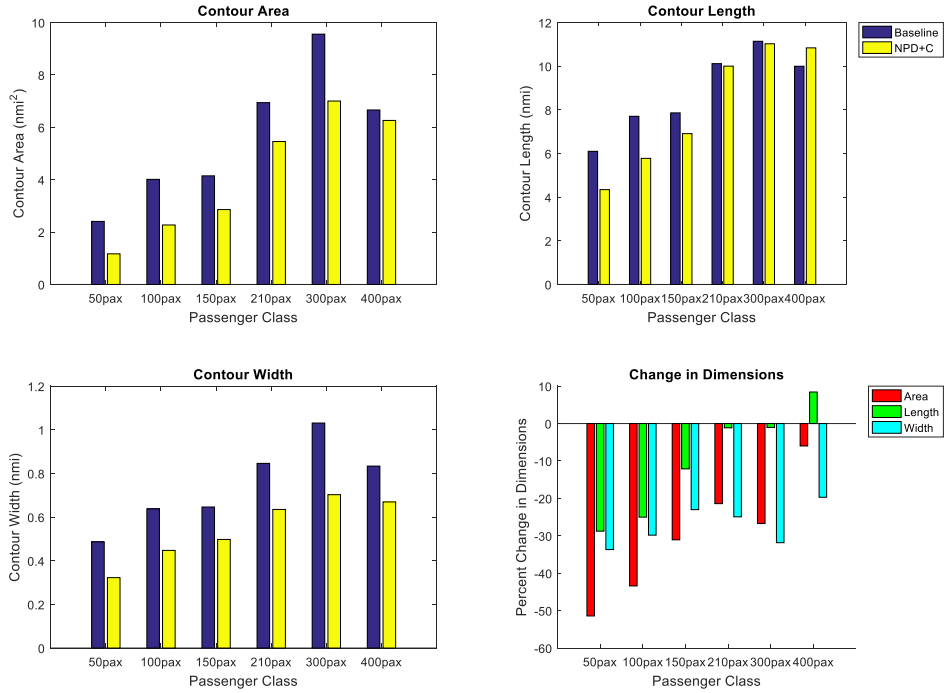


Figure 11. Study I.A Approach

As explained at the beginning of the current section, the duration adjustment has a large effect when including the speed dimension. This correction will either be negative if the reference velocity is higher than 190 kts, or positive should it be less than 130 kts. No correction is applied if the reference speed, during the operation, falls within the interpolation ranges as noise data is directly obtained within the bounds. This computation is explained physically by the fact that when the aircraft flies a given segment in less time, the segment contributes less to the overall total noise metric; same is true vice versa. Another factor important for the research is that the noise metrics (SEL & LAMAX) interpolated to the reference speed are significantly less/more in magnitude than the metrics obtained at 160 kts, when the aircraft is flying at 130/190 kts, respectively.

These features help explain the overall trend encountered in Figure 11. The smaller sized vehicles' segments are constantly discretized from lesser aircraft speeds with respect to the larger sized (210, 300, 400 PAX). This contributes to the upward linear trend. The effect of the duration adjustment is counteracted by the LAMAX and SEL values acquired from the noise power distance and configuration curves. At approach, the jet source noise is less relevant and thus a large difference is encountered from the velocities of the different flight procedures.

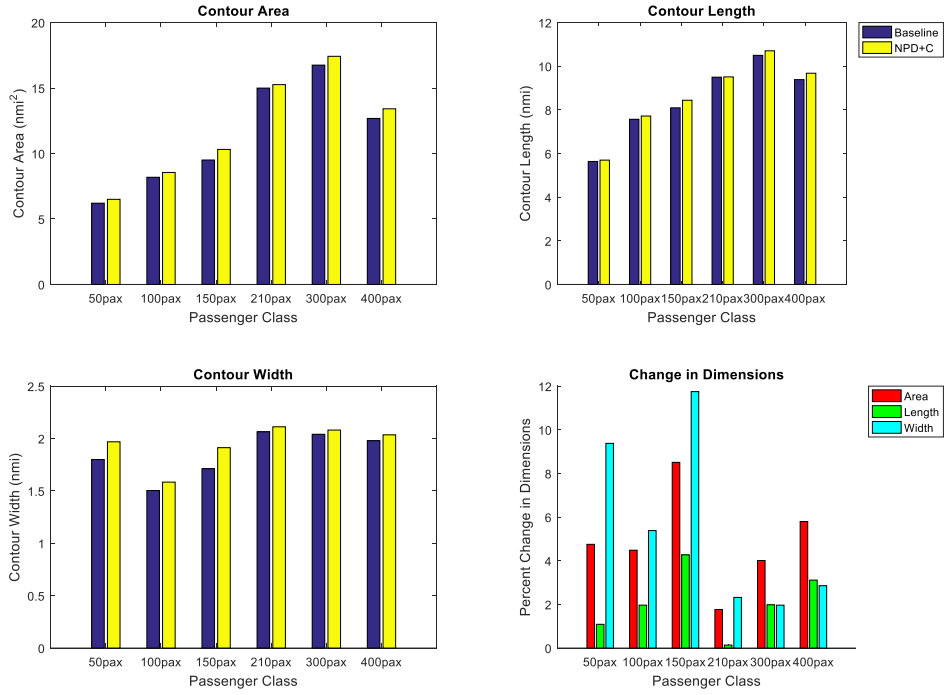


Figure 12. I.A Departure

In contrast to the approach procedure, departure operations present smaller change in magnitude between vehicles as the jet source noise has the largest effect on the contours. Figure 12 researches the effect of including the aircraft speed in the NPD+C AEDT output noise contour. The noise power distance curves have been obtained for constantly higher reference speeds thus increasing the total SEL value for each of the grid points.

Study I.B

Study I.B researches the impact of including control surfaces as part of the noise signature. For this case, the flap-slat combination setting (AEDT treats both settings in the same dimension) follows the procedure the aircraft is flying at approach and departure. As explained in the Task 1 section, the baseline noise SEL and LAMAX noise metrics are obtained at a flap-slat deflection of 15 ° with a constant reference speed of 160 knots. Study I.B interpolates from the superset of 12 NPD+Cs to obtain a metric specific to the flight procedure. At approach the mission follows a clean configuration to a deflection of 15 degrees; while on departure, the initial flap-slat configuration is set to 5°, which is then retracted to 1° during rotation, following a clean configuration for the rest of the procedure.

The results for the analysis match what's expected (explained further in detail below) from the understanding of the effect of control surface interference with the airflow. The sound exposure levels associated with a more/less deflected state, increase/decrease respectively as sound pressure levels change appropriately. The output noise contours for all of the vehicles during approach (Figure 13 top) now includes metrics corresponding to a descending clean configuration for the initial 7 segments of the path (on average). The percentage change is more pronounced for the 400 PAX because it includes double-slotted, double-flap configuration. The percentage change in area associated with the departure profile (Figure 21, bottom) is rationalized with similar logic. The baseline NPDs correspond to a 15° deflection which are then corrected, whilst the SEL and LAMAX inputs to AEDT – for the current study - are associated to the 5, 1, 0 setting. The percentage change is less pronounced than in approach because the engine source noise dominates the trend. Figure 14 is plotted from the algorithm's results and graphically shows the differences between the NPD and NPD+C for the most contributing segments.

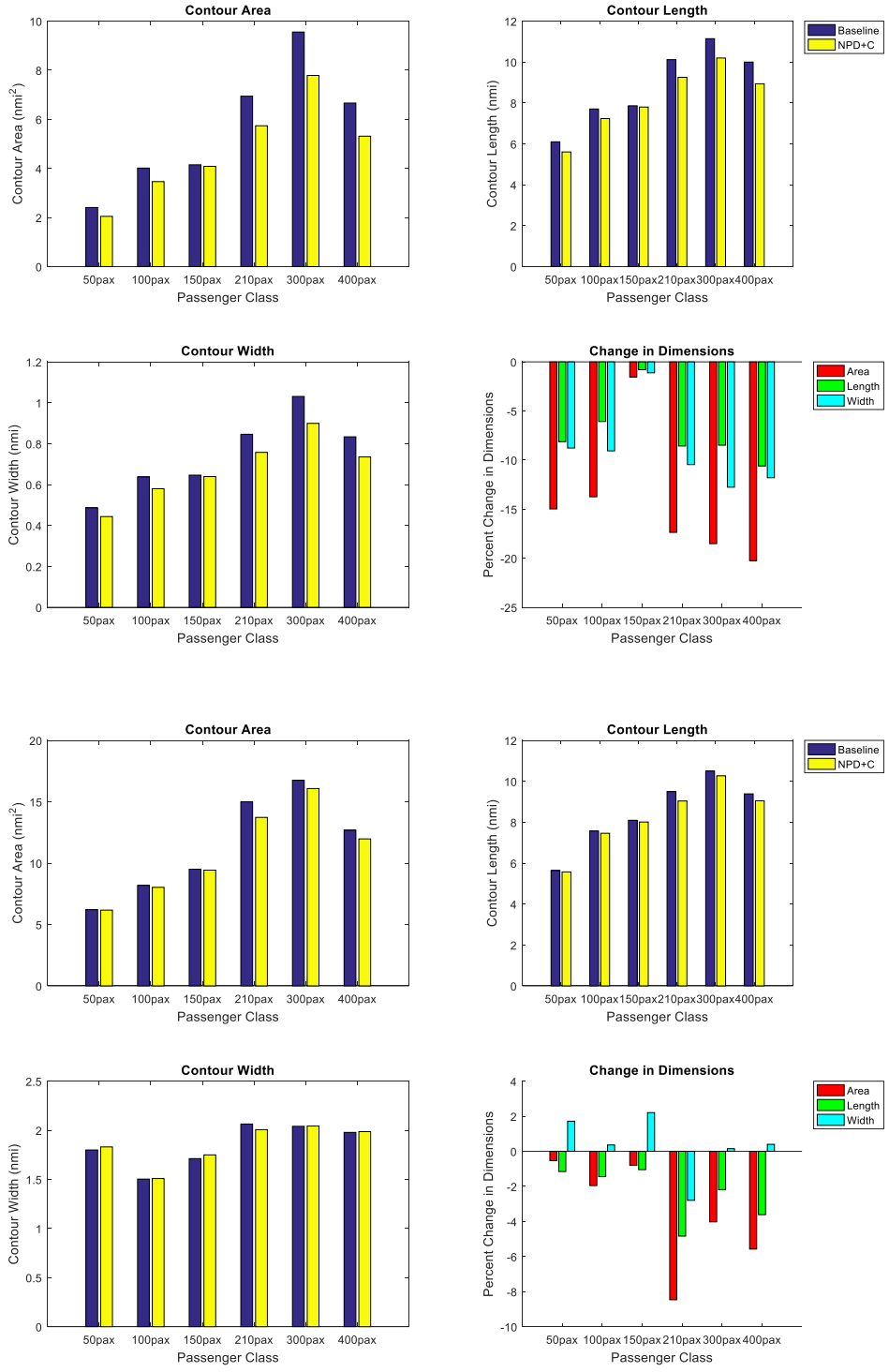


Figure 13. Study I.B Approach (Top) & Departure (Bottom) procedures

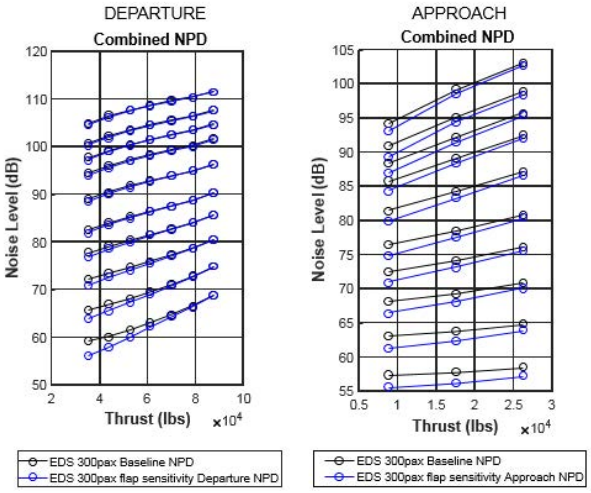


Figure 14. NPD vs. NPD+C most contributing segment. I.B

Study I.C

I.C researches the effect of including the gear setting as part of the NPD+C's interpolation procedure. The gear configuration includes two unique settings: gear-up and gear-down, which had to be defined in the acoustic computation process of AEDT as the initial source code did not include a parameter to analyze the differences with respect to this dimension. Gear-up is associated with a clean configuration and a flap-slat deflection of 1°, while the gear down setting is included to account for deflections at $5°, 10°, 15°, 30° \& 40°$. Figure 15 and 16 highlight the percentage change in dimensions for approach and departure, respectively.

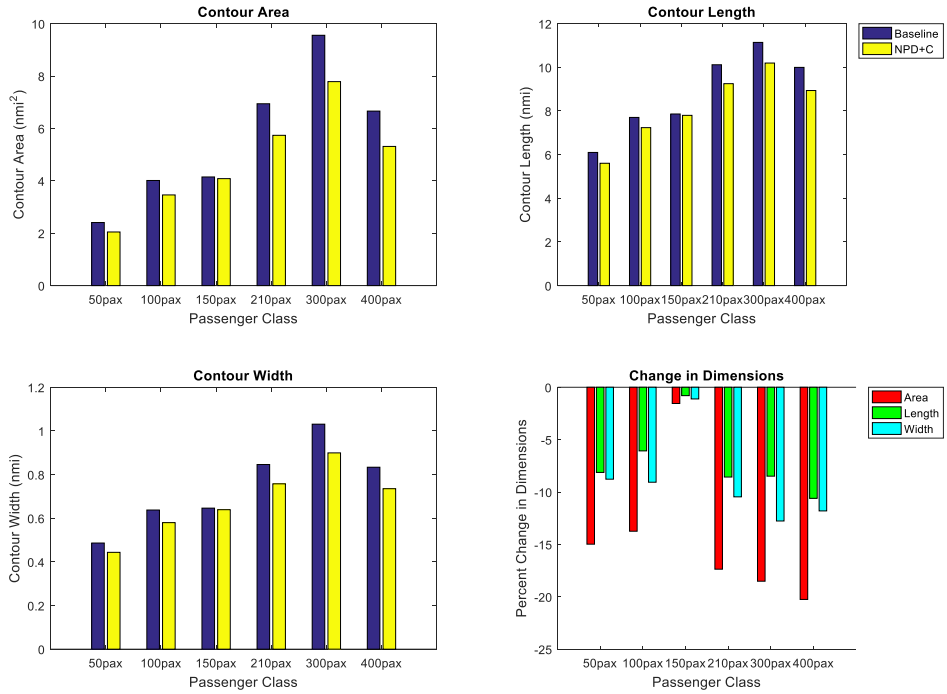


Figure 15. Study I.C Approach

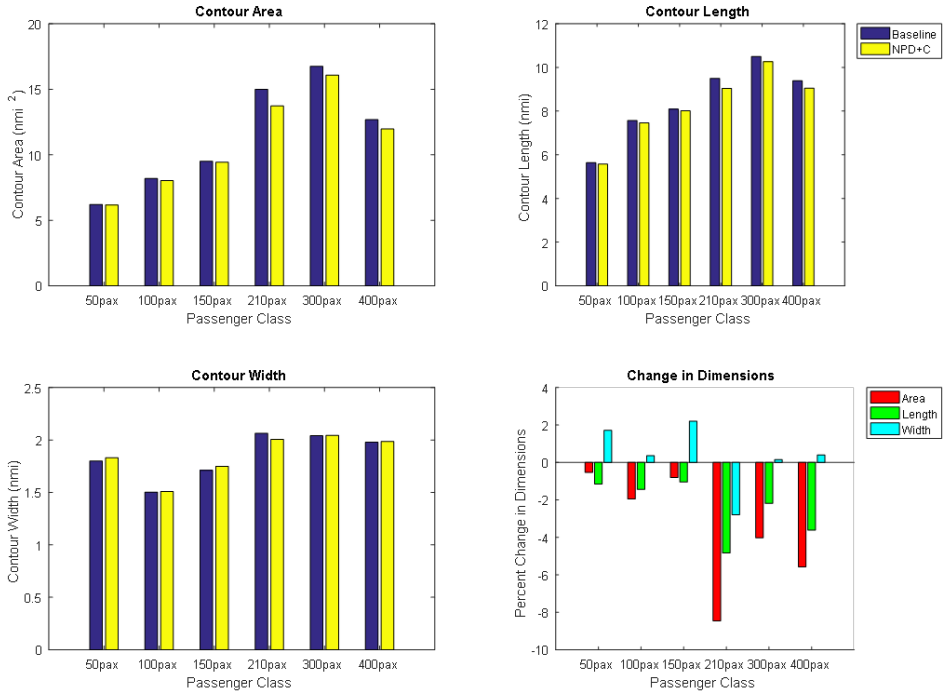


Figure 16. Study I.C Departure

By further analyzing the results, the Georgia Tech team observed that the percentage differences between including the flap setting or the gear setting as main effects were minimal for smaller sized vehicles during approach. This outcome is explained with the fact that for a single grid-point in the contour, the total SEL is computed by summing the noise exposure of the flown segments. There are, on average, 2 segments that contribute about 99% to the total SEL. In studies I.C, the smaller vehicle classes (50 – 100 – 150 PAX) had their respective total SEL maximum noise contribution from segments in which the parameters were equal (i.e. flap-slats at 15°, gear-down). The Pareto plot depicted in the Task 3 section, along with the vehicle-specific-impact (studies I & II) plots, and the detail research in the AEDT NPD+C Studies section of the report contain further detail.

$$E_{seg} = 10\text{^}\left[\frac{L_{E,NPD+C,ADJ} + NF_{ADJ} + DUR_{ADJ} - LA_{ADJ} + TR_{ADJ} + DIR_{ADJ}}{10}\right]$$

$$SEL = 10 * \log_{10}\left[\sum_{i=1}^{n_{seg}} E_{seg(i)}\right]$$

Cross-term combinations' impact

The AEDT NPD+ C Studies section provides the results and insights obtained from the investigation. Each study's main findings are explained after which summary plots are included following the same study order.

Study II.A

This research section analyzes the impact of including a combination of reference-speed-dimension-expansion and the finite gear setting. In order to properly analyze the impact of the combination, a comparison is performed against the results obtained from including the speed dimension only (I.A). There are two distinct behaviors between approach and departure procedures. At departure, the same logic applies as the one encountered in the comparison case. The jet source noise has the most significant impact on the noise signature. The higher reference speed range associated with the higher thrust setting yield larger values of the noise metrics acquired from the NPD+C (SEL & LAMAX). This factor overcomes the impact of the airflow noise created by the gear-down setting. The maximum contributing segments correspond to the same configuration between I.A and II.A, which is at a gear-down setting. The difference is minimal in this respect and the trend can be observed in yellow in Figure 17 which is provided as a reference for the percent area change between studies. In contrast, the approach procedure presents noticeable differences to I.A. The clean configuration for the initial segments, which is now adopted in the NPD+C interpolation yield a larger magnitude in percent reduction when juxtaposed to the baseline. The baseline approach procedure assumes a gear-down setting for all the segments. This is not the case in study II.A; therefore, the decrease in the 80-dB noise contour area matches the physical behavior. The complete results of study II are presented at the end of this section.

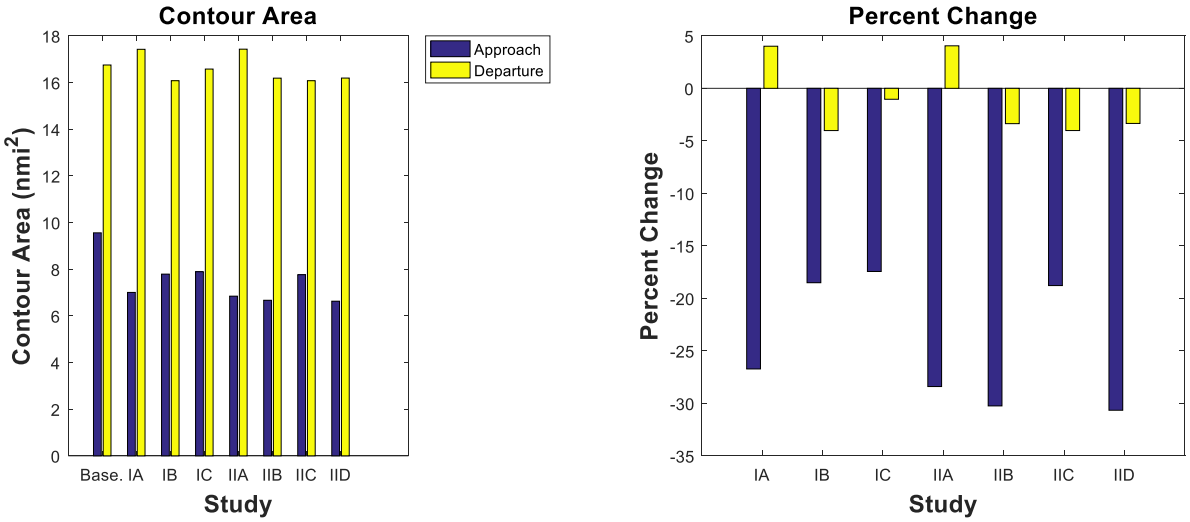


Figure 17. Aircraft-specific impact for studies I & II. 300 PAX

Study II.B

Having studied the effect of II.A, this research section analyzes the impact of including a combination of reference-speed-dimension-expansion and the flap-slat deflection. To follow the same line of analysis, the results are contrasted to the effect of including only speed as the extra-dimension, and to the previous study (II.A). Important to note is that by including the flap setting, the departure-operation noise-contour-change is now negative. This is expected, as in the baseline operation, the noise metrics are corrected from a flaps-slat deflection of 15°; while this is not the case for study II.B. The metrics are directly interpolated in AEDT NPD+C for the 5° → 1° → 0° settings. Nonetheless, the decrease of the contour is still less in magnitude than the effect observed during approach. This led the team to confirm that for departure paths, the effect of jet source noise dominates the response. Interestingly, by including the effect of speed with surfaces deflection instead of gear setting, a more substantial decrease in the total SEL contour is observed during approach (blue bars in Figure 17). Therefore, the effect of a 15-degree flap deflection is larger than a gear-down configuration in the AEDT algorithm. The vehicle specific studies are presented for all the aircrafts in the Task 2 section. The 300 PAX bar plot is shown as reference; however, there are slight differences in the trends encountered in each passenger class. The 50 – 100 – 150 PAX show insubstantial differences between studies II.A & II.B at approach. It is important to iterate that an exhaustive research of this tendency is given in the validation section (Task 3) of the report.

Study II.C

This research section analyzes the effect of an aircraft's variable configuration. The combination of flap-slat deflection with the gear setting provides a definition of the vehicle's configuration. I.B and I.C depict each dimension's impact by itself. It is interesting to note that the most substantial decreases for both the approach and departure procedures are accumulated in I.C. The reasoning behind the decrease lies in the procedure and surface interference with the airflow producing noise. This is explained in larger detail for the previous cases; thus, the reader is referred to those sections for the specifics of percentage area change with respect to each dimension. A salient feature form the study is that the combined effect of configuration settings is nonetheless less consequential than speed.

Study II.D

Study II.D is of essential importance to the goals specified in this research project. It is the initial study analyzing the complete effect of including the NPD+C superset while keeping trajectories constant with respect to the baseline. In II.D, the flap-slat deflection, gear setting, and reference speed, vary according to approach and/or departure. The specific procedures are explained further in detail in Task 2 section. With a validation and detail research of the results, the effect of changing trajectories within AEDT NPD+C to reflect more realist paths can be examined. Specific results for the 300 PAX study II.D are shown in Figure 18, Figure 19, and Figure **20**.

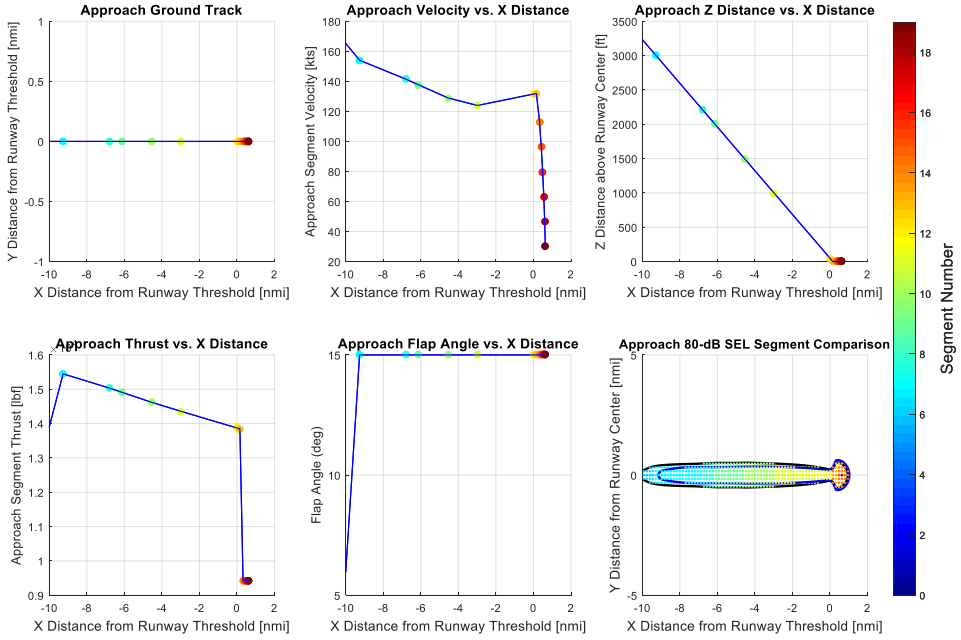


Figure 18. 300 PAX Study II.D – 1

The outcome of the modified AEDT which includes a NPD+C superset for all of the dimension follows the tendency expected as a result from all of the buildup-studies performed. It is evident that the speed impact is most substantial in the superset while keeping the trajectory constant with respect to the baseline. Both departure and approach procedure decrease in contour area magnitude, and a higher fidelity analysis with respect to the noise metrics acquired and the calculated corrections is performed.

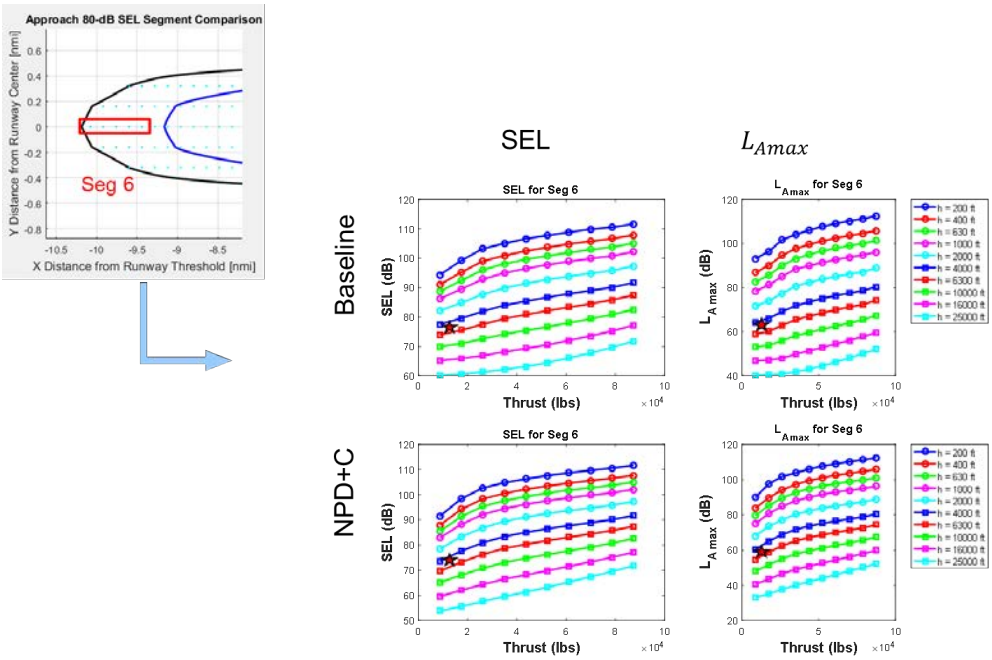


Figure 19. 300 PAX Study II.D – 2

(X = -10.24 nmi, Y = 0 nmi)

	Baseline	NPD+C
Distance (ft)	3706	3706
Thrust (lbs)	12875	12875
NPD Value (SEL dB)	79.1	76.1
LA max (dB)	66	63.5
Noise Fraction	0.760	0.788
Velocity Correction	-0.0895	0
Contour Area (nmi^2)	9.5576	6.6271
Total SEL	79.92	77.58

(X = -10.08 nmi, Y = 0 nmi)

	Baseline	NPD+C
Distance (ft)	4195	4195
Thrust (lbs)	12875	12875
NPD Value (SEL dB)	78.1	75.1
LA max (dB)	64.5	62
Noise Fraction	0.841	0.870
Velocity Correction	-0.0895	0
Contour Area (nmi^2)	9.5576	6.6271
Total SEL	80.17	77.82

(X = -9.92 nmi, Y = 0 nmi, seg 7)

	Baseline	NPD+C
Distance (ft)	4832	4832
Thrust (lbs)	12875	12875
NPD Value (SEL dB)	76.9	73.8
LA max (dB)	62.8	60.1
Noise Fraction	0.871	0.900
Velocity Correction	-0.0895	0
Contour Area (nmi^2)	9.5576	6.6271
Total SEL	80.40	78.07

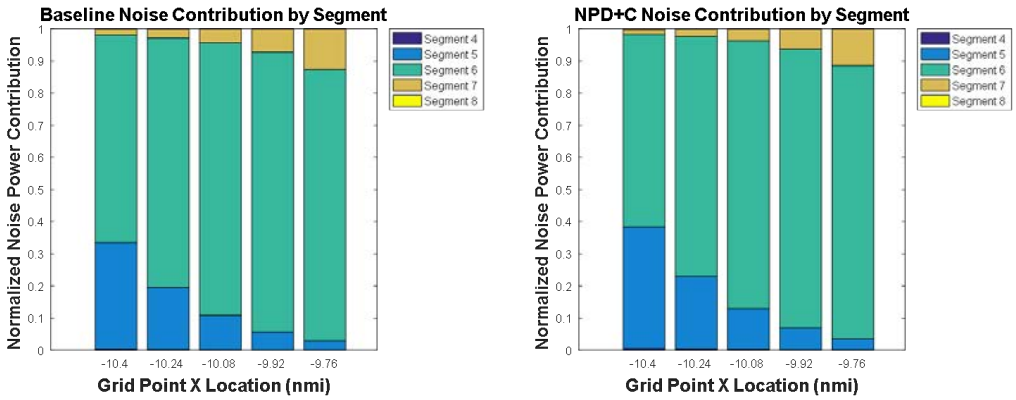


Figure 20. 300 PAX Study II.D – 3

Study II.A summary plots

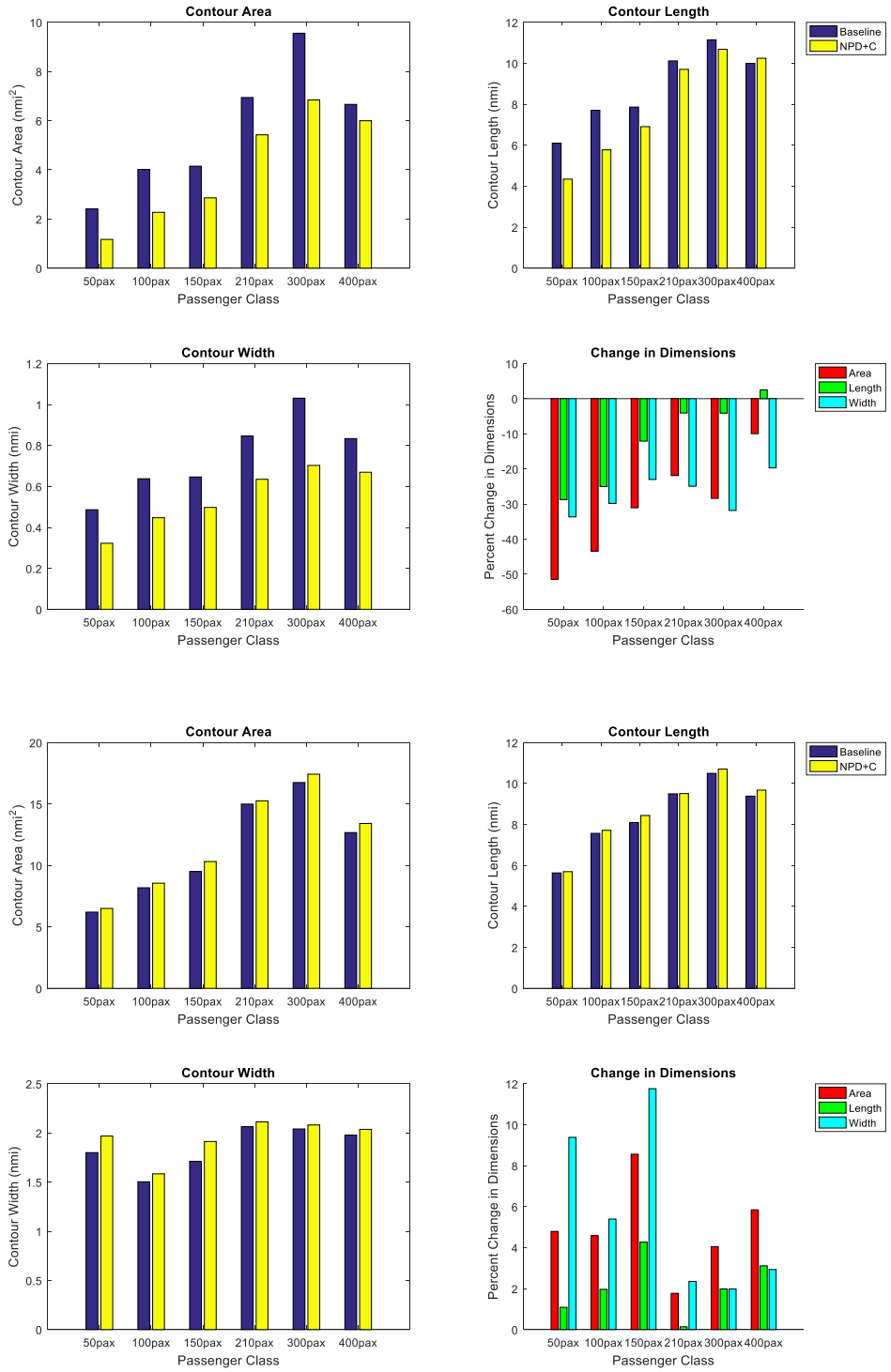


Figure 21. Study II.A Approach (top) – Departure (bottom)

Study II.B summary plots

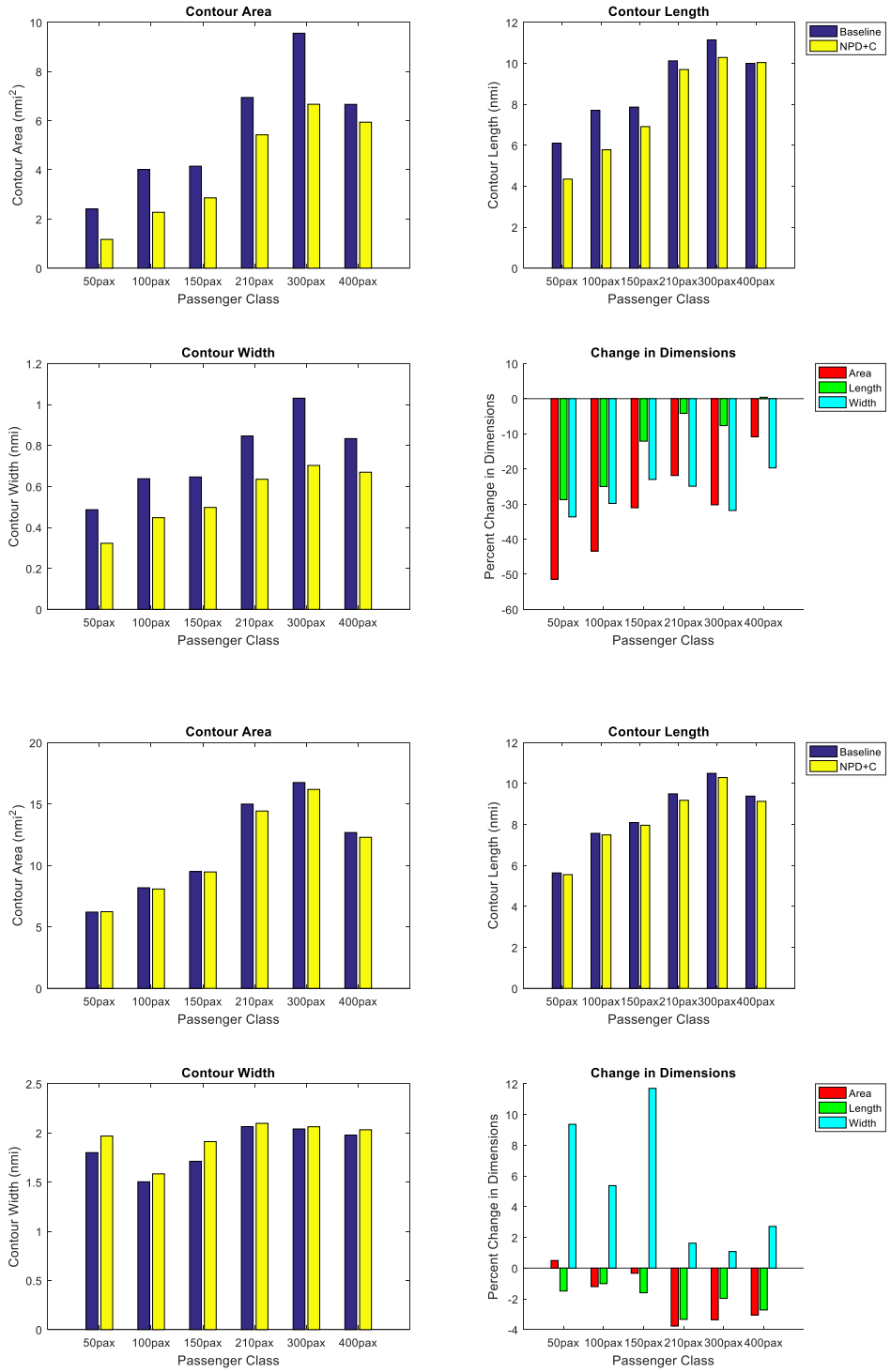


Figure 22. Study II.B Approach (top) – Departure (bottom)

Study II.C summary plots

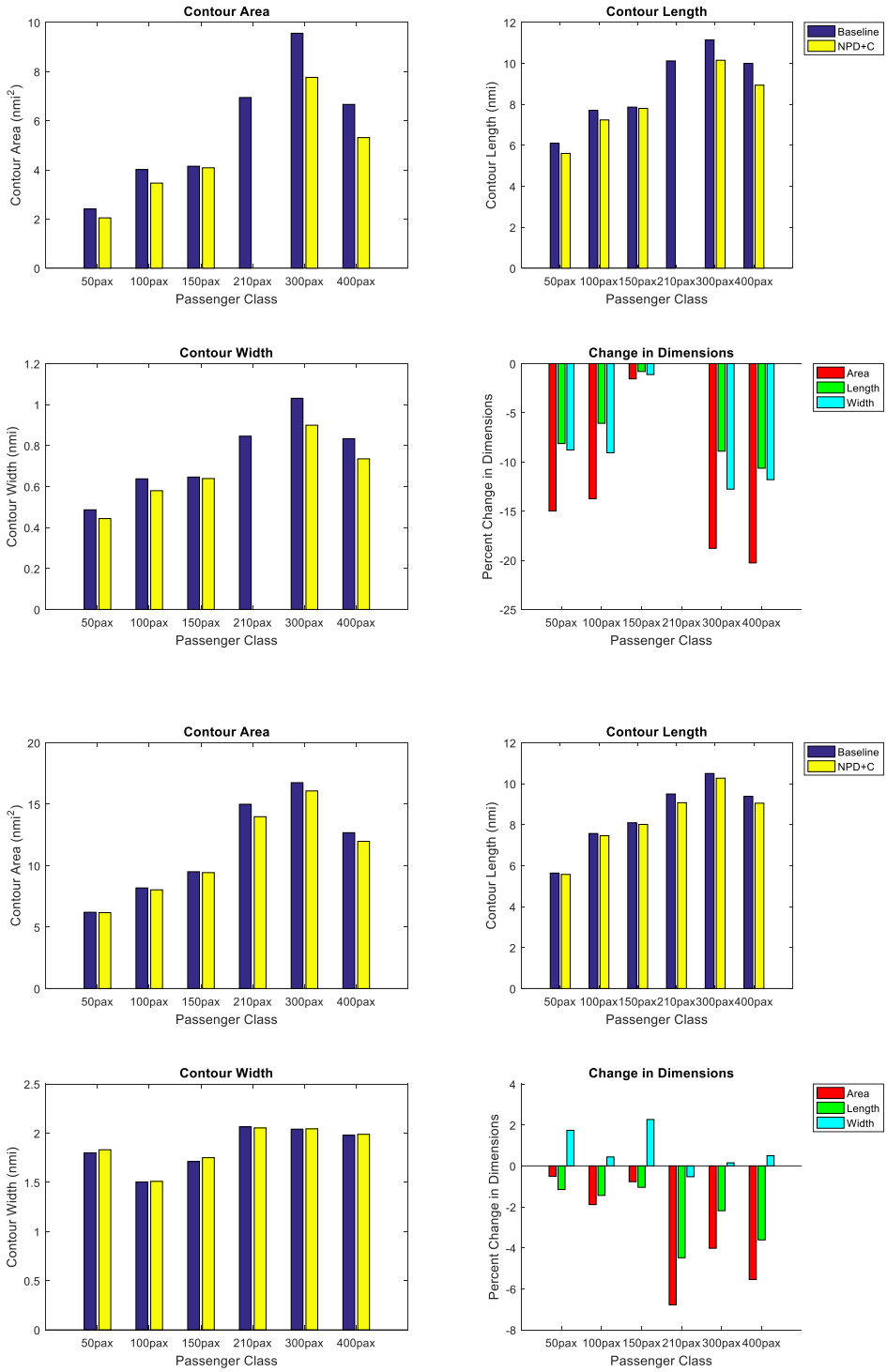


Figure 23. Study II.C Approach (top) – Departure (bottom)

Study II.D summary plots

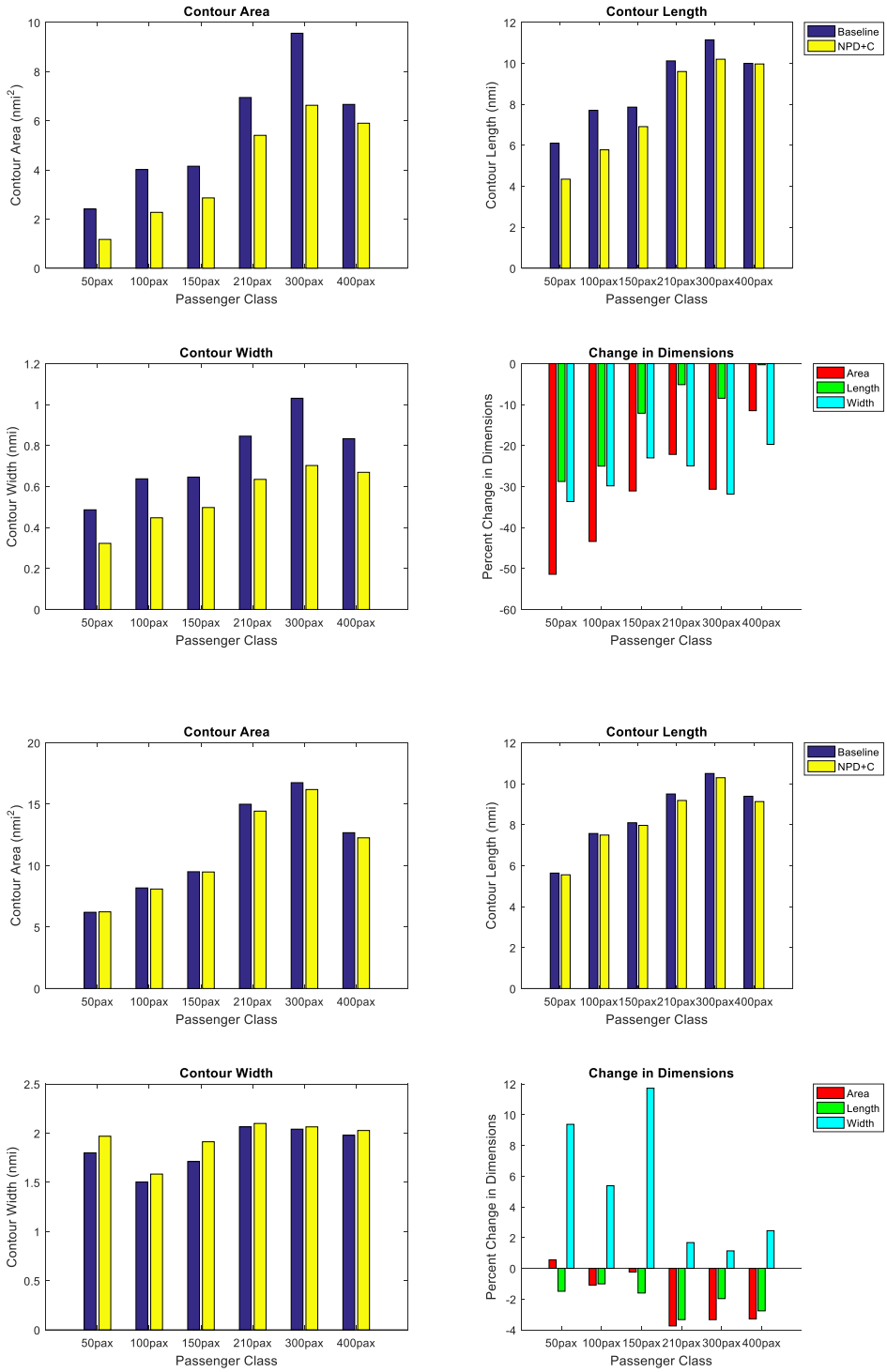


Figure 24. Study II.D Approach (top) - Departure (bottom)

Summary of results

Figure 25 includes a bar plot with a synthesis of the results obtained for the complete studies of I and II. The range of aircraft size classes is included with a quantile description of the mean, max and min values corresponding to the percent area change. These results are evident from the flight procedure which more closely corresponds to the noise procedure. At approach the clean configuration decreases the noise impact around the airport, while in departure, gear contributes to a larger contour. These results are analyzed in more detailed in Figure 26 and Figure 27. Both of these figures describe the area change for small & large size vehicles respectively. Recommendations from the combined findings are then explained in the NPD+C Recommendations section.

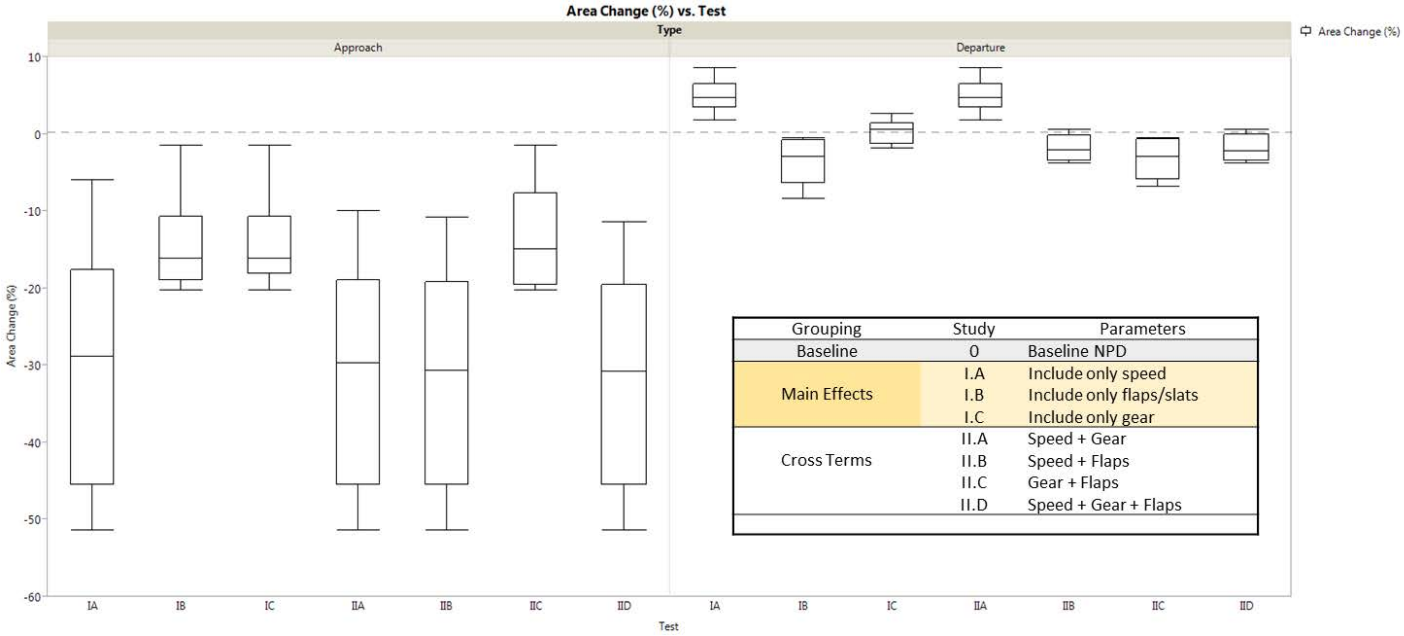


Figure 25. Noise contour area change (%) for all of the studies

The presence of the speed dimension in the NPD+C curves has the most significant impact in the overall noise contour obtained from running the modified AEDT environment for studies I and II. It is evident from the figure that departure procedures are less affected by the modifications. These impacts are observed to be explained by the following facts:

- Jet source noise is more relevant than airframe-configuration source noise, consequently explaining the configuration-dimension's lower impact
- Velocity corrections (duration adjustments) at higher reference speeds are negative, thus decreasing the total SEL value for the grid points obtained from higher noise metrics interpolated from the NPD+C
- Noise fraction adjustment show a similar behavior with respect to reference velocity and SEL vs LAMAX differences
- Impact of including the studies is mostly an area decrease during approach procedures due to:
- The initial procedures obtained at more deflected configurations
- The velocity corrections having a great impact in the final total SEL value for the given grid point
- The higher noise metrics with regards to the speed pertain to segment points further away from the observer.



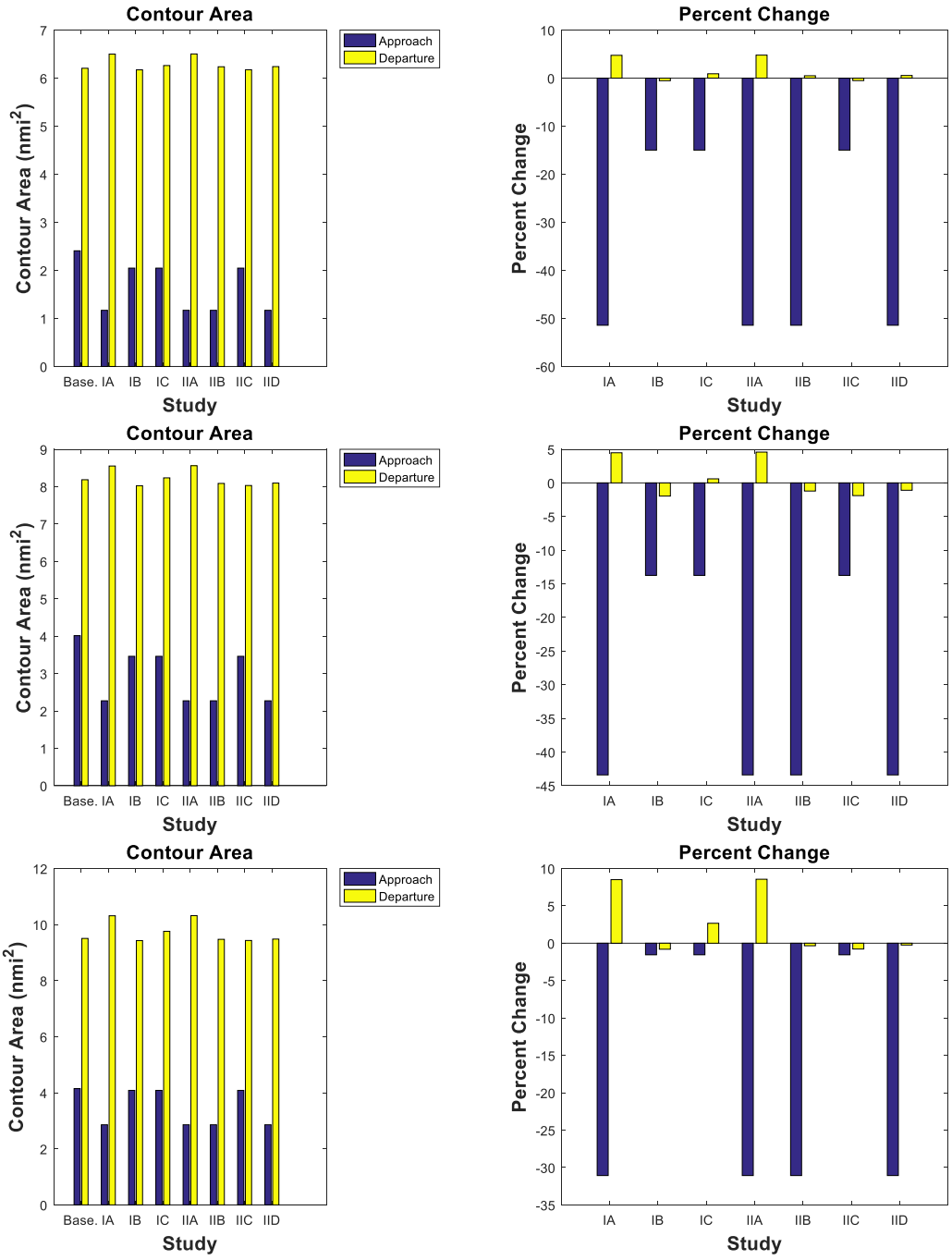


Figure 26. 50 – 100 – 150 PAX. Study I & II

Vehicle specific impacts - studies I & II – large sized aircrafts

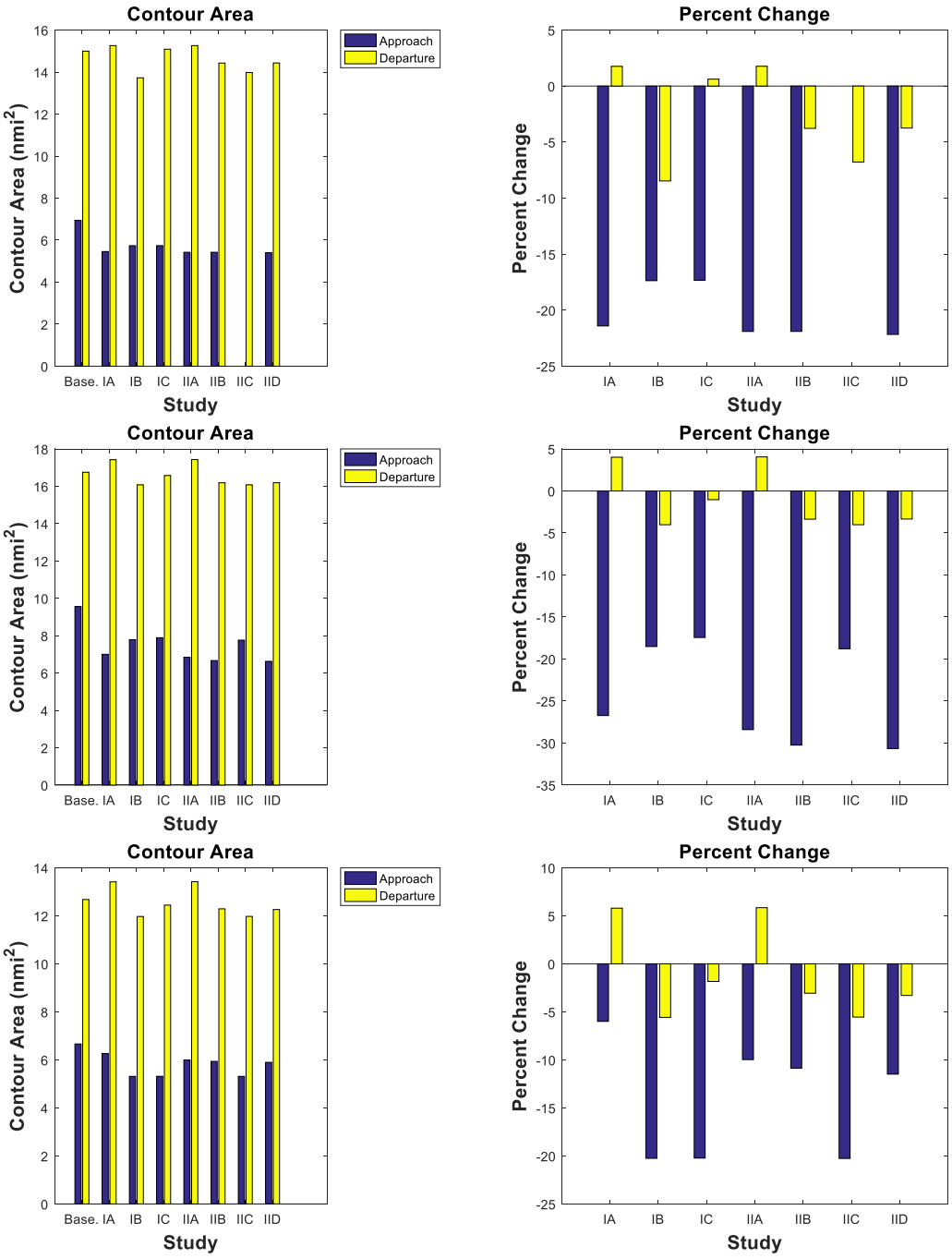


Figure 27. 210 – 300 – 400 PAX. Study I & II



NPD+C Recommendations

Figure 26 and Figure 27 provide insight into which dimensions should be expanded for a higher fidelity of the noise contours outputted by the AEDT NPD+C. Both the smaller and larger sized aircrafts demonstrate a large sensitivity to the reference velocity range of 130 – 190 kts. A substantial percent area decrease for approach operations (-25% to -50% area) and a significant increase in departure procedures (5% to 10%) is observed when the expanded range of reference velocities is included in the NPD+C input XML vehicle. Consequently, Georgia Tech recommends an increase in the NPD+C data which initially includes the velocity dimension. This initial consideration would require the minimum effort as there will be a maximum of two NPD sets.

The aircraft configuration, however, becomes increasingly relevant for the larger sized vehicles. A minor difference is observed between the gear and flap-slat setting effect, with the control surfaces having a more considerable impact. The optimum second expansion would be to include flap-slat setting noise metrics in the NPD+C superset data; nonetheless, this consideration would require the most effort. Accordingly, the second reasonable expansion is to acquire data with respect to gear-setting. Ultimately, both recommendations increase the NPD from a single set to a 4 set NPD+C input vehicle.

Task 3- Implementation Validation

Georgia Institute of Technology

Baseline vehicles validation

To validate the modifications made to AEDT, the noise contours generated by the modified version of AEDT must be compared to those generated by the unmodified version of AEDT using the original baseline vehicle. To allow for interpolation, the modified version of AEDT must be run using 12 sets of NPD+C data corresponding to the test matrix discussed previously. These results must be compared to the original version of AEDT, which only allows for one set of NPD data. To produce comparable results, the original baseline vehicle for each class is run using the original unmodified version of AEDT. This vehicle is referred to as the "Baseline" vehicle. To compare this with the modified version of AEDT, a new vehicle is defined using 12 sets of NPD+C data that are each identical to the single set of NPD data from the Baseline vehicle. This vehicle is referred to as "singleNPD1." By defining an NPD+C vehicle with all aircraft configuration (velocity, flap setting) information identical to the original baseline, it is possible to compare the results generated by the original and modified versions of AEDT. The results should be identical, since the interpolation scheme in the modified version of AEDT should always generate the baseline NPD data based on the 12 identical NPD+Cs. This simple validation test is performed to ensure that none of the modifications made to AEDT in this study have any effect on how AEDT is performing analysis, but is instead only affecting the NPD information that AEDT is provided at each segment. Table 8 provides a summary of differences between the baseline AEDT code and the modified version used for this work.

Figure 28 show the SEL contours of the validation study for approach and departure at both 60 and 80 dB. In each case, the contours generated by both the Baseline and singleNPD1 match identically. This shows that the modified version of AEDT developed in this study produces identical analysis to the original version of AEDT when provided identical NPD+C information. This study confirms that the modifications made to AEDT only work to change the NPD data that AEDT uses to perform analysis for each segment without changing any of the analysis methods.

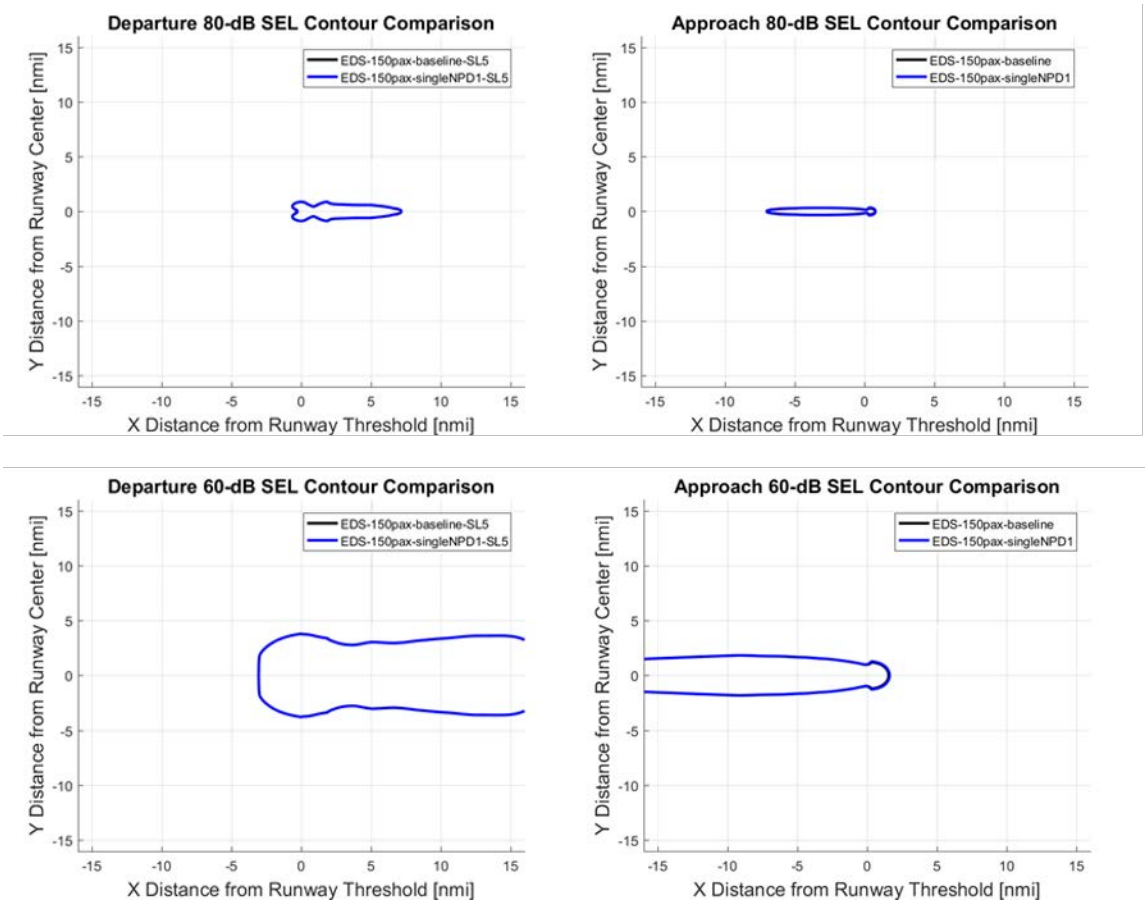


Figure 28. Validation Results for 150 PAX Vehicle Class

Table 8: AEDT Source Code Modifications

AEDT SOLUTION MODIFICATIONS FOR NPD+C IMPLEMENTATION				
Project	Class / File	Method / Class	Description	Related Mods
AAM (Aircraft Acoustic Module)	AA0MCompute.cs	RunComputeAcoustics()	Create new empty lists, of the modified noise matrix type, for the NPD+C's SEL & LAMAX values interpolated on configuration and speed	NpdData.cs
			String builder initializers for a faster output of the segment by segment noise power contribution, noise fraction, and velocity correction, to each grid point	MainContainer.cs
			Logic designed for obtaining, calculating and appending each-segment-each-grid point's information (coordinates in nm, noise fraction, velocity correction, noise power contribution translated to dB values) to the string builders	
			Logic included for writing the csv files, based on the string builders, depending on the operation type (approach, departure)	
		DetailedGridReport()	Adding noise fraction and velocity correction information to the local receiver object. Included in the detailedDataList and obtained from the segment storage information once it is expanded within the MainContainer	
	CDOAAMInterface.cs	CopyCDOTrajectorySegmenttoFlightPathSegment()	Include FLAP ID information to the flight path segment and subsequent objects	
		CopyCDONoiseParameterstoNPDObj()	Use the instance of the created object NoiseParameters_combined, which expands the NoiseParameters object in order to include the superset of 12 base NPDs. Use its respective thrust setting type	NoiseParameters_combined.cs
			The included algorithm obtains the data from all of the NPD curves (noisegroups as specified in the input XML vehicle). The 12 objects are each analyzed individually and cumulatively passed as an expanded object in NpdDataList_in. Once the operation mode for the logic is set, the reference values (flap, velocity and gear setting) are included in the newNpd expanded object.	NpdDataAircraft_combined.cs
	FlightPathSegment.cs	FlightPathSegmentAirplane : FligthPathSegmentBase	Included and encapsulated the flap id string for a given segment	
	MainContainer.cs	using	MathNet.Numerics package imported as "Interpolate." Used for faster interpolation with linear algebra extensions	
		Main Container	Internal NOISECURVE object for noise curves of a given aircraft to be interpolated. Include reference gear string	
		AircraftNoiseCurveStorage()	Assign the reference values (velocity, flap setting, gear setting) to the noisecurveStorage fullSet data	NpdDataAircraft_combined.cs
		Maximum()	Single event noise level is calculated from the senl_max() method whose constructor is updated to include the NPD+C SEL & LAMAX data	NpdData.cs
			Save velocity correction and noise fraction values to the segmentStorage list of objects	
		TimeAbove()	The NoiseInterpolation() and senl_max() functions are updated to include the NPD+C SEL & LAMAX data	NoiseInterpolation()
			Save velocity correction and noise fraction values to the segmentStorage list of objects	
		TimeAudible()	The NoiseInterpolation() and senl_max() functions are updated to include the NPD+C SEL & LAMAX data	
			Save velocity correction and noise fraction values to the segmentStorage list of objects	
		Exposure()	The NoiseInterpolation() and senl_max() functions are updated to include the NPD+C SEL & LAMAX data	
			The segment's aircraft velocity is included in the updated Noisefraction method	Noisefraction()
			Save velocity correction and noise fraction values to the segmentStorage list of objects	
		NoiseInterpolation()	Logic to assign the noise matrix object values based on the noise level type (SEL, LAMAX, EPNL, PNLTMAX, CW, CMAX)	
			Create temporary instances of the segment storage and aircraft object for interpolation considerations. Assign gear down & up reference setting values. Convert the flap setting string to a double and obtain aircraft velocity	
			Studies iA & IB: gear configuration is tied to the flap setting. Logic for including these effects	

			Interpolation algorithm discussed in great detail in the above sections of the report. Based on gear setting, the logic interpolates polynomial w.r.t. flap setting and linearly on velocity. This process is repeated for the 10 slant distances specified in the NPD superset. The resulting set of NPD+C for each segment is saved from this grid point and used for the subsequent grid points as the NPD+C list will be the same. It will then be interpolated based on thrust and distance.	
			Print both the SEL & LAMAX list of NPD+Cs for each segment of the aircraft's flight path for a high fidelity comparison of NPD vs NPD+C values	
			Use the temporary instances to interpolate on thrust and distance	
		SegmentContainer()	Include flap id and velocity correction information	
		Noisecorrection()	Logic for correctly implementing the velocity correction adjustment. Should the aircraft velocity be less than 130.35 kts, it would use this reference speed value; should it be higher than 190 kts, it will use this upper limit value. Otherwise, the reference speed will be the same as the aircraft velocity as it is within the bounds of the NPD+C data generation	
		Noisefraction()	An algorithm is included for the noise fraction adjustment to be correctly computed based on the aircraft's velocity and the respective reference speed at which the NPD+C was generated.	
			The S0 value (Ka in the source code) in the NF adj factor is computed as thoroughly explained in the respective sections of the report. This calculation uses a velocity in ft/s. and is dependent on the type of noise level used. The formulation is flexible to SEL, LAMAX, EPNL and CW metrics.	
	NpdData.cs	NOISE_MATRIX_TYPE	Cloneable interface for a member copy instead of referencing original class	
			Include double array internal values for reference velocities, reference flap settings and reference gear settings	
			Clone() method for noise matrix manipulation w/o altering original matrix	
		NOISECURVE	Cloneable interface for a member copy instead of referencing original class	
			Constructor inclusion of the fullSet values referencing the velocity, flap and gear reference settings	
			Constructor created for the interpolated noise curves values	
			Clone method logic created for a member-wise cloned instance	
AEDTTester	AircraftXmlReader.cs	AircraftXmlReader	Modified AEDT's reader schema to incorporate the new vehicle XML input containing the information of the superset of NPDs.	EDS2AEDTFLEET_3.xsd
		ReadAirplane()	Parameters are now obtained from the NoiseParameters_combined class which includes the set of 12 NPD curves. The object is expanded to include all the NPD+C relevant information. These are then included in the airplane instance	NoiseParameters_combined.cs
		GetNoiseParameters_combined()	Included logic to obtain the 12 different noise groups stated in the input vehicle XML file, with respective noise curves	
		NPD+CurveLongRecord_combined	The instance now includes the reference gear, flap setting, and velocity value for subsequent implementation in the code	
		GetNoisePowerDistanceCurves	The NPDs are obtained from the NPD+CurveLongRecord_combined () method developed for the input XML vehicle using the superset of NPDs. The aircraft data information also uses the expanded NpdDataAircraft_combined() which includes the reference values	NPD+CurveLongRecord_combined.cs, NpdDataAircraft_combined.cs
			The expanded object referring to NoiseParameters_combined is used to allow for 12 curve passing	NoiseParameters_combined.cs
	Program.cs	ProcessFlights()	The detailed noise reporting option is activated to allow for each-segment-each-grid point information output	
	ResultsCSVWriter.cs	SavePerformanceAndNoise()	Include flap setting information in the noise & performance report ouput	
(APM) Aircraft Performance Module	AirplaneProcedureStepModeler.cs	AirplaneProcedureStepModeler, PostComputeStep()	Include final and initial profile point flap id information for the given step	
	OagStep.cs	calcSegmentWeightChange()		
	ProcedureStep.cs	ProcedureStep()	Initialize the flapId in the default constructor	
	ProfilePoint.cs	ProfilePoint	Encapsulate the flap setting	
		initialize()	Initialize the flap setting after the method is called from main constructor	
	StepClimbout.cs	calcBadaAccel()	Assign the profile flap setting to the start and end of the segment	
		calcBadaClimb()	Assign the profile flap setting to the start and end of the segment	
	StepDescent.cs	calcDescendPhase()	Initialize the flap setting	

		calcBadaDecel()	Assign the profile flap setting to the start and end of the segment	
		calcBadaDescent()	Assign the profile flap setting to the start and end of the segment	
	AirplaneProfile.cs	AssignContextToStep()	Flap setting information passed to the procedure step and the computed profile	
	EventModeler.cs	PopulateCDOPerformnce EventResultFromFlightPa	Source segment flap setting passed to the target segment	
		ResolveSpeed()	Properties of the trajectory segment expanded to include flapsetting	
	ComputedProfile.cs	Computed Profile	Initialize the procedure step as well as the flap setting	
		trim_at_altitude()	Target altitude now includes the flap setting information	
		setThrustCutBack()	Include flap id information from the airplane procedure step	
	FlightPath.cs	compute_path_points()	Populate the new path point with the expanded configuration information	
		adjust_airplane_path_points()	Pass configuration information	
	FlightPathSegment.cs	FlightPathSegment	Initialize flap information	
		FlightPathSegment()	Initialize the flap configuration information in the default constructor	
	OagFligthPath.cs	createGateTogateFlightPathSegments()	In the creation of the segments from flight path points, include the flap configuration information	
		addAltIntervalPoints()	The new path point includes the previous path's information on flap setting	
		createDepartureFlightPathForHoldingPoints(), createApproachFlightPathForHoldingPoints()	The new path point includes the previous path's information on flap setting	
	IAirplaneProcedureStepExtensionMethods.cs	AsApmProdecureStep()	Including flap configuration information for the target step	
(CDO) Common Data Objects	IAirplane.cs	IAirplane : IAircraft	NoiseParameters_combined included in the airplane's interface	
	NoiseParameters_combined.cs	NoiseParameters_combined : NoiseParameters	Developed a new class for the noise parameters members that inherits from the original NPD noise parameters class included in AEDT.	
			Expanded all the methods and initialization to include 12 instances of the npd curve type, which has in interface defined in INoisepowerDistanceCurve	
	NpdDataAircraft_combined.cs	NpdDataAircraft_combined : NoisePowerDistanceCurve, INpdDataAircraft	Developed a new class that inherits from the original single NPD based noise power distance curves and the interface of the aircraft's npd data. The method is expanded to include reference settings; including velocity, flap, and gear configuration	
	TrajectorySegment.cs	TrajectorySegment : ITrajectorySegment	Initialize the flap id parameter for the trajectory segment constructor. Change the number of fields to include data array corresponding to the configuration	
			Backwards compatible increase in the data array for flap ID information. Include FlapID information in the trajectory subdivided by segments	

Segment-wise contribution build-up

The ability to analyze segment-wise noise contribution was instrumental to validate results obtained from the modified AEDT algorithm developed for the NPD+C studies. The build-up analysis enabled as well the assessment of the minor amount of cases with unintuitive behavior.

This was the case for a subset of the smaller-sized vehicles (50 – 100 – 150 PAX), which portray a similarity in the noise contour impact between gear-setting and flap-slat-configuration main-effect analyses. Specifically, the approach procedure 80 dB contours (for both studies - studies I.B & I.C are available through requesting from the authors) shared identical changes in the total SEL values for grid-points showing the largest difference with respect to the reference baseline.

Figure 29 depicts the graphical explanation of this behavior and Table 9 help explain the differences in the flight path characteristics. The graph's orange line represents the difference between the baseline value and the flap sensitivity output; the blue line represents the difference between the baseline value and the gear sensitivity output; and the gray line is the difference between the flap-slat and the gear sensitivity outputs.

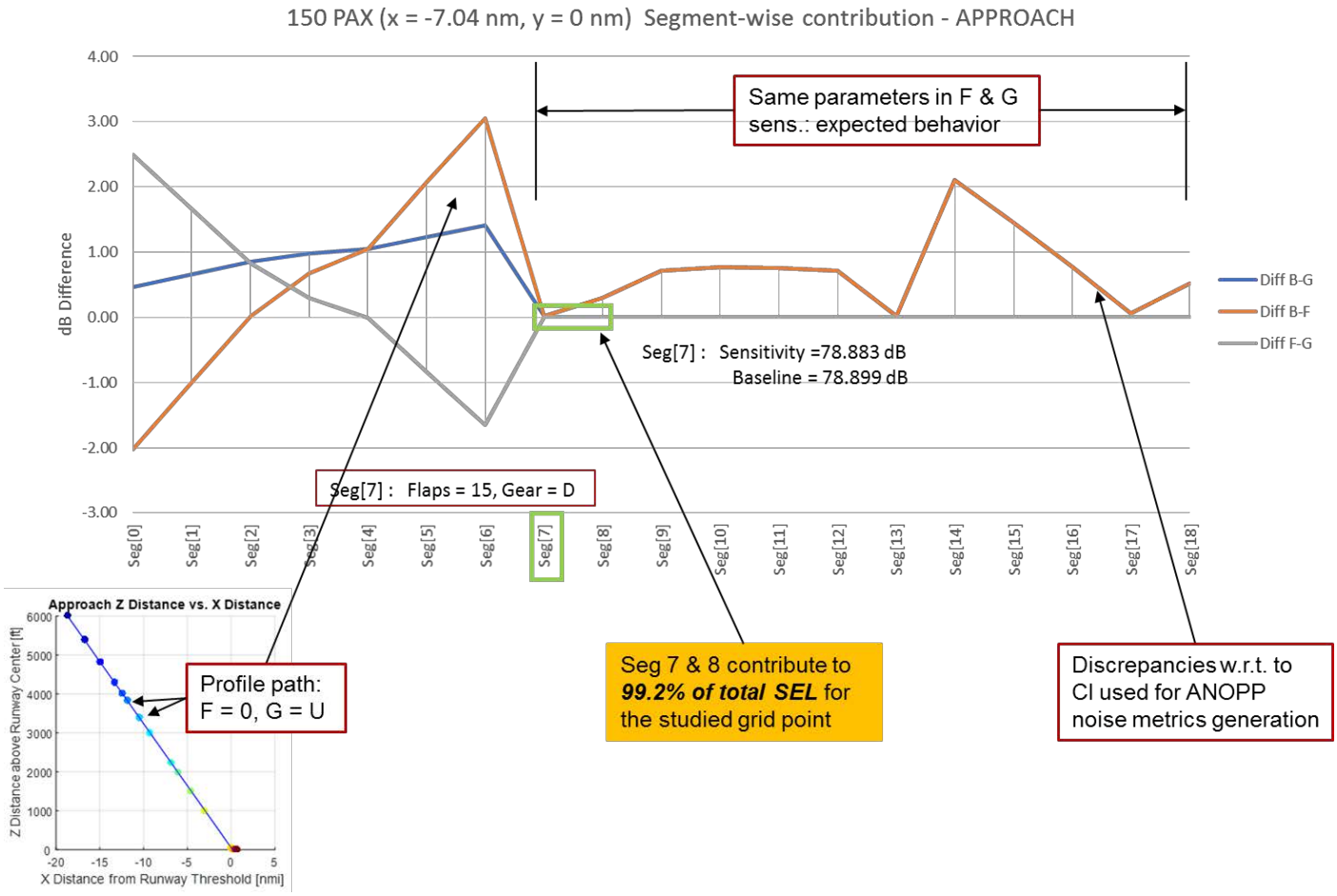


Figure 29. Segment-wise contribution – APPROACH 150 PAX

As explained in the Task 2 section, the changes in NPD+C's at approach lies in the initial segments having a clean configuration, gear-up setting. These differences are reflected until segment 7. Afterwards, the segment-wise noise metric



values with regard to the baseline should be zero (due to the instantaneous configurations being the same); however, it was then realized that the discrepancies were due to the rounded lift coefficient value ($C_l = 0.355$ for the baseline, $C_l = 0.354$ for the studies) in the 150 PAX case. Both gear and flap sensitivity studies converge to the same dB difference to the baseline, which is the expected behavior. The blue trend differs significantly from the orange trend during the initial segments (as expected due to the differences in aircraft configuration); nonetheless, these SEL values contribute very little to the total SEL value for the studied grid-point. As highlighted in the plot, segment 7 and 8 contribute 99.2% of the noise value (Figure **30.** Pareto plot for an NPD+C notional departure that can better describe the differences in contribution). For these segments, both gear and flap analyses converge to the same value as seen in the gray trend. Consequently, the detailed research performed explained the similarities in the calculated values.

Table 9. Segment-wise contribution research

Flight path differences				Grid 150 pax, x = -7.04 , y = 0						
Flap Base	Flap Sens	G Base	G Sens	Segment	gear	Flap	base	*Diff B-G*	*Diff B-F*	*Diff F-G*
15	0	D	U	Seg[0]	13.902	16.400	14.372	0.47	-2.03	2.498
15	0	D	U	Seg[1]	18.086	19.750	18.748	0.66	-1.00	1.664
15	0	D	U	Seg[2]	22.827	23.658	23.682	0.85	0.02	0.831
15	0	D	U	Seg[3]	24.834	25.136	25.810	0.98	0.67	0.302
15	0	D	U	Seg[4]	25.430	25.427	26.476	1.05	1.05	-0.003
15	0	D	U	Seg[5]	34.992	34.162	36.226	1.23	2.06	-0.830
15	0	D	U	Seg[6]	43.463	41.817	44.872	1.41	3.06	-1.646
15	15	D	D	Seg[7]	78.883	78.883	78.899	0.02	0.02	0.000
15	15	D	D	Seg[8]	73.257	73.257	73.558	0.30	0.30	0.000
15	15	D	D	Seg[9]	58.835	58.835	59.556	0.72	0.72	0.000
15	15	D	D	Seg[10]	40.998	40.998	41.767	0.77	0.77	0.000
15	15	D	D	Seg[11]	31.707	31.707	32.461	0.75	0.75	0.000
15	15	D	D	Seg[12]	10.334	10.334	11.046	0.71	0.71	0.000
15	15	D	D	Seg[13]	9.739	9.739	9.754	0.02	0.02	0.000
15	15	D	D	Seg[14]	9.132	9.132	11.237	2.11	2.11	0.000
15	15	D	D	Seg[15]	8.396	8.396	9.854	1.46	1.46	0.000
15	15	D	D	Seg[16]	7.714	7.714	8.487	0.77	0.77	0.000
15	15	D	D	Seg[17]	7.079	7.079	7.135	0.06	0.06	0.000
15	15	D	D	Seg[18]	6.508	6.508	7.035	0.53	0.53	0.000

Seg 7 & 8 contribute to 99.2% of total SEL for the studied grid point

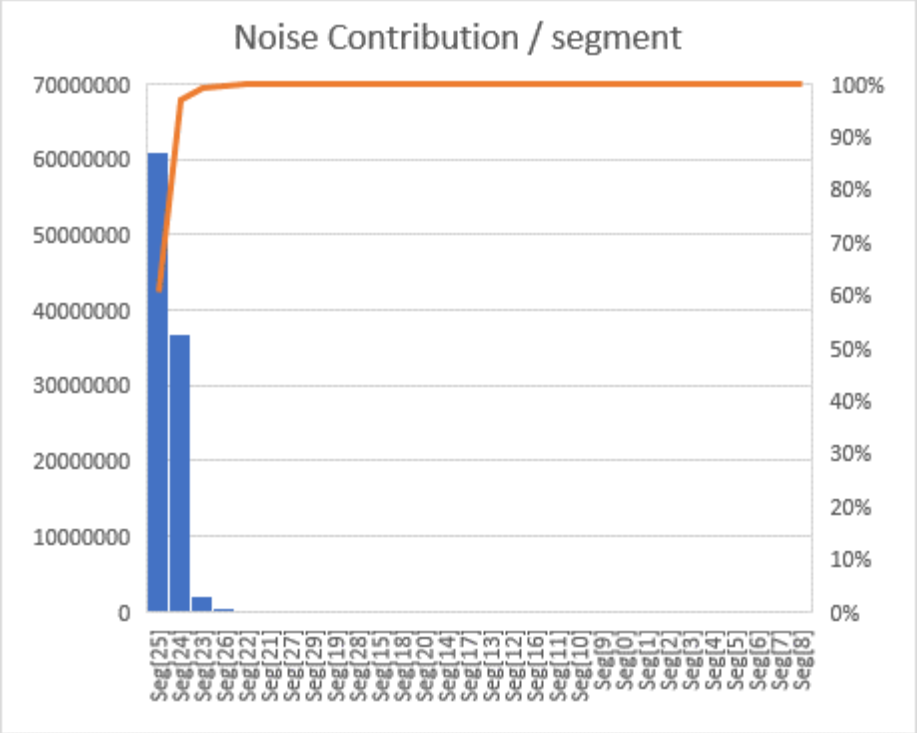


Figure 30. Pareto plot for an NPD+C notional departure

Task 4- Sensitivity Study of Noise Sources within ANOPP

Georgia Institute of Technology

A screening test was utilized in order to perform a sensitivity study to determine major noise sources within ANOPP. A screening test uses a high, low, and middle value of various inputs to show the spread of the data accurately with as few runs as possible. After the screening test, a predictor screening test was used to determine the main contributors.

Below is a flow chart that describes each step of this process. Phase one shows the research into each ANOPP module used in the study in order to look at important equations and relationships between parameters. This helps to identify important inputs that are used within the modules in order to generate the run matrix for the screening test. Understanding the relationships between important parameters helps to confirm findings found later on because it is understood why an input might be a large contributor.

Phase two explains the steps to each of the sensitivity studies. Phase two A describes the sensitivities studies done for each modules, while two B describes the sensitivities for all modules. A sensitivity study within airframe modules which include flaps, slats, landing gear, and wing, as well as engine modules which include jet, core, and fan. This shows what is the most influential parameter to noise results within each module as well as what module is most influential to noise results at each flight segment.

Phase three discusses the generation of the correction function by quantifying the sensitivity of each input and each module. The following studies were done for three different vehicle classes (50pax, 150px, and 300pax).

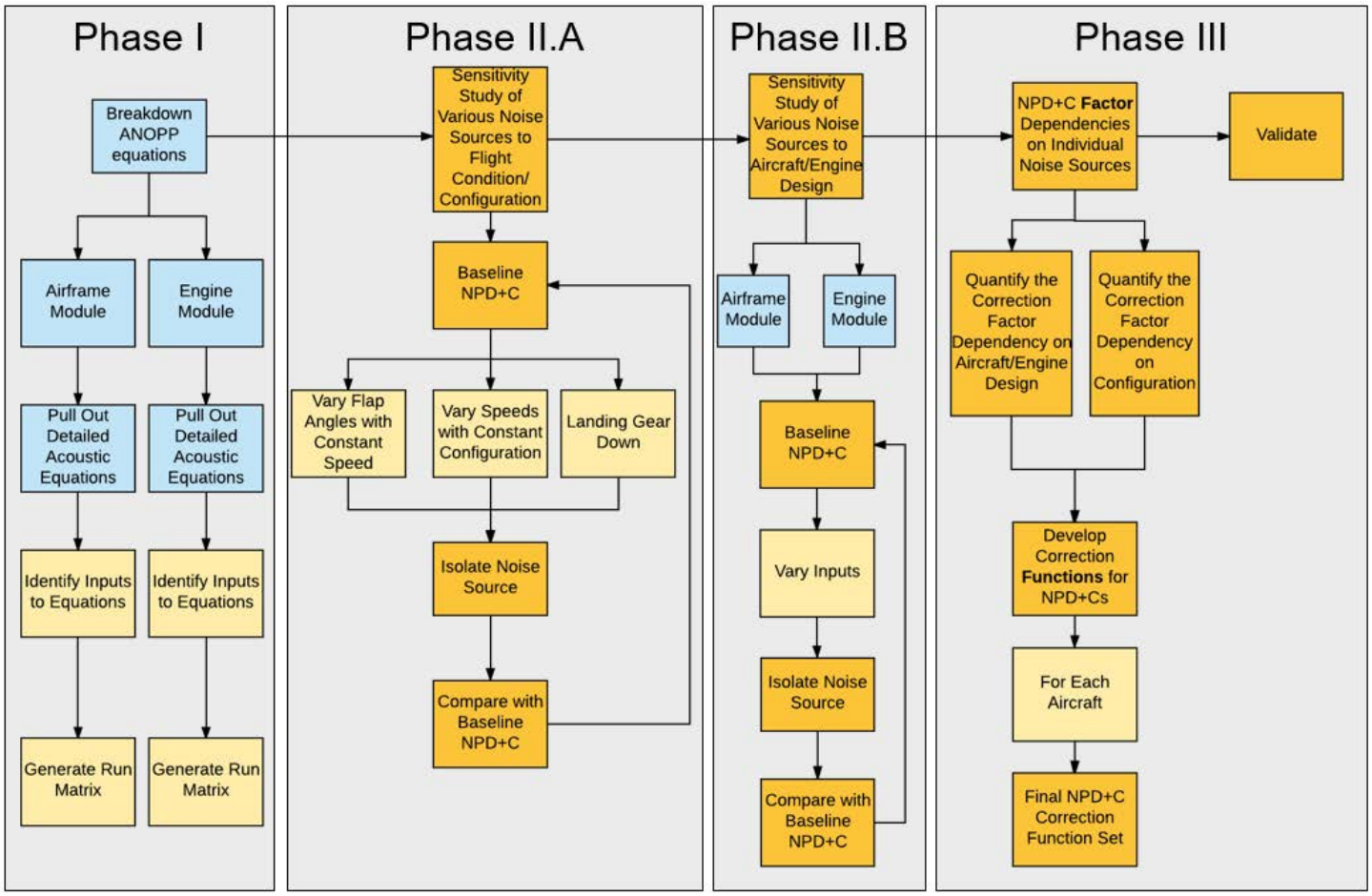


Figure 31. Flow Chart for Identifying Noise Sources

Phase I

The first step of the project was to investigate ANOPP which is the primary tool for this project. This involved research into the user manual and research papers that cover the experiments that were used to create ANOPP, primarily focusing on the equations and theory surrounding the calculations. The goal of this was to understand the empirically derived equations and main driving parameters. This was necessary to run an accurate and purposeful sensitivity study involving the found parameters. Later on in the study this confirms and validates the outputs given to see if it accurately correlates with the important equations and relationships found. This step was done for each module of importance within ANOPP focusing on engine and airframe modules.

Phase II

Phase two are the sensitivity studies and involved executing ANOPP in varying different inputs in order to identify the sensitivity of noise to the chosen parameters. Phase two A focuses on flight conditions and configurations. The flight speed, flap angle and gear setting with the airframe and engine modules were varied and the noise sources were then isolated using the subtraction method. The subtraction method is where the simulation is run with specific noise calculations and then run again without the noise calculation that is desired to be isolated. Logarithmic subtraction (due to the logarithmic nature of decibels) is then done to find the difference in noise and therefore isolate the noise source. This was implemented because calculations cannot be done without some results. For example, the simulation cannot isolate flaps similar to how flaps alone cannot generate noise in the same fashion as flaps attached to an aircraft. This phase provides insight on the most influential noise sources to the NPD+C and how sensitive they are to changes in flight configurations and conditions.



Phase two B is similar to phase two A, but focuses on various engine and airframe design parameters. This is another sensitivity study just focusing on different parameters. Instead of changing parameters such as flap angle, this study changes parameters such as flap chord length. The noise sources were isolated in the same manner as phase two A and provides insight on the most influential noise sources to the NPD+C and how sensitive they are to design changes. Phase two A and B were run in parallel. Both of the sensitivity studies gives an idea of the type of correction function desired.

Phase III

Phase three looks at the trends throughout the sensitivity studies across all parameters in order to decipher what the final correction function might look like. The goal of this step is to create a function that changes the correction factor due to the individual flight configurations, conditions and design variables. Correction factors are then used to create a NPD+C given a baseline NPD. For each vehicle class, the sensitivity studies were plotted to determine the most influential noise sources. Input parameters were plotted against NPD noise levels as well as against NPD to NPD+C correction factors. A function of best fit of the data is the correction function. This allows the use of correction factors on a wide range of baseline NPDs to generate NPD+C without the need to rerun ANOPP every time. Therefore the NPDs within AEDT will easily become NPD+Cs in order to better reflect actual data.

Summary of Results

Figure 32 shows the matrix of test conditions for one of the modules. The parameters chosen to vary were decided based off of the empirical equations found in ANOPP. This process helps to narrow down the many parameters that could potentially influence noise to major contributors. This process was repeated for the other modules, such as slat, gear, wing, jet, fan, and core. There are similar matrices for other modules.

Noise Source: FLAP		Min	Max
Configuration	Flight Velocity	130 knots	210 knots
	Flap Deflection Angle	0	40
Design Parameters	Vehicle Weight	-30%	30%
	Wing Area	-25%	25%
	Wing Span	-25%	25%
	Flap Span	-25%	25%
	Flap Chord	-25%	25%

Figure 32. Run Matrix for Flap

Figure 33 shows how relative importance of different parameters were ranked for a 150pax aircraft within the flap module at a height of 4000ft. This was done using JMP which is a statistical software which for this calculation uses 100 decision trees that consider a random subset of the predictors. The final prediction is the average of the predicted values for that response over all the decision trees. This was done for every height and thrust setting for approach and departure, for every

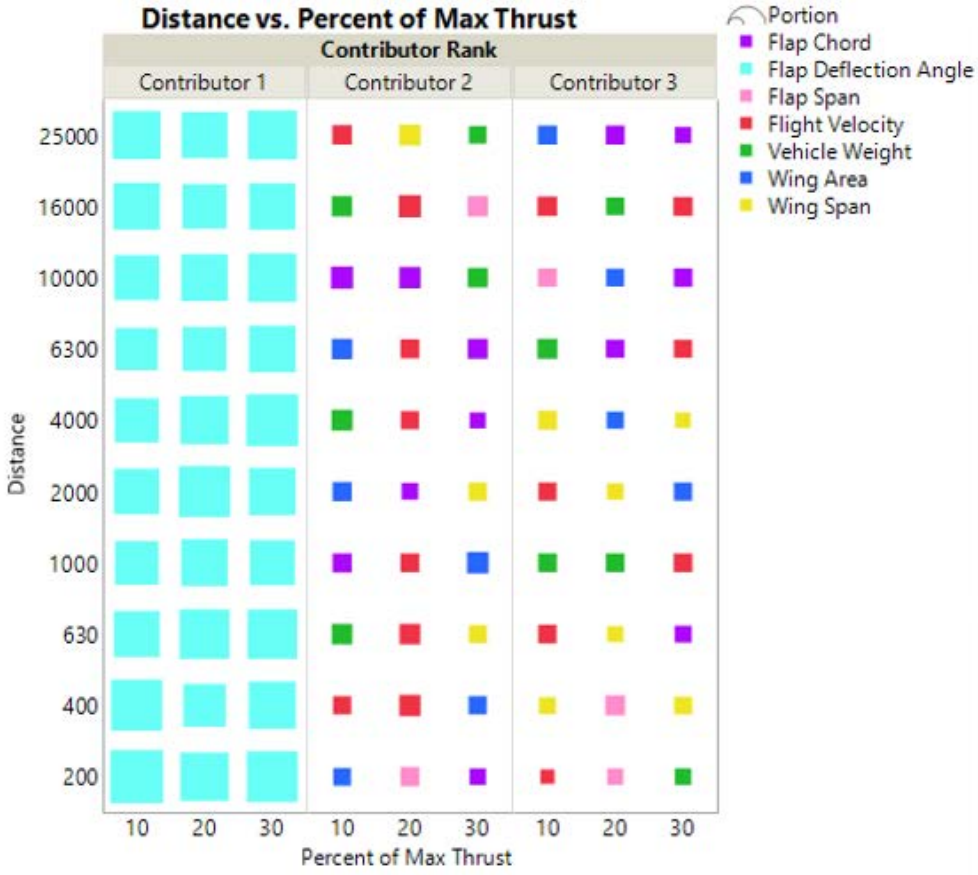
module, in addition to every vehicle class. After the repetition is done, it is then put into graphs like Figure 35 for easy comparison.

	L_4000			
Predictor	Contribution	Portion		Rank
Flap Deflection Angle	3.41832	0.2456		1
Flap Chord	1.88482	0.1354		2
Vehicle Weight	1.48983	0.1070		3
Flap Span	1.42878	0.1026		4
Wing Span	1.35327	0.0972		5
Flap Chord 2	1.31586	0.0945		6
Flight Velocity	1.30251	0.0936		7
Flap Span 2	1.03451	0.0743		8
Wing Area	0.69249	0.0497		9
THR_SET	0.00000	0.0000		10

Figure 33. Importance Calculation

Figure 34 shows the repeated results from the Flap module for approach for a 150pax aircraft varying flap chord length, flap deflection angle, flap span, flight velocity, vehicle weight, wing area and wing span. Only the top 80% of contributors are considered significant and the top three contributors make up a majority of that 80% so only the top three were graphed. The square sizes on the plot are determined by the relative contribution to the noise. It is seen in this graph that the primary contributor to flap noise for a 150pax aircraft, is the flap deflection angle. Therefore, at configurations where the flap deflection angle needs to be high the correction function will be highly correlated with flap deflection angle. The square sizes for the first contributor are relatively similar meaning that at every point the flap deflection angle is the same relative importance. While in the second and third contributors the sizes of the squares vary more meaning the relative importance varies in the secondary contributors.

Figure 34 displays at what points in descent different parameters are most influential. Some parameters that are uninfluential to the noise may be ruled out because their contribution is insignificant. It can be noted that as the aircraft is lower to the ground more parameters become significant, because as an aircraft is higher in the atmosphere it is more difficult to distinguish between sound sources. The thrust setting is the same at various heights within the graph even though this would not be typical of an aircraft in flight. Patterns or lack of patterns shown on graphs such as this help to show what the correction function will look like. This shows if a different correction function is needed for approach and descent or different vehicle classes. These graphs were generated for approach and departure, for other modules (slat, gear, wing, jet, fan, and core), for three vehicle classes (50pax, 150pax, 300pax).



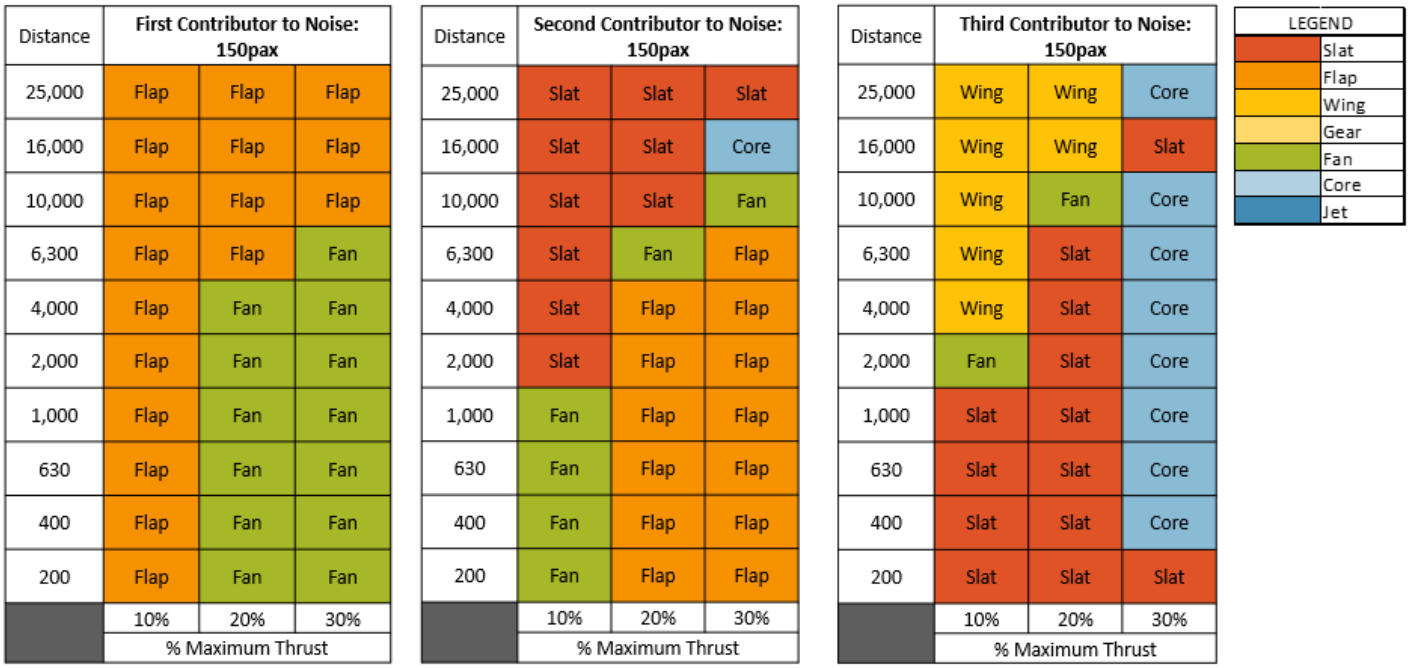
1st Noise Driver	
Driver	Count
Flap Deflection Angle	30
Flap Span	0
Flap Chord	0
Flight Velocity	0
Vehicle Weight	0
Wing Area	0
Wing Span	0

2nd Noise Driver	
Driver	Count
Flap Deflection Angle	0
Flap Span	2
Flap Chord	7
Flight Velocity	8
Vehicle Weight	5
Wing Area	5
Wing Span	3

3rd Noise Driver	
Driver	Count
Flap Deflection Angle	0
Flap Span	3
Flap Chord	5
Flight Velocity	7
Vehicle Weight	5
Wing Area	4
Wing Span	6

Figure 34. Sensitivity Study of Flap Module

Figure 35 shows the results from the sensitivity study from the module study for a 150pax aircraft. This shows at what point different modules are most influential to the noise generated so influential parameters can be considered at points in which the module is most influential. It is seen for a 150pax aircraft the flap module within ANOPP is most dominate at low thrust settings as well as high thrust setting when the altitude is high. When thrust settings are higher and altitude is lower the fan module from the engine is most dominate. Flap is still relatively important throughout because it is a secondary contributor even at high thrust settings and low attitude. This process was repeated for each vehicle class (50pax, 150pax, 300pax).



Distance	First Contributor to Noise: 150pax		
25,000	Flap	Flap	Flap
16,000	Flap	Flap	Flap
10,000	Flap	Flap	Flap
6,300	Flap	Flap	Fan
4,000	Flap	Fan	Fan
2,000	Flap	Fan	Fan
1,000	Flap	Fan	Fan
630	Flap	Fan	Fan
400	Flap	Fan	Fan
200	Flap	Fan	Fan
	10%	20%	30%
	% Maximum Thrust		

Distance	Second Contributor to Noise: 150pax		
25,000	Slat	Slat	Slat
16,000	Slat	Slat	Core
10,000	Slat	Slat	Fan
6,300	Slat	Fan	Flap
4,000	Slat	Flap	Flap
2,000	Slat	Flap	Flap
1,000	Fan	Flap	Flap
630	Fan	Flap	Flap
400	Fan	Flap	Flap
200	Fan	Flap	Flap
	10%	20%	30%
	% Maximum Thrust		

Distance	Third Contributor to Noise: 150pax		
25,000	Wing	Wing	Core
16,000	Wing	Wing	Slat
10,000	Wing	Fan	Core
6,300	Wing	Slat	Core
4,000	Wing	Slat	Core
2,000	Fan	Slat	Core
1,000	Slat	Slat	Core
630	Slat	Slat	Core
400	Slat	Slat	Core
200	Slat	Slat	Slat
	10%	20%	30%
	% Maximum Thrust		

LEGEND
Slat
Flap
Wing
Gear
Fan
Core
Jet

Figure 35. Sensitivity Study of Modules

Figure **36** shows the combination of Figure 34 and Figure **35** onto one graph to better see patterns and confirm the data follows logically. It is necessary to compare this figure with the segments of flight that show the most difference in noise when the configuration is included in the NPD. Some of the parameters of the configuration are not available within AEDT, but can be correlated or approximated from other known parameters. Many of these graphs were looked at and analyzed in order to determine the correction function. This process was repeated for each vehicle class (50pax, 150pax, 300pax).

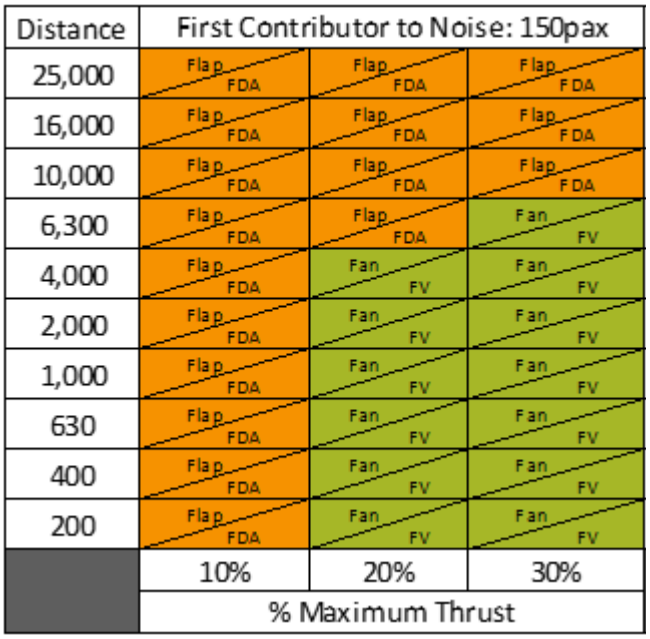
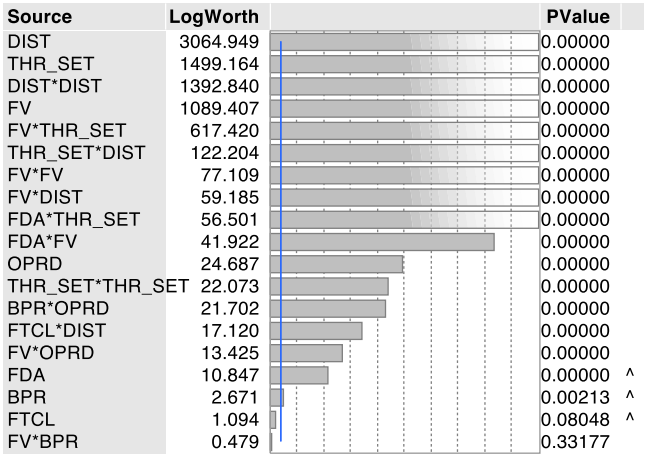


Figure 36. Combination of Important Parameters and Modules

Generating Correction Functions

Using the sensitivity from Figure **36**, a small study was undertaken to determine if reduced order correction functions could be applied to correct the baseline NPD+C noise as a function of correlating parameters (flap deflection angle and flight velocity), design parameters (OPR, FPR, Thrust), and NPD inputs (distance and operational thrust setting). As shown earlier, approach has the highest difference in noise prediction, therefore the approach portion of the NPD was used for testing generation of the correction function. A polynomial was regressed to predict the difference between the NPD+C generated using ANOPP and a conventional NPD, also generated with ANOPP. Fortunately, the regression showed that the change in SEL due to aircraft configuration is somewhat invariant to the engine design (OPR, BPR, design thrust) as shown Figure 37. This indicates it may be possible to make a correction that is invariant to aircraft design parameters and which may be applicable to many types of aircraft within a size class or type. To test this further, a regression was created which is only a function of NPD distance and power, flight velocity, and flap deflection angle.



Source	LogWorth	PValue	
DIST	3064.949	0.00000	
THR_SET	1499.164	0.00000	
DIST*DIST	1392.840	0.00000	
FV	1089.407	0.00000	
FV*THR_SET	617.420	0.00000	
THR_SET*DIST	122.204	0.00000	
FV*FV	77.109	0.00000	
FV*DIST	59.185	0.00000	
FDA*THR_SET	56.501	0.00000	
FDA*FV	41.922	0.00000	
OPRD	24.687	0.00000	
THR_SET*THR_SET	22.073	0.00000	
BPR*OPRD	21.702	0.00000	
FTCL*DIST	17.120	0.00000	
FV*OPRD	13.425	0.00000	
FDA	10.847	0.00000	^
BPR	2.671	0.00213	^
FTCL	1.094	0.08048	^
FV*BPR	0.479	0.33177	

Figure 37. Regression Function Variable Contributions

The resulting error in the prediction of the correction relative to the true SEL level is shown in Figure **38**. The error bars show the mean error along with upper and lower quantiles and upper and lower bounds. There is some scatter in the correction, but the prediction is generally within +/- 1 dB SEL. This is well within the predictive accuracy of ANOPP or the source noise models within AEDT. Furthermore, it is much smaller than the actual predicted difference between the NPD and NPD+C as shown in Figure **39**. The actual differences that result from including aircraft configuration range from +/- 5 dB SEL at the lower thrusts. This shows that a correction approach is possible and will be tested against operating data in future work.

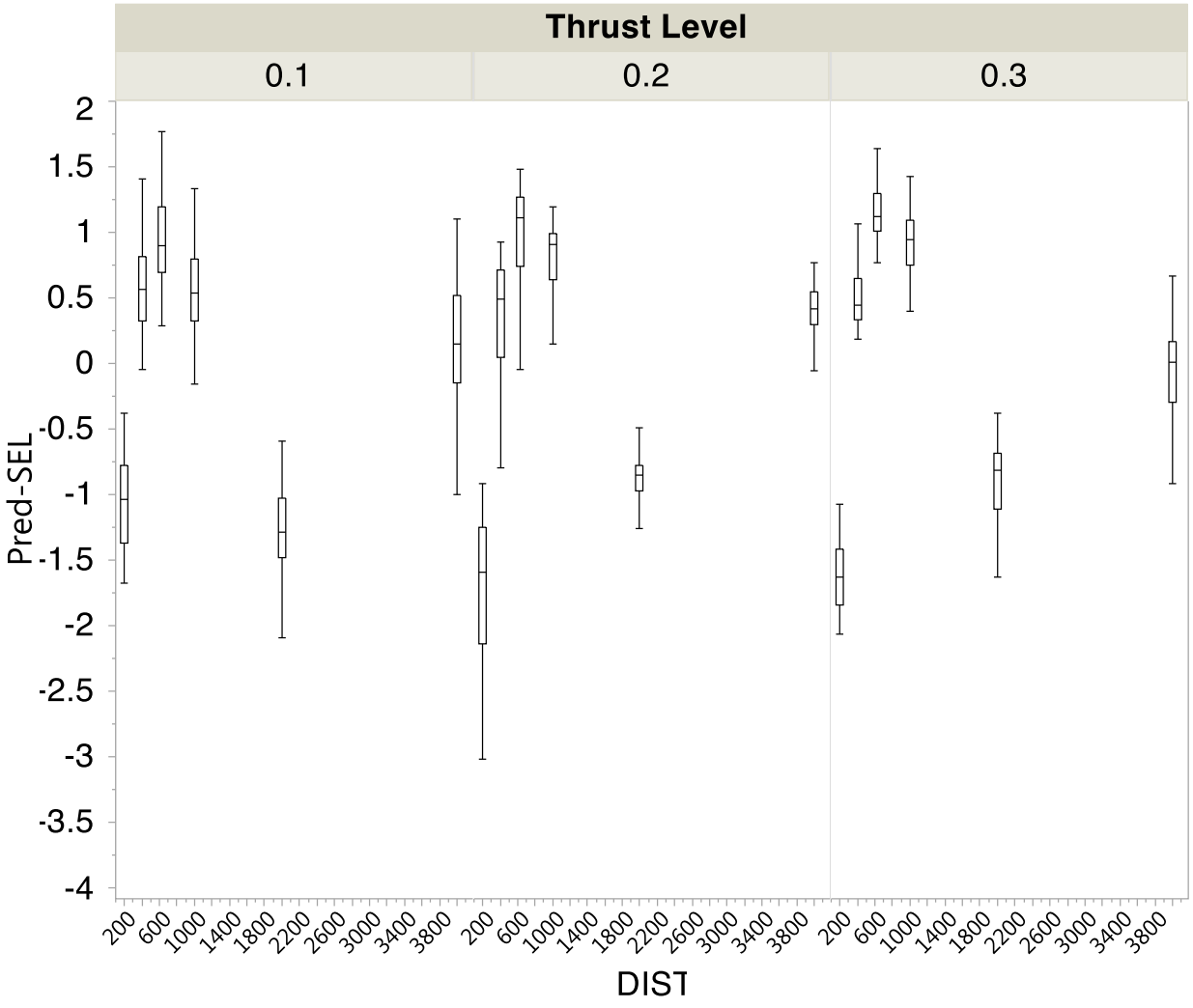


Figure 38. Error in SEL Prediction of Correction Function (150 pax)

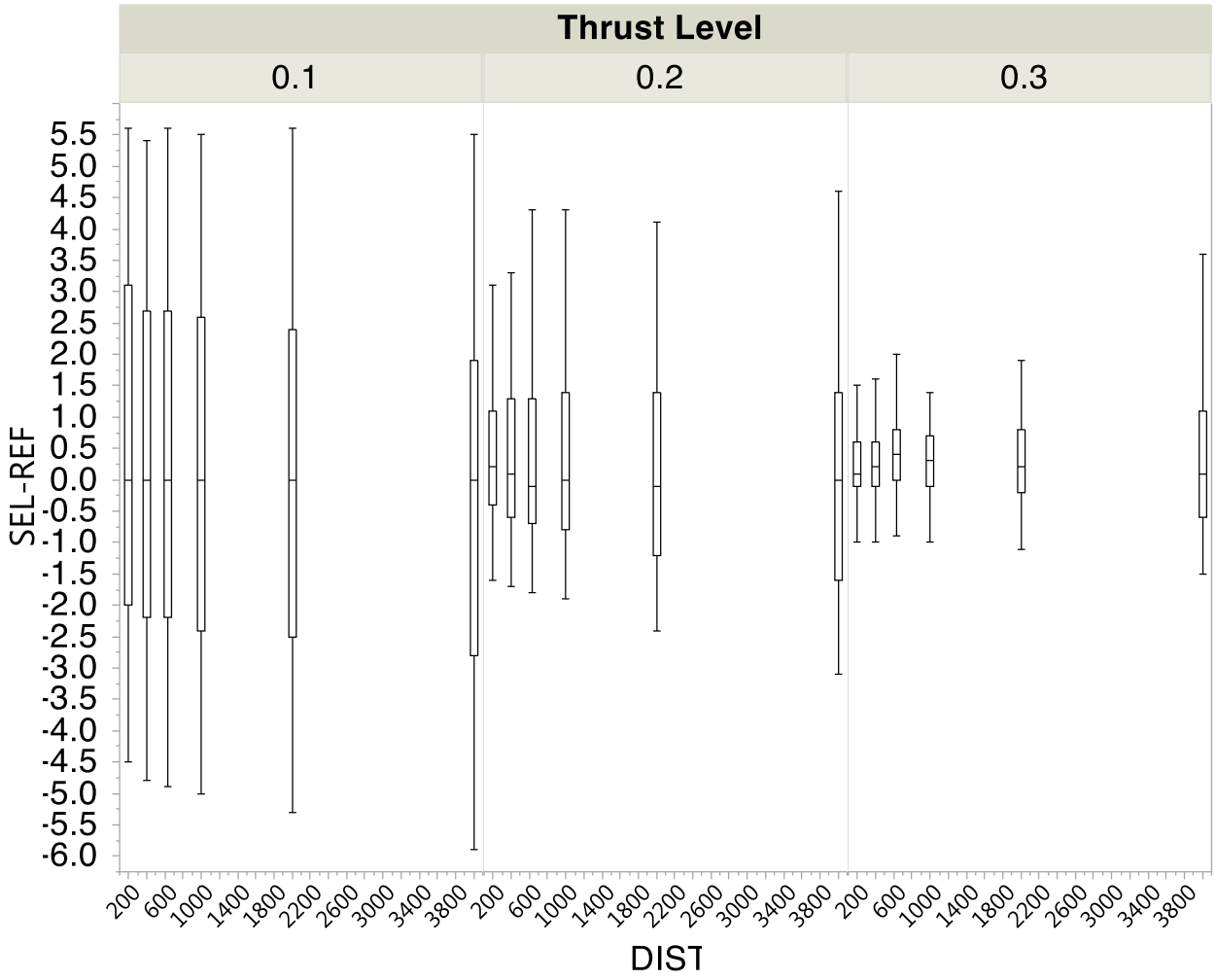


Figure 39. Difference Between NPD+C and NPD (150 pax)

Publications

A journal paper submitted to the AIAA Journal of Aircraft is expected from the research effort. Arturo Santa-Ruiz is the first author of the paper.

Outreach Efforts

Meetings with the ASCENT team were scheduled for subsequent work. Presentations at SAE A-21 meetings. FAA bi-weekly tools team presentations as appropriate.

Awards

None

Student Involvement

Kenneth Decker, Arturo Santa-Ruiz and Sara Huelsman were intimately involved in the day-to-day activities on this research. Kenneth worked on Task 1 in obtaining correct NPD+C input vehicles and developed appropriate plotting scripts. Arturo



developed and coded the AEDT NPD+C program and algorithm, included the segment-to-grid-point logic, performed Task 2 & Task 3, and analyzed results. Sara worked on the correction function and sensitivity studies in Task 4.

Plans for Next Period

Investigate Impact of Frequency Content on Standard NPD

AEDT currently uses a single set of spectral data which is assumed to be consistent with an observer directly underneath the flight path. The spectral data is used to correct noise attenuation as the atmosphere is shifted from a standard day. Incorrect spectral data can lead to gross over or underestimation of the community noise contour. As part of including more detailed aircraft configuration data in the NPD, the spectral data will change. This in turn leads to more fundamental questions about the accuracy of using a single set of spectral data for the entire NPD. To investigate the impact of these assumptions, Georgia Tech will use NASA's ANOPP noise prediction tool to generate a unique set of spectral data for each combination of thrust and distance for standard approach and departure NPD curves. Once generated, an XML format must be created so that this information can be used with a modified version of AEDT, developed in year 1 of this project. This modified AEDT version enables a unique NPD to be used for each flight segment (vs. a common NPD as is used now). Additional modifications to the source code will be made to input unique spectral information, generated by ANOPP, to be used in each AEDT flight segment.

Once modifications are made to AEDT, a sensitivity study will be performed to examine the impact of including unique spectral data for each thrust-distance combination. The 80 dB SEL contour will be examined for multiple aircraft sizes, including the regional jet, single aisle and twin aisle classes. The 80 dB SEL contour is examined first since it trends well with the resulting 65 DNL contour; however, complete grids will be generated which enable examination of any contour noise level. Other contour areas will be examined if further insight is required. This information will be used to inform the FAA of any possible prediction errors in the current AEDT approach.

Validate NPD+C Approach Using BANOERAC Data

Penn State has gained access to BANOERAC dataset. BANOERAC stands for "Background noise level and noise levels from en-route aircraft," and the data is owned by the European Aviation Safety Agency (EASA). It contains aircraft noise levels on the ground from a wide fleet-mix of aircraft, and recently the aircraft trajectory information was added through ASCENT Projects 5 and 40. Penn State will work to facilitate Georgia Tech gaining access to this dataset, to the extent possible, and to provide guidance on how that dataset works. Georgia Tech would then be able to use BANOERAC to assist in the validation of their ANOPP predictions for various aircraft. This will require Georgia Tech to use a full Environmental Design Space (EDS) model consisting of a complete engine and airframe definition using NPSS and NASA's FLOPS software. In addition, Penn State is planning to use ANOPP for a selected group of aircraft and to make comparisons between the Georgia Tech and Penn State predictions and the field measurements.

Validate NPD+C Approach Using Vancouver Airport (YVR) Data

Validation will also be attempted with data taken from Vancouver Airport (YVR). As is the case for Task 3, the dataset will be evaluated for usefulness and specific validation cases will be identified. Since this task involves an actual airport, instead of flyover data, AEDT will be used to model specific ground and sensor track paths using AEDT 3a. This task will consist of two validation steps. First, in order to assess the accuracy of the current AEDT 3a noise prediction, a baseline case will be established. Specific flights will be selected and compared to available measurement data during different weather conditions and at different locations relative to the runway. The objective will be to assess what drivers cause the largest sources of difference between the measurement locations and AEDT model predictions. Comparisons will be made for both SEL and LAmax metrics as these are the ones that fundamentally influence AEDT prediction of aircraft noise contour area.

The resulting trajectories will be used with ANOPP to generate NPD+C information which will be compared to the existing AEDT NPD predictions and the measurement data. For this task Georgia Tech will use the standard propagation models that exist within AEDT.

References

[1] U.S. FAA, "Aviation Environmental Design Tool (AEDT) Technical Manual Version 2c." DOT-VNTSC-FAA-16-11, 2016

[2] Aratani, Lori "D.C. residents suffer major setback in fight over plane noise from National Airport." The Washington Post, URL: https://www.washingtonpost.com/news/dr-gridlock/wp/2018/08/09/d-c-residents-suffer-major-setback-in-fight-over-plane-noise-from-national-airport [retrieved 12 August 2018]



[3] Federal Aviation Administration (FAA) "Aircraft Noise Issues." United States Department of Transportation, URL: https://www.faa.gov/about/office_org/headquarters_offices/apl/noise_emissions/airport_aircraft_noise_issues/ [retrieved 1 July 2018]
[4] U.S. DOT Volpe Center, FAA, ATAC Corp, CSSI, Inc, Metron Aviation, "Aviation Environmental Design Tool (AEDT) Technical Manual Version 2d," DOT-VNTSC-FAA-17-16, 2017
[5] John A. Volpe National Transportation Systems, "Integrated Noise Model (INM) Version 7.0 Technical Manual," FAA-AEE-08-01, 2008
[6] Raymer, Daniel P, *Aircraft Design: A Conceptual Approach,* 4th ed., AIAA Education Series, Reston, Virginia, 2006, pp. 197
[7] ANOPP, Aircraft NOise Prediction Program, Ver. 1.0, NASA, Langley, VA, 1998. Ref. LAR-16809-GS
[8] AEDT, Aircraft Environmental Design Tool, Ver. 2.c FAA, Washington, DC. 2016



Project 045 Takeoff/Climb Analysis to Support AEDT APM Development

Georgia Institute of Technology

Project Lead Investigator

Prof. Dimitri Mavris
Professor Dimitri N. Mavris
Director
Aerospace Systems Design Laboratory
School of Aerospace Engineering
Georgia Institute of Technology
Phone: (404) 894-1557
Fax: (404) 894-6596
Email: dimitri.mavris@ae.gatech.edu

Dr. Michelle R. Kirby, Co-PI
Chief, Civil Aviation Research Division
Aerospace Systems Design Laboratory
School of Aerospace Engineering
Georgia Institute of Technology
Phone: (404) 385-2780
Fax: (404) 894-6596
Email: michelle.kirby@ae.gatech.edu

University Participants

Georgia Institute of Technology (GT)

- P.I.(s): Prof. Dimitri Mavris, Dr. Michelle R. Kirby (Co-PI)
- FAA Award Number: 13-C-AJFE-GIT, Amendment 020 and 035
- Period of Performance: August 15, 2016 to December 31, 2018

Project Funding Level

FAA funded amount is $250,000 for the period of performance of August 15, 2016 to August 14, 2017. The Georgia Institute of Technology has agreed to a total of $250,000 in matching funds. Subsequently, the FAA funded amount is $75,000 for the period of performance of August 15, 2017 to August 14, 2018. The Georgia Institute of Technology has agreed to a total of $75,000 in matching funds. This total includes salaries for the project director, research engineers, graduate research assistants and computing, financial and administrative support. The institute has also agreed to provide equipment funds as well as tuition remission for the students paid for by state funds.

Investigation Team

Prof. Dimitri Mavris, Dr. Michelle Kirby, Dr. Don Lim, Dr. Yongchang Li, Dr. Holger Pfaender, Dr. Matthew Levine, and Mr. Jim Brooks. Graduate Students: Ameya Behere, Zhenyu Gao, Yee Chan Jin, Junghyun Kim.



Project Overview

Accurate modeling of aircraft performance is a key factor in estimating aircraft noise, emissions and fuel burn. Within the Aviation Environmental Design Tool (AEDT), many assumptions are made for aircraft performance modeling with respect to aircraft weight and departure procedure coupled with the fact that, typically the aircraft departure is modeled assuming full rated takeoff power/thrust is used. As operations around airports continue to evolve, there is a need to examine those assumptions and to improve the modeling accuracy with flight data. In recent years, flight data has been used more and more to enhance models and bring model estimation even closer to reality. Research is needed to build on prior work with a view to develop a robust set of recommendations for improved estimation processes for takeoff weight, reduced thrust takeoffs, and departure profiles within AEDT.

Task 1- Development of New Profile for Improving Weight and Thrust Modeling in APM

Georgia Institute of Technology

Objective(s)

In the previous year's P45 effort, Georgia Tech identified the AEDT assumptions in question, the validity of the physics behind the APM assumptions, and suggested improvements and the issues in data availability or modeling fidelity associated with the suggested improvements. Based on the literature review and analysis on the real world flight data, the research team found that AEDT underestimates the takeoff weight, and AEDT uses full thrust for takeoff while airlines use reduced takeoff thrust when it is possible. In addition, most airlines use NADP1 and NADP2 procedure instead of STANDARD, ICAO A or ICAO B procedures which are defined in AEDT. To improve AEDT's current APM assumptions, new profiles were developed for the major commercial and general aviation jets in AEDT. The new profiles contain reduced thrust, alternative weight, flap and speed schedule information.

New profiles for several aircraft were developed in order to help AEDT model real world aircraft operations. Before the implementation of this profile, most AEDT aircraft could only perform takeoffs using maximum climb thrust. Further, the weights which were assigned to the different stage lengths were significantly lower than what was observed from flight data. One of the reasons behind this was the assumption of a 65% load factor. In present times, average load factors of more than 80% are often observed. Due to the combination of these two factors, real world flight trajectories could not be modeled in AEDT. An additional factor is that aircraft use NADP profiles for takeoff rather than STANDARD or ICAO profiles. Currently, NADP profiles are not modeled in AEDT. This is an important area of improvement and will be the focus of attention for this project mobbing forward.

By the creation of these new profiles, users now have more options to choose when running environmental analyses. The implementation of reduced thrust and alternate weights will help users better match real world trajectories. This improvement in accuracy may help with future policy decisions by better informing the users of the real-world environmental effects of aviation.

Research Approach

The development of the new profiles involved multiple steps which are explained in this section. The new profiles were created as several Excel tables meant for importing in the AEDT Databases using SQL scripts. There were two aspects of modification of the existing profiles to create the new profiles – thrust and weight. It was decided that the STANDARD profile set be used as the baseline, this is because not all aircraft have ICAO A or ICAO B procedures defines, however, STANDARD departure profile is always present. Based on the STANDARD profiles, seven additional profiles with reduced thrust and alternative weight were created for all stage lengths for the batch of 90 aircraft.

Selection of aircraft

This section explains how the batch of 90 aircraft was selected for additional profile generation. First, the list of all aircraft was exported from the AEDT Database Table "FLT_ANP_AIRPLANES". The table was then filtered to include major commercial and general aviation jets with noise category 3 or 4. This process reduced the list to 92 aircraft. Of these, 2 had to be excluded as they contained point-based departure profiles and hence could not be used for alternate profile generation. Thus, the finalized batch of 90 aircraft was created.

Creation of modified weights and additional thrust types

It was previously found that AEDT tends to underestimate the takeoff weights assigned to the different stage lengths. These weights are defined in the SQL table "FLT_ANP_AIRPLANES_PROFILES". After a series of discussions among the AEDT development team and the FAA liaisons, it was decided that the weights should be increased for all stage lengths except for the maximum stage length. This increase would be in the form of updating the weights for a specific stage length to the average weight of the current stage length and the next stage length. This calculation is illustrated in Figure 1. The final stage length was excluded from modification as it was understood that it is typical for the aircraft maximum takeoff weight to be assigned to the final stage length.

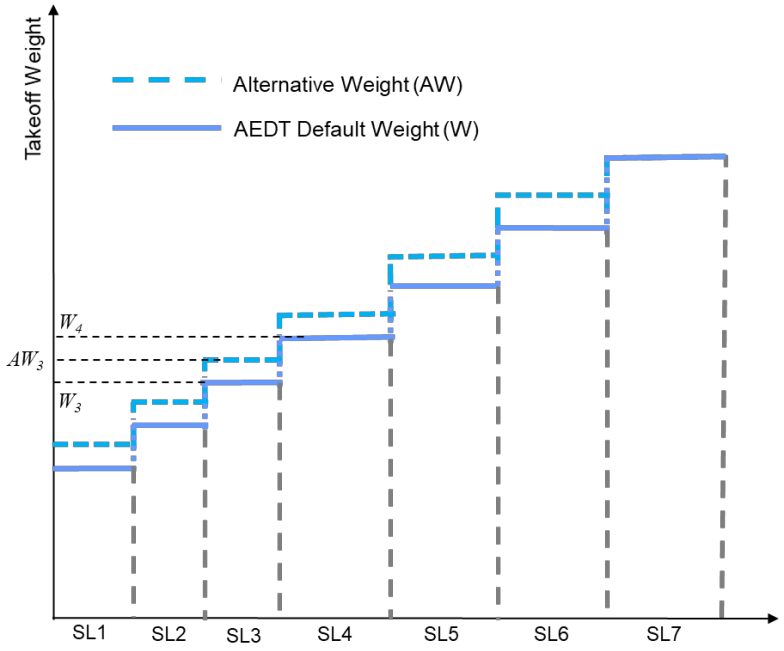


Figure 1. Calculation of alternate weights for profiles

The creation of additional thrust types was more involved. In AEDT, thrust is calculated with the help of thrust types such as "Takeoff" or "Climb". The thrust is calculated with the help of several thrust coefficients. Currently, AEDT uses the maximum available thrust for these two thrust modes. In order to implement reduced thrust departure procedures, new thrust types had to be defined and implemented in AEDT. Thrust types are defined in the SQL table "FLT_ANP_AIRPLANES_THRUST_JET". Takeoff thrust was implemented as either 5%, 10% or 15% reduction. Climb thrust reduction was implemented as a constant 10%, to be utilized only when the takeoff thrust reduction is 10% or more. Table 1 shows a typical thrust definition table for an aircraft. Note that not all aircraft have high temperature coefficients defined. It was decided that the high temperature coefficients not be derated as in a high temperature departure, it is unlikely that derated thrust will be used. This is illustrated in Figure 2. Note that although AEDT already had provisions for reduced climb and takeoff thrust, they were not implemented in AEDT itself, thus new derated thrust types had to be created.

Table 1. Description of new and existing AEDT thrust types

Existing AEDT Thrust Types	Description	New AEDT Thrust Types	Description	Based on
I	Idle	A	10% derated Max Climb (High Temp)	B
J	Idle (High Temp)	D	10% derated Max Climb	C
C	Max Climb	E	5 % derated Max Takeoff (High Temp)	S
B	Max Climb (High Temp)	F	5 % derated Max Takeoff	T
N	Max Continuous	W	10 % derated Max Takeoff (High Temp)	S
M	Max Continuous (High Temp)	X	10 % derated Max Takeoff	T
T	Max Takeoff	Y	15 % derated Max Takeoff (High Temp)	S
S	Max Takeoff (High Temp)	Z	15 % derated Max Takeoff	T
Q	Reduced Climb			
P	Reduced Climb (High Temp)			
H	Reduced Takeoff			
G	Reduced Takeoff (High Temp)			

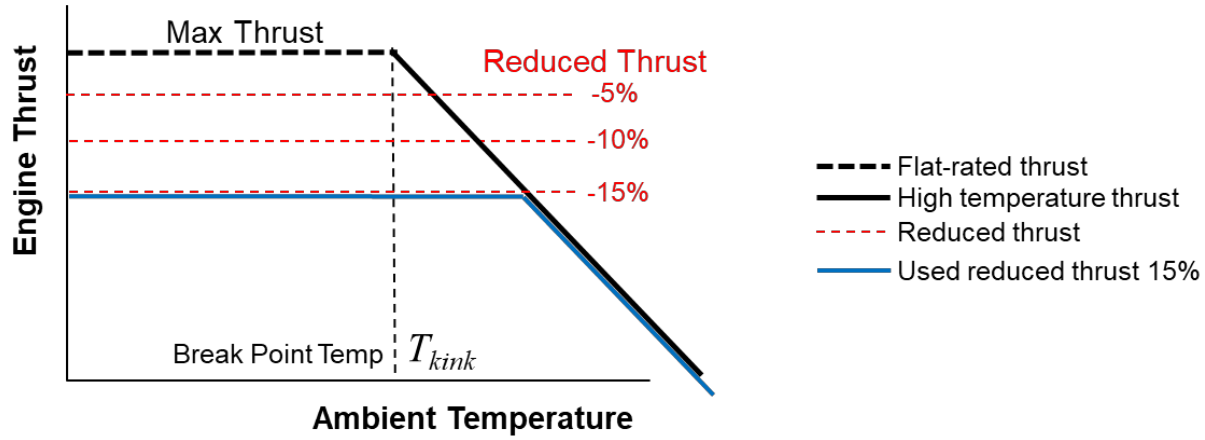


Figure 2. High temperature thrust calculations in AEDT

Creation of new profile and procedure tables

AEDT handles profiles through two separate SQL tables. The first is the "FLT_ANP_AIRPLANE_PROFILES" which contains information which is displayed in the AEDT GUI when a profile is to be selected. It contains the aircraft ID, operation type, profile name, stage length and weight information. For each of the batch of 90 aircraft, the new profiles were created for all stage lengths. Further, these new profiles were named as "MODIFIED_RT05", "MODIFIED_RT10", "MODIFIED_RT15", "MODIFIED_AW_RT05", "MODIFIED_AW_RT10", and "MODIFIED_AW_RT15". The weights were modified only for the profiles containing the "_AW" tag. Table 2 summarizes the type of changes made to each new profile set.



Table 2. Summary of new profile types

PROF_ID1	Weight	Takeoff Thrust Level	Climb Thrust Level	RoC/ES	Takeoff Thrust	Climb Thrust
STANDARD	Standard Weight	0% Reduction	0% Reduction	RoC	**T**	**C**
MODIFIED_RT05	Standard Weight	5% Reduction	0% Reduction	ES	**F** (new)	**C**
MODIFIED_RT10	Standard Weight	10% Reduction	10% Reduction	ES	**X** (new)	**D** (new)
MODIFIED_RT15	Standard Weight	15% Reduction	10% Reduction	ES	**Z** (new)	**D** (new)
MODIFIED_AW	Alternative Weight	0% Reduction	0% Reduction	ES	**T**	**C**
MODIFIED_AW_RT05	Alternative Weight	5% Reduction	0% Reduction	ES	**F** (new)	**C**
MODIFIED_AW_RT10	Alternative Weight	10% Reduction	10% Reduction	ES	**X** (new)	**D** (new)
MODIFIED_AW_RT15	Alternative Weight	15% Reduction	10% Reduction	ES	**Z** (new)	**D** (new)

The second table is the "FLT_ANP_AIRPLANE_PROCEDURES". This is the main table where all of the profile steps are defined. A typical AEDT procedural profile consists of a takeoff ground roll, initial climb, thrust cutback, acceleration and retraction of flaps and final climb to end of terminal area. The order and number of these steps vary from aircraft to aircraft but the general structure is the same. Each of these steps has a specific step type defined with it and based on this step type, AEDT uses extra information in the form of parameters. These parameters specify either climb rate, target speed or target altitude as appropriate.

The use of climb rate as one of the parameters posed a problem as it is strongly dependent on the aircraft weight. As we are also modeling additional weight profiles, it would not be accurate to use the baseline climb rates that were defined specifically for the existing AEDT weights. Fortunately, there is a simple solution to this as AEDT offers two types of accelerated climbs. The common type is to specify a climb rate and a target speed. AEDT will then calculate the required thrust for maintaining the climb and then allocate the remaining thrust to perform the horizontal speed acceleration. Alternatively, AEDT can also perform accelerated climbs using energy share percentage. In this, the procedure step specifies the percentage of energy which is to be allocated to climb and acceleration. AEDT will then calculate the climb rate using this information. A detailed explanation of this is provided in subsequent sections. Many AEDT aircraft use the first type of accelerated climb, a notable exception is the Boeing 787-800 which uses an energy share percent climb with a value of 55% and 50% for the final step. The climb rates for a given energy share percent are highly dependent on the instantaneous weight of the aircraft and the thrust level. It is difficult to estimate what this climb rate might be. However, when we look at this from the point of view of energy allocation, it turns out that the fraction of energy allotted to climb is roughly the same regardless of the aircraft weight and thrust level. Hence, this energy share approach proves to be very useful when creating the new profiles.

Defining the new procedural steps for the sets of 7 new profiles involved changing the accelerated climb step types, allotting the energy share percentage and assigning the appropriate thrust type. High temperature thrust coefficients never appear in these tables as they are not used explicitly. AEDT is designed to invoke the high temperature thrust coefficients as necessary. Further, the flap setting for each step was retained, no changes were made to the flap retraction schedule or to the flap setting used for takeoff.

Development and Validation of Energy Share

As mentioned in the previous section, the RoC of the STANDARD profile is not correct and cannot be used for the new profile any more when the takeoff weight and thrust change. This section will discuss how the new energy share (ES) based profiles are built to and validated for the RoC-based profiles. The new profiles are first built using the energy share method, and then tested and validated to make sure that they work properly and accurately. During this process, the energy share values are calculated analytically using potential energy and kinetic energy, given by the equation:

$$ES\,\% = \frac{\Delta KE}{\Delta KE + \Delta PE}$$

where the change in kinetic energy ΔKE is determined via aircraft speed and weight from performance calculating model, and the change in potential energy ΔPE is determined from the altitude and weight information. During the aircraft takeoff process, different energy share values are associated with different stage lengths. For example, an energy share value of 100% is used during ground roll in order to add kinetic energy; an energy share value of close to 0% happens during the constant speed takeoff when most of the excess power is used to add potential energy. In other climb stages, a typical energy share value varies from 40% to 70%. The energy share values for all 90 aircraft and all stage lengths were calculated and implemented in the new profiles.

After the initial calculations of the energy share values were finished, a validation analysis was conducted to test the validity of the ES-based profiles. The flowchart of the complete validation process is shown in Figure 3. The test was conducted for all stage lengths of 90 aircraft (409 cases total). As shown in Figure 3, first, the FLEET DB in SQL database is used to generate .xml files for all 90 aircraft, for RoC-based group and ES-based group, respectively. Then the AEDT tester, a tester that mimics the way aircraft are flown in AEDT, was run to generate performance and noise reports for all test cases. Then, a post-processing process was conducted to compare the flight trajectory and noise results between RoC- and ES-based profiles for each test pair to validate the new ES-based profiles.

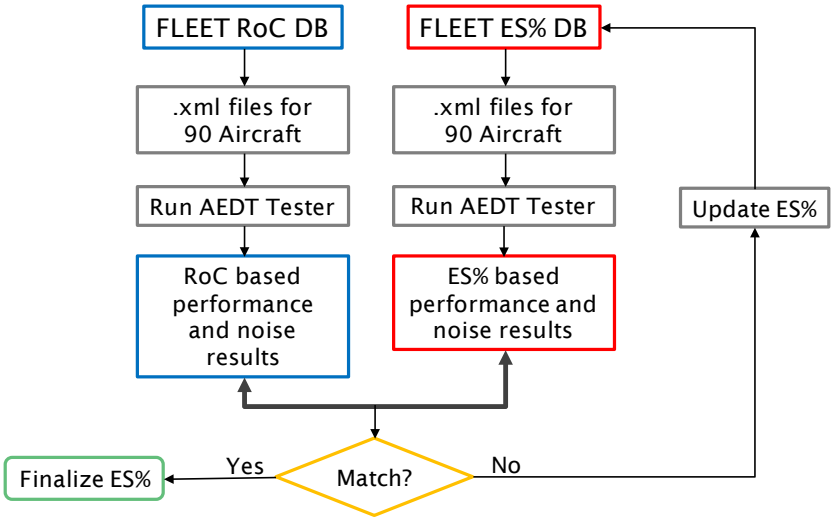


Figure 3. Energy Share DB Validation Process

Three different comparisons were considered in this process: flight trajectory, noise contour, and noise difference between ES- and RoC-based profiles. Examples of the three types of comparisons are shown in Figure 4-Figure 6. An excellent flight trajectory match is shown at the left of Figure 4. In this plot, for a given aircraft, flight trajectories of different stage lengths generated from the RoC and ES-based profiles are almost identical, with only minor differences. In a poor flight trajectory match shown at the right of Figure 4, large discrepancies exist between the two groups of flight trajectories. Similar to the flight trajectory comparison, the noise contour comparison provides another analytical way to validate the ES values for a profile. In an excellent noise contour match shown at the left of Figure 5, two groups of the noise contours show a high degree of agreement. A poor noise contour match shown at the right of Figure 5 indicates that the corresponding ES values are not accurate enough. The last comparison method utilizes the percentage differences in the magnitude of noise at all measurement points. An example of an excellent match is at the left of Figure 6 where the noise differences across all points are within the range of $\pm 0.06\%$. While in a poor noise difference match, the percentage difference at some points can go to as high as 6.5%. By examining the comparison plots for all 90 aircraft and all stage lengths, one can find out cases where the ES calculations are far from the target. For those ES values which don't provide a good agreement with the corresponding

RoC-based profile, such as the ones shown at the right of Figure 4-Figure 6, it is necessary to go back and modify the ES values until a good agreement between the RoC- and ES-based profiles is reached.

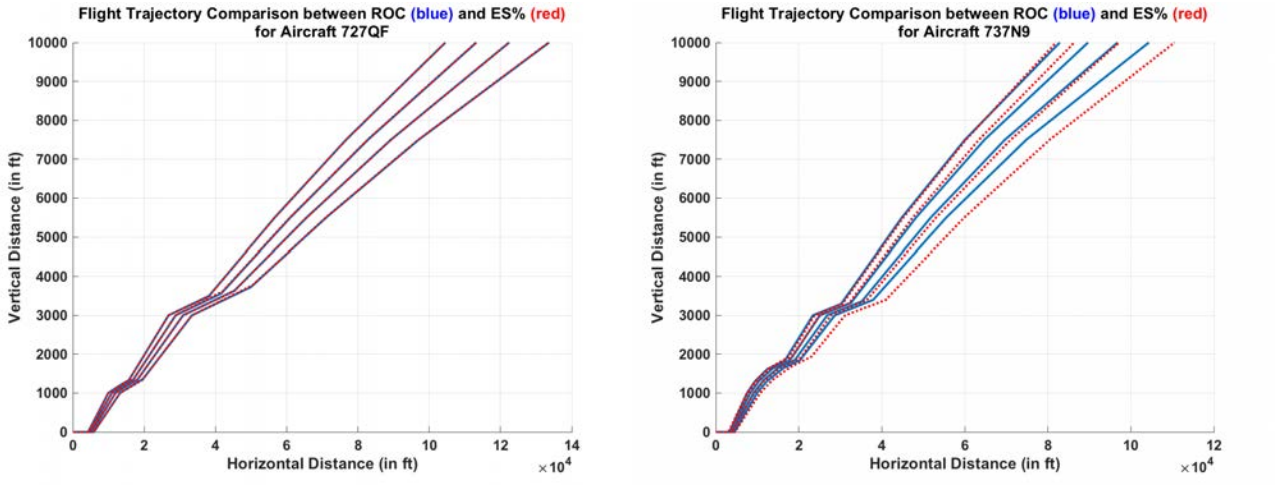


Figure 4. Example of Flight Trajectory Comparison: Excellent (Left) and Poor (Right) Matches

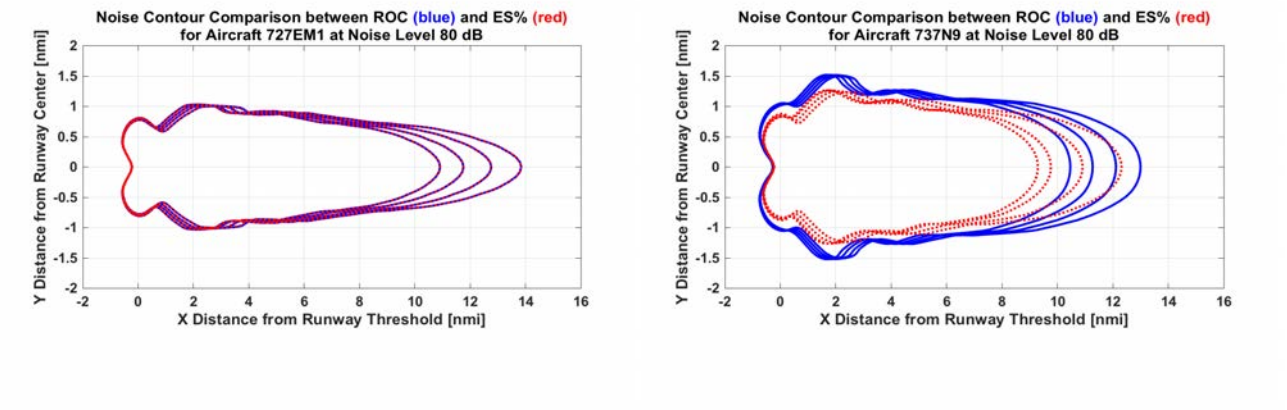


Figure 5. Example of Noise Contour Comparison: Excellent (Left) and Poor (Right) Matches

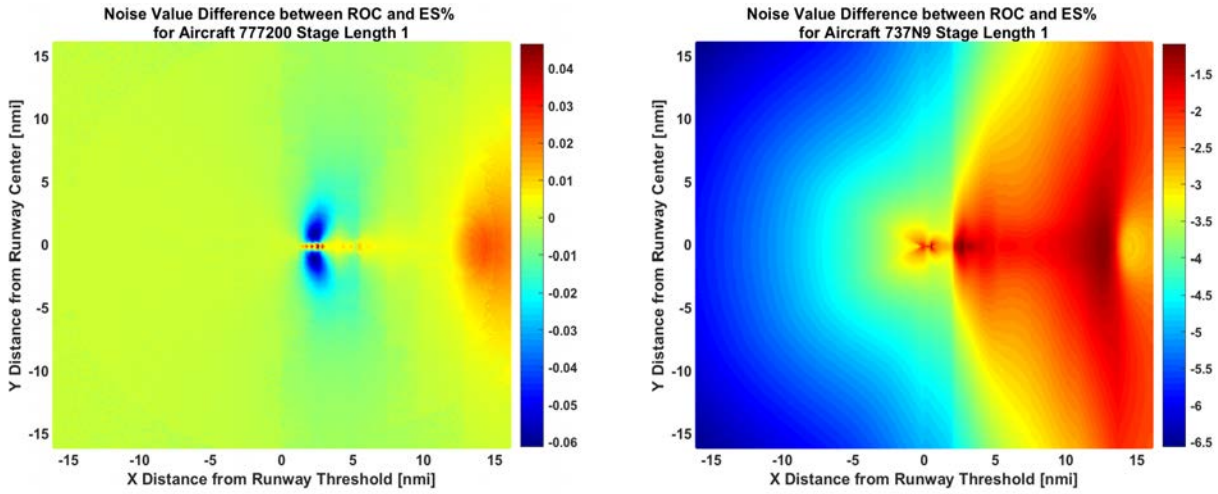


Figure 6. Example of Noise Difference Comparison: Excellent (Left) and Poor (Right) Matches

It was found out that between flight trajectory and noise plots, the flight trajectory comparison is a more rigorous criterion. That being said, if the flight trajectories between RoC- and ES-based profiles for a test case show excellent agreement, similar agreement can also be found in the relevant noise comparisons. However, an excellent agreement in the noise plots does not necessarily mean that the same agreement will also happen in the flight trajectory comparison. Based on this observation, the flight trajectory comparison results became the main reference in this validation process.

After the flight trajectory comparison was chosen as the main reference, a metric was developed to quantitatively assess the validity of an ES-based profile: the maximum trajectory difference in percentage (Max Diff %). At each trajectory segment, the altitudes of both the RoC and ES-based trajectories are obtained as y_{RoC} and y_{ES}, and the trajectory difference at the point is given by:

$$\text{Diff \%} = \frac{|y_{RoC} - y_{ES}|}{y_{RoC}} \times 100\%$$

The quantitative criterion for an excellent match is that, when the maximum of trajectory differences (Max Diff %) during the entire trajectory is less than 5%, the ES values for the corresponding case are deemed to be "good enough". When the Max Diff % for a case is greater than 5%, a process consisting of three step is taken to modify the ES values until satisfactory:

Step 1: Visually identify the takeoff segments in which the deviation in trajectories happens

Step 2: Identify the direction to modify ES values:

If the ES-based trajectory is below the RoC-based one: corresponding ES value is too large and should be reduced

If the ES-based trajectory is above the RoC-based one: corresponding ES value is too small and should be increased

Use the increment of modification to be plus or minus 5%, and reduce the increment if needed

If the ES value is not the reason behind a trajectory mismatch, look for other possible reasons

Step 3: Modify the ES values until the Max Diff % of the case is smaller than 5%.

The energy share development and validation process concluded when a trajectory Max Diff % of less than 5% is achieved for all the 409 STANDARD profiles. A histogram of the final Max Diff % results by aircraft and stage length can be found in Figure 7. Across the 409 STANDARD profiles, the set of final trajectory Max Diff % values has a mean of 1.40% and standard deviation



of 1.04%, indicating that the final ES values are accurate enough. After the final ES values are finalized, they are used to replace the RoC-based profiles in future studies.

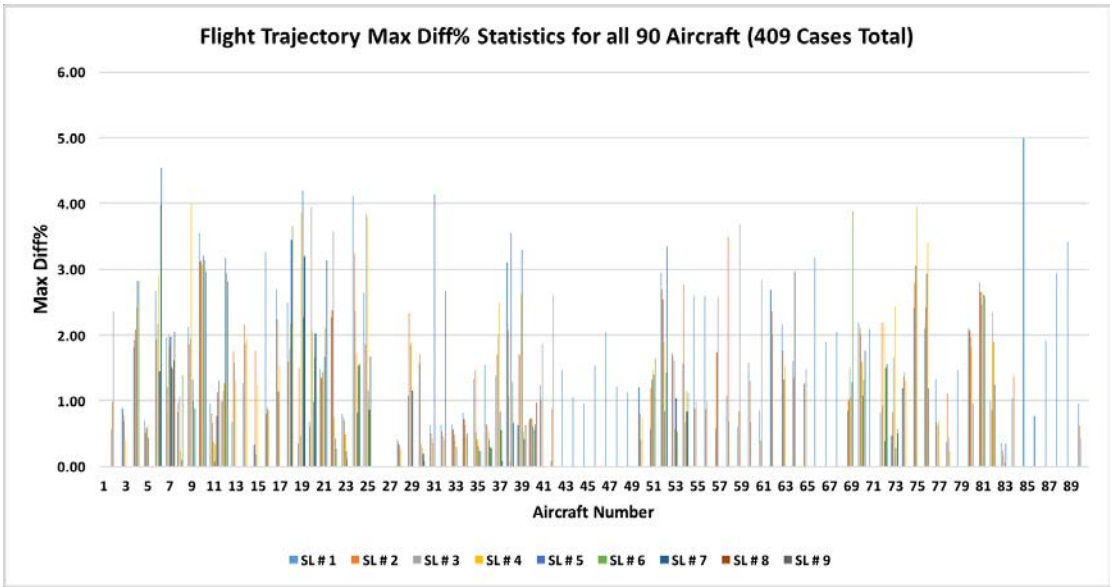


Figure 7. Final ES Validation Results: Statistics for the Max Diff %

Task 2- V&V Studies for Reduced Weight and Alternative Weight Profiles

Georgia Institute of Technology

Objective(s)

This task focused on V&V the newly developed profiles to verify if they are working properly for different aircraft at different stage length, airport, weather profiles, and conducted sensitivity analysis to compare the fuel burn, emission, and noise results of the new profiles to see how the reduced thrust and alternative weight impact the results. In addition, further analysis was performed to investigate the main drivers to the noise results.

Research Approach

V&V Study for Reduced Thrust Profiles

The reduced thrust and alternative weight profiles were developed to simulate real world operations practiced by airlines, and can more accurately model the takeoff operations. A comprehensive study is also conducted to analyze the performance, fuel burn, emissions and noise impacts of these new profiles. The study started with a full factorial experiment for selected airport and weather conditions within the ANP database, and the test matrix is listed below:

Test Matrix

- AEDT version: Sprint 106
- Aircraft: all 90 aircraft
- Airport: one airport, KIAH
- Runway: east-west for departure
- Weather Profile: sea level standard (temperature 59F, pressure 1013.25mb)



- Profiles: 1 STANDARD + 7 MODIFIED
- Stage Length: all stage lengths, ranging from 1-9 for different aircraft

The AEDT study was created by running a series of SQL scripts, and consisting a total number of 3,562 cases. The study was run with AEDT and the performance and noise reports generated were then extracted and analyzed through a large scale post-processing process. Through the study, the research team is interested in how the new profiles impact the performance, emissions and noise metrics:

- Performance: fuel burn
- Emissions: CO, NOx
- Noise: noise contour area, length, and width at different noise levels

When the experiment was finished, all the 3,562 cases were successfully run without any failure case. After that, all the performance and noise reports were further processed and analyzed by an integrated analysis code in MATLAB. The comparison results for the above metrics of interest across different profiles were summarized in two large tables, and visualized through box plots. In the following sections, performance, emissions and noise results will be summarized separately.

Performance and Emissions Results

As stated above, when comparing the aircraft takeoff performance and emissions across different profiles, the team is interested in three performance metrics: fuel burn, NOx emissions, and CO emissions. For each of the 90 aircraft, these metrics are calculated and compared across the 8 profiles for all the stage lengths. Table 3 shows an example of the performance metrics comparison across different profiles for aircraft 737-00 only. In this example table, the three metrics can be compared across new profiles against STANDARD profile, as well as different stage lengths.

With this table, several trends can be observed for a typical aircraft like the Boeing 737700. First, with more thrust reduction, all the three metrics display a monotonically increasing or decreasing pattern. Among the three of them, fuel burn and CO emission, in general, increase with more reduced thrust, compared to NOx emission which decreases with more reduced thrust. The increase in fuel burn is expected because the takeoff process is defined as the aircraft operation from the ground until the altitude of 10,000 ft AFE. With more reduced thrust, the aircraft has a shallower climbing slope, leading to a longer flight path and greater fuel consumption. This trend is also shown in Figure 8 with trajectory comparisons for the same aircraft with different profiles. In the meantime, with more reduced thrust, the CO emission also increases, but the differences are very slight compared to the fuel burn. The largest CO change in this case is 0.5%, which is one order of magnitude less than the fuel burn change. The NOx emission, however, decreases with more reduced thrust for aircraft 737700. This is because that when the thrust is reduced, the emission index of NOx is reduced which lead to the reduction in NOx. The second overall observation is that, the trends for different reduced thrust profiles are the same within each weight group (with or without 'AW'). The alternative weight group (AW) in general has larger positive changes in the three metrics compared to the Non-AW group. Lastly, the trends across different stage lengths are the same, with differences only in the magnitude of percentage changes.

Table 3. Example of the Performance Metrics Comparison

Profile	SL 1	Fuel Burn	Difference %	CO	Difference %	NOx	Difference %	SL 4	Fuel Burn	Difference %	CO	Difference %	NOx	Difference %
STANDARD		687.25	0	6463	0	10915	0		769.26	0	6506	0	12890	0
MODIFIED_RT05		687.65	0.06	6463	0	10792	-1.13		769.87	0.08	6506	0	12742	-1.15
MODIFIED_RT10		698.38	1.62	6469	0.09	10071	-7.73		784.83	2.02	6514	0.13	11922	-7.51
MODIFIED_RT15		698.8	1.68	6469	0.1	9929	-9.03		785.7	2.14	6515	0.14	11757	-8.79
MODIFIED_AW		697.7	1.52	6468	0.09	11165	2.29		798.63	3.82	6521	0.24	13593	5.45
MODIFIED_AW_RT05		697.94	1.56	6468	0.09	11035	1.1		799.25	3.9	6522	0.24	13435	4.21
MODIFIED_AW_RT10		709.29	3.21	6475	0.18	10303	-5.61		816.3	6.11	6531	0.38	12592	-2.31
MODIFIED_AW_RT15		709.75	3.27	6475	0.19	10158	-6.94		817.33	6.25	6532	0.4	12419	-3.65
Profile	SL 2	Fuel Burn	Difference %	CO	Difference %	NOx	Difference %	SL 5	Fuel Burn	Difference %	CO	Difference %	NOx	Difference %
STANDARD		707.3	0	6473	0	11397	0		826.95	0	6536	0	14276	0
MODIFIED_RT05		707.78	0.07	6474	0	11269	-1.12		827.83	0.11	6537	0.01	14112	-1.15
MODIFIED_RT10		719.78	1.76	6480	0.1	10528	-7.62		847.14	2.44	6547	0.17	13252	-7.17
MODIFIED_RT15		720.29	1.84	6481	0.11	10381	-8.91		848.36	2.59	6548	0.18	13071	-8.44
MODIFIED_AW		718.62	1.6	6479	0.09	11667	2.37		827.31	0.04	6537	0	14283	0.05
MODIFIED_AW_RT05		718.93	1.64	6480	0.1	11532	1.18		828.06	0.13	6537	0.01	14118	-1.11
MODIFIED_AW_RT10		731.65	3.44	6486	0.2	10781	-5.4		847.39	2.47	6547	0.17	13258	-7.13
MODIFIED_AW_RT15		732.21	3.52	6487	0.21	10630	-6.73		848.61	2.62	6548	0.18	13077	-8.4
Profile	SL 3	Fuel Burn	Difference %	CO	Difference %	NOx	Difference %	SL 6	Fuel Burn	Difference %	CO	Difference %	NOx	Difference %
STANDARD		728.88	0	6485	0	11916	0		827.41	0	6537	0	14287	0
MODIFIED_RT05		729.32	0.06	6485	0	11780	-1.14		828.29	0.11	6537	0.01	14123	-1.15
MODIFIED_RT10		742.23	1.83	6492	0.11	11009	-7.61		847.63	2.44	6547	0.17	13263	-7.17
MODIFIED_RT15		742.85	1.92	6492	0.12	10855	-8.9		848.86	2.59	6548	0.18	13082	-8.43
MODIFIED_AW		752.17	3.2	6497	0.19	12473	4.67		827.54	0.02	6537	0	14289	0.01
MODIFIED_AW_RT05		752.59	3.25	6497	0.19	12329	3.47		828.29	0.11	6537	0.01	14123	-1.15
MODIFIED_AW_RT10		767.06	5.24	6505	0.31	11537	-3.18		847.63	2.44	6547	0.17	13263	-7.17
MODIFIED_AW_RT15		767.79	5.34	6506	0.32	11377	-4.52		848.86	2.59	6548	0.18	13082	-8.43

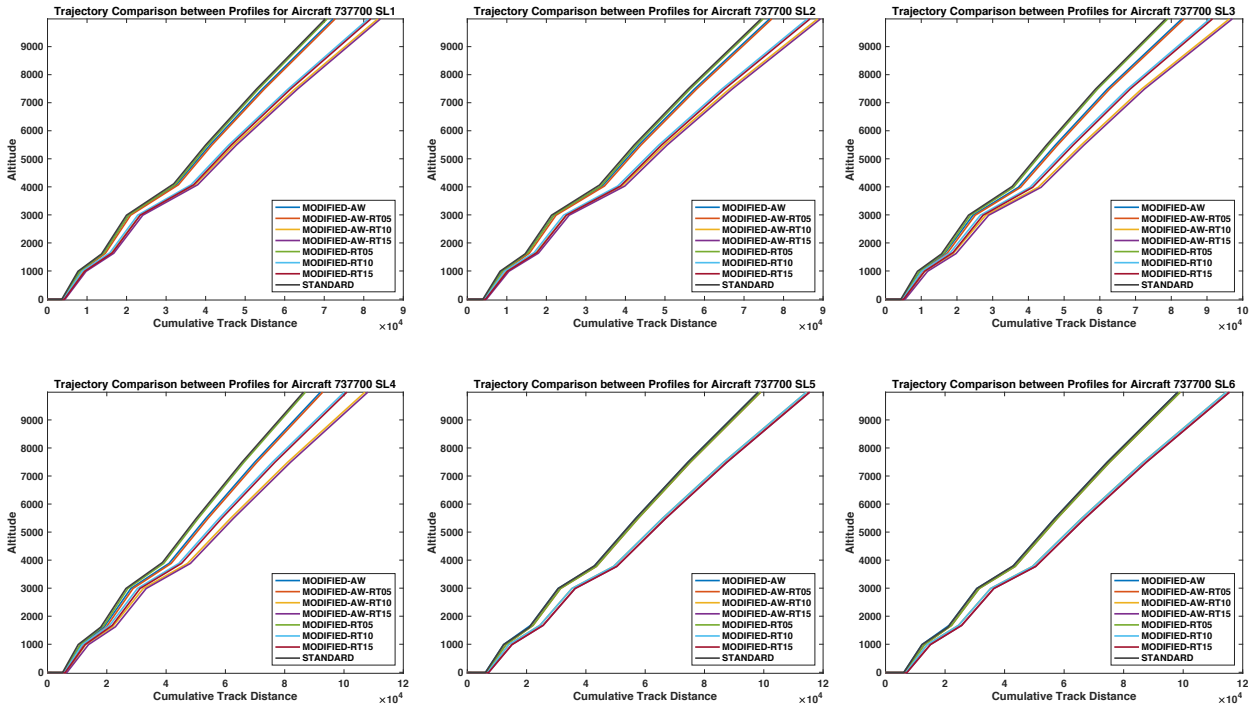
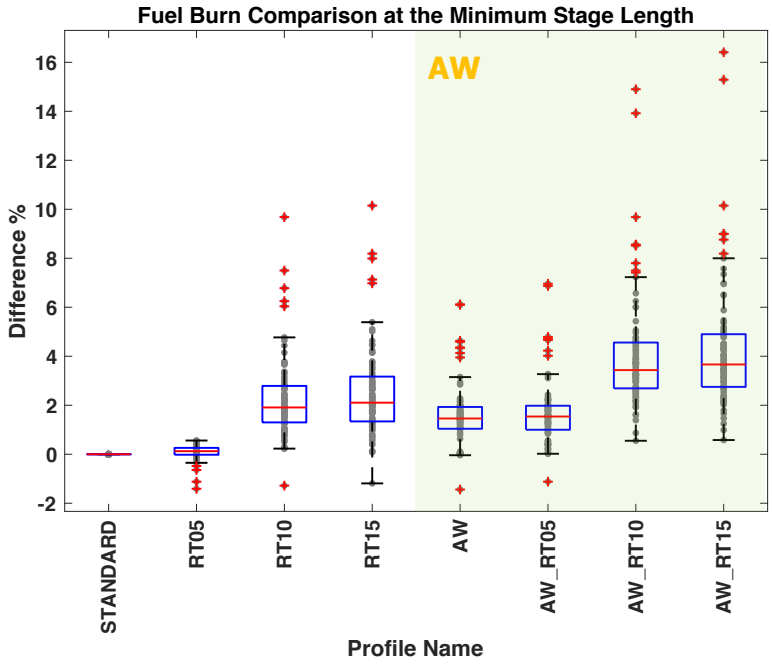


Figure 8. Trajectory Comparison for Different Profiles

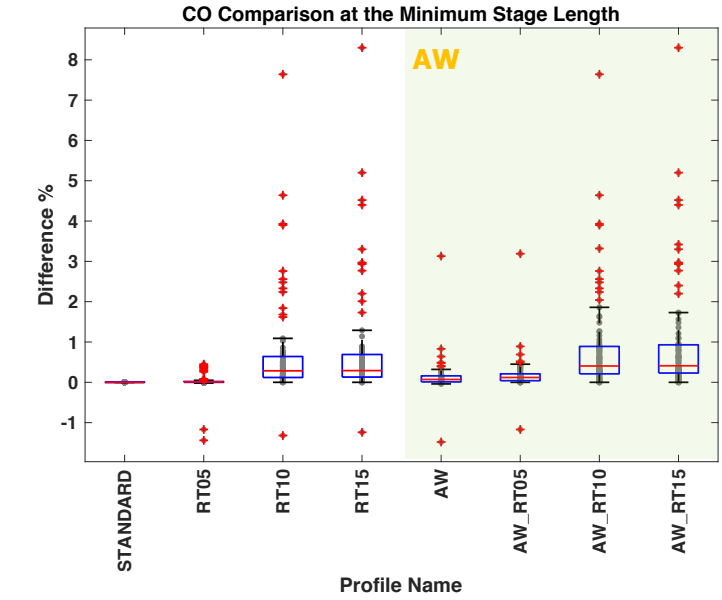
In addition to the comparison at aircraft level, the research team is also interested in investigating the pattern among the 8 profiles for all 90 aircraft at system level. Since different aircraft have different numbers of stage length ranging from 1 to 9, and considering the fact that some aircraft only have 1 stage length, only the minimum stage length is used in this comparison. The comparison results for fuel burn, NOx emission and CO emission are presented by box plots as shown in Figure 9 - Figure 11. Each box plot contains two different groups: with alternative weight (AW, in the right half), and without alternative weight (non-AW, in the left half). Within each group, results of the four different thrust levels (-0%, -5%, -10%, -15%) are displayed from left to right. Several descriptive statistics can be identified from the box plot, including the median (red horizontal line), first and third quartile (boundaries of the blue box), max and min (two ends of the whisker), and outliers (red dots). The mean values of the profiles are also shown below the box plot.



Median:	0	0.125	1.9100	2.105	1.460	1.540	3.435	3.665

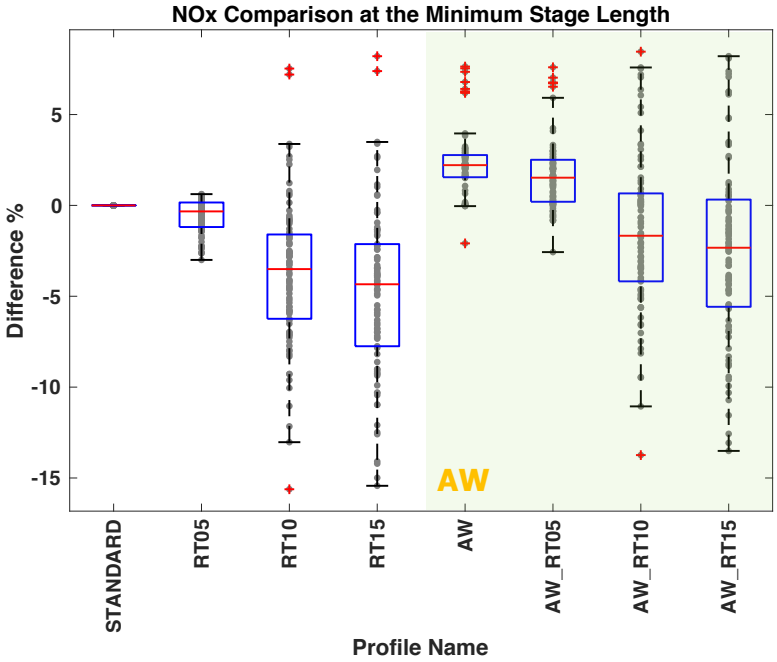
Figure 9. All 90 Aircraft Performance Comparison: Fuel Burn

Figure 9 shows the fuel burn comparison for the 8 profiles of all 90 aircraft. It can be observed that the overall trend is similar to the analysis of Boeing 737700, in which takeoff fuel burn generally increases with more reduced thrust. In the meantime, with the implementation of alternative weight (AW), each reduced thrust profile has a higher fuel burn value (approximately 1.5% higher) compared to its counterpart in the non-AW group. This general trend is exactly what was expected and can be used to further validate the effectiveness of the new reduced thrust and alternative weight profiles. Figure 10 shows the CO emission comparison for all 90 aircraft. Compared to the fuel burn results, now the CO emission results are in general less affected by the reduced thrust (the magnitude of the mean percentage changes are less than 1%), and have more outliers. Yet still, the results show that CO emission also increases with more reduced thrust, and is further increased by around 0.1% when alternative weight is added. Figure 11 shows the NOx emission comparison for all 90 aircraft. When compared to fuel burn and CO emission results, the NOx emission results have the fewest outliers and show a clear opposite trend: NOx emission generally decreases with more reduced thrust. One thing worth mentioning here is that for a number of aircraft, the NOx emission in fact increase with more reduced thrust, as shown by the left part of Figure 11. This is due to different characteristics of different aircraft and engines in which the increased fuel consumption is dominated the NOx calculation even though the EI of NOx is reduced.



Median: 0 0.010 0.285 0.290 0.070 0.120 0.405 0.410

Figure 10. All 90 Aircraft Performance Comparison: CO Emission



Median: 0 -0.330 -3.505 -4.340 2.215 1.525 -1.670 -2.330

Figure 11. All 90 Aircraft Performance Comparison: NOx Emission

Although individual differences can be significant among the 90 aircraft, the general trends of fuel burn, CO emission, and NOx emission changes for the new profiles are clear and interpretable. Below the general observations for the three metrics are summarized:

1. With more reduced thrust, the fuel burn increases
2. With more reduced thrust, the CO emission increases
3. With more reduced thrust, the NOx emission decreases
4. With the alternative weight, all of fuel burn, CO emission and NOx emission are increased by a certain level
5. Magnitude of change: NOx emission > Fuel burn > CO emission

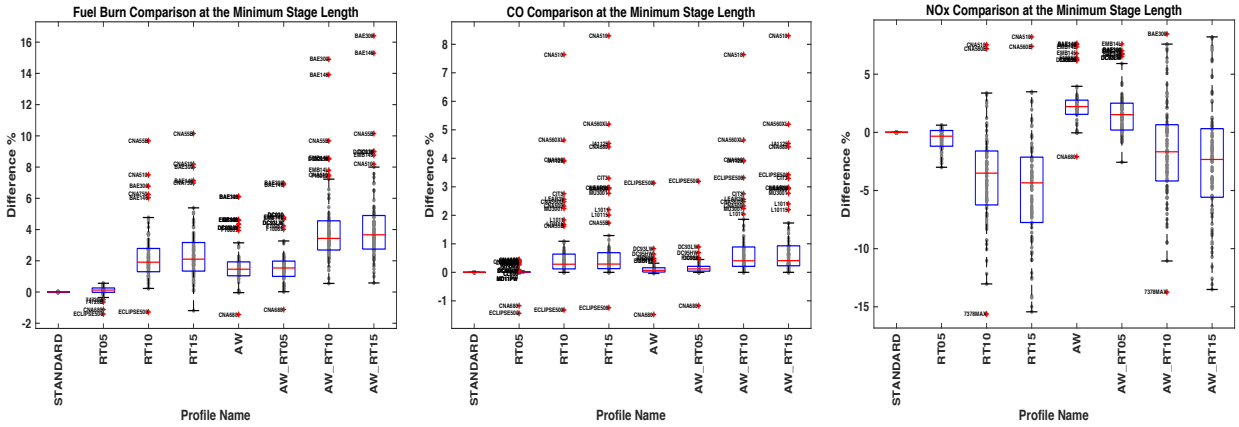


Figure 12. Outlier Identification for Performance Metrics Comparison

From the box plots shown in Figure 9 - Figure 11, there are outliers whose value are far from the median. It is necessary to identify all those outliers and see if further investigation or validation for some specific aircraft is needed. Figure 12 shows the identification of all the outliers directly from the box plots. Most of the outlier aircraft are repetitive in the three comparisons: CNA510, CNA560 series, CNA55B, BAE146, BAE300, ECLIPSE500, CNA680, DC930, DC93LW, L1011, L10115, F10062, F10065. Note that this short list of 13 aircraft contains no frequently-used aircraft in today's operation. Therefore, no further investigation is necessary to find out the reasons behind these outliers.

Nevertheless, when it comes to the NOx emission result, it was observed from the box plots and the outlier identification that the Boeing 737 Max 8 (737MAX8) aircraft is an outlier for the reduced thrust profiles. The difference compared to STANDARD profile was up to -15 % for the RT10 and AW_RT10 profiles. This large difference reduced slightly with increasing stage lengths but stood out consistently. To investigate this further, the performance and emissions data tables from AEDT were analyzed. It was observed that the percent difference in NOx was exactly the same as the percent difference in Fuel Burn, up to the "Terminal Climb" trajectory mode. To pinpoint the exact source of deviation, various plots were created to visualize the trajectory, cumulative NOx emissions, fuel flow rate, and segment fuel burn among many others. After detailed inspection, it was deemed necessary to replicate AEDT's NOx calculations independently. AEDT uses the Boeing Fuel Flow Method 2 for NOx calculations and the method is explained in detail in the Technical Manual. The investigation is done and it was found out that NOx EI for this aircraft was highly reduced for the profiles with reduced climb thrust which lead to big reduction in NOx results. This is an aircraft specific phenomenon which is not normal for other aircraft and engine.

Noise Results

Noise metrics are another major category to investigate with the results from the large scale experiment. A similar comparison was also conducted with the noise reports for all the 3,562 cases. The team identified 9 noise metrics of interest to calculate and analyze: 70 dB Noise Contour Area, 70 dB Noise Contour Length, 70 dB Noise Contour Width, 80 dB Noise Contour Area, 80 dB Noise Contour Length, 80 dB Noise Contour Width, 90 dB Noise Contour Area, 90 dB Noise Contour Length, and 90 dB Noise Contour Width. Figure 13 contains an example of the noise contour plots for aircraft 737700 stage

length 1, with the definitions of the noise contour area, length, and width. For each of the 90 aircraft, the 9 noise metrics are then calculated and compared across the 8 profiles for all the stage lengths. Table 4 shows an example of the noise metrics comparison across different profiles, for aircraft 737700.

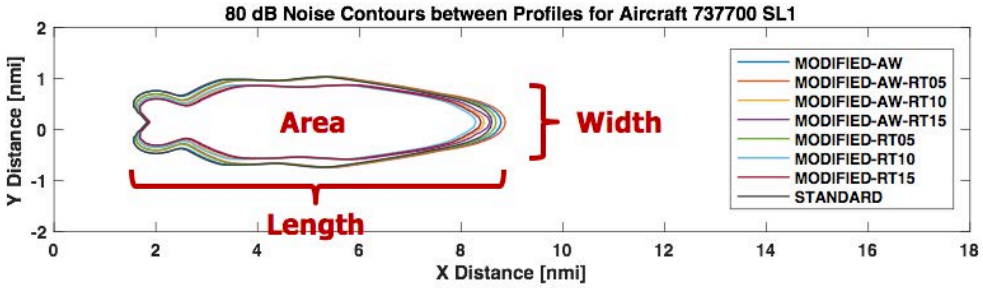


Figure 13. Example of the Noise Contour with Metrics Definition

Compared to the performance results, the noise results display more complex changing patterns. As can be seen from Table 4, among the changing patterns of contour area, length, and width at different noise levels, changes of contour area and width are consistent. When the thrust level is reduced from 0% to 15%, both the contour area and width monotonically decrease. It can also be observed that alternative weight (AW) profiles produce increased contour area by a certain amount compared to the non-AW profiles, but have almost no influence on the contour width. The changing pattern of contour length is relatively complicated and will be analyzed and discussed later.



Table 4. Example of the Noise Metrics Comparison

Profile	SL 1	Area - 70 dB	Difference %	Length - 70 dB	Difference %	Width - 70 dB	Difference %	Area - 80 dB	Difference %	Length - 80 dB	Difference %	Width - 80 dB	Difference %	Area - 90 dB	Difference %	Length - 90 dB	Difference %	Width - 90 dB	Difference %
STANDARD		44.841	0	12.928	0	3.9706	0	9.185	0	6.8526	0	1.7537	0	1.0903	0	2.4233	0	0.62981	0
MODIFIED_RT05		44.387	-1.01	12.92	-0.06	3.9654	-0.13	9.0282	-1.71	6.8867	0.5	1.7537	0	1.0397	-4.64	2.4751	2.14	0.57734	-8.33
MODIFIED_RT10		43.068	-3.95	14.144	9.41	3.5755	-9.95	7.3459	-20.02	6.438	-6.04	1.4569	-16.92	0.86341	-20.81	2.358	-2.69	0.50933	-19.13
MODIFIED_RT15		42.758	-4.65	14.17	9.61	3.5731	-10.01	7.3053	-20.46	6.5144	-4.94	1.4497	-17.33	0.8398	-22.98	2.4439	0.85	0.45745	-27.37
MODIFIED_AW		46.061	2.72	13.249	2.48	3.9759	0.13	9.3659	1.97	7.032	2.62	1.7577	0.23	1.1184	2.58	2.4849	2.54	0.62907	-0.12
MODIFIED_AW_RT05		45.532	1.54	13.242	2.43	3.9707	0	9.1926	0.08	7.0646	3.09	1.7557	0.11	1.0632	-2.49	2.5548	5.43	0.57191	-9.19
MODIFIED_AW_RT10		44.26	-1.3	14.519	12.31	3.5788	-9.87	7.5171	-18.16	6.6035	-3.64	1.4528	-17.16	0.88022	-19.27	2.4269	0.15	0.50226	-20.25
MODIFIED_AW_RT15		43.945	-2	14.549	12.54	3.5771	-9.91	7.4762	-18.6	6.6843	-2.42	1.4516	-17.23	0.85669	-21.43	2.516	3.83	0.45214	-28.21
Profile	SL 2	Area - 70 dB	Difference %	Length - 70 dB	Difference %	Width - 70 dB	Difference %	Area - 80 dB	Difference %	Length - 80 dB	Difference %	Width - 80 dB	Difference %	Area - 90 dB	Difference %	Length - 90 dB	Difference %	Width - 90 dB	Difference %
STANDARD		47.161	0	13.573	0	3.9522	0	9.5326	0	7.2086	0	1.7382	0	1.1369	0	2.556	0	0.61868	0
MODIFIED_RT05		46.647	-1.09	13.57	-0.02	3.9493	-0.07	9.3727	-1.68	7.2474	0.54	1.7382	0	1.0835	-4.7	2.6204	2.52	0.56719	-8.32
MODIFIED_RT10		45.434	-3.66	14.912	9.87	3.5603	-9.92	7.6732	-19.51	6.7919	-5.78	1.4435	-16.95	0.89768	-21.04	2.4923	-2.49	0.49945	-19.27
MODIFIED_RT15		45.114	-4.34	14.947	10.12	3.5578	-9.98	7.6317	-19.94	6.8751	-4.62	1.4346	-17.47	0.87451	-23.08	2.5872	1.22	0.44717	-27.72
MODIFIED_AW		48.493	2.82	13.924	2.59	3.9574	0.13	9.7775	2.57	7.4006	2.66	1.7422	0.23	1.1651	2.48	2.6202	2.51	0.61748	-0.19
MODIFIED_AW_RT05		47.936	1.64	13.922	2.57	3.9545	0.06	9.6067	0.78	7.4419	3.24	1.7418	0.21	1.1048	-2.82	2.6888	5.2	0.56122	-9.29
MODIFIED_AW_RT10		46.751	-0.87	15.33	12.94	3.5642	-9.82	7.8628	-17.52	6.9739	-3.25	1.4385	-17.24	0.91498	-19.52	2.5523	-0.14	0.49363	-20.21
MODIFIED_AW_RT15		46.428	-1.56	15.367	13.22	3.5603	-9.92	7.8177	-17.99	7.0593	-2.07	1.4352	-17.43	0.89107	-21.62	2.6571	3.96	0.44217	-28.53
Profile	SL 3	Area - 70 dB	Difference %	Length - 70 dB	Difference %	Width - 70 dB	Difference %	Area - 80 dB	Difference %	Length - 80 dB	Difference %	Width - 80 dB	Difference %	Area - 90 dB	Difference %	Length - 90 dB	Difference %	Width - 90 dB	Difference %
STANDARD		49.497	0	14.241	0	3.9397	0	10.065	0	7.6545	0	1.7242	0	1.1886	0	2.691	0	0.60703	0
MODIFIED_RT05		48.979	-1.05	14.237	-0.03	3.9371	-0.07	9.956	-1.08	7.6947	0.53	1.7232	-0.06	1.1296	-4.96	2.7727	3.04	0.55707	-8.23
MODIFIED_RT10		47.778	-3.47	15.685	10.14	3.5484	-9.93	8.1348	-19.18	7.2489	-5.3	1.4305	-17.03	0.93494	-21.34	2.6314	-2.21	0.48891	-19.46
MODIFIED_RT15		47.45	-4.14	15.726	10.43	3.5472	-9.96	8.0895	-19.63	7.3397	-4.11	1.418	-17.76	0.91211	-23.26	2.7361	1.68	0.43638	-28.11
MODIFIED_AW		52.217	5.5	14.97	5.12	3.9481	0.21	10.564	4.96	8.0608	5.31	1.7285	0.25	1.214	2.14	2.8486	5.86	0.59762	-1.55
MODIFIED_AW_RT05		51.615	4.28	14.974	5.15	3.9455	0.15	10.416	3.49	8.1097	5.95	1.7275	0.19	1.1747	-1.17	2.9309	8.91	0.54694	-9.9
MODIFIED_AW_RT10		50.538	2.1	16.559	16.28	3.5562	-9.73	8.5453	-15.1	7.6377	-0.22	1.421	-17.58	0.9752	-17.95	2.7846	3.48	0.47792	-21.27
MODIFIED_AW_RT15		50.198	1.42	16.608	16.62	3.5543	-9.78	8.4962	-15.59	7.743	1.16	1.4207	-17.6	0.94997	-20.08	2.9	7.77	0.4322	-28.8
Profile	SL 4	Area - 70 dB	Difference %	Length - 70 dB	Difference %	Width - 70 dB	Difference %	Area - 80 dB	Difference %	Length - 80 dB	Difference %	Width - 80 dB	Difference %	Area - 90 dB	Difference %	Length - 90 dB	Difference %	Width - 90 dB	Difference %
STANDARD		53.921	0	15.527	0	3.9016	0	10.947	0	8.4849	0	1.6846	0	1.2702	0	3.0066	0	0.58719	0
MODIFIED_RT05		53.364	-1.03	15.532	0.03	3.9016	0	10.807	-1.28	8.5428	0.68	1.6844	-0.01	1.2255	-3.52	3.1059	3.3	0.53441	-8.99
MODIFIED_RT10		52.23	-3.14	17.186	10.68	3.5116	-10	8.8558	-19.12	8.0481	-5.15	1.405	-16.6	1.0143	-20.15	2.9448	-2.06	0.4719	-19.63
MODIFIED_RT15		51.872	-3.8	17.248	11.08	3.5116	-10	8.7639	-19.94	8.1634	-3.79	1.3828	-17.92	0.99109	-21.97	3.0732	2.22	0.4358	-25.78
MODIFIED_AW		57.333	6.33	16.449	5.94	3.9105	0.23	11.585	5.83	9.0044	6.12	1.6896	0.3	1.3295	4.67	3.1948	6.26	0.57242	-2.52
MODIFIED_AW_RT05		56.729	5.21	16.466	6.05	3.9092	0.19	11.431	4.42	9.0734	6.94	1.6896	0.3	1.2807	0.83	3.2994	9.74	0.52278	-10.87
MODIFIED_AW_RT10		55.716	3.33	18.298	17.85	3.5198	-9.79	9.3783	-14.33	8.5596	0.88	1.3887	-17.57	1.063	-16.31	3.1364	4.32	0.47332	-19.39
MODIFIED_AW_RT15		55.343	2.64	18.373	18.33	3.5194	-9.8	9.2761	-15.26	8.6864	2.37	1.3833	-17.89	1.0378	-18.3	3.2785	9.04	0.43959	-25.14
Profile	SL 5	Area - 70 dB	Difference %	Length - 70 dB	Difference %	Width - 70 dB	Difference %	Area - 80 dB	Difference %	Length - 80 dB	Difference %	Width - 80 dB	Difference %	Area - 90 dB	Difference %	Length - 90 dB	Difference %	Width - 90 dB	Difference %
STANDARD		60.562	0	17.416	0	3.9169	0	12.071	0	9.5474	0	1.6426	0	1.3938	0	3.4152	0	0.57025	0
MODIFIED_RT05		59.893	-1.1	17.438	0.13	3.9181	0.03	11.928	-1.18	9.6273	0.84	1.6424	-0.01	1.3431	-3.64	3.5301	3.36	0.51849	-9.08
MODIFIED_RT10		59.076	-2.45	19.462	11.75	3.4719	-11.36	9.7856	-18.93	9.0959	-4.73	1.3741	-16.35	1.1121	-20.21	3.3439	-2.09	0.47674	-16.4
MODIFIED_RT15		58.691	-3.09	19.551	12.26	3.4728	-11.34	9.7228	-19.45	9.2379	-3.24	1.3507	-17.77	1.0874	-21.98	3.5034	2.58	0.44324	-22.27
MODIFIED_AW		60.611	0.08	17.418	0.01	3.9181	0.03	12.09	0.16	9.5474	0	1.6426	0	1.3948	0.07	3.4173	0.06	0.57043	0.03
MODIFIED_AW_RT05		59.92	-1.06	17.445	0.17	3.9181	0.03	11.931	-1.16	9.6273	0.84	1.6424	-0.01	1.3437	-3.59	3.533	3.45	0.51865	-9.05
MODIFIED_AW_RT10		59.102	-2.41	19.471	11.8	3.4719	-11.36	9.7891	-18.9	9.0959	-4.73	1.373	-16.41	1.1125	-20.18	3.3446	-2.07	0.47674	-16.4
MODIFIED_AW_RT15		58.719	-3.04	19.559	12.3	3.4728	-11.34	9.6855	-19.76	9.2469	-3.15	1.3499	-17.82	1.088	-21.94	3.505	2.63	0.44324	-22.27
Profile	SL 6	Area - 70 dB	Difference %	Length - 70 dB	Difference %	Width - 70 dB	Difference %	Area - 80 dB	Difference %	Length - 80 dB	Difference %	Width - 80 dB	Difference %	Area - 90 dB	Difference %	Length - 90 dB	Difference %	Width - 90 dB	Difference %
STANDARD		60.616	0	17.431	0	3.9181	0	12.078	0	9.5577	0	1.6426	0	1.3946	0	3.4177	0	0.57043	0
MODIFIED_RT05		59.946	-1.11	17.453	0.13	3.9181	0	11.938	-1.16	9.6384	0.84	1.6424	-0.01	1.3439	-3.64	3.533	3.37	0.51865	-9.08
MODIFIED_RT10		59.129	-2.45	19.479	11.75	3.4719	-11.39	9.7933	-18.92	9.102	-4.77	1.3729	-16.42	1.1127	-20.21	3.3474	2.06	0.47677	-16.42
MODIFIED_RT15		58.746	-3.08	19.569	12.27	3.4728	-11.37	9.6882	-19.79	9.2469	-3.25	1.3499	-17.82	1.0881	-21.98	3.5071	2.62	0.44324	-22.3
MODIFIED_AW		60.638	0.04	17.425	-0.03	3.9181	0	12.091	0.11	9.5477	-0.1	1.6426	0	1.3951	0.04	3.4196	0.06	0.57043	0
MODIFIED_AW_RT05		59.946	-1.11	17.453	0.13	3.9181	0	11.938	-1.16	9.6384	0.84	1.6424	-0.01	1.3439	-3.64	3.533	3.37	0.51865	-9.08
MODIFIED_AW_RT10		59.129	-2.45	19.479	11.75	3.4719	-11.39	9.7933	-18.92	9.102	-4.77	1.3729	-16.42	1.1127	-20.21	3.3474	2.06	0.47677	-16.42
MODIFIED_AW_RT15		58.746	-3.08	19.569	12.27	3.4728	-11.37	9.6882	-19.79	9.2469	-3.25	1.3499	-17.82	1.0881	-21.98	3.5071	2.62	0.44324	-22.3

Similar to the performance results, a comprehensive comparison using results for all 90 aircraft was also conducted. Still, only the minimum stage length was used to compare across different aircraft with different number of stage length. Figure 14 - Figure 16 contains the comparison results for all 90 aircraft for noise contour area, length, and width, respectively. Within each figure and noise contour metric, the three subplots show results for three different noise levels: 70 dB, 80 dB, and 90 dB. In each figure, one can compare between the 8 profiles for a certain noise level, or observe the differences across different noise levels by comparing the three subplots. Median of contour area, length and width for each noise level can be found in Table 5 - Table 7.

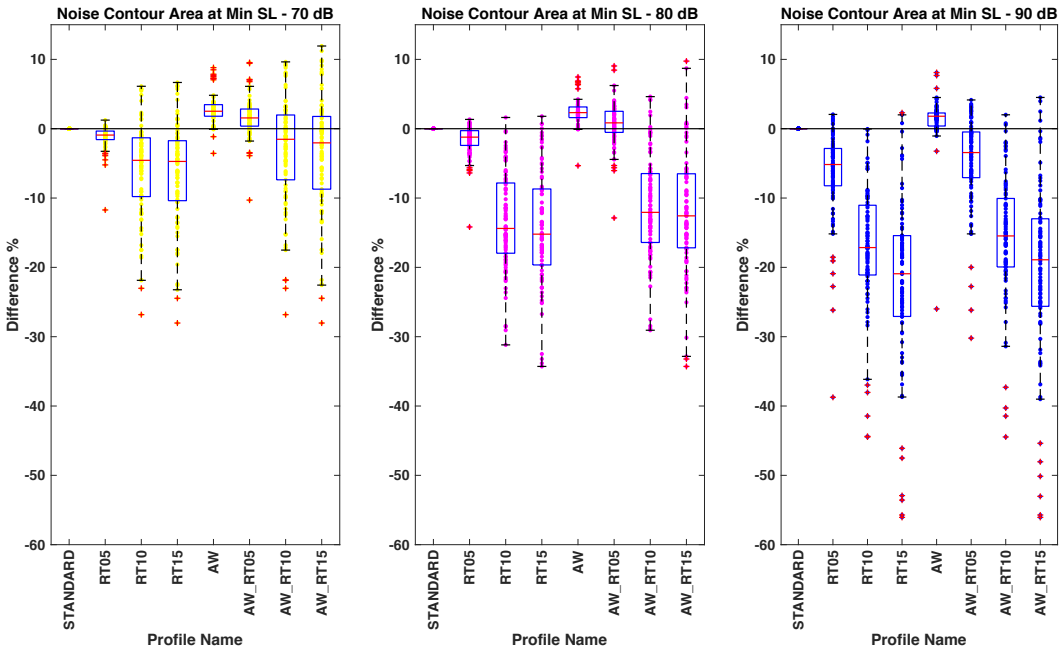


Figure 14. All 90 Aircraft Noise Comparison: Noise Contour Area

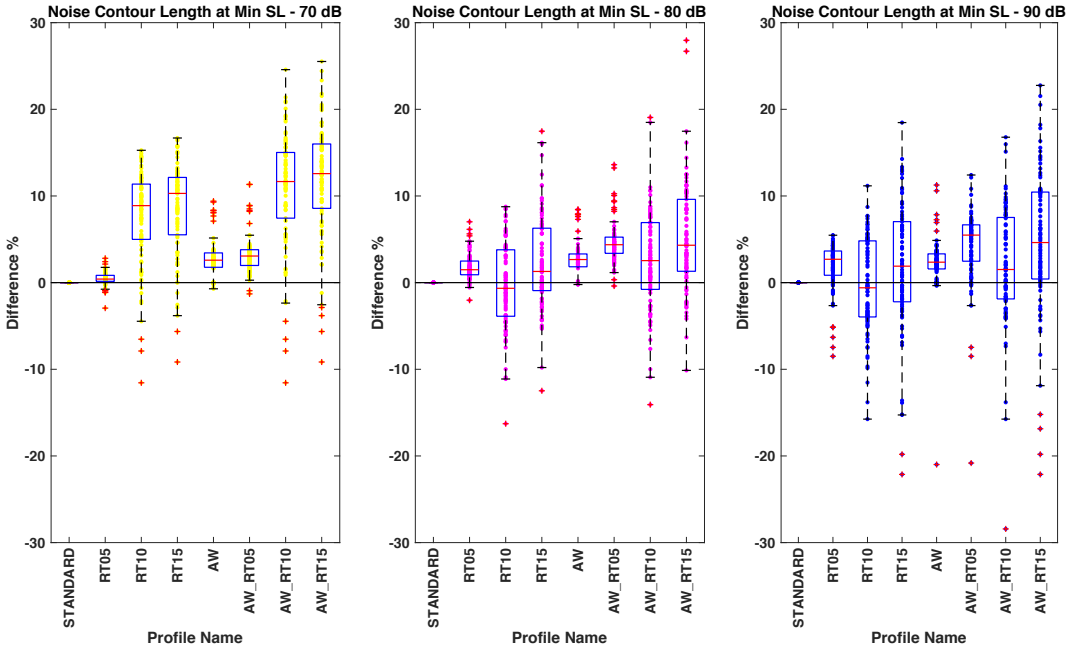


Figure 15. All 90 Aircraft Noise Comparison: Noise Contour Length

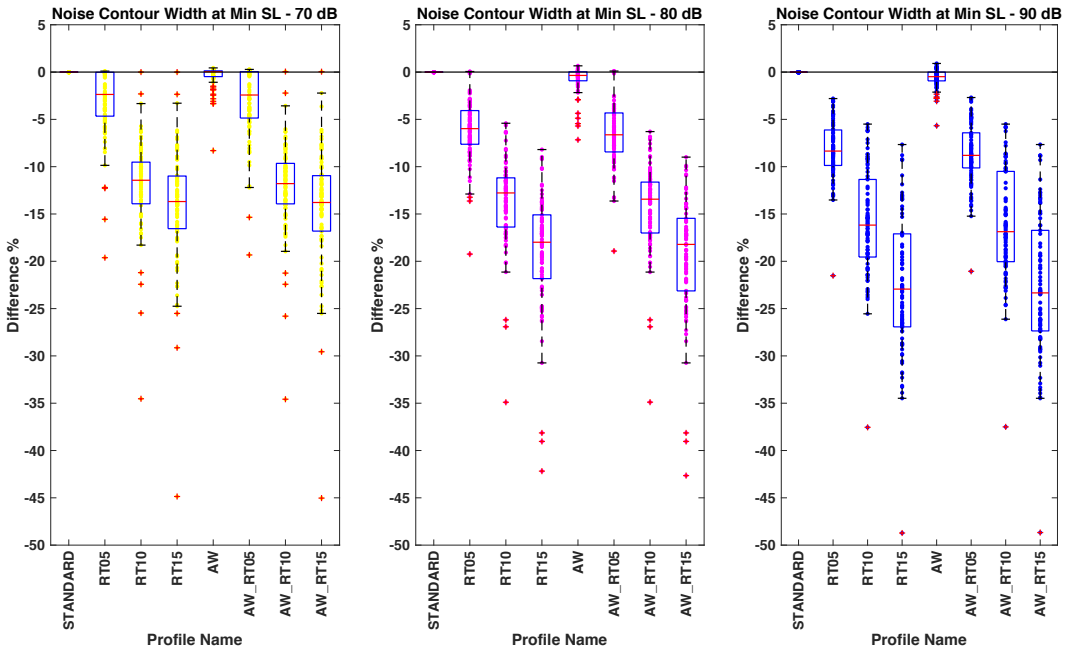


Figure 16. All 90 Aircraft Noise Comparison: Noise Contour Width

Table 5. Medians for Noise Contour Area Comparison for all 90 Aircraft

Profiles	STANDARD	MODIFIED RT05	MODIFIED RT10	MODIFIED RT15	MODIFIED AW	MODIFIED AW_RT05	MODIFIED AW_RT10	MODIFIED AW_RT15
70 dB	0.000	-0.915	-4.560	-4.720	2.520	1.555	-1.525	-2.040
80 dB	0.000	-1.215	-14.385	-15.210	2.320	0.845	-12.065	-12.570
90 dB	0.000	-5.165	-17.145	-20.920	1.800	-3.440	-15.465	-18.905

Table 6. Medians for Noise Contour Length Comparison for all 90 Aircraft

Profiles	STANDARD	MODIFIED RT05	MODIFIED RT10	MODIFIED RT15	MODIFIED AW	MODIFIED AW_RT05	MODIFIED AW_RT10	MODIFIED AW_RT15
70 dB	0.000	0.410	8.885	10.295	2.590	3.070	11.665	12.580
80 dB	0.000	1.490	-0.655	1.290	2.665	4.375	2.540	4.315
90 dB	0.000	2.695	-0.595	1.900	2.360	5.485	1.515	4.625

Table 7. Medians for Noise Contour Width Comparison for all 90 Aircraft

Profiles	STANDARD	MODIFIED RT05	MODIFIED RT10	MODIFIED RT15	MODIFIED AW	MODIFIED AW_RT05	MODIFIED AW_RT10	MODIFIED AW_RT15
70 dB	0.000	-2.365	-11.435	-13.685	0.040	-2.425	-11.790	-13.785
80 dB	0.000	-5.980	-12.775	-17.985	-0.355	-6.630	-13.435	-18.215
90 dB	0.000	-8.350	-16.175	-22.940	-0.485	-8.805	-16.870	-23.340



The integrated analysis for noise metrics for all 90 aircraft unveils general impacts of the new profiles on noise contour. Figure 14 and Table 5 show the noise contour area comparison among the 8 profiles at three different noise levels. Three general observations can be made from the contour area comparison. First, when the thrust level is further reduced, the noise contour area at all the three noise levels becomes smaller. This results shows that the reduced thrust takeoff operation can in fact abate the noise impact to the ground. Second, when comparing across the AW and non-AW groups (left and right four columns), the use of alternative weight increases the noise contour area by around 2.5%. Third, at a larger noise level, the noise contour area is reduced by a larger extent under the influence of reduced thrust takeoff. Figure 15 and Table 6 show the noise contour width comparison of this round. The changing pattern of the contour width is the most straightforward among the three: with more reduced thrust, the noise contour width decreases monotonically. It is less influenced by the alternative weight, and the percentage of reduction is larger at larger noise levels. Figure 16 and Table 7 show the noise contour length comparison between the 8 profiles. It can be observed that the changing pattern of the contour length is the most complicated one, as the changing trends are not consistent at three different noise levels. At the noise level of 70 dB, the contour length increases with more reduced thrust. Yet at 80 and 90 dB, the largest contour length happens when the reduced thrust level is -5%, and the trend is fluctuating as the reduced thrust level goes from 0% to -15%.

The difficulty of predicting the change of noise contour length is not a surprise, as the noise metrics are affected by a mix of several direct consequences brought out by a reduced thrust profile. On one hand, when the thrust level is reduced, the noise directly generated from the engine is expected to become smaller. On the other hand, with reduced thrust, the takeoff flight trajectory is also closer to the ground, as shown by Figure 8. A shallower trajectory amplifies the flight's noise impact to the ground. When both the plus (trajectory) and minus (engine) effects are added together, predicting the noise metrics impact requires the identification of the most dominant effects at different stages and noise levels. A quantitative study to uncover the reasons behind the complex changing pattern for noise metrics will be discussed later.

Although due to significant differences among the 90 aircraft and the complexity of noise metrics, the changing patterns of noise metrics are more complicated compared to the performance metrics, some general observations for noise metrics are summarized below:

1. With more reduced thrust, the noise contour area at different noise levels decreases
2. With more reduced thrust, the noise contour width at different noise levels decreases
3. With more reduced thrust, the change of noise contour length does not have a monotonic changing pattern, and displays different characteristics at different noise levels
4. With the alternative weight, the noise contour area and length are increased by a certain increment. Contour width is less influenced by the alternative weight
5. For noise contour area and width, the percentage change with reduced thrust is greater at higher noise levels.

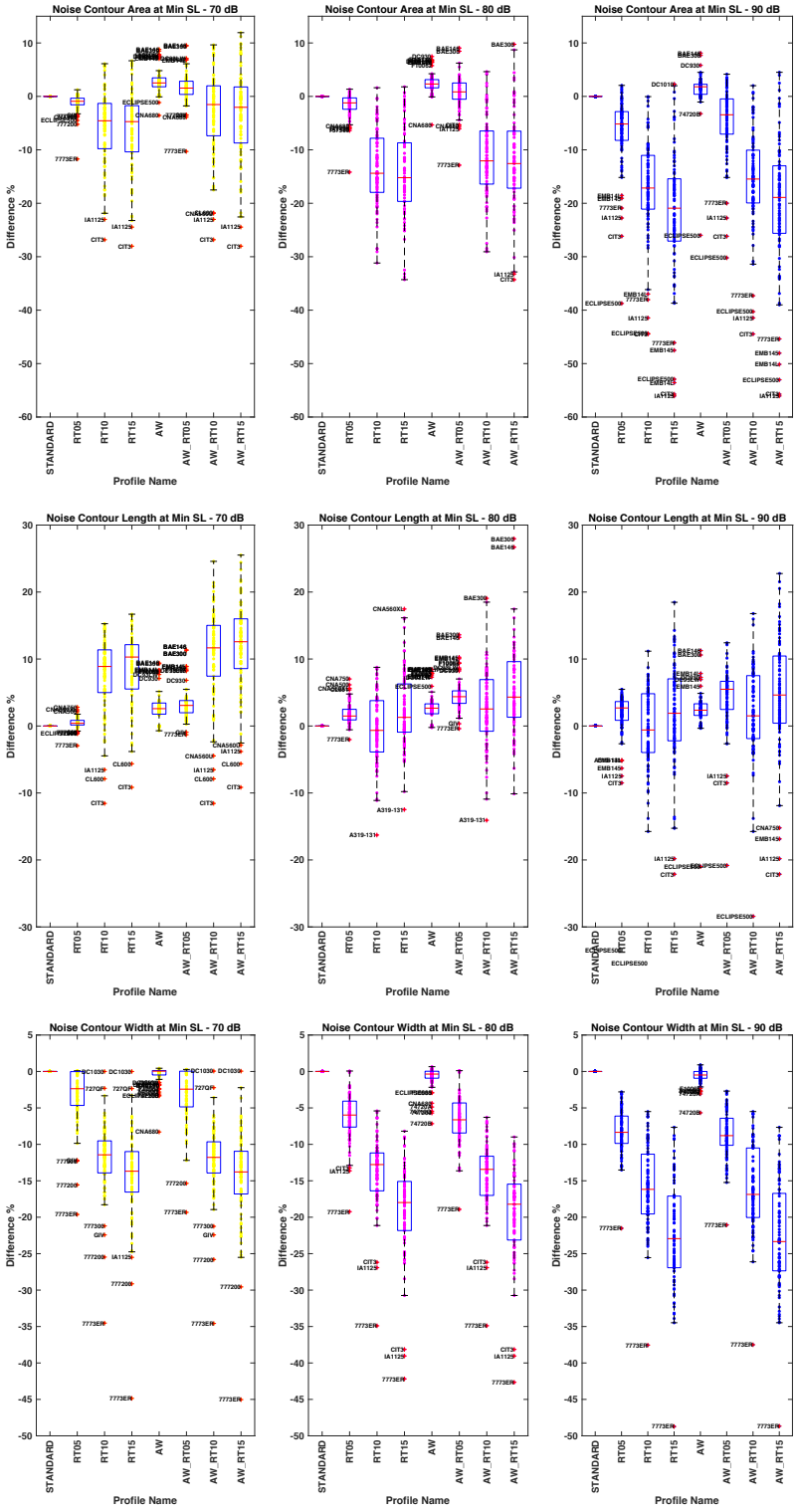


Figure 17. Outlier Identification for Noise Metrics Comparison



An outlier analysis was also conducted to identify and analyze outlier aircraft in the noise results. The outliers in Figure 14-Figure 16 are first identified and marked out in Figure 17. A complete list of outlier aircraft in noise results include: 717200, ECLIPSE500, IA1125, F10062, F10065, 74720B, 777200, 7773ER, 757PW, BAE146, BAE300, 727EM2, 727QF, CIT3, DC930, DC1030, DC93LW, 727QF, 767JT9, A300-622R, A319-131. From the list, it can be found out that most of the outlier aircraft are still aircraft that are old aircraft and not commonly operated in today's operations. Some representative aircraft, such as A319-131 and 777200, are outliers only in one of the metrics, or are not too far from the ends of the whisker. For those aircraft, there's no need to specifically investigate the reasons behind. However, for one aircraft, the Boeing 777-300ER (7773ER), it is a standing-out outlier in contour width comparison in all the three noise levels. Although the noise contour width changing trend for 7773ER is consistent with other aircraft, its contour width decreases much more than other aircraft (around 20% more compared to the median of the 90 aircraft). An investigation on the performance report of 7773ER was therefore conducted to further explain the reasons behind this outlier. After checking the performance data from various angles, no abnormal pattern has been found. A speculation of the reasons behind 7773ER being an outlier is that the 7773ER aircraft and engine data provided by the manufacturers may be relatively new compared to other aircraft. The more up-to-date data can cause better performance as of the environmental impacts.

Quantitative Root Cause Analysis on Noise Results

After the large scale AEDT study with all 90 aircraft and all stage lengths was conducted, the analysis results for key performance and noise metrics were presented in the previous sections. For the new reduced thrust profiles, while the changing patterns for the performance metrics are relatively straightforward and easy to be interpreted, the changing patterns for the noise metrics are more complex and require further in-depth analysis. In general, the observed changing patterns for the three noise metrics are:

- Noise Contour Area: monotonically decreases with more reduced thrust
- Noise Contour Width: monotonically decreases with more reduced thrust
- Noise Contour Length: does not have a monotonically changing trend with reduced thrust.

The reason why the changing patterns of the noise results are more difficult to explain is that, with a reduced thrust profile, the changes for all of contour area, length, and width are affected by two direct consequences caused by reduced thrust:

- Consequence 1 – Thrust Change: with reduced thrust, the magnitude of noise that directly comes from the engine is also reduced. This is a negative effect to the contour area, length, and width on the ground.
- Consequence 2 – Trajectory Change: with reduced thrust, the aircraft takeoff trajectory is closer to the ground. This is a positive effect to the contour area, length, and width on the ground.

Therefore, to better explain why for different reduced thrust profiles, the noise metrics change in the way we observed, an advanced statistical analysis is needed to identify the most influential factors to each noise metrics for different noise levels. When such influential factors are identified, the changing trends of the noise metrics should follow the directions given by the most influential factors. In the meantime, the study was done from a mode's perspective, in which the noise metrics contribution from four takeoff modes were distinguished. Overall, a takeoff process consists of four different modes according to the performance report:

Mode 1: Taxi

Mode 2: Takeoff Ground Roll

Mode 3: Takeoff Airborne

Mode 4: Terminal Climb

Because AEDT does not model Taxi noise, only Mode 2-4 are considered in this analysis. With all these information, the analysis is formulated as shown in Figure 18. In this whole analysis, we have 9 objectives to study, which are the 9 noise metrics: percentage of noise contour area, length, and width at 70, 80 and 90 dB levels, as shown at the left of Figure 18. In the meantime, there are 6 predictors of interest for each of the 9 metrics: percentage of thrust change and trajectory change for Mode 2-4, as shown in the middle of Figure 18. Then, each of the 9 noise metrics is a function of the 6 predictors, indicated by the matching at the right of Figure 18.

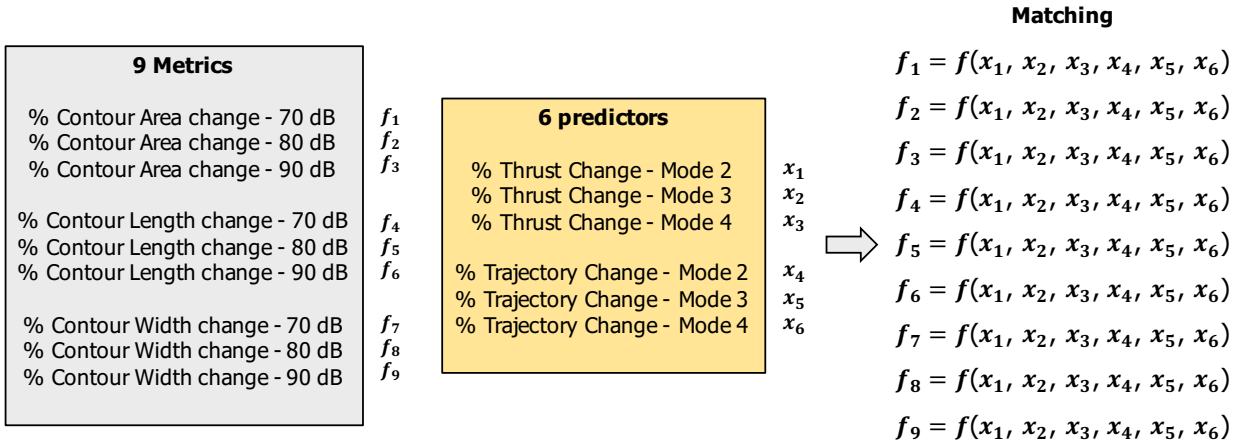


Figure 18. The Root Cause Statistical Analysis Set-up

After the analysis approach is formulated, information from the previous analyses must be re-organized for the statistical model selection process. The necessary information for the statistical analysis is calculated and organized into a table shown in Table 8. Due to the limited space, Table 8 only contains part of the complete table. With each row representing one case, the complete table has more rows and includes all the cases summarized above in Figure 14 - Figure 16 (the full factorial combination of all 90 aircraft, 8 profiles, and stage length 1). The table can be divided into two parts. The left part contains 9 columns that are highlighted in gray, and they correspond to the percentage changes of the 9 noise metrics. The right part contains 6 columns that are colored in yellow, and they correspond to the percentage changes of the 6 predictors. Among the 6 predictors, the definition of the percentage change in trajectory needs to be emphasized. Here, a 20% increase in trajectory means that compared to the old trajectory, the new one is 20% closer to the ground.

When the pre-analysis table is ready, statistical learning methods LASSO (**L**east **A**bsolute **S**hrinkage and **S**election **O**perator) and Elastic Net are used to identify the most influential predictors for each noise metric. Both the LASSO and Elastic Net are methods from the category of linear model selection and regularization. In a regression setting, a linear model can be written as

$$Y = \beta_0 + \beta_1 X_1 + \beta_2 X_2 + \cdots + \beta_n X_n + \epsilon$$

where Y is the metric of interest, $X_1, X_2, \ldots, X_n$ are the predictors and $\beta_1, \beta_2, \ldots, \beta_n$ are the coefficients. The first statistical method LASSO is an important statistical learning method for model selection (or in our context, predictor selection). For a certain model with many predictors, the LASSO is a shrinkage method and is able to remove the redundant predictors, select the most influential ones and rank among them. Mathematically, the LASSO estimate minimizes

$$\sum_{i=1}^{n}\left(y_i - \beta_0 - \sum_{j=1}^{n}\beta_j x_{ij}\right)^2 + \lambda\sum_{j=1}^{n}|\beta_j|$$

where $\lambda\sum_{j=1}^{n}|\beta_j|$ is called the LASSO penalty, and is controlled by the value of λ. As λ increases, more shrinkage is employed and more coefficients go to zero. In this process, a predictor is more influential if its corresponding coefficient remains non-zero for larger λ values.

The second statistical learning method considered, the Elastic Net, is a modified version of LASSO. It makes a compromise between LASSO and Ridge Regression (also a shrinkage method but uses different penalty function) and has a better performance when some of the predictors are highly correlated. The Elastic Net minimizes



$$\frac{1}{2}\sum_{i=1}^{n}\left(y_i-\beta_0-\sum_{j=1}^{n}\beta_j x_{ij}\right)^2+\lambda[\frac{(1-\alpha)}{2}\sum_{j=1}^{n}|\beta_j|^2+\alpha\sum_{j=1}^{n}|\beta_j|]$$

where the α is adjusted to assign weights between LASSO and Ridge Regression. It becomes LASSO when $\alpha = 1$, and Ridge Regression when $\alpha = 0$.

Table 8. The Format of the Pre-Analysis Table for LASSO and Elastic Net Analysis

70dB - Area	70dB - Length	70dB - Width	80dB - Area	80dB - Length	80dB - Width	90dB - Area	90dB - Length	90dB - Width	Mode 2 Trajectory	Mode 3 Trajectory	Mode 4 Trajectory	Mode 2 thrust	Mode 3 thrust	Mode 4 thrust
3.1588	1.5779	-0.38062	3.4496	3.3673	-1.4328	2.3895	2.6647	0.50695	5.1732	4.7263	3.5992	-0.054155	-0.24377	-0.076558
2.7004	1.9506	-0.4183	1.4505	4.7635	-3.9085	-6.1374	7.1547	-7.1943	10.554	11.343	4.2905	-5.0424	-5.2343	-0.43638
-11.559	2.9816	-12.266	-14.786	1.1476	-14.673	-15.922	7.8097	-13.452	16.528	18.836	20.507	-10.031	-10.218	-10.067
-12.184	1.6276	-12.266	-15.84	3.405	-20.372	-25.008	10.659	-19.173	23.204	27.422	21.413	-15.019	-15.209	-10.427
-0.58546	0.30644	-0.086675	-0.95648	1.4073	-3.0314	-8.9272	3.695	-7.729	5.1111	6.3017	0.63563	-4.9883	-5.0041	-0.32154
-4.332	-0.62945	-11.765	-16.802	-2.2197	-14.627	-18.252	3.9812	-13.832	10.785	13.44	16.137	-9.9765	-10.001	-9.9602
-14.981	0.0082823	-11.803	-17.834	0.017758	-19.634	-27.116	7.0402	-19.547	17.127	21.593	16.995	-14.971	-15.005	-10.32
3.6025	1.6911	-0.51979	3.3033	3.6755	-0.55653	2.5352	3.3939	-0.55611	5.2168	1.8129	4.0106	-0.047033	-0.11842	0
0.86749	1.9126	-13.533	-9.9929	4.9122	-15.416	-11.55	2.9899	-17.461	16.695	18.333	23.382	-10.034	-10.108	-9.999
-3.0394	1.4488	-12.99	-13.012	1.0383	-14.865	-13.917	-0.56798	-16.947	10.901	16.14	18.332	-9.9945	-10.007	-10.002
3.2783	1.4274	-0.74668	3.4448	3.8466	-0.88568	2.269	3.7718	-0.6217	5.1802	1.8319	3.9557	-0.034958	-0.10239	-0.026346
0.72056	1.5382	-2.8172	1.4405	4.6171	-9.551	-0.63526	6.6955	-10.67	10.631	9.1557	5.2763	-5.3695	-5.083	-0.4391
-9.0738	1.5562	-17.211	-28.81	-7.6572	-17.744	-19.938	-3.983	-20.372	16.688	17.681	22.479	-10.347	-10.078	-10.003
-10.938	1.6297	-25.177	-30.139	-6.3247	-25.524	-22.712	0.26214	-26.209	23.459	27.708	24.306	-15.325	-15.074	-10.433
-2.5899	0.11576	-3.0379	-2.087	0.75822	-8.8158	-3.1836	2.9591	-9.8316	5.1775	6.8904	1.3146	-4.999	-4.9805	-0.42153
-12.338	1.375	-16.61	-31.18	-11.12	-17.105	-21.96	-7.4264	-19.656	10.933	15.187	17.613	-10.313	-9.9832	-9.9939
-14.121	2.064	-24.6	-32.491	-9.7676	-24.929	-24.749	-3.2907	-28.693	17.365	24.93	19.38	-15.29	-14.986	-10.424
3.882	1.8777	-0.56688	3.0447	3.6836	-0.594	2.2488	3.3633	-1.3042	5.2715	2.5435	4.1136	-0.052079	-0.16406	-0.009827
1.975	1.2067	-2.0959	0.55301	5.4034	-9.4305	-4.5392	8.7792	-12.905	10.705	10.244	5.3005	-5.0448	-5.1515	-0.42256
-1.8734	0.3128	-2.2399	-2.5294	1.6326	-8.8671	-6.9189	5.0703	-11.894	5.1576	7.2505	1.152	-4.9922	-4.9955	-0.42256
3.1679	1.2385	0.10002	2.7325	3.1781	-0.50176	2.4321	3.2597	0.51201	5.1321	4.7486	3.4864	-0.084598	-0.3229	-0.076634
3.1959	1.0142	0.22708	2.7158	3.0102	-0.91851	2.1085	3.2903	-0.84	5.0776	4.6896	3.3715	-0.070179	-0.2884	-0.04462
-2.2168	1.3856	-15.184	-14.089	0.75329	-12.8	-17.962	-0.58589	-21.268	16.51	18.533	19.89	-10.046	-10.256	-10.04
-5.4398	1.0242	-15.281	-16.449	-2.4034	-12.197	-19.914	-3.5402	-20.722	10.871	13.201	15.847	-9.9754	-10.002	-10.001
3.1024	1.9944	0.22024	2.3673	3.1537	0.092513	2.2086	2.6205	-0.61409	5.0524	4.6894	3.3888	-0.077489	-0.28487	-0.03635
-2.8949	1.3551	-17.367	-16.397	-0.8288	-14.819	-21.072	-1.8803	-21.816	16.498	18.517	20.083	-10.049	-10.255	-10.033
-6.058	0.9935	-17.488	-18.432	-3.8805	-14.278	-22.883	-4.8858	-21.501	10.887	13.179	16.028	-9.9816	-9.9983	-9.9903
3.468	1.2007	0.1611	3.1476	3.2328	-0.22516	1.943	2.884	-1.6564	5.1773	4.7861	3.4667	-0.08285	-0.32121	-0.020789
-0.052058	1.4914	-10.117	-8.9204	4.1601	-11.011	-15.122	0.086293	-14.666	16.624	18.891	20.201	-10.052	-10.285	-10.02
-3.4254	1.1106	-10.19	-11.449	0.83137	-10.902	-17.177	-3.5018	-15.12	10.875	13.422	16.046	-9.9807	-9.9961	-9.9716
2.7207	2.483	0.13348	1.9695	2.618	0.22809	2.5773	2.542	-0.1175	4.2891	3.9362	2.8394	-0.054225	-0.22809	-0.17346
2.6186	1.6433	-0.50774	2.3709	2.8011	-0.79773	1.5439	2.4066	-1.1955	4.5846	2.8211	3.0451	-0.061232	-0.16494	0
0.71227	1.9563	-4.6692	-2.0578	4.072	-9.9668	-10.544	4.096	-13.23	9.9736	9.6245	4.4862	-5.0496	-5.1555	-0.47925
-2.455	1.2611	-13.444	-21.14	-4.9183	-18.905	-23.359	2.0633	-24.643	15.962	17.382	19.264	-10.038	-10.146	-10.002
-3.6052	1.3481	-14.919	-23.287	-2.6334	-25.167	-33.932	0.66624	-33.948	22.655	26.308	21.169	-15.026	-15.137	-10.482
-2.0587	0.2852	-4.8126	-4.0889	1.2905	-9.4623	-12.203	1.4786	-12.856	5.1496	6.5999	1.4086	-4.9924	-5	-0.47925
-5.2849	0.4533	-13.189	-23.018	-7.4888	-18.391	-24.966	-1.0401	-23.997	10.872	14.118	15.641	-9.9808	-10	-10.002
-6.4149	0.281	-14.943	-25.162	-5.3336	-24.749	-35.236	-1.9807	-33.284	17.266	22.76	17.473	-14.973	-15	-10.482
2.4809	1.5544	0	2.0605	2.3015	-0.30566	1.8375	1.9835	0.36672	3.4031	2.4471	2.685	-0.048703	-0.14621	0
2.6561	1.7881	-3.7756	2.8068	6.0833	-5.2622	-5.0095	2.716	-4.7644	8.7288	10.123	3.862	-5.0367	-5.1408	-0.42413
0.013834	1.359	-7.7738	-2.2358	6.8678	-10.115	-9.5325	4.4696	-8.9089	14.644	19.061	22.706	-10.025	-10.135	-10
0.6548	1.0249	-11.331	0.58916	12.489	-14.403	-14.768	5.7167	-12.742	21.255	29.614	24.324	-15.013	-15.125	-10.424
0.22134	1.2179	-3.5174	0.79159	3.6712	-4.777	-6.6998	0.16574	-5.1166	5.146	8.083	1.1341	-4.988	-4.9993	-0.42413
-2.4998	1.5437	-7.5512	-4.254	4.2758	-9.6122	-11.356	2.0477	-9.1795	10.864	16.804	19.248	-9.9801	-9.9986	-10
-1.8261	1.3705	-11.1	-1.5499	9.7436	-14.352	-16.505	3.2934	-13.05	17.252	27.081	20.83	-14.968	-14.998	-10.424
3.7603	1.5638	-0.40333	3.5231	3.6228	-0.60221	2.6965	3.3507	-0.64339	5.5332	2.4889	4.0872	-0.026441	-0.097209	0
2.5901	1.8634	-3.7861	2.1291	4.5374	-6.578	0.87292	6.0142	-8.6037	10.932	9.5938	5.1805	-5.0238	-5.0896	-0.40496
1.3061	1.6421	-12.884	-13.077	2.1311	-13.867	-19.268	-4.0877	-17.529	16.928	17.74	21.977	-10.015	-10.089	-9.9975
0.084028	1.6896	-16.811	-14.232	3.4097	-20.234	-21.894	-0.44958	-26.194	23.628	27.202	23.43	-15.017	-15.081	-10.402
-1.0009	0.23093	-3.8445	-1.1828	0.75475	-5.1883	-1.4191	2.4239	-7.358	5.1085	8.6728	1.02	-4.9907	-4.9928	-0.37121
-2.5171	1.2015	-11.739	-15.909	-1.6782	-12.56	-20.199	-7.5241	-16.543	10.783	16.726	16.899	-9.9881	-9.9917	-9.9722

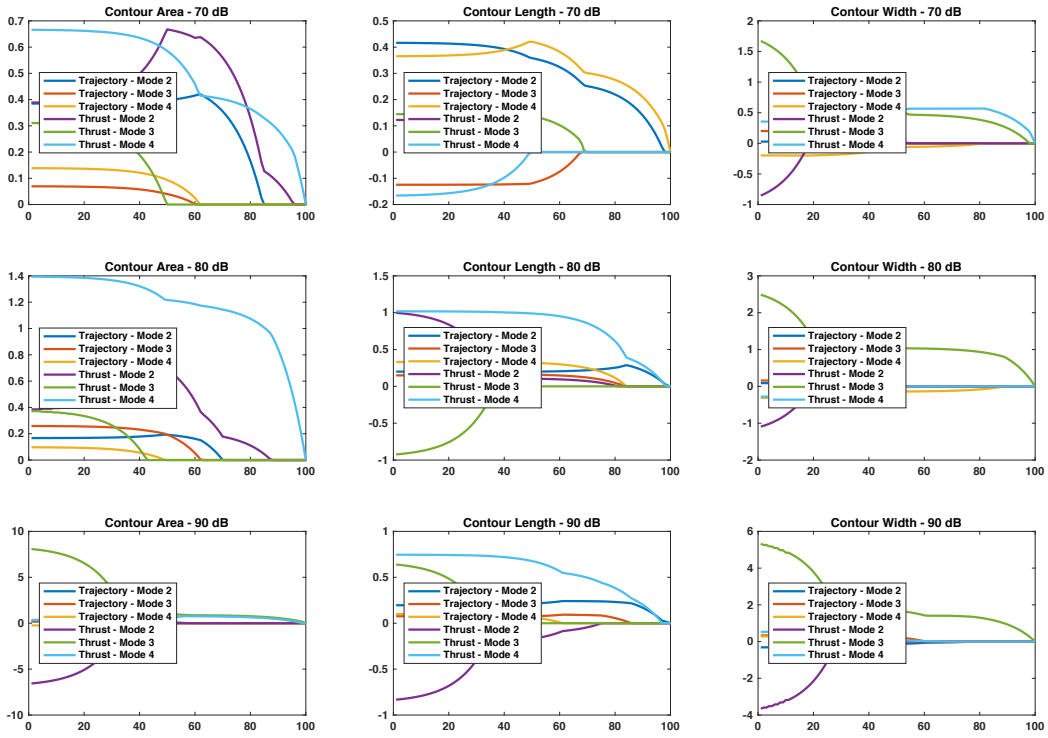


Figure 19. LASSO Results for the 9 Noise Metrics

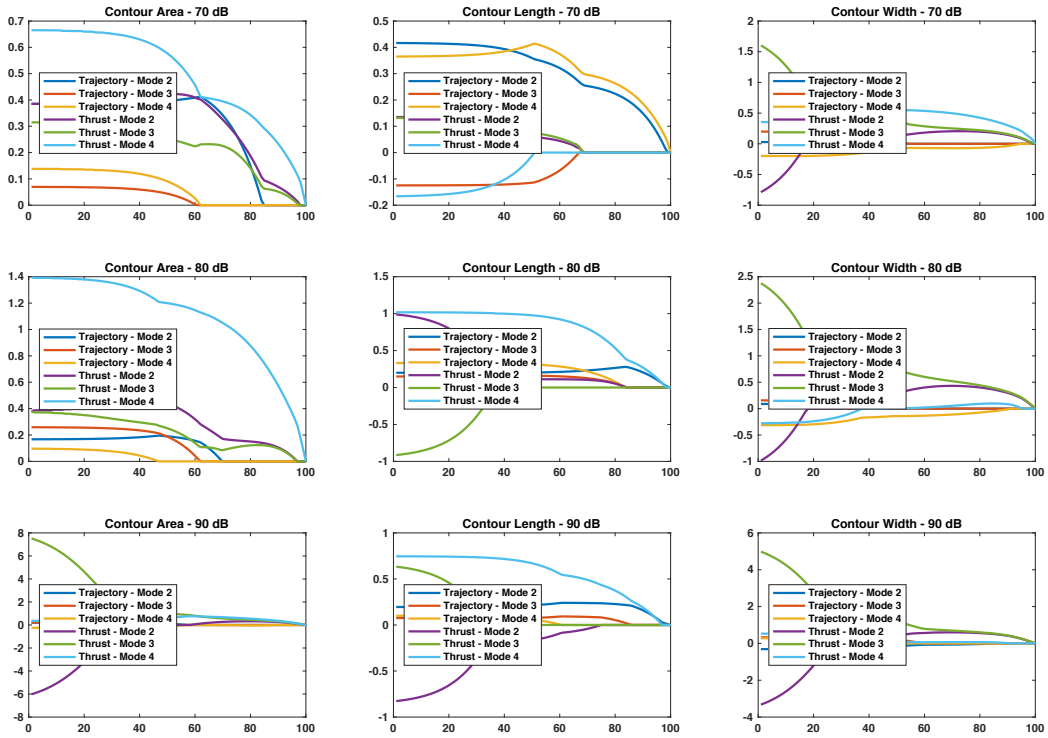


Figure 20. Elastic Nets Results for the 9 Noise Metrics

Both LASSO and Elastic Net were used in the analysis. It is worth mentioning here that the Elastic Net must be used carefully. Among the 6 predictors that we have, the correlations between them is not simple. On one hand, there are indeed correlations between the percentage reduced thrust and the percentage trajectory change. On the other hand, although the changing patterns are very similar within the groups of reduced thrust predictors and trajectory change predictors, it does not mean that the predictors within each group are also correlated – it is just a result of the setting. In the end, it was decided that LASSO and Elastic Net with a α value of 0.95 are both used in the analysis, and the results from the two methods are combined to make a judgment.

After the analysis is done, the graphical results are shown in Figure 19 and Figure 20. As can be seen from the Figures, when the penalty value (x-axis) increases, the later the corresponding coefficient goes to zero, the more important that predictor is. The graphical results in Figure 19-Figure 20 are also summarized in Table 9. In our study, due to its complexity and variations among different aircraft, the second 50% of the predictor ranking may not be precise. Therefore, only the results from the first 50% of the predictor ranking (first three most influential predictors) are extracted and studied.



Table 9. Statistical Learning with LASSO and Elastic Net – Results Summary

Contour Area - 70 dB			Contour Length - 70 dB			Contour Width - 70 dB		
Top Predictors	**Lasso**	**Elastic Net**	**Top Predictors**	**Lasso**	**Elastic Net**	**Top Predictors**	**Lasso**	**Elastic Net**
1	Mode 4 Thrust	Mode 4 Thrust	1	Mode 4 Trajectory	Mode 4 Trajectory	1	Mode 4 Thrust	Mode 4 Thrust
2	Mode 2 Thrust	Mode 3 Thrust	2	Mode 2 Trajectory	Mode 2 Trajectory	2	Mode 3 Thrust	Mode 3 Thrust
3	Mode 2 Trajectory	Mode 2 Thrust	3	Mode 3 Thrust	Mode 3 Thrust	3	Mode 4 Trajectory	Mode 2 Thrust
Contour Area - 80 dB			**Contour Length - 80 dB**			**Contour Width - 80 dB**		
Top Predictors	**Lasso**	**Elastic Net**	**Top Predictors**	**Lasso**	**Elastic Net**	**Top Predictors**	**Lasso**	**Elastic Net**
1	Mode 4 Thrust	Mode 4 Thrust	1	Mode 2 Trajectory	Mode 2 Trajectory	1	Mode 3 Thrust	Mode 3 Thrust
2	Mode 2 Thrust	Mode 3 Thrust	2	Mode 4 Thrust	Mode 4 Thrust	2	Mode 4 Trajectory	Mode 2 Thrust
3	Mode 2 Trajectory	Mode 2 Thrust	3	Mode 4 Trajectory	Mode 4 Trajectory	3		Mode 4 Thrust
Contour Area - 90 dB			**Contour Length - 90 dB**			**Contour Width - 90 dB**		
Top Predictors	**Lasso**	**Elastic Net**	**Top Predictors**	**Lasso**	**Elastic Net**	**Top Predictors**	**Lasso**	**Elastic Net**
1	Mode 3 Thrust	Mode 3 Thrust	1	Mode 2 Trajectory	Mode 2 Trajectory	1	Mode 3 Thrust	Mode 3 Thrust
2	Mode 4 Thrust	Mode 4 Thrust	2	Mode 4 Thrust	Mode 4 Thrust	2	Mode 2 Trajectory	Mode 2 Thrust
3		Mode 2 Thrust	3	Mode 3 Trajectory	Mode 3 Trajectory	3		Mode 2 Trajectory

It can be observed from Table 9 that, for most of the 9 noise metrics, the ranking of the top 3 predictors from LASSO and Elastic Net are in good agreement. For all the 9 noise metrics, the first most influential predictors from the two methods are the same. Most of the second most influential predictors from the two methods are also the same. For some LASSO results, there are only two influential predictors identified, because all the rest of the predictors are deemed redundant (or insignificant and relatively incomparable) by LASSO. When the Elastic Net results are further compared with the actual changing directions of the 9 noise metrics, a final result is given in Table 10. In this table, the changing directions of the top three predictors and the metrics are marked with different symbols: the green down arrow means decrease, the red up arrow means increase, and the yellow circle means fluctuation. As a reminder, Mode 2 is Takeoff Ground Roll, Mode 3 is Takeoff Airborne, and Mode 4 is Terminal Climb.



Table 10. Comparison between the Changing Directions of Noise Metrics and Their Top Predictors

Top 3 Predictors Ranking	70 dB Contour Area ▼	70 dB Contour Length ▲	70 dB Contour Width ▼	80 dB Contour Area ▼	80 dB Contour Length ◉	80 dB Contour Width ▼	90 dB Contour Area ▼	90 dB Contour Length ◉	90 dB Contour Width ▼
1st	Mode 4 Thrust ▼	Mode 4 Trajectory ▲	Mode 4 Thrust ▼	Mode 4 Thrust ▼	Mode 2 Trajectory ▲	Mode 3 Thrust ▼	Mode 3 Thrust ▼	Mode 2 Trajectory ▲	Mode 3 Thrust ▼
2nd	Mode 3 Thrust ▼	Mode 2 Trajectory ▲	Mode 3 Thrust ▼	Mode 3 Thrust ▼	Mode 4 Thrust ▼	Mode 2 Thrust ▼	Mode 4 Thrust ▼	Mode 4 Thrust ▼	Mode 2 Thrust ▼
3rd	Mode 2 Thrust ▼	Mode 3 Thrust ▼	Mode 2 Thrust ▼	Mode 2 Thrust ▼	Mode 4 Trajectory ▲	Mode 4 Thrust ▼	Mode 2 Thrust ▼	Mode 3 Trajectory ▲	Mode 2 Trajectory ▲

Some general conclusions can be made from the results in Table 10. First, the noise contour area and contour width metrics monotonically decrease with bigger thrust reduction, and this is because for all the 6 contour area and width metrics, their top 2 most significant predictors are the percentage changes in thrust (negative effect). Therefore, the changing directions of contour area and width follow the changing directions of thrust. The changing directions for noise contour length display two different patterns. At the noise level of 70 dB, it can be seen from the table that the top two predictors are the percentage changes in trajectory (positive effect). This explains why the contour length at 70 dB monotonically increases with more reduced thrust. At the noise level of 80 and 90 dB, now the contour length fluctuates with more reduced thrust. This can also be explained by the statistical learning results because the top 3 predictors for contour length at 80 and 90 dB consist of both the percentage change in thrust and in trajectory (a mix of positive and negative effects). To better predict the contour length changing direction, detailed analysis has to be done for individual aircraft. In the meantime, the above statistical learning results make sense from the mode's perspective. For example, when the noise level increases from 70 dB to 90 dB, the most influential predictors involve from the Mode 4 thrust or trajectory to ones from Mode 3 and Mode 2. This coincides with the real world situation: with a higher noise level, the noise contour becomes smaller and should be more influenced by the earlier modes during takeoff.

In conclusion, the above statistical learning analysis is a way to quantitatively explain the root causes behind the noise metrics change. When the change of a metric is complex and involves with different factors, these methods provides a path to distinguish the most influential factors, such that the overall trend can be predicted from the changing directions of a subset of predictors. The analysis explains the observed changing patterns of the noise metrics and concludes the study for the reduced thrust profiles.

Task 3- Improved Departure Procedure Modeling

Georgia Institute of Technology

Objective(s)

For most aircraft types in AEDT, the manufactures provided flight profiles for three departure procedures: STANDARD, ICAO-A, and ICAO-B. Under this research, the GT team conducted a literature review on departure procedures. The team also conducted interviews with airline pilots and flight engineers regarding the usage of departure procedures by the airlines. Based on the literature review, both ICAO-A and ICAO-B procedures are obsolete. ICAO PANS-OPS and FAA AC91-53 have adopted two noise abatement departure procedures (NADPs) in the 1990s. The PANS-OPS allows a maximum of two different takeoff procedure to be implemented by an airline: one to mitigate noise impact to the communities close to the airport and the other to mitigate the noise impact to the communities far from the airport. Literature review and the interviews confirmed that none of the airlines uses ICAO-A and ICAO-B procedures anymore. The ICAO-A and ICAO-B procedures were originally defined in ICAO PANS-OPS in 1993 and were replaced by NADP1 and NADP2 in 2004. Most airlines in the United States currently use NADP2. NADP1 is popular in Asia and Europe where communities tend to be closer to the airports.

In AEDT 3a, the new weight and thrust options were implemented to the existing STANDARD departure procedures. The AEE decided not to pursue the modeling of NADPs in AEDT 3a due to limited resources, including time constraint. The GT team has identified some challenges modeling NADP1 and NADP2 for the majority of the aircraft types in AEDT 3a timeframe. Therefore, the focus of the third year effort will be to address the ways to overcome the challenges. First of all, to be able to model NADPs in future AEDT versions, extensive NADP data should be collected for all major airlines and aircraft types. The GT team will continue to work with the FAA, airlines, and airports to obtain such data.

GT has conducted further literatures review on prior research to understand the work has been done in the area of improving departure procedure modeling. New profiles were developed under ACRP 02-55 project. GT reviewed the report of this project and see how to leverage NADP procedure with the work done under ACRP 55 project.

Research Approach

As part of process for improving the departure procedure modeling, the ACRP 02-55 project was reviewed. The ACRP 02-55 project is titled "Enhanced AEDT Modeling of Aircraft Arrival and Departure Profiles". The objective of the project is to help users of AEDT better model real world aircraft trajectories by providing them with more options. These options were created by observing real world radar data, and then matching that data with customized AEDT profiles. The result of this matching is that the resulting noise and emissions calculations will also be more accurate. In addition to the new proposed profiles, a Profile Customization Tool was also envisioned which can help users modify profiles to their liking without needing to know advanced programming skills of the details of AEDT database manipulation.

AEDT currently has several different methods to model aircraft operations. These are shown in Figure 21. Going from left to right, users have the option of performing higher fidelity analysis, at the expense of higher modeling effort and data requirements. As is evident from the figure, the ACRP 02-55 proposed methods are on the lower end of the fidelity spectrum and are meant to supplement the existing default profiles in AEDT.

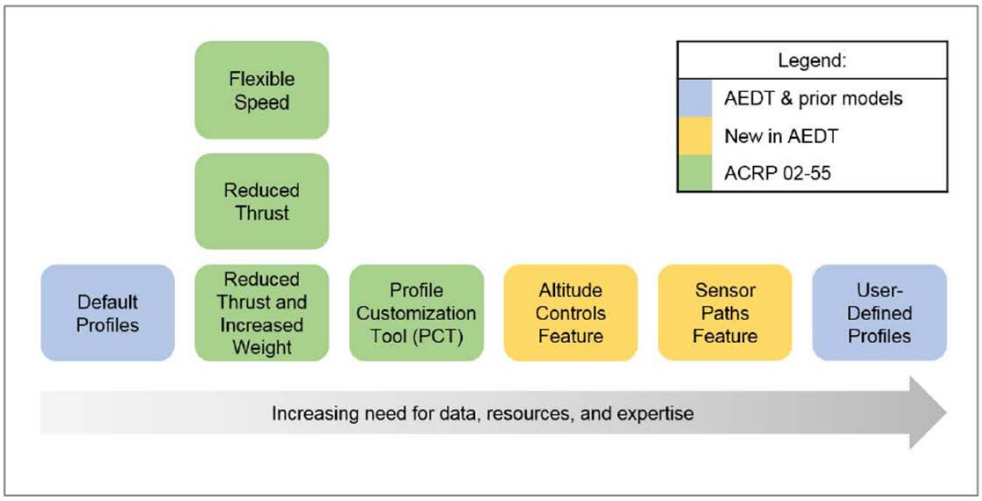


Figure 21. Available and proposed new options for operation modeling in AEDT

These new profiles for AEDT were created using extensive radar data from a large number of U.S. airports. Operation data for 29 U.S. airports over a period of 30 days were utilized. A total of 840 approach and 1,410 departure profiles were created. The general process of profile creation started with segregation of data based on aircraft type, category, runway, operation, stage length etc. Next, the radar tracks for these were visualized and a single candidate trajectory was created. This was then compared with the existing default modeling option in AEDT – the STANDARD profiles. Based on the amount of deviation of the AEDT option from the radar candidate profile, a prioritized list of aircraft and operations was created. The new profiles were then created for this prioritized set of aircraft. Figure 22 shows the flowchart for the modeling process.

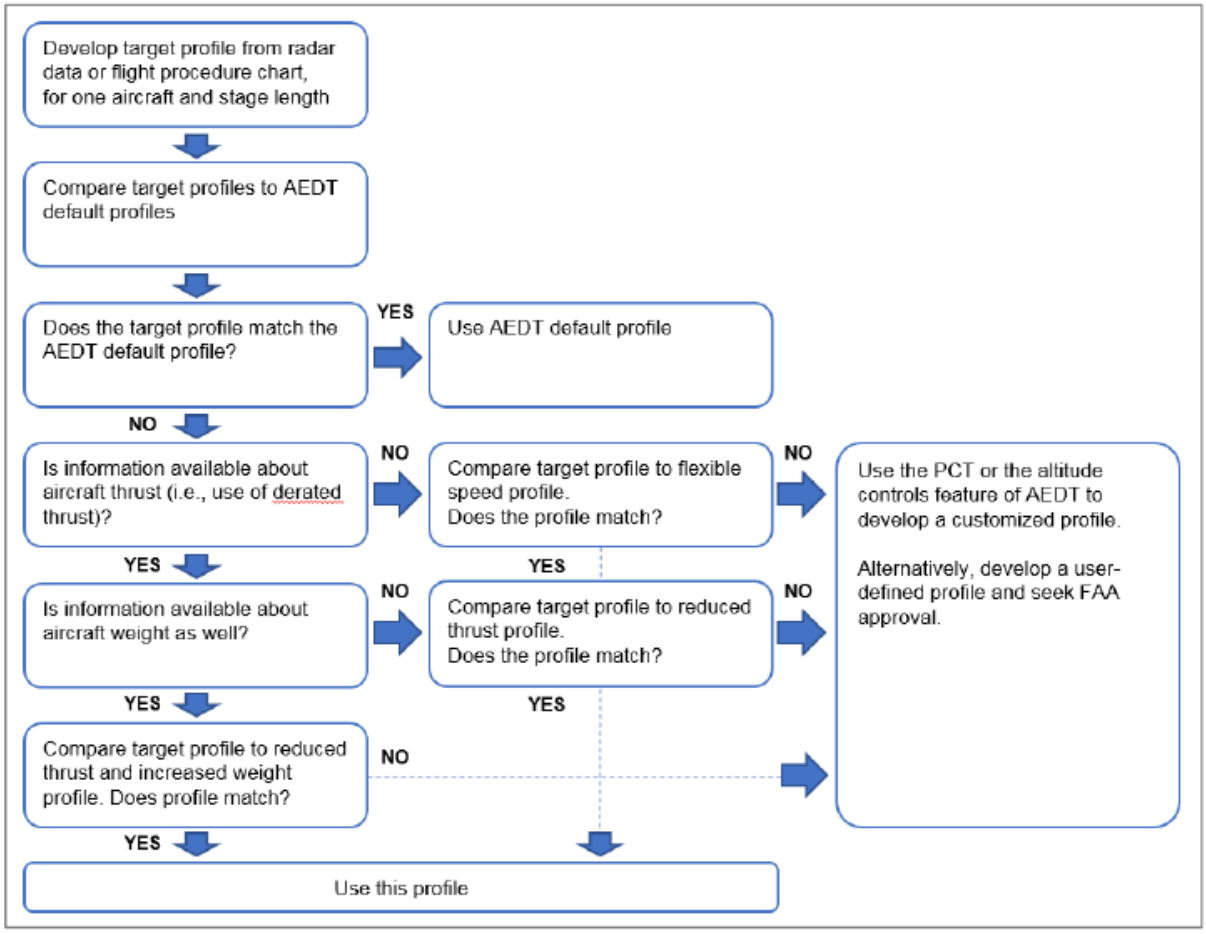


Figure 22. Profile Modeling Flow Chart (from ACRP 02-55 Guidance Document)

The approach profiles were created by adding "level off" segments to the single 3-degree glideslope constant descent which is common in many aircraft. While a few aircraft already make use of level segments, the altitude and duration of these segments could be varied to get new profiles. With these new and/or modified segments, the team able to achieve good match between the radar tracks and their profiles. Figure 23 shows a comparison of several alternate approach profiles.

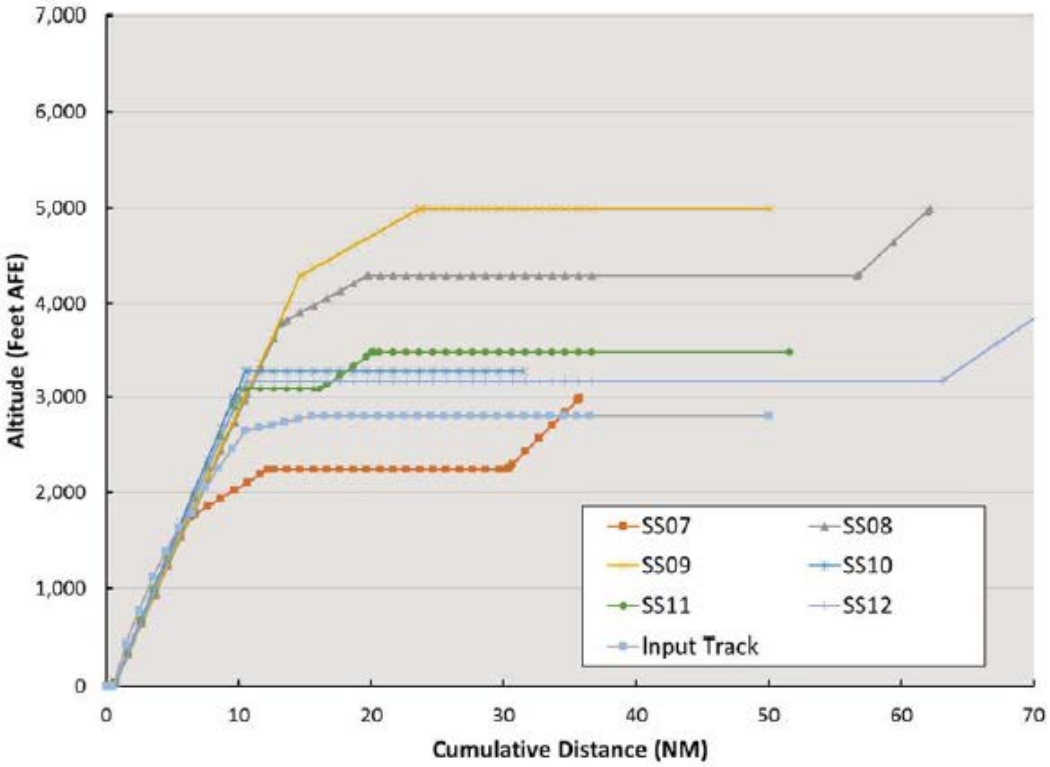


Figure 23. Trajectory comparison for several candidate alternate approach profiles

For departure profiles, it was seen that because real world operations used reduced thrust, there was a large difference between the target trajectory and what could be obtained in AEDT. To address this, three sets of profiles were proposed. The first set, called "Flexible Speed" profiles would remove the restriction on maximum speed of 250 KCAS below 10,000 ft. altitude. This would lead to any excess thrust being materialized into additional speed instead of higher climb rates; therefore, a closer match could be obtained. The second set utilized reduced thrust and reinstated the speed limit. Thrust reduction was varied as 0 to 44% in increments of 2% and the best match profile was chosen. The final set made the use of both reduced thrust and increased weight. The weight was varied between the BADA minimum and ANP maximum weight, in increments of 2% of the difference. It was observed that the average thrust reduction is about 25% and the average weight increase is between 0 to 12%. Figure 24 shows a comparison of several different candidate departure profiles.

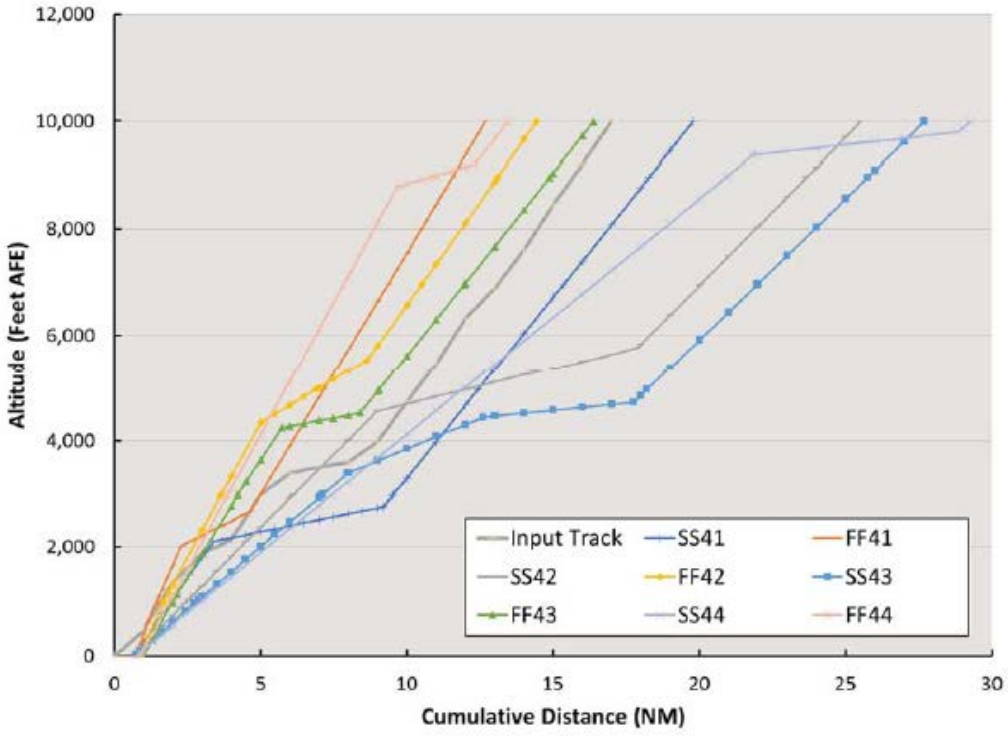


Figure 24. Trajectory comparison for several candidate alternate departure profiles

The methodology of the ACRP 02-55 project may have some applications in future modeling efforts of the ASCENT 45 project. Specifically, the trajectory comparison methods, grouping methods and radar trajectory candidate profile generation technique may all prove to be useful.

Milestone(s)

Milestone	Due Date	Estimated Date of Completion	Actual Completion Date	Status	Comments (Problems & Brief Resolution Plan)
Quarterly Report (Jan)	1/31/2018	1/31/2018	1/31/2018	Completed	
Quarterly Report (March)	3/31/2018	3/31/2018	3/31/2018	Completed	
ASCENT Meeting	4/3 - 4/2018	4/3 - 4/2018	4/3 - 4/2018	Completed	
Quarterly Report (June)	6/30/2018	6/30/2018	6/30/2018	Completed	
ASCENT Meeting	10/9 - 10/2018	10/9 - 10/2018	10/9 - 10/2018	Completed	
Quarterly Report (Oct)	10/30/2018	10/30/2018	10/30/2018	Completed	
Annual Report	11/30/2018	11/30/2018	11/30/2018	In Progress	



Major Accomplishments

- Developed new reduced thrust and alternative weight profiles for 90 major commercial and general aviation jets. Converted rate of climb in the procedure to energy share percentage for each stage length of the 90 aircraft.
- Validated the energy share value against the RoC based profiles.
- Conducted comprehensive tests and analysis on the new profiles to investigate the impact of the new profiles. In addition, carried out statistical analysis to study the main drivers on the noise results.

Publications

Matthew J Levine, Dongwook Lim, Yongchang Li, Michelle R Kirby, Dimitri, Mavris, Quantification of Error for Rapid Fleet-Level Noise Computation Model Assumptions, AVIATION conference, June 17-21, 2018.

Dongwook Lim, Matthew Levine, Vu Ngo, Michelle Kirby, and Dimitri Mavris, Improved Aircraft Departure Modeling for Environmental Impact Assessment, AVIATION conference, June 17-21, 2018.

Outreach Efforts

- Bi-weekly calls with the Project Managers.
- ASCENT annual meeting.
- FAA Noise workshop.
- FAA External tools calls.

Awards

None

Student Involvement

Ameya Behere, Zhenyu Gao, Yee Chan Jin, Junghyun (Andy) Kim– Graduate Research Assistant, Georgia Institute of Technology

Plans for Next Period

The primary focus for the next period will be:

- Improve each sensitivity assumption to AEDT
- Assessment of new assumptions at the airport level



Project 046 Surface Analysis to Support AEDT Aircraft Performance Model (APM) Development

Massachusetts Institute of Technology and Massachusetts Institute of Technology Lincoln Laboratory

Project Lead Investigator

Hamsa Balakrishnan
Associate Professor
Aeronautics and Astronautics
Massachusetts Institute of Technology
77 Massachusetts Ave., 33-328
Cambridge, MA 02139
617-253-6101
hamsa@mit.edu

University Participants

Massachusetts Institute of Technology

- P.I.(s): Hamsa Balakrishnan
- FAA Award Number: 13-C-AJFE-MIT, Amendments No. 021and 035
- Period of Performance: Sep. 1, 2017 to Aug. 31, 2018
- Task(s):
  - Phase 1
  - 1.1. Assess AEDT aircraft surface performance modeling needs
  - 1.2. Develop enhanced aircraft surface performance models
  - 1.3. Validate enhanced aircraft surface performance models
  - 1.4. Recommend AEDT APM enhancements
  - Phase 2
  - 2.1. Extend analysis to broader range of aircraft types that serve US domestic operations
  - 2.2. Extend analysis on airport-specific differences that significantly impact surface fuel burn to more US airports
  - 2.3. Identify AEDT surface APM enhancements to support emissions and noise inventories
  - 2.4. Recommend AEDT APM enhancements & Coordination with AEDT APM Developers

Project Funding Level

$75,000 FAA funding and $75,000 matching funds. Source of match is approximately $75,000 all from MIT.

Investigation Team

Prof. Hamsa Balakrishnan, Co-Principal Investigator (MIT)
Dr. Tom Reynolds, Co-Principal Investigator (Lincoln Laboratory, via separate contract)
Yashovardhan Chati (Graduate student)
Sandeep Badrinath (Graduate student)

Project Overview

The current taxi phase models in the Aviation Environmental Design Tool (AEDT) make a number of simplifying assumptions that reduce the accuracy of their fuel burn and emissions predictions. First, AEDT's current model assumes a constant engine specific thrust level (and resulting fuel flow rate) during taxi, determined from engine manufacturer certification data [1]. However, this assumption can be significantly different than actual characteristics during operational conditions for a given aircraft because of factors such as the age of the engine (as the engine gets older the amount of fuel it burns changes), as well as pilot technique (chosen taxi thrust level or "riding the brakes" instead of throttling down the engines when coming to a stop). Second, default taxi times are often assumed to be consistent with the standard certification Landing and Take-Off (LTO) cycle which assumes 26 minutes of taxi time on the airport surface, typically broken into 19 min taxi-out and 7 min taxi-in. Clearly different airports may have very different taxi times depending on topology, configuration, congestion levels, etc., that can lead to a large range of different taxi times. Using empirical data to determine realistic taxi time distributions can be effective, but these distributions need to be updated regularly to capture evolving airport conditions. Finally, the fuel burn contribution in the non-movement area from the gate time, pushback and engine start events (including engine and auxiliary power unit (APU) contributions) are typically neglected but can be quite significant. This project addresses these three issues by leveraging empirical data to build statistical and predictive models of fuel flow for a given airport and aircraft type. These analyses are designed to capture "first order" enhancements to provide recommendations for future development of tools such as AEDT.

Task Progress and Plans

Objectives

The objective of this research project is to identify and evaluate "first order" methods for improving taxi performance modeling in AEDT in order to better reflect actual operations. This objective will be met through analyses using surface surveillance (ASDE-X) and ASPM taxi time datasets, in combination with a statistical analysis of Flight Data Recorder (FDR) archives and other operational fuel burn data. Subsequent research phases may address potential higher order enhancement areas. Phase 1 of the work identified key gaps in the AEDT aircraft performance models and enhancements were developed in the areas of improved baseline fuel flow modeling, updated airport-specific taxi times and addition of pre-taxi fuel burn components. Phase 2 activities are refining and expanding and these areas. Tasks 2A.1-4 listed below correspond to the Tasks which were carried out between September 2017-Aug 2018 which are the main focus of this report. Subsequent Tasks 2B.1-4 correspond to the on-going activities in these task areas, which are discussed in the following section.

Research Approach

Task 2A.1 -Extend Phase 1 analysis to broader range of aircraft types: Phase 1 of ASCENT 46 (Jul 2016-Aug 2017) extended this approach by synthesizing such statistical models with surface traffic models obtained through the analysis of ASDE-X data [9]. A particular focus of this phase was the analyses needed to identify and extract first-order vs. higher-order effects on the fuel burn. To do so we considered fuel consumed in the non-movement area (including gate, push-back and engine start events that have previously not been studied in detail, as well as accounting for Auxiliary Power Unit (APU) fuel during these events), as well as the movement areas, including the relative effects of acceleration events on fuel burn, when compared to the baseline fuel flow rates.

Through a synthesis of prior work in ACRP 02-27 [10], ACRP 02-45 [11], AEDT documentation, stakeholder input, and data analysis, the following gaps were identified: (1) Need for improving/refreshing taxi times at different airports; (2) Absence of a surface-specific regression model, even for modeling the baseline fuel burn index; (3) No evaluation of the magnitude of non-movement area, engine-startup and/or APU fuel burn impacts; and (4) No consideration of acceleration events, and the resulting increase in the fuel flow rate. In addition, it was noted that the existing surface APM models were deterministic in nature and did not evaluate the uncertainty or variability associated with real operations.

Figure 1 shows a typical fuel flow rate profile (post-pushback and engine start) during taxi-out. It can be seen that the fuel flow rate profile (red curve) can be divided into two distinct regions: a baseline region and a fuel flow spike region. The baseline region is characterized by an almost constant (low variation) fuel flow rate having a low value. The fuel flow spike region is characterized by spikes in the fuel flow rate with values greater than the baseline fuel flow rate. Therefore, these two fuel flow rate regions need to be modeled separately.

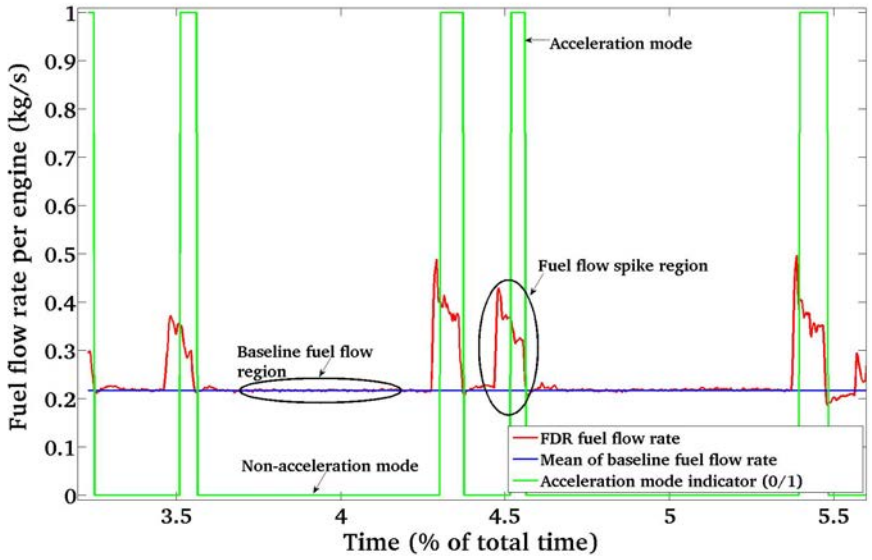


Figure 1. Typical fuel flow rate profile in taxi-out.

Phase 1 also analyzed different characteristics of the baseline fuel flow region for two example aircraft types: the A330-343 and the B777-300ER extracted from operational FDRs data and found that, on an average, more than 90% of the taxi-out fuel consumption occurs during the baseline fuel flow region. Therefore, in the current work, only the baseline fuel flow region is modeled and the fuel flow spikes are neglected. Figure 1 also shows a mean baseline fuel flow rate (in blue) obtained by averaging the baseline fuel flow rates for a particular taxi-out operation.

The values of aircraft acceleration during taxi are generally not explicitly recorded in the trajectory data. Hence, the raw trajectory data are smoothed in order to estimate the variables of interest (such as acceleration mode, shown in green in Figure 1). Finally, the mean baseline fuel flow rate per engine in taxi-out (blue curve in Figure 1) was regressed against the mean values of the selected predictor variables. An Ordinary Least Squares (OLS) regression approach is found to be sufficient to develop this simplistic model (which is still based on the same functional form as the current AEDT model). Table 2 shows the OLS-derived equations for modeling the fuel flow rate in taxi-out for the six aircraft types.

Table 1. OLS regression equations to model fuel flow rate per engine during taxi-out, along with the number of observations (flights) in the training dataset.

A/C Type	Engine Type	# Training Obs.	OLS Model Equation
A320-214	2 × CFMI CFM56-5B4/2	103	$0.812 \cdot \dot{m}_{f_{ICAO}} \cdot \delta_{\infty}^{-0.123} \cdot \theta_{\infty}^{-0.483}$
A321-111	2 × CFMI CFM56-5B1/2	46	$0.796 \cdot \dot{m}_{f_{ICAO}} \cdot \delta_{\infty} \cdot \theta_{\infty}^{0.209}$
A330-343	2 × RR Trent 772B-60	117	$0.779 \cdot \dot{m}_{f_{ICAO}} \cdot \delta_{\infty} \cdot \theta_{\infty}^{0.350}$
A340-313	4 × CFMI CFM-56 5C4/P	37	$1.019 \cdot \dot{m}_{f_{ICAO}} \cdot \delta_{\infty}^{-6.690} \cdot \theta_{\infty}^{0.597}$
B777-300ER	2 × GE GE90-115BL	81	$0.753 \cdot \dot{m}_{f_{ICAO}} \cdot \delta_{\infty} \cdot \theta_{\infty}^{0.717}$
C Series 100 (RJ)	2 × PW PW1542G	95	$0.966 \cdot \dot{m}_{f_{ICAO}} \cdot \delta_{\infty} \cdot \theta_{\infty}^{0.186}$

We also compare the predictions from such baseline fuel flow modeling with the estimates provided by AEDT, which uses the ICAO fuel burn indices in conjunction with the Boeing Fuel Flow Correction. Since the pressure and temperature ratios are approximately one for taxi operations, the multiplicative factor in Table 2 is the key differentiator from AEDT, which uses a constant value of 1.1 for all aircraft types. The results are shown in Table 3, and suggest that significant benefits may be achieved through such a data-driven methodology.



Table 2. Performance of the OLS-based baseline fuel flow rate models and the AEDT model to predict fuel flow rates on unseen test data during taxi-out. The number of flights in the test data are also shown.

A/C Type	# Test Observations from FDR	Mean error (%)		Mean absolute error (%)	
		OLS Model	AEDT	OLS Model	AEDT
A320-214	34	1.0	36.3	13.3	39.4
A321-111	14	3.8	47.1	14.9	50.1
A330-343	37	-3.0	36.4	5.8	39.1
A340-313	12	-0.7	7.8	9.1	12.5
B777-300ER	25	-2.2	42.3	3.1	43.1
C Series100 (RJ)	30	0.1	17.7	5.5	19.3

Task 2A.2- Extend Phase 1 findings on airport-specific differences that significantly impact surface fuel burn to more US airports: Airport-specific taxi out times are available in AEDT but have been found to be outdated. For this part of the study, taxi times were collected from the FAA's Aviation System Performance Metrics (ASPM). This dataset contains flight-specific taxi out times, available to the nearest minute. ASPM data from flights across 25 major U.S. airports was aggregated for dates between October 2016 and September 2017, to provide a more recent model of the distribution of taxi out times at a given airport. This analysis could be extended to other U.S. or international airports as needed.

Figure 2 below shows the updated taxi out time distributions for three sample airports: New York LaGuardia (LGA), Charlotte Douglas (CLT) and Washington Reagan (DCA). As expected, the times vary significantly within and between airports. For this particular set of airports, LGA is seen to have the largest peak and broadest spread in taxi-out time; this is not surprising given the high congestion levels at LGA. The peak in the total taxi-out time distributions for LGA, CLT, and DCA are 18, 15, and 13 minutes, respectively. Compared to the standard 19 minutes of taxi-out time assumed from the LTO cycle (shown by the dashed magenta line in Figure 2), these correspond to errors of 5.3%, 26.7%, and 46.2% of the typical taxi out times for these particular airports. This is indicative of the impact the LTO 19-minute taxi time has on the accuracy of the calculated fuel burn based on the simplified taxi time.

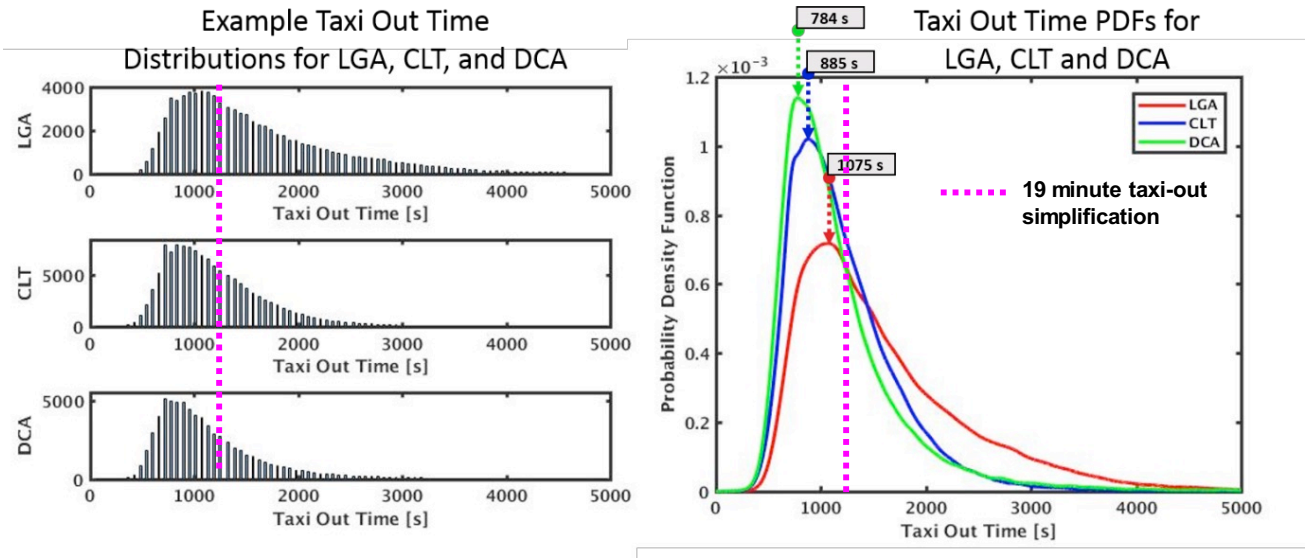


Figure 2. Example ASPM taxi-out time distributions for LGA, CLT and DCA airports

A similar comparison was conducted across the top 25 U.S. airports. Sometimes it is beneficial to reduce the number of taxi time distributions to a few clusters which capture the spectrum of differences seen in the taxi-out distributions for all

airports. To this end, each of the airport distributions were fitted to a cumulative distribution function (CDF) and the resulting curves were clustered. Since the CDF is a cumulative function, differences in the shape of the distributions will accumulate, and therefore better results are achieved by clustering on the CDFs instead of the probability density functions (PDFs). Clustering the data was accomplished through implementing a Mean Shift algorithm but other techniques could also be applied. The resulting number of clusters can be modified by changing the bandwidth parameter for the Mean Shift algorithm. There is a trade-off between the number of clusters and the error between each of the actual distributions and the corresponding cluster approximations. Fewer clusters allows for a simpler categorization of the different distributions, but results in higher error. A larger number of clusters will decrease this error, but at the cost of defeating the purpose of clustering. To determine the optimal number of clusters for the taxi-out distributions at these airports, the relationship between the error and the number of clusters was investigated. It was seen that the error continued to decrease steadily until around 6 clusters, at which point adding additional clusters had a reduced incremental impact on the total error, with zero error when there were as many clusters as airports. The box plot in Figure 3 allows a side-by-side comparison of all the airport taxi-out distributions across the 25 airports studied, as well as the differences between the six resulting clusters. The 19-minute taxi-out simplification is provided as a reference, along with the error between this assumption and median of each of the distributions. It is seen that for some clusters (such as cluster 1), the 19-minute approximation is relatively accurate. However, for other clusters (such as cluster 5), such an estimate would introduce significant error compared to the actual taxi-out time at the airports in this group. It is also interesting to note which airports are paired together. For example, JFK and LGA have been identified as airports with similar taxi-out characteristics. Both distributions have a higher spread and higher mean compared to the other airports. By contrast, Chicago Midway (MDW) is dissimilar enough from any of the other airports that it has been placed into a cluster by itself.

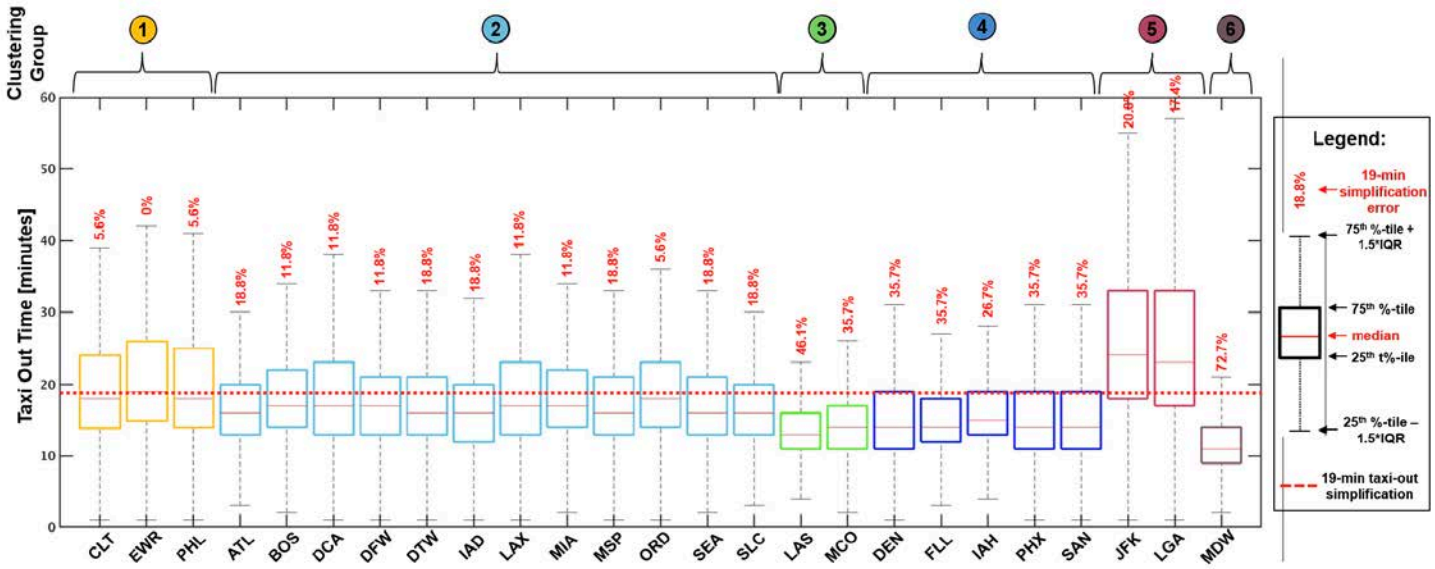


Figure 3. Boxplot of airport distributions by clustering group (outliers removed).

The 19-minute default taxi-out time assumption is intended to represent average airport taxi time. This chart shows that the errors in this estimate vary from 0% to 72.7% for these particular airports, which is one reason why users typically do not use the 19-minute default taxi time. By using recent historical data at an airport, the error resulting from predicting the taxi-out time for a given flight can be decreased drastically. In addition, if it is better to have fewer groups of airports, much of the error can still be reduced by clustering airport taxi-out data and using the respective cluster centroid as an estimation for the flight's taxi-out time.

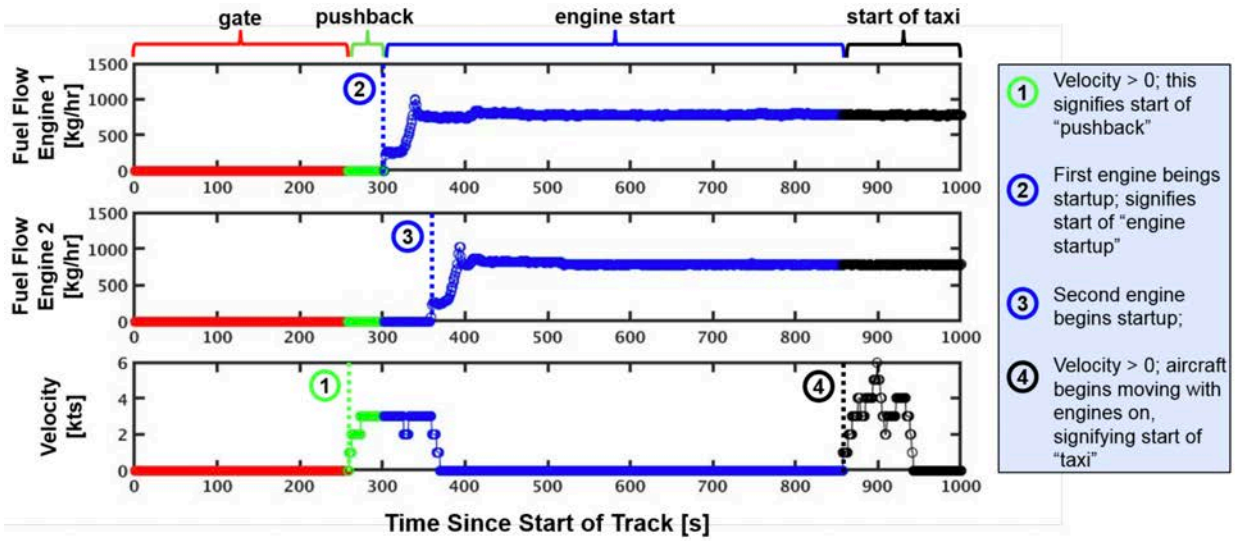


Figure 4. Example FDR data for a single flight gate, engine and push-back events.

Adding Gate, Push-back & Engine Start Fuel Estimates: In order to establish a more accurate model of the fuel burn at a given airport, the fuel consumed during engine startup up, as well as the APU contribution at the gate, pushback, and engine startup is also investigated in this study. Differences in fuel burn for these phases across different airports were found to be negligible, however the fuel burn distributions were found to vary significantly between different aircraft types. For this analysis, data from FDR was available for a European carrier for a selection of aircraft types. This contains a record over time of information specific to a flight, including fuel burn and velocity.

Figure 4 above shows the raw FDR data for a sample flight. For this part of the analysis, the flight was broken up into multiple segments, as the gate, pushback, and engine start have different APU and engine fuel burn settings. APU fuel burn rates were obtained from the ACRP 02-25 guidance document [3], which groups aircraft into categories (Narrow Body, Wide Body, Jumbo Wide Body, Regional Jet, and Turbo Prop) and gives the APU settings for the "no load" (gate), "environmental control systems" (pushback), and "main engine start" conditions for each aircraft category. The APU is turned on while still at the gate in the "no load" condition, after the aircraft has been disconnected from the gate's electricity. Through discussion with an experienced commercial pilot, it was determined that the APU is first turned on typically between 10-15 minutes before pushing back from the gate at large U.S. airports. Therefore, for all aircraft, the gate time was assumed to be 12.5 minutes, although different assumptions may be appropriate at other airports, for example where off-gate stands are more common. Pushback was defined from the point at which the aircraft began to move back from the gate, until the point at which one of the engines began burning fuel. As can be seen in Figure 4, most aircraft begin starting the first engine while still in the process of pushback by the tug from the gate, before halting and completing engine startup with the remaining engines. Engine startup was defined from the end of pushback to when the aircraft begins to move for taxi after all engines have started up and post-engine checklists are complete.

Much of the work incorporated pre-processing the data before performing the statistical analysis, as many of the flights had corrupted data, such as non-zero fuel or velocity at the beginning of the track. Once tracks had been corrected for these issues, the fuel burn totals for the gate/pushback/engine start processes were aggregated over all the flights of a given aircraft type available in the FDR data as a statistical approach to building the fuel burn histograms from historical data. The resulting fuel burn distributions for the types studied are shown in Figure 5 (left). The relationship between fuel burn and aircraft size was then investigated as a means to predict the fuel burn of the flights not within the FDR dataset. The maximum takeoff weight was used for each data type, pulled from the BADA 3.6 dataset. The total fuel burned during gate/pushback/engine start was seen to be linearly related to the weight of the aircraft type, and this correlation was used to then predict the approximate fuel burn for aircraft types not available in the FDR data set. Estimates for some example types using the observed correlation are presented as dashed lines in Figure 5 (left), and also on Figure 5 (right).

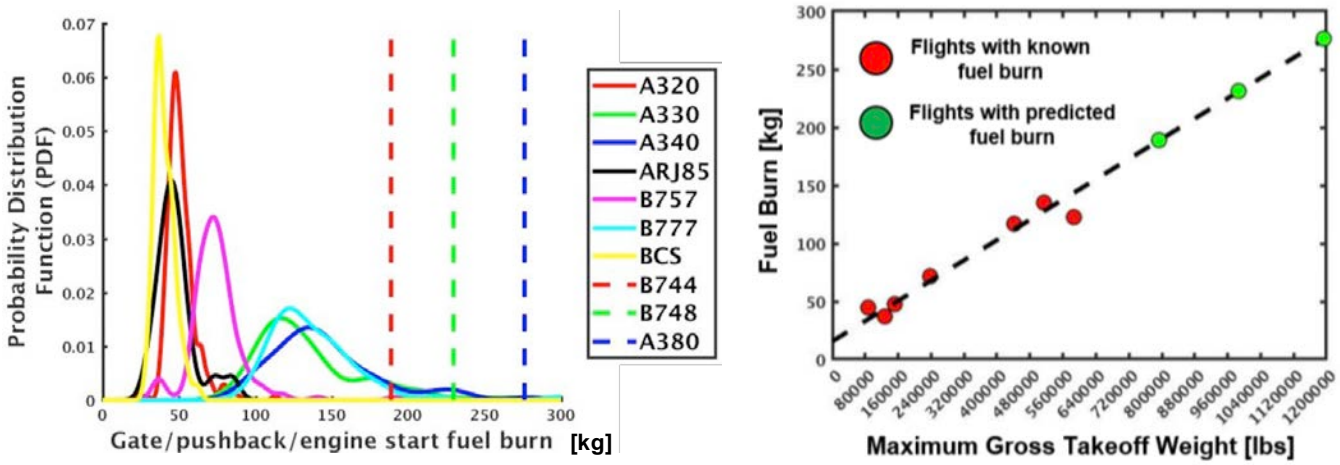


Figure 5. PDF curves for gate, pushback, and engine start fuel burn by aircraft type.

The total fuel burn between the gate to the point at which an aircraft begins to taxi is seen to vary significantly between aircraft types, and can be a significant fraction of total surface fuel burn. Figure 6 shows the percentage of pre-taxi fuel burn relative to total surface fuel burn from the types analyzed from the FDR data. For narrow body aircraft, this percentage of total fuel burn is seen to be higher than the larger body aircraft, as seen in the left plot of Figure 6. The right plot of the figure shows that the typical contribution of the pre-taxi fuel in comparison to the total fuel burned on the aircraft surface is between 10-40% on average, reinforcing the need to carefully consider this component of surface fuel burn.

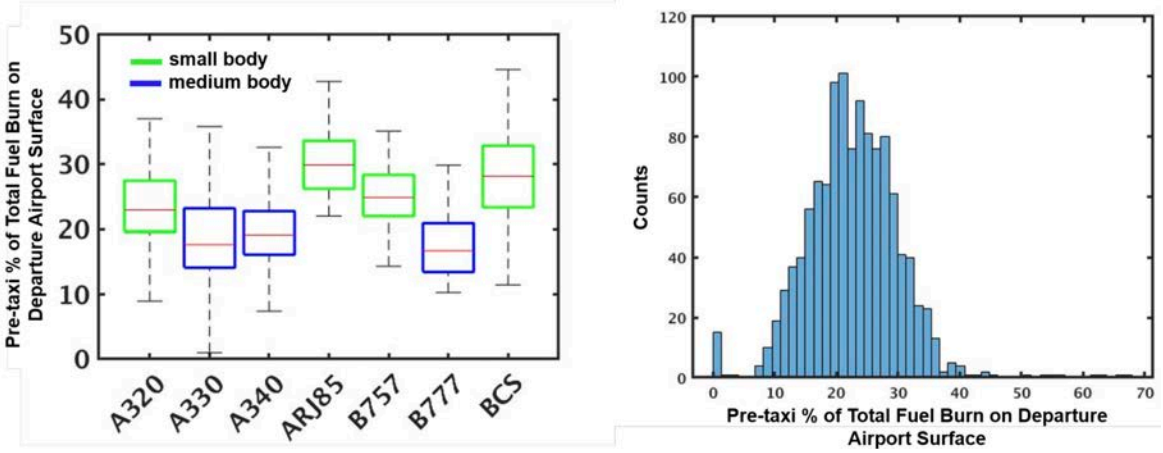


Figure 6. Pre-taxi fuel burn as a percentage of total fuel burned during departure from gate to wheels-off, per aircraft type (left) and aggregate distribution (right).

Task 2A.3- Identify AEDT surface APM enhancements to support emissions and noise inventories

The work to date has focused on the enhancement of AEDT surface APM to support fuel burn models. We have begun to conduct a preliminary study (based on prior literature) to identify potential first-order effects in the modeling of emissions and noise. Our literature survey for emissions modeling has considered literature on NOx (e.g., 'P3-T3' methods), HC, CO, and soot emissions. References [4]-[15] have been the primary sources reviewed for emissions modeling. In ongoing work, we are undertaking a similar exercise on noise modeling, beginning with ACRP 02-27 [16, 17].



Task 2A.4- Recommend AEDT APM enhancements & Coordination with AEDT APM Developers
Based on the modeling enhancements developed from this process, specific targeted recommendations for AEDT APM improvements for the surface domain will be made. Coordination will be required throughout with the primary AEDT APM developers—i.e., Volpe and ATAC—to ensure that the research is practical and will directly inform enhancements to the APM.

Milestone(s)

Phase 2A (Tasks 1-4) were carried out between September 2017-Aug 2018. Phase 2B (Tasks 1-4) are now ongoing. These tasks include:

Task 2B.1: Refine analyses in "1st order" improvement areas
Refine "1st order" AEDT surface fuel burn improvements initiated in prior phases in the areas of: (1) **Pre-taxi operations** (gate and engine start operations), e.g., extending fuel estimates to a wider range of aircraft types, more refined modeling of APU fuel burn rates and usage times to reflect differences between airports, airlines, etc. (2) **Baseline fuel flow rates**, e.g., extending estimates and correlation techniques to a wider range of aircraft types, operating conditions, etc. In particular, develop techniques that can leverage the A4A data, accounting for identified data-quality issues on the surface fuel burn components. (3) **Airport-specific taxi times**, e.g., extending to a wider set of airports (potentially the Core 30) and operating conditions, such as taxi time distributions conditioned on factors such as weather (VMC, IMC), airport congestion level, airport runway configuration, etc.

Task 2B.2: Extend surface fuel burn analyses to align with planned additional AEDT development aligned with different user classes
Based on engagement with AEDT developers in the prior phase of the work, investigate the functionality needed by different user classes, ranging from **basic users** wanting the ability to select "pre-canned" options representative of typical operating conditions, to **advanced users** who may want complete control over all aspects of aircraft and airport dynamics. In addition, the needs may vary depending on whether a user is interested in modeling inventories (i.e., the aggregate) or dispersions at an airport.

Task 2B.3: Undertake initial studies to extend AEDT capabilities to model surface noise and emissions impacts
Appropriate literature sources and the modeling enhancements initiated in the prior phase will be leveraged and extended to explore AEDT surface noise and emissions modeling enhancements. AEDT currently calculates surface emissions as the product of the taxi time, fuel flow rate, and emissions index. The refinements of taxi times and fuel flow rates, as conducted in Task 1, will therefore improve the emissions models within AEDT. The locations and times at which emissions occur are a necessary input for dispersion modeling in AEDT. In other words, the location at which emissions are generated, as well as the distance between the emission source(s) and a receptor (i.e., locations for which the model will derive estimated concentrations of pollutants), have a direct impact on the modeled pollutant concentrations. For surface noise impacts, we are using the findings of ACRP 02-27 as a starting point to identify the aircraft performance modeling needs.

Task 2B.4: Continued coordination with AEDT developers to transition key findings into development plan. Conduct regular analysis status and results review with FAA sponsors and AEDT developers. Based on relevant modeling enhancements identified in the tasks above, discuss specific targeted recommendations for AEDT improvements with developers. Coordinate to align research plans with AEDT development schedule as required.

Publications

E. Clemons, T.G. Reynolds, S. Badrinath, Y. Chati and H. Balakrishnan. Enhancing Aircraft Fuel Burn Modeling on the Airport Surface. AIAA Aviation 2018 Conference, Atlanta, June 2018.

Outreach Efforts

Presentation at the AIAA AVIATION 2018 Conference.

Awards

None

Student Involvement

Graduate students have been involved in all aspects of this research.

Plans for Next Period

Completion of Tasks 2B.1-4.

References

[1] International Civil Aviation Organization (ICAO), "ICAO aircraft engine emissions databank." [Online database], cited 12 February 2014.

[2] ACRP 02-45, "Methodology to Improve EDMS/AEDT Quantification of Aircraft Taxi/Idle Emissions", Transportation Research Board, 2016.

[3] ACRP 02-25, "Handbook for Evaluating Emissions and Costs of APUs and Alternative Systems", Transportation Research Board, 2012.

[4] Dopelheuer A., "Aircraft Emission Parameter Modelling," Air and Space Europe, Vol. 2, No. 3, 2000, pp. 34-37.

[5] Wasiuk, D.K., Lowenberg, M.H., and Shallcross, D.E., \An Aircraft Performance Model Implementation for the Estimation of Global and Regional Commercial Aviation Fuel Burn and Emissions," *Transportation Research Part D*, Vol. 35, 2015, pp. 142-159.

[6] Baughcum, S.L., Tritz, T.G., Henderson, S.C., and Pickett, D.C., "Scheduled Civil Aircraft Emission Inventories for 1992: Database Development and Analysis," NASA Contractor Report 4700, 1996. [Appendix D contains the Boeing Method 2 Fuel Flow Methodology Description].

[7] Kim B. et al., "System for assessing Aviation's Global Emissions (SAGE) Version 1.5, Technical Manual," John A. Volpe National Transportation Systems Center, Massachusetts Institute of Technology, and Logistics Management Institute, Report No. DOT-VNTSC-FAA-05-14, 2005.

[8] International Civil Aviation Organization (ICAO) Aircraft Engine Emissions Databank 2014, https://easa.europa.eu/document-library/icao-aircraft-engine-emissions-databank , [Online database: last accessed February 2014].

[9] Dopelheuer A., and Lecht, M., "Influence of Engine Performance on Emission Characteristics," RTO AVT Symposium on Gas Turbine Engine Combustion, Emissions and Alternative Fuels, Lisbon, October 1998.

[10] Martin, R.L., Oncina, C.A., Zeeben, J.P., "A Simplified Method for Estimating Aircraft Engine Emissions," Appendix C of Scheduled Civil Aircraft Emission Inventories for 1992: Database Development and Analysis by Baughcum, S.L. et al. 1996.

[11] Kyprianidis K.G., Nalianda, D., and Dahlquist, E., "A NOx Emissions Correlation for Modern RQL Combustors," Energy Procedia, Vol. 00, 2015.

[12] Deidewig, F., Dopelheuer, and Lecht., M., "Methods to Assess Aircraft Engine Emissions in Flight," Congress of the International Council of the Aeronautical Sciences, 1996.

[13] Schaefer, M., and Bartosch, S., "Overview on Fuel Flow Correlation Methods for the Calculation of NOx, CO, and HC Emissions and their Implementation into Aircraft Performance Software," DLR Report, 2013.

[14] M. Ahearn et al., "Aviation Environmental Design Tool (AEDT) Technical Manual, Version 2b, Service Pack 3," U.S. Department of Transportation John A. Volpe National Transportation Systems Center, Report No. DOT-VNTSC-FAA-16-11, 2016.

[15] Kim, B., and Rachami, J., "Aircraft Emissions Modeling Under Low Power Conditions," Technical Report, Observatory for Sustainability in Aviation, 2008.

[16] ACRP 02-27, "Enhanced Modeling of Aircraft Taxiway Noise, Volume 1: Scoping", Transportation Research Board, 2009.

[16] ACRP 02-27, "Enhanced Modeling of Aircraft Taxiway Noise, Volume 2: Aircraft Taxi Noise Database and Development Process", Transportation Research Board, 2013.



Project 048 Analysis to Support the Development of an Engine nvPM Emissions Standard

Massachusetts Institute of Technology

Project Lead Investigator

Steven Barrett
Associate Professor
Department of Aeronautics & Astronautics
Massachusetts Institute of Technology
77 Massachusetts Ave
Building 33-316
Cambridge, MA 02139
617-452-2550
sbarrett@mit.edu

University Participants

Massachusetts Institute of Technology

- P.I.: Prof. Steven Barrett
- Co-PI: Dr. Raymond Speth
- FAA Award Number: 13-C-AJFE-MIT, Amendment Nos. 027, 036, and 045
- Period of Performance: July 8, 2016 to Aug. 31, 2019 (Reporting here with the exception of funding level and cost share only for the period October 1, 2017 to September 30, 2018).
- Tasks:
  - Task 1: Develop and evaluate policy and stringency options
  - Task 2: Verify technology response provided by engine manufacturers
  - Task 3: Evaluate proposed fuel sensitivity corrections and ambient conditions corrections
  - Task 4: Map emissions from a short-list of representative engines to all engine/airframe combinations
  - Task 5: Conduct the cost-benefit analysis

Project Funding Level

$350,000 FAA funding and $350,000 matching funds. Sources of matching funds are approximately $105,000 from MIT, plus 3rd-party in-kind contributions of $87,000 from University College London and $158,000 from Oliver Wyman Group.

Investigation Team

Principal Investigator: Prof. Steven Barrett
Co-Principal Investigator: Dr. Raymond Speth
Co-Investigators: Dr. Jayant Sabnis
Graduate Students: Akshat Agarwal

Project Overview

The Federal Aviation Administration's Office of Environment and Energy (FAA-AEE) is working with the international community to establish an international aircraft engine non-volatile particulate matter (nvPM) standard for engines of rated thrust > 26.7 kN. The proposed nvPM standard will influence the development of future engine technologies resulting in reduction of nvPM emissions from aircraft engines. A reduction in nvPM emitted by aircraft engines will lead to improved human health and climate impacts of aviation. To this end, the FAA needs to understand and quantify how an nvPM standard might impact the total nvPM emissions for the National Air Space (NAS) as well as the globe, including overall system-wide environmental and monetary costs and benefits.



The objective of this project is to provide support for FAA decision-making related to the nvPM certification standard by analyzing scenarios involving different emission metrics, stringency options, and assumptions about technology and fleet evolution. The analyses being conducted include economic, climate, air quality, and noise impact assessments on both global and NAS-wide bases. Activities executed for this project year focus on identifying and evaluating nvPM metrics and stringency options, analyzing and developing methods to correct measurements based on fuel properties and ambient conditions, developing emissions inventories based on estimated technological responses to proposed regulations, and conducting cost/benefit analyses of proposed regulations. This research is also contributing to the understanding of how an nvPM standard may influence future engine development, fleet evolution, and associated fleet-wide nvPM emissions.

Task 1- Develop and Evaluate Policy and Stringency Options

Massachusetts Institute of Technology

Objective(s)

Aid the FAA and WG3 indeveloping potential stringency options that can be tested to identify and evaluate potential costs and benefit of nvPM mass and number regulation.

Research Approach

To develop reasonable stringency options, we must account for current technological capabilities and the difficulties faced by engines which are used in different aircraft. As such, we developed a variety of potential limit line shapes, which were presented to WG3 [CAEP11-WG3-PMTG6-WP11]. These options were updated based on feedback from WG3 and aided in developing consensus on a set of stringency options for both mass and number emissions.

Milestone(s)

Stringency options were accepted by WG3. Our analysis helped the group in defining suitable characteristics of the options. Thereafter we helped in processing the stringency options and presenting them in an overview to the group.

Major Accomplishments

Task complete

Outreach Efforts

A series of papers were presented to WG3 and several discussions held with members of the group to improve the options.

Student Involvement

Graduate student Akshat Agarwal was primarily responsible for conducting the analysis and presenting the work.

Plans for Next Period

Task complete

Task 2- Verify Technology Response Provided by Engine Manufacturers

Massachusetts Institute of Technology

Objective(s)

Independently verify the technology response provided by the engine manufacturers and assist the FAA in developing consensus.

Research Approach

OEMs supplied technology responses to WG3, which include the predicted cost to OEMs of reducing nvPM mass or number by a certain amount and also present potential emissions' trade-offs with other species. We used our expertise to evaluate the extent to which these responses are justified and provided feedback to the FAA on how to improve these responses. We used the range of data available in the ICAO emissions data bank (EDB) to compare how historic NO_x standards have led to adoption of combustor technologies affecting other emissions, in particular the smoke number (SN) which has been



shown to be well correlated with nvPM mass emissions. Thus, we can identify changes in SN due to improvements in combustor technology that lead to a reduction in NO_x emissions.

Milestone(s)
EDB data has been analyzed and results shared with the FAA in November 2017.

Outreach Efforts
None

Student Involvement
None

Plans for Next Period
Task complete

Task 3- Evaluate Proposed Fuel Sensitivity Corrections and Ambient Conditions Corrections
Massachusetts Institute of Technology

Objective(s)
Conduct an independent evaluation of the proposed fuel sensitivity corrections and ambient conditions corrections.

Research Approach
Since nvPM emissions are a function of both engine and fuel characteristics, the development of an engine emissions standard requires methods for correcting for variations in nvPM emissions due to changes in fuel composition. We began this process using in-house expertise (Speth et al. 2015), with presentations to WG3 of an approach that correlated emissions to fuel aromatics content. We have since worked with other members of WG3 to reconcile this approach with other approaches based on using the fuel hydrogen content. This collaborative work led to an additional modeling approach which we also presented to WG3. We have continued to provide feedback on the hydrogen-content based approach which has been accepted by the group.

Milestone(s)
- Presented the potential use of fuel aromatics content instead of fuel hydrogen content as correlating parameter.
- Collaborated with other WG3 members to develop an alternative modeling approach using fuel hydrogen content and presented this approach to WG3.

Publications
CAEP11-WG3-PMTG5-IP03, Fuel sensitivity corrections for nvPM measurements.
CAEP11-WG3-PMTG6-WP14, Fuel sensitivity corrections factors for nvPM mass and number.

Outreach Efforts
Regular presentations have been made to the FAA and the Metrics ad-hoc group within PMTG. These efforts are aimed at disseminating preliminary results, engaging in discussions about the approach and receiving feedback from WG3.

Student Involvement
Graduate student Akshat Agarwal is collaborating on the data analyses for this task.

Plans for Next Period
Task complete



Task 4- Map Emissions from a Short-list of Representative Engines to All Engine/Airframe Combinations

Massachusetts Institute of Technology

Objective(s)

Develop mappings between the set of representative engines that were analyzed during the measurement campaign and engine/airframe combinations currently in operation. This mapping will be used to develop projected nvPM emissions inventories for different policy options.

Research Approach

A major improvement from historical smoke standard developed by CAEP is the use of a new measurement method to more precisely estimate nvPM emissions from aircraft engines. The measurement campaign in support of developing an nvPM standard focused on a subset of all available aircraft engines. However, to model the effect of an emissions standard on the current fleet of aircraft, or a projected future fleet, it is crucial to have estimates of nvPM emissions from the full range of engines in use in such a fleet. This requires a mapping between measured and available engines.

We have developed the mapping iteratively, based on consultation with engine manufacturers communicating their own mappings, and MIT has been responsible for ensuring this mapping is reasonable, providing scientific and data-driven justifications. This mapping has now been completed, verified by OEMs, MIT and the FAA. The final step in this process is calculating the nvPM emissions (mass and number) for each of the “modeled” engines and ensure that they lie in the range that is expected. This process will allow for the use of these engines in understanding OEM responses to stringency options.

Milestone(s)

The mapping process has been completed and agreed upon by all parties involved.

Major Accomplishments

The mapping process has been completed and agreed upon by OEMs and the FAA. We have estimated the nvPM emissions from the mapped engines and presented results to WG3 in an information paper to PMTG7 [CAEP11-WG3-PMTG7-IP04]. With feedback from WG3 and PMTG, this was improved upon and presented to FAA and WG3 in February 2018.

Publications

Agarwal, A., Speth, R.L, “Metric values for the GRDB”, 2018, CAEP11-WG3-PMTG7-IP04

Student Involvement

Graduate student Akshat Agarwal is primarily responsible for conducting the mappings.

Plans for Next Period

Task complete

Task 5- Conduct the Cost-Benefit Analysis

Massachusetts Institute of Technology

Objective(s)

Estimate the climate and health impacts of the emissions, and the associated uncertainties, caused by each stringency option defined under Task 1. This task culminates in a report to the FAA to be presented to ICAO-CAEP as an information paper.

Research Approach

This task involves using various tools developed at MIT under the ASCENT projects. This include the APMT-Impacts Climate model developed by under ASCENT Project 21 and the APMT-Impacts Air Quality tool developed by under ASCENT Project



20. The climate model has been continuously improved upon since Marais et al. (2008) and allows us to rapidly estimate the climate impacts due to aviation, along with the uncertainty in this estimate. It has previously been used in the CAEP/8, CAEP/9 and CAEP/10 cycles. The air quality model employs a computationally-efficient adjoint approach to estimate the air quality impacts due to a set of emissions, requiring only multiplication of the pre-computed sensitivities with 3-D emissions (latitude x longitude x altitude). In all estimates, we quantify the uncertainty attributable to the concentration response functions that relate a change in concentration with a change in premature mortalities. In addition, for full-flight emissions, we also estimate the uncertainty due to ammonia emissions. Finally, high-resolution adjoint sensitivities have also been calculated for certain regions (North America and Asia-Pacific) and we use these sensitivities to estimate regional air quality impacts in addition to the global results.

Both the climate and global air quality models are able to compute not only the physical impacts (temperature change and premature mortalities respectively), but also to monetize these impacts for use in a cost-benefit analysis. This aggregate global environmental impact can be combined with estimates of the industry costs to give a net cost-benefit result. If the benefits are greater than the costs, then the regulation is cost-beneficial and vice-versa if the costs outweigh the benefits.

Milestone(s)

Emission datasets from Volpe were provided in July 2018 for all cases. This has allowed us to convert the input to a format that can be used by both models. Preliminary runs of the models have been conducted and regular updates have been provided to FAA project managers.

Outreach Efforts

We have presented our preliminary results to the FAA and will continue to update them as we work through our modeling chain.

Student Involvement

Graduate student Akshat Agarwal is primarily responsible for conducting the analyses.

Plans for Next Period

A paper describing the cost-benefit analysis results will be prepared for submission as an IP to the CAEP/11 meeting.

References

Dopelheuer, A., and M. Lecht. 1998. “Influence of Engine Performance on Emission Characteristics.” In *Symposium of the Applied Vehicle Technology Pane-Gas Turbine Engine Combustion, Emissions and Alternative Fuels, Lisbon, Portugal*. Citeseer. http://citeseerx.ist.psu.edu/viewdoc/download?doi=10.1.1.453.4717&rep=rep1&type=pdf.

Marais, Karen, Stephen P. Lukachko, Mina Jun, Anuja Mahashabde, and Ian A. Waitz. 2008. “Assessing the Impact of Aviation on Climate.” *Meteorologische Zeitschrift* 17 (2): 157–72. https://doi.org/10.1127/0941-2948/2008/0274.

Speth, Raymond L., Carolina Rojo, Robert Malina, and Steven R. H. Barrett. 2015. “Black Carbon Emissions Reductions from Combustion of Alternative Jet Fuels.” *Atmospheric Environment* 105 (Supplement C): 37–42. https://doi.org/10.1016/j.atmosenv.2015.01.040.

Stettler, Marc E. J., Adam M. Boies, Andreas Petzold, and Steven R. H. Barrett. 2013. “Global Civil Aviation Black Carbon Emissions.” *Environmental Science & Technology* 47 (18): 10397–404. https://doi.org/10.1021/es401356v.

Publications Index

Project 001

Twenty graduate students and three undergraduate students involved.

Publications

- Chen, Rui, Zhangcai Qin, Jeongwoo Han, Michael Wang, Farzad Taheripour, Wallace E. Tyner, Don O"Connor, James Duffield (2018). "Life cycle energy and greenhouse gas emission effects of biodiesel in the United States with induced land use change impacts." *Bioresource Technology* 251, pp. 249-258, https://doi.org/10.1016/j.biortech.2017.12.031.
- Yao, Guolin, Mark D. Staples, Robert Malina, and Wallace E. Tyner. "Stochastic techno-economic analysis of alcohol-to-jet fuel production." *Biotechnology for Biofuels* 10:18 (2017), 13 pages.
- McGarvey, Elspeth, and Wallace E. Tyner (2018). "A Stochastic Techno-Economic Analysis of the Catalytic Hydrothermolysis Aviation Biofuel Technology." *Biofuels, Bioproducts, & Biorefining* DOI: 10.1002/bbb.1863.
- Morgan, T.M., A. Youkhana, R. Ogoshi, S. Turn, and M. Garcia-Perez. Review of biomass resources and conversion technologies for alternative jet fuel production in Hawai'i and tropical regions. *Energy & Fuels*. Reviewed and under revision.
- Evan Markel, Burton C. English, Chad Hellwinckel, R. Jamey Menard (2018) Potential for Pennycress to Support a Renewable Jet Fuel Industry. in Ecology, Pollution and Environmental Science, *SciEnvironm* 1:121 accessed at http://hendun.org/journals/EEO/EEO-121.php.
- Sharma, B. 2018. Analyzing the Impacts of Policy Supports and Incentive Programs on Resource Management. Ph.D. dissertation. University of Tennessee.
- Suresh, P, R Malina, MD Staples, S Lizin, H Olcay, D Blazy, MN Pearlson, SRH Barrett, 2018. Life cycle greenhouse gas emissions and costs of production of diesel and jet fuel from municipal solid waste. *Environmental Science and Technology,* DOI: 10.1021/acs.est.7b04277
- Staples, MD, R Malina, P Suresh, JI Hileman, SRH Barrett, 2018. Aviation CO_2 emissions reductions from the use of alternative jet fuels. *Energy Policy,* 114, p. 342-354, DOI: 10.1016/j.enpol.2017.12.007
- de Jong, S, MD Staples, C Grobler, V Daioglou, R Malina, SRH Barrett, R Hoefnagels, A Faaij, M Junginger, 2018. Using dynamic relative climate impact curves to quantify the climate impact of bioenergy production systems over time. *GCB Bioenergy,* DOI: 10.1111/gcbb.12573
- Scott Geleynse, Kristin Brandt, Manuel Garcia-Perez, Michael Wolcott, Xiao Zhang, The Alcohol to Jet Conversion Pathway for Drop-In Alternative jet fuels: Techno-Economic Evaluation. ChemSusChem, 11,3728 –3741 (2018).
- Lewis, Kristin C., Emily K. Newes, Steven O. Peterson, Matthew N. Pearlson, Emily A. Lawless, Kristin Brandt, Dane Camenzind et al. 2018. US alternative jet fuel deployment scenario analyses identifying key drivers and geospatial patterns for the first billion gallons. Biofuels, Bioproducts and Biorefining. Doi: 10.1002/bbb.1951
- Martinkus, Natalie, Greg Latta, Kristin Lynne Brandt, and Michael P. Wolcott. 2018. A Multi-Criteria Decision Analysis Approach to Facility Siting in a Wood-Based Depot-and-Biorefinery Supply Chain Model. Frontiers in Energy Research, 6:124. Doi: 10.3389/fenrg.2018.00124
- Mueller, D., Hoard, S., Smith, P. M., Sanders, C., & Gaffney, M. (2019). Airport Management Perspectives on Aviation Biofuels: Drivers, Barriers, and Policy Requirements in the U.S. Pacific Northwest. *International Journal of Aviation Management*. https://doi.org/10.1504/IJAM.2019.098380
- Martinkus, N., Rijkoff, S.A.M., Hoard, S.A., Shi, W., Smith, P., Gaffney, M. & Wolcott, M. (2017). Biorefinery site selection using a stepwise biogeophysical and social analysis approach. Biomass and Bioenergy, 97, 139-148. doi:10.1016/j.biombioe.2016.12.022
- Rijkhoff, S.A.M., Hoard, S., Gaffney, M.J. & Smith, P.M. (2017). Communities ready for takeoff: Integrating social assets for alternative jet fuel site-selection modeling. Politics and the Life Sciences, 36(1):14-26. doi:10.1017/pls.2017.6
- Camenzind, D. 2018. Supply Chain Analysis for the Production of Alternative Jet Fuel from Oilseeds produced within the U.S. Pacific Northwest. MS Thesis. Washington State University.



Reports

- CAEP/11-AFTF/05-WP/04 – "Updates on Preliminary GTAP-BIO and GLOBIOM Results for Aviation Biofuels Induced Land use change Emission Values," Brasilia, October 2017.
- CAEP/11-AFTF/06-IP/04 – "GTAP-BIO Progress on Estimating Aviation Biofuel Induced Land Use Change Emission Values," Montreal, April 2018.
- CAEP/11-AFTF/06-WP/03 – "Updates on Preliminary Aviation Biofuel Induced Land Use Change Emission Values from GTAP-BIO and GLOBIOM," Montreal, April 2018.
- CAEP/11-AFTF/07-IP/05 – "GTAP-BIO Updates on Estimating Aviation Biofuel Induced Land Use Change Emission Values," Montreal, September 2018.
- CAEP/11-AFTF/07-IP/06 – "Sensitivity Analysis for Key Data and Parameters in GTAP-BIO and AEZ-EF," Montreal, September 2018.
- CAEP/11-AFTF/07-IP/07 – "Discussion of Creating Global or Regional Values for Aviation Biofuel Induced Land Use Change Emissions," Montreal, September 2018.
- CAEP/11-AFTF/07-IP/08 – "Updates of Comparisons between GTAP-BIO and GLOBIOM for Aviation Biofuels Induced Land Use Change Emissions," Montreal, September 2018.
- CAEP/11-AFTF/5-IP/03, Progress on calculation of default core life cycle analysis (LCA) values, presented at AFTF/5, October 2017, Brasilia, Brazil
- CAEP/11-AFTF/5-WP/03, Progress on the core LCA task group, presented at AFTF/5, October 2017, Brasilia, Brazil
- CAEP/11-AFTF/6-IP/06, Progress on calculation of default core LCA values, presented at AFTF/6, April 2018, Montreal, Canada.
- CAEP/11-AFTF/6-WP/04, Summary of the work of CLCA-TG since AFTF05, presented at AFTF/6, April 2018, Montreal, Canada.
- CAEP/11-AFTF/6-IP/08, Assessing LEC and REC for MSW-derived fuels within CORSIA, presented at AFTF/6, April 2018, Montreal, Canada.
- CAEP/11-AFTF/7-IP/11, Progress on calculation of default core LCA values, presented at AFTF/7, September 2018, Montreal, Canada.
- CAEP/11-AFTF/7-IP/04, Report on the progress of the MSW Crediting Small Group, presented at AFTF/7, September 2018, Montreal, Canada.
- CAEP/11-AFTF/7-WP/06, Core LCA progress, September 2018, Montreal, Canada.
- CAEP/11-AFTF/6-IP/05, Stochastic techno-economic analysis for quantitative policy assessment, presented at AFTF/6, April 2018, Montreal, Canada
- CAEP/11-AFTF/7-IP/14, Stochastic techno-economic analysis for quantitative policy assessment, presented at AFTF/7, September 2018, Montreal, Canada
- CAEP/11-AFTF/7-IP/12, Report on the progress of the feedstock classification small group, presented at AFTF/7, September 2018, Montreal, Canada
- CAEP/11-AFTF/7-IP/13, Reporting requirements for actual GHG emissions LCA values, presented at AFTF/7, September 2018, Montreal, Canada

Presentations

- Mueller, D., Hoard, S., Sanders, C. & Gaffney, M. 2018. *From Field to Flight: Using Community Capitals to Predict Sustainable Aviation Biofuel Scale-Up*. Poster, Washington State University Academic Showcase. Pullman, WA.
- Scott Geleynse, Xiao Zhang. Techno-Economic Assessment of Pulp Mill Infrastructure Integration with the Alcohol-to-Jet Pathway for Aviation Fuel Production. International Bioenergy & Bioproducts Conference, October 30, 2018
- Sharma, B., T.E. Yu, B.C. English, and C.N. Boyer. "Economic Analysis of Renewable Jet Fuels: A Game-theoretic Approach," Selected presentation at the 7th International Conference on Transportation and Logistics, Dalian, China. September 8-10, 2018.
- Sharma, B., T.E. Yu, B.C. English, C.N. Boyer, and J.A. Larson. "Stochastic Optimization of Cellulosic Biofuel Supply Chain under Feedstock Yield Uncertainty," Selected presentation at the 10th International Conference on Applied Energy, Hong Kong. August 22-25, 2018.
- Sharma, B., T.E. Yu, B.C. English, and C.N. Boyer. "Analyzing the Economics of Renewable Jet Fuels Using a Game-theoretic Approach," Selected Presentation at Applied and Agricultural Economics Association annual meeting, Washington D.C. August 5-7, 2018.
- Thomas, McKenzie, Kimberly Jensen, Christopher Clark, Dayton Lambert, Burton English, and Forbes Walker. (2019 forthcoming). Consumer Preferences for Potting Mix with Biochar. Paper to be presented at 2019 Southern Agricultural Economics Association Meetings, Birmingham, AL.



Project 002

Four undergraduate students involved.

Reports

- Data provided to ICAO working group 3 Particulate Matter Task Group in paper CAEP11-WG3-PMTG7-IP01

Presentations

- Reported at the ASCENT advisory board meetings held in Cambridge MA, April 2018 and Washington DC October 2018
- AEC Roadmap Meeting held in Washington DC in May 2018

Project 003

Two graduate students involved.

Publications

- Peters JL, Zevitas CD, Redline S, Hastings A, Sizov N, Hart JE, Levy JI, Roof CJ, Wellenius GA. Aviation noise and cardiovascular health in the United States: a review of the evidence and recommendations for research direction, Current Epidemiology Reports 2018; 5(2):140–152. doi.org/10.1007/s40471-018-0151-2.

Presentations

- Nguyen DD, Levy J, Hart JE, VoPham T, Simon MC, Malwitz A, Laden F, Peters JL. Characterizing temporal trends in aviation noise surrounding U.S. airports, ISES/ISEE 2018 Annual Joint Meeting, August 2018 (oral).
- Simon MC, Hart JE, Levy J, VoPham T, Lane KJ, Fabian MP, Nguyen DD, Laden F, Peters JL. Sociodemographic patterns of exposure to civil aircraft noise, ISES/ISEE 2018 Annual Joint Meeting, August 2018 (poster).
- Kim CS, Hart JE, Levy JI, VoPham TM, Simon MC, Nguyen DD, Malwitz A, Laden F, Peters JL. Time-varying aircraft noise exposure and incident hypertension in the Nurses' Health Study, ISES/ISEE 2018 Annual Joint Meeting, August 2018 (oral).

Project 005

Four graduate students involved.

Project 008

- Site developed and contents are published at www.noisequest.psu.edu

Project 010

Nine graduate students involved.

Publications

- Ogunsina, K., Chao, H., Kolencherry, N., Jain, S., Moolchandani, K., Crossley, W. A., and DeLaurentis, D. A., "Fleet-Level Environmental Assessments for Feasibility of Aviation Emission Reduction Goals," Proceedings of CESUN Global Conference 2018, Tokyo, Japan.

Presentations

- ASCENT 10: Aircraft Technology Modeling and Assessment, oral presentation to ASCENT Spring Advisory Committee Meeting, MIT, Cambridge MA, April 4, 2018.
- Ogunsina, K., Chao, H., Kolencherry, N., Jain, S., Moolchandani, K., Crossley, W. A., and DeLaurentis, D. A., "Fleet-Level Environmental Assessments for Feasibility of Aviation Emission Reduction Goals," 2018 Council of Engineering Systems Universities (CESUN) Global Conference, Tokyo, Japan.

Project 011(A)

Four graduate students involved.

Publications

- Jensen, L., "Data-Driven Flight Procedure Simulation and Noise Analysis in a Large-Scale Air Transportation System," *MIT ICAT*, 2018. http://hdl.handle.net/1721.1/116741

Presentations

- Aviation Noise Symposium – February 26, 2018 (briefing)
- ASCENT Advisory Committee Meeting – April 3-4, 2018 (briefing)
- FAA Joint University Program research update meeting briefing, April 19, 2018
- FAA Joint University Program research update meeting briefing, July 23, 2018
- ASCENT Advisory Committee Meeting – October 9-10, 2018 (briefing)
- FAA Joint University Program research update meeting briefing, October 22, 2018
- Airline Industry Consortium briefing, November 8, 2018

Project 017

Publications

- Basner, M., Clark, C., Hansell, A., Hileman, J.I., Janssen, S., Shepherd, K., Sparrow, V.: Aviation noise impacts: state of the science. Noise and Health 19(87): 41-50, 2017.
- Smith, M., Witte, M., Rocha, S., Basner, M.: Effectiveness of incentives and follow-up on increasing survey response rates and participation in field studies. Manuscript currently under FAA project manager review, to be submitted to Public Opinion Quarterly.
- Basner, M., Witte, M., McGuire, S.: Aircraft noise effects on sleep – results of a pilot study near Philadelphia International Airport. Manuscript currently under FAA project manager review, to be submitted to the International Journal of Environmental Research and Public Health.
- Rocha, S., Witte, M., Smith, M., Basner, M.: Survey results from a pilot sleep study near Atlanta international airport. Manuscript to be submitted to International Journal of Environmental Research and Public Health, in preparation.

Project 018

Four graduate students involved.

Presentations

- Dr. Kevin Lane presented an update of the Project 18 field monitoring and descriptive data analysis at the ASCENT Spring 2018 meeting.
- Dr. Kevin Lane presented on "Ultrafine Particulate Matter Monitoring and Source Apportionment", at the Aviation Emissions Characterization Meeting. National Academy of Sciences, DC, USA.
- Dr. Kevin Lane Presented and sat on a panel on "Monitoring and modeling aviation-related ultrafine particles from background concentrations", at the Aviation Emissions Characterization Meeting. National Academy of Sciences, DC, USA.



- Chloe Seyoung Kim presented an oral presentation on a portion of the major accomplishments of Project 18 at the International Society for Exposure Science annual meeting in October 2017.
- Dr. Matthew Simon presented an update of the Project 18 field monitoring and statistical analysis at the ASCENT Fall 2018 meeting.

Project 019

One graduate student involved.

Presentations

- Presentation at bi-annual ASCENT stakeholder meetings in Spring and Fall 2018, Alexandria, VA.
- Moniruzzaman, C. G. & Arunachalam, S. (2018). *An integrated modeled and measurement-based assessment of particle number concentrations from a major US airport.* Oral presentation, Presented at the 2018 Annual CMAS Conference, Chapel Hill, NC.
- Poster presentation at annual CMAS conference (October 2018)
- Poster Presentation at 2018 annual North Carolina BREATHE Conference (Raleigh, NC)
- Poster Presentation at 2018 International Technical Meeting on Air Pollution Modeling and its Application (Ottawa, Canada)

Project 020

Three graduate students involved.

Presentations

- Results were presented at the 2018 ASCENT Spring and Fall meetings

Project 021

One graduate student involved.

Publications

- Sierk de Jong, Mark Staples, Carla Grobler, Vassilis Daioglou, Robert Malina, Steven Barrett, Ric Hoefnagels, André Faaij, Martin Junginger. *Using relative climate impact curves to quantify the climate impact of bioenergy production systems over time*, Accepted to the journal GCB Bioenergy. FAA support under ASCENT Project 1 and ASCENT Project 21 was acknowledged.
- Internal report covering current state of contrail research and proposed plan for development of a reduced-order contrail model was compiled and made available to the FAA.

Presentations

- The modeling approach was presented at ASCENT advisory board meetings (Spring 2018 and Fall 2018).

Project 022

One graduate student involved.

Report

- Zhang and Wuebbles, Evaluation of FAA Climate Tools: APMT. Report for the FAA, March 2018

Presentations

- American Geophysical Union Fall Meeting – December 11-15, 2017 (Presentation)



- ASCENT Advisory Committee Meeting – April 3-4, 2018 (Presentation)
- ASCENT Advisory Committee Meeting – October 9-10, 2018 (Presentation)
- Dr. Wuebbles made a special invited presentation on the history of the understanding of environmental effects from supersonic aircraft at a FAA sponsored meeting in spring 2018.

Project 023

Three graduate students involved.

Publications

- "Block 1 Procedure Recommendations for Logan Airport Community Noise Reduction," 2017. Link: http://hdl.handle.net/1721.1/114038
- "Framework for Analyzing Aircraft Community Noise Impacts of Advanced Operational Flight Procedures," *Submitted for Review, Journal of Aircraft*, 2018.

Presentations

- ASCENT Advisory Committee Meeting – April 3-4, 2018 (poster)
- Presentation to FAA 7100.41 PBN Working Group, May 7, 2018
- FAA Joint University Program research update meeting briefing, July 23, 2018
- ASCENT Advisory Committee Meeting – October 9-10, 2018 (poster)
- Airline Industry Consortium presentation, November 8, 2018

Project 024(B)

One graduate student involved.

Publication

- Abrahamson, J. P., Zelina, J., Andac, M. G., & Vander Wal, R. L. (2016). Predictive Model Development for Aviation Black Carbon Mass Emissions from Alternative and Conventional Fuels at Ground and Cruise. Environmental Science & Technology, 50(21), 12048-12055.
- Abrahamson, J. P., Vander Wal, R. L., (2017). Gas turbine nvPM formation and oxidation semi-empirical model for commercial aviation. Paper 2E19. Topic: Gas Turbine Combustion. 10th US National Meeting of the Combustion Institute, The University of Maryland, College Pak, MD April 23rd - 26th, 2017.

Presentations

- Vander Wal, R. L. Abrahamson, J. P., ASCENT Project No. 24B, Emissions data analysis for CLEEN, ACCESS and other tests. FAA Center of excellence for alternative jet fuels and environment. Contractor's workshop. Alexandria, VA. Sept. 27th–28th, 2016.
- Abrahamson, J. P., Vander Wal, R. L., PM Emissions Analysis and Predictive Assessment: Update on nvPM predictive modeling from conventional and alternative jet fuels. Aviation Emissions Council (AEC) WEBEX seminar. Feb. 23rd, 2017.
- Vander Wal, R. L., Abrahamson, J. P., nvPM Emissions Analysis and Predictive Summary. Poster Presentation. Project 24B Report. FAA Center of Excellence for Alternative Jet Fuels & Environment (FAA COE AJFE). Alexandria, VA April 18th - 19th, 2017.
- Abrahamson, J. P., Vander Wal, R. L., (2017). Gas turbine nvPM formation and oxidation semi-empirical model for commercial aviation. Paper 2E19. Topic: Gas Turbine Combustion. 10th US National Meeting of the Combustion Institute, The University of Maryland, College Park, MD April 23rd - 26th, 2017.



Project 025

Three graduate students involved.

Publications

- S. Wang, T. Parise, S.E. Johnson, D.F. Davidson, R.K. Hanson, "A New Diagnostic for Hydrocarbon Fuels using 3.41-micron Diode Laser Absorption," Combustion and Flame 186 129-139 (2017)
- T. Parise, D.F. Davidson, R.K. Hanson, "Shock Tube/Laser Absorption Measurements of the Pyrolysis of a Bimodal Test Fuel," Proceedings of the Combustion Institute 36 281-288 (2017)
- H. Wang, R. Xu, K. Wang, C.T. Bowman, R.K. Hanson, D.F. Davidson, K. Brezinsky, F.N. Egolfopoulos, "A Physics-based approach to modeling real-fuel combustion chemistry - I. Evidence from experiments, and thermodynamic, chemical kinetic and statistical considerations," Combustion and Flame 193 502-519 (2018)
- R. Xu, K. Wang, S. Banerjee, J. Shao, T. Parise, Y. Zhu, S. Wang, A. Movaghar, D.J. Lee, R. Zhao, X. Han, Y. Gao, T. Lu, K. Brezinsky, F.N. Egolfopoulos, D.F. Davidson, R.K. Hanson, C.T. Bowman, H. Wang, "A physics-based approach to modeling real-fuel combustion chemistry - II. Reaction kinetic models of jet and rocket fuels," Combustion and Flame 193 520-537 (2018)
- J. Shao, Y. Zhu, S. Wang, D. F. Davidson, R. K. Hanson, "A shock tube study of jet fuel pyrolysis and ignition at elevated pressures and temperatures, Fuel 226 338-344 (2018)
- N. Pinkowski, T. Parise, Y. Ding, S. Johnson, Y. Wang, D. F. Davidson, R. K. Hanson, "High-temperature infrared absorption cross-sections to facilitate the study of hydrocarbon pyrolysis," submitted to Journal of Quantitative Spectroscopy and Radiative Transfer, August 2018
- Y. Wang, D. F. Davidson, R. K. Hanson, "A new method of predicting derived cetane number for hydrocarbon fuels," submitted to Fuel, September 2018
- N. Pinkowski, "Jet fuel chemical kinetics: shock tubes, laser diagnostics, and machine learning methods," ASCENT Program Student Paper Competition 2018

Project 027(A)

Six graduate students involved

Project 027(B)

Ten graduate students involved.

Publications

- Ek H., Chterev I., Rock N., Emerson B., Seitzman J., Jiang N., Proscia W., Lieuwen T., Feature Extraction from Time Resolved Reacting Flow Data Sets, Proceedings of the ASME Turbo Expo, Paper #GT2018-77051, 2018.
- Emerson, B., and Ozogul, H. 2018. Experimental Characterization of Liquid-gas Slip in High Pressure, Swirl Stabilized, Liquid-fueled Combustors, in Western States Section of the Combustion Institute – Spring 2018 Meeting.
- Chterev, I., Rock, N., Ek, H., Emerson, B.L., Seitzman, J.M., Lieuwen, T.C., Noble, D.R., Mayhew, E. and Lee, T., 2017. Simultaneous High Speed (5 kHz) Fuel-PLIE, OH-PLIF and Stereo PIV Imaging of Pressurized Swirl-Stabilized Flames using Liquid Fuels. In 55th AIAA Aerospace Sciences Meeting (p. 0152).
- Rock, N., Chterev, I., Emerson, B., Seitzman, J. and Lieuwen, T., 2017, June. Blowout Sensitivities in a Liquid Fueled Combustor: Fuel Composition and Preheat Temperature Effects. In ASME Turbo Expo 2017: Turbomachinery Technical Conference and Exposition (pp. V04AT04A022-V04AT04A022). American Society of Mechanical Engineers.
- Wei, S., Sforzo, B., and Seitzman, J., 2018, "Fuel Composition Effects on Forced Ignition of Liquid Fuel Sprays," *ASME Turbo Expo 2018: Turbomachinery Technical Conference and Exposition*, Oslo, Norway



Presentations

- Ek H., Chterev I., Rock N., Emerson B., Seitzman J., Jiang N., Proscia W., Lieuwen T., Feature Extraction from Time Resolved Reacting Flow Data Sets, ASME Turbo Expo, Paper #GT2018-77051, 2018.
- Emerson, B., and Ozogul, H. 2018. Experimental Characterization of Liquid-gas Slip in High Pressure, Swirl Stabilized, Liquid-fueled Combustors, Western States Section of the Combustion Institute – Spring 2018 Meeting.
- Wei, S., Sforzo, B., and Seitzman, J., 2018, "Fuel Composition Effects on Forced Ignition of Liquid Fuel Sprays," *ASME Turbo Expo 2018: Turbomachinery Technical Conference and Exposition*, Oslo, Norway

Project 028

Four graduate students involved.

Publications

- Yang Gao, "Model Reduction and Dynamic Adaptive Hybrid Integration for Efficient Combustion Simulations," Ph.D. thesis, University of Connecticut, 2017.
- Suo Yang, "Effects of detailed finite rate chemistry in turbulent combustion," Ph.D. thesis, Georgia Institute of Technology, 2017.
- Yang, S., Ranjan, R., Yang, V., Menon, S., Sun, W., "Sensitivity of Predictions to Chemical Kinetics Models in a Temporally Evolving Turbulent Non-premixed Flame," Combustion and Flame, Vol. 183, 224-241, 2017.
- Yang, S., Ranjan, R., Yang, V., Menon, S., Sun, W., "Parallel on-the-fly Adaptive Kinetics in Direct Numerical Simulation of Turbulent Premixed Flame," Proceedings of the Combustion Institute, Vol. 36, Vol. 2, 2025-2032, 2017.
- Yang, S., Ranjan, R., Sun, W., Yang, V., and Menon, S., "Sensitivity to Chemical Kinetics Models in Time Evolving Turbulent Non-Premixed Flames," 10th U.S. National Combustion Meeting, College Park, MD, April 23-26, 2017.
- Rieth, M., Ranjan, R., Kempf, A., and Menon, S., "On the Comparison of Finite-rate Kinetics and Flamelet Based Subgrid Models for LES of Turbulent Premixed Flames," 10th U.S. National Combustion Meeting, College Park, MD, April 23-26, 2017.
- Milan, P., Ranjan, R., Panchal, A., and Menon, S., "Flame Dynamics Sensitivity to Turbulent Combustion Models in a Swirl Spray Combustor," AIAA-2017-5079, 53rd AIAA/SAE/ASEE Joint Propulsion Conference, Atlanta, GA, 10-12 July 2017.
- Ranjan, R., Panchal, A., Hannebique, G., and Menon, S., "Towards Numerical Prediction of Jet Fuels Sensitivity of Flame Dynamics in a Swirl Spray Combustion System," AIAA-2016-4895, 52nd AIAA/SAE/ASEE Joint Propulsion Conference, Salt Lake City, UT, July 25-27, 2016.

Project 029(A)

Four graduate students involved.

Publications

- Veeraraghava Raju Hasti, Prithwish Kundu, Gaurav Kumar, Scott A. Drennan, Sibendu Som, and Jay P. Gore. "A Numerical Study of Flame Characteristics during Lean Blow-Out in a Gas Turbine Combustor", 2018 Joint Propulsion Conference, AIAA Propulsion and Energy Forum, (AIAA 2018-4955)
- Veeraraghava Raju Hasti, Prithwish Kundu, Gaurav Kumar, Scott A. Drennan, Sibendu Som, Sang Hee Won, Frederick L. Dryer, and Jay P. Gore. "Lean blow-out (LBO) computations in a gas turbine combustor", 2018 Joint Propulsion Conference, AIAA Propulsion and Energy Forum, (AIAA 2018-4958)
- Veeraraghava Raju Hasti, Prithwish Kundu, Gaurav Kumar, Scott A. Drennan, Sibendu Som, and Jay P. Gore. "Numerical Simulation of Flow Distribution in a Realistic Gas Turbine Combustor", 2018 Joint Propulsion Conference, AIAA Propulsion and Energy Forum, (AIAA 2018-4956)
- Veeraraghava Raju Hasti, Shuaishuai Liu, Gaurav Kumar, and Jay P. Gore. "Comparison of Premixed Flamelet Generated Manifold Model and Thickened Flame Model for Bluff Body Stabilized Turbulent Premixed Flame", 2018 AIAA Aerospace Sciences Meeting, AIAA SciTech Forum, (AIAA 2018-0150)



- Veeraraghava Raju Hasti, Gaurav Kumar, Shuaishuai Liu, Robert P. Lucht, and Jay P. Gore. "Large Eddy Simulation of Pilot Stabilized Turbulent Premixed CH4+Air Jet Flames", Presented at the 2018 AIAA Aerospace Sciences Meeting, AIAA SciTech Forum, (AIAA 2018-0675)

Presentations

- "Spray Characteristics at Lean Blowout and Cold Start Conditions using Phase Doppler Anemometry," A. J. Bokhart, D. Shin, N. Rodrigues, S. V. Naik, R. P. Lucht, J. P. Gore, P. E. Sojka, and S. E. Meyer, presented at the 2018 AIAA SciTech Meeting, Kissimmee, Florida, 8-12 January 2018.
- "Spray Characteristics of a Hybrid Airblast Pressure-Swirl Atomizer at Cold Start Conditions using Phase Doppler Anemometry," Dongyun Shin, D. Shin, A. J. Bokhart, N. Rodrigues, S. V. Naik, R. P. Lucht, J. P. Gore, P. E. Sojka, and S. E. Meyer, presented at ICLASS 2018 14th Triennial International Conference on Liquid Atomization and Spray Systems, Chicago, Illinois, 22-26 July 2018.
- Veeraraghava Raju Hasti, Prithwish Kundu, Sibendu Som, Robert P. Lucht and Jay P. Gore, "Lean blow-out mechanism in a swirl-stabilized turbulent spray combustion in a realistic gas turbine combustor, Presented at the 71st Annual Meeting of the APS Division of Fluid Dynamics, Sunday–Tuesday, November 18–20, 2018; Atlanta, Georgia, USA
- Veeraraghava Raju Hasti, Prithwish Kundu, Gaurav Kumar, Scott A Drennan, Sibendu Som and Jay P. Gore, "A computational investigation of lean blow-out in a realistic gas turbine combustor", Poster Presentation, 37th International Symposium on Combustion, 29th July – 3rd August 2018, Dublin, Ireland
- Veeraraghava Raju Hasti, Gaurav Kumar, Shuaishuai Liu, Robert P. Lucht and Jay P. Gore, "A computational study on turbulent premixed flames with CO2 dilution", Poster Presentation, 37th International Symposium on Combustion, 29th July – 3rd August 2018, Dublin, Ireland
- Veeraraghava Raju Hasti presented the work on "Computational modeling of fuel effects on engine combustion" at the 2018 Spring Reception Meeting, Office of Interdisciplinary Graduate Programs, Purdue University, West Lafayette, IN, USA
- Veeraraghava Raju Hasti, Prithwish Kundu, Gaurav Kumar, Scott A. Drennan, Sibendu Som, and Jay P. Gore. "A Numerical Study of Flame Characteristics during Lean Blow-Out in a Gas Turbine Combustor", Presented at the 2018 Joint Propulsion Conference, AIAA Propulsion and Energy Forum, (AIAA 2018-4955)
- Veeraraghava Raju Hasti, Prithwish Kundu, Gaurav Kumar, Scott A. Drennan, Sibendu Som, Sang Hee Won, Frederick L. Dryer, and Jay P. Gore. "Lean blow-out (LBO) computations in a gas turbine combustor", Presented at the 2018 Joint Propulsion Conference, AIAA Propulsion and Energy Forum, (AIAA 2018-4958)
- Veeraraghava Raju Hasti, Prithwish Kundu, Gaurav Kumar, Scott A. Drennan, Sibendu Som, and Jay P. Gore. "Numerical Simulation of Flow Distribution in a Realistic Gas Turbine Combustor", Presented at the 2018 Joint Propulsion Conference, AIAA Propulsion and Energy Forum, (AIAA 2018-4956)
- Veeraraghava Raju Hasti, Shuaishuai Liu, Gaurav Kumar, and Jay P. Gore. "Comparison of Premixed Flamelet Generated Manifold Model and Thickened Flame Model for Bluff Body Stabilized Turbulent Premixed Flame", Presented at the 2018 AIAA Aerospace Sciences Meeting, AIAA SciTech Forum, (AIAA 2018-0150)
- Veeraraghava Raju Hasti, Gaurav Kumar, Shuaishuai Liu, Robert P. Lucht, and Jay P. Gore. "Large Eddy Simulation of Pilot Stabilized Turbulent Premixed CH4+Air Jet Flames", Presented at the 2018 AIAA Aerospace Sciences Meeting, AIAA SciTech Forum, (AIAA 2018-0675)

Project 031(A)

One graduate student involved.

Publications

- UDRI Method FC-M-101, "Flow Modulation GCxGC for Hydrocarbon Type Analysis of Conventional and Alternative Aviation Fuels," UDR-TR-2018-40.
- UDRI Method FC-M-102, "Identification and Quantification of Polar Species in Conventional and Alternative Aviation Fuel Using SPE-GCxGC," UDR-TR-2018-41

Presentations

- Presentations on Project 31a were given at the April (Boston) and October (Alexandria) 2018 ASCENT meetings.



Project 033

Two graduate students involved.

Project 034

Four graduate students and three undergraduate students involved.

Publications

- Heyne, J., Peiffer, E., Colket, M., Moder, J., Edwards, J. T., Roquemore, W. M., Shaw, C., Li, C., Rumizen, M., and Gupta, M., "Year 3 of the National Jet Fuels Combustion Program: Practical and Scientific Impacts," 56th AIAA Aerospace Sciences Meeting, Kissimmee, FL: 2018, https://doi.org/10.2514/6.2018-1667
- Stachler, R., Peiffer, E., Kosir, S., Heyne, J., and Stouffer, S., "A Study into the Chemical Timescale for a Toroidal Jet-Stirred Reactor (TJSR)," Central States Section of The Combustion Institute, Minneapolis: 2018. (cssci2018-B604)
- Bell, D. C., Heyne, J. S., Won, S. H., and Dryer, F. L., "The Impact of Preferential Vaporization on Lean Blowout in a Referee Combustor at Figure of Merit Conditions," ASME 2018 Power and Energy Conference, Lake Buena Vista: 2018, https://doi.org/10.1115/POWER2018-7432
- Briones AM, Olding R, Sykes JP, Rankin BA, McDevitt K, Heyne JS. Combustion Modeling Software Development, Verification and Validation. ASME. ASME Power Conference, Volume 1: Fuels, Combustion, and Material Handling; Combustion Turbines Combined Cycles; Boilers and Heat Recovery Steam Generators; Virtual Plant and Cyber-Physical Systems; Plant Development and Construction; Renewable Energy Systems ():V001T01A012. doi:10.1115/POWER2018-7433.
- Peiffer, E., Heyne, J.S., Colket, M., "Characteristic Timescales for Lean Blowout of Alternative Jet Fuels in Four Combustor Rigs," Joint Propulsion Conference, Cincinnati, OH: 2018, https://doi.org/10.2514/6.2018-4914

Presentations

- Colket, Heyne, Lee, "NJFCP Update: Properties and Modeling to FOM Predictions," JetScreen Meeting, Paris, FR, December 2018.
- Heyne, Colket, Lee, "An overview of ASCENT research efforts to improve our understanding of how fuel composition and characteristics determine performance," CAAFI Biennial General Meeting, December 2018.
- Stachler, R., Peiffer, E., Kosir, S., Heyne, J., and Stouffer, S., "A Study into the Chemical Timescale for a Toroidal Jet-Stirred Reactor (TJSR)," Central States Section of The Combustion Institute, Minneapolis: 2018.
- Heyne, J., Edwards, T., "What makes a Great Jet Fuel?," Keynote, Tri-Lateral US-Mexico-Canada Bio-Jet Workshop, Pacific Northwest National Laboratories, May 2018.
- Bell DC, Heyne JS, Won S, Dryer FL. The Impact of Preferential Vaporization on Lean Blowout in a Referee Combustor at Figure of Merit Conditions. ASME. ASME Power Conference, *Volume 1: Fuels, Combustion, and Material Handling; Combustion Turbines Combined Cycles; Boilers and Heat Recovery Steam Generators; Virtual Plant and Cyber-Physical Systems; Plant Development and Construction; Renewable Energy Systems* ():V001T01A011. doi:10.1115/POWER2018-7432.
- Peiffer, Erin, Heyne, Joshua. 2018. "Combustor Rig Sensitivity to Derived Cetane Number for Lean Blowout and Ignition Results from Year Three of the National Jet Fuels Combustion Program." Dayton-Cincinnati Aerospace Sciences Symposium. Dayton, Ohio: ASME.
- Peiffer, Erin, Heyne, Joshua, Colket, Meredith. 2018. "Characteristic Timescales for Lean Blowout of Alternative Jet Fuels." Joint Propulsion Conference. Cincinnati, Ohio: AIAA.
- Joshua S. Heyne, Erin Peiffer, Meredith B. Colket, Aniel Jardines, Cecilia Shaw, Jeffrey P. Moder, William M. Roquemore, James T. Edwards, Chiping Li, Mark Rumizen, and Mohan Gupta. "Year 3 of the National Jet Fuels Combustion Program: Practical and Scientific Impacts of Alternative Jet Fuel Research", 2018 AIAA Aerospace Sciences Meeting, AIAA SciTech Forum, (AIAA 2018-1667)
- Heyne, Colket, "Overview and Results from the National Jet Fuels Combustion Program," CAAFI SOAP-Jet Webinar, Jan. 2018.
- Med Colket, Sang Hee Won, Stephen, Dooley, Bill Pitz, Charlie Westbrook, Josh Heyne, Fred Dryer, Steve Zeppieri, "Surrogates for Practical Fuels: Historical Perspective, Palettes, Selection, Use and Modeling," 2018 MACCCR Meeting, Sandia National Laboratories, Livermore, CA, 2018.



- Colket, Heyne, "NJFCP Update," JET SCREEN Meeting, Rome, October 2017.

Project 036

Four graduate students involved

Publications

- Yongchang Li, Dongwook Lim, Michelle Kirby, Dimitri Mavris, George Noel, Uncertainty Quantification Analysis of the Aviation Environmental Design Tool in Emission Inventory and Air Quality Modeling, AVIATION 2018 conference, June 17 – 21, 2018.
- Dongwook Lim, Yongchang Li, Matthew J Levine, Michelle R Kirby, Dimitri, Mavris, Parametric Uncertainty Quantification of Aviation Environmental Design Tool, AVIATION 2018 conference, June 17 – 21, 2018.
- Jung-Hyun Kim, Kisun Song and Seulki Kim, Yongchang Li, Dimitri Mavris, Aircraft Mission Analysis Enhancement by using Data Science and Machine Learning Techniques, Submitted to AVIATION 2019 conference

Presentations

- Yongchang Li, Dongwook Lim, Michelle Kirby, Dimitri Mavris, George Noel, Uncertainty Quantification Analysis of the Aviation Environmental Design Tool in Emission Inventory and Air Quality Modeling, AVIATION 2018 conference, June 17 – 21, 2018.
- Dongwook Lim, Yongchang Li, Matthew J Levine, Michelle R Kirby, Dimitri, Mavris, Parametric Uncertainty Quantification of Aviation Environmental Design Tool, AVIATION 2018 conference, June 17 – 21, 2018.

Project 37

One graduate student involved.

Project 038

One graduate student involved.

Project 039

Two graduate students involved.

Publications

- This work is currently being prepared for publication as a paper entitled "Techno-economic Assessment of Removing Jet Fuel Naphthalene to Reduce Aviation-attributable Non-volatile Particulate Matter Emissions."

Presentations

- Drew Weibel gave a presentation entitled "Naphthalene Removal Assessment: Cleaning up Jet Fuel for Reduced Environmental Impacts" at the CRC Aviation Meeting on May 3, 2018.
- Raymond Speth gave a presentation with an overview of the project at the Aviation Emissions Characterization Roadmap Meeting on May 23, 2018.

Project 040

Three graduate students involved.

Publications

- Patankar, H. P., and Sparrow, V. W. “Quantifying the effect of uncertainty in meteorological conditions on aircraft noise propagation." INTER-NOISE and NOISE-CON Congress and Conference Proceedings, 4745-4754.

Presentations

- Patankar, H. P., and Sparrow, V. W. “Quantifying the effect of uncertainty in meteorological conditions on aircraft noise propagation." 47th International Congress and Exposition on Noise Control Engineering, INTER-NOISE 2018.

Project 041

Three graduate students involved.

Publications

- J. Xu, V. Sparrow, “Investigation of deturbing methods for sonic boom signatures,” J. Acoust. Soc. Am. **143**(3, Pt. 2) 1913 (2018), 7-11 May 2018 Acoustical Society of America presentation, Minneapolis, MN, USA.

Presentations

- J. Xu, V. Sparrow, “Investigation of deturbing methods for sonic boom signatures,” 7-11 May 2018 Acoustical Society of America presentation, Minneapolis, MN, USA.

Project 042

Three graduate students involved.

Publications

- Z. Huang and V. W. Sparrow, "An improved Mach cut-off model based on a 3-D ray tracing method and realistic atmospheric data," *J. Acoust. Soc. Am.*, **143**(3), 1913 (2018), invited presentation at 175th Meeting of the Acoustical Society of America, Minneapolis, MN, USA, May 07-11, 2018.
- N. D. Ortega; M. C. Vigeant; V. W. Sparrow, “Perceptual characterization of Mach cut-off Sonic Booms,” J. Acoust. Soc. Am. **143** (3, Pt. 2) 1936 (2018). Presentation at ASA Spring 2018 in Minneapolis, MN, USA in May 2018.

Presentations

- Z. Huang and V. W. Sparrow, " An Improved Mach Cut-off Model Based on a 3-D Ray Tracing Method and Realistic Atmospheric Data," Poster for the Penn State Center for Acoustics and Vibration (CAV) Spring Workshop, University Park, PA, April 24-25, 2018.
- Z. Huang and V. W. Sparrow, "An improved Mach cut-off model based on a 3-D ray tracing method and realistic atmospheric data," invited presentation at 175th Meeting of the Acoustical Society of America, Minneapolis, MN, USA, May 07-11, 2018.
- N. D. Ortega; M. C. Vigeant; V. W. Sparrow, “Perceptual characterization of Mach cut-off Sonic Booms,” Presentation at ASA Spring 2018 in Minneapolis, MN, USA in May 2018.

Project 043

Four graduate students involved.

Publications

- A journal paper submitted to the AIAA Journal of Aircraft is expected. Arturo Santa-Ruiz is the first author of the paper.



Project 045

Four graduate students involved.

Publications

- Matthew J Levine, Dongwook Lim, Yongchang Li, Michelle R Kirby, Dimitri, Mavris, Quantification of Error for Rapid Fleet-Level Noise Computation Model Assumptions, AVIATION conference, June 17-21, 2018.
- Dongwook Lim, Matthew Levine, Vu Ngo, Michelle Kirby, and Dimitri Mavris, Improved Aircraft Departure Modeling for Environmental Impact Assessment, AVIATION conference, June 17-21, 2018.

Presentations

- Matthew J Levine, Dongwook Lim, Yongchang Li, Michelle R Kirby, Dimitri, Mavris, Quantification of Error for Rapid Fleet-Level Noise Computation Model Assumptions, AVIATION conference, June 17-21, 2018.
- Dongwook Lim, Matthew Levine, Vu Ngo, Michelle Kirby, and Dimitri Mavris, Improved Aircraft Departure Modeling for Environmental Impact Assessment, AVIATION conference, June 17-21, 2018.

Project 046

Two graduate students involved.

Publications

- E. Clemons, T.G. Reynolds, S. Badrinath, Y. Chati and H. Balakrishnan. Enhancing Aircraft Fuel Burn Modeling on the Airport Surface. AIAA Aviation 2018 Conference, Atlanta, June 2018.

Presentations

- E. Clemons, T.G. Reynolds, S. Badrinath, Y. Chati and H. Balakrishnan. Enhancing Aircraft Fuel Burn Modeling on the Airport Surface. Presented at the AIAA Aviation 2018 Conference, Atlanta, June 2018.

Project 048

One graduate student involved.

Publications

- Agarwal, A., Speth, R.L, “Metric values for the GRDB”, 2018, CAEP11-WG3-PMTG7-IP04



Project Funding Allocations by Federal Fiscal Year

Breakout by Project

Project		Funding Based on award date					
		2014	2015	2016	2017	2018	Total
001	Alternative Jet Fuel Supply Chain Analysis	$1,599,943	$1,425,000	$1,498,749	$1,855,461	$1,102,865	$7,482,018
002	Ambient Conditions Corrections for Non-Volatile PM Emissions Measurements	$2,800,000	$750,000	-$147,766	$725,500		$4,127,734
003	Cardiovascular Disease and Aircraft Noise Exposure	$200,000	$200,000	$200,000	$340,000		$940,000
004	Estimate of Noise Level Reduction	$150,000	-	-	-	-$8,845	$141,155
005	Noise Emission and Propagation Modeling	$212,000	$200,000	-	-		$412,000
006	Rotorcraft Noise Abatement Operating Conditions Modeling	$250,326	-	-	-		$250,326



007	Civil, Supersonic Over Flight, Sonic Boom (Noise) Standards Development	$100,000	$200,000	-	-		$300,000
008	Noise Outreach	$ 30,000	$ 50,000	$ 75,000	$ 25,000		$180,000
010	Aircraft Technology Modeling and Assessment	$899,979	$200,000	$310,000	$669,567	$764,185	$2,843,731
011	Rapid Fleet-wide Environmental Assessment Capability	$600,000	$270,000	$300,000	-		$1,170,000
012	Aircraft Design and Performance Assessment Tool Enhancement	$ 90,000	-	-	-		$90,000
013	Micro-Physical Modeling & Analysis of ACCESS 2 Aviation Exhaust Observations	$200,000	-	-	-		$200,000
014	Analysis to Support the Development of an Aircraft CO2 Standard	$520,000	-	-	-		$520,000
017	Pilot Study on Aircraft Noise and Sleep Disturbance	$154,000	$343,498	$266,001	$134,924		$898,423



018	Health Impacts Quantification for Aviation Air Quality Tools	$150,000	$150,000	$200,000	$270,000		$770,000
019	Development of Aviation Air Quality Tools for Airport-Specific Impact Assessment: Air Quality Modeling	$320,614	$369,996	-	$625,378		$1,315,988
020	Development of NAS wide and Global Rapid Aviation Air Quality	$150,000	$200,000	$250,000	$250,000		$850,000
021	Improving Climate Policy Analysis Tools	$150,000	$150,000	$150,000	$150,000		$600,000
022	Evaluation of FAA Climate Tools	$150,000	$30,000	$ 75,000	$100,000		$355,000
023	Analytical Approach for Quantifying Noise from Advanced Operational Procedures	-	$296,711	$250,000	$250,000		$796,711
024	Emissions Data Analysis for CLEEN, ACCESS, and Other Recent Tests	$244,975	-	$ 75,000	-		$319,975



025	National Jet Fuels Combustion Program – Area #1: Chemical Kinetics Combustion Experiments	-	$615,000	$210,000	$200,000	$ 2,556	$1,027,556
026	National Jet Fuels Combustion Program – Area #2: Chemical Kinetics Model Development and Evaluation	-	$200,000	-	-	-$ 2,556	$197,444
027	National Jet Fuels Combustion Program – Area #3: Advanced Combustion Tests	-	$1,010,000	$580,000	$265,000		$1,855,000
028	National Jet Fuels Combustion Program – Area #4: Combustion Model Development and Evaluation	-	$470,000	$ 55,000	-		$525,000
029	National Jet Fuels Combustion Program – Area #5: Atomization Tests and Models	-	$640,000	$360,000	$150,000		$1,150,000



030	National Jet Fuels Combustion Program – Area #6: Referee Swirl-Stabilized Combustor Evaluation/Support	-	$349,949	-	-		$349,949
031	Alternative Jet Fuels Test and Evaluation	-	$489,619	$744,891	$999,512	$183,019	$2,417,041
032	Worldwide LCA of GHG Emissions from Petroleum Jet Fuel	-	$150,000	-	-		$150,000
033	Alternative Fuels Test Database Library	-	$199,624	$119,794	$165,000		$484,418
034	National Jet Fuels Combustion Program – Area #7: Overall Program Integration and Analysis	-	$234,999	$635,365	$192,997	$374,978	$1,438,339
035	Airline Flight Data Examination to Improve flight Performance Modeling	-	$150,001	-	-		$150,001



036	Parametric Uncertainty Assessment for AEDT2b	-	$ 65,000	$175,000	$380,000		$620,000
037	CLEEN II Technology Modeling and Assessment	-	$200,000	$150,000	$170,000		$520,000
038	Rotorcraft Noise Abatement Procedures Development	-	$150,000	$150,000	$150,000	$150,000	$600,000
039	Nephthalene Removal Assessment	-	-	$200,000	$290,000		$490,000
040	Quantifying Uncertainties in Predicting Aircraft Noise in Real-world Situations	-	-	$218,426	$200,000		$418,426
041	Identification of Noise Acceptance Onset for Noise Certification Standards of Supersonic Airplane	-	-	$160,000	$221,000		$381,000



042	Acoustical Model of Mach Cut-off	-	-	$255,000	$150,000	$170,000	$575,000
043	Noise Power Distance Re-Evaluation	-	-	$150,000	$ 75,000		$225,000
044	Aircraft Noise Abatement Procedure Modeling and Validation	-	-	-	-	$350,000	$350,000
045	Takeoff/Climb Analysis to Support AEDT APM Development	-	-	$250,000	$ 75,000	$ 8,845	$333,845
046	Surface Analysis to Support AEDT APM Development	-	-	$ 75,000	$ 75,000	$ 75,000	$225,000
048	Analysis to Support the Development of an Engine nvPM Emissions Standards	-	-	$150,000	$200,000		$350,000



Breakout by University*

	Funding Based on award year						
University	**2013**	**2014**	**2015**	**2016**	**2017**	**2018**	**Total**
Boston University	$5,000	$350,000	$350,000	$400,000	$610,000		$1,715,000
Georgia Institute of Technology	$5,000	$1,660,000	$1,625,001	$1,435,000	$1,468,500	$650,000	$6,843,501
Massachusetts Institute of Technology	$10,000	$1,153,927	$1,179,073	$1,855,000	$1,690,000	$1,000,000	$6,888,000
Missouri University of Science and Technology	$5,000	$2,800,000	$750,000	-$147,766	$725,500		$4,132,734
Oregon State University	$5,000	-	$160,000	$80,000	$59,000		$304,000
Pennsylvania State University	$5,000	$862,301	$766,711	$958,426	$890,424	$320,000	$3,802,862
Purdue University	$5,000	$389,979	$1,030,000	$763,750	$747,067	$114,185	$3,049,981
Stanford University	$5,000	$380,000	$1,155,000	$345,000	$200,000		$2,085,000



University of Dayton	$5,000	-	$906,196	$1,349,087	$1,192,509	$574,944	$4,027,736
University of Hawaii	$10,000	-	$75,000	$100,000	$125,000		$310,000
University of Illinois	$5,000	$349,943	$553,000	$375,000	$265,000		$1,547,943
University of North Carolina	$5,000	$320,614	$369,996	-	$625,378		$1,320,988
University of Pennsylvania	$5,000	$154,000	$343,498	$266,001	$134,924		$903,423
University of Tennessee	$5,000	$200,000	$100,000	$100,000	$225,000		$630,000
University of Washington	$5,000	$60,000	$29,997	$15,000			$109,997
Washington State University	$20,000	$974,228	$864,968	$725,961	$796,039	$510,918	$3,892,114



Breakout by State*

	Funding Based on award year						
State	**2013**	**2014**	**2015**	**2016**	**2017**	**2018**	**Total**
California	$5,000	$380,000	$1,155,000	$345,000	$200,000		2,085,000
Georgia	$5,000	$1,660,000	$1,625,001	$1,435,000	$1,468,500	$650,000	$6,843,501
Hawaii	$10,000	-	$75,000	$100,000	$125,000		$310,000
Illinois	$5,000	$349,943	$553,000	$375,000	$265,000		$1,547,943
Indiana	$5,000	$389,979	$1,030,000	$763,750	$747,067	$114,185	$3,049,981
Massachusetts	$15,000	$1,503,927	$1,529,073	$2,255,000	$2,300,000	$1,000,000	$8,603,000
Missouri	$5,000	$2,800,000	$750,000	-$147,766	$725,500		$4,132,234
North Carolina	$5,000	$320,614	$369,996	-	$625,378		$1,320,988
Ohio	$5,000	-	$906,196	$1,349,087	$1,192,509	$574,944	$4,027,736
Oregon	$5,000	-	$160,000	$80,000	$59,000		$304,000
Pennsylvania	$10,000	$1,016,301	$1,110,209	$1,224,427	$1,025,348	$320,000	$4,706,285
Tennessee	$5,000	$200,000	$100,000	$100,000	$225,000		$630,000
Washington	$25,000	$1,034,228	$894,965	$740,961	$796,039	$510,918	$4,002,111

*Totals include administrative funds not associated with specific NFOs